Geotechnical Special Publication No. 208

Earth Retention Conference 3

Proceedings of the 2010 Earth Retention Conference

Edited by Richard J. Finno, Ph.D., P.E.,
Youssef M. A. Hashash, Ph.D., P.E., and
Pedro Arduino, Ph.D., P.E.

ASCE

G-I GEO-INSTITUTE ASCE

GEOTECHNICAL SPECIAL PUBLICATION NO. 208

EARTH RETENTION CONFERENCE 3

PROCEEDINGS OF THE 2010 EARTH RETENTION CONFERENCE

August 1–4, 2010
Bellevue, Washington

SPONSORED BY
The Geo-Institute of the American Society of Civil Engineers

EDITED BY
Richard J. Finno, Ph.D., P.E.
Youssef M. A. Hashash, Ph.D., P.E.
Pedro Arduino, Ph.D., P.E.

Published by the American Society of Civil Engineers

Library of Congress Cataloging-in-Publication Data

Earth Retention Conference (3rd : 2010 : Bellevue, Wash.)
Earth Retention Conference 3 : proceedings of the 2010 Earth Retention Conference, August 1–4, 2010, Bellevue, Washington / sponsored by the Geo-Institute of the American Society of Civil Engineers ; edited by Richard J. Finno, Youssef M. A. Hashash, Pedro Arduino.
p. cm.
Includes bibliographical references and index.
ISBN 978-0-7844-1128-5
1. Earthwork--Congresses. 2. Shoring and underpinning--Congresses. 3. Retaining walls--Congresses. I. Finno, Richard J. II. Hashash, Youssef M. A. III. Arduino, Pedro. IV. American Society of Civil Engineers. Geo-Institute. V. Title.

TA760.E17 2010
624.1'64--dc22 2010023353

American Society of Civil Engineers
1801 Alexander Bell Drive
Reston, Virginia, 20191-4400

www.pubs.asce.org

ISBN 978-0-7844-1128-5
Manufactured in the United States of America.

Preface

The 2010 Earth Retention Conference (ER2010) is the third in a series of conferences on earth retaining structures organized by the Earth Retaining Structures Committee of the Geo-Institute of ASCE. Held at 20-year intervals, ER2010 follows the highly successful earth retention conferences held in Ithaca, New York (1990) and (1970). The objective of the conference and the related proceedings is to review major developments in the design and construction practice of earth retaining structures worldwide over the past 20 years.

The conference organizing committee consisted of the following members who were responsible for the planning and execution of the conference:

Youssef M. A. Hashash, Ph.D., P.E., University of Illinois at Urbana-Champaign
Conference Chair

Richard Finno, Ph.D., P.E., Northwestern University
Technical Program Coordinator

Pedro Arduino, Ph.D., P.E., University of Washington
Student Program Coordinator

John R. Wolosick, P.E., Hayward Baker
Exhibitors and Field Demonstrations Coordinator

Kimberly A. Warren, Ph.D., University of North Carolina at Charlotte
Short Course Coordinator

Joe Cavanaugh, P.E., Tensar International Corporation

Hubert Deaton, P.E., Schnabel Foundation Company

Lawrence A. Hansen, Ph.D., P.E., AMEC Earth & Environmental, Inc.

Andrew J. Whittle, Sc.D., P.E., Massachusetts Institute of Technology

Carol W. Bowers, P.G., CAE, Director, Geo-Institute of ASCE

Lauren E. Tighe, Board and Meetings Specialist, Geo-Institute of ASCE

Stacey Ann P. Gardiner, CMP, Geo-Institute Conference Manager

A general call for abstracts was issued in the summer of 2009. Of the submissions made in response to this call, 72 papers were accepted and 38 abstracts/papers were declined. Each submission was reviewed by at least two reviewers. Internationally known experts were invited to cover specific topics of interest and contributed an additional 21 invited papers. All 93 papers published in the proceedings are eligible for ASCE awards.

Youssef M.A. Hashash
Conference Chair

Acknowledgements

The editors are grateful for the following individuals who reviewed abstracts and papers for this proceedings.

Robert Alperstein
Daniel Alzamora
Glen Andersen
Tom Anderson
Pedro Arduino
Jonathan Bennett
Shobha Bhatia
John Bickford
James Blackburn
Stan Boyle
Jonathan Bray
Lindsey Bryson
Kevin Cargill
Raymond Castelli
Joseph Cavanaugh
Armando Cazzola
Susan Chang
Ashok Chugh
Lucas deMelo
Gordon Denby
Elizabeth Dwyre
Ghada Ellithy
Clifton Farnsworth
Mitchell Fong
Karen Geraci
Robert Gladstone
Jesus Gomez
Jean Habimana
Lawrence Hansen
Mohamed Haque
Fransiscus Hardianto
Chu Ho
Terence Holman
Rupert Hon
John Horvath
Robert Jameson
Tae Ju
Karina Karina
Edward Kavazanjian
Dimitrios Konstantakos
Arvind Kumbhojkar
Walter Kutschke
Debra Laefer
Thomas Lee
Doug Lindquist
Barbara Luke
Daniel Mageau
Camilo Marulanda
Stephen McLandrich
Donald McMahon
William Neely
Charles Ng
Phillip Ooi
Nick O'Riordan
Ali Porbaha
Daniel Pradel
Susan Rafalko
Hosam Salman
John Sankey
James Schmidt
Lok Sharma
Raj Siddharthan
George Siller
Michael Simac
Alan Stadler
Bryan Sweeney
Harry Tan
Burak Tanyu
Gary Taylor
John Thornley
Ketan Trivedi
Edward Ulrich
Daniel Uranowski
Kimberly Warren
David Weatherby
Gregory Wilson
Xiangwu Zeng.

Richard J. Finno, M. ASCE
Youssef M. A. Hashash, M. ASCE
Pedro Arduino, M. ASCE
Proceedings Editors

This page intentionally left blank

Contents

Case Studies

Mechanically Stabilized Earth Retaining Walls

Overview

Design Issues

Case Studies

Seismic Evaluation of Retention Systems

Numerical Analyses of Retention Systems

Load and Resistance Factor Design

Other Walls

Landslide Stabilization

Indexes

Recent Trends in Supported Excavation Practice

Richard J. Finno[1], M. ASCE, Ph.D. P.E., D.GE.

[1] Professor, Dept of Civil and Environmental Engineering, Northwestern University, Evanston, IL, 60208, r-finno@northwestern.edu

ABSTRACT

This paper presents an overview of developments and trends in the practice of supported excavations since 1990. Soil mixed walls, ground improvement and hybrid support systems are more frequently used. Design has evolved such that stiffness based approaches are common in urban areas. LRFD based design is replacing traditional allowable stress design in a number of situations. Numerical analyses of support systems have become more prevalent, especially in situations where ground movements adjacent to an excavation are important. With developments in sensors and information technology, the observational approach is becoming more automated, with near real time data available to share holders. This paper summarizes these trends and speculates how they may evolve in the future.

INTRODUCTION

In no other situation are the design, construction and performance of geotechnical works more interrelated than deep supported excavations. The details of construction can have a decisive effect on the outcome of a particular project, and these impacts must be considered in design. This fact has been implicit in practice since Terzaghi and Peck (1967) published apparent earth envelopes for use in design of internally-braced excavations, and characterized zones of performance in terms of "average workmanship."

The practice of deep excavation support has advanced in the intervening 20 years since the state-of-the-practice was summarized in 1990 at the conference on Design and Performance of Earth Retaining Structures. A great deal of time at this conference will be spent discussing advances related to design, construction and performance of supported excavations. For example, new wall systems and innovative support methods have been introduced. Basic design philosophies are in flux with the introduction of LRFD. Stiffness-based design of support systems has become common for excavations made next to movement-sensitive structures. Numerical analyses of excavation support systems have become more prevalent because of the need to compute ground deformations associated with excavations and to more closely link support requirements with actual soil conditions. Furthermore, results of finite element simulations of excavations are being used to size support elements. Sessions will be dedicated to each of these issues. Manufacturers have not stood still, and the capabilities of construction equipment have been enhanced. Some of these capabilities are described in case studies presented at this conference. The ultimate measure of any design is indeed its performance and this theme is emphasized throughout the conference proceedings.

Because this paper serves as an overview of the recent developments and future trends and as an introduction to the portions of the conference related to deep supported excavations, it by necessity is a bare bones treatment. More detail can be found in the excellent topic-specific papers included in this proceedings volume. It is further influenced, probably unduly, by the author's experiences. That being said, this paper will summarize the trends since our last meeting in 1990, with some emphasis on the emergence of stiffness-based design and corresponding increase in numerical analyses of support systems. Future directions in the practice are projected.

TRENDS SINCE 1990

Many large-scale deep excavation projects have been undertaken in the past 20 years. In the US, the largest undertaking was the Central Artery and Tunnel project in Boston, which has been the subject of many publications and much discussion. In Europe, major excavation projects for public works have been undertaken in London, Berlin and Amsterdam. In the Americas, projects have been completed in Washington, D.C., Los Angeles, Toronto, Santiago, Mexico City, Bogata and Puerto Rico. In addition to these public works projects, many private developers took advantage of the booming economic conditions of the 1990s and early 2000s to finance construction of large commercial buildings, and their accompanying deep excavations. There has been explosive public and private development in Southeast Asia. Major underground work has been reported from projects in Hong Kong, Taipei, Toyko, Seoul, Osaka, Singapore and Shanghai. Many of these projects were summarized in a volume edited by Lambrechts et al. (1998).

A number of these excavations have been installed to greater depths than before in a given geologic setting, pushing the state-of-the-art in some locales. Ground movements induced adjacent to the excavations generally are now limited to smaller magnitudes than 20 years ago as a result of increased permitting and regulatory restrictions, increased awareness of adjacent property owners and threat of litigation. Excavations from a number of these projects are discussed in more detail in papers presented at this Conference.

Wall systems

While diaphragm slurry walls, cylinder pile walls and soil mixed walls all were introduced to practice by 1990, they have become much more commonplace since that time. Use of top down construction has increased as more developers have seen the benefit of taking the excavation portion of a project off the critical path. Top down methods use permanent walls and flooring systems as temporary support and thus the support systems are generally very stiff. Yet, there are conflicting data concerning whether resulting movements are smaller than that associated with bottom-up methods. For example, Long (2001) observed no discernible difference in the performance of internally supported, anchored, or top-down systems based on examination of 296 excavation case studies. In contrast, Kung (2009) reported results of 26 excavations made through Taipei silty clay which showed the maximum lateral wall deflection induced by the top-down methods were 1.3 times larger than that induced by bottom up methods. A portion of the ground movements associated with these wall systems arises from shrinkage of concrete floor slabs after they have been connected to the walls, and this should be considered when evaluating adjacent ground movements.

Deep mixing has also been used to create walls, usually reinforced with steel beams (e.g., O'Rourke and O'Donnell 1997; Porbaha et al. 1999; Parmantier et al. 2009). The technology to create these walls has been called various names depending on the manufacturer of the equipment: deep mixed walls, soil mixed walls or cutter soil mixed walls. The essential idea is the same, to mix in situ soil with additives to create a wall with adequate strength and stiffness. Quality control testing usually consists of unconfined compression tests. While adequate for this purpose, more detailed characterization of its constitutive behavior is warranted, particularly when the design of the wall system includes numerical evaluation. In this way, the data input would be compatible with the more sophisticated constitutive models used to represent soil behavior.

Hybrid support systems are those that combine different types of lateral support. These are becoming more common as space becomes more valuable in urban areas. Examples include combinations of internal braces and tiedback ground anchors (e.g., Finno et al 2002) and soil nails and tiedback ground anchors (e.g., Denby 2010). Another novel system is suspension wall shoring. This system consists of steeply angled pre-tensioned soil nails and near vertical compression soil nails arranged to suspend a prestressed shotcrete facing. The idea is to produce near at-rest lateral earth pressures so as to minimize soil deformations (Wolschlag et al. 1999). The arrangement of the nails permits installation around utilities, and is useful for excavations in granular and cemented soils above the water table. A challenge in using these systems is that there is no directly applicable precedent that applies, and as such close monitoring of field performance is warranted.

Since 1990, ground improvement techniques to stiffen and strengthen soil below the bottom of an excavation between the walls have been become more commonplace in some locales to minimize movements in excavations through soft clays (e.g., Ou et al 1996a; Ou et al 2008). The *in situ* soil is commonly strengthened by jet grouting or mechanical deep mixing. The improved ground acts as a strut to support the toe of a support wall and is most effective when the factor of safety against basal heave is low and the walls are closely spaced. Improved soil also has been used as a buttress for the same purposes (Tanaka 1993; O'Rourke and O'Donnell 1997; Uchiyama et al. 1999).

Design Issues

The design of deep supported excavations requires careful consideration of global stability, structural capacity of the support elements, ground deformations and control of ground water. Depending on site constraints, the selection of the support system elements will be governed by assumptions regarding either lateral loading or allowable ground deformations (serviceability). A stiffness based design approach has become the norm when serviceability controls the design. No matter what approach is taken, one should check the final design with expected performance under similar conditions. If serviceability governs the wall selection, one can check the precedent contained in the works of Peck (1969), O'Rourke and Clough (1990) and Long (2001), wherein deformations associated with excavation support systems under a variety of conditions have been summarized.

Lateral loadings: Terzaghi and Peck (1967) apparent earth pressure diagrams still form the basis of lateral loadings for many temporary support systems. A distinction must be drawn between sizing the structural members for axial force, shear and bending moments (stability), and computing deformations associated with the construction of a system (serviceability). With regards to the former, the apparent earth pressure envelopes were derived primarily on the basis of performance of relatively flexible support systems. Their use in design is most appropriate for these conditions. Kerr and Tamaro (1990) summarized methods to analyze stiff diaphragm walls for strut reactions and bending moments, including beam on elastic foundation assuming a subgrade reaction approach and equivalent beam on rigid supports assuming Rankine pressures. They stressed the importance of considering sequential excavation when computing maximum brace loads and bending moments and the relative insensitivity of the solutions to the subgrade modulus. However, these values are best selected on the basis of precedent in a given geologic setting.

Recommendations from FHWA (Sabatini et al. 1999) are appropriate for walls supported by tied back anchors. The distribution of apparent pressure in this approach depends on the location of the tieback on the wall, in recognition of the effect of the lockoff load, typically on the order of 75-100% of the design load. Unlike internal braces, in well-designed and constructed excavations, loads in tiebacks do not vary much during the excavation process, but remain close to the lockoff load (e.g. Schnabel 1990). Finno et al. (2002) presented data from an excavation with both cross-lot braces and tiebacks at the same section that shows this trend (Figure 1). Consequently the location of the tieback directly affects the apparent distribution of lateral pressure, and thus is reflected in the FHWA recommendation. Detailed information regarding this is presented by

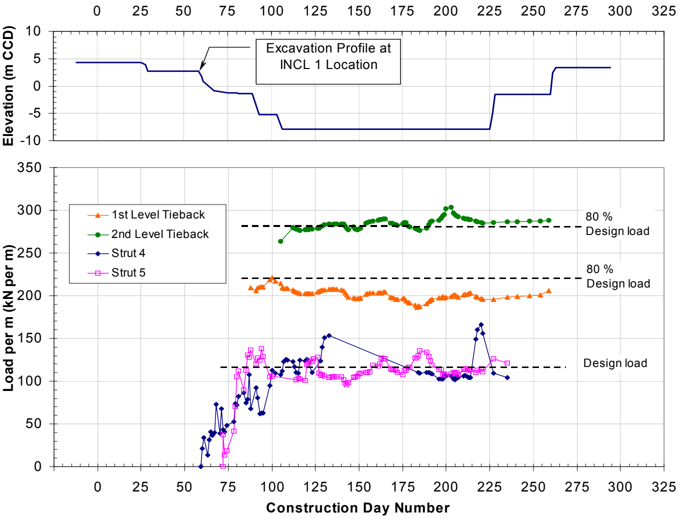

Figure 1. Forces in cross-lot braces and tiebacks

Weatherby (2010) in this conference for soldier pile and lagging walls supported by tieback ground anchors.

Numerical analyses recently have been used to size the structural support members of internally-braced systems. One must be careful regarding the capabilities of the numerical codes employed, as will be subsequently discussed. For example, when one expects significant variations in temperature over the service life of an internally-braced cut, then these effects must be explicitly considered since geotechnical-oriented commercial codes do not have routines to add the effects of temperature on the bracing responses. These effects may be quite significant, as noted by Boone and Crawford (2000), Hashash et al. (2003) and Blackburn et al. (2005).

Long-term loadings on walls usually are assumed to be those associated with at-rest conditions and a conservative selection of the permanent ground water table. However, ground deformations associated with the excavation process change the stresses in the ground, such that the soil stresses against a wall at the end of construction do not resemble at-rest values. While pore water pressures will eventually equilibrate to levels that depend on the degree of drainage around a structure, unless creep movements or swelling pressures develop, then little change in stress would occur after the pore water pressures equilibrate. While the at-rest approach is considered conservative, it likely does not represent the lateral loadings on the permanent structure. This aspect of the design process should be more closely examined.

Serviceability and allowable movements: Limits imposed on excavation-induced ground movements has made stiffness-based design of support systems more common, and a necessity when making deep excavations in urban areas. The stiffness of a support system, S, can be defined as:

$$S = \frac{EI}{\gamma_w h^4} \tag{1}$$

where *EI* is the bending stiffness of the wall, *h* is the average vertical spacing of the support and γ_w is the unit weight of water, used as a normalizing factor. For excavations in clay, Clough et al. (1989) developed a design chart based on finite element parametric studies that relates normalized lateral wall movement to S and factor of safety against basal heave. Their finite element simulations considered cycles of excavation and support. One must make allowance for movements associated with other activities, such as wall installation, deep foundation construction, consolidation, removal of existing foundations, etc. For all other soil conditions, and when one wants a more accurate representation of the entire construction process, either finite element or finite difference simulations are made to estimate ground deformations for a given support system. In this approach, the computed ground movements adjacent to the excavation depend on the system stiffness, constitutive responses of the soils and construction procedures.

Limits on allowable ground movements have become more restrictive, whether imposed by local regulatory agencies or by a general recognition of adverse effects of excessive ground movements of adjacent structures and utilities. Excavations in some urban areas have been subjected to movement limitations that are much smaller than even just 5 years ago. For example, excavations in Seattle are commonly built with a requirement that no more than 25 mm ground movement occurs, and excavations with 20 to 25 m deep cuts are common. Requirements for excavations in Chicago are now targeted for maximum ground movements of 35 to 50 mm, down from 100 mm just over a decade ago, a situation compounded in Chicago by the fact that excavations now are being made to depths of 25 m, much deeper than the typical depth at that time of 14 m. Some projects have been designed with distortions limited to 1/1000.

Ideally, the allowable movements are established based on the structure or utility affected by excavation. Burland and Wroth (1975), Boscardin and Cording (1989), Boone (1996), Son and Cording (2005) and Finno et al. (2005) proposed simplified methods of evaluating potential damage in terms of tensile strains to cause cracking. None of the models consider the strains that occur when the building settles under its own weight. Conceptually, one could estimate these "residual" strains and superpose them upon those arising during excavation. However, defining how much settlement would have occurred prior to attaching in-fill walls to a structural frame during the original building construction would be a difficult task. The movements to which these architectural portions of the structure would have been subjected are less than the total settlements. Given these uncertainties, either a conservative approach or a detailed structural analysis of an affected building is warranted when establishing allowable movements for an excavation. Cording et al. (2010) provides a summary of methods to assess building damage as part of these proceedings. Underpinning affected structures has become less common, and thus these deformation requirements present a challenge in design and construction of excavation support systems.

LRFD: LRFD is an approach that now is being applied to some excavation support systems worldwide, but its form is not uniform globally. The AASHTO-LRFD framework considers the strength (or ultimate), service and extreme event limit states to be applicable to supported excavations. The design of a wall typically is controlled by either the strength or the service limit state and then checked for applicable extreme events. This AASHTO framework has been used for permanent wall systems, but not temporary walls which typically are the province of the contractor in a design-bid-build format. While there is no AASHTO-LRFD platform for temporary walls, it may be that some agencies will simply adopt the available permanent-wall LRFD platform for this condition. Samtani and Sabatini (2010) discuss this framework in detail in this conference.

EUROCODE 7 (EC7) embraces the LRFD approach. This approach is discussed in detail by Simpson and Hocombe (2010) and Schweiger (2010) in contributions to this conference. Briefly, EC7 provides minimum requirements for design but is not proscriptive for many issues. It provides recommended values of partial factors, but leaves the choice of calculation methods to the designer. EC7 allows three different design approaches for specific load factors for ultimate state calculations. EC7 also requires consideration of serviceability limit states, both in terms of ground displacement, affecting existing structures, and deformation or cracking of the proposed structure. For retaining walls, displacements may be assessed by computations. Making judgments on the basis of previously recorded observations is allowed in the code. A formal approach to the observational method also is presented.

Seismic considerations: Lew et al (2010) reported a lack of damage to building basement walls retaining earth during recent US earthquakes and infrequent damage to building basement walls in foreign earthquakes. Although they noted many reports of damage to earth retaining walls during earthquakes, almost all of the reports were for either poorly constructed non-engineered walls or walls damaged because of a soil-related failure, with many being in marine or waterfront environments. Given that damage reports are quite rare, these observations suggest that temporary support systems need not be subjected to seismic earth pressures for design. However, Hashash et al. (2010) describes techniques applicable to temporary support. These methods apply smaller levels of ground shaking than needed for permanent systems. They also show the presence of a temporary system can increase the racking deformation for permanent box structure, if the temporary support system extends above or below the box structure. However, it is clear that walls that serve as permanent support must be designed for requirements from appropriate codes.

Numerical Analysis

Numerical analyses of excavation support systems have become more common in the past 20 years because of the need to compute ground movements as a function of system stiffness in a variety of ground conditions. Another factor in this trend has been the development and marketing of easy-to-use codes that were designed specifically for geotechnical applications, e.g. Plaxis, FLAC, SIGMA/W, etc. While users surely appreciate the pre- and post- processing capabilities of these and other commercial codes, one must be aware of the capabilities of the codes with respect to the desired output. One must not forget that ease of use does not equate to successful application.

Limitations inherent in numerical analyses: While it strictly is necessary to simulate all aspects of the construction process that affect stress conditions around an excavation to obtain an accurate prediction of behavior, the means needed for this are not always available in commercial codes. So one is always forced to make simplifications when making such simulations, and must be aware of the implications of such simplifications and assumptions. Key assumptions include selecting appropriate drainage conditions during excavation (Clough and Mana 1976; O'Rourke and O'Donnell 1997; Whittle et al. 1993; Li and Yang 2009), starting with appropriate initial effective stresses that include the effects of past construction activities at a site (Calvello and Finno 2003), and accurately defining the initial ground water conditions for a site (e.g. Finno et al. 1989; Zdravkovoic and Potts 2010). Top-down construction methods have become more common wherein the excavation moves off the critical path. Excavation durations up to 2 years may be expected, and the common assumption of undrained conditions in saturated clays for temporary support may not be valid. The duration of the excavation is long enough so that effects of excess pore water pressure dissipation or changes in water levels due to drainage may affect performance. In these cases, a coupled finite element formulation is useful to track the pore water pressures during excavation.

Many times the effects of the installation of a wall are ignored in a finite element simulation and the wall is "wished-into-place" with no change in the stress conditions in the ground or any attendant ground movements. However, there is abundant information (e.g. Clough et al. 1989; O'Rourke and Clough 1990; Finno et al. 1988; Koutsoftas et al. 2000) that shows ground movements may arise during installation of the wall, and, if ignored, these may have a significant impact on the accuracy of the computed responses, particularly in cases where one is attempting to limit the resulting ground deformations to small levels. One also must take care when representing the bracing system in a model. In typical plane strain simulations, application of prestress for cross-lot braces and installation of tiedback ground anchors can present problems under certain circumstances (e.g. Finno and Tu 2006).

A key factor in any finite element simulation is the selection of the constitutive model to represent soil behavior. Soils are inherently incrementally non-linear materials (e.g., Jardine et al., 1984; Clayton and Heymann 2001; Santagata et al. 2005; Callisto and

Calebresi 1998; Cho and Finno 2010) that exhibit complex behavior characterized by zones of high constant stiffness at very small strains, followed by decreasing stiffness with increasing strain. This behavior under static loading initially was realized through back-analysis of foundation and excavation movements in the United Kingdom (Burland, 1989) and is applicable to all soils. Stiffness also exhibits recent stress history effects, as measured from the most recently applied stress path (e.g., Atkinson 1990; Cho and Finno 2010). This latter type of behavior is not replicated in conventional elasto-plastic constitutive models included in commercial numerical codes. Several codes allow one to input a user-defined model, which has the possibility of representing these responses. However, these types of models are not part of the current state-of-the-practice.

Parameter selection is another important factor. One wants to compute responses in the field, and many parameter identification procedures depend on fitting data to laboratory results. This approach neglects the fact that soil structure is altered by sampling operations. Furthermore, application of good testing protocol is becoming a lost art.

It is clear that all models have limitations, and that parameter selection is not routine. Relatively simple models such as the Mohr-Coulomb elastic-perfectly plastic or Modified Cam-Clay have large regions with zones of constant elastic responses. Clearly a good deal of empiricism is required to make good predictions of deformations of any kind when a more sophisticated model is employed. As discussed later, optimization techniques can be used to find model parameters based on field performance data. In this way, one can define in a simulation the response of the *in situ* rather than the laboratory behavior of the soil.

Issues related to computing small movements: The state-of-the-art of predicting ground deformations has reached a point where advances in practice are required to make reliable design assessments when movements are limited to such small amounts. A number of factors that are not routinely considered in numerical simulations, especially those based on commercial codes, can have a significant impact when attempting to limit deformations to about 25 mm. These factors include small strain non-linearity of affected soils, non-linear stiffness of reinforced concrete or secant pile walls and, for top-down construction, creep and shrinkage of concrete floor slabs.

There are two main situations in which small strain non-linearity affects predictions of ground movements. The more recognized impact is predicting the distribution of ground movements with distance from the wall (e.g., Whittle et al 1993; Finno and Tu 2006; Schweiger 2010). Without including such capabilities in the constitutive model, one cannot compute the strain variations at distance from the wall. Ground surface settlements are the most commonly measured manifestation of this phenomenon. Unfortunately, limited quality field data sets are available, mainly because of difficulty of obtaining it in a crowded urban area.

The second impact is the possible effect on the inward movement of the toe of a support wall. Many walls are keyed into stiff layers at depths below the bottom of the excavation. This is the case for many cities around the Great Lakes. An unresolved issue when computing inward wall movements, especially for very stiff walls, is the interplay between small strain non-linearity of soil and the non-linear wall responses and their effect on movement of the toe of a wall. Given that the secant shear modulus can vary by a factor of 5 or more between strain levels <0.0001 and 0.1%, small-strain non-linearity in a model will affect the computed inward movements at the toe of such a wall. Furthermore, most finite element simulations of deep excavations assume the walls respond as a linear elastic material. Slurry and secant pile walls are quite stiff and brittle. Once the concrete cracks, the stiffness decreases with curvature. This reduction in stiffness impacts computed movements, especially when attempting to limit movements to small levels. Clearly more attention must be paid to adequately representing the wall stiffness, particularly when attempting to predict "small" movements.

ADAPTIVE MANAGEMENT APPROACH

When movements are a critical part of the design and construction of deep excavations, monitoring is usually incorporated into the specifications so that design assumptions can be verified, performance observed and adjustments to the construction procedure or support requirements made, if necessary. This observational approach has long been a part of geotechnical engineering, and is recognized as a valid approach to serviceability requirements by EC7. This is particularly applicable to deep excavation projects because of the assumptions made in numerical design calculations, especially when various construction activities are not explicitly modeled. Also, a contractor's procedures have such a large impact on the performance of the system, especially when excavation support and excavation are the responsibility of different subcontractors, as is typical for design-bid-build delivery systems. These planned procedures routinely change after a contract has been awarded, necessitating a change in the movement prediction.

Description

Developments in sensor technology, information technology and numerical analyses allow one to automate the cycle of observation and performance prediction updating. This automated observational approach can be thought of as adaptive management, and is summarized in Figure 2. The left hand column represents calculations made during the design and updating phases, and includes finite element computations when applied to deep excavations. Many times, inclinometer, optical survey and strain gage data are collected. These data can be incorporated into the optimization routine as observations against which the numerical predictions are evaluated. The center column is the optimization needed to update predictions based on the measurements. Examples of this approach applied to supported excavations are described by Finno and Calvello (2005), Hashash and Finno (2008), and Finno and Langousis (2007). Ideally, this process works automatically, all data collected in the field is transferred in real time to a host computer where it can be processed into format compatible with the numerical analyses, and updated performance predictions can be made in near real time.

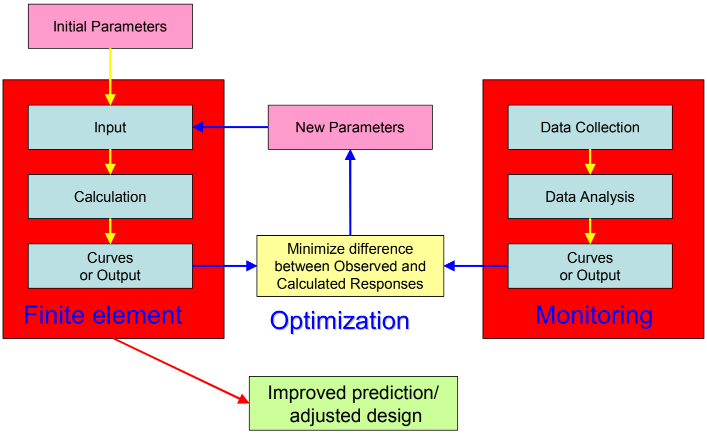

Figure 2. Flow chart for adaptive management procedure

Optimization is central to the process of adaptive management of geotechnical systems. Therein, various parts of a model are changed so that the measured values are matched by equivalent computed values until the resulting calibrated model accurately represents the main aspects of the actual system. Two main types of inverse analysis have been applied to geotechnics, optimization by iterative algorithms such as gradient methods (e.g., Ou and Tang 1994; Ledesma et al., 1996; Calvello and Finno 2004) and optimization by techniques from the field of artificial intelligence, including artificial neural networks (Yamagami et al. 1997; Hashash et al. 2006) and genetic algorithms (Levasseur et al. 2007). Optimization tools are readily available. UCODE (Poeter and Hill, 1998) is a computer code designed to allow inverse modeling posed as a parameter estimation problem and is free ware available from the US Geological Survey. Macros can be written in a windows environment to couple UCODE with any application software. MATLAB contains tool boxes with optimization routines, and these can be linked with commercial finite element codes as well.

Limitations

The assumptions inherent in any prediction limit the types of data that can be used as a basis of updating performance predictions. Consequently, one must carefully select the types of data, location of the measuring points, and the excavation conditions when applying an inverse technique. Inclinometer data based on measurements close to a support wall are most useful when typical elasto-plastic constitutive models are assumed to represent soil behavior, as is the case when employing commercial finite element codes. These data can be supplemented by ground surface settlements when using a constitutive model that accounts for small strain nonlinearities and dilation (e.g., Hashash and Whittle, 1996; Finno and Tu 2006; Zdravkovic and Potts 2010). Furthermore, other types of measurements, such as forces in internal braces and pore water pressures, conceptually can be used in conjunction with displacement measurements to make the computed results more sensitive to parameters selected for optimization (Rechea 2006).

While these different types of data can be handled within a properly formulated inverse analysis, the timely collection and screening of the data must be successfully accomplished. Furthermore, for any monitoring system to be fully automated, one must be able to track construction progress so that performance data can be correlated with the excavation activities. To correlate the numerical data with the causative actions of the excavation process, imaging technologies can be employed to provide an accurate and detailed record of construction activities. Su et al. (2006) used 3-D laser scanning to capture an accurate image of the geometry of the excavation to provide an accurate, as-built digital record of construction. Sections may be taken from these scans and imported into a finite element code to provide an accurate excavation surface for input to inverse analysis. Use of this imaging technology is not at the point where the results can be processed and incorporated into an adaptive management approach in near-real time, but likely will be so in the not too distant future. An internet accessible weather-resistant video camera has been used on several projects to allow remote visualization of the construction process in real-time, as well as a dated, photographic record of construction (Finno and Blackburn 2005).

If one is using an adaptive management approach wherein data is collected and compared with numerical predictions, then a 3D analysis would be required for most days as a result of the uneven excavated surface and timing of the support installation operations. If one is making a computation assuming plane strain conditions, then it is clear that one must judiciously select a data set so that planar conditions would be applicable to a set of inclinometer data. Even when a sufficiently extensive horizontal excavated surface is identified, 3-dimensional effects may still arise from the higher stiffness at the corners of an excavation. These boundary conditions lead to smaller ground movements near the corners and larger ground movements towards the middle of the excavation wall. Another, and less recognized, consequence of the corner stiffening effects is the maximum movement near the center of an excavation wall may not correspond to that found from a conventional plane strain simulation of the excavation, i.e., 3-dimensional (3-D) and plane strain simulations of the excavation do not yield the same movement at the center portion of the excavation, even if the movements in the center are perpendicular to the wall (Ou et al. 1996; Finno et al. 2007).

When conducting an inverse analysis of an excavation with a plane strain simulation, the effects of this corner stiffening is that an optimized stiffness parameter will be larger than it really is because of the lack of the corner stiffening in the plane strain analysis. This effect becomes greater as an excavation is deepened and conditions begin to depart from plane strain. This trend was observed in the optimized parameters for the deeper strata at the latter stages of the Chicago-State excavation project (Finno and Calvello 2005).

The calibration by inverse analysis can be very effective in minimizing the errors between the measured and computed results (Ou and Tang 1994; Ledesma et al 1996; Calvello and Finno 2004; Finno and Calvello 2005; Hashash et al. 2006). However, the convergence of an inverse analysis to an "optimal solution" (i.e. best-fit between computed results and observations) does not necessarily mean that the simulation is satisfactorily calibrated. A geotechnical evaluation of the optimized parameters is always necessary to verify the reliability of the solution. For a model to be considered "reliably" calibrated both the fit between computed and observed results must be satisfactory (i.e. errors are within desired and/or accepted accuracy) and the best-fit values of the model parameters must be reasonable.

An aid to communications

Keeping lines of communication open to all stakeholders in an excavation project can result in solutions that are economically feasible, yet not possible without such interplay. For example, a very stiff system is more expensive than a more flexible system, yet some times extra stiffness results in very little reduction in ground movements. The most feasible solution may be one where the system stiffness is selected which results in minor damage to an adjacent structure, and the cost of repairs is a line item in the bid documents. This type of solution requires that the owners of the adjacent property are engaged during the design phase of the project, and are kept aware of the effects of the progress of the excavation on the impacted facility. This can be accomplished by uploading performance expectations and field observation data to a website accessible to all interested parties. The author is aware of projects in Chicago, Boston and Seattle where this data sharing has been done with good success.

Speed of communication is quite important to keep pace with activities at excavation sites. Developments in information technology, automated data collection and remote monitoring have made real time information systems possible. There is a clear trend for more automated systems; the state-of-the-art was described in detail in the proceedings of FMGM conference held in Boston in 2007. With respect to deep excavations, remotely sensed total survey stations can be established to monitor the displacement of optical prisms (e.g. Finno and Blackburn 2005). In-place inclinometers can be deployed to remotely measure lateral movements of the walls of the support system and the adjacent ground, although systems which are stable over the time periods associated with excavations are still expensive. Current versions with MEMS-based sensors drift erratically and do not meet accuracy requirements over the time needed for excavation monitoring. Vibrating wire piezometers can be installed to monitor pore water pressures. Strain gauges can be mounted on structural supports. Tiltmeters can be placed on structural elements and results used to compute the angular distortion of an affected structure. A truly automated system of real time, remotely monitored performance and updated predictions likely will become a reality soon.

THE GREENING OF EXCAVATION SUPPORT

Green construction techniques are being introduced in deep excavation projects, and will become a factor in construction techniques employed in the future. Temporary support systems are redundant, and from a sustainability viewpoint, very inefficient since materials are left in the ground and energy wasted to install them. Walls that serve as both temporary and permanent support are starting to be employed as part of heating and cooling systems of the completed building. Recent developments in Europe are summarized by O'Brien (2010) in a paper presented at this conference. This holistic approach to building construction takes advantage of the fact that the earth is a geothermal energy source that may be harnessed for heating and cooling. A condition for successful application is an approximately constant ground temperature in the soil adjacent to a support wall. In many climates, this is satisfied and, under these conditions, heat pumps and cooling devices can be connected between absorber tubes within a concrete support wall and the mechanical heating/cooling systems of the building. Seasonal operation of a geothermal system uses the thermodynamic inertia of the ground to store energy there for later use. Structural design of the walls will have to consider the thermal changes in concrete during the cooling and heating cycles.

Construction equipment will be evaluated for its carbon dioxide footprint, and use of more 'carbon-efficient' construction materials will be emphasized, such as slag/flyash mixes or recycled materials from site. There are discussions in a number of states about making green building techniques a matter of statute, and there is no doubt that this trend eventually will make its way into deep excavation practice.

CONCLUDING REMARKS

Much has changed in the world of deep excavation support in the past 20 years, and this paper provides a rather brief and personalized summary. The Proceedings from this conference provide a much more detailed look. Practice has evolved regionally in different ways because engineers and contractors adapt to specific geologic conditions. Understanding these advances in terms of fundamental principles of geotechnics allows the advances in one geologic setting to be applied to others. As demands on performance of excavation support increase, we need to apply our understanding of constitutive responses of soils, take advantage of the relative ease of numerical simulations, and employ new information and sensor technologies. These can be incorporated into an adaptive management approach to design, which forces the design team to explicitly set realistic performance goals and plan for contingencies during construction while at the same time facilitates communication among shareholders in a particular project.

REFERENCES

Atkinson, J. H., Richardson, D., and Stallebrass, S. E. (1990). "Effect of recent stress history on the stiffness of overconsolidated soil." *Geotechnique*, 40(4), 531-540.

Blackburn, J.T., Sylvester, K. and Finno, R.J. (2005). "Observed bracing responses at the Ford Design Center excavation," Proceedings, 16th International Conference on Soil Mechanics and Geotechnical Engineering," Vol. 3, 1443-1446 .

Boone, S.J. and Crawford, A.M. (2000). "Braced excavations: temperature, elastic modulus and strut loads," *Journal of Geotechnical and Geoenvironmental Engineering*, ASCE, Vol. 126, No. 10, 870-881.

Burland, J.B. (1989). "'Small is beautiful' – the stiffness of soils at small strains: Ninth Laurits Bjerrum Memorial Lecture." *Canadian Geot. Jour.*, Vol. 26, 499-516.

Callisto, L. and Calebresi, G. (1998). "Mechanical behavior of a natural soft clay." *Geotechnique*, Vol. 48 (4), 495-513.

Calvello M. and Finno R.J. (2003). "Modeling excavations in urban areas: effects of past activities." *Italian Geotechnical Journal*, 37(4), 9-23.

Calvello M. and Finno R.J. (2004). "Selecting parameters to optimize in model calibration by inverse analysis." *Computers and Geotechnics*, Elsevier, Vol. 31, 5, 2004, 411-425.

Cho, W. and Finno, R.J., "Stress-Strain Response of Block Samples of Compressible Chicago Glacial Clays," *Journal of Geotechnical and Geoenvironmental Engineering*, ASCE, Vol. 136, No. 1, 2010

Clayton, C.R.I., and Heymann, G. (2001). "Stiffness of geomaterials at very small strains." *Geotechnique*, Vol. 51 (3), 245-255.

Clough, G.W. and Mana, A. I. (1976). "Lessons learned in finite element analysis of temporary excavations." *Proceedings, 2nd International Conference on Numerical Methods in Geomechanics*, ASCE, Vol. I, 496-510.

Clough, G.W. and O'Rourke, T.D. (1990). "Construction induced movements of insitu walls." *Proceedings, Design and Performance of Earth Retaining Structures,* Lambe, P.C. and Hansen L.A. (eds). ASCE, 439-470.

Clough, G. W., Smith, E.M., and Sweeney, B.P. (1989). "Movement control of excavation support systems by iterative design." *Current Principles and Practices, Foundation Engineering Congress,* Vol. 2, ASCE, 869-884.

Cording, E.J., Long, J.L., Son, M., Laefer, D. and Ghahreman, B. (2010). "Assessment of excavation-induced building damage," *Proceedings, Earth Retention 2010*, ASCE, R.J. Finno, Y. Hashash, and P.Arduino, eds.

Finno, R.J., Atmatzidis, D.K., and Nerby, S.M. (1988). "Ground response to sheet-pile installation in clay," *Proceedings, Second International Conference on Case Histories in Geotechnical Engineering*, St. Louis, MO.

Finno, R.J., Atmatzidis, D.K., and Perkins, S.B. (1989). "Observed Performance of a Deep Excavation in Clay," *Journal of Geotechnical Engineering*, ASCE, Vol. 115 (8), 1045-1064.

Finno, R.J. and Blackburn, J.T. (2005). "Automated monitoring of supported excavations," *Proceedings, 13th Great Lakes Geotechnical and Geoenvironmental Conference, Geotechnical Applications for Transportation Infrastructure,* GPP 3, ASCE, Milwaukee, WI., 1-12.

Finno R.J., Bryson L.S. and Calvello M. (2002). “Performance of a stiff support system in soft clay.” *Journal of Geotechnical and Geoenvironmental Engineering*, ASCE, Vol. 128, No. 8, p. 660-671.

Finno, R.J. and Calvello, M. (2005). “Supported excavations: the observational method and inverse modeling.” *Journal of Geotechnical and Geoenvironmental Engineering*. ASCE, 131 (7).

Finno, R.J., Blackburn, J.T. and Roboski, J.F., (2007). “Three-dimensional Effects for Supported Excavations in Clay,” *Journal of Geotechnical and Geoenvironmental Engineering*, ASCE, Vol. 133, No. 1, 30-36.

Denby, G. (2010). “Shoring system innovations in the Puget Sound area, Washington,” *Proceedings, Earth Retention 2010*, ASCE, R.J. Finno, Y. Hashash, and P.Arduino, eds.

Finno, R.J. and Langousis, M. (2007). “Real Time Monitoring at the Olive 8 Excavation,” Proceedings, FMGM 2007, 7th International Symposium on Field Measurements in Geomechanics, GSP 175, ASCE, Boston.

Finno, R.J. and Tu, X. (2006). “Selected Topics in Numerical Simulation of Supported Excavations,” *Proceedings, Numerical Modeling of Construction Processes in Geotechnical Engineering for Urban Environment,* T. Triantafyllidis, ed., Bochum, Germany, Taylor & Francis, London, 3-20.

Hashash, Y.M.A. and Finno, R.J. (2005). “Development of new integrated tools for predicting, monitoring and controlling ground movements due to excavations,” *Proceedings, Underground Construction in Urban Environments*, ASCE Metropolitan Section Geotechnical Group, New York, NY.

Hashash Y.M.A., Marulanda C., Kershaw, K.A., Cording, E.J., Druss, D.l., Bobrow, D.J. and Das, P.K. (2003). “Temperature correction and strut loads in Central Artery excavations,” *Journal of Geotechnical and Geoenvironmental Engineering*, Vol. 129, No. 6, 495-505.

Hashash Y.M.A., Marulanda C., Ghaboussi J. , Jung, S. (2006). “Novel approach to integration of numerical modeling and field observation for deep excavation.” *Journal of Geotechnical and Geoenvironmental Engineering*, 132(8), 1019-1031.

Hashash, Y.M.A. and Whittle, A.J. (1996). "Ground movement prediction for deep excavations in soft clay," *Journal of Geotechnical Engineering*, 122(6), 474-486.

Hashash, Y.M.A., Karina, K., Koutsoftas, K. and O’Riordan, N. (2010). “Seismic Design Considerations for Underground Box Structures,” *Proceedings, Earth Retention 2010*, ASCE, R.J. Finno, Y. Hashash, and P.Arduino, eds.

Jardine, R.J., Symes, M.J. and Burland, J.B. (1984). “The measurement of small strain stiffness in the triaxial apparatus.” *Geotechnique*, Vol. 34 (3), 323-340.

Kerr, W. C. and Tamaro, G.J. (1990). “Diaphragm walls - update on design and performance,” Design and Performance of Earth Retaining Structures, GSP 25, ASCE, ed. P.C. Lambe and L.A. Hansen, 576-594.

Koutsoftas, D. C., P. Frobenius, C.L Wu, D. Meyersohn, and R. Kulesza (2000). "Deformations during cut-and-cover construction of Muni Metro Turnback project," *Journal of Geotechnical and Geoenvironmental Engineering*, 126 (4), 344-359.

Kung, G. T.-C. (2009). "Comparison of excavation-induced wall deflection using top-down and bottom-up construction methods in Taipei silty clay," Computers and Geotechnics, Volume 36, Issue 3, April, 373-385.

Lambrechts, J.R. Hwang, R. and Urzua, A. eds (1998). *Big Digs Around the World*, GSP 86, ASCE, Boston, MA, 342 p.

Ledesma, A., Gens, A, and Alonso, E.E. (1996). "Estimation of parameters in geotechnical backanalysis – Maximum likelihood approach," *Computers and Geotechnics,* 18(1), 1-27.

Levasseur S., Malécot Y., Boulon M., Flavigny E., (2007). "Soil parameter identification using a genetic algorithm." *International Journal for Numerical and Analytical Methods in Geomechanics*, Vol. 34, No. 5, 471-491.

Lew, M. Sitar, N. and Al Atik, L. (2010). "Seismic Earth Pressures: Fact or Fiction," *Proc., Earth Retention 2010*, ASCE, R. Finno, Y. Hashash and P. Arduino, eds.

Li, L. and Yang, M. (2009). "Numerical evaluation of dewatering effect on deep excavation in soft clay," *Geotechnical Aspects of Underground Construction in Soft Ground*, Ng, C.W.W., Huang, H.W. and Liu, G.B. eds., Taylor & Francis Group, London, 147-152.

Long, M. (2001) "Database for retaining wall and ground movements due to deep excavations, " *J Geotech Geoenviron Eng, ASCE,* **127** (3), 203–224.

O'Brien, A.S. (2010). "Embedded Retaining Walls – A European Perspective on Design Developments and Challenges," *Proc., Earth Retention 2010*, ASCE, R. Finno, Y. Hashash and P. Arduino, eds.

O'Rourke, T.D. and O'Donnell, C.J. (1997). "Field behavior of excavation stabilized by deep soil mixing," *Jour. of Geotechnical Engineering*, ASCE, 123(6), 516-515-524.

Ou, C.Y., Chiou, D.C. and Wu, T.S. (1996b). "Three-dimensional finite element analysis of deep excavations." *Jour. of Geotechnical Engineering*, ASCE, 122(5), 473-483.

Ou C.Y., Tang Y.G. (1994). "Soil parameter determination for deep excavation analysis by optimization." *Journal of the Chinese Institute of Engineering*, 17(5), 671-688

Ou, C.-Y., Teng, F.-C. and Wang, I.-W. (2008). "Analysis and Design of Partial Ground Improvement in Deep Excavations," Computers and Geotechnics, 35(4), 576-584.

Ou, C.-Y., Wu, T.-S. and Hsieh, H.-S. (1996a). "Analysis of Deep Excavation with Column Type of Ground Improvement in Soft Clay," Journal of Geotechnical and Geoenvironmental Engineering, ASCE, , 122 (9), 709-716.

Peck R.B. (1969). "Deep excavations and tunneling in soft ground." *Proceedings, 7th International Conference of Soil mechanics and Foundation Engineering, State-of-the-ArtVolume*, 225-290.

Parmantier, D.M. Stow, R.P and Byrne, R.J. (2009). "Case study: cement-bentonite pre-trenching and cutter soil mixing for temporary shoring and ground water control,: *Contemporary Topics in Ground Modification, Problem Soils and Geo-Support,"*GSP 187, ASCE, Orlando, FL, 153-160.

Poeter E.P. and Hill M.C. (1998). "Documentation of UCODE, a computer code for universal inverse modeling." U.S. *Geological Survey Water-Resources investigations report 98-4080*, 116 pp.

Porbaha, A. Asada, H. and Fatemi, M.J. (1999). "Deep mixing technology for deep excavation," Geo-Engineering for Underground Facilities, GSP 90, ASCE, 1048-1057.

Santagata, M., Germaine, J.T. and Ladd, C.C. (2005). "Factors Affecting the Initial Stiffness of Cohesive Soils." *Journal of Geotechnical and Geoenvironmental Engineering*, ASCE, Vol. 131(4), 430-441.

Sabatini, P.J., Pass, D.G. and Bachus, R.C. (1999). "Geotechnical Engineering Circular NO. 4, Ground Anchors and Anchored Systems," Federal Highway Administration, report FHWA-SA-99-015, 281 p.

Samtani, N. and Sabatini, P.J., (2010). "LRFD for Earth Retaining Structures in U.S. Transportation Practice," Proceedings, Earth Retention 2010, ASCE, R.J. Finno, Y. Hashash, and P.Arduino, eds.

Schnabel, H. (1990). "A contractor's perspective on wall selection and performance monitoring," Design and Performance of Earth Retaining Structures, GSP 25, ASCE, ed. P.C. Lambe and L.A. Hansen, 67-84.

Schweiger, H.F. (2010). "Design of deep excavations with FEM – Influence of constitutive model and comparison of EC7 design approaches," Proceedings, Earth Retention 2010, ASCE, R.J. Finno, Y. Hashash, and P.Arduino, eds.

Simpson, B. and Hocombe, T. (2010). "Implications of modern design codes for earth retention structures," Proceedings, Earth Retention 2010, ASCE, R.J. Finno, Y. Hashash, and P.Arduino, eds.

Su, Y.Y., Hashash, Y.M.A. and Liu, L.Y. (2006). "Integration of construction as-built data with geotechnical monitoring of urban excavation," *Journal of Construction Engineering and Management*, Vol. 132, No. 12, pp pp. 1234-1241.

Tanaka, H. (1993). "Behavior of braced excavations stabilized by deep mixing method," Soils and Foundations, Vol. 33, No. 2 105-115.

Terzaghi, K. and Peck, R.B., (1967). Soil Mechanics in Engineering Practice, Second edition, John Wiley & Sons, New York, NY, 729 p.

Uchiyama, N., Katsura, Y. and Kamon, M. (1999). "New effective methods for reducing wall deformation in excavation using buttress-wall type ground improvement, " Proceedings of the Japan Society of Civil Engineers, Vol. 624, 91-100.

Weatherby, D. (2010). "Behavior of tiedback, H-beam walls and recommendations for their design," *Proceedings, Earth Retention 2010*, ASCE, R.J. Finno, Y. Hashash, and P.Arduino, eds.

Whittle, A.J., Y.M.A. Hashash, and R.V. Whitman (1993). "Analysis of deep excavation in Boston," *Journal of Geotechnical Engineering*, Vol. 119, No. 1, 69-90.

Wolschlag, C.J. Byrne, R.J. and Cotton, D.M. (1999). "Suspension wall shoring system," Geo-Engineering for Underground Facilities, GSP 90, ASCE, Urbana, Il. 200-211.

Yamagami T., Jiang J.C., Ueta, Y. (1997). "Back calculation of strength parameters for landslide control works using neural networks." *Proceedings of the 9th Int. Conf. on Computer Methods and Advances in Geomechanics*, Wuhan, China.

Zdravkovoic, L. and Potts, D.M. (2010). "Application of numerical analysis in geotechnical engineering practice," *GeoFlorida 2010: Advances in Analysis, Modeling & Design*, GSP 199, ASCE, 69-88.

Fill Walls – Recent Advances and Future Trends

Ryan R. Berg[1], P.E., F. ASCE

[1]Geotechnical Consultant, Ryan R. Berg & Associates, Inc., 2190 Leyland Alcove, Woodbury, MN 55125, RyanBerg@att.net

ABSTRACT: Significant advances in the past twenty years and anticipated advances over the next twenty years of fill wall structures are summarized herein. Advancement topics are presented in categories of: market drivers, materials, systems, performance, and analysis and design. Many of the future advancement topics can or should be interactive. Examples of interactive topics are presented. The purpose of this plenary paper is to stimulate discussion and debate on the future direction of fill walls, and to encourage work on moving these topics ahead.

1. INTRODUCTION

The purpose of this paper is twofold. First, is to document and discuss the significant advances in fill walls over the past twenty years. Second, is to discuss anticipated, or possible, significant advances in fill walls over the next twenty years. It is always constructive to look at recent history; both from an accomplishment viewpoint and to gauge the direction we are headed.

The term *fill wall* used herein is one method for classifying earth retaining systems (ERS). Fill wall construction technologies refer to a system in which the wall is constructed from the base of the wall to the top, i.e., *bottom-up* construction. Cut wall construction refers to a wall system in which the wall is constructed from the top of the wall to the base (i.e., *top-down* construction) concurrent with excavation operations. Cut wall technologies are not addressed within, except for hybrid fill-cut walls. Typical fill wall structures are listed in Figure 1. These are generally designed as permanent structures, with a typical design life of 75 or 100 years. Mechanically stabilized earth (MSE) slopes, or reinforced soil slopes (RSS), are listed in Figure 1. Structures with a face batter less than or equal to 20° as measured from vertical may be classified as a wall, and structures with a batter greater than 20° as a slope.

This paper is organized into two primary time periods: (i) 1990 – 2010 Advances and Trends; and (ii) Future Direction – Beyond 2010. Topics are organized within each section in categories of: (i) market drivers; (ii) materials; (iii) systems; (iv) performance; and (v) analysis and design. Several topics are briefly summarized under each of these categories, in both sections. Many of these topics can or should be interactive.

While this paper attempts to be comprehensive, it is not fully encompassing in its treatment of either the developments and trends in ERS over the past 20 years or in the future directions of ERS. Topics are based upon the experience of the author, with input from colleagues (see Acknowledgements). Opinions are that of the author. It is anticipated that this conference will add to and expand on the topics presented.

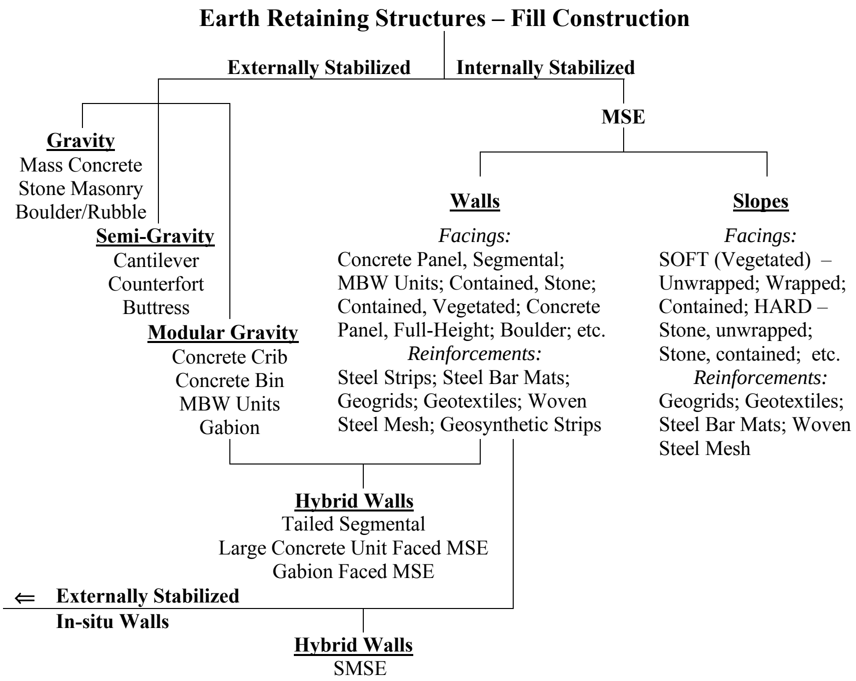

FIG. 1. Fill type earth retaining structures. (after O'Rourke and Jones, 1990)

2. 1990 – 2010 ADVANCES AND TRENDS

A look back over the past 20 years is historically interesting and offers some insights into what the next 20 years might bring. A summary of these recent trends and advances in fill walls follows. These are presented in categories of market drivers; materials; systems; performance; and analysis and design.

2.1 Market Drivers

Market Size: The market for fill walls grew significantly over the past twenty years as population growth fueled urban development of transportation and private works.

MSE Wall and Modular Wall System Suppliers: The model of a supplier providing a *system* to state transportation agencies has remained firmly entrenched. Material manufacturers (e.g., geogrids, MBW units, etc.) found that they needed to develop and market systems to state departments of transportation (DOT), and not just individual wall components. The use of a system has also developed for private works. Although in many cases this system is an assemblage of components (e.g., facing, reinforcements, design) by a subcontractor from individual suppliers, without a sole source responsibility of a system supplier.

Associations: Wall and material associations have influenced the growth and direction of fill walls. In highway works, the Association of Metallically Stabilized Earth (AMSE), National Concrete Masonry Association (NCMA), and Geosynthetic Materials Association (GMA) associations have contributed to refinement of the American Association of State Highway and Transportation Officials (AASHTO) specifications and Federal Highway Administration (FHWA) guidance. In private works, NCMA developed a design manual for gravity and MSE walls constructed with masonry retaining wall units (Simac et al. 1993) and has refined this guidance in subsequent manuals (NCMA, 1997, 2009; Collin et al. 2002).

FHWA/AASHTO: Very significant contributions to fill ERS have been made by both the FHWA and the AASHTO in the past twenty years. Foremost is that these two entities are working closely together and coordinating work to present consistent design and construction requirements and guidance. FHWA, in conjunction with state DOT, have contributed significant research into MSE walls (see Section 2.4). AASHTO has moved from an allowable stress design (ASD) platform to load and resistance factor design (LRFD) platform in the past decade.

Aesthetics: The importance of fill ERS aesthetics has continued to increase over the past twenty years. Wall system suppliers and design engineers have responded with a variety of wall aesthetics options. These include: (i) a wide variety of precast concrete finishes created with forms or formliners and coloring or staining; (ii) MBW units in a wide variety of finishes and colors; (iii) rock facing contained within steel mesh and/or geogrid; and (iv) vegetated, green facing.

National Review Mechanisms:
Highway Innovative Technology Evaluation Center (HITEC) – The HITEC program was initiated in 1994 and was managed by ASCE. The primary purpose of HITEC was to effectively introduce innovative technologies into highway construction without increasing the financial burden and resources that would be required by owners and designers (e.g., DOT). Though the ERS evaluation program quickly became the most successful of the HITEC programs, it is not fully working as initially intended, and its use has waned.

National Transportation Product Evaluation Program (NTPEP) – The key objective of NTPEP is to provide quality and responsive engineering for the testing and evaluation of products, materials, and devices that are commonly used by the AASHTO member DOT (www.ntpep.org). This program recently added geosynthetic soil reinforcement to the suite of materials that are evaluated. The primary use of the test results is to determine the nominal strength (in LRFD terminology), or long-term strength (in ASD terminology), of the soil reinforcements. NTPEP reports on geosynthetic reinforcements are available on their website. To stay current, complete evaluations of products are required every six years with a limited evaluation three years after the complete evaluation.

2.2 Materials

Modular Block Units: A material that has experienced significant increased use since 1990 is masonry retaining wall units, a.k.a. segmental retaining wall units or modular block wall units (MBW). There are a wide variety of proprietary MBW units commercially available. These are used to construct short gravity walls to tall MSE walls. MBW units are used in a wide range of projects – from landscaping, to residential and commercial development, to transportation works. The significant growth in use of this product has been spurred by several factors, including: aesthetics and variety of available units, a broad-based commercial interest of manufacturers and sales forces, a strong technical and commercial oriented trade association, and the ability to use MBW units to construct MSE walls.

Steel Wire: Welded wire mesh (WWM) and woven wire mesh is increasingly being used as MSE soil reinforcement. More recently, its use as MSE wall and slope facing on permanent and on temporary MSE walls and slopes has grown. Black steel WWM is used with a metal screen or a geotextile to face temporary walls. Wire mesh facing is used to construct walls and steepened slopes with vegetated or rock filled facings. Galvanized steel and select fill are used where permanent support is required. Steel or geosynthetic soil reinforcement is used in conjunction with this facing.

Green Facings: “Green” is in – even with earth retention systems. The use of green walls and reinforced slopes has grown, albeit slowly, in the U.S. over the past 20 years, and continues to grow. Stepped-faced and smooth-faced walls and slopes can be designed and constructed green. The “green” component is typically vegetation that is established and/or stabilized with an erosion control blanket or mat, bio-engineering, wrap-around grid or mesh, concrete elements with stepped openings, or geocells (typically with a green outer, exposed face). Recycled fill materials are another possible green wall component.

Non-Select MSE Fill: The *select granular fill*, defined by a gradation that limits particle size passing a No. 200 (0.075 mm) sieve to 15% and plasticity limit (PI) ≤ 6, is required for MSE walls in transportation works (AASHTO, 2007; FHWA (Berg et al. 2009)). Within the last two decades the use of *non-select,* lower quality reinforced fills (i.e., > 15% fines) has been the norm for the design and construction of MBW unit faced MSE walls for private and commercial works. The design and construction of MBW MSE walls generally follow the National Concrete Masonry Association (NCMA) design guidelines (NCMA, 2009) where the use of up to 35% fines is allowed. (Note, however, that many walls have been constructed with fine contents greater than 35%.) The difference between a maximum 15% to 35% fines is significant in terms of economics, construction, sensitivity to water; and in some cases in the performance of an MSE wall structure (see 2.4 Failures of MBW MSE Walls).

Research (Marr and Stulgis, 2010) on the use of non-select, lower quality reinforced wall fill for MSE highway walls has recently been completed. The purpose of the

National Cooperative Highway Research Project 24-22 (NCHRP 24-22) was to develop selection guidelines, soil parameters, testing methods, and construction specifications that will allow the use of a wider range fill (i.e., non-select) for highway MSE walls. See Section 3.2 for a discussion of the research findings.

2.3 Systems

A "system" may be defined as the components that when added to soil are an ERS. The systems discussed below are either new or their use has significantly expanded use over the last 20 years.

MBW Unit Faced, Geogrid Reinforced MSE Walls: This combination of materials was first used in the mid 1980s, but its use greatly expanded over the past twenty years. This growth was fueled by many factors including: aesthetics of the MBW units; large number of commercially available MBW products; masonry and geogrid sales forces, and the efforts of the masonry association – the NCMA. Growth into the private market was fairly rapid, due to aesthetics, availability, and cost; and was aided by the ability to use on-site soil in MSE walls. Growth in the transportation market has been slower due to block freeze-thaw durability concerns, problems with wall performance on private works (see Section 2.4), and other issues.

Reinforced Soils Slopes: The use of reinforced soil slopes (RSS) has significantly grown in both private and public works over the past twenty years. The design, specification, construction, and maintenance of the RSS facing are key to successful performance of a structure, and has been a challenge for engineers.

Shored MSE Walls: Shoring, most often in the form of soil nail walls, has been used to stabilize the back-cut in steep terrains for construction of MSE walls. If the shoring wall is designed as a permanent wall it can significantly reduce the long-term lateral pressures on the MSE mass and, thus, reduce the required width of the MSE mass. Details of Shored MSE (or SMSE) wall systems are presented in FHWA-CFL/TD-06-001 (Morrison et al. 2006) and FHWA NHI-10-024 (Berg et al. 2009).

Large Wet Cast Concrete Blocks: Several large precast concrete retaining wall block units are commercially available. Typical block sizes range in width (front to back) from 0.5 to 1.5 m (21 to 60 in.). Exposed face dimensions typically vary from 0.4 to 9.2 m (16 to 36 in.) high and 1.2 to 2.4 m (48 to 96 in.) wide. Units may be solid or bin shaped. These units are used to construct gravity walls and, for taller structures, combined with geogrids to construct MSE walls. Formliners and stain are used to create stone-like aesthetics. These units are used in private and public works, though currently their use on transportation works is not very widespread.

Geosynthetic Reinforced Soil (GRS) Walls: GRS is an MSE wall/abutment constructed with compacted granular fill and closely spaced layers of geotextile soil reinforcement. Researchers at the U.S. Forest Service and the Colorado Department of Transportation (CDOT) pioneered the early development of this system. FHWA, in conjunction with CDOT, has advanced this system through construction and testing of structures at its Turner-Fairbanks Highway Research Center. The GRS design procedure does differ from the AASHTO/FHWA procedure, and is documented in NCHRP Report 556 (Wu et al. 2006).

MSE Bridge Support Abutments: MSE walls with spread footings on top of the wall are used for bridge abutments. Growth has been slow since introduced in the 1970s, but has increased over the last ten years for walls constructed with steel strip soil reinforcement and precast concrete panel facing (Anderson and Brabant, 2005). However, the use of spread footing/MSE wall supported bridges remains relatively low as compared to traditional construction methods.

2.4 Performance

Heights: New heights have been reached in MSE structures in the U.S. The precast panel faced, steel strip reinforced soil West Wall at Seattle-Tacoma International Airport completed in 2005 has a total height of approximately 46 m (150 ft) and an exposed height of 43 m (142 ft) (Sankey et al. 2007). The geogrid reinforced soil slope at the Charleston, WV Airport has a 1:1 face slope and is 74 m (242 ft) high (Lostumbo, 2009). MBW unit faced, geogrid reinforced MSE walls have been constructed up to heights of approximately 21 m (70 ft).

Research: Several significant research projects on MSE walls and on seismic design of ERS have been completed in the last twenty years, as listed in Table 1. See references noted for summary or detailed information on the respective research projects.

Test Standards: ASTM International has standardized several test procedures for MSE walls over the past twenty years. Some of these tests were preceded by standardized NCMA or Geosynthetic Research Institute (GRI) test procedures. Tests include: (i) geosynthetic pullout; (ii) geosynthetic direct shear; (iii) geosynthetic creep, conventional; (iv) geosynthetic creep, stepped isothermal method; (v) connection strength; (vi) MBW units; and (vii) MBW unit freeze-thaw durability.

Table 1. MSE Wall Research Projects

Project	References
FHWA Soil Reinforcement Durability	see Elias et al. 2009
MSE Pooled Fund and GeoEngineering Centre at Queens-RMC	Allen et al. 2002; 2005 Bathurst et al. 2008a,b; 2009; 2010
NCHRP 12-70 Seismic Design	Anderson et al. 2008; (also see Berg et al. 2009)
NCHRP 24-28 Steel Corrosion	Fishman 2010
NCHRP 24-22 Non-Select MSE Fill	Marr and Stulgis 2010

Failures of MBW MSE Walls: Thousands of MBW MSE and gravity walls have been designed and constructed over the past two decades. This includes wall structures with heights around 21 m (70 ft). While the performance of MBW faced, MSE walls with non-select fill in private works generally has been excellent, the failure rate is too high (estimates range up to 5%) as compared to performance of other civil works. Failures are due to a variety of reasons, and often a combination of problems, including: (i) poor design judgment; (ii) poor design detailing; (iii) poor surface water drainage design/control; (iv) poor construction – e.g., low soil compaction, contamination of drainage materials, QC/QA, etc.; (v) poor project coordination between design disciplines; and/or (iv) lack of subsurface water drainage in proper locations. The MBW unit association, NCMA, has worked to provide design guidance for drainage considerations (Collin et al. 2002; NCMA, 2009) to lower the failure rate. An alternative solution, proposed by some, is to restrict or even eliminate the use of non-select reinforced fill on MSE walls.

2.5 MSE Wall Analysis and Design

Simplified Method: The *Simplified Method* of analysis has been used with allowable stress design (ASD) procedures since 1996. This method was developed using FHWA research (Christopher et al. 1990) and existing design methods (i.e., coherent gravity method, tie-back wedge method) as a starting point to create a single method for agencies and vendors to use (Elias and Christopher, 1997; Allen et al. 2001). The simplified method uses a variable state of stress for internal stability analysis. This variable state of stress is defined in terms of a multiple of the active lateral earth pressure coefficient, K_a, and is a function of the type of reinforcement used and depth from the top of wall.

The simplified method has been adapted to LRFD procedures in AASHTO (2007) and FHWA (Berg et al. 2009). Today, the use of the Simplified Method analysis model with the LRFD platform is recommended for the design of transportation MSE wall structures. Therefore, the latest guidance on MSE wall design using ASD procedures, i.e., AASHTO (2002) and FHWA NHI-00-043 (Elias et al. 2001), will not be updated. Any designers engineering MSE walls with the ASD procedures in the future may want to refer to current LRFD procedures for any updates which may also be applicable to ASD procedure designs (e.g., seismic loading for external stability analysis).

NCMA: The National Concrete Masonry Association (NCMA) method and analysis model was developed in 1993 (Simac et al.) specifically for, and is widely used with, masonry MBW unit faced (a.k.a. segmental retaining wall (SRW) blocks) walls, in private works. Both gravity walls and geosynthetic reinforced soil walls are addressed. Designs are based upon an ASD platform. The reference manual and procedures were updated in 1997 (NCMA) and in 2009 (NCMA).

Shored MSE Walls: FHWA has developed design and detailing guidance for SMSE walls (see Morrison et al. 2006), and updated guidance to LRFD (Berg et al. 2009).

Geosynthetic Reinforced Soil (GRS) Walls: GRS is an ASD wall analysis/design model. The GRS design method is documented in NCHRP Report 556 (Wu et al. 2006). This method was developed in Colorado specifically for geosynthetic soil reinforcements and wrap-around or block facings. The GRS design method is a modification of the Simplified Method (see above). The soil reinforcement model is based upon closely spaced vertically adjacent layers of reinforcement and soil arching, versus the FHWA method that is based upon a tied-back wedge model.

Additional principal differences between the GRS Method and the Simplified Method are: (i) the default vertical reinforcement spacing is 0.2 m (8 in.), and maximum spacing (for abutments) is 0.4 m (16 in); (ii) the soil reinforcement is specified on a basis of minimum ultimate tensile strength and a minimum tensile stiffness; and (iii) connection strength is not a design requirement where the maximum reinforcement vertical spacing is 0.2 m (8 in.) and reinforced fill is a compacted select fill.

Deep Patch RSS: *Deep patch* is a mitigation technique that is typically used on roads that suffer from chronic slide movements that are primarily the result of side cast fill construction. Deep patch repairs consist of reinforcing the top of a failing embankment with several layers of soil reinforcement. This technique is generally not expected to completely arrest movement seen in the road but rather slow it down to manageable levels. The design is based on determining the extent of the roadway failure based on visual observations of cracking and then using analytical or empirical methods for determining the reinforcement requirements. An empirical design procedure is presented in a U.S. Department of Agriculture Forest Service guide (Musser and Denning, 2005).

Numerical Techniques: A variety of numerical tools have been used over the past twenty years for research on the behavior of ERS, for comparison to measured performance, to investigate effects of construction methods, and to predict movements under static and seismic loading. Though not routinely used for design, these tools are used to enhance our understanding of ERS and the materials used to construct them. The use of such tools will become increasingly important to address ERS topics over the next twenty years.

3. FUTURE DIRECTION – BEYOND 2010

Current and emerging issues and trends that will influence design and construction of fill-type retaining walls are discussed below. These are presented in categories of market drivers; materials; systems; performance; and analysis and design.

3.1 Market Drivers

Many items may affect the near future of the fill wall markets, including the size of the market, commercial associations, professional organizations, and system suppliers, as discussed below. Recent initiatives will also affect the fill wall market, such as a national wall review program, SHRP2 research, and the Greenroads program summarized below.

Market Size: It is anticipated that the need for fill walls will remain strong and should increase as population growth continues to fuel urban development of transportation and private works. Demand will temporarily decrease, particularly for private works, in times of economic slowdowns.

Aesthetics: The importance of fill ERS aesthetics will continue to increase. Wall system suppliers and design engineers will develop more options and refine existing facing options. The use of vegetative/green solutions will increase significantly, due to aesthetics and to an increased attention to sustainability (e.g., see Greenroads).

Associations: Wall and material associations of AMSE, NCMA, and GMA will continue to influence growth and direction of fill walls. In highway works, associations will likely contribute to refinement of the AASHTO LRFD specifications and development of material specific resistance factors. In private works, association developed design guides (e.g., NCMA, 2009) will continue to be refined and used. Associations, and professional organizations, should work to lower the current MSE wall failure rate in private works. An active precast concrete wall association may be required to develop design guidance and promote growth of *heavy faced* MSE walls (see Section 3.5), and other precast concrete fill wall systems.

Professional Organizations: Professional organizations, such as the Geo-Institute, will continue to provide formats such as this conference, for presentation and discussion of technical aspects of fill walls. As noted above, professional organizations should also take an active role in lowering the current MSE wall failure rate in private works. And as noted below, the Geo-Institute should be a significant contributor to the proposed national based wall system review program.

MSE Wall System Suppliers: It is anticipated that the model of a supplier providing a *system* to DOT will remain the norm. Agencies have shown little interest in designing MSE walls in-house. Most DOT stay busy regulating/ approving systems and materials. The benefits of a national based review mechanism to aid DOT in regulating/approving materials and systems have been recognized. In the future, agencies will likely also be evaluating supplier proposed LRFD resistance factors.

It also appears that contractors providing a *system* to owners on private works will remain popular. Furthermore, the coordination of other design elements with the MSE wall design will continue to be problematic (see 2.4 Failures of MBW MSE Walls and 3.4 Private Works Project Design Teams) on private works.

National Review Mechanism: Although fill walls are widely used and generally a mature technology, there clearly is a need for a technical review of enhancements or advancements of existing products and of new products/systems coming to market. DOT's generally do not have the resources or budget to perform timely and thorough technical reviews of products and systems. This not only affects new products, but also existing products that may require technical review updates to check conformance to the AASHTO LRFD specification and/or to verify proposed system-specific LRFD resistance factor(s).

The FHWA has proposed the development of a three part program that provides a technical evaluation of wall components and systems, a process for approving components and systems by owners, and a framework for disseminating, maintaining and updating information compiled by the program. It is anticipated that the Geo-Institute, wall industry groups, DOT, and the FHWA will provide significant contributions to this program. Three distinct parts to the program are proposed, as follows: (i) technical review of products; (ii) owner approval of products; and (iii) warehousing and maintenance of program. Hybrid wall systems, which are not widely used or mature, also could and should be, reviewed under this program.

SHRP2: The Strategic Highway Research Program 2 (SHRP2) focused research program was established by Congress in 2006. SHRP2 targets goals in four interrelated focus areas of: safety, renewal, reliability, and capacity. The renewal objective is to “Develop design and construction methods that cause minimal disruption and produce long-lived facilities to renew the aging highway infrastructure.” (www.trb.org/StrategicHighwayResearchProgram2SHRP2)

The selection of a retaining wall system has traditionally been primarily based upon cost of the wall *system* (e.g. for MSE walls the design engineering and materials except soil). The SHRP2 program emphasizes a broader look at costs. The cost benefits of speed of construction (to minimize disruption to the traveling public), maintenance costs, and the potential life (beyond the traditional defined design life) are important aspects that may drive wall selection on future projects. Thus, the time to construct various wall types and systems will need to be documented in the near future to quantify the speed of construction cost benefits. Useable life projections will require the routine use of long-term (e.g., 75 to 100^+ years) instrumentation/ monitoring programs that can be used by future generations of engineers to assess the long-term structural life.

Greenroads: Greenroads is a sustainability performance metric for application to the design and construction of new and rehabilitated/reconstructed roadway projects. It is similar to the popular Leadership in Energy and Environmental Design (LEED) program for buildings. The ultimate goal of Greenroads is more sustainable roadways, i.e., less impact on the environment, lower life cycle costs, and more positive societal outcomes. Currently, retaining walls and other structures are not explicitly considered (nor explicitly excluded), but could be incorporated into future versions of Greenroads (www.greenroads.us).

Similar sustainability programs have been launched by individual states (e.g., New York DOT *GreenLITES* (www.nysdot.gov/programs/greenlites)). Such programs may affect future retaining walls by: (i) encouraging use of natural materials such as stone/rock and vegetated facings; (ii) use of on-site soils as fill; and (iii) better documentation of life-cycle costs of retaining walls via instrumentation and/or asset management (see Section 3.4) practices.

3.2 Materials

Non-Select MSE Fill: Highway works may relax MSE wall fill gradation and gradation criteria over the next twenty years, but if so, only with stringent detailing and QC/QA requirements. Four full-scale field tests were conducted as part of the NCHRP 24-22 research (see Section 2.2) to establish properties for *high fines* reinforced soils and associated design controls that provide acceptable MSE wall performance. The tests show that MSE walls can withstand substantial positive pore water pressures, provided they are designed to do so. The tests also show that increasing the pore pressure in the backfill causes lateral and vertical deformations of the wall that are as significant as those resulting from adding surcharge loads.

The tests show that soils with as much as 25% fines and a PI below 6 can be successfully used as reinforced fill in MSE structures, provided the design uses the appropriate material properties and addresses any positive pore pressures that may develop in the backfill over the life of the structure. Based upon test results and the professional judgment of the researchers, sand soils with up to 50% fines and PI up to 12% may be used in circumstances where the weather conditions permit proper placement of these materials, positive pore pressures are prevented in the backfill, surface water infiltration into the backfill is prevented, and construction is monitored by a qualified professional engineer to ensure that these requirements are fulfilled.

The researchers concluded that the best practice for using marginal fills in MSE structures is to adapt measures that minimize the potential of pore pressure build up in the fill. By preventing pore pressure build up, the marginal soils have adequate strength and stiffness characteristics to provide a wall which functions safely and with acceptable deformation. All potential sources of pore pressure build up in the reinforced zone should be considered in the design, including horizontal flow from the retained backfill, downward flow from surface water, and upward flow from the foundation. Where potential sources exist or may develop during the life of the project, the design should include specific measures to prevent flow of water into the reinforced fill in the form of a water barrier, a drain, or both.

In private works, the drainage requirements (Case III) recommended by NCMA (2009) guidelines, similar to those described above, should be stringently implemented for MBW faced walls when using lower quality fills. Additionally guidelines may need to be tightened, driven by the unacceptably high failure rate (see 2.3), to limit the use of lower quality fills. Recommendations might be tightened by wall height and fill gradation and plasticity limitations, and/or design detailing requirements, and/or design requirements (e.g., assumed water loads, target safety factors, etc.).

Wall Facings: Traditional gravity and MSE wall facings will continue to be used. However, market drivers will lead to facings which are faster to erect, more durable, and/or greener.

It is anticipated that research will continue into development of dry-cast MBW units that are more resistant to deicing salts and freeze-thaw degradation. This would broaden the current use of MBW materials, particularly in transportation works.

RSS Facings: The variety of RSS facings, including *green* vegetated, is an advantage of RSS systems versus concrete faced ERS. The key to successful RSS performance is the facing, particularly when selecting vegetation for green facings. It is anticipated that RSS facings will continue to challenge engineers and continue to limit use of this system until an industry association, AASHTO, and/or other organization develops comprehensive RSS facing selection guidelines with complementary design, details, specification, construction and maintenance guides.

3.3 Systems

Reinforced Soils Slopes: Reinforced soil slopes (RSS) will continue to be used in private and transportation works, and "green" initiatives may increase use of this ERS. Better recognition of a steepened reinforced slope as an ERS option could also increase its use. In transportation works, RSS are not addressed in the AASHTO (2007) Bridge Specifications where other ERS are. Inclusion in the AASHTO guide will likely increase the use of RSS ERS (though some may argue it might decrease usage). This does present some design challenges (see 3.5).

Use of RSS in transportation and private works should increase when facings are more thoroughly addressed (see above). RSS can be designed, supplied, and contracted as a system or can be designed by agency engineers or consultants with materials generically specified. Standardized reinforcement strengths and facing selection and detailing guidelines would enhance agency engineers and consultants' abilities to design and specify RSS structures.

Composite Gravity MSE Walls: The use of hybrid walls constructed of a MSE mass and large, heavy facing (see Section 2.3) is growing. The large "face" units are being used for aesthetic or other market driver reasons. The licensors and precasters of these large units are market drivers. Another potential driver is the rapid renewal aspect (see SHRP2 discussion) of constructing a MSE wall with large, self-supporting units that eliminate the need for temporary construction support bracing that is used with panel faced MSE walls. Economies with system could be gained by factoring the stabilizing affect of the large face units into the stability analyses (see 3.5).

MSE Bridge Support Abutments: It is anticipated that the use of MSE walls with spread footings to support bridge abutments will increase significantly over the next twenty years. A key factor in spurring growth is the change to a LRFD platform for design of transportation earthworks. This provides a logical methodology for estimating settlements, under serviceability limit states. Real-time instrumentation tools, now readily available, for monitoring movements during construction can be used to measure actual performance. Asset management programs and/or long-term monitoring of soil reinforcement corrosion (for steel) can be used to assess the design over time and, likely, to demonstrate a useable life greater than the calculated design life.

3.4 Performance

Transportation Asset Management: ERS are typically designed and constructed, and not revisited unless a problem with performance is noted. But walls are an important part of public and of private works, particularly when there are many structures owned, and as such constitute an important infrastructure asset. The National Park Service (NPS) and FHWA recently developed an asset management system for retaining walls, and have inventoried and assessed over 3,200 walls (Anderson et al. 2008). This management system can be used for life-cycle cost analyses, maintenance prioritization, safety evaluations, and project planning. The NPS/ FHWA system is a simple and versatile asset management tool (Anderson et al. 2008) for retaining walls that can be used for other public or private works.

Smart Walls: A significant increase in the instrumentation of ERS is anticipated. Instrumentation will be used for many reasons, including: (i) to define/refine LRFD resistance factors; (ii) monitor and document performance of new systems or materials; (iii) verification of new or refined design methodologies; (iv) asset management; and (v) document possible longer useable life of steel soil reinforcements. Smart reinforcement with strain gages embedded at the manufacturing facility, and with remote data acquisition, has already been developed by one manufacturer to facilitate this effort.

Private Works Project Design Teams: The performance of MSE structures, and other ERS, in private works can be enhanced with better coordination/communication amongst the project manager, project design consultants, and project contractors. Other project features, such as surface water control design, can negatively impact an MSE structure. Future improvements in project coordination/communication may be instigated by a professional organization and/or an ERS association. See the conference papers by Simac and Fitzpatrick, and by Schmidt, Harpstead and Christopher for detailed discussions on this issue.

3.5 Analysis and Design

LRFD: Transportation superstructures are designed using LRFD procedures, and logically the substructures and ERS supporting the superstructures should also be designed on a LRFD basis to provide design consistency on the overall project. Therefore, FHWA and the AASHTO Subcommittee on Bridges and Substructures established an October 1, 2010 deadline for implementation of LRFD in wall design. The current AASHTO LRFD Bridge Design Specification (2007, with 2008 and 2009

Interims) has retaining wall resistance factors calibrated by fitting to allowable stress design (ASD). Thus, the current code is a starting point for LRFD retaining wall design. Refinement of resistance factors through instrumentation, calibration, etc. is anticipated. LRFD should also facilitate innovation in design practice, and may lead to new design methods. But who will lead these efforts is to be defined – will it be researchers, system suppliers/vendors, independent DOT research, pooled fund DOT/FHWA research, and/or industry associations?

See the conference paper by Samtani and Sabatini for a detailed discussion on aspects LRFD for ERS in transportation works.

MSE Simplified Method: The simplified MSE analysis approach (Elias and Christopher, 1997; Elias et al. 2001) is also used in the LRFD platform (AASHTO, 2007; Berg et al. 2009). The internal lateral pressure is determined with the K_r/K_a relationship and a vertical earth load factor $\gamma_{EV\text{-}max} = 1.35$ (for Strength I limit states). It is anticipated that the K_r/K_a relationship will be refined for the wire bar/mesh soil reinforcement and will be defined for geosynthetic straps through research work, sometime in the near future.

MSE Design and Construction with Non-Select Reinforced Fill: Reinforced wall fills in transportation works with fines contents greater than the current 15% maximum (i.e., non-select fill) may increase in the future. The LRFD platform does not specifically address the use of finer grained, less permeable soils in load and/or resistance factors. Definition of load and resistance factors are required for wide spread use of lower quality reinforced wall fills. In addition to definition of LRFD factors, design details to prevent buildup of pore pressure (see 3.2 discussion) must be developed that correspond to the assumptions used in their definition.

Heavy Faced MSE Composite Walls: The use of hybrid walls constructed of a MSE mass and heavy face (see Sections 2.3 and 3.3) is growing. These walls are typically being analyzed as a MSE structure with treating the heavy face simply as a face (as other MSE wall systems are designed). Economies in design and construction can be realized by designing and analyzing the structures as a hybrid gravity/MSE wall structure. That is, incorporate the stabilizing effect of the heavy face mass in both the internal and external MSE stability assessments. However, the market drivers currently do not seem strong enough to initiate and complete the efforts to develop such a design procedure.

Mixed MSE Reinforcements: Current design guidelines and tools limit/assume a single type (e.g., steel strip, geogrid, steel bar mat, etc.) of soil reinforcement will be used throughout the reinforced soil volume. Different grades (strengths) of a reinforcement may be used, but of the same type. Design models and LRFD factors are calibrated to walls with a single type of soil reinforcement. However, in the future MSE walls might be designed and constructed with two (or more) soil reinforcement types, to provide better economies. For example, a reinforcement type with high tensile strength and an economical cross section may be used in the lower portion of a wall, with a lower strength, high pullout resistance reinforcement type in the upper portion of the wall. Numerical modeling design tools and instrumentation tools for performance monitoring should be used for the initial applications of multiple reinforcement types in a wall.

Two-Zone MSE Fills: Current design guidelines and tools limit/assume a single soil fill will be used throughout the reinforced soil volume. Design models and LRFD factors are calibrated to walls with a single, uniform reinforced wall fill soil. However, in the future MSE walls might be designed and constructed with two (or more) reinforced fill soil types. A two zone system with a coarser, stronger soil (e.g., No. 57 stone) in the lower portion of the wall and a lower strength, finer grained soil (e.g., silty sand) in the upper portion of the wall may provide economic and performance (e.g., decreased fill settlement) benefits for tall walls. A 1H:1V zone of high quality, free-draining fill could be used at the front of a wall, with non-select fill behind it, to handle seepage and drainage to provide an economic benefit.

The use of numerical modeling for design, along with the use of instrumentation to monitor performance, are tools that should be used for initial applications of a multiple MSE fill zones. Market drivers of: (i) potential use of non-select fills for transportation works, and (ii) desire to lower the rate of MBW MSE wall failures in private works may spur the development of two-zone MSE fills.

Numerical Modeling and Composite Material Design Methods: Future designs may be based upon numerical models within which the characteristics and behavior of the reinforced soil composite material can be evaluated. Both strength and service limits states could be evaluated with these methods. Numerical models will also allow designers to more effectively evaluate the potential consequence of using marginal or non-select fills for project specific conditions.

Reliability-Based RSS Design: Currently, there is not an LRFD slope analysis tool to check global and compound stability of MSE walls. Reliability analysis tool(s) should be developed in the future, though it is not clear how uncertainty will be addressed. Format could be similar to the AASHTO LRFD format, or could be in another reliability-based format.

Unified MSE Wall/RSS Design Method: MSE structures with batters of 20º or less (off vertical) are designed as walls and those with a greater batter as slopes. As questioned by Professor Holtz (2010) in his Terzaghi Lecture: "When does a very steep slope become a wall? Does the soil know the difference?" Historical practice and market drivers have led to this point, but should we continue along this path?

As noted above, we do not have an LRFD slope analysis tool to check global and compound stability of MSE walls. Furthermore, in both the LRFD and ASD platforms one tool is used to design the wall and then another tool is used to check compound and global stability. A unified approach, whether in a LRFD or other reliability-based platform, could provide a single tool for design/analysis.

4 SUMMARY

The purpose of this plenary session paper is to help initiate discussion and debate at this conference (and afterwards) as to what will be presented at a similar conference 20 years from now. But how do we get there? It is hoped that the future directions/ trends presented will inspire researchers and young engineers to seize hold of one of these new trends and research, develop, design, construct, and/or monitor performance of such structures and share experiences in technical venues. Likewise, associations, wall system suppliers, professional organizations, etc. may take one or more of the future direction topics/ideas and move them forward.

Many of the future direction topics can and should be interactive. For example, the use of MSE abutments should significantly expand: (i) due to market driven need for rapid construction; (ii) with use of an LRFD design platform, where serviceability is a specific design limit state; (iii) with a national review system/process for ERS; (iv) with instrumentation tools to monitor/document performance; and/or (v) with use of large, heavy precast facing members.

Another example is the future direction of MSE design. If a unified MSE wall/slope design method is developed should it be earth pressure or limit equilibrium based? If limit equilibrium based, is reliability better addressed in a non-LRFD platform?

Two of the topics seem to be at odds with one another. Historically, the failure rate of MBW faced, MSE walls on private works with non-select reinforced soil fills is unacceptably high, as compared to performance of other civil works (see Section 2.4). One possible method to reduce this failure rate is to restrict the use of non-select reinforced wall fill, or even eliminate its use. In contrast, research into the use non-select reinforced wall fill on transportation works has recently been completed. Highway works may relax MSE wall fill gradation over the next twenty years, but with stringent detailing and QC/QA requirements, and with due consideration of the lessons learned in private works over the past twenty years.

ACKNOWLEDGEMENTS

The input of many of my colleagues is sincerely appreciated. Thank you to: D. Alzamora, R. Barrows, R. Bathurst, B. Christopher, J. Collin, J. DiMaggio, R. Holtz, R. Koerner, D. Leshchinsky, S. Nichols, P. Sabatini, N. Samtani, M. Simac, V. Schaefer, R. Stulgis, and B. Tanyu.

REFERENCES

AASHTO (2007). *LRFD Bridge Design Specifications*. 4th Edition, with 2008 and 2009 Interims, American Association of State Highway and Transportation Officials, Washington, D.C.

AASHTO (2002). *Standard Specifications for Highway Bridges,* 17th Edition, American Association of State Highway and Transportation Officials, Washington.

Allen, T.M., Nowak, A.S. and Bathurst, R.J. (2005). *Calibration to Determine Load and Resistance Factors for Geotechnical and Structural Design*, Transportation Research Board Circular E-C079, Washington, D.C., 93p.

Allen, T.M., Bathurst, R.J. and Berg, R.R. (2002). "Global level of safety and performance of geosynthetic walls: an historical perspective", *Geosynthetics International*, (Vol. 9, Nos. 5-6), pp. 395-450.

Allen, T., Christopher, B.R., Elias, V.E. and DiMaggio, J. (2001) *Development of the Simplified Method for Internal Stability Design of Mechanically Stabilized Earth (MSE) Walls,* Washington State DOT Research Report WA-RD 513.1, 108 p.

Anderson D.G., Martin, G.R., Lam, I. and Wang, J.N. (2008). *Seismic Analysis and Design of Retaining Walls, Buried Structures, Slopes, and Embankments,* Project NCHRP 12-70, NCHRP Report 611, NCHRP, TRB, National Research Council, Washington, D.C.

Anderson, S.A., Alzamora, D. and DeMarco, (2008). "Asset management systems for retaining walls", Colorado ASCE Geotechnical Seminar Program in Lakewood, CO, pp 162 – 177.

Anderson, P.L. and Brabant, K. (2005). "Increased use of MSE abutments", presented at the International Bridge, Pittsburgh, PA.

Bathurst, R.J., Huang, B. and Allen, T.M. (2010). "Load and resistance factor design (LRFD) calibration for steel grid reinforced soil walls", *Georisk*, Taylor & Francis Group, London, U.K. (in press)

Bathurst, R.J., Nernheim, A., Miyata, Y. and Allen, T.M. (2009). "Predicted loads in steel reinforced soil walls using the AASHTO Simplified Method", A*SCE Journal of Geotechnical and Geoenvironmental Engineering,* (Vol. 135, No. 2), pp 177-184.

Bathurst, R.J., Miyata, Y., Nernheim, A. and Allen, T.M. (2008a). "Refinement of K-stiffness method for geosynthetic reinforced soil walls", Geosy*nthetics International*, (Vol. 15, No. 4), pp 269-295.

Bathurst, R.J., Allen, T.M. and Nowak, A.S. (2008b). "Calibration concepts for load and resistance factor design (LRFD) of reinforced soil walls", *Canadian Geotechnical Journal*, (Vol. 45, No. 10), pp 1377–1392.

Berg, R.R., Christopher, B.R. and Samtani, N.C. (2009). *Design and Construction of Mechanically Stabilized Earth Walls and Reinforced Soil Slopes*, FHWA NHI-10-024 Vol I and NHI-10-025 Vol II, Federal Highway Administration, Washington, D.C., 306p (Vol I) and 378p (Vol II).

Christopher, B.R., Gill, S.A., Giroud, J.P., Juran, I., Mitchell, J.K., Schlosser, F. and Dunnicliff, J. (1990). *Design and Construction Guidelines for Reinforced Soil Structures*, FHWA-RD-89-043, Federal Highway Administration, Washington, D.C.

Collin, J. G., Berg, R.R. and Meyers, M. (2002). *Segmental Retaining Wall Drainage Manual*, National Concrete Masonry Association, Herdon, VA, 96p.

Elias, V., Fishman, K.L., Christopher, B.R. and Berg, R.R. (2009). *Corrosion/ Degradation of Soil Reinforcements for Mechanically Stabilized Earth Walls and Reinforced Soil Slopes*, FHWA NHI-09-087, Federal Highway Administration, Washington, D.C., 146p.

Elias, V., Christopher, B.R. and Berg, R.R. (2001). *Mechanically Stabilized Earth Walls and Reinforced Soil Slopes, Design & Construction Guidelines*, Federal Highway Administration, Washington, D.C., FHWA-NHI-00-043, 418p.

Elias, V. and Christopher, B.R. (1997). *Mechanically Stabilized Earth Walls and Reinforced Soil Slopes, Design and Construction Guidelines*, Federal Highway Administration, FHWA SA-96-071, Washington, D.C., 371p.

Fishman, K.L. (2010). *LRFD Metal Loss and Service-Life Strength Reduction Factors for Metal Reinforced Systems in Geotechnical Applications*, Project 24-28, NCHRP, TRB, National Research Council, Washington, D.C., (publication pending).

Holtz, R.D. (2010). "Reinforced soil technology—from experimental to the familiar", 46th Karl Terzaghi Lecture, presented at the ASCE Geo-Institute GeoFlorida conference, West Palm Beach, FL.

Huang, B., Bathurst, R.J. and Hatami, K. (2009). "Numerical study of reinforced soil segmental walls using three different constitutive soil models, ASCE *Journal of Geotechnical and Geoenvironmental Engineering*, (Vol.135, No.10), pp. 1486-1498.

Lostumbo, J.M. (2009). "Yeager airport runway extension: tallest known 1H:1V slope in U.S."**,** *Proceedings of Geosynthetics 2009*, IFAI, Roseville, MN, pp. 593-598.

Marr, W.A. and Stulgis, R.P. (2010). *Selecting Backfill Materials for MSE Retaining Walls*, (Preliminary Draft, Final Report 2009), Project 24-22, NCHRP, TRB, National Research Council, Washington, D.C.

Morrison, K. F., Harrison, F. E., Collin, J. G., Dodds, A. and Arndt, B. (2006). *Shored Mechanically Stabilized Earth (SMSE) Wall Systems*, Federal Highway Administration, FHWA-CFL/TD-06-001, Washington, D.C., 212 p.

Musser, S.W. and Denning, C. (2005). *Deep Patch Road Embankment Repair Application Guide*, USDA Forest Service, 21p.

NCMA (2009). *Design Manual for Segmental Retaining Walls*, National Concrete Masonry Association, Bernardi, M., editor, 3rd Edition, Herndon, VA, 285p.

NCMA (1997). Desig*n Manual for Segmental Retaining Walls*, National Concrete Masonry Association, Collin, J.G., editor, 2nd Edition, Herndon, VA, 289p.

O'Rourke, T. D. and Jones, C.J.F.P. (1990). "Overview of earth retention systems: 1970-1990." *Design and Performance of Earth Retaining Structures*, GSP No. 25, ASCE, Reston, VA, pp. 22-51.

Sankey, J.E., Bailey, M.J. and Chen, B. (2007). "SeaTac third runway: design and performance of MSE tall wall," *New Horizons in Earth Reinforcement*, 5th Int. Symposium on Earth Reinforcement, IS Kyushu 2007, Fukuoka, Japan.

Simac, M.R., Bathurst, R.J., Berg, R.R. and Lothspiech, S.E. (1993). *Design Manual for Segmental Retaining Walls*, 1st Edition, National Concrete Masonry Association, Herndon, VA, 336p.

Wu, J.T.H, Lee, K., Helwany, S., and Ketchart, K. (2006). *Design and Construction Guidelines for Geosynthetic-Reinforced Soil Bridge Abutments with a Flexible Facing System*, NCHRP Report 556, Project 12-59, NCHRP, TRB, National Research Council, Washington, D.C.

Embedded Retaining Walls – A European Perspective on Design Developments and Challenges

A. S. O'Brien, BSc, MSc, DIC, C. Eng, FICE.
Geotechnics Practice Leader, Europe and Africa, Mott MacDonald;
Visiting Professor, Southampton University, UK
web: www.mottmac.com email: anthony.obrien@mottmac.com

Abstract

This paper provides a summary of major developments in the design of embedded retaining walls in heavily overconsolidated clays. These include wall installation effects, prop forces, wall and ground movements and observational method applications. Risks and opportunities are considered, examples are given of strengthening of old retaining walls and geothermal energy utilisation. Future industry challenges: better capabilities to assess/control groundwater pressures and associated clay softening; and improved training of engineers in advanced analysis are highlighted

1.0 Introduction

This paper provides an overview of developments in the design of embedded retaining walls in Europe during the last 25 years. Retaining wall design can involve complex soil-structure interaction, Figure 1 (a). A wide range of factors can significantly affect the structural forces, displacement, and stability of a wall. Behaviour will depend not just on the "theoretical" soil and structure response, but also on practical issues, such as the methods, sequence and timing of construction of the wall and its support system (both temporary and permanent). Embedded retaining walls are commonly used for constructing deep excavations in heavily populated

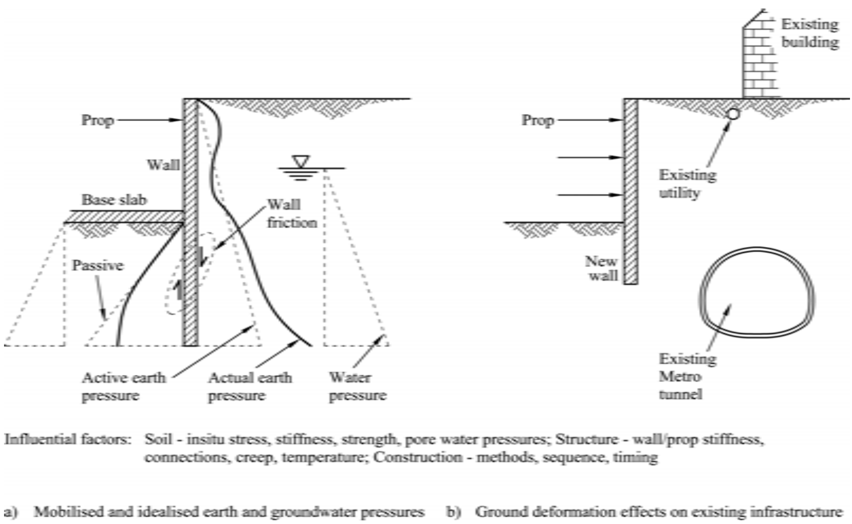

Figure 1: Embedded Retaining Walls: Soil – Structure Interaction

urban areas. Hence, there are usually concerns about the magnitude of ground deformation around the retaining wall, and the potential for damage to existing structures (surface and subsurface), Figure 1 (b). Most of the major developments are associated with the design of walls embedded in stiff, heavily overconsolidated clays; and this is the focus for this paper.

2.0 Uncertainties in the Early 1980's

In the early 1980's developments in insitu testing for horizontal stress measurements, (such as self-boring pressuremeter, spade cells, etc) together with easier access to more powerful analytical techniques (such as finite element methods), caused designers to more seriously question the reliability of conventional limit equilibrium methods. For example, Figure 2 provides a summary of output from some early finite element modelling, Potts and Fourie (1985) and Potts and Bond (1994). Figure 2 indicates that the wall bending moments and prop forces in stiff walls (such as reinforced concrete diaphragm or secant walls) could be far higher than predicted by limit equilibrium (l.e) methods (assuming simple active/passive earth pressures). It is important to note that the finite element analyses assumed the walls were "wished into place" (WIP), i.e. wall installation (and associated changes in insitu stress) was not modelled. In addition, the stress-strain behaviour of the soil was assumed to be linear elastic-perfectly plastic. The large forces implied by the type of analyses shown in Figure 2, were a major cause for concern for designers (for example, Hubbard et al, 1984). There were also a wide range of other uncertainties, Table 1. Geotechnical and structural design codes were difficult to use in a coherent way, due to fundamental differences in design philosophy. Even the geotechnical factor of safety against rotational failure was defined in several different ways; for example a popular design guide in the 1980's (CIRIA104, 1984) provided four different definitions. Two commonly used safety factors are: Factor of Safety on Strength, Fs; and Factor of Safety on Passive (or Gross) Pressure, Fp. Figure 3 provides a comparison between Fs and Fp for a cantilever and single propped wall in homogenous soil, with and without groundwater. For a constant Fs value of 1.2 the Fp value varies significantly with friction angle, wall type, and groundwater conditions. Because of the problems summarised above and in Table 1 there was considerable confusion, and uneconomic design/construction.

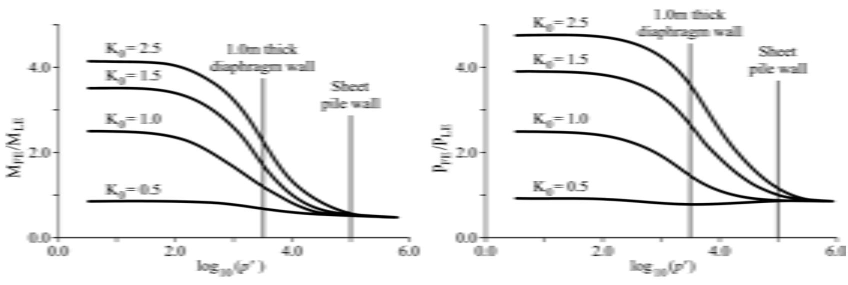

Note: FE - finite element, LE - limit equilibrium prediction. ρ' = normalised wall flexibility, Potts & Bond (1994). Wall installation effects not considered. Single prop at top of wall.

a) Maximum bending moment b) Maximum prop force

Figure 2: Simple Finite Element versus Limit Equilibrium, Wall Bending Moment and Prop Forces

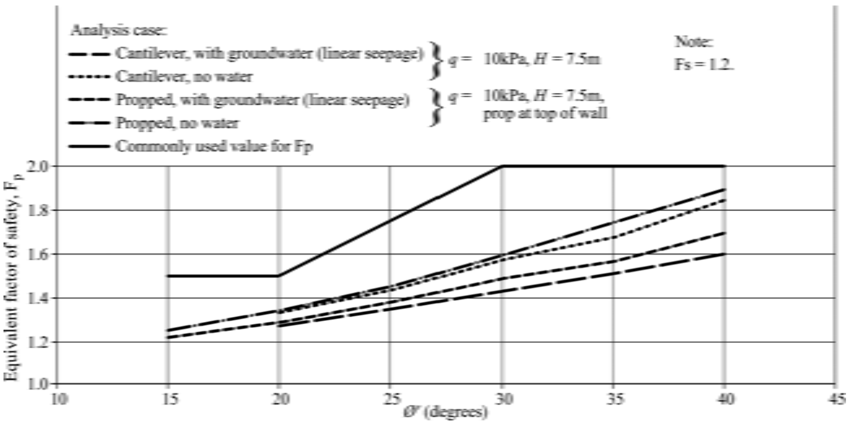

Figure 3: Variation of Factor of Safety on Passive Pressure, Fp; for Fs = 1.2

Table 1: Perceived Problems, Retaining Wall Design Early 1980's

Issue	Comment
Definition of Factors of Safety	Various definitions, all gave different answers; inconsistent results for various soil strengths
Temporary Works	Temporary Prop Loads - unsafe/too safe? Temporary Berms – how do they work? Observational Method – safe implementation?
Soil-Structure Interaction, High OCR Clays	Limit Equilibrium could be unsafe due to high Ko Long Term Increases in Ko over Time?
Ground Movements	Prediction of Movements, Appropriate Young's Moduli?
Integrate Geotechnical into Structural Design	Incompatibility between Structural (Limit State) and Geotechnical (Lumped Factor) codes
Changes in Strength over Time (for high OCR clays)	Reduction in undrained strength Reduction in effective cohesion

3.0 Overview of Major Developments

3.1 Wall Installation Effects

The Lion Yard project in Cambridge, UK (located about 100km north of London), provided an unusual opportunity to comprehensively monitor retaining wall and ground behaviour during construction of a 10m deep basement in a relatively homogenous layer of stiff clay. The site and monitoring have been described by Ng (1998). Figure 4 shows measurements of total horizontal stress against depth, before and after installation of the diaphragm wall (and prior to any excavation in front of the wall). Prior to wall installation, Ko values were between about 1.5 and 2.5. After wall installation the K value (horizontal effective stress divided by vertical effective stress) had dropped to values between 0.9 and 1.1. Other field measurements have provided similar evidence of the large stress changes which occur in stiff clay due to the installation of diaphragm, secant and contiguous bored piled walls (for example, Tedd et al, 1984; Symons and Carder, 1992). There is no evidence of earth pressures increasing with time (after retaining wall construction and excavation) and returning towards their original values, (Carder and Darley, 1998).

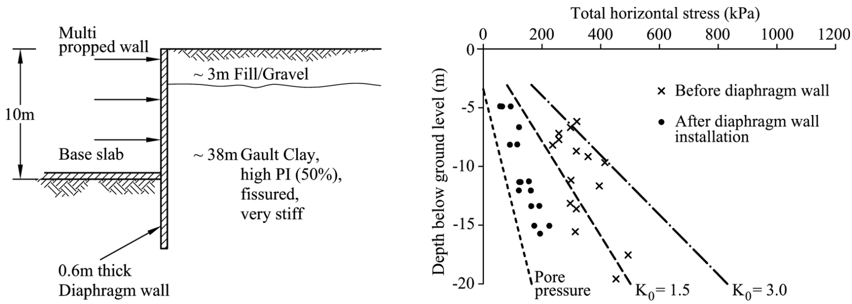

Figure 4: Lion Yard, Horizontal Stress, Before and After Wall Installation

3.2 Prop Forces

At Lion Yard, prop forces were carefully monitored, and comparisons were made with finite element predictions, Table 2.

Table 2: Lion Yard – Prop Forces

Prop location	Measured (Prop Force (kN/m)	Predicted Prop Force (kN/m)	
		WIP	WIM
L2	145	255	153
L3	119	216	155
L4	24	29	21

Notes: WIP – Wall "wished in place"; WIM – Wall installation modelled

It is clear that if (as is often the case) the effects of wall installation on insitu stresses are ignored, "WIP" assumptions, then in heavily overconsolidated deposits the prop forces can be significantly overpredicted. The combined effects of wall installation, plus the high stiffness of overconsolidated soils along relevant stress paths, Powrie et al (1998), leads to earth pressures dropping rapidly towards active limits.

Figure 5 summarises the monitoring of prop forces carried out at Canada Water (in the east of London, UK) for a metro project (Powrie and Batten, 2000). The value of these observations

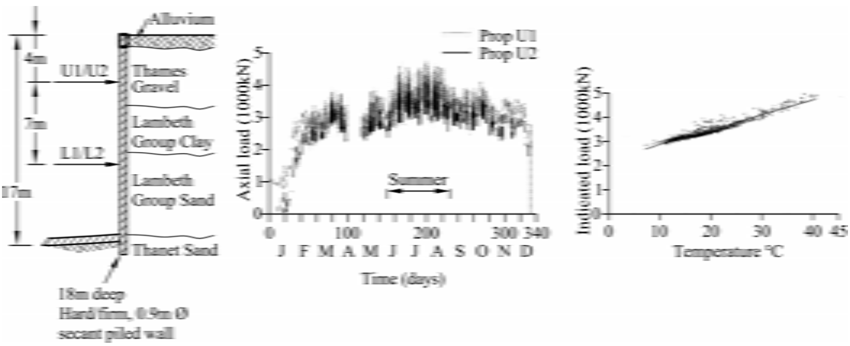

Figure 5: Prop Loads, Influence of Temperature

is that they were carried out over a period of nearly 12 months and the prop forces were monitored at two-hourly intervals using 8 vibrating wire strain gauges per prop. The prop forces were carefully correlated against temperature. In mid-summer, due to higher temperatures, the force in the upper props (which experienced the largest variations in temperature) was 50% higher than in winter, when they were installed. The magnitude of any temperature induced axial load depends not only on the temperature change, but also on the effectiveness of the restraint at the prop/wall connection. On the basis of a number of case histories Twine and Roscoe (1999) assessed the average end restraint to be in the range 40% to 60% for temporary props supporting stiff walls (secant/diaphragm walls) in overconsolidated deposits. Twine and Roscoe (1999) also provide a simple design method (called the "Distributed Prop Load" method) for calculating prop loads based on a modified version of Peck's earth pressure envelope. These recent observations of prop forces, highlight a few other important, but subtle, effects such as: the influence of thermal expansion of permanent concrete slabs (which can lead to the temporary reduction of prop forces in adjacent temporary props); the effects of clay permeability in dissipation of pore water suctions in retained soils, and associated time dependent increases in prop force; and non-uniform axial stresses due to "lack of fit" at the prop/wall connection, Batten and Powrie (2000).

3.3 Wall and Ground Movement

Perhaps one of the most significant developments in the last 25 years is the improved understanding of soil stiffness. At very small strains soil stiffness is extremely high, and with increasing strain amplitude soil stiffness can degrade by an order of magnitude or more. For heavily overconsolidated clays horizontal stiffness will be higher than vertical, Figure 6. Research in the UK and Italy (Lings et al, 2000; Lo Presti et al, 1999; Atkinson, 2000) has highlighted the range of factors which can influence small strain stiffness. Despite the improvements in understanding, practical implementation remains challenging. Careful back analysis and calibration of the chosen soil constitutive model and software against good quality case history data remains the most robust approach to selecting appropriate non-linear soil-stiffness parameters (for example, Chang et al, 2001; Scott et al, 2003). Experience has shown that realistic predictions of settlement and horizontal displacement around deep excavations requires sophisticated soil modelling, which allows for non-linear degradations of soil stiffness with

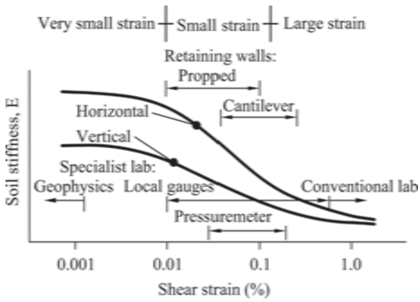

Figure 6: Variation of Soil Stiffness with Strain Amplitude

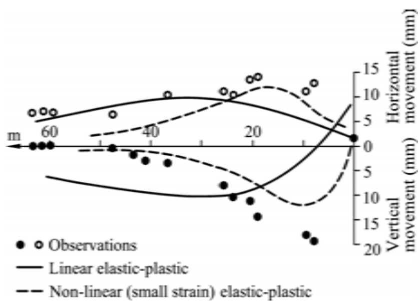

Figure 7: Ground Movements adjacent to a Deep Excavation, influence of soil model

strain amplitude, Burland (1989). Figure 7 illustrates the variation of settlement and horizontal displacement around the deep excavation for the House of Commons Car Park, Burland and Hancock, 1977. Predictions from two different analyses (linear elastic-perfectly plastic and a non-linear small strain model) are compared against observed movements. The non-linear small strain model predicts much more realistic differential movements. This is important since the risk of potential damage to existing infrastructure is largely governed by differential ground movements.

Cantilever walls form ideal temporary works, being simple, economic and rapid to build, leaving the site and its surroundings free of props or anchorages. Designers used to be reluctant to consider cantilever walls if excavations were deeper than about 4m or 5m. However, more recently cantilever walls have been used to retain deeper excavations. Long (2001) extended the work of Clough et al (1989) and reviewed 300 case histories of various retaining wall types (anchored, propped, cantilever, etc) embedded in stiff soils. The worldwide database for cantilever walls is shown on Figure 8 (a). More recently, Looby and Long (2007) have analysed the behaviour of cantilever walls in heavily overconsolidated glacial tills in Dublin, Ireland. The till has a low plasticity index of about 10%, and has little true clay minerals, the clay fraction (typically less than 20%) being ground up silica rock flour. Dublin cantilever wall case histories

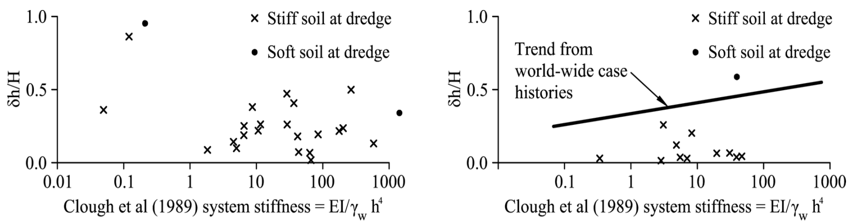

Notes:
1. Normalised maximum lateral wall movement = $\delta h/H$. 2. Observations typically for less than one year

a) World-wide case histories

b) Dublin Glacial Till case histories

Figure 8: Cantilever Retaining Walls, Short Term Movements

are shown in Figure 8 (b). Figure 8 (a) indicates δ_h/H values up to about 0.4 to 0.5%, (which includes clays of high plasticity) with an average value of about 0.25%. The cantilever walls in glacial till perform extremely well with δ_h/H values of less than 0.1%, for excavations up to 8m deep.

The displacement of a retaining wall can be only a small fraction of the overall ground movements induced by the various construction activities associated with a deep excavation. This is easy to overlook, since a lot of design effort (and most of the computer modelling) will naturally focus on the retaining wall itself. Figure 9 shows measurements of settlement plotted against time, for a 23m deep excavation adjacent to Harrods, London (Fernie et al, 2001). The

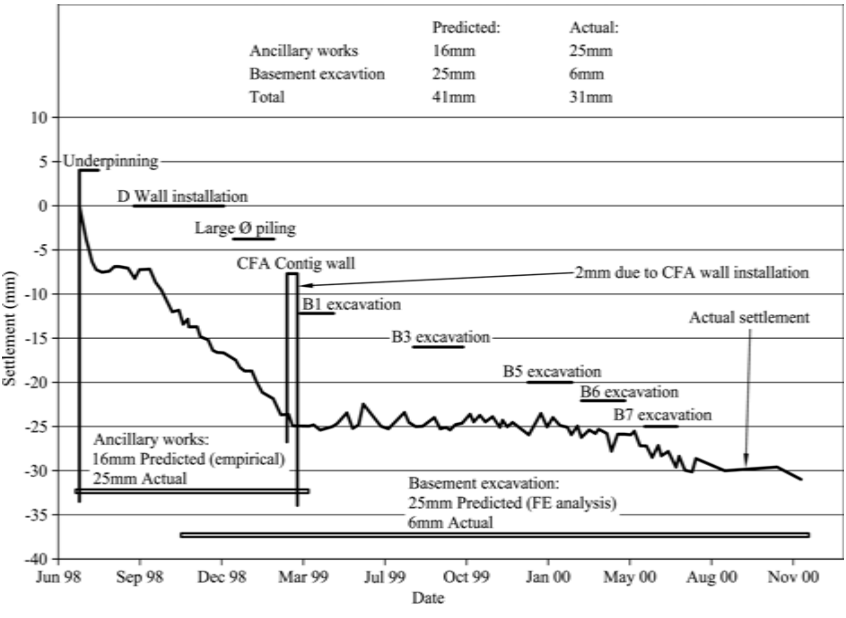

Figure 9: Sources of Ground Moment adjacent to the Deep Excavation at Harrods

retaining wall was an 800mm thick diaphragm wall about 29m deep. The wall was supported "top down" by 7 reinforced concrete slabs, at between 2.5 and 4.0m depth intervals. In addition, there were a range of ancillary activities, including: underpinning of adjacent buildings; installation of 70 bored piles (between 1.0 and 1.8m dia) which supported superstructure columns and the basement slab; and 600mm dia CFA piles for ramps into the basement. From Figure 9 it can be seen that about 80% of the observed settlement was due to these "ancillary" activities, with the residual 20% being within the scope of the finite element analysis of the retaining wall and basement excavation. Although this is an extreme example, it emphasises the need to consider ALL the potential sources of ground movement, irrespective of whether they can be simulated in a computer analysis.

3.4 Application of the Observational Method

The Observational Method, OM, (Peck, 1969) can lead to significant reductions in construction schedule and cost (for example, Powderham and Rutty, 1994). Maintaining safety is essential, and managing risk is central to the application of the OM. A key development has been the adoption of a step by step process known as "Progressive Modification", pioneered by Powderham (1998). A key uncertainty for retaining wall design and construction in stiff clays is the rate of softening of the clay as a result of stress relief induced by the excavation. Conventional design assumptions are usually quite conservative. A key benefit of OM is that it can fully exploit the short term strength of stiff clays. This usually allows temporary support to be minimised and construction to be carried out rapidly. Safe application of OM requires several key factors to be assessed Table 3. If any of the adverse factors outlined in Table 3 cannot be eliminated then OM cannot be applied. Successful OM implementation has often involved the exploitation of the beneficial effects of 3 dimensional geometries within an excavation.

Table 3: Adverse Factors for Observational Method Implementation

Factor	Comment
Brittle Failure	Adequate visual warning when approaching a ULS?
Progressive Collapse	Failure of one component, leads to rapid failure of overall system
Lack of Stakeholder Support	All parties in project need to be actively involved and supportive
Unable to obtain critical observations reliably	Control of works is dependant on obtaining pertinent data and acting on it.
Implementation of Contingency measures is too slow	The contingency plans need to be fully developed and able to be implemented within the available timescale

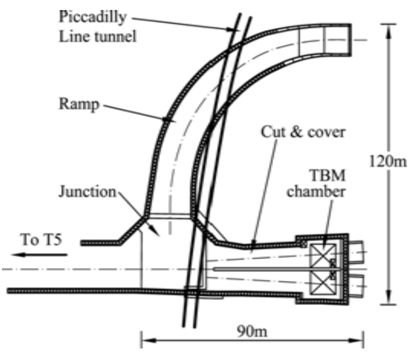

Figure 10: Heathrow T5, Plan of ART West Portal

The OM was successfully implemented recently for the new Terminal 5 at London's Heathrow Airport, which involved construction of an "Airside Road Tunnel" (ART), Powderham (2009). The west portal for the tunnel boring machine (TBM) launch chamber involved construction of a 17m deep retaining wall, Figures 10 and 11. The base case design required top down construction below the roof slab and temporary props at the mid-height of the walls. A conventional application of the OM would have used (as a contingency measure) temporary props similar to the base case design. However, the presence of this steelwork adjacent to the excavation would have reduced the potential benefits of OM. The innovative concept which facilitated application of OM was the use of intermediate "blinding struts" as a contingency lateral support measure. The use of blinding struts (simply a layer of unreinforced concrete cast on the excavated surface to support the retaining walls) required a suitable concrete mix design for early strength gain and the use of a strictly controlled excavation sequence using laser control. The use of OM was successful and wall deflections were less than 0.1% of the retained height and contingency measures were not required. The application of OM along subsequent sections of the western portal led to total savings of 275 tonnes of steelwork and 31 weeks on the construction schedule.

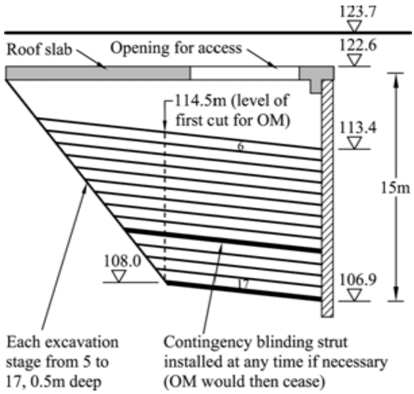

Figure 11: ART West Portal, OM Excavation Sequence

A PhD research programme has been initiated to assess the structural performance of blinding struts (Abela et al, 2008). The most likely failure mode is upheaval buckling. These studies have shown that blinding struts of reasonable thickness (300mm to 500mm) have sufficient strength to work effectively as alternatives to conventional props. However, a conservative approach is required for design due to the wide range of factors which may influence the buckling load and due to the brittleness of the failure mode.

3.5 New Design Codes and Methods of Analysis

The Eurocodes have been under development for some considerable time, for example, DDEN 1997-1 Eurocode 7 (EC7) for geotechnical design was issued in 1995. They are an inter-dependant set of documents, for example a sheet pile wall would be designed using EC7 and EC3 (design of steel structures), whilst a concrete wall would be designed using EC7 and EC2 (design of concrete structures). The main benefit of the Eurocode is that both geotechnical and structural design now uses the same limit state philosophy, which has not been the case historically. The recent retaining wall design guide CIRIA C580, (2003) collates the developments in design knowledge highlighted earlier in this paper, and has clarified many of the uncertainties outlined in Table 1. Hitchcock (2005) has carried out a comparison between old codes/guidance and new codes/guidance (CP2/CIRIA 104 and EC7/CIRIA C580 respectively), for the retaining walls for the Heathrow T5 project described earlier. This comparison showed that for propped walls under short term conditions, the new codes/guidance gave wall bending moments of about two-thirds of those derived from old codes/guidance. The principal reasons are the different approaches to selection of: K prior to wall excavation; undrained strength profiles; factor of safety. Modern analytical methods can also facilitate more economic design; Table 4 (CIRIA C580, 2003) provides a comparison between different methods of analysis for a 4m high cantilever wall and an 8m high single propped wall.

For the propped wall, the differences between analytical methods are significant. The reason for this is that FLAC can simulate the soil-structure interaction, which leads to stress redistribution along the back of the wall, whereas the limit equilibrium analysis cannot, Figure 1 (a).

Table 4: Comparison between Different Methods of Analysis

Wall Type	Limit Equilibrium			Beam/Spring		FLAC/Finite Difference	
		SLS	ULS	SLS	ULS	SLS	ULS
Cantilever Wall	Wall Depth	N/A	13.9	N/A	13.1	N/A	12.5
	BM	180	548	211	526	194	536
Single Propped Wall	Wall Depth	N/A	16.6	N/A	16.2	N/A	15.5
	BM	459	1159	340	910	470	836
	Prop Load	182	340	235	444	387	469

Notes: 1. Cantilever wall, 4m high, retaining wall stiff clay, Water Table 1mbgl
2. Propped wall, 8m high, single prop 2mbgl, retaining stiff clay, Water Table 1mbgl
3. Long term conditions, effective stress parameters only

4.0 Practical Applications of New Techniques (Risks and Opportunities)

4.1 General Comments

The ground engineering industry continues to be vibrant and innovative. The drivers for innovation are varied; historically reducing construction costs and schedule were predominant. Currently other drivers such as safety and sustainability are becoming more important. Sustainability is a broad topic covering issues (in the context of retaining wall design) such as reuse of lower quality material as engineering back fill; (Carley et al, 2007) and reducing the carbon footprint of new developments. The brief case histories outlined below (one successful, the other unsuccessful) highlight the risks and opportunities for designers and constructors.

4.2 Strengthening of Old Retaining Walls

The strengthening of old retaining walls is becoming an increasingly important task across Europe as infrastructure needs to be upgraded to meet 21st Century requirements. These projects can be relatively small, but can involve extremely complex soil-structure interaction and major uncertainties due to degradation of the old walls and unknown construction effects during the original wall construction. The project described below utilised an innovative design solution. Unfortunately, it led to a major dispute which was only resolved after a lengthy, complex and expensive series of legal proceedings through the High Court in London. The author acted as an expert witness over a period of about two years during this dispute. The original retaining wall which forms a dock in a busy UK port and the proposed strengthening works are outlined in Figure 12. The original retaining wall constructed in 1971 comprised the following elements:

- Driven sheet pile wall (a "larsson 6" with 28,6mm thick flange);
- A "stress relieving platform (SRP)", comprising a reinforced concrete slab;
- Beneath the SRP are driven vertical H-piles, and to anchor the SRP are raking H-piles at the landward end of the SRP

There were stiff competent soils, (the Bracklesham Beds, comprising interbedded heavily overconsolidated very stiff clays and very dense sands) about 3m below the SRP. Strengthening works were required to enable larger ships to berth in the port, hence the dredge level needed to be deepened from -12.8mCD to -16.0mCD. The works were let as a Design/Build contract and the winning tender (much cheaper than other tenderers) was highly innovative, comprising:

i) Pairs of interlocking jet grout columns, at 1.7m c/c along the dock wall (about one metre behind the wall) each column was reinforced by a 168mm dia. steel tube. The column dia was supposed to be 0.9m, and the column centres were at 0.7m centres. Hence, each pair of columns was meant to work "compositely" as a vertical reinforced concrete beam.
ii) Ground anchors were installed at 2.5m centres, just below the SRP.

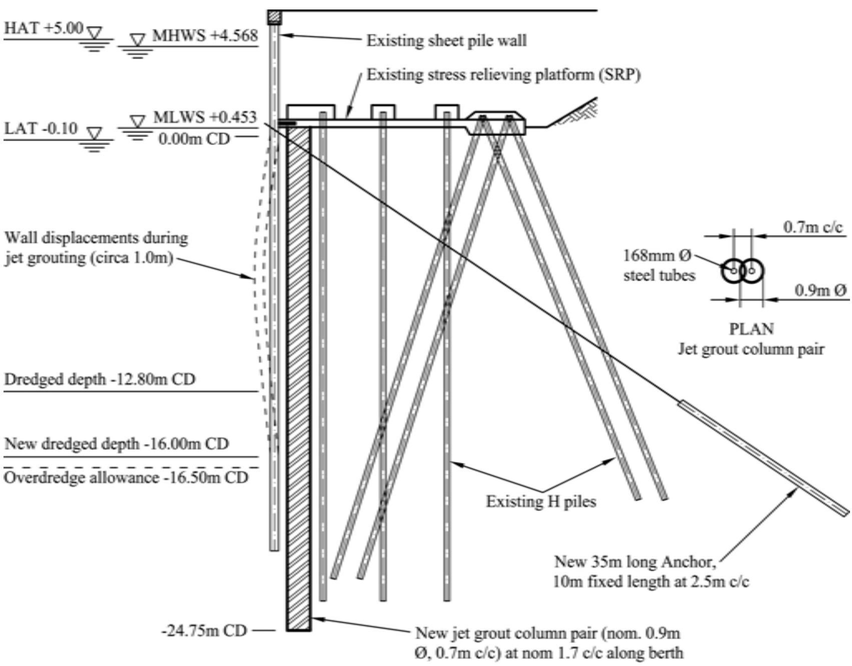

Figure 12: Strengthening of Old Dock Wall, Jet Grout Columns

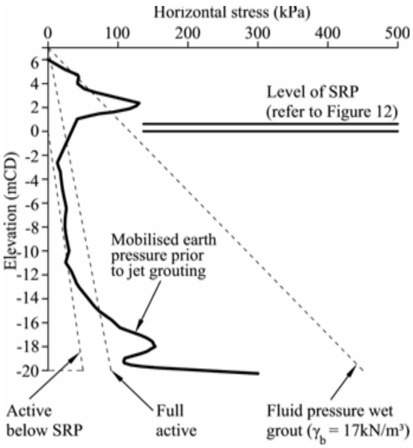

Figure 13 Horizontal Stresses on Old Dock Wall

The winning contractor/consultant team were highly experienced, and had carried out similar work across Holland/Belgium. Unfortunately, there were key differences in geology and type of retaining structure. Previous works were predominately in soft alluvial, post-glacial, deposits, and the retaining walls were mass gravity masonry walls. At this site there were numerous construction problems during jet grouting, including:

(a) The grout fluid pressures, Figure 13, caused large sheet pile wall displacements, up to one metre, forming a plastic hinge in the wall;
(b) The grout hardened rapidly in the overconsolidated soils at depth, which prevented the steel tubes being easily installed;
(c) Installation tolerances meant there was a loss of "composite" action below about -20mCD, hence the lower 5m of the new "beam" had negligible structural strength or stiffness

There were numerous other issues associated with the works and their anticipated "fitness for purpose". A critically important issue was the very low effective earth pressures which had developed behind the sheet pile wall due to soil arching (because the SRP is very stiff, both vertically and laterally, and the sheet pile wall is relatively flexible), Figure 13. The back analysis of the structure (using FLAC) indicates that in the mid-span area the effective earth pressures were less than the full active earth pressures from the top of the sheet pile wall. The failure to recognise that the existing insitu stresses acting on the sheet pile wall were very low was a critical error, and even a fraction of the fluid pressure (based on the wet grout density) would cause unacceptably large displacements of the old retaining wall. Issues which should also have been questioned at an early stage of the tender assessment process are listed in Table5.

4.3 Geothermal Energy

The ground contains a large potential geothermal energy source that can be used for heating and cooling purposes. The basic requirement is a reasonably constant ground temperature across the foundation/retaining wall depth. In most European climate zones the ground temperature varies between 10°C and 15°C. Heat pumps and cooling machines are connected between the closed loop absorber tubes within the foundation/retaining wall concrete and the heating/cooling systems of the building. A refrigerant fluid is circulated through the tubes and transfers heat energy between the heating/cooling system and the ground through conduction. Energy exchange occurs via a heat pump. In the mid to late 1980's geothermal energy was

Table 5: Potential Factors which could affect strengthening of old dock wall

Sheet Pile Driving History	Driving records (unavailable to tenderers) indicated extremely hard driving (potentially causing declutching of the sheets)
H-pile Driving	H-pile driving was also hard, with many piles requiring >1000 blows to drive the last 8ft. These could have caused local damage to the sheet piles, in vicinity of hard soil layers.
Tolerances for Jet Grout Columns	Critical for design concept. Practical?
Jet Grout Diameter	Inevitably would be highly variable, due to interbedded nature of cohesive/cohesionless soil. Tidal effects would also lead to irregular diameters.
Soilcrete Strength	Variable due to variable nature of interbedded soils. Cohesionless soils, soilcrete strength high; cohesive soils, soilcrete strength weak.
Analysis of Structure	Extremely complex soil structure interaction, influence of SRP is critical
Construction History	Important to understand, since affects current state of old structure and risk of "hidden defects"
State of Old Structure and Adjacent Areas	Risk of historic overdredging in front of wall? Corrosion of sheet pile wall? Risk of Obstructions behind wall?

first used in Switzerland and Austria, Brandtl (2006). Seasonal operation of a geothermal system uses the thermodynamic inertia of the ground in order to temporarily store energy in the ground for later use with reversed energy flow. This can produce energy equilibrium in the ground over a complete heating/cooling period during a year. Recent developments in Austria

Table 6: Examples of geothermal heating/cooling capacities

	EA Generali Centre	**Columbus Centre**	**Uniqa Tower**
Absorber units	4200 m^2 diaphragm wall	12400 m^2 diaphragm wall; 300 piles	7800m^2 diaphragm wall
Cooling capacity: kW	400	1428	240
Heating capacity: kW	600	370	420
Annual cooling output: MWh	220	1677	818
Annual heating output: MWh	630	660	646

have been described by Adam and Markiewiez (2009), and Table 6 gives examples of geothermal heating and cooling capacities.

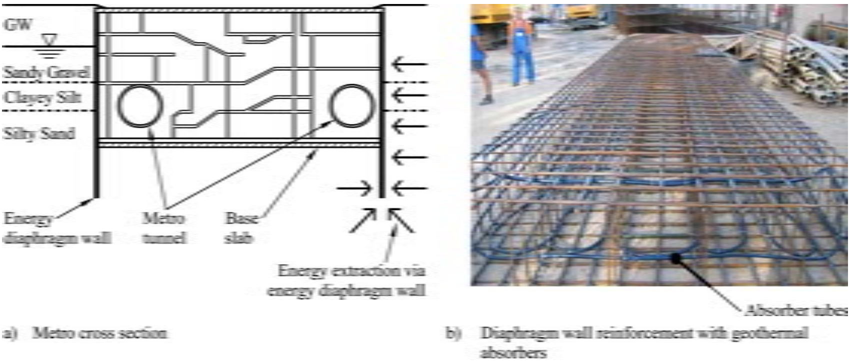

Figure 14: Viennese Metro Line U2, Geothermal Energy

Figure 14 illustrates a geothermal energy application for the new extension to the Viennese Metro, four new stations will be built and together they will have a heating power of 449kW and a cooling capacity of 231kW. Geothermal energy installation is a specialised task and a rigorous and systematic approach is needed to test the system components. Even with good workmanship some absorber loops can be damaged. For the Viennese metro the allowable failure rate is between 3% and 12%. For failure rates above 3% the contractor is penalised financially, but he has to guarantee that a 12% failure rate is not exceeded. Pressure tests are carried out at several stages during installation (Figure 15):

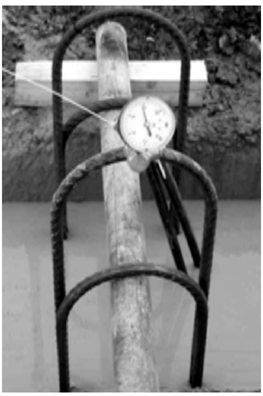

Figure 15: Top of Diaphragm Wall with Pressure Test Tubes and Manometer

(i) Before insertion of the cage
(ii) After concreting the diaphragm wall
(iii) After completion of the excavation, once the vertical absorber tubes are connected to base slab absorber tubes
(iv) At the handover stage between the Civil Engineering works contractor and the heating/ventilation contractors

Key aspects throughout the construction phase are protection of the absorber tubes and managing the interfaces between specialist contractors, and the below/above ground works. Current design methods are simple and based on highly idealised analytical models which usually assume radial heat flow resulting from a constant heat flux. These assumptions are valid for practical purposes for isolated small diameter boreholes of large aspect ratio (say 50m deep, 100mm dia), but for piles, and retaining walls, these simplifying assumptions are largely invalid due to their much smaller aspect ratio, Loveridge (2009).

Bourne-Webb et al (2009) have carried out an investigation of the influence of thermal cycles on the geotechnical resistance of a pile. This indicates that under normal operational conditions, the ultimate geotechnical resistance of a geothermal pile or wall is unaffected by heating/cooling. However, structural design needs to allow for thermally induced changes in concrete stress during cooling (pile/wall contraction) and heating (pile/wall expansion).

5.0 Future Challenges

5.1 Groundwater Pressures and Control, Clay Softening with Time

The assessment of potential changes in groundwater pressures, flow rates and associated reductions in the mobilised strength of stiff clays during retaining wall construction remains a major challenge. Even for apparently homogenous soils (such as London Clay) major differences in behaviour have been observed. Local variations in permeability and sources of water can have a marked effect, and permeability can be very sensitive to subtle changes in soil fabric, such as silt and sand lenses. Inadequate understanding of a site's hydrogeology, and rapid softening of competent soils is a common cause of retaining wall failures. Rowe (1986) describes a retaining wall failure due to seepage along thin silt/sand layers within a stiff clay. This led to a rapid change from undrained to drained conditions. The consequences of high or uncontrolled groundwater pressures can be catastrophic. The collapse of the 28m deep excavation in Cologne, Germany and adjacent buildings (causing two deaths) in March 2009 is still being investigated. However, early assessments indicate that groundwater problems are the most likely cause of the collapse.

5.2 Advanced Methods of Analysis – Engineer Competence

Modern methods of analysis are potentially extremely powerful. If used wisely they can facilitate more economic design. However finite element/finite difference modelling techniques can be easily mis-used. Numerical modelling software is readily available, and, because the software is user friendly, analyses can be run and results obtained. However, the results of benchmarking exercises indicate that analysis output is often unreliable. A benchmark problem organised by the German Society for Geotechnics (Schweiger, 1998) is fairly typical. The problem involved a 12m deep excavation supported by a 20m deep diaphragm wall, supported by two levels of props. The soil was assumed to be dry and all soil, wall and prop properties were defined together with the construction sequence. Hence, the participants only had to set up the mesh, input the defined properties and boundary conditions and run the analysis. Figure 16 summarises the results, from a dozen participants from several European countries for the initial cantilever stage. The magnitudes of predicted movement are all different, and there is no consensus on the direction of wall movement. Half the participants predicted the wall would move back into the retained soil, which is unrealistic. Some of the participants used the same software, and it was clear that human error rather than software problems was the principal cause of the erroneous results. Rapid advances in computer power and software means that sophisticated numerical modelling will become more common in the future. The challenge, therefore, in the future is to improve the competence of engineers carrying out numerical modelling and ensuring that the modelling is checked properly by engineers with appropriate expertise.

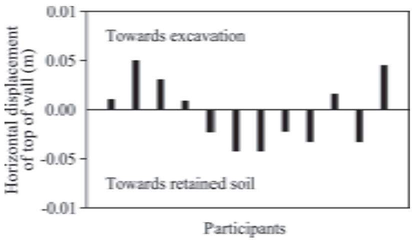

Figure 16: Predictions of Cantilever Wall Displacement results of benchmarking competition

6.0 Conclusions

There have been significant developments in the design of embedded retaining walls during the last 25 years. These developments have been facilitated by improvements in field instrumentation and numerical modelling of soil-structure interaction. For walls embedded in stiff clay, the effects of wall installation are significant in reducing high insitu horizontal effective stresses. This results in lower structural forces on an embedded retaining wall, particularly prop forces, compared with analyses which ignore wall installation effects. Non-linear small strain stiffness is important when assessing ground movements adjacent to retaining walls. There are many opportunities for more economic design and construction. For the unwary or those lacking expertise, there remains numerous risks, especially if the site geology/hydrogeology is misunderstood. Several industry wide challenges remain, perhaps the most important are:

(i) Better understanding and prediction of transient groundwater pressures around retaining walls during construction, and the associated effects on softening of stiff clays;
(ii) Improved training and higher levels of competence in using the numerical modelling software, which has now become widely available.

Energy use is a worldwide concern, and geothermal energy can make a positive contribution. Geothermal energy applications to date have been successful, and are typically used to supplement conventional fossil fuel energy sources. Further research will, however, be needed to address current knowledge gaps. Especially concerning potential thermal interactions between adjacent geothermal foundations (as ground energy utilisation becomes more intense) and long term behaviour (especially in ground affected by groundwater flow).

7.0 Acknowledgements

The author would like to express his thanks to Alan Powderham and Prof. William Powrie; discussions on retaining wall behaviour and observational method applications have given the author deeper insights into soil-structure interaction behaviour.

8.0 References

Abela, J. M., Vollum, R. L., Izzuddin, B. A., & Potts, D. M. (2008). Short and long-term effects on upheaval buckling of blinding struts. *Creating and Renewing Urban Structures, 17th Congress of IABSE,* Chicago.

Adam, D. & Markiewicz, R. (2009). Energy from earth-coupled structures, foundations, tunnels and sewers. *Geotechnique 59*, No. 3, p. 229-236.

Atkinson, J H (2000) "Non-Linear soil stiffness in routine design" *Geotechnique,* vol 50, no 5, pp 487-508

Batten, M and Powrie, W (2000) “measurement and analysis of temporary prop loads at Canary Wharf underground station, east London” In: *Proc Instn Civil Engrs, Geotechnical engineering,* vol 143, pp 151-163

Bourne-Webb, Amatya, Soga. (2009). “Energy pile test at Lambeth College London; geotechnical and thermodynamic aspects of pile response to heat cycles. *Geotechnique*, No. 3, p. 237-248.

Brandl, H. (2006). Energy foundations and other thermo-active ground structures. *Geotechnique 56*, No. 2, p. 81-122.

Burland, J B and Hanncock, R J R (1977) “Underground car park at the House of Commons, London: Geotechnical aspects” *Structural engineer*, vol 55, no 2, pp87-100

Burland, J. B. (1989). Ninth Laurits Bjerrum Memorial Lecture: Small is beautiful – the stiffness of soils at small strains. *Canadian Geotechnical Journal*, Vol. 6, No. 4, p. 499-516.

Carder, D R and Darley, P (1998) Long term performance of embedded retaining walls report 381,TRL, Crowthorne

Carley, S. W., O’Brien, A. S, Hsu, Y. S & Loveridge, F. A. (2007). Innovative use of clay backfill at the new Wembley Stadium, UK. *Proc. of the Int. Conf. Sustainability Construction Materials and Technologies*

Chang, J, Scott, J. M, and Pound, C. (2001). Numerical study of the Heathrow Cofferdam. *Proc. 2nd Int. FLAC Symp.* p163-170

CIRIA 104, Padfield, C. J. and Mair, R. J. (1984). Design of retaining walls embedded in stiff clay.

CIRIA C580 (2003). Embedded Retaining Walls, guidance for economic design, by Gaba, Simpson, Powrie, Beadman.

Clough, G W, Smith, E M and Sweeney, B P (1989) “Movement control of excavation support systems by iterative design procedure” *ASCE foundation engg:* current principles and practices, vol 1, pp 869-884

Fernie, R., Shaw, S. M, Dickson, R. A, St John, H. D, Kovacedic, N, Bourne-Webb, P. and Potts, D. M. (2001). Movement and deep basement provisions at Knightsbridge Crown Court, Harrods, London. *CIRIA, Int. Conf. Response of Buildings to Excavation Induced Ground Movements.*

Hitchcock, A R (2005) “Improving the delivery of underground transportation infrastructure: an observational method case history” *Engineering Doctorate Thesis,* University of Southampton

Hubbard, H W, Potts, DM, Miller, D and Burland, J B (1984) Design of the retaining walls for the M25 cut and cover tunnel at Bell Common” *Geotechnique,* vol 34, no 4, pp265-512

Lings, Pennington, Nash. (2000). “Anisotropic stiffness parameters and their measurement in a stiff natural clay”. *Geotechnique*, No.2, April 2000, p. 109-126.

Lo Presti, D. C. F., Pallara, O., Jamiolkowski, M. & Cavallaro, A. (1999). Anisotropy of small strain stiffness of undisturbed and reconstituted clays. *Proc. 2nd Int. Symp. on Pre-Failure Deformation Characteristics of Geomaterials,* IS-Torino 99, Torino, Vol. 1, p. 11-18

Looby, M. and Long, M. (2007). Deep excavations in Dublin - recent developments. *Presented at Engineers of Ireland, Dec. 07*, Transactions of Engineers – Ireland, Vol. 131, 2007 / 2008, pp. 1 – 15

Long M (2001). Database for retaining wall and ground movements due to deep excavations in: *ASCE Instn Civ Engrs, Geotechnical engg*, Vol127, no3, pp 163-172

Loveridge, F. A. (2009). Personal Communication

Ng, C. W. W. (1998). Observed performance of multi-propped excavations in stiff clay. *J. Geotech. & Geoenvir. Engng, ASCE,* 124 (9), p. 889-905.

Peck, R. B. (1969). Advantages and limitations of the observational method in applied soil mechanics, *Geotechnique*, Vol. 19, No. 2, p. 171-187

Potts, D. M and Fourie, A. B (1985). Effect of wall stiffness on the behaviour of a propped retaining wall. *Geotechnique,* Vol. 35, No. 3, p 347-352.

Potts, D. M and Bond, A. J (1994). Calculation of structural forces for propped retaining walls. *Proc. Int. Conf. Soil Mechanics and Foundations Eng. 13,* New Delhi, Vol. 2, p. 823-826.

Powderham, A. J. and Rutty, P. C. (1994). The observational method in value engineering. *Proc. 5th Int. Conf. on Piling and Deep Foundations,* Bruges.

Powderham, A. J. (1998). The observational method – application through progressive modification. *Proc. Journal ASCE/BSCE,* Vol. 13, No. 2, p. 87-110

Powderham, A. J. (2009) "The observational Method Using safety as a driver for innovation", proc osterreicheche Geotechniktagung, *Vienna Terzaghi Lecture*, OIAV, ISSMGE

Powrie, W., Pantelidou, H and Stallebrass, S. E. (1998). Soil stiffness in stress paths relevant to diaphragm walls in clay. *Geotechnique,* Vol 48, No. 4, p. 483-494.

Powrie, W. & Batten, M. (2000). Comparison of measured and calculated prop loads at Canada Water Station. *Geotechnique 50,* No. 2, p 127-140.

Rowe, P. W. (1986). The potentially latent dominance of groundwater in ground engineering. *Geol. Special Publication,* No. 3, p. 57-78.

Schweiger, H F (1998). Results from two geotechnical benchmark problems" *Proc 4th Eur Conf Number Methods Geotech Engng*, Springer Udine, Stuttgart, 645-654

Scott, J. M, Pound, C. & Shanghavi, H. (2003). Heathrow Airside Road Tunnel – wall design and performance. *Underground Construction 2003,* p. 281-292

Symons, I. F. and Carder, D. R. (1992). Field measurement on embedded retaining walls. *Geotechnique,* Vol. 42, No. 1, p. 117-126

Tedd, P., Chard. B. M, Charles, J. A. and Symons, I. F. (1984). Behaviour of propped embedded retaining wall in stiff clay at Bell Common Tunnel. *Geotechnique,* Vol. 34, No. 4, p. 513-532

Twine, D. and Roscoe, H. (1999) *Temporary Propping of deep excavations – guidance on design*. Publications 517, CIRIA, London

Performance of Deep Excavations in the Taipei Basin

Richard N. Hwang[1]

[1]Moh and Associates, Inc., Inc.,11F #3 Dunhwa S. Road, Taipei , Taiwan 10557; PH (886)958008393; FAX (886)25705566; email:richard.hwang@maaconsultants.com

ABSTRACT:

The concept of wall deflection path and reference envelope is introduced herein for evaluating performance of diaphragm walls. It has been found that, at a given site, wall deflection paths, which are plots of maximum wall deflections versus depths of excavation, converge to a narrow band as excavation goes beyond a depth of 10m or so. The envelope of a family of wall deflection paths, i.e., the so-called reference envelope, characterizes performance of diaphragm walls in a specific set of ground conditions. Based on the data obtained for deep excavations carried out in recent years, reference envelopes are established for the T2, TK2 and K1 Zones of the Taipei Basin and they can be used to evaluate the performance of individual walls.

1. INTRODUCTION

Due to the rapid economical growth in the past decades , the Taipei Basin has become densely populated and very congested. For gaining underground spaces, excavations tend to go deeper and deeper and protection of existing structures in the vicinity of excavations has thus become a serious concern. Because ground settlements, which are the major source of damages to adjacent structures, behind walls are closely associated with wall deflections, it is important to design retaining systems to limit wall deflections in deep excavations. The situation has become more and more critical since the commencement of the construction of the metro systems in the early 90's and excavations exceeding 35m in depth have become more and more frequent. Although it is possible to compute wall deflections by using computer software, the results of analyses are subject to limitations associated with the numerical schemes, and the difficulty in modeling complicated soil behavior often leads to confusions. Therefore, judgment based on field observations still plays a very important role in designs and back analyses.

Because of the presence of a thick layer of young sediments to a depth of, up to, 60m in the Taipei Basin, diaphragm walls are normally required for excavations exceeding 8m in depth. An enormous quantity of field data have been collected in recent years and the performance of diaphragm walls in deep excavations has been analyzed systematically. Deflections of diaphragm walls are routinely monitored by using inclinometers which are amazingly accurate and can be considered as one of the most reliable geotechnical instruments. However, this does not mean that inclinometers always report wall deflections faithfully. It is usually assumed that the toes of inclinometers will not move and the movements at other depths are computed accordingly. This assumption is certainly untrue unless the toes of inclinometers are embedded in competent strata for sufficient lengths. However, inclinometers often stopped at the same depths as diaphragm walls which do not necessarily have sufficient lengths to ensure the fixity of their toes and, as a result, the readings are often erroneous and have to be calibrated. Procedures have been established based on field observations for calibrating inclinometer readings and design charts have been recommended for estimating toe movements of diaphragm walls (Moh and Hwang, 2005; Hwang, Moh and Wang, 2007).

The performance of diaphragm walls will be most conveniently evaluated by studying the so-called wall deflection paths which are plots of maximum wall deflections versus depths of excavation in a logarithmic scale. Wall deflection paths at a certain site tend to converge to a narrow band as the excavation goes beyond a depth of 10m or so. The envelope of a family of wall deflection paths thus characterizes the performance of retaining systems with similar configurations for excavations with similar ground conditions. Based on the data obtained, the so-called reference envelopes have been established for the T2, TK2 and the K1 Zones in the Taipei Basin (Moh and Hwang, 2005; Hwang and Moh, 2007).

Numerical analyses have been performed to substantiate the concept of wall deflection paths and reference envelopes. Parametric studies have also been performed to investigate the influences of various factors on the performance of walls, including the wall thickness and length, width of excavation, the presence of buried slabs, etc. (Hsiung and Hwang, 2009b)

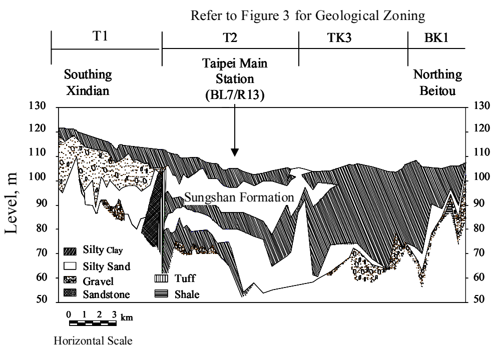

Figure 1. North-south geological section of the Taipei Basin

2. GEOLOGY OF THE TAIPEI BASIN

At the top of the Taipei Basin is the so-called Sungshan Formation of, up to, 60m in thickness underlain by the Chingmei Gravels. Figures 1 and 2 show the north-south and east-west sections, respectively, of the basin. As can be noted, the Sungshan Formation comprises an alternation of silty clay and silty sand sublayers and the six-sublayer sequence is most evident in the central city area where the Taipei Main Station (BL7/R13 Station of the Taipei Metro) is located. Toward the east and the north, the sandy sublayers diminish and clayey sublayers become dominating; and toward the west and the south, the stratigraphy of sublayers becomes rather complicated with silty sand and silty clay seams interbedded in these sublayers. Based on the information obtained in recent years, Lee (1996) proposed to divide the Basin into 22 geological zones as depicted in Figure 3 which is adopted herein for categorizing ground conditions.

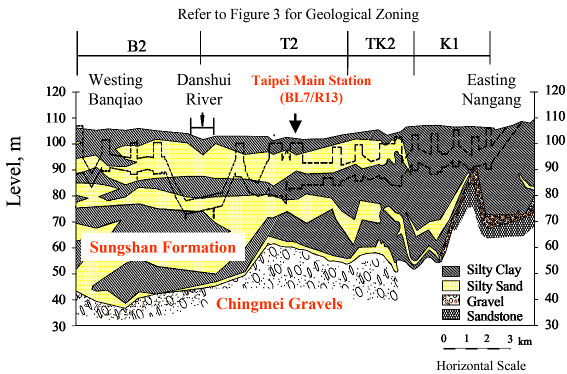

Figure 2. East-west geological section of the Taipei Basin

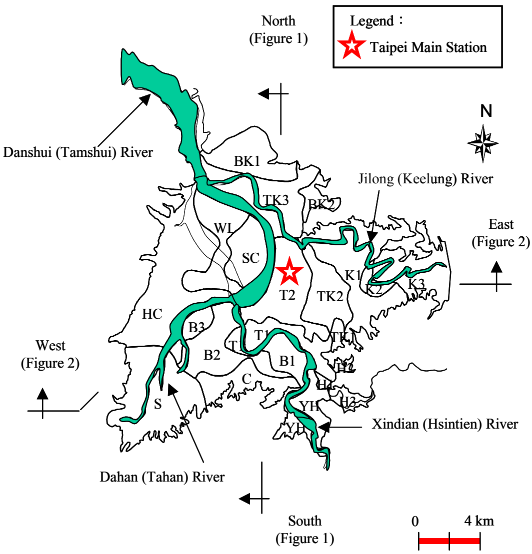

Figure 3. Geological zoning map of the Taipei Basin (Lee.1996)

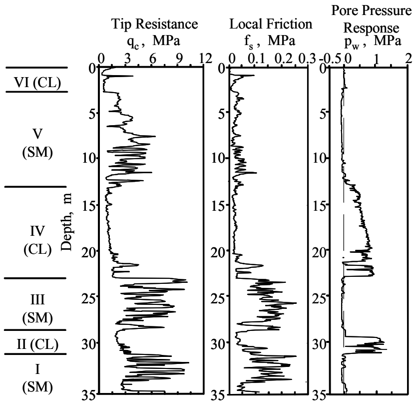

Figure 4. Typical results of CPT tests in the T2 Zone

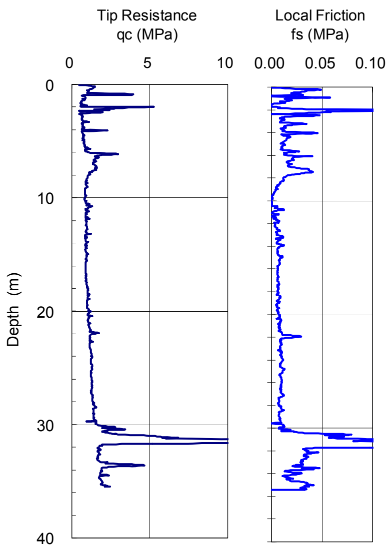

Figure 5. Typical results of CPT tests in the K1 Zone

Figures 4 and 5 show the typical CPT profiles obtained in the T2 and the K1 Zones. As can be noted that the six-sublayer sequence in the Sungshan Formation is clearly identifiable in the T2 Zone. The various soil sublayers can better be identified in the porewater pressure profile than tip resistance or local friction. In short, Sub-layers I, III and V consist primarily of silty sands and Sublayers II, IV and VI consist primarily of silty clays. The sandy sublayers, i.e., Layers I, III and V, thin out toward the east and the north of the basin and become unidentifiable in the K1 Zone as can be noted in Figures 1 and 2.

The Chingmei Gravels contains gravels, cobbles and boulders of various sizes and is extremely permeable. This gravelly layer is practically an underground reservoir and was responsible for several major failures during the first stage construction of TRTS. As can be noted from Figure 6, the piezometric levels in the Chingmei Gravels were lowered by as much as 40m in the 70's as a result of excessive pumping of groundwater for industrial and domestic usages. The sublayers in the Songshan formation have thus experienced consolidation to various degrees and the accompanying ground subsidence exceeded 2m. As pumping has been banned since the late 70's, the piezometric levels in the Chingmei Gravels recovered rapidly. The recovery of the piezometric levels in the Chingmei Gravels, however, has been slowed down as a result of dewatering for constructing the rapid transit systems starting from the early 90's.

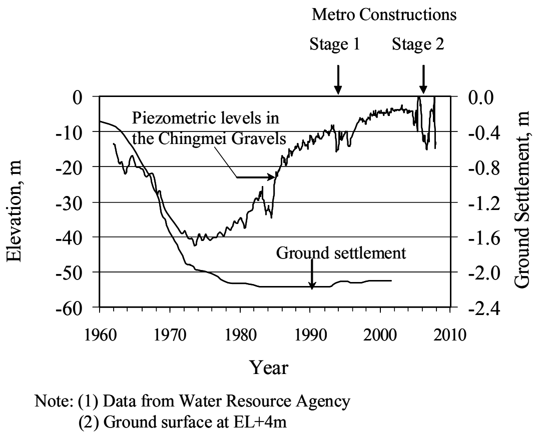

Figure 6. Piezometric levels in the Chingmei Gravels and ground settlements induced by the lowering of water heads in the central city area

In the early 90's, the piezometric levels in the Chingmei formation were below EL-10m, corresponding to a depth of 14m below surface as depicted in Figure 6. Take the soil profile shown in Figure 4 for example, the uplifting pressure acting on the bottom of Sublayer II, which acted as a impervious slab resisting water pressures, would be about 170 kPa and excavations would be able to be carried out, in general, to a depth of 20m in the T2 Zone with a sufficient factor of safety. As excavations for many metro stations and ventilation shafts exceeded this depth, large scale dewatering was necessary for these excavations to be carried out safely.

3. DEEP EXCAVATIONS IN THE TAIPEI BASIN

Numerous deep excavations have been carried out in the Taipei Basin for constructing basements and the metro systems. In addition, excavations have been carried out for constructing various types of infrastructures such as sewage and drainage systems, common ducts, etc., but to much shallower depths.

As shown in Figure 7, excavations for basements became deeper and deeper and have exceed 30m in depth. Since most of these excavations were located in the T2 Zone (i.e., the central city area as depicted in Figure 3), the typical stratigraphy of subsoils at Taipei Main Station is also shown in Figure 7 for comparison. The excavations deeper than 20m were mostly located in the TK2 and the K1 Zones in which the clayey sublayers are rather thick and, therefore, uplift was not a serious problem.

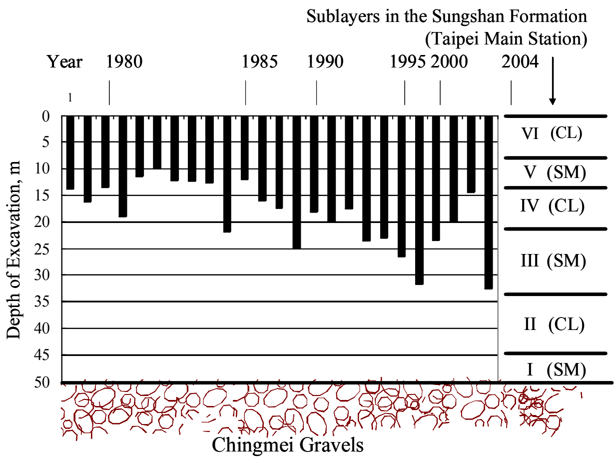

Figure 7. Depths of basement excavations in the Taipei Basin

The excavations for 3-level metro stations usually exceeded 20m in depth and pumping was necessary in later stages of excavations for maintaining sufficient factor of safety. In Stage 1 metro constructions, the excavations for 2 ventilation shafts in the T2 Zone exceeded 34m in depth and that for a ventilation shaft in the B2 Zone exceeded 28m in depth. Pumping was necessary to lower the piezometric levels in the Chingmei Formation by 10m or so and pumping rates ranged from 2800 cm/h to 4200 cm/h. The drawdown were as much as 2m even at a distance of 2km away indicating the extremely large transmissibility of the Chingmei Formation.

Figure 8 shows the deepest excavation carried out in the Taipei Basin. It was carried out to a depth of 40m at the west bank of the Danshui River for constructing a crossover in the Xingzhuang Line in Stage 2 metro construction. The pit was retained by diaphragm walls of 1.5m in thickness and 63m in length. Because of the absence of a clayey layer below the formation level, it was necessary to form a impervious slab at the toe level of the diaphragm walls to seal off seepage and to form a soil core inside the pit to resist water pressures at the bottom. This slab was installed by using high-pressure jet grouting. Even with this grouted slab, pumping was still required to lower the piezometric pressures in the Chingmei Gravels by 13m or so for maintaining a sufficient factor of safety against uplift (Woo, 2006). The entire section of the crossover is 126m long and was partitioned into 5 subsections by diaphragm walls. Excavations were carried out, from the east toward the west section by section. This reduced the maximum pumping rate to 3000 cm/h.

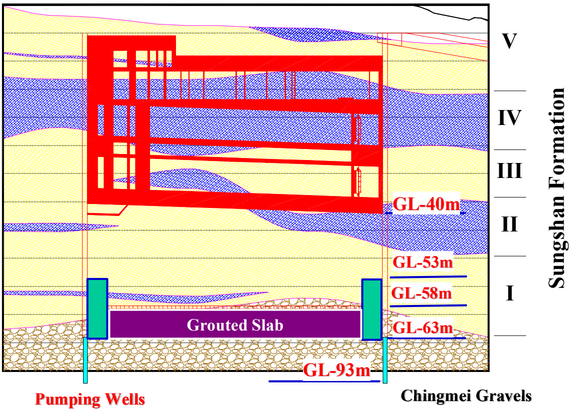

Figure 8. Crossover at the west bank of the Danshui River, Xinzhuang Line

4. PERFORMANCE OF RETAINING SYSTEMS

A large quantity of field data have been collected in recent years and it is therefore possible to conduct systematic analyses on the performance of retaining systems.

4.1 Corrections of inclinometer readings

Figure 9(a) shows the results normally expected from monitoring of wall deflections during deep excavations at sites with thick soft deposits,. Walls behave as cantilever plates in the first stage of excavation (i.e., the 1st dig) and significant movement would normally occur in soft ground before the struts at the first level are installed. During this stage of excavation, the stiffness of the wall contributes very little in reducing wall deflections. Once the struts at the first level are installed and preloaded, walls will behave as plates supported at their upper ends and the stiffness of the walls starts to play a major role in resisting earth pressures. In normal cases, walls will bulge in toward the pits in subsequent stages of excavation while the movements of the walls are mainly induced by the shortening of struts and are expected to be small once struts are preloaded,.

Since the tips of inclinometers are used as reference points and the readings at other depths were obtained accordingly, the results will be erroneous if they do move. It has become more and more frequent, unfortunately, that inclinometers were installed in diaphragm walls and stopped at the toe levels of the walls. Therefore inclinometer readings must be interpreted with great care.

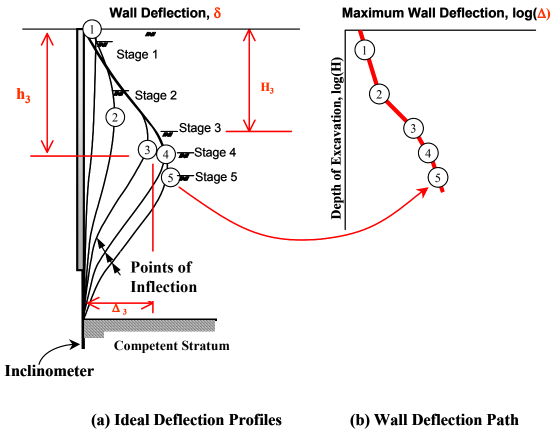

Figure 9. Ideal wall deflection profiles and wall deflection path

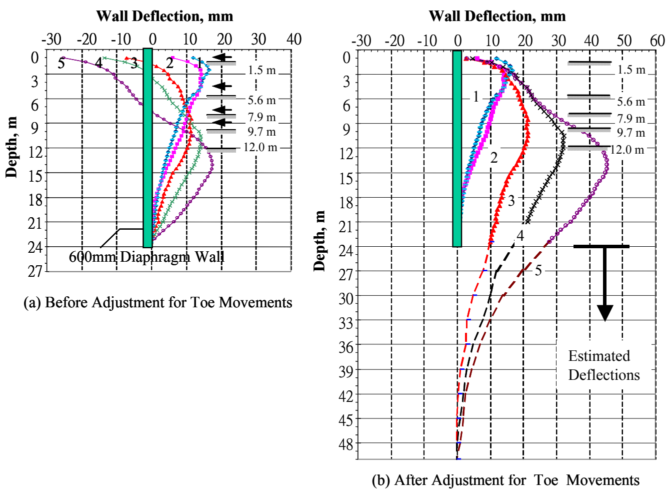

Figure 10. Correction of inclinometer readings for toe movements

Figures 10(a) shows, for example, the readings obtained by an inclinometer in an excavation carried out in the TK2 Zone. The excavation was carried out to a maximum depth of 12m in 5 stages. As can be noted, the top of the walls moved outward by as much as 25mm as indicated by inclinometer readings. At the first strut level of 1m below surface, the walls also moved outward by more than 20mm subsequent to preloading of struts. This certainly is unlikely to be realistic and the unreasonable phenomenon was most likely due to the toe movements of the diaphragm walls. The toe movements can be accounted for by assuming that the wall movements at the first strut level to be insignificant once the struts at this level were preloaded as illustrated in Figure 10(b).

Based on the observations made in several cases, Figure 11 is proposed for estimating the progressive movements of the toes of diaphragm walls in deep excavations in the T2, TK2 and K1 Zones (Hwang, Moh and Wang, 2007; Hsiung and Hwang, 2009a).

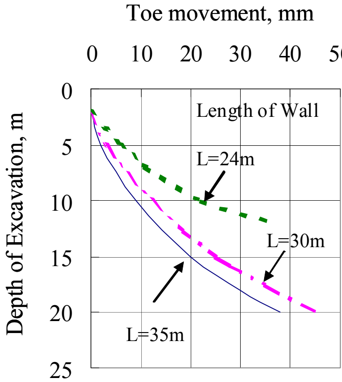

Figure 11. Progressive movements of toes of diaphragm walls for deep excavations in the Taipei Basin

4.2 Wall deflection paths and reference envelopes

As illustrated in Figure 9(b), the maximum deflections in the deflection profiles in each stage are plotted versus depths of excavations in a log-log scale and such a plot is designated as "wall deflection path" (Moh and Hwang, 2005; Hwang, Moh and Kao, 2006: Hwang, Moh and Wang, 2007). The envelope, designated as "reference envelope" herein, of a family of wall deflection paths can be considered as site characteristic curves for diaphragm walls and can be used for evaluating the performance of individual walls. Reference envelopes are defined by:

(a) wall deflections for shallow excavations, represented by deflections at depths of excavation up to 4m, i.e., Δ_4 ,

(b) wall deflections projected to a depth of excavation of 100m, i.e., Δ_{100}.

The depth of 4m is chosen because the first digs are usually within 4m and the depth of 100m is chosen for convenience because Microsoft Excel only plots full log-cycles. Furthermore, the extension of reference envelopes to this depth amplifies the differences in reference envelopes among various cases and makes it easier to study the effects of various factors affecting the performance of walls.

The deflection paths for diaphragm walls with thicknesses of 600mm, 800mm, 1000mm, and 1200mm for excavations in the T2 Zone are shown in Figure 12. Also shown in the figure are the reference envelopes which are the envelopes of respective deflection paths. Individual inclinometers are identified by suffixes such as A, B, C, etc, affixed to the site numbers.

Table 1 Comparison of reference envelopes for the T2, TK2 and K1 Zones

Wall Thickness, mm	Δ_4, mm			Δ_{100}, mm		
	T2	TK2	K1	T2	TK2	K1
600	10	12		1,600	1600	
700		12			1200	
800	10	12	30	800	800	800
900		12	30		600	600
1000	10		30	400		400
1200	10			200		

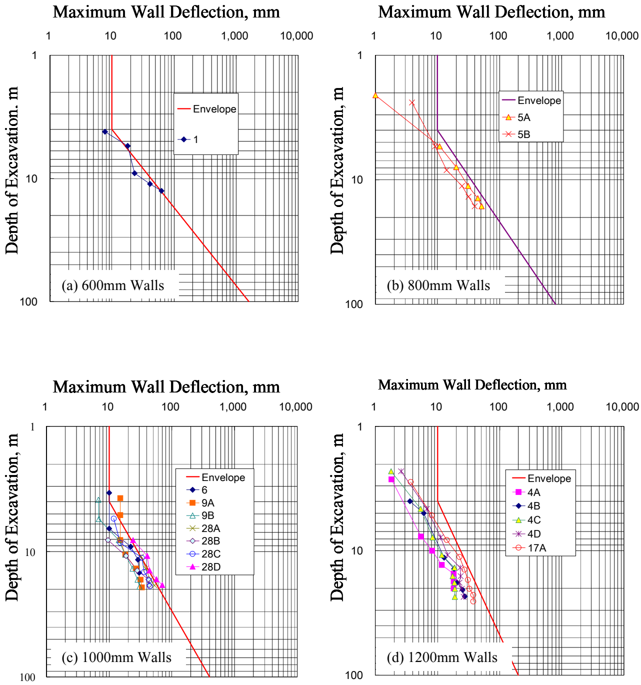

Notes: (1) for excavations using the bottom-up construction method
(2) no ground improvement other than localized treatment for stopping water leakages

Figure 12. Wall deflection paths and reference envelopes for the T2 Zone

There are numerous ways to draw reference envelopes based on the data presented and the decisions are inevitably subjective. The reference envelopes shown in Figure 12 were so drawn that, as shown in Table 1, deflections for depths of excavation of 4m or less, i.e., Δ_4, remain to be the same regardless of wall thickness while wall deflections for depths of excavation of 100m, i.e., $\Delta 100$ decrease by a factor of 2 as wall thickness increases from 600mm to 800mm, from 800mm to 1000mm, and from 1000mm to 1200mm.

Wall deflections for shallow depths of excavations are of little interest so the fact that some of the data points of Inclinometer 9A for excavations up to 5m go beyond the reference envelope for 1000mm walls in Figure 12(c) is of little concern. The fact that the data points for Inclinometer 28D in the range of 10m to 20m going beyond the reference envelope in the same figure is rather a disappointment but is considered to be an acceptable exception.

As illustrated in Figure 13, wall deflection paths are affected by many factors (Hwang, Moh and Kao, 2006). The wall deflection path which is unaffected by these factors is defined as "baseline wall deflection path", or simply, "baseline path" and can be used for evaluating the performance of walls. Wall deflection paths can generally be classified as follows:

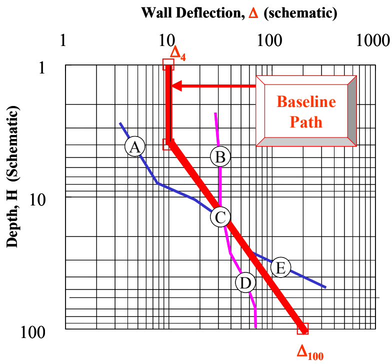

Figure 13. Patterns of wall deflection paths and baseline wall deflection path

Pattern A: The presence of basements, tunnels, retaining walls and foundation piles, etc., in the vicinity is likely to reduce wall deflections in the early stage of excavation. There could also be large culverts or drains which are lighter and more rigid than the soils replaced and tend to reduce ground movements.

Pattern B: On the other hand, surcharge loads, such as embankments, tall buildings and heavy storage tanks, etc., in the vicinity of excavation, if any, will increase wall deflections in the early stage of excavation.

Pattern C: Because the influence of adjacent structures and/or surcharges diminishes as depth of excavation increases, deflection paths tends to converge to a narrow band.

Pattern D: For walls with sufficient lengths beyond the formation levels and/or with their toes properly embedded in competent strata, wall deflections will increase at diminishing rates (in a log-log scale) and their deflection paths are expected to bend downward as excavation getting close to the rigid base.

Pattern E: On the other hand, if data points are plotted above the baseline path, it is most likely that the toe of the wall has become unstable because of insufficient length of the wall.

Since there are very likely to have buried structures, such as basements, tunnels, culverts, etc. in the vicinity of excavations in a densely populated city, wall deflection paths observed are most likely to belong to Pattern A. On the other hand, for properly designed walls with a sufficient stability of toes, the lower portion of wall deflection path will have Pattern D behave. Therefore, the reference envelopes established should be very close to baseline wall deflection paths.

4.3 Validation of the concept by numerical analyses

The concept of wall deflection path is founded on two observations:

(a) maximum wall deflections are insensitive to the stiffness of walls in the first stage of excavation. That means, the Δ_4 values will be about the same for walls with different thicknesses.

(b) the relationship between maximum wall deflection and depth of excavation, if plotted in a log-log scale, is linear in the range of depth of 10m to 20m.

To verify whether these two observations can be generalized, finite element analyses were performed using the computer program PLAXIS V8, released by PLAXIS BV of Amsterdam, the Netherlands (PLAXIS, 2002). The ground conditions and the excavation sequence for the case analyzed are shown in Figure 14 (Hsiung and Hwang, 2009a, 2009b).

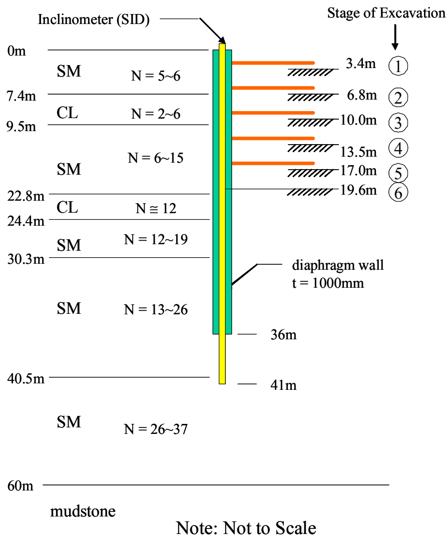

Figure 14. Case analyzed

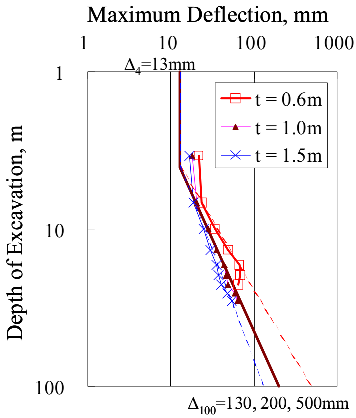

Figure 15. Influences of stiffness of walls on wall deflection paths

Analyses were performed for walls of 0.6m and 1.5m in thickness and the results are compared with those obtained for the case of interest, i.e., wall of 1m in thickness, in Figure 15. Firstly, as can be noted, the three wall deflection paths do intersect at Δ_4 = 13mm, indicating that wall deflections are insensitive to the stiffness of walls in the first stage of excavation. This finding is very useful because once the Δ_4 value is determined for walls of a certain thickness, the same value can be used for establishing the reference envelopes for walls with other sizes. Secondly, the relationship between the maximum wall deflections versus depths of excavation is indeed linear in the range of depths 10m and 20m. Since the analyses were performed for green field, the three wall deflection paths can be considered as the baseline paths for excavations with ground conditions similar to those depicted in Figure 14. The effectiveness of increasing the stiffness of walls in reducing wall deflection is readily apparent in Figure 15. Furthermore, Pattern D behavior can be observed for walls with a thickness of 0.6m.

5. CONCLUDING REMARKS

Inclinometer readings should be interpreted with care. Readings can be calibrated to account for toe movements by assuming wall movements at the first strut level are insignificant once struts at this level are installed and preloaded.

Performance of diaphragm walls can be evaluated by studying their wall deflection paths. Wall deflection paths are linear in the range of 10m to 20m, if plotted in a log scale, for excavations in thick soft sediments. Reference envelopes of a family of wall deflection paths can be defined by Δ_4 and Δ_{100}. The Δ_4 values are insensitive to the stiffness of walls and the Δ_{100} values are a function of the stiffness of walls. Wall deflection paths of individual walls can be compared with reference envelopes for studying the influences of various factors on wall deflections.

REFERENCES

Lee, S.H. (1996) Engineering Geological Zonation for the Taipei City, Sino-Geotechnics, vol. 54, April (in Chinese)

Hsiung, Benson B. C. and Hwang, R. N. (2009a). Correction of inclinometer readings for toe movements, Special Issue on Excavation and Tunneling in Geotechnical Engineering Journal of SEAGS

Hsiung, Benson B. C. and Hwang, R. N. (2009b). Evaluating performance of diaphragm walls by reference envelopes, Special Issue on Excavation and Tunneling in Geotechnical Engineering Journal of SEAGS

Hwang, R. N. and Moh, Z. C. (2007). Deflection paths and reference envelopes for diaphragm walls in the Taipei Basin, J. of GeoEngineering, v2, no. 1, April, Taipei, Taiwan, pp. 1~12

Hwang, R. N. and Moh, Z. C. (2008). Evaluating effectiveness of buttresses and cross walls by reference envelopes, J. of GeoEngineering, v3, no. 1, April, Taipei, Taiwan, pp. 1~11

Hwang, R. N., Moh, Z. C. and Kao, C. C. (2006). Design and construction of deep excavations in Taiwan, Seminar on “The State-of-the-Practice of Geotechnical Engineering in Taiwan and Hong Kong”, 20 January, Hong Kong

Hwang, R. N., Moh, Z. C. and Wang, C. H. (2007). Toe movements of diaphragm walls and correction of inclinometer readings, J. of GeoEngineering, v2, no. 2, August, Taipei, Taiwan pp. 61~72

Moh, Z. C. and Hwang, R. N. (2005). Geotechnical considerations in the design and construction of subways in urban areas, Seminar on Recent Developments on Mitigation of Natural Disasters, Urban Transportation and Construction Industry, 30 November-2 December, Jakarta Indonesia

PLAXIS (2002). Reference Manual, PLAXIS BV, Amsterdam, the Netherlands

Woo, S. M. (2006). Evaluation of the results of dewatering at Crossover, Contract 570C, Xinzhang Line, Taipei Metro

Shoring System Innovations in the Puget Sound Area, Washington

G. M. Denby[1], Ph.D., P.E.

[1] President, GeoEngineers Inc, 8410 154th Ave NE, Redmond, WA 98052; PH(425)861-6048; FAX(425)861-6050; email: gdenby@geoengineers.com

ABSTRACT

Innovations in shoring systems are occurring world-wide as new technologies accelerate our ability to design and construct. The paper highlights four different areas where innovation has been observed in the Puget Sound area: shoring design, shoring system components, construction methodology, and instrumentation and monitoring. These innovations are driven by constraints on the use of ground behind excavations to provide lateral restraint, the demand for deeper basements, and the continued advance of powerful numerical modeling capability. The current trend in shoring system design is clearly towards the more efficient and cost effective performance based design.

The paper also addresses future potential concepts in shoring design which are being driven by public demand for more sustainable solutions based on more effective use of energy and materials.

INTRODUCTION

Constraints on the use of ground behind excavations to provide lateral restraint and the demand for deeper basements, continue to drive innovation in shoring systems and their design. The continued advance of powerful numerical modeling capability and more dependable instrumentation and monitoring, is facilitating acceptance of new shoring concepts outside of the traditional design methodology.

In addition, the iterative cycle of more efficient software packages, supported by back-analysis of more instrumented case histories, is creating increased interest in performance based design. This cycle is yielding more reliability in the selection of the key soil deformational parameters and the modeling techniques for anchor and interface elements. Improved quality in the construction of shoring systems is also increasing our confidence in exploring non-traditional designs.

The paper highlights innovations in the Puget Sound area by reviewing two significant case histories where non-traditional designs were used for the no load zone and earth pressure diagrams. Some benefits of using vertical elements and post tensioning soil nails are presented, followed by observations on the evolution of single stage grouted tie backs and cutter soil mixed walls. The role and acceptance of increased instrumentation and monitoring is briefly discussed, followed by presentation of a few opportunities to respond to the need for more sustainable designs.

Innovation provides our profession with exciting opportunities to test our science, however innovation is hindered by a major obstacle – the inherent professional liability associated with designing outside the "Standard of Practice". Methods to overcome this obstacle are presented, including the Project Risk Analysis to enhance communication between the shoring designer and the shoring contractor.

HISTORIC PERFORMANCE

Shored deep excavations in the over-consolidated clays in the Puget Sound area developed a reputation for poor behavior in the early 1960s when excavation for the Interstate 5 highway through downtown Seattle resulted in large movements extending upslope for a distance up to 5 times the height of the excavation. In a report on the instability issues, Ralph Peck (1963) stated "The most suitable design would be one that permits the least possible relaxation of stresses within the soil mass". The solution for the highway construction was to control relaxation of the high lateral stresses with deep cylinder pile walls. Since then, typical apparent earth pressures for the over-consolidated clay soils have evolved to 20 to 25(rectangular or trapezoidal) times the height of the excavation in pounds per square foot, which has been found to successfully address the high lateral stresses and limit shoring wall displacement to tolerable limits on most excavations. A 25 mm (1 inch) wall movement criterion has been generally adopted by local city jurisdictions in the Puget Sound area for the issuance of excavation permits.

Numerical modeling was introduced to tieback shored excavations in the Seattle clay for the Bank of California Center project in 1971, (Clough et al 1971). Back-analysis of other instrumented tieback walls in Seattle, along with other published data, allowed a credible soil modulus value to be assigned to the Seattle clay. Inclinometer data obtained at intermediate steps during the excavation allowed comparison of actual and numerically predicted displacements during the successful construction of the 19.6 m (64 foot) high tied back wall. This project is considered to be the first use of real time feedback of shoring system performance. This approach, complemented by the more user friendly and visual computer program output from programs such as PLAXIS or FLAC, has increased geotechnical engineers' confidence in exploring new concepts in the design and construction of non-traditional shoring systems.

GEOLOGIC SETTING IN THE PUGET SOUND

Interpretation of the performance of soil/structure interaction systems will always include a vital geologic setting component; therefore, in describing the performance of innovative techniques it is appropriate to understand the geologic setting and appreciate its impact on shoring system performance.

The last glacial stage in Puget Sound occurred approximately 14,000 years ago and covered the area with up to 3000 feet of ice. In the upland areas where shored excavations are generally located, the glacial processes resulted in the deposition of complex sequences of recessional outwash, glacial till, advance outwash, and over-consolidated silts and clays. The urban environment typically also includes a surficial fill layer of varying depth.

Over-consolidation ratios for the glacially consolidated silt and clays typically are estimated to range up to 8 and the coefficient of horizontal earth pressure at rest (k_o) typically ranges up to 2.5. Slickensides are found inconsistently in the silt and clay and can adversely impact the performance of shored systems in the Puget Sound area.

SHORING DESIGN

The Olive 8 Project, Seattle. The project required a 23.2m (76 foot) deep excavation in downtown Seattle. A 4.9m (16 foot) wide alley with critical utilities exists between the west property line of the site and the 15.3m (50 foot) deep basement of an adjacent 33 story building (Winter et al, 2009). A hybrid shoring system was proposed using soldier piles, soil nails, and tie backs. See Figure 1.

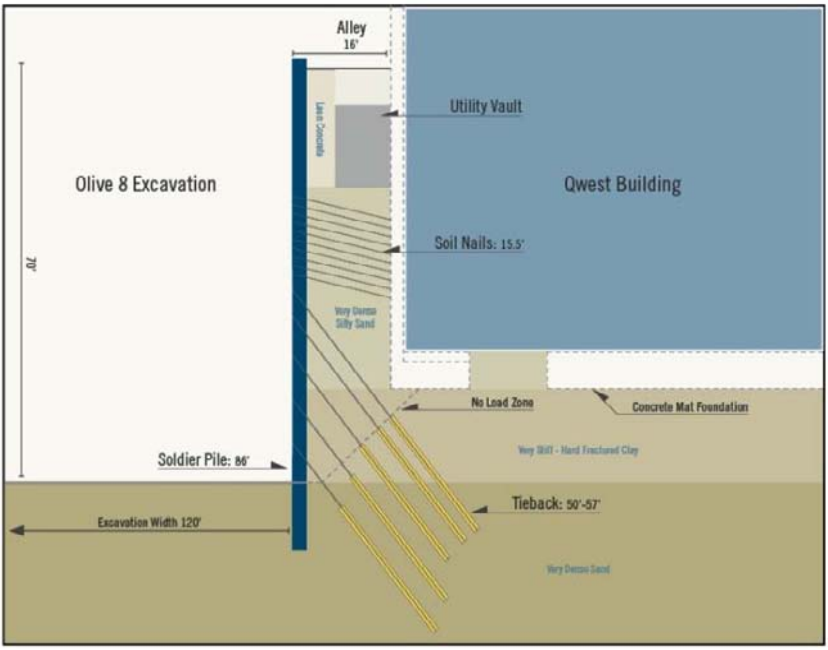

Figure 1 Cross Section Showing Hybrid Shoring Wall.

The system was designed using the software program PLAXIS. Sensitivity studies were used extensively to validate the analyses. The model simulated the following:

1) The change in the initial in situ stress state due to the construction (tied back wall) of the adjacent basement wall.
2) The placement of additional soil nails, 0.91m (3 feet) on center both ways, to stiffen the upper 15.3m (50 feet) of the soil mass
3) The reduced lateral restraint of the soil nails as the depth of excavation increased
4) The shear resistance at the soil/basement wall and soil/soldier pile interfaces.

5) The soil structure interaction of the shoring system and the prediction of the final wall displacement, required to be less than 25mm (1 inch) by the City of Seattle.

The wall was monitored by 3 inclinometers, tieback load cells, strain gages installed on soil nails, conventional optical survey techniques, and an automated optical survey system. The City of Seattle required a contingency plan to be in place in the event of excessive deflections. A photograph of the shoring system nearing completion is shown in the Figure 2.

Figure 2 Almost Completed Olive 8 Wall**.**

Final wall movement was 13mm (0.5 inch) with reasonable agreement between the predicted and actual wall shapes. This equates to 0.05H % where H is the height of the excavation. Typical wall movement would be expected to be in the range of 0.1 to 0.2H % (Clough and O'Rourke, 1990). Without the numerical modeling validation, it is very unlikely this system would have been able to be designed, constructed or permitted. The hybrid design saved the owner more than one million dollars in addition to decreasing the construction schedule by several months.

8th Ave and Virginia, Seattle.

The 8th and Virginia site is located at the north end of downtown Seattle, in the south Lake Union area where significant grading activities have occurred (Stauffer S.D. et al, 2010). The excavation for the project is 36.7m (120 feet) by 73.4m (240 feet) in plan and the depth of the north end of the east wall was 22.3m (73 feet). On the east side of the site a high rise condominium tower is located across a 4.9m (16 foot) wide alley. The condominium tower has a basement and is supported on deep foundations consisting of both piles and drilled shafts.

The fill thickness varies from 8.6m (28 feet) to 9.8m (32 feet) and consists of very loose to medium dense silty sand. Below the fill are glacially consolidated soils consisting of glacial drift and glacial till. The glacial till and the groundwater table were encountered near the base of the excavation at a depth of 19.0m (62feet) to 21.4m (70 feet.)

The innovative solution consisted of constructing two parallel soldier pile walls, with the outer wall on the property line and the inner wall 10.7m (35 feet) inside the property line, and then staging the excavation such that the outer wall was laterally supported by the completed building core.

The steps in the excavation were as follows:

1) The outer soldier piles were installed and the soil was excavated to a depth of approximately 8.6m (28 feet) leaving a berm in front of the outer wall.
2) The inner soldier piles, the rakers from the top of the inner wall to the outer wall and a reaction tieback were installed at the top of the inner wall.
3) The excavation proceeded to full depth installing tiebacks from the inner wall to the adjacent property line and removing the berm as shown in Figure 3.

Figure 3 Inner and Outer Walls with Raker Support

4) The building core was constructed to the top of the inner wall.
5) The excavation between the two walls was taken down in lifts with each lift being cross braced using the support struts. See Figure 4.
6) The floor slabs were constructed between the inner and outer walls from the bottom up removing the struts on the way out.

Displacements were consistent with the excavation steps – during step 1 the top of the outer wall moved outward 6 mm (0.25 inch); during step 2 the outer wall returned to close to its original position with a small bulge into the excavation near the bottom of the excavation; during step 3 the top of the outer wall moved

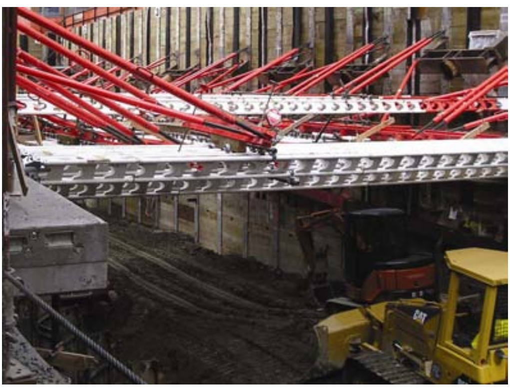

Figure 4 Struts between Inner and Outer Walls

inward 3mm (0.1inch) and the bulge increased to 3mm (0.1 inch). During step 3 the top of the inner wall moved into the excavation 12mm (0.5 inch). The final movement of the outer wall corresponded to a cantilever and was 22mm (0.84 inch), equivalent to 0.1H %.

Modified Non-traditional No Load Zone and Earth Pressure Diagrams

Both the Olive 8 and the 8th and Virginia shoring systems were designed using modified non-traditional no load zones and earth pressure diagrams. A typical no load zone, and truncated and modified no load zones are shown in Figures 5 a), b), and c).

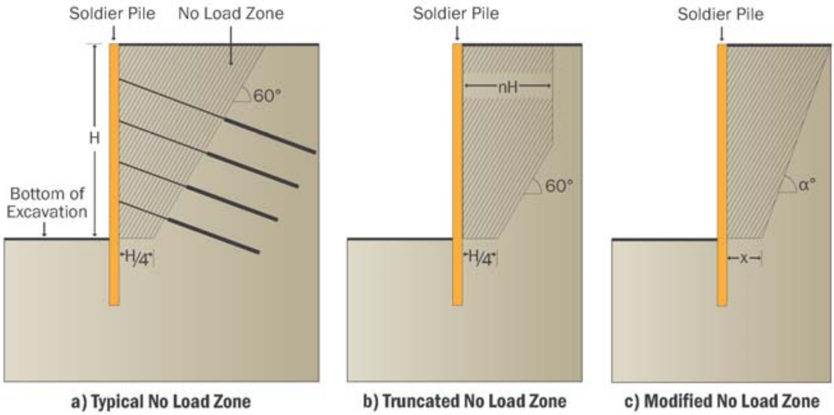

Figure 5 Modified No Load Zones

Modified no load zones may include a reduced horizontal setback and a steeper back plane angle as shown by x and α respectively in Figure 5 c). In order to use a reduced zone the analysis needs to include numerical modeling to evaluate wall displacements and system stability for each step of the excavation; system stability consists of anchor pull out and pile hinge development. The final step must also evaluate global stability of a failure surface extending below the base of the soldier pile.

The numerical analysis also needs to model the reduction in load capacity of the anchors as the excavation gets deeper and the critical failure surface moves into the bond zone. This can be modeled iteratively for each excavation step by reducing the capacity of the anchors, while maintaining constant stiffness, to reflect the effective bond zone behind the failure surface. The net effect of the reduction in capacity of the upper anchors is that the lower anchors need to be designed for higher earth pressures and a larger section soldier pile may be required. The iterative procedure may be expedited by completing the initial anchor design using a more triangular earth pressure diagram, especially for deep excavations.

It may be noted that both for traditional and non traditional no load zones, increasing the design earth pressures above traditional apparent earth pressures has the potential to reduce wall movements to less than the reported 0.1H % to 0.2H % values. In addition to basic construction method proficiency, the final wall movement will depend on the initial in situ stress state and the amount of relaxation that occurs between anchor row installations.

SHORING SYSTEM COMPONENTS

Vertical Elements. Most of the reported unanticipated movements of soil nail walls occur in the upper one or two lifts due to inadequate stand up time of fill or loose surficial soil. Vertical elements have been used very successfully with soil nail walls to solve this problem. Vertical elements consist of 150mm (6inch) to 450mm (18 inch) diameter controlled density fill or grout filled holes including small wide flange beams, pipe sections or threadbar/rebar. They are typically spaced at ½ to 1 times the horizontal soil nail spacing and extend into competent soils or below the base of the planned excavation. A typical soil nail wall with vertical elements is shown in Figure 6.

Figure 6 Vertical Elements for Face Support.

In addition to addressing the stand- up time issue, vertical elements have been used to provide lateral support for soil adjacent to utilities and vaults located behind the top of the wall, to underpin adjacent footings, and with wood lagging to provide lateral support in the presence of water. Vertical elements have been used extensively and very successfully in the Puget Sound area.

Special care needs to be taken in the design at the depth where the soil nail wall continues below the bottom of the vertical elements. In one such case there was a sudden movement of the wall as the excavation proceeded below the bottom of the vertical elements. This was considered to be caused by the removal of bearing support for the vertical elements.

Post Tensioning Soil Nails. Installing a soil nail shoring system adjacent to a building may result in unacceptable movements to activate the soil nails. It is not cost effective to use a second active shoring system to control displacements. In the case of stiff native foundation soils, soil nail systems without post tensioning have been successfully installed below adjacent buildings. In the case of fill or loose native foundation soils, post tensioning the nails has been used successfully below adjacent buildings on several projects. The post tensioning includes constructing the soil nail as a tieback using a polyvinyl chloride (PVC) sheath and post tensioning the nail to 100% of the design load.

CONSTRUCTION METHODOLOGY

Single Stage (SS) Grouting. The original concept of the tied back wall consisted of placing anchors behind a no load zone such that load transferred from the anchors to the soil did not occur in the failure wedge. Early anchor design specified structural grout in the bond zone and a less stiff material, such as a sand slurry, in the unbonded zone to prevent the anchor from developing capacity within the failure wedge. However, contractors in the Puget Sound region have long argued that acceptable performance can be achieved with anchors that are sheathed in the no load zone with structural grout placed the entire anchor length (for anchors with diameters of 8-inches or less).

SS grouting has been used extensively in the Puget Sound region over the last decade with acceptable performance. The stiffness contrast of the bond zone with the unbonded zone, straightening of the tieback tendons during proof-testing resulting in fracturing of the grout in the unbonded zone, and the small amount of movement, less than 6mm (0.25 inches), required at the anchor perimeter in the bond zone to transfer load to the adjacent soil, are factors that are considered to contribute to the successful performance of SS grouted anchors.

SS grouting is now used routinely in the Puget Sound area and proof testing of SS anchors shows consistent performance; however, a non-structural grout is typically still specified in the no load zone for the verification tests. Further, there is a reduced risk of loss of ground/caving with SS grouting. Where secondary grouting is implemented, SS grouting will typically result in higher anchor capacities due to the ability to apply higher secondary grouting pressures. Additional significant benefits associated with SS grouting are reduced construction costs and a shorter construction schedule.

Cutter Soil Mixed (CSM) Walls. Two CSM walls have been constructed successfully in Seattle to provide a water resistant shoring wall. CSM walls are similar in concept to the soil-cement auger-mixed walls developed by the Japanese in the 1980s. The walls are constructed using the cutter head technology from diaphragm walls and consist of soil mixed with cement slurry in situ. A single Kelly bar supports two cutter wheels which are pushed into the ground cutting

Figure 7 CSM Cutter Wheels

up the soil as bentonite slurry or cement slurry is injected. See Figure 7. Cement slurry is injected as the cutter head is retracted in a series of steps creating a rectangular panel. Steel reinforcing is inserted in the wall panel, which is typically 2.4m (8 feet) long by 0.76m (2.5 feet) to 0.92m (3 feet wide.) Panels are constructed alternately, similar to slurry trench walls.

The CSM methodology's greatest advantage is its sophisticated control system, which indicates the location of the cutter head relative to the footprint of the wall. The operator changes the direction of rotation of the cutters and moves the crane boom to adjust the location of the cutter head. The cutter head tracking system provides significantly increased confidence in the integrity of the wall in seepage cutoff applications.

At a Seattle waterfront site (Kvinsland and Plum, 2010) the CSM wall was selected over a secant pile wall based on reducing the construction schedule by 2 months and the construction cost by a million dollars. The CSM wall was able to overcome the challenges of encountering major obstructions, such as old timber piles, the impact of minor contamination on the soilcrete strength and leakage at the panel joints. The achievable 28 day soilcrete strength at this site was in the range of 690 to 2,000 KPa (100 to 300psi). Overall permeability of the soilcrete was less than 10^{-6} cm/sec. See Figure 8. With a single row of tiebacks, wall displacements were limited to 50 mm (2 inches.)

Figure 8 Finished CSM Wall

The CSM wall essentially performed as a concrete slurry wall, successfully providing both an effective seepage cut off and a temporary shoring wall.

Instrumentation/Monitoring

The use of numerical analysis allows the actual and predicted displacements to be compared at each step in the excavation. This provides an early warning system, which in the event of divergence of the actual with the predicted displacements, provides an opportunity to reconcile the design parameters with predicted performance and/or evaluate the construction methodology. The comparison must be based on reliable and comprehensive instrumentation data that accurately portrays performance.

Deviation from traditional shoring designs and the associated cost savings is accelerating the use of instrumentation in the Puget Sound area. Where non-traditional shoring designs are required, the use of inclinometers has been justified to owners on a value engineered basis and has provided reliable and valuable deformation data.

A total survey station, which provided 24/7 remote monitoring of inclinometer and survey instrumentation was installed at the Olive 8 project and performed acceptably well. (Finno, 2007). Total survey stations are justified at more performance-critical sites and can potentially save on the surveying cost while providing high quality data.

SUSTAINABILITY

With the latest innovations in shoring design, shoring system components, construction methodology and instrumentation and monitoring, there are significant opportunities for more cost effective use of materials and sustainable shoring designs. More credible numerical methods are facilitating the development and use of conventional and hybrid systems which support non-traditional no load zone and earth pressure diagrams for shoring walls. Comparison of predicted with actual performance by more prevalent instrumentation and monitoring, mitigates risk during construction.

There are also fundamental opportunities where we can make gains in designing more cost effective and sustainable structures. One of these opportunities is reducing the permanent earth pressures for the design of multi level basement walls. In the design of the lagging spanning between soldier piles, we observe a significant decrease in the earth pressure on the lagging due to the arching of the soil between the soldier piles and the flexure of the lagging boards in the horizontal plane. This concept may be applied to basement wall design where similar arching of the soil occurs between the floor slabs that act as supports in the vertical plane. By incorporating an arching factor in the design of the basement walls and accounting for creep effects, the maximum wall bending moments and the corresponding wall thickness should be able to be reduced.

Basement wall performance appears to be satisfactory based on the lack of reported failures in the literature, even after earthquake loading of walls not designed for seismic loading. The lack of reported failures/cracking suggests that there is an opportunity for more efficient design of permanent below grade basement walls.

In another opportunity for more sustainable shoring and basement wall design involving seismic loading of basement walls, Chin K. et al (2010) draw our attention to the benefits of permanent soil nails in resisting earthquake loading. The numerical modeling results indicate a significant reduction in earth pressures and maximum bending moments when the permanent nails are incorporated into the basement wall design.

The standard of practice in the Puget Sound area is to de-stress all tiebacks in the public right of way. However, an initial experiment to observe the effects of a tensioned tieback being severed by construction equipment was remarkably uneventful. The experiment involved severing two single stage grouted tiebacks (Smith et. al, 2010). By modifying public policy regarding the de-stressing of temporary tiebacks, significant cost savings and also improvement in the reliability of below grade waterproofing, may be realized.

Other opportunities to reduce the cost of shoring materials and hydro carbon emissions during construction include the use of plastic anchorage elements and spiral or helical nails. Spiral nails consist of a two inch ribbed steel box section that is twisted along its full length. The nail is driven into the soil and pullout resistance is mobilized in friction along the outer perimeter as well as bearing along the ribs. The ability to load the nails immediately after installation, instead of waiting for grout to set up, should have a significant positive impact on schedule. It is also possible to remove and reuse the nails as load is transferred from the nails to the structure.

RISK MITIGATION

Professional negligence is alleged when an adverse event occurs with a breach of the local "Standard of Practice". Innovation therefore includes an intrinsically higher risk of litigation by clients and third parties. The standard means of managing this risk is to incorporate increased exploration and analysis, to provide clear definition of the risk to the client, and to have the client formally accept the increased risk, preferably in writing.

Peck (1969) paved the way for innovation in geotechnical engineering by formalizing the "Observational Method", which is based on comprehensive instrumentation and monitoring, and a contingency plan in the event of misapplied science. This method was used on the Olive 8 project with mitigation measures incorporated into the shoring design in the event of excessive displacements.

A risk management program was used for the Olive 8 project consisting of a design engineer-generated identification of construction risks, the Project Risk Analysis. The purpose was to communicate to the contractor the risks that could impact shoring system performance. Some of the risks were readily apparent, such as over-excavation before installing a nail or anchor row; others were more subtle and included preventing rainfall infiltration behind the alley wall. The project risk analysis is common in Europe and is considered to have played an important role in the success of the Olive 8 project. Project risk analyses provide important risk mitigation when implementing new innovations in shoring systems.

SUMMARY

Shoring system design in the Puget Sound area continues to be challenged by the need for deeper excavations, spatial constraints associated with urban redevelopment and difficult soil conditions; this is driving innovation. A summary of observations related to these and future potential innovations is as follows:

1) Non-traditional no load zones and earth pressure diagrams are being developed to solve limited right of way and obstacle problems.

2) Reduction of the no load zone in combination with the use of higher design earth pressures is capable of yielding less wall movement than observed in traditional design.

3) The use of non traditional no load zones and earth pressure diagrams is more analytically challenging and requires checking wall movement and system stability for each excavation step, and global equilibrium at full depth.

4) The cost savings from innovative designs is justifying additional instrumentation and monitoring, which is supporting further innovation.

5) The use of vertical elements solves the challenge of inadequate stand up time and conditions where lateral support can not be provided by soil nails.

6) There is increased proficiency and consistency in soil nail and tied back shoring system construction which is allowing the inherent construction safety factor to be reduced.

7) New construction methods such as the cutter soil mixing method are providing cost effective shoring system alternatives where groundwater is an issue.

8) Demand for more sustainable designs is and will be driving further innovation.

9) Project risk analyses are an important part of mitigating risk and liability for implementation of innovative designs.

Permitting and regulatory agencies also play a role in facilitating more innovative and sustainable solutions. Application of the sound principals of the Observational Method, based on predicted and observed wall movements and an appropriate contingency plan, should mitigate the risk of damage to adjacent improvements and should allow the agencies to continue to accept innovation and more sustainable solutions in shoring system design.

ACKNOWLEDGEMENTS

The author would like to acknowledge the contributions and advice of John Byrne with Ground Support, John Kvinsland with Malcolm Drilling, and my co-authors King Chin, Matt Smith and Shaun Stauffer for their innovations and review comments.

REFERENCES

Chin K. et al, (2010), "Design of Permanent Soil Nail Walls using Numerical Modeling Techniques," ASCE Earth Retention Conference, Seattle, August.

Clough, G.W. Weber, P.R. and Lamont, J.L. Jr., (1972), "Design and Observation of a Tied-Back Wall," Proceedings of the ASCE Specialty Conference on Performance of Earth and Earth Supported Structures, Purdue University, June 11-14, ASCE, New York, pp.1367–1389.

Clough, G.W. and O'Rourke, (1990), "Construction Induced Movements of Insitu Walls", Geotechnical Special Publication No.25 on Design and Performance of Earth Retaining Structures, P.C. Lambe and L.A.Hansen, eds, ASCE, New York, p439-470.

Finno, R. J. et al, (2007), "Real Time Monitoring at the Olive 8 Excavation," Seventh International Symposium on Field Measurements in GeoMechanics.

Kvinsland J. and Plum R., (2010), "Cutter Soil Mixed Wall Shoring and Seepage Cut-off, Office Building near Waterfront," ASCE Earth Retention Conference, Seattle, August.

Peck, R. B. (1963), "Evaluation of Stability Problems, Seattle Freeway, South of Olive Way", Report dated July 8.

Peck, R. B. (1969), Advantages and Limitations of the Observational Method in Applied Soil Mechanics, Geotechnique 19.

Smith, M.W. et al, (2010), "Case History Investigating the Risks Associated with Allowing Temporary Tieback Anchors to Remain Stressed within Public Rights-of-Way," ASCE Earth Retention Conference, Seattle, August.

Stauffer, S. D. et al, (2010), "Design and Construction of an Innovative Shoring System at a Challenging Urban Site in Seattle, Washington," ASCE Earth Retention Conference, Seattle, August.

Winter, D. G., et al, (2009)," Creative Shoring Solutions for a Tight Urban Site: Olive 8, Seattle", Proceedings of the 34th Annual Conference on Deep Foundations, October.

Displacement-Based Design for Deep Excavations

W. Allen Marr[1] and Martin Hawkes[2]

[1]Geocomp Corporation, 1145 Massachusetts Avenue, Boxborough, MA 01719; PH (978) 635-0012; FAX (978) 635-0266; wam@geocomp.com
[2] Geocomp Corporation, 1145 Massachusetts Avenue, Boxborough, MA 01719; PH (978) 635-0012; FAX (978) 635-0266; mh@geocomp.com

ABSTRACT. Many structures located close to excavations are damaged by excessive ground movements during construction. This is partly due to limitations of commonly used methods to design the excavation support system. The authors propose using a displacement-based design method that focuses on designing to keep movements within allowable values. A step-by-step approach for the method is described and illustrated for a deep excavation into soft clay.

INTRODUCTION

Limiting movements that result from constructing deep excavations is becoming a significant design issue, especially in urban environments. Failure to control deformations can cause significant damage to adjacent structures and utilities. Consequences such as the following can become very costly:

- Collapse of Excavation Support System (ESS) with major damage and delays.
- Loss of bearing capacity of shallow foundations for an adjacent building.
- Cracking of adjacent buildings that cost time and money to resolve.
- Loss of factor of safety for basal heave, global instability, or bearing capacity such that work must be stopped until remedial measures are implemented.
- Shut down of the project and withdrawal of permits by government officials until a resolution can be found.
- Abandonment of the project, leaving an open hole in the ground.
- Poor relations with neighbors, which take management time.
- Lawyers and litigation.

Design is becoming more challenging due to increasing requirements for deeper excavations on poorer sites, tighter limits on allowable displacements for adjacent structures, and new methods of construction that extend beyond the experience base used to develop historical design methods. Increasingly, designs are controlled by the need to limit movements, which goes beyond the traditional approach of focusing on required support loads and avoiding collapse. These conditions require a new approach to design of excavation support systems, one that focuses on controlling displacements.

Designing to limit movements places the design emphasis exactly where it should be: How much movement is allowable? What is the optimal design to keep movements within the allowable values? What mitigation steps are possible if the allowable movements are exceeded?

Construction of a deep excavation involves unloading of the soil. For unloading, the movements of soil are small until the factor of safety for any soil failure mechanism drops below 1.1 to 1.2. Then the movements increase rapidly and the factor of safety decreases quickly. This condition can worsen rapidly as the excavation becomes deeper, a fact that catches many people by surprise and leaves little time to take preventive actions.

Designing to control movements became possible with the development of non-linear finite element analysis (FEA) in the early 1970's. However, it was not a practical design tool in its early versions. In recent years, finite element software has greatly improved. There are more realistic stress-strain models, more stable numerical methods, tools to ease the creation of the geometric model, and especially tools to provide powerful and useful graphical output for quick interpretation and presentation of results. Some products also compute a factor of safety against soil failure at any stage of the excavation. When done correctly, this method automatically gives the most critical failure mode for each level of excavation, whether it is global instability, basal heave or localized bearing capacity. FEA calculates displacements of all types at all locations, making a displacement-based design approach now possible. The ease-of-use of these programs allows quick parametric studies to examine sensitivity of the design to changes in key parameters and feasibility of various options to optimize the design. Additionally, the pool of engineers capable of using these programs has greatly increased. A large portion of graduating geotechnical engineers enters practice with FEA skills.

CAUSES OF DISPLACEMENTS

Figure 1 shows the various failure modes for a braced excavation. Similar failure modes occur for most types of lateral supports including struts, rakers, tiebacks and soil nails. To limit large movements from any of these failure mechanisms, it is necessary to provide an adequate factor of safety for each.

Excessive movements can occur without a failure mechanism occurring. Prefailure movements can result from:

- Elastic displacements of soil and support system.
- Plastic displacements of soil without stability failure.
- Strains in the structural support system due to lower stiffness or strength, load redistribution, or temperature changes.
- Slippage and give at the structural connections.
- Consolidation of some or all of the soil.
- Local loss of ground due to flow into the excavation.
- Installation of components behind the wall (tiebacks, soil nails, grouting for water control) that result in loss of soil from behind the supporting wall.

The first five in this list can be evaluated with geotechnical FEA programs. The last two cannot with any reliability. The best approach to preventing movements from water flow and ground losses is to adopt construction practices that keep these mechanisms from occurring. Once these mechanisms begin they are unpredictable and difficult to control.

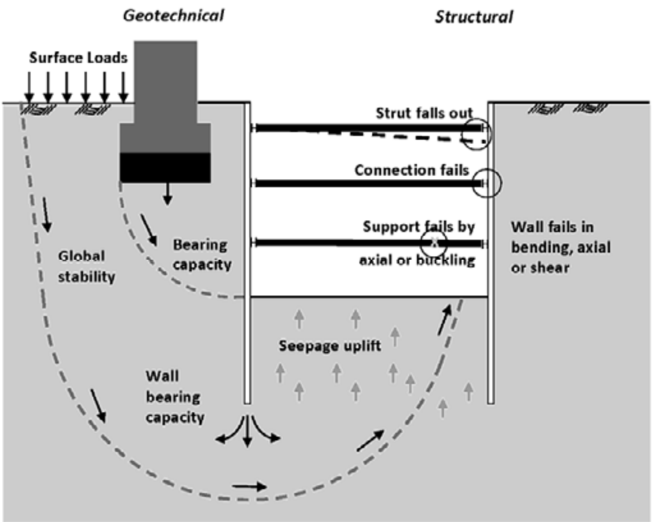

Figure 1: Failure modes for excavation support systems

A common practice in the US is for the designer of the excavation support system, usually a structural engineer, to ask a geotechnical engineer for design earth pressures. The geotechnical engineer will use the geotechnical data he has to develop a design earth pressure diagram. The earth pressure diagram is often based on forces computed from Rankine active and passive earth pressures or from an "equivalent fluid" pressure diagram based on local practice. The method based on Rankine earth pressures assumes the earth deforms to a failure state. This cannot happen if movements are to be limited. The equivalent fluid pressure method gives no indication of what movements might occur. Others may use the Terzaghi et al (1996) apparent earth pressure diagrams (hereafter referred to as the TPM method) which are considered to give an upper bound to the forces for design of the lateral support system. However, no guidance was given on using these diagrams when movement is to be controlled.

PAST APPROACHES TO PREDICTING DISPLACEMENTS

Using a displacement-based design approach requires a way to predict displacements for trial designs. For many years predicting displacements was empirical. Guidelines such as these were used:

- Ignore displacements in the design, and then modify construction if necessary.
- Use local experience from measurements on previous projects of similar type.
- Use rules of thumb such as "maximum lateral displacement may be up to 0.005 times the depth of the excavation, H."

- Limit displacements to elastic values by keeping the base stability number, $N_b = (\gamma_t H + q_s)/s_{ub}$ less than 4. γ_t is average total unit weight above bottom of excavation, q_s is the surface load and s_{ub} is the average undrained strength below the bottom of the excavation.
- Make estimates based on prior experience of summarized performance. For example, from NAVFAC DM-7 (1982):
  - Walls in sands and silts might displace laterally up to 0.002H.
  - Walls in stiff clays might displace laterally up to 0.005H.
  - Walls into soft clays might displace laterally up to 0.02H.
  - Walls into very soft clays might displace laterally more than 0.02H
  - Pre-loading the lateral supports can reduce these values by up to half.
  - Poor construction methods can increase these values significantly.
- Maximum settlement of outside ground about ½ to 1 times the maximum horizontal displacement of wall. However, if significant soil volume reduction might result from nearby vibrations of loose sands or consolidation of soft clays, a separate evaluation is required.

A major step forward occurred with Dr. Peck's state-of-the art paper at the 7th ICSMFE in Mexico (Peck, 1969). He compiled data from instrumented excavations located around the world and created charts showing settlement divided by depth of excavation versus distance from the supporting wall. He did the same for maximum horizontal displacement. He divided the data into three sets, varying from sand and hard clay to very soft clay. He differentiated the different sets using soil types and the base stability number. His work gave a rational basis to estimate the maximum lateral wall displacements and settlement behind the wall for different soil types. His results provided recommended envelopes of maximum displacement. Consequently, it generally should over predict movements where design and construction are managed to limit movements. Additionally, many of the construction methods used today, particularly stiffer walls and struts with preloading, wall embedment, pre-stressed tiebacks and soil nails, were not a part of his database. His work is still a valuable set of reference cases to evaluate the reasonableness of newer methods.

With the advent of computers in civil engineering in the middle 1960's, a numerical solution using the theory of "beam on elastic foundation" was developed to compute the stresses, moments and displacements of a wall." This approach became widely used particularly by structural engineers. Soil behavior was bundled into a set of springs that represented soil as an elastic material. It was never clear how to determine the values of spring constants to represent realistic soil behavior. The method typically uses Rankine active and passive earth pressure coefficients; however, excavation support systems designed to limit movements don't develop Rankine earth pressure conditions. Due to the nature of the method, the factor of safety of the excavation against global instability may be overlooked, resulting in severe consequences. This method is increasingly discredited as an applicable design tool (Poulos, 2000).

In the early 1970's, finite element programs became available that could model the non-linear stress-strain behavior of soils to include elastic and plastic components. One of the early applications of these new methods was to predict displacements for deep excavations (Clough et al, 1972 and Jaworski, 1973). After a few rounds of improvements, FEA was used to develop parametric charts that predict the maximum displacements resulting from an excavation. Principal among these were papers by Clough and his many co-authors. These culminated in the Clough et al (1989) paper with additional considerations by Clough and O'Rourke (1990). The key figure from Clough et al (1989) is reproduced in Figure 2. The figure includes some added data symbols that will be discussed later. This figure was especially significant because it showed the important relationships among factor of safety, system stiffness, and depth of excavation as the determinants of maximum displacement. The paper referenced other papers that provide approximate ways to account for other significant factors such as preloads, vertical strut spacing, lateral support stiffness, support preload, anisotropy in soil shear strength, variable soil conditions, water pressure, and construction influences. This chart uses Terzaghi's (1943) factor of safety against basal heave defined as $FOS_{BH} = \frac{1}{H} \cdot \frac{N_c s_{ub}}{\gamma_t - f \cdot s_{uu}}$ where Terzaghi's N_c value is typically replaced by Skempton's (1951) N_c (see Figure 3). s_{uu} is the average shear strength above the bottom of the excavation. f equals 1/D if D < 0.7B and equals 1/0.7B if D > 0.7B where B is the width of the excavation and D is the distance from the bottom of the excavation to firm soil.

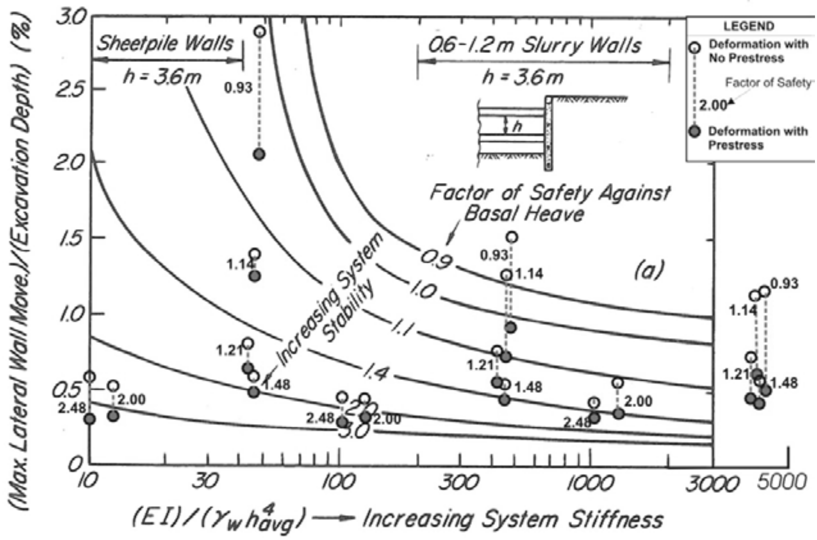

Figure 2: Design Curves to Obtain Maximum Lateral Wall Movement for Soft to Medium Clays (from Clough, et al 1989)

This chart is widely used to calculate displacement for a design. Clough et al (1989) described it as a first estimate tool. It has limitations because the effects of many factors on displacement are reduced to those in the chart. It uses a conservative upper bound of the data as design values. It is limited to the types of cases considered in its formulation, i.e. soft soils with undrained shear strength increasing with depth from the top of the ground. Many cases fall outside the conditions of the chart. The chart also focuses on maximum lateral wall movement and maximum settlement outside the wall but does not give angular distortion or horizontal strain that are required to assess impact of movements on adjacent structures. With the challenges facing designers and contractors to create less costly designs that meet stricter performance requirements in more complex subsurface environments, we need an improved way to make accurate predictions of displacement, horizontal strain and angular distortion that result from the construction of deep excavations with nearby structures.

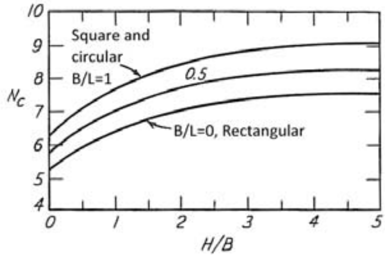

Figure 3: Skempton's (1951) Bearing Capacity Values

What is needed is a design method that is centered on controlling displacements to values that minimize damage caused by movements. Modern FEA software designed for geotechnical applications gives this capability.

PARAMETERS FOR FINITE ELEMENT ANALYSIS

Finite element analysis requires more information than traditionally used to design the ESS. A frequent argument is that this additional information is not available or will be too expensive to obtain. In consideration of the potential risks created by construction deep excavations, the cost to obtain the added information is small and is good engineering practice. Required parameters for FEA are:

- Geometry of the site, plan for the excavation, possible methods for ESS, and proposed sequence of work for construction expediency.
- Subsurface information to establish a model of the subsurface conditions that realistically simulates the actual conditions.
- Groundwater conditions with depth and as planned during the work.
- Soil parameters – density, Atterberg limits, drained and undrained shear strength, permeability and stiffness.
- Desired wall and lateral support methods and materials (such as struts or sheeting that already exist for the project or are readily available from suppliers).
- Desired lateral support type and spacing both vertically and horizontally for construction expediency.

Water pressure has a direct effect on strength of soils, pressure against the wall, and uplift of soil in the bottom of the excavation. Many situations are not hydrostatic before the work starts and change during the work. These conditions can be modeled in FEA, provided the initial water condition is known. At a minimum, depth to groundwater, pore pressure at the bottom of the excavation and pore pressure in any pervious layer up to 0.5H below the base of the excavation should be known.

Soil properties, especially strength, require careful attention because they are a key factor in the overall performance of the excavation support system. Soil strength below the bottom of the excavation becomes increasingly important for N_b values greater than 4. Special care should be used to define strength of low strength soils when N_b is greater than 6. There are at least a dozen methods to measure undrained shear strength and each method gives a different result. A qualified geotechnical engineer with experience in the design of deep excavations should soil strength parameters for the design.

Soft to medium clays may exhibit strength anisotropy, i.e. strength varies with the orientation of the failure surface. Very few FEM programs available in the US market can model strength anisotropy. Clough and Hansen (1981) showed that strength anisotropy can be considered by using the average of strengths measured with triaxial compression and triaxial extension tests on undisturbed samples or strengths measured in a direct simple shear device. These conclusions are consistent with Ladd's SHANSEP approach (Ladd and Foote 1974, Ladd 1991) and result in more realistic values of undrained strength for the FEA. Undrained strength values can also be obtained with cone penetration tests or corrected field vane tests. For projects where the consequences of a wrong prediction are high or there is little experience working with the soils, the stress path method by Lambe and Marr (1979) to determine soil strength and stiffness can be very helpful.

Table 1: Stiffness values for soils (modified from AASHTO 1996, 2002)

Soil Type	Soil Description	Range of E_{50} (kPa)	Range of E_{50} (ksf)
Clay	• Soft sensitive • Medium stiff to stiff • Very stiff	• 2,500 to 15,000 • 15,000 to 50,000 • 50,000 to 100,000	• 50 – 300 • 300 - 1,000 • 1,000 –2,000
Loess		• 15,000 to 60,000	• 300 – 1,200
Silt	• Silts, sandy silts, slightly cohesive mixtures	• 2,000 to 20,000 [400 $(N_1)_{60}$]	• 40 – 400 [8 $(N_1)_{60}$]
Fine sand	• Loose • Medium dense • Dense [Clean fine to medium sands and slightly silty sands]	• 8,000 to 12,000 • 12,000 to 20,000 • 20,000 to 30,000 [700 $(N_1)_{60}$]	• 160 – 240 • 240 – 400 • 400 – 600 [14 $(N_1)_{60}$]
Sand	• Loose • Medium dense • Dense [Coarse sands with little gravel]	• 10,000 to 30,000 • 30,000 to 50,000 • 50,000 to 80,000 [1,000 $(N_1)_{60}$]	• 200 – 600 • 600 – 1,000 • 1,000 – 1,600 [20 $(N_1)_{60}$]
Gravel	• Loose • Medium dense • Dense [Sandy gravels and gravels]	• 30,000 to 80,000 • 80,000 to 100,000 • 100,000 to 200,000 [1,200 $(N_1)_{60}$]	• 600 – 1,600 • 1,600 – 2,000 • 2,000 – 4,000 [24 $(N_1)_{60}$]

Strength values for stiff to very stiff clays and for silts and sands are less critical to the design of excavation support systems with soft clay below the bottom. For most cases, values can be estimated from empirical correlations with SPT tests or cone penetration tests. For a project involving stiff to very stiff clays, or silts and sands with no soft cohesive soils, strengths can be estimated from SPT tests or cone penetration tests and local experience.

Finite element methods require values of soil stiffness to make reasonable predictions of displacement; however, soil stiffness is less important than soil strength for values of N_b above 4. Soil stiffness values can be reasonably estimated from the values given in Table 1. Stiffness data can often be determined from the data used to obtain design strength. For clays, Figure 4 from Duncan and Buchignani (1976) is very useful. K is E_{50}/s_u. Values from Table 1 and Figure 4 are used as the secant Young's modulus at a shear stress of half the shear strength, E_{50} which is twice the initial tangent modulus. The unloading modulus is typically 3 to 5 times E_{50}. Kulhawy and Mayne (1990) and Sabatini et al (2002) contains extensive compilations of methods to estimate or measure stiffness and strength.

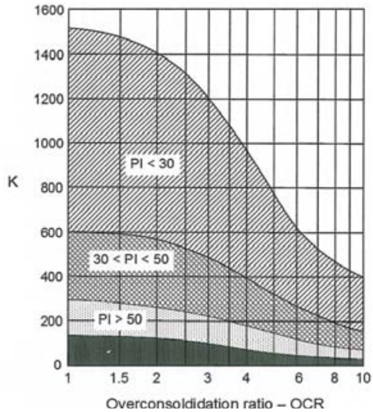

Figure 4: Generalized Undrained Modulus Ratio for Clays
(after Duncan and Buchignani 1976)

PROPOSED APPROACH TO DISPLACEMENT-BASED DESIGN

The proposed approach is to determine the allowable displacements that minimize potential damage, establish a trial design and analyze the performance of this design with FEA. Then compare results to the allowable displacements, revise the design and rerun the FEA until the predicted displacements are less than allowable values. The FEA software must have the following capabilities:

- Model non-linear stress-strain behavior for soils, including drained and undrained soil behavior for loading and unloading stress paths.
- Compute factor of safety against global instability.
- Model structural components of the wall and support system and their interaction with the soil, including slippage between soil and wall.
- Compute groundwater pressures and their change with time.
- Support removal of elements and correctly adjust nodal forces.
- Model the sequence of excavation to closely follow the steps of dewatering, excavation, support installation and support pre-stressing.

Current programs used in the US with these capabilities include PLAXIS, FLAC, SIGMA/W, midasGTS, CRISP, and others.

The following sections describe step-by-step guidelines to establish allowable displacements, then develop a design that deforms less than these values.

Allowable Displacements

Designing to limit movements requires knowledge of how much each structure within the influence zone can deflect without incurring excessive damage. Very few building codes give explicit limits for allowable displacements and these limits are not quantitative. Exceptions are codes for Shanghai, South Korea and some railway agencies in the US. Most of the codes that address this issue put the responsibility on the Builder to avoid damaging all neighboring structures. If not thoroughly familiar with local Code requirements, it is best to consult with a construction attorney familiar with these requirements.

Displacement limits depend on several factors, including the details of the foundation, loads, type of structural framing and exterior shell, and the existing condition of these elements. Many older buildings may have already undergone significant movement such that floor joists have limited bearing areas. For others, the structural members may have been significantly weakened by rot or insects, or their condition may be totally unknown because they are not visible for inspection. The limit values also depend on the consequences of any significant movement. A building where movement of one inch might cause a collapse and loss of life will

Table 2: Allowable Settlement and Tilt of Structures

Type of Movement	Limiting Factor	Maximum Settlement
Total settlement	Drainage	150 – 300 mm
	Access	300 – 600 mm
	Masonry walled structure Framed structures Smokestacks, silos, mats	25 – 50 mm 50 – 100 mm 75 – 300 mm
Tilting/ Differential movement	Tilting of smokestacks, towers	0.004L
	Stacking of goods, rolling of trucks, or similar	0.01L
	Machine operation-cotton loom	0.003L
	Machine operation – turbogenerator	0.0002L
	Crane rails	0.003L
	Drainage of floors	(0.01 to 0.02)L
	Framed buildings and reinforced load bearing walls: Structural damage Cracking in walls and partitions Open frames In filled frames Framed buildings	 1/150[1] 1/250[2] 1/200[3] 1/300[1] to 1/500[2] 1/300[6] 1/1000[6] 1/300[7]
	High continuous brick walls	(0.0005 to 0.001)L
	One-story brick mill building, wall cracking	(0.001 to 0.002)L
	Plaster cracking (gypsum)	0.001L
	Reinforced-concrete building frame	(0.0025 to 0.004)L
	Reinforced-concrete building curtain walls	0.003L
	Steel frame, continuous	0.002L
	Simple steel frame	0.005L
	Unreinforced load bearing walls: Sagging Hogging	 1/2500[2] L/H < 3; 1/3500 – 1/2500[3] L/H < 5; 1/2000 – 1/1500[3] 1/2500 at L/H = 1[5] 1/1250 at L/H = 5[5] 1/5000 at L/H = 1[5]

		1/2500 at L/H = 5[5]

Note: Data from Sowers (1962) unless otherwise indicated [1]Skempton &Macdonald (1956), [2]Meyerhof (1956), [3]Polshin & Tolkar (1957), [4]Bjerrum (1963), [5]Burland & Wroth (1975), [6]Meyerhof (1953), [7]Grant et al (1974).

no consequence to anything or anyone.

There are a number of publications on the allowable settlement and tilt for different types of structures. Table 2 summarizes recommendations from some of these as a useful reference to help set limit values for displacements. Boscardin and Cording (1989) developed a plot relating angular distortion and horizontal strain to building damage. Their plot is provided in Figure 5. It is useful in establishing allowable values for a structure.

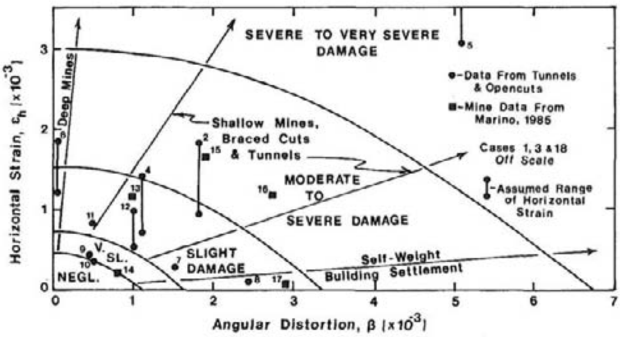

Figure 5: Angular Distortion and Horizontal Strain Limits

(after Boscardin and Cording, 1989)

The recommended approach to establishing displacement limits is as follows:

1. Review project information, local codes, ordinances and the Owner's requirements. Call these values ΔH_{max1} for maximum allowable lateral movement of the wall, ΔV_{max1} for maximum allowable settlement behind the wall, $\varepsilon_{H\ max1}$ for maximum allowable horizontal strain in of building behind the wall and $\Delta\alpha_{max1}$ for maximum allowable angular distortion of building outside the wall.
2. If displacements limits are not provided in Step 1, perform a site-specific evaluation. An engineer qualified in structural assessment of constructed facilities should inspect each building and utility within 4H of the ESS to determine its present condition and tolerance for additional settlement, horizontal strain and angular rotation. A larger zone should be evaluated if any significant alteration to the groundwater conditions outside 4H is anticipated. The result of this work should be limits for horizontal displacement of the ESS and settlement, angular distortion and horizontal strain of the ground outside the excavation for each structure. Call these values ΔH_{max2}, ΔV_{max2}, $\varepsilon_{H\ max2}$ and $\Delta\alpha_{max2}$.
3. If specific displacement limits are not provided from Steps 1 or 2, use the following method for each structure that might experience damage:
   a. Determine maximum allowable angular distortion, $\Delta\alpha_{max3}$, from Table 2 depending on building type and condition. Poor condition will lower the allowable values in Table 2.

b. Enter chart by Boscardin and Cording (1989), Figure 5, with allowable angular distortion and allowable damage to determine maximum allowable horizontal strain, ε_{Hmax3}.
c. Multiply ε_{Hmax3} by 3H for an estimate of the maximum allowable horizontal displacement of the wall that limits building damage, ΔH_{max3}.
d. Estimate maximum allowable ΔV_{max3} from values in Table 2 or from $\Delta V_{max3} = \Delta H_{max3} \cdot 0.16 \cdot e^{0.73FOS_{BH}}$ which is based on Clough et al (1989).

4. Take the smallest values from Steps 1-3 to obtain ΔH_{all}, ΔV_{all}, $\varepsilon_{H\,all}$ and $\Delta\alpha_{all}$.

Establish FEA Input

Finite element analysis is a very useful tool for design of ESS, but considerable care must be used by someone familiar with the software, its limitations and with the behavior of soils. The following gives a set of steps that can produce a trial design with 1 or 2 re-runs of the software once the finite element geometric model is correct.

1. Establish the subsurface conditions, including material properties. Especially important are strength and stiffness of soils below the bottom of the excavation and groundwater conditions before and during excavation. See section "Parameters for FEA" for guidance. Use expected value for each parameter.
2. Layout an ESS that works for constructability, i.e. type of wall, type of supports and horizontal and vertical locations for lateral supports. People with experience in constructability of ESS should participate in this step.
3. Compute FOS_{BH} using above equation. If less than 1.5, extra attention should be given to reduce any uncertainty about the shear strength of the soil below the excavation.
4. Use Terzaghi et al (1996), reproduced in Figure 6, to estimate lateral support loads per unit length of wall. Note that TPM for soft to medium soils has been revised from original Terzaghi and Peck method with the addition of ΔK based on Henkel (1971). $\Delta K = \frac{2.83d}{H}(1 - \frac{5.14s_u}{\gamma_t H})$. "d" is the lesser of 1.41B and D. ΔK can increase K for soft soils considerably. Use TPM lateral support loads and allowable axial stress to compute the structural area, A_s, for each support, including the effect of inclination of rakers or tiebacks.

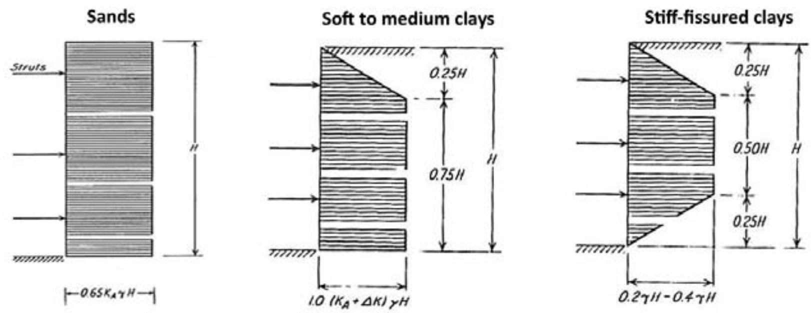

Figure 6: Apparent Earth Pressure Diagrams from Terzaghi et al (1996)

5. Compute stiffness of each support per unit length of the wall using $k_s=E_sA_s/L$, where k_s is the stiffness of the support member per unit of length, E_s is the modulus of elasticity for the support member, A_s from Step 4, and L is the length of the support member (half length for struts).
6. Compute moments in wall between each strut level and between lowest strut and the bottom of the excavation assuming hinges at each support location and at the bottom of the excavation. This can be done using $M=wl^2/8$, where M is the maximum moment, w is the average stress acting on the segment of length, l. Take the largest value to size the wall. For cantilevered walls and walls with embedment of more than the average strut spacing, h, the maximum moment will be below the bottom strut and should be computed using other methods such as those given in NAVFAC DM 7.2 (1982).
7. Use the maximum moment to compute required EI of wall so that allowable bending stress is not exceeded. Compute $I=M*y/\sigma_{allowable}$ where y is taken as ½ the thickness of the wall. Select thickness of wall based on required EI and wall type that contractor wants to use. I is moment of inertia of the wall.
8. Use Figure 2 with $\Delta H_{all}/H$ and FOS_{BH} to estimate the required system stiffness, $(EI/\gamma_t * h^4_{avg})$.
9. With I from Step 8, compute average vertical support spacing, h. Compare this spacing with that in Step 2 and adjust the spacing where constructability considerations allow or increase I to achieve the required system stiffness.
10. Use resulting EI per unit length of wall as input stiffness for the wall.

Prepare the FEA Model

1. Establish the finite element model giving consideration to the soil layering, the location of lateral supports, depth of the wall, the depth of each excavation stage, and the locations of any external loads.
2. Input information from above and check that all is correct.
3. Input the construction sequence for the FEA. Include steps to calculate FOS for the full excavation and for other levels where stability might be a concern.

Do the Finite Element Analysis

1. Make the finite element run.
2. Examine contour plots of stresses, strains and displacements for discrepancies, anomalies and unusual patterns. If these are present, examine the input data and results for each excavation step to locate the cause of the anomaly. Challenge any result that contradicts engineering judgment. Correct errors and rerun the analysis before proceeding to the next step.
3. Compare FEA forces in the supports to those calculated with TPM and the allowable stresses. The important part of this step is that the total loads are comparable and that any differences are understandable and explainable.
4. Compare the maximum moment in the wall to the value computed with TPM and the allowable moment. The FEA value will typically be similar to the value from TPM if the wall embedment is less than h. It may be much larger if the wall embedment exceeds h.

5. Compare maximum horizontal displacement of the wall, maximum vertical displacement of ground surface outside the excavation, horizontal strain at the ground surface outside the excavation and angular rotation of the ground surface to the values established in section "Allowable Displacements."

Revise the Trial Design

1. Multiply the FEA lateral support loads by 1.3 to account for variability that TPM indicates for support design. Adjust the size of lateral support members to meet structural design requirements for these loads. Resize the wall dimensions to satisfy structural code using the maximum moment from the FEA analysis.
2. Apply preload of 50% to 100% to supports, if further reduction in the computed displacements is required.
3. If lateral displacement of the wall exceeds ΔH_{max} by more than a factor of 2, increase the support stiffness by a factor of 5. If FEA maximum settlement outside the wall is considerably more than the allowable value and more than the FEA maximum horizontal displacement of the wall then, consider increasing the embedment of the wall.
4. Repeat the steps under "Do the Finite Element Analysis." Multiple adjustments and repeats may be required to find the optimal design. A point may be reached where further increases in strut or wall stiffness will not be very effective and the support loads will increase significantly. If the displacements remain larger than the allowable values, the value of h may have to be decreased.

These steps do not consider the effects of uncertainties in the soil profile and properties. The ease-of-use of modern FEA programs allow multiple parametric studies and reliability assessments. The computed deflections, loads, stresses, moments and FOS from these analyses must be less than the allowable values.

Structural Design

Following TPM, the axial capacity of the lateral supports computed in the FEA should be increased by 33% to account for individual variability that can occur in any one support. The envelope of maximum values computed with the FEA can be used as the design moments and shear forces for design of the wall.

Some agencies require an evaluation of the removal of any one lateral support element. This can be simulated in a two-dimensional FEA by removing the lateral support one level at a time and examining the effects on the moments and shear in the wall and forces in the lateral supports. This is a conservative approach. The FEA forces in the adjacent lateral supports need not be increased by 33% for design since this is a check on an extreme load condition.

Temperature changes can greatly increase strut loads in hot conditions and decrease them with possible additional movements in the cold. These need to be considered in the structural design or steps be taken to reduce temperature changes. Freezing of ground behind the all can also create large forces in the lateral support system and wall. This condition cannot be reliably analyzed and should be avoided.

Settlement and bearing capacity failure of the wall base can cause additional movement when lateral supports are inclined or vertical load is added to the wall. The FEA will detect this condition and automatically consider it in the analysis.

DEMONSTRATION OF THE DISPLACEMENT-BASED APPROACH

Figure 7 shows a project where the Owner wants to construct a four-level parking garage. He would be elated with five levels. The site conditions are typical of some locations in the US but have been generalized to avoid any similarity to actual projects. The four-level garage requires excavation to 42.5 ft depth and the five-level garage requires a 52.5 ft deep excavation. Older design methods usually limited excavations in these conditions to two or three levels. An evaluation of nearby structures using the approach described above results in allowable displacement values of $\Delta H_{max} < 1$ inch; $\Delta V_{max} < ¾$ inch; $\Delta\alpha_{max} < 0.001$ and $\Delta\varepsilon_{max} < 0.001$. Below the excavation is a normally consolidated soft clay with shear strength at a depth of 45 feet of 620 psf increasing to 1260 psf at 100 ft deep. It is not clear what shear strength to use to compute FOS_{BH} because the method considers constant shear strength with depth. FOS_{BH} for the example was computed using the strength at the mid-point of the soft soil below the bottom of the excavation.

Analyses with PLAXIS using the procedures outlined in this paper gave the results in Table 3. Case 1a is for 42.5 ft deep excavation without preload and Case 1b is with 100% preload. Cases 2a and 2b are for the 52.5 ft deep excavation without and with preload. The preload reduces movements but the values are well above the limit values.

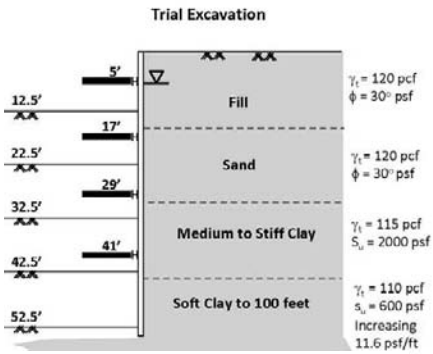

Figure 7: Hypothetical Project

Table 3 summarizes calculations of strut forces and maximum bending moments using Terzaghi et al (1996) for both depths. Also included are the values determined from FEA. Cases 1a, 1b, 2a and 2b are structurally stable but the displacements are much more than the allowable values. The sum of the strut loads computed by PLAXIS are 3 to 26% higher than computed by the TPM method. The loads are considerably higher than the TPM conclusion that actual earth pressures should, on average, be 25% less than loads computed with their method. The maximum moments computed by PLAXIS are considerably higher than those by TPM method, which contradicts the TPM conclusion that generally the actual moments should be less than those computed from the TPM method. These higher forces and moments result from increasing the wall and strut stiffness to reduce deflection, something the TPM method does not take into account.

Another interesting result in Table 3 is the FOS information. From calculations on many different types of facilities, it has been determined that the PLAXIS FOS is equal to or better than other methods because it finds the most critical failure surface of any shape and computes a value equal to or slightly lower than that obtained with limit equilibrium using Spencer's method. This capability is particularly useful for design of excavations where strength varies with depth in ways that other solutions cannot consider.

Figure 8 illustrates the critical surfaces determined by PLAXIS for a case where it reaches to the bottom of the soft soil and another case where it passes through the middle of the soft clay. Note that FOS_{BH} from FEA is similar to that calculated with the basal heave equation using the average undrained strength below the excavation. For Case 3, the PLAXIS FOS is considerably more than the basal heave value because of the added embedment and increased stiffness of the wall that the basal heave method cannot consider. Also note the differences in failure surface. Case 1b develops a shallower failure surface than Case 2b. Basal heave assumes failure at the bottom of the soft soil.

Table 3: Comparison of PLAXIS Results to Results from Peck Diagrams (forces in kips/ft, moments in kip-ft/ft)

Case	Total Strut Load TPM	Max. M TPM	FOS Basal Heave Eq.	Pre-load	Total Strut Load PLAXIS	Max. M PLAXIS	FOS PLAXIS	H_{max} (in)	V_{max} (in)	ε_{HOR} (%)	α_{MAX}
1a	108	80.6	1.14	0	125	138	1.10	8.36	4.85	0.97	0.003
1b	108	80.6	1.14	100	136	189	1.10	6.49	3.76	0.82	0.003
2a	189	84.7	0.93	0	195	413	1.03	18.2	10.02	1.5	0.007
2b	189	84.7	0.93	100	214	434	1.03	13.2	7.78	0.95	0.005
3	108	80.6	0.93	100	209	1040	1.77	2.03	0.86	0.10	0.0005
4	189	84.7	N/A	100	220	1670	N/A	0.99	0.54	0.10	0.0003

Several options can be examined with FEA to determine how to reduce movements. Additional runs were made on the hypothetical case to examine strut stiffness, strut spacing, wall stiffness, and wall embedment. The final variation that keeps the movement of a building on the surface close to the allowable values for the 42.5 ft deep excavation is to increase wall stiffness 210 times, strut stiffness by 6 to 13 times, embedment of wall from 2.5 ft to 22.5 and use a 100% preload. The results are summarized in Table 3 as Case 3. Similarly for the 52.5 ft deep excavation the wall stiffness was increased 200 times, strut stiffness by 5 to 10 times with 100% preload and embedment all the way to a firm base at 100 ft depth for Case 4. Note that for Case 3, the maximum horizontal displacement exceeds the 1 inch limit but this occurs at the bottom of the stiff, extended wall. Maximum settlement, horizontal strain and angular distortion are within the allowable limits for the hypothetical case.

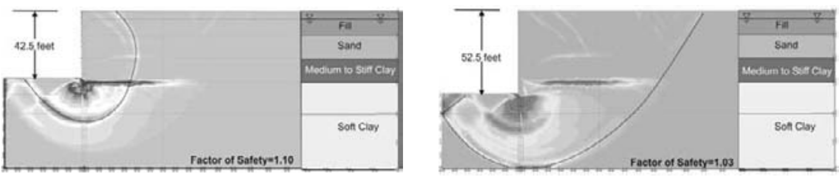

Figure 8: Shear Strain Contours at Failure for Cases 1b and 2b

There are some other interesting results in Table 3. Very large struts with high preloads and a very stiff wall are required to minimize horizontal displacement and settlement; but, a stable solution is found. Increasing the stiffness of the wall and struts greatly increases the maximum moment in the wall as shown for Cases 3 and 4.

It may not be economical to build these solutions but the FEA results show that constructing the excavation to 52.5 ft and meeting the tight displacement limits is possible, even with the soft soil conditions at the bottom of the excavation.

With additional parametric studies other alternatives might be found that would be less expensive to construct. A considerable number of variations were considered to find the results for Cases 3 and 4. The results computed from PLAXIS are plotted onto Figure 2 to compare with Clough et al's 1989 results. There is general agreement with the values for cases where struts are not preloaded in the FEA. Preloading in general reduces the predicted movements relative to those one would calculate from Figure 2. The good agreement in Figure 2 shows that the PLAXIS calculations give results comparable to what Clough et al (1989) obtained and hence, comparable to compiled field cases. The value of performing site-specific FEA rather than relying on the Clough et al (1989) chart is that variable soil profiles, variable soil properties, site specific conditions and ESS details can be included in the analysis. When designing for displacement control, these differences may cause substantial differences in computed wall movement and wall moment. A site-specific FEA may give a solution with less displacement than determined with the Clough et al (1989) chart. Additionally as shown in Table 3, the FEA predicts settlement, horizontal strain and angular rotation outside the wall, which Boscardin and Cording (1989) showed must be considered to limit damage to buildings close to the wall.

A-site-specific analysis also avoids having to resort to rules of thumb or limited empirical data to estimate movements. One generality that is commonly used is that the maximum settlement of the ground behind the excavation is usually between ½ to 1 times the maximum horizontal displacement of the wall. Figure 9 shows values obtained with PLAXIS for the considerable number of parametric studies used in this work. Most of the points compare with the generality, but there are a number of points where the settlement is much larger. These points are cases with large preloaded struts and limited wall embedment. The horizontal displacements of the wall were reduced but plastic flow of soil beneath the wall allowed settlement of the ground surface and angular distortions that would damage many buildings. It is not obvious which conditions will violate this generality.

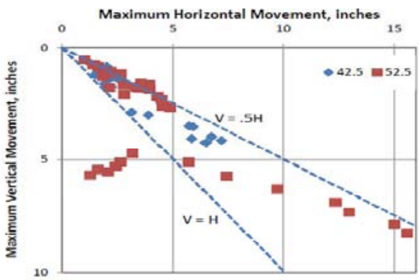

Figure 9: Computed Values of Maximum Horizontal and Vertical Displacements

These analyses assume careful control over construction operations to ensure that the wall is sound in all respects, the lateral supports and connections are installed as tightly as possible with preloads locked off at the required values and over excavation does not occur prior to installing the next level of struts. Failure to do any of these can increase the movements considerably.

One useful outcome of the displacement-based design approach is that a number of alternatives can be simulated with a consistent approach to determine which have the best performance and which may produce problems. This information can be combined with construction cost estimates to help determine the optimal design.

DISPLACEMENT MONITORING TO REDUCE RISK

Even when a careful evaluation and analysis are done to design an excavation support system, there remain sources of uncertainty that can result in poor performance and damage the complete works or adjacent structures. There is also the unknown effect of quality of the construction workmanship and attention to detail. Contractors are production oriented people who resist actions that slow them down. Limiting depth of excavation until lateral supports are installed, preloading supports with lock off at design levels, reducing strut spacing and controlling ingress of water and soil particles are steps many contractors resist. These mechanisms can increase lateral wall movements and ground settlements by factors of two or more. Detection of unexpected behavior during the excavation process can only be done with performance monitoring from start to finish. An effective monitoring program must be a part of the design for any excavation where the consequences of larger than expected movements are significant. Marr (2007) discusses benefits of performance monitoring programs that are applicable to deep excavations.

CONCLUSIONS

Design of excavations in urban areas is becoming more complex due to increasing requirements for deeper excavations on poorer sites, tighter limits on allowable displacements for adjacent structures, and new methods of construction that extend beyond the experience base used to develop previous design methods. Increasingly, limiting movements control ESS design, not avoiding collapse. This requires a new approach to designing ESS, one that focuses on controlling movements.

The step-by-step design approach laid out in this paper will result in a design that limits movements, provides adequate factors of safety against soil failure and provides realistic forces and moments to design the structural members. Each site has a unique set of conditions that may violate generalities and rules of thumb used in the past. With tighter restrictions and more demanding situations, site-specific finite element analyses permit more accurate prediction of horizontal deflection of the wall and settlement, angular rotation and horizontal strain outside the wall.

The application of the proposed method to a hypothetical project shows that despite very difficult conditions involving excavation into soft clay, ways can be found that meet strict displacement limits. These involve stiff struts with 100% preloads, stiff walls and significant wall embedment. The solutions may or may not be economically feasible but they show the power of using FEA to provide a consistent and rational method to design excavation support systems that meet specific displacement criteria.

REFERENCES

AASHTO (1996) *Standard Specifications for Highway Bridges," 16th Edition.* Washington, D.C. and 2002 17th Edition.

Bjerrum, L. (1963) "Discussion session IV." *Proc, European Conf. on Soil Mech. and Found. Engr.,* Wiesbaden, Germany, II, 135-137.

Boscardin, M.D. and Cording, E.J. (Jan. 1989) "Building Response to Excavation Induced Settlement." *ASCE:JGE,* Vol. 115, No. 1.

Burland, J.B. and Wroth, C.P. (1974) "Settlement of buildings and associated damage." *Proc Conf. on Settlement of Structures,* Pentech Press, London, England.

Clough, G.W., Weber,P.R. and Lamont, J. (1972) "Design and Observation of a Tied-Back Wall," *Proc. Specialty Conf. on Performance of Earth and Earth Supported Structures, Purdue University*, pp. 1367-1390.

Clough, G.W. and Hansen, L.A.(1981) "Clay Anisotropy and Braced Wall Behavior." *ASCE:JGED* Vol. 107, No. CT7, July 1981, pp. 893-914.

Clough, G.W, Smith, E.M. and Sweeney, B.P.(1989) "Movement Control of Excavation Support Systems by Iterative Design." *Proc. ASCE, Foundation Engineering: Current Principles and Practices, Vol. 2,* pp. 869-884.

Clough, G.W. and O'Rourke, T.D. (1990) "Construction Induced Movements of In-situ Walls." *Proc, ASCE Conf. on Des. And Perf. of Earth Retaining Struct., Geotech. Spec.Publ. No.25,* ASCE, New York, 439-470.

Duncan, J.M. and Buchignani, A.L. (1976) "An Engineering Manual_for Settlement Studies." Department of Civil Engineering, University of California, Berkeley.

Goldberg, D.T., Jaworski, W.E. and Gordon, M.D.(1976) "Lateral Support Systems and Underpinning." *Report FHWA-RD-75-128, Vol. 1,* FHWA, Washington, D.C.

Grant, R., J. T. Christian, and E. H. Vanmarcke (1974), "Differential Settlement of Buildings," *ASCE:JGED*, Vol. 100, No. GT9, pp. 973-991.

Hana, A.I. and Clough, G.W.(1981) "Prediction of Movements of Braced Cuts in Clay." *ASCE:JGD,* Vol. 107, No. GT6, pp. 759-778.

Jaworski, W.E. (1973) "An Evaluation of the Performance of a Braced Excavation," Ph.D. Thesis, Massachusetts Institute of Technology.

Henkel, D. (1971) The calculation of earth pressure in open cuts in soft clays," *The Arup Journal* London, 6, No 4. pp. 13-15.

Kulhawy, F. H. and Mayne, P.W. (1990) *Manual on Estimating Soil Properties for Foundation Design.* EPRI Report No. EL-6800.

Ladd, C.C. and Foote, R. (1974) "A new design procedure for stability of soft clays." *ASCE:JGED,* Vol. 100, No. GT7. pp. 763-786.

Ladd C.C. (1991) "Stability Evaluation During Staged Construction." The Twenty-Second Karl Terzaghi Lecture, *ASCE:JGE* Vol. 117, No. 4, 540-615.

Lambe, T.W. and Marr, W.A. (1979) "Stress Path Method-Second Edition", *ASCE:JGED*, Vol. 105, No. GT6, pp. 727-738.

Marr, W. A (2007) "Why Monitor Performance?" *ASCE: GSP 117*. Keynote paper presented to 7th International Symposium on Field Measurements in GeoMechanics, Boston.

Meyerhof, G.G. (1953) "Some recent foundation research and its application to design." *Struct Engr. Vol. 31*, pp. 161-167.

Meyerhof, G.G. (1956) "Discussion paper by Skempton et al – Settlement analysis of six structures in Chicago and London", *Proc. ICE*, 5, No.1, p170.

NAVFAC (1982) *Design Manual DM-7*, Department of Navy, Washington, D.C.

Peck, R. B. (1969) "Deep Excavations and Tunneling in Soft Ground." *State-of-the-Art-Report, 7th ICSMFE, Mexico City, State-of-the-Art Volume, pp. 225-290.*

Polshin, D.E. and Tolkar, R.A. (1957) "Maximum Allowable Nonuniform Settlement of Structures, *Proc. 4th ICSMFE*, Vol.I, p. 402.

Poulos H.G. (2000) "Foundation Settlement Analysis – Practice Versus Research." 8th Spencer J. Buchanan Lecture, Texas A&M University, College Station, Texas

Sabatini, P.J., Bachus, R.C., Mayne, P.W., Schneider, J.A. and Zettler, T.E. (2002) *Geotechnical Engineering Circular No. 5: Evaluation of Soil and Rock Properties.* FHWA-IF-02-034.

Skempton, A.W. (1951) “The bearing capacity of clays,” *Proc. British Bldg, Research Congress*, pp. 180-189.

Skempton, A.W. and MacDonald, D.H. (1956) “The allowable settlement of buildings.” *Proc. Inst. of Civ. Engrs., Part III,* 5, 727-784.

Sowers, G.F. (1962) *Shallow Foundations, Foundation Engineering*, G.A. Leonards (ed.) McGraw-Hill Book Co., New York, NY, pp. 525-632.

Terzaghi, K. (1943) *Theoretical Soil Mechanics*, John Wiley & Sons, Inc., New York, NY.

Terzaghi, K. Peck, R.B. and Mesri, G. (1996) *Soil Mechanics in Engineering Practice: Third Edition*. John Wiley & Sons, Inc.

Assessment of excavation-induced building damage

E. J. Cording[1], J. L. Long[2], M. Son[3], D. Laefer[4], B. Ghahreman[5]

[1]Professor Emeritus, University of Illinois at Urbana Champaign, P O Box 125, Savoy, IL 61874; cordingconsult@gmail.com
[2]Associate Professor, University of Illinois at Urbana Champaign, 2230 Newmark CE Lab, 205 N. Mathews, Urbana, 61801; jhlong@illinois.edu
[3]AssistantProfessor, Department of Civil Engineering, Daegu University, Jilyang, Gyeongsan, Gyeongbuk, South Korea, 712-714; mson@daegu.ac.kr
[4]Head of Development, School of Architecture, Landscape & Civil Engineering, University College, Newstead, Belfield, Dublin 4, Ireland; debra.laefer@ucd.ie
[5]Geotechnical Engineer, Black & Veatch, 200 Wheeler Road, Burlington, MA 01803; bidjan7@hotmail.com

ABSTRACT

Ground movements during excavation have the potential for major impact on nearby buildings, utilities and streets. Increasingly ground movements are controlled at the source. They are assessed by linking the ground loss at the excavation wall to the volume change and displacements in the soil mass, and then to the lateral strains and angular distortion in structural bays or units, and are related to damage using a damage criterion based on the state of strain at a point. Numerical and physical models of excavation-induced building damage were used to vary parameters and develop procedures for assessing distortion and damage. Examples of building distortion and damage are presented for brick bearing wall structures of the 1800's and early 1900's, as well as later frame structures, that illustrate how geometry, era of construction, stiffness, and condition influence building response to ground movement.

INTRODUCTION

Increasingly, ground movements are controlled at the wall of the excavation, with less reliance on underpinning or ground modification, although such procedures may be used to reduce the risk of impacts from ground movement. The impacts are assessed by linking the magnitude of ground loss at the source to the volume change and lateral and vertical displacements in the soil mass, and then to the lateral strains. angular distortion, and resulting damage in the structure, using a damage criterion based on the average state of strain in a structural bay or unit.

In this paper, emphasis is placed on relating the given ground displacements to the building response. The settlement slope, tilt, and change in ground slope across the structure serve as a basis for assessing angular distortions, which will be modified by the geometry, condition, stiffness, and strength of the building. Added to this are the lateral ground strains imposed on the building foundation. The distribution of lateral strains throughout the structure will be affected by bending or rotation at the foundation level and modified by the lateral stiffness and variation in stiffness of the structure. Grade beams and continuous, reinforced foundations will limit – or eliminate -- lateral strains in the base of the structure. At upper levels of a structure, structural frames and floors tied to the walls will limit lateral strains induced by both lateral ground strain and by bending. Structural weaknesses such as construction joints, windows, stair wells, and poor connections at façade walls and between walls and floors will allow concentration of lateral strains.

The damage criterion is based on the average state of strain, determined from lateral strains and angular distortions near the base and in upper levels of a given structural bay or unit. The sensitivity of the structure to damage and the significance of the structure must also be considered in evaluating the impact of the damage and the cost of pre-emptive measures or required repairs.

Numerical and $1/10^{th}$ scale physical models of brick bearing walls adjacent to excavation walls in sand were used to vary parameters and develop procedures for assessing building distortion and damage. Examples are presented of building distortion and damage for brick bearing wall structures of the 1800's and early 1900's, as well as later frame structures, that illustrate how the geometry, era of construction, stiffness, and condition of the building influence its response to ground movement.

SOURCES OF GROUND MOVEMENT

Lateral displacement of excavation wall

The lateral displacement of the excavation wall that develops during excavation is largely controlled by relative soil/wall stiffness, which is a function of the EI of the wall and the distance, L, excavated below a strut or tieback level before setting struts or tiebacks at the next level. Distortion of adjacent buildings can be controlled by placing a stiff wall with small enough vertical spacing between brace levels and by limiting the depth of excavation below brace levels before installing the tiebacks or struts. In sands and stiff clays, a relationship relating wall/soil stiffness (EsL^3/EI) to normalized lateral wall displacements can be used where Es is the secant Young's modulus of the soil in the stress range of interest. Numerical analyses provide a means of assessing the effect of soil/wall stiffness on lateral wall displacement. Papers describing excavation wall displacements in clays as a function of wall stiffness and factor of safety against basal heave due to excavation include Clough and O'Rourke, 1990 and Hashash and Whittle, 1994.

Lateral wall movement patterns include cantilever deflection due to excavation prior to placing the first brace, and bulging deflections that develop below brace levels as the excavation is deepened. Mueller, et al (1994), based on model tests of 1/4-scale tieback walls in sand, observed a third lateral deflection pattern when the toe depth and capacity of the soldier pile was inadequate and the vertical component of tieback force caused penetration of the pile. The resulting lateral wall displacement at the tieback level was s_{wall} tan a where s_{wall} is wall settlement and a is tieback angle.

A standard approach during excavation is to monitor the lateral and vertical settlement at the top of the soldier piles and on the adjacent building wall. Inclinometers installed in the wall provide a profile of lateral displacements over the wall height. To obtain a complete record of the causes of lateral wall deflection, measurements should be made every time the excavation is deepened and lateral braces are installed. To measure deep-seated movements that may occur below the tip of the pile, inclinometer casing is extended below the bottom of the wall.

Displacement due to wall installation

Ground losses can also occur due to installation of the vertical wall elements, such as excavation of a slurry trench for a concrete diaphragm wall, or installation of timber lagging in a soldier pile wall. Lateral displacements immediately adjacent to slurry wall installation have typically been reported in the range of 0 to 20 mm, and are dependent on soil type, slurry density and panel width. Local ground losses due to installation of the excavation wall are of greatest concern when building foundations are immediately adjacent to the wall, which is commonly the case where building walls are set on the property line. In this case, underpinning may be used or an excavation wall provided that will limit movements of the adjacent foundation during wall installation, as shown for the case in Figure 1b. Inclinometers and settlement points placed adjacent to the excavation wall, prior to its installation, can be used to record lateral displacements due to both wall installation and, later, excavation.

Control of excavation wall movement

Early experience on the Washington Metro with excavation walls of soldier beams and lagging in medium-dense sands and stiff clays, resulted in maximum settlements ranging between 0.1% to 0.3% of the excavation height (O'Rourke and Cording, 1975). Most walls were supported with cross-excavation struts. The larger settlements developed when excavation was extended far enough below strut levels before installing the next strut to allow passage of excavation equipment. Additional displacements also developed as the station structure was built and backfilled and the struts were removed. For an 18-m-deep excavation at G St, lateral movement averaged 15 to 20 mm and produced vertical settlements of 35 mm at a distance of 3 m behind the wall. The volume of lateral wall displacement and the volume of surface settlement were approximately equal at 0.4 cu m/m.

Tighter control of excavation wall displacements has been achieved on other projects, and is particularly important in order to limit damage to decorative finishes in historic buildings and other sensitive structures.

Such a case was the historic Masonic Temple in Philadelphia, built in 1870 (Figure 1). It is a 24-m- high masonry bearing-wall structure with interior plaster finishes and decorative murals. Initially, in 1975, the plan was to support the exterior bearing wall with pit underpinning prior to excavating a cut and cover structure for an adjacent subway. As the initial pits were being installed, cracking of plaster walls developed in the bay adjacent to the bearing wall, on all floor levels (Figure 1a). Crack patterns showed both diagonal shear cracks above doorways as well as vertical cracks between the bearing wall and adjacent cross walls. Opening of pre-existing cracks was observed in non-public areas. Estimated angular distortion was 1.5×10^{-3} (very slight to slight damage, point A in Figure 2).

To prevent further distortion, the underpinning operation was terminated and a 12-m high wall was installed adjacent to the footing with sufficient stiffness to limit lateral wall displacements and prevent further settlement of the bearing wall. It consisted of tangent H piles and tiebacks at close vertical spacing (Figure 1b). A row of tiebacks was installed immediately below the bearing wall foundation before excavating below foundation level. The next 2 tieback levels were at close 2-m vertical spacings.

The wall was designed to have an average lateral displacement of 3 mm, using beam-on-elastic-foundation and finite element analyses correlated with the data from the more flexible excavation walls in Washington, DC.

The measured lateral displacements were in the anticipated range, with a maximum of 5 mm and average of 3 mm (0.25% of excavation wall height, H), and displacement was held to zero when excavating the first 2 m below footing level. Lateral wall displacement volume was 0.05 cu m/m. There was no further extension of damage in the building.

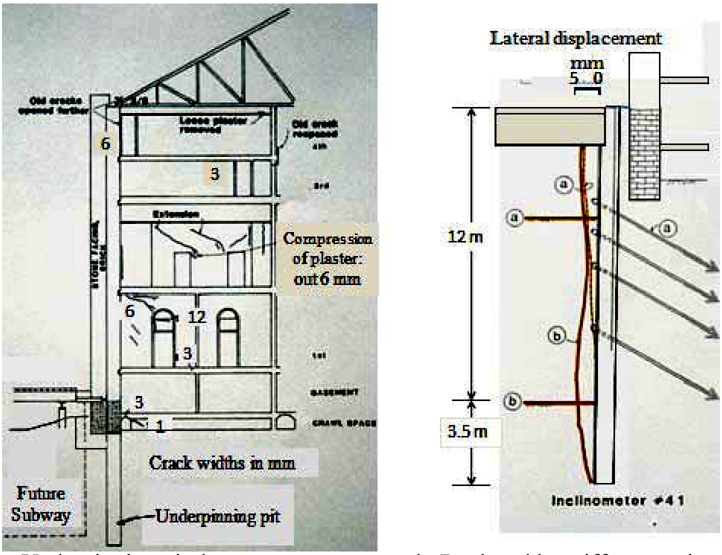

a. Underpinning pit damage b. Replaced by stiff excavation wall

Figure 1. Masonic Temple: a) Damage due to excavation of underpinning pits and b) displacement of tied back tangent pile wall, with no further damage.

PATTERNS OF GROUND MOVEMENT

Settlement at the ground surface

The volume of the surface settlement trough can be estimated from the volume of lateral wall displacement. In dense sands, the volume of the surface settlement will be less than or equal to the volume of the lateral wall displacement but they can be assumed to be equal. For soft clays, the volume of the settlement trough will initially be approximately equal to the lateral displacement volume and will increase with time due to drainage and consolidation of the clay.

The boundaries of the settlement profiles for excavations in clay were described by Peck (1969). Observed settlements adjacent to a series of excavations in soft clay, sands, and stiff to very stiff clays were summarized in Clough and O'Rourke (1990). The envelope of ground displacements is shown to extend laterally a distance of 2 to 2.5 the excavation height. For sands, the envelope of the settlement zone is shown to be a triangular region extending laterally from the excavation wall a distance of twice the excavation depth, H. Deep seated movements in soft clays will cause displacements to extend to greater distances, which are a function of the height of the zone of lateral displacement extending below the excavation bottom.

Field measurements show that an individual settlement profile typically exhibits a decreasing slope with distance away from the excavation wall. The maximum settlement is near the excavation wall, although there may be a reduced settlement close to the wall due to the soil shear stresses developed on the excavation wall, which, if it has good bearing, will settle less than the soil mass. Large scale-model tests in sand also show a similar pattern (Mueller, 1994, Laefer, 2001).

A parabola can be used to approximate the settlement profile so that structural distortions can be estimated. Often, the measured settlement profile adjacent to an excavation is not precise enough to obtain accurate measure of changes in slope and curvature, but the parabola provides a sense of the parameters controlling distortion. Settlement with respect to the maximum settlement is simply $\delta/\delta_{max} = (1\text{-}x/l)^2$ where x is distance from excavation wall and L is the length, L, of the settlement profile. The settlement slope decreases with distance, x, and is equal to 2(1-x/L). A unit or bay of a structures distorting with a parabolic settlement pattern between 0 and x = L/2 would have an average settlement slope of 1.5 δmax/L. Although the parabola can be assumed to extend a distance of L = 1.5 to 2H from the excavation in sands and stiff clays, the displacements beyond 0.75 L are likely to be in the range of the precision of the survey measurements (less than 1.5 mm for a maximum settlement of 25 mm near the wall)

Lateral displacements of the ground surface

For the cantilever deflection of a braced excavation, which occurs prior to installing the first brace level, lateral displacement of the ground surface will be high, on the order of 1 to 1.5 times the vertical displacement. For the bulging displacements that develop as excavation proceeds below strut and tieback levels, lateral displacements at the surface will be on the order of 0.5 to 1.0 times the vertical. (Milligan, 1974), O'Rourke, et al, 1977, Clough and O'Rourke, 1990.

Measurements of lateral and vertical displacement were made for model excavation walls in sand. Wall height was 2 m for a ¼ scale wall constructed of soldier beams and steel lagging (Mueller et al, 1994) and 1.8 m height for 1/10 scale wall of sheet steel (Laefer, 2001).

For the bulging displacements, the field and lab data show that the vectors of near-surface soil displacement are steepest near the wall and flatten further from the wall. To estimate lateral displacements from the vertical settlement profile, it is recommended that 0.5 δl/δv be used near the excavation wall and that it be increased to 1.0 at and beyond a distance of 0.75 L where L is the length of the settlement profile.

With deep-seated displacements on weak, flat-lying clay seams or sheared surfaces extending behind the excavation, lateral displacements will predominate and can be concentrated at lateral distances well in excess of the excavation depth, H. In several projects, large ground movements did not develop until the braced excavation approached full depth. Deep-seated movements on weak layers have caused lateral displacement of the overlying ground mass and produced opening of cracks at distances behind the excavation from 1 to 3 times the excavation depth, H. In these cases, significant cracking did not develop near the excavation wall.

BUILDING DISTORTION AND DAMAGE

Damage criterion for assessing building distortion and damage

The damage criterion presented in Figure 2 compares damage levels to the angular distortion and lateral extension strain that develops within a structure due to lateral and vertical ground movements acting on the structure foundation. It is applicable to a full range of building geometries and distortions and strains, and is not limited to a single value of building length/height ratio (L/H). The relationship gives the state of strain at a point, which is used to describe the average strain within a structural bay or unit. Each of the boundaries between damage categories represents a constant principal extension strain, determined from the combination of angular distortion and lateral strain. (Cording et al, 2001). The structure is strained by the ground movement acting along its base (Figure 3). The angular distortion, or shear strain, is equal to the average settlement slope minus the tilt of a structural bay or unit. The lateral strain at the base is equal to the extension of the base divided by the base length. Separate values of lateral strain may be estimated for the lower and upper portions of the building unit. In the upper portions of the building, lateral strains may reduce due to the stiffness and restraint provided by the upper floors, or, conversely, they may increase due to bending or rotation for a convex (hogging) soil settlement profile, and will concentrate in areas where the building is weak in tension.

The state of strain at a point criterion was developed from, and is almost identical to, the criterion developed by Boscardin and Cording (1989); There is a only a minor adjustment in boundaries between damage levels so that each boundary represents a constant value of maximum principal extension strain, rather than the relationship for a deep beam with L/H =1. Additionally, as recommended by Burland (1995) the zone of moderate damage is not described as moderate-severe.

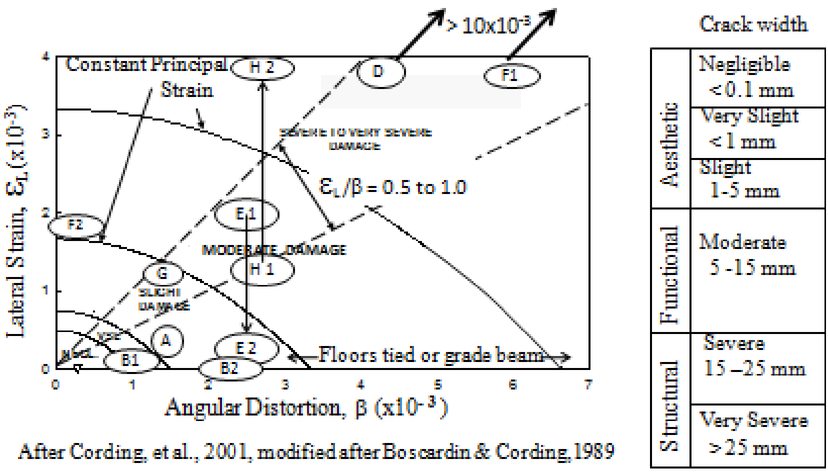

Figure 2: Damage criterion based on state of strain at a point

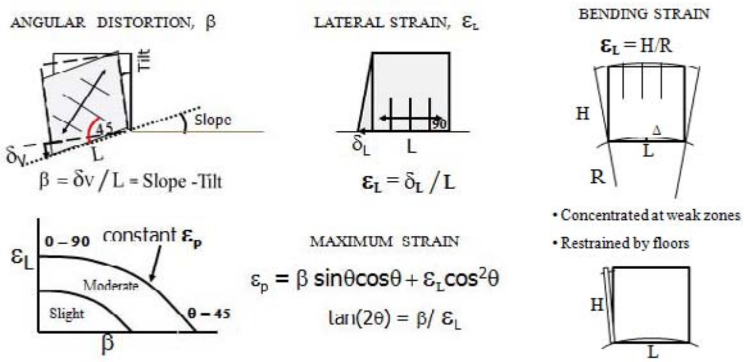

Figure 3: Angular distortion and lateral strain in a structural element due to ground movement

Burland and Wroth (1974) used beam theory to describe the effect of the length/height ratio (L/H) on distortions for different ratios of Young's modulus to shear modulus (E/G) and provided the relationships for brick and mortar structures with a higher ratio of E/G than an elastic continuum, and therefore shear strains would be critical for larger L/H ratios than would be predicted for an isotropic elastic continuum. From their observation of bending cracks in upper levels of the historic Westminster cathedral due to excavation of an adjacent car park, they concluded that criteria should be based on bending, not shear distortion alone, as had been described by Skempton and MacDonald (1956).

Boscardin and Cording (1989) added to this relationship the lateral strain imposed by the ground movement. They observed that, for many settlement profiles adjacent to excavations and tunnels, the portions of a structure impacted by ground movement have a relatively low length/height ratio and a low effective shear stiffness so that they act as deep beam, and shear distortions control damage. They set damage levels for the lateral strains to correspond with criteria used by the National Coal Board (U.K) for lateral displacements imposed on structures due to deep coal mine subsidence where the settlement profile is so large that buildings are subject to lateral strain and tilt, and not angular distortion. In setting damage levels for angular distortion they considered the relationships developed by Skempton and MacDonald (1956) for buildings settling under their own weight.

The relationships for bending of a continuous beam provides an estimate of damage due to bending in the central portion of structures distorted over a low L/H ratio that are weak in tension. However, for a deep beam that is continuous and elastic, significant bending and extension cannot develop near the façade, whereas cracks and lateral extension in the upper portion of the structure often are concentrated near the façade wall along pre-existing weaknesses, such as the boundary between a façade wall and a bearing wall, or along shear cracks that have extended up the wall because of large angular distortion. The equations for bending of an elastic continuous beam are not applicable to this case. One way to assess the potential lateral strain at the top of the wall is to determine the radius of curvature of the settlement trough for the unit of the building that is expected to have pre-existing cracks or joints or a low enough tensile strength that a crack can form and separate, and then calculate the maximum lateral displacement at a weak point from the strain in the upper portion of the structure (Figure 3). The procedure is similar to the strain superposition method proposed by Boone (1996, 2008). However, once the façade wall of a building separates, the displacement magnitude becomes unpredictable. The primary effort should be to limit ground movements at the base so that lateral strains do not amplify in the upper portion of the structure, as described in Section 4.7.

The description of each of the damage categories was developed by Burland et al (1977). It was developed for brickwork and stone masonry and can be applied to plaster work, and was not intended for reinforced concrete structural elements. Crack sizes for each of the categories are indicated in Figure 2, but Burland (2008) states: "The strong temptation to classify the damage solely on crack width must be resisted. It is the ease of repair which is the key factor in determining the category of damage." The categories are summarized as follows:

Aesthetic damage, including very slight to slight damage, affects interior finishes. Slight damage may require some re-pointing of visible masonry cracks. Redecoration may be required.

Moderate damage affects building function and results in masonry cracks requiring patching and may require some re-pointing of brickwork.. "Doors and windows stick, service pipes may fracture, and weather-tightness is often impaired."

Severe and Very Severe categories result in structural damage. Severe damage involves…"breaking-out and replacing of sections of walls, especially over doors and windows, distorted windows and frames, sloping floors, leaning or bulging walls, some loss of bearing in beams and disrupted service pipes." "Very severe damage often requires…partial or complete rebuilding, beams lose bearing, walls lean and require shoring, and there is a danger of structural instability."

It is understood that the impact of a given distortion will differ for different buildings, depending on their sensitivity and significance, and they should be evaluated on a case by case basis. As Burland (2008) notes, the descriptions relate to standard domestic and office buildings and may not be appropriate for a building with valuable or sensitive finishes. (Plaster finishes such as crown moldings and wall murals in historic structures are of particular concern in the aesthetic damage range.)

Physical and numerical models of ground movement and building damage

Relationships between ground deformation and building distortion and damage were obtained in research programs conducted at the University of Illinois at Urbana Champaign. The work consisted of a combination of physical modeling and numerical analysis, as well as correlations with field measurements and case histories, for brick-bearing wall and frame structures adjacent to excavations.

Physical modeling of excavation walls was first carried out in a large model test pit constructed of segmental blocks, designed and utilized by M. Hendron for testing of tied back and soil nailed excavation walls. It was then used in a program of testing of ¼ scale (1.8 m high) excavation walls with single and double tiers of tiebacks (Mueller, et al, 1994). The test pit was moved to a new University of Illinois test facility, Schnabel Laboratory, where, for the first time, the testing program combined the modeling of excavation walls with adjacent building walls. Tied back excavation walls in sand were constructed adjacent to 600-mm-high, 2-story brick bearing walls and frame walls in order to observe the effect of ground movement patterns on building distortion and damage (Laefer, 2001). The strength and stiffness of the buildings were scaled with the 1/10 scale structure dimensions. The results of the model tests produced realistic settlement and lateral displacement patterns in the ground. Down-drag of the façade walls against the bearing wall caused concentration of shear distortions and cracking between the windows nearest the excavation wall. The data was correlated with the numerical models which were then used to conduct parametric studies.

Two types of numerical analyses were conducted. Distinct element analyses (UDEC) were conducted of brick bearing walls in which each brick was modeled as a block element and the mortar was modeled as the contact shear and normal stiffness and strength between blocks (Son, 2003). A parabolic pattern of ground settlement and lateral displacement was imposed on a system of elastic springs and contact elements modeling the soil at the foundation level of the structure. A series of runs were conducted to correlate the numerical results with the physical model tests. Additional runs were conducted using the dimensions of full scale structures. Finite element analyses were conducted in which the full excavation, excavation wall, sandl mass and adjacent building were modeled (Ghahreman, 2004). The two and three- dimensional numerical models used an Abaqus platform and a hypo-plastic constitutive model that produced displacement patterns consistent with field observations .

In both the physical and numerical models, lateral and vertical displacements at the top and base of the wall were recorded at four sections along the length of the building wall. From this data were obtained the tilt and angular distortion and their variation along the length of the wall, as well as lateral strains at both the base and top of the wall. The tilt and bending could not be determined from a settlement profile alone, but required the measurement of lateral displacement over the height of vertical sections along the wall. It was apparent that the tilt of the bearing wall structure was not simply the average slope of a chord extending over the settlement profile, as is the assumption when using beam theory, but was usually a lesser value, which depended on the distribution of the ground displacements beneath the building, the effect of façade downdrag, building stiffness, and mortar cracking.

The more flexible bearing wall had a deflection pattern close to the imposed soil displacements, whereas stiffer bearing walls would have a flatter settlement profile and smaller imposed angular distortions with respect to the change in ground slope. Once cracking developed in the walls, the angular distortions would increase, approaching the ground settlement slope or change in slope.

Estimating angular distortion from slope, change in ground slope, and tilt

Figures 4 and 5 illustrate the method for estimating angular distortion for a building flexible enough to settle with the soil profile. For a building extending beyond the outer portion of the settlement profile, with the first unit spanning a significant portion of the settlement profile, there is no tilt, and the angular distortion, or shear strain, is approximately equal to the average slope of the settlement trough (Figure 4a). In Figure 4b, the structure also extends beyond the settlement profile but consists of several units that have different slopes on the parabolic settlement profile. Unit 1 has an angular distortion equal to approximately 1.5 times the average ground slope, δ_{max}/L. whereas Unit 2 has an angular distortion equal to the ground slope that is approximately 0.5 times δ_{max}/L. Thus, damage levels for unit 1 would be greater in the case of Figure 4b than the case of Figure 4a.

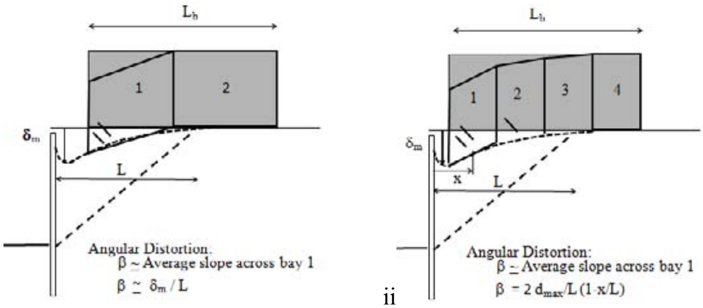

a. Single bay across settlement slope b. Multiple bays

Figure 4: Building moves with ground and extends beyond settlement zone

For cases in which the building is narrower than the settlement profile, as in Figure 5, the slope minus the tilt is a measure of the angular distortion. In Figure 5a, all the distortion is concentrated in unit 1, either because of the down drag of the façade wall on unit 1, increased curvature under unit 1, or because unit 1 has a lower shear stiffness than unit 2. As a result, the slope of unit 2 represents the tilt, and the change in ground slope between unit 1 and 2 is the angular distortion.

In Figure 5b, sidesway of units 1 and 2 results in increased tilt and reduces the angular distortion in unit 1. At the extreme, it could reduce the angular distortion in unit 1 to one half of the case in Figure 5a, and cause an equal and opposite angular distortion in unit 2.

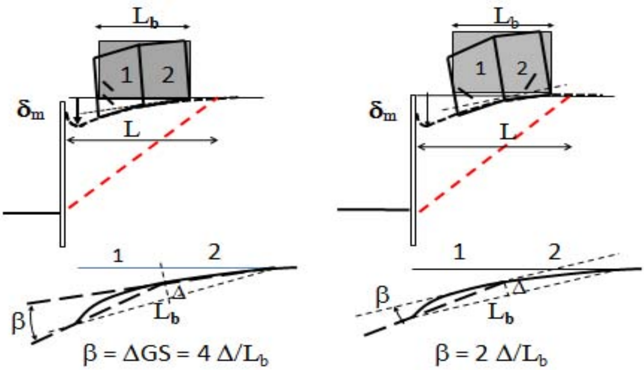

a. Distortion concentrated in unit 1 b. Sidesway reduces distortion in unit 1

.

Figure 5: Buildings moves with the ground, Tilt reduces angular distortion.

A beam analysis is consistent with the assumption of Figure 5b. In this case, the tilt of the structure is assumed equal to the slope of the chord extending across the settlement profile. The slope of the chord is considered in much of the literature to represent the structure's tilt, and damage criteria based on the deflection ratio, Δ/L make this assumption. However, the actual tilt should be measured from the tilt of vertical sections within the structure.

Although the angular distortion, β, changes by a factor of 2 from Figure 5a to Figure 5b, the deflection ratio, Δ/L remains the same because it does not consider the difference in tilt between the two cases and will predict the same level of damage for both cases. The deflection ratio damage criterion proposed by Burland (1995) based on beam theory is consistent with the damage criterion based on angular distortion (Figure 3) for the conditions described in Figure 5b but it underestimates the damage level for the conditions described in Figure 5a.

The series of UDEC numerical analyses by Son (2003) showed values of β that ranged from the conditions in Figure 5a (β= 4Δ/L) to Figure 5b ((β= 2Δ/L). The distortions of Figure 5a occurred with the brick bearing walls in which there was downdrag of the façade wall and where cracking developed in the structure. The symmetrical distortions of Figure 5b were more characteristic of elastic beams and uniform, open, continuous frames that are narrow enough that they will sidesway, as is shown in the finite element analysis by Ghahreman (2004). Sidesway of the frame caused shear distortions within the third bay that were approximately equal and opposite to those in the first bay (Figure6). In this case, in the absence of a continuous foundation or grade beam, lateral ground displacements caused significant bending strains in the columns between the foundation and the first concrete floor level. Such a condition caused cracking and structural damage to the columns at foundation level of a reinforced concrete parking structure at Heathrow Airport due to lateral displacements generated by adjacent tunneling (Powderham et al, 2004).

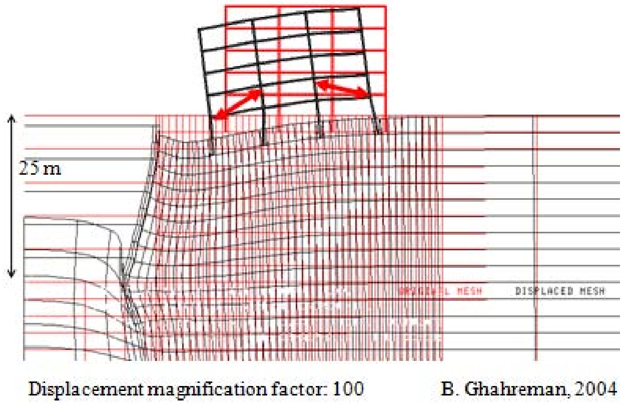

Figure 6 Distortion of concrete frame adjacent to excavation in sand, finite element analysis with hypo-plastic soil model.

Finno, et al (2005) described and analyzed a Chicago school building in which distortions due to adjacent excavation in clay were concentrated in the first bay of the structure, consistent with the pattern of Figure 5a. The brick bearing walls were clad with limestone and floors were concrete, which limited lateral extension strains in the building. Shear strains and cracking were concentrated in the first bay, which was on the steeper portion of the settlement slope. Damage consisted of shear and horizontal cracks, typically less than 3 mm, as well as some distortion of doorways, requiring replacement. The settlement slope beneath the first bay, after consolidation of the clay took place, was $2.7x10^{-3}$.

As noted by Boone (2008), analysis of the Chicago structure as a beam, using the beam analysis with the deflection ratio, Δ/L, underestimates the actual damage level. The beam analysis assumes that the chord of the settlement across the structure represents tilt, and distortions are equal and opposite at the ends of the beam as illustrated in Figure 5b. Based on this assumption, the tilt is relatively high ($1.2 \ x10^{-3}$), which, when subtracted from the bay 1 settlement slope of $2.7x10^{-3}$, results in an angular distortion of $1.5 \ x10^{-3}$, in the very slight range (Point B1 in Figure 2).

The distortion pattern was more typical of Figure 5a, where unit 2 tilts but does not distort. Although there is no information on the actual tilt of the structure, it appears from the building sections and the steeper settlement profile near the excavation wall that distortions would be concentrated in the first bay of the structure and that the tilt would be represented by the slope of the 2nd and 3rd bays. Their tilt was relatively low ($0.3 \ x \ 10^{-3}$), which when subtracted from the settlement slope of $2.7x10^{-3}$ in bay 1 results in an angular distortion of $2.4x10^{-3}$ (Point B2 in Figure 2), in the slight damage range, consistent with the observed damage.

Structural analysis of the building confirmed that the distortions were concentrated in the first bay. Finno, et al, used a laminate beam model to analyze the structure in which the floors of the building acted as diaphragms and shear displacements predominated, and obtained results close to those that were observed for the onset of cracking. Boone analyzed the structure using his strain superposition approach and also obtained results consistent with the observed damage.

Reduction in lateral strain due to building stiffness

In cases where the building is relatively stiff, the green-field ground movements will be modified, and the distortions of the structure will be less than those estimated assuming the structure conforms to the shape of the green-field settlement profile. Boscardin and Cording (1989) give a relationship between the axial soil/beam stiffness of grade beams and the reduction in lateral building strain from the green-field lateral ground strain. Large reductions in lateral strain imposed by the ground will result if the foundation has grade beams, reinforced wall footings, or structural slabs on grade. In such cases, the lateral strain across the structural unit can be assumed zero. Additionally, the lateral strain imposed by the ground or by bending in the upper portions of a building will be reduced if the upper floors are reinforced and tied to the walls. Such a condition existed in the case of the school described above (Finno, et al, 2004), and in the case of a 3-story apartment building in Evanston, Illinois constructed in the early 1900s, described in a following section entitled "Brick bearing wall structures with concrete floors." In both cases shear distortions developed in the portion of the building nearest the excavation or tunnel subjected to the greatest angular distortion.

Reduction in angular distortion due to building stiffness

Parametric studies using a series of UDEC analyses were conducted to evaluate the reduction in the ratio of angular distortion, β, with respect to the change in greenfield ground slope, ΔGS, between adjacent structural units due to the shear stiffness of a masonry bearing wall for both downdrag cases and no downdrag cases.

The ratio is a function of relative building/soil shear stiffness and also the level of distortion and cracking in the structure. Window penetrations of 30% will reduce the effective building shear stiffness.

For a medium to stiff soil, and structure with lime rich mortar (type N), the soil/wall shear stiffness is $E_S L^2/GHb = 10$, where E_S is soil stiffness, L is the distorted span of the structure, G is the effective shear stiffness of the building, including reduced stiffness due to window penetrations, H is building height, and b is the width of the wall. For this stiffness, cracking results in $\beta/\Delta GS = 1$. The value of $\beta/\Delta GS$ reduces to less than 0.5 only for elastic deformations or for very small cracks at very low values of ΔGS. For a stiffer wall or softer soil ($EsL^2/GHb = 1$), $\beta/\Delta GS = 1$ for larger changes in ground slope ($\Delta GS \geq 3x10^{-3}$) and $\beta/\Delta GS$ reduces to less than 0.5 for $\Delta GS \leq 1.5x10^{-3}$ (Son and Cording, 2005, Cording et al, 2008).

Era and type of building construction

Brick bearing wall structures with timber floor joists. A large number of brick bearing wall structures were constructed in cities and towns throughout the U.S. in the mid to late 1800s and early 1900s. They usually have only one basement level, and the brick walls are on brick or rubble wall footings, although in some cases, structures are on timber piles.

In the early 1800's, many of the brick bearing wall buildings in older towns along the eastern seaboard had both bearing and facade walls tied together with a pattern of alternating headers and stretchers (Flemish bond).

In the late 1800's and early 1900's, the hidden walls (party walls, alley walls and basement walls) of almost all the masonry structures in the U.S. consisted of a common bond consisting of multiple wyths of stretchers tied together, usually every 6 rows, with a row of headers. The building facades were cladded with a veneer of a running bond (stretchers, no headers) mortared against the common brick wall behind the façade.

When evaluating buildings adjacent to a proposed excavation, existing damage and deterioration need to be recorded so that they can be separated from any damage that results, or is alleged to result, from the adjacent excavation and, in addition, to determine if the structure's condition will affect its response to excavation-induced ground movements. Over the long term, façade walls with brick cladding tend to be more susceptible to cracking or displacement due to deterioration and environmental effects than the common brick walls. Separation of the brick or stone cladding on the façade from the common wall behind, as well as separation of the façade wall from a perpendicular bearing wall can occur due to deterioration or distortion. Often, the brick cladding, although mortared against the common wall behind, is not well tied to the common wall. Details of window support are important, and their condition is often unrelated to settlement. Wood lintels are subject to shrinkage and can cause cracking and lateral displacement of a wedge of bricks above the windows. Iron or steel angles placed as a lintel to support the brick may be subject to rust jacking if leakage occurs, which causes the brick above the lintel to be pushed outward.

Brick-bearing wall townhouses built in the 1800's and early 1900's typically have bearing walls with timber joists spanning approximately 6 m between adjacent brick bearing walls. The joists are seated in pockets on the bearing wall, usually one wyth (100 mm) wide. The joists are set in the pocket, they are not usually tied to the wall, unless the wall has been repaired or retro-fitted. One of the critical concerns is rotting of the joist ends due to water and moisture coming through the wall or leaking from drains. The end of the joist may have a tapered fire cut (shorter joist length at the top) that allows it to fall out of the wall more readily in a fire, without causing the wall to collapse, an important detail that would prevent progressive collapse of a row of townhouses with common bearing walls during a fire.

Larger masonry bearing wall structures. Structures with wider spans may have an intermediate timber bearing wall between the exterior brick bearing walls. In some structures, the upper level floors sag toward the center of the building because of shrinkage of the timbers. This is the case for several of the historic houses in Washington DC, built in the early 1800's. Door frames were observed to have undergone shear distortion, with the side of the door frame toward the center of the building displacing downward due to the sag in the center of the building.

Larger commercial brick bearing wall structures in the 1800's had intermediate supports of timber posts and beams supporting the timber floor joists between brick bearing walls. Monumental structures, such as the Masonic Temple built in 1870 in Philadelphia had masonry bearing walls and floors consisting of I beams spaced approximately 1.2 to 1.5 m on center with jacked arches of brick between the beams, set on the lower flange. For the Masonic Temple, the beams were seated in pockets in the brick bearing walls but were not tied so that lateral displacement and settlement of the bearing wall during pit underpinning produced the damage shown in Figure 1a.

Bearing wall perpendicular to excavation, lateral displacement reduces floor-joist bearing. Figures 7a and 7b illustrate a case where bearing walls perpendicular and adjacent to an unsupported basement excavation were subject to settlement and lateral displacement in the range of 40 to 75 mm. The lateral displacement at the building foundation wall caused loss of 58 mm of joist bearing at the first floor level, reducing the remaining joist bearing to less than 50 mm. The joists on all floors had to be supported with temporary posts and beams and the building was subsequently demolished. The average lateral strain between adjacent bearing walls exceeded 10×10^{-3}, in the very severe damage range (point D1, off the plot in Figure 2).

ε_L > 57 mm/ 6m = 10 x 10^{-3} - Very severe damage, loss of joist bearing

Figure 7. Concentrated lateral and vertical displacement of bearing wall

Brick bearing wall structures with concrete floors. In the early 1900's, many of the larger brick bearing wall structures were constructed with reinforced concrete floors. In some structures a T beam was formed by rows of clay tile set in the bottom of the form to fill the space between the concrete beams. Some of the floors structures consisted of T beams with a top slab of concrete and the T consisting of an I beam encased in concrete. Concrete floors, unlike timber joists, were tied to the masonry walls preventing lateral extension and loss of bearing of the floors.

One such structure, a 3-story apartment structure built in the early 1900's in Evanston, Illinois, had no grade beams or structural slabs in the basement floor, but upper floors were concrete and tied into the brick bearing walls. Tunneling in the street adjacent to the building resulted in a settlement of 30 mm and a lateral extension in the 11.7 m wide bay of 17 mm that produced cracking of the basement slab and opening of cracks on the wall perpendicular to the tunnel axis. A vertical crack, open 5 mm at the basement level between bays 1 and 2, narrowed and ultimately terminated at the level of the reinforced concrete floor. Angular distortions at foundation level in the first bay were 2.7×10^{-3} and lateral strains were approximately 2×10^{-3} (moderate damage, Point E1 in Figure 2). A diagonal shear crack, open 5 mm, developed in the brick of the exterior wall, immediately adjacent to the bearing wall nearest the tunnel at the ground level, and there was some shear cracking and fall of plaster in a third floor apartment. In the upper floors, the absence of lateral strains reduced the damage level from that observed in the first floor level (slight damage, Point E2 in Figure 2).

The connection of the floor to the wall should be checked. In one case, post-tensioned pre-cast concrete T beams were attached to a concrete block wall with a short rebar that was embedded in the bottom of the beam but not tied to the reinforcement. Lateral extension of 25 mm across the bay of the structure could not be caused a continuous crack to form at the end of the beam, separating the beam from the wall. Temporary posts were placed on all the beams to prevent collapse.

Extension of cracks and lateral displacement in upper floor levels

Tunneling beneath 7th St with an open face shield in sands on the first phase construction of the Washington Metro in the early 1970's resulted in running of the sands into the tunnel face and surface settlements on the order of 70 mm of an adjacent brick bearing wall building (Figure 8). Cracks of 50 mm developed in the basement wall due to lateral ground displacement. Both angular distortion and lateral strain at the foundation of the building are on the order of $10x10^{-3}$ (point F1, off the chart in Figure 2). The settlement resulted in diagonal shear cracks in the first and second vertical rows of windows located on the bearing wall adjacent to the façade. Shear displacements were concentrated near the façade wall as a result not only of the low shear stiffness of the windows, but also the downdrag of the façade wall on the bearing wall. The building behaves as a box structure, not as a single wall or beam. The shear cracks extended almost to the roof of the four story building and separated the façade wall from the bearing wall, causing an outward lateral displacement of 25 mm near the top of the façade wall (Point F1 in Figure 2). Fall of portions of the cornice and bulging of the masonry finishes developed.

Minor bending cracks developed at the top of the bearing wall, toward the center of the building. Based on the estimated curvature across the structure, the lateral strain at the top of the bearing wall is $1.8x10^{-3}$, (moderate damage, Point F2 in Figure 2). Other buildings along the street were similarly affected by the large shear distortions and lateral strains at the building wall. Facades and cornices required temporary bracing and ties to prevent their collapse.

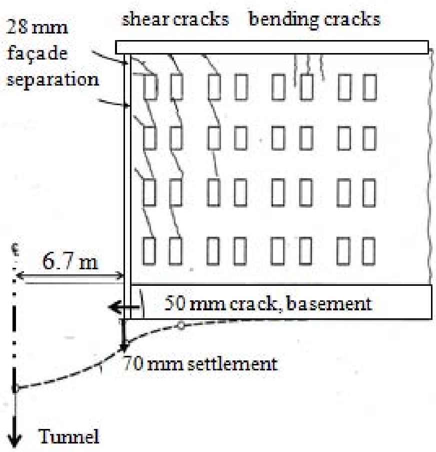

Figure 8: Washington Metro, 7th Street, bearing walls perpendicular to tunnel: shear cracks over height of wall caused façade wall to displace laterally.

The effect of downdrag is illustrated by two UDEC numerical analyses of a 4-story brick bearing wall structure (Son, 2004). Figure 9a shows the results for no façade wall downdrag. Maximum settlement was 34 mm and angular distortion in the first bay was $1.4x10^{-3}$. Shear cracks were concentrated in the second vertical row of windows from the façade wall. Lateral strain was $1x10^{-3}$ at foundation level of the first bay and in the upper level of the first bay (Slight damage, point G in Figure 2).

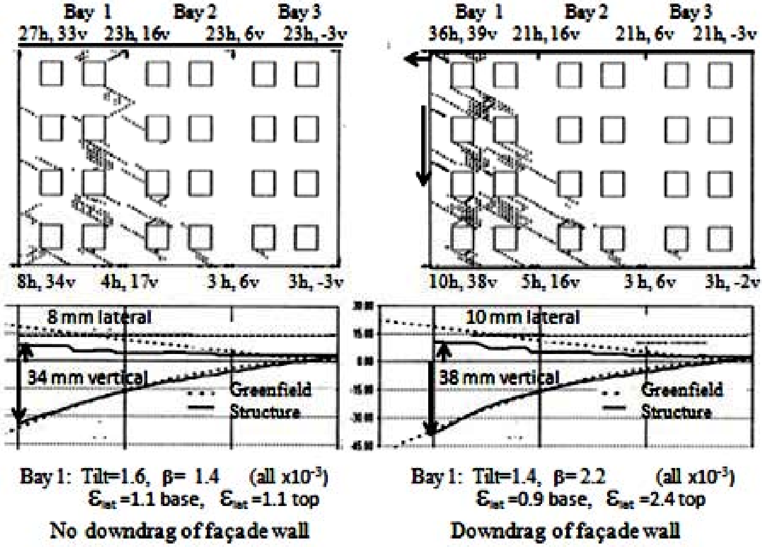

Figure 9: Numerical analysis of brick bearing walls

Figure 9b illustrates the effect of downdrag of the façade wall on the same structure. Downdrag of the façade caused slightly greater settlement at the wall (38 instead of 34 mm) and higher angular distortion in the first bay ($2.2x10^{-3}$). Lateral strain at the foundation level of the first bay was $0.9x10^{-3}$) (Point H1 in Figure 2) and lateral strains increased to 2.4x10-3 in the upper row as shear cracks caused separation of the portion of the wall nearest the façade wall (Point H2 in Figure 2).

Separation and rotation of either a non bearing façade wall or a bearing walls can occur due to settlements caused by excavation or tunneling. Lateral displacements can occur on the upper wall with the propagation of shear fractures or as a result was of pre-existing weaknesses on or between the walls or at the connection between the wall and floors. Structural floor diaphragms tied to walls prevent such cracks. Even for the older brick bearing wall structures, loaded floor joists, roof structures, or cross walls perpendicular to the displacing wall may reduce the opening of cracks due to bending. Investigation of the wall/floor connections and the condition of the building allows the potential strain distributions in the structure to be estimated.

When undergoing settlement, brick walls may rotate outward at the top when the following conditions are present:

1. For façade walls:
    a. Poor or deteriorated connection of façade wall to bearing wall
2. For bearing walls: floor joists seated in the bearing wall may prevent outward displacement, except when the follow occurs:
    a. Low floor loads on joists seated on the bearing wall,
    b. Intermediate walls, such as cross walls or non bearing walls pick up the load of the floor joists as the bearing wall settles causing the joists to become unloaded on the bearing wall.
    c. Water causes rotting and loss of joist bearing in their seats.

   d. Floor joists are absent due to open areas, such as stair wells, adjacent to the wall.
3. For both bearing and façade walls:
   a. Reduced strength of bond between bricks in side walls due to uncontrolled drainage off roof, water damage, deterioration, lack of maintenance, lack of repointing of mortar joints in the side wall.
   b. Downdrag, angular distortion, and lateral strain result in shear and tension cracks extending over the height of the side wall, usually between window openings close to the end wall.

CONCLUSIONS

Understanding the characteristics of structures from a given period and in a given region or country --- both how they were built and how they deteriorate and are maintained --- will aid in determining the potential strains and distortions within the structure for assumed greenfield ground displacements. Structural and ground/structure analyses for structural types adjacent to the project site, or for specific structures can follow as needed. In both cases, the damage criterion based on strain and distortion within bays or units of the structure can be utilized. The following outlines steps in the process of evaluating potential distortions and damage.

1. Determine if structure is within the estimated width of the settlement profile.
2. For structures within the anticipated settlement zone, a first level of evaluation is to impose the estimated ground settlement and lateral displacement on the structure.
   a. The volume of lateral soil displacement is estimated from the wall type, wall stiffness and support installation sequence. For sandy and stiff soils, the volume of surface settlement, Vs will approach the volume of wall displacement, V_L, as the wall displacements increase. For soft clays, Vs/VL = 1, and will increase with time due to consolidation.
   b. For a parabolic settlement profile, the maximum surface settlement is 3Vs/L, where L is the length of the settlement profile, and the slope at a distance, x from the wall is 2(1-x/L). Lateral displacements can be estimated in the range of 0.5 to 1.0 times the settlement for bulging wall displacements. For a bay close to the excavation that is less than half the length, L, of the settlement profile, a maximum slope in the range of 1.5 to 2 times the average slope, δ_{max}/L.
   c. Assuming the building distorts with the ground and spans beyond the settlement zone, estimate building distortions and strains equal to the ground slope and lateral ground strain. The average slope across the settlement profile may be used, but, if bays or building units are significantly narrower than the settlement profile, the slope across the bay should be estimated.
3. Distortions will be reduced from those estimated in item 2 if the settlement profile is wider than the structure. Determine the expected changes in ground slope and potential tilt across units or bays of the structure. In selecting the building units that will tend to concentrate distortion or lateral strain, consider geometry and weaknesses in the structure (spacing of columns or bearing walls, presence of construction joints, stair wells, connection of brick cladding to wall).
4. Assess condition of the structure: pre-existing distortion and displacements, cracking of masonry and finishes, deteriorated masonry, leakage through walls, rotted floor joists, damaged lintels above windows and doors.

5. Consider lateral strains in upper levels of structure
   a. Due to bending of a beam with displacement pattern imposed over a large L/H value, and weak in tension
   b. Due to rotation and opening along shear cracks or pre-existing weaknesses within or between walls. Consider influence of downdrag and amplification of strains with increasing ground displacement.
6. Reduce lateral strains due to lateral and bending stiffness of the structure:
   a. If there is a structural grade beam or reinforced continuous foundation, then lateral ground strains can be ignored. Lateral displacements will concentrate at construction joints, if present.
   b. In frame structures, or structures with concrete floors tied to the wall, significant lateral strains due to bending or lateral ground strain will not develop in the upper levels of the frame. The detail of the wall/floor connections should be checked.
   c. For a frame with columns on isolated foundations, lateral ground displacements will be imposed on the lower level columns, and can cause bending and damage to the columns.
   d. In brick bearing wall structures with joists in seats, lateral strains in upper floors may be low if there is sufficient load on the joists to keep walls from displacing or if structure has been retrofitted by tieing joists to walls.
7. Reduce Angular distortion, β, due to shear stiffness of the structure.
   a. $\beta/\Delta GS$ reduces to less than one with reduction in E_sL^2/GHb.
   b. $\beta/\Delta GS$ increases to one with increasing ΔGS due to cracking of masonry, which reduces shear stiffness.
   c. Consider shear stiffness due to strength of mortar, percentage of window penetrations, presence of shear walls and infilled walls, and retrofitting with diagonal braces. (Braces set in second bay to reduce drift during seismic events will not increase stiffness of first bay, rather, shear strains due to settlement may be concentrated in first bay.)
8. Select specific structures or classes of structures for a detailed structural analysis in which strain distributions throughout the structure are determined based on building geometry and stiffness.

In the cases illustrated, the structures themselves served as indicators of the type and causes of distortions and damage that were imposed on them. The ability to observe and read the building response is aided by an understanding of the chain of relationships that extends from the excavation wall to the building distortion and damage.

Excavation wall stiffnesses and construction practices should be required that limit wall movements and prevent unacceptable building response. Observations and analysis show that ground movements as well as distortions and building damage are non-linear and increase at an increasing rate as the magnitude of wall displacement increases.

To properly assess building behavior – both distortion and damage -- it is necessary to understand not only the ground movement patterns but also the building's structural characteristics and finishes: when and how the building was built, maintained, and repaired. Often the effects of excavation are superposed on pre-existing distortions and deterioration. In many cases, pre-existing conditions are separate from, and unrelated to, the excavation-induced damage. In other cases, the deterioration of the building reduces its strength and stiffness, causing more severe distortion and damage for relatively small displacements.

ACKNOWLEDGMENTS

The research on excavation-induced building damage was conducted at the University of Illinois at Urbana-Champaign with the support of the National Science Foundation and Schnabel Foundation Company.

REFERENCES

Boone, S.J. (1996). "Ground-Movement-Related Building Damage," *Journal of Geotechnical Engineering*, ASCE, Vol 122, No. 11, pp 886-896.

Boone, S.J. (2008). "Evaluating Risks of Construction-Induced Building Damage for Large Underground Construction Projects," *Jornada Tecnica 16-12-08, Movimientos de Edificios Inducidos por Excavaciones: Criterios de dano y gestion del riesgo,* Escola Tecnica Superior d'Enginyers de Camins, Canals i Ports de Barcelona, Universitat Politecnica de Catalunya.

Boscardin, M. & Cording, E. J. (1989). "Building Response to Excavation-Induced Settlement," *Journal of Geotechnical Engineering, ASCE,* Vol. 115, 1-21, January.

Burland, J.B and Wroth, C.P. (1974). "Settlement of Buildings and Associate Damage," *Proceedings of a Conference on Settlement of Structures*, Cambridge, pp. 611-654.

Burland, J. B., Broms, B. B., & De Mello, V. F. B. (1977). "Behavior of foundations and structures," *State of the Art Report. Proc. 9th Intl. Conf. on Soil Mech. and Foun. Engr.,* II, 495-546, Tokyo.

Burland, J.B. (1995), "Assessment of risk of damage to buildings due to tunneling and excavation," *Proceedings of 1st International Conf. on Earthquake Geotechnical Engineering*, IS-Tokyo.

Burland, J. B. (2008). "The assessment of the risk of damage to buildings due to tunnelling and excavation." *Jornada Tecnica 16-12-08, Movimientos de Edificios Inducidos por Excavaciones: Criterios de dano y gestion del riesgo.* Escola Tecnica Superior d'Enginyers de Camins, Canals i Ports de Barcelona, Universitat Politecnica de Catalunya.

Clough, G.W. and O'Rourke, T.D. (1990), "Construction induced movements of insitu walls," *Geotechnical Special Publication*, ASCE, No. 25, pp.439-470.

Cording, E. J., Long, J. H., Son, M., and Laefer, D. F. (2001). "Modeling and analysis of excavation-induced building distortion and damage using a strain-based damage criterion," *London Conference on Responses of Buildings to Excavation-Induced Ground Movements,* Imperial College, London.

Cording, E. J., Son, M., Laefer, D.F, Long, J. H, and Ghahreman, B. (2008). "Examples of building response to excavation and tunneling," *Jornada Tecnica 16-12-08, Movimientos de Edificios Inducidos por Excavaciones: Criterios de dano y gestion del riesgo.* Escola Tecnica Superior d'Enginyers de Camins, Canals i Ports de Barcelona, Universitat Politecnica de Catalunya.

Finno, R. J., Voss, F, T, Rossow, E. and Tanner J. (2005). "Evaluating Damage Potential in Buildings Affected by Excavation," *Journal of Geotechnical and Geoenvironmental Engineering*, ASCE, 131(10),1199-1210.

Ghahreman, B. (2004) "Analysis of ground and building response around deep excavations in sand." *Ph.D. Thesis*, University of Illinois at Urbana-Champaign.

Hashash, Y. and Whittle, A. (1994), " XXX

Laefer, D.F. (2001). "Prediction and assessment of ground movement and building damage induced by adjacent excavation." *Ph.D. Thesis*, University of Illinois at Urbana-Champaign.

Milligan, G.W.E. (1974). “The behavior of rigid and flexible retaining walls in sand,” *Ph.D. Thesis,* Cambridge University.

Mueller, C. G., J. H. Long, E. J. Cording, and D. E. Weatherby, (1994), "Ground Movements from Tieback Wall Construction," *ASCE Symposium on Vertical and Horizontal Deformations for Foundations and Embankments*, Geotechnical Special Publication No. 40, pp. 1337-1352.

O'Rourke, T.D. and Cording, E. J., (1974). “Observed loads and displacements for a deep subway excavation. *Proc. 2nd Rapid Excavation and Tunneling Conference*, Vol. 2, Ch. 84, San Francisco.

O’Rourke, T. D., Cording, E. J. and Boscardin, M., (1977). “Damage to brick-bearing wall structures due to adjacent braced cuts and tunnels,” *Conference on large ground movements and structures*, UWIST and Institution of Civil Engineers, Cardiff, July.

Peck, R. B. (1969). “Deep excavations and tunneling in soft ground, State of the Art,” *Proc. 7th Intl Conf. on Soil Mech. and Found. Engr.*, p.225-290, Mexico City.

Powderham, A., Huggins M. and Burland, J. B. (2004), Induced subsidence on a Multi-storey car park, *Proc. Intl. Conf. on Advances in Geotechnical Engineering, The Skempton Conference*, Thomas Telford, London, pp 117-1130.

Skempton, A.W. and MacDonald, D.H (1956), “The allowable settlements of buildings,” *Proc. Inst. of Civ. Engrs*. Part II, 5, 727-768.

Son, M. (2003). “The response of buildings to excavation-induced ground movements.” *Ph.D. Thesis,* University of Illinois at Urbana-Champaign.

Son, M. and Cording (2005), “Estimation of Building Damage to to Excavation-Induced Ground Movements,” *Journal of Geotechnical and Geoenvironmental Engineering*, 133(8), 995 -1002.

Recommendations for Assessing Bending Moments for Stiff Wall Systems

A. Liu[1], C. Pound[2] & M. Wongkaew[3]

[1]Hatch Mott MacDonald, Los Angeles, CA, andrew.liu@hatchmott.com
[2]Mott MacDonald, Croydon, UK, chris.pound@mottmac.com
[3]Hatch Mott MacDonald, Seattle, WA, mike.wongkaew@hatchmott.com

ABSTRACT

Empirical Apparent Earth Pressure (AEP) diagrams, such as those proposed by Terzaghi and Peck (1967), are regularly used for assessing support loads for propped or anchored retaining structures. This approach has been used successfully on many flexible wall projects over the years in the United States. Initially developed for assessing support loads, these diagrams are now commonly being used to assess bending moments and shear forces developed in the retaining structures by application of the AEP diagrams to a beam simply supported at the position of each of the struts or tiebacks (Sabatini et al., 1999). While this approach may achieve satisfactory results for relatively flexible wall systems, many authors have recommended more sophisticated analysis methods for stiff wall systems.

This paper presents the results of comparisons of the empirical AEP diagram with a beam on rigid supports (RIGID) analysis to "beam on spring" (Winkler) and numerical analysis methods for the assessment of structural forces in deep multi-propped excavations. Comparisons are provided for a stiff slurry diaphragm wall system and a flexible soldier pile and lagging wall system. For the stiff slurry diaphragm wall with tiebacks, the RIGID approach was found to be highly non-conservative for estimating bending moments in the retaining structure. The reason for this is shown to relate to the staged excavation, tieback installation sequence adopted, and locked-in deformation of the ground below the excavation level, which are not considered in the RIGID analysis. The Winkler and numerical analyses, however, both consider these effects and result in global deflection of the wall which in turn leads to large bending moments. The analyses show that the magnitude of these deformation-induced bending moments far exceed those resulting from the distributed load between rigid supports. For the flexible soldier pile with lagging wall, the RIGID analysis still estimated smaller bending moments than the Winkler or numerical approach but by a much smaller degree of difference than the stiff diaphragm walls. In view of the limitations associated with using AEP diagrams with the RIGID analysis for stiff wall systems, it is recommended that a more sophisticated analysis method be the minimum requirement for assessing structural forces in these walls.

BACKGROUND AND STATE OF PRACTICE

Apparent Earth Pressure (AEP) diagrams proposed by Terzaghi and Peck (1969) were initially developed for assessing excavation support (bracing or tieback) forces of relatively flexible retaining structures with regular support spacing, open-sheeting, and penetration into a competent stratum. Though intended for estimating support forces, AEP diagrams have been used successfully in conjunction with a beam on rigid support

(RIGID) analysis for assessing bending moments and forces in flexible walls for many years. Because of the success and simplicity of this approach for flexible wall systems, its usage started being carried over to the design of stiff wall systems.

However, because of inherent problems with transferring this approach from a flexible wall system to a stiff wall system, multiple authors provided warnings against the usage of AEP diagrams with a RIGID analysis for stiff walls such as slurry diaphragm walls (Kerr and Tamaro, 1990; Tamaro and Gould, 1992; Ratay, 1996; Strom and Ebeling, 2001, 2002; and Mikhail et al, 2000). Despite these warnings and the rise of usage of slurry diaphragm walls in the United States for sensitive structures such as building basements and underground transit stations, many practitioners continue to use this approach with the common misconception that AEP diagrams were developed as an envelope of all wall systems. The following sections present comparative analyses conducted to quantify the underestimation of bending moments described by the above authors.

COMPARATIVE APPROACH

To assess the differences between common approaches used in current practice for estimating bending moments, a series of comparative analyses were performed for a stiff slurry diaphragm wall. Three approaches were used for comparison as follows:

1) RIGID analysis consisting of a continuous beam on rigid supports with AEP diagram,
2) A beam on elastic foundation (Winkler analysis), and
3) A finite difference numerical analysis.

The RIGID analysis is the subject of this paper and applies an AEP diagram, as shown in Figure 1, on a beam with rigid supports at locations of bracing or tiebacks. Because of the rigid supports, the displacements at these locations are always equal to zero, which result in moment reversals. At the point of zero net pressure below subgrade (where the earth pressure on the active side is equal to the earth pressure on the passive side), a fictitious support is assumed and the wall below this point is neglected in the analysis (Kerr and Tamaro, 1990). While this method is easy to use, it does not provide any wall or ground movements and is known to be the least accurate of the three for predicting bending moments.

The second method is the beam on elastic foundation, or the Winkler approach. This approach uses a continuous beam where the brace supports are represented by a spring with a k value and the active pressures and passive resistance are represented by a series of soil springs that are a function of the soil's modulus of subgrade reaction. This method provides more realistic strut reactions at lower levels compared to the RIGID analysis and also provides insight for inward wall movement and therefore wall bending moments.

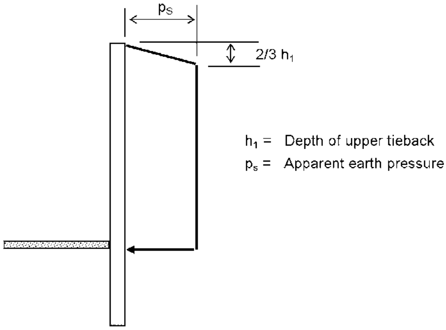

Figure 1. AEP diagram applied to RIGID analysis.

The third method is a numerical approach by finite difference method (FDM). This method depends on user-inputted in-situ stress conditions, soil strength and deformation properties, and groundwater levels but derives earth pressures from the results of the analysis. The ability to compute earth pressures for a specific stage of excavation allows the wall to be analyzed at a more realistic state of stress. The method also computes wall and ground movement, which are dependant on the soil deformation properties entered. While the requirement for soil deformation properties may make this application impractical for smaller projects, the cost and time associated with running the numerical analysis is becoming less cumbersome with modern computing speeds and increased familiarity.

For the comparisons presented in this paper, the RIGID analyses were carried out manually with a spreadsheet implementing a stiffness matrix analysis of a continuous beam on rigid supports being loaded by pressures derived from AEP diagrams. The Winkler analyses were carried out using the computer program WALLAP (Geosolve, 2005) and the numerical analyses were carried out using the finite difference program FLAC (Itasca, 2007). The analyses considered the excavation of a 19m deep excavation in a sequence of clays, sands and gravels. The geotechnical properties adopted in the Winkler and numerical analyses are provided in Table 1. The excavation is supported by an approximately 1m thick slurry wall with nine levels of tie-backs.

The analyses assume that excavation progressed 0.6m below the level of the relevant tieback prior to tieback installation. The tiebacks have a cross-sectional area of 5.6 cm^2 for the upper 6 levels of tiebacks and 7 cm^2 for the lower 3 levels of tiebacks. The unbonded length and prestress force for the tiebacks are provided in Table 2. All tiebacks were modeled at an angle of 15° measured from the horizontal.

Table 1. Geotechnical Properties

Stratum	Unit (kN/m^3)	Young's Modulus Top (MPa)	Young's Modulus Increase (MPa/m)	Poisson's Ratio	Cohesion (kPa)	Friction (°)	Coefficient of Earth Pressure at rest
CL1	18.8	42		0.25	0	32	1
SM1	18.8	76		0.3	0	33	1
CL2	18.8	42		0.25	0	32	0.92
CL3	20.1	46		0.25	0	32	0.7
CH1	20.1	52	0.18	0.25	0	28	0.7
CL4	20.1	64	0.29	0.25	0	32	0.7
SM2	20.1	174	0.3	0.3	0	33	0.7
CL5	20.1	104	0.18	0.25	0	32	0.7
SG1	20.1	212	0.42	0.3	0	37	0.7
CL6	20.1	137	0.2	0.25	0	32	0.7
SG2	20.1	268	0.42	0.3	0	37	0.7
CL7	20.1	179	0.29	0.25	0	32	0.7
CH2	20.1	229	0.19	0.25	0	28	0.7

Table 2 – Tieback unbonded lengths and pretension forces

Tieback Level	Unbonded Length (m)	Pretension Force (kN)
1	20	516
2	18	494
3	17	525
4	15	507
5	14	489
6	12	552
7	10	641
8	8	703
9	6	770

RESULTS

The resulting bending moments from the three comparative methods are shown in Figure 2. As seen in this figure, there is a major difference in the predicted magnitude and distribution of bending moments between the RIGID approach and the other two approaches. Though bending moments were only computed at the supports for the RIGID analysis, it is clear that the maximum bending moment will occur at these points. For the RIGID analysis, the maximum bending moment is 100 kN-m/m whereas for the Winkler approach and numerical approach, the maximum bending moments range between 1000 kN-m/m to 1300 kN-m/m. It is important to note that the face of the wall with the maximum predicted tensile stress is the soil face in the RIGID analysis and the excavation face in the Winkler and numerical approaches.

It is also important to note that the Winkler approach and numerical approach yield similar bending moment estimates. This is largely due to the fact that the Winkler approach was carried out assuming staged construction and incremental installation of tiebacks similar to the numerical analysis. The two methodologies only have minor differences with slightly higher bending moments in the Winkler analysis that may be explained by reviewing the wall deflections at the final stage of excavation shown in Figure 3. This figure shows reasonable similarity between the two wall deflection profiles, with the maximum movement for both curves occurring near the final excavation level. However, near the top of the wall, the Winkler analysis predicts that the wall will move towards the soil, whereas the numerical analysis predicts that the wall will move towards the excavation. Evaluation of the numerical analysis at earlier stages in the excavation sequence shows that the wall also moves towards the soil during pre-stressing of the tiebacks but begins to move away from it as the excavation proceeds. This greater restraint at the top of the wall in the Winkler approach is presumably the reason for the slightly higher bending moments shown in Figure 2. However, the general comparison between a Winkler approach that accounts for excavation sequence and a numerical approach does not yield significantly different results.

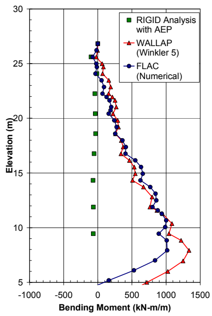

Figure 2. Stiff wall Bending moments.

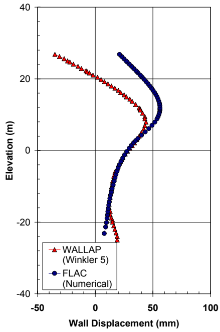

Figure 3. Stiff wall Displacements.

With that, we use the simpler Winkler approach for further analysis to obtain a better understanding of the key reasons for the difference between the RIGID analysis and the Winkler and numerical analyses. To do this, the Winkler analysis was repeated multiple times with modifications to make the analyses more similar to the RIGID analysis. Five analyses were carried out as follows:

Winkler 1: An initial analysis assuming an arbitrarily very stiff, strong rock below excavation level with very stiff strut supports (9 in total) located at the tieback elevations. All elements of the structure including surcharge and ground water levels were ‘wished in place’ without considering excavation sequence.

Winkler 2: The same as Winkler 1, but with actual soil properties substituted for the arbitrary rock properties below excavation level.

Winkler 3: The same as Winkler 2, but with the excavation and strut installation being carried out in progressive stages. This also involved lowering the water table progressively on the passive side with the phreatic surface being maintained approximately 0.6m below the relevant excavation level. Note that this case continued to retain the very stiff strut supports adopted in Winkler 1.

Winkler 4: The same as Winkler 3, but with untensioned tiebacks substituted for the very stiff strut supports assumed above.

Winkler 5: The same as Winkler 4, but with pretensioned tiebacks with the unbonded lengths and pretensioning values being those adopted in the original analysis.

Figures 4a and 4b show the predicted wall deflections and bending moments for the five Winkler analyses described above. From these results, the following conclusions can be drawn:

1. With very stiff supports, stiff ground in the passive zone and wished-in-place construction sequence the deflections and bending moments are similar to the RIGID analysis.

2. Modeling of realistic soil stiffness in the passive zone increases deflections and bending moments at excavation level.

3. Modeling of sequential excavation and installation of struts increases deflections and bending moments significantly.

4. Use of untensioned tiebacks result in larger movements and bending moments.

5. Pre-tensioning of tiebacks significantly reduces deflections and maximum bending moments.

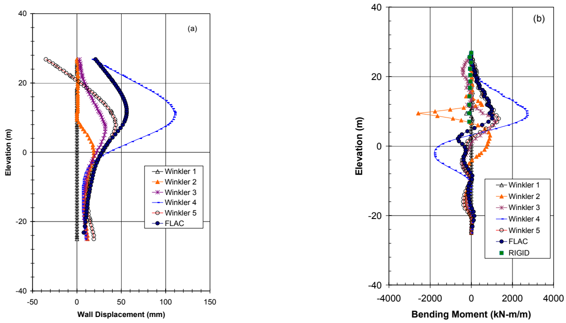

Figure 4. Wall displacement (a) and bending moments (b) from Winkler 1 – 5 analyses.

For comparative purposes, the original analyses were made for a flexible soldier pile (HP14 x 89 at 1.8m centers) with lagging system which has a stiffness value approximately 38 times smaller than the slurry diaphragm wall system. The resulting maximum bending moments for the flexible wall, as shown in Figure 5, are much smaller than bending moments of the stiff wall and the underestimation by the RIGID approach is far less pronounced for the flexible wall. In fact, the RIGID analysis provides a comparable estimate for the upper 12m in the case of the flexible wall.

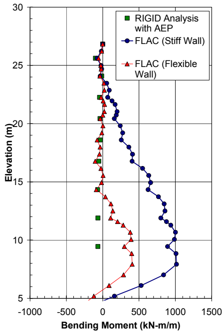

Figure 5. Comparison of bending moments for stiff and flexible wall.

LIMITATIONS WITH A RIGID ANALYSIS USING AEP DIAGRAMS

The preceding sections have shown the significant limitations with the RIGID analysis using AEP diagrams. As the name of the pressure diagrams indicate, these are apparent earth pressures based on the loads measured in struts and do not necessarily represent accurately the actual earth pressures applied to the wall. The actual earth pressures applied to the wall depend on many factors including the nature of the soil (including the at rest state of stress) the stiffness of the wall, the support system and the excavation sequence including dewatering.

Potentially of greater significance to this approach though are the oversimplifying assumptions of the RIGID analysis itself. The assumption of rigid supports that cannot deflect at tieback locations results in smaller bending moments and moment reversals. In addition, the RIGID analysis does not consider that the support system is incrementally installed but assumes that the wall, supports and excavation are wished-in-place. The method therefore cannot determine the wall movements occurring before installation of the supports and as a result does not correctly calculate the bending moment associated with the global wall movements. In principle an analysis of this form could be carried out with a modified RIGID analysis with non-rigid supports, by considering each of the stages of excavation as a separate AEP analysis with the appropriate number of supports in place at each stage and with the deflection state for the previous stage considered as the starting point of the next, but this would approach would require more effort than a Winkler analysis and also be more prone to produce inaccurate results.

Finally, the RIGID analysis does not adequately consider movements and support to the wall below the base of the excavation. The development of earth pressures below excavation level can be complex depending on the soil types, groundwater conditions and wall stiffness and is shown to have a substantial impact on bending moments. Also, movement of the wall is governed not only by the earth pressure mobilized on the active and passive side of the wall, but also by heave of the ground beneath the excavation. This factor can only be fully considered by numerical analysis.

CONCLUSION AND RECOMMENDATIONS

This paper presents the results of a comparison of the empirical Apparent Earth Pressure (AEP) diagram combined with a RIGID analysis to "beam on spring" (Winkler) and numerical analysis methods for the assessment of bending moments in a deep multi-propped excavation. For the example chosen of a stiff slurry wall with tiebacks, the RIGID approach was found to be highly non-conservative for estimating bending moments in the retaining structure. The reason for this difference is shown primarily to relate to the staged excavation, tieback installation sequence adopted, and locked-in deformation of the ground below the excavation level. These features are not considered in the RIGID analysis method and result in global deflection of the wall which in turn leads to large bending moments. The analyses show that the magnitude of these deformation-induced bending moments far exceed those resulting from a distributed load between rigid supports. Though the limitations are significantly more pronounced for stiff walls than flexible wall systems, the RIGID approach still underestimates bending moments by a factor of 3 for the flexible wall example discussed herein. In view of the limitations associated with using AEP diagrams with a RIGID analysis for both stiff and flexible walls, it is recommended that this approach be abandoned for more sophisticated analyses methods such as a Winkler analysis or numerical analysis for assessing structural forces.

REFERENCES

Sabatini, P.J., Pass, D.G., and Bachus, R.C. (1999). "Ground Anchors and Anchored Systems," *Geotechnical Circular No. 4*, USDOT FHWA, *Rpt. No. FHWA-IF-99-015*.

Geosolve (2005). Computer software "Wallap for Windows".

Itasca (2007). Computer software FLAC (Fast Lagrangian Analysis of Continua).

Kerr, W.C. and Tamaro, G. J. (1990). "Diaphragm walls—Update on design and performance." *Proceedings, ASCE specialty conference on design and performance of earth retaining structures, Geotechnical Special Publication 25*. ASCE, Reston, VA.

Mikhail, R.A., Kucker, M.S., Fischer, G.R., Robinson, R.A., and Godlewski, P.M. (2000). "Earth Pressures on Deep Shafts," *Proceedings, North American Tunneling*, Balkema, Rotterdam.

Ratay, R.T. (1996). *Handbook of Temporary Structures in Construction, 2nd edition*, McGraw-Hill, New York.

Tamaro, G.J. and Gould, J.P. (1992). "Analysis and design of cast in situ walls (diaphragm walls)," Retaining Structures, *Proceedings, Conference of the Institute of Civil Engineers,* London, England, pp 343-352.

Terzaghi, K. and Peck, R.B. (1967). *Soil Mechanics in Engineering Practice*, John Wiley and Sons, New York.

Strom, R.W. and Ebeling, R.M. (2001). "State of the Practice in the Design of Tall, Stiff, and Flexible Tieback Retaining Walls," *USACE Rpt. ERDC/ITL TR-01-1*.

Strom, R.W. and Ebeling, R.M. (2001). "Simplified Procedures for the Design of Tall, Stiff Tieback Walls," USACE Rpt. ERDC/ITL TR-02-10.

Steel Sheet Pile Used as Permanent Foundation and Retention Systems – Design and Construction

Chad A. Underwood, M. ASCE, P.E., P.G.[1] and Richard M. Greenlee, P.E.[2]

[1] Principal, Engineering Partners International LLC, 9001 East Bloomington Freeway, Suite 123, Bloomington, MN, 55420 USA; www.engineeringpartners.net; PH (612) 751-8648; FAX (952) 884-0491; cunderwood@engineeringpartners.net
[2] Principal, Engineering Partners International LLC, 9001 East Bloomington Freeway, Suite 123, Bloomington, MN, 55420 USA; www.engineeringpartners.net; PH (952) 884-0481; FAX (952) 884-0491; rgreenlee@engineeringpartners.net

ABSTRACT: This paper summarizes the design and construction of steel sheet pile walls for permanent building foundations and earth retention on four projects in and around Minneapolis, Minnesota USA. The buildings have one to two levels of below grade parking and up to six above grade floor levels. In each case, the below grade parking slabs and the perimeter walls and columns of the superstructure are supported by the sheet pile foundation. The sheet pile are designed to carry uniform wall loads in the range of 5 to 12 kips per linear foot and concentrated loads of up to 251 kips.

The perimeter sheet pile walls are designed for both temporary (during construction) and permanent earth retention. Utilizing the perimeter earth retention system as the permanent foundation maximizes the building footprint on a site and allows building construction in a “top-down” manner. Top-down construction reduces the need for temporary internal bracing or tiebacks to support the earth retention walls by using the building floor slabs to resist lateral earth pressures. It also permits construction of the above grade levels to start before the below grade levels are completed; this can save critical time during the early stages of a project.

Design of the sheet pile for both temporary and permanent earth retention follows conventional design methodology, with special attention to each stage of construction. The interior building excavation and construction sequence is staged to reduce the cantilevered length of sheet pile until permanent floor slabs are constructed, thereby limiting pile deflection.

The evaluation of vertical bearing capacity of the sheet pile foundations is based on conventional analyses for friction piles. The vertical bearing capacities estimated by static methods were verified in the field using high strain dynamic testing with a Pile Driving Analyzer (PDA).

INTRODUCTION

Construction of buildings with below grade levels in urban environments often requires temporary excavation support systems to keep excavation limits from encroaching on neighboring properties or rights-of-way. A typical construction process for this type of building involves installation of a temporary earth retention system around the perimeter of the site, often using tieback anchors or internal bracing, excavating to the lowest floor slab subgrade elevation, forming and pouring the perimeter footings and foundation walls and interior footings and columns for the building, and then constructing the elevated slabs one floor at a time.

Significant time and cost savings can result from incorporating the temporary excavation support system into the permanent building foundation. For instance, installing an earth retention system that serves as the perimeter building foundation wall can shorten the construction schedule several weeks compared to constructing separate earth retention systems and foundation walls.

Using the perimeter foundation wall as the temporary and permanent earth retention systems also permits building construction to proceed using “top-down” (or “up-down”) construction. Top-down construction allows construction of above grade levels of a building to start while below grade levels are still being built. The ability to start construction of above grade levels before the below grade levels are completed can shorten the construction schedule several weeks.

Using conventional temporary earth retention systems with cast-in-place foundation walls requires that the perimeter building line be offset up to 4 to 5 feet from the face of the earth retention system to provide sufficient space to form and pour the perimeter foundation walls. This reduces the allowable building footprint on a site and lowers the revenue generating capacity of the structure, whether from loss of commercial/retail space, residential space, or parking stalls.

There are several types of earth retention systems that can be designed for use as permanent building foundation systems. Tangent or secant pile walls, slurry diaphragm walls, and sheet pile walls all have the structural characteristics to resist both lateral earth pressures and vertical building loads. This paper focuses on the use of steel sheet pile as permanent foundation walls. To our knowledge, the use of sheet pile foundations together with the construction sequencing described in this paper are among the first of their kind in the United States.

SHEET PILE FOUNDATIONS IN MINNESOTA

Engineering Partners International LLC (Engineering Partners) has designed sheet pile foundations for four projects in and around Minneapolis, Minnesota USA since 2005. The buildings have one to two levels of below grade parking and up to six above grade floor levels. In each of the four projects, both the below grade parking slabs and the perimeter walls and columns of the superstructure are supported by the sheet pile foundations. In two of the projects, the sheet pile foundations were designed as end bearing pile (bearing on relatively shallow bedrock); the other two were designed as friction pile. A summary of each project is provided in Table 1.

Table 1. Summary of Sheet Pile Foundation Projects

Project Name	Project Location	No. of Below Grade Levels	No. of Above Grade Levels	Max. Column or Point Load	Max. Uniform Wall Load	Bearing Condition
Flour Sack Flats	Minneapolis, MN	2	5	111 k	5 klf	End Bearing, Skin Friction(1)
Blue Apartments	Minneapolis, MN	2	6	153 k	12 klf	Skin Friction
St. Cloud Police Sta.	St. Cloud, MN	1	1	N/A	7 klf	Skin Friction
Mill District City Apts.	Minneapolis, MN	2	5	251 k	9 klf	End Bearing

Footnotes:
(1) Sheet pile supporting concentrated loads were designed as end bearing on relatively shallow bedrock; sheet pile supporting uniform wall loads designed as friction pile.

Notes: k = kip = 1,000 pounds klf = kips per linear foot

The projects discussed in this paper had excavation depths up to 24 feet below grade to accommodate the below grade parking. To achieve these excavation depths without temporary bracing or tiebacks, yet minimizing the sheet pile section, required staged excavation and slab construction in a top-down manner. With top-down construction, the building floor slabs for the below grade levels are used to resist the lateral earth pressures. A typical construction sequence for a two level below grade parking structure is summarized on Figure 1.

Similar construction sequences can be used for buildings with more than two below grade levels. However, the design of buildings with more than two levels below grade requires special considerations which are beyond the scope of this paper.

EARTH RETENTION ANALYSIS

Analysis of lateral earth pressures on the permanent sheet pile walls must consider both construction stage loading and final (permanent) loading conditions. Until the first floor slab connection is made at the top of the sheet pile, pile top deflection (δ) for the cantilevered wall must be maintained between ½ inch to ¾ inch to avoid unnecessary bending stresses and eccentric loading on the sheet pile once the axial load (P) from perimeter walls of the superstructure are applied (Figure 2). Pile top deflection during the construction stage often controls both pile selection (by requiring a higher moment of inertia) as well as the required mass of soil comprising the temporary construction slope (i.e., controls the elevation of the top of the construction slope and/or steepness of the slope).

The pile embedment depth below final excavation elevation that is required to satisfy wall stability is often greater under the temporary or construction stage loading conditions (i.e., when the sheet pile wall is completely cantilevered, Figure 1, Stage 3) than under final loading conditions when the P1, P2 and First Floor slabs are in place (Figure 1, Stage 8). The required pile embedment depth to satisfy bearing capacity of sheet pile foundations acting as friction piles must also be analyzed.

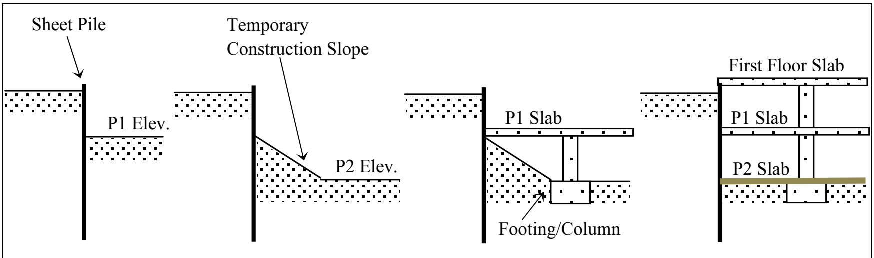

Stage 1, 2 *Stage 3* *Stage 4, 5* *Stage 6, 7, 8*

Stage 3

Stage 4, 5

Stage	Description
1	Drive sheet pile along perimeter walls of building.
2	Excavate to the first below grade parking level (P1); typically a 10 to 12 foot excavation.
3	Maintain the P1 subgrade elevation at the sheet pile wall then slope the excavation down to the second parking level (P2) subgrade elevation (referred to as the temporary construction slope). The P2 subgrade elevation is typically 20 to 24 feet below exterior grade. The sheet pile wall is cantilevered (no tiebacks or temporary internal bracing).
4	Construct interior footings and columns while the temporary construction slope is in place.
5	Place the P1 slab (either precast or post-tensioned) and complete connections to the sheet pile wall (see Figure 3). The P1 slab pins or braces the sheet pile wall prior to removal of the temporary construction slope.
6	Excavate the temporary construction slope from below the P1 slab while construction continues above the P1 level.
7	Pour the P2 slab on grade.
8	Place the first floor slab and complete first floor connection to top of sheet pile (see Figure 3). *(Note: Stages 7 and 8 could occur in opposite order, whereby the first floor slab is in place before P2 slab construction is completed.)*

Figure 1. Typical sheet pile foundation construction sequence using a modified top-down approach.

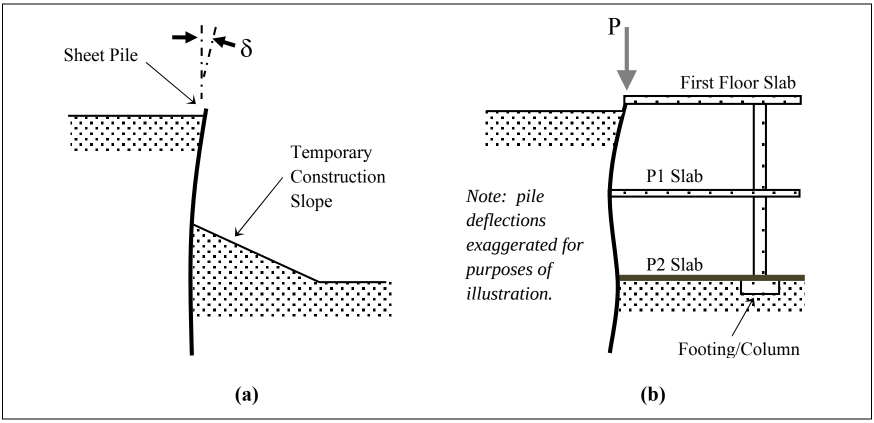

Figure 2. Typical sheet pile deflection patterns during (a) construction stage and (b) final stage loading (pile deflections exaggerated for purposes of illustration).

SHEET PILE BEARING CAPACITY EVALUATION

Evaluation of vertical bearing capacity of sheet pile foundations is based on conventional analyses for piles (Terzaghi and Peck, 1996; USACE, 1991). The relatively large surface area of the sheet pile wall can yield high bearing capacities from skin friction alone, and tip resistance from end bearing is generally neglected for conservatism, unless the pile bears on competent bedrock. For example, a single sheet of AZ19-700 pile, which is 2.3 feet wide, has a surface area (both sides of the sheet) of 6.10 ft^2 per vertical linear foot of pile. As a comparison, a pipe pile of the same outside surface area would have a diameter of 1.9 feet.

Unit skin friction values were estimated based on the author's experience with driven pipe pile and H-pile, together with literature values for skin friction parameters (Winterkorn and Fang, 1991; Terzaghi and Peck, 1996; USACE, 1991; NAVFAC, 1986), including relationships developed from full-scale load tests and pull-out tests on instrumented sheet pile walls and box pile (Bustamante and Gianeselli, 1991).

Vertical bearing capacities were verified in the field using high strain dynamic testing with a Pile Driving Analyzer (PDA). Capacities in the range of 150 kips to 250 kips per single sheet pile were estimated based on the PDA results.

SHEET PILE STRUCTURAL ANALYSIS AND DESIGN

The structural capacity of the sheet pile considers combined axial loading and/or eccentric loading due to uniform wall loads and point loads, together with bending moments due to the lateral earth pressure. The structural analysis treats the sheet pile foundation as a steel column subject to axial loads and bending moments. The following is a summary of the structural analysis and design process.

- Sheet pile shear, deflection, and bending moments (from lateral earth/surcharge pressures) are determined for each stage of construction.

- Eccentric moments from superstructure loads are added to the earth/surcharge pressures to compute the total bending moment.
- Axial loads from above grade floor levels are added to the sheet pile.
- Combined axial and bending stresses in the sheet pile are evaluated using American Institute of Steel Construction (AISC) interaction formulas.

For three of the four projects described above, the sheet pile foundations support elevated slabs (i.e., first floor and P1 slabs shown on Figure 3a) constructed of hollow core precast concrete plank. The precast plank is supported by precast concrete beams that span interior reinforced concrete columns. Where the precast beams meet the sheet pile wall, the beams are supported by brackets (Figure 3d) welded to the flanges of the sheet pile. Where the brackets are welded to the sheet pile flange, a yield line analysis is used to evaluate the flange thickness with respect to the bracket plate shear force and moment.

Where the precast plank for P1 slabs is perpendicular to the precast beams supporting the plank, the plank is supported at the sheet pile wall using a bearing angle (Figure 3c). The bearing angle is continuous along the sheet pile wall and welded to the inside face of flanges at each pair of pile. To accommodate support of precast plank or post-tensioned slabs for the first floor level at the top of the sheet pile, a continuous steel plate is welded to the top of the pile (Figure 3b).

CONCLUSIONS

Permanent sheet pile foundations can be cost effective where it is necessary or desirable to construct one or more below grade levels with building foundation walls close to the property lines. A sheet pile foundation system is conducive to top-down construction, which can eliminate temporary tiebacks or bracing of the sheet pile wall and can greatly reduce the overall construction schedule by allowing construction of above grade levels to begin before below grade levels are completed.

Construction stage loading typically controls the sheet pile section, and often controls the required pile embedment depth below the bottom of excavation. The embedded portion of the sheet pile has a high surface area that can generate relatively high vertical bearing capacities from skin friction alone. The structural design of the sheet pile must consider both axial stresses from the superstructure and bending stresses from earth/surcharge pressures and from eccentric building loads.

With a deep foundation along the perimeter of the building and spread footings on the interior of the building, differential settlement between the different foundation types must be evaluated. The expected differential settlement must be within the tolerable limits of the structural framing system.

The finished sheet pile walls provide a profile distinctly different from concrete walls, and are typically painted (Figure 4) for aesthetics and corrosion protection. Skyline Steel provided the sheet pile for each project described in this paper, and has performed extensive testing of its AZ series sheet pile for use as permanent structural building elements. This testing includes fire rating, corrosion, and waterproofing (Abbondanza, 2009). Detailed discussion of these aspects of sheet pile foundation design is beyond the scope of this paper, and can be obtained from Skyline Steel.

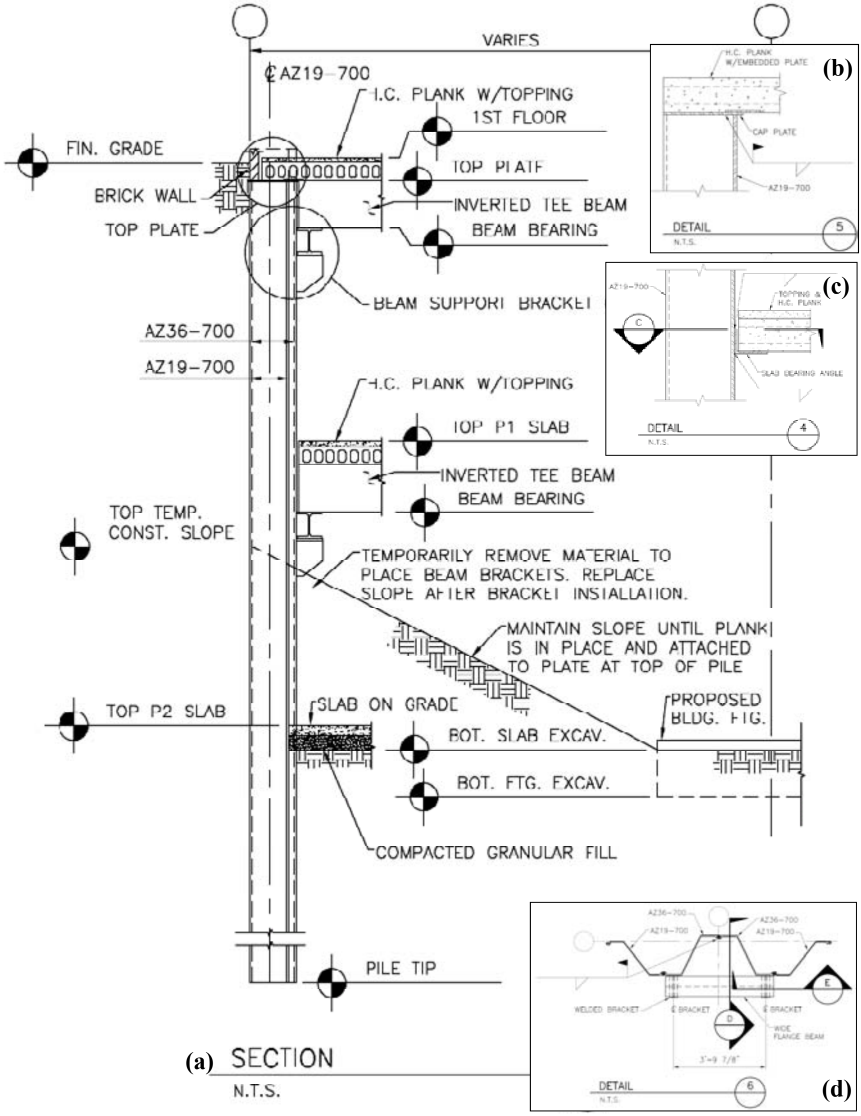

Figure 3. Typical sheet pile foundation section for two levels of below grade parking (a), and standard details for the sheet pile top plate (b), precast plank bearing angle (c), and precast concrete beam bearing bracket (d).

(a) **(b)**

Figure 4. Finished sheet pile foundation walls in below grade parking garages. Precast plank bearing at the top of sheet pile (a) and precast beam bearing on a bracket welded to the flanges of the sheet pile (b).

ACKNOWLEDGMENTS

These sheet pile foundations for these projects were designed and constructed using the design-build project delivery method. We thank the contractors whom we worked for to design these foundation systems: Carl Bolander & Sons, Inc. of St. Paul, Minnesota, Frana Companies of Hopkins, Minnesota, and Ramsey Excavating of Minneapolis, Minnesota. We also thank our partner Bruce Weber, P.E. and associates Bogdan Winiarczyk, P.E. and Steve Redfield who contributed significant design time to each project and were key to the success of these projects.

REFERENCES

Abbondanza, D. (2009). "Steel innovation: changing the economics of below grade foundations." *Contemporary Topics in Ground Modification, Problem Soils, and Geo-Support*, GSP No. 187, ASCE, Reston/VA: 57-64.

Bustamante, M.G. and Gianeselli, L. (1991). "Predicting the bearing capacity of sheet piles under vertical load." *Proc. 4th Intl. Conference on Piling and Deep Foundations.*, Italy: 9 p.

NAVFAC, 1986. *Foundations and Earth Structures*. Naval Facilities Engineering Command Design Manual 7.02.

Terzaghi, K. and Peck, R. B., 1996. *Soil Mechanics in Engineering Practice*, 3rd ed., John Wiley & Sons, Inc., New York, NY.

USACE (1991). *Design of Pile Foundations*. US Army Corps of Engineers Engineering Manual EM 1110-2-2906.

Winterkorn, H. F. and Fang, H. Y. (1991). *Foundation Engineering Handbook*, 2nd ed., Kluwer Academic Publishers, Norwell, MA.

ADAPTATION: Block 75 Redevelopment Shoring and Dewatering

R. Jameson[1], L. West[2] and J. Bishop[3]

[1] Malcolm Drilling Company, Inc., 3503 Breakwater Court, Hayward, CA 94545; PH (510) 780 9181; FAX (510) 780 9167; rjameson@malcolmdrilling.com
[2] Kleinfelder 14710 NE 87th Street Suite 100, Redmond, WA; PH (425) 636-7900; FAX (425) 636-7901; lwest@kleinfelder.com
[3] Geotechnical Design Systems, Inc., 865 East 4800 South, Suite 140, Salt Lake City, Utah 84107; PH (801) 262-1942; FAX (801) 262-1943, jerry@geosystems-inc.com

ABSTRACT

The City Creek Block 75 Project encompasses a large city block in Salt Lake City, involving excavations to 90 feet below street grade and over 40 feet below groundwater. Earth retention, in combination with dewatering systems, was installed to support five adjacent high rise structures and three major streets abutting the site. Ground conditions are comprised of dense cobbles and gravels overlying interlayered lakebed deposits with incised stream deposits which provide conduits for groundwater recharge from the ancestral City Creek. The design and construction scheme provided the flexibility required and often emphasized by Terzaghi to adjust in response to actual underground conditions using the available means and methods. This case history traces the innovative modifications to dewatering and shoring systems implemented in response to subsurface conditions identified during Block 75 shoring and dewatering construction.

Initial subsurface projections allowed for a dewatered approach using a complex multi-stage wellpoint system combined with soil nail and shotcrete shoring, supplemented by soldier or secant piles and post-tensioned elements for added stiffness at critical sections. In general, the wellpoint systems reduced pore pressures within the upper aquifer, but groundwater remained perched in an intermittent zone of interlayered silts and clays along the east wall. Modified shoring design, dewatering systems and changes to construction procedures were required to complete this wall. Consequently, the north perimeter of the project was redesigned as a composite shoring and groundwater cut-off system combining secant piling, jet grouting and soil nailing. The revised shoring and dewatering configurations from the east and north walls are presented with performance data for these unique earth retention systems.

SITE AND PROJECT DESCRIPTION

City Creek comprises a 20 acre redevelopment for mixed residential, retail and commercial use with five levels of underground parking and facilities. Block 75 is the central segment of the project, located adjacent to Temple Square in downtown Salt Lake City. The site extends 650 feet south from South Temple to 1st Street, and

450 feet east from Main Street to the Key Bank Tower. The existing retail structures on the site were demolished, leaving driven piles abandoned in place. Existing high rise commercial structures were located at each corner of the site, and remained in operation throughout construction. A site layout plan is presented as Figure 1.

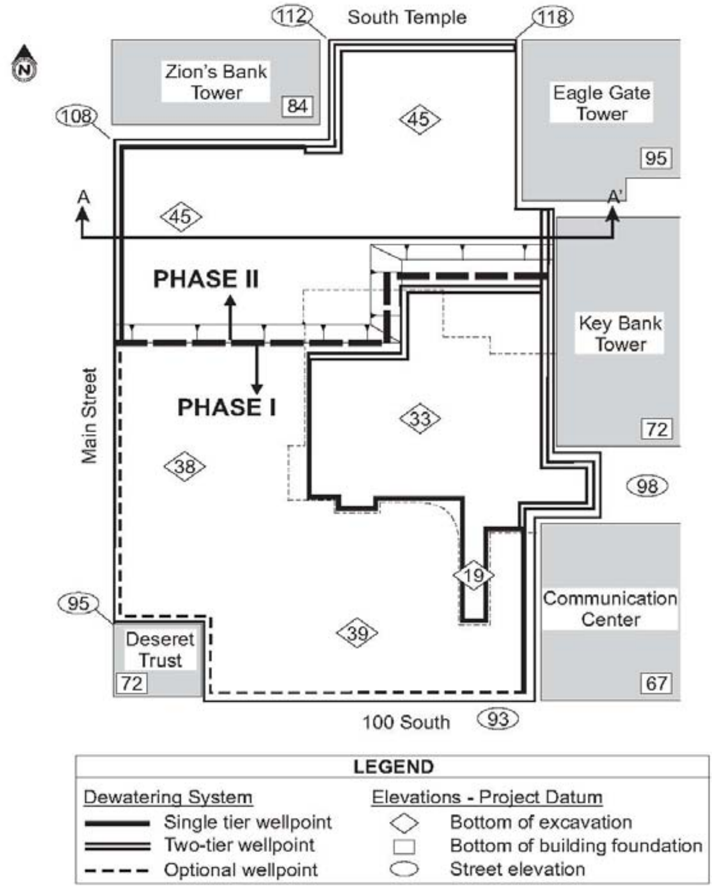

Figure 1. Site Plan

The topography of the project site and surrounding area generally slopes from project El. 118 in the northeast corner down to El. 92 at the southwest. Project El. 100 correlates to 4320 feet above Mean Sea Level. The base of excavation was at approximately El. 45, with a deepened zone along the east wall extending down to El. 33. The truck elevator in the southeast corner reached down to El. 19. The resultant shoring depths were approximately 75 feet from street level at the north wall and 55 feet along the south, with 99 feet overall vertical grade change between the high and low points. The excavation and shoring were performed in two phases. Phase I, extending over the southern two thirds of the site, was completed in 2008. Phase II, the remaining northern segment, was performed in 2009.

SOIL AND GROUNDWATER ENVIRONMENT

Initial evaluation of the subsurface data indicated a stratified soil profile sloping from northeast to southwest across the site, consistent with the surface topography (See Figure 2). Variable fill materials extend down to existing foundation level 25 feet below street grade. The natural soils are gravel with some clay and silt which in-turn overlay silty sand and clay lenses. This unit of predominantly non-cohesive soils served as an unconfined aquifer which required dewatering. The underlying aquitard (lean interlayered clay and silty sand) has a typical thickness ranging from 30 to 50 feet, thinning to 15 to 20 feet in the northwest corner, and separates the upper aquifer from a lower, confined aquifer. Historical records and the soils data show that ancient streams meandered through the site from northeast to southwest, creating intermittent incised zones in the aquitard. The deeper confined aquifer consists of highly permeable gravel and sand with occasional lenses of clay.

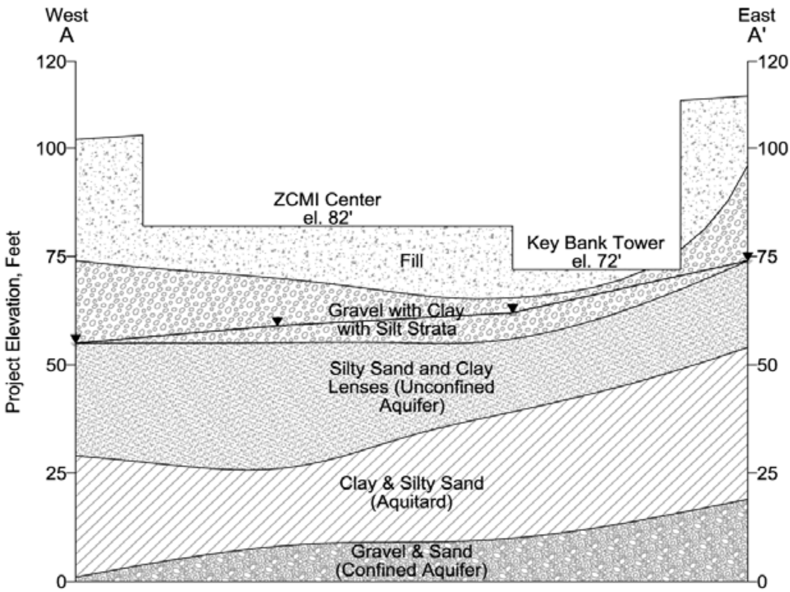

Figure 2. Block 75 subsurface cross-section A-A'

At the time of geotechnical studies, groundwater was encountered in the unconfined aquifer around El. 60 at the northeast corner and El. 42 at the southwest corner. Based on historical water level data, the geotechnical investigation concluded that design water levels could be about 10 feet higher. Groundwater levels in the confined aquifer were measured at around El. 33 feet during site pumping tests.

Borehole and water level data showed a strong correlation between direction of groundwater flow and inclination of fine-grained soil layers. The hydraulic conductivity of the finer grained soils is several orders of magnitude lower than the gravels and indicated these units may not readily yield groundwater to wells.

EXCAVATION SUPPORT PLAN

Soil nails and shotcrete was selected as the primary shoring system based on consideration of ground conditions and construction cost. This system requires dewatering to relieve hydrostatic pressure on the wall and maintain face stability. Soil nail and shotcrete shoring allows for flexible geometry to accommodate the existing structures and utilities which could not be exposed and dimensioned until demolition was nearly complete. Soil nails were relocated to mitigate any direct conflicts with obstructions, but maintained a minimum density across the excavation face, and in some cases were threaded through existing pile clusters behind the shoring walls. Vertical elements, comprising lengths of reinforcing steel encased on grout, were installed from grade before the start of excavation to improve face stability in the dense gravels. The specified deflection allowance was 1-inch for all shoring walls. The estimated soil nail wall deformations were consistent with the specified criteria for work adjacent to existing streets. Excavation support adjacent to the existing structures was evaluated on a case specific basis, with focus on enhanced deformation control using vertical and inclined micropiles and soldier pile elements in combination with post-tensioned nails and anchors to maintain confinement of retained soil and furnish shoring systems with significantly lower estimated deflections. Low yield systems were chosen to provide structural support while limiting deformation. Elements were sized with lateral pressure theory, recognizing the need to maintain low unit stresses and maximize use of composite soil-structure interaction. A variety of local and global stability analyses were employed to complete the design process.

DEWATERING APPROACH

Initial analyses suggested the majority of groundwater inflow could be controlled by measures implemented along the north and east sides of the excavation. Deep pumped wells and pressurized eductor or ejector wells were considered in project planning; however, the presence of existing buildings and access restrictions outside of the excavation footprint, prevented their use. The selected design employed vacuum wellpoints drilled through shoring walls at six to seven foot centers. Additional wellpoint systems were installed at the base of excavation to accommodate construction sequencing and deepened areas (see Figure 1). The dewatering scope was divided into required systems on north and east perimeters of both Phase I and II areas, and optional systems to be implemented as dictated by site conditions in other areas.

A two-tiered vacuum wellpoint system was used to manage groundwater up to 30 feet above the base of shoring along the Phase I north and east perimeter, with supplemental wells around the deepened east wall excavation and truck elevator pit.

Sumping was evaluated along the south and west walls; however since the soils did not readily yield groundwater, the optional wellpoint systems were installed. The Phase II work area was located north of Phase I and required new wellpoint systems along this up-gradient perimeter. A two-tier vacuum wellpoint system was designed along South Temple Street; however, the Eagle Gate Tower perimeter was designed as a combined shoring and cut-off wall due to risk of dewatering induced settlement.

Anticipated groundwater flows to attain drawdown behind the shoring wall were 240 GPM in gravels and 50 GPM in sand/silt for a 400 foot long wellpoint system. Actual flow rates typically ranged from 100 to 200 GPM at the initiation of a new wellpoint system to less than 50 GPM at stabilization. Total flow from the entire dewatering system never exceeded 300 GPM.

EXCAVATION SUPPORT CHANGES DURING CONSTRUCTION

The dewatering systems performed as anticipated throughout Phase I with the exception of the eastern wall. The Communications Center and the Key Bank Tower were located adjacent to this segment of the site perimeter (see Figure 1). Perching layers within the aquifer, the presence of utility backfills and leaking water pipes all contributed to increased hydrostatic pressure behind the soil nail walls. The evidence of these conditions included water emanating from discrete perforations in the shoring, discharge of soil and non-native materials as well as discovery of steady mid-summer flows into a storm-drain.

The east wall groundwater conditions compromised excavation face stability and applied excess hydrostatic loads against the shoring system. The project team considered multiple solutions in order to progress shoring along this wall. Some supplemental weep holes were installed, but due to difficulty in targeting the zones of free groundwater a full additional level of wellpoints was added, effectively halving the spacing to 3 feet. This reduced some of the hydrostatic pressure measured behind the wall, but did not effectively stabilize zones of non-cohesive soils, and hence excavation could not advance without risk of ground loss undermining previously constructed shoring elements. The soil face exposed during construction was minimized by reducing shotcrete lift height and working in only limited lengths of wall. This combination of slot cutting, supplemental weeps and additional wellpoints allowed completion of the east wall, but required thickened shotcrete and additional soil nails to resist the increased hydrostatic loading. The Phase II shoring systems were re-evaluated based on the conditions encountered during construction on the east wall. This resulted in modified excavation support schemes using secant piles and grouting to provide full-face pre-excavation stabilization, combined with supplemental anchorage to accommodate lateral loading from retained groundwater.

EXCAVATION SUPPORT SYSTEM CROSS-SECTIONS:

Communications Center. Excavation depths of 45 ft were required along the north and west sides of the Communications Center, located at the southeast site corner. Face of shoring was limited to be only 2 ft offset from the edge of this concrete framed structure, however an easement allowed for temporary anchorage elements to extend below. This layout constraint did not allow sufficient clearance for soldier pile drilling and placement so the design used deep hollow-bar soil nails as the primary retention element. Micropile A-frames, spaced at 3 ft centers, added flexural stiffness and overall deflection control to the wall face. The shoring configuration is illustrated in Figure 3. Settlement control was enhanced by post-tensioning of all the soil nails against the reinforced shotcrete facing. The micropiles were terminated slightly below the main shoring face in order to avoid a "hard spot" beneath the footing. This allowed structure loads to transfer within the support system and dissipate through the soil mass. A shallow grade beam was added all along the top of the wall to enhance fixity of the drilled elements before start of excavation. The two-tier wellpoint system was designed to capture groundwater behind the excavation face and lower hydrostatic pressures. Wellpoint tips were located within five to ten feet of the shoring face to minimize dewatering induced consolidation.

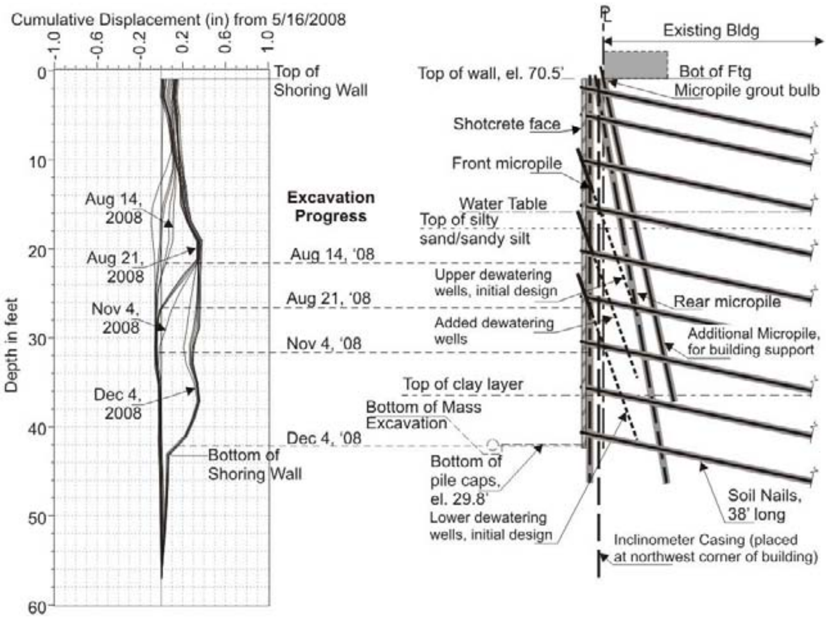

Figure 3. Communications Center inclinometer data and shoring cross-section

During construction an unanticipated layer of soft saturated silt was identified within the face of the excavation. It became apparent that wellpoints were not effectively dewatering this material. Consequently, the design was modified to include additional rows of nails and a ten-inch thick, reinforced shotcrete face. The inclinometer records show that the soil nails, which were tensioned after initial grout and shotcrete cure, effectively pulled the shoring face back into the soil near to the top of wall, countering some settlement induced by the dewatering and excavation. After a temporary hold in excavation for design and installation of the supplemental support, the cut was completed with total outward movement measured by the inclinometer casing of approximately 0.5-inch. Settlement surveys by the owner show a total settlement of the building at 0.52-inches. The use of closely spaced, small diameter vertical and horizontal shoring elements accommodated the geometric constraints of this wall. This provided sufficient stability to allow excavation to final grade through extremely difficult soil conditions. Settlement matched the 0.5 inch maximum estimated during initial shoring design.

Eagle Gate Tower. This high-rise commercial building is supported on a mat foundation at El. 95, approximately 50 feet above the planned adjacent excavation. To avoid dewatering induced settlement, the project team proposed a secant wall with four rows of strand tieback anchors, designed to support hydrostatic head up to 20 feet above excavation grade. The secant wall was to be placed in a four-foot wide strip of ground along the west edge of the exposed building foundation.

After demolition was completed to El. 100, the abandoned foundations were exposed along the shoring alignment. Groups of driven pipe piles were identified within the shoring zone on 14 foot centers, and consequently a continuous secant wall could not be completed. The shoring and groundwater cut-off scheme was revised to combine segments of secant wall between the existing pile groups, with jet grouting, vertical spiling and shotcrete providing enclosure and sealing around the pipe piles, as shown in Figure 4. Some of the abandoned driven piles were out-of-plumb, requiring substantial real-time adjustments to secant pile and grouting configurations.

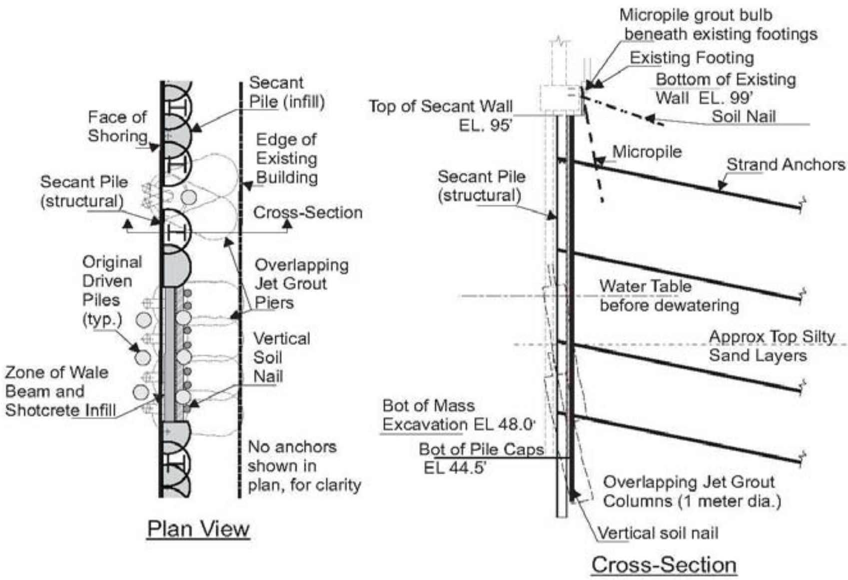

Figure 4. Eagle Gate Tower shoring details

During excavation, the deep tieback anchors were installed and stressed against either the secant pile reinforcing beams or wale beams bearing onto the existing pipe piles. Some supplemental hollow-bar anchors were placed in zones which required reconfiguration due to obstructions. The jet grouting was installed using a steeply inclined drilling pattern at three different vertical intervals in order to work around the existing pipe piles. The resultant wall consisted of alternating vertical panels of secant piles and composite shoring elements, all intended to mobilize uniformly for support of the highly loaded mat foundation.

Two inclinometers were installed in this wall, but both were damaged during excavation and limited data was obtained. Optical surveys showed the maximum lateral movement of the wall was 0.54-inches and settlement was 0.26-inches during the 50 foot excavation extending below groundwater level. No collateral distress was identified in the building or on the actual shoring wall face.

South Temple Street. This 75 foot high shoring wall was the tallest vertical cut on the project and was scheduled under Phase II construction. The original design employed soil nails and shotcrete wall with a two-tier wellpoint system. However, based on experience gained during Phase I, the owner elected to redesign the wall as a composite shoring and groundwater cut-off system. The lower 40 feet utilized a tied-back secant pile wall while the upper 35 feet (above groundwater) remained a soil nail structure to minimize overall cost. The upper soil nail wall was set-back 3 feet in order to accommodate the lower tier secant pile installation, but existing utilities limited nail length to only 12 foot in the upper half of this wall section. Existing driven piles were exposed at 14 foot centers directly in front of the shoring zone and therefore jet grouting was used in combination with segments of secant piling to complete the wall. Tieback anchors were stressed against the secant piles during excavation.

The upper soil nailed section of South Temple shoring behaved erratically during construction. The west-end of this system terminated at a deep utility vault excavation. This outside corner, which was supported by short nails from the main shoring wall construction and by a simple corner brace in the vault area, indicated a trend of outward movement in both directions. A tie-rod bracing system was added to give adequate face support. The total settlement was consistent with the pre-construction estimate of 0.6 to 1.0 inch. The shoring cross-section is presented in Figure 5 with corresponding lateral deformation as measured by inclinometer.

SUMMARY & CONCLUSIONS

Block 75 was a large and complex excavation which required a variety of shoring and dewatering systems. Soil nail shoring and wellpoints provided the necessary flexibility to accommodate the range of site conditions and geometry. The initial excavation support scheme performed well for Phase I, with the exception of the east wall, where modified design details and construction methods were necessary for completion. Drawing on this experience, the north site perimeter was redesigned as a composite shoring and groundwater cut-off system combining secant piles, jet grouting, anchors, soil nails and shotcrete. The excavation and shoring was successfully completed with wall deformations consistent with pre-construction predictions. Geo-structure performance on this project underscores the flexibility of composite design.

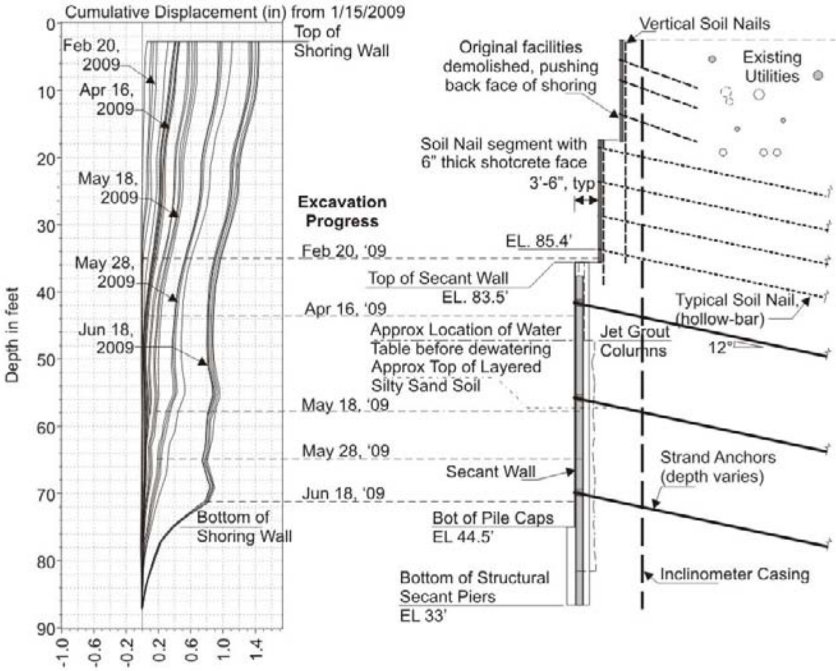

Figure 5. South Temple Street inclinometer data and shoring cross-section

ACKNOWELDGEMENTS

The Authors wish to acknowledge the extensive team which contributed to successful completion of this project, and in particular, City Creek Reserve, Inc., the Owner, and Big-D Construction, the General Contractor.

REFERENCES

Applied Geotechnical Engineering Consultants, Inc. (2006). "Geotechnical Investigation Block 75 and 76." *Prepared for Property Reserve, Inc.*

Difficult Geologic Conditions Mandate Retaining Wall Redesign

Donald R. McMahon, P.E., M.ASCE[1], Andrew J. Nichols, P.E., M.ASCE[1] and Brian T. Contino, P.E.[2]

[1] Principal Engineer and Project Manager, McMahon & Mann Consulting Engineers, P.C., 2495 Main Street, Buffalo, NY 14214
[2] Director of Business Development, dck north America, P.O. Box 18505, Pittsburgh, PA 15236-0505

ABSTRACT

This paper discusses a case history where hard boulders embedded in a residual clay matrix prevented completion of a top-down retaining wall. Observations of soil conditions in excavations during construction allowed an indirect estimate of soil shear strength properties, which were used to analyze the stability of an approximately 27-foot deep excavation with a vertical side. This excavation was necessary to construct a concrete cantilever retaining wall as an alternative to the top-down wall. The design of the cantilever wall within the limited right-of-way is discussed. The construction monitoring program used to verify soil properties and protect workers is also discussed.

INTRODUCTION

This case history involves the widening of the Outer Loop of Interstate Highway 695 (I-695), northwest of Baltimore, Maryland, south of the interchange with I-70. The existing Outer Loop of the Baltimore Beltway was two southbound lanes and the project required widening it to three lanes. It also included construction of several retaining walls due to the topography, which sloped upwards from the edge of the highway in some locations along the alignment. To widen the highway, retaining walls were required for grade separation because the resulting ground surface would have been too steep without them.

One such retaining wall, RW-8, was designed as a top-down cantilever wall in which the contractor was required to drill 3-foot diameter holes with a drilled shaft rig, place a specially fabricated soldier pile inside the hole, fill the hole from the soldier pile tip elevation to the bottom of the pavement with reinforced concrete, excavate the ground in front of the wall to the back flange of the piles, slide pre-cast concrete panels between the flanges of adjoining piles, fill the zone between the native ground and the back flange of the pre-cast panels with drainage material and construct a cast-in-place reinforced concrete facing on the front side (highway side) of the wall.

Retaining wall RW-8 was 688 feet long and required 87 drilled shaft excavations spaced 8 feet apart. The wall height ranges from 3.5 to 20 feet.

Excavation of the drilled shafts became a problem that increased with difficulty as the project progressed, eventually requiring the contractor to develop an alternative approach to complete the project. Obstructions in the ground in the form of boulders hindered the drilled shaft subcontractor in advancing the excavations to the design elevations.

This paper describes the alternative approach taken when the ground conditions prevented the original design from being constructed.

SITE AND GEOLOGIC CONDITIONS

The site topography can be described as rolling. Within the limits of RW-8, the highway grade rises gently to the north, but the ground on the outside of the pavement slopes upward about 20 to 25 feet. Thus, the highway widening required a wall to maintain a manageable slope outside the highway limits. Figure 1 shows a section view of the proposed top-down wall and the ground surface conditions.

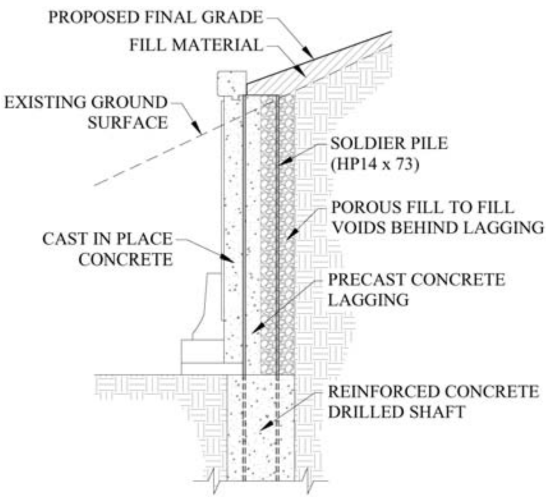

Figure 1. Top-down retaining wall section.

The property line is 18 feet from the front face of the wall and there were no opportunities to obtain a temporary easement for construction of an alternative wall type due to historical properties adjacent to the proposed wall. A fence was located along the right-of-way, separating the highway from an asphalt driveway and parking lot.

The site is located in the Piedmont Region and has residual soils resulting from the chemically weathering of the native bedrock. Bedrock at this site is amphibolite and soil is silty clay.

Nine test borings were drilled near the proposed RW-8 alignment during design. In general, the boring logs show soil above the pavement elevation that consists of stiff to hard silty clay. The boring logs show that the conditions beneath the pavement elevation consist of silty clay with layers of amphilobite. The drillers collected core samples of the amphilobite and the logs note the presence of soil seams in some of the core samples. At some boring locations, rock was penetrated with the split spoon sampler, revealing saprolite, a very weathered rock. A soil sample collected during construction from an excavation had a liquid limit of 96 percent and plastic index of 46. The borings extended to below the tip of the drilled shaft elevations. The top of competent rock elevation varies erratically between borings.

Groundwater levels were measured in the borings at various times following completion, but installation of piezometers was not included in the subsurface exploration program. Water levels in the borings ranged from about 12 feet above to 15 feet below the pavement elevation. These data were insufficient to characterize the groundwater regime. During construction, water accumulated in the base of the retaining wall excavations, but was never observed seeping from the side slopes.

CONSTRUCTION ISSUES

Construction of the wall began in late 2003 with the drilled shaft excavations, but problems emerged from the outset. The drillers encountered hard boulders making progress much slower than anticipated. The caisson contractor attempted several techniques to advance the drilled shaft excavations including augering with different diameter augers, core barrel drilling, cluster drilling with small diameter percussion drills and down-hole hammer method. All proved largely unsuccessful due to boulders embedded in the soil matrix. The augers could not penetrate the boulders and coring through a mixed face (part of the base of the hole was soil and part was rock) at the base of the hole was not successful because the ground stiffness varied with the boulders present, causing the core barrel to wander off alignment.

The contractor's approach was then to advance the auger to refusal and then place a laborer inside the hole with a jack hammer and rock splitter to break and remove the boulders. The contractor then continued augering until refusal was encountered again. Then, the boulder breaking process was repeated. This significantly extended the time required to advance the holes such that by August 2004, excavation for the piles in a 142-foot length of the wall had not yet begun.

ALTERNATIVES ANALYSIS

The contractor considered other options for constructing the 142 feet of the retaining wall including a conventional cast-in-place concrete cantilever wall. However, it was considered that construction of this wall type would require installation of a sheet pile or soldier pile wall along the right-of-way to support the excavation.

Installation of piles was rejected because the boulders embedded in the soil matrix that hindered advancement of the drilled shafts would also prevent piles from being advanced. Additionally, lateral support necessary for the shoring was not feasible. Tiebacks could not be used because a temporary easement was unavailable. Rakers could not be used because they would interfere with the retaining wall construction.

The contractor had successfully completed drilling some excavations for the soldier piles and had placed them in the drilled excavations. It excavated the sloped soil in front of the soldier piles, extending the excavation with an unsupported vertical face to the back flange of the soldier piles, as shown in Figure 2 to allow installation of the concrete lagging between the soldier piles and drainage material behind the lagging. These excavations allowed an indirect measure of the soil undrained shear strength.

In two locations along the RW-8 alignment, the contractor had left excavations between the soldier piles for the lagging (similar to the conditions shown in Figure 2) open for several weeks before installing the lagging. The excavations appeared stable and the ground surface at the top of the excavations showed no indication of lateral movement, such as tension cracks or sloughing. The excavation height was 16.5 feet.

The contractor then excavated a test pit along the retaining wall alignment to observe the soil conditions and check the soil mass for features, such as fissures, slickensides, etc. that cold adversely affect the stability of a vertical excavation slope. The test pit revealed a silty clay matrix mixed with hard amphilobite boulders. The soil matrix was hard. A thumbnail could be indented about 1/16 to 3/16 inches into the soil matrix only with much difficulty. Peck (1974) relate penetration of the soil mass to unconfined compressive strength. The amount of difficulty observed at this soil mass indicates the unconfined compressive strength exceeds 4 tons per square foot (tsf).

Figure 2. Top-down wall before lagging installation.

The test boring logs along RW-8 were reviewed and the least favorable boring had an average Standard Penetration Test N-value of 15. Based on the Terzaghi and Peck correlation appearing in Department of the Navy (1971), the unconfined compressive strength could be inferred as 2 tsf. However, considering the Sowers and Sowers correlation for “clays of high plasticity” (the PI of a sample was 46), the unconfined compressive strength could be 3.7 tsf.

Construction of a cast-in-place concrete cantilever retaining wall would require an excavation along the property line that would be 26.8 feet high. Using the Taylor Chart, Peck (1974), for a vertical slope, the N_c term equals 3.85. Using an estimated unit weight of 125 pounds per cubic foot, and an unconfined compressive strength of 2 tsf, the factor of safety for a 26.8-foot vertical excavation is about 2.4.

The contractor left the test pit open and observed the response of the ground with time. The excavation side slopes were nearly vertical and remained stable for at least five weeks. No secondary features manifested themselves during this period.

The results of these observations and estimates of the soil undrained shear strength allowed a cast-in-place cantilever wall to be considered as an alternative because they indicated that the overburden could be excavated with a vertical side slope.

ALTERNATIVE WALL DESIGN

A conventional cast-in-place cantilever wall was proposed such with the identical facing and architectural elements as the specified top-down wall so that this portion of the wall would not be distinguishable from the highway. Many challenges faced the designers in that the wall height was specified and the alternative wall needed to fit within the restricted space behind and in front of the wall.

The alternative wall was designed following conventional approaches by achieving factors of safety against sliding and overturning specified by the American Association of State Highway and Transportation Officials (1996) and for bearing capacity. Drained soil strength parameters were used for design. The soil mass was assigned an angle of internal friction of 28 degrees, based on the Atterberg limit data. Many iterations were necessary to achieve the specified factors of safety and fit the cantilever wall within the limited space. The width of the toe was limited by the specified location of a pavement drain that needed to be installed in front of the toe. The heel needed to be limited in width to keep the theoretical failure plane within the backfill to the extent possible. This resulted in an unusual configuration having a relatively wide toe and a narrow heel.

The designers elected to include a shear key to assist with sliding resistance and specified a uniformly graded crushed stone for backfill. This material was estimated to have an angle of internal friction of 38 degrees and an estimated unit weight of 100 pounds per cubic foot, Alva (1981). This friction angle placed a majority of the theoretical failure plane within the backfill. The high friction angle and low unit weight also reduced the lateral forces on the wall. Figure 3 shows a typical section of the alternative wall.

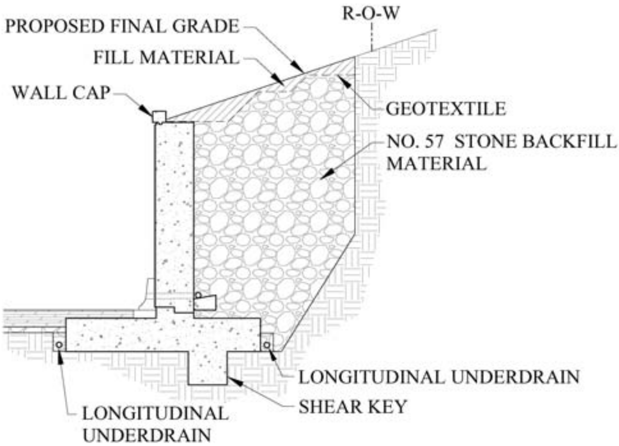

Figure 3. Alternative retaining wall section.

Although the estimates of the soil shear strength indicated that the excavation slopes would remain stable for the duration of construction, the designers elected to divide the length of the cast-in-place wall into four approximately 35-foot sections for construction. The first section was excavated and the wall was built and backfilled before the adjacent wall section excavation was begun to take advantage of any soil arching that might exist between the wall sections to assist in maintaining the vertical slope stable. The construction sequence (see Figure 4) was:

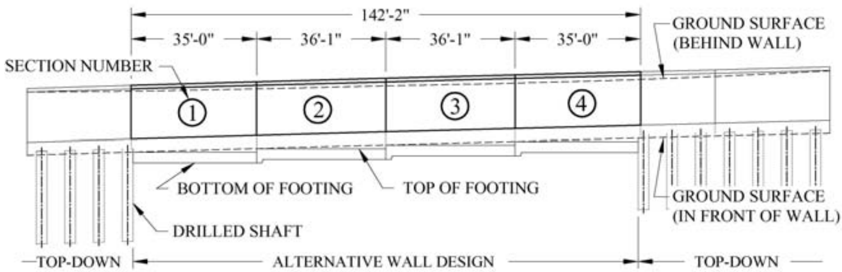

Figure 4. Alternative wall profile.

Excavate and build Section 1 (southernmost section)
Excavate and build Section 3
Excavate and build Section 2
Excavate and build Section 4

The contractor placed a Jersey barrier along the top of the slope, about 7 feet from the crest to prevent traffic from applying a surcharge to the top of the slope.

CONSTRUCTION OBSERVATIONS

Two concerns about this approach existed that led to a construction monitoring program. The primary concern was for the safety of workers building the wall next to the vertical slope because of the potential exposure of workers to falling soil clods and/or cobbles from the excavation face. Another concern existed for a general slope failure into the excavation. This would damage adjacent property and could injure workers and the general public using the facility at the top of the slope. A landslide was considered possible if soil conditions (i.e., soil strength and/or soil composition) or groundwater conditions (e.g., seepage through the excavation side slopes) along the alignment differed from those observed in excavations and test pit. Therefore, a monitoring program was initiated to address these issues.

A series of frequent observations of the ground behind the excavation were initiated. These included measuring the position of six hubs installed in the ground behind the excavation slope and monitoring the width of cracks in the pavement at the top of the slope that had existed before construction. Movement of the hubs or opening of the cracks would alert the contractor that the excavation slope was behaving differently than planned.

Since the excavations were made during the dry fall weather when the soil would dry, slake and fall into the excavation, the condition of the excavation face was inspected twice daily, at the start of work and following lunch. The inspector used a man-basket on a crane to inspect the slope condition and to scale any loose soil clods or rocks from the excavation face.

Additionally, the contractor placed a tarp over the slope during non-working hours to slow drying (and slaking) of soil on the excavation face and to prevent erosion into the excavation. This tarp was removed during work periods so the slope could be inspected.

Figure 5 shows the excavation of Section 1 in progress and the boulders removed from the excavation. This amount of boulders was the cause for the drilling difficulties.

CONCLUSIONS

This case history demonstrates the critical importance of accurately characterizing subsurface conditions. In this case, test pits could have proved useful for identifying the boulder condition. Test borings often do not accurately identify the extent boulders embedded in a soil matrix.

Drilled shaft equipment can successfully excavate through soil with augers and through rock with core barrels (or rock loosening tools), but is ill-suited to excavate soils laden with hard boulders.

Figure 5. Excavation of Section 1.

The solution to the construction problem at this site involved the observational approach. Utilizing observations of soil behavior in excavations and a test pit together with test boring data allowed the concept of an approximately 27-foot high excavation with nearly vertical side slopes to be considered. Once the feasibility of such an excavation was demonstrated, a monitoring program was initiated to check that the estimates made during design were valid. The design estimates proved valid and the alternative wall design was successfully constructed.

REFERENCES

Alva-Hurtado, J. E., McMahon, D. R. and Stewart, H. E. "Apparatus and Techniques for Static Triaxial Testing of Ballast" *Laboratory Shear Strength of Soil*, ASTM STP 740, R. N. Yong and F. C. Townsend, Eds., American Society for Testing and Materials, 1981, pp. 94-113.

American Association of State Highway Officials (AASHTO). (1996). *Standard Specifications for Highway Bridges,* Washington, D.C.

Department of the Navy, Naval Facilities Engineering Command. (1971). Design Manual Soil Mechanics Foundations and Earth Structures, Alexandria, VA

Peck, R. B., Hanson, W. E. and Thornburn, T. H. (1974) *Foundation Engineering, Second Edition,* Wiley, New York.

Direct Approach for Designing an Excavation Support System to Limit Ground Movements

L. Sebastian Bryson[1] and David G. Zapata-Medina[2]

[1]Department of Civil Engineering, 161 Raymond Bldg, University of Kentucky, Lexington, Kentucky 40506; PH (859) 257-3247; FAX (859) 257-4404; email: bryson@engr.uky.edu

[2]Department of Civil and Environmental Engineering; Northwestern University; 2145 Sheridan Road; Evanston, IL 60208

ABSTRACT

Traditionally, excavation support systems are designed solely on the basis of satisfying limit equilibrium, using apparent earth pressure diagrams. Using this approach, the support system design becomes a function of the maximum anticipated earth pressure and is governed by overall structural stability as opposed to maximum allowable horizontal or vertical deformation. This approach produces a support system that is adequate with regards to preventing structural failure, but may result in excessive wall deformations and ground movements.

This paper presents a design methodology that facilitates the sizing of all components of the excavation support system in such a way that limits the maximum lateral and vertical excavation-induced deformations. Based on the fundamental approach of the presented design methodology, structural and basal stability is guaranteed.

INTRODUCTION

Conventionally, excavation support systems are designed based on structural limit equilibrium. Although these approaches will prevent structural failure of the support wall, they may result in excessive wall deformations and ground movements. Existing design methods that do consider deformations, relate lateral wall movements to excavation support system stiffness and basal stability. However, these design methods were developed using a limited number of wall types and configurations. These methods do not include considerations for differing excavation support systems, whose performance is highly dependent on construction techniques; the three-dimensional (3D) effects of the wall construction and the excavation process;

the effects of different support types; the influences of the excavation geometry and sequencing; or complex site geology.

This paper presents a design methodology that facilitates the sizing of all components of the excavation support system in such a way that limits the maximum lateral and vertical excavation-induced deformations. The design methodology is a semi-empirical approach that was developed from observations of several case histories reported worldwide and a fully 3D finite element analysis that realistically modeled the excavation geometry, the excavation support system, and the excavation activities. Based on the fundamental approach of the presented design methodology, structural and basal stability is automatically achieved.

EXCAVATION-INDUCED GROUND MOVEMENTS

As was previous mentioned, current design methodologies satisfy structural stability first and then check deformation conditions. This approach does not guarantee that excavation-induced ground movements will not cause damage to the adjacent infrastructure. Thus, the most efficient approach for designing excavation supports systems is to design the systems such that the excavation activities will not cause damage to the adjacent infrastructure. Researchers (Son and Cording, 2005; Kotheimer and Bryson, 2009) have linked damage in buildings adjacent to excavations, to vertical ground movements. These approaches typically relate semi-empirical damage criteria to building distortions. These excavation-induced building distortions are then related to changes in ground slope. Changes in ground slope can be predicted via settlement profiles, given the maximum settlement value.

Ground movements adjacent to deep excavations occur in response to lateral deflections of the excavation support system. In soft clay, these movements are influenced by the stiffness of the support system, the soil and groundwater conditions, the earth and porewater pressures, and the construction procedures. Clough et al. (1989) presented a design chart for clays that allows the user to estimate lateral movements in terms of effective system stiffness ($EI/\gamma_w h_{avg}^4$) and the factor of safety against basal heave. The EI is the wall flexural stiffness per horizontal unit of length (E = the modulus of elasticity of the wall element and I = the moment of inertia per length of wall), h = the average vertical spacing between supports, and γ_w = the unit weight of water. The factor of safety against basal heave used in the Clough et al. (1989) work is that given by Terzaghi (1943). The Clough et al. (1989) chart was created from parametric studies using plane strain finite element analyses of sheet piles and slurry walls.

A link between excavation-induced settlement and lateral wall deformations is made by evaluating case data. Researchers (Clough et al, 1989; Hsieh and Ou, 1998) have reported that the maximum ground settlement adjacent to deep excavations is directly related to the maximum lateral displacement of the support system. Finno et al. (2002) found that for undrained unloading conditions in saturated soils the lateral deformation envelop closely matched that of the ground settlement. For this study, a definite relationship between maximum settlement and maximum lateral deformation was sought for input into the proposed design methdology. Zapata (2007) investigated the excavation-related ground movements by evaluating data from several case histories. A partial listing of the case history information is given in Table 1. Additional detail of the case history data can be found in Zapata (2007).

Table 1. Partial case history database.

Soil Type	Reference	Wall Type	H [m]	He [m]	$\delta_{H(max)}$ [mm]	$\delta_{V(max)}$ [mm]
Stiff Clay	Ng (1992)	Diaph.	16.3	9.57	18	10
	Burland and Hancock (1977)	Diaph.	30	18.5	24	20
	Hsieh and Ou (1998)	Diaph.	33	20	125	78
	Whittle et al. (1993)	Diaph.	25.6	20.2	54	45
	Becker and Haley (1990)	Diaph.	26	20	47	102
Medium Clay	Ou et al. (1998)	Diaph.	35	19.7	107	77
	Finno and Roboski (2005)	Sheet	19	12.8	63	74
	Hsieh and Ou (1998)	Diaph.	31	18.4	63	43
	Miyoshi (1977)	Steel-Conc.	32	17	177	152
	Finno et al. (1989)	Sheet	19.2	12.2	173	256
	NGI (1962)	Sheet	16	11	224	200
	Wang et al. (2005)	Diaph.	38	20.6	48	31
	Peck (1969)	Sheet	14	8.5	229	210
Soft Clay	Finno et al. (2002)	Secant	18.3	12.2	38	27
	Hu et al. (2003)	Diaph.	21	11.5	15	7
	Baker et al. (1987)	Diaph.	18.3	8.5	37	37
	Koutsoftas et al. (2000)	Soldier	41	13.1	48	30

H=Height of wall; He=Depth of excavation; $\delta_{H(max)}$=maximum lateral deformation; $\delta_{V(max)}$=maximum settlement

The case data presented in Table 1 is divided into stiff, medium, and soft clay. These distinctions are made on the basis of undrained shear strength found at the bottom of the excavations. Soft clay is defined as clay deposits with undrained shear strengths between 0 kPa to 25 kPa. Medium clay is defined as undrained shear strengths between 25 kPa and 50 kPa, and stiff clay are deposits with undrained shear strengths greater than 50 kPa. Figure 1 shows the maximum lateral movements as a function of the maximum vertical movements for the case histories. The purpose of Figure 1 is to provide an estimation of the maximum lateral deformation based on an inputted value of the maximum settlement. The maximum lateral deformation can subsequently be used to estimate the required support wall stiffness. This approach is considered appropriate for design of support systems in urban areas because presumably the limiting criteria for design will be the maximum settlement of the ground behind the support wall.

In the Figure 1, the maximum lateral deformations are normalized with respect to the depth of wall and the maximum vertical movements are normalized with respect to the depth of the excavation. This approach follows the implications of data presented by Bryson and Zapata (2007). Their work showed that lateral deformations tended to be more influenced by the physical characteristics of the support system (i.e. length of wall, wall stiffness, etc.), while the vertical deformations tended to be more influenced by the soil behavior. Subsequently, the soil behavior at deep excavations is typically influenced by the depth of excavation.

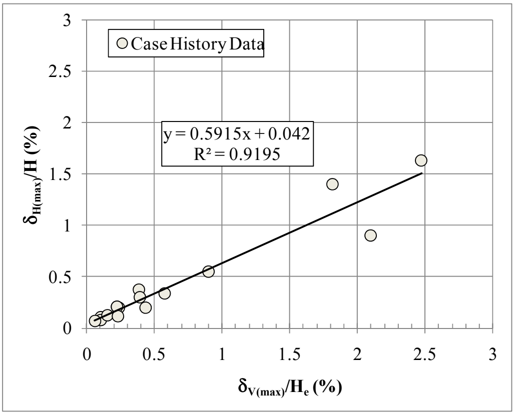

FIGURE 1. CORRELATIONS BETWEEN MAXIMUM HORIZONTAL DEFORMATIONS AND MAXIMUM VERTICAL DEFORMATIONS.

From Figure 1, it is seen that an expression relating the maximum horizontal and vertical deformations can be developed by plotting a linear regression line through the case data. The expression is given by:

$$\frac{\delta_{H(\max)}}{H} = 0.591\left(\frac{\delta_{V(\max)}}{H_e}\right) + 0.042 \tag{1}$$

It is noted that both the normalized maximum horizontal deformation and the normalized maximum vertical deformation in Equation 1 are in percent.

BASAL STABILITY

Basal stability is an important parameter in the analysis and design of excavation support systems in soft soils. Lateral movements of an excavation support system tend to increase dramatically as a result of plastic yielding in the soil beneath and surrounding the excavation. The extent of the plastic yielding can be quantified with the use a factor of safety against basal heave.

Basal stability analyses can be carried out using limit equilibrium methods. Limit equilibrium methods assume two-dimensional conditions and are based on bearing capacity (Terzaghi, 1943). The most common bearing capacity methods were developed before the introduction of stiffer insitu wall systems such as diaphragm walls and secant piles. As a result, these methods ignore the effect of the depth of the wall penetration below the base of excavation, soil anisotropy, and other factors. Ukritchon et al. (2003) presented a modified version of the Terzaghi (1943) factor of safety against basal heave that included the effects of the wall embedment. Figure 2 shows the excavation geometry used in the modification. The expression for the factor of safety is given by:

$$FS_{(heave)} = \frac{s_u N_c + \sqrt{2} s_u (H/B) + 2 s_u (D/B)}{\gamma_s H_e} \tag{2}$$

where the terms $s_u N_c$ and $\sqrt{2} s_u (H/B)$ represent the shear capacity and the shear resistance of the soil mass, respectively and $2 s_u (D/B)$ represents the adhesion along the inside faces of the wall assuming a rough surface.

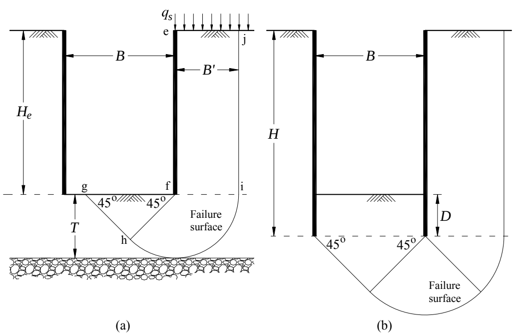

FIGURE 2. FACTOR OF SAFETY AGAINST BOTTOM HEAVE: (A) WITHOUT WALL EMBEDMENT; AND (B) WITH WALL EMBEDMENT.

Note that Terzaghi (1943) used $N_c = 5.7$, which originally assumed resistance at the interface of the base of the footing and the soil (i.e., perfectly rough foundation). For basal calculations, this implies some restraint at the base of the excavation. However, it is assumed that the base of the excavation is a restraint-free surface. Thus, $N_c = 5.14$ (i.e., perfectly smooth footing) is more appropriate.

RELATIVE STIFFNESS RATIO

As was previously discussed, lateral deformation is a performance parameter of the excavation support system and has traditionally been shown to be a function of the factor of safety against basal heave and the effective system stiffness. These relations are shown in the chart developed by Clough et al. (1989). Unfortunately, the chart was developed using a limited number of wall types and configurations. Furthermore, the chart does not include the 3D nature of the excavation.

To address the deficiencies of the Clough et al. (1989) chart, a new relative stiffness ratio is presented. This new ratio was formulated using dimensional analysis of the excavation support system stiffness problem. The relative stiffness ratio is given as

$$R = \frac{E_s}{E}\frac{s_h s_v H}{I}\frac{\gamma_s H_e}{s_u} \tag{3}$$

where R = relative stiffness ratio; E_s = reference secant modulus of the soil at the 50 percent stress level; E = elastic modulus of the wall; I = moment of inertia per unit length of the wall; s_h = average horizontal support spacing; s_v = average vertical support spacing; H = height of the wall; H_e = excavation depth; γ_s = average unit weight of the soil; and s_u = undrained shear strength of the soil at the bottom of the excavation. In Equation 3, the terms E_s/E, $S_H S_V H/I$, and $\gamma_s H_e/s_u$ represent the relative stiffness resistance, the relative bending resistance, and the excavation stability number, respectively.

The relative stiffness ratio was compared with data obtained from a 3D finite element parametric study. The parametric study consisted of a 3D system model and 3D ground movements. Figure 3 presents maximum lateral wall displacements obtained from the parametric study versus the relative stiffness ratio, *R*, for different factors of safety against basal heave.

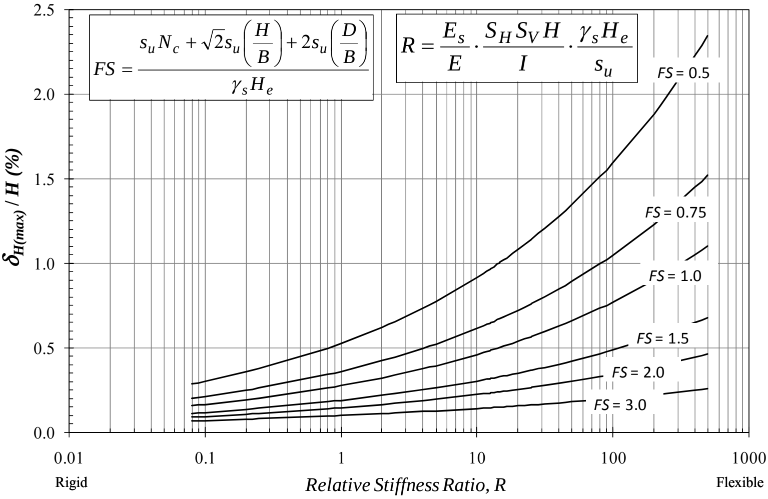

FIGURE 3. RELATIVE STIFFNESS RATIO.

In the figure, the lateral movements are normalized with respect to the height of the wall, and the factors of safety are calculated using Equation 2, which includes the effects of the wall embedment depth below the base of excavation. For details of the parametric study and the development of Figure 3, the reader is referred to Zapata (2007). Figure 3 allows the designer to predict maximum lateral wall movements for deep excavations in cohesive soils based on simple soil data and excavation geometry. These data can then be used to predict maximum settlement using Equation 1.

ELEMENTS OF EXCAVATION SUPPORT SYSTEM DESIGN

The proposed direct design methodology is illustrated in the flow chart presented in Figure 4. The proposed methodology allows the designer to size all the elements of the excavation support system, given the maximum allowable settlement of infrastructure adjacent to the excavation. The proposed methodology also allows the designer to predict final ground movements (horizontal and vertical), given data about soil and support system.

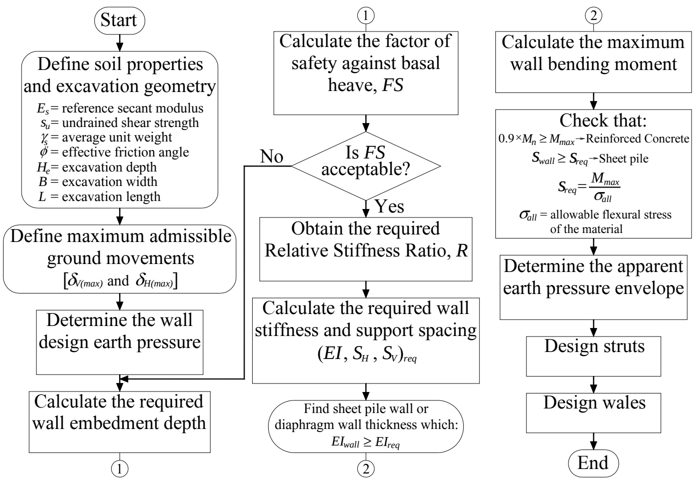

FIGURE 4. FLOW CHART FOR DESIGNING EXCAVATION SUPPORT SYSTEMS USING THE DIRECT APPROACH.

CONCLUSIONS

This paper presents a deformation-based design methodology based on both observation of case histories and fully 3D finite element analyses that realistically model the excavation support system and the excavation activities. This semi-empirical approach allows for the design of excavation support systems based on deformation criteria including the influences of the inherent 3D behavior of the excavation support system and the associated excavation. The proposed approach will also allow the designer to predict final ground movements, given data about soil and support system or size all the elements of the excavation support system, given the allowable soil distortion of adjacent structures.

It is important to mention that the new design procedures proposed in this investigation is only applicable to clays similar to those studied and must be verified and validated with real case history data.

ACKNOWLEDGEMENTS

The material presented in this paper is based upon work supported by the National Science Foundation under grant No. CMS 06-50911, under program director Dr. Rick Fragaszy. This financial support was greatly appreciated.

REFERENCES

Bryson, L.S. and Zapata-Medina, D.G. (2007). “Physical Modeling of Supported Excavations,” *Proceedings of Geo-Denver*, Denver, CO, 18-21 February 2007.

Clough, G. W., Smith, E. M., and Sweeney, B. P. (1989). “Movement Control of Excavation Support Systems by Iterative Design.” *Current Principles and Practices, Foundation Engineering Congress*, ASCE, Vol. 2, pp. 869-884.

Finno, R. J., Bryson, L. S., and Calvello, M. (2002) “Performance of a Stiff Support System in Soft Clay.” *Journal of Geotechnical and Geoenvironmental Engineering*, ASCE, Vol. 128(8), pp. 660-671.

Hsieh, P-G. and Ou, C-Y. (1998). “Shape of Ground Surface Settlement Profiles Caused by Excavation.” *Canadian Geotechnical Journal*, Vol. 35(6), pp. 1004-1017.

Kotheimer, M.J. and Bryson, L.S. (2009). “Damage Approximation Method for Excavation-Induced Damage to Adjacent Buildings,” *International Foundations Congress and Equipment Expo (IFCEE09)*, Orlando, FL, 15-19 March, 8 pp.

Son, M. and Cording, E. J. (2005). “Estimation of Building Damage Due to Excavation-Induced Ground Movements,” *Journal of Geotechnical and Geoenvironmental Engineering*, ASCE, Vol. 131(2), pp. 162-177.

Terzaghi, K. (1943). *Theoretical Soil Mechanics*, John Wiley and Sons, New York.

Ukritchon, B., Whittle, A. J., and Sloan, S. W. (2003) “Undrained Stability of Braced Excavations in Clay.” *Journal of Geotechnical and Geoenvironmental Engineering*, ASCE, Vol. 129(8), pp. 738-755.

Zapata. D.G. (2007), “Semi-Empirical Method for Designing Excavation Support Systems Based on Deformation Control.” *Master Thesis*, University of Kentucky, Lexington, KY.

Development of Project-specific p-y Curves for Drilled Shaft Retaining Wall Design

Jiun-Yih Chen[1], S.M. ASCE, Emad Farouz[2], M. ASCE, P.E. and
Paul Landers[3], M. ASCE, P.E.

[1]Doctoral Candidate, The University of Texas at Austin, 1 University Station C1792, Austin, TX 78712; jychen@mail.utexas.edu
[2]Principal Engineer, CH2M HILL, Inc., 15010 Conference Center Drive, Suite 200, Chantilly, VA 20151; emad.farouz@ch2m.com
[3]Project Engineer, CH2M HILL, Inc., 15010 Conference Center Drive, Suite 200, Chantilly, VA 20151; paul.landers@ch2m.com

ABSTRACT

This paper presents the development of project-specific p-y curves for the analysis and design of tangent and secant pile walls in the Marquette Interchange Project. The passive soil resistance, characterized by non-linear p-y curves, available to the embedded part of the wall is one of the key elements in the analysis for geotechnical and structural designs of the wall. In this project, p-y curves were developed using pressuremeter tests in various soil types encountered along the wall alignments. Several design categories were developed to group p-y curves with similar soil conditions and lateral resistance. An average p-y curve was developed for each design category using a hyperbolic model. These project-specific p-y curves were calibrated against the measured pile deflection profiles from three lateral pile load tests. A design example is presented to illustrate the design procedure incorporating project-specific p-y curves. This procedure is proven to work satisfactorily in full scale.

INTRODUCTION

The $810 million Marquette Interchange Project is a reconstruction of an interchange that connects three major interstate highways in downtown Milwaukee. A total of 42 retaining walls were designed and constructed between 2002 and 2008. The majority of walls are cut walls, among which tangent and secant pile walls are the dominant types. Tangent and secant pile walls are constructed of continuous and overlapping drilled shafts and used in the top-down construction scheme for temporary excavation support or permanent grade separation purposes.

More than 400 soil borings with 45 groundwater observation wells were drilled to characterize subsurface conditions. Pressuremeter tests (PMTs) were performed at

24 locations near the walls and 15 locations near the bridge piers to characterize the lateral resistance in different soil strata. PMT results were used to develop site-specific p-y curves. Several design categories were developed to group site-specific p-y curves with similar soil conditions and lateral resistance. An average p-y curve was developed for each design category. These average p-y curves are project-specific p-y curves that were used to design pile foundations and tangent and secant pile walls. The data from three lateral pile load tests performed in the design phase of the project were used to calibrate and validate the use of project-specific p-y curves.

PRESSUREMETER P-Y CURVES

The relationships between mobilized lateral resistance and pile displacement at any points along the pile are characterized by p-y curves. They are regularly used in the soil-structure interaction analyses to design laterally loaded piles and drilled shafts. Conventional p-y curves were developed experimentally at the University of Texas in the 1970's (Matlock 1970 and Reese et al. 1974 and 1975) in response to oil industry's demand to build offshore structures that can sustain relatively large horizontal loads from waves. A school of thought considered in situ testing a better way to develop p-y curves because materials tested in situ are generally less disturbed than those sampled and tested in the laboratory (Briaud et al. 1984 and Robertson et al. 1985). The method proposed by Robertson et al. (1985) and validated recently by Anderson et al. (2003) using PMT data was adopted and used in this project.

This method utilizes the reloading part of the corrected PMT curve. Raw PMT data, consisting of pressure (p_r) and volume (v_r) readings, from the PMT control unit were corrected for membrane resistance, hydrostatic pressure, initial reading and system compressibility to obtain the corrected pressure acting against the borehole wall (p_c) and increase in volume of the PMT probe (v_c), according to Briaud (1989). Figure 1 (a) presents a set of raw and corrected PMT curves from this project. This set of PMT curves were obtained from a test performed at a depth of 6.1 m in a material characterized as stiff brown clay with a Standard Penetration Test (SPT) N-value of 21 blows per 0.3 m.

The corrected pressure (p_c) and volume (v_c) were then used to develop a site-specific p-y curve using the following equations:

$$p = (p_c)(\phi)(\alpha) \quad (1)$$

$$y = [v_c/(2V_p)](\phi/2) \quad (2)$$

where:

ϕ= pile diameter, α= multiplying factor, and V_p= initial volume of the PMT probe.

The multiplying factor (α) is a function of soil type and testing depth. If the testing depth is greater than 4 pile diameters, α is equal to 1.5 for cohesionless soils and 2.0 for cohesive soils. At a depth less than 4 pile diameters, α is reduced linearly to 0.0 for cohesionless soils and to 0.67 for cohesive soils at the ground surface.

The unload-reload procedure was not carried out for the PMT shown in Figure

1 (a). As such, engineering judgment was exercised to determine what would have been the reloading part of the corrected PMT curve. In this case, the point of the maximum curvature along the initial part of the curve was determined and the slope of the curve immediately beyond this point was used to extrapolate the curve back to a pressure of 0 kPa. Finally, this modified PMT curve was used to obtain a site-specific p-y curve, as shown in Figure 1 (b), using Equations (1) and (2).

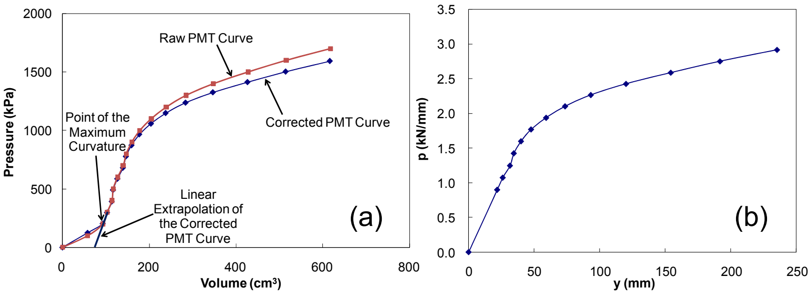

Figure 1. An example set of (a) raw and corrected PMT curves and (b) site-specific p-y curve derived for piles with a nominal diameter of 356 mm.

A total of 45 site-specific p-y curves were developed for bridge foundations in the Core segment of the project. Figure 2 shows several site-specific p-y curves and Table 1 summarizes their important attributes. They were all developed using a nominal pile diameter of 356 mm. These site-specific p-y curves fall into two clusters according to their lateral resistance. As such, two design categories were developed, one for medium stiff and the other for very stiff to hard silty clay/ clayey silt.

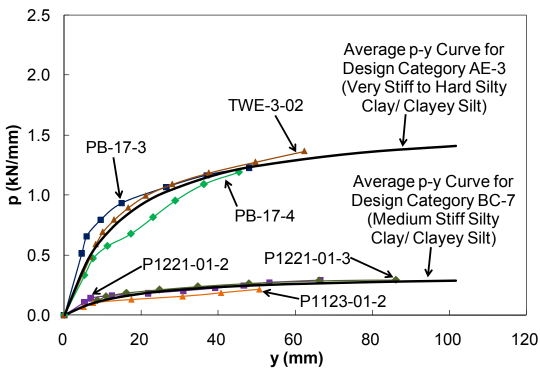

Figure 2. Selected site-specific p-y curves and average p-y curves for design categories BC-7 and AE-3.

An average p-y curve was developed for each design category. A hyperbolic model was used to characterize the average p-y curve. The hyperbolic model can be expressed using one of the following equations:

$p= y/(a+by)$ (3)
$y/p= a+by$ (4)
where:
a= inverse of the initial slope and b= inverse of the ultimate lateral resistance of the average p-y curve.

Table 1. Attributes of Selected Site-specific p-y Curves.

Designation	Testing Depth (m)	Soil Type	SPT N-value (blows per 0.3 m)	Consistency
P1221-01-2	4.2	Silty Clay	5	Medium Stiff
P1221-01-3	4.7	Silty Clay	5~7	Medium Stiff
P1123-01-2	3.0	Silty Clay	7	Medium Stiff
PB-17-3	6.6	Clayey Silt	9	Very Stiff
PB-17-4	12.1	Silty Clay	22	Very Stiff
TWE3-02-3	12.5	Silt	22~40	Very Stiff to Hard

The model parameters (a and b) for each design category can be determined by transforming all site-specific p-y data in the design category to the y/p-versus-y space and determining the intercept (a) and slope (b) of the best-fit line through all transformed data points using least squares. For example, a and b for design category BC-7 (Figure 2) are 52.1 mm^2/kN and 3.0 mm/kN, respectively. Likewise, a and b for design category AE-3 (Figure 2) are 9.4 mm^2/kN and 0.6 mm/kN, respectively.

CALIBRATION AND VALIDATION OF PROJECT-SPECIFIC P-Y CURVES

Three lateral pile load tests were performed in the design phase of the project. Test piles were driven closed-ended pipe piles backfilled with high-strength (41.4-MPa) concrete. Lateral deflections along the piles were measured using inclinometers. Project-specific p-y curves developed for the design of bridge foundations in the Core segment were used to estimate the pile deflection profiles under various lateral loads using computer program LPILE. A reasonable agreement between the measured and estimated pile deflection profiles was reached for all three load tests. Figure 3 shows the measured and estimated deflection profiles of the north pile at Test Site A. The diameter and wall thickness of this test pile are 356 mm and 13 mm, respectively.

The following principles were followed in the calibration process in order to reach a reasonable agreement between measured and estimated pile deflections.

1. The lateral resistance at the ground surface is very low. For practical purposes, it was assumed to be zero, equivalent to assigning two points, (0 mm, 0 kN/mm) and (100 mm, 0 kN/mm), for the p-y curve at the ground surface.
2. The lateral resistance of sandy fills near the ground surface depends significantly on the confining pressure (or depth). Therefore, project-specific p-y curves for sandy fills were assigned at the average depth where PMTs were performed.
3. When project-specific p-y curves were only recommended at the bottom of a particular soil layer, other project-specific p-y curve recommended at the bottom of the overlying layer was assigned to the top of this layer for a smooth transition of

lateral resistance across the artificially defined layer boundary.

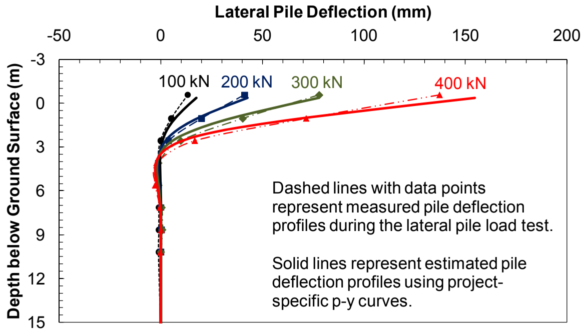

Figure 3. Measured and estimated pile deflections of the north pile at Test Site A.

DESIGN P-Y CURVE CATEGORIES FOR RETAINING WALLS

A total of 25 site-specific p-y curves were developed for the tangent and secant pile walls in the West Leg and Core segments of the project. Site-specific p-y curves with similar soil conditions and lateral resistance were grouped into a design category. Table 2 summarizes these design categories and Figure 4 presents project-specific p-y curves for these design categories. These p-y curves were developed using a nominal pile diameter of 914 mm. Farouz et al. (2005) compared project-specific and conventional p-y curves. The initial stiffness exhibited by project-specific p-y curves is sometimes higher and sometimes lower than that shown in conventional p-y curves. However, the ultimate lateral resistance in project-specific p-y curves is generally higher than that in conventional p-y curves for the same material.

EXAMPLE SECANT PILE WALL DESIGN

Retaining Wall R-40-341 is located in the Core segment of the project. This wall, along with Wall R-40-340, provides permanent grade separation for a two-lane below-grade ramp, which is at the lowest level of the entire interchange. The maximum exposed wall height of these walls is 10.1 m. Parts of these walls also support the abutments of Michigan Street Bridge and Wisconsin Avenue Bridge.

The use of project-specific p-y curves in the analysis and design of secant pile walls is illustrated using Wall R-40-341 cross-section at Station 15+50. The design cross-section is presented in Figure 5. The long-term design height is 6.4 m, whereas the short-term design height is 7.0 m, to install the footing supporting the precast facing panel and storm drain in front of the wall. Design soil parameters shown in Figure 5 were used to develop the lateral earth pressure acting on the wall, which was expressed as an equivalent fluid pressure of 6.3 kN/m^3 and 6.0 kN/m^3 under the short-term and long-term conditions, respectively. A rectangular lateral earth pressure of 3.3 kPa as a result of traffic surcharge was also applied on the wall for both short-term and long-term conditions. Because groundwater table is above the excavation levels, water pressure was also applied on the wall below the groundwater table. The above pressure components were applied on the secant pile wall above the excavation levels. In this case, the short-term condition governs the design because the short-term wall height and equivalent fluid pressure are both higher than those under the long-term condition. As such, design analysis was performed only for the short-term condition.

Table 2. Design p-y Curve Categories for West Leg and Core Retaining Walls.

Design Category	Soil Type	Consistency or Relative Density	Application Location
WC-1	Sandy Silt Fill	Stiff	Bottom of Layer
WC-2	Silty Clay Fill	Very Stiff	Bottom of Layer
WC-3	Silty Clay Fill	Hard	Bottom of Layer
WC-4	Organic Silty Clay	Stiff	Top and Bottom of Layer
WC-5	Silty Sand	Medium Dense	Bottom of Layer
WC-6	Silt and Sand with Gravel	Very Dense	Bottom of Layer
WC-7	Silty Clay	Stiff to Very Stiff	Top of Layer
WC-8	Silty Clay	Stiff to Very Stiff	Bottom of Layer
WC-9	Silty Clay/ Clayey Silt	Very Stiff to Hard	Top of Layer
WC-10	Silty Clay/ Clayey Silt	Very Stiff to Hard	Bottom of Layer
WC-11	Silty Clay	Hard	Top of Layer
WC-12	Silty Clay	Hard	Bottom of Layer

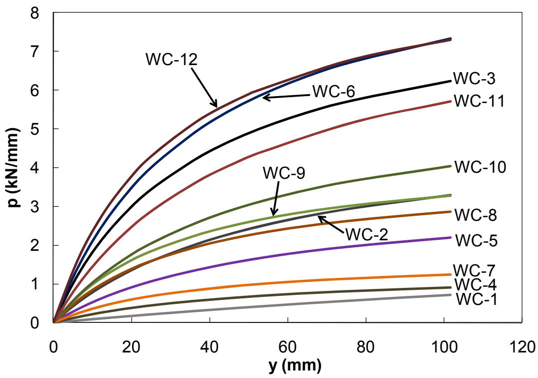

Figure 4. Project-specific p-y curves for West Leg and Core retaining wall design.

Project-specific p-y curves developed for West Leg and Core retaining walls were specified at the top and bottom of each soil layer based on the soil type, consistency or relative density (Figure 5). Note that design category BC-2 was originally developed for bridge foundations in the Core segment. However, it was converted for a nominal pile diameter of 914 mm and adopted for this analysis because very soft to soft organic silty clay and organic silt are not represented by any design categories for West Leg and Core retaining walls. Computer program FB-MultiPier was used in the design analysis. The FB-MultiPier model consisted of a single drilled shaft. Design earth pressure, including traffic surcharge and water pressure, was converted to concentrated forces applied at the nodes, spaced at 0.3 m, along the drilled shaft. It is imperative to use a p-multiplier of 0.5 to reduce the lateral resistance because the drilled shafts are closely spaced (Reese and Van Impe 2001). The center-to-center spacing and diameter of drilled shafts herein are 813 mm and 914 mm, respectively.

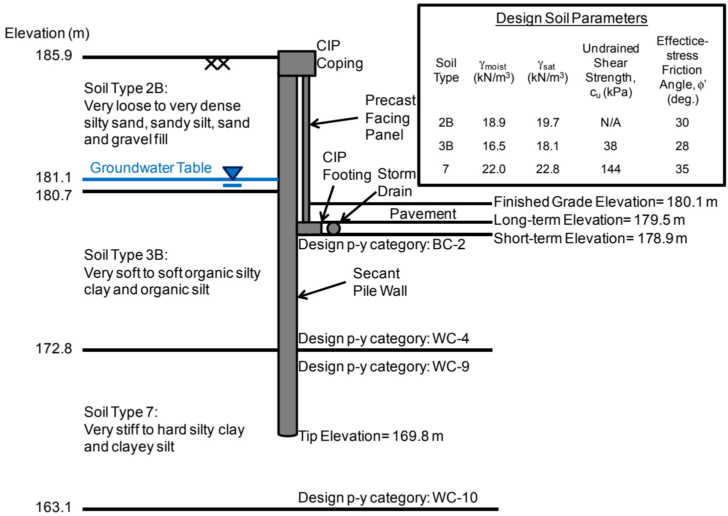

Soil Type	γ_{moist} (kN/m³)	γ_{sat} (kN/m³)	Undrained Shear Strength, c_u (kPa)	Effectice-stress Friction Angle, ϕ' (deg.)
2B	18.9	19.7	N/A	30
3B	16.5	18.1	38	28
7	22.0	22.8	144	35

Figure 5. Design cross-section of Wall R-40-341 at Station 15+50.

Two design analyses were performed. Service load analysis was performed to check the deflection of the wall. Allowable deflection in this project was established to be one percent of the exposed wall height, which was 58 mm for this design section. The maximum lateral deflection was 57 mm at the top of the wall with a shaft tip elevation of 169.8 m. Note that the shaft tip elevation was often governed by long-term global stability requirement from a limit-equilibrium analysis. Load factors were selected according to AASHTO (2002). Factored load analysis was performed to check the demand-to-capacity (D/C) ratio and detail the reinforcement in the drilled shaft. Default values of AASHTO (2002) strength-reduction factors in FB-MultiPier were used to determine the D/C ratios in various shaft segments. A rebar cage consisting of 10 Metric No. 32 longitudinal rebars with a cage diameter of 508 mm was specified for all drilled shafts in this section. The compressive strength of concrete was specified to be 35 MPa. The corresponding maximum D/C ratio in the drilled shaft was 0.95.

Potential cost savings as a result of using project-specific p-y curves were discussed by Farouz et al. (2005). Savings typically come from elimination of the need for tieback anchors and reduced shaft diameter, embedment or reinforcement.

CONCLUSIONS

Site-specific and project-specific p-y curves were successfully developed from PMTs for the Marquette Interchange Project. These p-y curves were calibrated against measured pile deflection profiles from three lateral pile load tests. Project-specific p-y curves were used to design all tangent and secant pile walls in this project. A design example is presented to illustrate the design procedure incorporating project-specific p-y curves. Most walls have been in service for about five years and have performed satisfactorily. As such, the procedure presented herein is proven to work in full scale.

ACKNOWLEDGMENTS

The authors acknowledge the support from their colleagues including: Bob Gilbert, Brian Powell, Jan Hansen, John Yao, Karl Schmid, King Sampaco, Mark Maday, Roger Failmezger, Steve Maxwell, Therese Koutnik and Van Komurka. The opinions expressed herein are those of the authors alone and do not necessarily reflect those of any of the organizations, parties or individuals involved in this work.

REFERENCES

AASHTO (2002). *Standard specifications for highway bridges*, American Association of State Highway and Transportation Officials, 17th edition.

Anderson, J.B., Townsend, F.C. and Grajales, B. (2003). "Case history evaluation of laterally loaded piles," *Journal of Geotechnical and Geoenvironmental Engineering*, ASCE, Vol. 129, No. 3, pp. 187-196.

Briaud, J.L., Smith, T. and Meyer, B. (1984). "Laterally loaded piles and the pressuremeter: comparison of existing methods," *Laterally Loaded Deep Foundations: Analysis and Performance*, ASTM STP 835, pp. 97-111.

Briaud, J.L. (1989). *The pressuremeter test for highway applications*, Publication No. FHWA-IP-89-008, U.S. Department of Transportation, Federal Highway Administration, 148 p.

Farouz, E., Chen, J.Y., Koutnik, T.E. and Powell, B.L. (2005). "The use of in-situ testing to optimize retaining wall design in the Marquette Interchange Project," *Geotechnical Applications for Transportation Infrastructure: Featuring the Marquette Interchange Project in Milwaukee, Wisconsin*, ASCE, pp. 13-27.

Matlock, H. (1970). "Correlations for design of laterally loaded piles in soft clay," Offshore Technology Conference, OTC 1204.

Reese, L.C., Cox, W.R. and Koop, F.D. (1974). "Analysis of laterally loaded piles in sand," Offshore Technology Conference, OTC 2080.

Reese, L.C., Cox, W.R. and Koop, F.D. (1975). "Field testing and analysis of laterally loaded piles in stiff clay," Offshore Technology Conference, OTC 2312.

Reese, L.C. and Van Impe, W.F. (2001). *Single piles and pile groups under lateral loading,* A.A. Balkema, 463 p.

Robertson, P.K., Campanella, R.G., Brown, P.T., Grof, I. and Hughes, J.M.O. (1985). "Design of axially and laterally loaded piles using in situ tests: a case history," *Canadian Geotechnical Journal*, Vol. 22, No. 4, pp. 518-527.

BEHAVIOR of TIEDBACK, H-BEAM WALLS and RECOMMENDATIONS for THEIR DESIGN

David E. Weatherby[1], Member, ASCE

ABSTRACT: Tiedback H-beam and wood lagging walls are commonly used for temporary excavation support systems and permanent earth retaining structures. FHWA recognized that there was an opportunity to improve the design of tiedback walls and initiated a research program to study the behavior of these walls and to develop new design recommendations. As part of the study, a 25-foot high wall was constructed. Important aspects of the walls behavior are discussed. Recommendations for; apparent earth pressures, axial load in soldier beam toes, controlling wall and ground movements, using limiting equilibrium methods for design, and checking different construction stages are presented.

INTRODUCTION

Our understanding of the behavior of tiedback, H-beam and wood lagging earth retaining structures has improved since the 1990 Design and Performance of Earth Retaining Structures Conference at Cornell University. Some of the important additions to our practice are based on measurements made on a tiedback H-beam and wood lagging test wall built in coarse-grained soils.

TEST WALL

A 25 foot high, instrumented, tiedback H-beam and wood lagging wall was constructed at Texas A&M's National Science Foundation site for Geotechnical Experimentation. Four instrumented soldier beams were supported by two rows of tiebacks, the two-tier wall section, and four instrumented beams were supported by one row of tiebacks, the one-tier wall section. The wall was built in an alluvial sand deposit. The soils had an angle of internal friction of 32° and a total unit weight of 115 pcf. The groundwater table was located approximately 33

[1] Vice President of Research and Product Development, Schnabel Foundation Company, 45240 Business Court, Sterling, VA 20166, dave@schnabel.com

feet below the ground surface. Figure 1 shows a section through the wall and a typical soil profile. Weatherby et al. (1998) provides additional information regarding the wall.

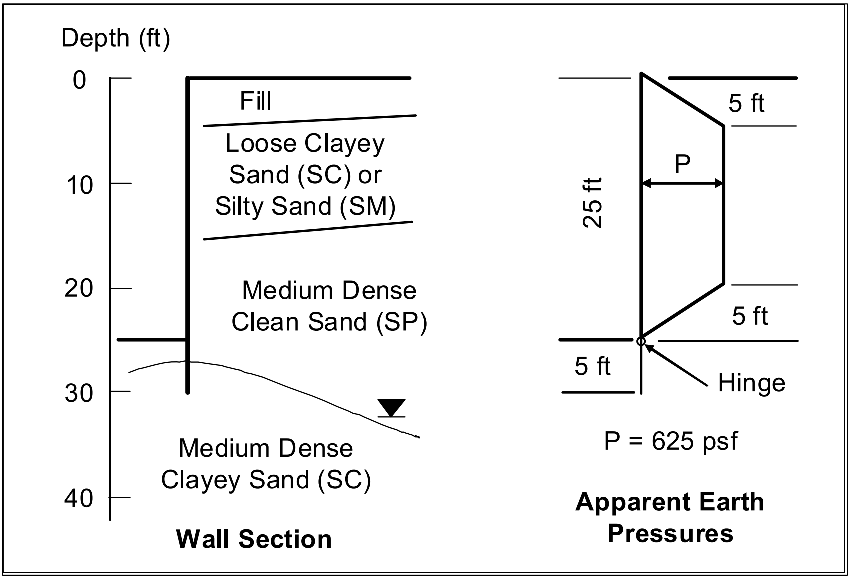

Figure 1. Wall Section, Soil Profile and Apparent Earth Pressures

The wall sections were designed to support the Schnabel (1982) apparent earth pressure diagram, Figure 1. Bending moments and tieback loads were calculated assuming a hinge at subgrade. Figure 2 shows the design bending moment diagrams, tieback loads and subgrade reactions for the wall sections. A hinge was assumed in the beam at the lower tieback in the two-tier wall section. Soldier Beams 7-10, two-tier section, were WF 6X25 beams with welded angle gauge protection. Beams 7-10 had an area of 10.9 in^2 and a moment of inertia of 132.9 in^4. Beams 13-16, one-tier section, were HP 10X57 beams with welded angle gauge protection. They had an area of 19.68 in^2 and a moment of inertia of 417.8 in^4. Soldier beams were spaced 8 feet on center and they had a 5 foot toe below subgrade. Three inch thick wood lagging was used to span between the beams. The wood lagging boards were secured to the soldier beams using 0.5 inch welded studs.

Vibrating wire strain gauges were installed on 1 foot centers along the front and back flanges of the instruments beams. Custom built, concrete embedment strain gauge tubes were installed in the concrete or low strength fill used to backfill the toes of the drilled-in soldier beams. Vibrating wire loads cells were installed on the tiebacks. A datalogger read and recorded all of the vibrating wire instruments. Plastic inclinometer casings were installed between the flanges of each instrumented beam. The inclinometer casings extended approximately 12 feet below the bottom the beams.

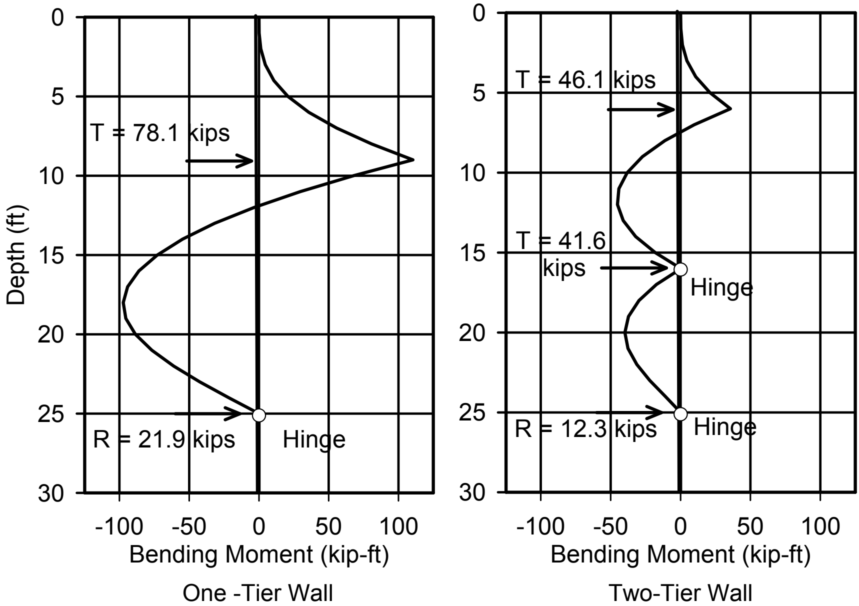

Figure 2. Soldier Beam Bending Moment Diagrams

Driven Beams 7, 8, 15 and 16 were installed using a MKT 9B3 double acting air hammer supported in swinging leads. Drilled-in Beams 9, 10, 13 and 14 were installed in cased holes. Eighteen inch casing was used for Beams 9 and 10 and 24-inch casing was used for Beams 13 and 14. A truck mounted drill removed the soil from the casings. Holes for Beams 9 and 14 were backfilled with lean-mix fill. Holes for Beams 10 and 13 were backfilled with structural concrete in the toe and with lean-mix backfill above the bottom of the excavation. The lean-mix fill had an average 28-day compressive strength of 87 psi and the concrete had an average 28-day compressive strength of 4770 psi.

Pressure-injected tiebacks were used to support the wall. The tiebacks were installed at 30 degree from the horizontal in order to apply a significant axial load to the soldier beams.

WALL BEHAVIOR

Soldier beam bending moments and axial loads were calculated from the measured strains. During construction unreasonably large axial loads were calculated at all exposed gauge locations. Investigation revealed that welding of the lagging studs to the beams increased the compressive strains in the front flange gauges above the bottom of the excavation. The induced compressive strains in Beams 7-10 caused the calculated axial loads to be about 14 kips higher than the actual loads. The calculated axial loads in Beams 13-16 were about 24 kips higher than the actual loads. Figures 3 and 4 show the uncorrected axial loads. Since the axial load errors were significant, the axial loads reported in the remainder of this paper were computed from strain gauges located below the bottom of the excavation, beyond the influence of the welding. The calculated bending moments were affected by the welding induced strains but the error was relatively small, -4.11 kip-ft for Beams 7-10 and -7.74 kip-ft for Beams 13-16.

One-Tier Wall Section

Bending moment curves, axial load curves, soldier beam inclinometer plots and soldier beam settlements for the one-tier wall section, Beams 13-16, at completion of construction, are shown in Figure 3. The tieback design load for the one-tier section was 90.2 kips. The average lock-off load was 67.7 kips. The average tieback load upon completion of construction was 72.5 kips. Figure 2 shows that the maximum design bending moment was 110.8 kip-ft and it was located at the tieback. After stressing of the tiebacks, excavation at 10 feet, the average bending moment at the tiebacks was 95.4 kip-ft. Upon completion, excavation at 25 feet, the bending moments at the tieback averaged 113 kip-ft, Figure 3. The average maximum moment was 102% of the design value.

The maximum design bending moment below the tieback in the one-tier wall section was -97.1 kip-ft, Figure 2. Measured bending moments below the tieback increased as the excavation deepened. The maximum measured moments below the tieback averaged 49.4 kip-ft upon completion of the wall, Figure 3. They were only 51 % of the design moment. Figure 3 shows small bending moments below the tieback and moments near zero in the toe.

Bending moments for the drilled-in beams were calculated using steel section properties. Figure 3 shows that the drilled-in beams had lower bending moments than the driven beams over the lower portion of the wall. This difference may be the result of partial composite action between the steel beams and the concrete or lean-mix backfill. Bending moments calculated assuming full composite action between the steel and the backfill concrete or lean-mix were unreasonably high.

Axial load curves for Beams 13-16 are shown in Figure 3. The average axial load in Beams 14, 15 and 16 at a depth of 26 feet, one foot below the bottom of the excavation and beyond the influence of the stud welding, was approximately 43 kips when the excavation was completed. The vertical component of the tiebacks supporting these beams was 36.3 kips. Therefore, the average axial load was 6.7 kips greater than the vertical component of the tieback force. The axial load in Beam 13 at a depth of 26 feet was 5 kips. A significant portion of the load in Beam 13 was transferred to the ground between 21 and 26 feet. Beam 13 settled more than the other beams in the one-tier wall section and as it settled it transferred load to the supported ground above the bottom of the excavation. Plotted loads in Figure 3 ignored composite action between the concrete and the

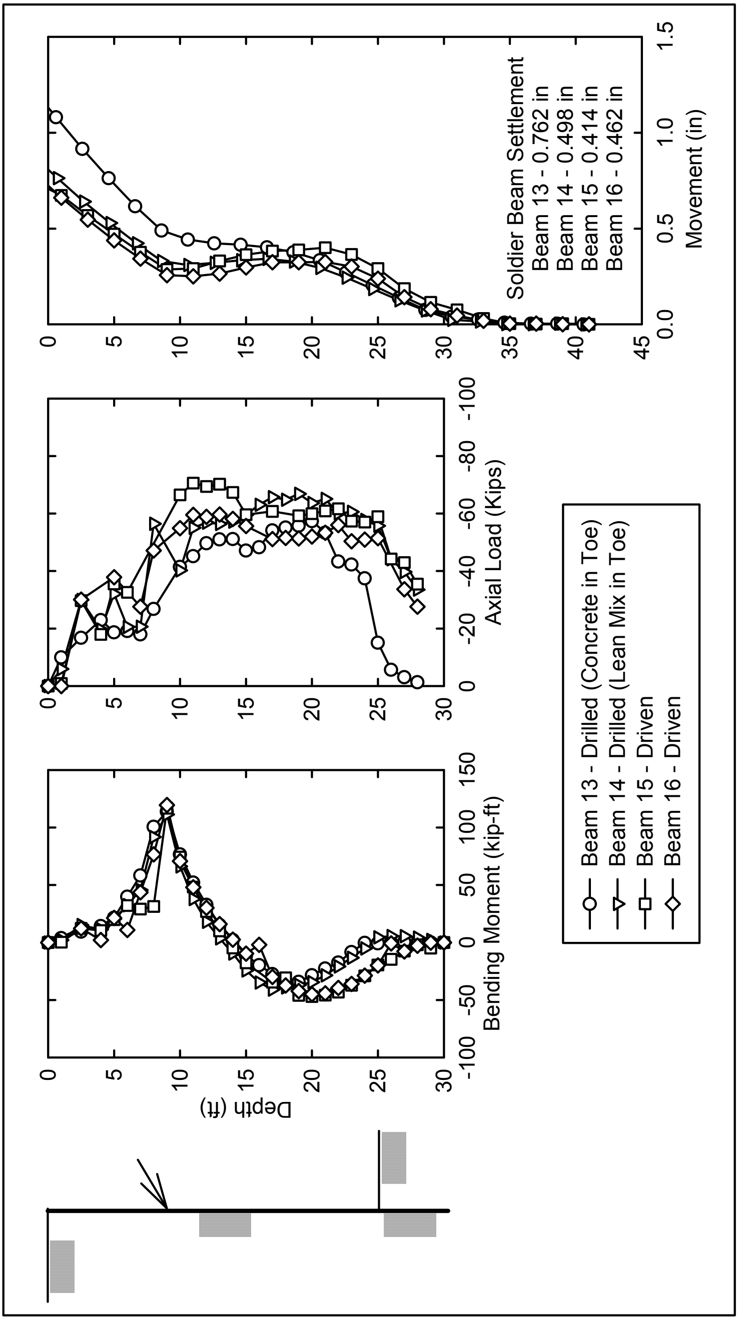

Figure 3. One-Tier Wall Bending Moments, Axial Loads, Lateral Movements and Settlements

beam in the toe. If the toe behaved as a partial composite section, then actual loads would be higher than those shown in Figure 3.

Lateral wall movements and beam settlements for the one-tier section are shown in Figure 3. Average lateral wall movement of the tops of Beams 14 – 16 was 0.25% H, and the lateral wall movement of the top of Beam 13 was 0.38% H. The vertical settlement for Beams 14 – 16 averaged 0.15% H and the settlement for Beam 13 was 0.25% H. Clough and O'Rourke (1990) reported the average lateral and vertical wall for similar walls to be 0.2% H and 0.15% H, respectively. Movements for Beams 14-16 were in this range.

Driven Beams 15 and 16, and drilled-in Beam 14 had similar lateral movements. Drilled-in Beam 13 experienced larger movements its upper half. Beam 13 settled about 1.65 times more than the other beams in the one-tier section and the larger lateral movements were a direct result of the additional settlement.

All four beams settled sufficiently to fully mobilize skin friction along the toe. Beam 13 continued to settle after construction was completed. The end bearing resistance of Beam 13 was fully mobilized. Beams 14 - 16 mobilize some end bearing, but settlement did not continue upon completion of the wall. Beam 14 was backfilled with lean-mix backfill and it behaved better than Beam 13 which was backfilled with structural concrete.

Two-Tier Wall Section

Beams 7-10 were instrumented in the two-tier wall section. In the two-tier wall section, one tieback was used to support two adjacent soldier beams at each support level. The tieback was installed in the center of a wale that spanned between the beams. The design load for the top tier tieback was 106.5 kips and the design loads for the lower tier tieback was 96 kips. Upper tier tiebacks were locked off at an average load of 82.4 kips and the lower tier tiebacks were locked off at an average load of 71.5 kips. Upon completion of construction the average upper tier tieback load had increased to 90.9 kips and the average lower tier tieback load essentially remained unchanged after tieback stressing.

Bending moment curves, axial load curves, soldier beam inclinometer plots and soldier beam settlements for the two-tier wall section, Beam 7-10, at completion of construction are shown in Figure 4. The design bending moment at the upper tieback was 35.8 kip-ft, Figure 2. Upon completion of the excavation, the average measured bending moment at the upper tieback location was 44.9 kip-ft, Figure 4. The difference between the design and the measured bending moment at the upper tieback resulted from the shape of the apparent earth pressure diagram and the moment "locked" into the beam during testing of the tieback.

The maximum design bending moment below the upper tieback level was 45.8 kip-ft. The maximum average bending moments below the upper tieback occurred at the second tier tieback and it was 28.1 kip-ft, Figure 4. The moment at the second tieback was 61% of the design moment for the lower portion of the wall. The design assumed a hinge, zero moment, at the second tier tieback and

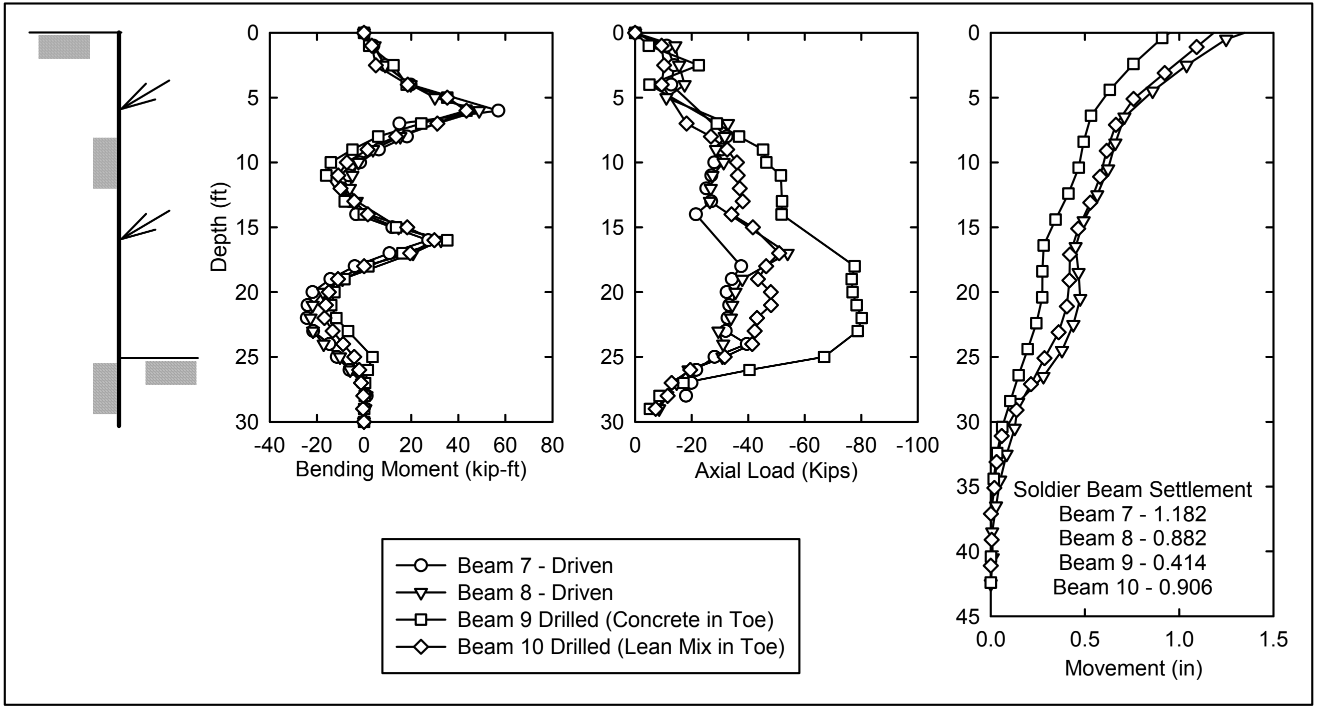

Figure 4. Two-Tier Wall Bending Moments, Axial Loads, Lateral Movements and Settlements

at subgrade. Hinges break the wall into simple spans for ease of calculations and give conservative bending moment estimates. The average maximum bending moment in the span between the upper and lower tier was -10.6 kip-ft and the average maximum moment below the lower tieback was -19.4 kip-ft. These values are 23% and 42% of the design values at these locations.

Figure 4 shows that both drilled-in beams had lower bending moments than the driven beams below the lower tieback. Similar to the one-tier wall, this difference may be the result of the development of a partial composite section along the lower portion of the beam.

The average axial load in Beams 7, 8 and 10 at a depth of 26 feet, one foot below the bottom of the excavation and beyond the influence of the stud welding, was approximately 20 kips when the excavation was completed. The vertical component of the tiebacks supporting Beams 7 and 8 was 37.8 kips. Therefore, 17.8 kips of the vertical load in the beams was transferred to the ground above the bottom of the excavation. Beam 9 settled less than the adjacent beams and had an axial load of 40 kips at a depth of 26 feet when the excavation was completed. The vertical component of the tiebacks supporting Beam 9 was 43.5 kips. The axial load in Beam 9 was similar to the load in Beams 14-16. Beam 9 and Beams 14-16 settled between 0.4 and 0.5 inches while Beams 7, 8 and 10 settled about 1 inch.

Lateral wall movements and beam settlements for the two-tier wall section are shown in Figure 4. The inclinometer probe could not reach the bottom of the Beam 7 casing. Therefore, no lateral movement curve is shown for Beam 7. Average movement of the top of Beams 8 and 10 was 0.42% H and the vertical settlement for Beams 7, 8 and 10 averaged 0.32% H. Lateral movement at the top of the wall at Beam 9 was 0.3% H and the vertical settlement for Beam 9 was 0.14% H. Wall movements for Beams 7, 8 and 10 are in the upper range of movements reported by Clough and O'Rourke (1990).

All four beams settled sufficiently to fully mobilize skin friction along the toe. Beams 7, 8 and 10 continued to settle after construction was completed indicating that their end bearing resistance was fully mobilized. Beam 9, drilled beam with structural concrete in the toe, did not continue to settle and had some additional end bearing capacity.

Axial Loads, Settlements and Lateral Wall Movements

Axial loads in the instrumented soldier beams depended on the vertical component of the tieback force and the relative movement of the beams with respect to the supported ground. The load was greater than the vertical component of the tieback force when the supported ground settled relative to the soldier beams and less than the vertical component of the tieback force when the beams settled relative to the ground.

As stated earlier, the axial behavior of the wall during construction was studied by examining the loads computed from the strains one foot below the excavation level. These strains were not affected by welding. Axial load curves for Beams

7, 8 15 and 16 are shown in Figure 5. Load in the driven beams is presented to eliminate possible effects of composite behavior. Open triangles represent the average vertical component of the tieback load and open circles represent the average axial load in the soldier beams 1 foot below the excavation level at each stage of construction. Average soldier beam settlements and the volume of lateral wall movement per inch along of wall are shown in the figure.

Small axial compressive loads were measured in the soldier beams before installing the tiebacks. An average axial load of about 2 kips was measured in Beams 7 and 8 when the excavation extended to a depth of 8 feet. An average axial load of 6 kips developed in Beams 15 and 16 when the excavation reached 10 feet deep. These axial loads occurred as the soldier beams moved out allowing the supported soil to move down relative to the beam.

After the tiebacks were stressed, the axial load in the soldier beams was less than the vertical component of the tieback force. The average compression load at 9 feet in Beams 7 and 8 was 19.0 kips and the vertical component of the ground tieback force was 20.7 kips. After stressing the tiebacks supporting Beams 15 and 16, the average axial load in the beams at 11 feet was 28.9 kips, while the average vertical component of the tieback force was 33.7 kips. Beam settlement was negligible. When the tiebacks were stressed, the normal stress between the beams and the ground increased allowing load to be transferred from the beams to the ground with small relative movement.

As the excavation deepened to 17 feet, the axial load in the beams increased above the vertical component of the tieback force. This indicates that the supported ground moved down relative to the soldier beams as the excavation deepened. Figure 5 shows that the average axial load in Beams 7 and 8 was approximately 12.0 kips greater than the vertical component of the tieback force, and that the average axial load in Beams 15 and 16 was about 11.6 kips greater than the applied force. Settlement was negligible, and axial loads and lateral movement volumes were similar for the one-tier and two-tier driven beams when the excavation depth was 17 feet.

A second row of tiebacks was installed to support Beams 7 to 10 while the excavation was 17 feet deep. The effect of locking-off these tiebacks is shown in Figure 5. The increase in the axial load in Beams 7 and 8 was about the same amount as the vertical component of the second row tieback force. Beams 7 and 8 did not settle significantly as the second row tieback was stressed.

When the excavation reached 21 feet deep, the axial loads in Beams 7 and 8 decreased to approximately equal vertical components of the tiebacks that supported the beams. At this time, Beam 7 had settled 0.28 in and Beam 8 had settled 0.19 in. When the excavation in front of Beams 15 and 16 reached 21 feet deep, the axial loads in these beams increased. With the excavation 21 feet deep, Beam 15 had settled 0.09 in and Beam 16 had settled 0.11 in. The behavior of the wall at the 21 foot deep excavation confirms the observation that the relative movement of the beams with respect to the supported ground affects the magnitude of the axial load in the beams. The vertical component of the tieback loads in each beam was about the same for all beams. However, Beams 7 and 8

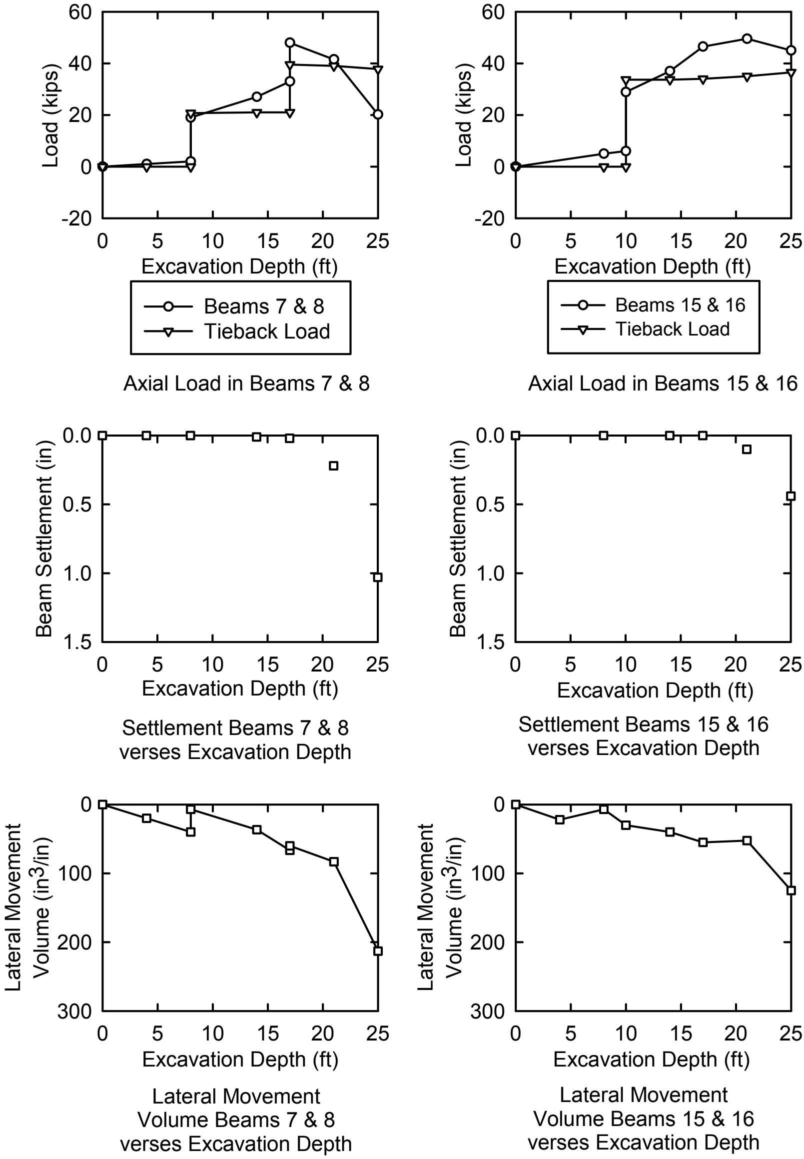

Figure 5. Average Axial Load, Vertical Component of Tieback Load, Beam Settlements and Lateral Movement Volume for Beams 7, 8, 15 and 16

settled an average of 0.13 inches more than Beams 15 and 16, and the average axial load in Beams 7 and 8 was 13.5 kips less than the average axial load in Beams 15 and 16. Beam settlements between 0.1 and 0.15 inches were required to the transfer significant load from Beams 7 and 8 to the ground. At the 21 foot depth, the total settlement of Beams 7 and 8 equaled 0.09% H, and the maximum lateral movement equaled 0.26% H. The movements are typical for well designed walls.

Upon excavating from 21 to 25 ft, the average settlement of Beams 7 and 8 exceeded 1 inch, and the axial load in these beams dropped below the vertical component of the tieback. Figure 5 shows that the lateral movements increased as the beams settled. At the 25 foot deep excavation, Beams 15 and 16 had a total settlement of about 0.45 inches. The axial load dropped from the value measured when the excavation was 21 feet deep, but the load was still 9 kips greater than the vertical component of the tieback force. Figure 5 shows that the lateral movement of Beams 7 and 8 was about 170% of the movement of Beams 15 and 16. Most of the lateral wall movement occurred as the beams settled.

Backfilling Drilled-in Soldier Beam Toes

Structural concrete was used to backfill the toes of drilled-in Beams 9 and 13. Beams 10 and 14 were backfilled with lean mix backfill. Beams 9 and 14 had less settlement than the other drilled-in beams. Beam 9 had structural concrete in the toe and Beam 14 had lean-mix fill in the toe. The performance of the drilled-in beams did not depend upon the type of backfill used. It is likely that the conditions at the bottom of the drilled shafts affected the end bearing resistance. The bottoms of the drilled shafts for Beams 9 and 14 were likely well cleaned while the bottoms of the drilled shafts for Beams 10 and 13 probably were disturbed.

RECOMMENDATIONS

A series of recommendations for the design of free-drained, tiedback walls were made to the FHWA in a Design Manual, Weatherby (1998). Some of the recommendations are presented below.

Earth Pressure Diagrams

Apparent earth pressure diagrams should be used for the design of one-tier and multi-tier walls. A new diagram is discussed and recommendations for using apparent earth pressure diagrams for the design of tiedback walls are presented.

Use Apparent Earth Pressure Diagrams for the Design of One-Tier Walls

Rankine, triangular, active earth pressure diagrams are still being used to design walls supported by one level of tiebacks or to check early construction stages of multi-tier walls. The research clearly showed that a trapezoidal apparent earth pressure diagrams should be used for design of one-tier walls.

Figure 6 compares the average bending moments in Beams 15 and 16, with those computed from the Schnabel diagram and those computed using a Rankine triangular active earth pressure diagram. The active Rankine pressures were determined using an active earth pressure coefficient of 0.307 and a total unit weight of 115 pcf. Passive toe pressures were determined using a passive earth pressure coefficient of 6.44, and they were applied over 3 times the soldier beam width. The passive earth pressure coefficient included wall friction and was determined using a chart from NAVFAC (1982) Design Manual 7. A wall friction angle of 21.5 degrees was selected. Active pressures were applied over the width of the beam below the bottom of the excavation. A continuous beam, no subgrade hinge, was used in the Rankine design.

The total load from the Schnabel diagram was 100 kips and the total Rankine load above the bottom of the excavation was 88.3 kips. The horizontal component of the tieback load from the Schnabel diagram was 78.1 kips and the horizontal component of the tieback load from the Rankine diagram was 60 kips. The Schnabel diagram required the toe to develop about 22 kips of lateral resistance while the Rankine diagram required the toe to develop 28 kips.

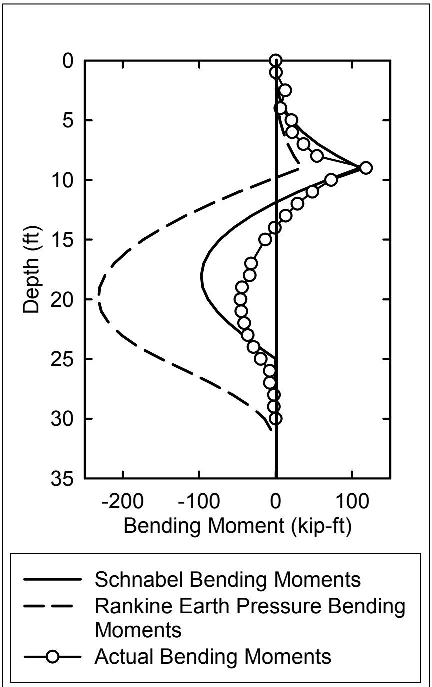

Figure 6. Schnabel, Rankine and Measured Moments for the One-Tier Wall

Figure 6 shows the Rankine bending moment at the tieback to be 34 kip-ft with the tieback at 9 feet from the top of the beam. In the span below the tieback, the maximum Rankine moment is 232 kip-ft. It is necessary to check intermediate construction stages when designing for Rankine pressures. At a depth of 10 ft, the minimum excavation necessary to allow for the installation of a tieback at 9 feet, the computed cantilever bending moment was 86.5 kip-ft. This moment is 78% of the Schnabel bending moment at the tieback. At the tieback level, the apparent earth pressure bending moment was 110.8 kip-ft. In the span between the tieback and the bottom of the excavation the maximum Schnabel bending moment was 97.1 kip-ft. The maximum Rankine bending moment below the tieback was 209% larger than the maximum design moment. Small bending moments were measured in the lower portion of the wall and in the toe. The apparent earth pressure diagram gave conservative bending moments for the lower portion of the wall. Using a Rankine triangular earth pressures did not accurately model the behavior of the wall and it would have unnecessarily doubled the design bending moments without any benefit.

Based on the measurements and the above discussion it is clear that apparent earth pressure diagrams should be used for the design of one-tier tiedback walls. This behavior was confirmed by the model tests reported by Mueller et al. (1998).

Intermediate Construction Stages

Some specifications require that the design check different construction stages using Rankine pressures. This practice probably is a carryover from designing one-tier walls for Rankine active pressures. It is unnecessary to check intermediate construction stages if apparent earth pressure diagrams are used for design. Apparent earth pressures are envelops of measured strut loads during all stages of construction and they are substantially greater than the Rankine pressures at shallow depths. As an example, the Rankine bending moment (86.5 kip-ft) when excavating to a depth of 10 feet is 78% of the cantilever Schnabel bending moment (110.8 kip-ft). There are two exceptions; when the wall is a structural cutoff wall with significant water pressures and when low strength soils are present below the tieback or at the bottom of the excavation. In these situations, intermediate construction stages should be checked.

New Apparent Earth Pressure Diagrams

Figure 7 shows the average bending moments from Beams 7 and 8 with those predicted from the Schnabel diagram. Using the same earth pressure diagram for the one-tier and the two-tier section underestimated the bending moment at the upper tieback in the two-tier section. Figures 7 also shows the bending moments predicted using the Terzaghi and Peck (Terzaghi et al. (1996)) apparent earth pressure diagram for sand. The Terzaghi and Peck diagram is rectangular and it gave large bending moments at the top tieback. The actual earth pressures in a coarse-grained soil are zero at the ground surface and the new apparent earth pressure diagram discussed below starts with zero pressure at the ground surface. Measured bending moments along the toe of all the beams were small indicating that the earth pressures were small over lower portions of the walls. Model wall tests described by Mueller et al. (1998) also showed small earth pressures over the lower portion of the wall. The measured bending moments clearly showed that the wall distributes the tieback force to the ground. A new trapezoidal apparent earth pressure diagram was developed based on the measurements from the full-scale and model-scale wall tests.

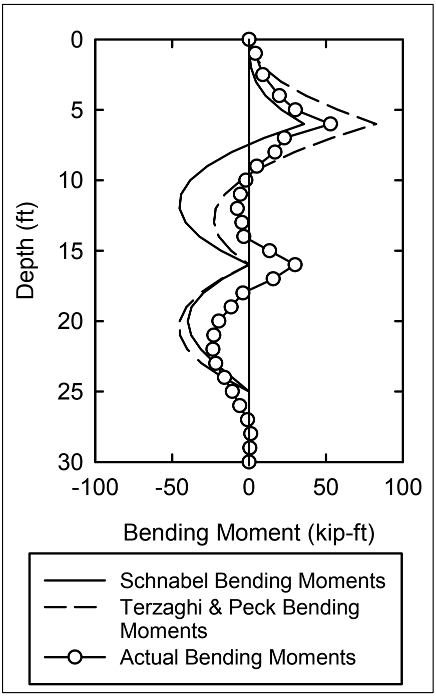

Figure 7. Schnabel, Terzaghi & Peck and Measured Moments for the Two-Tier Wall

Figure 8 shows the new trapezoid apparent earth pressure diagrams for one-tier and two-tier walls. The shape of the trapezoid is determined by the locations of the supports and the load is zero at the top of the wall and the bottom of the excavation. The total load distributed by these diagrams is equal to the total load given by the traditional apparent earth pressure diagrams or that determined by limiting equilibrium analysis. Figures 8 and 9 show the bending moment plots for the new apparent earth pressure diagrams and the Schnabel diagram. Measured bending moments are also shown. The moment curves match the measured data better than design moment curves. Weatherby et al. (1998) provides additional details regarding the new apparent earth pressure diagram.

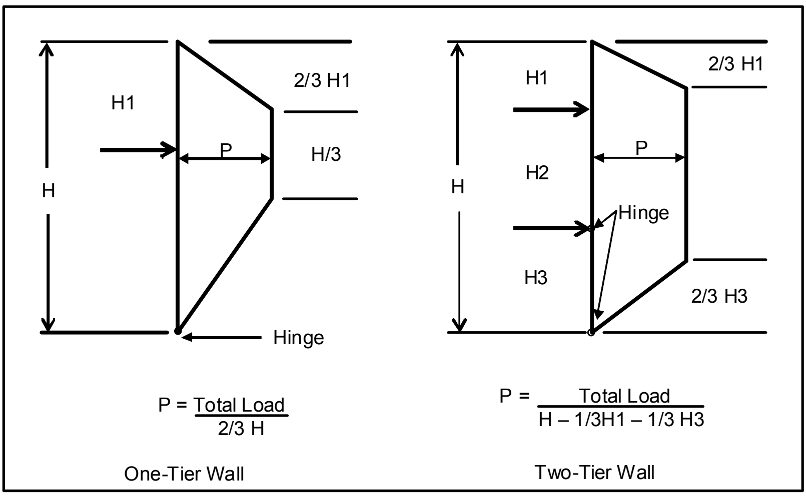

Figure 8. New Trapezoidal Apparent Earth Pressure Diagrams

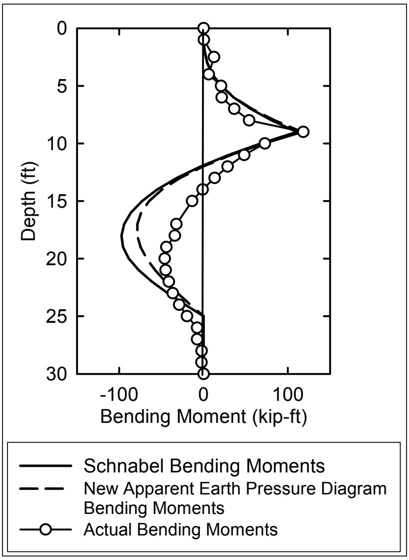

Figure 9. New Apparent Earth Pressure Diagram, Schnabel and Measured Moments for One-Tier Wall

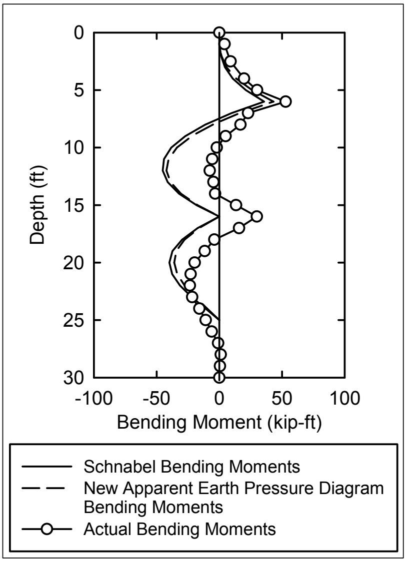

Figure 10. New Apparent Earth Pressure Diagram, Schnabel and Measured Moments for Two-Tier Wall

Subgrade Hinge

Bending moment calculations using apparent earth pressure diagrams assume a hinge at bottom of the wall. The full-scale and model-scale walls show that assuming a pin connection at the bottom of the wall gives reasonable bending moments for design. A subgrade hinge is not appropriate for walls with poor soils at subgrade or for structural cutoff wall supporting significant water pressures.

Moment Reductions

The apparent earth pressure diagrams predict bending moments below the upper tieback that are larger than those measured, Figures 6, 7, 9 and 10. Peck et al. (1974) recommended designing the soldier beams to resist bending moments equal to 2/3 of the computed bending moments. The performance of the walls indicates that soldier beam design moments below the upper tieback can be 66% of the moments computed from the apparent earth pressure diagram.

Determining Total Earth Pressure Loads Using Limiting Equilibrium Methods

General purpose slope stability computer programs are used to determine the total lateral earth load to be distributed by an apparent earth pressure diagram.

Before using a computer program for determining tieback loads, compare the total loads from the program with the loads from both the Terzaghi and Peck sand and soft-medium clay earth pressure diagrams. Use planar failure surfaces for sands and circular surfaces for clays. Use a factor of safety of 1.3 on the shear strength of the soil for the computer runs. See Long et al. (1998) for justification for selecting a factor of safety of 1.3. The failure surface must go through the bottom of the excavation and the tieback force must be horizontal. The loads from the apparent earth pressure diagram and the computer program should be similar and the shape of the failure surface should be reasonable.

When using slope stability computer programs for the design of tiedback walls the tiebacks will be modeled differently depending upon how the vertical component of the tieback force is being resisted. If the tieback is being used to support a wall that penetrates the failure surface, then the tieback should be modeled as a horizontal load and the load should equal the horizontal component of the tieback force. If the tieback load is applied to an element that does not penetrate the failure surface, then the full tieback load should be used and the load should be applied at the proposed tieback angle. This is illustrated in Figure 11. When the vertical component of the tieback is applied to the ground above the failure surface, the load increases the driving force. It also increases the normal force on the failure surface and the shear resistance along the failure surface of frictional soils.

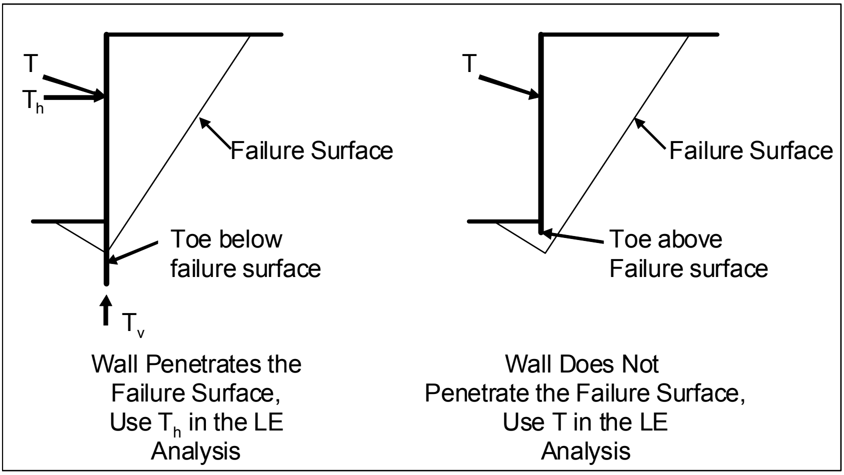

Figure 11. Modeling the Tieback in Limiting Equilibrium Analysis

Axial Load and Axial Capacity

Soldier beam toes should be designed to carrying the vertical component of the tieback force. The vertical force can be reduced by installing the tiebacks at shallow angles. Wall movements will increase if the beams settle, but collapse is not likely if the wall settles excessively.

Side friction along the toe is mobilized first, and as the beam settles end bearing is mobilized. Small movement is required to mobilize side friction. Wall movement can be limited by designing the toe to carry load in side friction. This will increase the costs, but should be considered when sensitive structures are located behind the wall.

Lean-mix is suitable for backfilling drilled soldier beam toes. Care must be taken to ensure that the end bearing resistance of drilled-in beams can be developed.

Tip resistance for driven soldier beams is more reliable than the end bearing resistance for drilled-in beams.

CONCLUSIONS

The following conclusions and recommendations for the design of tiedback walls were presented in the paper.

- Use apparent earth pressure diagrams for the design of one-tier walls.
- It is unnecessary to check intermediate construction stages when designing for apparent earth pressures.
- A new trapezoidal apparent earth pressure diagram was developed. The shape of the diagram is determined by the location of the tiebacks.
- Use a subgrade hinge when calculating soldier beam bending moments.
- Below the upper tieback, design bending moments can be 2/3 of the moments computed by the apparent earth pressure diagrams.
- Axial load in the soldier beams depended on the vertical component of the tieback force and the relative movement of the beams with respect to the supported ground.
- Tieback wall movements depend upon soldier beam settlement.
- Minimize axial load and settlement by installing the tiebacks at flat angles.
- Take care to maintain good end bearing resistance when using drilled-in soldier beams.
- When it is necessary to limit movements, design the toes to carry most of the axial load by side friction.
- Lean-mix backfill can be used to backfill soldier beam toes.
- Driven pile tip resistance is more reliable than drilled shaft end bearing resistance.

REFERENCES

Clough, G. W. and O'Rourke, T. D. (1990) "Construction Induced Movement of In-situ Walls," Proceedings ASCE Specialty Conference Design and Performance of Earth Retaining Structures, Cornell University, Ithaca, NY.

Long, J. H., Weatherby, D. E., and Cording, E. J. (1998) *Summary Report of Research on Permanent Ground Anchor Walls*, "Volume I: Current Practice and Limiting Equilibrium Analyses," FHWA-RD-98-065, FHWA, Mclean, VA.

Mueller, C. G., Long, J. H., Weatherby, D. E., Cording, E. J., Powers III, W. F., and Briaud, J-L. (1998). *Summary Report of Research on Permanent Ground Anchor Walls*, Volume III: Model-scale Wall Tests and Ground Anchor Tests," FHWA, McLean, VA.

NAVFAC (1982). *Foundations and Earth Structures Design Manual 7.2*, Dept. of the Navy, Naval Facilities Engineering Command, Alexandria, VA.

Peck, R. B., Hanson, W. E., and Thornburn, T. H. (1974) *Foundation Engineering*, John Wiley & Sons, New York, NY.

Schnabel Jr., H. (1982). *Tieback in Foundation Engineering and Construction*, McGraw-Hill, New York, NY.

Terzaghi, K., Peck, R. B., and Mesri, G. (1996). *Soil Mechanics in Engineering Practice*, 3rd Edition, John Wiley & Sons, New York, NY.

Weatherby, D. E., (1998). *Design Manual for Permanent Ground Anchor Walls*, FHWA-RD-97-130, FHWA, McLean, VA.

Weatherby, D. E., Chung, M., Kim, N-K., and Briaud, J-L., (1998). *Summary Report of Research on Permanent Ground Anchor Walls*, "Volume II: Full-scale Wall Tests and a Soil-Structure Interaction Model," FHWA-RD-98-066, FHWA, McLean, VA.

ACKNOWLEDGEMENTS

The research work was funded by the Federal Highway Administration and Schnabel Foundation Company. The work at Texas A&M was under the direction of Professor Jean-Louis Briaud and the work at the University of Illinois was under the direction of Professors James H. Long and Edward J. Cording. Graduate students M. Chung, N-K Kim, and W. F. Powers at Texas A&M and C. G. Mueller at the University of Illinois devoted an amazing amount of time, energy and creative thinking during this research effort. This work would not have been possible without their efforts.

APPENDIX I. CONVERSION TO SI UNITS

Feet (ft) X 0.305 = meter (m)
Inch (in) X 25.4 = millimeter (mm)
Kip (kip) X 4.448 = kilo-newtons (kN)
Pounds per ft^3 (pcf) X 0.157 = kN/m^3
Pounds per in2 (psi) X 6.895 = kilo-pascal (kPa)

Case History: Investigating the Risks Associated with Allowing Temporary Tiebacks to Remain Stressed

Matthew W. Smith, PE, M.ASCE[1], Lindsay C. Flangas, PE, A.M.ASCE[2], and Daniel P. Ciani, A.M.ASCE[3]

[1] Associate, GeoEngineers, Inc., 8410 154th Avenue NE, Redmond, WA 98052, msmith@geoengineers.com
[2] Project Engineer, GeoEngineers, Inc., 8410 154th Avenue NE, Redmond, WA 98052, lflangas@geoengineers.com
[3] Staff Engineer, GeoEngineers, Inc., 8410 154th Avenue NE, Redmond, WA 98052, dciani@geoengineers.com

ABSTRACT

The City of Seattle, like many municipalities, requires that tiebacks installed in the City right-of-way be de-stressed at the conclusion of the project. For buildings where basement walls are constructed adjacent to temporary shoring walls, de-stressing tiebacks is costly and time-consuming, and often diminishes both the waterproofing and aesthetic characteristics of the basement wall. These factors raise the questions: "Is it necessary or good practice to de-stress tiebacks?" and "What are the risks of not de-stressing tiebacks?"

To help answer these questions, a demonstration was conducted to assess the risk when tiebacks are de-stressed along the embedded strand rather than at the tieback head, simulating the condition where the tieback is de-stressed during future improvement projects. The demonstration was designed to evaluate the behavior of the tieback when de-stressed with an excavator and to assess the impact to a basement wall upon immediate release of tieback load. An auxiliary goal was to evaluate the portion of the anchor capacity derived from the grout located in the no-load zone of the tieback.

The demonstration involved installing two sacrificial tieback anchors on soldier piles at an active project site. After excavation exposed the no-load zone of each tieback, one tieback was severed with an excavator and the other with a hydraulic shear. Video cameras recorded the demonstration, and survey measurements were made of the soldier piles before and after the tiebacks were de-stressed. Tieback load cell readings were taken at different stages of the excavation.

The demonstration did not reveal significant safety concerns or risk of potential adverse impacts to existing improvements or the adjacent basement wall when the tieback was de-stressed along the embedded strand. Additionally, the load cell measurements indicate that very little capacity of the tieback was derived from the anchor no-load zone.

INTRODUCTION

The City of Seattle's municipal code requires that temporary tiebacks installed in the City right-of-way be de-stressed prior to project completion. The primary reason for this requirement is concern that loaded tiebacks could represent a hazard to worker safety and/or to existing improvements when encountered as part of future construction in the City right-of-way. To comply with this code, a typical construction sequence is to block-out the tieback head, cast the permanent basement wall and building diaphragms, de-stress the tieback, and patch the waterproofing membrane (where present) and basement wall. The de-stressed tiebacks are typically abandoned in place because the City's municipal code does not require removal of shoring elements located more than 4 feet below the ground surface.

Figure 1 is a photograph depicting block-outs for tieback de-stressing on a project in the City of Seattle. This process is expensive and results in a less reliable waterproofing system and an aesthetically less desirable basement wall. Given the expense and undesirable impacts of this policy, a demonstration project was conducted to investigate the risks associated with stressed tiebacks.

Figure 1. Typical tieback block-out

The purpose of the demonstration project was to observe the behavior of tiebacks and impacts to surrounding improvements when the tiebacks are de-stressed along the embedded strand rather than at the tieback head. The demonstration was planned to model the situation in which tiebacks are not de-stressed from inside the building prior to the completion of construction, but rather are de-stressed from outside the building in a manner that would likely occur during new construction of improvements adjacent to the property.

The primary goal of this demonstration project was to provide a well-documented case history to assess the risk of leaving stressed tiebacks in the City right-of-way and to provide recommendations for future study regarding this topic. To this end, the study included: (1) monitoring the load in the tiebacks during excavation and removal of grout from the no-load zone/bond zone interface; (2) observing the response of a stressed tieback anchor being de-stressed by an excavator and by a hydraulic shear device; (3) observing the response of a mock concrete basement wall constructed adjacent to the tieback head during instantaneous de-stressing of the tieback anchor by means of a hydraulic shear device; and (4) monitoring the deflection of the soldier pile after de-stressing the tieback.

A secondary goal of the demonstration was to evaluate the portion of the anchor capacity derived from the grout located in the no-load zone for tiebacks constructed using high strength steel strands with a sheathed no-load zone and single-stage grouting of the anchor.

DESCRIPTION OF DEMONSTRATION SETUP

The tieback de-stressing demonstration consisted of installing two sacrificial tieback anchors at an active construction site and severing the tiebacks in the tieback no-load zone under controlled conditions. The approximate geometry of the excavation completed to sever the tiebacks is shown in Figure 2.

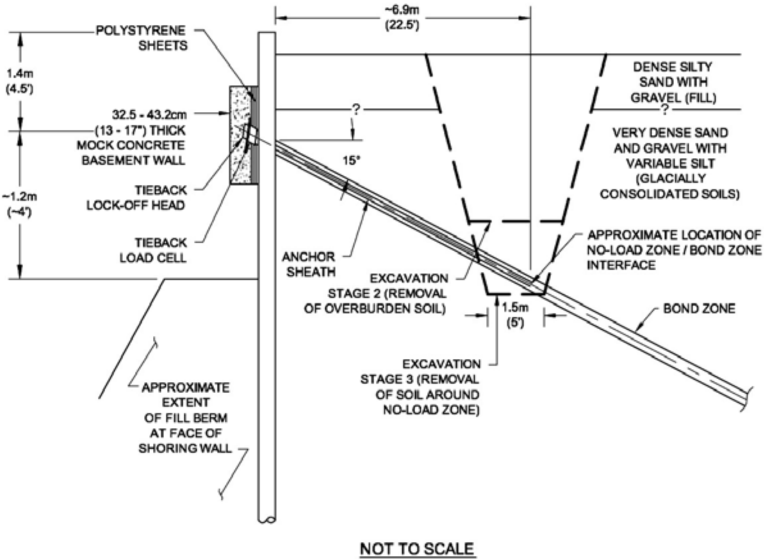

Figure 2. Test section

The tiebacks were installed using a Davey DK 725 air-rotary drill rig with 6-inch-diameter casing. The soil profile generally consisted of several feet of fill overlying glacially consolidated soils. The soils that the tieback anchors were installed into consisted of very dense sand and gravel with variable silt and cobble content. The groundwater table is located well below the tieback bond zone. The tieback anchors each had a 7.6 m (25 ft) bond zone, a 7.6 m (25 ft) no-load zone and a 1.2 m (4 ft) tail. The tieback no-load zone was isolated from the grout column with grease-filled polyethylene sheathing. Both tiebacks consisted of four 1.5 cm (0.6 in) diameter, 7-wire, low-relaxation strands with an ultimate tensile stress of 1862 MPa (270 ksi). Neat cement grout was mixed on-site and pumped into the holes after inserting the tieback using a 1.3 cm (½ in)-diameter polyvinyl chloride (PVC) tremie pipe. The grouting was completed in a single stage (grouted to the face of the wall prior to stressing the tiebacks). The tiebacks were post grouted approximately three days after installation by using a 1.3 cm (½ in)-diameter PVC pipe with grout ports located within the bond zone of the tieback.

The tiebacks were installed on two soldier piles (designated BB5 and BB6), which consisted of W18x65 wide flange steel beams inserted in 91.4 cm (36 in)-diameter drilled shafts that were backfilled full depth with lean concrete. The heads of the sacrificial tiebacks were located approximately 1.1 m (3.5 ft) below the ground surface, and the tiebacks were installed with 15-degree declinations. The tiebacks were proof-tested to 133 percent of the design load [445 kN (100 kips)]. Each of the sacrificial tiebacks was instrumented with Geokon Model 4900 vibrating wire load cells with a maximum range of 1334 kN (300 kips).

A mock concrete basement wall was constructed in front of and adjacent to the tieback head at pile BB5 in order to evaluate whether adverse impacts to the concrete or waterproofing would occur if the tieback were instantaneously severed.

A layer of geocomposite drainage board and a layer of a sodium bentonite waterproofing membrane were placed between the soldier pile and lagging and the concrete, with the waterproofing membrane placed over the top of the tieback head. The mock basement wall consisted of an approximately 1.2 m (4 ft) wide by 1.2 m (4 ft) high by 33 to 43.2 cm (13 to 17 in)-thick cast-in-place concrete panel located immediately adjacent to the tieback head. The panel was lightly reinforced with two vertical and two horizontal #4 reinforcing bars spaced approximately 0.3 m (1 ft) apart. The panel was attached to the shoring wall with four #4 reinforcing bars.

The tieback at soldier pile BB6 was completed with a steel cap covering the tieback head assembly (but not touching the tieback head). The cap was installed in order to contain the tieback head, wedges and strands in the event that these elements moved into the excavation. Figure 3 is a photograph of the demonstration setup.

Figure 3. Demonstration setup (from within excavation)

DESCRIPTION OF DE-STRESSING PROCEDURES

The tieback de-stressing demonstration was designed to observe the response of severing the tiebacks through the use of an excavator (tieback BB6) and through the use of a hydraulic shear (tieback BB5). Severing the tieback using an excavator created a likely condition in which a stressed anchor would become de-stressed either intentionally or inadvertently during future excavation. The instantaneous severing using the hydraulic shear would represent a 'worst case' condition for releasing the tieback load.

In order to sever the tiebacks, an excavation was completed to expose 1.5 to 2.1 m (5 to 7 ft) of the no-load zone of each tieback while only slightly exposing the interface between the no-load zone and the bond zone. Figure 2 shows the approximate geometry of the excavation. The size of the excavation was limited in order to reduce the potential for the excavation to cause movement of the soldier pile toward the bond zone of the anchor, which would result in loss of load in the anchor.

Each de-stressing demonstration was recorded by two video cameras mounted on tripods near the excavation and by one camera set near the tieback head.

OBSERVATIONS

One notable observation prior to de-stressing both of the tiebacks was the significant difference in the nature of the neat cement grout observed in the no-load zone compared to the grout in the bond zone. The neat cement grout in the no-load zone was observed to be brittle, fracturing easily and 'flaking' off of the polyethylene sheathing encapsulating the tieback strands when touched by the excavator bucket. The grout in the bond zone was observed to be competent and did not break or fracture when touched by the excavator bucket. The brittleness of the no-load zone grout is interpreted to result from the tieback stressing sequence. Once the tieback is placed in the hole after drilling, there is some inherent sag between centralizers. When the tieback is stressed, the strands located in the un-bonded portion of the tieback straighten. Because the un-bonded portion of the tieback is allowed to freely elongate, the cable straightening effect may create fractures within the no-load zone grout which may contribute to the brittle nature of the grout observed in this demonstration.

Tieback BB6 was the first tieback to be de-stressed. A Komatsu 400 series excavator was positioned perpendicular to the tieback, and the bucket was positioned within the no-load zone and immediately adjacent to the bond zone. The excavator bucket was first placed below the tieback anchor and was then lifted vertically until the tieback was severed. The tieback broke easily at the interface between the no-load zone and the bond zone.

Subsequently, tieback BB5 was de-stressed by means of a large hydraulic shear device mounted on a Kobelco SK 330 excavator. The hydraulic shear instantaneously severed the tieback in the no-load zone immediately adjacent to the bond zone.

The load recorded in the tieback load cell for each tieback remained relatively constant [between 329.6 and 331.4 kN (74.1 and 74.5 kips) for BB6 and 484.9 and

493.8 kN (109 and 111 kips) for BB5] during the following stages of excavation: (1) prior to excavation; (2) after removal of the overburden soil down to 0.6 m (2 ft) above the tieback strand; (3) after removal of the soil around several feet of the tieback no-load zone; and (4) after removal of grout in the no-load zone near the no-load zone/bond zone interface. The recorded load in each tieback load cell was zero after severing the tieback.

Grout and soil were observed to fall away from the tieback strands of both BB6 and BB5 as they were severed, but no significant flying debris was observed from either tieback.

The upward motion of the excavator bucket lifted the BB6 tieback strands into the air when the strands broke, but the strands returned to near the previous tieback alignment after the excavator bucket was removed from the excavation. The BB5 tieback strands remained near their original position and were not observed to move significantly out of axis after being severed. The strands were observed to be stiff when the hydraulic shear device moved away from the tieback after severing the strands, and the strands quickly rebounded to their original position. No uncontrolled or sudden movement of either the BB6 or BB5 tieback strands was observed when the strands were severed.

No movement of the BB6 pile/tieback head toward the bond zone was observed as a result of the excavator pulling on the tieback strands. The video of tieback BB6 and BB5 de-stressing captures the sound of the tieback strands breaking followed by a sudden movement of the pile/tieback head away from the tieback bond zone. These observations are consistent with survey measurements of the tops of piles BB6 and BB5 taken by the contractor (the survey documented that each pile moved into the excavation 0.8 cm (5/16 in) after the tieback was de-stressed).

After the steel cap was removed from the head of tieback BB6 and the mock concrete basement wall panel removed from the head of tieback BB5, the wedges and strands were still observed to be firmly seated in the tieback stressing head assembly for both anchors. This condition is anticipated to be typical because the wedges and tieback stressing heads are designed such that the wedges become firmly seated. No damage was observed in the mock concrete basement wall after the tieback was severed. Although difficult to ascertain without testing under water pressure, it is considered unlikely that the sodium bentonite waterproofing membrane was damaged when tieback BB5 was instantaneously severed.

DISCUSSION OF OBSERVATIONS

The tieback de-stressing demonstration provided valuable information regarding the response of loaded tiebacks being de-stressed by excavating/severing the tiebacks at the tieback no-load/bond zone interface. Additionally, the results of the demonstration provide valuable insight into the use of single-stage grouting of tieback anchors and the question about load transfer into the no-load zone.

Practicability

Typical tiebacks can be readily excavated using conventional earthwork equipment. Tieback BB6, which consisted of a four-strand anchor, was excavated with the

Komatsu 400 series excavator. Given the ease with which the tieback was excavated, it is anticipated that the use of an excavator to de-stress/remove tieback anchors would be the preferred means of de-stressing a tensioned tieback.

Impact to Existing Improvements

For reinforced concrete basement walls cast in front of tiebacks that are not de-stressed, the potential for damage resulting from future de-stressing of the tieback from behind the basement wall is anticipated to be low. By casting the basement wall adjacent to the tieback head, the tieback head is effectively contained.

Provided that the building diaphragms are designed to resist the permanent earth pressures, no adverse impacts are anticipated from de-stressing of the tiebacks and resultant movement of the soldier pile toward the building. This condition is similar to that encountered when tiebacks are de-stressed using conventional techniques. The risk of damage to the basement wall or the waterproofing membrane, if present, is considered low provided that the soldier pile is not attached to the permanent building wall.

The risk of damage to the waterproofing membrane resulting from severing tensioned tiebacks located adjacent to the waterproofing membrane is considered low—much lower than the risk of water damage resulting from patching waterproofing systems after tiebacks are de-stressed using conventional block-outs at the basement walls. Further study may be appropriate to more fully investigate the risk of damage to waterproofing membranes; however, detailing such as welding a steel cap over the tieback or specification of a redundant/resilient waterproofing detail are alternative measures that can be implemented to manage the risk to the waterproofing system, if considered necessary.

Safety

No significant flying debris or erratic response of the tieback strands was observed when severing the tiebacks. The tieback strands were observed to be stiff and to return to or remain near their original position after being severed. These observations indicate that tiebacks can be safely de-stressed using an excavator or a hydraulic shear. An additional demonstration designed to investigate the response of de-stressing tiebacks using a cutting torch or a saw would be helpful to further assess the risk associated with leaving temporary tiebacks in their stressed condition.

Single-Stage Grouting

Single-stage grouting with polyethylene sheathing was used for the two sacrificial tiebacks, and the load in the anchor did not significantly change during excavation or removal of grout from near the no-load zone/bond zone interface. The load cell data demonstrate that nearly the full anchor capacity was derived from the tieback bond zone, with no significant capacity in these tiebacks derived from the grout located within the no-load zone.

The significant stiffness contrast between the bond zone (stiffer) and no-load zone (softer) is believed to be a factor contributing to no significant tieback capacity being derived from the no-load zone. Another likely factor is that tensioning of the tieback strands in the no-load zone is anticipated to straighten the strands and result in cracking of the grout encapsulation.

Given the significant advantages of using single-stage grouting of tiebacks (such as reducing the potential for caving of materials in the no-load zone, quality control of the anchor bond zone location, cost of construction, speed of construction and enhanced post-grouting performance/higher anchor capacity), continued routine use of single-stage grouting of tieback anchors should be considered.

CONCLUSIONS

Based on the results of the tieback demonstration, the considerable expense associated with de-stressing tiebacks at the face of the shoring wall after the permanent building walls and building diaphragms are in place, the reduction in the reliability in waterproofing systems and increased risk of water intrusion, and the undesirable aesthetics associated with patching the permanent building walls, consideration should be given to allowing temporary tiebacks to remain stressed for future projects where temporary tiebacks are specified. Alternatively, consideration should be given to allowing tiebacks to remain stressed if they meet specific criteria (for instance, deeper than a threshold depth and located below existing utilities). If significant concerns or questions still remain, it is recommended that future demonstration projects, such as the one described herein, be completed to provide case histories to help assess these concerns.

ACKNOWLEDGEMENTS

The authors would like to acknowledge IRIS Holdings, LLC and the Seneca Real Estate Group for helping to facilitate this demonstration. Additionally, the authors would like to acknowledge Sellen Construction, Malcolm Drilling and Hos Brothers Construction for assisting with the demonstration.

Load Transfer Mechanism of Small-Diameter Grouted Anchors

N. John Bingham, PE[1], P. Erik Mikkelsen, PE[2], Gary L. Petersen, CEG[3]

[1]Hart Crowser Inc., 120 Third Ave. South, Suite 110, Edmonds, WA, 98020; (425) 329-1161; john.bingham@hartcrowser.com.
[2]Geometron Inc. PS, 16483 SE 57th Place, Bellevue, WA 98006; (425) 746-9577; mikkelsen.pe@comcast.net.
[3]Shannon & Wilson Inc., 3990 Collins Way, Suite 100, Lake Oswego, OR 97035; (503) 479-6251; glp@shanwil.com

ABSTRACT

Results from instrumented 187 mm (7-3/8 in.)-diameter (nominal) tremie grouted multi-strand tendon anchors are presented. Unique instrumentation consisting of strain gages mounted to PVC pipe sections were used to measure strains in the grout column in the bonded and unbonded zone. This is difficult and rarely done in small diameter anchors due to the small clearance between tendons and the borehole wall. The results provide useful data indicating progression of tension and compressive strains down the anchor during loading, contribution of grout in the unbonded zone to anchor capacity, and additional support that high radial stresses (greater than overburden pressures) contribute to high anchor adhesion values.

INTRODUCTION

Small diameter tieback anchors are routinely used for earth retention systems around the U.S. Many studies have been performed with instrumented tiebacks for larger diameter tiebacks (about 305 mm [12 in.] diameter or larger) that indicate load transfer mechanisms (e.g., Mueller et al. 1998, Briaud et al. 1998, Stoupa et al. 1990). However, there appear to be relatively few studies where small diameter tiebacks (less than about 190 mm [7-1/2 in.] diameter) have instrumented the steel tendon/ bar to confirm the load transfer mechanism (Shields et al. 1978). The authors are not aware of studies where small diameter anchors have instrumented the grout to determine whether load transfer occurs above the tendon bond zone up into the unbonded zone. The difficulty of avoiding damage to instrumentation in the small annular grout space between steel tendons/bars and the borehole wall likely is the reason for the limited data. This paper provides such data and discusses plausible load transfer mechanism(s) that may account for high adhesion values in excess of those computed using overburden and limiting skin friction values.

BACKGROUND

General

Data contained in this paper is from work conducted by L.R. Squier Associates (1986a, 1986b) for the US Army Corps of Engineers at the Bonneville Locks. The site is located on the Columbia River forty-two miles east of Portland, Oregon. The project included construction of temporary and permanent anchored retaining walls for construction of new navigation locks. A tieback test program was conducted to confirm design capacities and configuration for these retaining walls.

The L.R. Squier Associates reports did not discuss the load transfer mechanism associated with the high adhesion values achieved.

Geology

The temporary and permanent walls are located near the toe of the Tooth Rock Landslide and retain(ed) landslide debris from this massive landslide. The geologic cross section (A-A') on Figure 1, illustrates representative geologic conditions for the temporary wall section that is pertinent to this paper.

The Tooth Rock Landslide is composed of two primary materials: large to massive displaced slide blocks (SB unit) and unconsolidated slide debris (SD). Slide blocks range in size from tens of feet to hundreds of feet. The slide debris (SD) unit consists of a chaotic mixture of angular rock-fragments to large boulders (up to 6.1 m [20 ft.]) in a clay-rich matrix of granulated, decomposed rock materials.

The test tieback anchor zones exist within the Reworked Slide Debris (RSD) unit that was formed by erosion and reworking of the SD unit by the Columbia River. The RSD unit contains a heterogeneous mixture of materials ranging in size from silt to large boulders. It is thought that much of the unit consists of hard angular rock fragments that are boulder-size to small slide block-size material. Distinct silt and sand beds are also present, at least near the ground surface. Recent (Holocene) River Deposits (RD) locally overlie the RSD and SD units at the ground surface.

TIEBACK INSTALLATION

Tiebacks were drilled using ODEX rotary percussion drilling methods because of its capability to drill through cobbles and boulders. A 152 mm (6 in.)-diameter button bit with an eccentric reamer on a down-hole hammer was used. This resulted in a borehole diameter of about 187 mm (7-3/8 in.). The majority of the unbonded zone was cased with standard well casing (152 mm [6 in.] inside and 168 mm [6-5/8 in.] outside diameters, respectively) as shown on Figure 2. Compressed air with drilling foam was used as the drilling fluid to flush cuttings from the hole.

Six tiebacks were successfully installed and tested. Four were installed in the RSD geologic unit, the primary overburden material present in the vicinity of the proposed temporary wall. Two tiebacks were installed in the SB-Tw geologic unit, which is present at depth along the upstream portion of the permanent buttress wall.

Since the focus of this paper is on the load transfer mechanism, only data for instrumented Tiebacks 1 through 3 with bond zones in the same RSD unit are presented. Each of these tiebacks were tremie grouted until grout returned at the top of casing. Grout was flushed with water from 4.6 m (15 ft.) above the bonded zone to the ground surface. Surface gage grout pressures ranged between 138 and 414 kPa (20 - 60 psi). Table 1 summarizes key tieback installation data for these tiebacks.

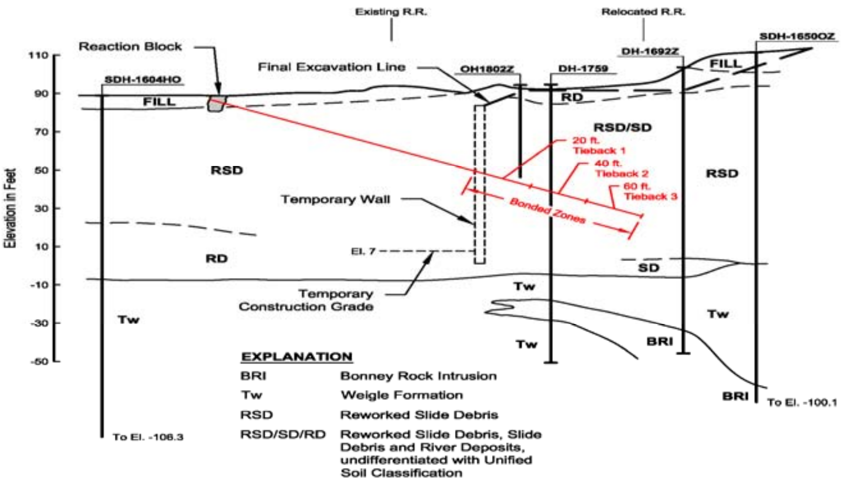

Figure 1. Geologic Cross Section A-A' at Tiebacks 1 and 2 (after L.R. Squier Associates 1986b).

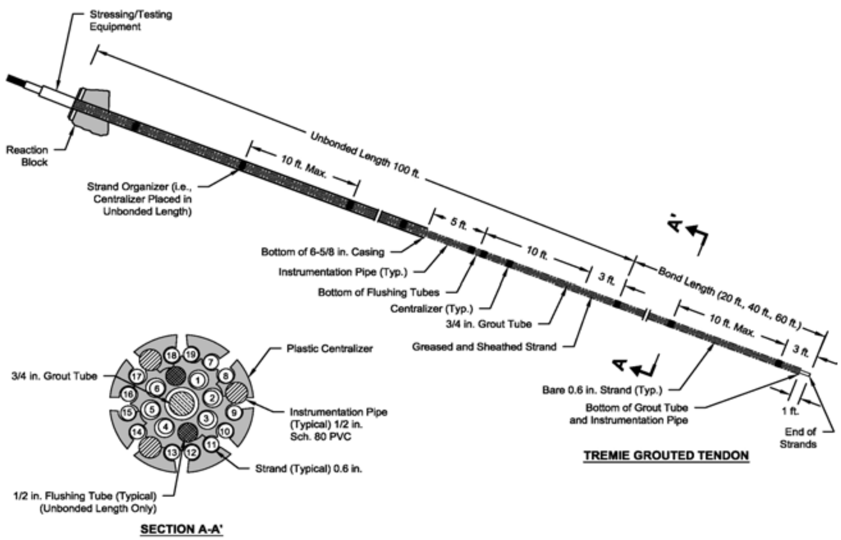

Figure 2. Tieback typical sections (after L.R. Squier Associates 1986b).

DOWN-HOLE INSTRUMENTATION

Down hole instrumentation was used to evaluate the mechanism of load transfer. Instrumentation consisted of electrical resistance strain gages bonded within 0.61 m

Table 1 - Tieback (TB) Installation Data[a]

TB No.[b]	Installed Bond Length (m)	Approx. Grout Vol. Placed (m^3)	Theoretical Hole Vol.[c] (m^3)	Static Grout Pressure[f] (kPa)	Grout Compressive Strength[d] (kPa)
1[e]	6.1	0.63[e]	0.72	285	30833
2	12.2	1.54	0.88	333	30833
3	18.3	1.63	1.05	389	31005

Notes:

a. Adapted from L.R. Squier Associates 1986b. Data for similar anchors (i.e., similar geology, location, and grouting methods) are presented for the purposes of this paper. All tieback anchor bond zones discussed are within the RSD geologic unit and were tremie grouted.
b. Anchors consisted of 19 strands (7-wire, 0.6 in. outside diameter), unbonded lengths (grease filled sheathed strands) of 30.5 m (100 ft.), and were angled 20 to 23 degrees below horizontal.
c. Excluding volume of tendon and associated components.
d. Strengths based on 10- to 13-day compressive tests.
e. Initial tieback location abandoned due to installation difficulties, but reinstalled 2 feet away.
f. Grout pressure (unit weight ~145 pcf) at average anchor bond zone depth below top of casing.

(2 ft.)-long PVC pipe segments (Figure 3). The strain gages were mounted within the PVC pipe segments at the Slope Indicator manufacturing facility in Seattle, Washington (design by Erik Mikkelsen and Pat Smith). The individual strain-gaged pipe segments were then shipped to the site and incorporated into full length flush-coupled, strain gage pipe assemblies in a warehouse on site. Strain gage wiring was threaded through the pipes to protect against damage during installation and grouting.

Each tendon was fitted with three instrumentation pipes, each containing five strain gages. As shown on Figure 2, the instrumentation pipes were positioned at the outside of the tendon bundle, as close as practical to the grout-soil interface.

The position of each strain gage in the anchor zone and in the 3.05 m (10-foot) unbonded segment is shown on Figures 4a and 5a for the 6.1 and 12.2 m (20-, and 40-foot) bond lengths. The strain gage data are included in a later section.

The survivability of the strain gages during the installation process was generally good. A few strain gage pipes joints were broken during the assembly and installation process. However, all pipe breaks were repaired in the field using external PVC couplers and cement or plastic pipe and epoxy. Repaired pipe sections appeared to work reasonably well during testing.

INSTRUMENTATED TIEBACK TESTING RESULTS

General

Tieback performance testing consisted of cyclically loading and unloading the instrumented multi-strand tendons, with creep tests at loads near maximum capacity. Tests measured applied loads, total and residual anchor movement, and strain in the grout. None of the tiebacks discussed herein failed during testing. Tieback test results pertinent to load transfer discussion are summarized in Table 2.

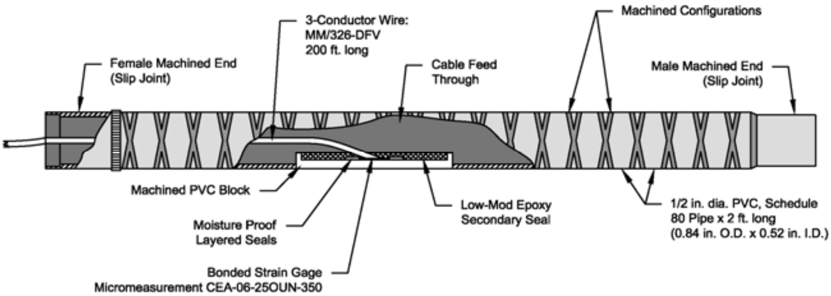

Figure 3. PVC pipe strain gage detail by Slope Indicator Co. (after L.R. Squier Associates 1986b).

Table 2 - Tieback Test Results[a]

TB No.	Max. Test Load (kN)	Installed Bond Length (m)	Avg. Load Transfer Length[b] (m)	Avg. Ultimate Adhesion (kPa)	Approx. Grout-Soil Interface Friction[c] (kPa)
1	3914[d]	6.1	7.5	891	135
2	3647[e]	12.2	7.6	813	159
3	3914[d]	18.3	7.2	929	186

Notes:

a. Adapted from L.R. Squier Associates 1986b.
b. Determined from strain gage data, where measured, including unbounded and bonded lengths.
c. Based on mass concrete on silty or clayey gravel interface friction of 0.5 x vertical effective stress assuming average soil unit weight of 19.6 kN/m^3 (125 pcf).
d. Tested to maximum capacity of tendon (i.e., 0.8 guaranteed ultimate tensile strength [GUTS]), but ultimate load of soil grout interface was not reached.
e. Two strands damaged during instillation were not loaded (i.e., maximum test load reduced).

Comparison of the average ultimate anchor adhesion (based on the average load transfer length from strain gage data) to the approximate grout-soil interface friction indicates ultimate adhesions are between 5 and 6.5 times those estimated. Although not as high as for some pressure injected anchors, the difference is noteworthy. One possible explanation for the high adhesion values are high radial stresses due to restrained dilation (Wernick 1978 and, Schlosser 1990), also termed suppressed dilation (Shields et al. 1978). Optimum conditions for dilation reaction in the soil may be provided in one or more ways, such as densification of the soil due to the installation/grouting process and formation of a dense filter cake in the grout at the borehole wall as water is pushed out under pressure (Shields et al. 1978). Littlejohn (1990) mentions a similar mechanism just before anchor failure where the grout bursts and expands into adjacent loose/soft soils that do not provide lateral constraint.

Strain Gage Data

Results of strain gage data for Tiebacks 1 and 2 (generally similar soils, grouting methods, and location) are shown on Figures 4 and 5.

The strain gage data revealed that the bond zone carries load in both compression and tension, and that the portion of the anchor in compression increases as the load increases. The strain gage data also revealed that the unbonded portion of the tendon immediately above the bonded zone carries load in compression, and needs to be considered part of the anchor zone. Since load tests did not exceed the soil grout adhesion, strain gage data were used to determine the load transfer length of the anchor and the "average" ultimate soil-grout adhesion (Table 2) effective at the maximum test load.

The 1986 report on the testing simply concluded that: *"The mechanism of load transfer between steel and grout, and in turn, between grout and soil or rock is complex. The use in design of "average" bond stress along the anchor zone is obviously a gross simplification."* Heterogeneity within geologic units also made it difficult to fully understand these complex mechanisms. The strain gage results from Figures 4 and 5 reveal a significant contrast in load transfer mechanism.

Tieback 1 has a 6.1 m (20 ft.) bond zone and is, according to the strain readings in Figure 4(b), entirely supported by high compression in the grout at the highest load. Tieback 1 encountered relatively uniform ground conditions in the grouted zone, and a notable lack of cobbles and boulders. At lower loads, the grout is in tension up to a strain of about 300 micro-strain or less. For additional increase in load, the strains reverse to compression as the same effect migrates to gages below. This is evidence of grout first cracking in tension and subsequently is restrained from radial dilation with further loading. The high radial stresses are created and provide increased friction with load. For this anchor, both geologic and construction conditions provided the radial rigidity to suppress dilation.

The load transfer mechanism is somewhat different for Tieback 2. The bond zone is 12.2 m (40 ft.) long and encountered a cobbley zone (near gage No. 9) and a large boulder (near gage No. 4). Gage 9, just 0.6 m (2 ft.) below the unbonded zone, shows the tension/compression characteristic described above. Gage 7 below it shows increasing tension to about 1750 micro-strain, too high for any grout to sustain elastically. One must conclude that only steel-grout-soil shaft adhesion is at work without the benefit of suppressed dilatency. The lower 6.1 m (20 ft.) of the anchor did not exhibit load transfer. A large boulder penetrated by the anchor at the top of this zone appears to have influenced strain transfer deeper into the bonded zone.

However, both anchor tests show compression in the grout at the top of the bonded zone and above. Five strain gages were located at 0.6 m (2 ft.) intervals 3.3 m (10 ft.) into the unbonded zone. The top gages (No. 15) did not show significant compression. Most of the compression was within 1.5 m (5 ft.) of the bonded zone.

CONCLUSIONS

1. Load in the anchor is carried in both compression and tension.
2. The zone of compression extends above the bonded length of the anchor.
3. When present, compression generally increases with increasing loads.
4. High grout compression in the bonded zone only occurs when conditions for restrained or suppressed dilation exist. That is, compression occurring in the

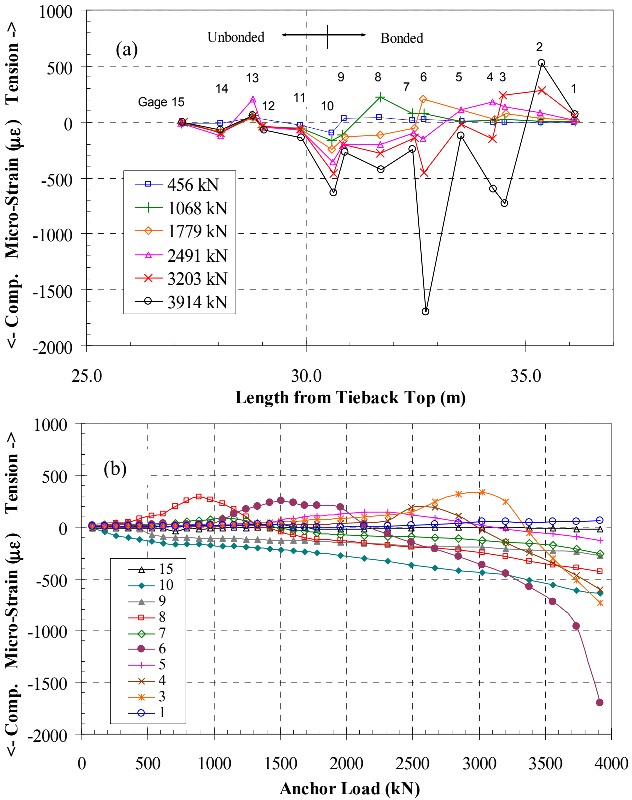

Figure 4. Tieback 1 a) strain-location and b) strain-load data (after L.R. Squier Associates 1986b).

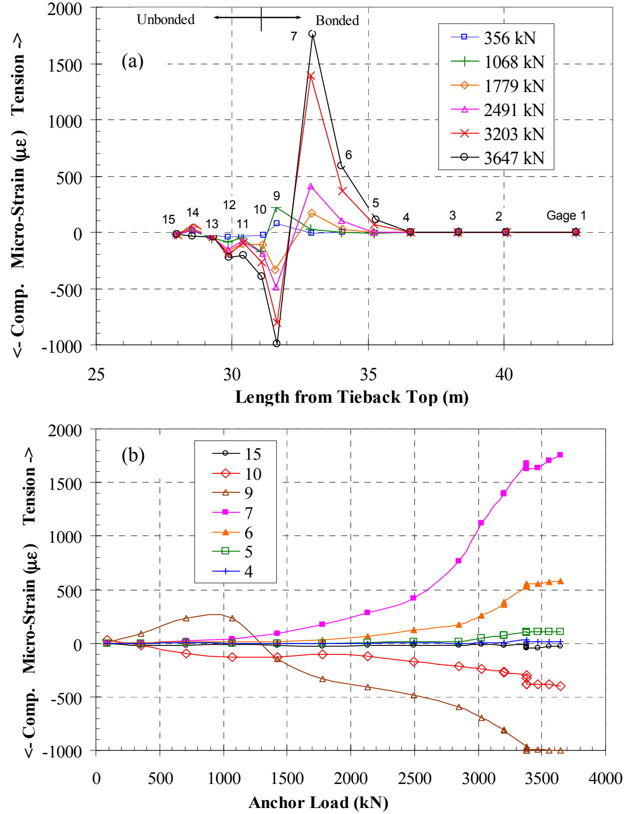

Figure 5. Tieback 2 a) strain-location and b) strain-load data (after L.R. Squier Associates 1986b).

upper portion of the bond zone causes the grout body to expand radially, increasing the grout-soil contact pressure, and enhancing the anchor adhesion.

5. Traditional assumptions for straight shaft friction govern when anchor conditions allow unrestrained dilation.
6. The results indicate strong support for the opinion held by some that higher anchor performance is gained by moving the unbonded part of the tendon deeper into the load zone.

APPLICATION TO LOCAL PRACTICE

Differing opinions exist within local Seattle practice as to whether or not single stage grouting (i.e., bonded and unbonded zone at one time) of small-diameter, high-pressure injected tiebacks should be allowed for performance tests (200% of design load). Data presented here for low-pressure grouted, small-diameter anchors suggest load is transferred in the grout from the bonded to unbonded zone. Additional strain gage data in the grout column across the bonded-unbonded zone would be invaluable in evaluating this load transfer, actual effective bond lengths, and more realistic average adhesion values.

ACKNOWLEDGEMENTS

The authors would like to acknowledge the contributions of David Weatherby and Ron Chapman of Schnabel Foundation Company for their insight into the original work for this project. We would also like to thank Matt Veenstra of Hart Crowser for assisting with data reduction and compilation for preparing this paper.

REFERENCES

Littlejohn, G.S. (1990). "Ground Anchorage Practice," *Design and Performance of Earth Retaining Structures (Conference Proceedings)*, ASCE, GSP No. 25, 1990.

L.R. Squier Associates (1986a). "Phase I Tieback Testing Program Bonneville Navigation Lock," US Army Corps of Engineers, Portland District, May 1986.

L.R. Squier Associates (1986b). "Phase II Tieback Testing Program Bonneville Navigation Lock," US Army Corps of Engineers, Portland District, November 14, 1986.

Mueller, C.G., Long, J.H., Weatherby, D.E., Cording, E.J., Powers III, W.F., and Briaud, J.-L., (1998). "Summary Report of Research on Permanent Ground Anchor Walls, Volume III: Model-Scale Tests and Ground Anchor Tests," Pub. No. FHWA-RD-98-067, September 1998.

Schlosser, F. (1990). "Mechanically Stabilized Earth Retaining Structures in Europe," *Design and Performance of Earth Retaining Structures (Conference Proceedings)*, ASCE, GSP No. 25, 1990.

Shields, D.R., Schnabel H., Weatherby, D.E., (1978). "Load Transfer in Pressure Injected Anchors," Jrnl. Geot. and Env. Engrg., ASCE, Vol. 104, No. GT9, September 1978.

Stoupa, J. Anderson, D., Sharp, K., Majewski, H. (1990) "Installation and Testing of Instrumented Tieback Anchors," *Proceedings of the 15th Annual Members Conference – Lessons of the 80s – Strategies of the 90s*, Deep Foundations Institute, Seattle, WA.

Wernick, E., (1978). "Stresses and Strains on the Surface of Anchors," Revue Francaise de Geotechnique, Vol. 3, 113-119.

Diaphragm Walls at the Canton Dam Auxiliary Spillway

Michael P. Walker, P.E., M. ASCE[1], Mary C. Nodine, P.E., M. ASCE[2] and Rick Deschamps, P.E., PhD, M. ASCE[3]

[1] Michael P. Walker, P.E.; M. ASCE; P.E.; GEI Consultants, Inc.; 400 Unicorn Park Drive, Woburn, MA 01801; mwalker@geiconsultants.com; 781-721-4057.

[2] Mary C. Nodine, P.E.; A.M. ASCE; GEI Consultants, Inc.; 4601 DTC Boulevard, Suite 900, Denver, CO, 80237; mnodine@geiconsultants.com; 303-264-1090.

[3] Rick Deschamps, P.E., PhD; M. ASCE; Nicholson Construction, 12 McClane St. Cuddy, PA 15031-9754; RDeschamps@NicholsonConstruction.com; (412) 221-4500 EX 202.

ABSTRACT

Canton Lake Dam is a U.S. Army Corps of Engineers (Corps) flood control project located in north-central Oklahoma. When it became necessary to increase the spillway discharge capacity to pass the probable maximum flood (PMF), the Corps decided to construct an auxiliary spillway through the right abutment. The auxiliary spillway channel is 450 feet wide, with walls totaling 1,470 feet in length retaining up to 50 feet of soil and rock in the dam abutment. The spillway training walls consist of 2-foot-wide concrete diaphragm walls with up to two rows of prestressed strand anchors. This site was geotechnically challenging, with relatively weak and erodible rock and soil.

This paper presents a case study of the design and construction of the training walls for the Canton Lake Dam auxiliary spillway. The walls were designed as reinforced concrete hydraulic structures in accordance with Corps of Engineers guidelines. A combination of methods was used for design, including soil-structure interaction software (WALLAP), slope stability and seepage analysis software (SLOPE/W and SEEP/W), and conventional techniques.

The application of diaphragm wall construction for permanent training walls of the spillway channel provided unusual challenges, including the design of tiebacks for extreme flood water levels behind the wall. Limited guidelines and standards for the design of permanent tiebacks also made the selection of appropriate load cases and factors of safety challenging.

INTRODUCTION

Canton Lake Dam was built in the 1940's to provide flood control and recreational facilities northwest of Oklahoma City. The dam is owned and operated by the U.S. Army Corps of Engineers (Corps) Tulsa District. The dam is a 15,100-foot-long (4,600 m) rolled earth filled embankment with a maximum height of 73 feet (22 m). The crest of the dam is at El. 1,648 ft. The dam has an 800-foot-wide (244 m) service spillway at the right abutment.

For more than 30 years there has been concern about the stability of the existing spillway and the flood capacity of the dam. The 2002 Dam Safety Assurance Program Evaluation Report specifically cited that the spillway had an inadequate factor of safety against sliding, and that the spillway was unable to discharge the probable maximum flood (PMF), which could result in overtopping of the embankment. The allowable storage level of the dam was reduced due to these safety deficiencies, and the dam has since been unable to provide the level of flood control for which it was designed – the service spillway is only able to safely discharge 59.5% of the PMF. In 2006, anchors were installed in the existing spillway to increase its factor of safety against sliding. The Corps then planned an auxiliary spillway that would safely pass the PMF, thereby restoring the dam's storage capabilities.

The Corps' auxiliary spillway design included a channel excavated into the right abutment of the dam, adjacent to the existing spillway (Figure 1). The channel would have nine 53.3-foot-wide (13.3 m) fusegates on the spillway sill which would be triggered in the event of the PMF. The proposed channel walls were a total of 1,470 feet (448 m) long with a maximum height of 50 feet (15 m) and would consist of 2-foot-thick (0.6 m) anchored diaphragm walls. Diaphragm wall construction techniques would allow the auxiliary spillway to be built adjacent to the existing spillway without disrupting existing dam or reservoir operation. The use of diaphragm walls in this application is unusual, and the project was one of the first uses of diaphragm walls in a Corps of Engineers design.

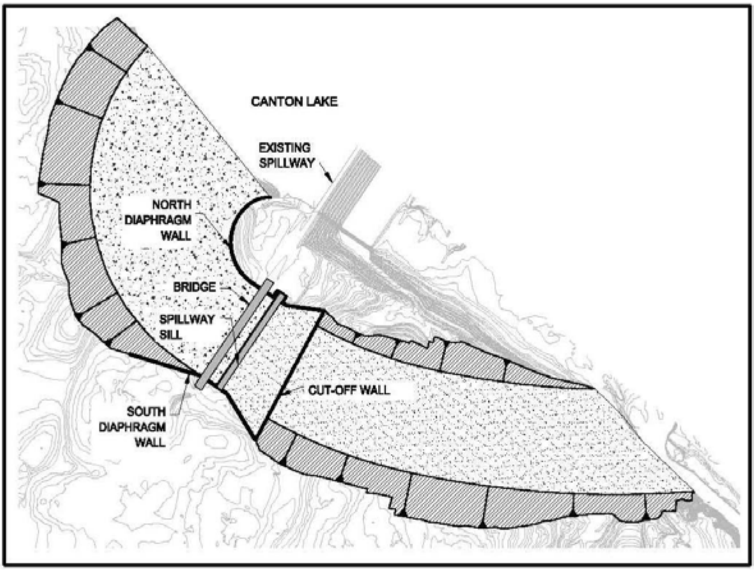

Figure 1. Schematic plan view of the Canton Lake Dam auxiliary spillway.

The process of designing the diaphragm walls for the auxiliary spillway at Canton Lake Dam highlighted the limited number of guidelines and standards available for the design of diaphragm walls and permanent tiebacks. The Corps specified the use of their own Engineer's Manuals as well as such sources as the Post Tensioning Institute (PTI) Manual and the Federal Highway Administration (FHWA) guidelines. Ultimately a feasible design was completed using these and other guidelines, but the experience made it clear that a comprehensive set of standards specifically written for the design of diaphragm walls with permanent tiebacks would be useful in the industry.

SUBSURFACE CONDITIONS

The soil profile at the auxiliary spillway location consists of four primary strata. A silt stratum includes overburden soil and decomposed rock extending from the ground surface to between about 10 and 45 feet (3 to 14 m) deep. The silt is underlain by siltstone, the weak rock predominant in the profile. Shale is present under the siltstone between about 50 and 70 (15 to 21 m) below grade. The shale was found to have higher strength and stiffness parameters than the siltstone based on field observations and field and laboratory test data. However, due to limited test data in the shale and the variability of the shale-siltstone interface depth along the diaphragm wall alignment, strength and stiffness properties of the shale were assumed to be the same as those for siltstone. The strength and stiffness values used for design are shown in Table 1.

Table 1. Soil Parameters used for Design.

Stratum	Undrained Friction Angle (ϕ)	Undrained Cohesion (c)	Elastic Modulus (E)
Silt	30°	0	2.5×10^4 psf/ft
Siltstone	30°	1,300 psf	3.4×10^7 psf
Shale	30°	1,300 psf	2.0×10^7 psf
Breccia	0	4,000 psf	2.0×10^7 psf

A section of the diaphragm wall with a typical soil profile is shown in Figure 2.

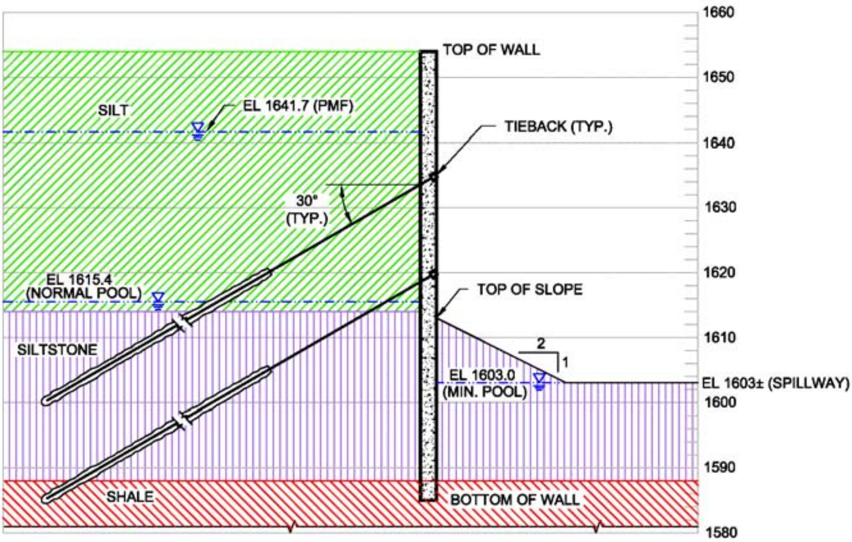

Figure 2. Section of diaphragm wall in spillway channel wall with two tiebacks.

DIAPHRAGM WALL MODELS

Staged Construction Modeling using WALLAP

Internal stability of the spillway walls was evaluated at critical sections using WALLAP, a computer program that analyzes soil-structure interaction using a beam-on-elastic foundation model. Preliminary analyses using PLAXIS, a two dimensional finite element analysis program, were also prepared for one design section. There was good agreement between the results of the PLAXIS and WALLAP analyses. Therefore, the simpler WALLAP model was used for analyses of the remaining design sections.

WALLAP can be used to model all stages of wall construction. It calculates moments, shear stresses, and anchor loads in the wall as well as wall deformation at each stage. Soil in WALLAP is assigned Mohr-Coulomb strength parameters and an elastic modulus, and is modeled as an elasto-plastic material. Material behavior is assumed to be linear-elastic for shear stresses below the Mohr-Coulomb failure criterion (when strengths are fully mobilized), and is in a state of full plastic yield when stresses reach the failure criterion. This material model simulates active and passive limit states similar to those described in classic earth pressure theory for soils. A typical model created using WALLAP, including the soil profile, wall, surcharge, and tieback loads, is shown graphically in Figure 3 along with corresponding output plots of shear forces and moments, displacements and active and passive pressures.

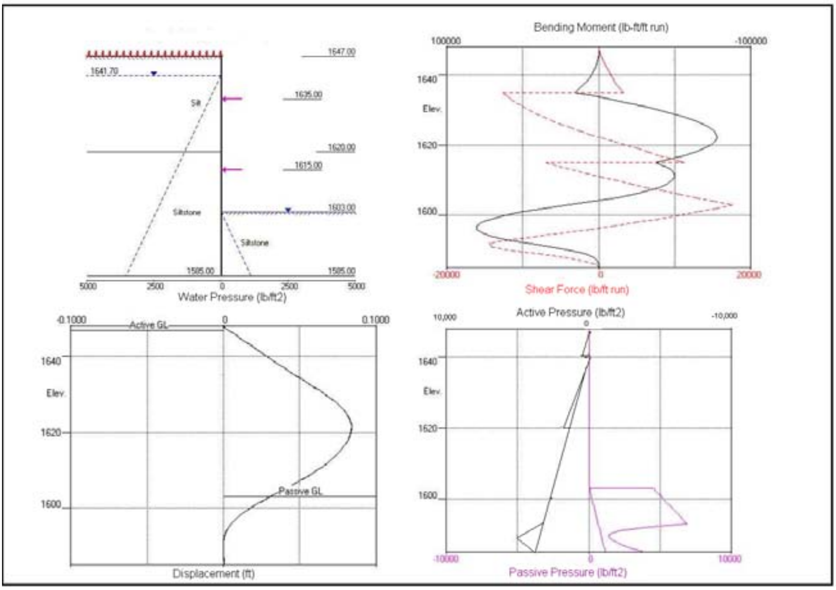

Figure 3. (Clockwise from top) WALLAP model of two-tieback section of diaphragm wall showing PMF load case; Bending moment and shear force plot; Displacement plot; Active and passive pressure plot.

External Stability and Seepage

The design of the diaphragm walls at Canton Lake Dam was controlled by the internal stability model created using WALLAP, but the design was also checked for external stability (global slope failure). External stability of the diaphragm walls was modeled using SLOPE/W, a limit equilibrium slope stability computer program. Failure surfaces in the global stability analyses were assumed to extend outside the wall and tiebacks, since the design of the wall and tiebacks was evaluated using WALLAP.

The diaphragm wall design was also checked to assess whether seepage and exit gradients might be a safety concern. SEEP/W, a two-dimensional finite element computer program, was used to perform steady state seepage analyses of water flow around the toe of the diaphragm wall.

DIAPHRAGM WALL DESIGN

The auxiliary spillway walls at Canton Dam were designed as 2-foot-thick (0.6 m) diaphragm walls with up to two horizontal rows of prestressed strand anchors (tiebacks). The quantity of tiebacks was optimized depending on the height of the wall and the depth of the weak silt layer at a given location. The wall was constructed with approximately 21-foot-wide (6.4 m) panels, and tiebacks were equally spaced horizontally at two per panel. Specific challenges encountered in design of the wall are discussed in the following sections.

Safety Factors for Internal and External Stability

The diaphragm walls were designed as reinforced concrete hydraulic structures in accordance with Corps of Engineers guidance documents, including EM 1110-2-2100: Stability Analysis of Concrete Structures. This document specifies that structures be analyzed for Construction, Normal Pool (El. 1615.4), PMF (El. 1641.7) and Rapid Drawdown conditions as well as for seismic conditions. Required factors of safety for each load case are shown in Table 2:

Table 2. Load Cases and Associated Safety Factors.

Load Case	Factor of Safety
Construction	1.7
Normal Pool	1.7
PMF	1.1
Rapid Drawdown	1.1
Operating Basis Earthquake: $a_h = 0.02g$	1.3
Maximum Credible Earthquake: $a_h = 0.17g$	1.1

When the PMF occurs at Canton Dam, water in front of the spillway walls (inside the spillway channel) is at or near the top of the walls. The water in the soil behind the wall could be as high as the PMF elevation, but may not reach this elevation due to the low permeability of the rock. As the flood recedes, the water in front of the walls will drain rapidly, while the water behind the wall will drain more slowly. The critical load case, therefore, is that with the water at its highest elevation behind the wall but completely drained in front of the wall. This load case effectively combines the PMF and the Rapid Drawdown load cases. (The relative water elevations used are somewhat conservative, but the precise configuration of the water in front of and behind the wall would be difficult to estimate with reasonable confidence.)

A typical diaphragm wall constructed in dry land conditions is designed to withstand hydrostatic pressures from the water table behind it, but the design is usually governed by the loads applied during construction. In the case of the Canton Dam spillway walls, the siltstone and shale behind the wall are essentially free-standing, and the limiting factor in design is the wall's ability to withstand the hydrostatic pressures placed on it under PMF loading conditions.

Movement Criteria

Determination of movement criteria was a challenge in the design of the diaphragm walls. Typical allowable deflections for diaphragm walls due to excavation are in the range of ¾-inch to 1.5 inches (2 to 4 cm) depending on the proximity of buildings to the wall and the sensitivity of the structure to movement. We referred to work by Boscardin and Cording (1989) and Clough and O'Rourke (1990) to investigate consequences of diaphragm wall movement. Boscardin and Cording (1989) relate historic building damage to angular distortion and horizontal strain of building foundations, while Clough and O'Rourke (1990) relate vertical settlement behind a wall to horizontal movement of the wall. The nearest building to the walls is the Lake Building located behind the south wall, which is relatively modern compared to the buildings discussed by Boscardin and Cording (1989), and can therefore withstand about twice as much movement as a more brittle historic structure.

Ultimately we chose a limiting movement criterion of 1.5 inches (4 cm) for construction and normal operating conditions of the diaphragm wall. Using the sources referenced above, this amount of movement is expected to cause negligible to slight damage to the adjacent building and less than ½-inch (1.3 cm) of settlement. For the extreme PMF loading condition, we chose a limiting movement criterion of 2.5 inches (6.5 cm).

Geotechnical Capacity of Tiebacks

Limited guidance is available to determine the appropriate factor of safety for the geotechnical capacity of permanent tiebacks subject to increased temporary loads during their service life. The Corps specified that guidelines published by the Post Tensioning Institute (PTI) and the Federal Highway Administration (FHWA) be used for design of tiebacks in the Canton Lake Dam diaphragm wall. Tiebacks are typically proof tested to a load greater than their nominal design load. PTI recommends that tiebacks be tested at a load of 133 percent of the design load, and the FHWA recommends testing to between 120 and 150 percent of the design load. Another frequently-used reference, NAVFAC Design Manual 7.3 recommends that permanent anchors be tested to 150 percent of their design load.

The tiebacks on the Canton Dam spillway walls were designed to withstand loads from the PMF, which is an extreme event that imposes short-duration loads on the walls. The general design requirement for extreme events and load cases is that the structure must survive without collapse, but some non-catastrophic displacement or damage may occur. The difference between the tieback loads resulting from normal pool conditions and PMF conditions is as much as a factor of two.

Testing the tiebacks at loads significantly greater than the PMF load was considered unnecessary. We ultimately chose to test tiebacks at 150 percent of the load experienced in normal pool conditions, which is the upper bound of the recommendations in the manuals listed above. For PMF conditions, we allowed a 33 percent overstress above the normal pool design load. This ensures that the tiebacks are proof-tested during construction to a load greater than the controlling extreme event (PMF) load case and consistent with the safety factor shown in Table 1.

CONSTRUCTION

The use of diaphragm wall technology allowed the Canton Dam Auxiliary Spillway to be constructed in close proximity to the existing spillway without disrupting the operation of the reservoir, since the walls would be formed in place prior to excavation of the spillway channel. Another advantage of the diaphragm wall technique for this project is that it allows flexibility in wall construction. In the case of the Canton Dam Auxiliary Spillway, construction is being completed in three phases. The diaphragm wall installation was complete in February 2010. At the time this paper was submitted (April 2010) excavation of the first cantilever section had been completed and no negligible movements had been recorded. The initial phase of construction will also include excavation of the channel downstream of the cutoff wall and installation of the cutoff wall. The upstream channel will also be excavated during this phase, with the exception of a plug adjacent to the fuse gates consisting of about 1 million cubic yards of material. The bridge across the channel will be constructed in the second phase of construction. The final phase will include construction of the spillway sill, the fuse gates and appurtenant structures and the downstream apron. Excavation of the plug upstream of the fuse gates will be the final step before the spillway is fully operational. The project is scheduled for completion in 2014.

CONCLUSION

Design of the diaphragm walls at Canton Lake Dam presented several unusual challenges, including determination of appropriate factors of safety for stability and for the geotechnical design of tiebacks, and determination of deflection criteria. These issues originated in part from a lack of guidelines that specifically address diaphragm wall design, as well as the unusual use of a diaphragm wall structure in a hydraulic application. As diaphragm walls have become more widely used, common methodologies have evolved for their design, but no universal, standard procedure has been established. Some engineering judgment was therefore required in determining which standards and guidelines were appropriate in the various aspects of design of the walls. It would be useful for future projects if practitioners in the diaphragm wall industry created standards that would take into account design methodologies and performance specific to diaphragm walls for a wide range of applications.

REFERENCES

1. Post Tensioning Institute Manual (6^{th} Edition)
2. United States Army Corps of Engineers (CORPS), (2005). EM 1110-2-2100: "Stability Analysis of Concrete Structures," December 1.
3. Boscardin, M.D. and Cording, E.J. (1989). "Building Response to Excavation-Induced Settlement", ASCE, Journal of Geotechnical Engineer, Vol. 115, No. 1, pp 1-21.
4. Clough, G.W. and O'Rourke, T.D. (1990). "Construction Induced Movements of Insitu Walls", Proceedings ASCE Specialty Conference, Cornell, ASCE Geo Special Publication 25.
5. Department of Transportation, Federal Highway Administration (FHWA) (1999). Geotechnical Engineering Circular No. 4: Ground Anchors and Anchored Systems"
6. Department of the Navy, Facilities Engineering Command (NAVFAC), (1983). Design Manual 7.3: "Soil Dynamics, Deep Stabilization, and Special Geotechnical Construction"

Innovations and Advances in Tied-Back Soldier Pile Shoring in Seattle

David G. Winter[1], Garry E. Horvitz[2], and Tom A. Armour[3]

[1]Senior Principal, Hart Crowser, Inc., Seattle, Washington
[2]Senior Principal, Hart Crowser, Inc., Seattle, Washington
[3]President, DBM Contractors, Federal Way, Washington

ABSTRACT

Since the 1970s soldier pile and tieback anchor shoring in the Seattle downtown core has supported more than 40 deep excavations and has become substantially more economical and predictable in its performance. Design and construction efficiencies have been made possible using a growing database of performance results. Recent development sites have often been partial blocks surrounded by buildings with basements, vital utility corridors, and narrow streets. These conditions have challenged development teams and led to new solutions that have made tough site development practical. This paper analyzes published and unpublished data to demonstrate how soldier pile and tieback shoring in Seattle has changed, how a greater emphasis on observed behavior and calibrated predictive tools has led to more efficient designs, and how much more cost-effectively these designs can be installed in today's market.

SHORING HISTORY IN SEATTLE

In 1972 the Bank of California Center helped open an era of high-rise/deep excavation development in Seattle that continues today. Clough, et al (1972) documented the design and construction results, and provided some of the first published information on tied-back shoring in the region. The paper described the characteristics of the overconsolidated sand, silt, and clay that dominates the downtown Seattle core, and reminded the reader that not only was there meager soldier pile and tieback shoring wall deflection data available for comparison, but that the accepted design methods published by Terzaghi & Peck (1967) were developed for normally consolidated soils. The wall was nonetheless designed using the Terzaghi & Peck approach, with a maximum lateral pressure of 0.4*120pcf*H=48H psf and a trapezoidal distribution. Based on laboratory test results and a finite element analysis the predicted maximum wall deflections were about 2 inches. The observed pressures were very close to the design values but the wall deflected only about ¾ inch. The authors concluded that the wall pressures reflected the lock off load of the anchors, instead of the actual lateral pressures on the wall. After nearly 40 years of additional data we can conclude that the authors were correct about the wall pressures, and offer that the low observed deflections meant the wall was overdesigned.

Other Seattle engineers faced similar challenges. The authors reviewed the design criteria for five downtown excavations deeper than 50 feet and seven excavations 30 to 50 feet deep (between 1963 and 1979) as reported by Gurtowski and Boirum, (1989). Of the five deep shoring walls, only one appears to have strayed from the Terzaghi & Peck approach, since all had design pressures typically 40H psf or higher. The one excavation with a lower design pressure was in more of a sand profile, with a uniform distribution of pressure calculated as 0.65*Ka*H=21H psf.

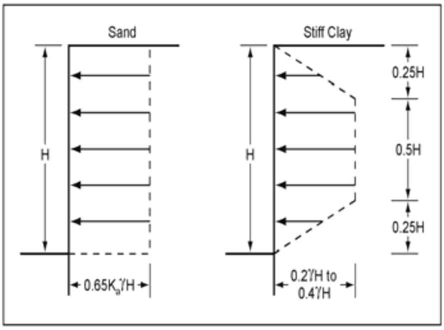

Figure 1. Terzaghi & Peck Design Envelope

One designer had a particularly challenging problem. The geotechnical engineers prepared a design for the 50-foot deep 1111 Third Avenue excavation that encountered both layers of sand and layers of clay in the profile. The design called for a pressure of 22H psf, based on a Terzaghi & Peck approach for sand, and a belief that the pressures used in the past for clay were conservative.

But city reviewers believed that the clay layers ought to have higher design values than the sand, and thus a pressure envelope that jumped between 22H and 36H resulted. Not only was such an envelope difficult to translate into an easily constructed tieback system (because of the changing loads on each tieback) but it was also based on an assumption of soil layering consistency that was impossible to verify until the 120 or so soldier piles were installed. Even though over the next 10 years there were a few projects with similar variable pressure envelopes designed and constructed most designers understood that variable design from layer to layer suggested a precision in both the methodology and the understanding of the subsurface profile that didn't exist. The more reasonable approach, and the one that increasingly gained favor among the primary downtown geotechnical engineers, was to:

- Estimate a single combined representative or average soil profile
- Design the pressure envelope for the soil profile, based on the results of past successful projects, and check against the established empirical methods, and
- Include a monitoring program for wall deflections and tieback pressures.

With this approach various elements of tied-back shoring design advanced.

ADVANCES IN PRESSURE ENVELOPE DESIGN

Just as important as a realization that lateral soil pressure envelopes for overconsolidated soil profiles couldn't be directly developed using methods based on normally consolidated soil data, was the growing recognition that pressures for very deep excavations were not directly comparable to those for shallow excavations. In other words, a pressure envelop of 36H for a 40 foot deep cut might be reasonable and result in an economical design in a mixed clay and sand profile, but 36H for an 80 foot deep cut resulted in huge pressures; and very large soldier piles, long tiebacks, and thick lagging boards, thus making construction unnecessarily expensive. On several very deep excavations in the 1980s (Seafirst 5th Avenue Plaza – 75 feet, Madison Hotel – 70 feet, First Interstate Bank – 80 feet, Columbia Center – 120 feet, 1201 Third Avenue – 85 feet, and Pacific First Center – 80 feet), consideration of maximum pressures regardless of depth began. At the First Interstate Bank excavation of a predominantly clay profile resulted in a pressure envelope of 30H psf. The trapezoidal shape of the envelope allowed elimination of the bottom row of ties during design. The City of Seattle reviewer objected to the bottom truncation of the trapezoid and required another row of ties to be designed within just a few feet of the bottom of the excavation. The designers used load cells, inclinometers, and optical survey monitoring to document the small movements of the wall during the excavation. By the time the excavation reached the bottom row they had a convincing case for the City that the wall was performing better than expected and the last row of tiebacks was eliminated without issue.

Five years later designers working on the 1201 Third Avenue project just three blocks from First Interstate built on the observations of that earlier instrumented excavation. They advanced the pressure envelope design by instrumenting tiebacks with hydraulic load cells and trying to isolate a section of the instrumented wall to get results more representative of the true pressures. The instrumented section was comprised of the soldier pile with the load cells on each tieback plus the two soldier piles on each side of the instrumented pile. All of the tiebacks on the five solder piles in this 35 foot wide section were locked off at 50% of the design load, instead of the usual 100%, after proof testing. By isolating a section of the wall at 50% of the design load there was a better chance of recording actual pressures instead of just lock-off values. The field observations verified the validity of the approach and the designers concluded that pressures even lower than the 20H design were appropriate for this soil profile and depth. They concluded that a pressure envelope as low as 17H psf would have been a reasonable design for this deep excavation (Winter, et al, 1987).

Note that 17H for an 85 foot deep excavation gives a maximum pressure of 1,445 psf, about the same as 36H on a 40 foot deep cut. The First Interstate and 1201 Third Avenue results supported a belief that overconsolidated soils reached a maximum pressure at a relatively shallow depth, and if the shoring system was properly designed and constructed, the same pressures could be applied to much deeper excavations resulting in a significant construction cost savings. Subsequent excavations and different Seattle designers verified this conclusion and shoring walls for just about any overconsolidated soil type and depth greater than 50 feet were designed for a maximum pressure envelope of less than 30H psf and typically 20H to 25H, representing about a 60% reduction in pressures from the conventional designs of the 1970s.

Other elements of the wall pressure and soldier pile/tieback design were similarly considered and adjusted for observed conditions. They included:

- Wall pressures in corners were reduced in recognition of three-dimensional resisting effects of the adjacent perpendicular wall. Often pressures within 30 to 50 feet of corners were reduced by as much as 50% (4th and Madison, Chase Center).

- The upper section of the shoring wall that includes the cantilever portion and the first tieback often deflected away from the excavation, suggesting the prestressing of the upper tieback was jacking load into the soil rather than resisting pressures from the soil. These observations allowed the location of the first tieback to be deepened thus reducing interference with adjacent shallow utilities (Olive 8).
- Design of crossing tiebacks supporting re-entrant corners was subject to debate. Four significant excavations (Columbia Center, Westlake Center, Pacific First Center, and 4th and Madison) included re-entrant corners. Observations at these sites supported three conclusions: 1) each of the "re-entrant walls" can be designed as if the other wasn't present; 2) lower pressures exist near the corner so prestressing required caution; 3) pressure grouted ties required careful pressure monitoring to avoid overstressing the perpendicular wall.

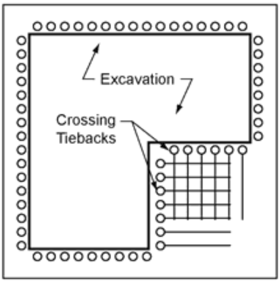

Figure 2. Re-entrant Corner.

ADVANCES IN NO LOAD ZONE CONFIGURATION

The designers of the Columbia Center excavation faced a significant challenge: The conventional no load zone design for this 120 feet deep excavation extended as far as 90 feet from the excavation face at the ground surface. However, 5th Avenue, on the high side of the excavation was only about 70 feet wide. The upper rows of tiebacks would thus extend as much as 20 feet beyond the property line, requiring easements and often intersecting basements. To address this problem the designers proposed a truncated no load zone, set back from the base of the excavation a distance of about 40 feet. The no load zone represents the area of potentially unstable soil just behind the wall behind which all tiebacks must attain their support. The practical effect of a truncated no load zone is shorter tiebacks for the upper rows. The uncertainty is how much additional wall deflection could result. At Columbia Center the wall deflected only about 1/2 inch. The designers concluded that the shorter ties in the truncated no load zone "provided satisfactory stability for the shoring wall without excessive movement" (Grant, 1985).

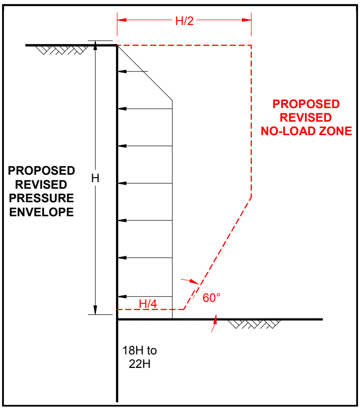

Figure 3. Revisions proposed by Winter, Loesch, and Hollister (2001)

Similar no load zone truncations with similar results occurred at 4th and Madison (95 feet deep) and Olive 8 (85 feet deep). The maximum deflections at 4th and Madison were about 2 inches and minor repair work was required for cracks opened at the property line across the street (Winter, et al, 2001). At Olive 8 deflections were less than 1 inch. At none of the sites was stability of the wall threatened by the truncation.

ADVANCES IN ESTIMATING AND MEASURING WALL DEFLECTIONS

The success of a shored excavation is not solely expressed in the ability of the system to safely retain the earth loads imposed on the system. Success, in the context of a design acceptable to the reviewing agencies, is the avoidance of adverse impacts to adjacent utilities, rights-of-way and buildings. Thus the attention given to deformation of the shoring system and potential settlement behind the wall has justifiably increased.

In early shoring system designs for excavations shallower than 60 to 70 feet, empirical approaches to estimating deflections were accurate enough. But non-standard site geometry and deeper excavations challenge traditional limit equilibrium models. Recently the state of the practice has evolved to include the use of soil/structure interaction models to predict not only the deformations of the shoring system but the deformations of the adjacent soil mass within the right-of-way and the potential vertical and lateral movement of nearby building foundations. The use of finite element models such as PLAXIS or finite difference methods such as FLAC have enhanced the industry's ability to more reliably predict these deformations. With repeated use we can "calibrate" the models' predictive ability by back-calculating input parameters for results that match past observations, and use those adjusted parameters at future sites.

An example of this approach is the Chase Center. The excavation for this building extended to deeper than 100 feet at the corner of 2nd Avenue and Union Street. This depth required the use of a truncated no load zone which increased the likelihood of greater deflections. In addition the mainline tracks of the BNSF Railroad travel through a century-old tunnel located within 25 feet of the edge of the excavation which extends down to the invert of the tunnel. The tunnel is highly settlement sensitive and a design focus was to avoid adverse impacts to the tunnel and structures across the street. FLAC was used to model the interaction of the shoring elements, adjacent soil mass, tunnel and existing building foundations. The model predicted 0.9 inches of deflection at the tunnel and 1.2 inches at the shoring face. Optical survey monitoring and inclinometer casing attached to the soldier piles showed magnitudes of vertical and horizontal displacement matching those predicted.

At Olive 8 (Winter, et al, 2009) the site was surrounded by narrow streets and existing buildings. One of those buildings had a deep basement (about 50 feet) that could not be accessed, and was separated from the excavation by a narrow alley with utilities that could not be moved or abandoned. The Olive 8 excavation was to extend about 85 feet deep. On the wall facing the 16-foot wide alley and adjacent deep basement the designers developed a hybrid shoring solution consisting of:

- Soldier piles on a normal spacing,
- Short soil nails on a tight grid pattern between the soldier piles and extending just back to the adjacent basement wall, and

- Tieback anchors extending below the adjacent basement and designed for the surcharge loads from the adjacent footings.

The PLAXIS model and the design and performance of the shoring wall showed that the hybrid system actually performed better than predicted by the model, with deflections well under 1 inch for most of the instrumented areas. These two results demonstrate that creative solutions to difficult site problems are possible, and made easier and more dependable by the competence of the overconsolidated Seattle soils, and the confidence recently gained in predictive modeling of deflections.

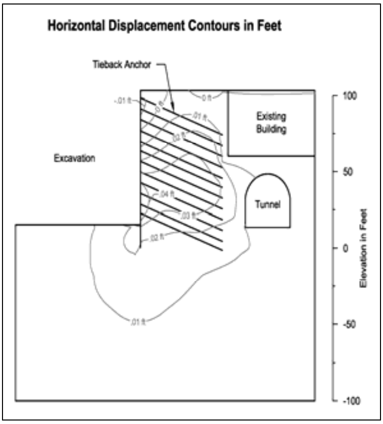

Figure 4. Chase Plaza FLAC Model

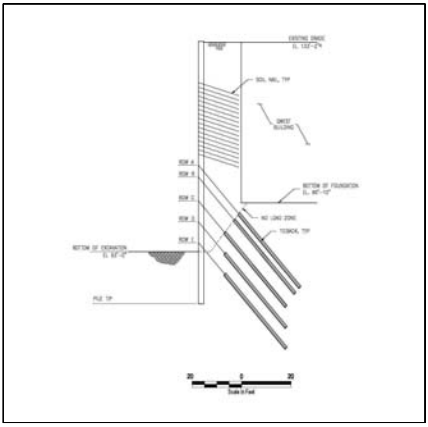

Figure 5. Olive 8 Hybrid Shoring

ADVANCES IN CONSTRUCTION METHODS AND APPROACH

In addition to the consistent and incremental advances in wall design, contractors, equipment manufacturers and material suppliers have improved construction elements to cut costs and meet schedule demands. Addressing site, soil, and neighborhood challenges require foundation contractors working closer than ever with their project partners during design development as well as construction. Since the Bank of California Center Project in 1972 innovations in procurement, equipment, tooling, and field process have helped owners and engineers "pencil out" difficult to build on properties that at one time seemed too expensive to develop. In the early 1980's foundation contractors introduced smaller European hydraulic drill rigs. More efficient anchor designs were now possible with this new ability to install longer anchors, pressure grout bond zones, and anchors at varying angles - all in less required space and at a faster rate. Continuing this European trend, specialty soldier pile drill rigs were introduced in the late 1980's. These more compact and powerful drills, designed for the tight urban confines of European cities allowed more efficient installation of deeper soldier piles enabling the project owners to add more usable space to their buildings. Tooling innovations have played an integral role as well. Drill augers, core barrels and cleanout buckets are constantly being improved to process a hole faster and safer. Auger flight and drill tooth designs are specific to ground conditions. Much improved overburden drill tool systems are more readily available allowing higher quality lower cost anchor installations in difficult ground. Dual rotary systems, oscillators, and casing rotators perfected in the late 1990's allow independent and synchronized rotation and advancement of a casing and a drill tool.

Over the last thirty years process improvements have also played a critical role in the Seattle excavation support market. Engineers, contractors and manufacturers have become more knowledgeable of concrete mix designs, mineral and polymer slurry and shotcrete placement. Advances have improved the constructability of excavation soldier pile/tieback systems allowing more economical and safer designs to be installed. As an example, for a typical moderate depth soldier pile and tieback excavation and comparing costs from the 1970's to today (assuming the same labor and material unit prices), by incorporating today's advancements (both design and construction) owner unit cost savings are in the range of \$8/s.f. to \$12/s.f of wall face. This represents a 30% to 45% savings in shoring costs.

Figure 6. 4th and Madison

Alternative design delivery and contract procurement methods are becoming more common. Owners often request design/build proposals based on stated wall performance criteria or allow foundation contractors to provide design/build options (as cost reduction incentives) to owner provided designs. Two recent project examples include the 505 1st Avenue and 635 Elliott Avenue projects. At 505 1st Avenue the owner provided designs for an anchored secant pile wall to provide the necessary temporary groundwater cutoff barrier and a constructible wall system through buried wood debris. The successful shoring contractor proposed an alternate design which relied on pre-trenching through the wood debris before installing a deep anchored cutoff wall. On the 635 Elliott Avenue Project the owner designed a conventional permanent anchored secant pile wall system due to the difficult soil conditions with a high water table. The selected contractor designed modifications that reduced costs and tightened a tough schedule. Congested sites and challenging ground conditions require early and active contractor participation in order to maximize efficiency.

CONCLUSIONS AND FUTURE IMPROVEMENTS

Summarizing the conclusions reached previously and supported herein:

- Lateral pressures on shoring walls in overconsolidated soils can be more accurately predicted from previous observations than from established design methods.
- Lateral pressures on excavations deeper than about 40 feet appear to reach a limiting value, and do not necessarily increase with depth.

- No load zones can be safely truncated.
- Numerical modeling should be routinely used to predict wall deflections and area settlements.
- Instrumentation to measure wall performance is key to continuing improvement in wall design.
- Early participation from contractors can optimize designs.

The authors believe future studies should emphasize:

- Lighter soldier piles, shorter anchors, and thinner lagging – all are indirectly tied to lower wall pressures.
- Additional modeling of hybrid systems – combinations of soldier piles, tiebacks, soil nails, and corner bracing to produce the most efficient solution to variable site conditions.
- Adaptation of conventional construction equipment for specific site conditions to allow more efficient installation of shoring elements.

REFERENCES

Clough, G., Weber, P., and Lamont, J. (1972). "Design and Observation of a Tied-Back Wall." *Proc., Performance of Earth and Earth Supported Structures*, ASCE, Purdue University.

Grant, W.P. (1985). "Performance of Columbia Center Shoring Wall." *Proc., 11th International Conf. on Soil Mechanics and Foundation Engr.* San Francisco.

Gurtowski, T.M. and Boirum, R.N. (1989). "Foundations and Excavations for High-Rise Structures in Downtown Seattle." *Engineering Geology in Washington, Vol. II,* Washington Division of Geology and Earth Resources Bulletin 78.

Terzaghi, K. & Peck, R. (1967). *Soil Mechanics in Engineering Practice.* John Wiley & Sons, New York.

Winter, D., Loesch, D.and Hollister, R. (2002). "Shoring Wall and Subsurface Structural Systems, IDX Tower, Seattle, Washington." *Proc., Challenges and Future Directions for Tall Buildings.* Los Angeles Tall Buildings Structural Design Council.

Winter, D., Macnab, A. and Turner, J. (1987). "Analysis of 85-Foot-Deep Shored Excavation in Seattle." *12th Annual Meeting and Seminar.* Deep Foundations Institute. Hamilton, Ontario.

Winter, D., Smith, M., Chin, K. and Carnevale, R. "Creative Shoring Solutions for a Tight Urban Site." *34th Annual Meeting and Seminar.* Deep Foundations Institute. Kansas City, Missouri.

Selection and Construction of a Permanent Anchored Soldier Pile Wall

By Steven R. Lowe,[1] P.E., Frederick C. Rhyner,[1] P.E.,
and Edward J. Schluter,[2] P.E.

1. Mueser Rutledge Consulting Engineers, New York, NY; 2. Yonkers Contracting Company, Inc., Yonkers, NY

ABSTRACT: An access road to a new 34.5 hectare (85 acre) multi-use development in Yonkers, New York required the use of an unconventional, permanent tied-back soldier pile wall to accommodate steep cross slopes, limited Right-of-Way (R.O.W.), and unfavorable subsurface conditions. The subsurface conditions were 1.5 to 9 meters (5 to 30 feet) of uncompacted boulder-laden fill, standing at its angle of repose and underlain by thin natural soil and irregular bedrock. In many places the rock level was above final grade, thus the wall had "mixed-face" conditions. The 183 meter (600 foot) long wall varied from 0.5 to 7.5 meters (2 to 25 feet) high on its exposed face. It was constructed of drilled-in steel H-piles for the soldier piles, timber lagging for temporary soil support and reinforced concrete infill "lagging" for the permanent condition. Rock anchors were installed at steep angles to remain within the R.O.W. This paper discusses the issues leading to the wall type selection and the various challenges encountered during construction of the wall.

INTRODUCTION

Two new roads were required to access a new development on a 34.5 hectare (85 acre) hilltop site in Yonkers, New York. One of the access roads traverses land adjacent to a major utility company's largest electrical substation. Available land in this area was in short supply so the alignment was located up against the substation and its width was constricted to preclude the use of typical embankment side slopes. The profile grade line dropped at 10 percent throughout most of the alignment to accommodate the 59 meter (195 foot) change in elevation from the hilltop site to the collector road. The upper 213 meters (700 feet) of the roadway was situated in a stable rock cut; from there, the cross-section quickly transitioned to a side-hill condition for about 290 meters (950 feet). Within this segment, the cross slope of existing topography varied from about 1:2 to 1:1. See Figure 1 for a typical section through the access road.

Because of limited R.O.W., a tied-back soldier pile retaining wall was used to support the cut on the uphill side of the roadway and precast concrete T-walls to support the fill on the downhill side. The remaining segment of the road was typically constructed in fill supported by T-walls.

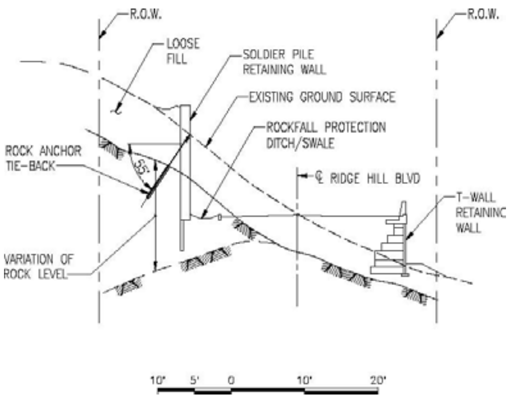

Figure 1. Typical Cross Section

The most difficult portion of the alignment from the design and construction viewpoint was the central 183 meters (600 feet) of side-hill condition. In this segment the topography was so inaccessible that during the design phase of the project it was not possible to make borings, even with a tripod rig. The investigation relied on hand-dug test pits, expecting to locate shallow rock. Instead, 3 of the 4 test pits encountered fill or natural soil to 1.2 meters (4 feet) deep, without encountering rock. Figure 2 shows the existing conditions after clearing and grubbing.

Figure 2. Existing Conditions

The bid-phase design called for a precast concrete retaining wall on the uphill side of the roadway and the bidding proceeded with the assumption that rock would be at

1.5 meters (5 feet) below ground surface, but recognized that additional borings were necessary prior to construction. The Contractor built a temporary access road and made six borings along the proposed wall alignment. These borings generally confirmed the presence of thick, loose granular fill overlying gneissic bedrock. The elevation of the bedrock surface varied dramatically. At several locations outcrops were visible, but elsewhere, rock was 11 meters (36 feet) below grade. The loose fill was standing at or close to its angle of repose, judging from the slides observed during construction of the temporary access road.

Soon after construction began, the utility company disclosed that it had long ago dumped fill materials on the uphill portion of the slope. It advised that the fill materials consisted of shot rock and other waste excess soil generated during the construction and expansion of its substation. It also provided an historic rock contour map, created before the substation was constructed. Shot rock refers to the waste material generated from blasting operations. In this instance it consisted of a loose soil matrix with a wide and inconsistent gradation of particle sizes from boulders of several feet in diameter to layers of silt, with predominant group symbols of SM and GP per the Unified Soil Classification system. After the site was cleared, the Owner obtained an updated topographic contour, because the earlier design-phase topographic survey was obscured due to dense vegetation. By comparing the new topographic survey to the original rock contour plan, it became evident that the dumped fill materials were from 1.5 to 7.5 meters (5 to 25 feet) thick.

The bid-phase design had called for a 6 to 9 meter (20 to 30 foot) deep cut along most of the length of the wall. Given the newly discovered subsurface conditions, the Geotechnical Engineer and Contractor quickly came to the conclusion that the precast retaining wall design would not work: the width of the wall required to support the soil above the rock would have to extend past the R.O.W. Instead, it was decided that a soldier pile and lagging wall, which could be converted to a permanent wall would be the least expensive solution. The solider piles could adapt to the erratic top of rock (i.e. the tip of piles could be extended as required for toe of wall support), timber lagging would provide temporary support for the loose fill and a concrete in-fill panel would provide the permanent exposed face. The most difficult aspect of the redesign was being able to install permanent tie-backs into rock that would not extend beyond the R.O.W. As part of the redesign effort, the Contractor proposed a major cost-saving idea: raise the profile grade line by 4.5 meters (15 feet), to reduce the length of the wall, the quantities of excavation and the required height of the uphill retaining wall. This change was adopted and as a consequence, the precast retaining wall on the downhill side of the roadway became 4.5 meters (15 feet) higher, but the net effect was a major cost and schedule savings.

WALL TYPE SELECTION AND DESIGN PARAMETERS

Once it was determined that the top of rock was much lower than expected, a redesign of the uphill retaining structure was performed. The new design needed to address the challenging site conditions, including the unstable slopes, variable subsurface conditions, close proximity to the R.O.W. line, high voltage overhead power lines and a maximum 10% roadway gradient (dictating the exposed height of wall). The resulting design was a soldier pile and lagging wall that initially acted as a temporary support of excavation (SOE) and then formed to be a permanent wall. The wall varied along the alignment from a cantilevered condition, up to 3.5 meters (12 feet) high, to a braced wall 7.5 meters (25 feet) high with one or two anchor levels based on the top of rock elevation. See Figure 3 for a typical section through the wall.

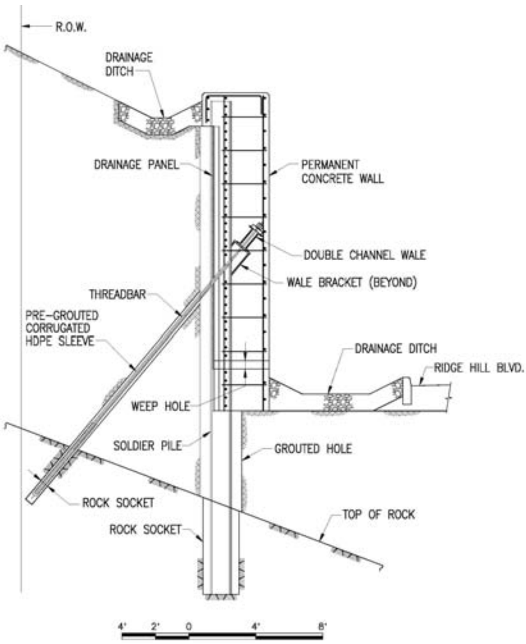

Figure 3. Typical Wall Section

The geotechnical parameters used for the design were:

Fill: dry unit weight = 11.7 kN/m^3 (115 lbs/ft^3)
angle of internal friction = 30°
slope of material behind the wall = 30°
Rankine active earth pressure coefficient = 0.75
Rankine passive earth pressure coefficient = 3.0

Rock: nominal active pressure for sound rock = 138 kPa (20 lbs/ft^2)

The variable grades, both behind and in front of the retaining wall, and the variable top of rock elevations resulted in multiple design sections. Four design sections were initially considered and were expanded to ten after additional top of rock information was available from the soldier pile installation. Each design section was analyzed for the temporary construction stages and for the final constructed condition.

The permanent wall was designed and detailed with the following elements to improve the long term performance of the wall:

- Prefabricated, heavy duty drainage board behind wall
- Additional weep holes
- Epoxy coated reinforcement
- Coal tar epoxy coated soldier piles
- Double corrosion protected rock anchors
- Concrete encapsulation of the soldier piles for additional corrosion resistance
- Zinc rich primer coating on the wales and wale brackets
- A minimum of 76 mm (3 inches) of concrete cover on all reinforcement and embedded steel
- Control joints at all piles and wales

During construction it was also revealed that a relatively thick layer of decomposed rock was present at the north and south ends of the wall. The design was checked and it was determined that the soldier piles in these areas should either extended 1.5 meters (5 feet) into sound rock or a minimum of 6 meters (20 feet) into decomposed rock. The reduced strength of the decomposed rock also required that the wall be designed for reduced capacity rock anchors. A combination of additional anchors and lightweight fill (expanded shale) were required to provide adequate wall stability since the anchors could not lengthened beyond the R.O.W. line.

WALL CONSTRUCTION

A number of site conditions had to be overcome to install the wall. The first was site access. Clearing and grubbing of the existing slope was required. A level work bench had to be installed over the steep slopes to accommodate the soldier pile drill rig and its five accompanying compressors, solider pile deliveries, support equipment and concrete deliveries. The temporary work bench height and width was driven by requirement of the drill rig to sit level and at the elevation of the hole to be drilled. The 11 meter (36 foot) wide bench was constructed by importing approximately 23,000 cubic meters (30,000 cubic yards) of material from a rock blasting operations on other portions of the project.

One of the principal hurdles was how to drill a large diameter hole through an un-compacted steep slope riddled with large boulders. Since the top of sound rock varied from less than a meter to 11 meters (2 to 36 feet) below the existing ground surface, a temporary casing would be required to maintain the loose fill for drilling the rock socket. Given that the design required that the solider piles be fully encased in the concrete wall, a permanent casing was not an option. The selected drill rig had to be cable of installing and removing the temporary casing and capable of drilling a rock socket 1.5 to 3 meters (5 to 10 feet) deep. The Bauer BG-40 was selected due to its dual rotary capability, its enormous torque capacity and its ability to quickly switch to a down the hole hammer (pneumatic hammer run by five Ingersoll Rand 1170 high output compressors in series) necessary to make the rock sockets.

Once the temporary access bench was constructed the drill rig was mobilized to the site and drilling began. After the first few holes it became apparent that modifications had to be made to stay within the 76 mm (3 inch) plan tolerance for the solider piles. The shot rock overburden and irregular top of rock surface caused the temporary casing to drift. In order to address this problem the temporary casing was increased from 76 to 107 cm (30 inch to 42 inch) diameter to accommodate a 92 cm (36 inch) diameter rock socket rather then the 66 cm (26 inch) diameter rock socket assumed in the redesign. Additionally, a hydraulic hammer was utilized at some pile locations to level the steeply sloped rock to facilitate rock socket drilling.

Excavation and installation of temporary timber lagging proceeded after the solider piles were installed and the drill rig was demobilized. The excavation was limited to two feet below the proposed brace level prior to installing and testing the rock anchors. See Figure 5.

Figure 5. Installation of the permanent rock anchors

The rock anchors were tested as per the Post Tensioning Institute's recommendations. The tests included water pressure testing the rock socket and tension load testing the grouted anchors. The majority of the anchors failed the initial water test which indicated that the rock was fractured and had to be grouted, re-drilled and water tested again. All the anchors were load tested to 133% of the design load and held for a minimum of 10 minutes for the proof tests and 300 minutes for the performance tests. After testing the anchors were locked off to 80% of the design load.

Construction of the concrete portion of the permanent wall began when the excavation and lagging had extended to the final subgrade. A leveling pad was constructed at the bottom of the proposed wall and stepped as required between the solider beams to support the reinforcing bars and formwork. DOKA Framax panels were used as the formwork and were supported by back to back C8x11.5 channels blocked behind the flanges of the solider piles. See Figure 6**.**

Figure 6. Wall reinforcement and formwork

CONCLUSIONS

An inaccessible site, prior to the bid-phase of the project, made it difficult to assemble information on the existing subsurface conditions. As a result, the initial design had to be based on an assumed top of rock estimated from a few hand excavated test pits. Supplemental borings were possible once the Contractor was able to clear, grub and install temporary site access roads. The borings indicated that the top of rock was much lower than originally assumed, making the construction of a gravity retaining wall impossible within the available R.O.W.

Once the design parameters and site limitations were better understood, it was determined that a soldier pile and lagging wall, readily adaptable to the variable site conditions, would be the most appropriate and economical wall type. The advantages of the soldier pile wall were:

- The soldier piles could be installed to variable depths for sockets into the variable depth of rock.
- Temporary timber lagging could be installed as a backside form for the permanent wall and also provide excavation support to excavate to final subgrade.

- Rock anchors could be added as necessary to provide support within the R.O.W.
- The required quantity of rock excavation could be minimized since the wall did not need to extend beyond the soldier piles.

The redesigned wall required construction of a temporary access road and level work benches for the pile installation. The installation was complicated by the unstable slopes, unfavorable shot rock fill and variable top of rock elevations. The permanent rock anchor installation revealed the rock to be highly fractured and additional steps were required to water test, grout and load test the anchors. Minor changes to the proposed wall drainage system were required due to the excavated surface of the rock.

In the end, a successfully constructed permanent anchored soldier pile wall was achieved through the cooperative efforts between the Geotechnical Engineer and the Contractor. See Figure 7 for the completed wall.

Figure 7. Completed wall

REFERENCES

American Association of State Highway and Transportation Officials (AASHTO). "Standard Specifications for Highway Bridges, 17th Edition" (2002).

New York State Department of Transportation. (NYSDOT) "Geotechnical Design Procedures for Flexible Wall Systems" (2007).

Post Tensioning Institute. (PTI) Recommendations for Prestressed Rock and Soil Anchors" (2004).

THOUGHTS ON SOIL NAIL TESTING & DESIGN

Thomas D Richards, Jr.[1]

Abstract

Soil nail testing is a crucial aspect to design and is critical to ensure that parameters assumed during design are verified. The need to define a bond stress rather than "design load" in Contract Documents is explained. The needs to test a grouted length shorter than total nail length and to create an ungrouted free length are discussed. FWHA GEC7 provides clear instructions on procedures for design. However, these procedures have conservative and unconservative aspects. Punching shear and bar yield are shown to potentially be treated unconservatively. Recommendations for proper handing of punching shear and bar yield are presented.

Introduction

Soil nail design, testing, and construction are well documented in FHWA(2003), hereafter referred to as GEC7. Readers are urged to review GEC7 for general soil nail design and construction background not covered in this paper prior to reading this paper.

The following topics are presented:

- Soil nail testing details
- Soil nail acceptance criterion errata in GEC7
- Punching shear
- Bar strength

The guidance for nail testing is clear and thorough; however, this author has found many users misunderstanding key points.

The guidance on punching shear and bar strength are unconservative in this author's opinion.

This author finds GEC7 to be a valuable document and presents these points for clarification or improvement.

Soil Nail Testing – What is "design load" of a nail?

The general load distribution used in soil nail design is shown in Figure 1. The key design parameter is the bond, qall, in force/unit length which is the slope of the load versus length plot in Figure 1. In SNAIL (Caltrans 1991), this bond is input as a bond stress and hole diameter and then

bond = bond stress * π* hole diameter.

[1] Chief Engineer, Nicholson Construction Company,12 McClane St.,Cuddy, PA 15031
email : trichards@nicholsonconstruction.com

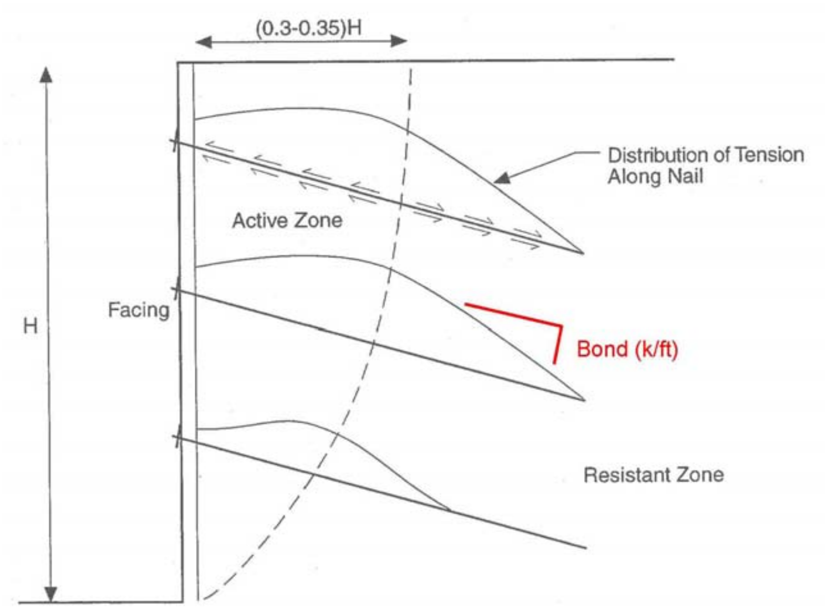

Figure 1. Load distribution in soil nails (modified from FHWA 1998)

The goal of verification and proof testing is then to prove the design bond used in design. GEC7 then provides useful equations on page E-8 through E-11 for determining the maximum test bond length and "Design Test Load" (DTL) and the maximum bond length. This author has seen several projects where Engineers have defined a "design load" of the nail. This has led to confusion about what grouted length should be tested and what the defined "design load" means.

Soil Nail Testing – Why not test a full length nail ?

This author has found confusion among Engineers and Contractors about testing a fully grouted nail. This confusion seems to stem from experience with ground anchors. A key difference between soil nails and anchors is that soil nails are fully bonded including on the "active" side of the critical surface.

Figure 2 shows the "Design Test Load" that would be required for a fully grouted nail to prove a bond which was used in design. Note that this "Design Test Load" exceeds the maximum load in the nail near the critical surface for which the nail bar steel was designed also shown on Figure 2.

Table 1 used the equations in pages E-8 through E-11 for an example bond of 3 kips/ft. Even with a fairly large #10 Grade 75 bar, the maximum test load of 85.5 kips (90% of yield) is exceeded for a grouted bond length over 14.2 ft testing for a verification test to a factor of 2.0 and 18.9 feet for proof tests to a test factor of 1.5. These lengths are significantly less than the typical nail length especially for a #10 Grade 75 bar.

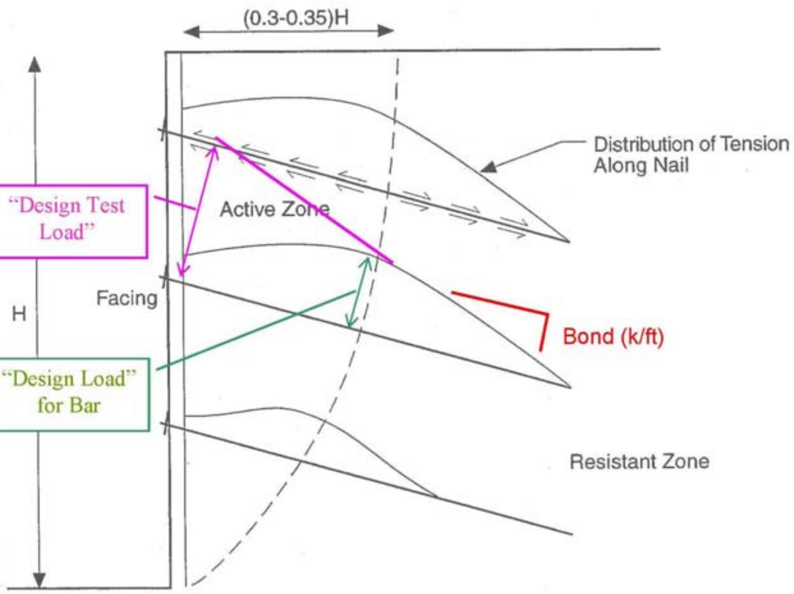

Figure 2. Design Load for a full length grouted nail (modified from FHWA 1998)

SOIL NAIL MAXIMUM TEST BOND LENGTH

VERIFICATION TEST FACTOR =		2			
BAR SIZE FS in Verification Test FS_{Tver} =		2	must be greater than Test Factor and preferably 2.5 to 3		
PROOF TEST FACTOR =		1.5			
BAR SIZE FS in Proof Test FS_{Tproof} =		1.5	must be greater than Proof Test Factor and preferably 1.7		
HOLE USED IN ANALYSIS	in	4	4	4	
DESIGN BOND	psi	20	20	20	
MODIFIED HOLE DIAMETER	in	6.3	6.3	6.3	
TEST BOND on MOD DIAMETER	psi	25	25	25	
BOND = Qall	k/ft	3.0	3.0	3.0	
TEST BOND	k/ft	6.0	6.0	6.0	
BAR YIELD = f_Y	ksi	75	**75**	150	
C_{RT}		0.9	0.9	0.8	
MIN BAR AREA FOR L_{BVT} = 10 ft	in^2	0.89	0.89	0.50	
BAR		#8	**#10**	1.25"	
BAR DIAMETER	in	1.00	**1.27**	1.25	
BAR AREA = At	in^2	0.79	**1.27**	1.23	
MAX LOAD ON BAR = C_{RT}*At*f_Y	kips	53.0	**85.5**	147.3	
$L_{BVTmax} = C_{RT}$*At*f_Y/(Qall*FS_{Tver})	ft	8.8	**14.2**	24.4	**Maximum Verification Test Bond Length**
$L_{BPTmax} = C_{RT}$*At*fY/(Qall*FS_{Tproof})	ft	11.7	**18.9**	32.6	**Maximum Proof Test Bond Length**

Table 1. Example of maximum test bond length

Soil Nail Test – Minimum Free length

GEC7 requires a minimum unbonded length of 3 feet. However, there is no explanation provided as to why, and this presents some opportunities for confusion. As shown conceptually in Figure 3, one possible and good reason is so that radial ground stresses on the hole from the bearing of the reaction system, which is typically close to the hole, do not falsely increase the confinement and bond and cause a "pulling up on your bootstraps" effect.

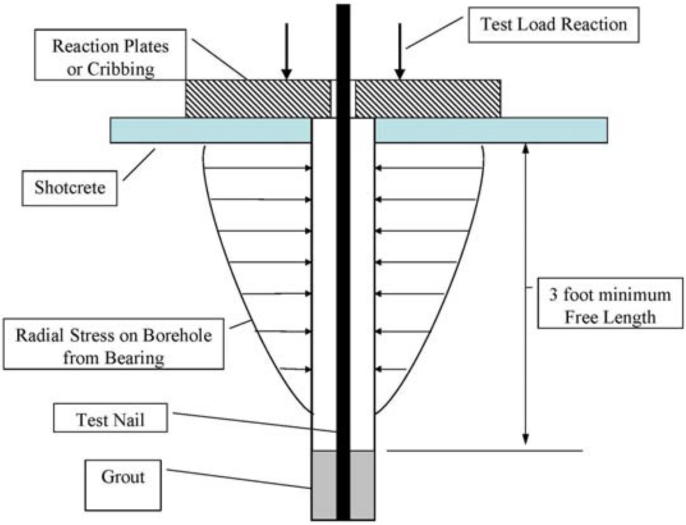

Figure 3. Radial Stress from Reaction System

Soil Nail Test – Use of Bond-Breakers

Some feel that the minimum unbonded length or the limited bond length discussed above can be accomplished using a bond-breaker over part of the nail length (Figure 4). While this can reduce the potential for false capacity in the uppermost portion test nail, it is likely that the grout in the "unbonded" portion of the bar does provide indirect capacity to the test nail by resisting the up-hole movement of the bonded portion of the test nail and causing compression in the grout above the bottom of bond-breaker. In this scenario shown in Figure 4, the bonded length bears against the unbonded grout body above, possibly gaining capacity, and this leads to questions about the real bond length. This concept is a concern for soil nails rather than ground anchors since:

1. the test load of soil nails is small relative to the strength and stiffness of the grout column,
2. ground anchor free lengths extend past the critical surface and often into stiffer ground, and
3. every ground anchor is tested

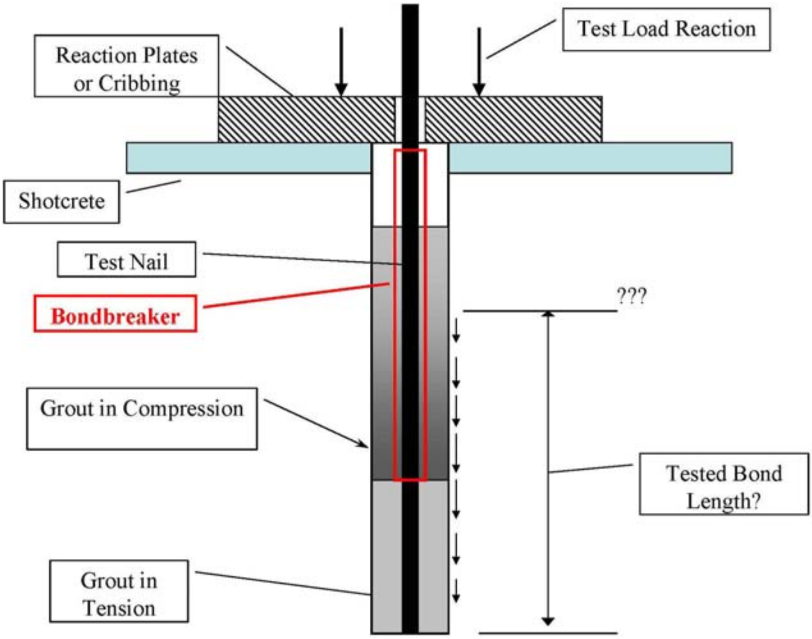

Figure 4. Compression Effect with Bondbreaker

GEC7 Nail Test Acceptance Criteria

The soil nail test acceptance criteria in GEC7 sample specification page E-12 includes the statement "A pullout failure does not occur at 3.0 DTL under verification testing …". However, throughout GEC7, the factor of safety on bond used in design is 2. Therefore, a verification test on a well designed soil nail wall should be expected to fail above 2 DTL, but not necessarily above 3 DTL. The Anchored Earth Retention Committee of ADSC submitted to FHWA a proposed correction to "A pullout failure does not occur at 2.0 DTL under verification testing…". FHWA and the authors of GEC7 have agreed to this correction and errata to GEC7 are available on the FHWA website.

GEC7 Punching Shear

For calculation of global stability (factor of safety on soil strengths), GEC7 Page D-15 states " To ensure that pullout failure controls over tensile or punching shear failure, artificially large values of nail diameter and facing capacity are entered in SNAIL." Then in the facing design sections, the punching shear strength of the facing is designed for semi empirical working load without comparison to the input for SNAIL.

The result of this procedure is that bottom rows of nails have much higher forces and contribution to the factor of safety. However, as shown in Figure 5, the limiting load from the bottom rows is really from the facing to the failure plane.

This procedure is considered to be unconservative. A reasonable solution is to input the punching shear resistance of the actual planned facing into SNAIL.

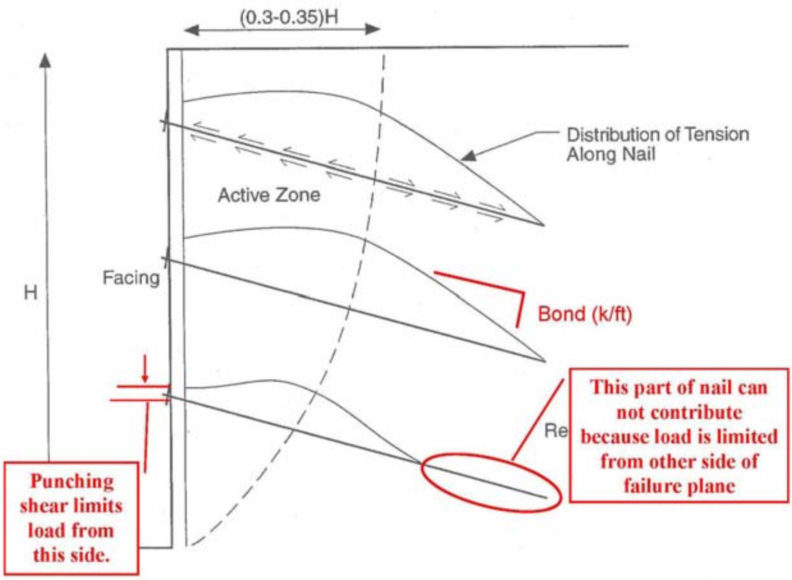

Figure 5. Limiting contribution of lower rows (modified from FHWA 1998)

GEC7 Bar Strength

The same quote from GEC Page D-15 applies to bar strength where "nail diameter" is understood to mean diameter of reinforcement based on "To ensure that pullout failure controls over tensile". The same logic and concern expressed for punching shear then apply but to a lesser degree since

1. bars are ductile and
2. the bar strength exceeds the maximum load in the bar in the global factor of safety in the example in GEC7. This may not always be the case.

Therefore, this procedure may be unconservative. A reasonable confirmation would be to input proposed bar strength and size into SNAIL.

Conclusions

Proper testing procedures as presented in GEC7 need to be properly understood and properly implemented to verify the critical design parameter of bond. Several key points which are often missed or overlooked are presented and further explained above. The minimum pullout load needs to only exceed 2 times design test load as documented in errata to GEC7.

GEC7 provides good guidance on the design of soil nails walls. However, punching shear and bar strength could be limiting conditions in the "global stability" factor of safety calculations. Punching shear resistance of the proposed facing and strength of the proposed bars should be input into SNAIL or similar programs.

References

CALTRANS (1991). "A User's Manual for the SNAIL Program, Version 2.02 – Updated PC Version," California Department of Transportation, Division of New Technology, Material and Research, Office of Geotechnical Engineering, Sacramento, California.

FHWA (2003) . "Soil Nail Walls." *FHWA Geotechnical Engineering Circular No. 7, Report No. FHWA0-IF-03-01*, FHWA, March 2003

FHWA (1998) . "Manual for Design and Construction Monitoring Soil Nail Wall." *FHWA Report No. FHWA-SA-96-069R*, FHWA, November 1996 (Revised October 1998)

Soil Nail and Shotcrete Earth Retention for Construction of a Coal Plant Rotary Railcar Dump and Conveyor

J.R. Hill[1], M.G. Iffert[2], and S.J. Farr[3]

[1]Area Manager, Hayward Baker Inc., 1530 South Second Street, Saint Louis, Missouri 63104; Phone: 314-802-2923; jrhill@haywardbaker.com
[2]Project Engineer, Hayward Baker Inc., 1530 South Second Street, Saint Louis, Missouri 63104; Phone: 314-802-2925; mgiffert@haywardbaker.com
[3]Division Manager, Hayward Baker Inc., 1350 West Lake Street, Roselle, IL, 60172; 630-339-4300; sfarr@haywardbaker.com

ABSTRACT

A new limestone unloading structure consisting of a rotary railcar dump and conveyor was planned for construction in Marissa, IL, at the largest coal fired power plant in the U.S. An earth retention system was necessary to facilitate the underground construction. The original design included a system of braced sheetpiling. The geotechnical contractor provided a soil nail and shotcrete alternative including design and construction of 161.5 meters (530 lineal feet) of soil nail wall and over 1,672 square meters (18,000 square feet) of shotcrete earth retention around the proposed limestone unloading structure and conveyor.

This paper describes the design and construction of the earth retention system and quality control measures.

BACKGROUND

Near Marissa, Illinois, the construction of the largest coal-fired power plant in the United States is underway. The power plant will have a capacity of 1,600 megawatts of power, enough to serve 2.5 million families. A 213.3 meter (700 feet) tall concrete stack, approximately 21.3 meters (70 feet) taller than the St. Louis Arch, was erected during early phases of the construction schedule. Near the base of the stack and proposed steel structures, a limestone unloading structure consisting of a rotary railcar dump and conveyor is planned for construction. The new power plant will cover up to 2.8 square kilometers (700 acres) upon completion, most of which consists of cleared farmland.

SITE CONDITIONS

The site access and logistics plan is shown in Figure 1. These conditions eliminated the option of laying back the excavation at a reasonable slope and therefore required earth retention near the structure's footprint. With the close proximity of the existing stack and the ongoing construction of the surrounding steel structures, the available open real estate for crane access and material lay-down could not be sacrificed to an open excavation. Therefore, the excavation for the unloading structure required earth retention. The proposed unloading structure foundation was planned to be up to 18.2 meters (60 feet) below grade. The soil profile consisted of 13.7 meters (45 feet) of relatively stiff silty clays overlying layers of shale and sandstone.

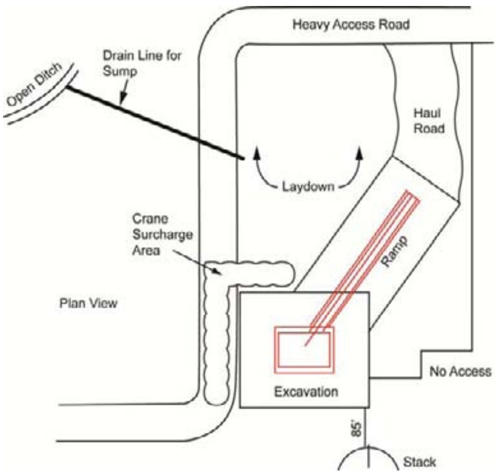

Figure 1. Site access and logistics plan.

SOIL CONDITIONS

The soils on site appeared to represent typical central-southern Illinois stratigraphy: 3 to 4.5 meters (10 to 15 feet) of loessial deposits overlying stiff silty clay glacial till scattered with a few water bearing sand pockets generally 0.3 to 0.6 meters (1 to 2 feet) thick, followed by shale, sandstone and limestone. Standard penetration N-values, within the loessial deposits ranged from 8 to 21 with moisture contents in the low to mid 20s. The glacial till N-values varied between 15 and 28 while the moisture contents remained consistently in the mid to upper teens. Because the soils were shown to be predominantly cohesive within the applicable borings, the water encountered at a depth between 3 to 4.5 meters (10 to 15 feet) below grade was assumed to be a perched water table and was discounted during the bidding period.

DESIGN CONCEPT

The originally specified earth retention system for the proposed structure consisted of approximately 155.4 meter (510 linear feet) of braced, hot-rolled sheet piling to be designed by the geotechnical contractor. The sheet piles were specified to extend from grade (Elevation 138.3 meter [454 feet]) to the top of rock (Elevation 124.9 meters [410 feet]). The excavation below the top of rock was assumed to stand freely without additional bracing. Because the sheet piles were specified to sit directly on top of the shale bedrock, developing passive resistance from the sheet pile "toe" was not possible. Instead, an additional bracing level would be required near the sheet pile base.

Despite the scattered water bearing pockets of sand, the requirement of the sheet piling did not appear essential for the excavation. At least three levels of bracing were required, spaced fairly close together due to the cut height and construction surcharge loads. These factors combined and resulted in a costly retention system which seemed inefficient in regards to the surrounding environment and current soil conditions.

Soil Nail and Shotcrete Alternative

In consideration of costs associated with the specified retention system, the geotechnical contractor provided an alternative consisting of the design, furnishing, and installation of 161.5 meters (530 lineal feet) of a soil nail and shotcrete earth retention system for the proposed limestone unloading structure and conveyor. The proposed alternate retention system provided potential cost savings for the owner of nearly 50%.

Alternative System Design

A plan view of the alternative design is presented in Figure 2. The alternative system was designed for a top of rock elevation of 124.9 meters (410 feet) with a back batter of 15 degrees from vertical as shown in Figures 2 through 5. Below the top of rock, the geotechnical contractor provided an option to shotcrete the top 1.5 meters (5 feet) of shale to prevent weathering. Global stability analysis indicated that nails were not required in the shale bedrock. The existing grade was approximately elevation 138.3 meters (454 feet) while the top of the earth retention system was designed to be 1.5 meters (5 feet) below the existing grade, requiring a 1.5 meter (5-foot) pre-cut slope at 1.5 horizontal to 1 vertical up to grade, as shown in Figure 4. The design included a construction surcharge of 11.97 kPa (250 psf) around the east, south and west sides of the pit and east side of the ramp. In order for the general contractor to set forms for the structure, the north side of the pit and west side of the ramp were designed for a 150 ton crane surcharge approximately 6 meters (20 feet) from the face of the proposed structure.

The retention system design included 7 rows of nails beginning at elevation 136.5 meters (448 feet), spaced on 1.8 meter (6-foot centers both horizontally and vertically, and installed in a 152 mm (6 inch) or 203 mm (8 inch) diameter hole. The nails within the top five rows for the pit were typically #10 Grade 75 threaded bar, and 11.8 meters (39 feet) long, while the ramp nails were typically #9 Grade 75 threaded bars, and 8.2 meters (27 feet) long. The nails along the north side of the pit and west side of the ramp were extended three to five feet to cover the additional load presented by the crane surcharge. The lower two rows were considerably shorter due to bonding within the shale in lieu of the overburden. The facing of the system included welded wire mesh, waler rebar and a 102 mm (4 inch) thick shotcrete overlying 0.6 meter (2-foot) wide strips of drain board on 1.8 meter (6-foot) oc.

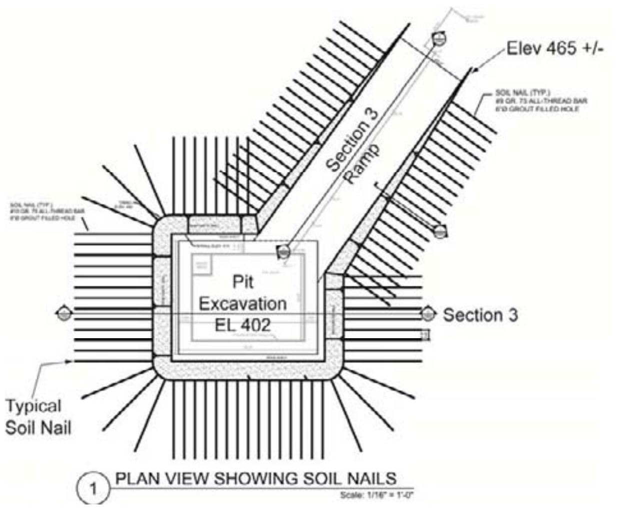

Figure 2. Plan view of the pit and ramp and ramp displaying the extent of nails.

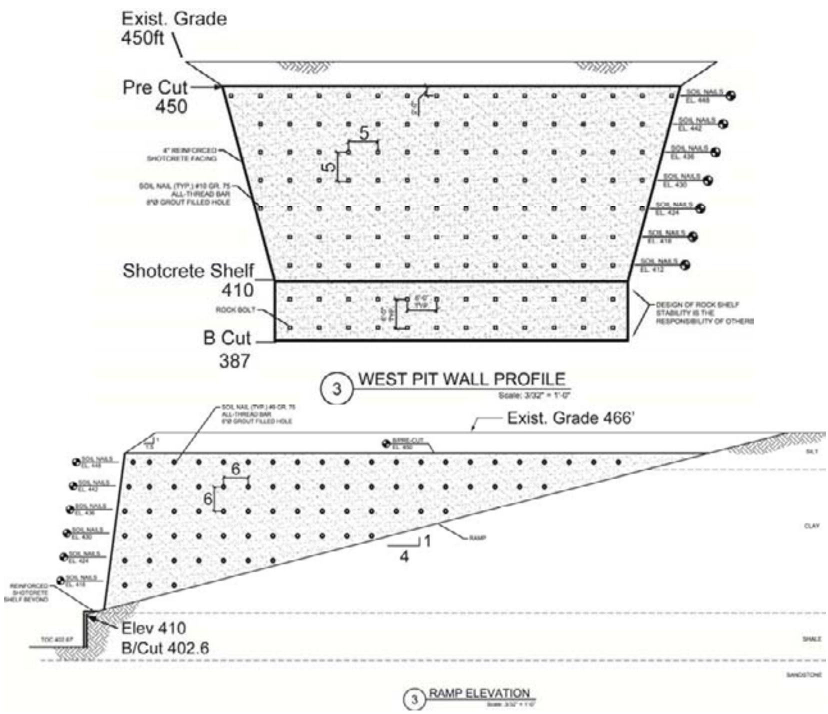

Figure 3. Profile views of pit (top) and ramp walls (bottom) with nail layout.

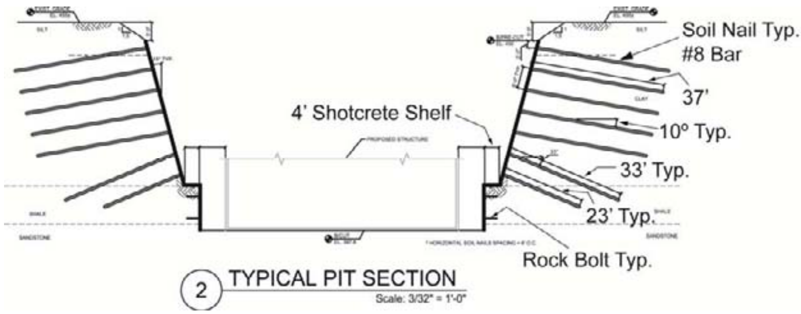

Figure 4. Cross section view of the main pit and ramp

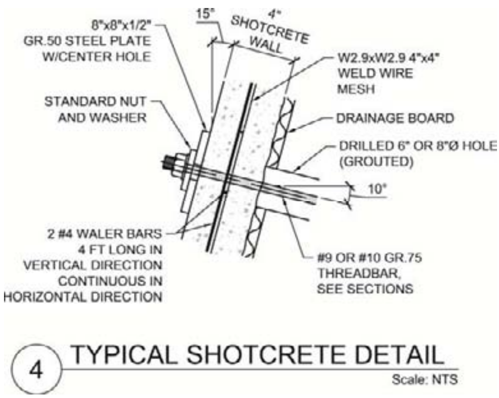

Figure 5. Typical shotcrete detail.

CONSTRUCTION

The loessial soils were not cohesive enough to facilitate an oversized bit without material sloughing into the excavation as illustrated in Figure 6. The contractor implemented several different bit types and drilling speeds to drill 152 and 203 mm diameter holes, while preventing sloughing of the soils. The soil nail design included 152 and 203 mm (6 and 8 inch) diameter holes. In order to maximize the bond capacity, the geotechnical contractor attempted to use an over-sized bit (nearly 254 mm [10 inch] diameter) with a 203 mm (8 inch) auger.

Water control became a problem for both the general contractor and geotechnical contractor before construction began. Because the job entailed excavating a deep hole on a flat site, surface run-off eventually drained to or near the pit area from almost the entire site. Although the project team employed water control measures that included sump pumps, berms and drain lines prior to excavating, the period between the initial excavation and the installation of the retention system experienced multiple heavy rain events, which lead to very wet conditions for the retention and excavation crews, as shown in Figure 7. The excessively wet site slowed construction considerably. Earth retention crews utilized extra drainage material in front of active seeps. Some active water seeps required the removal and then re-application of shotcrete, prior to the shotcrete curing. The excavators connected the vertical drains to discharge pipes that were then directed to a sump for pumping away from the site.

Figure 6. Photograph illustrating the sloughing of soil during the first lift drilling of the soil nails.

Figure 7. Photograph of wet conditions after excavation of the first lift.

Despite the project beginning with unforeseen setbacks, the soil nail and shotcrete installation was well coordinated with the excavating to ensure continuous production. The remainder of the excavation below the first lift became more stable as the groundwater conditions improved. Control of the groundwater conditions was improved with measures which included additional sump pumps and drainage board. A total of 512 soil nails were installed and over 1,672.2 meters (18,000 square feet) of shotcrete was applied, and was completed approximately two weeks ahead of the projected schedule. Figure 8 demonstrates the nearly completed walls. Note the lack of active water seeps through the shotcrete facing.

Figure 8. Left: Soils nails being installed on the ramp; Right: Soil nails being installed on the 7th row.

QUALITY CONTROL

Prior to the start of construction of the soil nails and shotcrete, shotcrete was applied onto two mock panels. The panels were comprised of the reinforcement that mimicked actual wall conditions overlying a 102 mm by 203 mm (4-inch by 8-inch) plywood surface. The reinforcement is shown in the shotcrete detail, Figure 5.

Cores were taken from the panels and observed prior to the installation of any production shotcrete. The target strength for the shotcrete was 27.5 MPa (4,000 psi) at 28 days while the cores reflected strengths of over 34.4 MPa (5,000 psi) at 7 days.

Five performance tests and 25 proof tests were conducted on production nails. The tests were distributed across the seven rows of nails to ensure that each soil stratum was capable of achieving the designed bond resistance. A graph of one of the typical proof tests is shown in Figure 9. Grout cylinders were also taken daily during nail installation to verify that adequate strength was reached prior to testing. The load tests were conducted to 1.33 times the design load. This corresponds to a design bond stress of 0.09 MPa (14 psi) in the overburden soil. The design bond stress in the shale was 0.2 MPa (40 psi).

Based on visual observations no signs of movement at grade or in the face of the wall were observed. At times, large scale construction equipment was active within the active soil wedge of the wall, and the wall performed as expected.

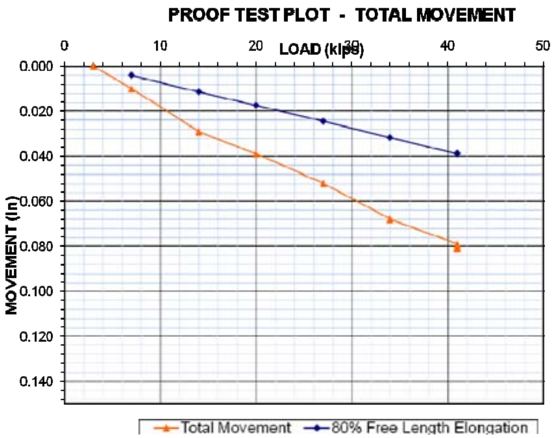

Figure 9. Soil nail proof test.

CONCLUSION

Soil nailing and shotcrete can be an effective means of earth retention on complex project sites, even with challenging ground water conditions. This system was more economical to install than the originally specified tied back hot rolled steel sheeting, and provided acceptable performance to allow for excavation and backfilling of the excavation.

REFERENCES

Lazarte, C., Elias, V., Espinoza, R, and Sabatini, P. (2003) "Geotechnical Circular No. 7, Soil Nail Walls", FHWA0-IF-03-017.

Permanent Soil Nail Wall Utilizing Chemical Grout Stabilization

Keith LaRue, P.E., M.ASCE[1]

[1]Moretrench, 100 Stickle Avenue, Rockaway, NJ 07866; PH (973) 400-3629; FAX (973) 586-7265; email klarue@mtac.com

ABSTRACT

A permanent soil nail wall was constructed to support an existing bridge abutment of an active major interstate. During the construction of the wall, poorly graded sand with trace silt (SP) was encountered directly beneath the abutment footing. The soil did not posses sufficient "face stability" to permit soil nail wall construction to proceed as originally designed. Further investigations determined this soil condition to be present the full depth of the proposed excavation support system thus requiring an alternate solution to be implemented. Due to restrictions associated with future roadway construction, sodium silicate based chemical grouting of the excavation face along the full height of support was selected to temporarily stabilize the poorly graded sands and permit the originally designed soil nail wall to be constructed. This paper discusses the conceptual design and construction procedures utilized to carry out the grouting program and soil nail wall construction.

INTRODUCTION

In an effort to improve traffic flow between two major thoroughfares, New Jersey Department of Transportation (NJDOT) is in the process of constructing two new ramps at the Garden State Parkway (GSP) Interchange 142 with I-78. As part of the ramp construction between the northbound GSP and westbound I-78, road widening of the GSP directly adjacent and beneath the east abutment of the eastbound I-78 was required (Figure 1). To achieve this requirement, the project's engineering consultant designed a 450.6 m^2 (4,850 ft^2) permanent soil nail wall system with a cast in-place concrete facade to retain a 4.88 m (16 ft) deep vertical cut. The support system allowed the sequential removal of the existing slope present in front of the existing bridge abutment and permitted the necessary widening required for future ramp construction. Prior to the actual construction of the soil nail wall structure, an interim measure of lateral stabilization of the existing abutment was required. This interim measure consisted of permanent double corrosion protected strand anchors being installed, tested, and pre-stressed against the existing abutment providing both the initial stabilization of the existing roadway abutment as well as becoming an integrated part of the final support system.

Figure 1. Pre-construction photo of east abutment condition where soil nail system was to be installed

TIEBACK DESIGN AND INSTALLATION

Preliminary stabilization of the existing abutment required the installation and testing of 24 permanent strand tiebacks each with a design capacity of 258 kN (58 kips). The anchors were initially designed to be installed at a 15 degree inclination through 178 mm (7 in.) diameter coreholes in the concrete abutment at elevation +26.67 m (+87.5 ft) (Figure 2). However, due to conflicts with the drilling equipment and the existing skewed bridge girders the tieback system was redesigned to be installed at a 10 degree inclination at elevation +25.76 m (+84.5 ft). The horizontal spacing was also changed to permit the drill rig boom to be extended between the girders as required for installation. The tiebacks were installed in less than 3.05 m (10 ft) of headroom using rotary-percussive duplex drill methods from a 6.10 m (20 ft) wide earthen berm constructed in front of the abutment. Due to the variable fill conditions encountered during the drilling process, the tiebacks were single-stage post-grouted prior to testing to ensure the capacities would be achieved, thus preventing any potential delays to the operation. All anchors were performance tested to 133% of the design load and locked off against the abutment.

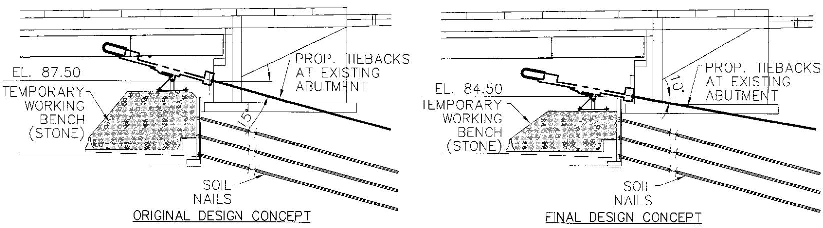

Figure 2. Original and final design concept for tieback installation

INITIAL SOIL NAIL CONSTRUCTION

During initial excavation for construction of the soil nail wall system, a poorly graded sand with trace silt (SP) was encountered. This material provided insufficient standup time to permit soil nail wall construction resulting in excessive caving as noted immediately upon excavation (Figure 3).

Figure 3. Poorly graded sand condition encountered during initial excavation for soil nail wall construction

Further investigations determined this unstable condition to be present for the full depth of the proposed soil nail excavation support, requiring an alternate solution to be investigated. Numerous alternatives were evaluated including the use of different underpinning/earth support methods, however, all were quickly eliminated given the existing conditions and restraints imposed by future lower roadway construction. Accordingly, the project team focused on methods of ground improvement which would provide sufficient face stability to permit soil nail wall construction.

Initial considerations were given to the use of a system of vertical grouted reinforcing elements along the alignment which the contractor had utilized successfully on previous projects (Figure 4). However, this scheme was not deemed feasible due to structural concerns associated with the numerous 152 mm (6 in.) diameter core holes required to be made through the existing footing to permit the installation of these elements. Considerations were also given to positioning the reinforcing elements in front of the footing, however, due to issues associated with installation tolerances the elements could not be guaranteed to not impede concrete facade construction and future roadway construction.

Figure 4. In-place vertical grouted reinforcing elements installed successfully on previously completed project

In the end, stabilization using sodium silicate based chemical grouting of the excavation face along the full height of support was the selected method of treatment. Grouting offered numerous advantages including the ability to excavate the grouted soil layer on the original alignment using conventional excavation methods and the ability to adjust the treatment procedures for varying ground conditions including performing multiples injections, if required. Grouting also provided the added benefits of serving as both temporary underpinning of the existing structure and as an additional movement reduction measure.

CHEMICAL GROUTING PROGRAM

A sodium silicate based grouting program using a two (2) row system of tube-a-manchette (TAM) grout pipes and needles were positioned on three (3) foot center to center spacing along the alignment to chemically stabilize a theoretical three (3) foot wide soil block (Figure 5). The preliminary concept was to install the TAM pipes at 5 degree batter just in front of the abutment footing. However, this geometry would result in much of the assumed grout influence zone at top of the wall being installed on the outside face of the excavation. Due to concerns with the possibility of "pulling" the grout body out from under the footing during excavation of the upper portion of the wall, small 25 mm (1 in.) diameter grout needles were utilized to grout the upper 2.13 m (7 ft) of grout wall construction. This would ensure that a better concentration of the grout injected would be present in the upper portion of the cut.

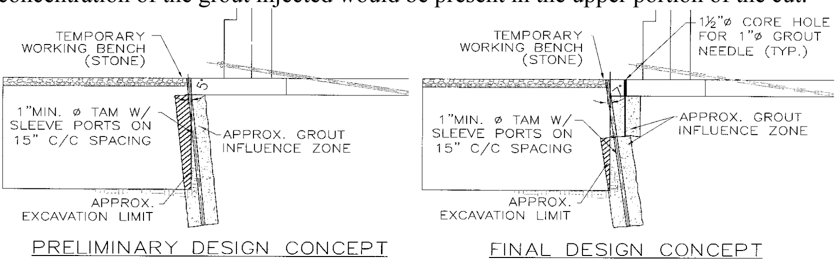

Figure 5. Preliminary and final chemical grout design concepts

TAM pipes were installed in 2.44 m (8 ft) of headroom utilizing wet rotary external flush method with a lost point. Once the design depth was reached, the lost point was ejected from the bottom of the casing and a bentonite-cement grout was injected via tremie the full length of the hole. The 25 mm (1 in.) diameter TAM pipes with sleeve ports on 381 mm (15 in.) center to center spacing were installed in sections due to the limited headroom conditions. It should be specifically noted that during TAM installation a change in silt content was noted in the wash water in certain areas which could have impacted the groutability of the soil. Accordingly, water tests were performed at pre-selected TAM pipes by positioning the slide packer at each individual port and injecting water using a small portable piston pump type setup. Both pressure and rate of injection were recorded at each port and used to estimate the soil porosity and grout injectibility along the alignment. This information was later utilized to determine the required grout viscosity and gel times as well as injections pressures for grouting at each TAM pipe.

Grout needles consisting of 25 mm (1 in.) diameter flush-coupled drill rods with a lost point system were installed through 38 mm (1 ½ in.) diameter cored holes in the footings prior to grouting of the TAMs. Due to the limited headroom and the minimal depth of injection required, the grout needles were installed using a hand-held conventional post driver. Once driven, a casing extractor was positioned on the hole and the grout header hooked up to needle for subsequent injection (Figure 6).

Figure 6. Grout needles through abutment footing with header system attached

Grout injection was carried out utilizing a continuous mixing, plural component chemical grout plant equipped with progressive cavity Moyno pumps for grout delivery. The containerized system was designed and built by the contractor and permitted multiple injections to be carried out simultaneously. The initial proposed starting grout mix was a 50% sodium silicate, 45% water, and 5% organic reactant by volume. However, this was quickly adjusted to a 40% sodium silicate, 55% water, and 5% organic reactant by volume to reduce the mix viscosity and permit better penetration into the areas with higher silt contents. TAM grouting was performed using packer grouting at both primary and secondary grout ports. A higher percentage of the targeted grout volume was directed to primary ports with secondary ports used for “tightening” between primary injections. To increase the visibility of occasional grout escapes, the contractors opted to dye the chemical grout. Upon discovery of grout escapes, the contractor would then adjust the percentage of sodium silicate, water, and organic reactant utilized to limit further grout losses. Grouting pressures varied from 68.9 kPa (10 psi) to as high as 413.7 kPa (60 psi) at deeper grouting depths. Continuous monitoring of the structure was carried out with a laser level with no visible signs of movement detected.

Grouting started at the northern end of the abutment and proceeded in a southerly direction. Grouting of the needles was performed prior to TAM grouting to minimize installation issues that could arise by attempting to drive needles into grouted ground. Multiple header connections were run simultaneously. The grouting was monitored via pressure gauges and magnetic flowmeters and recorded with a data acquisition system. Gel tests were performed periodically to determine set times and permit adjustments as required. A test section of the grout wall was exposed during the initial grouting operation which confirmed the effectiveness of the grout program to provide the necessary stand up time to permit soil nail construction. Unconfined compressive strength testing of grouted sand samples were performed in general accordance with ASTM D4219. Results yielded unconfined compressive strengths of between 861.8 kPa (125 psi) and 1378.0 kPa (200 psi).

Grouting during the first cycle of injections yielded a total of approximately 85,172 liters (22,500 gallons) of chemical grout injection representing approximately 90% of the anticipated grout yield anticipated at the start of grout program. Subsequent re-injections were then performed at TAM locations in areas where lower grout takes were documented to ensure sufficient coverage had been achieved.

SOIL NAIL WALL CONSTRUCTION

After completion of the grouting program, the soil nail wall construction resumed and was installed to full depth. The effectiveness of the chemical grouting was confirmed during excavation with significant increases in the excavation face stability noted at all soil nail levels (Figure 7).

Figure 7. Excavation first and second tier of soil nails after chemical grouting

The wall was excavated in 1.22 m (4 ft) vertical lifts with a 101 mm (4 in.) temporary shotcrete facing placed prior to nail installation. Due to the permanent nature of the wall, geocomposite drainage board was installed on 1.22 m (4 ft) center spacing the full depth of the wall and integrated into a toe drainage structure at base of the wall to prevent hydrostatic buildup. Nails consisting of #32M (#10) epoxy coated thread bars, over-sized for additional corrosion protection, were installed to a depth of 12.2 m (40 ft) using rotary-percussive duplex drilling methods (Figure 8). Both proof and verification nail tests were performed to confirm the required bond capacity was achieved. The upper two rows of nails were pre-tensioned with a calibrated torque wrench to 17.8 kN (4 kips) to limit movement during construction. Careful attention to wall verticality during construction was made to ensure that the wall did not encroach into future roadway construction (Figure 9). It should be specifically noted that the chemical grouted soil assisted in this endeavor and permitted a very uniform shotcrete facing to be constructed.

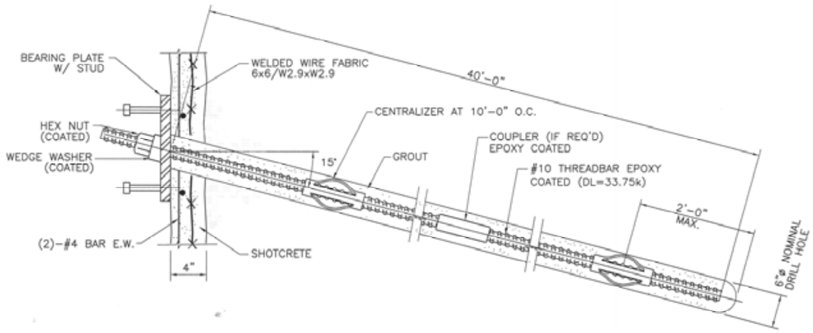

Figure 8. Typical soil nail detail

Figure 9. Completed wall construction with reinforced concrete facing installed

INSTRUMENTATION AND MONITORING

Due to the sensitive nature of construction in the vicinity of active roadways, instrumentation and monitoring of the wall construction was performed through out the construction process. Optical survey measurements were performed to monitor both vertical and lateral movement of both the abutment and soil nail wall. In addition, a system of biaxial tiltmeters was established at three points along the wall alignment and at two distinct elevations. Designated soil nails were instrumented with spot weldable strain gauges installed at third points along the bar length to monitor loads induced in the nails during and after wall construction. Two strain gauges were positioned on either side of the bar at each location in the event that a bending condition was present. Instrumentation stations were established at two points along the wall which could be lowered as the excavation proceeded and permit time critical readings to be performed.

Optical survey points on the abutment and temporary shotcrete facing indicated that vertical movements of less than 6.35 mm (1/4 in.) and lateral movements of less than 1.5 mm (1/16 in.) had occurred. The strain gauge field data indicated an interpreted maximum tension load in the soil nails of 31.1 kN (7 kips) along the upper portion of the nail. The nail loads recorded were relatively low with respect to the maximum nail service load of 151 kN (34 kips) and are believed to be a function of the long nail lengths, dense nail pattern, and the effectiveness of the chemical grouting to reduce the impacts of lateral stress relief. Further evidence of this was seen in the tiltmeter data which indicated less than one degree of outward rotation.

CONCLUSION

Unanticipated poorly graded sand provided insufficient face stability for soil nail construction which the contractor was able to overcome through the use of sodium silicate based chemical grouting. Chemical grouting using TAM grouting methods provided flexibility in construction by permitting changes in mix design to suit actual ground conditions encountered as well as permitting construction in limited access conditions. The effectiveness could be assessed both during and after grouting prior to soil nail wall construction with supplementary grout injections performed as required. Additional benefits of grouting prior to soil nail wall construction included temporary underpinning of the abutment as well as assistance in maintaining verticality and permitting longer stretches of shotcrete runs during soil nail construction.

ACKNOWLEDGEMENTS

The project was successful in large part due to the group efforts of the project team including representatives from the NJDOT, the soil nail wall designer Gannett Fleming, and the general contractor Union Paving. It was with input and ideas from all parties that appropriate solutions to the problems encountered were implemented in a timely manner.

Soil Nailing in Glacial Till: a Design Guide Evaluation Based on Irish and American Field Sites

James Joy[1], Tom Flahavan[2], and Debra F. Laefer[3], M.ASCE, PHD

[1]University College Dublin (UCD), School of Architecture, Landscape, and Civil Engineering (SALCE), Urban Modelling Group (UMG), Newstead, Belfield, Dublin 4, Ireland; PH(61- 43 062 5554); email: jamesjoy86@gmail.com

[2]UCD, SALCE, UMG, Newstead, Belfield, Dublin 4, Ireland; PH(353-87 077 5001); email: tom.flahavan@kpmg.ie

[3] UCD, SALCE, UMG, Newstead, Belfield, Dublin 4, Ireland; PH(353-1-716-3226); email: debra.laefer@ucd.ie

ABSTRACT

The French in-situ earth retaining system soil nailing began in 1970 and benefited greatly from that government's investment in the 1986 study 'Clouterre'. As such, French geology strongly influenced both practice and expectations world wide over the past 4 decades. Yet, recent studies in glacial till, a non-French soil type, have shown significant strength under-estimation using conventionally accepted design approaches. This paper reconsiders skin friction expectations for soil nail installations in till. Installation at 3 till sites (1 American and 2 Irish) are examined in detail. Traditional British, French, and American design methods and parameters are applied. Conventional methods under-predicted capacity by more than 50%, thereby raising serious questions as to the appropriateness of such design guidelines in tills. New correlations based on pile installation design are proposed.

INTRODUCTION

Soil nailing began as a French earth retention system in 1970. The approach uses long steel inserts to generate frictional resistance between the nail and soil, thereby forming a coherent unit resistant to horizontal and vertical loads (fig. 1). Popularity grew following the French 1991 publication of 'Clouterre', which summarizes the entire soil nail design and construction processes. Recent installations in Irish glacial tills indicated a strong conservatism by applying such correlations (Menkiti and Long 2008). In fact, soil nailing adoption in Ireland has lagged significantly behind other developed countries. In the United Kingdom (UK) more than 60,000m^2 of face area of soil nailing was installed in 2002 alone (CIRIA 2005), with huge growth having occurred in the 1990's especially for infrastructure projects. In contrast, Irish practitioners cite a paucity of expertise, lack of knowledge, protectionism related to older techniques, and inadequate design guides as reasons why Irish soil nailing usage lags (O'Dowd 2009). While several design guidelines exist [e.g. Clouterre (1991), UK's Highways department HA68/94 (1994), BS8081 (1981), and CIRIA (2005)] none specifically address performance expectations in glacial tills.

The prominence of glacial tills in Ireland challenges the applicability of current design guides for the Irish context. Currently most work is conducted based on contractor experience, and little is known about long-term performance in such widely encounter tills as Dublin Boulder Clay (DBC). This paper investigated a more accurate means of predicting skin friction for soil nails in glacial tills.

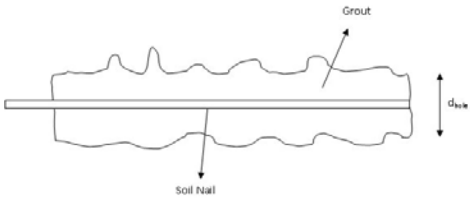

Fig. 1 Profile of Embedded Section of Soil Nail

BACKGROUND

DBC can stand at angles up to 80° in natural slopes for indefinite periods without additional support, despite having negligible cohesion (O'Dowd, 2009). The short-term stability has been attributed to the materials' very low permeability (10^{-8}-10^{-10} m/s) combined with suction created during excavations (Menkiti and Long, 2008). This unique ability allows for greater excavation cuts in DBC than most materials; previously, Bruce and Jewell (1986b) observed that in over-consolidated clays cuts were often greater than the industry standard of 2m for granular soils. DBC, however, is variable and may include local sand/silt seams. According to O'Dowd (2009), Irish soil nailing first occurred in Cork in 1978. Initial Irish usage concentrated on slope stabilization and deep basements. The 1981 British Government's decision to require BS8081 (1981) for soil nailing design; thereby mandating full double corrosion protection, effectively ended Irish soil nail usage (O'Dowd 2009) until after the introduction of HA68/94 (1994) more than a decade later.

SCOPE

This project examines current practices in soil nailing in glacial tills with regard to establishing a further understanding of performance and best practice. Although numerous factors influence performance, the key interaction and the most difficult parameter to assess in design is skin friction, which is currently obtained from design guides or pull out tests on sacrificial nails. To investigate this, a four-part approach was taken: (***1)*** data and information gathered through personal interviews conducted with Ireland's soil nailing contractors, (***2)*** survey issued to soil nailing specialists worldwide, (***3)*** review of design guides used for predicting skin friction, and (***4)*** pull-out test results from two case studies in Dublin, Ireland and one in Washington, United States (US) were examined. The project compared the design codes, results obtained, opinions, and previous research conducted over the past 40 years to make recommendations as to which design guide most closely predicts the values of skin friction measured during a number of case studies in glacial tills.

METHODOLOGY

Interviews were held with both of Ireland's soil nailing contractors: P.J. Edwards's Geotechnical Consultants Ltd. and PHI Ireland Ltd. regarding Ireland's relatively slow soil nail adoption rate, perceptions about potential barriers, and challenges to soil nail installation in glacial tills. This informed the survey creation, which was sent to 22 soil nail contractors and designers worldwide representing the membership of the Soil Nailing Committee of the Deep Foundation Institute (DFI); 6 responses were received. The aims were to inquire as to how frequently soil nailing was used, where, with what designs guides, and whether skin friction values used in design were considered conservative. Finally, data from three field sites dealing with skin friction in glacial till were evaluated alongside data from pile design in DBC (Gavin 2009) (Table 1). Three of the projects were located in or around Dublin Ireland and the fourth in the American state of Washington, where Vashon Till (VT) was present (Mitchell et al. 2007). All of the soil nails were drilled and grouted nails. Unfortunately Irish soil nails are rarely tested to failure due to cost.

Table 1 Soil Properties

Project	**Menkiti and Long (2008) – DPT**	**O'Dowd (2009) - Trinity College**	**Mitchell et al. (2007)**	**Gavin (2009)**
Soil Type	Glacial till (DBC)	Fill overlaying Glacial Till (DBC)	Glacial till (Vashon till - VT)	Glacial till (DBC)
Description	Very stiff to hard dark-grey slightly sandy clay with some gravel and cobbles zones	10 m of fill overlaying very stiff to hard dark-grey slightly sandy clay with some gravel and cobbles zones	Silty, gravelly sand to sandy clay ("hardpan"); cobbles and boulders; very dense to hard	Very stiff to hard dark-grey slightly sandy clay with some gravel and cobbles zones
Location	Dublin	Dublin	USA	Dublin
Friction Angle (φ')	32.5°	30°	45° *	32.5°
γ	20.5 kN/m^3	18 kN/m^3	20 kN/m^3	18 kN/m^3
C_u / SPT (N)	220kPa	Not available	SPT: 50 (HWA Geosciences 2007)	SPT: 20 to 80

*Based on typical SPT value of 50 and look as a well-graded sand and gravel (Smith and Smith 1998).

At the DPT (Dublin Port Tunnel) pull out tests were conducted to obtain skin friction values on sacrificial nails at varying depths across the height of the excavation generating ultimate and maximum skin friction 212-550kPa; maximum skin friction occurs where the nail and gout interface fail, as opposed to ultimate skin friction where the soil and grout interface fail. Not dissimilarly, Mitchell et al. (2007) collected ultimate skin friction values 300-950 kPa in VT in Washington based on micropile installation.

At a soil nailed retaining wall at Trinity College Dublin (TCD) in fill overlaying DBC, proof tests to 150% of the design working load were performed on 5% of the nails in accordance with BS8081 (1989) to confirm assumed skin friction values. The TCD site exhibited a maximum measured skin friction of 70kPa at strains ranging from nearly 10% to 14%, at which point testing was discontinued. For the purpose of design, the contractors used conservative values of friction angle and bulk density (Table 1) [O'Dowd 2009].

Adapting Results

Developing dimensionless analysis to allow for relevant comparisons to be made between results was necessary for developing a better understanding of nail performance in glacial till. In particular, nail loads measured during testing on the TCD site were converted to skin friction values, which are independent of nail length and spacing. This conversion was necessary for comparing results from different sites. Nail load was converted to skin friction values using eq 1 (Clouterre 1991).

$$q_s = T_f / \pi L_e d_{hole} \qquad \textbf{(eq 1)}$$

where q_s = skin friction (kPa), T_f = load in the nail (kN), d_{hole} = nail hole diameter (mm), and L_e = effective length of the nail (mm).

The TCD information is not as straightforward as the nails were not pulled to failure. Thus, it only gives an indication of how the nail performs up to 150% of its designed working load. To conduct dimensionless comparisons skin friction calculated for the TCD site were compared with strain (ε) in the nail (eq 2)

$$\boldsymbol{\varepsilon = s / L_e} \qquad \textbf{(eq 2)}$$

where s = displacement at the nail head (mm).

Data collected from Gavin (2009) included results from SPT tests carried out in DBC's across the Dublin area. SPT (N) values can easily be converted to undrained shear strength (C_u) using eq 3 (Gavin 2009).

$$\boldsymbol{C_u = 6\,N} \qquad \textbf{(eq 3)}$$

Calculating Skin Friction

To compare actual performance and current design, the skin friction suggested by current design guides in use in Ireland was calculated. The design guides examined were: CIRIA (2005), HA68/94 (1994), and BS8081 (1989). While Clouterre is not used directly, most of the codes reference it and hence skin friction results suggested by Clouterre (1991) were also considered (Table 2). Using these design guides ultimate skin friction was calculated. In contrast, CIRIA (2005) details a number of methods for predicting skin friction all of which were used in the report (see Table 3). Table 3 shows values suggested for pull out resistance for Boulder Clay and glacial tills.

Table 2 Clouterre Skin Friction

Soil	Limit Pressure	Skin Friction
Clay	200kPa	50kPa
Clay	2600kPa	125kPa
Sand	500kPa	50kPa
Sand	3000kPa	125kPa

Table 3 Information extracted and tabulated from Ciria (2005)

Source	Values
FHWA (1998 and 2003)	40–100 kPa
Pull out test data for DBC	177–235 kPa
Effective Stress Methods	As per HA 68/94
Undrained Shear Strength Methods	As per BS8081
Correlations with Pressuremeter tests	As per Clouterre

Dublin Port Tunnel Performance

In Fig. 2 the solid black squares represent soil values in DBC obtained from O'Dowd (2009), and the open circles represent values from Menkiti and Long (2008). Optimal values of skin friction were achieved using the highest bulk density and friction angle; however at low depths (around 2m) the effects of friction angle and bulk density on skin friction are minimal. For calculations according to BS8081 (q_s=C_u.α) 2 values of alpha were considered (α=0.45, 0.75), with α a 'fudge' factor to reduce shear strength to account for changes in the soil state (e.g. dilation) as piles are installed. As a result, α varies with soil and installation method; α for bored piles in stiff clay (e.g. DBC) should be taken as 0.45 (Craig 2004). Gavin (2009) also suggested that α for driven piles in Boulder Clay span 1.0 at C_u=80kPa, to 0.45 when C_u exceeds 200kPa and that for piles in DBC α can be as high as 0.75 for bored pile design, contingent upon field verification. Fig. 3 shows results of calculations using SPT (N) values taken from Gavin (2009) and converted to Cu values using eq 3.

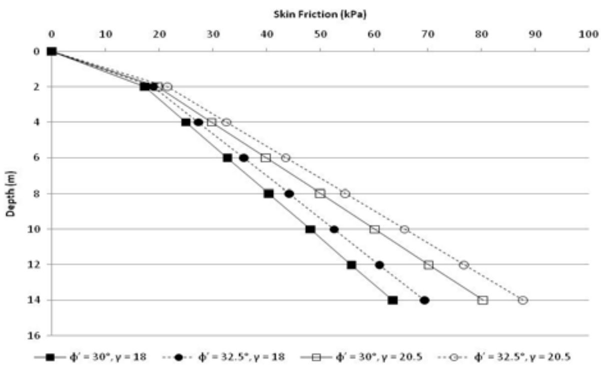

Fig. 2 DBC, DPT, HA68/94 Changing γ and ϕ

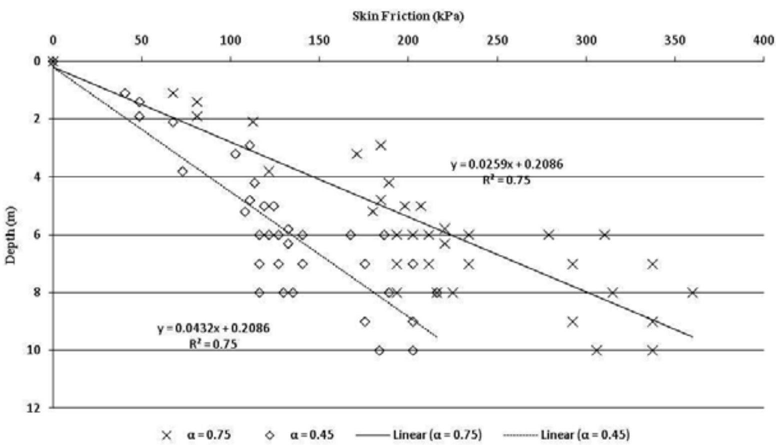

Fig. 3 DBC, DPT, Skin Friction by BS 8081 (α=0.45, 0.75) [Cu from (Gavin, 2009)]

As shown in fig. 4, the skin friction predicted for DBC using HA 68/94 greatly underestimated the values obtained from Menkiti and Long (2008), by a factor of approximately four. The pull-out results predicted by CIRIA are extremely conservative compared to the field results reported by Menkiti and Long (2008) (Fig. 5). Skin friction from design guides CIRIA (FHWA) and Clouterre was also plotted and was found to be even more conservative (Fig. 5). The maximum value obtained from these design guides was for the upper limit of Clouterre (125kPa), which was well below the lowest ultimate skin friction (212kPa).

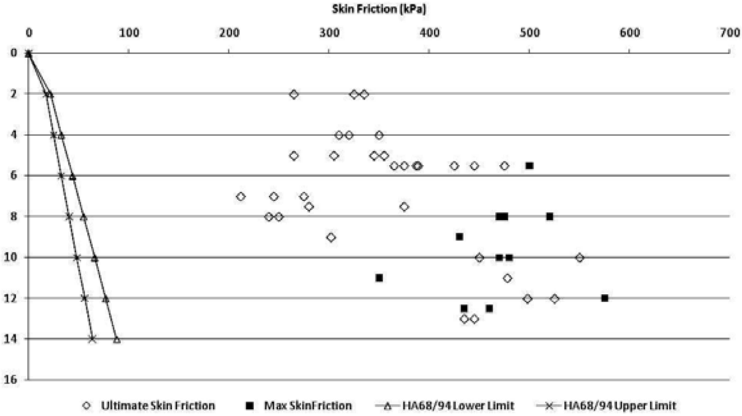

Fig. 4 DBC, DPT, HA 68/94

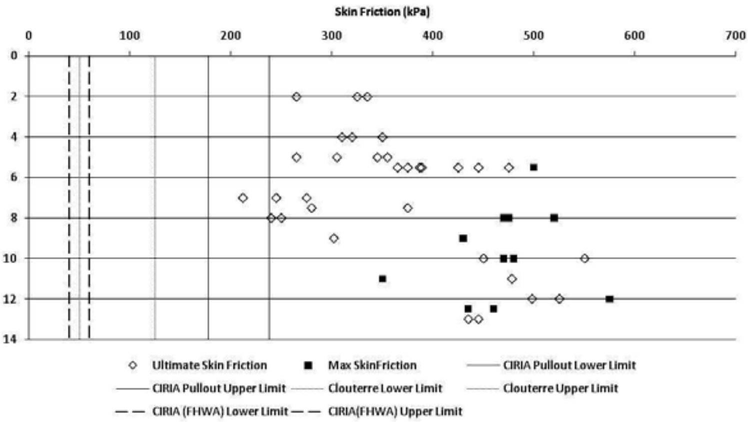

Fig. 5 DBC, DPT, CIRIA pullout, CIRIA (FHWA), and Clouterre

Fig. 6 shows predicted skin friction values using the undrained shear strength method with α=0.45 and 0.75 based on Gavin (2009). This is the first case where a clear correlation can be noticed between predicted and measured results.

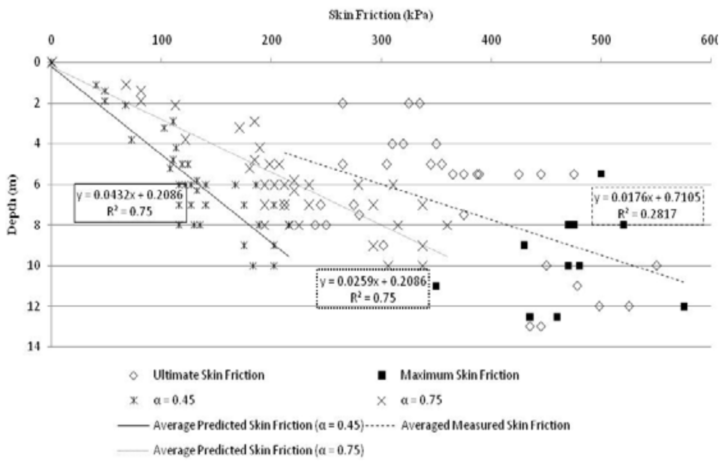

Fig. 6 DBC, DPT, BS8081 [Cu from (Gavin 2009)]

Trinity College Dublin Performance

The results of maximum skin friction for the TCD retaining wall were compared against that obtained from CIRIA, Clouterre, and HA68/94 (Fig. 7). The maximum measured skin friction of 72 kPa correlates well with the suggested skin friction of Clouterre, but these nails were not tested to a very high load. Correlations with BS8081 were not carried out here, as the skin friction predicted using BS8081 (Fig. 3) was more that three times that recorded at the site.

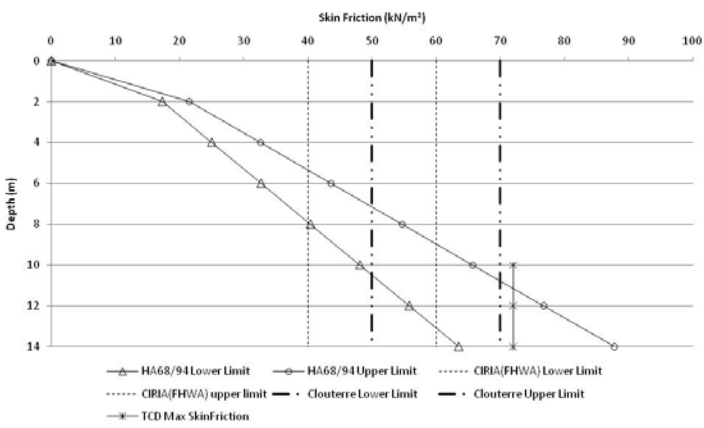

Fig. 7 DBC, TCD measured vs predicted

Vashon Till Performance

Figure 8 shows overly conservative skin friction results predicted in VT by HA68/94 (1994) and those suggested by Clouterre compared to results reported by Mitchell et al. (2007). Results are regularly underpredicted by at least half.

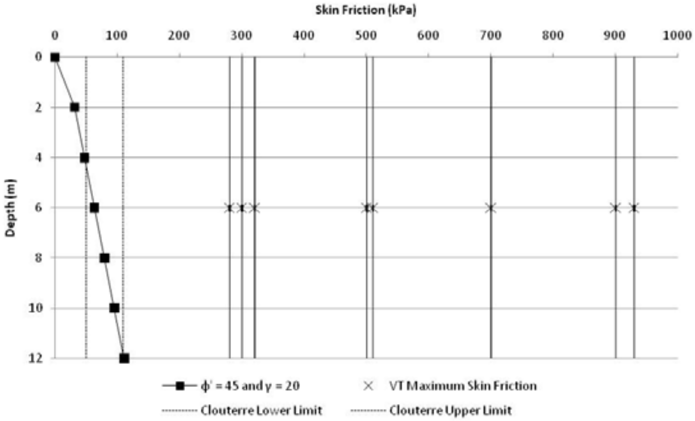

Fig. 8 VT, HA68/94 and Clouterre vs skin friction Mitchell et al. (2006)

Summary

Table 4 summarizes the results of using the primary design guides (HA68/94, BS8081, CIRIA, and Clouterre) for glacial till. Where the nails were pulled to ultimate capacity, under prediction was by as much as four fold. Only at the TCD site, where the nails were not full stressed did HA 68/94, Clouterre and CIRIA provide reasonable correlations (Fig. 7). Undrained shear strength methods of predicting skin friction provide the closet match to the measured values of skin friction for DBC (Fig. 6), where a critical design value is α.

Table 4 Design Guide Performances

Design Guides	Project / Soil Type		
	DPT – DBC	TCD – DBC	VT
BS8081 (1989)	Satisfactorily predicts (α is key)	Inconclusive *	--
HA68/94 (1994)	Underestimates greatly	Satisfactory	Underestimates greatly
CIRIA (2005)	Underestimates	Inconclusive *	--
Clouterre (1991)	Underestimates	Inconclusive *	Underestimates

*Inconclusive results were obtained for some of

Table 4 particularly at the TCD site. In these cases it was not possible to make comparisons, as the nails were simply not loaded sufficiently.

FURTHER ANALYSIS

The undrained shear strength method (BS8081) for predicting skin friction provided the most accurate results for ultimate skin friction (Fig. 6). A value of α as 0.75, only marginally underestimated the average skin friction in DBC. In contrast, the effective stress methods (Fig. 4 and Fig. 8 for DBC and VT respectively) greatly underestimated skin friction. Using a value of α=1.1 [instead of the previously proposed value of 0.75 (Gavin 2009)] provided the best fit between the predicted and measured results (Fig. 9).

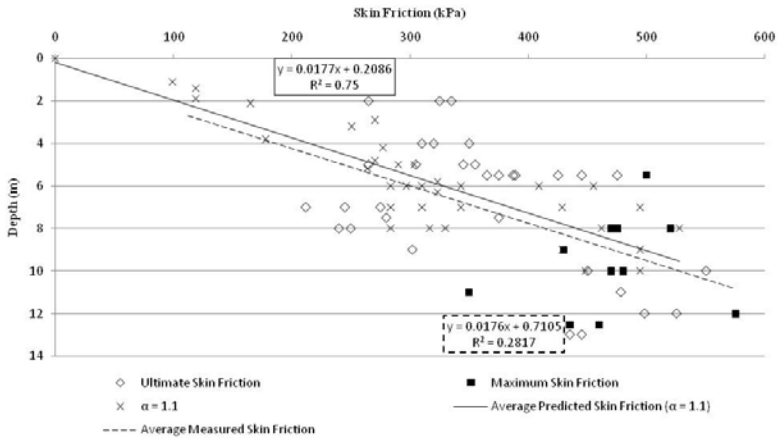

Fig. 9 DBC measured versus predicted skin friction [α = 1.1, Cu from (Gavin (2009)]

Alpha values for piles are based on a displacement (*s*) over diameter (*D*) ratio of 5% (Fig. 10). Because of the comparatively small diameters and large lengths of soil nails, an s/D of 10% may be in the range of 10mm, and if of concern could be mitigated by pre-tensioning the top row of nails as suggested by Wolosick (1988).

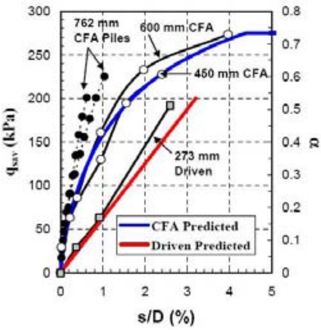

Fig. 1. Measured and Predicted pile skin friction, extracted from (Gavin 2009).

Craig (2004) suggested that α values should not exceed 1.0 as this would imply more than the soil shear resistance was being mobilized. However a value of α=1.1 could be justified in soil nails due to the irregularities created during the installation of the grout around the nails (Fig. 1). These irregularities protrude into the soil potentially generating extra resistance shear strength of the soil through shear keys.

While the findings presented are extremely promising in terms of predicting skin friction of Glacial Tills, it is important to remember that data sets for only one case study were considered in terms of assessing a new value of α for glacial tills. To substantiate the findings and significantly more data are needed, especially as α is an empirical value.

SURVEY RESULTS

Survey results showed the primary American design guide used was FHWA GEC 7, with 5 of the 6 respondents citing this document as a good reference, but even so 40% of those with experience nailing in glacial tills suggesting that current designs under estimate the pull out resistance. Additionally 83% of respondents noted that soil nailing design relies heavily on local experience, so it is likely that they have developed their own proprietary correlations for skin friction in the same way as has been done in Ireland (O'Dowd 2009).

CONCLUSIONS

Primary design guides (HA68/94, BS8081, CIRIA, and Clouterre) to predict the performance of soil nails in glacial till generate conservative results. As such, use of undrained shear strength methods (BS8081) is proposed to predict skin friction. Gavin's suggestion of α=0.75 (Gavin 2009) would be better for nail design in glacial tills, and simple correlations based on one project showed that a value of α=1.1 might be appropriate for Dublin Boulder Clays. However since α is an empirical value further confirmation and verification is needed.

REFERENCES

British government, BS8081:1989, "*British code of practice for ground anchors*".
Bruce, D.A., Jewel, R.A., 1986a, "*Soil Nailing: Application and Practice – Part 1"*, Ground Engineering Nov., 10-15.
Bruce, D.A., Jewel, R.A., 1986b. "*Soil Nailing: Application and Practice – Part 2"*, Ground Engineering Nov., 27-33.
Clouterre, 1991, "*Soil nailing recommendations"*, French research project, France
CIRIA C637, 2005, "*Soil Nailing – best practice guidance*", ISBN 0-86017-637-1.
Craig, R.F., 2004, "*Craig's soil mechanics*", 7th edition ISBN: 978-0-415-32708-9
Gavin, K., 2009, "*Development of Design Practice for Piles in Stiff Glacial Till"*, DFI Journal 3(1) 57-68.
HWA Geosciences Inc, 2007, "*Geotechnical investigation: Ingraham HS – New Building & Parking area Seattle Washington. HWA Project No. 2007-121-21. Prepared for DKA for Seattle Public Schools Dept of Facilities*", Nov. 8.
Menkiti, C.O., Long, M., 2008, "*Performance of Soil Nails in Dublin Glacial Till",* Canadian Geotechnical Journal 45, 1-14.
Mitchell, C., Mathieson, W., Hopkins, T., 2007, "*Micropile load transfer rates and bond stresses in the Puget sound region of Washington state, USA*", 8th International Workshop on Micropiles, Toronto, Canada, Sept. 26-30.
O'Dowd, T., Director PJ Edwards and Company Ltd, 28th Jan. 2009, "*Personal Interview in PJ Edwards offices, Palmerstown, Ireland"*
Smith, G. N., Smith, I. G.N., 1998, "*Elements of soil mechanics*", 7th edition, ISBN: 0632041269, Owford: Blackwell Science.
UK Department of transport, HA68/94, 1994, "*Design methods for the reinforcement of highway slopes by reinforced soil and soil nailing techniques"*, Design manual for roads and bridges, 4: Part 4, UK.
Wolosick, J. R., 1988. *"Soil nailing: A Nashville fault zone"*, Deep Foundations Institute 13th Annual Meeting, USA, 44-54.

Results of an Instrumented Helical Soil Nail Wall

Donald Deardorff, P.E[1], Mike Moeller[2]and Eric Walt[3]

[1]Senior Application Engineer, Foundation Supportworks, Inc., 12330 Cary Circle, Omaha NE 68128; don.deardorff@foundationsupportworks.com
[2]President, Structural Anchor Supply, 11730 Brockton Lane North, Osseo, MN 55369; mike.moeller@structuralanchorsupply.com
[3]Former Business Development Manager, Structural Anchor Supply, 11730 Brockton Lane North, Osseo, MN 55369; eric.walt@structuralanchorsupply.com

ABSTRACT

This paper describes the results of an instrumented helical soil nail wall project. Design of helical soil nails differ from grouted tendons due to the bond strength resulting from shear strength of the soil at the helices versus bond strength between the grout/soil interface. The instrumented helical soil nail walls were constructed during 2005 by the Missouri Department of Transportation (MoDOT) at the Route 169 and 68th Street Bridge in the City of Raytown, Missouri to allow widening of 68th Street into 4 lanes. The walls are approximately 3.7 m (12 ft) high at the center and have a 2:1 sloped backfill from the top of wall to the front of abutment. Prior to construction of the permanent facing, verification and proof testing was performed at several nail locations. The north and south walls were instrumented with load cells and inclinometers at the east, west and center of the two wall lengths. The description of the helical soil nail wall design and construction, along with the results of the initial and follow up instrument readings are presented herein.

INTRODUCTION

Soil nail wall technology began in Europe in the early 1960's, with the use of the New Austrian Tunneling Method in rock formations in 1961 and then carried over to unconsolidated soil retention, primarily in France and Germany. Soil nail walls were first used in North America for temporary excavation support in the late 1960's and continued to gain recognition during the 1970's and 80's for higher profile projects including highway applications. Much of the soil nail wall research performed in North America was funded by the Federal Highway Administration (FHWA) and other State Highway Agencies during the 1990's. Although helical anchors have been used by A. B. Chance as tiebacks since the early 1950's, helical soil nails are a relatively new alternative to grouted soil nailing with the first documented use for a 6.7 m (22 ft) high permanent soil nail wall project in 1996 (Bobbitt 1996).

A helical soil nail typically consists of square shaft lead and extension sections with small diameter helical flights spaced evenly along the entire shaft. The helical soil nail shaft serves a twofold purpose of transmitting axial and torsional stresses to the helical bearing plates, the latter of which is only needed during installation. The soil nail acts as a passive bearing element, which relies on soil movement and subsequent active earth pressure to mobilize the shear strength along the nail whereas a tieback anchor is prestressed to mobilize shear strength. As a result, soil nail walls typically experience more movement than tieback walls of similar height; however soil nail walls have less load at the nail head for tieback walls of the same height and therefore, allow a more economical wall face design.

Two permanent helical soil nail walls were constructed in 2005 at the Route 169 and 68th Street Bridge in the City of Raytown, Clay County, Missouri by the Missouri Department of Transportation (MoDOT). The retained soils were instrumented with slope inclinometers, and load cells were installed at select nail heads to monitor wall performance after construction. The site work was required to facilitate widening of 68th Street under the Route 169 overpass. This paper describes the helical soil nail wall construction details and results of wall instrumentation recordings.

68th STREET HELICAL SOIL NAIL WALL DESIGN

A soils investigation was performed by MoDOT during July 2003. However, due to the steepness of the existing abutment soils, the top of boring elevations were below the top row of proposed soil nails. The soils information available below the second row of soils nails generally consisted of very stiff lean clay in the upper 2.1 m (7 ft) underlain by stiff lean clay to depths ranging from about 3.4 to 4.3 m (11 to 14 ft) where soft shale was observed.

The north soil nail wall design included a temporary condition with 3.7 m (12 ft) of exposed wall face and a permanent condition with 2.6 m (8.6 ft) of exposure. The south wall had a temporary condition of 3.7 m (12 ft) and permanent condition of 2.8 m (9.3 ft) of exposure. The abutment soils slope up from the top of wall at a 2:1 horizontal to vertical ratio to the edge of abutment. The existing abutment footings consist of driven H-piles and vertical battering of the soils nails at the south wall east side was part of the design to preclude impact with the existing foundations. The design required shotcrete for the temporary wall facing and a permanent cast-in-place (CIP) concrete facing. Typical cross-sections of the north and south walls are shown on Figures 1 and 2.

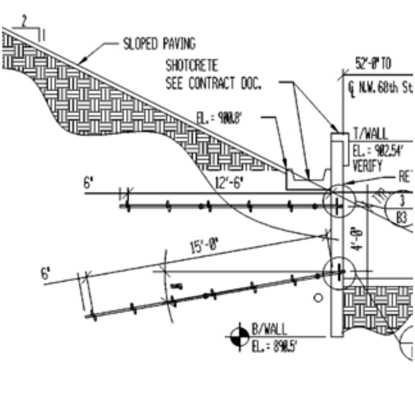

Figure 1: North Helical Soil Nail Wall

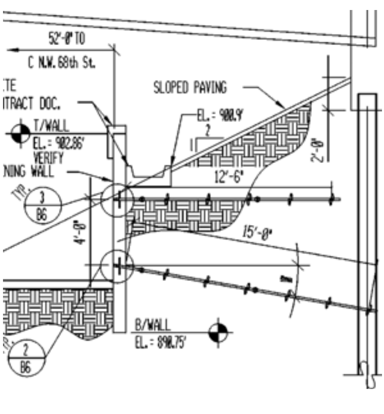

Figure 2: South Wall Helical Soil Nail

The design was performed with several software packages including SNAILZ (CALTRANS 1999) for design of the helical soil nail wall internal stability, HeliCAP (Chance 2001) for determination of soil nail capacity and bond pressures and XSTABLE (Sharma 1994) for global stability analysis. The design generally followed the methodology recommended in FHWA design guides (Byrne, Cotton et al. 1996; Lazarte, Elias et al. 2003). The design required a Factor of Safety (FS) equal to 1.5 for the temporary condition and 2.0 for the permanent condition.

The results of the SNAILZ analysis required two rows of CHANCE SS5-8 helical soil nails with design loads of 67 kN (15 kip). The top row was generally located 0.61 m (2 ft) below the top of wall and the second row was located 1.8 m (6 ft) below the top of the wall. For both walls, the design included helical soil nails 3.5 m (12.5 ft) long with no batter for the top row and 4.6 (15 ft) long with a 10 degree batter for the bottom row at both walls. Horizontal nail spacing was selected as 1.8 m (6 ft) during the design.

HELICAL SOIL NAIL WALL CONSTRUCTION

Soil nail installation is performed from top to bottom with the upper nails installed first and temporary shotcrete facing applied prior to excavation and installation of the next row of soil nails. This process continues to the final depth of the wall face. The specified Chance helical soil nails consisted of 20.3 cm (8 inch) helical flights generally spaced every 61 cm (24 inches) along a 3.8 cm (1.5 inch) diameter square steel shaft. A typical lead and extension section are shown on Figure 3.

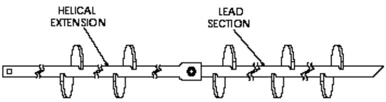

Figure 3: CHANCE Helical Soil Nail Lead and Extension Section

The helical soil nails were installed with a gear motor capable of 6779 N-m (5,000 ft-lbs) attached to a New Holland LS170 skid steer. The installation equipment was calibrated using an in-line Chance Dial Torque Indicator to determine the gear motor differential pressure versus torque curve prior to the start of construction.

A preconstruction verification/creep test was performed in accordance with FHWA requirements on July 26, 2005 to demonstrate the required 67 kN (15 kip) design load capacity. The verification test was taken to 134 kN (30 kip) with a maximum net deflection of 2.5 cm (0.98 inches). A total of 111 helical soil nails were installed during August and September 2005 including 31 nails in the north wall upper row, 26 nails in the north wall bottom row, 29 nails in the south wall upper row and 25 nails in the south wall bottom row.

Actual nail lengths generally exceeded design lengths in order to meet torque specification requirements of 4067 N-m (3,000 ft-lbs). Average soil nail lengths ranged from 4.3 m (14 ft) at the south wall-center bottom row to 6.7 m (22 ft) at the north wall-center top row. Several nails along the south wall required lateral battering in order to meet the torque requirements and avoid impact with the existing foundations.

The helical soil nails transition to a 2.54 cm (1 inch) diameter Dywidag Grade 150 bar at the shotcrete wall face. The temporary wall face consists of 10.2 cm (4 inch) thick shotcrete with 152x152-MW19xMW19 (6x6-W2.9xW2.9) W.W.F. and 25.4 x 25.4 cm (10 x 10 inch) bearing plates. The requirements for minimum shotcrete strength at 3 and 28 days was 96 kPa and 192 kPa (2,000 and 4,000 psi), respectively. The permanent face design consists of 15.2 cm (6 in) thick CIP concrete reinforced with #4 Grade 60 vertical bars on 0.4 m (1.3 ft) centers and #5 Grade 60 horizontal reinforcement walers. The nail heads are connected to the permanent CIP concrete face with four 1.3 cm (0.5 in) studs attached to the 25.4 x 25.4 cm (10 x 10 in) bearing plate. The requirement for minimum concrete strength at 28 days was 216 kPa (4,500 psi). Details of the temporary and permanent soil nail head connection at the wall face is shown in Figures 4 and 5.

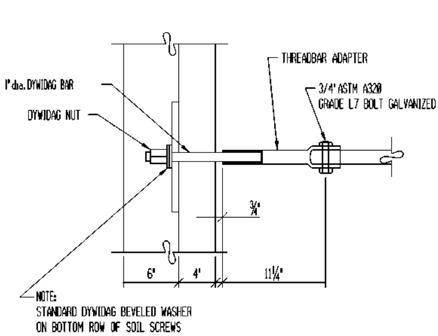

Figure 4: Detail of Helical Soil Nail Wall Connection

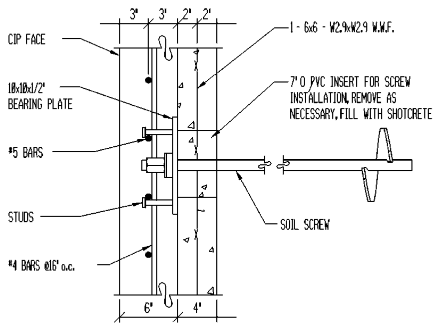

Figure 5: Detail of Shotcrete and Permanent Wall Facing

Drainage is provided at the top of wall by a concrete culvert running adjacent and parallel to the top of wall face. The retained soils are drained with 30.5 cm (12 in) wide vertical geocomposite drainage medium installed between each soil nail at the soil/shotcrete interface. The drainage medium is connected to a 10.2 cm (4 in) PVC drain pipe installed at the toe of the soil nail wall and ultimately drains into the storm sewer system. The existing concrete cover was utilized for slope protection behind the soil nail walls extending up to the face of the abutments.

Prior to construction of the permanent wall face, more than 5% of the helical soil nails were proof/creep tested to 1.5 times the design load to confirm capacity; including three at the north wall top row, two at the south wall top row, three at the north wall bottom row and three at the south wall bottom row. The proof and creep testing was performed in accordance with FHWA requirements.

WALL INSTRUMENTATION

Six slope inclinometers and six load cells were installed during construction of the soil nail walls in general accordance with FHWA requirements. The slope inclinometers were installed at the east, center and west areas of the north and south soil nail walls. The upper row of soil nails on the north wall was instrumented with load cells at the west, west-center, center and east region. At the south wall, load cells were installed on the top row of nails at the center and west region.

The inclinometers were constructed with 7 cm (2.75 inch) OD, internally grooved plastic casing. The casing extends approximately 7.3 m (24 ft) below the top of grade and is located approximately 1.0 m (3.3 ft) behind the shotcrete wall. All site readings were taken with the same Slope Indicator Digitilt Model 50302150 probe. The load cells installed at the site are Slope Indicator Model 513510 center hole 445 kN (50 ton) cells wired to a Campbell Scientific CR10X data storage and acquisition system.

INSTRUMENTATION RESULTS

Load cell readings were collected during August 2005, February 2006, March 2009, May 2009 and September 2009. Subsequent to the initial lock off readings taken during August 2005, the average helical soil nail head loads ranged from 3.04 to 7.94 kip (13.52 to 35.32 kN). Some of the load cells were not operable during reading operations which limits the amount of data, particularly for the south wall nails T-15 and T-25. The average helical soil nail loads are shown on Table 1.

Table 1: Soil Nail Load Cell Readings

Average Nail Head Loads (Kip) [kN]						
Period	North Wall West T-7	North Wall West Center T-12	North Wall Center T-17	North Wall East T-28	South Wall Center T-15	South Wall West T-25
Aug-05 (Lock-off)	(2.60) [11.58]	(2.53) [11.25]	(2.48) [11.03]	(2.49) [11.08]	(2.61) [11.61]	(2.62) [11.65]
Feb-06	(4.21) [18.73]	No Reading	(5.04) [22.42]	(4.57) [20.33]	(5.08) [22.69]	(5.25) [23.35]
Feb-09	(3.19) [14.19]	No Reading	(7.94) [35.32]	(7.06) [31.40]	No Reading	No Reading
Mar-09	(3.14) [13.97]	No Reading	(7.32) [32.56]	(6.18) [27.49]	No Reading	No Reading
May-09	(3.04) [13.52]	(4.52) [20.11]	(7.17) [31.89]	(4.18) [18.59]	No Reading	No Reading
Sep-09	(3.21) [14.28]	(3.27) [14.55]	(5.49) [24.42]	(6.08) [27.05]	No Reading	No Reading

Prior to construction of the wall, inclinometer readings were taken on August 10, 2005 and August 15, 2005. Post wall construction inclinometer readings were collected on October 6, 2005 and form the baseline reading for all subsequent inclinometer readings. Additional readings have been taken on May 22, 2009 and September 16, 2009. The post wall construction results at each inclinometer relative to the October 6, 2005 readings are shown on Figures 6 to 11.

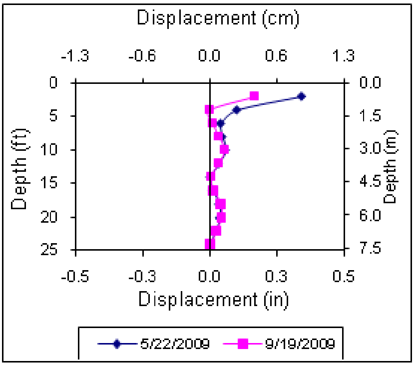

Figure 6: Post Construction Cumulative Displacement at the NW-West

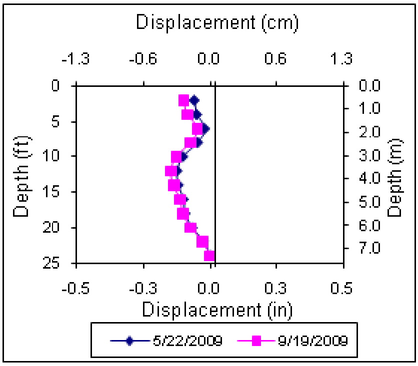

Figure 7: Post Construction Cumulative Displacement at the NW-CTR

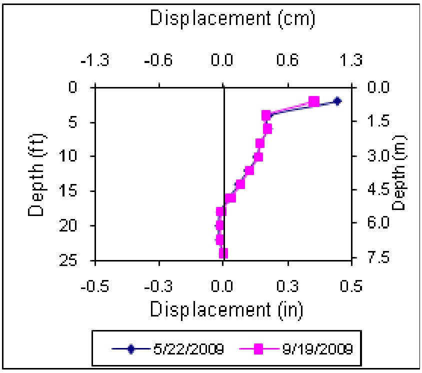

Figure 8: Post Construction Cumulative Displacement at the NW-East

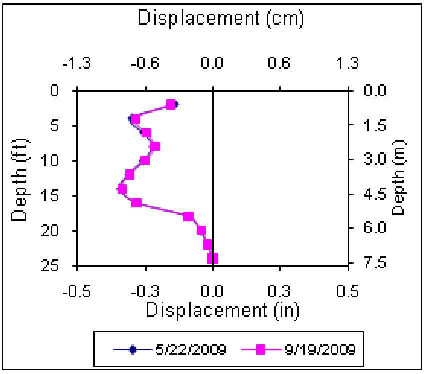

Figure 9: Post Construction Cumulative Displacement at the SW-West

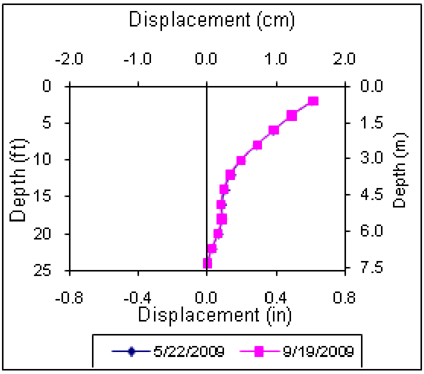

Figure 10: Post Construction Cumulative Displacement at the SW-CTR

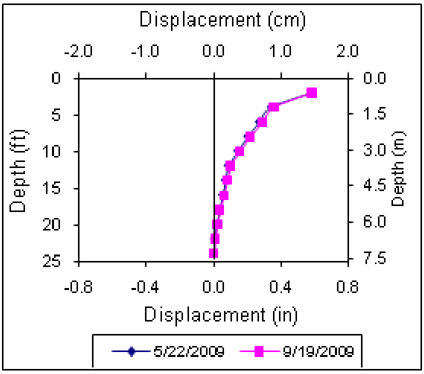

Figure 11: Post Construction Cumulative Displacement at the SW-East

Maximum cumulative displacements and associated depths at the maximum value for the inclinometer readings are shown on Table 2.

Table 2: Inclinometer Maximum Cumulative Displacements Relative to October 2005

	North Wall West		North Wall Center		North Wall East		South Wall West		South Wall Center		South Wall East	
Date	Disp (in) [cm]	Depth (ft) [m]	Disp (in) [cm]	Depth (ft) [m]	Disp (in) [cm]	Depth (ft) [m]	Disp (in) [cm]	Depth (ft) [m]	Disp (in) [cm]	Depth (ft) [m]	Disp (in) [cm]	Depth (ft) [m]
Oct-05	Baseline Reading Post Wall Construction											
May-09	(0.34) [0.86]	(2.0) [0.6]	(-0.13) [-0.32]	(12.0) [3.7]	(0.45) [1.13]	(2.0) [0.6]	(-0.34) [-0.87]	(14.0) [4.3]	(0.62) [1.56]	(2.0) [0.6]	(0.59) [1.49]	(2.0) [0.6]
Sept-09	(0.17) [0.42]	2.0 [0.6]	(-0.15) [-0.37]	(12.0) [3.7]	(0.35) [0.90]	(2.0) [0.6]	(-0.34) [-0.86]	(14.0) [4.3]	(0.62) [1.56]	(2.0) [0.6]	(0.59) [1.49]	2.0 [0.6]

The 2009 inclinometer readings relative to the Oct 2005 reading show maximum positive displacements (towards the wall) ranging from 0.86 cm (0.34 in) at the North Wall West to 1.56 cm (0.62 in) at the South Wall East inclinometer locations. The depth of the maximum positive displacement was 0.6 m (2 ft) at the 4 locations that experienced positive soil movement. Negative soil displacements were recorded at the North Wall Center and South Wall West inclinometers with maximum displacements of -0.38 cm (-0.15 in) to -0.86 cm (-0.34 in). The depth of maximum negative displacement was 3.7 m (12 ft) and 4.3 m (14 ft), respectively for these 2 locations.

DISCUSSION OF RESULTS

The results of the load cell and inclinometer data show wall performance within design guidelines. Inclinometer displacements are greatest at the South Wall Center and South Wall East locations with cumulative movements of 1.56 cm (0.62 in) and 1.49 cm (0.59 in), respectively. This may be a result of shorter bottom row nail lengths in this region due to existing foundation restrictions. There is a significant gap in data collection between October 2005 and May 2009, therefore the wall performance immediately subsequent to wall construction cannot be determined. Minimal soil movements were recorded during the two inclinometer readings performed in 2009 with a maximum differential cumulative displacement of 0.42 cm (0.17 in) occurring at the North Wall West inclinometer. Based on the May and September 2009 readings, it appears that minimal wall movement is occurring and the wall has stabilized, however further readings are necessary to confirm this. Visual reconnaissance of the wall face at both the north and south helical soil nail walls showed no indication of movement or distress during the May and September 2009 site visits.

The negative soil displacements observed at the North Wall Center and South Wall West inclinometers were not expected since soil nail wall movement is typically outward (away from the retained soils). The amount of negative soil displacement at the North Wall Center is negligible with a maximum cumulative displacement less than 0.38 cm (0.15 in) whereas the negative soil displacement at the South Wall West inclinometer is slightly higher with a maximum cumulative displacement of 0.86 cm

(0.34 in). A possible cause for this negative displacement may be soil shrinkage at localized areas due to moisture reduction from the internal and external wall drainage system. The depth of maximum negative cumulative and incremental displacement for these two inclinometers are in the a region where stiff clay with preconstruction moisture contents of about 25% were present. There is also the possibility that systematic errors were introduced, particularly during the data collection for the baseline readings taken during October 2005.

The load cells installed at the top row along select nails at the north and south walls show loads below the estimated design loads for the periods recorded. Unfortunately, the load cell data is sporadic due to intermittent operation of some cells resulting in no recording events (excluding the pre-tensioning performed during August 2005) where all six load cells are operational.

In order to provide quality instrumentation data, it is recommended that the non-operational load cells be repaired or replaced. The CR10X is battery powered which looses charge after a couple days of readings and must be recharged each site visit, therefore installation of a permanent power supply to the CR10X unit is warranted to provide continuous load cell monitoring. The inclinometer and load cell monitoring should continue on a quarterly basis to document seasonal fluctuation of nail loads and soil movement.

ACKNOWLEDGMENTS

The authors would like to thank Mr. Nathan Juliana and Mr. Kevin McLain of the Missouri Department of Transportation for their assistance in the collection and interpretation of the wall instrumentation data. Also, representatives of Campbell Scientific and Slope Indicator provided valuable programming assistance to clarify and modify the CR10X code.

REFERENCES

Bobbitt, D. E. (1996). Chance Case History; Freightliner Truck Company Soil Screw Retention Wall System Report. Chance Soil Screw Retention Wall System Report. Centralia, MO, Chance Civil Construction**:** 2 pp.

Byrne, R. J., D. M. Cotton, et al. (1996). Manual for Design and Construction Monitoring of Soil Nail Wall. Washington, D.C.**:** 530.

CALTRANS (1999). Manual of Instructions for SNAILZ, California Department of Transportation.

Chance (2001). HeliCAP computer program. Centralia, MO.

Lazarte, C. A., V. Elias, et al. (2003). Geotechnical Engineering Circular No. 7 - Soil Nail Walls. Washington, D.C., Federal Highway Administration**:** 182 pp.

Sharma, S. (1994). XSTABLE computer program, University of Idaho.

INNOVATIVE WATERFRONT RETAINING WALL SYSTEM SAVES A CONDOMINIUM

Andrew E. Sparks, A.M. ASCE, P.E.[1], Jonathan L. Robison, P.E.[2], and Robert D. Hotz, II, E.I.T.[3]

[1]GeoEngineers, Inc., 3050 South Delaware Avenue, Springfield, Missouri 65804; PH: (417) 831-9700; FAX: (417) 831-9777; email: asparks@geoengineers.com
[2]GeoEngineers, Inc., 3050 South Delaware Avenue, Springfield, Missouri 65804; PH: (417) 831-9700; FAX: (417) 831-9777; email: jrobison@geoengineers.com
[3]GeoEngineers, Inc., 3050 South Delaware Avenue, Springfield, Missouri 65804; PH: (417) 831-9700; FAX: (417) 831-9777; email: rhotz@geoengineers.com

ABSTRACT: Following record spring precipitation in April 2008, Table Rock Dam, located in Southwest Missouri, opened all ten of its flood gates to lower the water level of Table Rock Lake and prevent flooding within the basin. The subsequent flow into Lake Taneycomo below was the highest on record and resulted in damage to the lake channel and many structures downstream. Significant scour along the banks of the lake resulted in multiple slope failures. The slope below one condominium building fell away leaving a portion of the building hanging unsupported over the lake below. To save this building and protect several other buildings in the area, GeoEngineers developed an innovative solution to support the building, regain lost waterfront property and protect the bank from future flood events. Because the river is an important fish habitat and tourist destination, the solution had to be integrated into the surrounding vegetation and geology and not unduly impact the river water quality during construction.

INTRODUCTION

Following two months of record precipitation, Table Rock Dam opened all ten of its floodgates in April 2008 to lower the level of Table Rock Lake, thereby preventing flooding within the basin and potential overtopping of the dam, see Figure 1. The subsequent flow into Lake Taneycomo below was the highest on record since the dam was constructed in 1958 and resulted in damage to the river channel and many structures downstream.

Figure 1. Table Rock Dam releasing flood water.

Significant scour along the banks of the river led to multiple slope failures. The slope below one condominium building fell away leaving a portion of the building hanging without support over a 9-meter (30-feet) drop to the lake below.

PROJECT BACKGROUND/HISTORY

Building History

Lake Taneycomo was formed in 1913 in the White River Basin following the construction of Powersite Dam in Forsythe, Missouri, roughly 20 miles downstream of the project site. In 1958, Table Rock Dam was constructed by the United States Corps of Engineers (USACE). Lake Taneycomo, became a popular trout fishing and outdoor activity area. Many resort complexes and condominiums were constructed along the banks to provide accommodations for anglers, tourists and outdoor enthusiasts.

The condominiums in the project area were constructed in the 1990s along the left bank of the lake approximately 3.2 kilometers (2 miles) downstream of the dam. The bank is approximately 9 meters (30 feet) high and the soil units consist primarily of stiff, silty clay and medium dense, clayey fine sand overlying dolomitic bedrock near the channel bottom, see Figure 2.

Figure 2. Condominiums along left bank of lake.

The buildings are three-story, wood-framed structures with 12 individual units and screen porches at the corners. Exterior stairways provide access to the units. Six buildings are located along the bank and are set back between 10 and 50 feet from the top of the slope. Design bearing pressure for the building foundations is approximately 96 kilopascals, kPa (2,000 pounds per square foot, psf). The ground floor elevations of the buildings range between 223.7 and 224.3 meters (734 and 736 feet).

Lake Taneycomo

Unlike its riverine past, the hydraulic character of present-day Lake Taneycomo is dependent on the amount of water released above and below the lake from Table Rock and Powersite dams. The flow fluctuates on an hourly basis between 0.57 and 368 cubic meters per second, cms (20 and 13,000 cubic feet per second, cfs). This results in daily water level elevations at the project site typically ranging between 213.7 and 216.4 meters (701 feet and 710 feet). When the flow is reduced to a minimum level required to maintain aquatic life (0.57 cms, 20 cfs) the hydraulic character of the water is similar to slow moving streams in the region. However, when releases from the dam are above about 28.3 cms (1,000 cfs), the water behaves like a river system with water velocities between 0.61 and 2.1 meters per second, (2 and 7 feet per second).

The lake channel winds through the White River basin and near the project site it is constrained by bedrock along the right bank and in the channel bottom. Along the left bank, the dip of bedrock is flatter, and the bedrock is overlain by residual soil consisting of silty clay and clayey fine sand. Where bedrock is present, the channel is stable, but the residual soil on the left bank is susceptible to erosional forces.

In the vicinity of the condominiums, the thalweg of the stream is pushed over towards the left bank by the curvature of the channel upstream. This results in higher velocities and increased erosional force along the bank just below the buildings.

SERIES OF EVENTS LEADING TO SLOPE FAILURE

Record-Breaking Precipitation

Repeated storm events in Southwest Missouri resulted in record precipitation between February and April 2008. The prolonged precipitation saturated the ground in the region resulting in widespread flooding. The floodwaters in the drainage basin filled Table Rock Lake to a record 284.46 meters (933.25 feet).

The additional inflow into Table Rock Lake prompted the USACE to open the floodgates to draw down the lake and prevent overtopping of the dam. With all ten floodgates open, peak discharge reached the highest flow since the construction of the dam. The flow of 1,413 cms (49,900 cfs) into Lake Taneycomo resulted in a water level elevation in the lake below the dam greater than 220.1 meters (722 feet).

Damaged Buildings and Slope Failures

The flood waters flowed downstream inundating buildings and roads and damaging many slopes along the banks. Many boats and several dock structures were either swept downstream or heavily damaged.

During the highest flows, the water reached an estimated elevation of 220.1 meters (722 feet) at the condominium site. The flood waters caused the bank to erode and several trees toppled into the lake. During the flood event, more than 150 meters (500 feet) of shoreline were eroded in the vicinity of the condominiums and the downstream marina was damaged beyond repair. The most significant slope failure was adjacent to Building 7 where the toe of the slope was apparently eroded by the eddying water in a drainage swale downstream. The subsequent loss of toe support caused shallow slope failures that eventually undercut the corner of the building leaving the northeast corner of the building suspended about 9 meters (30 feet) above the lake. The undercut slope was nearly vertical for about 3 meters (10 feet) under the building corner, see Figure 3. Below the vertical scarp, colluvium embedded with trees and vegetation formed a roughly 1H:1V (horizontal to vertical) slope to the lake bottom. Elsewhere, the slopes ranged from nearly vertical adjacent to Buildings 7 and 8 to approximately 2H:1V near Buildings 9 and 10.

Figure 3. Building 7 undercut from sliding soil.

GeoEngineers was contacted by the owner in June 2008 to visit the site, observe the damage, and develop a scope of services to complete a geotechnical evaluation of the slope failure.

A subsurface exploration program was completed to evaluate the stability of the slopes. The exploration program consisted of drilling 12 borings to depths ranging between 5.8 and 9.9 meters (19 and 32.5 feet) below ground surface. The borings were drilled into bedrock to confirm the elevation and condition of the underlying bedrock.

Inclinometer casings were installed in five of the borings to assess slope movement over time. The subsurface conditions as indicated by the borings consisted of residual soil overlying dolomitic bedrock. The residual soil consisted of stiff, silty clay overlying medium dense, clayey fine sand. The bedrock elevation along the top of the bank ranged between 215.2 and 215.8 (706 and 708 feet), while the bedrock elevation near the toe of the slope (a horizontal distance of approximately 15 meters (50 feet) ranged between 213.1 and 214.0 meters (699 and 702 feet). No evidence of deep-seated failure planes was noted in the subsurface exploration program or the data obtained from the inclinometers. The slope failures appeared to be limited to the surface failures observed along the banks.

RETAINING WALL SELECTION AND DESIGN

Once the probable failure mechanism was understood, the next action was to evaluate the most appropriate solution to stabilize the slopes, reclaim lost ground, and support Building 7 and protect Buildings 8-10. Several stabilization options were evaluated including boulders, gabions, segmental concrete blocks, riprap and various structural retaining walls. A significant consideration in selecting the most appropriate solution was reducing the risk of erosion behind the slope protection system in future flood events. As a result, riprap and a structural retaining wall were selected as the preferred options. These options were discussed with the USACE, which indicated that a riprap slope would be acceptable, but the required slope would extend beyond allowable limits into the lake. As a result, the riprap slope option could not be used.

Based on these site limitations, a soil nail wall was selected as the preferred stabilization option. However, what normally would have been the retained soil slid into the lake during the flood. As a result, the design for this project required an alternate approach. The ultimate innovation was a bottom-up design using conventional soil nails, vertical elements for vertical support, and a launchable riprap toe to protect the bottom of the wall from scour and provide a platform for construction operations, see Figure 4. The soil nail wall design concept was approved by the USACE and was authorized as an emergency repair to protect the buildings. Because the project area is in a highly visible tourist area, and the portion of Lake Taneycomo adjacent to the project is considered a Blue Ribbon fishing area, the USACE also required that the retaining wall blend into the surroundings as much as possible.

The vertical elements provided vertical wall support and a rigid framework for the shotcrete back-form. The vertical elements also provided the rigidity required to allow a cantilever wall section at the top of the wall, which eliminated the top row of soil nails and reduced the overall cost of the project. The vertical elements consisted of W12x26 steel sections placed in 61-cm (24-inch) diameter holes spaced 1.8 meters (6 feet) on center and drilled to bedrock.

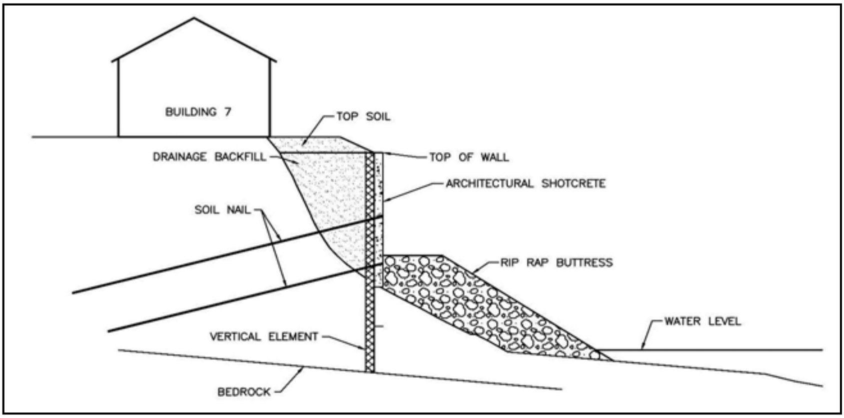

Figure 4. Typical cross section of retaining wall.

Although more than 150 meters (500 feet) of the slope were damaged in the flood event, the final wall design consisted of only 96 meters (314 feet) of retaining wall extending from Building 8 north to approximately 30 meters (100 feet) north of Building 7, see Figure 5.

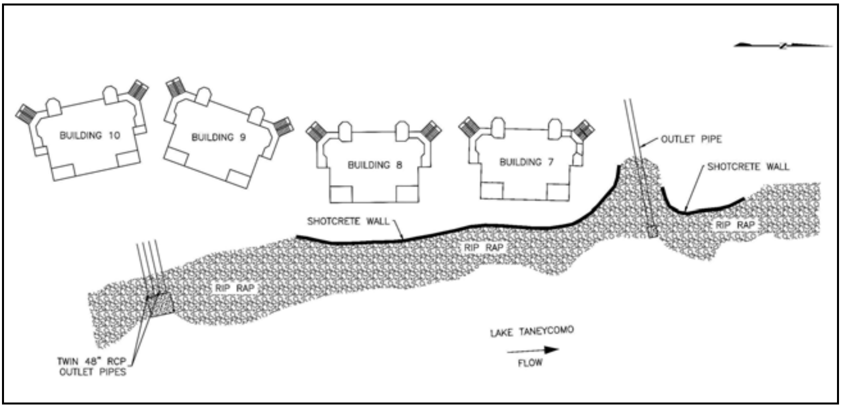

Figure 5. General site plan of soil nail wall and riprap.

The wall was turned into the drainage swale and a drainage pipe was installed to transport stormwater from the development upslope. Riprap was placed at the ends and in the drainage swale for slope and scour protection. The flatter slope between Buildings 8 and 10 allowed the placement of riprap to buttress the slope and provide slope protection without exceeding the allowable limits established by the USACE.

Along the bottom of the wall, launchable stone riprap was placed from an elevation of 219.2 meters (719 feet) sloping down to the channel bottom. The launchable stone riprap consisted of additional stone placed along the toe so scour below the riprap would cause the excess stone to fill in the lost soil while maintaining protection of the wall. This launchable stone toe allowed the contractor to complete the work without excavating through the river channel to tie the riprap into the bedrock. As a result, very little construction was required below the adjacent lake level. This was particularly helpful given the daily fluctuations of water level of 3 meters (10 feet) or more. It also greatly reduced the discharge of soil fines into the adjacent lake.

The soil nails consisted of Number 8, grade 75, epoxy coated steel bar grouted in place with lean cement grout. The holes were drilled using a 20-cm (8-inch) diameter continuous flight auger. The soil nail bond lengths were 9.1 meters (30 feet) in the native soils. In addition, a series of 15 micropiles along the bank-side of Building 7 were designed to reduce the surcharge-induced lateral loads on the wall and support the building during construction operations. The micropiles were 10-cm (4-inch) diameter steel pipe piles drilled through the residual soil and founded on the dolomitic bedrock.

CONSTRUCTION SEQUENCING

Construction began in February 2009 with an access road built through the drainage swale north of Building 7 to provide access to the toe of the slope, see Figure 6. Cobble and boulder-sized shot limestone rock was pushed out along the toe to provide a working platform for construction equipment.

Figure 6. Access road constructed north of Building 7.

Once access was established, the slope was cleared of the remaining vegetation and trees. During clearing and grubbing, it became evident that the slopes adjacent to Buildings 7 and 8 were steeper than initially anticipated and showed indications of additional slope instability. Following clearing and grubbing, a flash coating of shotcrete was placed on the slope to protect the bare soil from runoff erosion.

The micropiles were installed along the east and north walls of Building 7. The 10-cm (4-inch) diameter steel pipes were drilled through the residual soil using 15-cm (6-inch) diameter continuous flight augers and socketed approximately 30 cm (12 inches) into the underlying bedrock. The drilled holes were filled with neat cement grout before installing the micropiles. After curing, the micropiles were connected to the building foundation using steel support chairs. The grout had a minimum 28-day compressive strength of 144 kPa, (3,000 psi) and the micropile lengths ranged between 25 and 27 feet. Based on a full-scale load test, the allowable axial capacity of each micropile was approximately 107 kN (24 kip).

Figure 7. Vertical elements in place below buildings.

The vertical elements consisted of W12x26 steel sections placed in 60 cm (24 inch) diameter holes drilled to refusal on bedrock and spaced 1.8 meters (6 feet) on center, see Figure 7. The vertical elements were placed into the drilled holes and backfilled with structural concrete. The vertical elements also formed the framework for the wall and provided a rigid back-form for the shotcrete placement.

The back-form for the shotcrete consisted of corrugated steel decking attached to the vertical elements by steel impact-nails. After the steel decking was in place, holes were cut in the decking to drill the soil nails, see Figure 8. The soil nail holes were drilled by using 15-cm (6-inch) diameter continuous-flight augers mounted to a Klemm 2510 drill rig. The holes were drilled to a depth of 9.1 meters (30 feet) into the bank. The soil nails consisted of Number 8, grade 75, epoxy coated steel bar grouted in place with lean cement grout. Because the wall was designed to be backfilled after construction, PVC sleeves were placed in the unbonded zone between the bank and the wall.

Figure 8. Drilling soil nails through partially completed decking.

A drainage board was placed between the vertical elements to provide drainage behind the wall. Weep holes were placed at the bottom of the wall and where the native soil contacted the back of the wall. The weep holes penetrated the decking and drained to the wall face.

Steel reinforcement consisted of welded wire reinforcement placed full height on the wall. The soil nails were tied into the wall with continuous horizontal waler and vertical punching shear reinforcement. Because the wall was constructed full height prior to backfilling, the shotcrete was placed in two 10-cm (4-inch) thick, full-height lifts instead of the typical horizontal lifts, see Figure 9 on the next page. This allowed for a continuous wall face without horizontal cold joints. Steel plates, beveled washers and nuts were wet-set after the final lift of shotcrete was placed. Two verification nail tests were completed in each of the two soil types to 200

Figure 9. Completed shotcrete placement.

percent of the design loads. One in ten production soil nails were proof-tested to 150 percent of the design loads.

After shotcrete placement, the wall was backfilled with 5-cm (2-inch) clean, crushed rock to approximately 0.6 meters (2 feet) from the top of the wall. A needle-punch non-woven geotextile fabric was placed on the crushed rock before topsoil was placed up to the top of the wall. The topsoil was graded and sloped toward the wall for positive drainage. Downspouts from the buildings were routed over the top of the wall and down the face.

To comply with the requirements of the USACE, an architectural shotcrete facing was placed on the completed wall. The shotcrete was stained and shaped to resemble the native dolomitic outcroppings common in the area, see Figure 10.

When the wall was completed, the riprap used for the access road was pulled back to the wall face and shaped to cover the bottom 1.2 meters (4 feet) of the wall to provide scour protection. Topsoil and trees were then planted within the riprap slope to increase the hydraulic roughness of the slope below the wall.

Figure 10. Completed soil nail wall with architectural shotcrete application.

CONCLUSIONS

Because the slope failures occurred on a slope with existing structures at the top, site limitations required an innovative bottom-up hybrid retaining wall system incorporating both vertical elements and soil nails to support the threatened buildings. Significantly, due to the incorporation of the launchable stone toe into the hybrid system, which also served as a work platform, very little impact to the surrounding environment was experienced during construction. The completed project had the added benefit of integrating into the native surroundings without having a negative visual impact on the fishing or tourism.

Quality Assurance of Soil Nail Grout for
Provo Canyon Reconstruction Project

Clifton B. Farnsworth[1], M. ASCE, P.E.,
Blaine Leonard[2], F. ASCE, P.E., and Darin Sjoblom[3], P.E.

[1]Assistant Professor, Department of Civil Engineering, The University of Texas at Tyler, 3900 University Blvd., Tyler, TX 75799; clifton_farnsworth@uttyler.edu
[2]Research Program Manager, Research Division, Utah Department of Transportation, 4501 South 2700 West, Salt Lake City, UT 84114-8410; bleonard@utah.gov
[3]Geotechnical Engineer, Geotechnical Division, Utah Department of Transportation, 4501 South 2700 West, Salt Lake City, UT 84114-8405; dsjoblom@utah.gov

ABSTRACT: In 2007, construction was completed on the most current segment of Provo Canyon reconstruction, US-189 Wildwood to Deer Creek, widening an 8 km stretch of existing 2-lane highway to 4-lanes. Many of the cut slopes throughout the project required either ground nail or tieback reinforcement. A neat cement grout, consisting of a 0.5 water-cement ratio (by weight), was used for both tieback and ground nail installation. The primary means of quality assurance of the cement grout, by specification, included random sampling of the wet grout for grout cube generation, and laboratory testing the compressive strength of the cubes at specified intervals of time. An alternative method was also adopted for quality assurance of the grout, measuring the specific gravity of the wet grout with a mud balance and drawing the potential compressive strength of the grout from specific gravity and compressive strength correlations. Periodic cube sampling of the grout was continued throughout to verify the strength correlations, and both test methods were evaluated simultaneously. The findings support utilizing both methods in conjunction with each other.

INTRODUCTION

In 2007, construction was completed on the most current segment of Provo Canyon reconstruction, US-189 Wildwood to Deer Creek. US-189 is a principal arterial highway that runs from Provo, Utah, paralleling the Provo River up into the Wasatch Mountains, to Heber City, Utah. This $85 million construction project was undertaken to widen an approximate 8 km stretch of the existing 2-lane highway to 4-lanes.

The Provo Canyon Reconstruction Project was located in a very challenging geologic setting, with numerous steep, highly fractured limestone and quartzite slopes, susceptible to weathering. Another section of the highway traversed a large historic deep seated landslide area that had been locally creeping for decades, and the highway was completely realigned through this to a more stable location upon the slide mass. To create sufficient room for the widened highway, large cuts towering as high as 55 m were required in the adjacent slopes. To ensure stability of these large cut slopes, ground nails (i.e., soil nails and rock dowels) with reinforced shotcrete were utilized. More than 12,700 ground nails varying from 3 m to 15 m in length (totaling more than 70,000 lineal meters), and nearly 5,000 cubic meters of structural shotcrete, were used to support the steep soil/rock cut slopes. Tiebacks were utilized through the landslide area as a means of slope stabilization, including approximately 300 tiebacks up to 49 m in length, totaling around 10,200 lineal meters. A neat cement grout (consisting of only cement and water) was used for both ground nail and tieback applications.

The primary means of quality assurance for the cement grout, as specified in the contract documents, was obtaining daily cube samples from the project site to be later laboratory strength tested at specified time intervals (UDOT 2004). An alternative method for quality assurance was suggested, using specific gravity testing with a mud balance along with periodic cube samples gathered for strength testing. Rather than completely abandon the daily cube sampling in lieu of mud balance testing, it was determined a better alternative would be to study the feasibility of using the mud balance for future applications by continuing to take daily grout cubes in conjunction with mud balance testing. This paper summarizes the findings of that study and the complete summary of this testing is discussed in Farnsworth et. al (2007).

GROUT PRODUCTION

Ground nails, or more specifically soil nails and rock dowels, were used extensively on the Provo Canyon Reconstruction Project. Installation of the ground nails took place as the excavation of the cut slope proceeded in a top down fashion following the basic procedure described in FHWA (1994). To facilitate the enormous amount of ground nailing being performed throughout the project, there were as many as 5 drills located across the project. Each drill (or set of drills where they may have been working in tandem) had a paddle-type grout mixer located with it, and the nails were all grouted toward the end of each workday. One batch of grout was generally sufficient to fill 2 to 3 short (~5 m) holes. However, for longer drill holes or holes that were prone to grout loss, more than one batch of grout had to be mixed to fill just that single hole. Either way, there were numerous batches of grout mixed at several different locations throughout the project each day.

Tiebacks were also used at two different locations on the Provo Canyon Reconstruction Project. Installation of tieback reinforcement generally followed the same installation process as the ground nails, except that each tieback was grouted immediately upon installation. The mixing tank used for tieback grout was much larger than those used for soil nail grout, and therefore required less batches of grout to be mixed for an equivalent length of drill hole. Furthermore, the tiebacks were tensioned after the grout had achieved sufficient strength, typically after several days of curing time.

The grout utilized on the Provo Canyon Reconstruction Project for both ground nail and tieback reinforcement application consisted of a neat cement grout, or simply water and cement. The target water-cement ratio was 0.5, by weight. Grout production therefore consisted of simply mixing a certain number of bags of cement with a certain volume of water, with an equivalent weight ratio of 0.5. As an example, 6 bags of cement (approximately 45 kg each) were often mixed with 132 liters of water (~136 kg total weight), to achieve a grout batch with a water-cement ratio of 0.5.

The project specifications required the use of a cement grout with a minimum compressive strength of 10.3 MPa (1,500 psi) within 24 hours after placement, and a minimum compressive strength of 27.6 MPa (4,000 psi) within 28 days after placement. The specification also required unconfined compressive strength test results from two grout cube samples taken from the grout mix during each working day, where the strength tests were conducted at 14 and 28 days. Unfortunately, the specifications did not contain the specific means to test the 24 hour strength requirement.

GROUT CUBE TESTING

Throughout the duration of the project, two grout cube samples were taken from random grout mixing stations each day, as required by specification. These cube samples were later broken in a laboratory upon curing for 14 and 28 days, to ensure that the grout had reached adequate strength, following the grout cube sampling and testing procedure detailed in ASTM C109, Compressive Strength of Hydraulic Cement Mortars (ASTM, 2006).

The grout cubes were created on site using brass grout cube molds. To create the grout cubes, the cube molds were first assembled and gently lubricated with a light oil to keep the cement grout from bonding to the mold. A sample of the grout was then collected from the grout mixer and poured into the molds. Since the cubes can be prone to some slight shrinkage, the cubes were slightly overfilled. To minimize disturbance to the wet grout cubes, the molds were stored in an insulated storage container for approximately 24 hours. The molds were then stripped and the cubes removed and transferred to a moisture room at the laboratory where they continued to cure until they were later tested.

Negative issues associated with preparing and testing grout cubes include the following:

1. Preparation and testing of the cubes is quite labor intensive and thus quite costly (preparation of the samples in the field, removal from the site the following day, storage, compression testing, and all associated tracking and reporting)
2. Sample disturbance from movement, especially during the first day of curing
3. Adverse effects of extreme temperatures and/or moisture
4. Inconsistent grout cube dimensions due to shrinkage of grout
5. Inconsistent break results depending on equipment and testing methods used

To minimize any inconsistencies, the project team made every effort to ensure that the same techniques and procedures were utilized throughout the project. Furthermore, care at every level of sampling and testing was used to ensure that error could be minimized. While the testing was conducted in a laboratory under fairly controlled conditions, the grout cubes were created in the field where there were a number of variables (weather, vibration, unclean environment, etc.) that simply could not be controlled.

There are two additional points of concern associated with using grout cube testing that the authors wish to note. First, the compressive strength results are not known for at least two weeks after the ground nail has been installed. In many instances, the bench may have been excavated down in the meantime and if the break showed that the grout was not achieving an adequate strength, it is not easy to get back up to the level of nails with the inadequate grout. A second drawback is only gathering two grout cube samples per working day from the project. With several grout mixing stations located throughout the project and a number of batches being mixed at each mixing station, gathering only two cube samples becomes a random attempt at finding a representative batch and assuming that all batches are the same.

Additionally, when a cube sample is to be taken, it takes some time to get everything set up in preparation. The person working the grout mixer is given sufficient time to recognize that a test is going to be taken and the person may increase the cement in the grout to achieve better results. It would be very impractical, however, to consider doing more extensive grout cube testing based on the associated cost and time.

MUD BALANCE TESTING

The mud balance test measures the specific gravity of a liquid, in this case cement grout. According to the Post-Tensioning Institute (2004) the behavior of neat cement grouts (consisting of only cement and water) without admixtures is well understood. Mud balance testing provides the ability to ensure that grouts are mixed with the desired water to cement ratio. The strength of the grout can be predicted based on strength to water-cement ratio correlations. The mud balance itself consists of a mud cup at one end of the beam with a fixed counterweight on the other. A sliding-weight rider is moved along the graduated scale to provide the specific gravity of the mud within the cup. It is important that the reader ensure that the mud cup is filled completely, wiped clean of any residual spilling, and placed on a level surface to ensure accurate readings are taken.

The compressive strength of the cement grout and the rate of strength gain are dependent upon the ratio (by weight) of mixing water to Portland cement and the method of mixing. Since water and cement are the only items used in the neat cement grout, the relationships between the specific gravity, water-cement ratio, and compressive strength are well defined (PTI 2004).

The use of the mud balance provides a significant advantage over grout cube testing. The adequacy of the cement grout is known immediately, prior to even grouting the nails, as opposed to having to wait for two weeks to find out the strength results. The mud balance test is conducted very quickly and tests can essentially be run anytime and anywhere that grout mixing is taking place.

PROJECT DATA

The data gathered during construction consisted primarily of 14 and 28 day compressive strengths from laboratory grout cube testing and the corresponding specific gravities obtained from mud balance testing of the neat cement grout while making the cube samples. Although, not required by specification, there were additional grout cubes tested at 1, 3, and 7 days for some of the samples taken, to further investigate the early strength gain of the grout. The target specific gravity of the cement grout for this project was 1.85, which correlates to an approximate water-cement ratio (by weight) of 0.5 (PTI 2004). However, specific gravity values measured on the project varied from 1.70 to 1.91.

Figure 1 shows a plot of the average compressive strengths of the field cube samples tested in the laboratory vs. the specific gravities measured in the field at 7, 14, and 28 days. This figure also shows the linear trendlines for each of the data sets. It should be noted that there is tremendous overlap in the raw readings between the three datasets, a fact not demonstrated in the figure, since only the average values are shown. However, as seen in the figure, the linear trendlines are approximately parallel to each other, thus representing a consistent trend in strength gain between the three different days tested. This illustrates that despite the tremendous overlap in the data, there is a distinct difference between the datasets and that the difference is statistically significant. In general, the linear trendlines exhibit two distinct characteristics. First, there is a change in the slope intercept, demonstrating that there is an increase in strength gained over time. Second, the increasing slope of the trendlines shows that there is also an increase in strength with an increase in cement content within the grout.

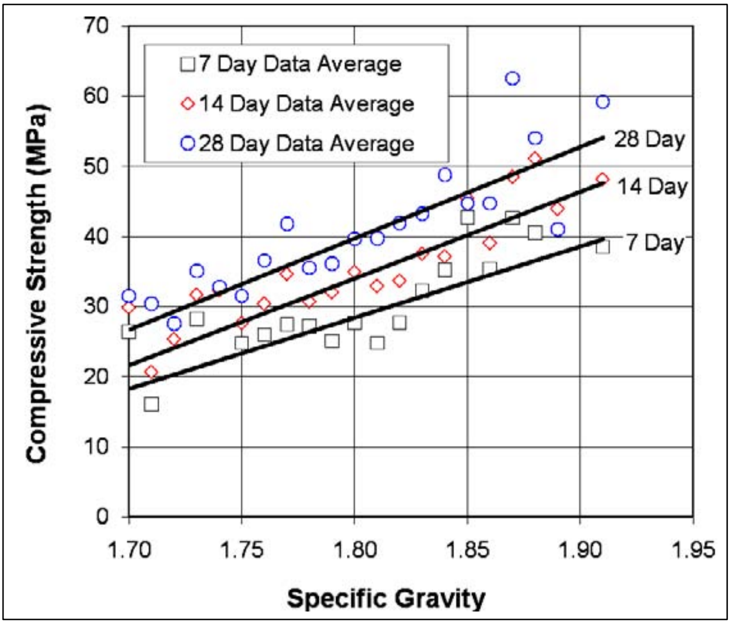

Figure 1. Average compressive strength vs. specific gravity; days 7, 14, and 28.

The average compressive strength vs. time for several different specific gravity values is shown in Figure 2, including the approximated values for a specific gravity of 1.85 from PTI (2004). This figure shows the rate at which strength is obtained in the cement grout as it cures. Furthermore, this figure demonstrates that there is an increase in compressive strength as the specific gravity increases.

There are several additional items to note about Figure 2. This figure indicates that with a cement grout specific gravity of around 1.88, the average compressive strength meets the 27.6 MPa (4,000 psi) minimum value after about 3 days. With the lower specific gravity of around 1.75, the average compressive strength is only about 24.1 MPa at day 7, reaches 27.6 MPa about day 14, and finishes up around 31.0 MPa at day 28. This meets the minimum required strength. However, the values shown are an average and therefore do not leave much room for values falling below this average to meet the minimum strength. The lower specific gravities shown (1.72 and 1.75) barely reach or remain slightly beneath the minimum compressive strength value of 27.6 MPa (4,000 psi) within the 28 days, for the average value. This suggests that it may be better to establish a higher minimum specific gravity (perhaps 1.80) to ensure that there is some factor of safety in meeting the minimum compressive strength. Figure 2 also demonstrates that the time for sufficient strength gain prior to excavating below for subsequent rows of nails should be determined by the target specific gravity. Finally, this figure includes approximated values of compressive strength vs. age for a specific gravity of 1.85 from the Post Tensioning Institute (2004). The shape of the PTI curve in general resembles the shapes of the curves obtained in this study. However, the rates of strength gain from the data within this report exhibit more rapid strength gain initially, with a milder strength gain later. The PTI data is shown simply as a point of reference. The differences do seem to suggest that establishing project specific correlations at the beginning of the project, utilizing the specific type of cement, mixing procedure, etc., would be wise.

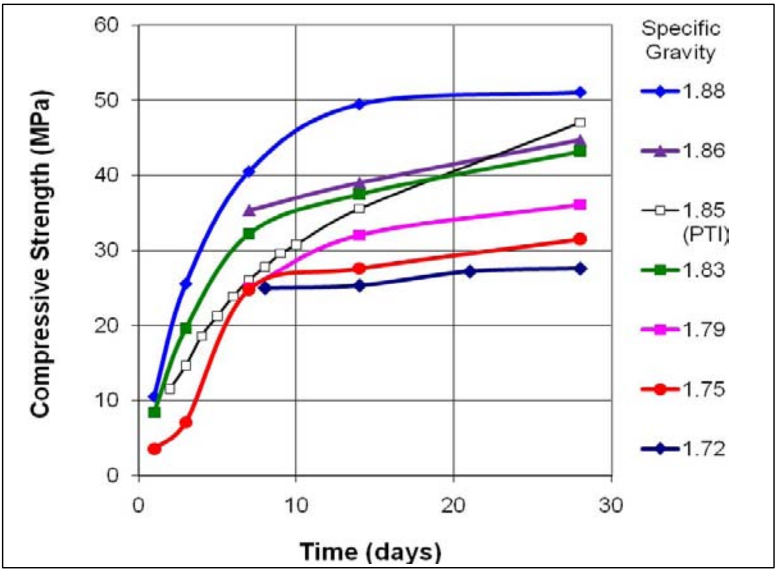

Figure 2. Average compressive strength vs. time for varying specific gravities.

The specification requirement for the grout to reach a minimum compressive strength of 10.3 MPa (1,500 psi) within 24 hours of grout placement is only met for the average compressive strength from a specific gravity of 1.88, or higher, as shown in Figure 2. This single requirement seems to govern the minimum specific gravity rather than the 28-day compressive strength. If this requirement is to be utilized for future jobs, it appears that the minimum specific gravity would need to be set sufficiently high to ensure that this requirement is met.

For this project, the minimum acceptable 28-day grout strength was established at 27.6 MPa (4,000 psi). The specifications further required that the ground nails be replaced if the grout cubes did not meet this tolerance. Although the averages value for each specific gravity level tested met the 28 day strength, there were many individual compressive strength tests that did not meet the minimum acceptable value. In the majority of the instances it was determined that the lower values were simply a function of external influences such as adverse temperature conditions or improper preparation and handling of the grout cubes rather than inadequate grout strength. Re-installation of the nails was therefore not required. However, this brings several key design issues to mind for situations where the grout truly may be inadequate. First, it would be useful to have a better understanding of how the factor of safety of a soil nail wall is affected by the grout strength. In other words, how critical is the grout strength of 27.6 MPa (4,000 psi) in the soil nail design? Second, can an acceptable penalty be established for grout cubes that may exhibit results below the minimum acceptable value rather than simply requiring re-installation of the soil nails? Finally, it may be prudent to ensure that minimum specific gravity thresholds be utilized that adequately account for the large standard error associated with testing grout cubes. These issues should be addressed up front during the design phase of the project and the information passed along to the construction engineers. The current project did not specifically address these issues, but it would have been valuable to have had a better understanding of each.

Finally, it should be noted that the grout cube dataset contained within this paper is an actual sample of the type of results that can be generated while performing quality assurance of a cement grout by means of grout cube testing. Because the actual strength of the grout was not measured in-situ, it is unknown how much error was introduced into the break data by the grout cube testing process and therefore how representative these results are of the actual strength of the in-situ grout. It seems that the actual in-situ grout strength would still have some variance with it, but probably not as large of error as that introduced by the grout cube testing process. However, the quality assurance of the cement grout is still dependent upon the values obtained from the grout cube testing and tolerances should probably be set for the expected minimum values as opposed to the expected average values. Similar minimum thresholds for using the mud balance as a means of quality assurance should also be utilized.

CONCLUSIONS

Specific gravity testing should be used as part of the quality assurance program for ground nail grout, because these tests can be performed quickly, at any time, without interfering with the work and provide an immediate indication as to the quality of the mixed grout. This provides the ability to perform regular testing throughout the day where numerous batches of grout are being produced at several locations throughout the project. The use of specific gravity testing simply provides the ability to eliminate the waiting to see if the grout was good or not. On the Provo Canyon Project the use of the mud balance proved to be very beneficial when disputes arose about the adequacy of the grout to be installed.

The project results indicate that a reasonable estimate for meeting the minimum 28 day compressive strength is to establish a minimum allowable specific gravity of 1.80, accounting for those test values that fall below the average results. For projects where the time to strength gain is a consideration, especially if the work is progressing rapidly and excavation needs to take place for additional rows of nails, it is necessary to have sufficient strength much sooner than 28 days. For very-rapid construction sequencing situations, the minimum specific gravity should be increased to reflect adequate strength gain in the desired duration of time. These results suggest that a minimum specific gravity of 1.83 allows the minimum compressive strength to be met within about a 5-day period, and likewise, a minimum specific gravity of 1.88 for a 3-day period.

To verify that the cement-grout follows previously established curves or to simply reestablish the correlations, grout cube and mud balance testing could be performed within a laboratory setting at the beginning of the project. This process can be used to assist in establishing the minimum specific gravities to be allowed. Furthermore, rather than completely eliminate the use of grout cubes on the project in lieu of the mud balance test, periodic cube sampling should still take place. This testing can be performed on a cement volume and/or time basis. These periodic cube samples are used to verify that the cement powder being used is still providing consistent results and that the correlated compressive strengths are still being met.

There will be variability in the grout mixing process (due to differences in temperature, humidity, quality of cement and water, type of mixer utilized, etc.), and the strength of the installed grout due to these external variables is not taken into account with specific gravity testing. For instance, colloidal grout mixers tend to produce higher strength results than paddle-type grout mixers. Likewise, the actual difference between the strength of the grout placed in situ and the cube sample strength is not verified through this process. However, the specific gravity testing still provides an immediate indication as to what compressive strength will ultimately be achieved, and the periodic cube samples provide an indication as to what compressive strength was ultimately achieved. Together, they provide an effective quality assurance program.

ACKNOWLEDGMENTS

The authors appreciate the support of the Utah Department of Transportation.

REFERENCES

ASTM International (2006). "Standard test method for compressive strength of hydraulic cement mortars (using 2-in. or [50-mm] cube specimens)." Cement; Lime; Gypsum, ASTM International Book of Standards, Vol. 04.01, September 2006.

Farnsworth, C. B., Golden, J. W., Wallwork, B. (2007). "Assessment of Specific Gravity Testing with a Mud Balance for Quality Assurance of Cement Grout in Ground Nail Installation." UDOT Report No. UT-07.04, Salt Lake City, Utah, August 2007.

Federal Highway Administration (1994). "Soil Nailing Field Inspectors Manual – Soil Nail Walls." FHWA Report No. FWHA-SA-93-068, Washington D.C., April 1994.

Post-Tensioning Institute (2004). "Recommendations for prestressed rock and soil anchors, 4th Edition." Post-Tensioning Institute, Phoenix, Arizona.

Utah Department of Transportation (2004). Contract Special Provisions, NH-0189(12)14, SR-189, Provo Canyon; Wildwood to Deer Creek. October, 2004.

Hollow Core versus Solid Bar Soil Nails for Support Applications in Karst Terrain: What We Learned!

Jesús Gómez[1] Ph.D., P.E., Andrew Baxter[2] P.G., E.I.T., Melinda Dirdal[3], E.I.T.

[1]Principal Engineer, Schnabel Engineering, LLC, 510 East Gay Street, West Chester, PA 19380; jgomez@schnabel-eng.com
[2]Senior Scientist, Schnabel Engineering, LLC, 510 East Gay Street, West Chester, PA 19380; abaxter@schnabel-eng.com
[3]Staff, Schnabel Engineering, LLC, 510 East Gay Street, West Chester, PA 19380; mdirdal@schnabel-eng.com

ABSTRACT: The Crystal Bridges Museum of American Art is currently under construction in Bentonville, Arkansas. Most of the proposed buildings involve cuts up to 15 m (49 ft) and the construction of significant temporary and permanent retaining walls.

The site is within a karst region and soil nail walls were selected for excavation support. They provided sufficient flexibility to adapt to the architectural contours of the structures and the varying rock surface. They also presented significant advantages in installation through soft zones in the soil, hard rock, and significant voids within the rock mass.

This paper describes the installation of the soil nail walls and issues encountered during construction. It presents a comparison between the installation efficiency of hollow core bars and pre-drilled solid bars in this karst geology. Finally, data is presented that shows that measurement of specific gravity of the fresh grout is suitable for quality control of the grout in both hollow core bar and pre-drilled solid bar nails.

INTRODUCTION

Crystal Bridges Museum of American Art (Crystal Bridges) is located along a valley stream northeast of Bentonville, Arkansas. The 9,300 sq m (100,000 sq ft) facility will be both a gallery and a community/culture center. The buildings, up to five stories in height, are cut into the steep slopes extending up from the creek. The unique setting and layout of the structures results in deep and long vertical excavations following the curved buildings.

The site is underlain by moderately fractured, near horizontally bedded limestone and chert with moderately stiff gravely clay overburden. The soil rock interface is highly variable with typical karstic features including ledges, boulders, pinnacles and cutters. Unconfined compressive strength of the limestone and chert bedrock ranged from 13.8 MPa (2,000 psi) to 68.9 MPa (10,000 psi). The Engineering Rock Mass Rating was generally II or Good Rock (Bieniawski, 1989).

Installation of soil nails at the site involved drilling through a varying profile that included soft to stiff clay and silt, weathered rock, hard rock, and frequent solution features.

SOIL NAIL WALL CONSTRUCTION

Soil nail walls were utilized for temporary and long term excavation support. Temporary soil nail walls consisted of 40/20 IBO-Titan hollow core bars supplied by Con-Tech Systems, Ltd. Hollow core bars use a one-step drilling process in which grout is injected at the ground surface through the center hole of the bar. Upon exiting the drill bit at the tip of the bar, the grout exit velocity undercuts the soils and flushes the drill cuttings to the ground surface along the annular space of the bar.

The soil nail wall contractor, Foundation Specialties Inc. (FSI), drilled the hollow core nails with neat cement grout that was de-sanded and re-circulated during each nail drilling operation. Once the final nail length was reached, a final grout mix was pumped through the bar to flush the drilling grout and cuttings. The final grout mix consisted of a mix 9.5 L (2.5 gallons) of water per 21.3 kg (47-pound) bag of cement, yielding a specific gravity of about 1.8 to 1.9 for the fresh grout. The nails were installed using a TEI 300 rock drill mounted to a CAT 314C excavator.

In locations where open-hole drilling was feasible and grout losses through large open voids precluded hollow core bar installation, pre-drilled soil nails were used. The holes were drilled using TEI Rock Drills Models RDS350 rotary drill and HEM 300 feed system with a downhole hammer. These nails were reinforced with No. 11 Grade 75 All-Thread Rebar supplied by Williams Form Engineering Corp. These nails were installed using the same final grout mix as for the hollow core nails, and were subject to similar quality control procedures.

Figure 1 illustrates a typical soil nail wall section. The soil nail walls extend down to the top of hard rock deemed stable. Nine-gauge chain link fencing with a 5 cm (2-inch) maximum opening extending to the bottom of the cut was used to protect against rock fall. Figure 2 shows one of the completed excavations.

Drainage of perched water from behind the soil nail wall was provided by 30.5 cm (12 in) wide geocomposite drainage strips, spaced approximately at 3 m (10 ft). A drainage grate was provided at the bottom of the wall to allow the water to exit.

QUALITY CONTROL

Schnabel Engineering, LLC (Schnabel) performed extensive quality control of the soil nails. The information recorded during installation of the nails included type of soils/rock drilled, voids and seams within the rock, specific gravity of the grout, grout volume, drilling rate, and grout cube strength.

Specific gravity was the primary control for the grout, and was measured at the top of each nail using a mud balance (see Figure 3). Grout cubes were tested as a confirmation of the primary quality control parameter. The drilling rate was recorded excluding down time for splicing bars or drill rods, etc. This is a useful parameter that allows a better interpretation of the soil/rock conditions within one site. However, it cannot be directly extrapolated to other equipment or other sites.

FSI performed nine verification and 33 proof tests. The tests were designed to verify the design bond strength of the nails in various strata.

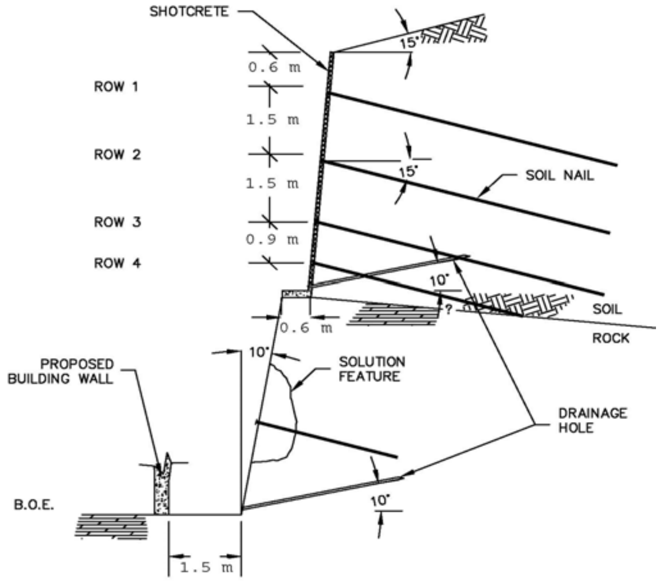

Figure 1. Soil Nail Wall Section

Figure 2. Completed Excavation at Building A234

Figure 3. Measuring Specific Gravity of Grout

LONG-TERM HOLLOW CORE NAILS

One of the challenges associated with long-term use of hollow core bars as soil nails or anchors is corrosion protection. These bars can be purchased from the supplier with galvanizing, metallizing, epoxy coatings, or a combination thereof. In the authors' experience, corrosion-protection coatings are susceptible to wear and tear during the drilling process. An FHWA-sponsored study currently under development has shown that significant damage occurs to protective surface layers in test hollow core bars drilled through granular materials. Epoxy-coated bars were especially susceptible to damage.

In this project, metallizing was chosen as the corrosion protection layer for the long-term nails. Because the soils at the site are not typically coarse-grained, damage to the metallizing was not considered to be significant. In addition, sacrificial steel was used in order to extend the life of the nails after full loss of the metallizing to corrosion. It is important to note that the soils at the site are not considered aggressive based on the Post Tensioning Institute (PTI) guidelines (PTI 2004).

SOIL NAIL INSTALLATION

Drill Times and Production Rate

Figures 4a and 4b show the installation drill times of hollow core bar and traditional soil nails. The drill times shown consider actual drill time per foot of drill strand, and do not consider time spent flushing the holes, changing drill strings, or other delays. The average drill time of hollow core bars was greater than that of the traditional, pre-drilled nails.

In soils, drilling time for installation of traditional solid bars was about 50 percent shorter than the drilling time for hollow core bars. However, this larger installation rate for traditional solid bars is offset by the subsequent installation of the solid bar itself and grouting, which takes place simultaneously during drilling of hollow core bars. For the solid bar, an open hole was drilled using a downhole hammer. The sacrificial drill bit installation method was used for the hollow core bars. Both systems provided similar overall production rates with a slight advantage of the hollow core bars over the traditional solid bars. In rock, traditional predrilled solid bar installation was clearly more efficient than hollow core bars.

The authors believe that the development of such a database of effective drill times for each project is an invaluable tool for quality control and decision making, especially in large projects. However, it is noted that the drill times measured in one project should not be directly extrapolated to other sites, or even to other drilling crews within the same site.

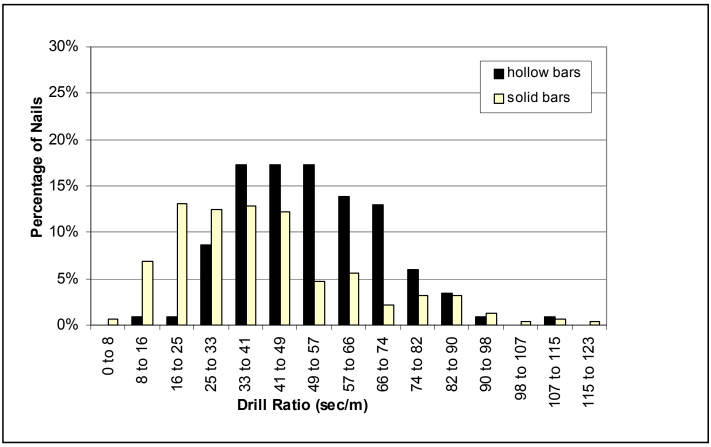

Figure 4a. Effective Drill Time in Soil (Continuous Drilling)

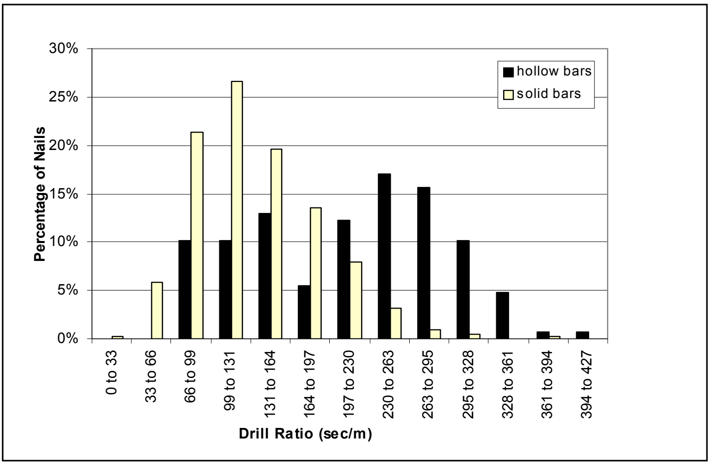

Figure 4b. Effective Drill Time in Rock (Continuous Drilling)

While hollow core bars have greatly increased production in many cases, that was not the case on this project. On average, the production rate using hollow core bars was only slightly higher than the production rate using traditional drill methods.

A significant number of soil nails encountered voids within the rock mass. In some cases the size and frequency of the voids required significant grout volumes, which caused a large drop in production rate.

When using the traditional pre-drill methods, the voids were noticeable through the loss of air return, increase in drilling ratios, and at times air return coming through an adjacent hole. When communication was observed between two holes, the driller stopped drilling, grouted the voids, and re-drilled once the grout set. This method prevented the air in the hammer from blowing out weak soil, which would create more voids and plug previously drilled holes.

Grout Strength

Figure 5 is a diagram that relates the measured values of the specific gravity (Gs) with the compressive strength of the grout for the traditional solid bars. The gray shaded area highlights the range of test results from a study performed by Schnabel Engineering and PKF Mark III (Gómez et al, 2007).

Preparation and compression-testing of the cubes followed ASTM C109. The specific gravity test sample was taken from fresh final grout at the top of the soil nail hole. The plot shows that the strength of the grout was consistently higher than 27.6 MPa (4,000 psi), with an average 28-day compressive strength of 46.8 MPa (6794 psi) and an average Gs of 1.86. In Figure 5, there are two test specimens that fall below the specified grout strength at the 28-day test; however, the 56-day strengths exceeded 27.6 MPa (4,000 psi) in both cases.

This diagram illustrates that specific gravity determination during nail installation is a suitable quality control parameter and offers immediate confirmation of the quality of the grout before or during grout installation.

GROUT-TO-GROUND BOND VALUES

The contractor performed nine verification and 33 proof tests. Of these tests only one reached geotechnical failure. This test nail was installed with a hollow core bar and was loaded to 150% of the design bond stress prior to failure. All other verification tests were loaded to 250% to 400% of the design bond stress.

The load testing procedure included several unload-reload cycles. Interpretation of the results of the verification and proof tests consisted of calculating the apparent elastic length of the nail tendon based on the results of the unload-reload cycles. The estimated apparent elastic length was then used to estimate the ultimate bond strength along fully mobilized portion of the nail. This procedure was detailed by Gómez et al. (2007).

Table 1 summarizes the mobilized bond stress values interpreted from the load tests for traditional pre-drilled solid bar and hollow core bar soil nails. In clay, the interpreted bond strength values are significantly larger than those recommended by FHWA. This is likely due to the undercutting action of the hollow core bars, grout filling voids, and displacement of soft materials under grout pressure. It is noted that the values shown on the table are based on the nominal hole diameter and not on the actual grout body diameter.

In rock, there was a significant variability of the interpreted bond strength values, which is consistent with the variability of the rock at the site. However, the average bond strength was within the typical range of values used for design.

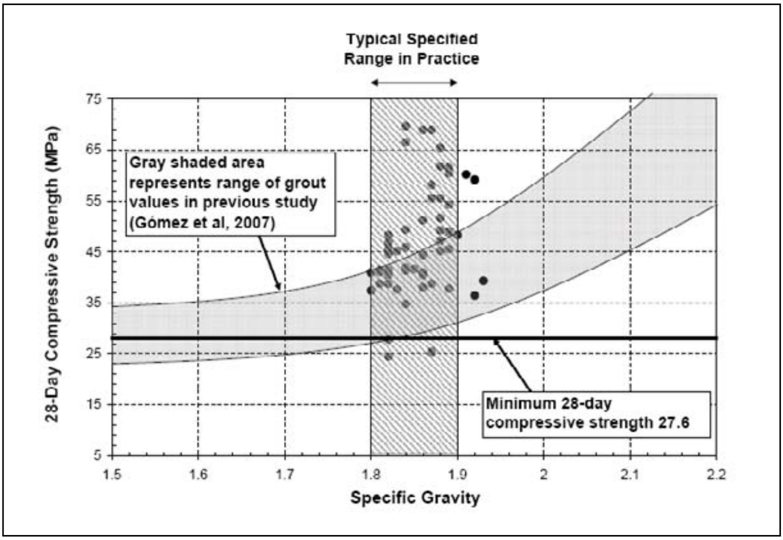

Figure 5. Grout Strength vs. Specific Gravity (adapted from Gómez et al, 2007)

Table 1. Comparison of Observed Bond Strength and FHWA Bond Strength

Soil Type	Average Mobilized Bond Stress in Proof Tests kPa (psi)	Bond Strength Suggested By FHWA (psi)
Clay	138 (20)	35-48 (5-7)
Limestone	262 (38)	303-400 (44-58)

CONCLUSIONS

The implementation of soil nail walls at Crystal Bridges was an effective solution for irregularly shaped excavations in karst terrain. In the clayey soils of this site, installation of hollow core bars was slightly faster than installation of traditional, pre-drilled soil nails. In rock sequences, however, predrilled solid bar nail installation was faster thon hollow core bars.

Comparison between specific gravity and grout cube strength confirm that specific gravity is an effective indicator of the quality of grout, even for hollow core bar soil nails. We believe that compressive testing of grout cubes can be used as a secondary indicator of grout quality, or may not be used at all in some cases.

There was a significant variability of bond strength values for soil nails installed in limestone sequences. This suggests the need for augmented soil nail testing programs in this type of geology. The bond values interpreted from test soil nails in clay were larger than those typically used for design, possibly due to the formation of a grout body significantly larger than the nominal bit diameter. This is advantageous but it is also difficult to predict during design.

ACKNOWLEDGEMENTS

We thank Schnabel Engineering for providing their support and resources during preparation of this paper. Especially, we thank Helen Robinson, P.E., and Johanna Mikitka, E.I.T. We want to acknowledge Paul Gintonio of Foundation Specialties, Inc. for his help during field testing. We also thank Winchester Falbe, and Michael Rysdorp of Buro Happold, Denise Richards of Keast and Hood Co., representatives of Moshe Safdie and Associates, and members of the Crystal Bridges Foundation Team for their support during the design and construction of the project.

REFERENCES

ACI (2002), ACI 318R-02, Building Code Requirements for Reinforced Concrete and Commentary, 2002

ASTM Standard C109, 2000, "Specification for Cement; Lime; Gypsum," ASTM International, West Conshohocken, PA, 2000, DOI:10.1520/C0109-00

Baxter, A. and Gómez, J. "Design and Construction of Micropiles Each Subject to 110 Kips of Lateral Load," DFI 33rd Annual Conference on Deep Foundations, New York, NY, October 2008.

Bieniawski, Z.T. (1989). Engineering Rock Mass Classifications, New York, NY

FHWA, Geotechnical Engineering Circular No.7: Soil Nail Walls. Publication No. FHWA0-IF-03-017, March, 2003.

Gómez, J.E., Cadden, A.W., Bruce, D.A., "Micropiles in Rock. Development and Evolution of Bond Stresses under Repeated Loading," 12th Pan-American Conference on Soil Mechanics and Geotechnical Engineering, Cambridge, MA, June 2003. Gomez et al. interface research and papers

Gómez, J.E., Rodriguez, C.J., Robinson, H.D., and Keough, L. "Hollow Core Bar Micropiles – Design Parameters Interpreted From 260 Load Tests," DFI 32nd Annual Conference on Deep Foundations, Colorado Springs, CO, October 2007.

Post-Tensioning Institute, "Recommendations for Prestressed Rock and Soil Anchors," Post-Tensioning Institute, Phoenix, AZ, 2004.

Wilder, D., Gómez, J., Cadden, A.W., Traylor, R.P., and Pilkington, M. (2005). "Compressive Load Transfer in Micropiles through Concrete Footings: A Full Scale Test Program." Companion paper in Geo3 Conference Proceedings.

Prototype Test of Soil-Cement Shoring Walls for the Transbay Transit Center, San Francisco

Brandon Kluzniak[1], Demetrious Koutsoftas[2], and Nick O'Riordan[3]

[1]Engineer, Arup, 560 Mission Street, Suite 700, San Francisco, CA 94105; email: brandon.kluzniak@arup.com
[2]Consultant; email: deme@dkgeotech.com
[3]Principal, Arup; email: nick.oriordan@arup.com

ABSTRACT

The Cement Deep Soil Mixing (CDSM) method was selected to construct shoring walls for temporary support of deep excavations for the Transbay Transit Center in San Francisco. The CDSM method is also planned to be used for ground treatment to improve the strength characteristics of soils to depths up to 150 ft (45.7 m) to protect adjacent structures from the potential impacts of excavation-induced deformations. Because of the unprecedented depths of the anticipated CDSM treatment, a prototype test was undertaken to evaluate the feasibility of the CDSM method to achieve the intended depths of treatment while maintaining the required quality in terms of strength, permeability, and continuity. This paper presents the results of the field tests, including the variation of soil-cement strengths and permeability.

INTRODUCTION

The project involves the construction of an underground station box for the Transbay Transit Center (TTC) in San Francisco, which will require an excavation approximately 1,500 ft (457.2 m) long, 185 ft (56.4 m) wide, and 57 to 62 ft (17.4 to 18.9 m) deep. The excavation shoring system will require construction of deep shoring walls that will function both as cut-off for groundwater control and as temporary retaining structures. The CDSM method is also being considered for improvement of the soils to depths of up to 150 ft (45.7 m) as a means of protecting adjacent structures from the potential effects of excavation-induced deformations.

The specialist contractor contacted during the planning stages of the prototype test could not verify whether in-situ soil-cement mixing could be accomplished to the planned depths without pre-treatment. It was explained that pre-treatment, consisting of pre-drilling two of the three soil-cement columns of every panel, might be necessary to loosen the soils so that the mixing augers could penetrate to the planned depths.

The prototype test was undertaken to demonstrate that the CDSM method could be used to construct continuous, relatively impervious, shoring walls, as well as to consistently improve the ground to the required depths. The information of interest includes: (1) maximum depth of penetration that could be achieved; (2) quality of the shoring walls in terms of integrity, permeability, strength, and continuity; (3) production rates under prototype conditions at the TTC site, including both CDSM panel and steel soldier pile installation.

SITE CONDITIONS

The subsurface conditions at the prototype test location consist of approximately 15 ft (4.6 m) of fill underlain by a layer of medium dense to dense, fine dune sand. The dune sand is very similar in gradation to the overlying fill, and in some instances it is difficult to distinguish between the two layers. Underlying the dune sand is a 15 to 20 ft (4.6 to 6.1 m) thick deposit of soft Holocene marine deposits, consisting of medium stiff to stiff clay known locally as Bay Mud, which is underlain by relatively thin deposits of marine clayey sands. Below the marine deposits is Colma Sand, a dense to very dense, terrestrial sand deposit with occasional clay layers. The thickness of the Colma Sand reaches 65 ft (19.8 m) at the test site. Underlying the Colma Sand is a layer of very stiff to hard, fat clay, known locally as Old Bay Clay, up to 110 ft (33.5 m) thick. The Old Bay Clay is underlain by residual soil and bedrock at a depth of approximately 220 ft (67.1 m). An idealized soil profile of the prototype test location with Atterberg limit, moisture content, and density data is shown in Fig. 1.

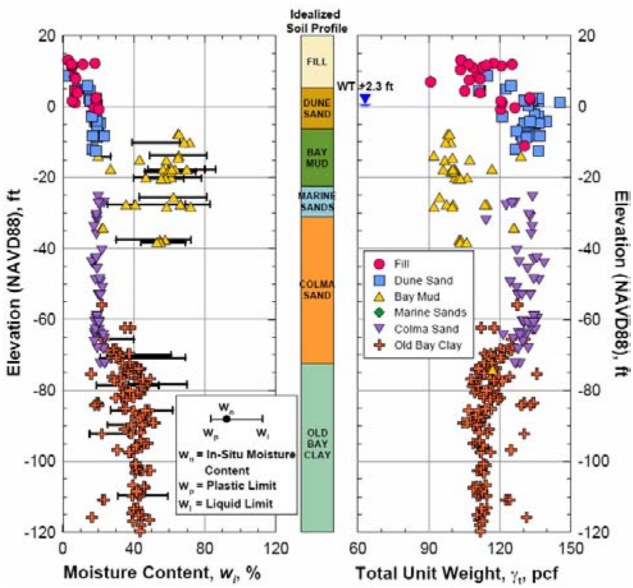

Fig. 1. Atterberg limit, moisture content, and density data in soils at the test site

Preliminary analyses indicate that the excavation may require construction of shoring walls to depths of 100 to 150 ft (30.5 to 45.7 m). As part of the test program, the design team needed to confirm that the CDSM method could penetrate through the very dense Colma Sand and the hard Old Bay Clay crust to reach the intended depths for the shoring walls and ground treatment. Moreover, verification was needed that proper mixing could be achieved to meet the requirements for watertightness, continuity, and integrity of the shoring walls.

PROTOTYPE TEST DESIGN

The test program for the CDSM shoring walls consisted of a single 50 ft (15.2 m) long by 25 ft (7.6 m) wide cell laid out within the selected test site as shown on Fig. 2. An additional 25 ft (7.6 m) long wall was constructed at an adjacent location to accommodate further testing, which was deemed necessary after review of the results of the initial test program, to evaluate additional factors affecting the installation of the shoring walls and the steel soldier piles.

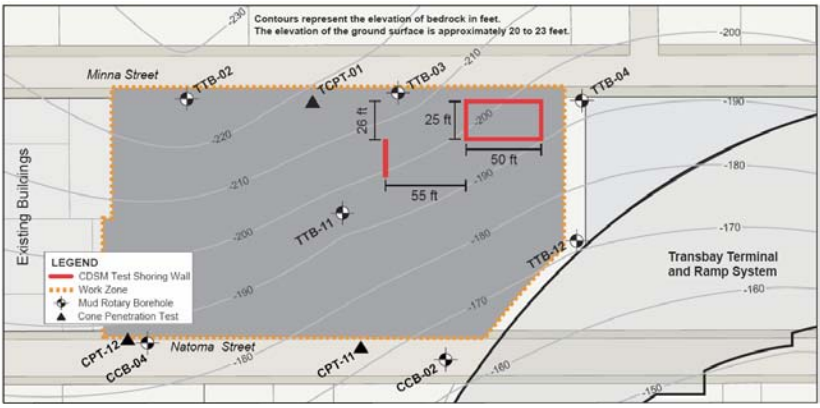

Fig. 2. Site layout for CDSM prototype test

The test cell was constructed of overlapping CDSM panels using a 608 triple-auger rig (O'Rourke and McGinn, 2006) with 36 in (914 mm) diameter augers. Because continuity is critical to construct relatively impervious shoring walls, the overlapping between adjacent CDSM panels included full re-drilling of the outer columns of each primary panel.

The typical installation sequence involved drilling two primary panels first, by skipping a space equal to the diameter of one column minus the normal overlap between adjacent columns. Once the primary panels were completed, the panel between them, referred to as the secondary panel, was installed. During installation of the secondary panels, the two outer soil-cement columns of the previously installed primary panels were redrilled. The panel installation sequence is shown in Fig. 3.

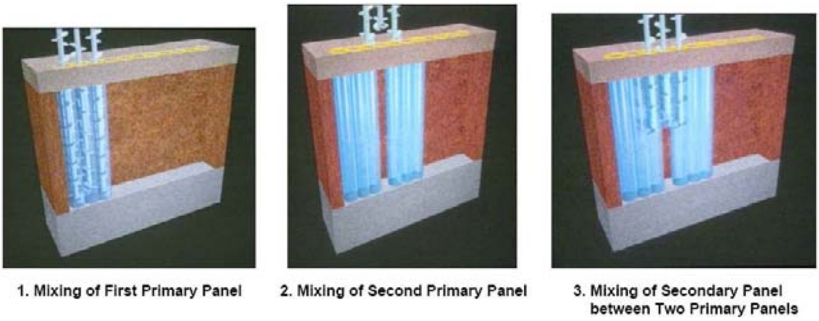

Fig. 3. CDSM panel installation sequence (courtesy of Raito, Inc.)

The slurry mix was prepared at an on-site batching facility and pumped from the batching plant through the two exterior CDSM shafts discharging at the tip of the two outer augers. All slurry mix designs used Type II Portland cement, with a cement factor (Filz, 2005) of 18.7 pcf (300 kg/m^3) and a bentonite-water ratio of 1%. To enhance the mixing process, air was pumped through the middle auger during the drilling and mixing program. Mixing began near the surface, by pumping slurry and air through the augers while advancing the augers at a relatively constant penetration rate. When the multi-auger system reached the bottom of each panel, a process called "bottom-mixing" was performed as a means of improving the mixing of the deeper soils. The bottom-mixing process involved raising the triple-auger system 5 to 30 ft (1.5 to 9.1 m) from the bottom of the panel, then re-mixing the lower portion of the panel by advancing the augers to the bottom of the panel. Generally, about two-thirds of the slurry is injected on the penetration of the triple-auger system, followed by one-third on the withdrawal (O'Rourke and McGinn, 2006). Auger penetration rates generally varied from approximately 2.0 to 3.0 ft/min (0.6 to 0.9 m/min) on the downstroke, to 5.0 to 6.0 ft/min (1.5 to 1.8 m/min) on the upstroke. The augers operate at two mixing settings, 20 rpm (low) and 40 rpm (high). Typically, each CDSM panel is started in low rotation speed within the upper 10 to 20 ft (3.1 to 6.1 m), and then mixed in high rotation speed when stiffer soils are encountered. Ground conditions at the test site generally did not require mixing in low rotation speed at depths beyond the upper 20 ft (6.1 m).

INSTALLATION OF SOLDIER PILES

Three pairs of steel soldier piles were installed to evaluate the effect of pile size and mix design on the ease or difficulty of installation. The steel soldier piles consisted of the following: (1) two W24 x 162 sections; and (2) four W27 x 217 sections. A summary of each soldier pile installation is presented in Table 1.

Table 1. Soldier pile installation summary

Panel Location	Furnished Length (ft)	Soldier Pile Section Size	Water-Cement Ratio (%)	Penetration Achieved (ft)
B-11/B-12	105	W24 X 162	220	105
B-7/B-8	105	W24 X 162	190	75
C-1/C-2	120	W27 X 217	250	117
C-4/C-5	120	W27 X 217	250	62
E-1/E-2	110	W27 X 217	250	77
E-5/E-6	110	W27 X 217	250	70

Results indicate the depth of penetration of the soldier piles was not affected by the slurry mix design within the range of parameters tested (water-cement ratio of 190% to 250%).

In the four trials in which the soldier piles did not reach full depth, the penetration of the piles stopped quite abruptly, which suggests that the piles hung up on the sides of the soil-cement columns due to inadequate verticality. This may be explained in part by the large size of the piles relative to the diameter of the soil-cement columns, which reduced the margin for error in maintaining verticality of the pile with the support crane during installation. Additionally, soldier pile sections were field welded in some cases to produce full length sections for installation. Imprecision in the design of these welded steel sections likely contributed to the difficulties reaching the intended depths.

QUALITY ASSURANCE

The prototype test program included post-construction verification testing to evaluate the quality of the in-situ CDSM walls. Six cores were taken to provide samples to evaluate strength, permeability, and quality of mixing. Cores were retrieved by the specialist CDSM contractor using a 2.5 in (64 mm) diameter double core barrel with a flexible inner membrane and a carbide bit.

The following criteria were set as targets for the coring program: (1) minimum core recovery of 90%; (2) Rock Quality Designation (RQD) of at least 70% of the recovered core; and (3) all cores shall be advanced to at least two-thirds of the depth of the CDSM wall.

Additionally, criteria were established for evaluating the quality of the mixed material: (1) the sum of all pockets/lenses of unmixed/poorly mixed material not to exceed 10% of the total length of the core; and (2) the thickness of any individual zone of unmixed/poorly mixed material not to exceed 2 in (51 mm).

Statistical analyses of core recovery, RQD, and poorly mixed core percentages are presented is Fig. 4. Results show a mean recovery of 96.4%, a mean RQD of 87.4% of the recovered core, and a mean percentage of poorly mixed core of 7.6%.

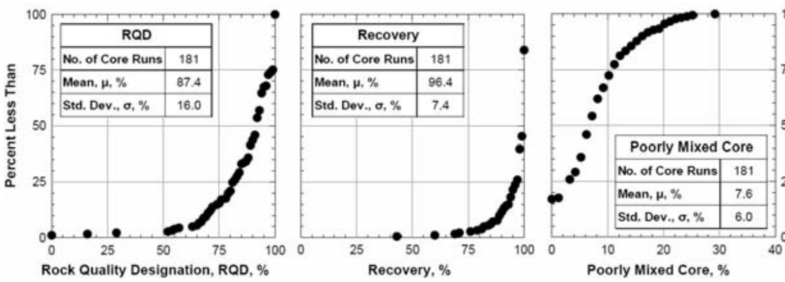

Fig. 4. Statistical analysis of RQD, core recovery, and percentage of poorly mixed core

LABORATORY TESTING

Strength Tests

47 unconsolidated undrained (UU) triaxial compression and 66 unconfined compression (UC) tests were performed on selected cores. CDSM strengths from UU and UC tests are plotted versus elevation in Figure 5. A target strength of 120 psi (827 kPa) was established for the CDSM stabilized material and may be considered within the appropriate range for excavation support applications (Andromalos and Bahner, 2003). Included in Fig. 5 are the strengths of the untreated and in-situ soils for comparison. The strength of the CDSM was 2.8 to 3.4 times the strength of the in-situ soils.

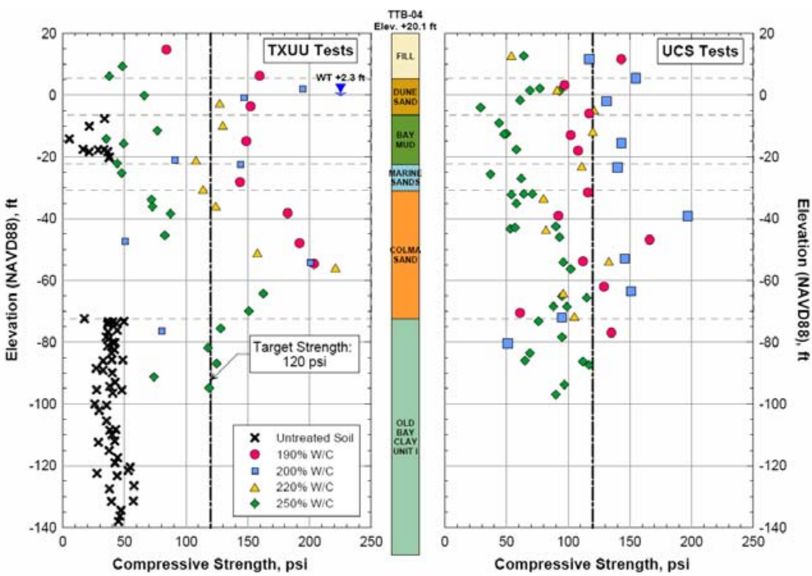

Fig. 5. UU and UC strengths by coring location

Statistical analyses of strength test results indicate mean strengths of 140.5 psi and 94.6 psi (968.7 and 652.2 kPa), respectively, for UU and UC tests, as shown in Fig. 6. On average, strengths from UU tests were about 49% higher than the strengths from UC tests, as shown in Fig. 7. UC tests were performed on samples cured 28 to 35 days, while UU tests were performed on samples cured for 28 to 83 days. Fig. 8 indicates strength gains continuing beyond 60 days of curing. The strength gain with time is more pronounced in samples with a lower water-cement ratio.

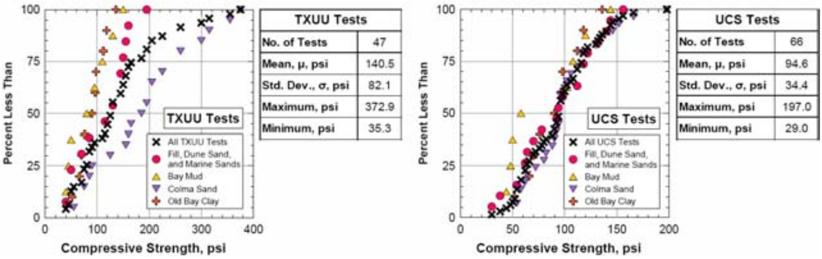

Fig. 6. Statistical analysis of UU and UC strengths

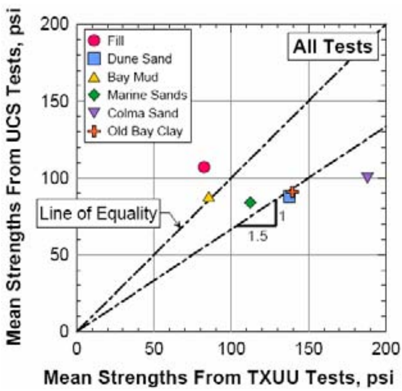

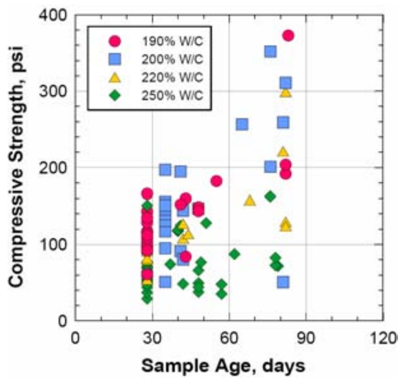

Fig. 7 Comparison of mean UU and UC strengths and Fig. 8. Variation in compressive strength with sample age

Permeability Tests

Two sets of laboratory permeability tests were performed on samples of CDSM cores retrieved from the Colma Sand layer— the most permeable layer of concern. The first set was performed on core samples; the second set of tests was performed on wet grab samples.

The results of permeability tests performed on CDSM cores indicate permeabilities between 2.57 x 10^{-9} and 1.89 x 10^{-8} ft/sec (7.82 x 10^{-8} and 5.76 x 10^{-7} cm/sec). Tests performed on wet grab samples indicate permeabilities between 3.6 x 10^{-9} and 3.9 x 10^{-8} ft/sec (1.1 x 10^{-7} and 1.2 x 10^{-6} cm/sec). For comparison, typical in-situ permeabilities of Colma Sand range between 3.3 x 10^{-6} and 3.3 x 10^{-5} ft/sec (1.0 x 10^{-4} and 1.0 x 10^{-3} cm/sec).

Additionally, in-situ rising-head permeability tests were performed in five standpipe piezometers installed in core holes drilled through the CDSM walls. In-situ permeabilities ranged between 5.9 x 10^{-10} and 1.3 x 10^{-8} ft/sec (1.8 x 10^{-8} and 3.9 x 10^{-7} cm/sec), slightly lower than the laboratory permeabilities. These results suggest that lower in-situ permeabilities may be due to sample disturbance from core retrieval and handling, rather than from cracking or poor continuity of the soil-cement itself. Microcracks may develop in cores due to factors such as bend in the borehole, rigidity of the sampler, locking of the sampler, and rotation of the core within the sampler (Porbaha and Dimillio, 2004).

Figs. 9a and 9b show the effects of water-cement ratio on the strength and permeability, respectively, of the soil-cement cores. Results indicate that water-cement ratio was critical in achieving the target 120 psi (827 kPa) strength and significantly influenced the permeability of the shoring walls. The vast majority of cores tested from the 250% water-cement ratio mix failed to meet the target strength.

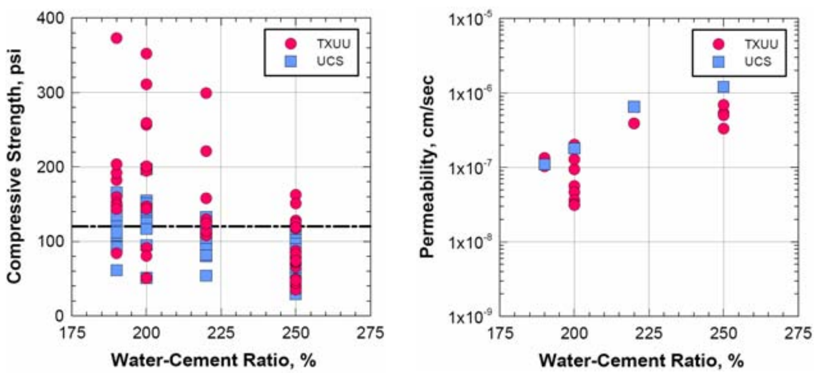

Fig. 9. Variations in a) compressive strength and b) permeability with water-cement ratio

CONCLUSIONS

Based on the results of the prototype test program for the Transbay Transit Center (TTC) project the following conclusions can be drawn:

1. The triple-auger system was able to treat soils at the test site to a depth of 150 ft (45.7 m) without pre-treatment. This finding eliminated uncertainty with regard to penetration difficulties, and provided valuable information about cost and production rates. Even under the test conditions, it was possible to achieve production rates of up to 25 lf (7.6 lm) per shift.
2. The results of coring at six panel locations showed that the requirements

for strength, permeability, and uniformity of mixing could be met. However, in order to meet the strength requirements for a 120 psi (827 kPa) compressive strength, water-cement ratios would have to be kept at, or below, 200%.

3. The program involved placement of six soldier piles consisting of wide-flange W24 and W27 sections into the soil-cement, immediately after completion of selected panels. Based on the difficulties encountered with soldier pile installations, it was concluded that either the size of the soldier piles would have to be reduced to W21 wide-flange sections or the diameter of the augers be increased from 36 to 42 in (914 to 1067 mm).
4. The results of vertical permeability tests on core samples and wet grab samples indicate permeabilities which are 2.5 to 5 times higher than in-situ horizontal permeability tests performed in the depth interval corresponding to the Colma Sand layer.

ACKNOWLEDGEMENTS

Drawings were provided courtesy of the Transbay Joint Powers Authority (TJPA). The authors would like express their gratitude to the TJPA, Raito, Inc., and their colleagues at Arup Geotechnics in San Francisco for their efforts on this project.

REFERENCES

Andromalos, K. B., and Bahner, E. W. (2003). "The Application of Various Deep Mixing Methods for Excavation Support Systems." *Grouting and Ground Treatment*, ASCE, GSP No. 120, pp. 515–526.

Filz, G. M., et al. (2005). “Standardized Definitions and Laboratory Procedures for Soil-Cement Specimens Applicable to the Wet Method of Deep Mixing.” *Innovations in Grouting and Soil Improvement,* ASCE, GSP No. 136.

O’Rourke, T. D., and McGinn, A. J. (2006). “Lessons Learned for Ground Movements and Soil Stabilization from the Boston Central Artery.” *Journal of Geotechnical and Geoenvironmental Engineering*, ASCE, Vol. 132, No. 8, pp. 966–989.

Porbaha, A. and Dimillio, A. (2004). “Engineering Tools for Design of Embankments on Deep Mixed Foundation Systems.” *GeoSupport 2004*, ASCE, GSP No. 124, pp. 850–861.

Taki, O. (2003). “Strength Properties of Soil Cement Produced by Deep Mixing.” *Grouting and Ground Treatment*, ASCE, GSP No. 120, pp. 646–657.

Cutter Soil Mixing Excavation and Shoring in Seattle's Pioneer Square District

Doug Lindquist[1], Ben Upsall[1], and Garry Horvitz[1]

[1]Hart Crowser, 1700 Westlake Avenue North, Suite 200, Seattle, WA 98109; 206-324-9530; Doug.Lindquist@hartcrowser.com, Ben.Upsall@hartcrowser.com, Garry.Horvitz@hartcrowser.com

ABSTRACT

In order to make a 13.1 m (43 ft) deep excavation, a 20.7 m (68 ft) Cutter Soil Mixing (CSM) groundwater cutoff shoring system was constructed in Seattle. The wall alignment was pre-trenched to remove obstructions and the wall was constructed using cement-bentonite slurry technology. The lower aquifer was depressurized to stabilize the base of the excavation while the upper aquifer was monitored closely for unexpected drawdown, which could result in unacceptable settlement of adjacent structures. Underpinning micropiles were installed below the perimeter footing of an adjacent 8-story building. The southern portion of the new building is supported on drilled shafts where the site's triangular shape made excavation less efficient. Permanent tie-downs were installed to resist hydrostatic uplift forces after the dewatering wells are shut off because the water pressure on the base of the foundation is greater than the building's weight.

INTRODUCTION

This paper presents a case history of the shoring system for the 505 First Avenue Building using Cutter Soil Mixing (CSM) technology in Seattle's historic Pioneer Square district. CSM is a relatively new technology developed in 2003-2004 by combining the technology from two European firms, Soletanche Bachy and Bauer (Mathieu et al. 2006). This shoring system was selected for an excavation 13.1 m (43 ft) below the ground surface and 11 m (36 ft) below the groundwater table. Challenging subsurface conditions included very soft soil containing wood debris, abandoned timber piling, and numerous other obstructions. Also, a lower aquifer required depressurization to avoid blowout of the excavation base.

There have been a number of excavations performed to depths greater than 25 m (82 ft) in downtown Seattle using soldier pile and tieback shoring methods with timber lagging, and numerous excavations performed to shallower depths using soil nail shoring methods. This project, however, is located south of downtown Seattle on a portion of reclaimed land where buildings are typically constructed with no more than one level below grade because of the high groundwater table.

The site also had challenges: the new structure required anchoring to the subgrade soils to counteract hydrostatic uplift pressure on its foundation, an adjacent 8-story building required underpinning, new tiebacks had to be installed between and through the adjacent building's existing piles and the presence of a nearby pile supported on-ramp to the settlement-sensitive Alaskan Way Viaduct. A discussion of each challenge and its solution is addressed in this paper along with a description of the shoring system's performance.

SITE AND SUBSURFACE CONDITIONS

Site. The site is located in an area south of downtown Seattle that has been reclaimed from Elliott Bay as part of multiple historical regrading projects. The property was initially developed as a wharf on pilings for timber mill-related businesses. Fill material was deposited in the late 1880s and early 1890s and included sawdust from adjacent sawmills, wood planks and pilings, ship ballast, and burn debris from the Great Seattle Fire of 1889. Figure 1 shows the site's proximity to the historical shoreline and low tide.

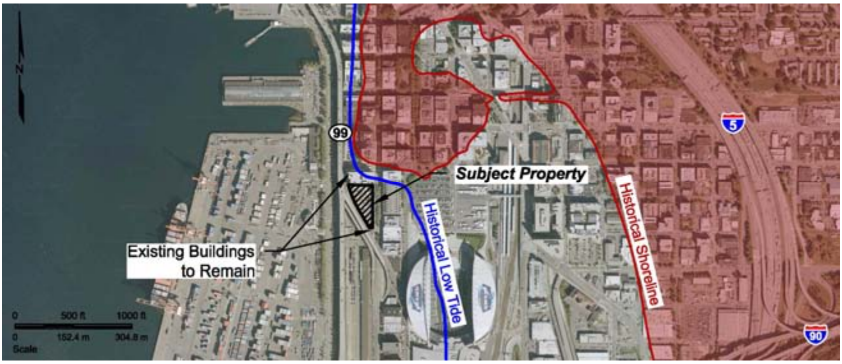

Figure 1. Vicinity Map Illustrating Historical Shoreline

The project site is bounded to the south by the historic, 3-story Triangle Pub building and to the north by the 8-story 83 King Street building (Figure 2). Three structures were demolished prior to site development; two historic building facades were preserved. The historic west facade was removed and rebuilt in kind, while the east façade was stabilized and kept in place during construction.

Soil. Subsurface conditions were based on 12 geotechnical borings extending into the bearing layer and two test pits performed within the fill. The soil conditions were generalized as 7.3 to 10.4 m (24 to 34 ft) of fill consisting of an upper crust of silty sand over wood debris, brick, silt and sand (upper aquifer) over marine silts and sands (historical beach deposits), over dense silts and silty sands (aquitard) over outwash sands (lower aquifer).

Groundwater. Groundwater conditions were evaluated based on seven shallow wells and two deep wells. Prior to construction, the lower and upper aquifers had piezometric head depths averaging 1.3 m (4.2 ft) and 2.3 m (7.5 ft) below the ground surface, respectively (i.e., the lower aquifer was under pressure).

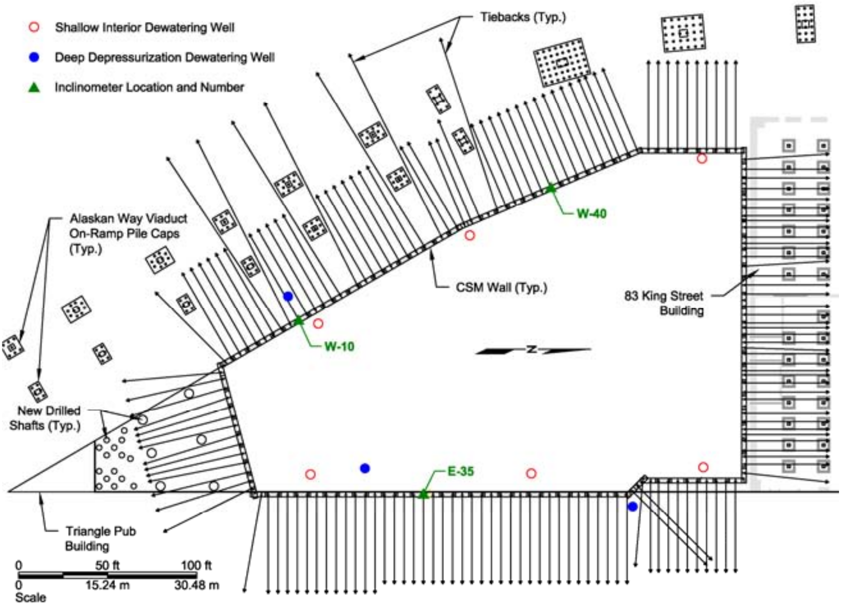

Figure 2. Site Plan Illustrating Tieback Layout

CSM SHORING SYSTEM AND CONTRACTOR SELECTION

At the time of design, secant piles and ground freezing were the primary methods of shoring below the water table in Seattle. To coordinate details of the shoring system, underpinning, and dewatering these options were submitted to local shoring contractors to develop costs and select a shoring contractor early in the design process. The secant pile system was less costly than the soil freeze system; however, the estimates excluded the cost of delays for obstructions, which were known to exist. The contractor was selected for their alternate design-build approach consisting of cement-bentonite slurry pre-trenching and CSM cutoff wall (Parmantier and Giwosky 2009). This alternative was selected because the pre-trenching would remove the obstructions and potential delay costs. The CSM shoring system was considered superior to a secant pile wall system because of the reduced number of joints in CSM panels compared to overlapping secant piles (Brunner et al. 2006).

The contractor performed cement-bentonite slurry pre-trenching with an excavator to a depth of 10.4 m (34 ft) to remove wood debris. The CSM shoring consisted of 108 overlapping panels 0.8 m thick by 2.8 m wide (2.6 ft by 9.2 ft) installed to a depth of 20.7 m (68 ft) around the 263 m (861 ft) site perimeter. While the cement/grout was still wet, soldier piles were placed through the panels on 1.7 m (5.4 ft) centers to a depth of 18.3 m (60 ft). During excavation, the panels were chipped away to expose the soldier piles and tiebacks were installed through sockets within the soldier piles. The overlapping CSM panels created a virtually water-tight shoring system.

DESIGN AND CONSTRUCTION CHALLENGES

Some of the design and construction challenges on this project are described here.

Design Earth Pressures. The challenging subsurface conditions described previously led to the unique pre-trenching and CSM shoring. The design earth pressure diagram used to develop the tieback layout for the CSM shoring system is shown in Figure 3 along with a schematic of the soil profile.

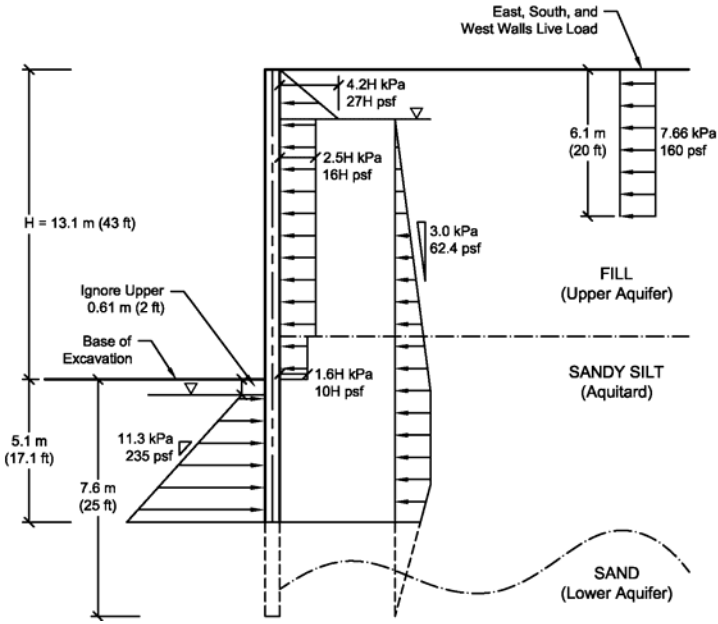

Figure 3. Design Earth Pressure Diagram and Soil Profile

Dewatering and Cutoff Wall. The project required the excavation to extend 11 m (36 ft) below the static water table with limited drawdown allowed in the upper aquifer. The designers estimated that a drawdown of the lower aquifer of approximately 12.5 m (41 ft) would be required to avoid blowing out the base of the excavation and that a maximum drawdown of 1.5 m (5 ft) of the upper aquifer would be acceptable to avoid settlement of adjacent structures. Recharging the upper aquifer from the dewatering wells was considered in case the low permeability aquitard was found to be discontinuous during construction dewatering.

Excavated soils had to be dewatered to facilitate transport off site. Six shallow interior wells were installed in the upper aquifer to dewater the excavated soils and two deep dewatering wells were installed outside of the site to depressurize the deep aquifer (Figure 2). One deep well was located interior to the site but was decommissioned early in construction because it was obstructing the excavation. Dewatering monitoring results are described in the Construction Monitoring section.

Hydrostatic Uplift Pressure. Upon recharge of the lower aquifer, the building, which was designed to be essentially water-tight, has an unbalanced hydrostatic uplift force in excess of the building weight acting on the foundation. This required the installation of 360 tiedown micropiles to hold the building in place.

Adjacent Structures. The adjacent 8-story 83 King Street building required micropile underpinning of its perimeter footing to replace existing pile support that encroached on the subject property. Piles located below the 83 King Street building and the Alaskan Way Viaduct on-ramp required accurate installation of tiebacks around existing timber foundations (Figure 2). The nearby on-ramp required tiebacks as long as 41 m (135 ft) to limit changes in soil stress near those piles.

CONSTRUCTION MONITORING

Construction monitoring is critical to verify that below ground construction and conditions conform to the design assumptions and that the performance is as anticipated. Site monitoring included measurement of site movement (i.e., inclinometers and optical surveys) and groundwater levels within the two aquifers. Quality assurance and quality control of the CSM wall included visual inspection of the panels during excavation as well as strength testing of the CSM soil-cement mix.

Inclinometers. Three inclinometers were used to measure the lateral displacement of the CSM shoring system. The inclinometers were installed on three soldier piles at the locations shown on Figure 2. Deflection readings are shown on Figure 4, with positive deflection indicating movement into the excavation. The results indicate initial movements into the excavation followed by movements back into the soil after the top row of tiebacks were stressed. Upon further excavation, the movement went back toward the excavation. In general, these lateral movements were less than 25 mm (1 in) in either direction and were considered acceptable.

Optical Monitoring. The optical monitoring plan consisted of over 200 survey points located near the top of every other soldier pile, on the buildings adjacent to the site, on the sidewalk next to the excavation, in the street, and on the adjacent Alaskan Way Viaduct on-ramp columns. The largest recorded lateral movement was approximately 4 cm (1.5 in) of movement into the soil on a pile located on the west side of the excavation. When lateral deflections of greater than about 25 mm (1 in) into the excavation were observed for any given monitoring point, the project team discussed the exceedance, visually inspected the shoring and adjacent CSM panels, and continued to monitor those deflections very closely. Deflections larger than about 50 mm (2 in) or visual signs of CSM panel or shoring system distress would likely have called for a more thorough review accompanied by corrective actions such as installation of whaler beams with additional tiebacks. There was negligible movement of many points including those on the pile-supported Alaskan Way Viaduct on-ramp columns.

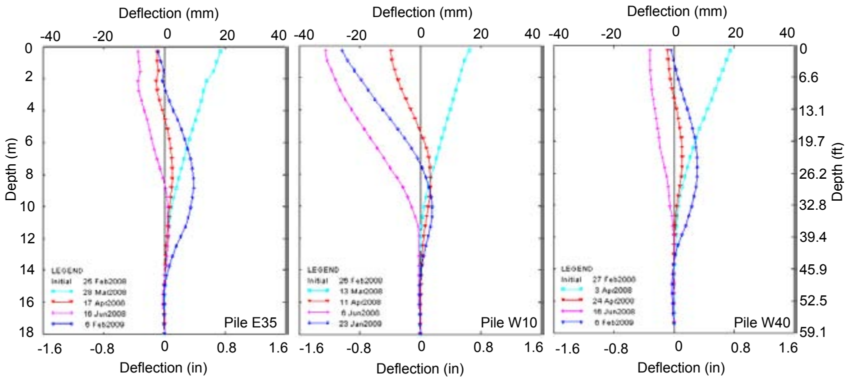

Figure 4. Inclinometer Results

Visual Inspection of CSM Panels. During excavation the condition of the CSM wall was observed visually and probed with a 13 mm (0.5 in) diameter T-probe to identify cracks, seeps, and voids or pockets of weaker-strength materials. Tieback pockets, seeps and cracks were generally filled with expanding epoxy material. The largest voids and pockets of weaker-strength material were encapsulated with a steel plate spanning between adjacent soldier piles and then backfilled. In general, the CSM wall had increased quality and consistency with depth.

CSM Strength Testing. The design called for 1.4 MPa (200 psi) 28-day compressive strength of the CSM panels. Wet samples were collected from the panels following installation for laboratory testing. Approximately 95 percent of the samples exceeded the design strength. Low strength test results required one of the CSM panels to have additional grouting on the outside of the wall to improve performance in that area.

Groundwater Monitoring. Groundwater monitoring was performed beginning 8 months prior to the start of depressurization of the deep aquifer, which began in February 2008, until the dewatering system was shut off in September 2009 following construction of the building to its full height and placement of exterior brick cladding. Monitoring was observed using two deep wells within the lower aquifer and seven shallow wells within the upper aquifer. Steady state pumping of 75 lpm (20 gpm) at the site resulted in a depressurization of approximately 16 m (52 ft) of water in the lower aquifer while the upper aquifer showed only 0.3 to 0.7 m (1 to 2 ft) of variation in the 7 monitoring wells, which was well within the criteria of 1.5 m (5 ft) established during design to minimize impacts to adjacent structures and utilities. Figure 5 illustrates the monitoring well data including the depressurization and recharge of the deep aquifer.

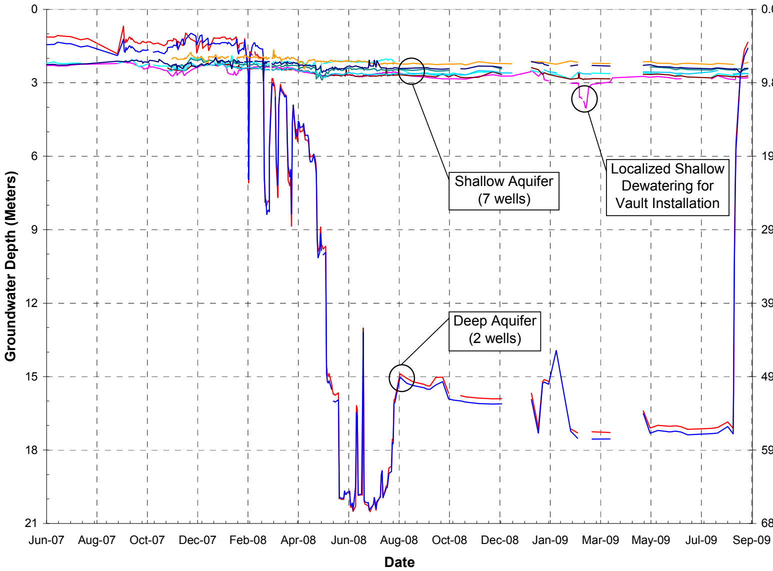

Figure 5. Dewatering Performance as Illustrated by Monitoring Wells

DISCUSSION ON LATERAL SHORING MOVEMENTS

The largest lateral movement of the shoring system was into the soil, which is not common. This is attributable to the shoring designer using total anchor design loads approximately 25 percent higher than would be inferred from the design earth pressure diagram to control intermediate stages of construction with only three tieback rows (Parmantier et al. 2009). Portions of the fill (e.g., the wood debris) also likely had a lower earth pressure than assumed in design.

SHORING CONSTRUCTION COSTS

The project consisted of approximately 11,300 m^2 (37,000 ft^2) of exposed shoring wall. The shoring contractor's design and construction costs (e.g., CSM design and installation, soldier piles, tiebacks, dewatering, micropile underpinning of north wall, facade support, etc.) were approximately \$8.5 million, or \$750/m^2 (\$230/ft^2). These were the contractor's costs and do not include the owner's design team, who were the designers of record with the city and provided design and construction support.

CONCLUSIONS

This paper presents a case history of the successful use of CSM technology to perform a 13.1 m (43 ft) deep excavation in an area with a high water table and challenging subsurface conditions. It also demonstrates the value of retaining a specialty shoring contractor early in the design process for a unique excavation solution. The contractor-proposed pre-trenching and CSM shoring performed well and reduced risk for obstruction-related delays compared to secant pile shoring methods used in Seattle in these difficult soils. Figure 6 is a picture of the project site near the end of excavation including the temporarily supported historic east facade.

Figure 6. Photo Looking North Following Final Tieback Row Installation

REFERENCES

Brunner, W.G., Fiorotto, R., Stötzer, E., and Schöpf, M. (2006). "The Innovative CSM-Cutter Soil Mixing for Constructing Retaining and Cut-Off Walls." *GeoCongress 2006 - Geotechnical Engineering in the Information Technology Age*, ASCE.

Mathieu, F, Borel, S., and Lefebvre, L. (2006). "CSM: An Innovative Solution for Mixed-In-Situ Retaining Walls, Cut-Off Walls and Soil Improvement." *10th International Conference on Piling and Deep Foundations*, DFI/EFFC.

Parmantier, D. and Giwosky, D. (2009). "Cutter Soil Mixing Comes to Seattle." *Foundation Drilling*, ADSC, February 2009, 21-31.

Parmantier, D.M., Stow, R.F.P., and Byrne, R.J. (2009). "Case Study: Cement-Bentonite Pre-Trenching and Cutter Soil Mixing (CSM) for Temporary Shoring and Groundwater Cutoff." *Contemporary Topics in Ground Modification, Problem Soils, and Geo-Support*, ASCE, GSP 187, 153-160.

CUTTER SOIL MIXED WALL
SHORING AND SEEPAGE CUT OFF
OFFICE BUILDING NEAR WATERFRONT

By
John Kvinsland – Malcolm Drilling Company, Kent, Washington
Bob Plum – ASCE, P.E., Principal Kleinfelder Consultants, Redmond, Washington

ABSTRACT:
This paper will present several aspects of the soil mixed CSM wall installed as part of an office building project completed in 2009 near the Seattle waterfront in an area underlain by fill and loose beach deposits with a shallow groundwater. The project involved construction of a 5-story office building with below grade parking that extends below the groundwater table. Constraints included an adjacent dry cleaner with a groundwater contamination plume, an adjacent railroad track, adjacent main arterial, loose liquefiable soils, and significant long term costs associated with discharging groundwater into the City storm drain system. A perimeter Cutter Soil Mixed Wall (CSM) was proposed by the contractor and selected. The CSM wall acted as a temporary shoring wall, a temporary seepage cutoff wall and a permanent seepage cutoff wall. The paper presents the basis for the wall design, and a description of various construction aspects including the CSM wall installation, tiebacks and dewatering. Field testing, instrumentation and laboratory testing results are described that provided critical data on wall permeability, dewatering effectiveness, wall deformation, and other aspects of the performance.

INTRODUCTION
The project site is located off of Elliot Avenue just north of the Seattle CBD near Elliot Bay. The area was at one time near the general location of the old Elliott Bay shoreline with much of the site originally below water. Over the years the area had been filled in such that the shoreline is now located 90 to 120 m (300 to 400 feet) to the west of the project site. At one time the site included a saw mill such that encountering wood debris was a potential issue. The project includes two five-story commercial office buildings, a plaza area, and two levels of below grade parking underlying the entire complex. The lowest parking level slab is at elevation +0.6 m (+2 feet) or some 3.3 to 6 m (11 to 19 feet) below the pre-construction site grades. During construction, deeper temporary excavations were required to install pile caps. Main line RR tracks are located just to the west of the site, a main City street arterial is located just to the east with a Dry Cleaners located to the north of the site.

The site is underlain by about 6 to 11 m (20 to 35 feet) of fill and loose beach deposits over a stiff, glacially over-consolidated clay unit as shown on the idealized cross-section in Figure 1. The fill was variable but generally consisted of loose to medium dense silty sands with wood debris. The beach deposits ranged from loose clean sands to loose sandy silt. The underlying stiff clay thickness generally ranges from about 4.6 to 7.6 m (15 to 25 feet). An older glacial sequence underlies the clay consisting of a very dense till-like deposit and very dense sandy silt overlying a very dense sand and gravel that extended beyond the depth of the borings at about 90 feet. Pre-construction groundwater was measured at an elevation of about 3.7 m (12 feet). Thus, the lowest parking garage level at an elevation of +0.6 m (+2 feet) was about 3 m (10 feet) below the original pre-construction groundwater levels. The Dry

Cleaners located just to the north of the site has a known groundwater contamination plume of chlorinated hydrocarbons that is spreading generally to the west. The chlorinated hydrocarbons were known to occur in the northern third of the new office building site adjacent to the Dry Cleaners. In addition, petroleum based hydrocarbons were located in the north east corner. These contaminants were a concern since they could interfere with the ability of soilcrete to develop the required strength and permeability properties.

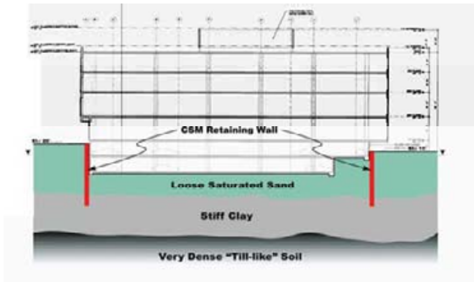

Figure 1. Generalized Soil Conditions

Based on the engineering and cost evaluations, the project design included an auger cast pile foundation; a perimeter Cutter Soil Mixed Wall (CSM) which functioned as temporary shoring and a temporary\permanent groundwater cut-off wall; vertical steel H beams and tiebacks installed as part of the CSM wall providing structural integrity; and a permanent underdrain system inside the CSM wall and below the slab. Liquefaction risks were considered in the overall design. Although the perimeter CSM walls were designed for hydrostatic pressures, the slab was not since it was isolated from the outside water pressures by the CSM wall penetrating into the underlying clays. The CSM wall isolated the effects of the excavation on the groundwater and the adjacent Dry Cleaner's contamination plume. To improve construction conditions, it was decided to install a temporary dewatering system consisting of wells and well points inside the excavation. The intent was to dewater the soils to a depth of about 4 feet below the construction excavation levels. The dewatering system was installed and operated before the excavation reached the original groundwater levels.

WALL SELECTION AND DESIGN

There were numerous issues relating to the selection of the perimeter foundation wall type including impacts on the adjacent Dry Cleaner's contamination plume, long term underdrain flow rates, hydrostatic pressures on the walls and slab, construction risks, and cost. The owner's strong preference was a system which would have minimal impacts on the Dry Cleaner's contamination plume. The City of Seattle charges a substantial fee for disposing of underdrain flows into the City sewer system which would be imposed over the entire life of the building. Thus the owner had a strong desire to limit the flows, both during and following construction. Due to the size of the building, designing the lower slab to resist hydrostatic uplift would have added significant costs to the project. Based on these and other considerations, the design decision was to take advantage of the site geology which allowed the below grade perimeter wall to penetrate into the underlying clay unit to form an effective seepage cut-off. This significantly reduced both construction and long term groundwater inflows and allowed the lower slab to be designed with underdrains to eliminate any uplift pressures. Both a drilled concrete secant pile wall and a CSM wall were initially considered with the CSM wall selected due to costs and schedule. It is estimated that using the CSM wall saved two months and a million dollars compared with the more conventional secant pile wall. The main disadvantages of the CSM wall were the risks of encountering major obstructions and the risk of encountering contamination that would adversely impact the soilcrete strengths. Neither concern was a major issue during construction. The permanent below grade earthpressures were supported with the permanent wall poured up against the CSM wall and braced with the building floors.

Unlike conventional slurry walls and diaphragm walls that utilize concrete, soil mixing relies on mixing the soils in situ with a cement and bentonite slurry to create a soil-cement wall. Cutter Soil Mixing technology utilizes two sets of vertically mounted cutting wheels rotating about a horizontal axis to produce rectangular panels of treated soil as shown on Figure 2. By overlapping the soil mix panels, a continuous rectangular wall is constructed, as opposed to circular columns created with conventional single-axis or multiple axes deep soil mixing systems. Upon completion of an individual panel, two 460 mm (18 inch) wide flange beams are inserted into the wet “concrete like” soil cement material to provide structural strength to the non-permeable mix. Later, following excavation of the interior of the foundation, tieback anchors can be installed to further increase the shoring capacity of the CSM cutoff wall.

Figure 2. CSM Cutting Head

Figure 3. Completed CSM Wall

The CSM wall had to provide two critical functions: 1) be an effective temporary/permanent cut-off wall; and, 2) support the temporary excavation earth pressures. This is unusual since the CSM wall can normally be optimized for either strength or low permeability depending on its function. For this project, the soilcrete properties had to meet both criteria. The cut-off wall function was satisfied by extending the wall at least 2.3 m (7.5 feet) into the underlying clay, constructing tight joints between the CSM panels, and developing a soilcrete mix that had a low permeability. The achievable 28-day soilcrete strength at this site was in the range of 690 to 2,000 kPa (100 to 300 psi). At this relatively low strength, the soilcrete could not provide the necessary structural integrity to support the earth pressures. Thus, the wall design included vertical H beams installed in the CSM wall at about 1.07 m (3.5 foot) centers as shown on Figure 3. Due to easement constraints on the west site, the west side excavation next to the RR included a lower cut slope section to reduce the wall height such that the wall functioned as a cantilever wall. On the other sides of the building footprint, the excavations were deeper and one row of tiebacks was installed to provide lateral support. Structurally, the loads were resisted by the steel beams and tiebacks with the soilcrete functioning as the lagging. In some areas, the hole drilled through the wall to install the tieback was below the groundwater table. Installing the tieback below the water table turned out not to cause a significant leakage issue as there was minimal loss of ground and seepage during installation and after installation, the holes were effectively plugged by non shrink grout. In a handful of cases, minor leakage occurred which was sealed by injecting semi-rigid injection grout.

The nominal minimal acceptable long term leakage for the entire below grade area was selected by the owner and design team as 64 liters/minute (17 gpm). A series of calculations were made to estimate the required clay and wall permeability to meet the 64 liters/minute (17 gpm) criteria. The calculations indicated that the majority of the inflow would be through the wall with the wall needing to have a gross overall average permeability less than about 5 x 10^{-6} cm/sec with an assumed maximum permeability of the underlying clay of 10^{-6} cm/sec. It was felt that much of the flow through the wall might be due to leaks at joints, cracks and/or areas of poor quality soilcrete. Accordingly, it was required that the soilcrete samples obtained a laboratory permeability less than 10^{-6} cm/sec and all identified leaks in the wall had to be sealed, even if the flows were small.

The owner did not want any actual seepage, wet areas or wall seepage discoloration within the below grade space. Even with the low expected seepage rates, it was felt that the owner's requirement would likely not be met by the CSM and permanent walls alone. Thus, a geosynthetic drainage mat was installed between the CSM wall and the adjacent permanent wall. Any drainage mat flow will drain down the mat into a perimeter underdrain pipe. Even though the flows are low, a watertight slab will eventually develop full hydrostatic uplift pressures. According, a full slab underdrain system consisting of a drainage layer with perforated pipes was installed below the slab. This collects the long term seepage flowing up through the clay and eliminates any seepage pressures on the slab. All of the underdrains flow into sumps under the slab with the water pumped out of the building into the City's sewer system.

CSM WALL DESIGN AND INSTALLATION ISSUES

Cutter Soil Mixing (CSM) was selected as the method of choice based on price and schedule relative to a Secant Pile wall. The decision was also based on the CSM's ability to construct a permanent, high quality soil-cement wall even in the gravels and stiff plastic clays, its capacity to key into the glacial till, and its ability to produce a soil-cement material with a minimum strength of 690 kPa ((100 psi) and a maximum permeability of 5 x 10-6 cm/sec.

Initial concerns related to several issues. It was known and anticipated that Chlorinated Hydrocarbons existed throughout the northern third of the site. In addition, petroleum based hydrocarbons were located in the north east corner. It was uncertain how the injected grout recipe would react with these contaminants and how it would impact permeability and compressive strengths. Another concern was the ability to develop a mix design that was able to meet the performance specifications in three completely different soil conditions. Lastly, it was uncertain how the cutter head would perform when encountering buried obstructions such as driven wooden piles which were prevalent in this area of Seattle at the turn of the century.

Given the concerns mentioned above, an intensive test program was undertaken before wall production installation to help identify site hazards and at the same time develop a mix recipe that would meet the specified criteria in every potential environment. A secondary exploration program was undertaken by the contractor to identify locations of existing wood piles and the occurrence of any buried rip-rap that might have been part of an old sea wall. The sampling also obtained more information on the occurrence and composition of contaminants. Once the samples were obtained, the contractor developed three separate mix designs which were used to construct three test panels. Cement was the primary component in the mix with bentonite making up only 7.5% of the cementitious. When the results for the various tests were provided by the independent testing firm, the results were better than anticipated. It was determined that the chlorinated hydro-carbons essentially burned off during the hydration of the sample. Testing of soilcrete mixed with high levels of petroleum hydrocarbon contaminated soils indicated unacceptably low strengths. It was later determined that the single phase mixing process diluted the limited zones of high contamination to a point where it has minimal effect if any on the mix. With the various ground conditions at the site, a single phase system was utilized to insure a homogenous product.

Based on the experience gained on this project, it was concluded that the CSM method dealt well with obstructions. Unlike a drill that cuts in one direction such as in conventional DSM installations, the cutter wheels run on independent drives and are capable of being steered. This aspect proved invaluable, for the operator was able to adjust the speed of the cutter wheels via the variable speed controls and essentially manipulate the pressure applied on the obstruction. For the most part, underground piles were reduced to splinters which floated to the top of the mix where it was pumped to the spoils pile. Due to the size of the cutter, hard obstructions such as cobbles were able to be moved to the surface. Thus obstructions were not a significant issue and only tended to marginally slow progress in some areas. Had boulders or old concrete blocks over about 3 feet been encountered, the CSM might have been stopped requiring that the boulder was broken up. However, these conditions were not encountered.

INSTALLATION CONTROLS

The CSM installation equipment includes a computer control and recording system. The touch screen computer system allows the rig operator to monitor and control the position of the cutter head to within tenths of an inch, independently control the cutter wheels, and monitor grout and hydraulic pressures. The data from each panel and corresponding batch of grout was stored on memory cards which were then transferred to a laptop computer allowing software to create graphical logs of each panel. These logs were submitted to the project team on a daily basis, providing real time quality control and assurance. During panel installation, the real time data enabled the operator to make on-the-fly corrections to account for obstructions and changes in soil types. In cases where obstructions caused significant positional deviations, the contractor was able to determine immediately whether re-digging the panel to achieve proper position and overlap was required since vertical tolerances were critical.

The computer installation data, which was provided to the engineers, proved to be helpful to the QC/QA monitoring of the installation.

TESTING

Based on the design, the main CSM criteria were that the QC/QA testing demonstrates a minimum 28-day strength of 690 kPa (100 psi) and have a permeability less than 10-6 cm/sec.

QC/QA field and laboratory testing were performed throughout the wall installation process. In general, this involved taking samples of the soilcrete mix (referred to as wet samples) and completing laboratory strength and permeability testing. Initially attempts were made to obtain in-situ samples from the wall after the soilcrete had cured. These attempts were unsuccessful even though several drilling methods were tried including coring. It was concluded that the high gravel content of the soilcrete was making the in-situ sampling impractical. In general, seven wet samples were taken for material being installed when the panel was at 2.7 and 7.6 m (9 and 25 feet) for one out of every four panels which included back-up samples. Laboratory testing included unconfined compressive strength testing and flexible wall permeameter testing. The strength testing included samples tested at 5 days, 7 days, 14 days and 28 days.

Initially, the strength test results were erratic with many of the results less than the requirements. It was determined that the samples were often being transported to the laboratory with too little field curing time and the method of transportation was not protecting the samples from vibration and disturbance. It was apparent that the samples were very sensitive and easily disturbed early in the curing process. Subsequently, all samples were transported on 3 inches of soft foam only after they had cured for at least 2 to 4 days. This transportation procedure resulted in higher, more consistent results that met the strength criteria. On site vibration monitoring indicated that the installed CSM wall was exposed to minimal vibration levels felt to be well below harmful levels.

More than half of the permeability results were below the 10-6 cm/sec criteria with many of the results being below 10-7 cm/sec. Less than half exceeded 10-6 cm/sec but very few exceeded 5 10-6 cm/sec. The average result was below the criteria. As the excavation proceeded and the wall exposed, minor leakage was identified generally at joints and cracks. These leaks had been anticipated and the contractor was prepared to seal the leaks using water activated foam. Once identified, the contractor was able to seal the leaks and essentially eliminate known leaks. Leaks that may have developed below the base of the cut could not be observed and were not repaired unless identified above the cut and "chased" below the cut level.

In addition to the testing and leak repair, observation wells monitoring the water levels in the granular formations above the clay were installed outside of the excavation near the wall. These were installed to demonstrate that the excavation had no measurable impact on the groundwater levels outside of the excavation. Although the monitoring would not identify minor leaks, any major leaks would have lowered the water levels next to the wall. None of the exterior wells measurements indicated wall leakage.

TIEBACK INSTALLATION ISSUES

The tiebacks were installed using air pressure which resulted in water being evacuated from the nearby observation wells during the installation process. Concurrently with the tieback installation, ground cracks and settlement were observed near the excavation which extended to the adjacent arterial street on the east side of the project. The maximum settlement of about 1 to 3 inches was measured at the curb line. Settlements occurred quickly and the area stabilized after the tiebacks were installed though an area. Fortunately, the City was about to grind and repave the road such that the settlement impacts were minimal. The City did require that the curb was replaced and any voids below the pavement filled.

It was theorized that the settlement was caused by the installation of the tiebacks, specifically the air and water pressure used to advance the tieback hole. These pressures may have induced localized liquefaction of the loose soils below the water table and above the stiff clays. Although the significance is not known, it was felt that the CSM wall, which acts as an underground dam, likely increased the impacts of the installation pressures as the pressures could not dissipate towards the inside of the excavation.

The settlement problems likely would have been minimized had a drilling method been used that did not require high pressure air.

WALL PERFORMANCE

To date, the cut-off wall performance has been excellent with the actual inflows generally less than 4 liters/minute (1 gpm) once the permanent slab and underdrains were installed. This is less than the design goal of 65 liters/minute (17 gpm) and indicates that the effective wall permeability is quite low. Using the 4 liters/minute (1 gpm) as a leakage value, the likely macro permeability of the underlying clay is on the order of 10-7 cm/sec with an effective wall permeability on the order of 4 x 10-7 cm/sec. The low rates also indicate that sealing the leaks at the tieback holes and wall cracks were successful. Virtually all of the wall leaks occurred at the panel joints with the worst leakage problems occurring in the area of the one re-entrant corner along the wall. A re-entrant corner develops minimal compression or even tension loads at the corner.

The temporary wall performed well with deflections similar to a standard soldier pile and tieback wall. The main performance issue related to the tieback installation procedure using high pressure air which did cause ground cracking and settlement as discussed under Tieback Installation Issues above.

CONCLUSION

Based on the experienced gained on this project, several conclusions can be made relating to the design and use of a CSM wall for both a permanent low permeability cut-off wall and a temporary shoring wall. These include:

- GENERAL CONCLUSION: The CSM wall successfully provided both an effective seepage cut-off and temporary shoring wall. The CSM wall likely achieved an overall large scale permeability of less than 10-6 cm/sec. The CSM process also proved to be robust dealing with obstructions, leaks and variability in the soil conditions.
- CONSTRUCTION DEWATERING: The temporary construction dewatering of the soils above the clay inside the excavation was effective in stabilizing ground, facilitating excavation and providing an adequate subgrade for construction activities.
- LEAKAGE CRACKS: Some leakage at panel joints occurred but was effectively sealed. Other than the tieback holes, the wall leaks appeared to occur at panel joints with a re-entrant corner providing an adverse condition for joint leakage.
- SOILCRETE WET SAMPLE SENSITIVITY: It was found that the wet soilcrete samples were sensitive to movement and vibration until they had time to cure. It is important to establish a procedure for handling and transporting the samples.
- POSSIBLE WALL EFFECTS ON TIEBACK INSTALLATION: As discussed above, the CSM wall, which acts as an underground dam, may have increased the impacts of the installation pressures as the pressures could not dissipate towards the inside of the excavation as it would with a normal soldier pile installation.
- SPOILS CONTROL: On this project a single phase system was utilized meaning that wall was cut with the same mix that was extracted to insure a homogenous product. If the soil conditions had been more uniform, a two phase mix which cuts with Bentonite and water might have been used to cut down on spoil removal and disposal costs by reusing the cutter mix and separating out the solids with de-sanders and de-silters.

Earth Retention Using the TRD Method

Ed Garbin[1], Ph.D., P.E., A. M. ASCE, James Hussin[2], M. ASCE, Chikashi Kami[3]

[1]Chief Engineer, Hayward Baker Inc., 6850 Benjamin Road, Tampa, FL 33634; PH (813) 884-3441; FAX (813) 884-3820; ejgarbin@haywardbaker.com
[2]Director, Hayward Baker Inc., 6850 Benjamin Road, Tampa, FL 33634; PH (813) 884-3441; FAX (813) 884-3820; jdhussin@haywardbaker.com
[3]Chief Civil Engineer Deputy General Manager, Tenox Corporation, 13-7, Akasaka, 6-Chome, Minato-KU, Tokyo, Japan; PH +81 (3) 35825168; FAX +81 (3) 35824714; kami-t@tenox.co.jp.com

ABSTRACT

The Trench Remixing Deep (TRD) method of wall construction is an innovative method of deep soil mixing developed in Japan that employs a tool resembling a "vertical chainsaw" to simultaneously cut and mix soil and grout in place without creating an open trench. Ideally suited for projects requiring a high quality wall or for conditions where typical construction methods would be difficult, TRD has been used to construct earth retention walls with great success.

This paper covers the design and construction of the TRD method to construct high quality earth retention walls.

INTRODUCTION

The TRD method of in-situ wall construction results in a highly uniform vertical wall. The tooling consists of a tracked rig mounted full-depth post equipped with a revolving chain with cutter teeth that chip away the in-situ soil from the trench face while mixing it with binder slurry as the post advances horizontally. Slurry composition varies according to specified wall properties. The slurry consists of water mixed with cementitious binder, typically Portland cement and/or ground granulated blast furnace slag (GGBFS), and clay (typically bentonite) when low permeability is required.

The TRD method has been used in the United States since 2006 and for the past 20 years in Japan, where the technology was developed. Previous use of the TRD method in Japan has been extensive and highly successful (Aoi et al. 1996 and Aoi et al. 1998). The TRD method's unique vertical mixing process results in a high degree of wall uniformity, which is its foremost advantage over other in-situ mixing methods. This quality is demonstrated in this paper with sample data from the extensive quality control (QC) testing program at Herbert Hoover Dike (HHD) at Lake Okeechobee, Florida.

THE TRD CONSTRUCTION PROCESS

Wall continuity and full vertical mixing are the primary differences between TRD and other wall construction techniques. The TRD process is continuous, with a full-depth cutter post that extends to the wall tip elevation. The cutting teeth vertically mix the entire soil profile to a high degree of homogeneity as they revolve around the cutter post, thus eliminating any natural layering that may have been initially present. The TRD machine horizontally advances the cutter post along the wall alignment as it mixes, leaving a wall free of joints (Figure 1).

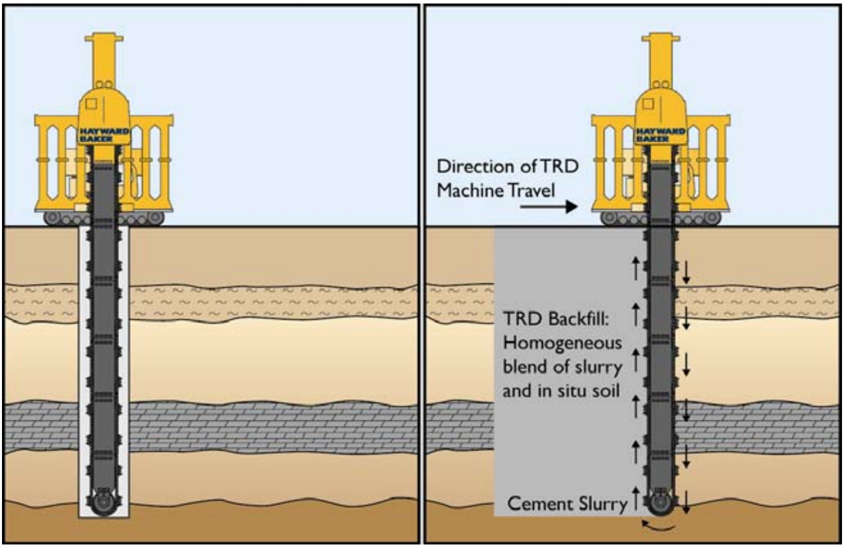

Figure 1. Illustration of the TRD walling method. Post is inserted full-depth (left) and then mixing proceeds horizontally (right).

The TRD method provides a high degree of control over the wall's verticality and positioning, whether at shallow or extreme depths [over 46 m (150 ft)]. The TRD machine is also able to install battered walls at up to 45 degrees from horizontal. It can cut through rock layers having a compressive strength of 20 MPa (~3000 psi) and can key into bedrock having a strength of 70 MPa (~10000 psi). Further, the TRD can cut through boulders up to 1 m in diameter, and has been used to cut through granite. Over the past 20 years in Japan, more than 1,486,448 m² (16,000,000 ft^2) of wall has been constructed to depths as great as 56.7 m (186 ft) (AK Chemical, 2006).

DESIGN

Earth retention systems constructed with the TRD method are designed as soldier pile and lagging walls, with the mixed soil-cement acting as the lagging. Horizontal spacing of the soldier piles is governed by the strength of the soil-cement and the soil and water pressures acting on the wall. In the past, a maximum spacing of about 1.5 m (5 ft) has been used. For permanent wall applications, modified H beams with interlocking flanges have been installed acting as a steel reinforcing cage. If the required depth of excavation is such that predicted wall movements exceed tolerable levels, one or more levels of tieback anchors may be incorporated into the design.

Several limitations inherent in traditional soldier pile and lagging walls are avoided by using the TRD. For example, soil arching between the soldier piles prior to lagging is not a concern with the TRD method, since the entire wall is constructed, full-depth prior to excavation. Where excavation below the water table is not feasible using traditional soldier pile and lagging walls, a TRD wall can be designed with low permeability to prevent inflow, though if the TRD wall is not keyed into an aquiclude, basal stability and flow beneath the wall must be evaluated during the design.

CONSTRUCTION

The wall construction process continuously produces a soil mix wall along a straight or curved line. Structural steel reinforcement is added, typically by inserting steel H beams or a similar steel section in the wet soil mix wall immediately behind the cutter post (Figure 2).

Figure 2. Steel beam being inserted vertically into the wet soil mix wall (left), and tops of soldier piles visible in TRD wall (right).

The post is initially inserted into the ground in sections, much the way that a drill rig advances drill steel (Figure 3).

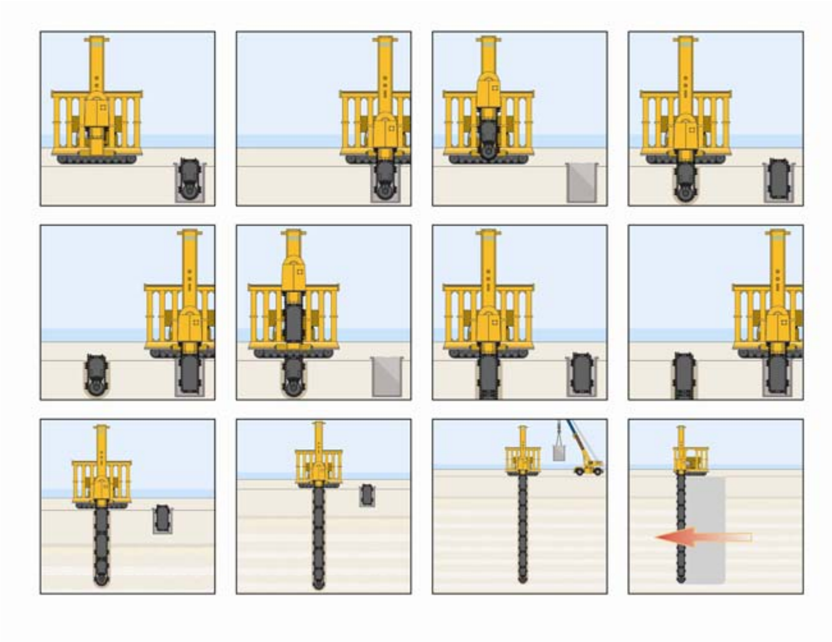

Figure 3. Sequence of initial installation of the cutter post.

After reaching a corner location, the post is removed by disconnecting the top of th post from the post drive unit and then pulling the post, generally in one piece, with a crane (Figure 4) to minimize the removal and reinsertion time.

Figure 4. Removal of cutter post in one section.

The post is laid on the ground and as each segment is unbolted it is reinserted along the next wall alignment as initially installed (Figure 3).

TRD QUALITY CONTROL

Quality control (QC) of TRD constructed walls begins with a pre-construction laboratory mix design program, mixing pre-selected grouts with full depth soil/rock samples. During construction, QC continues with careful monitoring of the grout components and the specific gravity (SG) of the neat grout at the batch plant. This ensures consistency between batches, and helps to achieve the highly uniform wall typical of the TRD method. SG is monitored in real-time using a mass flow sensor mounted on the TRD rig, with the data displayed in the cab and also recorded for later incorporation into QC reports (Figure 5). This same sensor also measures and records the flow rate, volume and temperature of the grout being pumped through the system. It is typical to also verify SG several times each shift using a mud balance, as a check test for the instrumentation.

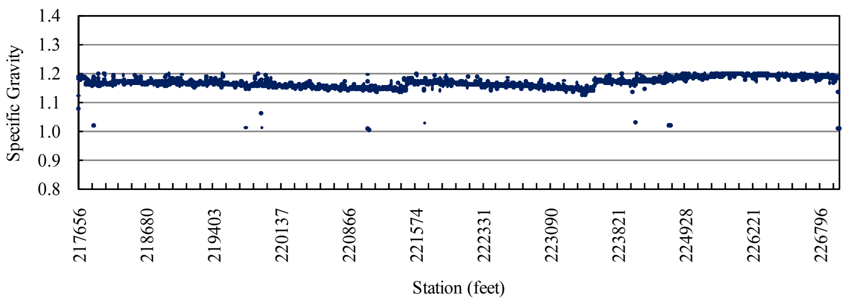

Figure 5. Plot of SG Data from the HHD project

Additionally, the wet soil mix material from the trench is sampled and subjected to flow table testing in order to assess the mix viscosity. Maintaining the flow table value within a certain range ensures proper material flow around the cutter post, which is essential for uniform full-depth mixing. The flow table testing apparatus and sample test results from the HHD project are shown in Figure 6.

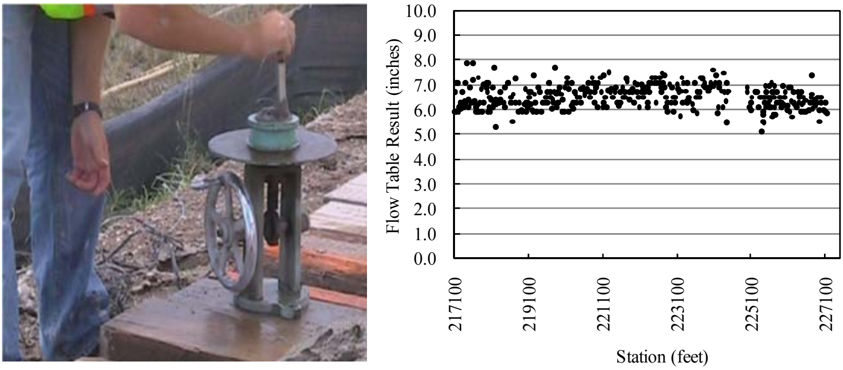

Figure 6. Flow table test apparatus and test results from the HHD project.

Wall verticality is controlled by the operator and monitored in real-time using inclinometers installed inside the TRD cutter post at various elevations. Additionally, the position of the cutter post can be tracked using a differential GPS, as well as with routine surveys using a total station. This inclinometer and GPS data are displayed in the cab and also recorded.

The strength and permeability of the cured soil mix material may be ascertained by testing specimens that have been collected wet and cast into standard cylinder molds. Careful control and monitoring of the grout quality during batching and quantity during mixing with the soil produces a homogeneous wall with the desired properties. (Figures 7).

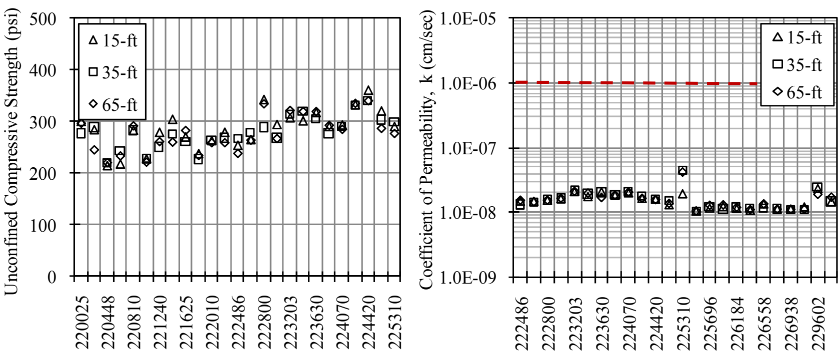

Figure 7. Deep grab sample laboratory strength and permeability test results from the HHD project demonstrates wall homogeneity over depth & length.

In addition, the material may be cored using rotary drilling techniques to retrieve samples for visual inspection, or to allow for the use of a down hole camera. Highly destructive by its nature, coring is not recommended except on a limited basis, as it can adversely impact the integrity of the wall. Where coring has been performed, down hole cameras have verified the high homogeneity and continuity of the TRD-constructed walls with depth (Figure 8).

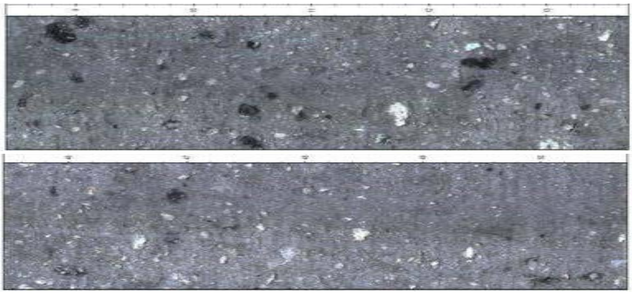

Figure 8. Down hole camera images at depths of 2.4-4.2 m (8-14 ft) [above], and 12.4-15.5 (45-51 ft) [below], from the HHD project, showing evenly distributed rock fragments from the bedrock layer.

PAST PERFORMANCE

Since the early 1990s, approximately 400 projects have been performed using the TRD method. Approximately two thirds have been structural retaining walls and one third were cut off walls. The retaining walls have ranged from 550 mm (21.6 in) to 800 mm (31.5 in) wide and as deep as 56.7 m (186 ft). The walls have been constructed in a wide range of subsurface conditions, including clay, silt, sand, gravel, boulders, peat, mudstone, limestone, weathered rock, and granite. The excavations were for various types of projects including housing, schools, offices, hotels, museums, airports, underground parking, roads, railroads, subways, tunnels, power plants, treatment plants, pump stations, utilities, canals, reservoirs, and dams. An example of a TRD earth retention wall project is presented in Figure 9.

LIMITATIONS

The TRD is a versatile tool which has been successfully used to install walls in a multitude of geologic conditions, ranging from soft soils to hard rock. TRD may not be cost-effective for shallower trenches or soils that can be readily excavated by traditional methods. Deep walls, excavation below the water table, boulders and hard rock, and other conditions that would impede traditional methods are ideal for TRD. Depth is limited to roughly 60 m (~200 ft). Wall thicknesses of 550 mm to 800 mm (1.8 ft to 2.6 ft) are possible with presently available equipment.

Figure 9. Isogo Pumping Station for a reservoir in Yokohama City, Japan. Top of TRD wall with exposed soldier pile (left) and TRD wall exposed after excavation (right).

CONCLUSIONS

The TRD method has a successful 20 year track record of shallow and deep earth retention for a wide range of construction projects and subsurface conditions. For earth retention applications, steel beams are inserted in the freshly constructed wall to provide the required lateral strength. The TRD method of wall construction provides the highest quality continuous mixed-in-place wall of any method available.

REFERENCES

AK Chemical Co., Ltd., (2006). "TRD Performance Records in Japan & USA." Internal Publication, Prepared for Hayward Baker.

Aoi, Minori, Fumio Kinoshita, Shigeki Ashida, Hiroaki Kondo, Yuji Nakajim, Motohiko Mizutani. (1998). Diaphragm Wall Continuous Excavation Method: TRD Method. *Korbelco Technology Review,* No. 21.

Aoi, M., T. Komoto and S. Ashida. "Application of TRD Method to Waste Treatment on the Earth." M. Kamon (ed.), *Environmental Geotechnics: Volume 1* (1996): 437-440, Rotterdam, Balkema.

Cedergren, Harry R., (1988). Seepage, Drainage and Flow Nets. 3rd Edition. John Wiley & Sons, Inc.

Evans, J.C., (2007). "The TRD Method: Slag-Cement Materials for In Situ Mixed Vertical Barriers." Conference Proceedings, *GeoDenver 2007*.

Fordham, E., 2006, "Flow Modeling as a Tool for Designing and Evaluating a Seawater Barrier Demonstration Project," MODFLOW and More 2006: Managing Ground-Water Systems - Conference Proceedings, Poeter, Hill & Zheng eds., International Ground Water Modeling Center, p. 796-800.

Gularte, F., Fordham, E., Watt, D., Weeks, J. and Johnson, T., (2007) "First use of TRD Construction Technique for Soil Mix Cutoff Wall Construction in the United States" *Proceedings of GeoDenver 2007*.

Influence of Tip Movements on Inclinometer Readings and Performance of Diaphragm Walls in Deep Excavations

Hsiao-Chou Chao[1]; Richard N. Hwang[2];and Chung-Tien Chin[3]

[1] Moh and Associates, Inc., 11F #3 Dunhwa S. Road, Taipei, Taiwan 10557; PH (886)919387869; FAX (886)25705566; Email: hsch.chao@maaconsultants.com
[2] Moh and Associates, Inc., 11F #3 Dunhwa S. Road, Taipei, Taiwan 10557; PH (886)958008393; FAX (886)25705566; Email: ct.chin@maaconsultants.com
[3] Moh and Associates, Inc., 11F #3 Dunhwa S. Road, Taipei, Taiwan 10557; PH (886)917631631; FAX (886)25705566; Email: richard.hwang@maaconsultants.com

ABSTRACT

Experience indicates significant movements at tips if inclinometers were not properly anchored in competent strata and, as a result, readings often indicated false outward wall movements in later stages of excavation. On the other hand, it has been observed that the changes in lengths of struts are minimal once these struts are preloaded; therefore walls can be assumed to be steady at corresponding strut levels in the subsequent excavation. Inclinometer readings can then be calibrated accordingly. Procedures have been proposed previously based on the experience learned from deep excavations carried out in the Taipei Basin. These procedures are substantiated herein by finite element analyses using the computer program PLAXIS.

INTRODUCTION

Inclinometers are often installed in diaphragm walls and stop at the toe levels. Since readings are obtained by using the tips of inclinometers as reference points, any movements at the tips will lead to misinterpretation of wall movements. Readings can be calibrated if the movements at the top of the inclinometers are measured by survey but this is rarely done. It has been proposed to calibrate inclinometer readings based on the assumption that walls at a specific level will no longer move or move inward by only small amounts, once the struts at this level are installed and preloaded (Moh and Hwang, 2005; Hwang et al., 2007). It is the purpose of this paper to validate this assumption by numerical analyses.

PREVIOUS STUDY

Figure 1 shows idealized profiles for wall movements. Inward movements of walls will lead to shortening of struts and increase in strut loads while outward movements of walls will result in lengthening of struts and reduction in strut loads. Therefore, the validity of aforementioned assumption can be verified by studying the performance of struts. Field data with an excellent quality were obtained during the construction of BL8 Station (Shandao Temple Station) of the Taipei Rapid Transit Systems (Taipei Metro). It is thus possible to correlate wall deflections with shortening of struts (Moh and Hwang, 2005; Hwang, et al., 2007).

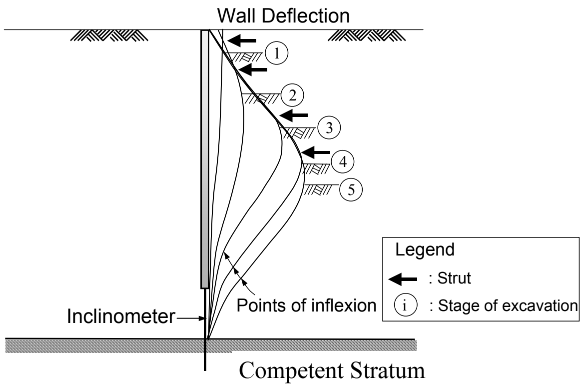

Figure 1. Ideal profiles of wall deflections

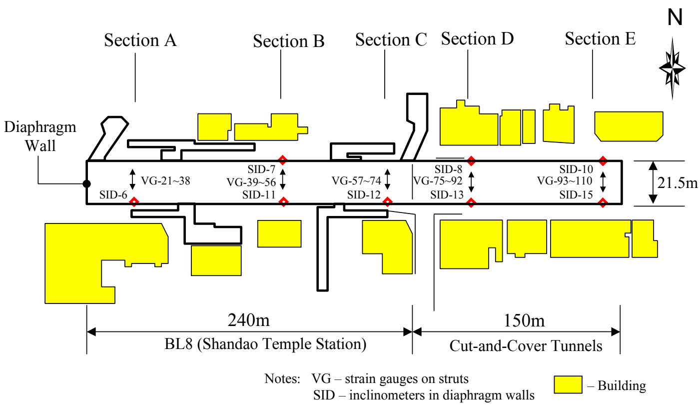

Figure 2. Site Plan and locations of instruments, Shandao Temple Station

Figure 2 shows a site plan for the station and the cut-and-cover section of tunnels to the east of the station. The station is 240m in length and 21.5m in width and the tunnel section is 150m in length with the same width. Excavation was carried out to the final depth of 18.5m in 7 stages as depicted in Figure 3. The pit was retained by diaphragm walls of 1m in thickness and 30.5m in length. Strain gauges were available in 5 sections for monitoring strut loads and Figure 4 shows, for example, the readings obtained at the top 4 levels in Section B. Take the strut at Level 1 for example, the maximum increase in loads was 52 kN/m subsequent to preloading, corresponding to a shortening of the strut of only 1.4mm computed based on the E value (Young's Modulus) of 200,000 N/mm^2 and strut length of 21.5m. Wall movements at the two ends of this strut would be a half of this value, ie., less than 1mm. Similarly, the shortening of the strut at the second level was 3.2mm maximum and the inward movements the wall at the two ends would be about 1.6mm after preloading. As the movement of a diaphragm wall at the tip is expected to be much more significant, the connecting points where the struts joined the wall, rather than the tips of inclinometers, can be selected as reference points for calibrating inclinometer readings (Moh and Hwang, 2005; Hwang, et al., 2007).

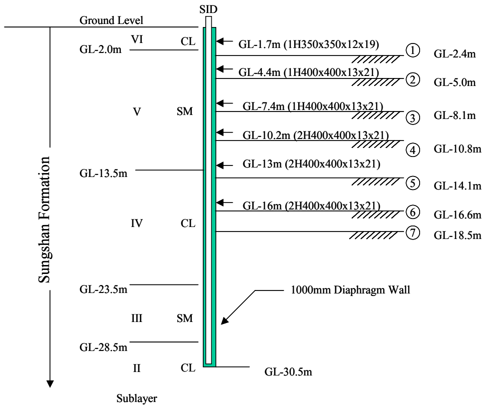

Figure 3. Soil profile and retaining system, Shandao Temple Station

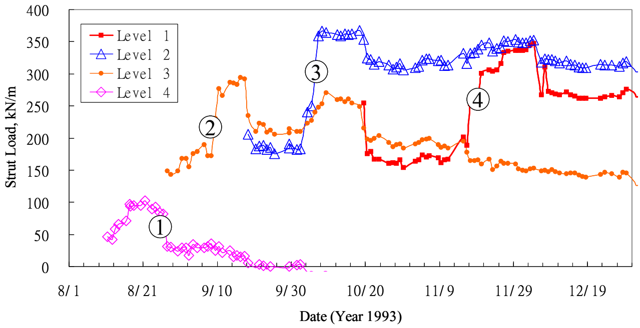

Figure 4. Strut loads recorded in Section B, Shandao Temple Station

There were a total of 8 inclinometers for monitoring wall movements in these 5 sections and the corresponding locations are shown in Figure 2. The readings obtained by Inclinometers SID-7 and SID-11 installed in opposite walls in Section B are shown in Figures 5(a) and 6(a) respectively. As can be noted, the top of the walls moved outward by as much as 20mm in both cases. At the first strut level of 1.7m below surface, the walls also moved outward by more than 15mm subsequent to preloading of struts in both cases. If these inclinometer readings were truly reliable, the strut at the first level would have been elongated by more than 30mm. This certainly cannot be true.

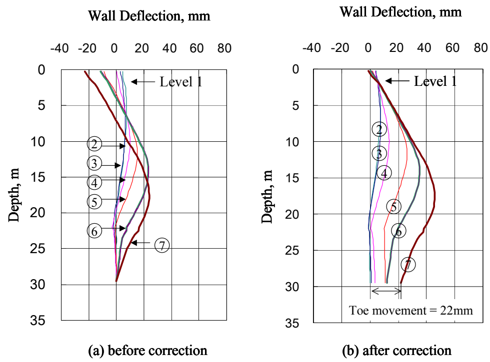

Figure 5. Wall deflection profiles, SID7, Shandao Temple Station

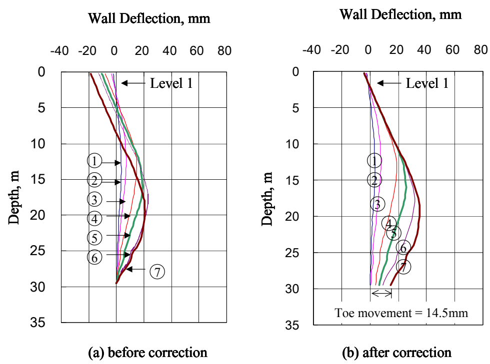

Figure 6. Wall deflection profiles, SID11, Shandao Temple Station

Figures 5(b) and 6(b) show the wall deflection profiles obtained by adjusting inclinometer readings so the wall movements at the first strut level become negligible subsequent to the preloading of the strut at this level. These profiles well resemble the ideal profiles shown in Figure 1. The corrections made to the readings correspond to the movements at the tips of the inclinometers and were found to be as much as 22mm for Inclinometer SID-7 and 14.5mm for Inclinometer SID-11.

The calibrated movements at the tips of all the 8 inclinometers are plotted versus depths of excavation in Figure 7. The final tip movements varied from 5mm to 31mm. The movements of Inclinometers SID-10 and SID-15 were smaller than those of others because these two inclinometers were very close to the eastern wall that helped to reduce wall movements. Although Inclinometer SID-6 was also located at the corner of the site, grouting was carried out to stop leakage on the diaphragm wall at this location and presumably increased the movement at the tip of this inclinometer.

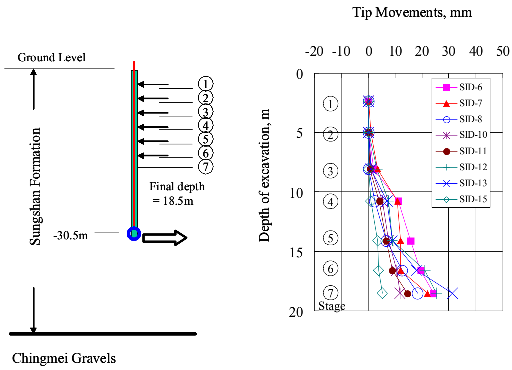

Figure 7. Progressive toe movements of diaphragm walls, Shandao Temple Station

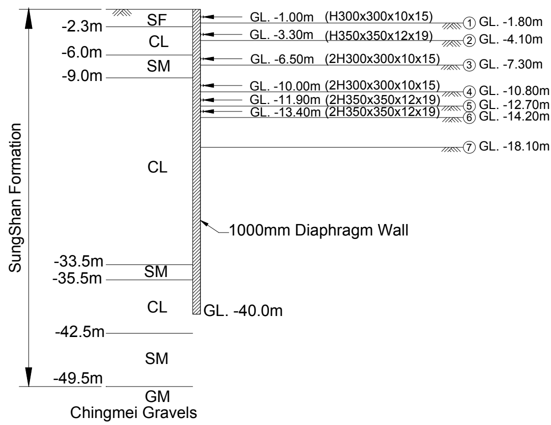

Figure 8. Soil profile and sequence of excavation, this study

VALIDATION OF THE APPROACH

The above-mentioned approach is founded on the assumption that walls at a specific level will no longer move, or move inward by only small amounts, once the struts at this level are installed and preloaded. The finite element computer program PLAXIS (PLAXIS, 2002) was used to analyze the performance of diaphragm walls in an excavation for a basement of an 8-floor above ground and 4-floor below ground commercial building to evaluate if this assumption is valid. The site of interest is located in the K1 Zone of the Taipei Basin. As illustrated in Figure 8, at the surface is a thick layer of young sediments, the so-called Sungshan formation, underlain by a sandy gravel layer at a depth of 49.5m. Excavation was, roughly, 50m by 60m in size and was carried out to a depth of 18.1m in 7 stages. The retaining structures were composed of diaphragm walls of 1m in thickness and 40m in length. The internal bracing structures were composed of 6 levels of cross-lot H-shaped steel struts with a typical horizontal spacing of 4.5m.

Table 1. Soil parameters adopted in the PLAXIS analyses

Depth (m)	Soil Type	γ_t (kN/m^3)	N-value	Su (kPa)	c' (kPa)	Φ' (degrees)
0~2.3	SF	19.0	4	30~33.2		
2.3~6	CL	18.1		33.2~38		
6~9	SM	19.0	4		0	33
9~23.5	CL	18.6		43~64		
23.5~33.5	CL	19.2		64~141		
33.5~35.5	SM	19.5	25		0	35
35.5~42.5	CL	19.9		156~210		
42.5~49.5	SM	19.9	30		0	35
49.5~70	GM	20.0	100		0	38

This sandy gravel layer, the so-called Chingmei formation, underlying the Sungshan formation is a competent bearing stratum and the movements in this formation are expected to be small. However, to remove doubts, the rigid boundary of the finite element model was lowered to a depth of 70m. Soils were modeled by 15-node elements and the elastic-perfect plastic model was adopted to simulate soil behavior during excavation. The groundwater table was at a depth of 2m below ground surface. Table 1 shows the soil parameters inferred from the results of field or laboratory tests and adopted in the analyses. Clayey soils (Type CL) were assumed to be undrained materials with a Poisson's ratio of 0.45 and with Young's moduli E of 500 Su. Sandy soils (Type SM) were assumed to be drained materials with a Poisson's ratio of 0.3 and with Young's moduli E of 4000 N (in kPa)

The wall deflection profiles obtained from finite element analysis are compared with the inclinometer readings in Figure 9. It is noted the readings are available for the upper section above a depth of 36m only and the first stage of excavation were not taken presumably due to mismanagement. Nevertheless, the movements corresponding to subsequent excavation stages were measured and the readings were calibrated accordingly. Results of comparison show both the computed and measured profiles resemble what is shown in Figure 1 and agree with each other quite well in magnitude. Also, Figure 10(a) shows the toe movements of the diaphragm wall are noticeable in the first stage of excavation and reached 17.2mm at the end. The wall movements computed at the depth of 36m are compared with the inclinometer readings at the same depth in Figure 10(b) and the agreement between the two sets of data is quite encouraging even though the potential forces induced by temperature effects via struts to walls have not been taken into consideration in the Plaxis analyses.

The computed strut loads are shown in Figure 2. Unfortunately, readings are unavailable for the site of interest for a direct comparison. The loads in the struts at the first level increased from 75 kN/m to 187 kN/m during Stage 2 excavation immediately subsequent to preloading. The struts, with a pitch of 4.5m and a span of 50m, would have been shortened by 10.3mm, giving a wall movement of 5.1mm at each end. The loads in the struts dropped to 87 kN/m and the net wall movements would be 0.6mm accordingly. Similarly, the shortening of the struts at the second level would be 10.6mm in the third stage of excavation and reduced to 7mm at the end of excavation. The wall movements at the two ends would be half of these values as depicted in Figure 11.

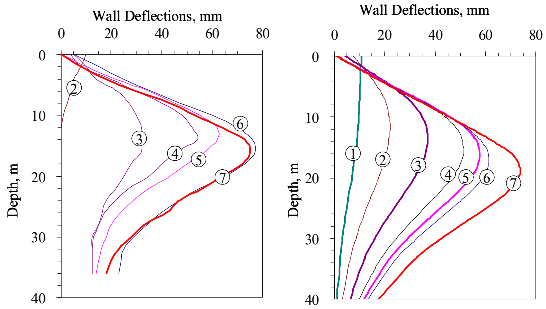

(a) Inclinometer Readings (b) Results of PLAXIS Analyses

Figure 9. Wall deflection profiles

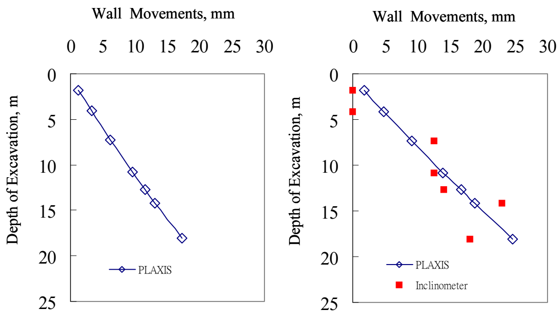

(a) GL-40m (b) GL-36m

Figure 10. Progressive wall movements

CONCLUSIONS

The results of analyses indicate wall movements of 6mm or less at the first two strut levels for excavations with a width of 50m. Such movements are small in comparison with the maximum wall deflections observed in deep excavations and also the movements at diaphragm wall toes. Wall movements would be smaller for narrower excavations. It is thus evident that the approach of calibrating inclinometer readings by assuming that, once struts are installed and preloaded, wall movements at the upper two strut levels are minimal is valid. Nevertheless, if feasible, it is suggested to extend the inclinometer to a competent stratum in practice such that the obtained information can be more reliable.

Table 2. Computed loads in struts

	Level 1	Level 2	Level 3	Level 4	Level 5	Level 6
Preload (kN/m)	75	115	200	120	160	250
Stage	Loads in struts (kN/m)					
1						
2	187					
3	154	282				
4	104	258	480			
5	93	249	491	294		
6	91	240	472	284	313	
7	87	226	440	278	395	610

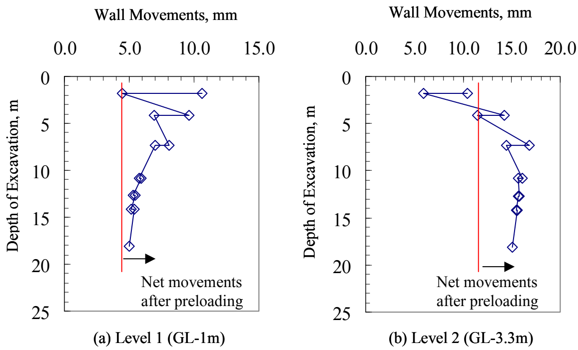

Figure 11. Computed progressive movements at strut levels

ACKNOWLEDGEMENTS

The authors are grateful to Dr. Za-Chieh Moh for his support in preparation of the manuscript.

REFERENCES

Hwang, R. N., Moh, Z. C. and Wang, C. H. (2007). Toe movements of diaphragm walls and correction of inclinometer reading, Journal of GeoEngineering, 2(2), 61- 71

Moh, Z. C. and Hwang, R. N. (2005). Geotechnical Considerations in the Design and Construction of Subways in Urban Areas, Seminar on "Recent Developments on Mitigation of Natural Disasters, Urban Transportation and Construction Industry" 30 November – 2 December, Jakarta Indonesia

PLAXIS (2002). Reference Manual, PLAXIS BV, Amsterdam, the Netherlands

Design and Construction of an Innovative Shoring System at a Challenging Urban Site in Seattle, Washington

Shaun D. Stauffer [1], P.E., Member, Geo-Institute, King H. Chin[2], P.E., Member, Geo-Institute and John Byrne[3], Ph.D., P.E.

ABSTRACT

This paper presents the design and construction of an innovative shoring system at the 8th Avenue and Virginia Street project (8V project) in Seattle, Washington. Shoring was completed using tieback soldier pile walls. A truncated no-load zone was used for tieback design because of limited right-of-way and existing foundation and utility conflicts. Easements along the east side of the site could not be obtained from the adjacent property owner because the existing foundations could not accommodate the installation of tiebacks. Therefore, the design and excavation had to be completed in two phases using two shoring walls connected with a raker. Implementation of this complex shoring system made the project possible. Instrumentation data for the shoring showed total horizontal and vertical deflection of less than 2.5 cm (1 in).

[1]Associate Engineer, GeoEngineers, Inc., 8410 154th Avenue NE, Redmond, WA 98052; sstauffer@geoengineers.com; Project Geotechnical Engineer
[2] Senior Engineer, GeoEngineers, Inc., 8410 154th Avenue NE, Redmond, WA 98052; kchin@geoengineers.com; Project Geotechnical Engineer
[3]Principal Engineer, Ground Support PLLC, 2475 152nd Avenue NE, Redmond, WA, 98052; johnb@groundsupport.com: Project Shoring Designer

INTRODUCTION

The 8V project consists of development of a 34-story mixed-use retail/office tower with below-grade parking. The excavation for the project is approximately 36.6 m by 73.2 m (120 ft by 240 ft) in plan and varies in depth from about 19.2m (63 ft) along the north side of the site to about 22.3 m (73 ft) along the south side of the site.

The site is located in a congested urban environment. City streets with a 19.8 m wide (65 ft) right-of-way are located along the north and west sides of the site. A pile-supported commercial building is located approximately 18.3 m (60 ft) away from the south side of the site. The conditions along the east side are the most complex. A high-rise condominium tower is located across an alley with a separation distance of 4.9 m (16 ft). The condominium tower has a below-grade level and is supported on deep foundations consisting of both concrete piles and drilled shafts.

The shoring system for the project consisted of temporary soldier pile and tieback walls. Several innovative design and construction methods, such as a truncated no-load zone for the tieback anchors and a two-phase shoring system for the east side of the excavation, were employed to successfully complete the excavation.

SUBSURFACE CONDITIONS

Soil conditions encountered at the site consist of fill overlying native glacially consolidated soils. The fill consists of loose to medium dense granular soil with variable debris (wood, concrete, etc.) and was about 9.1 m (30 ft) thick. The native glacially consolidated soils consist of glacial drift and glacial till. The glacial drift is interbedded layers of sand, silt and clay which is typically medium dense to very dense/stiff to hard. The glacial drift extended to the base of the excavation, where glacial till, consisting of very dense silty sand and gravel, was encountered.

Groundwater was encountered at depths of 18.9 to 21.3 m (62 to 70 ft), near the base of the planned excavation. Underslab and wall drainage was included in the building design. Groundwater did not pose problems during construction.

SHORING DESIGN

North, South and West Walls. Apparent earth pressure (AEP) diagrams were developed for the shoring walls using the procedures outlined in Geotechnical Engineering Circular No. 4 (Sabatini et al., 1999). The soils were modeled as a single soil unit by using a weighted average of the individual soil units and their relative thickness within the depth of excavation. The maximum AEP was calculated as 3.5H kPa/m (22.4H psf/ft). Figure 1 presents the design earth pressure diagram for the north, south and west walls.

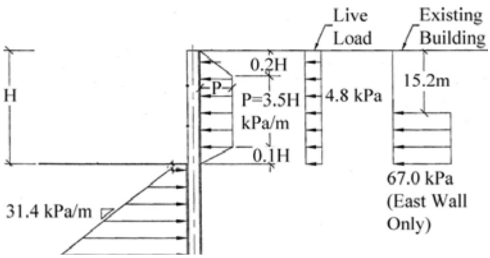

Figure 1. Design Earth Pressure Diagram for North, South and West Walls.

The biggest challenge for the shoring design related to the tieback anchors. The tiebacks along the north and west sides could not extend beyond the right-of-way. With excavation depths up to 22.3 m (73 ft), a conventional no-load zone (defined as a horizontal line extending H/4 at the excavation base, then extending upward at an angle of 60 degrees) was not practical. The upper row of tiebacks for a conventional no-load zone would have bond lengths as low as 4.6 m (15 ft) and utility conflicts did not allow additional rows of tiebacks.

To address insufficient right-of-way, we used a truncated no-load zone defined as a horizontal line extending H/5 at the excavation base, extending the line upward at 60 degrees, then truncating the line at H/2 behind the shoring wall. H/2 was selected as it mimics the assumed failure surface. This allowed the upper tieback row to have up to 4.6 m (15 ft) of additional bond length. Figure 2 illustrates the truncated no-load zone.

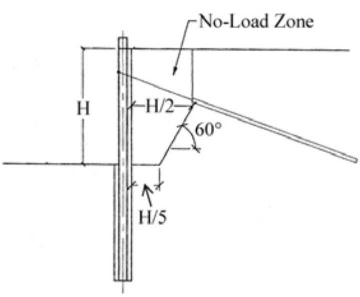

Figure 2. Truncated No-Load Zone.

The truncated no-load results in "softening" of the upper tiebacks as the excavation reaches the design height, potentially resulting in increased wall deflections and decreased stability. To counteract this effect, larger soldier pile beams are used and/or the lower tiebacks are designed for higher loads to "stiffen" the wall response.

For the south shoring wall, the tiebacks had to be threaded through deep foundations supporting the commercial building to the south. The truncated no-load zone was used to maintain a spacing of 3 diameters at the splayed tieback ends.

East Wall. The excavation on the east side of the site was completed adjacent to a 4.9 m (16 ft) wide alley, and three separate design conditions were evaluated. The middle portion was designed using the same methodologies described above. The discussion below presents design conditions for the north and south ends of the east wall.

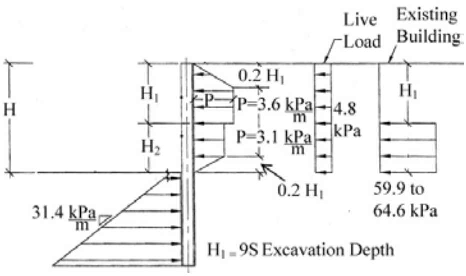

Figure 3. Earth Pressure Diagram for South End of East Wall.

At the south end, the 9th & Stewart (9S) project, which had the same owner/developer as 8V, was under construction directly across the alley. The excavation base for the 9S project was 7.6 m (25 ft) higher than the excavation base for the 8V project. Horizontal tierods were installed from the 9S site below the alley to allow connection of the shoring systems. The tierods were designed to support the AEP associated with the 12.2 m (40 ft) high wedge of alley soil between 9S and 8V. Below the 9S excavation base, the shoring was designed using AEPs and included the alley wedge surcharge and the adjacent 9S building surcharge. High-capacity tiebacks were required in the lower portion of the wall to satisfy global stability requirements. Figure 3 shows the earth pressure diagram used for the south end of the east wall. A typical cross section is presented in Figure 4.

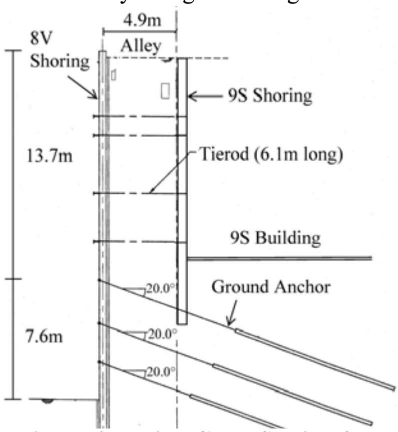

Figure 4. Design Cross Section for South End of East Wall.

Several design challenges were associated with north end. The adjacent condominium tower across the alley is supported on a foundation system consisting of perimeter 0.6 m (24 in) diameter concrete piles and interior columns on 1.5 m (5 ft) shafts. The foundation elements extended 15.2 m (50 ft) below the alley. Easements could not be obtained from the adjacent owner because tiebacks could not be "threaded" through the existing foundation system.

The design was completed for two phases. Phase I consisted of two soldier pile walls connected with a raker system. The outer wall, with a design excavation depth of 8.5 m (28 ft), was located on the property line along the alley and included one raker level. For this phase of the excavation, the outer wall was designed using an AEP of 3.6H kPa/m (23H psf/ft). The rakers were designed to connect the outer wall with the top of the inner wall, located approximately 10.7 m (35 ft) inside the property line and 8.5 m (28 ft) lower in elevation. Tiebacks for the inner wall were designed with a truncated no-load zone. For Phase I, the design of the walls did not need to account for surcharge loading from the adjacent condominium building. Figure 5 presents the AEP diagram used for design of the inner wall. Figure 6 presents the design cross section for Phase I.

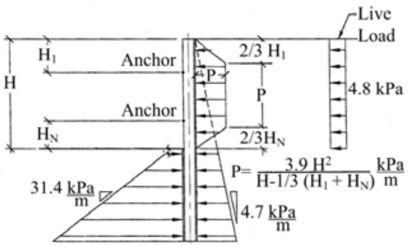

Figure 5. Apparent Earth Pressure Diagram for Inner East Wall.

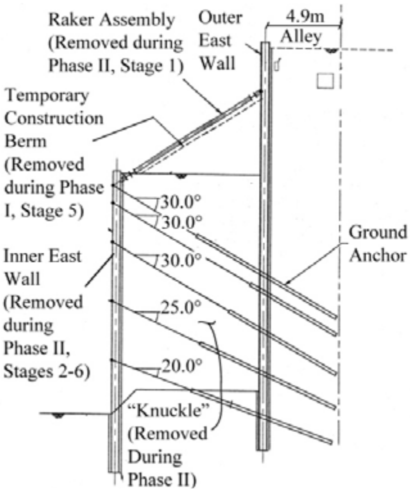

Figure 6. Design Cross Section for the Phase I East Walls.

Phase II consisted of removal of the inner wall, connecting raker system and soil (herein referred to as the "knuckle") and utilizing the recently constructed building core to provide lateral support for the outer wall. The AEP diagram presented in Figure 1 was used for this phase of the design. Additionally, a 67.0 kPa (1,400 psf) uniform rectangular building surcharge was applied below a depth of 15.2 m (50 ft).

A key component for Phase II was designing the outer wall piles for unsupported lengths of 5.5 m (18 ft) (two building floor levels). The design also considered temporary unsupported lengths and widths of 7.6 m (25 ft) because of the construction means and methods of the "knuckle" removal. The pile size was larger than typical because of the unbraced lengths. The bracing used between the outer wall and the building floor levels consisted of Peri Formwork, which is typically used to support concrete floors during pouring and curing. The bracing loads at each level were evaluated using the AEPs previously presented (Figure 1) and were dependent on the construction sequence and the unsupported pile length during each excavation stage. The design team provided bracing loads required at each bracing level, and the contractor designed the Peri Formwork (size, spacing and number of forms) at each level. Bracing loads for the various levels ranged from 321.1 to 656.7 kN/m (22 to 45 kips/ft) of linear wall. Figure 7 presents a photograph of upper level of Peri Formwork bracing.

CONSTRUCTION PERFORMANCE

General. The City of Seattle requires that horizontal and vertical movements of shoring walls be 2.5 cm (1 in) or less. Performance was evaluated during construction using optical survey and inclinometers. Optical survey points were installed on the top of the walls and behind the walls on adjacent buildings and curblines. Monitoring frequency was twice weekly.

Figure 7. Peri Formwork Bracing for Phase II Excavation.

A pair of inclinometers was installed behind the east wall (one each at the inner and outer walls) to evaluate lateral wall movements with depth. Data were collected from both inclinometers during Phase I excavation and from the outer wall inclinometer during Phase II excavation. Survey points were also installed at various heights on the outer east wall face to evaluate Peri Formwork bracing response.

North, South and West Walls. Construction of these walls occurred over a 5 month period. The monitoring data at the top of the wall was typical of soldier pile wall construction; movement was incremental as excavation proceeded. The walls met the performance expectation of less than 2.5 cm (1 in) of horizontal and vertical movement. The north wall experienced the most movement (2.3 cm (0.9 in)), which coincided with the location of the loose fill soils.

Horizontal movement of curblines was less than 0.6 cm (0.25 in). Vertical settlement up to 5.7 cm (2.25 in) was observed at the north curbline, most likely due to soil settlement caused by truck vibrations during soil export.

East Wall. Construction of the south end of the east wall consisted of installing soldier piles along the alley, excavating to connect the 8V piles with the existing tierods installed from the 9S site, and then excavating and installing tiebacks below the alley and 9S building. Construction occurred over a 5 month period.

Survey monitoring data for this short segment of wall indicated that the top of the wall moved outward up to 1.9 cm (0.75 in) during tierod connection. Vertical settlement of the wall was negligible. The horizontal wall movement was likely the result of not pre-tensioning the tierods during construction. Survey monitoring during excavation and installation of the tiebacks showed upwards of 0.6 cm (0.25 in) of vertical settlement of the piles. However, no additional horizontal movement of the wall was observed. The end result is that south wall section met the performance specification of less than 2.5 cm (1 in) of horizontal or vertical wall movement.

As discussed above, the design and construction of the north end of the east wall was completed in two phases. Phase I of the shoring system consisted of installing two soldier pile walls connected with a raker system. Phase I construction occurred over a 5 month period and consisted of eight major stages:

- Stages 1 and 2 consisted of installing the outer soldier piles and excavating a 1H:1V berm in front to prepare for raker and inner soldier pile installation.
- Stages 3 and 4 consisted of installing the inner wall solder piles, the connecting raker and reaction tieback and the upper row of tiebacks for the inner wall.
- Stage 5 consisted of installing the third row of tiebacks and removing the temporary 1H:1V berm between the walls. This resulted in an excavation depth of 8.5 m (28 ft) directly in front of the outer wall.
- Stages 6 through 8 consisted of installing the bottom two tieback rows and completing the excavation at the inner wall to 14.0 m (46 ft). Total depth of excavation at the inner wall was 22.3 m (73 ft) below preconstruction grades.

Figure 8 shows the inclinometer data plots for the outer (left side) and inner (right side) walls for each stage of construction. For the outer wall, the data show horizontal movement of up to 0.6 cm (0.25 in) into the excavation during the first two stages of construction, consistent with cantilever wall movement. When the rakers and prestressing tiebacks were installed, the wall was pushed away from the excavation. The top of the wall continued to move away from the excavation during subsequent stages, finally stopping at 0.3 cm (0.1 in) away from the baseline reading. The lower portion of the outer wall, however, began to bulge slightly (as much as 0.3 cm (0.1 in)) into the excavation during construction stages 6 through 8.

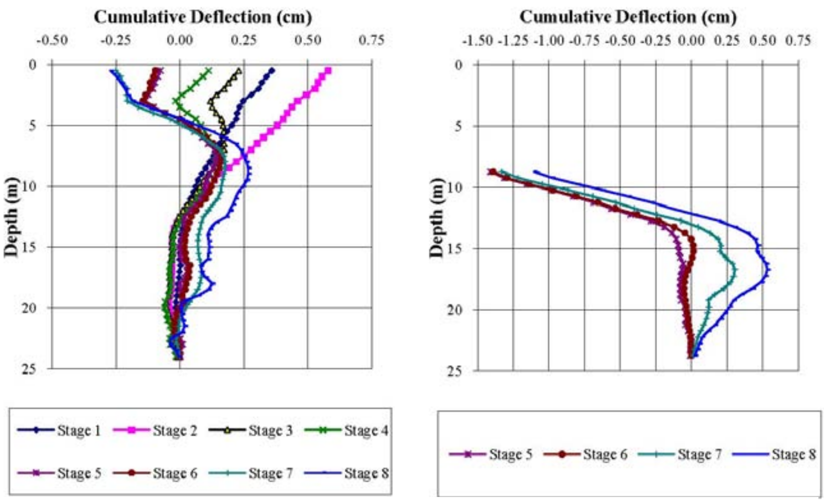

Outer Wall **Inner Wall**

Figure 8. Inclinometer Data for Outer and Inner Walls – Phase I Construction

Inclinometer readings for the inner wall could be completed only for stages 5 through 8 because of safety issues. At the end of stage 5, the data show that the top of the wall had moved away from the excavation 1.4 cm (0.5 in). This is consistent with the outer wall movement during raker and prestressing tieback installation. As subsequent construction stages occurred, the inner wall moved back 0.5 cm (0.2 in), as expected.

The response of the inner and outer walls was closely tied to the raker system. The rakers behaved as load transfer elements between the two walls and helped control the top movement. Figure 9 presents a photograph of the excavation at the end of Phase I excavation.

Figure 9. End of Phase I Construction.

Phase II consisted of excavation of the "knuckle" and construction of the permanent floor slabs within the "knuckle". Twelve major stages of construction occurred during Phase II over a 10 month period:

- Stage 1 consisted of installing the first level of Peri Formwork and removing the rakers and reaction tiebacks installed on the inner wall (see Figure 7).
- Stages 2 through 6 consisted of sequential excavation, Peri Formwork installation and tieback removal to the excavation base. Excavation depth was 21.9 m (72 ft).
- Stages 7 through 10 consisted of sequential removal of Peri Formwork and construction of the floor slabs for the lower four levels of the building. Effective excavation depth was about 9.1 m (30 ft) at the end of stage 10.
- Stages 11 and 12 consisted of sequential removal of Peri Formwork and construction of the floor slabs for the upper two levels of the building.

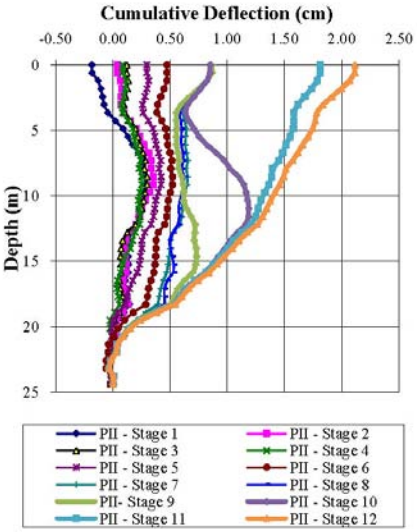

Figure 10. Inclinometer Data for the Outer East Wall – Phase II Construction

Figure 10 shows the inclinometer data for the outer wall for each Phase II construction stage. The data show that 0.7 cm (0.3 in) of cumulative outward wall movement (about 0.5 cm (0.2 in) from baseline) occurred during the "knuckle" excavation (stages 1 through 6). The authors believe that the movement is the result of the small amount of time (about 2 weeks) that occurred during these construction stages. Essentially, Peri Formwork installation occurred within hours to days after excavation occurred. However, construction during stages 7 through 12 was slow because of weather delays and construction scheduling. Each of these stages took about 1 month, which resulted in more "relaxation" of the shoring system. During stage 10, a "bulge" occurred because of the construction delay between removal of Peri Formwork bracing and construction of the floor slab. The outward wall movement continued during stages 11 and 12, resulting in a final wall movement of 2.2 cm (0.8 in). Although the total movement was within acceptable levels, the incremental movement during these stages could have been reduced with proper construction sequencing and scheduling.

The optical survey data for the outer east wall, alley and adjacent building showed similar results when compared to inclinometer data for both Phase I and Phase II of the construction, indicating reliability of the inclinometer data.

Two survey points along the north end of the outer wall showed horizontal movement in excess of 2.5 cm (1 in). This was the direct result of construction sequencing. At the end of stage 10, wall movement was at 1.3 cm (0.5 in). Stages 11 and 12 were completed concurrently in this area, resulting in an unsupported soldier pile length of 9.1 m (30 ft) for several soldier piles. Approximately 2.0 cm (0.8 in) of wall movement occurred as a result of this construction sequencing, bringing the total horizontal wall movement in this area to as much 3.3 cm (1.3 in).

Negligible movement of the adjacent condominium occurred during construction.

CONCLUSIONS AND RECOMMENDATIONS

As presented in this paper, innovative shoring solutions can be implemented in congested urban environments. Based on this case study, the authors conclude that:

1. Congested urban environments present multiple challenges for shoring systems. A thorough evaluation of the existing soil conditions, utilities and adjacent structures is required in order to design and construct shoring systems in this environment.
2. A truncated no-load zone can be successfully used in granular soils and wall deflections can be limited to less than about 2.5 cm (1 in) with proper design and construction. The authors caution the use of a truncated no-load zone in cohesive soils or where multiple rows of tiebacks are affected by the truncated zone. Numerical modeling should be completed for these situations.
3. Tierods from adjacent shoring systems can be used successfully, provided that the connection details on both shoring systems are designed for this purpose. The authors believe that horizontal wall deflections could have been significantly reduced by prestressing the tierods during construction.
4. The raker system connecting the outer and inner east shoring walls was effective in controlling the movement of the shoring system during Phase I of the excavation.
5. Peri Formwork can be used successfully to provide lateral support during excavation. Development of a detailed construction sequencing plan, along with proper implementation by the contractor, is critical when using this type of system.
6. The large soldier piles installed for the outer east wall helped control wall deflections, even when the design unsupported length was exceeded.

REFERENCES

Sabatini P.J., Pass D.G., and Bachus R.C. (1999). *"Geotechnical Engineering Circular No. 4, Ground Anchors and Anchored Systems."* Report FHWA-IF-99-015, Federal Highway Administration, Washington D.C.

DESIGN AND CONSTRUCTION OF AN UNDERPINNING AND EARTH-RETAINING SYSTEM FOR LEHIGH VALLEY HOSPITAL BUILDING

Rupert K Hon, MASCE[1,] and Michael R Demcsak, MASCE[2]

[1] Layne GeoConstruction, A division of Layne Christensen Co., Chief Engineer, 60 Fireworks Circle, Bridgewater, MA 02324; PH (508)588-8889; FAX (508)588-8989; email; rhon@laynegeo.com
[2] Lippincott Jacobs Consulting Engineers, Director of Geotechnical Services, 1 N. Pavilion Ave., Riverside, New Jersey 08075; PH (856)461-1100; FAX (856) 461-3166; email; mdemcsak@ljce.net

ABSTRACT

The foundation construction of Lehigh Valley Hospital New Medical Building required the installation of an underpinning and earth-retaining system along two existing buildings. Because of the drastic changes in geological conditions, a mixed face of weathered limestone rock and residual soil, a vertical wall of underpinning and an earth-supporting structure was required at the face of existing building foundations. This earth-retaining system consisted of drilled mini-piles for underpinning; a combination of mini-piles and jet-grouted walls as the main part of the earth-retaining wall system; an A-frame structure to support the wall at the shallow rock section; and jet-grouted anchors to stabilize the wall at the deep rock section.
This paper will describe details of the design and construction of various structural elements for this wall system.

BACKGROUND AND INTRODUCTION

The project is part of the expansion of the Lehigh Valley Hospital, Cedar Crest Campus off Highway I-78 in Allentown, PA. A new 7-story Medical Building Tower was to be constructed up against an existing one-story General Services Building to the South and an existing 3-story Anderson Building to the East. Both of these buildings are supported on shallow spread footing foundations. The new seven-story Medical Building has a deep basement and was designed on spread footings, which are up to 20 ft. below the bottom of the spread footings of the existing buildings. At certain locations, the new spread footing foundation extended underneath the existing footings and those portions of the existing footings had to be cut off. In order to construct the new foundation, and basement wall, an earth retaining wall along the foundation line of the 2 existing buildings was required. Also the existing buildings' foundations had to be underpinned. The existing buildings had to remain in full service throughout construction. The general project layout is shown on Fig. 1.

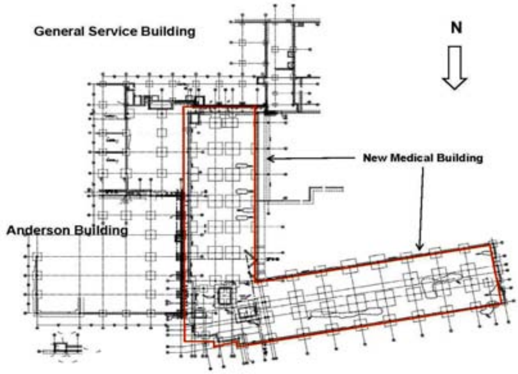

Fig. 1. Lehigh Valley Hospital Expansion Plan

Due to the extremely variable overburden soil and weathered limestone rock conditions, limited mobility-compaction grouting had previously been performed beneath all proposed footings throughout the tower footprint to densify the overburden soil and improve the rock by filling voids and weathered seams. Also, the construction of deep elevator shafts in shallow rock for the new medical building required light, bedrock blasting within the construction site which increased the horizontal pressure and introduced vibration onto the earth retaining walls. Layne GeoConstruction was awarded a design-construct contract for the earth support system and underpinning as an extension of their contract to perform the limited mobility/compaction grouting, designed by Lippincott & Jacobs Consulting Engineers (L&J), for support of the tower foundations. The earth support/underpinning system allowed the basement construction to proceed without problems or settlement of the existing structures, and the 7-story hospital tower has been successfully completed.

GEOTECHNICAL CONDITIONS:

Test borings drilled for the geotechnical investigation, by L&J show that the general soil profile consists of residual soil overburden, a mixture of Silt, Sand, and Clay, overlying a layer of extremely weathered limestone bedrock which varies in depth and has clay seams and voids. The borings revealed erratic shallow and deep depths to weathered and sound rock along the east side of the proposed tower where the existing Anderson Building abuts the tower. In the southern portion of the tower there are areas of very deep rock, up to 125 ft deep, with deeply weathered zones. At the southern end of the proposed tower, where it connects with the General Services Building, the residual soil and weathered rock conditions were also found to be very variable. In general, the rock is very weathered and fractured, with limestone pinnacles, ledges, and boulders, with abrupt changes from soil to rock to soil both laterally and vertically.

Conventional steel sheet piling or soldier piles and wood lagging to retain the soil would present many problems in penetrating the erratic weathered and fractured rock, possibly leaving unstable fractured rock below the sheeting in some areas and less than certain underpinning capabilities. Moreover, a sheeting line located away from the face of the building would interfere with new footings that extended beneath some existing footings. Layne GeoConstruction proposed jet grouting combined with drilled mini-piles to penetrate and reinforce the rock to underpin the buildings and support a vertical excavation face at the building line. The combined system could also allow some undercutting to construct the new footings extending beneath existing footings where necessary.
The complex geological profiles are shown in Figs. 2 & 3.

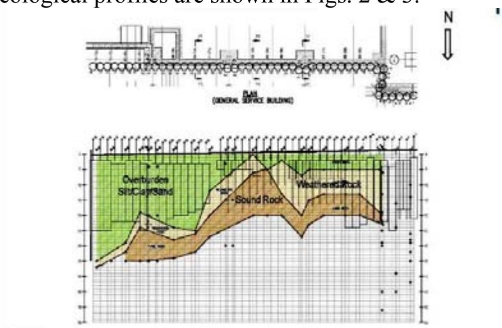

Fig. 2. General Services Building Geological Profile

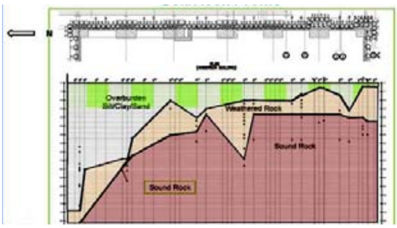

Fig. 3. Anderson Building Geological Profile

EARTH-RETAINING STRUCTURE DESIGN:

The project required an excavation from 15 ft (4.57 m) to 20 ft (6.1 m) below ground surface for the spread footing construction of the New Medical Building Tower. Large new building footing foundations are immediately adjacent to the existing buildings and, at certain locations, the new footings protrude underneath the existing footings due to the heavy column loads. The excavation adjacent to the General Services Building and the Anderson Building required a vertical excavation cut and the existing foundations had to be underpinned. An earth-retaining wall was required

to support the soils underneath the buildings. Light rock blasting was expected for the construction of nearby elevator shafts, which extended into bedrock .
The surface of rock varies from 5 ft (1.52 m) to more than 70 ft (21.34 m) below the existing ground surface within a relatively short distance of 200 to 300 ft. (61 to 92 m).
With all the challenges of foundation plan layouts and the difficult geological conditions, including various soil types in the overburden, extremely weathered and fractured rock in the upper section of bedrock, and drastic changes in the depth to bedrock surfaces in short distances, Layne GeoConstruction proposed a design/construct underpinning and earth retaining wall system which consisted of a combination of several structural elements to serve the project design purposes.

DESIGN METHODOLOGY

1) For underpinning, use mini-piles to support the structure loads of the adjacent General Services Building and Anderson Building foundations.
2) For earth support, use mini-pile and jet-grouted columns to form a continuous earth retaining wall to support the lateral earth pressure, structural and live loads on floor slabs of the existing buildings, and additional horizontal force induced from nearby blasting activities.
3) In shallow bedrock sections, design an A-frame self-standing structure (one vertical pile and one battered pile), to resist horizontal loads imposed onto the earth retaining wall.
4) In deep bedrock sections, design jet-grouted anchors for the earth retaining wall to resist the horizontal loads imposed onto the wall.

LOADS CONSIDERED IN THE DESIGN OF MINI-PILES AND EARTH RETAINING STRUCTURE

1) Maximum Column Loads of existing buildings adjacent to the New Medical Building Tower:

   The existing foundations of the General Services Building and Anderson Building are on shallow spread footings. The exterior curtain walls are supported by reinforced concrete grade beams which transfer the wall loads onto concrete column piers and the spread footings. The total maximum structural loads (dead loads and live loads) for the footings along the column lines provided by the structural engineer, varied from 85 to 140 kips (378 to 623 kN) and 100 to 220 kips (445 to 979 kN) for the General Services Building and Anderson Building respectively .

2) Earth pressure: Horizontal soil pressure from earth loads.

3) An Additional Load:

The ground floors of existing buildings were designed as slabs on grade, so that the structural load on the ground floor slab did not add onto the total column loads. However, in addition to the structural loads, the activities (live loads) on the ground floors will impose additional horizontal load onto the earth-retaining structure. The live loads used in design for the General Service and Anderson Buildings were 100 and 50 psf (4.8 & 2.4 kN/m^2), respectively.

4) The Additional Load due to Blasting for the construction of elevator shafts:

The construction specification specified that the maximum allowed peak ground velocity generated by the blasting shall not exceed 2 in/sec. (5.08 cm/sec.). Based on the Graph in "Soil Dynamics", by Shamsher Prakash, the Coefficient of dynamic earth pressure = 0.075 at peak velocity of 2 in/sec (5.08 cm/sec). With the Coefficient of dynamic earth pressure = 0.075, the additional horizontal pressures on the earth-retaining wall were calculated.

MINI-PILE DESIGN ASSUMPTIONS FOR UNDERPINING OF EXISTING FOOTINGS AND FOR THE EARTH RETAINING WALL.

1) Mini-pile Design

   a) Mini-piles will have a grouted diameter of 9 inches (23 cm).
   b) Steel reinforcement to be 7-inch (18 cm) O.D. x 0.5-inch (1.27 cm) wall thickness, N-80 steel casing.
   c) Bearing strata to be in natural stiff Silt/Clay/Sand or Limestone Bedrock.
   d) Minimum unconfined compressive strength of grout to be 4,000 psi (27,580 kN/m^2).
   e) Allowable skin friction in stiff Silt/Clay/Sand to be 5.6 psi. (38.6 kN/m^2).
   f) Allowable skin friction in weathered rock to be 20 psi. (138 kN/m^2).
   g) Allowable skin friction in mass intact rock to be 40 psi. (276 kN/m^2).
   h) The mini-pile will have a structural compression capacity of 276 kips (1228 kN) and a geotechnical capacity of 70 to 85 kips (311 to 378 kN) with various pile lengths depending on pile locations and the soil/rock conditions.

2) The underpinning mini-piles would be installed as close to the footing columns as possible, however, certain eccentricities could not be avoided, so the piles would be designed to have the capacity to resist the additional bending moment induced from the eccentricity.

3) In order to install the mini-piles, Layne GeoConstruction had to core through the existing footings. It was found that the existing footings were too thin to

resist the punching shear of the mini-pile. Additional reinforced concrete caps, doweled into the footings, were added above the top of the footings at the piles.

JET-GROUTED COLUMN TEST PROGRAM

Prior to starting the project, a jet-grouted column test program was performed. Single fluid jet grouting was used in this project. Three test sections with different jetting pressures and retraction rates were used. The columns were exposed and measured to determine the optimum jetting pressure and retraction rates to be used for construction. The unconfined compressive strength of grout at 28 days ranged from 5,200 to 6,600 psi (35.8 to 45.9 Mpa).

EARTH-RETAINING WALL DESIGN ASSUMPTIONS

The earth-retaining wall would consist of mini-piles and jet-grouted columns installed in between the mini-piles. This earth-retaining wall would be stabilized laterally by adding a battered mini-pile to form an A-frame structure in the shallow bedrock section and a jet-grouted anchor in the deep bedrock section.

1) The design of mini-piles for the earth-retaining structure will be the same as that used for underpinning.
2) Jet-grouted column in between the mini-piles (based on the test program).
   a) Jet-grouted column diameters would be 2.5 to 3.0 ft (76 to 91 cm), with a min. of 2.5 ft. (76 cm).
   b) Soilcrete would have a minimum unconfined compressive strength of 500 psi (3448 kN/m^2) and an allowable compressive strength of 165 psi (1138 kN/m^2) for design.
   c) Maximum allowable compressive capacity would be 117 kips (520 kN).
   d) At certain locations the jet-grouted columns would have to be installed at the edges of the existing footings. The bearing area on the jet-grouted column would be reduced to 1/3, and the maximum allowable compression capacity would be reduced to 39 kips (173 kN).
   e) Geotechnically, the jet-grouted columns would be supported by skin friction and end bearing.
   f) Allowable skin friction of the jet-grouted column in stiff Silt/Clay/Sand to be assumed 2/3 of that of mini-pile, 3.7 psi. (25 kN/m^2).
   g) Allowable bearing pressure in stiff Silt/Clay/Sand to be 4 ksf. (191.3 kN/m^2).
   h) Allowable bearing pressure in bedrock to be 20 ksf. (956 kN/m^2).
   i) The jet-grouted columns will be terminated at bedrock surface or 5 ft (1.5 m.) below the bottom of excavations in deep rock sections.

j) A reinforced concrete capping beam added on top of the jet-grouted column wall, would allow the wall to act as a unit.

The underpinning piles, earth-retaining structure mini-piles, jet-grouted columns, A-framed structures, and jet-grouted anchors were shown on the Jet-grouted Column Layout Plans for General Services Building Fig. 4, and Anderson Building, Fig. 5, respectively.

The basic function of the underpinning mini-piles was to support the total building loads so that generally no load would be imposed onto the earth-retaining structure. However at certain locations where the new footing protruded underneath the existing footing, the mini-piles would serve dual purposes of both underpinning and earth retaining. The mini-piles in A-frame structures and the vertical mini-piles together with the jet-grouted anchors in the earth-retaining wall were the skeleton support of the wall. The jet-grouted columns in between were filled in to retain the soil behind the walls. A reinforced concrete capping beam on top would hold different elements together to make the wall act as a unit.

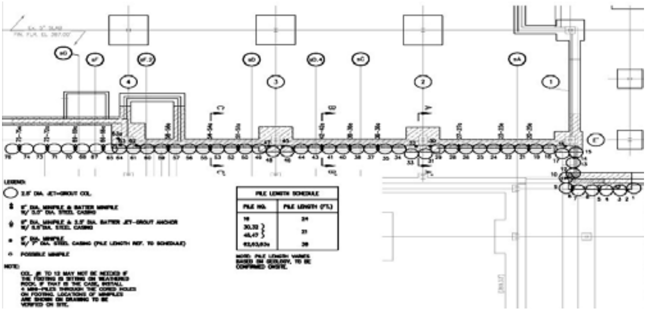

Fig. 4. General Services Building Mini-pile/Jet-grouted Column Layout Plan

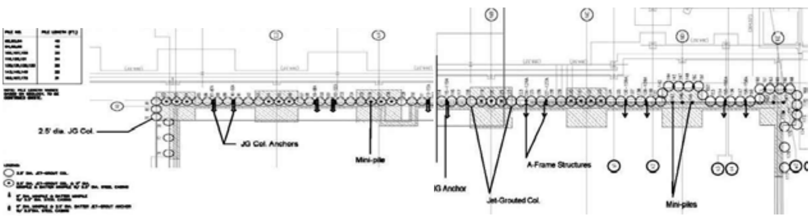

Fig. 5. Anderson Building Mini-pile/Jet-grouted Column Layout Plan

UNDERPINNING AND EARTH-RETAINING WALL DETAILS

1) The mini-piles for underpinning were installed at the edges of the column pilasters or walls. A 12-inch (30.5 cm) diameter hole was cored through existing concrete footings, and a 9-inch (23 cm) diameter pile with a 7-inch (17.8cm) diameter N-80 steel casing as reinforcement was installed through the hole. The pile lengths varied depending on the depth of bedrock encountered. The mini-piles either penetrated a min. of 6-ft (1.83m) into rock in shallow sections, or 18-ft (5.5m) into a stiff Silt/Clay soil layer to achieve the required design capacity. The average thickness of the existing footings was approximately 14 inches (35.5 cm), which is inadequate to take the punching shear load. A reinforced concrete block was constructed on top of the footings over the pile and anchored into the footing to increase the shear area. The jet-grouted columns would be installed around the footings to retain the soils. The columns would seat on top of bedrock if it was shallow or extend 5 ft (1.5m) below the bottom of excavation if bedrock was not reached. Fig. 6 shows this typical arrangement.

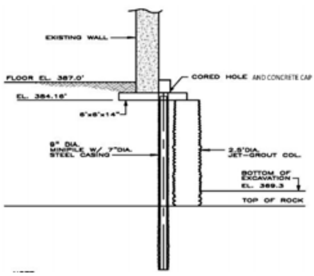

Fig. 6. Mini-pile and Jet-grouting for Column Footing Underpinning

2) A continuous row of jet-grouted columns will form the wall between column footings. The wall would either be stabilized by A-frame mini-pile structures or vertical mini-piles with jet-grouted anchors.
    a) Where the bedrock is shallow, the earth retaining wall will be stabilized by A-frame structures, placed at approximately 5 ft (1.5m) on center, composed of one vertical and one battered pile with a reinforced concrete capping beam on top to tie them together. The vertical load from the existing wall was minimal. The main load came from the ground floor live load and the earth pressures. The vertical pile would be in compression and the battered pile, in tension. The jet-grouted columns in between would have to resist the lateral pressures. The A-frames would act as the end supports. The mini-piles had to penetrate into rock below the bottom of excavation. Fig. 7 shows a section of the A-frame structure.

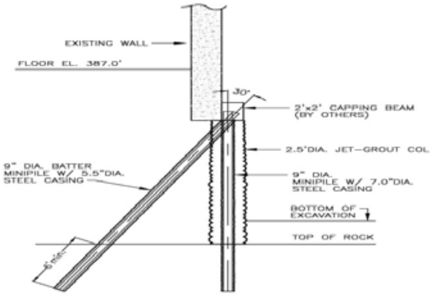

Fig. 7. A-Frame Structure in Earth Retaining Wall

b) Where the bedrock is at greater depth, the earth retaining wall will be stabilized by the jet-grouted anchors. This anchor is different from the conventional anchors, using the jet-grouting technique to create the bond zone with a steel pipe as a tension member. Fig. 8 shows a typical section of the jet-grouted anchors in the earth retaining wall.

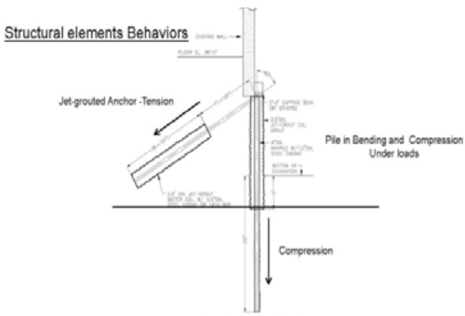

Fig. 8. Earth Retaining Wall Jet-grouted Anchor

CONSTRUCTION PHOTOS

Installation of mini-pile and jet-grouted columns at Anderson Building


Exposed Wall and New Building Foundations at the Anderson Bldg and General Service Bldg.

ACKNOWLEDGEMENTS:

The earth-retaining/underpinning walls in this project were successfully built, completed on time and they performed very well during new foundation excavations. We would like to thank the diligent efforts of the Layne GeoConstruction field crew personnel. We appreciate all assistance, and co-operation by the General Contractor /CM Whiting-Turner Company of PA.; Architect Freeman White, NC; Geotechnical Engineer Lippincott & Jacobs, NJ; and Structural Engineer O'Donnel & Naccarato, Inc, PA.

REFERENCES:

Terzaghi K and Peck R. B. (1968). "Soil Mechanics in Engineering Practice" Wiley, New York.

Prakash S. (1981). "Soil Dynamics" McGraw-Hill Book Company, New York.

Department of the Navy (1982). "Foundations and Earth Structures, Design Manual 7.2" Alexandria, VA.

US Department of Transportation FHWA-SA-97-070 (2000). "Micropile Design and Construction Guideline Implementation Manual"

Design of an Anchored, Cast-in-Place, Backfilled Retaining Wall

Steven Van Shaar[1] P.E., Katy Cottingham[2] P.E.,
Andrew Walker[3] P.E. Associate Member, Rich Barrows[4] P.E.

[1] Project Engineer, Golder Associates Inc., 18300 NE Union Hill Road Suite 200, Redmond, Washington 98052, svanshaar@golder.com

[2] Project Engineer, Golder Associates Inc., 18300 NE Union Hill Road Suite 200, Redmond, Washington 98052, kcottingham@golder.com

[3] Senior Consultant, Golder Associates Inc., 18300 NE Union Hill Road Suite 200, Redmond, Washington 98052, awalker@golder.com

[4] FHWA Geotechnical Engineer, Federal Highway Administration, Western Federal Lands Highway Division, 610 East 5th Street, Vancouver, Washington 98661, Rich.Barrows@dot.gov

ABSTRACT

Several retaining walls for a road widening project had been designed as Mechanically Stabilized Earth walls. However, the excavation necessary to construct the reinforced zone of the MSE Walls would require extended road closures. One of the MSE walls was re-designed as a backfilled anchored wall with a cast-in-place concrete facing. Excavation shoring necessary for construction of the wall was also designed. The excavation shoring consists of reinforcing a temporary cut slope with up to three rows of passive ground anchors connected to steel mesh at the face of the excavated slope. The excavation shoring was designed to allow construction of the concrete wall while limiting the duration of road closures to a few hours at a time. The maximum height of the concrete wall is approximately 6 m.

Micropiles were designed to support the axial load of the concrete facing, while the ground anchors were designed to support the lateral loads of the soil. The anchor tendons extend through the concrete wall facing and the zone between the concrete wall and reinforced slope is backfilled with structural fill. A field testing program confirmed the design bond strength of the ground anchors and micropiles.

INTRODUCTION

Limitations on road closures during a road widening project along Salmon River Road near Riggins, Idaho required the design of an innovative excavation shoring system and permanent concrete anchored wall. The excavation shoring was designed to support the existing road without extended road closures and allow construction of the concrete wall face. Ground anchors from the reinforced slope are to be extended and structurally connected to the concrete wall. A description of the project, the subsurface conditions at the site, and the methodology used in the design of the wall is presented herein. The results of field testing of anchors and micropiles are also presented.

PROJECT DESCRIPTION

Improvements are being completed along a 6.82-km corridor of Salmon River Road. Widening of the road is generally accomplished by addition of walls on the fill side of the road rather than extension of cuts into the steep and sometimes marginally stable hillside terrain above the roadway.

Several retaining walls were originally designed as mechanically stabilized earth (MSE) walls. However, the excavation necessary to construct the reinforced zone of the MSE walls requires extended road closures.

A revised design for Wall 6 was completed, with the potential for application to other walls on the project. The MSE wall design at Wall 6 was replaced with a design for a backfilled anchored wall with cast-in-place concrete facing. The new design included excavation shoring to allow construction of the concrete wall while limiting the duration of road closures to a few hours at a time. The maximum height of Wall 6 is approximately 6 m and the length of the wall is approximately 220 m.

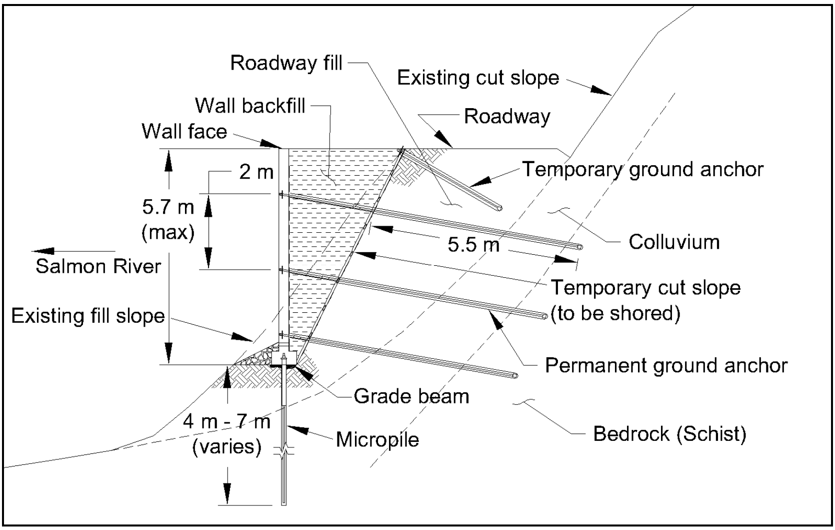

FIG. 1. Typical section of anchored wall.

A typical section of the wall design is shown in Figure 1. The temporary excavation for construction of the wall is a 0.5 horizontal to 1 vertical shored slope. The excavation shoring is installed from the top down as excavation proceeds, with anchors installed from the road above the slope. The shoring consists of passive ground anchors connected to steel mesh at the slope face. Up to three rows of anchors are used to support the excavation. When excavation is completed, micropiles are installed to support the dead load of the facing and the vertical component of anchor loads. A grade beam was designed to transfer the loads from the permanent facing to the micropiles. The permanent wall facing is then cast, and the ground anchors extended through and connected to the wall face, starting with the lowest anchor. A small pre-tension load is applied to the ground anchors after connection to the wall face. The excavation between the temporary slope and the permanent facing is backfilled with structural fill as the anchors are connected to the wall face.

SUBSURFACE CONDITIONS

A field investigation was performed to evaluate the subsurface conditions at the site (NTL 1999). The investigation program consisted of a combination of field reconnaissance, boreholes, and laboratory testing.

The Salmon River Road alignment extends through the geologic unit known as the Riggins Group, which is a series of schist and gneiss bedrock. Gravel and cobble deposits can be observed on the slopes above the road alignment. These deposits were interpreted to be a Pliocene alluvium. Subsequent erosion and deepening of the river valley have eroded and stranded the older alluvium on the valley walls and allowed a cover of colluvium to develop. The colluvium was described as rounded to sub-rounded, cobble to gravel-size deposits. The colluvium was used as a borrow source for construction of the fill slopes, and therefore the fill has a similar gradation to the undisturbed colluvium.

The existing road alignment was constructed as a balanced cut and fill. Many of the existing road cuts have steep colluvial slopes which are experiencing surficial raveling and debris fallout. Fill edge stability is also marginal at numerous locations due to steep, loose sliver fills and runoff erosion.

The colluvial soils exhibit an average standard penetration test (SPT) resistance of about 17 blows per 0.3 m. Sampler refusal occurred in approximately 10 percent of the tests conducted.

The fill soil exhibited an average SPT resistance of about 7 blows per 0.3 m. In many cases, it was difficult to discern fill from colluvium during exploration because the fill had similar visual properties (given that the colluvium was used as a borrow source for fill material). The looseness of the fill meant it would not be acceptable for foundation support of the retaining wall due to low shear strength and increased settlement potential.

Groundwater seepage was not noted along the Wall 6 alignment, although evidence of intermittent seepage locations was noted on the hillsides above the roadway at the interface between bedrock and colluvium.

A uniform soil profile was used for design. Design geotechnical parameters used in the design are presented in Table 1.

TABLE 1. Geotechnical design parameters.

Ultimate cohesion, kPa	0
Ultimate friction angle, deg.	38
Unit weight, kN/m^3	20.4
Ultimate soil-anchor bond, kN/m	58
Ultimate soil-micropile bond, kN/m	58

WALL DESIGN

The overall design was carried out in accordance with load and resistance factor design (LRFD) principles as published by the American Association of State Highway and Transportation Officials (AASHTO 2004). However, a few components of the design were based on allowable stress design principles (AASHTO 1996). Standards published by the Federal Highway Administration were used for design of excavation shoring (Byrne et al 1996), ground anchors (Sabatini et al 1999 and Samtani and Nowatzki 2006), and micropiles (Armour et al 2000).

The excavation shoring was designed as a soil nail reinforced slope using the GOLDNAIL computer program developed by Golder Associates. Anchors consist of hollow “self-drilling” bars (Titan 40/16 by Contech Systems) spaced 2 m apart horizontally and vertically in a rectangular pattern. The facing consists of flexible steel mesh with 75-mm openings (Tecco by Geobrugg) held in place by bearing plates connected to the anchors. The dead load of the mesh is supported by a temporary anchor at the top of the excavated slope.

Apparent pressure diagrams were used to calculate lateral loads on the concrete wall. A uniform horizontal live load surcharge of 3 kPa (equivalent to 12 kPa vertically) was included to account for typical traffic and construction loads. A uniform horizontal surcharge representing a seismic load was calculated to be 250 Pa per meter height of the wall, using the Mononobe-Okabe method (AASHTO 2004).

The wall was analyzed for resistance to lateral loads independently in the horizontal (i.e on a horizontal strip) and vertical (i.e. on a vertical strip consisting of one micropile, one column of anchors, and a portion of concrete facing equal in width to the anchor and micropile spacing) directions. Load effects in the vertical direction due to lateral loading were calculated using the hinge method as implemented in the CT-SHORING computer program by Civiltech. The vertical strip was also analyzed using normalized soil reaction versus displacement curves (i.e. the p-y method) as implemented in the LPILE computer program by Ensoft.

The vertical load of the concrete wall and the vertical component of the ground anchor load are designed to be carried by a row of micropiles installed in the colluvium/fill soils. The top of the micropiles are encased in a reinforced concrete grade beam prior to casting of the wall face.

The cast-in-place facing was designed to be 300 mm thick, with a 28-day compressive strength of 28 MPa. Uncoated reinforcing steel conforming to ASTM A706M was specified.

The anchors used for the excavation shoring are designed to be extended and structurally connected to the concrete wall. The anchor extensions are not bonded to the soil; they were designed with a sleeve to reduce the potential for load transfer to or from the soil. The anchor extensions are installed from the bottom up as backfilling proceeds. A minimum of two rows of anchors are included at all locations.

Additional design provisions included the following:

- Permeable backfill was specified to reduce water pressure buildup on the wall. In addition, a vertical strip of 1.2-m wide drainage geocomposite connected to a weep hole is provided every 2 m along the length of the wall.
- The fill wedge is expected to settle as backfill proceeds. To protect anchors in the fill zone from excessive bending stress, a protective cover was specified with at least 50 mm clear between the top of the tendon and the inside face of the cover. After completion of backfilling operations, the annulus between the tendon and the cover is grouted.
- The design accommodates the dead load from a 50-mm thick architectural finish at the wall face.
- Reinforcing steel was designed with adequate concrete protection for corrosion resistance. However, the anchor tendons and micropile reinforcement may be subject to corrosion. Therefore, the design includes sacrificial steel that allows the tensile or compressive stress to be within allowable limits even after 75 years in a mildly corrosive environment.
- Structural concrete was specified with air-entrainment to provide cold weather protection.
- The toe of the concrete facing is backfilled with a 0.6-m thick wedge of riprap.
- The design includes a standard penetration detail to accommodate culverts up to 610 mm in diameter.
- The design includes two inclinometer casings at locations of maximum wall height and optical survey monitoring points on the wall facing. The wall will be monitored for one year.

WALL CONSTRUCTION

Sacrificial micropiles and ground anchors were installed prior to wall construction to confirm the anchor and micropile adhesions used in the design. The design ground anchor diameter and micropile drill hole diameter was 115 mm. Verification tests were performed on the ground anchors and micropiles assuming an ultimate pullout capacity of 58 kN/m in the colluvium. The ultimate pullout measured on the three verification tests on micropiles ranged from 61 kN/m to 85 kN/m. The ultimate pullout measured on the two verification tests on the ground anchors ranged from 83 kN/m to 101 kN/m.

The ultimate pullout capacity was confirmed by the verification tests. Due to the potential variability in subsurface conditions along the wall alignment, the design team did not increase the ultimate pullout capacity beyond 58 kN/m.

Installation of the production anchors of the wall is complete. Construction of the concrete wall face and backfill is currently underway.

DISCUSSION

The following key insights were identified during the design process:

- The maximum service anchor load is approximately 130 kN.
- As backfilling proceeds, the micropiles develop lateral resistance first on the front side of the pile, then on the back. After the second anchor is installed, the micropile develops a negligible lateral resistance on the front. The upper 1.2 m of the micropile includes a 115-mm outside diameter 102-mm inside diameter pipe casing which helps resist bending loads during backfilling.
- The maximum moment in the concrete facing is developed for the interim case just before installation of the topmost anchor.
- Total lateral deflection of the wall is estimated to be 17 mm. The calculation included the effects of soil-anchor bond development, axial elastic deformation of ground anchors, mobilization of lateral soil resistance at the grade beam and micropile, flexural deformation of the concrete facing, and rigid body motion of the reinforced concrete grade beam and facing.
- The critical stage in expected lateral movement is when the first (bottom) anchor has been installed and soil has been placed above the level of the first anchor. In this case, the top of the micropile translates toward the backfill and the anchor translates forward, causing rotation of the facing. If the entire height of facing were cast and backfill were placed up to the second anchor, the calculated deflection at this stage would exceed 25 mm. The design specifies casting of the face in 3-m maximum heights to limit the total deflection at the top of the finished structure.
- The seismic load case (Extreme Event I in AASHTO 2004) did not govern any significant aspect of the design.

CONCLUSIONS

An innovative wall design was completed. The design includes an excavation shoring system that allowed re-use of anchors and facing mesh. The permanent wall was designed to resist lateral and vertical loads corresponding to strength and service limit states. A system of permanent ground anchors and concrete facing was designed to resist lateral loads. Vertical loads are resisted by micropiles. The design allowed construction to proceed while greatly reducing the amount and length of traffic closures.

The design values for micropile-soil bond and ground anchor-soil bond were confirmed by field tests.

ACKNOWLEDGEMENTS

Funding for the design described in this paper was provided by the Federal Highway Administration.

REFERENCES

AASHTO (2004). *AASHTO LRFD bridge design specifications*. Third ed., customary U.S. units. American Association of State Highway and Transportation Officials. Washington, D.C.

AASHTO (1996). *Standard specifications for highway bridges*. Sixteenth ed. American Association of State Highway and Transportation Officials. Washington, D.C.

Armour, T, P. Groneck, J. Keeley, and S. Sharma (2000). *Micropile design and construction guidelines: implementation manual*. Report no. FHWA-SA-97-070, Federal Highway Administration. Washington, D.C.

Byrne, R.J., D. Cotton, J. Porterfield, C. Wolschlag, and G. Ueblacker (1996). *Manual for design and construction monitoring of soil nail walls*. Report no. FHWA-SA-96-069R, Federal Highway Administration. Washington, D.C.

NTL Engineering and Geoscience (1999). "FHWA geotechnical report no. 18-99: Salmon River Road; ID PFH60; Riggins, Idaho; Nez Perce National Forest". Dated 9/13/1999. Great Falls, Montana.

Sabatini, P.J, D.G. Pass, and R.C. Bachus (1999). *Geotechnical engineering circular no. 4: ground anchors and anchored systems*. Report no. FHWA-IF-99-015, Federal Highway Administration. Washington, D.C.

Samtani, N.C. and E.A. Nowatski (2006). *Hollow-core soil nails: state of the practice*. Federal Highway Administration. Washington, D.C.

Design and Construction of Circular Cofferdams for Earth Retention in a Flyash Disposal Basin

Gordon Elliott, Ph.D., M. ASCE, P.E.[1], Paul Martin[2], and Daniel D. Uranowski, M. ASCE, P.E.[3]

[1] Technical Director, Geotechnical Services, Lachel & Associates, Inc., Wexford, PA
[2] Drilling & Grouting Group Manager, Brayman Construction Corporation, Saxonburg, PA
[3] Chief Engineer, Foundation Division, Brayman Construction Corporation, Saxonburg, PA

ABSTRACT: The construction of new Limestone Unloading and Reclaim Structures, and associated conveyor tunnels, required excavation and retention of over 12m (40-ft) of fly ash and fill material. The presence of a high ground water table and a relatively thin layer of soil below the excavation also provided for challenging geotechnical conditions to be overcome by the design/build team. A traditional rectangular excavation with a perimeter consisting of soldier piles and lagging or sheet piles would require several levels of significant interior wales and struts which would interfere with excavation and construction of the new structures. Ground and site conditions dictated that tieback installation would be costly. To accommodate the requirement to provide a cost effective "dry and unrestricted" deep excavation, the design/build team opted to build a pair of circular cofferdams, incorporating cast-in-place concrete compression rings to provide the required lateral support. This paper presents the innovative design and construction techniques that were successfully implemented during the project, resulting in significant savings in cost and time over conventional excavation support methods.

INTRODUCTION

The site of a retired fly-ash disposal basin (Figure 1) had been chosen for the construction of a 21.95m (72-ft) by 16.46m (54-ft) Limestone Rail Unloading Building and an 11.58m (38-ft) by 10.36m (34-ft) Limestone Reclaim Building as part of a new scrubber construction project at a coal-fired power plant. These structures, together with associated inclined conveyor tunnels up to 49.07m (161-ft) in length, were to be founded on mat foundations, and required excavations up to 12.80m (42-ft) deep to be made.

Subsurface investigations at the site had determined that the basin consisted of up to 9.14m (30-ft) of fly ash constructed on what appeared may have been a 1.22m (4-ft) thick hard clay layer (residual shale) overlying bedrock, and capped with 1.22m (4-ft)

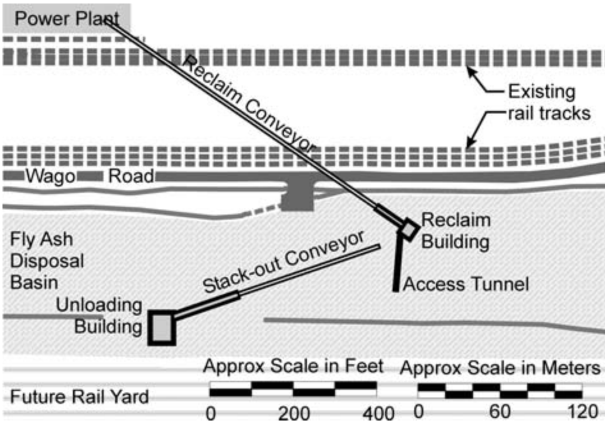

FIG. 1. Site Layout

of silty sand, clay and gravel fill that incorporated a geocomposite liner 0.61m (2-ft) below grade (see Figure 2). The relative density of the bottom 7.16m (23.5-ft) of fly ash was typically very loose to loose, whilst the upper 1.98m (6.5-ft) was typically medium dense to dense.

Approximately 7.62m (25-ft) of standing water was present within the fly ash, and chemical analyses indicated that this water contained elevated concentrations of arsenic, chromium and mercury, amongst other non-organic chemicals. Tight specifications and associated high costs of the treatment of extracted groundwater meant that it was impractical to select continuously operating well-points or other methods to draw down water levels. Therefore, the selected support-of-excavation design would have to incorporate a waterproof barrier, and be able to withstand the high hydrostatic pressures present.

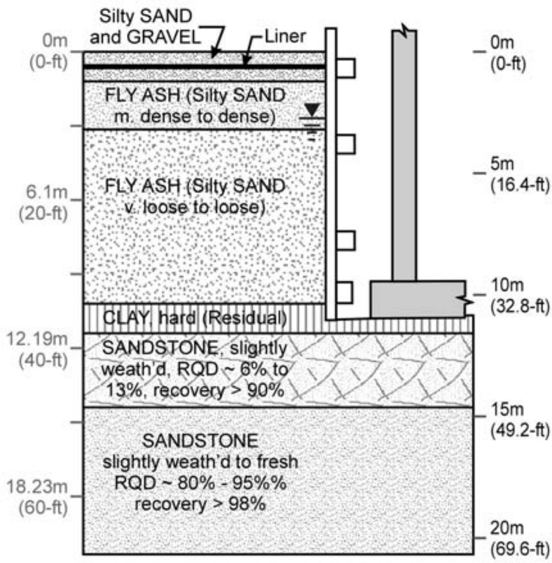

FIG. 2. Typical Geologic Section

The design of a support-of-excavation structure that closely conformed to the shape of the structures to be constructed would have required the inclusion of an expensive multi-level bracing system. The use of an internally braced system would have entailed construction of a significant system of wales and cross-lot struts that would have hindered construction of the final structures. The use of an externally tied-back system would have entailed the construction of water seals through the perimeter wall through which to drill and install the anchors. Tieback length and quantity, and wale connections also contributed to the expected high cost and time required to construct a more conventional excavation support system.

Since space was not at a premium at this site, it was decided instead to build a circular excavation for the main structures, and to use driven sheet piles braced internally by multiple levels of reinforced concrete compression wales. This solution, more usually seen in offshore construction and for deep shafts, not only allowed unrestricted overhead access to the excavation for soil and fly ash removal and building construction, but also minimized schedule and made best use of the combined resources of the construction team.

DESIGN

This solution was not without its challenges. The internal diameter of the two excavations would be 33m (108.5-ft) and 18.5m (60.7-ft) for the Unloading and Reclaim structures respectively. By design the reinforced concrete wales would be cast in-situ and it would not be possible to preload the sheets at the bracing points. The bracing system would therefore behave as a series of passive compression rings. Since the reinforced concrete sections were designed on the basis of limiting strain the expected lateral displacements of the wall were not expected to be any larger than those observed for other types of braced, anchored, or nailed walls (Clough and O'Rourke 1990).

The presence of the hard clay layer dictated that the sheets could only be driven to the base of the excavation and as a result, the sheet pile tips would ultimately be exposed. To prevent the toe from kicking in during construction, the elevations and hence quantity of the bracing points on the perimeter wall was controlled by the excavation sequence. The conveyor and access tunnels to the floors of the structures were linear and inclined, and would also be braced using reinforced concrete wales and struts. Hence the bracing for the tunnels included dead-man ties at the top of the wall, and struts at lower elevations that were required to achieve excavation to full depth, but would need to be removed prior to construction of the tunnel structures.

The design was based on the geotechnical parameters presented in Table 1, some of which had been determined by laboratory testing. A shear strength of 1.44MPa (15-tsf) was used for the low RQD rock immediately below the hard clay. Using the unloading building as the example, the imposed ground and surcharge pressures acting on the outside of the perimeter wall for each stage of construction are illustrated in Figure 3. Space was available at the site to keep the cranes and other heavy construction equipment a sufficient distance back from the rim of the excavation as to be out of the zone of influence. Therefore, the live load surcharge was limited to light traffic and materials storage.

Table 1. Geotechnical Parameters

Material	Soil Strength Parameters		Unit Weight	
	Effective Friction Angle	Effective Cohesion	Moist	Saturated
m. dense to dense silty sand and gravel	32°	0-kPa (0-psf)	19.0kN/m^3 (121-lbf/ft^3)	19.6kN/m^3 (125-lbf/ft^3)
v. loose to loose silty sand	26°	0-kPa (0-psf)	17.3kN/m^3 (110-lbf/ft^3)	19.6kN/m^3 (125-lbf/ft^3)
hard clay	26°	0-kPa (0-psf)	18.9kN/m^3 (120-lbf/ft^3)	20.9kN/m^3 (133-lbf/ft^3)

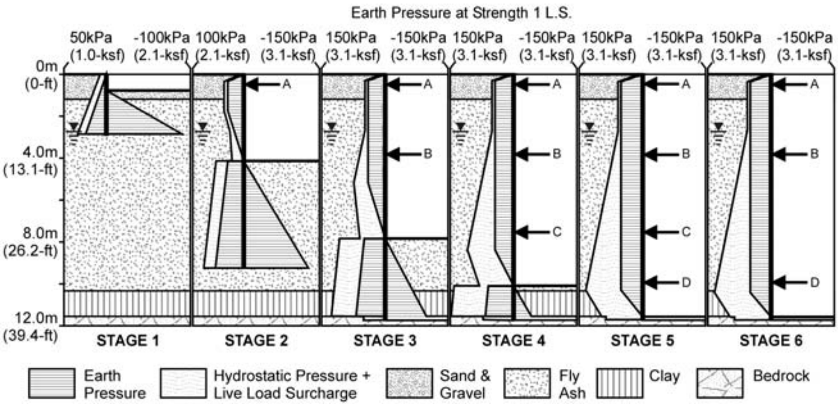

FIG. 3. Assumed Loading Conditions

The design was carried out using Load and Resistance Factor Design methods, and each stage of construction was checked for limiting equilibrium. The groundwater level within the perimeter wall was assumed to be maintained at approximately the elevation of the bottom of the excavation as the excavation was brought down. The calculated design parameters for the cofferdam walls and bracing system are presented in Table 2. The compressive force in the ring wales was calculated on the basis that the bracing force on each of the sheets was distributed uniformly around the perimeter of the excavation, and acted radially.

TABLE 2. Calculated Design Parameters

		STAGE 1	STAGE 2	STAGE 3	STAGE 4	STAGE 5	STAGE 6
At Strength 1 Limit State:							
Design Shear		11.35kN/m (0.78-kip/ft)	121kN/m (8.29-kip/ft)	275kN/m (18.84-kip/ft)	222kN/m (15.21-kip/ft)	187kN/m (12.81-kip/ft)	312kN/m (21.41-kip/ft)
Design Moment		13.29kN-m/m (36-kip-in/ft)	214.1kN-m/m (577.6-kip-in/ft)	556.5kN-m/m (1,501kip-in/ft)	203.1kN-m/m (548-kip-in/ft)	127.6kN-m/m (344-kip-in/ft)	419.4kN-m/m (1,131-kip-in/ft)
Bracing Loads	Row A	--- ---	136.6-kN/m (9.36-kip/ft)	94.7-kN/m (6.49-kip/ft)	102.4-kN/m (7.02-kip/ft)	95.9-kN/m (6.57-kip/ft)	95.9-kN/m (6.57-kip/ft)
	Row B	--- ---	--- ---	366.9-kN/m (25.14-kip/ft)	229.8-kN/m (15.75-kip/ft)	254.3-kN/m (17.43-kip/ft)	360-kN/m (24.67-kip/ft)
	Row C	--- ---	--- ---	--- ---	397.0-kN/m (27.20-kip/ft)	301.9-kN/m (20.69-kip/ft)	--- ---
	Row D	--- ---	--- ---	--- ---	--- ---	305.9-kN/m (20.96-kip/ft)	502.1-kN/m (34.40-kip/ft)
Compr'n Ring Load	Row A	--- ---	2.25MN (506-kip)	1.56MN (351-kip)	1.69MN (380-kip)	1.58MN (355-kip)	1.58MN (355-kip)
	Row B	--- ---	--- ---	6.05MN (1,360-kip)	3.79MN (852-kip)	4.20MN (944-kip)	5.94MN (1,335-kip)
	Row C	--- ---	--- ---	--- ---	6.55MN (1,472-kip)	4.98MN (1,120-kip)	--- ---
	Row D	--- ---	--- ---	--- ---	--- ---	5.05MN (1,135-kip)	8.28MN (1,861-kip)
At Service 1 Limit State:							
Displacement at top of sheet		0.01mm (0-in)	5.4mm (0.21-in)	2.9mm (0.11-in)	2.2mm (0.09-in)	-0.7mm (-0.03-in)	-3.6mm (-0.14-in)

The circular cofferdams were constructed using PZC18 Gr.345 (Gr.50) sheet piles braced at four levels (one of which was temporary because it had to be broken where the Stack-Out Conveyor Tunnel entered the main excavation) (see Figure 4). The reinforced concrete ring wales were designed on the basis of an unconfined compressive strength of 20.7MPa (3-ksi), but the concrete mix was specified to have a design strength of 41.3MPa (6-ksi) at 28-days so that forms could be removed and downward excavation continued approximately 3-days after the concrete had been poured.

Whilst the sheet interlocks could be sealed using proprietary water-stop material to prevent inflows into the excavation from the soil, there was still concern that under the high phreatic surface, groundwater could seep beneath the tips of the sheets, "float" the perimeter wall, and flood the excavation. The geologic logs of the investigation boreholes described the hard clay as residual, suggesting that it might have originated from shale strata, and therefore could not be relied upon to provide a tight seal when subjected to the vibratory hammering of the sheet pile tip. In situ packer tests had determined that the hydraulic conductivity of the massive sandstone underlying the site was on the order of $1.6\text{x}10^{-3}$ cm/sec. The hydraulic conductivity of the low RQD sandstone near the surface was expected to be much higher, and the possibility of high ground water pressure beneath the hard clay could not be ignored. To ensure that groundwater seepage did not occur through the open discontinuities, and to avert the possibility of piping of the low RQD rock material, the installation of the sheets also included a phased in situ grouting program of the upper rock strata, and the installation of tie-down anchors that would be bonded into the underlying massive sandstone. Given that the total core recovery from the subsurface investigation boreholes was typically better than 95% in the upper bedrock zone it was assumed that those fractures present are likely to be quite small in aperture and that under moderate grout injection pressures, a radius of penetration of approximately 1.37m (4.5-ft) could be achieved. Therefore, a continuous grout curtain could be created if injection holes were drilled at approximately 2.44m (8-ft) on center around the perimeter of the excavation. The installation of one 1.1MN (246-kip) anchor for every 16 sheets (10.2m (33.3-ft) perimeter distance) provided adequate tie-down force to prevent uplift from groundwater trying to pass beneath this 4.57m (15-ft) deep and 9-ft wide cut-off wall.

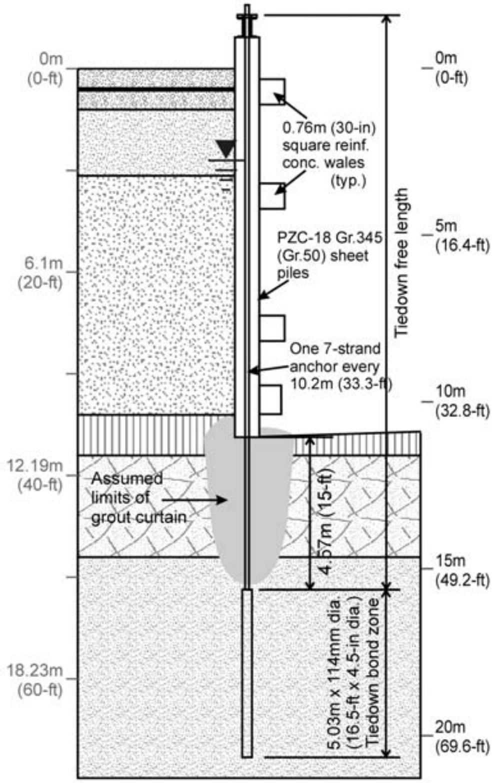

FIG. 4. Typical Section

CONSTRUCTION

Installation of the sheet piling was accomplished with the use of a Bauer BG-16 rig with each pile driven individually to refusal. The rationale for selection of the PZC-18 sheet was that the configuration of each sheet with a ball and interlock design permitted the flexibility to pivot individual sheet during placement, thus ensuring the appropriate circular configuration. A proprietary water-stop material was used to line the interlock during installation so that full perimeter seal from top to tip of the sheet piles would be created as soon as the ring was closed.

A tight tolerance on diameter and symmetry was required by the design in order to eliminate moments in the reinforced concrete wales. To maintain the critical circular configuration during pile placement a specially designed template was used. The template design consisted of a center pin and radius section to accommodate eight sheets per set-up. The template was rotated and re-placed incrementally around the entire circumference to ensure appropriate pile alignment. Although simple in design, this concept eliminated the need to procure and fabricate the full circular template

a) 33m (108.5-ft) Dia. Excavation

b) 18.4m (60.5-ft) Dia. Excav’n

FIG. 5. Construction Photos

normally used for each of the cofferdams. Thus significant savings in material, fabrication costs, and time were achieved.

After the sheeting was installed, excavation proceeded unrestricted inside the cofferdam (Figure 5). The elevation across the floor was maintained fairly uniform in order to maintain the symmetry of loading. As the level of each successive wale was reached, excavation would temporarily cease to allow the reinforced concrete ring to be formed and poured. Then, after allowing three days for concrete cure, as mentioned previously, excavation would proceed to the next wale level.

Tiedown anchors were installed and stressed, and grouting was performed around the perimeter of the cofferdam as excavation proceeded within.

Cofferdam work began in April of 2007 and was completed in approximately two months – well ahead of the originally anticipated schedule. Residual inflows to the excavation were handled using a standard sump pump, indicating that the design and construction had been successful in achieving a largely watertight system. Any deflections that may have occurred were not significant enough to be worthy of note.

CONCLUSIONS

This paper has described the design and construction of a pair of circular sheet pile cells, one 33m (108.5-ft) in diameter and the other 18.5m (60.7-ft) in diameter, which were built to provide the support of excavation for two 12.80m (42-ft) deep excavations in a saturated fly ash disposal basin containing elevated concentrations of several inorganic compounds. These PZC18 sheet pile cells were internally braced using multiple levels of 0.76m (30-in) and 0.51m (20-in), respectively, square reinforced concrete wales. The excavations were maintained watertight under a 7.62m (25-ft) hydrostatic head by the use of proprietary water stop material in the sheet interlocks, a program of injection grouting to form a cut-off wall in the low RQD rock beneath the sheet pile tips, and tie-downs to oppose the residual uplift.

This experience has shown that where space allows, this form of excavation support can offer significant benefits over alternate construction methods. These benefits not only include savings in cost and schedule, but also benefits in maintaining a clean and tidy site where potentially contaminated soils exist, eliminating troublesome wales and cross-lot struts, and enabling the different skill sets of the general and specialty contractors to be optimized.

REFERENCES

Clough, G.W. and O'Rourke, T.D. (1990). "Construction Induced Movements of Insitu Walls." *Design and Performance of Earth Retaining Structures* (GSP 25), ASCE, Reston/VA: 439-470.

Sabatini, P.R., Pass D.G., and Bachus, R.C. (1999). "Geotechnical Engineering Circular No. 4, Ground Anchors and Anchored Systems." *FHWA-IF-99-015*. Federal Highway Administration, Washington D.C.: 51

Terzagi, K. and Peck, R.B. (1967). *Soil Mechanics in Engineering Practice*, 2nd ed. John Wiley and Sons, Inc.: 192 and 263.

Design and Construction of Temporary Excavation Support at a Water Intake Structure

Gordon Elliott, Ph.D., M. ASCE, P.E.[1] and Gary Pate, P.E. [2]

[1] Technical Director, Geotechnical Services, Lachel & Associates, Inc., Wexford, PA
[2] Project Manager, G.M. McCrossin Inc., Bellefonte, PA

ABSTRACT: The construction of the Water Intake Structure for a new Cooling Tower at a power plant required excavation of a 16.76m (55-ft) deep pit beside the Susquehanna River south of Harrisburg, PA. The grading for the excavation was confined by a lined fly ash landfill on one side, an unlined fly ash waste area on another and the outlet channel from the existing operating power plant on a third. With top of rock being little more than 1.52m (5-ft) beneath the normal pool in the outlet channel, and rises in pool level in the Susquehanna River expected to be as much as 5.5m (18-ft) during construction, the site presented challenging conditions to be overcome by the design/build team. In addition to providing a description of the different ground support structures used in this project, this paper will focus on the innovative design and construction techniques implemented to construct the river wall in the dry, maintain a water-tight barrier, and provide for unfettered wall removal and channel restoration.

INTRODUCTION

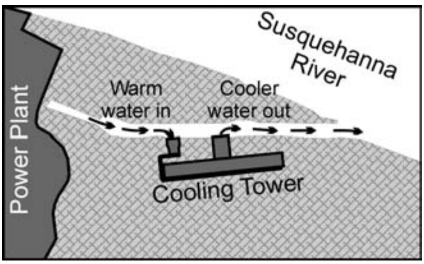

FIG. 1. Site Map

A 34-cell cooling tower capable of cooling 1.89 million liters (a half million gallons) of water every minute has recently been constructed at a power plant south of Harrisburg, PA. The plant uses water from the Susquehanna River as coolant in the power generation process. The cooling water is then returned to the river. However, in the summer months, when low flows in the river and higher water temperatures have the greatest impact on aquatic life, the temperature of the returning water needs to be reduced. This reduction will be achieved by passing it through the cooling tower (Figure 1).

Construction of the water intake and feed pipe required the excavation of a 16.76m (55-ft) deep pit immediately beside the discharge channel to the Susquehanna River, and a 6.4m (21-ft) deep trench (Figure 2). The grading for the excavation was confined by a lined fly ash landfill to the north, an unlined fly ash disposal basin to the west, and the outlet channel from the existing operating power plant to the east. With top of rock being little more than 1.52m (5-ft) beneath the normal pool in the outlet channel, and rises in pool level in the Susquehanna River expected to be as much as 5.5m (18-ft) during construction, the site presented challenging conditions to be overcome by the design/build team.

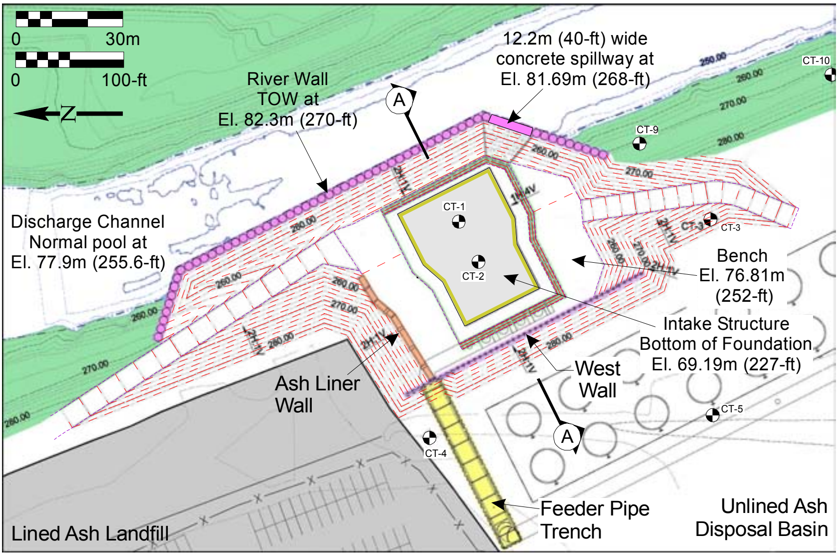

FIG. 2. Site Layout

SITE CONDITIONS

Subsurface investigations at the site had determined that the banks of the discharge channel consisted of a layer of alluvial silt above a layer of silty gravel and sand that overlaid bedrock (Figure 3). The relative density of silt was loose to medium dense, whilst the gravel and sand was medium dense to dense. Inland from the discharge channel, the area had been developed as an unlined fly ash disposal basin. The fly ash was described as very loose to medium dense silt and silty sand, which varied in thickness with increasing distance from the discharge channel until it appeared to have been placed directly on bedrock. The bedrock elevation formed the bottom of the discharge channel at approximately El. 76.2m (250-ft), and then rose in elevation slowly westward. The underlying bedrock was a weathered sedimentary formation variously described as sandstone, siltstone, and shale, and whereas the core recovery

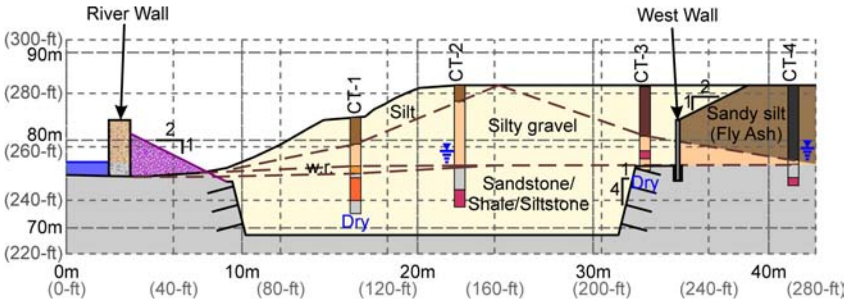

FIG. 3. Geologic Section A-A

was typically better than 90%, Rock Quality Designation was anywhere from 0% to 70%.

SUPPORT METHODS

Several different ground support methods were used in conjunction with conventional grading to create a 17m (56-ft) deep excavation through soil and rock. Early on in the design process, it was decided to take the initial excavation down to top of rock, and there create a 12.2m (40-ft) wide bench on three sides of the deeper rock excavation on which to locate the cranes that would be needed to construct the water intake structure. Cement grouted rock bolts and wire mesh were used to provide stable walls to the nominally 7.62m (25-ft) pit in which the mat foundation and wet wells would be constructed.

On the north side of the excavation, grading was constrained by the presence of the lined fly ash landfill, where the lining could not be damaged. Therefore, along this side of the excavation, a 3.05m (10-ft) high, 30.46m (100-ft) long and nominally 1.52m (5-ft) thick concrete block wall was used to provide grade separation.

On the west side of the excavation, a 5.49m (18-ft) high, 73.7m (242-ft) long non-gravity cantilever wall (West Wall) was constructed using W460x158 Gr.345 (W18x106 Gr.50) steel soldier piles set in 0.76m (30-in) holes drilled 1.52m (5-ft) into rock and backfilled with sandy gravel. The piles were lagged with pairs of PZC13 sheet piles driven down to top of rock to retain the materials in the fly ash disposal basin. At the north end of this wall, where it tied into the Feeder Pipe Trench, the wall reached 7m (23-ft) high, and W838x176 Gr.345 (W33x176 Gr.50) soldier piles were used. Previous experience with these material found that although these materials can be graded at 3H:1V, and even 2H:1V, stable slopes, they tend to "flow" and become quite unmanageable during heavy rainfall events. Therefore, the wall limited the area of fly ash that would be disturbed during construction of the intake structure.

A braced sheet pile trench was used to provide ground support for the buried portions of the 3.66m (12-ft) diameter high pressure feeder pipe that would convey the warm water from the intake structure to the rear of the cooling cells. The approximately 50.9m (167-ft) long, 5.79 (19-ft) wide, and 6.4m (21-ft) deep trench was constructed using PZC13 Gr.345 (Gr.50) sheet piles driven to rock. As a result of the shallow depth of rock below the dredge line (2.29m (7.5-ft)), the sheets needed to be braced at two levels in order to reach the required excavation depth. A 0.3m (12-in) thick mud mat was placed across the bottom of the excavation to provide a compression strut so that the lower bracing could be removed to leave room to place and assemble the 3.66m (12-ft) diameter feeder pipe sections. The design was formulated so that work within the trench could progress sequentially from one end of the excavation to the other, giving the contractor the flexibility to reuse some of the bracing elements.

The final element of the excavation support system was the River Wall. Since the east side of the intake structure projected out into the discharge channel, it was necessary to construct an impermeable barrier out in the river that would not only limit the obstruction to the flow of water in the discharge channel to less than 50% of its existing capacity (so that operation of the power plant could continue uninterrupted), but also provide a dry excavation within which to carry out the construction. The contract documents further required that the River Wall be removed at the end of construction and that the discharge channel be restored to its existing condition.

Data for the pool level in the discharge channel had been recorded for 5-years prior to the project being advertised for bid (Figure 4). The data indicated that whilst the depth of water typically varied between 1.52m (5-ft) and 4.27m (14-ft), about once per year on average the depth of water exceeded 4.88m (16-ft). Since the contractor wanted to limit the risk of flooding the excavation during construction, the river wall would need to be designed for at least this depth of water.

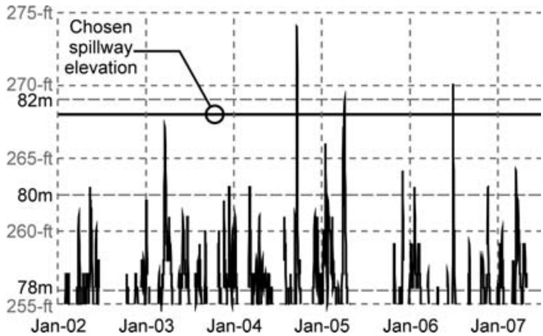

FIG. 4. River Gage Data

Given the relatively shallow depth of water in the channel, and somewhat irregular bottom, it was not feasible to bring in barges from which to stage construction of another soldier pile wall. Therefore, the only feasible solution was to construct some type of gravity wall system. The method that was ultimately constructed was a cellular wall supported on the land side by a rock fill buttress (Figure 5). This method took advantage of the normally shallow pool for placing an initial layer of rockfill to create a causeway on which construction equipment could move about to install the cells "in the dry".

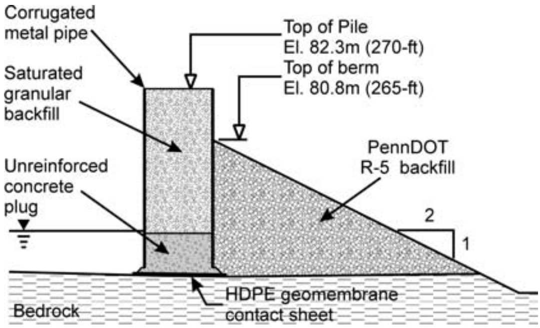

FIG. 5. Cross-section through River Wall

The main components of the cellular wall were inexpensive 2.44m (8-ft) diameter corrugated metal pipe sections that were conveniently supplied in lengths 6.1m (20-ft) long. These could be easily transported and placed side-by-side in the river bottom to form a row of upright metal cells. At the design stage, it was envisaged that the irregularities of the river bottom could be overcome by setting the cells in wet concrete. This would be achieved by first standing the pipe on-end at the desired location in the river, and then placing approximately 0.61m (2-ft) of concrete in the bottom. While still wet, the pipe would be lifted slightly to let this concrete slump out of the bottom and spread slightly before setting the pipe back down with the top of the pipe at the desired elevation. In this way, not only would the vertical irregularities be accommodated, but also the spreading concrete from one pipe would meet the spreading concrete from the adjacent pipe to create a continuous water tight barrier along the base of the wall. A 2mm (0.08-in) thick HDPE contact sheet placed between the concrete and the river bottom would provide an adhesion break so that at the end of the project, each cell and its concrete plug could be easily lifted and removed without disturbing the river bottom. Bedrock formed the river bottom and the wet concrete would mold the contact sheet around the natural irregularities. Small amounts of seepage beneath the contact sheet were tolerable. After the concrete had set, the depth of concrete inside the cells would be increased to 1.52m (5-ft) in order to create greater stability during later stages of construction, and later the remainder of the cell would be filled with saturated site fill to add weight and rigidity.

In the design, the gap between adjacent cells would be closed by constructing a vertical plug (Figure 6). First, a 0.91m (3-ft) arc section of corrugated metal pipe would be placed across the gap and tack-welded to the outside of the pair of cells to be plugged to form a guard plate. A 0.61m (2-ft) diameter sock, made from a non-woven geotextile tube closed at one end using heavy gauge tie wire, would be lowered into the void bounded by the adjacent cells and the guard plate. The sock would then be filled with a

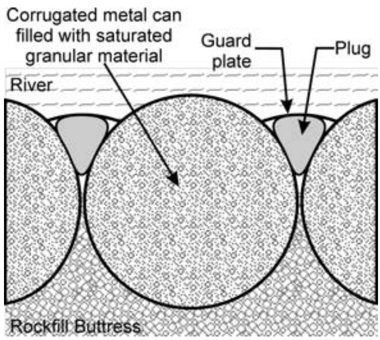

FIG. 6. Plan of wall components

low strength bentonite/cement grout to create a vertical plug that would conform to the shape of the corrugations of the pipes. As the fill material hardened, it would not only create a low permeability plug, but would also provide a degree of plasticity so that as the level of water in the discharge channel rose, the plug would want to squeeze into the gap between the adjacent cells, thereby providing a tighter seal.

When the construction of the line of cells was complete, the rockfill buttress on the land side of the wall could be raised. The purpose of the buttress was to provide resistance against overturning and sliding of the cellular wall when the water level on the river side was at the design elevation. The height of the buttress was constrained by the need to maintain outward stability of the cellular wall when the water level on the river side was at normal pool elevation. Several analyses of different granular materials having different angles of internal friction were evaluated during the design to provide an optimal balance between the performance requirements and availability.

As indicated by the gage data, when the river levels reach their maximum values, they tend to rise rather quickly. In order to avoid the possibility of losing the wall during flood events as a result of the overflowing water eroding away the buttress material and potentially knocking over the cells, it was decided to incorporate a concrete lined spillway into the wall design (Figure 7). The crest width and elevation were set on the basis of the hydrological considerations that the water level in the flooding excavation would rise sufficiently quickly to balance the river level before it reached the top of the cells. Conversely, sufficient pumps were sized to be able to draw down the water inside the excavation at the same or similar rate to the fall in river level as the water receded.

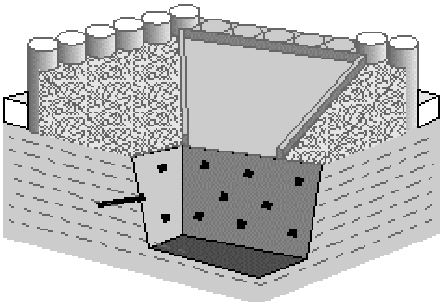

FIG. 7. Proposed Concrete Spillway

CONSTRUCTION

Although the cellular wall was designed to be constructed off a causeway that would become part of the final buttress, the contractor decided to install a 1.82m (6-ft) high, inflatable Aqua-Dam® in the discharge channel around the perimeter of the work and then dewater the land-side. This would facilitate cleaning the thin layer of alluvial sediments off the top of rock before the HDPE contact sheet was put down, and would allow for the placement of a continuous 0.15m (6-in) thick concrete slab on top of the contact sheet along the entire length of the cellular wall. The latter would provide a flat and level surface upon which to stand the cells plumb and eliminate the risk of the cells becoming out of plumb as concrete plug was placed. It would also facilitate the placement of the guard plates which could easily be stick welded to the cells working off ladders. The dam would then be removed when construction of the wall was completed.

The socks used to create the plugs between the cells were made from tubes of non-woven geotextile, which were backfilled in-place with a mixture of bentonite powder and sand in the proportions 1:9 by weight instead of the bentonite cement grout indicated in the drawings. These materials were mixed dry in a pug mill and poured into the open end of socks. Water was not added since it was assumed that sufficient water would penetrate the mix from the river to hydrate the bentonite. However, by not mixing the materials with water in a concrete mixer prior to placement in the socks, and by constantly pulling up on the geotextile as the fill was placed, it was suspected that the material might not have fully filled the corrugations in the cells, and the materials themselves might not have been mixed thoroughly enough to achieve the uniform, low permeability plug that was expected. Hence, when the Aqua-Dam® was deflated, the system leaked at an unacceptable rate. To reduce the inflows, a supplemental liner system made from overlapping lengths of standard rubber roofing material was placed on the outside of the cells. 7.62m (25-ft) wide sheets of this material were suspended from wooden planks fixed in place at the top of the cells and jutting out just so far to prevent the sharp metal edges from damaging the rubber. These sheets were overlapped 1.22m (4-ft) in the down-stream direction, and were weighted down in the river using sand bags and rock fill. The combined system reduced inflows to the excavation that could easily be handled using three 75mm (3-in) electrical submersible pumps that ran continuously during the construction period.

FIG. 8. Completed River Wall During Construction of the Intake Structure

Construction of the intake structure was completed between July 2008 and February, 2009, during which the water level in the discharge channel rarely rose above El.

79.25m (260-ft). The entire cellular wall was then removed over a two-week period, by first removing the rock fill down to El. 77.7m (255-ft) and then removing the cells working from one end towards the other. The rock fill was re-used on the banks as fill and erosion protection. Each cell was removed by first making two vertical cuts down to this elevation on the land-side. This enabled a portion of the cell wall to be peeled away, to allow the soil backfill to be easily removed from within. With the soil backfill removed, the perimeter of the cell was cut at El. 77.7m (255-ft), and the upper portion removed together with the guard plate to the next cell and the geotextile sock that had plugged the gap in between. The remaining concrete filled section and base slab, weighing approximately 160kN (36-kips), could then be lifted out of the river to be broken up on-shore and disposed of. After cell and slab removal, the causeway and remaining buttress material was removed, starting in the center and working out both north and south, resulting in the channel being left in the same condition as it was found prior to construction. By following this approach, the removal plan eliminated the need for dirt/silt containment in the discharge channel.

CONCLUSIONS

This paper has described the design and construction considerations for a water tight barrier that was successfully constructed in the Susquehanna River to enable the construction of the water intake structure that was part of a new Cooling Tower project at a power plant. By not over-complicating the design, but instead focusing on the details of construction and removal, a gravity wall system made from corrugated metal pipe sections stood on end, backfilled with site soils and supported on the land side by a rockfill buttress resulted in significant savings in cost and time over conventional barrier support systems.

Key elements of the wall were not constructed as planned, which lead to leaks that had to be addressed after the fact. Whilst the methods shown in the design drawings were simple and were embraced by the contractor at the design stage, they were unusual and were changed when work started. Given a second chance, the contractor would have first trained his on-site personnel using a trial wall constructed on land before starting work in the river, and thereby avoided the unwanted leaks.

Recent Advances in the Top-Down Construction of a 26.4 Meter Deep Soil Nail Retention System—Bellevue Technology Tower

D. M. Cotton[1] and R.D. Luark[2]

[1] Kleinfelder, 14710 NE 87TH Street, Suite 100, Redmond, WA, 98052
Email: dcotton@kleinfelder.com
[2]Kleinfelder, 14710 NE 87TH Street, Suite 100, Redmond, WA, 98052
Email: rluark@kleinfelder.com

ABSTRACT

This paper covers several aspects of the Bellevue Technology Tower Project in downtown Bellevue, completed in 2007 after a project start in 2001. The base of the excavation was completed 26.4 m below 108th Avenue NE, with an additional 2.1 m excavation for the mat foundation which extended the total depth of the excavation to approximately 28.5 m below street grade. It is believed that this was the deepest soil nail wall, built to date in the U.S., with a top-down construction procedure. The top-down building procedure includes construction of the permanent 31 - 46 cm thick shotcrete basement wall for the building as the facing for the temporary soil nail shoring in lifts, eliminating the requirement for temporary facing. During the excavation and shotcrete placement on the bottom row of the excavation, at an average depth of 22.7 m, the 2001 Nisqually Earthquake occurred with an Mw 6.8 event. No ground loss was experienced, and only nominal permanent lateral displacements were measured after the earthquake.

Recent advances that were implemented during the design and construction included the use of strut nails to support vertical loads and limit deflections in the first lift where fill is typically encountered, use of a composite soil nail wall with vertical elements to support an 8 story building along the south property line, use of splayed nails in a re-entrant corner with a 3 story building surcharge, and use of nails to carry vertical loads of the conveyor for excavated soils.

Finally, an extended life study of the system was completed after the project was put on hold prior to completing the floor slabs for the garage structure. The temporary soil nail system was only designed for the life of the excavation which in this case was approximately one year. In addition, a temporary wall is not designed for earthquake resistance, although the static factor of safety does provide for some inherent resistance. The soil nails are not designed with any corrosion protection for the extended life. After evaluating the corrosion rate and seismic recurrence of critical earthquakes an extended life of 4 to 8 years was determined for the temporary soil nail retention system.

INTRODUCTION

The top-down soil nail wall for the Bellevue Technology Tower included the following features:

The use of strut nails for face stabilization and deflection control;
The use of strut nails to carry vertical loads;
The use of splayed nails for a re-entrant corner;
A composite soil nail system with vertical elements to carry vertical loads and for face stabilization;
The use of top-down construction to build the permanent basement wall with temporary nails to the deepest recorded depth in the U.S. to date at 26.4 m, (2001);
A stable seismic response of the soil nail wall during an Mw 6.8 earthquake event, and;
A stable performance of the soil nail wall for 4 years beyond the original design life following an analysis of the seismic risk and corrosion of the steel nails.

The proposed Bellevue Technology Tower excavation encompassed an area slightly smaller than a city block, 59.1 by 50.9 m in downtown Bellevue, Washington. A site plan is shown on Figure 1, which illustrates that the project site is bounded on two sides by city streets and existing buildings on the other two sides. The shape of the excavation also includes a re-entrant corner. The Key Bank Tower, located on the west boundary of the excavation, has three levels of below grade parking garage. An 8 story office tower on top of the garage is set back from the excavation face approximately 6 m. The planned development was to include a twenty story building with eight stories of below grade parking. The below grade floor slabs at 8 levels were intended to provide for the final lateral load support. However, due to an economic downturn in the local market the project construction temporarily ceased following the excavation and foundation construction. Therefore, an evaluation of the soil nail system for an extended period beyond the 12-month planned designed life needed to be completed after construction ceased.

The base of the excavation was constructed to a depth of 26.4 m, below 108th Avenue N.E. It is believed that this is the deepest soil nail wall, built to date in the US, with a top-down construction procedure. The top-down building procedure includes building the permanent 300 mm to 450 mm thick shotcrete basement wall, with a double curtain of steel reinforcing, as the excavation progresses, installing the temporary nail system to a maximum depth of 26.4 m. A 2.1 m thick mat foundation was excavated approximately 6 m inside the excavation line extending the total depth of the excavation to approximately 28.5 m below street grade. The excavation required approximately 5,060 square m of permanent shotcrete wall construction. During the excavation and shotcrete placement of the last level of nails, at an average depth of 74.5 feet, the 2001 Nisqually Earthquake occurred with an Mw 6.8 event. No ground loss was experienced, and only nominal permanent lateral displacements were measured after the earthquake.

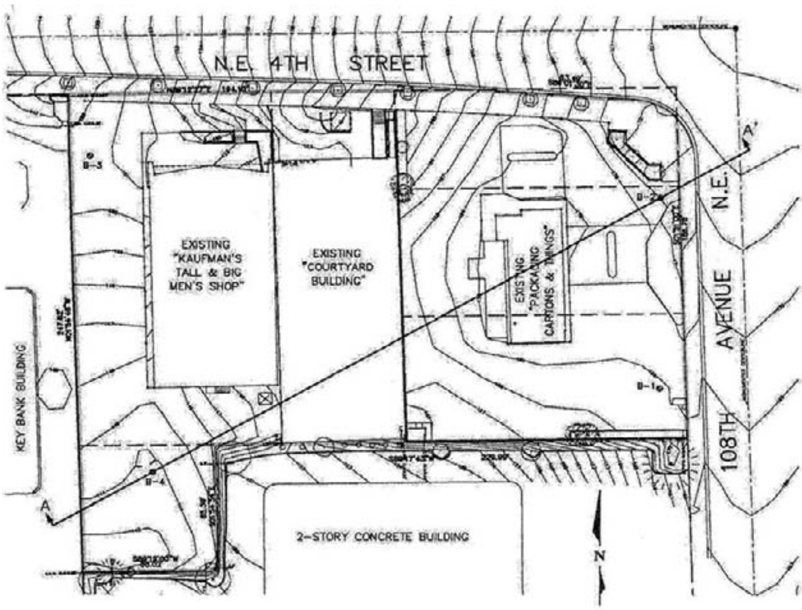

Figure 1

In general, the site is underlain by variable, minor amounts of fill, overlying dense till, dense advance outwash sands and gravels, and glaciolacustrine deposits of silt. The fill varied in thickness from less than 0.3 m to 4.3 m in the northwest corner of property, and consisted of loose to dense gravel and sand on the west side of the site, and soft to hard silts with sand and gravel on the east side. The native glacial till is generally a dense sandy silt, with little gravel, and ranged from 10 m thick on the east side to zero feet on the west. The advance outwash gravel was

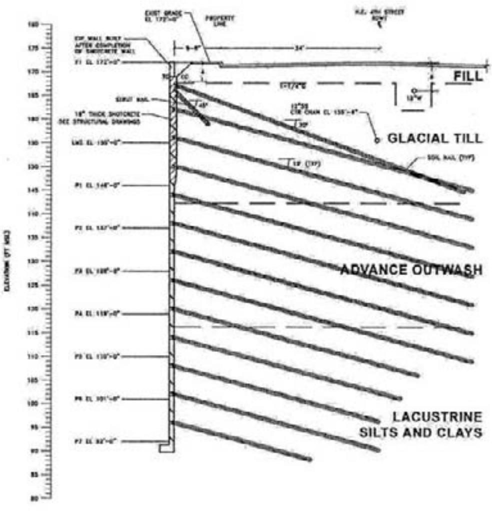

Figure 2

generally very dense gravel, with some fine to coarse sand and trace silt. Below the advance outwash gravels were the advance outwash sands, consisting of a very dense fine to coarse sand, with trace silt and some gravel. The advance outwash sand and gravels extended to an average depth of 19 m where the glaciolacustrine deposits were encountered. The glaciolacustrine silts were generally hard and very dense silt and clayey silt with a trace of very fine sand and subrounded gravel. Groundwater was encountered at or near the base of the excavation, at an average depth of 22 m below street level. Groundwater appears to be perched on top of the glaciolacustrine deposits.

SOIL NAIL WALL DESIGN

The soil nail wall design consisted of up to thirteen rows of nails on a 1.8 m by 1.8 m nail pattern. The upper row of nails included a strut nail system used to support vertical loads in the upper fill materials, as shown in Figure 2. Strut nails were also used to support the weight of a conveyor about midway down the north wall, which was being used to

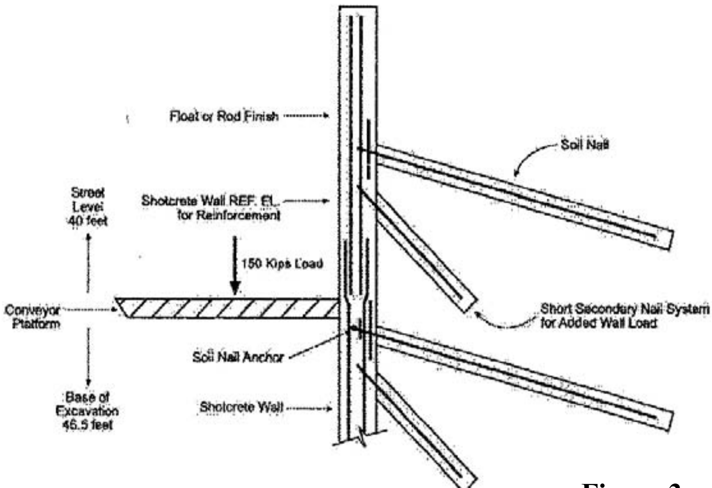

Figure 3

remove soil from the base of the excavation. The platform load was approximately 150 kips, supported by 5 strut nails, and is shown schematically in Figure 3. The maximum wall height on the north wall, 26.4 m, included nail lengths that ranged from a maximum for 20.1 m in the upper eight rows to decreasing lengths of 16.5, 15.2, 13.7 and 9.1m. The bar sizes ranged from 32 mm diameter 150 grade steel to 25 mm diameter 150 grade steel. The bars were typically inclined at 15 degrees, except for the upper row which was inclined at 20 degrees to avoid utilities. Strut nails were inclined at 45 degrees. A typical section is shown in Figure 2. The splayed layout for the southwest re-entrant corner is shown in Figure 4. The splayed nail design is done simply by taking the 2D analysis performed using the program GoldNail, and then increasing the length of the nail according to the geometric orientation of each nail splayed.

The stability analyses were performed using the program GoldNail, Verison 3.11 on five critical sections for each of the five walls surrounding the project. The soil design parameters used in the analysis were based on the field tests completed during the site investigation, laboratory testing, and the author's experience in the Bellevue area and Puget Sound Region.

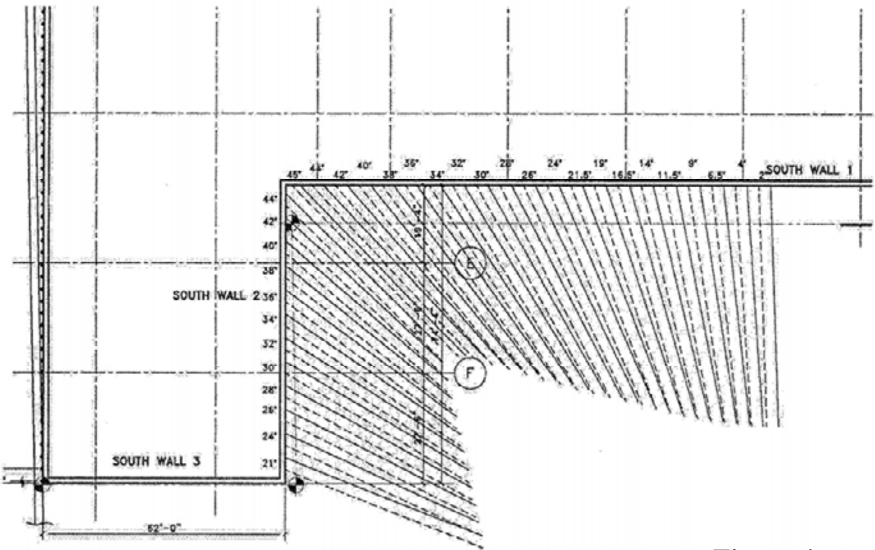

Figure 4

Specifically the soil nail design parameters used in the final analysis were:

TABLE 1.

Soil Unit	Unit Weight (PCF)	Friction Angle (Degrees)	Cohesion (PSF)	Ultimate Out Resistance (Kips/Ft)
Fill	120	34	100	6.3
Glacial Till	135	40	300	12
Advance Outwash	125	40	100	8.4
Lacustrine Silts and Clays	125	34	300	4.2

A factor of safety of 2 was utilized for nail pull out and a factor of safety of 1.35 on the soil strength parameters.

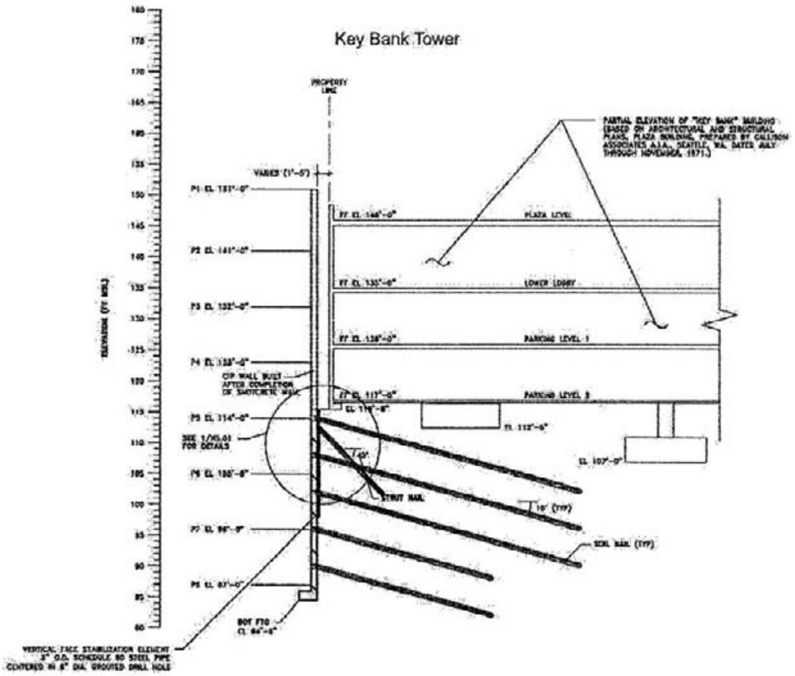

Figure 5

Another one of the features on this project was the use of vertical elements to stabilize a potential ground loss problem at the face of the excavation on the west side. The excavation section is shown in Figure 5, which illustrates the Key Bank Tower parking garage and tower footings. Anticipated lateral stresses at the face of the excavation combined with excavating 2.4 m vertical faces in the relatively clean advance outwash sands and gravels, led to the decision to include the use of vertical face stabilization elements. These are shown in Figure 5 and consisted of 76 mm O.D. schedule 80 pipe in a 150 mm diameter drill hole filled with grout and spaced 0.9 m on center. Vertical elements were extended 5.5 m below the basement footing for the bank tower, which included three rows of nails. It was felt that adequate confinement would be provided at this level so that no loss of ground support would be experienced below the footing. Also shown in Figure 5 is the use of strut nails which were included to control deflection, carry imposed vertical loads from the adjacent building, and improve face stabilization during excavation.

PERFORMANCE

The excavation began in October 2000 and was finished in March 2001. During excavation and construction of the excavation support wall, optical survey monitoring was performed that recorded maximum horizontal displacements on the order of 0.001H to 0.002H, where H is the maximum wall height. This resulted in permanent displacements at the top of the wall ranging from 6 mm (west wall) to 50 mm (north wall). These displacements during excavation and construction of the wall are normal and within the range for the soil type at the site.

The soil nail system performed well during the Nisqually earthquake of February 28, 2001, which occurred during excavation of the deepest lift of the excavation with only nominal movements of the soil nail wall. Maximum movements of 6 mm were noted on the re-entrant corner of the excavation, typically regarded as the weakest point of the structure. This movement was well within the design criteria for the wall. Additionally, no structure damage to neighboring buildings was discovered. The peak ground accelerations produced by the Nisqually Earthquake in Bellevue were on the order of .11g, about one-third of the design earthquake for permanent structures in the Seattle area.

EXTENDED LIFE ANALYSIS

Finally, an extended life study for the system had to be completed since the project was put on hold prior to completing the floor slabs for the garage. A temporary soil nail system is only designed for the life of the excavation which in this case was approximately one year. Therefore the owner requested an evaluation of the soil nail system for an estimated life of reasonable performance. A temporary wall is not designed for earthquake resistance, although the static factor of safety does provide for some inherent resistance. This was certainly the case for the resistance provided during the Nisqually earthquake. In addition, the soil nails are not designed with a corrosion protection for extended life performance. Based on the results for an extensive seismic analysis of the as built condition it was determined that the existing temporary excavation support system was adequate to resist the UBC design earthquake over the next 4 to 8 years.

CONCLUSIONS

The project involved several features that were innovative at that period of time in the United States, which included the construction of the permanent building walls from the top down, eliminating the need for temporary shoring facing. In addition, vertical elements were used to provide face stability to allow soil nailing shoring to support adjacent building foundation surcharge loads. Also, the use of strut nails was employed to support the vertical load of the permanent building wall as well as temporary construction loads. Finally, due to an economic down turn, the project was placed on hold, requiring an evaluation of the existing temporary support system for seismic loading and long term corrosion potential. The use of these innovative features resulted in significant cost savings to the project.

The Behavior of a Deep Retained Excavation in Soft San Francisco Bay Mud

Gregory P. Wilson, Ph.D., P.E., M.ASCE[1]

[1]Assistant Professor, Department of Industrial Engineering and Technology, Texas A&M University-Commerce, P.O. Box 3011, Commerce, TX. 75482-3011: PH (903) 886-5474; FAX (903) 886-5960; email: Gregory_Wilson@tamu-commerce.edu.

ABSTRACT

This paper presents portions of a five-part study done to further investigate the behavior of a deep braced excavation and improve upon existing techniques for estimating the magnitude of the transitory forces in such structures. This year-long project, constructed in San Francisco Bay Mud, was completely instrumented and monitored throughout the construction process. This initial part of the research provided the measured geotechnical and structural data with which to compute and compare load predictions made at various stages of construction. The second part of the study consisted of the development of a three-dimensional finite element structural model to allow for the application and study of various earth pressure theories proposed in the literature as well as a new earth pressure hypothesis developed and presented for this project. Comparisons were calculated and tabulated in the third and fourth parts of the study which included the evaluation of the relative performance of each model in predicting structural loads. Conclusions and recommendations were presented within the fifth part.

With respect to the five earth pressure models selected for comparison, those with triangular shapes performed slightly better in the prediction of structural loads than did those with trapezoidal configurations. For the new model proposed and developed, the use of the Tributary Area method along with earth pressures from K_o effective stress plus best-estimate pore pressures without reshaping of the newly suggested earth pressure diagram is recommended.

Bending stresses within specific strut members were found to be surprisingly high with measured values averaging approximately 85% of P/A stresses. Augmentation of the predicted compressive stresses by 150% is recommended until further studies are completed. The finite-element structural model developed was a valuable research tool but incredibly labor intensive. Continued use of the Tributary Area Method is recommended for routine design of braced excavations.

INTRODUCTION

The use of braced cuts and deep retained excavations in varying soil conditions for the purpose of installing subsurface structures has long been a major concern of geotechnical engineers. Considerable research has been conducted with respect to the design and subsequent behavior of these transitory structures. There is even evidence which suggests that efforts to model the behavior of such excavations, predict performance and measure the resulting responses were made as early as the nineteenth century (Peck, 1973).

This type of system which may cover several blocks in plan consists basically of a water-tight flexible wall structure. Site congestion in addition to the protection required for public utilities and access requirements to the project itself invariably require the use of vertically cut walls in both granular and clay-type soils. In addition, the location of many such projects and the type of subsurface conditions often encountered present a series of design problems which are unique to the support systems of this nature.

Braced excavations are frequently required in metropolitan areas which are often located on or near navigable water systems. The soils on which these cities are located were deposited under water; they may possess very low shear strength and be extremely compressible. Further, these urban areas are often built on fill which consisted of poor material deposited with little to no compactive effort (Lambe, 1970). These site conditions, in addition to the complex interaction between the soil and the structural components of the bracing system, serve to further compound the complexity of assessing the necessary design parameters.

The system itself must be designed with economic constraints yet perform acceptably. Engineers often call for very large structural sections because of their desire to minimize lateral movements and to create large factors of safety. These large sections are difficult for the contractor to handle as seen in the excavation study presented within this document; welding and fabrication costs are higher; the equipment necessary to handle and place these sections once at the jobsite becomes proportionately larger and further adds to the expense of the project.

The bracing system must restrain the movement of the large soil masses and structures adjacent to the opening, in addition to prohibiting the deep seated failures of the soil masses below the excavation which are generally associated with construction such as this. The predictability of the performance of such a structure then becomes paramount in importance from a safety and liability standpoint.

Project Description

For this study, a large retained excavation measuring 30.5 m x 61 m in plan with a depth of approximately 14.1 m done in San Francisco Bay mud was fully instrumented to compile additional documentation concerning the performance of such structures. See Figure 1 on the following page. This instrumentation consisted of (1) vibrating wire strain gages for measuring the axial deformations in the cross-lot strut system, (2) inclinometers set on two sides of the excavation for determining the lateral movements of the sheet piles, (3) survey monuments mounted both on the inside of the excavation and the outside to monitor surface subsidence adjacent to the site, lateral movements of the walers inside the excavation and relative movements of any structures in close proximity to the project, and (4) shallow and deep well points installed to monitor the fluctuations in the elevation of the ground water table both inside and outside the excavation.

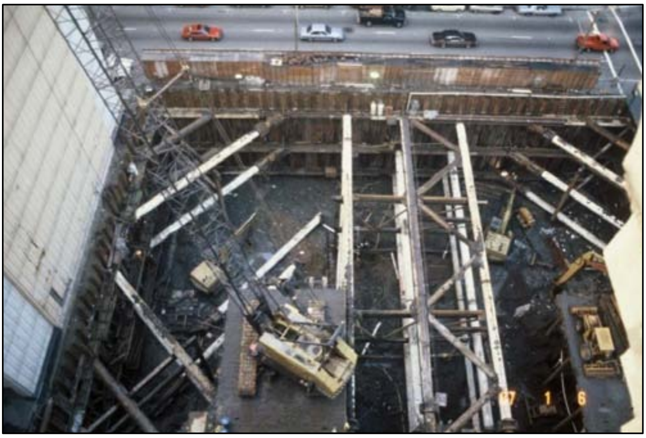

Figure 1. Aerial View of Excavation

Impact of the Construction Sequence

With respect to the construction sequence, Lambe (1970) recommended that

"The satisfactory performance of an earth-retaining structure is highly dependent upon the procedures used to build the structure. It thus becomes essential that the engineer not only design these structures but follow carefully their construction."

In an effort to determine the possible effects on the structural behavior of the support system, the construction sequence, including equipment used by the excavation contractor and its subsequent location within the jobsite, was systematically photographed as seen in Figure 1 above and Figure 2 below. This data was subsequently correlated with the measured strut loads and discussed in the results of the study.

Figure 2. Impact of Construction Sequence

Collection and Correlation of Data

Data has been compiled from strain gages mounted on the nine cross lot struts, inclinometers located behind sheet pile walls, well-point monitoring and phreatic surface fluctuation data in addition to significant surveying data collected both inside and outside the excavation. It was reduced, plotted, and correlated for use in determining the behavior of the excavation over the entire duration of the construction process. This data too, was correlated to the extensive amount of subsurface geotechnical data available from the project geotechnical engineer, a portion of which is detailed below in Figure 3. More specifically, this data served as the basis for the development of the active and at-rest earth pressure diagrams and subsequently all of the earth pressure models developed for this study.

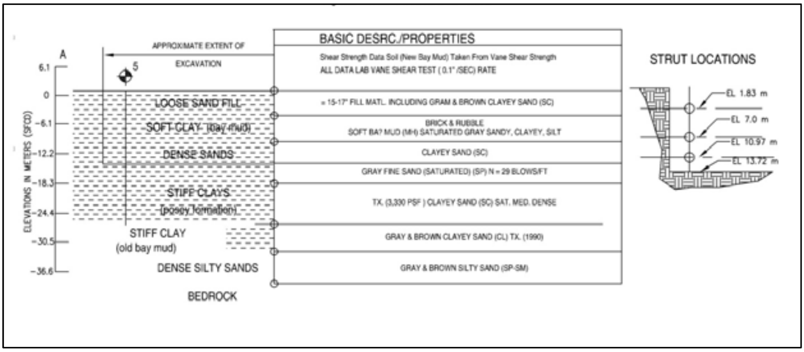

Figure 3. Subsurface Geotechnical Data

Evaluation of Lateral Earth Pressure Models

Following the completion of the data gathering phase of the project, the earth pressure models selected from the literature for comparison were used to predict strut loads and their resulting stresses within the excavation. The earth pressure diagrams selected for use from the literature included those proposed by Duncan, Peck, Tschebotarioff, and Harding Lawson, the project geotechnical consultant. While space does not permit the presentation of each proposed diagram, the trapezoidal model suggested by Duncan is developed in detail to demonstrate the analysis methods used in this study and shown in Figure 5 on the following page.

All hand and computer-based calculations were based upon the K_a (active) and K_o (at-rest) earth pressure diagram presented in Figure 4 on the following page and applied as shown in the Duncan model presented in Figure 5 (Duncan, 1985). Portions of the earth pressure diagrams given in Figure 4, depending upon the depth of the excavation and the strut levels installed are plotted, their areas calculated, and those areas transformed into the various shapes of the earth pressures shapes suggested in the literature. Note that Area 1 is made equal to Area 2 in Figure 5 below. This method is consistent throughout all model analysis.

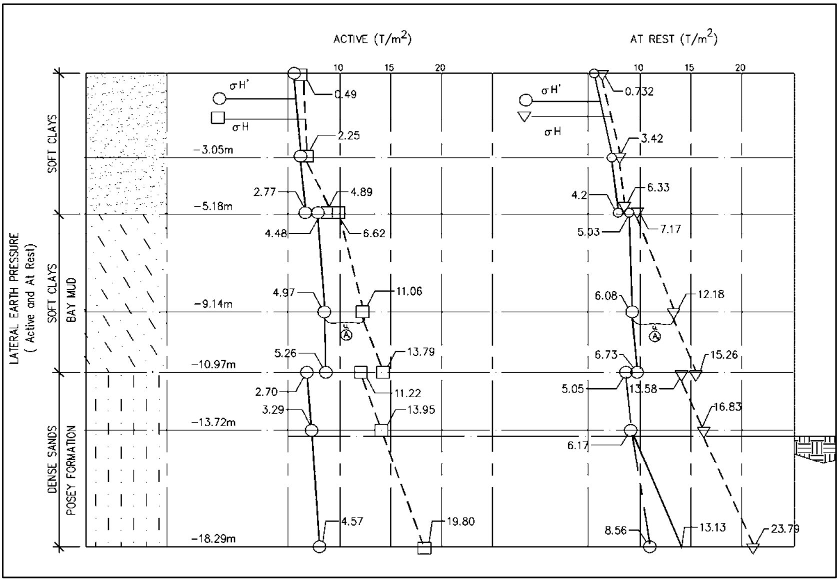

Figure 4. Active and At-Rest Earth Pressures (t/m²)

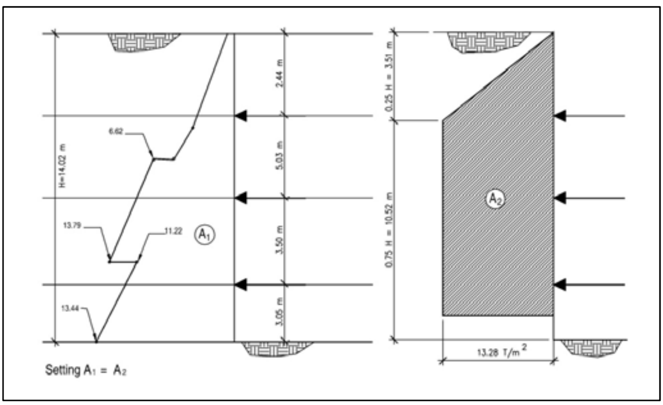

Earth Pressures from Figure 4 (t/m²) Duncan Trapezoid

Figure 5. Reshaping of Earth Pressure Diagram to Duncan Trapezoid

Hand calculations were performed in addition to extensive computer analysis using a finite element structural model developed specifically for this study with which to compare axial loads and stresses (CASA/GIFTS, 1995). The "deformed" shape of the bracing system (FEM) is shown in Figure 6 below. Note that only half of the excavation was modeled to save computer analysis time in addition to ensuring clarity of the results. Note too that the depth of the sheet piles sections shown is approximately 18.29 m while the length of the excavation is approximately 61 m. The width of the section shown is approximately 15.3 m. The FEM was programmed to exaggerate the horizontal deflections of the sheet pile sections by several hundred times. Those shown on this particular model represent deflections on the order of 1.6 cm to 2.54 cm (Clough and Hansen 1979).

See Figs 3 and 6, pg 4 and below for the configuration of the three strut levels, 1, 3, and 4 in their final positions. Table 1 contains the comparison of predicted strut loadings to measured values for these cross-lot strut locations.

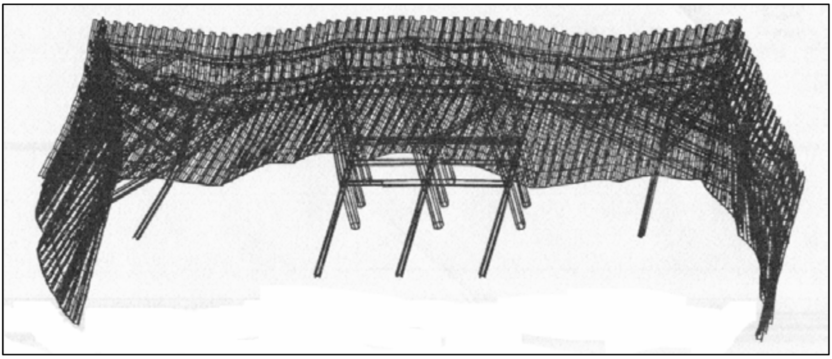

Figure 6. Finite Element Structural Model ("Deformed" after analysis)

Development of New Earth Pressure Model

This phase of the investigation centered on the development of an additional lateral earth pressure model for use on this project. A study of existing models was done to identify areas for possible improvement. Estimated strain rates within the retained soil were evaluated, at least qualitatively, to "build" the earth pressure model suggested by the author. Attention was also given to the dewatering methods and water table fluctuation as monitored and reported by the project engineer to determine its subsequent impact on water pressures calculated within the soil mass surrounding the excavation.

This portion of the study was developed under the supervision of Dr. William Houston during the preparation of the author's doctoral thesis at Arizona State University and represents a significant departure from the typical earth pressure model theory given that it evaluates soil parameters and behaviors below the dredge line. Additional details will be presented in other publications with respect to the performance of this particular model but specifically it was developed in eleven steps as follows and further detailed in Figure 7 and will be presented in complete detail in future publications relating to the data from this project.

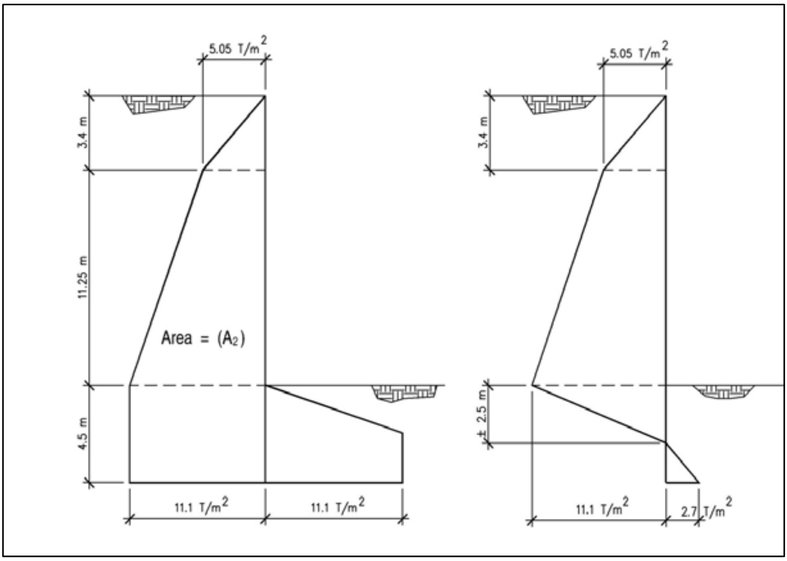

Figure 7. Wilson/Houston Earth Pressure Model

Comparison of Measured to Predicted Results

Table 1 below presents average measured strut loads as compared to predicted strut loads using both the finite element structural model (GIFTS) and hand-calculated strut loads using the tributary area method for sake of brevity and clarity. Additional data was collected and calculated for each of the three strut levels including bending stresses and the impact of construction processes and methods that will be presented in future publications about this project.

Data was collected from the four vibrating wire strain gauges located on each of the 3 cross-lot struts located at Levels 1, 2, and 4. Details regarding these comparisons are presented in the Results and Conclusions sections of this paper for further review, analysis, and comment.

Level No.	Avg. Meas. Load (knts)	Avg. Predicted Load FEM Model (kilonewtons)		Avg. Predicted Load Tributary Area (kilonewtons)	
		Tschbotarioff	796	Tschbotarioff	778
		Wilson/Houston	992	Wilson/Houston	1139
1	449	Peck	1904	Peck	1890
		Harding/Lawson	1948	Harding/Lawson	2149
		Duncan	2406	Duncan	2656
		Tschbotarioff	2153	Tschbotarioff	1753
		Wilson/Houston	2264	Wilson/Houston	1877
3	1330	Peck	2976	Peck	2406
		Harding/Lawson	3452	Harding/Lawson	2740
		Duncan	4204	Duncan	3385
		Tschbotarioff	1637	Tschbotarioff	1664
		Wilson/Houston	1833	Wilson/Houston	1962
4	1232	Peck	2086	Peck	2229
		Harding/Lawson	2571	Harding/Lawson	2749
		Duncan	3069	Duncan	2909

Table 1. Comparison of Average Results

RESULTS

An incremental quantitative analysis was performed for the excavation using the design trapezoids suggested by Peck (1969c), Tschebotarioff (1973b) in addition to recommendations given by Duncan (1982) and the model developed by the project soils engineer, Harding Lawson (1985). The fifth model used was that developed and proposed by the author for implementation during this study. While analyses were done and presented for four different strut levels (Times A, B, C, and D as given in the results) incrementally installed during the construction process, only the data and comparisons are presented for the deepest excavation level, Time D, (14 m). Three strut levels are in place at this stage of the construction and offer the most data available for computation, comparison, and model performance review.

CONCLUSIONS

(1) The vibrating wire strain gages performed quite well. Some measured strut loads were quite anomalous, reasonable explanations were found for their behaviors. a) twelve gauges were "calibrated/checked" when struts 4, 5, and 6 were preloaded while measurements were being taken b) eleven additional gauges were checked to a lesser degree by the fact that the average load on struts 2 and 3 tracked so closely with the strut 1 load in response to construction operations. c) for all struts, the four gauges on each strut tended to track together and d) all gauges were responsive and functioning until removal.

(2) The FEM structural model was very useful in accounting for the effects of variable stiffness within the system components. This model was considered the best possible method to calculate loads and thus was used as a basis for evaluating the Tributary Area Method. While performing very well, it was not possible to be faithful to each detail of the construction operation. For example, the sequential preloading of struts 2 and 3 was not modeled. It did however perform very well in explaining the reduction in Level 1 loads when Level 2 was preloaded.

(3) The Tributary Area Method (TAM) of determining strut loads appears to be generally satisfactory. The ratios presented in the RESULTS section which compare loads calculated by TAM to those calculated by the FEM model suggest a value of very nearly one. While some of the differences are not entirely negligible, they are small compared to the anomalies in the measured loads. It is therefore concluded that the differences between the TAM strut values and the FEM values are insufficient to justify the development of other FEM models even though they are very valuable for research. Continued use of the TAM for routine design appears justified.

(4) The stresses due to bending were found to be surprisingly high averaging approximately 85%n of the P/A stresses. The data suggested that P/A stresses plus about 150% of P/A stresses envelop about 80% of the measured strut values. It appears that it would not be overly conservative to take use these values to estimate maximum compresses stresses in similar strut members. These conclusions relative to bending stresses however do not necessarily dictate a substantial change in design practice but the results may be very helpful in showing what the real factors of safety are in current design practice.

(5) The relative performance of the five earth pressure models studied was presented in Table 1. The model developed and proposed by the author was used to predict strut loads at Time (D) only. Note that its performance ranged from moderate to good for Levels 1 and 3 to significant over-predictions at Level 4. It should be noted that modifications to the author's model showed insignificant effect on strut loads when K_o was reduced sharply and only slight improvement noted when reduced water pressures were assumed in the bottom 3.1 m of the Bay Mud (as well as the Posey layer below the Bay Mud), provided that the pressure diagram was reshaped as shown in Figure 4. However, when the model was modified to that of Figure 4 (at-rest) with reduced water pressures in the bottom 3.1 m of Bay Mud and no reshaping, then the predicted results by the Tributary Area Method matched the measured loads for Time (D) very well with no under-predictions.

(6) Although the importance of water pressures on lateral earth pressures on bracing systems is spelled out in many textbooks and technical publications, it is nevertheless easy to devote excessive attention to soil properties such as shear strength, unit weight, and earth pressure coefficients. The study showed once again that a major portion of predictive analysis should be devoted to predicting probable water pressures.

RECOMMENDATIONS

The FEM model is very useful for research studies, and perhaps for certain special cases of complex bracing systems. However, for routine bracing system design, continued use of the Tributary Area Method is recommended.

(1) Unless the earth pressure model is known to be conservative (consistent over-prediction) in predicting strut loads, the predicted P/A stresses should be augmented by an additional increment of 150% of the P/A stresses to get an estimate of total maximum compressive stress for design. These high stress values may be induced by equipment loads operating within close proximity to bracing members and should be considered when evaluating the equipment types and excavation methods early in the project planning stages. See Figure 2 on Page 3.

(2) The study of this excavation and the scope of work completed during its investigation represent a significant percentage of the data collected in the 1980's. Nevertheless, this research represents only one set of data points. Therefore, it would not be appropriate to make recommendations on which earth pressure models should be used on the basis of this research alone.

REFERENCES

Clough, G. W. and Hansen, L.A. (1979). "Design Aides for Estimating Movements of Excavation Support Systems." Stanford University, Civil Engineering Department. Photocopied.

Clough, G.W. and B. Schmidt. (1977). Design and Performance of Excavations and Tunnels in Soft Clay. A State of the Art Report. In *Proceedings of the International Symposium on Soft Clays in Bangkok, Thailand.* 1-76.

Duncan, J.M. (1982) Comments taken from lectures given at Cal Berkeley regarding behavior and performance of braced excavations. Class and lectures notes provided for the preparation of the author's doctoral thesis. W.N. Houston, 1991.

Harding Lawson and Associates. (1985). Geotechnical Investigation and Report prepared for Embarcadero Project. Hotel and Office Building Complex. San Francisco, CA. Initial report dated 7/1/1985.

Lambe, T.W. (1972). "Predicting the Performance of Braced Excavations. *Proceedings of the Specialty Conference on Performance of Earth and Earth-Supported Structures.* Vol. 3. Purdue University, Lafayette, Indiana. June 11-14. School of Civil Engineering, Purdue University and Soil Mechanics and Foundation Division, ASCE: 255-356.

Peck, R. B. (1969c) "Deep Excavations and Tunneling in Soft Ground." State of the Art Report. Proceedings of the Seventh Annual Conference on Soil Mechanics and Foundation Engineering: 225-290.

Tschebotarioff, G.P. (1973b) Foundations, Retaining and Earth Structures. 2nd. Edition, McGraw-Hill Book Co. 415-457.

Excavation Support for Jacking and Receiving Shafts on the East Boston Sewer Relief Project

Kevin M. Dawson [1]

[1]**Hayward Baker Inc., 9 Whipple Street, Cumberland, RI; PH (401) 334-2565; FAX (401) 334-3337; email: kdawson@haywardbaker.com**

ABSTRACT

Construction of new 914 mm, 1,219 mm, and 1,676 mm diameter sewer pipes by microtunneling on the East Boston Branch Sewer Relief Project for the Massachusetts Water Resources Authority (MWRA) required installation of 19 excavation support structures at jacking and receiving shaft locations. Three methods of excavation support were used: drilled soldier piles and lagging, drilled micropiles and contact lagging, and drilled secant piles. Jet grout bottom seals were installed at two excavation support structures. Jet grouting was also utilized to seal around existing utilities at one excavation support structure. The typical depth of excavation varied from 5.8 to 13.4 m.

The excavation support method used at each jacking and receiving shaft was determined after evaluation of the existing soil conditions and logistical site constraints. Since portions of the tunnel alignment intercepted made-ground (fill), the soil conditions varied considerably along the tunnel alignment. Each excavation support structure was constructed in a congested urban environment. Presence of overhead and underground utilities and proximity to existing buildings impacted the excavation support method chosen for each shaft location.

This paper presents an overview of the rationale used to determine the excavation support method utilized at each drop shaft, a review of the construction techniques used to build the excavation support structures, and the major lessons learned.

PROJECT OVERVIEW

Nineteen excavation support structures ranging in depth from 5.8 to 13.4 m were constructed for microtunneling jacking shafts and receiving shafts on the East Boston Branch Sewer Relief Project as detailed in Table 1. Three methods of excavation support were used: drilled soldier piles and lagging, drilled micropiles and contact lagging, and drilled secant piles. Jet grout bottom seals were also installed at two drop shaft locations to mitigate potential basal instability.

Drop Shaft Location	Excavation Depth (m)	Excavation Support System	No of Piles	Length of Piles (m)
RS-1A	6.4	Micropile & Lagging	15	9.1
JS-10A	7.0	Micropile & Lagging	23	10.7
RS-11A	7.9	Micropile & Lagging	16	9.1
JS-12A	5.8	Micropile & Lagging	20	9.1
JS-13A	6.7	Micropile & Lagging	20	9.1
RS-14A	7.3	Micropile & Lagging	15	10.7
JS-9	9.9	Secant Pile	32	12.5
RS-8A	11.4	Secant Pile	45	12.8
JS-8A	11.6	Secant Pile	32	14.0
JS-7A	10.5	Secant Pile	24	12.2
JS-6A	13.4	Secant Pile	24	15.5
RS-3A	9.1	Secant Pile	21	10.7
RS-2	7.3	Secant Pile	22	9.1
JS-1A	6.7	Secant Pile	21	10.7
RS-6A	9.2	Steel Sheeting	28	11.0
RS-9A	11.6	Soldier Pile & Lagging	7	14.3
JS-5A	10.2	Soldier Pile & Lagging	12	12.5
JS-4A	13.0	Soldier Pile & Lagging	12	15.2
JS-3	11.0	Soldier Pile & Lagging	12	13.7

Table 1. Summary of excavation support system used at each drop shaft location

The soil and groundwater conditions at each shaft location varied. The spatial variability of the soil and groundwater conditions influenced the choice of excavation support method at each drop shaft location. Site logistics also constrained the choice of excavation support method. A total of 18 out of 19 excavation support structures were constructed in active city traffic zones. A total of 10 out of 19 excavation support structures were constructed in close proximity to existing structures.

SOIL CONDITIONS

Although the soil profile varied across the project, the profile consisted of a combination of the following seven soil types, listed in general order of depth from the ground surface: fill, organic deposits, sand and gravel, marine clay, sand and clay, glaciomarine deposits, and glacial till (Boscardin, 2008).
The soil conditions present at four representative earth support structures are shown in Figure 1. The soil conditions at these four shaft locations are representative of the soil conditions present at other shaft locations where the same method of earth support was utilized.

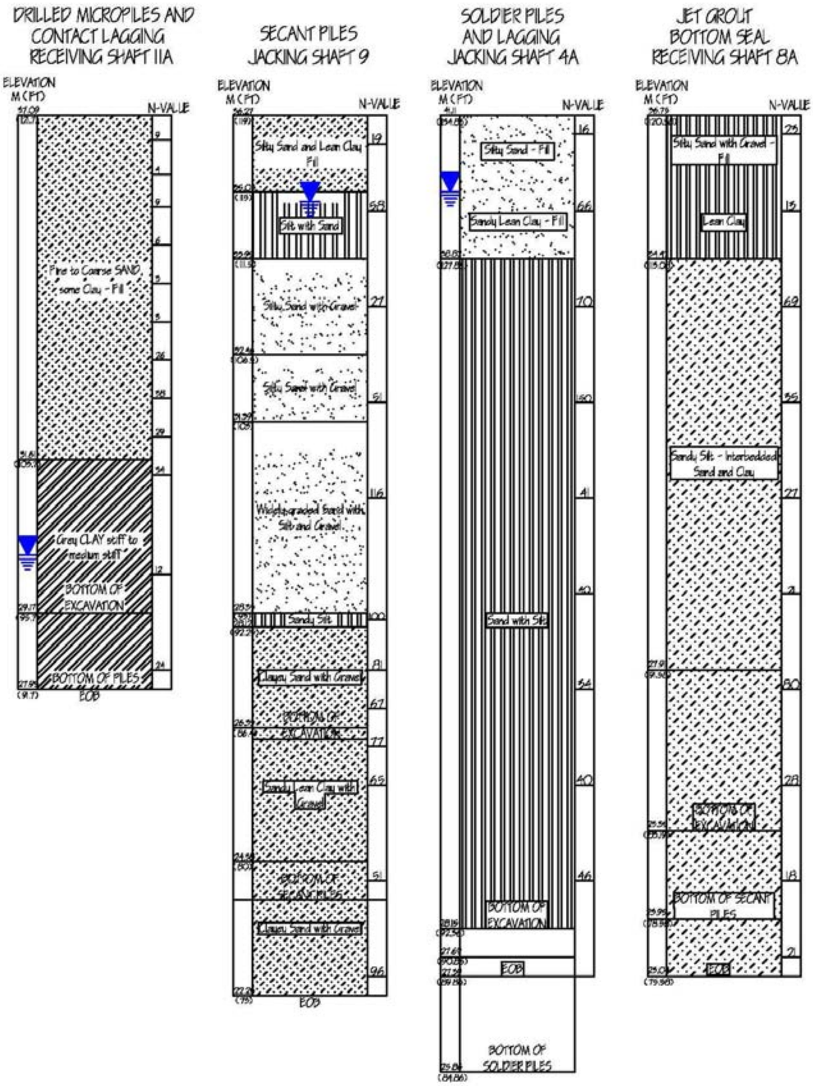

Figure 1. Design soil profiles at four representative drop shaft locations

EXCAVATION SUPPORT CHOICES

The method of excavation support utilized at each drop shaft location was chosen based on three main factors: proximity of drop shaft location to existing buildings and utilities (overhead and underground), the anticipated soil and groundwater conditions, and the overall cost of the excavation (including soil removal and dewatering costs). Since the site and soil conditions varied considerably across the project, a single method of excavation support would not offer the best value. Rather, three types of excavation support were used: drilled micropiles and contact lagging, drilled secant piles, and drilled soldier piles and lagging.

Drilled micropiles and contact lagging excavation support was used at locations where groundwater control issues did not exist, soil conditions were amenable to lagging, and site constraints did not permit use of larger soldier pile drilling equipment. The use of smaller, more maneuverable micropile drilling equipment permitted installation of drilled piles in close proximity to existing underground utilities and beneath low overhead utilities within one meter of existing structures.

Drilled soldier pile and lagging excavation support was used at drop shaft locations where groundwater control issues did not exist, soil conditions were amenable to lagging, and site constraints permitted use of large drill rigs. Drilled soldier pile and lagging earth support systems are generally more cost efficient than drilled micropile and contact lagging earth support systems since fewer soldier piles with higher section modulus can be installed.

Drilled secant pile earth support was used at drop shaft locations where groundwater control issues existed, a stiff excavation support system was required, and site constraints permitted use of large drill rigs. Many of the deeper shaft locations penetrated layers or pockets of sand and gravel below the water table. Control of the groundwater in these layers would not have been possible with pervious excavation support methods without significant dewatering.

Jet grouted soilcrete bottom seals were installed at two drop shaft locations where the subgrade of the excavation was below the water table and the soil at subgrade consisted of loose to medium sand or sand and gravel. Groundwater infiltration or piping through the pervious material could have caused basal instability due to a loss of strength in the subgrade soil at these locations. Jet grouting was also used at one earth support structure as a means to seal gaps below existing utilities and to seal between the existing utilities and the secant pile earth support system.

CONSTRUCTION TECHNIQUES

Drilled Micropiles and Contact Lagging

Drilled micropiles and contact lagging were used to support 5.8 to 7.9 m deep excavations at three jacking shaft and three receiving shaft locations due to difficult site access conditions. Site access restraints included overhead wires that could not be relocated, existing utilities that could not be relocated prior to excavation of the jacking or receiving pit, and constrained site geometry that could not accommodate traditional soldier pile drilling equipment.

A plan view of receiving shaft 11A, a typical drilled micropile and contact lagging earth support structure, is shown in Figure 2. Photographs of the installation of the drilled micropiles and lagging at this structure are shown in Figure 3.

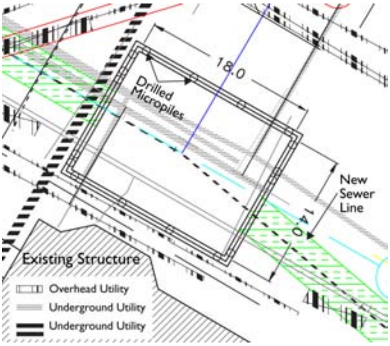

Figure 2. Plan view of drilled micropiles at one shaft location, and locations of various utilities that were negotiated.

Figure 3. Drilled micropile and contact lagging installation

The 244.48 mm diameter micropiles were drilled using a rotary hydraulic drill rig. External flush drilling techniques with water flush were used to advance the drill casing to depth. Once all the piles at an individual shaft location were advanced to depth, all the piles in the group were grouted simultaneously using a sand cement grout. Contact lagging and bracing was installed as each excavation was advanced.

Drilled Soldier Piles

Drilled soldier piles and lagging earth support was used to support excavations at three jacking shafts and one receiving shaft. The excavation depths at these shafts ranged from 10.2 to 11 m and soldier piles lengths ranged from 12.5 to 15.25m. A plan view and a construction photo of the excavation support system installed at jacking shaft 4A (a typical soldier pile supported shaft) is shown in Figure 4.

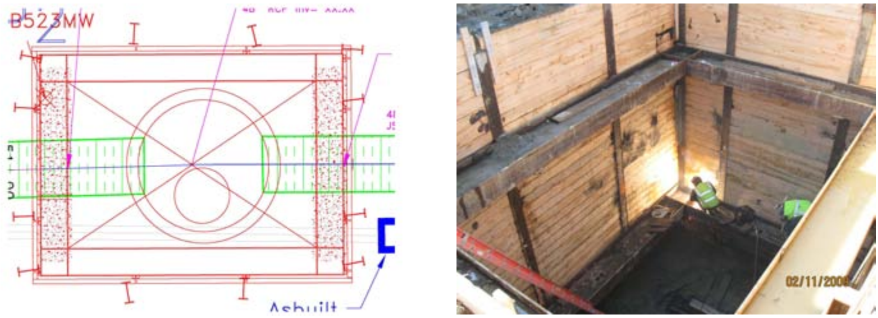

Figure 4. Plan view and construction photo of soldier pile and lagging earth support system installed at jacking shaft 4A

Each soldier pile was drilled using a hydraulic track drill rig with a kelly bar and rotator. Once each soldier pile drill hole was advanced to the tip elevation, the vertical beam was installed, the hole was backfilled with flowable fill and the temporary drill casing was removed. Timber lagging and internal bracing was installed as the excavation was advanced.

Drilled Secant Piles

Excavation depths ranging from 6.7 to 13.4 m at five jacking shafts and three receiving shafts were supported with 1,000 mm diameter drilled secant piles. The individual secant pile lengths ranged from 8.5 to 15.5 m. Six of the eight secant pile earth support structures were unreinforced circular drop shafts with diameters ranging from 4.27 m to 6.7 m. Two of the secant pile support structures were rectangular and were reinforced with vertical steel soldier piles and internal bracing. A plan view of the secant piles installed at jacking shaft 9 and a construction photo of a typical circular secant pile supported jacking shaft are show in Figure 5.

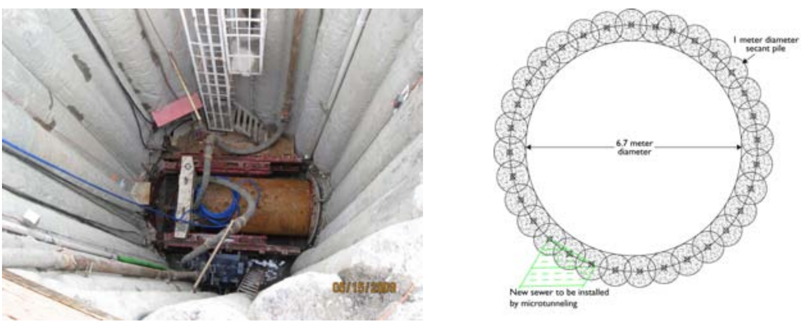

Figure 5. Plan view of secant pile retention system installed at jacking shaft 9 and construction photo of a typical non-reinforced circular secant pile supported jacking shaft

The 1,000 mm diameter drilled secant piles were typically spaced on 762 mm centers in order to maintain 228 mm overlap at each pile interstice. The secant piles were drilled in a primary secondary sequence using a hydraulic track drill rig with a kelly bar and rotator. Once each secant pile was advanced to final depth, concrete was placed in the shaft and the temporary drill casing was removed. Vertical beams (where required) were installed in the shafts after the concrete was placed.

Jet Grouting

Double fluid and Superjet grouting, an enhanced form of double fluid jet grouting, were utilized to create soilcrete bottom seals at two drop shaft locations. In a double fluid jet grouting system, grout and air are pumped through separate high pressure hoses to the jet grout monitor at the bottom of the drill string where high velocity coaxial air and grout form the erosion medium. Figure 6 shows a plan view and a construction photograph of the jet grout bottom seal and wall seals that were constructed at receiving shaft 8A.

Superjet grouting was utilized at receiving shaft 8A to create jet grout column diameters ranging from 2.4 to 3 m. The bottom seal at this shaft location was approximately 3 m thick and was installed from 11.6 to 14.6 m below the ground surface. Superjet grouting was used at this location to create large diameter columns beneath an existing 914 to 1,041 mm diameter sewer pipe.

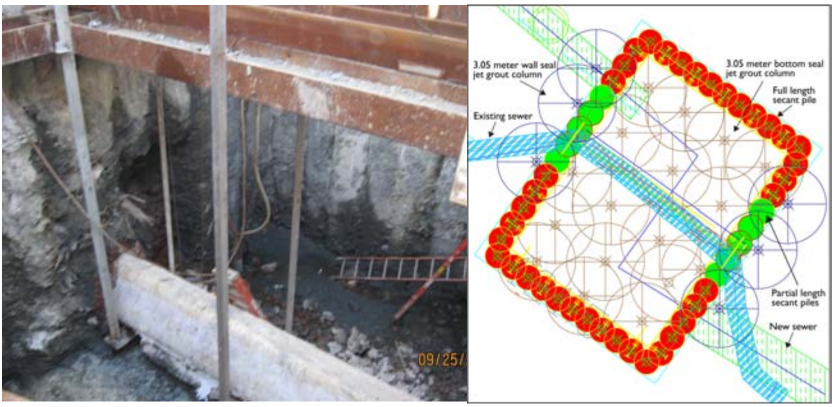

Figure 6. Plan view showing jet grouted soilcrete bottom and wall seals, secant piles, and existing and new sewer.

CONCLUSION AND LESSONS LEARNED

Construction of large scale sewer improvement projects in urban environments with variable soil conditions requires the use of a broad array of excavation support methods. Physical constraints and soil conditions directly impact the choice of an appropriate excavation support system. Drilled micropiles and contact lagging offer a cost effective means of installing excavation support systems in constrained sites with overhead restrictions, assuming groundwater control is not a required characteristic of the system. Drilled soldier piles and lagging excavation support is a cost-effective means of excavation support for drop shafts where overhead restrictions do not exist, underground utility locations are known, and groundwater control is not a required characteristic of the system. Drilled secant piles earth support is a cost-effective means of excavation support for drop shafts where water cutoff is required, obstructions or nearby structures prevent installation of driven sheetpiles, and a stiff excavation support wall is required. Jet grouting can be a cost effective method to mitigate basal instability in excavation support systems and to seal between existing utilities and other excavation support elements.

Although the cost to install a secant pile earth support system is higher than the cost to install a soldier pile and lagging or micropile and contact lagging earth support system, the overall cost of excavation of a secant pile supported excavation support system can be less than the overall cost of excavation of the other two systems. Time related costs (slower excavation) and heavier bracing requirements can inflate the overall cost of excavation using soldier pile and lagging or micropile and lagging support systems.

The average cost per square meter (of exposed earth support) to install a secant pile excavation support system on the East Boston Sewer Relief Project was 1.4 to 1.6 times the cost per square meter to install drilled soldier pile and lagging and drilled micropile and contact lagging earth support systems, respectively. However, the average cost per ton of excavated soil using a secant pile earth support system was 82 to 65 percent of the cost per ton of excavated soil using drilled soldier pile and lagging and drilled micropile and contact lagging earth support systems respectively. The additional excavation cost for drilled micropile and lagging and soldier pile and lagging is due to time-dependent costs associated with lagging, bracing, and water control during excavation. The circular secant pile drop shafts on the East Boston project did not require internal bracing. Consequently, the time related excavation costs were minimized and the overall cost of excavation was reduced. Contractors and owners alike should consider the cost benefit of using secant pile earth support structures where they are applicable.

REFERENCES

Boscardin, M. D. (2008). "Geotechnical Baseline Report, Massachusetts Water Resources Authority Construction Contract No. 6257 East Boston Branch Sewer Relief Project East Boston, Massachusetts." GEI Consultants, Inc and Boscardin Consulting, Woburn, Massachusetts.

Jet Grout Dike for Temporary Excavation Support in Soft Clay

C. E. Ho[1] Sc.D., Member, ASCE

[1]Associate, Arup, 155 Avenue of the Americas, New York, NY 10013, USA, chu.ho@arup.com

ABSTRACT

This paper describes the innovative application of jet grouting to enable fast track delivery of a large-scale basement project in soft marine clay. A self-stabilized jet grout dike was formed across the width of a basement to retain a temporary excavation 12m to 17m deep. The jet grout dike was designed to act as a rigid gravity retaining structure. Lateral stability was maintained by a horizontal jet grout slab confined within the surrounding diaphragm walls. Overturning stability was provided by the foundation piles integrated within the jet grout slab, which acted like a piled raft beneath the jet grout dike. The jet grout dike was trimmed in stages as the excavation progressed. This approach allowed simultaneous excavation for the basement to proceed, while foundation works were still in progress at the ground surface on the retained side of the jet grout dike. The main advantage for adopting a jet grout dike was the elimination of the activities involving installation and removal of temporary sheet pile walls and associated diagonal struts from the construction schedule.

INTRODUCTION

The critical path for a project is often governed by the bulk excavation for the substructure construction. To speed up this activity, the site may be divided into several zones, so as to allow simultaneous excavation activities to proceed in certain sections of the site while construction is still in progress at the ground surface in the other areas. A temporary separation wall is commonly installed at the internal boundary between two interfacing construction zones, with diagonal steel struts braced against the perimeter retaining walls for temporary support. This approach has been successfully applied for projects located in congested urban sites (Ho and Wallace 1994).

In this paper, an alternative method of temporary excavation support is introduced, using ground modification techniques to form a temporary dike within the ground in place of the sheet pile wall at the interface boundary. By eliminating the need for installation and removal of the temporary separation wall and associated bracings, construction staging is greatly simplified, resulting in significant reduction in overall construction time. The following sections describe the case history of a jet grout dike implemented at the Singapore Post Center site in Singapore.

PROJECT DESCRIPTION

The Singapore Post Center is a very large development comprising a 15-story tower block, a 10-story podium and a 2 to 3 level basement. The site is approximately 250m long and 100m wide. The basement covered virtually the whole site and was constructed using permanent diaphragm walls all round. The width of the basement varied between 88m and 94m between the diaphragm walls. The buildings were designed to be supported on large diameter bored piles and barrette foundations.

The site was filled over by a layer of sandy clayey material about 2.5m to 4m thick. The fill was underlain by soft peaty clay and marine clays up to 31m from ground surface. A layer of stiff desiccated clay was present within the marine members. A thin stratum of fluvial sand was found within a localized area at the middle of the site beneath the desiccated clay. A thick underlying bed of dense alluvium consisting of clayey silty sand was present across the site, undergirded by weathered granite bedrock. The water table was located about 1m to 1.5m below the ground surface.

Excavation depths for the basement ranged from 12m to 15.5m in general, with localized excavations for pile caps up to 17m. The diaphragm walls were braced by four to five levels of temporary steel struts. The final excavation levels were located within normally consolidated soft marine clays with field vane shear strengths between 19 kPa and 25 kPa. Figure 1 shows the excavation support design for the project.

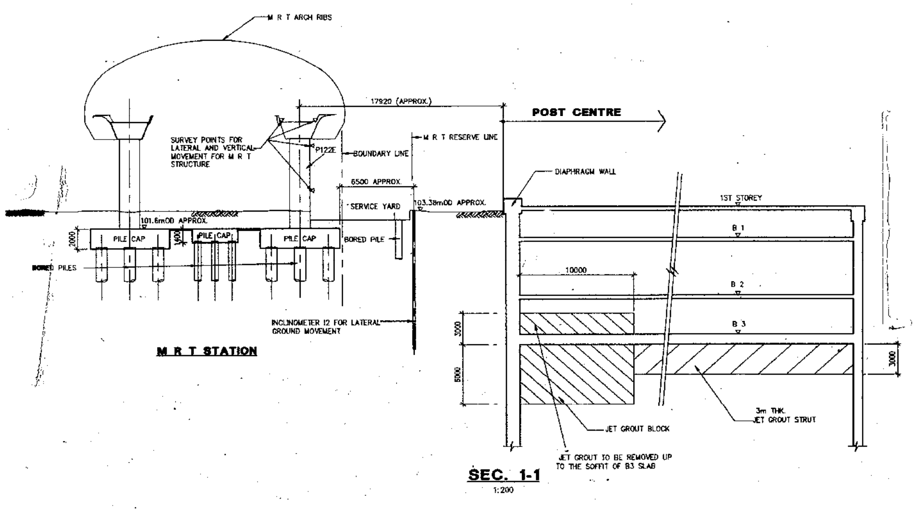

Figure 1. Excavation support design

Ground modification was implemented prior to the basement excavation as a mitigation measure to limit induced ground movements. A jet grout slab 3m to 4m thick was formed for the whole plan area of the basement, to act as a continuous buried strut for transmitting lateral loads between the diaphragm walls (Ho et al. 2005). Along the length of basement immediately adjacent to a running mass rapid transit viaduct, a 9m deep and 10m wide jet grout block was formed to enable better control of inward wall deflections at the earlier stages of excavation (Ho and Hu 2006). The jet grout columns were 1.8m in diameter spaced in a triangular grid of 1.55m center to center, with a design unconfined compressive strength of 0.6 MPa and Young's modulus of 150 MPa. Triple fluid jetting system was adopted for better control of ground displacements during jet grouting in soft marine clay (Ho, 1995).

CONSTRUCTION STAGING

As part of a fast track delivery strategy, construction of the substructure was carried out in three phases, 1A, 1B and 2 using bottom-up sequence (Figure 2). Excavation works commenced at Phase 1A and proceeded towards Phase 2. At the interface of each of the two phases, a sheet pile wall was originally planned to separate the adjacent construction activities. The sheet pile wall would be braced against the completed permanent diaphragm walls to allow simultaneous excavation within Phase 1A, while foundation construction at ground surface continued to progress at the retained ground in Phase 1B. This sequence would be repeated for the substructure works in Phase 1B and Phase 2.

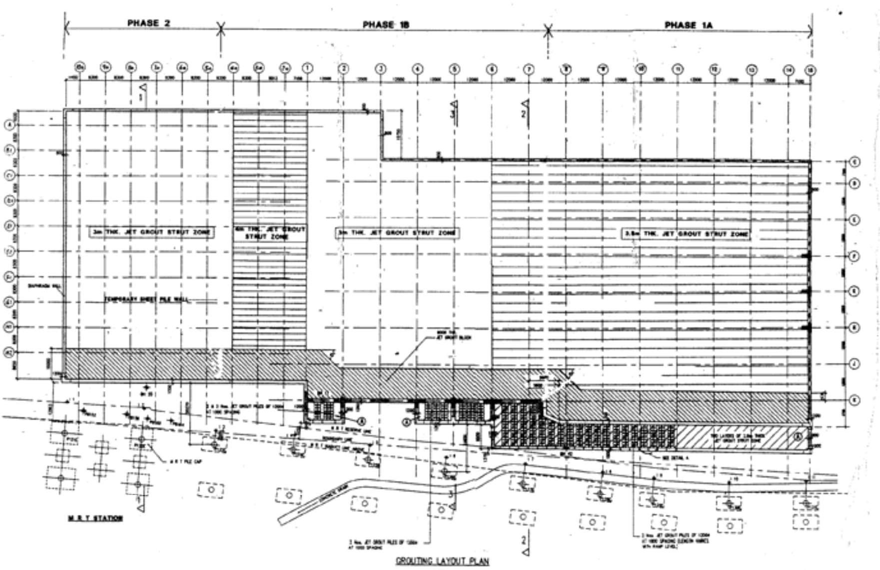

Figure 2. Phased construction staging

As the substructure contractor completed his work up to the ground floor level within each phase, it was sequentially handed over to the superstructure contractor to proceed with the above-ground structural works. Figure 3 shows the phased construction in progress.

Figure 3. Phased construction for basement excavation

JET GROUT DIKE FOR INTERNAL SUPPORT

During implementation of the project, the sheet pile walls were eliminated and replaced with a temporary self-stabilized jet grout "dike" between Gridlines 6 and 7.5, to improve staging of construction activities (Figure 4). This approach allowed for a less congested working space within the initial excavation in Phase 1A for the contractor. The grouted soil mass within the dike enabled a steeper slope to be cut within the excavation, up to about 40 degrees from the horizontal. The creation of the dike was made possible by simply extending the original jet grout columns within the jet grout slab upwards to form inter-locking columns.

The top levels of the jet grout columns were terminated at different levels to form terraced side slopes on the front and back. The terraced steps on the front slope were 1.3m high. The top level of the dike was designed to be about 0.9m below the general excavation level for installation of the first row wale beams and primary struts that braced against the permanent diaphragm walls. Above this level, a temporary cut of 1:2 slope within the fill material was sufficiently stable. The retained height between ground surface and the general excavation platform was about 12m, with a maximum height difference of 15.5m at areas of pile cap construction. In adopting this alternative scheme, the bored piles have to be installed through the jet grout dike. To ensure that the integrity of the dike was maintained, all bored piles located within the jet grout dike were backfilled with structural concrete up to at least the top of the terraces.

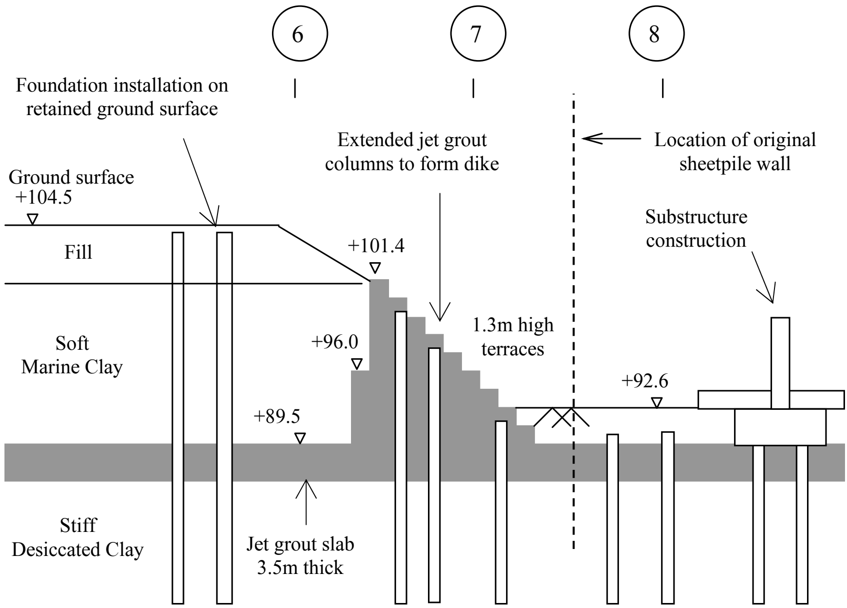

Figure 4. Configuration of temporary jet grout dike

STABILITY CONSIDERATIONS

The jet grout dike was assumed to behave as a rigid gravity retaining structure with its base seated on the jet grout slab and permanent foundation piles. Because the jet grout slabs were integrally linked with the foundation piles, it would act as an equivalent piled raft system. Further, as the jet grout slab extended laterally in all directions in full contact with the diaphragm walls, the permanent foundations were fully confined and no appreciable lateral displacement of the foundation elements was envisaged. The key considerations for design of the jet grout dike were (1) shearing resistance at the interface between the base of the dike and the jet grout slab against the imposed lateral earth pressure behind the dike, (2) horizontal bearing stress imposed on the jet grout slab at the toe of the dike that may induce crushing of the grout material, and (3) overturning moment that would increase the vertical bearing pressure on the underlying jet grout slab causing potential punching failure through the jet grout columns. The most critical factors relate to the available strength of the jet grouted marine clay and the resistance at the interfaces of the jet grout columns that would ensure stability of the dike.

Jet grout strength. Quality control testing on cores taken through the jet grout slab at 16 locations in plan provided data on the jet grout strength achieved insitu. The positions of coring were targeted at the intersections of jet grout columns. Unconfined compression tests on intact cores produced strengths (q_u) averaging 2.52 MPa, with a standard deviation of 1.60 MPa (Ho et al. 2005). However, four out of the total 19 tests (21%) gave results ranging from 52 kPa to 428 kPa that were lower than the design unconfined compressive strength of 600 kPa. The standard deviation for the data is large, reflecting the heterogeneous nature of the jet grouted soil mass, particularly at the intersection of jet grout columns. It is known that the grout at the interface between jet grout columns is usually weaker than the grout within the main body of the jet grout column due to dissipation of hydrodynamic energy with distance from the jet nozzle. Hence, the quality of grouted soil within the interior of the jet grout columns would be expected to be better than that shown by the test results.

The lateral imposed earth load on the back of the jet grout dike was estimated to be 2250 kN, including allowance for a construction loading of 20 kPa at the ground surface. Based on the width of jet grout dike of about 15.5m, the induced shear stress at the base of the dike is 145 kPa. Taking the design strength to be equal to the mean value of the above test results less one standard deviation i.e. 920 kPa, the factor of safety against sliding failure at the base would be of the order of 6.3, which is more than adequate.

Further, assuming the imposed lateral load is resisted entirely by horizontal bearing on the 3.5m thick jet grout slab at the toe of the dike, the horizontal bearing stress in the jet grout slab is estimated to be 642 kPa. The corresponding factor of safety against potential crushing of the grout material would be at least 1.4, which is satisfactory.

Jet grout column interface resistance. Back-analyses of load tests carried out on bored piles installed through the jet grout slab indicated that the ultimate bonding resistance at the jet grout-pile shaft interface ranged from 414.5 kPa to 1648.4 kPa for compression loading (Ho et al. 2002). Assuming that the pile is resisted by load transfer to three overlapping jet grout columns, a conservative estimate for the available interface friction at the perimeter of the jet grout columns would be 170.8 kPa to 751.4 kPa.

The maximum vertical bearing stress imposed at the base of the jet grout dike is estimated to be 325 kPa, based on a net overturning moment of 8590 kNm. Assuming punching shear takes place along the perimeter of a single jet grout column, the induced shear stress at the column interface would be about 42 kPa. Using the minimum interface resistance of 170 kPa back-computed from the pile load tests, a factor of safety of 4.0 is obtained, indicating that the design is sufficient.

ADVANTAGES OF JET GROUT DIKE

The main advantage for adopting a self-stabilized jet grout dike for temporary excavation support was the elimination of the activities involving installation and removal of temporary sheet pile walls and associated diagonal struts from the construction schedule. The only additional cost was the extra length of jet grouting performed to form the dike. There was no significant increase in the production period for the additional jet grouting, since the basic sequence of jet grouting operation remained unchanged from that required for forming the jet grout slab.

When the full depth of excavation in Phase 1A was completed, the exposed jet grout dike and base of the excavation was dry and provided a convenient working environment for cutting pile heads, and laying of reinforcements and formwork for pile caps, basement slab and structural columns.

Because the grouted marine clay was not of exceptionally high strength, subsequent demolition of the jet grout dike was easily accomplished using standard mechanical backhoe and pneumatic breakers as the excavation progressed in Phase 1B.

Figure 5 depicts the working conditions at the bottom of an excavation stabilized by jet grouting.

Figure 5. Construction of foundations within jet grout stabilized excavation

CONCLUSION

The Singapore Post Center project demonstrated the innovative application of jet grouting to form a self-stabilized jet grout dike for temporary support of a 12m to 15.5m deep excavation in soft marine clay. Lateral stability of the jet grout dike was maintained by confinement of the pre-installed horizontal jet grout slab and the surrounding diaphragm walls. Overturning stability was provided by the foundation piles integrated within the jet grout slab, which acted like a piled raft beneath the jet grout dike. The main advantage for adopting a self-stabilized jet grout dike was the elimination of the activities involving installation and removal of temporary sheet pile walls and associated diagonal struts from the construction schedule. There was no significant increase in the production period for the additional jet grouting, since the basic sequence of jet grouting operation remained unchanged from that required for forming the jet grout slab. At the locations where the jet grout dike protruded into the basement area, the grouted soil mass was easily trimmed using mechanical backhoe and pneumatic breakers. The jet grout dike allowed phased excavation of the basement, while foundation works were still in progress at the ground surface on the retained side.

REFERENCES

Ho, C. E. (1995). "An instrumented jet grouting trial in soft marine clay." *Verification of Geotechnical Grouting*, GSP No.57, M. J. Byle and R. H. Borden, eds., ASCE, 101-115.

Ho, C. E. and Hu, S. (2006). "Numerical analysis of jet grout elements for braced excavation in soft clay." *Proc. GeoCongress 2006: Geotechnical Engineering in the Information Technology Age*, D. J. DeGroot, J. T. DeJong, J. D. Frost and L. G. Baise, eds., ASCE, CD-ROM.

Ho, C. E., Lim, C. H. and Tan, C. G. (2002). "Characteristics of bored piles installed through jet grout layer." *J. Performance of Constructed Facilities*, 16 (4), ASCE, 160-168.

Ho, C. E., Lim, C. H., and Tan, C. G. (2005). "Jet grouting applications for large-scale basement construction in soft clay." *Innovations in Grouting and Soil Improvement*, GSP No.136, V. R. Schaefer, D. A. Bruce, and M. J. Byle, eds., ASCE, CD-ROM.

Ho, C. E. and Wallace, J. C (1994). "Geotechnical aspects of a deep basement construction in soft ground". *J. Institution of Engineers Singapore*, 23 (5), 35-41.

Instrumentation of Underpinning Piles in a 94-ft Deep Excavation

R.D. Luark[1], K.S. Cottingham[2], and F.S. Shuri[3]

[1]Kleinfelder, 14710 NE 87TH Street, Suite 100, Redmond, WA, 98052; PH (425) 636-7900; Email: rluark@kleinfelder.com
[2]Golder Associates Inc., 18300 NE Union Hill Road, Suite 200, Redmond, WA, 98052; PH (425) 883-0777; email: kcottingham@golder.com
[3]Golder Associates Inc., 18300 NE Union Hill Road, Suite 200, Redmond, WA, 98052; PH (425) 883-0777; email: fshuri@golder.com

ABSTRACT

Deep foundation construction in urban settings poses the unique challenge of working with deep excavations in a relatively confined area while preserving the integrity of nearby structures. A 94-ft-deep vertical excavation for a 31-story residential tower adjacent to an existing building in downtown Seattle, Washington, presented an opportunity to monitor shoring system performance in real time. Additionally, the analysis of monitoring data allowed for validation of the original design parameters. The shoring system consisted of a soldier pile and tieback walls. Underpinning piles were designed to support the adjacent building while minimizing deflections. The shoring system was designed to limit total lateral deflection adjacent to the existing structure to less than 1/2-inch to minimize the potential for damage. An instrumentation program was designed to monitor loads and deflections in the shoring system. The instrumentation consisted of strain gages, load cells, vertical inclinometers, and optical survey monitoring. Where the adjacent building prevented the use of an inclinometer, two underpinning piles were instrumented with vibrating wire strain gage pairs. Strain gage pairs were installed to: 1) monitor total axial load, 2) monitor the axial load in pile versus depth, and 3) monitor combined axial loading and bending in the pile. Load cells were installed on tiebacks on instrumented underpinning piles to monitor changes in the load during the excavation. The underpinning pile data was monitored remotely. This paper provides a discussion of the design and construction of the shoring system and an analysis of monitoring data collected from the instrumentation system.

Key Words: Deep Excavation, Soil-Structure Interaction, Soldier Pile and Tieback, Underpinning, Remote Data Acquisition, Strain Gages, Load Cells, Inclinometers

INTRODUCTION

A 31-story residential tower was constructed in downtown Seattle, Washington. Nine stories of underground parking were designed for the building, resulting in temporary excavation depths up to 30.8 meters. Soldier pile and tieback walls were designed to support the excavation. On one side of the excavation, an existing three story concrete building was underpinned by the soldier piles. An instrumentation program was developed and implemented to monitor the performance of the shoring system and confirm design assumptions.

PROJECT BACKGROUND

Site Description

The project site was located in downtown Seattle, Washington. The site measures 35.4 m by 78.7 m in plan dimension. The site is bound immediately by Virginia Street to the north, a 3.6 m wide alley to the east, an existing 3-story structure to the south, and 4th Avenue to the west. Across Virginia Street to the north is a 10-story hotel located 20 m behind the shoring wall. Buildings located across the alley east of the shoring wall consist of concrete and masonry structures ranging in height from two to five stories above grade with up to one story below grade. The existing concrete and masonry building to the south was constructed in 1926 and is located at the south property line of the project site. The site slopes down from the north-west corner to the south-east corner, with total elevation drop on the order of 3.3 m. A photograph of the project site after completion of the shoring system is shown in Figure 1.

Geologic Conditions

The near-surface geologic units encountered in the downtown Seattle core generally consist of glacial soils. The uppermost soil unit across the site was advance outwash sands, which were deposited in front of glaciers and subsequently overridden. The advance outwash sands consisted of dense to very dense fine, silty sands ranging in thickness from 7.6 m to 13.7 m. Underlying the advance outwash sands was a layer of hard, interbedded glaciolacustrine silts and clays, which were deposited in lakes formed in front of the advancing glaciers then subsequently overridden by the glaciers. Fractured zones and polished surfaces, locally referred to as “slickensides” were observed in the hard clays present in glacial lacustrine deposits. The glaciolacustrine silts and clays were present to depths of 27.4 m to 29 m below the existing ground surface. Very dense glacial till was encountered beneath the glaciolacustrine layer. The till consisted of silty sands with occasional gravel. The excavation generally terminated in the hard silts with the toe of the soldier piles embedded into the glacial till. Groundwater water was present at approximately 10 m below the existing ground surface with the outwash sand unit and glaciolacustrine silts and clays.

SHORING SYSTEM DESIGN AND CONSTRUCTION

A soldier pile and tieback shoring system was selected to support the excavation required by the project. The shoring system was designed using the following apparent active earth pressures:

- 1.10H kPa truncated from 0.2H to the top of the pile along the north, east, and west walls, where H is the depth of the excavation in meters.
- 1.20H kPa uniform along the south wall to limit deflections of the adjacent underpinned building.

Passive earth pressures represented by an equivalent fluid weight of 11.97 kPa were used for resistance below the base of the excavation. The upper 0.6 m of passive resistance was ignored in the analyses. A horizontal traffic/construction surcharge of 4.79 kPa was added to the above lateral earth pressures on the north, east and west walls. As-built records of the existing buildings were used to compute the building weight and estimate surcharge loads impacting the shoring walls. The axial load transferred to the underpinning soldier piles from the building to the south was computed to be 789.5 kN per soldier pile.

Soldier piles were designed with 2.4 m (8 ft) center to center spacing along the north, east, and west walls. Soldier piles on the south wall were spaced at approximately 2.1 m (7 ft) on center to support the building at the center of footings shown in the as-built drawings. The steel sections of the soldier piles on the north, east, and west walls were either W18x76 or W24x104 and were designed to satisfy shear and bending moments, while limiting the total calculated horizontal deflection to less than 25 mm. The underpinning piles on the south wall were W16x67 and were sized to limit calculated deflections to less than 12 mm to limit the potential for damage of the existing structure.

The no-load zone for the tiebacks used in the design was defined by a horizontal line extending from the base of the excavation back a distance of H/5 (where H is the total excavation depth) and then extending up at 60 degrees above the horizontal to the ground surface. An allowable soil/tieback bond adhesion of 5.4 kN/m was used in the design based on experience in similar soils. Tieback anchors consisted of wire strands installed in a 200 mm diameter cased drill hole and the bonded zone pressure grouted. Design loads ranged from 449 kN to 929 kN. Verification tests of anchors to 200% of the design load were successfully completed. The uppermost row of tiebacks was located to maintain required utility clearance. Subsequent rows of tiebacks were located to avoid conflict with the floor slabs of the proposed parking garage. The total number of tieback rows ranged from ten on the north and west walls to eight on the south wall. Tiebacks were installed at an angle of 30 degrees below horizontal. Tiebacks were tested to 130% of the design load and locked off at loads ranging from 85% to 95% of the design load to allow re-distribution of loads during excavation.

The transfer of the axial load within the soldier pile to the surrounding soil was evaluated for all soldier piles. Axial loads on the north, east, and west piles consisted of the vertical component of the computed tieback load. The axial load on the underpinning piles on the south wall also included the building surcharge. The following values were recommended in the geotechnical report for load transfer to the surrounding soil:

- 1.92 MPa end bearing
- 47.8 kPa side friction below the first row of tiebacks (acting on half the drilled pile surface area)
- 47.8 kPa friction below the base of the excavation.

The soldier piles were installed in nominal 0.9 m diameter drill holes which were backfilled below the base of the excavation with structural concrete and above the base of the excavation with lean concrete.

The underpinning piles were designed in accordance with the AISC steel code for combined loading. This design methodology results in a significant reduction in both axial and bending capacities of the steel pile section relative to piles subjected solely to axial or bending forces. Confirming the magnitude of load transfer to the surrounding soil could reduce the design load in the soldier pile, allowing a more efficient steel section to be used in future temporary wall designs.

INSTRUMENTATION

Objectives

The instrumentation system was developed to confirm design assumptions and monitor shoring system performance during the excavation. Reducing uncertainties in lateral earth pressures and load transfer to surrounding soils can potentially result in a significant cost savings to future projects.

System

Two of the 15 underpinning soldier piles along the south wall of the site were instrumented with strain gages and load cells. Nine strain gage pairs were placed at the centerline of the front and back of the soldier pile at 2.9 m vertical spacing along the soldier piles. Steel angles were installed over the strain gages and instrumentation leads to reduce the chance of damage during pile installation and excavation. Load cells were installed on 4 of the 8 tiebacks on each of the two instrumented underpinning piles.

The strain gages and load cells were wired to four multiplexers and a datalogger. The system was connected to a telephone modem to allow for remote data acquisition.

Inclinometers were installed at the midpoint of the north, east, and west walls. The inclinometer casing was fixed to the back of the soldier pile and installed in the same drill hole as the soldier pile.

Optical survey monitoring was completed twice weekly. Monitoring points included the top of every other soldier pile around the perimeter of the excavation, existing structures within a distance of 30 m from the excavation, and at the curb and centerline of streets adjacent to the excavation.

Monitoring frequency of the automated acquisition system was established as once per hour. Inclinometers were read manually on a weekly basis, unless the construction progress dictated an increased or decreased frequency.

RESULTS OF INSTRUMENTATION

Strain Gages

Axial Load versus Depth of Pile

The theoretical axial load in the pile versus depth was computed based on allowable side friction values of 47.9 kPa (1 ksf). Based on the vertical component of the tieback combined with the computed building load, the axial load within the soldier pile should be transferred to the surrounding soil entirely by side friction with no axial load in the tip of the soldier pile. Based on the ultimate soil/concrete adhesion of 95.7 kPa (2 ksf), the maximum design axial load was 1005 kN (226 kips) and was theoretically was located at the first tieback. The maximum axial load measure in the underpinning piles is approximately 1068 kN (240 kips). The maximum axial load in the pile generally increased with depth along the pile, achieving the highest value just below the bottom row of tiebacks. The axial load measured by the strain gages at the tip of the pile was 89 kN (20 kips). Figure 2 illustrates the theoretical axial load in the pile 14 verses the measured load. The results indicate that the axial load from the building did not transfer to the underpinning pile until the excavation had advance to approximately 12 m below the building's foundation. Below 12 meters, the measured load in the pile was close to the calculated load transfer used in the design.

Tieback Loads

The change in tieback load after stressing was monitored through the use of vibrating wire load cells. The instrumentation shows the maximum change in tieback load was less than 10% of the lock-off load at installation. The change in tieback load over time is shown for the Row 1 tiebacks on the two instrumented piles are shown in Figure 3.

Deformations

Lateral deformations were measured by inclinometers installed near the midpoint of the north, east, and west shoring walls. Optical surveying was also performed at the top of alternating soldier piles around the perimeter of the excavation, at varying distances behind the excavation, and all structures sensitive to movement. Results of optical surveying were in general agreement with deformations recorded from the inclinometers. Deformations of approximately 25 mm to 36 mm were observed at the top of the soldier pile walls. The measured deformations from the inclinometer installed on the west shoring wall are shown in Figure 4.

CONCLUSION

The instrumentation of the 94 deep solider pile and tieback anchor shoring system showed that the majority of the tieback vertical loads and the foundation loads of the underpinned building are transferred to the soil though adhesion (friction) above the base of the excavation. More design load was measured at the tip of the pile than that assumed for the design, but within the allowable axial design capacity of the soldier piles. Based on the instrumentation results, the vertical load from the building did not load the piles until the excavation depth achieved a depth of 12 meters, which is considered reasonable as load is transferred from the spread footing foundation to the soldier piles as the excavation deepens. Some unexplained results were measured at approximately 8 m and 22 m in depth, with the upper strain gages measuring slightly less axial load than predicted in the pile, and the lower strain gage measured higher axial load. The load cell measurements indicated that the tieback anchor loads increased over the 90% lock off load, but were less than the design load. In summary, the instrumentation system validated the assumptions used in the design and did show that the design parameters were slightly conservative.

Figure 1. Photograph of site looking toward underpinned building.

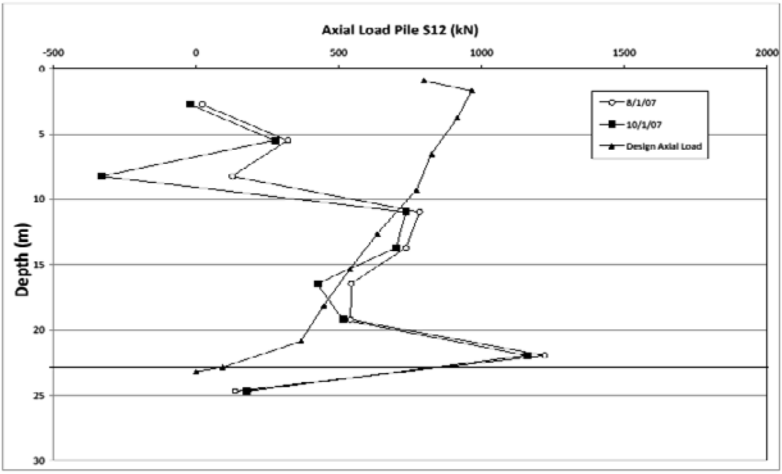

Figure 2. Measured Axial Load versus Depth

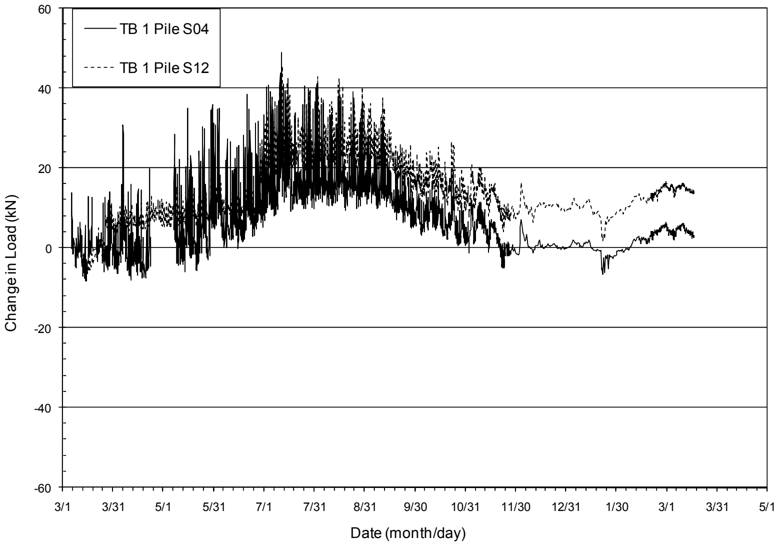

Figure 3. Change in Measured Tieback Load versus Time

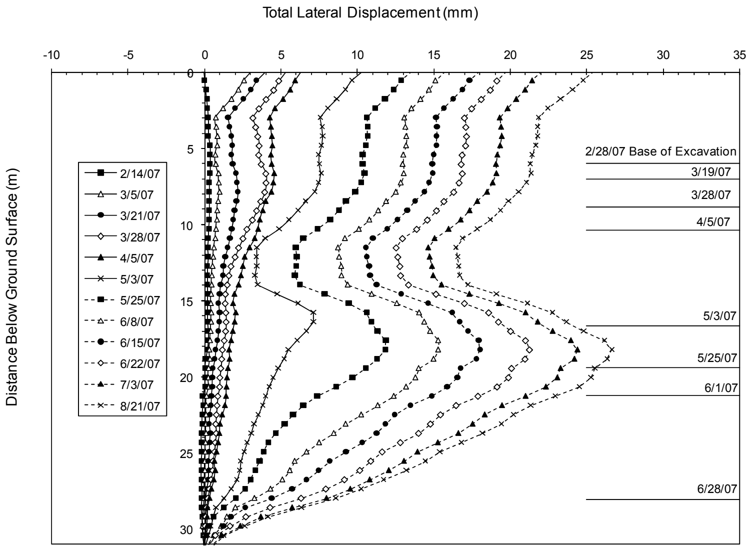

Figure 4. Measured Lateral Displacement versus Depth

Innovative Use of Jet Grouting for Earth Retention, Underpinning and Water Control

Tom Hurley[1] and Richard Crockford[2]

[1]District Manager Nicholson Construction Company, Salt Lake City, UT 84054
[2]Regional Manager Nicholson Construction Company, Sparta, NJ 07781

ABSTRACT

In recent years jet grouting has been implemented in innovative ways to solve earth retention, underpinning and ground water control issue on very complex sites in difficult soil conditions. This paper will prove case histories of the innovative applications and discuss why the jet grouting technique was chosen for each case.

The examples chosen span soil conditions from soft clay to coarse gravel and all contended with relatively high water tables.

Three of the case histories combined jet grouting with other geotechnical techniques to enhance the load carrying capabilities of the jet grout installations.

CASE HISTORY 1 – THE WORLD TRADE CENTER

PROJECT OVERVIEW

The World Trade Center Site redevelopment has employed a large and diverse range of geotechnical techniques in the sub grade construction work. Jet grouting was chosen to join the east and west basement slurry walls around and beneath the live No 1 subway line. Weekend closures were scheduled to allow the completion of the works during 2007.

DESIGN CONSIDERATIONS AND SOIL CONDITIONS

The soil succession in this part of lower Manhattan comprises about 10 feet of fill sitting on 15 feet of loose to medium dense sand underlain by up to 40 feet of highly mobile "bulls liver" silt then 5 feet of dense till which extends onto a thin layer of weathered mica schist, which transitions into hard competent bed rock. The water table sits at about the mid height of the subway box. These soils are well disposed to jet grouting and difficult to treat using either permeation grouting or structural support and dewatering. The silt gives up water slowly and settlements can be experienced over a large radius from well points.

However in this case, Jet Grouting was used beneath the live subway primarily because few other techniques could be installed under such tortuous conditions to provide a large monolithic block of permanently modified ground to withstand lateral earth pressures and to underpin the subway box. The 10 foot thick block had to be propped by tie backs at approximately 10 feet intervals to limit the jet grout span and this in turn necessitated the installation of micro piles within the jet grout block to carry the vertical component of the tie back restraining load down into the rock. The total supported height of soil beneath the subway had to be around 40 feet to reach bedrock. At any one time the jet grouting was only exposed in about 15 feet lifts prior to a reinforced concrete liner wall being erected in front of it supported on a further row of micro piles.

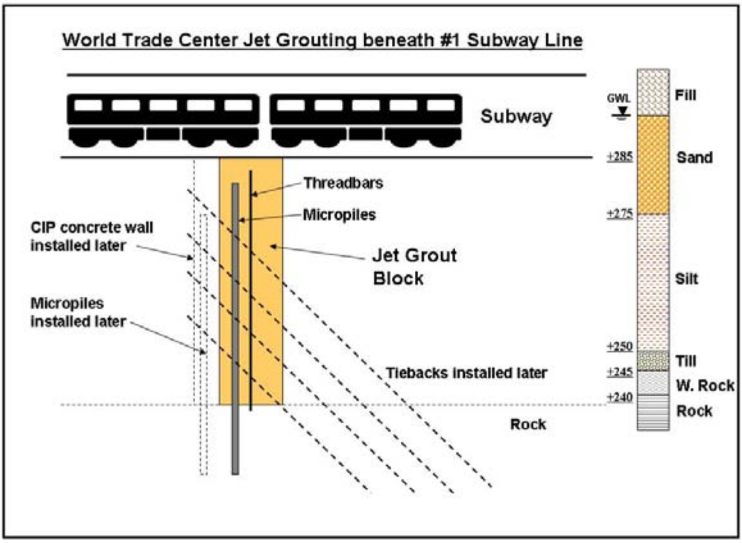

Figure 1 - Schematic of jet grout installation

TEST PROGRAM AND PRODUCTION WORK

An extensive trial program was undertaken, which has been described previously (1) prior to the production works commencing.

The first operation was to set thread shoes into the subway invert slab to accept spoil diverters and allow the completed column to be sealed prior to trains running after each GO. As expected the jet grout block location conflicted with the subway bent frame layout particularly at Liberty Street. This required a very detailed survey of the subway structure at the locations of the jet grout blocks in order to determine where jet grout columns could be located to miss obstructions (i.e. subway duct banks, steel beams, etc.), while still providing the geometry necessary to produce the jet grout mass required by contract drawings. The result of the time required for the preconstruction survey, and the time required to drill the invert slab, was that several GOs were expended with multiple coring and breaking crews to get to the point of starting to drill holes ahead of jet grouting.

While the Liberty Street work area was relatively clear of utilities, the Vesey Street end had a 24 inch diameter steam line in the worst position possible to be in conflict with the jet grout columns. After much discussion and coordination the PA and Phoenix (CM) worked with Con Edison (the utility company that owns the steam line) to temporarily remove the steam line for a period of about 3 months to allow work to proceed from above the subway (FIGURE 1).

Figure 2 - Jet Grout rig sitting over subway as seen from within and outside of subway

While the constraints mentioned above were the most significant, they were not the only ones (2). It was also required to locate the jet grout columns to miss the existing rock anchor tiebacks from the existing Greenwich St. slurry wall of the west basement, which extend under the subway structure.

It was recognized from the outset of the project that the effective handling of discharge spoil in the subway tunnel would be critical to the overall success of the operation. The spoil control needed to be conducted in such a way and with enough contingency plans in place so that all stake holders were satisfied that there was no risk of the subway being unable to re-open on Monday mornings. Sufficient time had to be built into the GO work planning to allow for final clean up to be made and the area inspected and approved mindful all the time of other activities such as track re-instatement that had to be undertaken simultaneously.

The collection and movement of spoil underwent a succession of developments responding in part to changing methods and in part to refining the process. It was always essential to have several back up methods of containing the spoils. Initially spoils were contained within a tube connected to the thread shoe with a side outlet to either a suction hose, pump priming hose or gravity fed hose to a skid pan for subsequent pumping. In case of problems becoming apparent with this system the work area was sand bagged such that about 10 cubic yards could be contained around the hole entry point. This proved sufficient for most fall back situations save for some minor spillage outside this immediate area. Vacuum suction tankers were used either exclusively or in combination with pumping to transfer the spoils to nearby curing pits. At the very least two suction tankers remained on stand by to intervene if other methods failed.

Figure 3 - Exposed Jet Grouting beneath Liberty Street Subway, tieback casing installed

Quality assurance was maintained throughout the work by sampling grout cubes and spoil cubes and performing breaks on both, along with taking spoil density readings throughout each jet grout lift to measure consistency, compatibility with the trial test sections, and to identify likely diameter of influence. Jet grout parameters were monitored both manually and with the aid of a Jean Lutz data recording system.

In early 2009 the jet grouting beneath the subway began to be excavated for the first lift of liner wall and tie back installation. Very competent jet grout material was uncovered at both Liberty and Vesey Street (FIGURE 2). The reality of the treatment's function was brought home graphically standing beneath the subway as 300 ton subway trains thundered overhead supported by the previously installed micro piles and the jet grout blocks at each end of the site.

CLOSING

About 100, 4ft and 6 ft diameter jet grout columns were installed between April and September 2007 predominantly on weekend railway closure periods enabling excavation below the ground water table in otherwise highly mobile ground conditions. Settlements of less than 0.1" were experienced by the subway in the process of executing the jet grout works.

CASE HISTORY 2 – OVERPECK VALLEY, NJ
PROJECT OVERVIEW

A series of tunnel launch and reception shafts were sunk using sheet piles and these were then excavated under water and tremie slabs formed prior to dewatering. To allow water control and early tunnel alignment jet grout break out and break in blocks were formed on the outside of these shafts between the desired tunneling top and bottom elevations. For the drive that passed underneath the heavily used New Jersey Turnpike a jet grout block some 30 feet long was made to allow additional directional adjustment of the tunnel prior to it boring beneath this critical highway. A total of 7 break in / break out blocks were formed around 4 shafts.

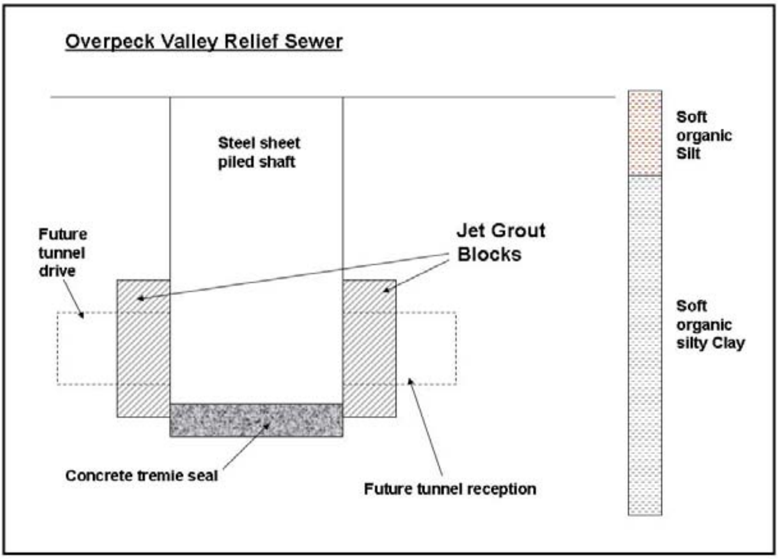

Figure 4 - Schematic layout and soil conditions

DESIGN CONSIDERATIONS AND SOIL CONDITIONS

Whilst the soft alluvial soils near the Hackensack River are ideal for sinking shafts and sympathetic to driving tunnels they are not the easiest soils to jet grout. Weight of rod blow counts masked the cohesive properties of this inorganic clay of low to medium plasticity (CL) which nevertheless contained traces of gravel and sometimes changed to a sandy or silty clay. From the borings you could deduce that the clay was at times lean but in other places fat. High plasticity fat clay soils have been responsible for some severe jet grout problems around the world and need to be treated very carefully. When designing the jet grout parameters for this work we were torn between using single or double system jet grouting. We opted for double system due to the variability of the boring information such that we could develop sufficient energy should the lean sandy and silty clays predominate. We noted however to keep a weather eye on the effects of jetting with a view to switching if necessary. In such soils columns that are formed too large can be just as problematic as columns of inadequate diameter. If a large column extends beyond the center line of an adjacent column shadowing can occur when forming that adjacent column. This would then result in the jet energy being dissipated in hardening grout and failing to cut the desired column diameter.

TEST PROGRAM AND PRODUCTION WORK

Despite this being a relatively small jet grouting scope of work we undertook a significant trial to determine the column diameter likely to be achieved. A Soletanche proprietary “Cyljet” geophysical assessment was made of a trial column which suggested that a column of about 7 to 8 feet diameter had been formed in the target elevation zone. We had been shooting for 6 feet. This was correlated using the drill rig to push the drill rods, with no rotation, down through the very soft soils at radii from the column center until strong resistance from the top of the column was met. This validated in situ strength to some degree also. When the rods failed to find hard cemented soil the column was proven to be smaller than the radius then being probed. This method was only possible due to the extreme soft nature of the soil. This technique proved a column diameter greater than 8 feet but less than 10 feet. The jetting parameters were thus adjusted to target a 6 to 7 feet diameter column.

Production works then proceeded well albeit the spoil returns were very cohesive in nature and did not flow well away from the mouth of the bore hole. This is not uncommon in such soils and makes spoil handling, and curing more difficult and time consuming. Figure 3 shows the Jet Grout face upon tunnel eye break out and water pressure through a sheet pile clutch where jet grouting was not installed demonstrating the effect of the 30 feet of water head.

Figure 5 - Jet Grout face upon tunnel eye break out and water pressure through a sheet pile clutch where jet grouting was not installed

CLOSING

The tunneling proceeded as planned with the help of the jet grout break in and break out blocks. The jet grout had developed about 1000 psi (6.8 MPa) strength upon excavation and was effective in mitigating soil and water flows.

CASE HISTORY 3 – WARNERVILLE PUMPSTATION, QUEENS, NYC

PROJECT OVERVIEW

The Warnerville Pumping Station in Queens was commissioned by the New York City Department of Environmental Protection as part of the area's new combined sewer overflow system. The shaft was constructed with driven sheet piles. Permeation grouting originally was specified for the shaft's bottom plug, but Nicholson proposed and designed a less expensive and technically superior solution using jet grouting. After the sheet piles were driven, and micro piles were installed at the base of the shaft, Nicholson installed 209, 5.5-foot diameter jet grout columns to create a completely watertight seal at the base of the shaft.

DESIGN CONSIDERATIONS AND SOIL CONDITIONS

In Queens south of JFK airport the ground conditions comprise uniform medium to medium dense sands extending for many hundreds of feet below ground level. The fine sands present at the site were assessed as very good jet grouting soils likely to combine very well with the jet grout to form a highly competent end product.

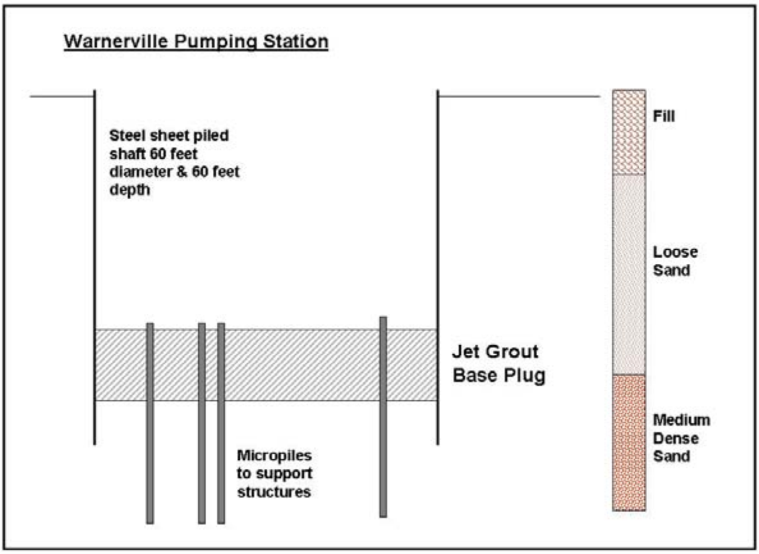

Figure 6 - Schematic layout and soil conditions

TEST PROGRAM AND PRODUCTION WORK

Owing to the nature of the uniform sandy soils a limited trial was undertaken ahead of the production works deploying radius tubes and hydro phones to detect strong vibrations at defined radii as the jet rotated around the drill string. This gave qualitative indications that the desired column diameter was being achieved which combined with back analysis of spoil return densities allowed confidence to proceed with the production works. Again the uniform nature of the soils allowed the reasonable interpretation of back density calculation. Such analysis must be used with caution in stratified or mixed soils as demonstrated at the World Trade Center (1).

The site's high water table presented some challenges. As a result, work platform stability was a constant concern. The work platform was prepared each evening by grading off spoils and adding clean stone to replace soils lost into collapsing surface column matrial. Platform stability problems diminished once 25 percent of the jet grout columns were installed. The high water table also meant the jet grout bottom plug had to withstand 55 feet of water pressure trying to displace it. Even one small leak would have caused major problems during the shaft excavation.

The requirement to have micro piles supporting the pump station structure above the jet grout base plug whilst shedding load to a bond zone below the jet grout slab presented some difficulties of installation. The piles ideally would be de-bonded from the jet grout slab but at the same time they could not allow leakage flow paths to develop between pile and jet grout. We elected to install the piles through the jet grout, withdraw the pile casing to a position above the jet grout slab immediately after grouting and then plunge it through the slab within the micro pile grout such that a thin layer of grout existed between the casing and the jet grout slab to prevent leakage whilst the casing provided a measure of resistance to early load transfer. It seemed to work as no leakage problems occurred during construction. On the other hand it is impossible to tell whether all load is being shed below or into the jet grout slab. Either way no excess settlement has been experienced.

Figure 7 - Shaft excavation nearing completion with micro piles protruding through the jet grout slab.

CLOSING

A 60 feet diameter base plug was successfully installed and by excavation proven to be watertight (Figure 4). The water coming through sheet pile clutches also testified to its presence and mobility. Some spectacular failures have occurred around the world where the design depth of base slabs employed has been cut to depths where tolerances of installation could not be deployed to effect full closure. Great care and attention must be paid to layout, rig set up geometry and parameter control to successfully form such slabs.

CASE HISTORY 4 – SALT CITY PLAZA, UT
PROJECT OVERVIEW

Salt City Plaza Phase I is the first phase of a US$100 Million project encompassing an entire city block (approximately 10 acres or 81,000 Sq M) in the heart of Salt Lake City, Utah. The overall project involves the demolition of existing hotel structures, excavation for underground parking structures, and construction of 3 new hotels and 1 office building 5 blocks south of Historic Temple Square. The focus of this paper is the Phase I portion of the project which involves relocation and new construction of the hotel lobby with underground basement between two existing hotel units. The relocation of the lobby is necessary to make way for the demolition and new construction of the overall project.

DESIGN CONSIDERATIONS AND SOIL CONDITIONS

Excavation was required up to 16ft (4.8m) below grade and by as much as 14ft (4.3m) directly below adjacent buildings supported by shallow foundations. Controlling movement of the earth retention system and adjacent buildings was of critically important.

The native soil stratigraphy consists of Holocene, marsh deposits overlying Pleistocene Lake Bonneville deposits, which are primarily comprised of clay, silt and fine sand. The soil encountered during the depth of the excavation was primarily very soft clay (CL) with Sandy Clayey Silt (ML) layers. The clay becomes medium stiff at a depth of 22ft below grade. The depth to existing groundwater is approximately 8ft (2.4m) below grade.

Careful consideration was applied to evaluate the various excavation support systems. The merits of each system were evaluated considering the requirement of excavations through soft soils below the groundwater table, directly adjacent to and below structures on shallow foundations. In addition the earth retention system was required to maximize usable space for the new basement construction and therefore needed to be as near to the vertical plane of the existing structure as possible.

Sheet piling, as well as soldier pile and lagging systems were evaluated for the project. Each of these systems was eliminated because they would encroach upon the new construction and eliminate usable space. In addition the soldier pile and lagging system would require face placement (installation of lagging boards) of the shoring system below the groundwater table in potentially flowing ground. Equipment constraints played a role in these decisions due to the proximity to the existing building and the vibration potential that would have been induced.

A dewatering system was evaluated however, the main concerns were two fold. 1) The dewatering system was to be located in a zone of fine material with low hydraulic conductivity, requiring many small diameter wells at a very close spacing and 2) the potential for removal of fines by the dewatering process could lead to settlement.

Ultimately, and anchored jet grout wall was selected as the integral underpinning and earth retention system for the project for the following reasons: 1) Jet grout columns could be installed adjacent to and below the existing foundations to underpin and provide a positive connection to the existing foundation, 2) Jet grout minimized encroachment of new construction, 3) Jet grouting would provide water cutoff, 4) Jet Grouting eliminated the risk of flowing ground during excavation. The jet grout walls were anchored using 2 to 3 levels of soil nails.

In order to verify that the earth retention system was performing as designed, inclinometers were placed within the jet grout wall and daily readings were taken to compare predicted deformations with actual values. In addition, deformation points were set and read during and jet grouting operations and during excavation to monitor building movements.

TEST PROGRAM AND PRODUCTION WORK

Prior to commencing production jet grouting, a jet grout field test program was instituted to optimize injection parameters and to confirm jet grout element geometric and mechanical properties. The test program involved the construction of 3 individual test columns using the single fluid method of jet grouting. The single fluid method of jet grouting is the technique where a single fluid, typically neat cement grout, is injected at high velocity through horizontal radial nozzle(s) to directly erode, and mix with, the in-situ soil. The injection times were varied for each set of test columns, while all other parameters remained constant. The grout mix consisted of Portland Cement Type II and potable water. The test columns were exposed by excavation and geometric properties obtained by direct measurement. The target column diameter was 3ft (1.2 m) and the target unconfined compressive strength (UCS) was 300psi (2.07Mpa). One test column achieved 2.75ft diameter, the second test column achieved the target diameter of 3ft and the third test column achieved 4ft diameter. All test columns achieved the UCS requirements. The jet grouting parameters that achieved the targeted 3ft (1.2m) diameter were selected for production work.

Two jet grout walls were constructed consisting of a single row of 27ea overlapping secant columns and connected below the existing 2 story buildings. The primary jet grout columns were installed to a depth of 25ft to ensure the bottom of column was embedded a minimum of 3ft (0.93m) into the medium stiff clay. The transition from the very soft clay into medium stiff clay was detected during drilling of each primary column. Secondary jet grout columns were installed to a depth of 18ft to ensure the bottom of column was a minimum of 2 feet below the bottom of excavation. Jet grout columns were installed in a hybrid “Primary-Secondary” (P/S) and “Fresh to Fresh” (F/F) sequence, where a Primary group of three columns were installed successively (F/F) then allowed to harden before installing the overlapping adjacent Secondary set of three columns. The fresh to fresh sequence involves jet grouting elements successively without waiting for the grout to harden in the overlapping elements. When constructing successive columns, it is very important that the pilot hole is advanced using cement grout as the drilling fluid so as not to dilute the adjacent “freshly completed” column. The fresh to fresh sequence generally produces a more monolithic jet grout wall.

Because the jet grout columns are directly underpinning the existing structure, distances greater than 10ft under existing footing temporarily unsupported by fresh jet grout columns was not desirable, therefore the hybrid P/S and F/F installation sequence. We started by installing three fresh to fresh columns and closely monitoring the building for response during each jet grout column installation. No movement was detected and the three F/F column sequence was validated. For the production work, three jet grout columns were installed successively as F/F then three column locations were skipped so that no more than 8ft of continuous existing footing was unsupported. During the installation of jet grout columns, the existing building was continuously monitored for deformation by laser level. No building movements were detected during the entire course of the jet grouting campaign. Had building movement been detected, a more conservative P/S sequence would have been implemented. Figure 5 shows the anchored jet grout walls.

Figure 8 - Jet Grout Walls exposed during excavation

CLOSING

54ea, 3ft diameter jet grout columns were installed in a 6 day period enabling excavation below the ground water table in very soft clay for the new lobby basement. 2 to 3 levels of 25ft long temporary hollow bar soil nails were installed to anchor the jet grout walls. The design expected horizontal walls movement of 0.75” and less than 0.1” was experienced at the site.

CONCLUSIONS

Jet grouting is a difficult technique to implement to tight design specifications. However, with adequate knowledge and experience it can be used to good effect across a wide range of earth support applications and soil conditions provided that conservative, bulk strength or modulus characteristics are used in design to account for the somewhat variable nature of the product constructed. Early contractor involvement is recommended to adequately size jet grout elements to fulfill the end use in the given soil conditions and to sequence any combination with other supporting geotechnical installations.

REFERENCES

1. “Underpinning the No. 1 Subway Line at the World Trade Center,” Crockford, Lizzo & Wise; DFI 33rd Annual & 11th International Conference on Piling & Deep Foundations, New York (Oct 2008)

2. “An overview of Geotechnical Work at the World Trade Center,” Crockford; ASCE 24th Central Pennsylvania Geotechnical Conference, Hershey, PA (Nov 2009)

A Perspective on Mechanically Stabilized Earth Walls
Pushing the Limits or Pulling Us Down

Robert C. Bachus[1], M. ASCE, Ph.D., P.E., and Leslie M. Griffin[2], M. ASCE, P.E.

[1]Principal. Geosyntec Consultants. 1255 Roberts Boulevard, Suite 200, Kennesaw, GA 30144. rbachus@geosyntec.com
[2]Senior Engineer. Geosyntec Consultants. 1255 Roberts Boulevard, Suite 200, Kennesaw, GA 30144. lgriffin@geosyntec.com

ABSTRACT

Many will argue that fill walls, particularly mechanically stabilized earth (MSE) walls, represent a boom to the U.S. geotechnical practice and are a testament to the valuable and innovative contributions by geotechnical practioners. Many examples can be cited to demonstrate the profession's ability to push the limits in terms of wall height and creative applications. These success stories notwithstanding, there have been several reported MSE wall failures that should give the profession pause for concern. There are indications today that the profession's lack of attention and focus has started to reverse the impressive trends of innovative practice. These failures should remind us that we have to remain ever mindful of the basic tennants of good geotechnical engineering practice and that we cannot afford to lose sight of important geotechnical considerations and perspective regarding the design and construction of MSE walls and slopes. Unfortunately, the lessons that have been identified by others from past failures have apparently fallen on deaf ears....because we continue to experience failures. This paper strives to once again highlight important lessons regarding the design and construction of MSE walls from both big and small projects. Most importantly, the authors offer specific recommendations to halt this disturbing trend before it has potentially severe consequences.

BACKGROUND

From the relatively simple design concepts proposed by Vidal in 1963, mechanically stabilized earth (MSE) walls and (subsequently) reinforced soil slopes (RSSs) have provided geotechnical engineers with yet another tool for innovative solutions to both difficult and routine geotechnical problems. The track record has been impressive, as described by others at this conference. Encourgaed by the past performances, the profession is also beginning to look ahead towards the next 20 years (Berg 2010), as likely will be presented by others at this conference. Without sounding like the proverbial "Chicken Little," the authors also note that recent publications (i.e., Koerner and Koerner 2009), presentations (i.e., Holtz 2010), and specific project experience by the authors have shown that MSE wall failures are apparently becoming more common. The reasons for these failures (sadly) often can be attributed to factors long recognized by geotechnical engineers, yet the problems persist and the important lessons outlined by others apparently have not been heeded.

Rather than merely providing a summary of previous “lessons”, the authors would like to build upon these contributions and provide specific recommendations that not only identify the challenges but heightenen the awareness and the importance of robust design and diligent construction . The not-so-subtle observations by the authors is that if current trends persist, the years of successful design, innovative solutions, and excellent performance of the literally thousands of MSE structures will be diminished as the failures will tend to represent an albatross around the neck of design professionals. Should this happen, we will only have ourselves to blame. The authors note that if current project experience defines the standard of care, then the standard needs to change.

THE GOOD, THE BAD, AND THE UGLY

The intention of this paper is not to provide a comprehensive list of accomplishments, to provide a recitation of case histories, nor to repeat the numerous lessons that should have been learned and heeded. Other speakers (and many of the exhibitors) at this conference will provide illustrative examples of the successes and advancements that have been experienced by the profession. Many speakers will likely highlight lessons from previous case histories. To provide illustrative examples of success and failure, Figures 1 through 3 provide what the authors identify as examples of “the good, the bad, and the ugly” MSE walls. To borrow and modernize the famous poem by Henry Wadsworth Longfellow regarding the curly headed girl….

> There were geotechnical engineers, who designed MSE walls
> And to Seattle in August they fled.
> And when they were good, they were very, very good,
> But when they were bad… they were horrid.

- The Good (Figure 1)
  - A. Very close to this venue, the third runway at the SEA-TAC airport presents a 42 m (142-ft) tall crowning achievement to MSE innovation.
  - B. A series of MSE walls at the Babylon Landfill on Long Island changed both the aesthetics and the perception of a former dump site. These wall systems were subsequently requested by the local public when asked to comment on an expansion permit application for the facility.
  - C. Innovative design and construction monitoring of a RSS on Cherry Island over soft dredge spoil and sediment adjacent to the Delaware River has provided exceptional performance despite more than 2 m (6 ft) of (anticipated) settlement.

A

B

C

FIG. 1. The Good….
Innovative and Successful Applications of MSE and RSS Structures

- The Bad (Figure 2):
  - A. Failure to consider the adverse impacts of foundation soil settlement led to failure of an otherwise impressive 14 m (45-ft) high MSE wall.
  - B. In an attempt to squeeze useful space at an apartment complex, this MSE wall with wire facing remain was used. The lack of vegetation and proximity to the buildings seem an example of bad decisions by the developer.
  - C. Global stability is always shown on sketches that present the "modes of failure" for MSE structures. When walls are developed and constructed for private (as compared to public) owners, it is a bad idea to rely on a homeowner and/or developer to complete this geotechnical assessment.

C

FIG. 2. The Bad….
Failures Occur in the Absence of Good Geotechnical Practices

- The Ugly (Figure 3):

  A. "Green" walls and slopes address a growing demand for sustainable innovation, but when the vegetation is stressed and/or dies, the entire structure is viewed to not live up to expectations.

  B. When attractive and aesthetically pleasing MSE walls fail to meet expectations, the commonly recommended soil nailed solution detracts from the original good intentions.

  C. Water infiltrating through a ditch and loading the back of an MSE wall that had shorter-than-design reinforcement lengths contributed to sliding and overturning failures. This single example has caused the owner to consciously re-think their decisions at all of its facilities across the U.S.

A

B

C

FIG. 3. The Ugly….
Examples of " but when they were bad… they were horrid"

WHAT HAVE WE LEARNED AND APPARENTLY FORGOTTEN

As referenced in the Background, the observations that there are too many failures resonate across the country…Bob Holtz (Seattle, WA), Bob and George Koerner (Philadelphia, PA), and the authors (Kennesaw, GA). An excellent summary of the reported failures was compiled by Koerner and Koerner (2009) who cite that the first of 82 reported failures was noted in 1987, followed by a gradual increase in reported problems that have been occurring since 1996 at a rate of five per year. These are the cases that have been reported (read as "published"). A survey of the audience today would of course identify a rate that significantly exceeds this, as litigation often prevents publication of informative case history studies that could provide additional constructive lessons.

For engineered structures, an isolated failure might be expected, but repeated occurrences of the same problems seem to be a characteristic of the MSE wall failures, despite the published lessons that have been "learned" from these problems. Consider the following summary statistics (Koerner and Koerner 2009) on geosynthetic reinforced walls:

- Non-technical Factoids
  - Ownership: 100 percent of failures are privately owned;
  - Facing: 76 percent of failures involve masonry block, with 24 percent fairly evenly spread among weld wire, wrap around geosynthetics, precast concrete, and timber;
  - Height: All (published) wall failures occurred in walls between approximately 3.7 to 11 m (12 to 36 ft) in height (though taller walls have failed);
  - Occurrence: 67 percent of the failures occurred within two years following completion of construction; and
  - Contributors: 65 percent of the failures were attributed to the design, while 33 percent were attributed to the contractor; the remaining 2 percent were attributed to a facing failure; notably, none of the failures were attributed to a defect in the manufactured geosynthetics or steel reinforcements.
- Technical Factors
  - Soil Type: Fine-grained (i.e., > 50% fines) reinforced wall fill materials were involved in 76 percent of the failures while 24 percent involved granular reinforced wall fills; and
  - Soil Compaction: 50 percent of the problems involved soils that were believed to be poorly compacted while 30 percent of the failures involved soils that were reported to be moderately compacted; the remaining 20 percent of the failures involved soils that exhibited "good" compaction.

Koerner and Koerner (2009) report that virtually 100 percent of the failures could be attributed to either the properties of the soil or the influence of water. While this should not be particularly surprising to most geotechnical engineers, Table 1 presents an interesting summary regarding the allocation of soil and water that is either internal or external to the MSE wall.

Table 1. Allocation of Soil and Water to MSE Wall Failures
(after Koerner and Koerner, 2009)

	Internal	**External**
Soil	26 percent	6 percent
Water	46 percent	22 percent

This compilation should put private developers on notice that they might want to carefully consider the selection of a designer and contractor for their 11-m (36-ft) high wall constructed using masonry blocks and native fine-grained materials, particularly if the system does not include provisions for drainage and if they prefer to not include construction quality assurance (CQA) personnel to control compaction. Furthermore, the developer (and the designer) should probably be nervous for similar projects built within the last two years!

Geotechnical engineers are well acquainted with the influence of water and soil type on retaining walls. For example, a qualitative rating of soils for use as retaining wall backfill by Sowers and Sowers (1970) is presented in Table 2. Have MSE wall designers forgotten that this information is applicable to reinforced structures?

Table 2. Rating of Retaining Wall Backfill
(Sowers and Sowers, 1970)

SOIL	RATING & COMMENTS
GW, SW, GP, SP	Excellent, well-draining backfill.
GM, GC, SM, SC	Good if kept dry but requires good drainage. May be subject to some frost action.
ML	Satisfactory if kept dry but requires good drainage. Subject to frost. Neglect cohesion in design.
CL, MH, OL	Poor. Must be kept dry. Subject to frost.
CH, OH	Should not be used for backfill because of swelling.
Pt	Should not be used.

WHY GOOD IDEAS CAN GO WRONG

The previous section identified the factors that were found to contribute to the failures of MSE walls. Furthermore, the authors note that many of these factors have long been recognized as potentially contributory to instability of engineered structures. The key question to address is… "With all of this prior knowledge and experience, are there explanations as to why we still continue to have problems?" In general, the authors believe that there are potentially logical (but admittedly unacceptable) explanations for the factors that were identified in the previous section. The explanations can be broadly placed into the following three categories: (i) inexperience, poor understanding, and forgetting first principles: (ii) wishful thinking; and (iii) market pressure. Each of these explanations presents often subtle but potentially increasingly insidious challenges to the profession.

- Inexperience, Poor Understanding, and Forgetting First Principles: One of the major problems with the MSE technology is that it can be used to construct walls to a height of 1.2 m, 12 m, or 42 m (4 ft, 40 ft, or 140 ft). The concepts for these different designs are similar; but unfortunately the reality of actual construction and performance is much different. Many engineers (or "builders") faced with the opportunity to build an MSE structure fail to see the difference between systems constructed to different heights. This likely explains why the majority of the failures occur in walls that are between 3.7 m and 12.2 m (12 and 40 ft) in height. Most will agree that there is limited engineering required for a 1.2- to 1.8-m (4- to 6-ft) tall landscape wall where you can procure the materials at a local building supply store. Similarly, few would likely argue that when the walls are >30 m (100 ft) in height, extensive design and experience are required. For structures that are within the "mid-height" region of 3.7 m to 12.2 m (12 to 40 ft), there is likely a tendency to adopt the "I can do that" attitude and actually design by "rule of thumb" guidelines. Designers often tend to forget that many of the design details come from experience and that experience gained from a low-height MSE wall explicitly cannot and should not be extended to mid-height walls. It would seem a good practice to re-think the current approach and realize that any structure over about 1.8 m (6 ft) in height should be considered and "engineered structure" and treated as such. Simply changing this perspective would likely alleviate many of the problems. The authors recognize that there will be several practitioners (and constructors) that believe this recommendation is too severe, but with this proposed change in perspective, many of the first-principle retaining wall concepts of geotechnical engineering hopefully will not be overlooked. The areas that currently seem to be overlooked due to inexperience and poor understanding of MSE wall systems include (not surprising) drainage, strength, and compaction as highlighted above. In many cases, it appears that the "designers" failed to consider the *engineering* aspects of these structures.

- Wishful Thinking: In the previous category, it was postulated that the designers or builders of the MSE systems did not realize the fact that MSE walls are engineered structures. For this second category, the authors believe that the designers may be experienced engineers, but they simply want to solve a problem and want their solution to work. We term this "wishful thinking" as the concepts are *generally* adopted and the materials are *probably* acceptable. The problems are realized when attention to the details of engineering design are forgotten or not applied. Three specific examples are cited.

- Soil Type: While both coarse-grained and fine-grained soils used in construction are geotechnical materials, the engineering properties can be dramatically different in terms of long-term strength, time-dependent creep characteristics, and permeability. Engineers should require more site-specific testing, particularly as the grain size of the backfill materials includes silt and clay materials, and should remember the information presented in Table 2 regarding retaining wall backfill soils.
- Water: Virtually every geotechnical engineer knows the problems that water can present to virtually any geotechnical project, particularly walls. Where many often fail is in the consideration of the various and numerous ways that water can get into their structure/project. As most geotechnical engineers realize, however, Mother Nature will find a way! Therefore, we should not "wish" or "hope" that water is not a factor. The design of MSE walls should either consider that water will find its way into the wall and therefore: (i) should be accounted for in the design; or (ii) be controlled by explicitly providing a means for drainage….period.
- Maintenance: Many engineers of substructures (i.e., spread footing, piles, drilled shafts, and cutoff walls) have the luxury of burying their work products. By contrast, most walls (and slopes) are visible for their entire life. Maintenance of these engineered structures is often a relatively foreign concept to many geotechnical engineers. For MSE walls, particularly welded-wire baskets that include vegetation, we are learning the valuable and importance of planned and executed maintenance.

- <u>Market Pressures</u>: This explanation is perhaps the most disturbing, because in the worst case scenario it implies that a design engineer's principles can be compromised by external pressures from the market, whether those pressures come from competitors or clients. In an attempt to make the client happy, get the job, or to get a lower price, there may be an unconscious (or potentially conscious) impact to overlook some aspect of the design. This includes adding notes on the design drawings to indicate that certain aspects of design (e.g., global stability, settlement, etc.) are the responsibility of someone other than the wall designer. Taken to its extreme or cycled through several iterations, it may be difficult to remember all of the compromised steps. In this case, a failure is likely inevitable. It has often been cited that there is a perception that the contributions of geotechnical engineers are "unappreciated" and "not valued." While the authors have experienced the frustration of this perception, we also feel that succumbing to market pressures essentially validates the same perception. While this last explanation may represent the exception rather then the rule, the authors note that the actions of even a few can ruin the good efforts of majority. Consider the following:

- In the Southeastern U.S., the term "blow count engineer" and "sample fetcher" is often applied to the geotechnical engineer, as these terms connote the lack of value for the geotechnical work product. An extension of this to the topic at hand is a concept that a MSE Wall design can be "bid" on a ¢ per ft^2 basis regardless of subsurface conditions, wall height, materials, etc.
- The authors are aware of MSE wall projects where geotechnical exploration programs are not executed prior to design. This has recently extended to a project where the geotechnical investigation was conducted but the report was explicitly not provided to the MSE wall designer by the owner for fear of potential implied owner liability for the MSE wall design.
- In many cases, the MSE wall designer is forced to submit stamped design drawings that include limitations regarding external stability and settlement analyses. These limitations state that these assessments are explicitly not the responsibility of the wall designer. While the authors may agree with this in concept due to absence of foundation parameters, it begs the questions: (i) who is responsible for external stability and settlement calculations; and (ii) how can a design be executed in compliance with recognized design methodologies, if the design does not include external stability assessments? Should the design drawings be stamped and issued for construction without verification that these analyses have been performed?

In an effort to control (read as "reduce") costs, CQA personnel are often not employed during construction and in many cases their reports seem to provide "lip service" to the concept and really do not act on behalf of the owner to assure that the designer's field conditions and/or assumptions are achieved. A landscaper that is experienced in building 2 m (6 ft) high walls likely does not have the construction quality control (CQC) experience or knowledge for constructing the 11 m (36 ft) high walls they are now building.

WHAT WE NEED TO LEARN

The previous sections summarized the various causes for failures and identified potential reasons and/or explantions for the problems, despite our apparent understanding of the causes. The authors believe that there is a need for specific guidelines and/or recommendations. It is too simple to believe that just because we know the reasons for the failures, we will be able to minimize and/or eliminate them. This "simple" solution is, unfortunately, in the author's opinion another example of "wishful thinking", as numerous case histories have repeatedly identified lessons....and yet problems persist. The Koerner and Koerner (2009) report repeats some previously cited and recognized recommendations as a means of reducing the incidence of failures: (i) use granular materials, (ii) provide adequate compaction to the backfill; (iii) control storm water at the site; (iv) minimize impact of external sources of water; and (v) be sure that the software adequately models the as-built conditions. These are excellent recommendations, but the authors believe that stronger and more specific recommendations need to be advanced. This section identifies five initial specific recommendations that should be implemented and considered part of the standard of care for MSE wall designs.

- The Buck Stops with the Designer: The wall designer plays a critical role in improving the practice and in reducing the incidence of failures. The authors believe that if we are to change practice: (i) change has to start with the designer; and (ii) ultimately the designer should assume responsibility for the engineered system. To accomplish this the designer has to insist that adequate geotechnical investigations be performed and inform the owner that design parameters are to be identified in the report. This action will reduce the requirement for extensive limitations on the design drawings and the designer should minimize the number of limitations, conditions, caveats, etc. that are included on the design drawings. This may involve interaction between the geotechnical engineer who prepared the report and the MSE wall designer. An MSE wall design can not (and should not) be "designed" as though it is placed on an "flat parking lot" if the actual site conditions includes slopes at the toe of the wall and foundation conditions that indicate a potential for slope stability and settlement.

- Drainage: In many regards this should be the easiest recommendation to accomodate. Simply stated, if the MSE wall design does not include loading due to water pressure, than the MSE wall should be designed either to: (i) be freely draining (i.e., open graded, permeable, granular) backfill, or (ii) include a base and/or chimney drain. Guidelines for these drainage systems are available in numerous design guidance documents. They should be followed explicitly or specific equivalency calculations need to be provided – i.e,. always include drainage unless it is specifically engineered out of the design (Berg et al. 2009). As summarized previously, water can generally be traced to the root of most geotechnical problems, including those with MSE walls.

- CQA Monitoring: Owners should budget for and designers should insist on qualified CQA monitoning during construction for all walls larger than approximatelt 3 m (10 ft) in hieght. The geotechnical engineer who provides oversight should assume responsibility for assuring that the design parameters and conditions are achieved. The author's experience is that qualified CQA monitors are extremely beneficial and influencial in achieving high quality work products. The responsibilities of the field monitors needs to be explicit and should include: (i) assuring compaction and calibration requirements; (ii) understanding all relevant design details; (iii) reviewing laboratory test results; and (iv) assuring all materials meet the project specifications.

- Laboratory Testing: In recent years, there seems to have been a reduced emphasis on laboratory testing for both soil and soil/geosynthetic interface materials. There seems to be more emphasis on assumed (and potentially "wished") properties. This trend needs to be reversed, particually when fine-grained soils are considered in the design. Testing should assess the long-term strength and settlement of fine-grained soils and the strength and creep characteristics at the soil/geosyntehtic interface. Designers need to assess potential "what if" design conditions and testing needs to be performed to model these potential conditions. Upon review of the test results, the designer needs to interpret these results and suggest appropriate design recommendations.

- Maintenence: There is an increased emphasis on long-term, life-cycle cost assessment for current construction projects. There is also strong interest in sustainable development. As mentioned previously, walls are engineered structures that are visible and accesible for their entire service life. Designers need to consider potential maintenance requirements and have these recommendations be included in the design report. Owners need to budget for and then implement the maintenance recommendations. With regards to MSE walls, this is particularly important for welded-wire basket facing that support vegetation. In all cases this will mean controlling vegetaion from adversely impacting the face by removing trees from the face that will become established as volunteer growth. In some cases this may mean providing irrigation (i.e., introducing water) to the soils at the face and developing specific topsoil specification for materials placed in the front of the wirs baskets. In the author's experience, lack of maintenance for these welded wire structures often leads to a perception that the walls themselves are failing.

To assure that these recommended actions are included in the design and the operations documents, it is recommended that forms be developed to help assure that these guidelines are included in design packages. In cases where concurrence needs to be achieved between owners, engineers, and contractors, forms should similarly be developed and executed.

CLOSURE

This paper started with an appropriate historical quotation. It seems fitting to end with a similar timely citation from the Spanish philosopher George Santayana who noted in 1905 that ..."Those who cannot remember the past are condemned to repeat it." The authors note that there have been numerous examples where "lessons learned" have been reported, but apparently not fully heeded by the MSE design and construction community. The goal of this paper is to slow the incidence of failures by: (i) identifying the key elements that cause the problems; and (ii) defining specific actions to address these causes.

Geotechnical enginners provide a tremendous service and can represent significant value to a project. However, if we allow failures to continue at anywhere close to the existing rates, we will see an impressive history of innovation slowly recede because the public will not trust us to provide MSE walls that will serve as durable engineered structures. As an example, in suburban Atlanta, one municipality banned all MSE walls because of the high incidence of failure. The ban was lifted only after prescriptive requirements for investigation, independent review, and final construction confirmation by a third party were adopted. In a final disturbing trend, the increased market pressures and (a potentially correlated lucrative litigation environment) has caused some designers to concede and leave the ranks of innovative design. If these trends continue we will only have ourselves to blame as we will essentially pull down the good works of earlier generations of geotechnical engineers.

REFERENCES

Berg, R. (2010). “Fill Walls – Recent Advances and Future Trends.” *Earth Retaining Structures 2010*, ASCE.

Berg, R.R., Christopher, B.R. and Samtani, N.C. (2009). “Design and Construction of Mechanically Stabilized Earth Walls and Reinforced Soil Slopes.” FHWA NHI-10-024 Vol I and NHI-10-025 Vol II, Federal Highway Administration, Washington, D.C., 306p (Vol I) and 378p (Vol II).

Holtz, R. (2010). “Reinforced Soil Technology: From Experimental to the Familiar.” Terzaghi Lecture, *GeoFlorida*, Palm Beach, Florida.

Koerner, R.N. and Koerner, G.R., (2009). “A Database and Analysis of Geosynthetic Reinforced Wall Failures.” GRI Report No. 38 (Members only distribution).

Sowers, G.B. and Sowers, G.F. (1970). *Introductory Soil Mechanics and Foundations*, MacMillan Publishing Co., Inc., New York, NY, 556 p.

Facing Displacements in Geosynthetic Reinforced Soil Walls

R.J. Bathurst[1], Y. Miyata[2] and T.M. Allen[3]

[1]GeoEngineering Centre at Queen's-RMC, Department of Civil Engineering, Royal Military College of Canada, Kingston, Ontario, K7K 7B4 Canada; PH (613) 541-6000 (ext. 6479/6347/6391); FAX (613) 541-6218; email: bathurst-r@rmc.ca
[2]Department of Civil and Environmental Engineering, National Defense Academy, 1-10-20 Hashirimizu, Yokosuka 239-8686 Japan; PH +81 (468) 41-3810; FAX: +81 (468) 44-5913; email: miyamiya@nda.ac.jp
[3]State Geotechnical Engineer, Washington State Department of Transportation, State Materials Laboratory, Olympia, Washington, 98504-7365 USA; PH (360) 709-5450; FAX (360) 357-3814; email: AllenT@wsdot.wa.gov

ABSTRACT

The paper summarizes current recommendations for anticipated and specified maximum horizontal deformation of geosynthetic reinforced soil wall facings found in a number of codes of practice. Recommended limits on verticality are compared to a database of wall performance data collected by the writers. In most cases, end of construction (EOC) measured facing deformations for walls on firm foundations are within recommended limits. Anticipated deformations for walls extrapolated out to a design life of 75 years are also reported. The results of a careful set of full-scale wall tests show that EOC deformations are influenced by both compaction effort and global reinforcement stiffness when other factors remain unchanged. The paper is of value to design engineers by providing example deformation data to estimate the additional facing batter required to satisfy intended design alignment and to provide adequate clearance for adjacent structures.

INTRODUCTION

Geosynthetic reinforced soil walls are now an established technology for earth retaining walls in civil engineering works. Their use in North America can be traced back to the early 1970s when the first wrapped-face walls were constructed in northwestern USA by the US Forest Service (Allen et al. 2002). Today there are guidance documents available to design these soil retaining wall systems that are classified as mechanically stabilized earth (MSE) walls in USA terminology. Most design methods are limit equilibrium-based and adopt variants of classical notions of active earth theory (e.g. AASHTO 2009; FHWA 2008; NCMA 2009). These design methods have proven to be conservative (i.e. safe) when predicted reinforcement loads are compared to measured loads at end of construction (e.g. Allen et al. 2002). This has led to an empirical-based working stress design method (K-stiffness Method) that has been shown to give more accurate estimates of reinforcement loads and their distribution under operational conditions compared to current methods (e.g. Allen et al. 2006; Bathurst et al. 2008; WSDOT 2006).

Nevertheless, as interest towards performance-based design increases and limit states design codes are developed which include serviceability limit states, there is a need to estimate what facing deformations can be anticipated or tolerated for geosynthetic reinforced soil walls during and after construction. Furthermore, designers may be interested in the magnitude of outward deformations that may be anticipated for different types of wall structures so that a pre-batter may be designed into the facing to achieve a target batter at the end of wall construction or to provide minimum clearances with adjacent structures. At present there are no analytical methods available and estimates of facing deformations have been restricted to a design chart first proposed by Christopher et al. (FHWA 1989) and reproduced in subsequent FHWA and AASHTO design guidelines. Numerical modeling has also been used but credible predictions have been restricted to Class C predictions of a small number of instrumented structures.

Over the last decade the writers have collected case study records of the quantitative performance of full-scale walls constructed in North America, Europe, Japan and elsewhere. The core data are taken from case studies with sufficient quantitative information on the properties of the component materials (e.g. reinforcement and soils) and construction records to allow the writers to compare measured reinforcement loads at end of construction to predicted values using the current limit-equilibrium method in North America (called the "tie-back wedge" or Simplified Method) and the K-stiffness Method. A collateral benefit of this collection is that it can be used to summarize observations on the magnitude of lateral facing deformations for different types of walls that are judged to have performed well and a few that have not. A number of other field walls with less comprehensive monitoring data but with good quality horizontal deformation data from survey or inclinometers have been added to the database for this study.

The objectives of this paper are to summarize current recommendations for anticipated horizontal facing displacements and specified tolerances from current codes of practice in the USA and other countries/regions, and from other sources. Reported deformations from high quality instrumented and monitored full-scale walls are reviewed and compared to recommended values. The paper is restricted to horizontal deformations since the walls in the core database were either built on rigid foundations in the laboratory or on firm competent foundations in the field. Furthermore, vertical settlements have been recorded infrequently in the literature with the exception of a few instrumented walls built specifically on soft foundations. Finally, the results of a series of carefully constructed full-scale geosynthetic reinforced soil walls are used to examine the influence of compaction, reinforcement stiffness and spacing on facing deformations.

CURRENT GUIDELINES AND SPECIFICATIONS FOR FACING HORIZONTAL DISPLACEMENTS AND TOLERANCES

Table 1 summarizes anticipated horizontal out-of-alignment and specified tolerances for different geosynthetic reinforced soil wall types. Guidelines typically report

Table 1. Guidelines for anticipated and specified horizontal facing deformations.

Source	Criterion No.	Wall type	Maximum displacement from target batter over wall height, H	Verticality ($\Delta x/H$)	Anticipated	Specified
FHWA (2008), AASHTO (2009)	1	All walls	-	Variable (4% to 0.9% without surcharge) [f]	√	
Bathurst et al. (1995)	2	Segmental	-	1% for H ≤ 8 m 1.5% for H > 8 m	√	
NGG (2005)	3	All walls	-	0.1% to 0.3%	√	
EN 14475 (2006)	4	Vertical and sloped concrete panel, king post system, incremental concrete panel	± 25 mm	-		√
	5	Segmental	± 50 mm			
	6	Welded wire and gabion face	± 100 mm			
BS8006 (1995), Geoguide 6 (2002)	7	All walls	-	0.5%		√
NCMA (2009)	8	Segmental	-	3.5%		R
PWRC (2000)	9	All walls	± 300 mm	3%		√
WSDOT (2005)	10	Welded wire [a]	-	1.3% in 3 m		√
	11	Concrete panel[b], Segmental [c]	-	0.4% in 3 m		
	12	Wrapped face – Permanent [d]	-	1.7% in 3 m		
	13	Wrapped face – Temporary [e]	-	2.5% in 3 m		

[a] The maximum outward bulge of the face between welded wire faced structural earth wall reinforcement layers shall not exceed 50 mm. [b] The maximum allowable offset in any precast concrete facing panel joint shall be 20 mm. [c] The maximum allowable offset in any concrete block joint shall be 9 mm. [d] Maximum outward bulge of the face between backfill reinforcement layers shall not exceed 100 mm. [e] Maximum outward bulge of the face between backfill reinforcement layers shall not exceed 150 mm. [f] Increase displacements by 25% for every additional 25 kPa of surcharge. R = recommended

facing deformations as maximum horizontal value (Δx measured perpendicular to the running length of the wall) over the entire face of a wall or as an equivalent rotation over the height of the wall ($\Delta x/H$) from design batter (verticality). For example, a value of 1% verticality in the table corresponds to an equivalent rotation of 10 mm/m of wall height. Most guidelines have recommendations or specifications for horizontal alignment tolerances at the base or along elevation lines above the base. Deviations from these values were not investigated in this study since these are almost exclusively controlled by construction quality control. The table shows that limits for facing deformations and verticality vary widely between sources and between wall types. For example the WSDOT (2005) specifications for facing tolerances are very detailed and specific with respect to wall type. In contrast, current Japanese specified tolerances (PWRC 2000) are very general and least restrictive. An explanation for the 300 mm limit on outward deformations is that cohesive-frictional fills are used routinely in Japan while they are avoided in North America (at least by government DoTs). The Japanese approach for geosynthetic reinforced soil walls for railway embankments is to build a wrapped-face wall and once deformations have ceased, cast a reinforced concrete face against the wrapped face (Tatsuoka 1993; Kojima et al. 1996). There are no horizontal deformation criteria for these walls. However there is a limit of 100 mm post-construction settlement for these structures (Miyata et al. 2003).

The anticipated deviations from verticality reported by Bathurst et al. (1995) were based on analysis of deformations of two field segmental walls that were monitored during construction. The remaining sources are design guidance documents from the USA (FHWA 2008; AASHTO 2009; NCMA 2009; WSDOT 2005), Scandinavia (NGG 2005), Europe (EN 14475 2006), United Kingdom (BS8006 1995), Hong Kong (Geoguide 6 2002) and Japan (PWRC 2000).

In the USA, the design chart for anticipated deviations from verticality originally reported by Christopher et al. (1989) is likely most familiar to designers and appears in current FHWA (Holtz et al. 2008) and AASHTO (2009) guidelines. This is an empirically-based chart developed from finite element analyses, small-scale tests and limited measurements from 6-m high test walls available at that time. However, as carefully pointed out by the original authors in the original and subsequent republications, this chart should be used with caution. The footnotes to this chart point out that soil type, compaction quality, initial slack in the reinforcement and overall quality of construction can all influence facing deformations. The chart is recommended for use as a first order estimate of lateral displacements during construction of simple MSE structures built on firm foundations.

WALL DATABASE

The majority of case studies in the current investigation were taken from studies described in detail in earlier papers by the writers (Allen et al. 2002, 2006; Miyata and Bathurst 2007a,b; Bathurst et al. 2002, 2008). Additional performance data focused largely on reinforcement loads and strains can be found in the papers by Allen and Bathurst (2002a,b). In the current study, designations for walls such as GW9 and GW17 that appear later are taken from this original database. Some additional case studies with high quality wall deformation data and supporting information have been found in the literature and these case studies have been added to the original database and used in this paper (e.g. GW43 and GW44). A total of 42 wall sections were used to generate the data in this paper (not including the recent RMC test walls described at the end of the paper). Of the 42 wall sections, 11 were segmental (modular) block type, seven were full height concrete panel, four were incremental concrete panel, six were wrapped face, four were gabion basket face and three were constructed using sandbags for the facing. Seven of the walls are identified

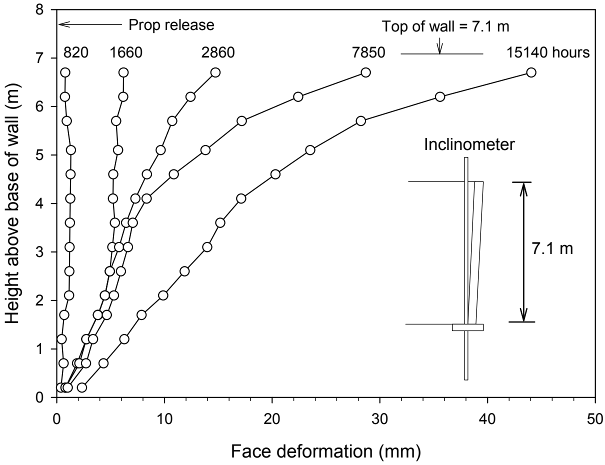

Figure 1. GW17 London wall (propped concrete panel wall) (after Bathurst 1991).

as miscellaneous walls; these were experimental walls with wood or aluminum panels, EPS block facing and in one case a steel reinforced concrete panel cast against a wrapped face. Of the 42 wall sections, 30 were constructed with uniaxial HDPE geogrids, four with biaxial PP geogrids, five with woven PET geotextiles and three with nonwoven geotextiles. Today, uniaxial HDPE geogrids and woven PET geogrids are the most common soil reinforcement materials in North America for geosynthetic reinforced soil walls.

EXAMPLE WALL FACING DEFORMATIONS

Bathurst (1993) reported the instrumentation monitoring results of a 125-m long wall (GW17) in London, Ontario constructed with 150-mm thick reinforced concrete panels 2.4 m wide and varying in height from 1.25 m to 7.1 m. The panels were braced externally (propped) during construction and seated on a concrete strip footing. The walls were constructed with a single type of uniaxial HDPE geogrid and a high quality granular fill. The deformations were recorded by inclinometers mounted against the back of three facing panels of height 7.1 m, 6 m and 5.2 m. Deformations were recorded for almost 2 years after construction. Figure 1 shows wall deformations measured after prop release of the 7.1-m high section. For clarity not all recorded deformation profiles are shown. Immediately after prop release the wall displacements were from 2 to 7 mm. However, time-dependent outward deformations continued thereafter as shown in the figure. Interestingly, the maximum recorded post-construction deformations were 44 mm, 55 mm and 60 mm for the 7.1-m, 6-m and 5.2-m high panels, respectively. The relative deformations are in the reverse order expected based on wall height. One explanation is that the relative "reinforcement density" measured as number of reinforcement layers divided by

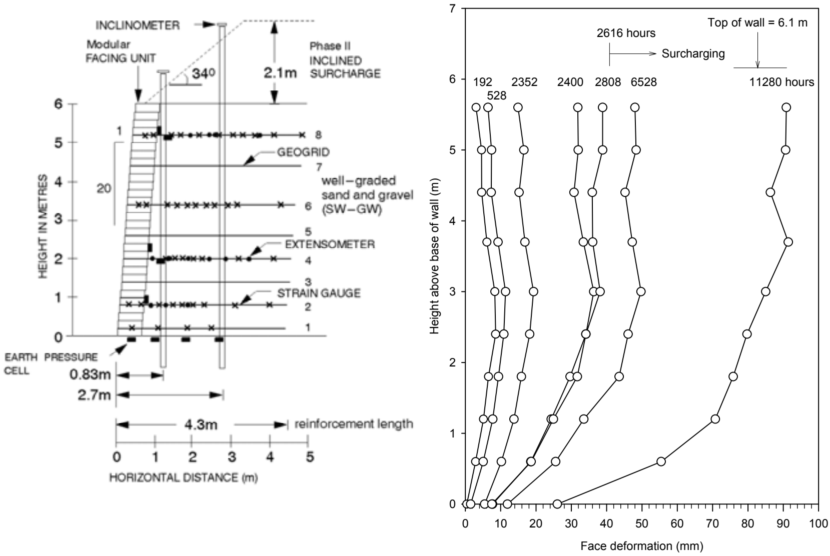

a) cross-section

b) wall deformations with respect to end of construction

Figure 2. GW9 Algonquin wall (segmental wall) (after Bathurst et al. 1993).

height of wall was 0.96, 1.17 and 1.27 for the 5.2 m, 6 m and 7.1 m panels, respectively. Hence, assuming that all panels sections were constructed to the same level of care, the relative deformations suggest that reinforcement density (or global reinforcement stiffness introduced later) may influence wall deformations when all other factors remain the same. The maximum strains in the reinforcement were about 3.5% which puts this wall at the limit of walls estimated to have good performance based on a set of criterion proposed by Allen and Bathurst (2002a). High connection strains were also detected due to the downward movement of the soil behind the vertically rigid panel sections. Nevertheless, the wall remains in service today after 20 years with no evidence of poor performance.

A reinforced segmental retaining wall (GW9) was constructed at a site in Algonquin Illinois as part of a research program by the FHWA (Figure 2a) (Bathurst et al. 1993). The facing units were dry-stacked hollow masonry units with toe-to-heel dimension of 600 mm. The reinforcement was a woven PET geogrid. The wall was purposely under-designed to encourage detectable wall deformations and reinforcement strains. End of construction movements were estimated to be about 60 mm but time-dependent outward movements of about 30 mm continued while the wall remained at the 6.1 m height for about 100 days. Thereafter the wall was surcharged. Wall deformations with respect to end of construction are shown in Figure 2b and were taken from an inclinometer located behind the modular block facing. Total outward movements with respect to beginning of construction were 150 mm at the end of the surcharging. The wall deformation profiles during surcharging show that most of the movement occurred over the bottom half of the wall. Despite being under-designed the maximum reinforcement strains were about 1.2% which is well below limits that would be expected to lead to long-term rupture of the geogrid reinforcement.

SUMMARY OF NORMALIZED FACING DISPLACEMENTS

Deformation data for hard-faced walls are summarized in Figure 3. Normalized displacements $\Delta x/H$ were computed for end of construction (EOC) or during construction and are plotted against L/H and H, where L is the base reinforcement length. Also included in these figures are post-EOC data for the Berkeley (segmental) wall (GW44) and GW9 discussed earlier. The Berkeley wall data includes wall creep data taken while the wall was kept at a constant height of 10.4 m for about 16 days (final height was 14.4 m) (Bathurst et al. 1995). Projected time-dependent wall deformations for this structure are discussed later in the paper. The minimum reinforcement ratio specified in design guidance documents is L/H = 0.6 or 0.7. It can be noted that there are many data points with L/H greater than minimum specified values. Most of these data correspond to wall deformations recorded as the wall was constructed. Hence at low wall height, L/H will be greater than the final design L/H value corresponding to end of construction.

With the exception of GW21 and GW23, all walls deformed less than 1.5% of the wall height at the end of construction (EOC). GW21 was an experimental wall constructed at the PWRI in-door laboratory in Japan. The 4-m high wall was purpose-constructed using 1-m high plywood panels with a single reinforcement layer attached at mid-height of each panel and a relatively large vertical reinforcement spacing S_v = 1 m (Miyata and Bathurst 2007). A biaxial geogrid was selected with low stiffness and strength and was oriented in the weak direction. This combination of materials and geometry makes the wall facing relatively unstable and susceptible to local deviations from vertical alignment. Nevertheless, the data is useful since it demonstrates the conditions necessary to generate large facing deformations (e.g. poor panel-reinforcement geometry, large vertical reinforcement spacing and low stiffness reinforcement). GW23 was another experimental PWRI incremental panel wall (H = 6 m). This wall was constructed with concrete panels and stiffer reinforcement, large reinforcement spacing (S_v = 1 m) and relatively short reinforcement lengths (L/H = 0.58). This wall generated out-of-vertical deformations that were only just in excess of 1.5%. Compared to the shorter GW21 wall, the greater stability of the concrete panels plus stiffer reinforcement is likely the reason that this wall deformed less based on deformations relative to wall height.

Wall GW5 was one of the first production (field) propped concrete panel walls constructed in North America (1984) (Berg et al. 1986). The concrete panels were cast with short loops of uniaxial HDPE geogrid that were then connected to the primary reinforcement layers (same geogrid) using a PVC pipe bodkin. Wall GW6 was another propped concrete panel wall constructed about the same time (1985) (Berg et al. 1986). The reinforcement layers were not attached directly to the facing panels. Geogrid tabs 1.3 m long were cast into the concrete panels and these tabs overlapped with the primary reinforcement layers with a 75-mm thick layer of soil

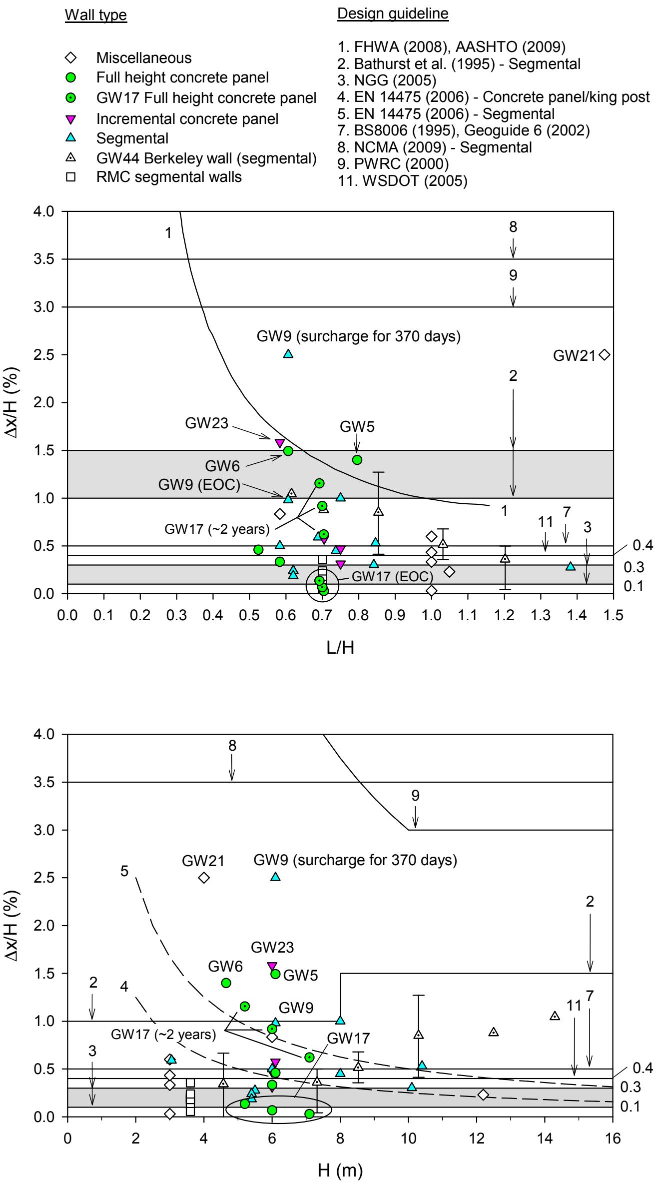

a)

b)

Figure 3. Normalized horizontal deformation for <u>hard-faced walls</u> Δx/H versus: a) reinforcement length ratio (L/H); b) wall height (H).

between the two layers. To the best of the writers' knowledge this technique is no longer used in North America. The lack of a direct connection may explain the relatively large deformations. The normalized wall deformations for GW17 with less deformable connections were smaller than GW6 and GW5 even after almost two years of in-service creep measurements. These observations give support to the hypothesis that increasing slack or play in the connections for reinforced soil walls may create greater wall deformations. However, the vertical compliance of deformable connections can have the advantage of reducing connection strains. The connection strains in GW17 with more rigid connections were in excess of 3% which is considered large compared to strains recorded in the database of monitored walls collected by the writers.

Wall GW9 (segmental) discussed in the previous section, exhibited large relative deformations compared to all other walls but only after a large surcharge was applied for more than a year. Recall that this wall was purposely under-designed.

In general, curve 1 in Figure 3a is judged to serve well as an upper limit on anticipated deformations for hard-faced walls at the end of construction despite its empirical basis. For non-surcharged *segmental* retaining walls, a value of $\Delta x/H = 1\%$ at end of construction is considered a reasonable upper limit for anticipated deviations from verticality for walls of 8-m height or less. Current recommendations by the NCMA (2009) and PWRC (2002) easily captured measured wall deformations for this wall category.

The data reviewed in Figure 3 is useful to compare measured wall deformations with guideline values but difficult to use to isolate trends. Deformation data collected from the Berkeley wall (GW44) (Bathurst et al. 1995) has been plotted in Figure 4 and some insightful trends are apparent. This wall was a temporary segmental retaining wall (final wall height H = 14.4 m) used to support the side of a deep excavation. However, the contractor was unprepared for the magnitude of lateral deformations that occurred for this wall despite the observation that the movements (in hindsight) are close to or below anticipated values using the FHWA/AASHTO design curve that was available at that time. From the contractor's point of view the wall had failed. Multiple deformation readings were taken at six stations along the 73-m length of the wall as the structure was built. Deformations can be seen to increase non-linearly with wall height. Furthermore, the range of deformations can be seen to increase with height of wall. The smallest deformations at any wall height were measured at the stations closest to the end of the wall where the structure was tied into 90 degree corners with conventional soldier pile and lagging board support systems. As noted earlier, the deformations are generally below the FHWA/AASHTO curve for anticipated deformations (Figure 4b). The predicted non-linear trend of decreasing normalized deformation with increasing L/H is seen in the physical survey data. However, most walls are built with L/H in the narrow range of 0.6 to (say) 1.0 where there are only small predicted changes in normalized wall deformations. From a practical point of view, the influence of reinforcement length ratio on $\Delta x/H$ is likely masked by the influence of reinforcement density (or global reinforcement stiffness), compaction method and unavoidable sources of construction variability for these discrete modular block facing systems.

Figure 5 presents deformation data for soft-faced walls. GW10 is a wrapped-

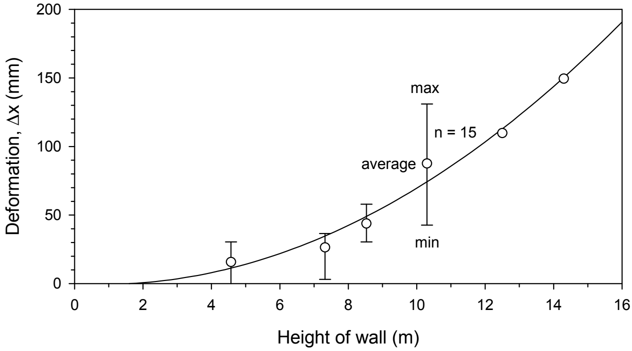

a)

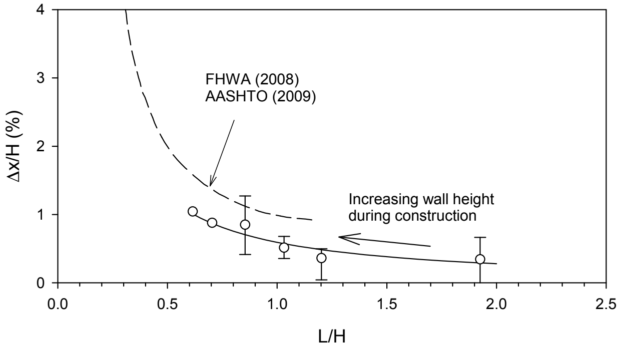

b)

Figure 4. Berkeley wall (GW44) deformations during construction: a) Δx versus wall height (H); b) Δx/H versus reinforcement length ratio (L/H). Note: n is number of measurements across the running length of the wall.

face wall that was constructed as part of the FHWA study at Algonquin Illinois mentioned earlier. The 5.9-m high wall was purposely designed and constructed to produce internal stability failure. The wall was supported externally over the bottom half during construction. The support was released leading to large deformations (150 mm) and reinforcement strains up to 3%. Nevertheless, these deformations were at or within recommendations for temporary walls according to WSDOT (2005) and PWRC (2000), respectively.

Wall GW16 (Figure 6) was a temporary wall 12.6 m high constructed to support preload fills at a large freeway interchange in Seattle, Washington (Allen et al. 1992). This wall was the highest wall of its type in North America at the time of construction and supported an additional 5.3 m of sand surcharge. The structure was instrumented and monitored for one year after construction and has provided valuable performance data for geosynthetic reinforced wall structures. The wall was constructed using a moving formwork approach and reinforcement layer spacing of

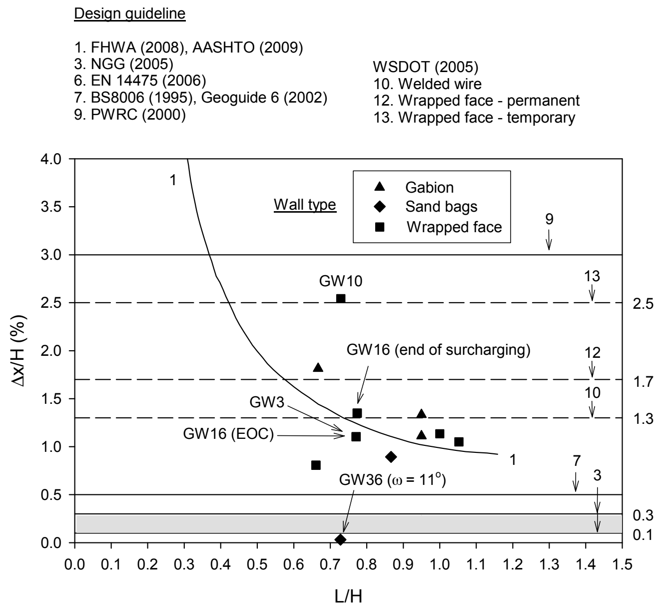

a)

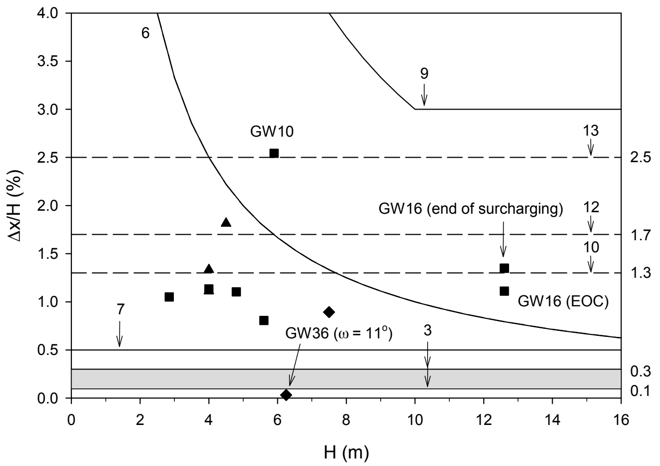

b)

Figure 5. Normalized horizontal deformation for soft-faced walls Δx/H versus: a) reinforcement length ratio (L/H); b) wall height (H).

S_v = 0.4 m. Four different geotextile products were used. The geotextiles were arranged in four different zones roughly matching the demand for increasing

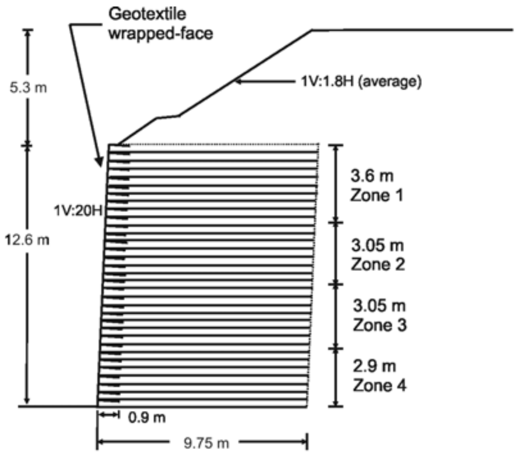

Figure 6. Cross-section of wall GW16 - WSDOT Rainier Ave wrapped-face geotextile wall.

reinforcement load capacity with depth below the wall crest according to conventional tie-back wedge methods of design. The maximum normalized wall deformations after a year of surcharging were about 1.3% which is well within the WSDOT specification of 2.5%.

GW36 was a sandbag wall that was constructed to a facing batter of 11 degrees from the vertical and geotextile reinforcement spacing of $S_v = 0.25$ m. The experience of the writers with the test walls constructed at RMC is that wall deformations and reinforcement loads decrease with increasing wall batter when all other factors remain unchanged. This is not unexpected based on conventional notions of active earth pressure theory.

Taken together the data in Figure 5 leads to the conclusion that current WSDOT (2006) tolerances for soft-faced walls at end of construction are reasonable and the FHWA/AASHTO curve does well in the range of $0.7 \leq L/H \leq 1.0$. The current Scandinavian code (NGG 2005) is satisfied in only one instance despite the observation that all walls in this figure with the exception of GW10 have performed satisfactorily.

LONG-TERM FACING DEFORMATIONS

Most of the data presented in Figures 3 and 5 are for deformations measured at or soon after the end of construction. It is well known that polymeric reinforcement materials will creep under load, particularly geosynthetics manufactured from polyolefins (high density polyethylene and polypropylene). Indeed, current design practice is to use creep-limited tensile strength values in Europe and Japan, and tensile strengths from creep-to-rupture tests in North America to estimate tensile strengths available at design lifetime (e.g. after 75 years for permanent structures).

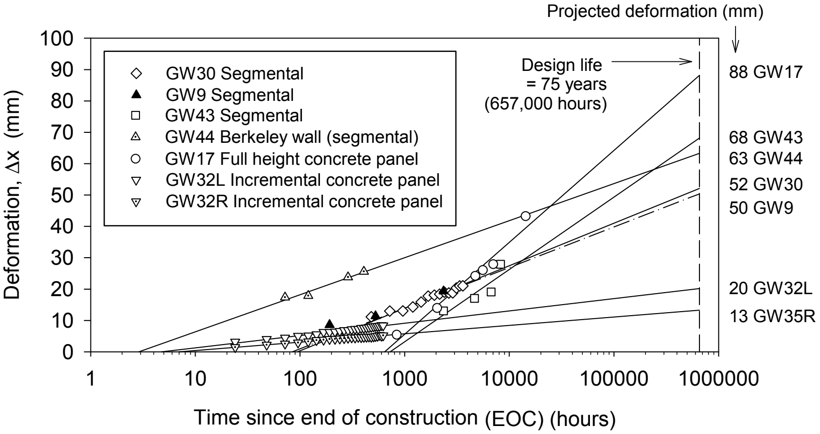

a)

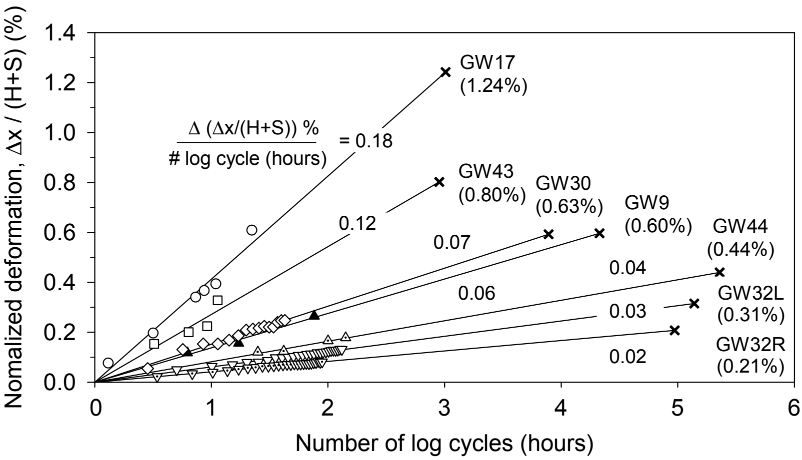

b)

Figure 7. Projected post-EOC deformations at 75-year design life: a) Δx versus time since EOC; b) Δx/(H+S) versus number of log time cycles since start of creep deformation readings.

Since geosynthetic reinforcement materials will creep under load (as will granular soils but less so) if loads are high enough, it may be expected that the wall facing will continue to deform over time as well; if so will these deformations exceed limits discussed in the previous section? A number of case studies collected by the writers have data that can attempt to answer this question.

Figure 7a shows maximum facing deformations recorded against log-time for walls with post-construction wall deformation measurements. The data have been

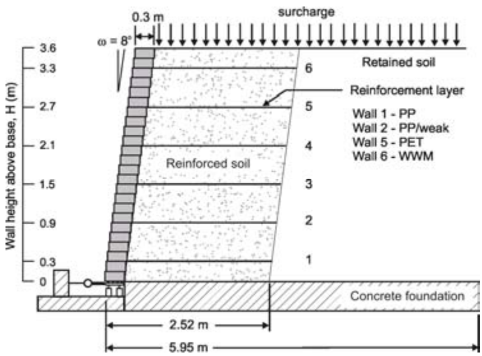

Figure 8. Cross-section of RMC wall with segmental (modular block facing).

extrapolated out to 75 years using the regressed log-linear line fitted to each data set. At low geosynthetic strains typical of the walls in the available database, creep of the reinforcement layers is considered to be very low and may have for practical purposes stopped soon after the wall was completed. Hence, the projections shown are considered to be upper-bound values. The largest projected deformations of 88 mm in the figure correspond to the 7.1-m high (GW17) concrete panel wall discussed earlier. Many of the walls are segmental type and the additional projected deformations for these walls vary widely from 13 mm to 68 mm. In order to isolate wall creep rates, the data in Figure 7a have been re-plotted using the intersection of the regressed line with horizontal axis as datum. The rates of change of normalized deformation (slopes of the lines) are shown in Figure 7b. The wall height is expressed as (H+S) in this plot since in some cases there was a small uniform surcharge (q) applied to the wall backfill surface and it is expressed as an equivalent height $S = q/\gamma$ where γ is soil unit weight. The maximum post-EOC normalized creep rate for GW17 is computed as 0.18% of the wall height per log cycle time in hours. The projected additional deformation as a percent of wall height is 1.24% which is effectively the total 75-year deformation since there were only a few millimeters of initial movement at prop release. The 1.24% value is still below the FHWA/AASHTO curve shown in Figure 3a for this particular panel.

INFLUENCE OF REINFORCEMENT STIFFNESS AND COMPACTION

An experimental program of instrumented full-scale reinforced soil walls has been recently completed at the Royal Military College of Canada (e.g. Bathurst et al. 2000, 2009). A total of 11 walls, 3.6 m in height were constructed in-doors. The control wall in the test series was a segmental retaining wall constructed to a target batter of 8 degrees from vertical. Each subsequent wall was constructed with one change from the control structure (Figure 8). For example, Walls 3 and 7 were nominally the same as Wall 1 but with four and 11 layers of reinforcement, respectively. The other parameters that were changed between walls were: 1) strength and stiffness of the reinforcement layers; 2) facing type (segmental, wrapped face, incremental concrete panel; 3) facing batter (8, 13 and 25 degrees). The strategy was to isolate the contribution of each of these parameters on wall performance.

Following construction, the walls were uniform surcharged in stages to levels well in excess of working stresses in order to encourage large deformations and reinforcement strains. An advantage of this experimental program was that performance trends that are masked between field walls due to a large number of unquantifiable factors were largely avoided by using the same backfill material (high quality medium sand) and construction technique/quality. As noted earlier, the reinforcement density (e.g. number of reinforcement layers per wall) can be expected to influence wall deformations when all other factors remain the same. A similar quantity that better captures the influence of both number of reinforcement layers and reinforcement stiffness is the global reinforcement stiffness value S_{global} computed as (Allen et al. 2003):

$$S_{global} = \frac{1}{H}\sum_{i=1}^{n} J_i$$

Here: J_i = T/ε = the secant tensile stiffness of an individual reinforcement layer, where T = tensile load in units of force per running length of wall and ε = strain; n = number of reinforcement layers, and; H = wall height. Examination of this equation shows that global stiffness increases with stiffness of the reinforcement. The stiffness of the reinforcement can be computed in many ways. However, the writers have demonstrated that the operative stiffness of the reinforcement is best computed using laboratory constant load tests (or temperature-accelerated creep testing) or constant rate-of-creep tests taken out to 1000 hours or more and corresponding to the strain level in the reinforcement layer (Walters et al. 2002).

Figure 9a shows maximum out-of-vertical deformations at end of construction for six of the RMC walls. Segmental retaining walls are constructed in layers. Hence each row of blocks has a different (moving) datum. The deformations shown in this plot are maximum relative deformations as opposed to deviations from the target wall batter commencing at the wall toe (which was essentially fixed). During the experimental program the compaction equipment was changed from a gasoline driven plate tamper to a heavier electrical jumping jack compactor in order to avoid gasoline fumes in the enclosed laboratory space. Both devices were shown to give the same final density but the heavier device generated more lateral force against the wall facing (ratio of dynamic contact pressure estimated to be a factor of 2.6). Hence, the relative deformations of the walls were seen to decrease with increasing reinforcement global stiffness but the heavier compacted walls experienced about 60 to 80% greater deformation at end of construction (Bathurst et al. 2009).

Figure 9b shows maximum recorded post-construction deformations for the same set of walls after uniform surcharging had reached 30 kPa. The same trend of decreasing displacement with increasing global reinforcement stiffness is apparent. However, the influence of compaction intensity is judged to have disappeared. In this experimental program the initial effects of compaction were considered to have been

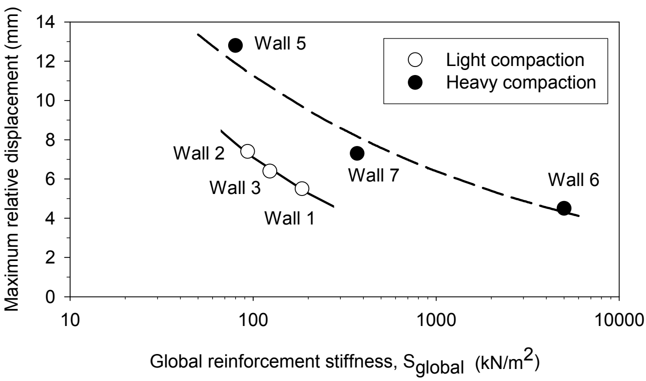

a)

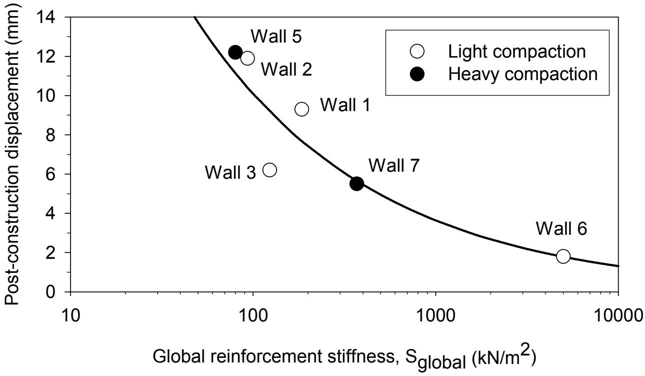

b)

Figure 9. Influence of compaction and reinforcement global stiffness on facing displacements: a) EOC relative displacements versus S_{global}; b) Post-construction maximum facing displacements at 30 kPa surcharge versus S_{global} (after Bathurst et al. 2009).

erased after the addition of 30 kPa surcharge pressure or higher. This threshold surcharge level corresponds to about 1.5 m of equivalent fill height.

CONCLUSIONS

Reinforced soil walls are complex structures and there are at present no reliable analytical models to assist design engineers to predict facing deformations. The paper has focused largely on comparison of measured facing deformations and recommendations for anticipated movements or specified tolerances found in design guidelines. Deformation limits in codes of practice vary widely. However, current FHWA and AASHTO recommendations are found to provide reasonable upper limits in most cases for end-of-construction movements for walls constructed on firm foundations. The database of observed full-scale wall deformations summarized in this paper is of value to engineers as examples to select wall facing pre-batter angles and to provide post-construction clearances for adjacent structures.

REFERENCES

Allen, T.M. and Bathurst, R.J. (2002a). Soil reinforcement loads in geosynthetic walls at working stress conditions. *Geosynthetics International*, 9(5-6): 525-566.

Allen, T.M. and Bathurst, R.J. (2002b). Observed long-term performance of geosynthetic walls, and implications for design. *Geosynthetics International*, 9(5-6): 567-606.

Allen, T.M. and Bathurst, R.J. (2006). Design and performance of an 11-m high block-faced geogrid wall. *Proc. 8th International Conference on Geosynthetics*, Yokohama, Japan, September 2006, pp. 953-956.

Allen, T.M., Bathurst, R.J. and Berg, R.R. (2002). Global level of safety and performance of geosynthetic walls: An historical perspective. *Geosynthetics International*, 9(5-6): 395-450.

Allen, T.M., Bathurst, R.J., Holtz, R.D., Walters, D.L. and Lee, W.F. (2003). A new working stress method for prediction of reinforcement loads in geosynthetic walls. *Canadian Geotechnical Journal*, 40(5): 976-994.

American Association of State Highway and Transportation Officials (AASHTO). (2009). *Interim LRFD Bridge Design Specifications*. 4th ed., Washington, D.C., USA.

Bathurst, R.J. (1991). Case study of a monitored propped panel wall. *Proc. International Symposium on Geosynthetic-Reinforced Soil Retaining Walls*, Denver Colorado, August 1991, pp. 159-166.

Bathurst, R.J., Allen, T.M. and Walters, D.L. (2002). Short-term strain and deformation behavior of geosynthetic walls at working stress conditions. *Geosynthetics International*, 9(5-6): 451-482.

Bathurst, R.J., Miyata, Y., Nernheim, A. and Allen, T.M. (2008). Refinement of K-stiffness method for geosynthetic reinforced soil walls. *Geosynthetics International*, 15(4): 269-295.

Bathurst, R.J., Nernheim, A., Walters, D.L., Allen, T.M., Burgess, P. and Saunders, D. (2009). Influence of reinforcement stiffness and compaction on the performance of four geosynthetic reinforced soil walls. *Geosynthetics International*, 16(1): 43-59.

Bathurst, R.J., Simac, M.R., Christopher, B.R. and Bonczkiewicz, C. (1993). A database of results from a geosynthetic reinforced modular block soil retaining wall. *Proc. Soil Reinforcement: Full Scale Experiments of the 80's*, ISSMFE/ENPC, Paris, France, November 1993, pp. 341-365.

Bathurst, R.J., Simac, M.R. and Sandri, D. (1995). Lessons learned from the construction performance of a 14 m high segmental retaining wall. *Proc. Geosynthetics: Lessons Learned from Failures*. Nashville, Tennessee, February 1995, 15 p.

Berg, R.R., Bonaparte, R., Anderson, R.P. and Chouery, V.E. (1986). Design, construction, and performance of two geogrid reinforced soil retaining walls. *Proc. Third International Conference on Geotextiles*, Vol. 2, Vienna, Austria, April 1986, pp. 401-406.

BS8006 (1995). *Code of Practice for Strengthened/Reinforced Soil and Other Fills.* British Standards Institution, Milton Keynes, U.K.

Christopher, B.R., Gill, S.A., Giroud, J.P., Mitchell, J.K., Schlosser, F. and Dunnicliff, J. (1989). *Reinforced Soil Structures: Vol I, Design and Construction Guidelines; Vol II, Summary of Research and Systems Information*. FHWA RD 89-043, Federal Highway Administration, Washington, D.C.

EN 14475 (2006). Execution of special geotechnical works – Reinforced fill. European Standard.

Geoguide 6 (2002). *Guide to Reinforced Fill Structure and Slope Design*. Geotechnical Engineering Office, Hong Kong, China.

Holtz, R.D., Christopher, B.R. and Berg, R.R. (FHWA) (2008). *Geosynthetic Design and Construction Guidelines.* FHWA NHI-07-092, Federal Highway Administration, Washington, D.C.

Kojima, K., Sakamoto, N., Tateyama, M. and Maruyama, 0. (1996). Geosynthetic-reinforced soil retaining wall using clay on a very soft ground for Hokuriku bullet train yard in Nagano. *Proc. International Symposium on Earth Reinforcement*, Fukuoka, Japan, Vol. 1, pp. 227-232.

Miyata, Y. and Bathurst, R.J. (2007a). Development of K-stiffness Method for geosynthetic reinforced soil walls constructed with c-ϕ soils. *Canadian Geotechnical Journal*, 44(12): 1391-1416.

Miyata, Y. and Bathurst, R.J. (2007b). Evaluation of K-stiffness Method for vertical geosynthetic reinforced granular soil walls in Japan. *Soils and Foundations*, 47(2): 319-335.

Miyata, Y., Fukuda, N., Kojima, K., Konami, T. and Otani, Y. (2003). Design of reinforced soil wall - Overview of design manuals in Japan. *Proc. International Symposium on Earth Reinforcement*, Fukuoka, Japan, Vol. 2, pp. 1107-1114.

NCMA (2009). *Design Manual for Segmental Retaining Walls*, (3rd ed.). National Concrete Masonry Association, (ed. M. Bernardi), Herndon, VA, USA.

Nordic Geosynthetic Group (NGG) (2005). *Nordic Guidelines for Reinforced Soils and Fills*. Nordic Geosynthetic Group, www.sgf.net

PWRC (2000). *Design and Construction Manual of Geosynthetics Reinforced Soil*, (revised version). Public Works Research Center, Tsukuba, Japan, 305 p.

Tatsuoka, F. (1993). Roles of facing rigidity in soil reinforcing, Keynote Lecture. *Proc. Earth Reinforcement Practice*, Fukuoka, Japan, Vol. 2, pp. 831-870.

WSDOT (2006). *Geotechnical Design Manual*, M 46-03, Chapter 15 Abutments, retaining walls, and reinforced slopes. Washington State Department of Transportation, Olympia, Washington, USA.

Walters, D.L., Allen, T.M. and Bathurst, R.J. (2002). Conversion of geosynthetic strain to load using reinforcement stiffness. *Geosynthetics International*, 9(5-6): 483-523.

Recent Research and Future Implications of the Actual Behavior of Geogrids in Reinforced Soil

Florian Bussert[1], Joseph Cavanaugh[2]

[1] Tensar International Ltd., Cunningham Court, Shadsworth Business Park, Blackburn BB12QX, United Kingdom, email: fbussert@tensar.co.uk
[2] Tensar International Corporation, 5883 Glenridge Drive, Suite 200, Atlanta, GA 30328-5363, USA, email: jcavanaugh@tensarcorp.com

Abstract: Over the last 20–30 years the design methods used for geosynthetic reinforced soil structures have become well-proven and accepted. These methods generally are based on a "tied back wedge", or similar, approach to the design. These methods are considered to be very conservative in determining the required reinforcement strength and density for geogrid reinforced structures. This has been validated by monitoring results of instrumented structures which have demonstrated a significant discrepancy between predicted design tensile loads (strains) in geogrids and actual in-situ measured values. Recent research findings indicate that this is the result of the complex mechanisms of geogrid-soil interaction and the influence of planar layers of reinforcement vs. discrete strips which are not considered sufficiently in actual design. Most current design methods in use throughout the world give guidance on the determination of serviceability limit state (SLS) based on geosynthetic material properties. These proved to be impractical to calculate structural deformation at different design stages (e.g. a specific design life).

INTRODUCTION

The basic assumption in reinforced soil design is to divide the reinforced soil into an active and passive zone. The weight of the active zone results in a downward force which has to be "tied back" (in equilibrium) by tensile forces along potential failure surfaces (figure 1). The activated tensile forces are transferred into the passive zone. Each geogrid layer therefore needs sufficient tensile strength to withstand the theoretical tension force and a sufficient length to avoid geogrid pull-out out of the passive zone.

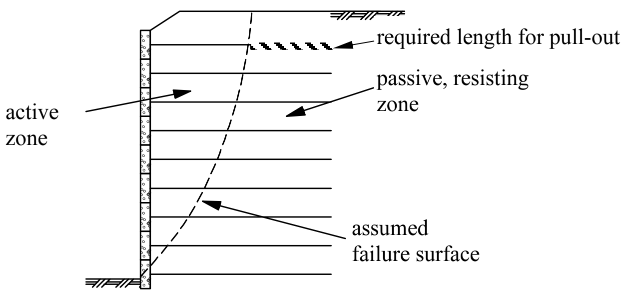

Figure 1. Determination of different areas

These basic design assumptions were derived for "inextensible" steel strip reinforcement and, with the advent of geogrids, were subsequently modified to consider the specific material properties of "extensible" geogrid reinforcements. Emphasis was placed on the available strength; mechanical differences of discrete strip reinforcements to a "full coverage" open mesh grid structure and differences in interaction between soil and reinforcement were neglected in the basic design assumptions. The design assumptions were derived for Ultimate Limit State (ULS) and have been adapted for Serviceability Limit State (SLS) in various design procedures (e.g. AASHTO, 1996, BS8006, 1995, Dt. Inst. f. Bautechnik, 1990, EBGEO, 2010). Variations in the design procedures exist in the use of soil shear strength (peak or constant volume), derivation of long term characteristic geogrid strength as well as the pull-out and shear resistance at the soil-geogrid interface.

Fundamental in all design approaches is the independent assessment of soil shear resistance and geogrid strength. The total resistance is then based on a superposition of both; no influence of soil/geogrid interaction is considered in the design and no consideration for how the presence of the geogrid structure changes and/or improves the soil properties adjacent to the geogrid is considered. Numerous discussions of the importance of specific parameters (e.g. Leshchinsky, 2001; Steiner, Rüegger, 1992) or possible design improvements (e.g. Ehrlich, Mitchell, 1994; Bathurst et al., 2005) were published in the past, indicating that the current design methods are safe and reliable but contain parts for possible improvement. It was reported that the theoretically calculated failure loads can be significantly exceeded in actual field trials (e.g. Bräu, Bauer, 2001; Carruba et al, 1999).

To define SLS the allowable strain increase over the design life is defined by the type of structure. A theoretical geogrid elongation over the design life is calculated by the activated tensile strength in each geogrid layer. The integrated strains over the geogrid length are assumed to be equal to structural deformation. This has, however, proven impractical and the calculated deformations have not been measured.

MEASURED STRUCTURAL BEHAVIOR

Motorway BAB A9, Germany

As part of the widening of the A9 (Berlin – Nuremberg) a 15m high reinforced 60^{o} slope with an 8m high top berm was constructed, Stiegeler, Floss (1999).

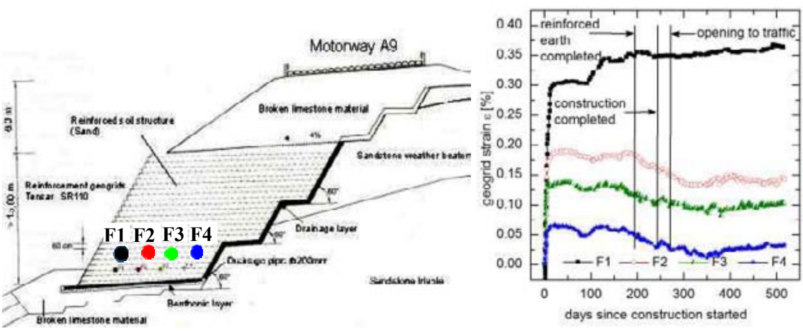

Figure 2. Cross section, measured geogrid strains during first 1.5 years

The reinforced soil structure was constructed using silty/clayey fine and medium sand as the fill material. The shear resistance, depending on the degree of compaction, was established with triaxial tests. Geogrid strains, earth pressures and face deformations were measured from the beginning of the construction period and continued after opening to traffic. A typical cross section and typical geogrid strains are indicated in figure 2. To achieve a redundant measurement system, deformations within the structure were also measured by inclinometers. It can be seen that around 95% of the strains were activated during the placement and compaction of the soil directly above the instrumented geogrid layer. Further construction (i.e., placement and compaction of layers of fill above the instrumented layers) resulted only in small strain increase. The strain development was therefore primarily a function of compaction energy, geogrid geometry, soil inhomogenities as well as the geogrid properties. The measurement results indicated that the strains are non-uniform within a single layer; the largest strains were measured near the front and decreased with distance from the face. After completion, the measured strains showed either a minor strain increase or even a decrease. Only measurement F1 indicated a small increase in strain after the structure was opened for traffic. In the first nine month after opening to traffic (250 days construction start) no creep strains were observed. The reduced initial strains resulted in reduced creep characteristics.

Extensive analysis was carried out to investigate the difference between measured and predicted strain data. Unfavorable slip lines for different methods of calculation were used, for example Bishop (circular slip lines), Janbu (straight slip lines) and rigid block mechanisms (sliding wedge method) which differ from each other regarding the fault mechanism and the safety definitions. While the method of Bishop refers to the safety of shear parameters of the ground according to Fellenius' safety definition, the safety at the rigid block mechanism (as required by the general approval for the use of DIBt refers to the comparison between the retention required for the horizontal balance, as well as for the allowable and available reinforcement element. The latter are restricted by the design value of the tensile strength and pull out resistance of the geogrid (Stiegeler, Floss, 1999). All methods do not vary substantially in the required geogrid tension force but result in significantly larger required geogrid tension forces than measured.

Founders/ Meadows Bridge abutment, Colorado, USA

Structures supporting deformation sensitive structures require reliable information on the expected deformations during serviceability. To limit deformation of reinforced soil walls BS8006 (1995) suggests a reduction in creep strain during the design life. For structures supporting bridge abutments the allowed strain increase during the design life is reduced from 1.0% to 0.5%. This leads to larger initial geogrid tensile strength to be used for sensitive structures. Abu-Hejle et al. (2002) published the results of an 8.9 m high bridge abutment that was built at the intersection of Highway 25 and 86 in Colorado, figure 3. The reinforced fill was constructed using crushed rock with a maximum fill size of 19mm. The shear parameters by a conventional shear box were investigated to 40.1^o and a cohesion of 17kPa. Different parameters were measured in large scale tests. Design shear parameters did not consider cohesion and used a friction angle of 34.0^o.

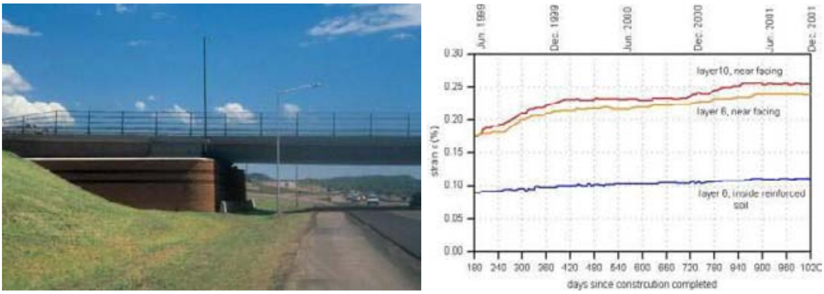

Figure 3. Meadows bridge abutment after opening to traffic, measured strains

The structure was designed according to AASHTO (1997) and used different strength geogrid reinforcements depending on the theoretical strength required from the design method. This resulted in an optimized utilization ratio according to the theoretical assumptions in the design method. During construction the measured geogrid strains increased nearly linear with height. After completion the measured strains were in an order of 0.2% and significantly lower than the theoretical design values. The strain increase due to loading by the superstructure was significantly lower than estimated. The measured strain increase in the first three years decreased from 0.09% to 0.04% and 0.02%. Even with conservative predictions the strain will not reach design values during the design life.

LIMITATIONS OF ACTUAL DESIGN APPROACH

To ensure serviceability excessive deformations must be prevented; measurements taken in the past indicate that the concentration on ULS in the design methods does not allow meaningful predictions of deformation characteristics in SLS. The assumed load transfer mechanism (development of a distinct failure surface between active and passive wedge) cannot be derived from measurements in instrumented structures. This fundamental design assumption in ULS is therefore not reliable to determine deformations in SLS.

Four main problems are obvious in current design methods:

1. Geogrid strains are activated during compaction of overlying soil, and, in contrast to design fundamentals, nearly no subsequent strain increase.
2. Activated geogrid strains after construction are lower than minimum strains to ensure equilibrium between active and passive zone.
3. With no occurrence of a distinct shear plane, stress transfer in the reinforced soil is different from the design assumptions.
4. Current design methods do not give reliable information on expected deformations in SLS.

It is questionable whether the basic design assumptions represent the mechanical interaction of geogrid reinforcement and soil sufficiently. It has been shown by measurements in the past that a superposition of resisting parameters does not represent true material behavior (Ochiai et al., 1996). For these reasons, the main parameters that influence deformation need to be investigated to be able to develop a strain based design approach, particularly for deformation sensitive structures.

BIAXIAL APPARATUS

To identify the stress transfer, deformation characteristics and the interaction of geogrid and soil, it is necessary to construct a test device that is capable of modelling a full representative unit or element out of a structure (figure 4). Also, realistic load transfer characteristics need to be incorporated; in real structures the load is transferred from the soil to the geogrid which is fundamentally different to usual laboratory tests, i.e. pull-out tests. The test apparatus should not introduce a specific failure plane and should allow deformation characteristics to be investigated.

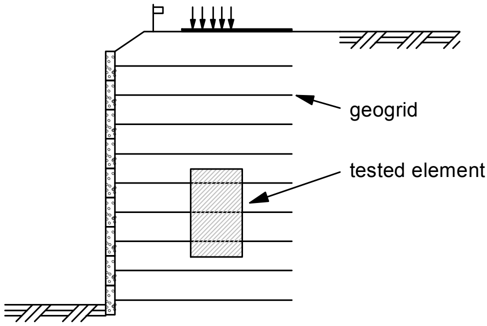

Figure 4. Investigated element out of a structure

The biaxial apparatus used enables plain strain deformations while allowing the development of a three-dimensional stress state. The apparatus had dimensions of 1.0 /1.0 /1.5 (length/ width/ height) and consisted of a base plate and four rigid side elements (1) connected by rigid rods (4) (figure 5). One side element was connected to a movable plate (7) inside the massive frame that can be moved outwards with an accuracy of $^{1}/_{10}$ mm by plug gages (5) while the vertical pressure was kept constant (Bussert, 2006). The stress controlled vertical load was applied via a hydraulic cylinder connected to a loading frame. The applied vertical stress, horizontal stress on the movable plate, stress acting perpendicular to the movement as well as settlement of the loading plate and displacement of the plate were measured throughout the test.

With increasing horizontal deformation under a constant vertical stress, shear stresses are activated within the test material by reducing the stresses on the movable side. From the horizontal stresses measured at the movable side wall, the load transfer and deformation characteristics in the test material were derived. After reaching a residual stress state, higher vertical stresses were applied and further movements activated to derive material properties for multiple surcharges. Additional tests showed that the initial activation of shear stresses in the first loading step does not influence the final stresses achieved under higher pressures.

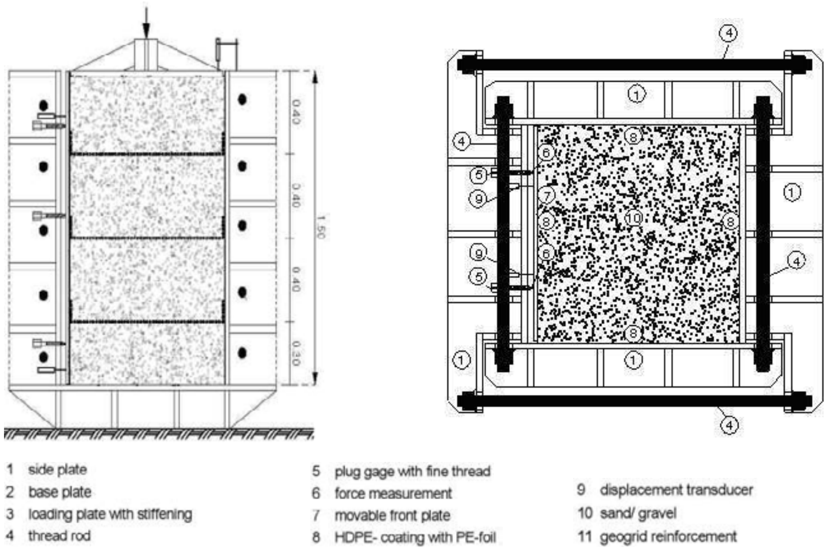

Figure 5. Cross-section and top view on biaxial apparatus

96 tests were carried out in which the soil properties (grain size distribution), geogrid layer spacing, geogrid type and strength as well as manufacturing method were varied. Layer spacing in the tests varied from 0.2m to 1.0m; the geogrids were slightly folded at the side during installation to ensure continuous strain. After the vertical pressure was applied, the movable plate was shifted outwards in increments of 0.1mm under constant vertical stress. Dependent on the geogrid-soil interaction and the load transfer within the material, the pressure on the movable side decreased.

TEST RESULTS AND COMPOSITE MATERIAL PROPERTIES

In analyzing the data, no relationship could be established between geogrid tensile strength or soil shear strength and the measured stress reduction. The soil geogrid interaction leads to significantly enhanced material properties which combine the advantages of geogrid and soil. The result is a composite material which properties have to be described appropriately. As such, new notations and definitions were derived. The chosen descriptions, indicated in figure 6, are based on a comparison of horizontal composite stress to the earth pressure at rest, k_0. After sufficient movement, the horizontal pressure in an unreinforced soil reduces from k_0 to k_a.

- A k_c of ~0.45 represents the ratio k_a/k_0 for soil. This requires continuous horizontal support or tensile reinforcement to avoid further deformation.
- A k_c of 1.0 indicates that all horizontal stresses are absorbed within the composite and no horizontal support or tensile force is required (σ_{Ph}=0).
- Intermediate values require either lower tensile reinforcement or horizontal support than soil (remaining pressure σ_{Ph}=1-k_a/k_0).

Changing soil or geogrid properties (layer spacing, aperture size and shape, stiffness, geometrical properties or bars and ribs) results in a new composite with different material properties.

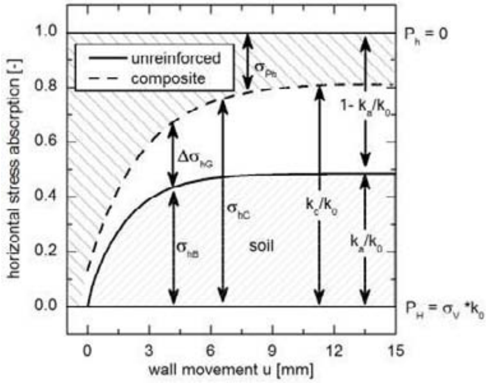

Figure 6. Definitions of stress absorption in the reinforced system

Layer spacing

The influence of layer spacing was investigated for one specific geogrid and soil combination, resulting in a unique composite material. The continuous black line indicates the activated shear stresses of unreinforced sand. With increasing wall movement the horizontal stress reduced from the earth pressure at rest (k_0) to the active earth pressure (k_a), which is described as activation or absorption of stresses within the material. After reaching a residual stress state no additional stresses can be activated within the system.

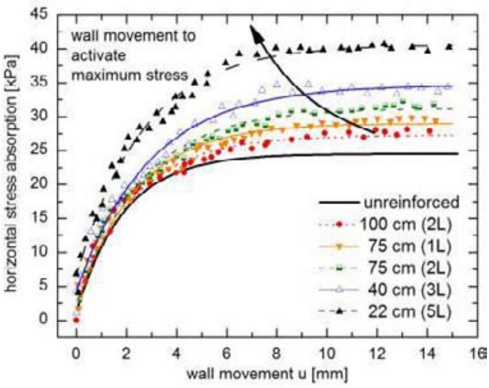

Figure 7. Layer spacing vs. horizontal stress absorption, σ_v=120kPa, sand

The composite in contrast absorbs higher stresses. Dependent on the layer spacing an increase in horizontal stress absorption (figure 7) was measured. Comparable to unreinforced soil no additional stresses can be absorbed by the composite after the residual stress state is reached. With decreasing layer spacing, the deformation required to activate maximum stress absorption reduces, leading to a stiffer material behaviour. The left line in figure 8a indicates k_c as the ratio of k_a/k_0 for the test results from figure 7. A reduction in layer spacing below 0.75m leads to an exponential increase in absorbed stresses. The shape of the composite stress absorption curve changes for every geogrid type. The absorbed stress is, in contrast to design methods, independent of the tensile forces available.

Particle size

Figure 8a indicates the layer spacing versus stress absorption for different composites (similar geogrids, varying soil properties). Changing the soil properties within the composite does not change the shape of the stress absorption curve but results in a horizontal shift. The composites achieved by the change of soil properties have an increased stress resistance when the layer spacing remains unchanged. However, similar stress resistance can be achieved even under changing geogrid layer spacing.

Figure 8b indicates the maximum stress absorption for different composites. Changes in soil properties are expressed by grain size d_{90}. The layer spacing for three different geogrids is kept constant at 0.6m for all tests. It can be seen that for every individual composite a maximum stress absorption can be developed which depends on the grain size distribution and the d_{90} for normal graded soils.

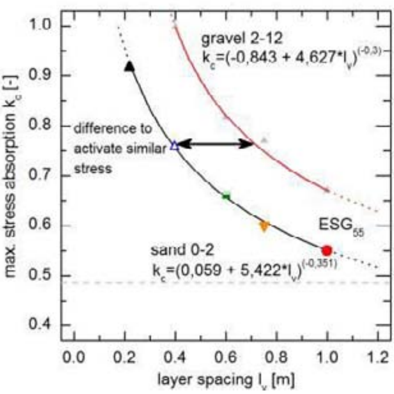

Figure 8a. Stress absorption vs particle size distribution, varying spacing, σ_v=120kPa, sand

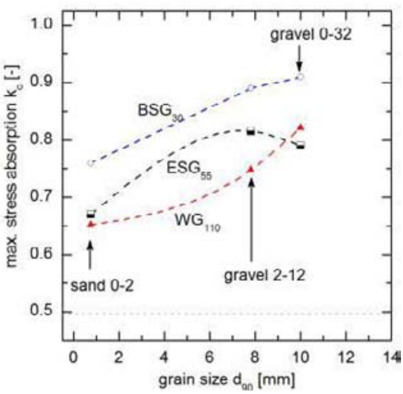

Figure 8b. Stress absorption vs. d_{90}, spacing: 0.6m, σ_v=120kPa, sand

ESG_{55} develops optimum composite material properties at a d_{90} of 8mm, increasing the diameter to 10mm results in decreased stress absorption. In contrast BSG_{30} shows a reduced rate of stress absorption with increasing particle size, indicating composite properties are near maximum. WG_{110} shows a strong increase in material resistance with d_{90}, maximum composite resistance is not developed yet.

Aperture size and shape

Similar effects were observed for other geogrid properties. A geogrid was modified to investigate the influence of aperture size and shape.

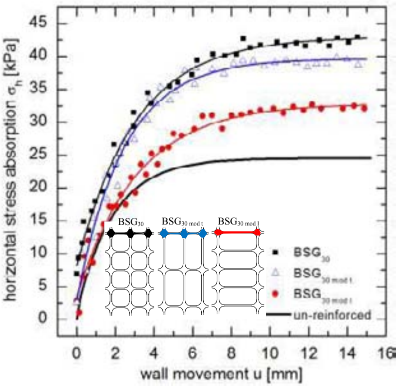

Figure 9a. Stress absorption vs wall movement, mod. geometry; spacing: 0.4m, σ_v=120kPa

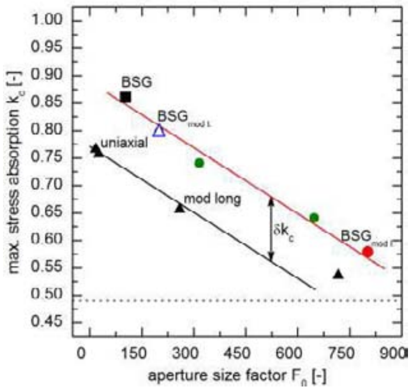

Figure 9b. Stress absorption vs. shape factor F_0, layer spacing: 0.4m, σ_v=120kPa, sand

Figure 9a indicates the absorbed stresses achieved for these geometrical modifications. With increasing aperture size, particle movements can occur within the aperture due to reduced confinement. Apart from aperture size and orientation, aperture geometry, rib height, width and shape as well as aperture orientation influences composite material behavior.

Figure 9b indicates maximum stress absorption for the tests in figure 9a based on the achieved k_c value vs. a shape factor, F_0. Based on the derived shape factor a linear reduction of maximum stress absorption with increasing shape factor can be established (dimensions in mm). In addition, the results of a modified geogrid, manufactured by a different process, are indicated, resulting in a vertical offset δk_c.

$$F_0 = \frac{\dfrac{b^{1,8}}{t_r}}{\left(\dfrac{1000}{a + 2 * \dfrac{r_a}{2}}\right) \bullet \left(\dfrac{1000}{b + 2 * \dfrac{r_b}{2}}\right)}$$

The shape factor depends on the aperture geometry, transverse rib heights and aperture width (Bussert, 2006). With increasing shape factor, F_0, the efficiency to prevent particle movement in the aperture reduces, resulting in smaller stress absorption potential.

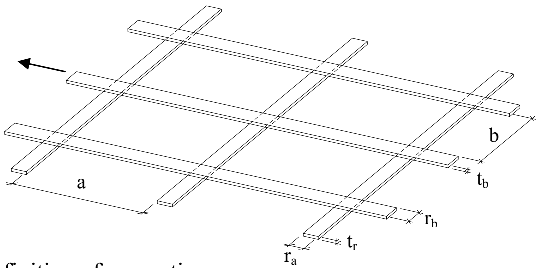

Figure 10. Definition of properties

No relationship between composite stress absorption and grid tensile strength could be derived, figure 11. This indicates the importance of particle confinement within the aperture which is independent of the geogrid tensile strength.

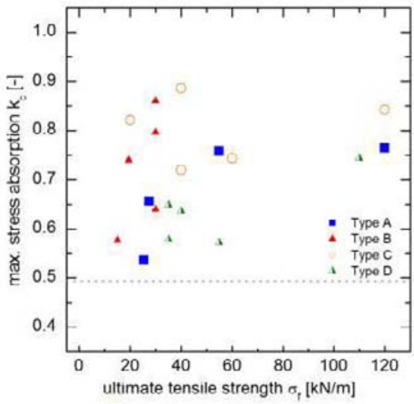

Figure 11. Stress absorption vs. tensile strength, spacing: 0.4m, σ_v=120kPa, sand

Particle movement

To identify the stabilizing mechanism in the composite, particle movements were investigated. The results are mirrored at the centerline between two geogrids (figure 12). After 3mm wall movement the activated movement within the composite is nearly constant with a slight reduction in the geogrid vicinity. After 7mm movement (max. stress absorption) a distinct increase in particle movement in the unconfined area between the geogrid is noted. These unconfined particles exhibit stress-strain characteristics similar to unreinforced soil.

The more efficient the particle confinement is, the larger the stabilized or influenced area around the geogrid. Introducing further wall movement results in additional soil movement between the geogrid layers, no changes were observed within the geogrid layer.

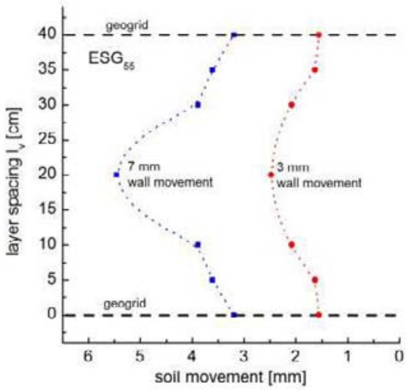

Figure 12. Soil movement in the composite, σ_v = 120kPa, sand

The results are a function of the aperture stability, geometry and geogrid rib shape and the stiffness of the material at low strains. Dependent on the geogrid aperture size, soil particles are forced into the apertures of the geogrid. For the activation of soil shear strength, relative movement between individual particles is required. In dense granular fill, as used in reinforced soil walls, these relative movements take place in shear zones which prevents uniform deformation in the soil continuum. Within these around 10 particles thick shear zones soil particles are able to rotate which results in an increase in mechanical roughness and prevention of further expansion of the zone (Gudehus, 2008).

However, dependent on the aperture size, the development of a shear zone, together with the required volume increase representing dilatancy is restricted within the composite by the geogrids. The geogrid properties therefore restrict particle movement and therefore the development of a continuous shear plane that is required to determine a ULS. Additionally, the restricted particle movement results in a complex interaction between geogrid and soil by increasing the confining stress σ_3 within the soil mass leading to an increase in the shear resistance. The degree of restriction depends on the ability to restrict particle movement within the aperture. A main key in determining the structural capacity and deformation of a geogrid reinforced structure is to assess the geogrid soil interaction as a function of varying geogrid and soil parameters.

NUMERICAL INVESTIGATIONS

Due to the size of geogrid apertures and soil stress variations in full scale or laboratory models, residual stresses within actual geogrid apertures cannot be measured reliably. Therefore, alternative investigations need to be undertaken to identify the stress level, influenced zone height and the involved mechanism as well as the main influencing parameters controlling the behavior. Discontinuum methods such as distinct element method (DEM) or particle codes are well-suited to model distinct particles (e.g. soil particles) and physical penetration through elements (e.g.

geogrids). The interaction between individual elements is a function of the contact law used. The development of contacts between particles, soil-soil and geogrid-soil, and the displacements and forces involved can be studied on a micro-mechanical level.

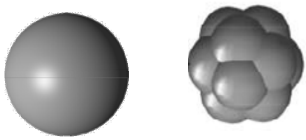

Figure 13. Single and clumped particle

The micro-mechanical particle parameters (shear and normal stiffness, surface friction and density) are calibrated to represent specific macro-mechanical soil properties. The macro-mechanical properties are derived by integration over multiple particles. Tensile properties for the geogrid are modelled by contact bonds between particles. The contact forces between the incompressible particles are derived based on particle overlap and the chosen contact law. The contacts can be specified as elasto-visco-plastic, for single as well as for clumped particles which represent angularity, see figure 13.

The calculation procedure is a repetition of contact force determination for particles in contact with particles or walls, based on the force-displacement law. Newton's Laws of motion is then applied to determine new particle/wall positions resulting in new contact forces. As a result, contacts between particles or particles and walls can develop or break up any time of the calculation.

Soil and geogrid calibration

The particle generation for the geogrid is based on defined geometrical positions while a random generation for the soil ensures different mathematical solutions even under similar boundary conditions. A random particle generation, comparable to a laboratory test, results in varying results under constant boundary conditions. Triaxial (10cm diameter, 20cm height) and shear tests (30x30cm) were modelled to verify that the chosen micro-mechanical properties represent measured laboratory macro mechanical properties. Measured and simulated stress- strain curves are shown in figures 14a and 14b. The dotted lines represent laboratory results; numerical simulations are plotted as solid lines.

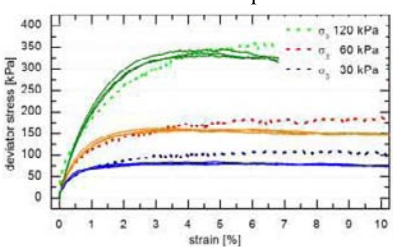

Figure 14a. σ–ε curves for triaxial test

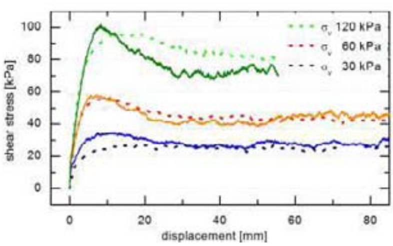

Figure 14b. Shear displacement curves

The geogrid properties were calibrated by tensile tests of single and multiple elements of longitudinal (MD) and transverse (TD) bars according to BS EN ISO 10319 (1996) wide width test for geosynthetics. To determine the influence of aperture stability, tensile tests at 45º orientation were modelled. As the investigation focused on small strains (<1.0%) a linear contact model was used for the parallel-bonds connecting the geogrid particles.

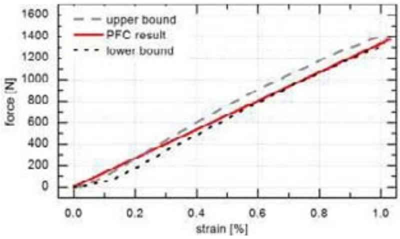

Figure 15a. σ–ε curves in MD

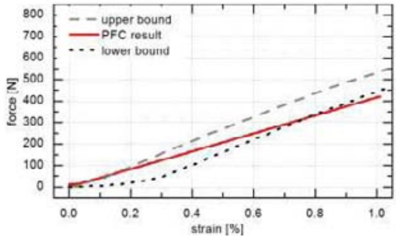

Figure 15b. σ–ε curves at 45º orientation

Figures 15a and 15b show upper and lower boundaries of laboratory quality control tests stress-strain curves as well as the numerical solution for the specific geogrid. The used contact model results in small differences to the laboratory properties which does not affect the geogrid-soil interaction or composite material properties significantly.

Stresses in geogrid apertures

Strains after the soil particle installation process were in the order of 0.05-0.20%. The final geogrid strains are non-uniform over the geogrid length and independent of the initial strain level. Comparable findings have been reported from field (Abu-Hejleh et al, 2002; Meyer et al, 2003) and laboratory measurements (McGown et al, 1990). Average values were calculated as the stresses in the apertures are non-uniform in individual areas.

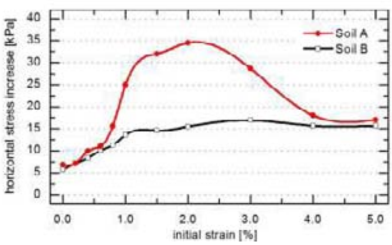

Figure 16a. Activated horizontal stress

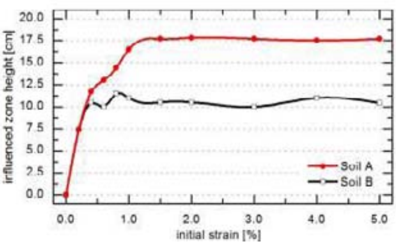

Figure 16b. Activated influenced zone

The results of two different soils stabilized with the same geogrid are shown in Figures 16 indicating the average stress increase measured within the geogrid apertures and the influence zone height around the geogrid. The stress increase is calculated relative to the stresses in an unreinforced system. The maximum horizontal stress depends on the activated geogrid strain and the soil properties. The level of stress increase that can be achieved depends on soil properties, especially angularity, and geogrid properties as rib height, aperture size, stability, and shape as well as junction efficiency. The influenced zone height reaches a maximum after small initial strains and remains constant afterwards. The influenced area is a function of the soil properties. For models reinforced with more than one geogrid layer a larger influenced area has been observed as a result of interaction between geogrid layers and the stabilising effect taking place above and below the geogrid.

Figure 17 indicates typical contact forces between particles after geogrid activation. The thicker the lines, the higher the contact forces between the particles and, integrated over an area, the higher the stresses. The stresses activated depend on particle size distribution and the largest stresses do not occur necessarily directly in one aperture as bridging effects can result in stresses interacting between the adjacent bars. Secondary effects due to bridging over multiple apertures lead to even larger additional horizontal stresses which result in increased resistance against deformation.

It can be seen that the horizontal stresses in the geogrid vicinity exceed the vertical stresses, indicating higher horizontal forces. Additionally, the confining stresses are also generated perpendicular to the direction shown due to three-dimensional load distribution between particles.

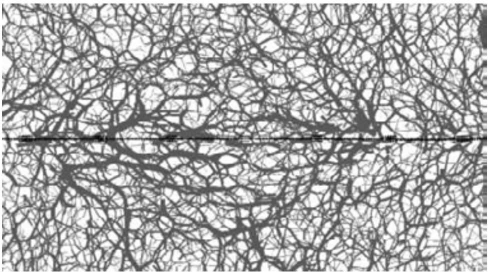

Figure 17. Contact forces after composite material installation

The confining stresses are perpendicular to the principal stress orientation of an unreinforced soil and influence principal stress orientation in the geogrid vicinity. A change in principal stresses changes the composite stress-strain characteristics compared to unreinforced soil and alters the load transfer within the composite.

TRIAL TEST WALL

Based on the investigated composite material properties a 9.6m high trial test wall was constructed (figure 18). To identify the validity and the influence of composite material properties on the deformation characteristics in the field, the wall was divided into six sections with individual composite properties out of which two were constructed with a 70^{o} slope. The design was based on the results of the laboratory tests and did not consider soil shear parameters. Instead the grain size distribution resulting in improved or reduced confinement was used as main design parameter.

The particle size distribution was combined with the geogrid aperture size, layer spacing and geogrid stiffness. Stresses, strains and structural deformations were measured after placement of each soil layer. To minimize facing influence on the measured deformation a flexible geogrid mesh was used backfilled with coarse material to prevent soil erosion.

Figure 18. Structure at full height, 9.6m

Figure 19 shows measurements from two different composite sections. In contrast to current design methods, the tensile geogrid strength in both sections is not sufficient to ensure stability in short or long term. The composite properties were changed by varying particle size distribution and geogrid parameters (aperture shape, manufacturing process and layer spacing).

The particles used for composite_II have a maximum grain size of 12mm; the layer spacing was designed to 0.6m. In agreement with current design methods, measured geogrid strains in composite_II increase nearly linear with the overburden stress. This is present at different height levels (figure 19, left). A constant increase in strain is noted as the grain size was chosen to result in a material with limited confinement potential. However, the strains at the end of construction result in lower activated tensile strength than required to achieve equilibrium between the active and passive wedge. At a height of 8m construction was stopped for 3 month which did not lead to a strain increase. When construction was completed, the strains increased with increasing overburden, but at a lower strain rate.

Soil stresses measured show the effect of reinforcement on the stresses in a similar manner. While the vertical stresses are equal to the overburden stress, the horizontal stresses show a significant reduction below theoretical active earth pressures after small initial strains were activated. The stresses remain constant afterwards at extremely low levels indicating that the stress flow stress transfer characteristics within the composite material are altered.

Composite_IV was constructed with a lower tensile strength than composite_II. The layer spacing was chosen to 0.4m, the maximum grain size to 36mm. According to current design methods, the geogrid used should result in increased creep characteristics and large structural deformations. Composite_IV indicates a substantially different behavior. The measured strains are smaller than in composite_II even though larger strains would be required to activate sufficient tensile strength for equilibrium between active and passive wedge.

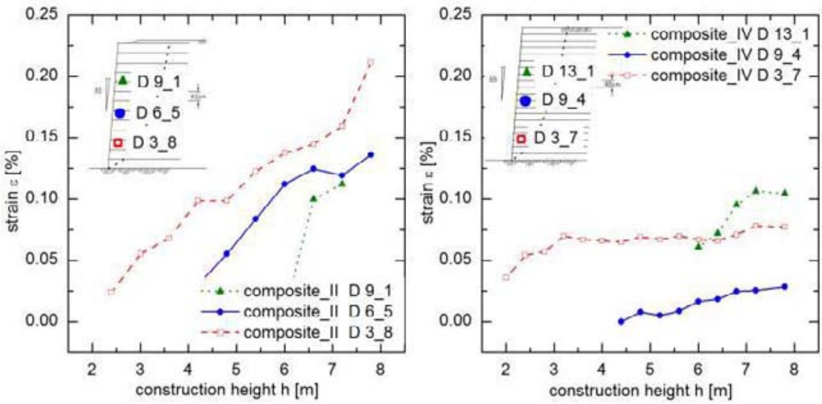

Figure 19. Typical measurement results for two sections of the test wall

Fundamentally different strain properties were measured during the construction of the wall segment. After placement and compaction of a small overburden above the measurement section, no further strain increase is noted in the geogrids. The initially activated strains depend on the compaction energy introduced to compact the overburden material. Little increase is noted after compaction of subsequent soil layers which still has an impact on the soil layers below. The activated strains remain unchanged even though the overburden stress is increased by nearly 150kPa which is in contrast to the fundamental assumptions made in current design methods. This identifies the importance of the improved particle confinement within the geogrid layer which prevents particle movement and increases material resistance.

Figure 20 shows the measured facing deformation for three different composites. Variation were measured based on the facing type: gabion facing, steel mesh at 0.6m spacing (composite_II) and steel mesh at 0.4m spacing (composite_IV). Variations in the upper part of the structure are comparable even though the activated geogrid strains differ quite significantly. One measurement point of the steel mesh with 0.6m spacing was destroyed during construction. A linear extrapolation (dotted line) from higher measurement points, indicating an upper boundary, is indicated in figure 20.

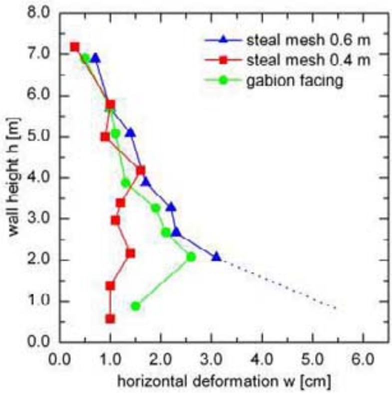

Figure 20. Measured facing deformation

Most important however is that the deformations for composite_IV are smaller than for other composites. In line with the geogrid measurements, the deformations of composite_II increased continuously with increasing structural height. Deformations of composite_IV however stopped after a small overburden. Any further increase did not change the deformations at the lower height of the structure. No increase in deformation was measured within the first five years after construction which proved that the currently used assumptions are very conservative and unpractical.

SUMMARY

Extensive laboratory and field tests, backed by numerical investigations were undertaken to investigate the load transfer characteristics and deformation behavior of the composite material formed by the inclusion of geogrids into soil. The results indicate that the design approaches in common use today do not reflect the stress flow within the composite adequately. From laboratory and numerical studies the main influencing parameters governing the deformation characteristics were derived. The findings were demonstration in a full scale structure in the field. Reliable deformation predictions are required to be able to determine SLS and ULS.

REFERENCES

AASHTO (1996): “Standard Specification for Highway Bridges“, 16th Edition, as amended by 1997 Interim Revisions, American Association of State Highway and Transportation Officials, Washington DC, USA

Abu-Hejleh, N., Zornberg, J.G., Wang, T., Watcharamonthein, J. (2002): “Monitored displacements of unique geosynthetic-reinforced soil bridge abutments”, Geosynthetics International, Vol. 9, No. 1

Bathurst, R.J., Allen, T.M., Walters, D.L. (2005): “Reinforcement loads in geosynthetic walls and the case for a new working stress design method”, Geotextiles and Geomembranes 23, 2005, pp 287 – 322

Bräu, G., Bauer, A. (2001): “Versuche im Boden mit gering dehnbaren Geogittern”, 7. FS-KGEO, 2001, Munich, DGGT
BS 8006 (1995): “Code of practice for strengthened/ reinforced Soils and other Fills”, British Standard
BS EN ISO 10319 (1996): Geotextiles. Wide-width tensile test, British Standard
Bussert, F. (2006): “Verformungsverhalten geokunststoffbewehrter Erdstützkörper – Einflußgrössen zur Ermittlung der Gebrauchstauglichkeit“, Schriftenreihe des Institutes für Geotechnik und Markscheidewesen, Technische Universität Clausthal, Heft 13/2006
Carruba, P., Moraci, N., Montanelli, F. (1999): „ Instrumented soil reinforced retaining wall: Analysis of measurements“, Proc. of the Conf. On Geosynthetiocs 1999, pp. 921 - 934
Gudehus, G. (2008): „Die Rauhe Welt der Bodenmechanik“, Abschiedsvorlesung G. Gudehus 25.07.2008, Karlsruhe, Germany
Ehrlich, M., Mitchell, J.K. (1994): “Working stress design method for reinforced soil walls“, Journal of Geotechnical Engineering, Vol. 120, No.4 April 1994, pp.625 - 645
Jenner, C., Nimmesgern, M. (2001): “Geogrid reinforced railway embankment – excavation after 10 years of loading”, Proc. of the 7th Int. Conf. on Geosynthetics, Nice, France
Leshchinsky, D. (2001): “Design Dilemma: Use peak or residual strength of soil”, Geotextiles and Geomembranes 19, 2001, pp 111 – 125
McGown, A., Yeo, K.C., Yogarajah, I. (1990): “Identification of a dynamic interlock mechanism”, Proc. of the int. Reinforced soil conf., Univ. of Strathclyde, Glasgow
Meyer, N., Bussert, F., Obermeyer, H. (2003): “Measurements of the deformations of a high retaining structure”, GTMM, Karlsruhe, Germany
Ochiai, H., Yasufuku, N., Yamaji, T., Xu, G.-L., Hirai, T. (1996): “Experimental evaluation of reinforcement in geogrid-soil structure“, Proc. of the int. Symp. On Earth Reinforcement, Vol. 1, pp. 249 – 254
Rüegger, R., Steiner, P. (1992): “Steilböschungen aus geotextilbewehrtem Erdmaterial: Vergleich verschiedener Sicherheiten und Bemessungsmodelle”, 2. FS-KGEO 1992, Luzern, Switzerland, DGGT
Stiegeler, R., Floss, R. (1999): “Geogitterbewehrte Steilböschung am Hienberg (BAB A9 Nürnberg – Berlin)“, 6. FS-KGEO, 1999, Munich, DGGT

Applying Lessons Learned in the Past 20 Years of MSE Wall Design & Construction

Daniel L. Harpstead, P.E.[1]
James M. Schmidt, P.E., P.Eng., D.GE.[2]
Barry R. Christopher, P.E.[3]

[1] Kleinfelder, 180 Sheree Blvd., Exton, Pennsylvania 19341; PH (610) 430-7866; FAX (610) 594-2743; email: dharpstead@kleinfelder.com
[2] Kleinfelder, 4815 List Drive, Colorado Springs, Colorado 80919; PH (719) 632-3593; FAX (719) 632-2468; email: jschmidt@kleinfelder.com
[3] Christopher Consultants, 210 Boxelder Lane, Roswell, Georgia 30076; PH (770) 641-8696; FAX (770) 645-1383; email: barryc325@aol.com

ABSTRACT

For the past 20 to 30 years, the design and construction of Mechanically Stabilized Earth (MSE) walls has transformed the available options for development. While this is an excellent technology, our design methods are relatively conservative, and tens of thousands of structures have been safely constructed, it appears that the lessons learned from this past experience are not sufficiently contributing to advancement of the MSE wall technology, specifically related to design. Design issues and resulted in various problems including serviceability issues (i.e., construction and post-construction occurrence of vertical and horizontal movement), construction delays, and other local performance issues including collapse continue to occur at a relatively high rate. One of the causes of these problems is that MSE walls are often not treated with the same diligence and care as other engineered structures (e.g., concrete cantilever retaining walls) in terms of the geotechnical investigation, the design review and/or the quality control/quality assurance requirements. Another principal cause is poor communication between all parties that should be involved in decisions from the concept stage and design phase through construction. Communication issues and other causes, which continue to complicate the success of MSE wall projects, are summarized and discussed in this paper. Recommendations to improve the ways MSE walls are designed and built are provided, which if implemented, will enhance the performance of MSE wall systems.

INTRODUCTION

Do we really have 20 years of experience with the design and construction of MSE walls or can it be argued that we have one year of experience 20 times? It appears that geotechnical, civil, and structural engineers, MSE wall designer, and MSE wall constructor routinely accept the absence of communication between themselves during MSE wall design and construction, which can, and often times does, contribute to significant problems in the execution of MSE wall design, construction, and ultimately performance. From their 20 to 30 years of experience with MSE wall design and construction, the authors can cite numerous cases where communications failed and the significant consequences thereof. If we improve key communication issues outlined within this paper, we will have a better record of MSE wall design and performance in the future.

The lessons learned based on the combined experience of the authors is discussed in this paper and include:

- lessons learned on wall designs in general,
- wall design engineering professionals,
- critical wall components (drainage systems and reinforced soil fill materials), and
- wall construction and construction monitoring.

The third author published a paper on these same subjects 10 years ago (Christopher and Stulgis, 1999). In preparation of this paper, the first two authors collaborated with the third author to provide new insight as to how far we have come in the last decade. Based on this combined experience, it appears that there remain a number of challenges for improvements in wall design and construction to achieve success in tomorrow's MSE wall building environment.

THE WALL DESIGN LESSON

Soong and Koerner (1999) reported MSE wall failures at a rate of approximately 1 in 1,000 (26 failures reported for approximately 35,000 walls). Many failures (including unacceptable wall movement and local wall problems) go unreported throughout the United States and world, especially where litigation is involved. For example, the authors are aware of at least 3 times the number of reported failures and of course we are not aware of all projects where significant problems have occurred. Whitman (1984) states that appropriate (conservative) structural designs should have a failure rate in the range of 1 in 1,000 to 1 in 10,000. These failure rates imply that MSE wall construction is currently not on par with other civil engineering structures.

The authors suggest modifications to the current design practices so that MSE walls are recognized as engineering structures. Because MSE wall design contains elements of both structural engineering and geotechnical engineering including soil-structure interaction, qualified geotechnical and structural engineers should be involved in the design, either directly or, as a minimum, in a review capacity.

THE WALL DESIGN ENGINEERING PROFESSIONALS LESSON

In current MSE wall design practice there is often a disconnect between the project design professionals including the geotechnical, civil, and structural engineers, and wall engineer. Often during the project design phase, the geotechnical engineer is not aware that MSE walls are planned for the project and hence does not provide design recommendations (such as soil strength parameters) or construction recommendations (such as soil strength verification testing requirements and frequencies) specific to MSE wall design. Further, the civil engineer will typically not prepare 100 percent plans and specifications, but rather the civil design includes a 30 percent MSE wall design, presenting line and grade and a typical MSE wall cross section in the design package. The actual wall designer is subsequently contracted to the general contractor and/or the wall system supplier. This approach completely removes the geotechnical, civil, and structural engineers from the design process. Without first hand knowledge of the project, the wall designer may not fully understand the issues impacting the MSE wall design and performance (such as drainage, material availability, and constructability). Unless this contracting method is performed under a design build contract with a performance specification, one could question the professional ethics of this practice (i.e., bidding the engineering as part of the construction contract and the wall design engineer often being employed by the wall system provider).

The authors believe that the geotechnical engineer should assume responsibility for designing MSE walls and preparing the plans and specifications as MSE wall design is based on soil-structure interaction. Given their unique understanding of soil-structure interaction, geotechnical engineers are highly qualified to perform MSE wall designs and must take an active role in the design. Facing details including connections, structural steel in the concrete to handle bending stresses, and structural frames often used for obstruction avoidance should be designed and reviewed by a structural engineer. Geotechnical engineers must collaborate with the project civil and structural engineers in optimizing the design. Otherwise, key foundation, drainage, and soil-structure interaction issues will often be overlooked and not be addressed.

CRITICAL WALL COMPONENTS LESSONS

This lesson relates to the drainage behind the wall facing and the soil used within the reinforced zone. An evaluation of MSE wall failures indicate that either the designer or the contractor often does not understand the importance between each element of the MSE wall and the requirement that each element perform as expected. These issues are further discussed below:

Drainage Systems

"Drainage, drainage, drainage!" After numerous wall failures because of poor drainage behind the MSE wall, we should recognize that the "customary methods of designing retaining walls disregard the effect of rainstorms on earth pressures…A rainstorm may increase the earth pressure by as much as 33%. Hence, it is not surprising that the failure of retaining walls usually occurs during heavy rainstorms."

This is a quote from Karl Terzaghi in 1943 in discussing the fallacy of assuming a vertical drain at the back of the wall face will resolve seepage problems, a practice that is often used today for MSE walls. Terzaghi goes on to show that placing a vertical drain at the back of a wall face actually creates a higher stress condition during rain events, and that to eliminate this problem, an inclined drain (or base drain and backdrain) must be included in the wall design. Unless free draining backfill (i.e., minimal to no fines) is used, then drainage must be included or water pressure accounted for in both internal and external stability. It should always be assumed that water would enter the reinforced soil structure and appropriate drainage features included (e.g., base drains and back drains) unless the design engineers can prove that drainage is not required. (This is also the current recommendation of the FHWA (Berg et al., 2009))

In addition to ground water, surface water must also be controlled both during and after construction. The ground surface above and behind the MSE wall should be sloped to direct surface water runoff away from the MSE wall during construction, and if possible after construction. A number wall failures have occurred during construction from surface water runoff that has been directed to the wall face, where hydrostatic pressures have built up and exceed the wall design capacity or reinforced fill is eroded through, beneath and around the wall face. Surface water infiltration during and after construction creates seepage forces on the wall unless controlled. Pavement above a wall may actually contribute to this problem, if not properly drained and sloped away from the structure; pavement drainage is often not included to remove water from base course layers and these layers can pond water above the wall. Methods for control of surface water are covered in the Federal Highway Administration MSE wall design manual NHI-09-083 and GEC 011 (Berg et al., 2009).

Reinforced Fill

As the quantity of quality fill becomes more scarce and expensive, the use of marginal fill in the reinforced zone has become more and more prevalent. The risks for using marginal fill increase significantly as the percent fines increase. For example, 20 out of 26 case histories on geosynthetic MSE wall failures identified by Soong and Koener (1999) were constructed with low permeable silts and clays.

Designers and contractors must recognize the following when using marginal soils:

- The friction angle of the soil is reduced, correspondingly the horizontal stress is increased and the soil/reinforcement interaction characteristics are decreased.
- Construction deformations will increase and soil creep may be an issue.

- Drainage and water problems are increased, both during and after construction. Additional layers of drainage material may be required within the reinforced zone.
- Settlement of the reinforced fill will induce down drag stress at the reinforcement/face connection, and differential settlement between the reinforced fill and retained fill is likely; thus, a tension crack should be anticipated at the back of the reinforced section.
- Soil strength values, interface friction values, and soil-reinforcement interaction values cannot be assumed and tests must be performed at both drained and undrained conditions. Additional testing must be performed during construction to verify the conditions used for design.
- The soil will become wet, especially if there is a poorly drained paved parking facility above the wall (i.e., pavements leak, which is why highway engineers use edge drains). Water dissipation takes a considerable amount of time, thus there is a potential for softening of the reinforced zone soil leading to a reduced in soil strength.
- Consideration must be given to stresses induced by frost heave and shrinkage and swelling of marginal soils.

These issues lead to increased uncertainty, which means that internal and external factors of safety should be increased when using marginal soils.

MSE WALL CONSTRUCTION AND CONSTRUCTION MONITORING LESSONS

The major lesson learned with regard to construction is the need for both contractor's quality control (QC) and owner's quality assurance (QA) in the field. Often the design and construction team confuse the roles and in many projects the authors find one or both activities being excluded from the construction process. The disconnect between the project design professionals and the wall engineer can also lead to the misunderstanding of QA and QC of key components of the MSE wall design, specifically soil strength parameters.

As with design, many contractors believe MSE wall construction is simple and rapid so no special skills are necessary. Consequently, contractors and owners don't require full-time QC and QA, respectively. When QC and QA firms are present, their representatives often have no appreciation for the detail required to correctly construct and monitor MSE wall construction. Most field inspectors (if they are present at all) think that checking the backfill compaction is all that is required.

As reported by Schmidt and Harpstead (2009) QA comprises a broad general view of the entire MSE wall design and construction process and verification that QC is performed in accordance with the plans and specifications. QA should be performed by an engineering firm under contract with the project owner. The QA consultant should have experience with construction of MSE walls including forensic evaluation of MSE walls that have not performed as designed.

Historically, project specifications have excluded the requirement for verification of soil strength parameters. The geotechnical engineer is typically the best qualified and most knowledgeable entity to perform the QA activities. The geotechnical engineers also understand the importance of verifying the soil strength parameters that they provided for the design. This further supports the authors' believe that the geotechnical should prepare MSE wall designs. The QA consultant should, at a minimum, conduct the following reviews, checks, and assessments:

- Review the geotechnical report
- Review the civil engineering plans showing the locations of the proposed MSE walls
- Evaluate site design issues such as fencing, guide rails, storm water drainage, water distribution pipelines, irrigation, and proposed landscaping as these items may impact the proposed MSE design
- Review the MSE design engineer's plans and specifications
- Review the MSE wall design/shop drawings
- Check the MSE wall background conditions and design calculations
- Review the proposed construction QC plans
- Assess existing conditions affecting stability factors of safety (global stability, bearing capacity, sliding, and eccentric loading).

QC is performed at the time of construction and includes the collection of samples for the MSE wall components, performance of field measurements and testing, and developing a record of activities related to the MSE wall construction. In many cases, the QC agency is under contract to the general contractor; however, some owners prefer to have the QC agency independent of the general contractor and retain the project QC consultant directly. In either case, the contractor should have a quality control plan with a list of items that construction personnel should document and report to the QC and QA personnel and owners' engineering representatives.

The QC consultant should perform the minimum following functions and report the results in the DFR:

- Note foundation improvement conducted
- Collect soil samples, proof roll and/or perform tests (e.g., DCP) to verify foundation soil strength parameters contained in the MSE wall design
- Measure the reinforcement length and spacing
- Verify and note the reinforcement is placed in the proper direction
- Verify the supplier and model number of the reinforcement supplied

- Sample and measure the retained soil parameters and compare those parameters to the MSE wall design assumptions
- Routinely collect samples of the reinforced zone soils for laboratory measurement of grain size distribution, moisture-density relationship, and strength parameters
- Compare reinforced zone materials being used for construction to the materials specified in the MSE wall design assumptions (strength and unit weight)
- Collect samples of and certification for other materials such as bearing/compression pads, geotextile filters, etc. and confirm that they meet specification requirements
- Measure the location (thickness and height) of wall drainage materials
- Document that the leveling pad and subsequent facing lifts are level
- Measure facing units with respect to tolerance requirements
- Measure the lift thickness in the reinforced zone
- Measure soil densities and moisture contents and record the horizontal and vertical location of the tests performed in the reinforced zone
- Measure wall face batter and alignment during construction to confirm that it meets specification requirements
- Record progress using photographs

A more detailed example list of QC requirements is contained in the FHWA MSE wall design manual (Berg et al., 2009).

CONCLUSION

The authors experience over the past 20 to 30 years indicate that the lessons learned that past experience is not sufficiently contributing to advancement of MSE wall design. While this is an excellent technology that has successfully been used over centuries, quite often, the design approach utilized today over-simplifies the critical details and is inappropriate. Qualified geotechnical and structural engineers should be involved in the design and review capacity. MSE wall designers must be in direct communication with the project civil engineer in order to identify features that may negatively impact the wall design and work together to avoid these issues, if possible. The consequences of such features and their potential impact on long-term maintenance should be explained to the Owner. MSE wall plans and specifications must be completed with the project civil and structural drawings and specifications.

MSE wall design is based on soil-structure interaction, which geotechnical engineers are familiar. The authors believe that the geotechnical engineer should assume responsibility for designing MSE walls and preparing the plans and specifications, given their unique understanding of soil-structure interaction. Geotechnical engineers must collaborate with the project civil and structural engineers to optimize the design and verify that specific concerns are addressed. Otherwise, key foundation, drainage, and soil-structure interaction will be overlooked.

The major lesson learned with regard to construction is the need for both QC and QA. Often the design and construction team confuse the roles and in many projects the authors find one or both activities being excluded from the construction process. The disconnect between the project design professionals and the wall engineer can also lead to the misunderstanding of QA and QC of key components of the MSE wall design, specifically soil strength parameters. Proper QA and QC are essential for the successful performance of MSE walls.

REFERENCES

Berg, R.R., Christopher, B.R., and Samtani, N.C. (2009) Design of Mechanically Stabilized Earth Walls and Reinforced Soil Slopes, U.S. Department of Transportation, Federal Highway Administration, Washington DC, FHWA NHI-09-083 and FHWA GEC 011, 668 p.

Christopher, B.R. (1993), Deformation Response and Wall Stiffness in Relation to Reinforced Soil Wall Design, Ph.D. dissertation, Purdue University, 352 p.

Christopher, B.R., Zornberg, J.G. and Mitchell, J.K. (1998), "Design Guidance for Reinforced Soil Structures with Marginal Soil Backfills," Proceedings of the Sixth International Conference on Geosynthetics, Atlanta, GA, pp. 797-804.

Christopher, B.R. and Stulgis, R.P., (1999) "The Future of Geosynthetics: Mechanically Stabilized Earth (MSE) Walls," Geosynthetics in the Future: Year 2000 and Beyond, GRI Conference Series GRI-13, Koerner, R.M., Koerner,G.R., Hsuan, Y. and MarilynV. Ashley, Editors, Geosynthetic Institute, Folsom, PA, pp.172 - 182

Harpstead, D.L. and Schmidt, J.M (in Print), "Construction QA and QC for Mechanically Stabilized Earth (MSE) Retaining Walls", to be presented at GeoFlorida Conference.

Schmidt, J.M and Harpstead, D.L. (2009), "Redefinition of the Design and Construction of Mechanically Stabilized Earth (MSE) Retaining Walls for Highway Projects", 60th Geologic Highway Symposium, Buffalo, New York.

Soong, T. and Koerner, R.M. (1999), Geosynthetic Reinforced and Geocomposite Drained Retaining Walls Utilizing Low Permeability Backfill Soils, GRI Report #24, Geosynthetic Research Institute, Folsom, PA, 140 p.

Whitman, R.V. (1984), "Evaluating Calculated Risk in Geotechnical Engineering," ASCE Journal of the Geotechnical Engineering Division, Vol. 110, February.

Sustainability Measures for MSE Walls and Baseline Environmental Impact Evaluations

S. D. Rafalko[1], J. E. Sankey[2], and N. Freitag[3]

[1]The Reinforced Earth Company, 8614 Westwood Center Dr. Suite 1100, Vienna, VA 22182; PH (703)821-1175 ext. 242; FAX *(703)734-5794; email:* srafalko@reinforcedearth.com

[2]The Reinforced Earth Company, 8614 Westwood Center Dr. Suite 1100, Vienna, VA 22182; PH (703)821-1175 ext. 229; FAX *(703)734-5794; email:* jsankey@reinforcedearth.com

[3]SoilTech R&D division, Terre Armée Internationale, 1 bis, rue du Petit Clamart, Bât. D, 78148 Vélizy-Villacoublay Cedex – France; PH +33 (0)1 46 01 84 84; FAX +33 (0)1 46 01 86 87*; email:* nicolas.freitag@terre-armee.com

ABSTRACT

Over the past few decades, greater emphasis has been placed on environmentally responsible ("green") engineering and development of more sustainable products, structures and systems. Although Mechanically Stabilized Earth (MSE) walls are inherently more sustainable than many retaining wall systems, little has been done to evaluate or further increase the sustainability of the basic MSE wall concept. This paper describes a life cycle assessment (LCA) study that was performed to establish a baseline for the environmental impact of MSE walls from the "cradle" to dismantling and recycling the wall. This study consisted of identifying the goal and scope, performing an inventory analysis, assessing the impact and interpreting the results. The assessed impact categories are energy consumption, abiotic depletion, climate change, photo-oxidant formation and acidification. For comparison purposes, the environmental impact of a gravity wall is also evaluated using similar methods developed from the LCA study.

INTRODUCTION

Mechanically Stabilized Earth (MSE) walls are retaining walls made of earth fill stabilized with layers of soil reinforcements. This composite structure retains the earth pressure with facing elements that are connected to the soil reinforcements. Figure 1(a) shows a cross section of a typical MSE wall system compared to that of a typical concrete gravity wall as shown in Figure 1(b). Common MSE wall applications include retaining walls by themselves and bridge abutments.

As there becomes a greater awareness of the impact to development and increasing requirements for more environmentally responsible engineering, the reduction of environmental impact by products, structures and systems has become more important to society. Before environmental impacts can be reduced, however, an assessment method must be developed so that the most significant contributing factors can be identified. The ISO 14000 environmental management standards have established an outline of a life cycle assessment (LCA) method to evaluate the environmental impact of products, structures and systems. Guinée et. al (2001) have also provided a detailed step-by-step procedure for performing a LCA study in the *Life Cycle Assessment: An operational guide to the ISO standard*.

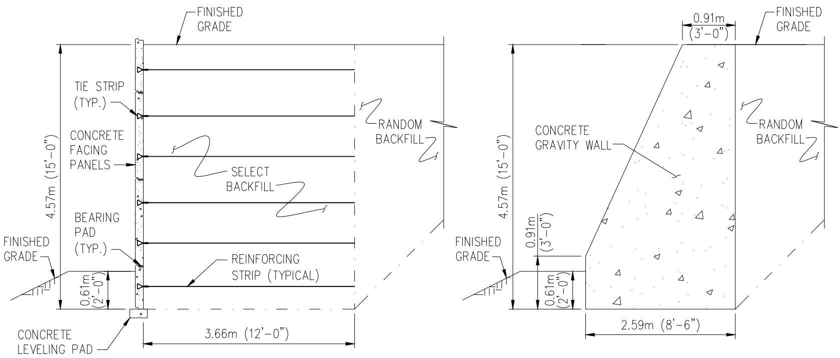

(a) MSE wall **(b) Gravity Wall**

Figure 1. Retaining wall cross sections.

The purpose of this paper is to outline the methodology of how to perform a LCA study that evaluates the environmental impact of MSE walls. A comparison of the environmental impact of a MSE wall and a gravity wall is also presented for demonstration purposes.

LIFE CYCLE ASSESSMENT

The LCA study is performed by first defining the goal and scope, then performing an inventory analysis and finally assessing the environmental impact. In addition, interpreting the results should be performed at discrete steps throughout the entire LCA study.

Goal and Scope

The first step of a LCA study is to define the goal and scope of the assessment. The most common goal of a LCA study is to determine the baseline of the environmental impact of a product, structure or system, such as a MSE wall. In addition to establishing a baseline, the goal of this study is to also compare the baseline environmental impact of a MSE wall to other wall systems, such as a gravity wall. While not discussed herein, an additional goal of the study is to compare the impact of alternative wall components for product development.

Depending on the goal of the evaluation, the scope of the assessment may vary greatly. For the study presented in this paper, a MSE wall supplier is considered under a scope that includes the complete environmental impact of a MSE wall beginning at the “cradle" (extraction or mining of material) to the dismantling and recycling of the wall. Note that if the study is performed for a contractor building the wall, then the scope may only include the environmental impact beginning at the “cradle” to material delivery at the job site such that the contractor may compare alternative wall systems. Therefore, identification of the user needs to be established at the outset of a LCA study.

The materials that are included in the evaluation may vary as well. At the beginning of a project, assessment of all elements may be necessary. On the other hand, the MSE wall supplier may be requested by the contractor to provide an assessment of the impacts only due to the supplier’s scope of work, which generally excludes backfill materials.

As another point of consideration in defining the goal and scope of the study, a functional unit must be defined. The appropriate unit is chosen based on the function of the final product and the goal of the study. The most obvious functional units for the evaluation of retaining wall systems are “per wall” or “per surface area” of wall. For this study, the functional unit of “per wall” is found to be the most appropriate, although the functional unit of “per surface area” of wall may be appropriate for certain applications where the wall size may change. The functional unit can also be defined on a time basis, for example “per year”. In that sense, if the service life of the wall is expected to be 75 years per AASHTO specifications, then the full impact (including manufacturing, transportation, construction and dismantling) may be divided by 75 to give a “per year” value. This approach was not taken in this study, but is worth mentioning as a way to promote more “durable solutions”.

Inventory analysis

After defining the goal and scope, an inventory analysis is performed. An inventory analysis is an itemized list of all the inputs and outputs of the defined system. Inputs consist of materials and energy going into the system and outputs consist of air emissions, water emissions, solid waste and radiation leaving the system. These inputs and outputs can be found in databases that are available to the public for various extraction processes, manufacturing processes and modes of transportation. For the evaluation of MSE walls in this paper, the inventory analysis is broken down into four main stages: the manufacturing of MSE wall components, transportation of MSE wall components, construction of the MSE wall and dismantling of the MSE wall. Before databases and datasets can be used in the LCA study, a check must be performed to determine their appropriateness in addition to their quality and accuracy. Since life cycle assessments are still relatively new, especially in the United States, it is anticipated that databases and datasets will become increasingly more detailed and accurate as additional information is made available. As a result, a LCA study should be considered a live document, where the inventory may be continuously updated to reflect the most current information.

Manufacturing of MSE Wall Components

The manufacturing of MSE wall components for this study is considered from the “cradle” to the manufacturing of the wall components. Even though this stage focuses on the manufacture of materials, it also includes the extraction and/or mining of the base materials, as well as representative transportation between locations of extraction and/or mining of materials to the manufacturing plants. In general, since the extraction and/or mining of material to the manufacture of a product is not under the control or direct supervision of the MSE wall supplier, the data used in this stage is based on general data available to the public (CPM 2008, US NREL 2008, PlasticsEurope: Association of Plastics Manufacturers 2005, Ecoinvent Centre 2009 and US EPA 1994). In certain cases, where the MSE wall supplier takes part in the manufacture of the product, the specific data is used instead of the general data, e.g. the casting of the wall facing panels. The MSE wall components that are found to have a significant impact in the manufacturing stage include the backfill materials, facing elements (including accessories) and the soil reinforcements (including fasteners). Other minor wall components are not included that have less than a 1% impact compared to the total manufacturing impacts.

Transportation of MSE Wall Components

The transportation of MSE wall components includes transportation from a manufacturing plant to the jobsite or from a manufacturing plant to a storage facility then the jobsite. The transportation included in this stage is much more specific than the transportation included in the manufacturing stage and is based on actual locations of the manufacturing plants, storage facilities and jobsites to determine the impact, since this data is available to the MSE wall supplier. In this study, trucks are considered to be the main mode of transportation for the United States, while in other countries either trucks or cargo vessels are considered. Railways have not been included at this point in time, since their use is found to be insignificant compared to transportation by truck or cargo vessel. Data for the transportation stage is based on CPM (2008).

Additional MSE wall components are included in the transportation stage, which are not considered in the manufacturing stage, such as bolt sets, adhesive and lifting inserts for the facing panels. Unlike the manufacturing of materials, transportation is not just a function of the amount of material, but also the distance the material must be transported. MSE wall components that have less than 1% impact under consideration of their transportation are excluded from the analysis.

Construction of the MSE Wall

The activities that are evaluated for the construction of the MSE wall include the excavation of the in situ soil with an excavator; the transportation of select backfill, random backfill and in situ soil around the jobsite with a dump truck; the placement of select backfill, random backfill and in situ soil with a front wheel loader; and the compaction of select backfill, random backfill and in situ soil with a roller. Placement of the concrete facing panels and soil reinforcements are not included in the analysis as these activities are assumed to have little impact in comparison to the activities mentioned above.

Dismantling of the MSE Wall
The activities involved in dismantling the MSE wall that are accounted for in the analysis are the removal of the select backfill, random backfill and in situ soil with a front wheel loader; the excavation of the in situ soil with an excavator; the transportation of select backfill, random backfill and in situ soil around the jobsite with a dump truck; and the recycling of the concrete facing panels with a mobile concrete crusher unit. Transportation of any ready-to-use recycled materials produced at the site should be part of the impact assessment of the next project.

The references used for creating the inventory for the construction and dismantling of the MSE walls include CPM (2008) and US EPA (2005).

Electricity
In this study, all extraction processes, manufacturing processes and modes of transportation between countries are assumed to be essentially the same; however, one large difference between countries that is not and cannot be assumed to be the same is the electricity used in a database. The environmental impact per megajoule of electricity varies greatly from one country to the next. For example, Table 1 shows the difference between how electricity is generated in the United States and France. Between these two countries, the United States has a much higher emissions of carbon dioxide due to the high percentage electricity generated from coal, while France generates greater levels of radiation due to the high percentage of nuclear energy per megajoule of electricity. Depending upon where materials are extracted, manufactured and transported, this difference in generation of electricity for each country must be accounted for in the inventory analysis.

Table 1. Generation of Electricity in the United States and France in 2007.

Location	Coal (%)	Natural Gas (%)	Nuclear Energy (%)	Hydroelectric Energy (%)
United States	49	22	19	6
France	4	4	77	12

Energy Information Administration (2009)
Ministère de l'Écologie, de l'Energie, du Développement durable et de la Mer (2008)

Impact Assessment

After determining all the inputs and outputs in the inventory analysis, the impact of the MSE wall is assessed. Guinée et. al (2001) provide a list of impact categories that include energy consumption, abiotic depletion, biotic depletion, climate change, photo-oxidant formation, acidification, radiation, stratospheric ozone depletion, eutrophication, water consumption, toxicity, land usage, waste, heat, odor, noise and desiccation. The impact categories that are found to be meaningful and can be measured in this study include the following:

- **Energy Consumption** – energy consumed during extraction, production, manufacture and transportation, but does not include feedstock energy

- **Abiotic Depletion** – evaluates the effect of the depletion of inorganic natural resources and the impact is evaluated using antimony equivalents
- **Climate Change** – evaluates the effect of air emissions that contribute to increased global temperatures and the impact is evaluated using carbon dioxide equivalents
- **Photo-Oxidant Formation** – evaluates the effect of air emissions that contribute to increased levels of ozone and the impact is evaluated using ethylene equivalents
- **Acidification** – evaluates the effect of air emissions that contribute to increased levels of acid and the impact is evaluated using sulfur dioxide equivalents

Water consumption and radiation were also considered for the assessment of impact categories, but the available input and output data did not appear detailed enough to report. Biotic depletion (the depletion of organic natural resources) was also considered, but a method for evaluating this impact category has yet to be well developed.

With the exception of energy consumption, all of the impact categories listed above are evaluated with equivalents, which are calculated by multiplying each input or output by a specified factor. Guinée et. al (2001) provide tables of materials or chemicals that have been found to be significant in each impact category and their corresponding factor. Guinée et. al (2001) references Guinée (1995) for abiotic factors, Jenkin and Hayman (1999) and Derwent et. al (1998) for photo-oxidant factors, and Hauschild and Wenzel (1998) for acidification factors. Guinée et. al (2001) includes climate change factors, but the climate change factors for this study are taken from the Solomon et. al (2007) for more up-to-date factors.

Interpretation of Results

The interpretation of results includes evaluations relating to consistency and completeness, an analysis of the results relating to sensitivity and uncertainty, and conclusions and recommendations based on the results.

STUDY OF A MSE WALL AND GRAVITY WALL

To illustrate the results of a LCA study, the environmental impact of an actual MSE wall at the Washington Dulles International Airport was evaluated. The MSE wall components that were included in the scope of the evaluation included the select backfill (not including random backfill) as distinguished in Figure 1(a), facing elements (including accessories) and soil reinforcements (including fasteners). The MSE wall evaluated in the study had a length of about 131 m (430 ft) and an average height of 4.6 m (15 ft), and the foundation and retained soil had a unit weight of 19.6 kN/m^3 (125 pcf) and a friction angle of 30 degrees. A traffic surcharge of 12 kPa (250 psf) was also included in the analysis. Figure 1(a) shows the dimensions of the MSE wall under evaluation.

Table 2 presents the results of the LCA study for the four stages of the MSE wall life cycle. For all four stages, the analysis showed that the select backfill had the greatest environmental impact, since MSE walls consist mostly of select backfill. In addition to the select backfill, the concrete panels and soil reinforcing strips significantly contributed to the environmental impact of the MSE wall in the manufacturing stage.

Table 2. Environmental Impact of the Four Main Stages of a MSE wall.

	Inputs		Output Air Emissions		
Stage	Energy Consumption (GJ)	Abiotic Depletion (kg Sb eq.)	Photo-oxidant Formation (kg C_2H_4 eq.)	Acidification (kg SO_2 eq.)	Climate Change (kg CO_2 eq.)
Manufacturing	860	700	69	540	99,000
Transportation	129	34	20	100	11,100
Construction	18.8	9.7	1.6	9.4	1,600
Dismantling	4.6	2.3	0.6	2.8	450

For comparison, the environmental impact of manufacturing material for a gravity wall was evaluated against the impact of manufacturing MSE wall components. The gravity wall was assumed to consist solely of concrete and had the same length and height as the MSE wall. The gravity wall design also used the same foundation and retained soil parameters and traffic loading as those used in the MSE wall design. Figure 1(b) shows the cross section of the gravity wall used in the study. Table 3 presents the environmental impact of both the MSE wall and gravity wall.

Table 3. Environmental Impact of Manufacturing Material for a MSE Wall and a Gravity Wall.

	Inputs		Output Air Emissions		
Wall System	Energy Consumption (GJ)	Abiotic Depletion (kg Sb eq.)	Photo-oxidant Formation (kg C_2H_4 eq.)	Acidification (kg SO_2 eq.)	Climate Change (kg CO_2 eq.)
MSE Wall	860	700	69	540	99,000
Gravity Wall	2,200	910	147	1,310	420,000

CONCLUSION

MSE wall solutions have long since proven to hold major advantages over other solutions for retaining wall applications such as less cost, quick construction and reduced labor and construction equipment needs. The study presented in this paper is only preliminary but already clearly shows that common MSE solutions are extremely efficient in terms of environmental impacts. In addition, by performing this study, components that contribute significantly to the environmental impact of a MSE wall can now be identified. If those components are replaced with more sustainable or recyclable material, then the overall MSE wall solution will become even more efficient and environmentally friendly.

REFERENCES

Center for Environmental Assessment of Product and Material Systems (CPM). (2008). *CPM Life Cycle Analysis Database*, http://www.cpm.chalmers.se/CPMDatabase/Scripts/AdvGeneral.asp (April 2, 2009).

Derwent, R.G., M.E. Jenkin, S.M. Saunders and M.J. Pilling (1998). "Photochemical ozone creation potentials for organic compounds in Northwest Europe calculated with a master chemical mechanism." *Atmosperic Environment*, 32, 2429-2441.

Ecoinvent Centre (2009). *Ecoinvent Database*, http://www.ecoinvent.com (October 9, 2009).

Energy Information Administration (2009). *Electric Power Industry 2007: Year in Review*, http://www.eia.doe.gov/cneaf/electricity/epa/epa_sum.html (April 17, 2009).

Guinée, J.B. (1995). *Development of a methodology for the environmental life-cycle assessment of product; with a case study on margarines*. Thesis, Leiden University.

Guinée, J.B., M. Gorree, R. Heijungs, G. Huppes, R. Kleijn, A. de Koning, L. van Oers Anneke Wegener Sleeswijk, S. Suh, H.A. Udo des Haes, H, de Bruijn, R. van Duin, and M. Huijbregts (2001). *Life Cycle Assessment: An operational guide to the ISO standard*. Centre of Environmental Science - Leiden University, Delft University of Technology, Fuels and Raw Materials Bureau, and University of Amsterdam.

Hauschild, M and H. Wenzel (1998). "Environmental Assessment of Products." *Volume 2: Scientific background*. Chapman & Hall, London.

Jenkin, M.E. and G.D. Hayman (1999). "Photochemical ozone creation potentials for oxygenated volatile organic compounds: sensitivity to variations in kinetic and mechanistic parameters." *Atmospheric Environment*, 33, 1775-1293.

Ministère de l'Écologie, de l'Energie, du Développement durable et de la Mer (2008). "L'Electricité en France en 2007: une analyse statisque." *énergies & matières premières*, http://www.statistiques.developpement-durable.gouv.fr/IMG/pdf/elec-analyse-stat_cle29435b-1.pdf (April 2, 2009).

PlasticsEurope: Association of Plastics Manufacturers (2005). *Eco-Profiles of the European Plastics Industry*, http://lca.plasticseurope.org/index.htm (April 2, 2009).

Solomon, S., D. Qin, M. Manning, Z. Chen, M. Marquis, K.B. Averyt, M. Tignor, and H. Miller. (2007). *Climate Change 2007: The Physical Science Basis. Contribution of Working Group I to the Fourth Assessment. Report of the Intergovernmental Panel on Climate Change*. Intergovernmental Panel on Climate Change.

United States Department of Energy: National Energy Renewable Laboratory (NREL). (2008). *U.S. Life-Cycle Inventory Database*, http://www.nrel.gov/lci/database/default.asp (April 2, 2000).

United States Environmental Protection Agency (US EPA). (1994). *Test Car List Report*, http://www.epa.gov/otaq/tclrep.htm (April 6, 2009).

United States Environmental Protection Agency (US EPA). (2005). *NONROAD2005*, http://www.epa.gov/otaq/nonrdmdl.htm#model (April 6, 2009).

Mobilization of Reinforcement Tension within Geosynthetic-Reinforced Soil Structures

Kuo-Hsin Yang[1], Jorge G. Zornberg[2] and Richard J. Bathurst[3]

1. Assistant Professor, Construction Engineering Dept., National Taiwan University of Science and Technology; E-mail: khy@mail.ntust.edu.tw
2. Associate Professor, Civil, Environmental and Architectural and Environmental Engineering Dept., The University of Texas at Austin, E-mail: zornberg@mail.utexas.edu
3. Professor, Civil Engineering Dept., Royal Military College of Canada, E-mail: bathurst-r@rmc.ca

ABSTRACT

This paper examines the mobilization of reinforcement tension within geosynthetic-reinforced soil (GRS) structures at working stress and at large soil strains. Fully-mobilized reinforcement tension is assumed in most current design methods for the internal stability of GRS structures. In these methods the mobilized reinforcement tensile load is assumed to be equal to mobilized horizontal soil forces computed using active earth pressure theory. However, comparison with reinforcement tension loads measured in the field has shown that this approach is conservative (excessively safe) by as much as a factor of two. This observation has prompted the current study in which stress data obtained from a numerical study and two instrumented large-scale GRS retaining walls were used to examine the relationship between mobilized reinforcement tensile load and mobilized soil shear strength. The results show that the ratio of reinforcement tensile load and mobilized soil shear strength is not constant Only when the average mobilized soil shear strength exceeds 95%, is reinforcement tensile capacity mobilized significantly. Nevertheless, less than 30% of reinforcement strength is mobilized when the average mobilized soil shear strength reaches peak soil shear capacity. These results help explain why current design methods lead to computed reinforcement loads that are very high compared to measured loads under operational conditions.

Keywords: Reinforcement tension, GRS structure, Finite element analysis

INTRODUCTION

In FHWA design guidelines for Mechanically Stabilized Earth (MSE) retaining wall structures (Elias et al. 2001), earth pressure theory is used to predict reinforcement tensile loads for internal stability calculations. The design rationale assumes that the tensile loads developed in reinforcement layers are in local equilibrium with lateral earth pressures generated in MSE walls. The soil stress state within Geosynthetic-Reinforced Soil (GRS) structures along potential internal failure surfaces is assumed to be at active conditions due to the relative flexibility of geosynthetics which allows the surrounding soil to deform. Therefore, the internal stability design of GRS structures simply assumes that the mobilized reinforcement tensile load is equal to the soil horizontal forces developed at active conditions.

Christopher et al. (2005) reported that the maximum reinforcement loads estimated by using the lateral active earth pressure approach could over-predict actual loads by as much as a factor of two. Allen et al. (2003) and Bathurst et al. (2008, 2005) investigated quantitatively the accuracy of reinforcement loads predicted by earth pressure theory using careful interpretation of a database of 30 well-monitored full-scale walls. They also concluded that loads predicted using earth pressure theory were excessively conservative. The predicted loads for GRS walls were *on average* three times greater than estimated values for full-scale instrumented walls. To overcome these deficiencies, Allen et al. (2003) and Bathurst et al. (2008, 2005) proposed a new empirical-based working stress method for estimation of reinforcement loads in GRS walls (K-stiffness Method). However, the K-stiffness Method is empirical-based and thus does not provide insight into the actual physical mechanisms that lead to mobilization of soil shear strength and reinforcement load capacity. The objective of this paper is to examine the mobilization of reinforcement tensile loads within GRS structures at working stress conditions (operational conditions) and at large soil strains approaching an ultimate soil state. The results provide useful insight into mechanisms that lead to different rates and magnitude of mobilization of soil shear strength and reinforcement loads.

MODELING OF GRS SLOPE

Centrifuge Test

A series of centrifuge tests on GRS reinforced slopes was conducted by Arriaga (2003) to investigate the response of GRS slopes to various design factors, e.g. backfill relative density, slope angle, reinforcement vertical spacing and reinforcement type. One centrifuge test (slope M1), was selected for numerical simulation and verification.

The dimensions and reinforcement layout of slope M1 are illustrated in Figure 1. Monterey No. 30 sand with a target relative density of 70% was used as the backfill and foundation soil. For this relative density, the peak friction angle was 36.5^o under triaxial compression conditions and 42.0^o under plane strain conditions. The unit weight of the backfill was 16.0 kN/m^3. The reinforcement used in the centrifuge study was a commercially available nonwoven geotextile. The average unconfined tensile strength from wide-width tensile tests was 0.03 kN/m. The confined tensile strength value, obtained from back-calculation at failure in the centrifuge slope models, was 0.124 kN/m (Arriaga 2003). Each slope model was loaded to failure and the g-level N_g required to fail the slope was recorded. Slope failure was determined by a sudden large increase in settlement measured by a LVDT at the front crest of the slope.

Finite Element Simulation

Finite element modeling was carried out using the in-house developed finite element program, Nonlinear Analysis of Geotechnical Program (ANLOG). ANLOG is coded in FORTRAN. The initial conditions for the slope M1 model are shown in Figure 1. An 8-node quadratic quadrilateral element under plane strain condition was used for the solid elements. Four gauss points were assigned to each solid element.

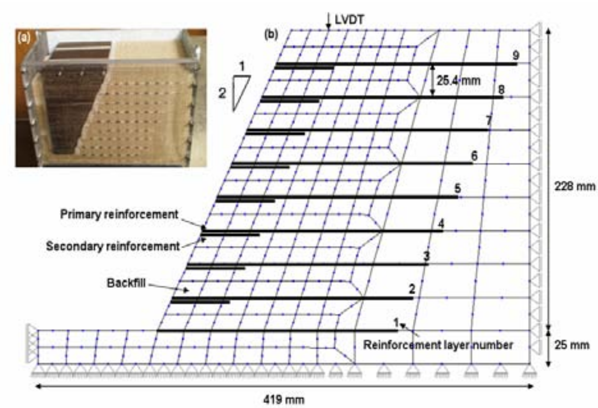

Figure 1. Slope M1 dimensions and layout

Standard boundary conditions were imposed to simulate confinement at the edges of aluminum centrifuge box. A small isotropic stress of 0.01 atm was applied to the first filled soil layer as initial stress field. Staged (layer by layer) construction was simulated. Mesh updating was used to account for large model deformations. The centrifugal force of the centrifuge was simulated by increasing the body force on each element. Each loading stage was applied in 5g increments. A total of 10 loading stages were applied. Hence, the final target g-level in the simulation was 50g.

The Lade-Kim elastoplastic constitutive model (Kim and Lade 1988; Lade and Jakobsen 2002; Lade and Kim 1995, 1988, and 1988b) and a proposed soil softening model (Yang 2009) were implemented in program ANLOG to model soil behavior at various stress states. As soil strength changes from hardening (pre-peak) to softening (post-peak), the yield surface changes from expansion to contraction. The yield surface contraction is governed by a soil softening model proposed by Yang (2009). The model captures the soil softening behavior using an inverse sigmoid function with the following features: 1) provides a smoother transition from hardening to softening after soil peak strength; 2) limits the decrease in size of the yield surface to a minimum (residual) yield surface during softening.

Reinforcement layers were simulated using bar elements with only one degree of freedom in the horizontal direction. A nonlinear elastic reinforcement model based on a second order polynomial was used to equate tensile load to tensile strain (Karpurapu and Bathurst 1995). The reinforcement model parameters were calibrated using the load-strain data from wide-width tensile tests.

Although the interaction and relative movement between reinforcement layers and backfill can be modeled using the interface element in the ANLOG program, the interface element was not applied in the numerical model to prevent numerical difficulty and to reduce computational cost. The approach used in the numerical modeling was supported by the visual observation that reinforcement specimens ruptured rather than failed due to pullout in the centrifuge tests. The readers are referred to Yang (2009) for more computational details of the finite element model simulation.

Model Verification

The simulation results were compared with centrifuge results to verify the accuracy of the proposed finite element model. Figure 2 shows that there is good qualitative agreement between physical and numerical deformation patterns at the moment of slope failure. In making comparisons the following observations are important: 1) sliding of the slope mass, 2) settlement at the top of the slope, and 3) failure surface above the slope toe. Both the centrifuge and numerical model showed a similar pattern of sliding of the slope mass and settlement at the location of the top LVDT. The settlement can be detected by comparing the original and deformed meshes at the slope top in the numerical model in Figure 2b. The failure surface in the vicinity of the toe was expected to pass through the toe based on conventional analysis. However, as shown in Figure 2a, the failure surface in slope M1 passed through the slope face at the second layer of reinforcement. This may be influenced by the boundary constraint due to the shallow thickness of foundation. This behavior was also captured in the numerical simulation as shown in Figure 2b.

The accuracy of the numerical model was also verified by quantitatively comparing the location of the failure surface, settlement at the slope crest with g-level and displacement along each reinforcement layer. In this regard, all predicted and measured results were judged by Yang (2009) to be in satisfactory agreement.

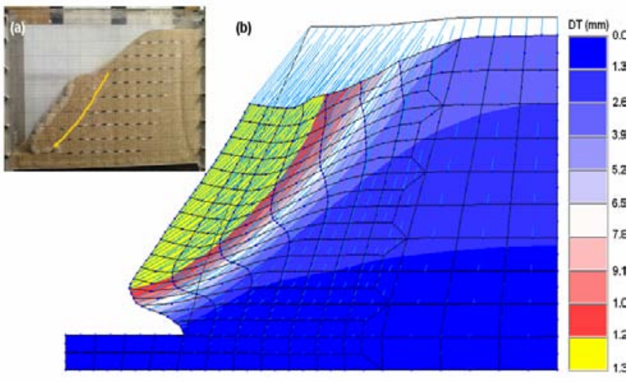

Figure 2. Comparison of deformation pattern: (a) Centrifuge model; (b) FE model (deformation x 20)

RESULTS FROM NUMERICAL SIMULATION

Definition of Strength Mobilization

The mobilization of soil shear strength can be quantified using soil stress level S defined in the Lade-Kim soil model as follows:

$$S = \frac{f_n}{\eta_1} \quad (1)$$

where f_n is the stress state on the current failure surface and η_1 is the corresponding failure criterion. One can also view the soil stress level S as an index of soil strength mobilization; i.e. the ratio of current mobilized soil shear strength to peak soil shear strength. Figure 3 shows a typical simulation result of soil stress level contours and the corresponding stress states. The value of S is less than 1.0 when the current soil stress state is below the soil peak shear strength (Figure 3a). S equals 1.0 when the current soil stress state reaches the soil peak shear strength (Figure 3b).

When the current soil stress state exceeds the soil peak shear strength, the soil shear strength will decrease. This soil softening (post-peak) behavior can be modeled using the contraction of the yield surface in the soil softening model. As a result, the soil stress level S defined in Eq. (1) would be less than 1.0 during softening. In order to distinguish between soil stress levels during hardening and softening stages, it is necessary to define the soil stress level S during softening as follows:

$$S = 1 + (1 - \frac{f_n}{\eta_1}) \tag{2}$$

Here, the current soil stress state reaches the peak soil shear strength, $f_n = \eta_1$ and S = 1.0 in Eq. (2) and is consistent with Eq. (1) at peak shear strength mobilization. In the soil softening region, the range of S is from 1.0 to 2.0.

Similar to the definition for the mobilization of soil shear strength, the reinforcement stress level S_R is defined to quantify the mobilization of reinforcement tensile capacity as follows:

$$S_R = \frac{T_m}{T_{ult}} \tag{3}$$

where T_m is the mobilized peak reinforcement tension in each layer of reinforcement and T_{ult} is the ultimate tensile strength of the reinforcement.

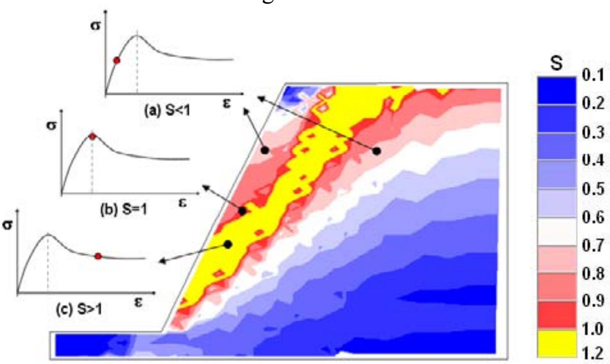

Figure 3. Soil stress level contours and illustration of corresponding stress states

Mobilization of Soil Shear Strength and Reinforcement Tension

The concurrent mobilization of reinforcement tensile load and soil strength is investigated in this section. Because soil shear strength and reinforcement loads along the failure surface are critical factors for the evaluation of system stability, the focus of this study is on the failure surface. The soil stress level S is obtained at the Gaussian point that is closest to the location of peak reinforcement load level S_R in each reinforcement layer. The results are presented in Figure 4. Relatively large variations in S (scatter in horizontal direction in Figure 4) are observed at low g-level and relatively large variations of S_R (scatter in vertical direction in Figure 4) are observed at high g-level. This suggests that mobilization of soil shear strength is not uniform along the failure surface at low g-level (or at low S values) but becomes more uniform at high g-level (or at high S values when S approaches 1.0). In contrast, the mobilization of reinforcement tensile load at each layer is uniform at low g-level and becomes non-uniform at high g-level. Because of the scatter, average and upper bound values on reinforcement load level are provided. The average value of reinforcement load level is obtained by averaging all reinforcement layer loads. The upper bound value represents the mobilization of maximum peak reinforcement tensile load at each g-level increment.

In Figure 4, the most important observation is that the mobilization of reinforcement tensile load capacity does not increase linearly with the mobilization of soil shear strength; rather, there are two stages. In the first stage, the mobilization of reinforcement tensile load increases slowly to approximately 10% of its ultimate tensile strength until the average mobilized soil shear strength along the failure surface reaches about 95% of its peak shear strength. During the second stage, when the average mobilized soil shear strength exceeds 95%, reinforcement tensile load capacity is mobilized rapidly. Nevertheless, more than 30% of reinforcement strength is still available even when the average mobilized soil shear strength reaches the peak shear strength value (S = 1).

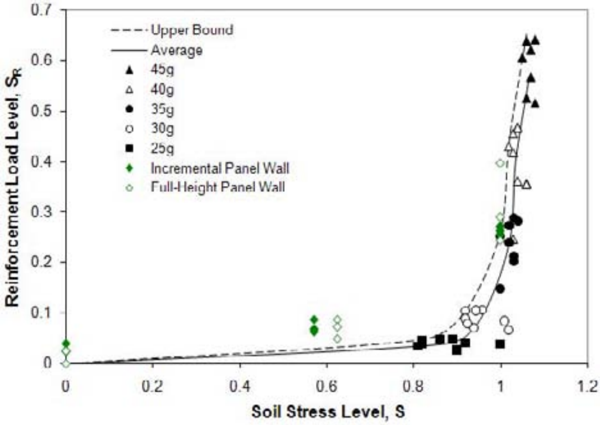

Figure 4: Comparison of the mobilization of reinforcement tensile load capacity and soil stress level (plus data from two full-scale instrumented walls)

RESULTS FROM TWO LARGE-SCALE TEST WALLS

Two instrumented large-scale GRS retaining walls 3m in height were tested to failure in the Royal Military College (RMC) retaining wall test facility(Bathurst 1993, Bathurst and Benjamin 1990, Bathurst et al. 1989, Karpurapu and Bathurst 1995). The GRS walls were constructed with a dense sand fill and layers of extensible geogrid reinforcement attached to two different facing treatments: incremental panel and full-height panel. Both walls were taken to collapse under uniform surcharge pressure applied to the top of the backfill. The strains developed at each reinforcement layer were seen to increase as surcharge pressure was increased in steps. Reinforcement strains can be used to compute reinforcement tensile load in the physical tests using the load-extension response reported by Bathurst (1993). S_R can then be computed using the ultimate tensile strength of the reinforcement (reported as 12 kN/m) and S_R compared to numerical predicted values.

The soil failure mechanism in the large-scale GRS wall tests was detected during careful wall excavation by tracing a well-developed shear plane propagating through the reinforced soil zone commencing at the heel of the facing. Therefore, the average soil stress level S corresponding to this stage along this failure surface is assumed equal to 1.0 or slightly larger than 1.0. Because the soil stress levels along the failure surface before and after soil failure were not measured, the development of soil stress levels is assumed uniform along the failure surface and proportional to the magnitude of applied surcharge. Hence, S is taken as zero at end of construction before the application of surcharge and possible mobilization of soil shear strength during construction is neglected in this analysis.

Results obtained from the two instrumented walls are also plotted in Figure 4 and fall on the band of data obtained from numerical analysis of the centrifuge tests. The reinforcement load level S_R is generally higher than values obtained from numerical analysis of the centrifuge tests when $S < 1$. The difference may be due to compaction during wall construction which is not included in the numerical analysis.

DISCUSSION AND CONCLUSIONS

In this paper, stress data obtained from a numerical study of a centrifuge model slope and two physical full-scale instrumented GRS retaining walls were used to examine the relationship between mobilized reinforcement load capacity and mobilized soil shear strength. The results indicate that mobilization of reinforcement tensile load capacity does not increase linearly with mobilized soil shear strength up to soil failure. Rather reinforcement tensile load increases slowly to approximately 10% of its ultimate tensile strength until the average mobilized soil shear strength along the failure surface reaches about 95% of its peak shear. Even after the soil is at a post-peak shear strength state the reinforcement still retained an additional 30% of its original tensile load capacity.

The results obtained in this study help to explain the observation that measured reinforcement loads in geosynthetic reinforced soil walls under operational conditions are much less than predicted values using current force-equilibrium based design methods. This is because the soil shear strength within GRS structures is computed using classical active earth pressure theory and thus soil shear strength is assumed to be fully mobilized. However, based on the results shown in Figure 4, less than half of the reinforcement strength is mobilized at $S = 1$. Therefore, the over-prediction of maximum reinforcement loads by as much as a factor of two may be expected for walls at end of construction and under operational conditions.

In fact, soil and reinforcement strains and load are developed due to internal displacement of GRS structures. Hence, mobilized reinforcement tensile load in GRS structures are a function of the type of elongation and stiffness of the geosynthetic layers as they interact with and potentially influence and improve the confining soils. Consequently, design methodologies based on force equilibrium cannot be expected to predict accurate reinforcement loads. Rather, displacement-based analysis and design methods hold promise as alternative approaches for the selection of reinforcement materials and for the internal stability analysis of GRS structures.

REFERENCES

Allen, T.M., Bathurst, R.J., Holtz, R.D., Walters, D. and Lee, W.F. (2003) "A New Working Stress Method for Prediction of Reinforcement Loads in Geosynthetic Walls", *Canadian Geotechnical Journal*, v 40, n 5, p 976-994.

Arriaga, F. (2003) "Response of Geosynthetic-Reinforced Structures under Working Stress and Failure Conditions", PhD Dissertation, Department of Civil Engineering, the University of Colorado, Boulder.

Bathurst, R.J. (1993) "Investigation of Footing Restraint on Stability of Large-Scale Reinforced Soil Wall Tests", *46th Canadian Geotechnical Conference*, p 389-398.

Bathurst, R.J., Allen, T.M. and Walters, D.L. (2005) "Reinforcement Loads in Geosynthetic Walls and the Case for a New Working Stress Design Method", *Geotextiles and Geomembranes*, v 23, n 4, p 287-322.

Bathurst, R.J. and Benjamin, D.J. (1990) "Failure of a Geogrid Reinforced Soil Wall", *Transportation Research Record*, 1288, Washington, D.C., p 109-116.

Bathurst, R.J., Benjamin, D.J. and Jarrett, P.M. (1989) "An Instrumented Geogrid Reinforced Soil Wall", *Proceedings of the Twelfth International Conference on Soil Mechanics and Foundation Engineering*, Rio de Janeiro, 13-18 August 1989.

Bathurst, R.J., Miyata, Y., Nernheim, A. and Allen, T.M. (2008) "Refinement of K-Stiffness Method for Geosynthetic Reinforced Soil Walls", *Geosynthetics International*, v 15, n 4, p 269–295.

Bathurst, R.J., Vlachopoulos, N., Walters, D.L., Burgess, P.G. and Allen, T.M. (2006) "The influence of facing rigidity on the performance of two geosynthetic reinforced soil retaining walls", *Canadian Geotechnical Journal*, v 43, n 12, p 1225-1237.

Christopher, B.R., Leshchinsky, D. and Stulgis, R. (2005) "Geosynthetic-Reinforced Soil Walls and Slopes: US Perspective", *International Perspectives on Soil Reinforcement Applications. ASCE Geotechnical Special Publication No. 141,* ASCE Press, Reston, Virginia, January 2005, ISBN 0-7844-0769-X, 166 p.

Elias, V., Christopher, B.R. and Berg, R.R. (2001) "Mechanically Stabilized Earth Walls and Reinforced Soil Slopes Design and Construction Guidelines", Report No. FHWA-NHI-00-043, *National Highway Institute, Federal Highway Administration*, Washington, D.C. March.

Karpurapu, R.G. and Bathurst, R.J. (1995) "Behaviour of Geosynthetic Reinforced Soil Retaining Walls Using the Finite Element Method", *Computers and Geotechnics*, v 17 n 3, p 279-299.

Lade, P.V. and Jakobsen, K.P. (2002) "Incrementalizaton of a Single Hardening Constitutive Model for Frictional Materials", *International Journal for Numerical and Analytical Methods in Geomechanics*, v 26, p 647-659.

Lade, P.V. and Kim, M.K. (1995) "Single Hardening Constitutive Model for Soil, Rock and Concrete", *International Journal Solids and Structures*, vol. 32, n.14, pp. 1963-1978.

Lade, P.V. and Kim, M.K. (1988) "Single Hardening Constitutive Model for Frictional Materials– II. Yield Criterion and Plastic Work Contours" *Computers and Geomechanics*, 6, pp. 13-29

Lade, P.V. and Kim, M.K. (1988b) "Single Hardening Constitutive Model for Frictional Materials – III. Comparisons with Experimental Data." *Computers and Geomechanics*. 6, pp. 31-47.

Kim, M.K. and Lade, P.V. (1988) "Single Hardening Constitutive Model for Frictional Materials- I. Plastic Potential Function" *Computers and Geomechanics*, 5, pp. 307-324.

Yang, K-H. (2009) "Stress Distribution within Geosynthetic-Reinforced Soil Structures", PhD Dissertation, Department of Civil Architectural and Environmental Engineering, the University of Texas, Austin.

Factors Affecting the Development of MSE Wall Reinforcement Strain

Armin W. Stuedlein[1], Ph.D., P.E., M. ASCE, Tony M. Allen[2], M.S., P.E., M.ASCE, Robert. D. Holtz[3], Ph.D., P.E., D.GE, Dist. M. ASCE, and Barry R. Christopher[4], Ph.D., P.E., M.ASCE

[1] Assistant Professor, Oregon State Univ., 220 Owen Hall, Corvallis, OR, 97331
[2] State Geotechnical Engineer, Materials Laboratory, Washington State Dept. of Transportation, Tumwater, WA 98511
[3] Professor Emeritus, Univ. of Washington, Box 352700, Seattle, WA 98195
[4] Geotechnical Consultant, 210 Boxelder Lane, Roswell, GA 30076

ABSTRACT The grade raising associated with the construction of a new runway at Seattle-Tacoma International Airport required construction of two near vertical tall reinforced earth walls that included the two tier 26 m North wall and the four tier 46 m tall West wall. Twenty reinforcement strips at critical wall cross-sections were instrumented with approximately 550 strain gages, and performance data were obtained during initial installation and backfill placement. The performance data facilitated the assessment of factors affecting the development of strains within the MSE walls. A simplified method to determine the amount of reinforcement strain due to installation of the reinforcement strip and subsequent compaction of fill is presented. Estimates of the initial reinforcement strain, fill thickness up to which compaction effects were noted, and the initial and geostatic reinforcement strain rate in terms of microstrain per meter of fill placed are tabulated and discussed. The local reinforcement stiffness contributes to the accumulation of initial reinforcement strain, but is found to play a significant role in controlling the rate of strain due to normal geostatic stresses. Implications for the design of very tall MSE walls are also given.

Keywords: Soil stabilization, retaining walls, performance, instrumentation

INTRODUCTION

Due to growing restrictions on right-of-way, wetlands, or other space-limiting conditions (Sankey and Soliman, 2004), the design and construction of tall MSE walls (greater than 20 m high) are increasing worldwide. Case histories, especially on instrumented structures, provide critical information for understanding construction and long-term behavior, as well as provide data for aggregate database analysis. Although the critical design goal for MSE walls is selecting the reinforcement strip strength and distribution for internal and external stability in a completed state, it is also important to understand the development of reinforcement strain during construction. Consider the behavior of an MSE wall on a weak foundation; the ability to discern the reinforcement strains developed due to normal construction activities from those due to compound wall/foundation instability could be critical. The focus of this paper is to discuss the factors affecting the development of reinforcement strain in steel-reinforced earth walls and to compare reinforcement strain predictions for intermediate construction stages.

BRIEF DESCRIPTION OF THE THIRD RUNWAY MSE WALLS

The North MSE wall supports the north safety area of the Third Runway at Seattle-Tacoma International Airport (STIA). This wall is approximately 350 m long and 25.9 m high at the tallest section, from the bottom to the top of the reinforced zone, and has a 2.4 m setback near mid-height forming two tiers (Figure 1). The exposed height at this section is 23.6 m. The West MSE wall is approximately 436 m long, has four tiers formed by 2.4 m setbacks, and is 45.7 m high at the tallest section. The exposed height of the MSE wall is 41.9 m at this location, not including the unreinforced 2H:1V soil slope, with a crest height of 4.5 m (Figure 1). Behind the crest, the backslope is a negative 3 percent for drainage. To the authors' knowledge, this is the tallest MSE wall in the Western Hemisphere. For a full discussion of project background, design aspects, and instrumentation of these MSE walls, see Stuedlein et al (2007), Stuedlein et al (2010a), and Stuedlein et al (2010b).

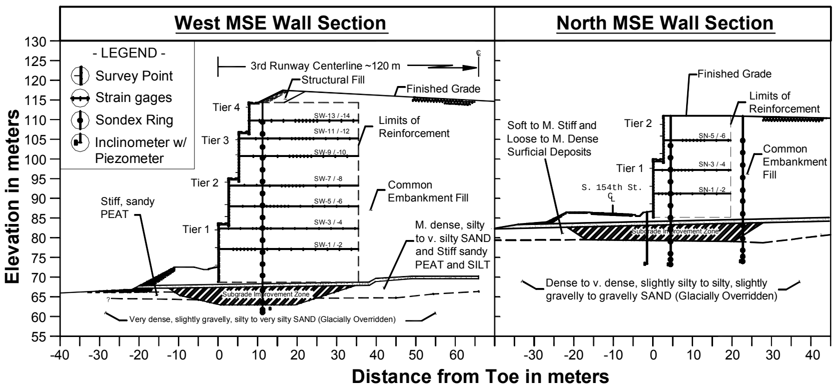

Figure 1. Instrumented section of the North and West MSE walls.

THE DEVELOPMENT OF REINFORCEMENT STRAIN

Sources of tensile strain in the reinforcement strips include:

1. Movement and adjustment of the wall components as initial lifts of backfill are placed to reach an initial equilibrium,
2. Compaction of backfill over the reinforcement and near wall face panels as the panels react to the soil and compaction-induced lateral earth pressure,
3. Vertical drag force applied to the reinforcement at its connection to the wall face as the compaction of the soil compresses the backfill,
4. Continued placement of overburden, increasing earth pressures on wall face panels and drag forces at reinforcement strip connections,
5. Resistance to geostatically induced shear strain in backfill as an active soil zone develops, and
6. Potential development of differential settlement within the foundation transverse to the wall face.

Strain measurements reported herein that were recorded during construction were taken at midnight to minimize the effects of construction-related vibrations, to prevent the measurement of live, construction-induced loading, and to reduce thermal influences.

Reinforcement Strain Developed Due to Initial Installation Effects and Compaction

The effects of initial installation and compaction are presented in terms of reinforcement strains. The compaction equipment used by the contractor was a Caterpillar model CS-563D vibratory roller. The smooth 10,875 kg drum roller had a 1.55 m diameter, 2.13 m width, and supplied static and dynamic compaction forces of 26.4 kg/cm and 127.5 kg/cm, respectively. The initial strain induced in the reinforcement strip results from the proximity of fill spreading and compaction activities to the strip and the initial development of strain in the system as the wall components achieve initial equilibrium. Evidence of the effects of initial take-up and compaction has been presented by, e.g., Anderson et al., 1987; Neely, 1993; and Mitchell and Ehrlich, 1994.

Strain rates are typically assessed in the time domain, since rapid application of load typically results in rapid straining for metallic materials. Because the filling time history, or loading rate, of any given MSE wall construction cannot be estimated with certainty prior to construction, it is convenient to assess strain rate in terms of overburden placement (i.e., strain per m of fill placed). Strain assessed in terms of the latter formulation may then be easily compared to walls of similar construction types. Figure 2(a) shows the development of tensile strain as a function of overburden for instrumented reinforcement strips placed within the West MSE wall. Initially, the accumulation of strain is rapid, ranging from approximately 40 to 100 microstrain ($\mu\varepsilon$) per meter of fill. Following 1 to 2 m of overburden placement, the strain rate slows to 15 to 25 $\mu\varepsilon$ per meter of fill placed as the level of initial installation and compaction effects diminishes and the fill approaches normally consolidated, geostatic stress states.

Figure 2(b) illustrates the method used to estimate and differentiate strains due to initial installation and soil compaction effects in contrast to strains due to the normal accumulation of overburden stress. The strain due to initial take-up and soil compaction has been assumed to be the difference in strain at points A and B, where point A represents a marked change in rate of strain accumulation and point B represents the intersection of the observed overburden strain rate and the amount of fill in meters corresponding to point A. For the reinforcement strip shown in Figure 2(b), the initial take-up and compaction-induced strain determined is 115 $\mu\varepsilon$. Table 1 presents the mean fill thickness, mean strain caused by compaction and initial installation effects, mean initial strain rate, and mean overburden strain rate estimated from the analysis of strain accumulation as illustrated in Figure 2. The estimates represent average values observed for strain gages within the zone of maximum stress as defined by Elias et al. (2001) plus an additional 2 m; therefore, the approximate boundary between the active and resisting zones is considered. The estimates did not include the strain gages nearest the wall face. The average amount of estimated fill above an instrumented reinforcement strip that produced strain caused by compaction and initial installation effects is 1.52 m, with an estimated coefficient of variation

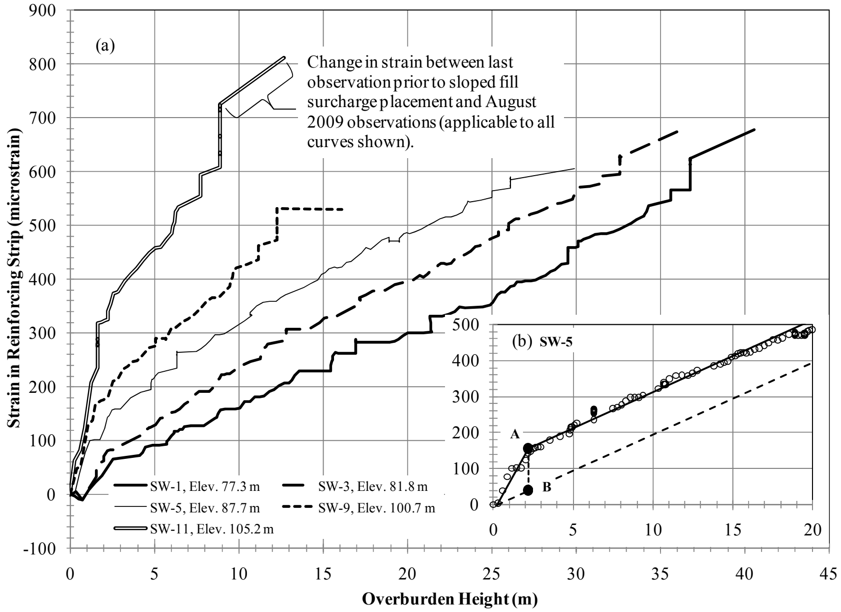

Figure 2. Tensile reinforcement strain in West MSE wall: (a) accumulation of strain during construction (some strips omitted for clarity), (b) method used to differentiate initial installation effects from overburden placement.

(*COV*) of 10 percent per individual strip and 54 percent overall. The average estimated strain caused by compaction and initial installation effects is 93 $\mu\varepsilon$ with a corresponding *COV* of 25 percent per strip and 51 percent overall. In terms of strain rate, the mean and *COV* of initial strain rate is 90 $\mu\varepsilon$ and 24 percent percent, respectively. In comparison, the average strain rate due to placement of overburden is approximately one fourth of the strain rate due to compaction activities and other initial installation effects. The results of the simple analysis presented in Table 1 quantify a marked difference in strain accumulation between initial installation and compaction effects and the general overburden placement.

Reinforcement Strain Time History

Figure 3 presents the strain time history for reinforcement strip SW-5 (Figure 1), corresponding to elevation 87.7 m at the West MSE wall. For clarity, only five strain time histories are shown. This reinforcement strip was installed within the soil mass on day 90 of the West MSE wall construction. Decreases in strain within the instrumented reinforcement strips were observed during pauses in wall construction. Following completion of Tier 2 on day 113 and cessation of fill placement, peak reinforcement strain at individual gage pairs occurred, with subsequent decrease in strain, whereas other gages indicated increases in strain. For example, the gage pair located 0.2 m behind the wall face peaked on day 115 with 137 microstrain, followed

Table 1. Effects of Initial Installation and Overburden on Reinforcement Strip Strain Behavior. Note, no significant initial effects were observed for strip SW-8.

Instrumented Strip Designation	Mean Thickness of Fill Up to which Initial Effects Noted (m)	COV for Fill Thickness per strip (%)	Mean Strain Caused by Initial Effects ($\mu\varepsilon$)	COV for Initial Strain per strip (%)	Mean Initial Strain Rate ($\mu\varepsilon$/m)	COV for Initial Strain Rate per strip (%)	Mean Overburden Strain Rate ($\mu\varepsilon$)	COV for Overburden Strain Rate per strip (%)
SW-1	1.61	2	47	14	42	8	13	8
SW-2	1.30	3	77	16	73	14	14	12
SW-3	1.35	8	68	21	63	9	13	24
SW-4	1.93	8	71	20	53	13	16	20
SW-5	1.96	4	77	21	56	15	17	30
SW-6	3.27	9	94	18	44	18	15	27
SW-7	1.38	8	30	24	40	15	18	20
SW-8	0.00	-	0	-	17	31	17	31
SW-9	2.86	14	122	30	62	34	18	32
SW-10	2.68	15	154	17	79	20	21	26
SW-11	1.95	12	143	55	100	62	24	75
SW-12	2.09	29	110	61	82	57	24	45
SW-13	1.12	2	108	47	122	48	25	50
SW-14	0.95	4	84	29	112	36	23	63
SN-1	0.84	8	51	27	84	25	21	11
SN-2	0.44	5	43	20	117	17	20	15
SN-3	0.73	12	125	14	197	14	25	20
SN-4	0.83	20	136	19	195	26	25	30
SN-5	1.47	2	200	12	162	14	25	27
SN-6	1.67	9	121	9	97	10	24	5
MEDIAN	1.42	8	89	20	80	18	20	26
MEAN	1.52	9	93	25	90	24	20	28
COV (%)	54		51		55		22	

by a decrease of 21 percent to 108 microstrain on day 122. Gage pairs located up to 13 m behind the wall face indicated moderate increases in strain following Tier 2 completion. Similarly, some segments of the reinforcement strip exhibited up to a 10 percent decrease in strain whereas other segments experienced an increase in strain over the 28 day pause between the end of Tier 3 and start of Tier 4 construction. This behavior indicates the: (1) potential relaxation of locked-in compaction stresses within the backfill, and/or (2) development of the active zone, leading to redistribution of tensile strain within the reinforcement strip.

No decrease in strain was observed following end of Tier 4 construction; rather, strains continued to accumulate at a decreasing rate. The strain accumulation is thought to be associated with outward wall movement, of which 5 to 35 mm occurred along various elevations of the wall following completion of Tier 4 (Stuedlein et al.; 2010a). Tensile reinforcement strains approach a stabilized value at approximately 125 days following the end of Tier 4 construction, during which the rate of lateral wall face displacement decreased. Unfortunately, no strain observations were available during the placement of the sloped fill surcharge; however, the latest readings from August 2009 (Figure 2a) show strains that developed in the completed wall.

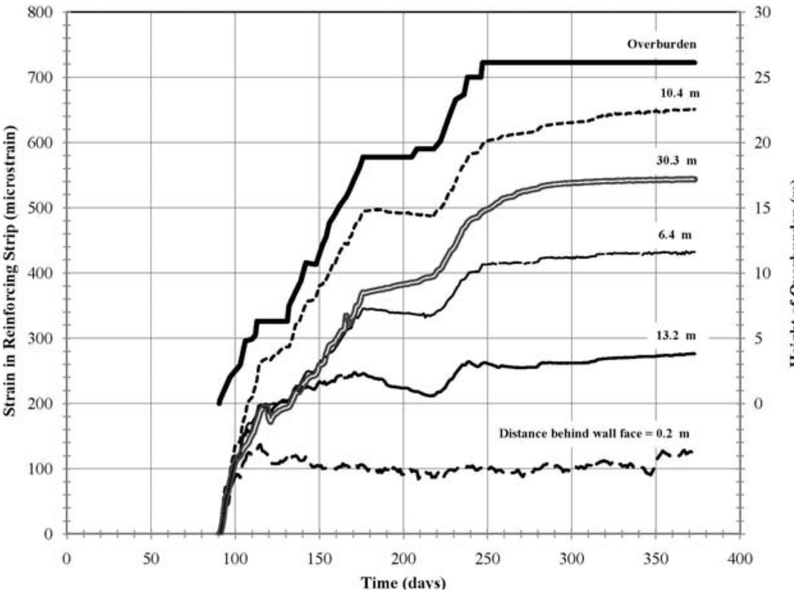

Figure 3. Strain time history for instrumented reinforcement strip SW-5.

PREDICTION OF REINFORCEMENT STRAIN DEVELOPMENT

Comparison of observed reinforcement strains to those predicted using existing design procedures is of interest to identify areas for improvement in the methods. The Coherent Gravity (Schlosser, 1978; Juran and Schlosser, 1978; Schlosser and Segrestin, 1979) and Simplified (Allen et al., 2001; Elias et al., 2001) methods are the procedures fully accepted by state departments of transportation; the K-Stiffness method (Allen et al., 2004) is an optional method for design of walls in Washington State. Another method considered here is that developed by Ehrlich and Mitchell (1994), which attempts to explicitly account for the effects of compaction-induced earth pressures and reinforcement stiffness. Note that the friction angle used for design was 37° and the reinforcement strains predicted during design are not discussed herein. The actual measured direct shear friction angle of 41° is used for the predictions presented here. With the exception of the Ehrlich and Mitchell method, which cannot readily be modified for battered walls, predictions of reinforcement strain considered the horizontal component of active earth pressure to account for the effect of the tiered walls. See Stuedlein et al (2010b) for a complete description of the reinforcement strain predictions.

The development of reinforcement strain with the placement of overburden is presented for reinforcement strips SW-1 and SW-2 in Figure 4, and SW-5 and SW-6 in Figure 5 (refer to Figure 1 for locations). Also shown are the predictions in strain using the four selected design methods. The K-Stiffness and Ehrlich and Mitchell methods, which consider the effects of reinforcement stiffness, predict the observed

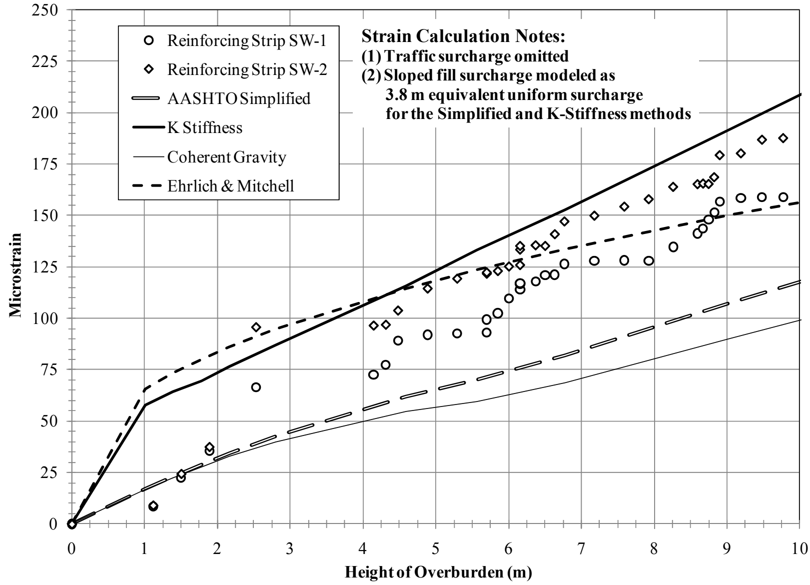

Figure 4. Observed and predicted development of tensile reinforcement strain, elevation 77.3 m.

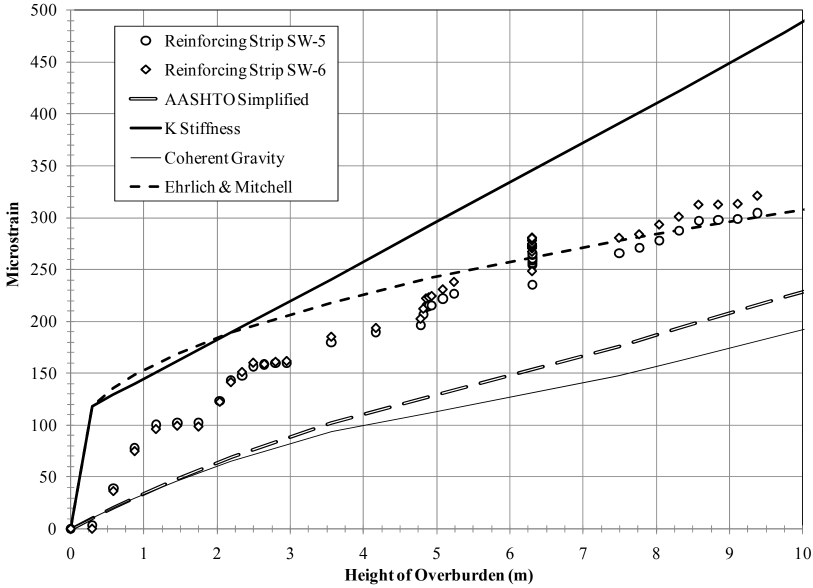

Figure 5. Observed and predicted development of tensile reinforcement strain, elevation 87.7 m.

initial reinforcement strains fairly well. The K-Stiffness method performs better with increasing overburden thickness for the more stiffly reinforced elevation (i.e., 77.3 m) than at elevation 87.7 m, an effect of the assumed load distribution D_{tmax}. In contrast, the Ehrlich and Mitchell strain prediction becomes more accurate with increasing overburden height. The Simplified and Coherent Gravity methods, which do not account for reinforcement stiffness, generally under-predict the tensile strain for the duration of filling in Figures 4 and 5 and at the end of construction (not shown). See Stuedlein et al (2010b) for a complete comparison of reinforcement strain prediction and bias.

DISCUSSION OF FACTORS AFFECTING REINFORCEMENT STRAIN

The great height and high global reinforcement stiffness of the North and West MSE walls are two characteristics that place them outside the range for which the considered design methods were empirically derived or compared to during their development. In general, the Coherent Gravity, Simplified, and K-Stiffness methods are likely to work best for walls that are approximately 18 m in height or less, and for walls with a global reinforcement stiffness of 150 MPa or less (Allen et al., 2001; Stuedlein et al, 2010b). As recognized by Christopher et al. (1990), Ehrlich and Mitchell (1994), Neely (1995), and Allen et al. (2004), among others, the local and global reinforcement stiffness is one of the most important design parameter for MSE walls constructed with conventional granular backfill and compaction methods. Figure 6 plots the rate of tensile strain accumulation presented in Table 1 against the local reinforcement stiffness for each of the twenty instrumented strips. The initial rate of strain accumulation at the location of the peak strain during placement and compaction of the first lifts of fill indicates that reinforcement stiffness plays a moderate role in the initial uptake of strain, that is, it accounts for 41% of variability in strain rate. However, as additional fill is placed and a normally consolidated stress state is achieved, the effect of local reinforcement stiffness on accumulation of strain becomes more significant, explaining 71 and 81% of the variability in the peak and average rate of strain accumulation, respectively. The differences in local reinforcement stiffness from elevation to elevation explain the relatively large overall variability in Table 1. Therefore, only methods that consider reinforcement stiffness will be able to accurately predict reinforcement strains at intermediate stages of construction.

Other factors that control reinforcement strain include the shear strength and modulus of the backfill, type of compaction equipment, facing batter, degree of toe restraint, and quality of the foundation. These factors, while significant, are not considered herein. Additionally, the observed reinforcement strains exhibit variability, a fact that must be considered when evaluating predicted strains. Measurements of reinforcement strains were obtained in two nominally identical wall sections for both the North and West MSE walls, and differences in reinforcement loads between the nominally identical sections were observed (e.g., Figures 4 through 6, Table 1). Potential sources of variability include the: (1) material properties and dimensions; (2) placement of reinforcement and backfill; (3) the uniformity of the fill surface onto which the reinforcing strips were placed; (4) compaction effort; (5) foundation stiffness; (6) strain measurements (e.g., measurement error, adhesive creep, etc.); and, (7) other unidentified sources.

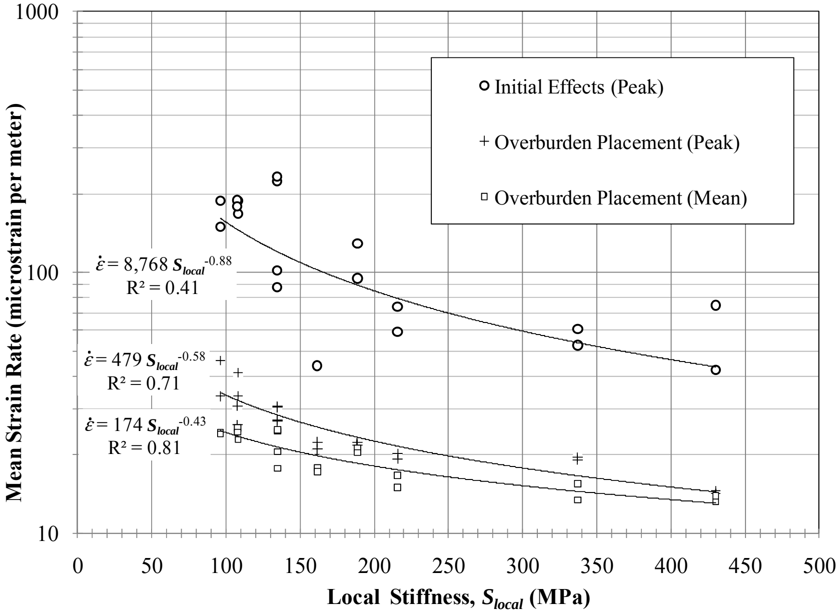

Figure 6. Effect of local reinforcement stiffness on peak initial and overburden placement induced tensile strain rate.

SUMMARY AND CONCLUSIONS

Reinforcement strain performance data were presented and discussed for two very tall steel reinforced earth walls. An analysis of twenty instrumented reinforcement strips found that on average, 1.52 m of backfill (+/-9% per strip, +/-54% overall) contributed to initial installation and compaction-related reinforcement strain, the average and *COV* of which was 93 $\mu\varepsilon$ and 25% per strip, respectively. The mean and *COV* of initial strain rate was found to be 90 $\mu\varepsilon$ and 24%, respectively. The average strain rate due to continued placement of overburden was one fourth of the initial strain rate due to compaction activities and other initial installation effects. The K-Stiffness and Ehrlich and Mitchell methods, which consider the effects of reinforcement stiffness, predict the observed initial reinforcement strains fairly well, whereas the Simplified and Coherent Gravity methods under-predict initial strains for the reinforcement strips evaluated. Local reinforcement stiffness was found to play a significant role in the rate of strain accumulation in the steel reinforcement strips, and explains up to 81% of the variability in the rate of strain for normal overburden placement activities at the third runway MSE walls.

ACKNOWLEDGEMENTS

We thank the Port of Seattle for providing helpful information about the wall construction and HNTB Corp. who provided project management and civil engineering services for the MSE walls. We gratefully acknowledge the contributions of Mike Bailey of Hart Crowser, Inc., the geotechnical engineer of record, and the contractor's Instrumentation Engineer, P. Erik Mikkelsen of GeoMetron, Inc., and Instrumentation Specialist, Dave Yonemitsu, of Yonemitsu Geotechnical Services.

REFERENCES

Allen, T. M., Bathurst, R. J., Holtz, R. J., Walters, D., and Lee, W. F. (2004). "New method for prediction of loads in steel reinforced soil walls." *J. of Geotech. and Geoenv. Engrg.,* Vol. 130, No. 11, ASCE, pp. 1109-1120.

Allen, T. M., Christopher, B. R., Elias, V., and DiMaggio, J. A. (2001). "Development of the simplified method for internal stability design of mechanically stabilized earth (MSE) walls." WSDOT Research Rep. WA-RD 513.1.

Anderson, L. R., Sharp, K. D., and Harding, O. T. (1987). "Performance of a 50-foot high welded wire wall." *Proc., Soil Improvement—A Ten Year Update*, GSP No. 12, J. P. Welsh, ed., ASCE, New York, 280–308.

Christopher, B. R., Gill, S. A., Giroud, J.-P., Juran, I., Mitchell, J. K., Schlosser, F., and Dunnicliff, J. (1990). *Reinforced Soil Structures, Vol. 1 Design and Construction Guidelines*" *FHWA Rep. FHWA-RD-89-043*, U.S. Department of Transportation, Federal Highway Administration, Washington D.C., 301 p.

Ehrlich, M. and Mitchell, J.K. (1994) "Working Stress Design Method for Reinforced Soil Walls,"*J. of Geotech. Engrg.*, Vol. 120, No. 4, ASCE, pp. 625 – 645.

Elias, V., Christopher, B. R., and Berg, R. R. (2001). "Mechanically stabilized earth walls and reinforced soil slopes—Design and construction guidelines." *FHWA-NHI-00-043*, Federal Highway Administration, Washington, D.C., 394 p.

Juran, I., and Schlosser, F. (1978) "Theoretical Analysis of Failure in Reinforced Earth Structures," *Proceedings, Symposium on Earth Reinforcement*, ASCE, Pittsburgh, pp. 528-555.

Neely, W.J. (1993) "Field Performance of a Retained Earth Wall," *Renforcement des Sols: Experimentations en Vraie Grandeur des Annees 80*, Paris, pp. 171-200.

Neely, W.J. (1995) Discussion of "Working Stress Design Method for Reinforced Soil Walls," *J. of Geotech. Engrg.*, Vol. 121, No. 11, ASCE, pp. 818 – 820.

Sankey, J. E., and Soliman, A. (2004) "Tall Wall Mechanically Stabilized Earth Applications," *Geo-Trans 2004,* GSP No. 126, Reston/Virginia, pp. 2149-2158.

Schlosser, F. (1978) "History, Current Development, and Future Developments of Reinforced Earth," *Symposium on Soil Reinforcement and Stabilizing Techniques*, sponsored by New South Wales Institute of Technology and the University of Sidney, Australia.

Schlosser, F., and Segrestin, P. (1979) "Dimensionnement des Ouvrages en Terre Armee par la Methode de l'Equilibre Local," *Int. Conf. on Soil Reinforcement: Reinforced Earth and Other Techniques*, Paris, Vol. 1, pp. 157-162.

Stuedlein, A.W., Mikkelsen, P.E., and Bailey, M.J. (2007) "Instrumentation and Performance of the Third Runway North MSE Wall at Seattle-Tacoma International Airport," *Field Measurements in Geomechanics 2007*, GSP No. 175, ASCE, J. DiMaggio and P. Osborn, Eds., Reston, Virginia. pp. 1-14.

Stuedlein, A.W., Bailey, M.J., Lindquist, D.D., Sankey, J., and Neely, W.J. *(*2010a*)* "Design and Performance of a 46 m High MSE Wall," *J. Geotech. and Geoenv. Eng.*, Vol. 136, No. 6. ASCE.

Stuedlein, A.W., Allen, T.M., Holtz, R.D., and Christopher, B.R. *(*2010b*, Submitted)* "Assessment of Reinforcement Strains in Very Tall MSE Walls," *J. Geotech. and Geoenv. Eng., Manuscript submitted for publication.*

Coherent Gravity: The Correct Design Method for Steel-Reinforced MSE Walls

Peter L. Anderson, P.E., M.ASCE[1], Robert A. Gladstone, P.E., M.ASCE[2], James L. Withiam, Ph.D., P.E., D.GE, M.ASCE[3]

[1]The Reinforced Earth Company, 133 Park Street North Reading, MA 01864; PH (978) 664-2830; FAX (978) 664-2831; Email: panderson@reinforcedearth.com

[2]Association for Metallically Stabilized Earth, P.O. Box 9142, McLean, VA 22102; PH (703) 749-3033; FAX (703) 749-3034; Email: bobgladstone@amsewalls.org

[3]D'Appolonia, 275 Center Road, Monroeville, PA 15146; PH (412) 856-9440; FAX (412) 856-9535; Email: jlwithiam@dappolonia.com

ABSTRACT

The Coherent Gravity Method has been used for more than three decades for design of Mechanically Stabilized Earth (MSE) structures. This paper discusses the history and essential characteristics of the Coherent Gravity Method and compares it to other available design methods such as the tie-back wedge, structure stiffness and simplified methods, and to monitored wall performance. These comparisons show that the Coherent Gravity Method accurately models the behavior of MSE structures reinforced with steel reinforcements, demonstrating why it is the design method recommended by the MSE industry and preferred by state departments of transportation.

INTRODUCTION

At the invitation of the Federal Highway Administration (FHWA), Reinforced Earth® structures were introduced in the US in 1971. The success of this new technology spawned competing systems, the generic name Mechanically Stabilized Earth (MSE), and a new and vibrant industry. Design of MSE walls with inextensible (steel) reinforcements has, from the beginning, been performed by assuming the MSE structure behaves as a rigid body, sized to resist external loads applied by the retained soil and by any surcharge, while internal stability is verified by checking against reinforcement pullout and tensile rupture. This design method, derived from basic soil mechanics, is known as the Coherent Gravity Method.

In the 1970s, the Coherent Gravity Method was refined by several MSE-specific research studies to include a bi-linear internal failure plane and a variable state of stress based on depth within the structure. From extensive usage, reinforcement pullout resistance parameters were developed for both ribbed reinforcing strips and welded wire mesh reinforcement and the behavior of steel-reinforced MSE structures became well understood and accepted. The development of extensible (geosynthetic) reinforcements, in the late 1970s, necessitated use of the Tieback Wedge design method to account for differences in both internal stress distribution and deformation characteristics evident in MSE structures reinforced with extensible reinforcements. There was some confusion among engineers due to differences between these two design methods, giving rise to two additional design methods which are also discussed below. Meanwhile, the validity of the Coherent Gravity Method was being proven in tens of thousands of highway and other structures and it became the MSE structure design method either accepted or required by the majority of state departments of transportation (DOTs).

THE COHERENT GRAVITY METHOD

The Coherent Gravity Method was developed by postulating MSE structure behavior, observing actual structures, and interpreting observations in terms of the fundamentals of statics and soil mechanics. This process spanned a decade, culminating in three symposia dedicated to this increasingly accepted technology: the *Symposium on Earth Reinforcement* (Pittsburgh, 1978), the *Symposium on Soil Reinforcing and Stabilizing Techniques* (Sydney, 1978) and *The International Conference on Soil Reinforcement*, (Paris, 1979). The proceedings, containing the works of recognized geotechnical and MSE experts such as Vidal, Schlosser, Long, Juran, Segrestin, Baquelin, Guilloux, McKittrick, Mitchell and many others, include the extensive research on Reinforced Earth begun in 1969 by the French Highway Administration and carried forward by many of the symposium authors.

Studies reported at these symposia included model and full scale test walls and 10 years of instrumentation of in-service structures (Baquelin, 1978), theoretical modeling of the forces in Reinforced Earth structures (Juran and Schlosser, 1978), and the keynote address to the Sydney symposium, "Reinforced Earth: Application of Theory and Research to Practice" (McKittrick, 1978). In 1979, Schlosser and Segrestin reported on a "Local Stability Analysis Method of Design of Reinforced Earth Structures", and Schlosser and Guilloux presented, "Friction Between Soil and Strips in Reinforced Earth Structures." Later that year the French Ministry of Transport issued "Reinforced Earth Structures, Recommendations and Rules of the Art" (Ministry of Transport 1979). Collectively, these works defined the Coherent Gravity Method for the design of Reinforced Earth (generically, MSE) structures. The method included a bi-linear internal failure plane, a state of stress varying with depth within the structure, and high-pullout-resistance reinforcements (originally ribbed strips, with data becoming available later for welded wire mesh reinforcements). High pullout resistance and minimal reinforcement movement and elongation are among the principal characteristics of this design method.

The effects of externally applied loads on the reinforced soil mass, and the tendency of those loads to increase vertical and horizontal stresses within the structure, were confirmed by an extensive finite element study of 6-m and 10.5-m high walls conducted by the lead author of this paper in 1983. In 1987, the Coherent Gravity Method was presented in its entirety, including worked example calculations, by Mitchell, et al in NCHRP Report 290 (NCHRP, 1987). The finite element studies were further discussed by Schlosser at the 1990 *Specialty Conference on Design and*

Performance of Earth Retaining Structures at Cornell University (Schlosser, 1990). Characteristics of the Coherent Gravity Method, shown in Figure 1, are:

- A rectangular cross section ("block") defined by the structure height, H, and the reinforcement length, L;
- Application of vertical and horizontal forces to the block, creating eccentric loading;
- A Meyerhof bearing pressure distribution at the base of the structure to determine foundation reactions and the repeated use of Meyerhof to determine the vertical earth pressure at each reinforcement level (Meyerhof, 1953);
- A state of stress decreasing from at rest (K_o) at the top of the structure to active (K_a) at a depth of 6 m and more;
- The resulting tensile forces in the reinforcements, determined from the horizontal earth pressure multiplied by the tributary area of the wall face restrained by the reinforcement at that level;
- The bilinear failure surface (envelope of maximum tension) that separates the active from the resistive zone; and
- The inextensibility and high pullout resistance of the reinforcements which maintain the internal stability of the block.

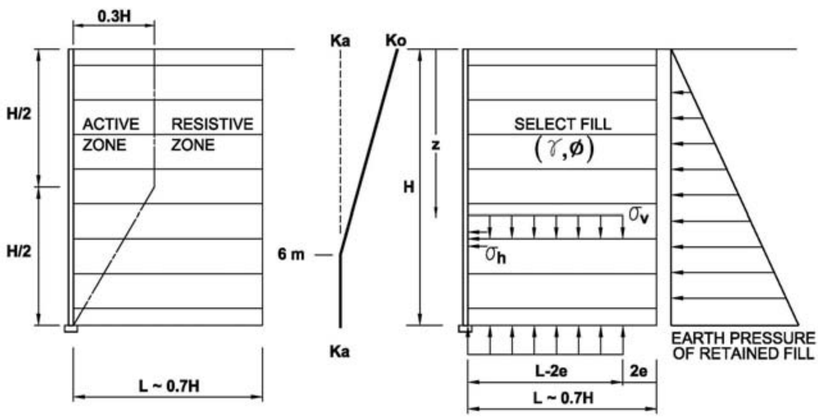

Figure 1. Characteristics of the Coherent Gravity Method

THE TIEBACK WEDGE METHOD

The Tieback Wedge Method was developed by Bell, et al. (1975) as an extension of the trial wedge method from traditional soil mechanics (Huntington, 1957), and has always been the appropriate design method for geosynthetic-reinforced MSE walls. In an MSE wall with geosynthetic reinforcements, the failure plane is assumed to develop along the Rankine rupture surface defined by a straight line oriented at an angle of 45+ϕ/2 from the horizontal and passing through the toe of the wall. Sufficient deformation is assumed to occur for an active earth pressure condition to exist from top to bottom of wall. The Rankine failure plane is not modified by inclusion of the extensible geosynthetic reinforcements. Therefore, reinforcement strain actually allows the failure plane to develop and the geosynthetic reinforcements, acting as tiebacks, restrain the active wedge from failing. This contrasts sharply with the Coherent Gravity Method where the shape of the bilinear failure plane is based on the location of maximum reinforcement tension, the failure plane does not actually develop, the active wedge does not displace, and the inextensibility of the steel reinforcements prevents structure deformation.

THE STRUCTURE STIFFNESS METHOD

The Structure Stiffness Method was developed by Christopher, et al. (1990) based on instrumentation of full scale test walls and review of data reported in the literature from instrumented in-service walls. The Structure Stiffness Method is similar to the Tieback Wedge Method, however a bi-linear failure plane is assumed for inextensible (steel) reinforcements and a Rankine failure plane angled at $45+\phi/2$ from the horizontal is assumed for extensible (geosynthetic) reinforcements. The lateral earth pressure coefficient, K_r, is based on a complex formula that takes into account the global stiffness of the reinforcement, where the global stiffness is directly related to the area of tensile reinforcement times the reinforcement modulus of elasticity. Therefore, as the reinforcement density increases, the global stiffness and the resulting coefficient of earth pressure, K_r also increase. This method was not adopted by state DOTs and, therefore, does not appear in any AASHTO specifications. However, the method did lead to development of the earth pressure ratio K_r/K_a, now used in the Simplified Method.

THE SIMPLIFIED METHOD

The Simplified Method was developed to create a single design procedure applicable to MSE walls reinforced with either inextensible or extensible reinforcements. The term "simplified" refers to the elimination of the requirement to determine the vertical stress at each reinforcement layer for inextensible (steel) reinforcements, as required in the Coherent Gravity Method. Instead of calculating the increase in internal vertical stress due to overturning, the Simplified Method applies a multiplier of 1.2 to the soil overburden, γz, at each (inextensible) reinforcement level. However, no such multiplier is used with extensible reinforcements. The Simplified Method uses the Coherent Gravity Method's bi-linear failure plane for walls reinforced with inextensible reinforcements, and the Rankine failure plane at an angle of $45+\phi/2$ from the horizontal, for extensible reinforcements. In general, the Simplified Method is the Tieback Wedge Method with K_r/K_a ratios adopted from development of the Structure Stiffness Method.

COMPARING THE DESIGN METHODS

Prior to development of the Simplified Method, the Coherent Gravity Method was used for design of MSE walls reinforced with inextensible (steel) reinforcements and the Tieback Wedge Method was used for design of MSE walls reinforced with extensible (geosynthetic) reinforcements. Design guidance for these methods was published in 1990 by Task Force 27 (AASHTO, 1990) and was included in the AASHTO Standard Specifications for Highway Bridges the following year (AASHTO, 1991). The Simplified Method was added to the AASHTO Standard Specifications in 1997 (AASHTO, 1997), but the Coherent Gravity and Tieback Wedge methods continued to be permitted for design under AASHTO, subject to approval by the applicable DOT. Today, both the Coherent Gravity Method and the Simplified (Tieback Wedge) Method are outlined in Section 11 of the 2009 AASHTO LRFD Interim Bridge Design Specifications (AASHTO, 2009).

The following sections explain the behavior differences between inextensible (steel) and extensible (geosynthetic) reinforcements. This discussion clearly demonstrates that the Coherent Gravity Method should be used for design of MSE walls with inextensible reinforcements, and that the Simplified (Tieback wedge) Method should be used for design of MSE walls with extensible reinforcements.

Differences in Reinforcement Behavior. Pullout tests on inextensible and extensible soil reinforcements begin the same, regardless of reinforcement type. The reinforcements are placed between layers of compacted soil in a pullout box and an overburden load is applied to the soil by an air bladder or mechanical means. The pullout force is applied to the leading end of the soil reinforcement and the pullout force and resulting displacement of the reinforcement are measured at frequent intervals. The pullout resistance of the reinforcement should be determined at a displacement of 20 mm (Christopher et al, 1990).

The applied pullout force and resulting displacement of the reinforcement are measured simultaneously, but this is where the similarities between the reinforcement types ends. Because inextensible reinforcements experience virtually no elongation, displacement is measured at the leading end where the load is applied. For extensible reinforcements however, displacement is measured at the trailing end, opposite from the end where the load is applied. This difference is necessary because significant elongation of the extensible reinforcement occurs, but by measuring displacement at the trailing end, deformation of the geosynthetic reinforcement is eliminated from the measurement. Recognizing this major difference in test protocol is fundamental to understanding why different design methods should be used for inextensible and extensible reinforcements.

Inextensible (Steel) Reinforcement. With inextensible reinforcements, the displacement at the leading end is nearly the same as the displacement at the free end because reinforcement strain is negligible. The friction developed between the reinforcement and the soil is determined for a leading edge displacement of 20 mm, and the transfer of load to the soil via friction is uniformly distributed over the full length of the reinforcement.

In an actual structure, the load is applied to the reinforcement by the soil within the active zone, which is trying to escape through the wall face. The magnitude of this earth pressure depends on the vertical stress and the coefficient of lateral earth pressure. Vertical stress is a function of the overburden pressure, which increases with depth in the structure, while the coefficient of lateral earth pressure varies from at rest (K_o) at the top of the structure to active (K_a) at a depth of 6 m and deeper. The horizontal earth pressure becomes tension in the reinforcements through the mechanism of friction.

The tension in the reinforcement is greatest at the line of maximum tension (the potential failure surface) (Figure 2), and decreases gradually over the full reinforcement length until near the free end, where the tension decreases rapidly to zero. Significant tension is observed over the full length of the reinforcements.

Figure 3 presents reinforcement maximum tensile loads, calculated from post-construction strain measurements, at seven reinforcement levels within the tallest (45-m high) Reinforced Earth wall at Sea-Tac International Airport in Seattle (Stuedlein, 2005). The line in the figure labeled "Coherent Gravity" shows the reinforcement tensions from the project design calculations. Note the excellent agreement between actual reinforcement loads and those calculated by the Coherent Gravity Method.

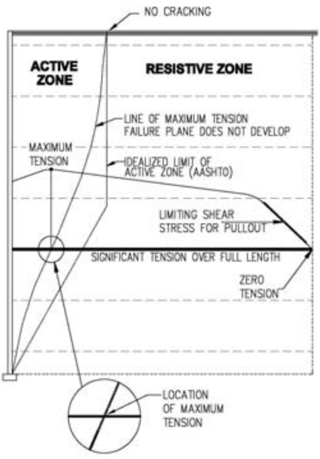

Figure 2. Inextensible Reinforcement Tension

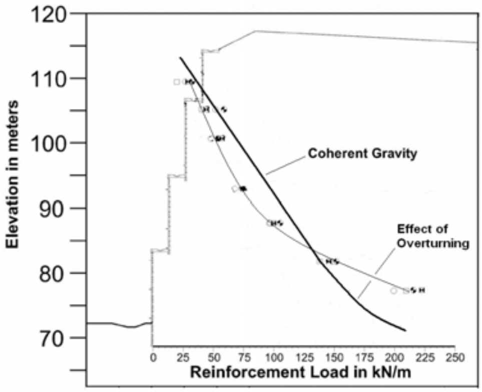

Figure 3. Measured Loads in Inextensible Reinforcement

As was shown in Figure 2, the tension is distributed over nearly the entire reinforcement length. The compressive strength and shear strength of the soil combine to make the MSE structure behave as a rigid body. This rigid body behavior is also evident in Figure 3, in the magnitude of the maximum reinforcement tension, which increases significantly toward the bottom of the wall. The increase is magnified by the overturning effect of the externally applied loads. This overturning effect, determined by the Meyerhof (1953) calculation, is considered by the Coherent Gravity Method but is not considered by the Simplified Method.

Extensible (Geosynthetic) Reinforcement. When performing pullout testing on extensible (geosynthetic) reinforcement, displacement must be measured at the trailing end of the reinforcement, not the end at which the load is applied. This is because extensible reinforcement undergoes significant strain under load, meaning when the leading edge has displaced 20 mm, the trailing end typically will not have displaced at all. Until trailing end displacement equals 20 mm, the length over which shear stresses have developed is unknown and load transfer from the soil to the reinforcement cannot be calculated over the full reinforcement length.

Terre Armee Internationale studied the difference in pullout resistance between inextensible and extensible reinforcements (Segrestin and Bastick, 1996). In this study, 40-mm wide ribbed steel strips and 100-mm wide polyester straps, in 6-m and 8-m lengths, were tested and compared in pullout. The steel strips are inextensible; the geosynthetic straps, though extensible, are among the least extensible geosynthetic soil reinforcements available. Figure 4 and Figure 5 show Segrestin's results for the 6-m long reinforcements; results for the 8-m long reinforcements were similar.

Figure 4 shows that, for a 40 mm leading edge displacement, the trailing end of the inextensible (steel strip) reinforcement displaced 38 mm while the trailing end of the polyester strap had zero displacement. In addition, the displacement of the polyester strap at its mid-point was only 1.6 mm, indicating that virtually no load was induced on the back 3 m of this 6.0-m long reinforcement. Figure 5 shows the tensile load developed in the reinforcements during the pullout test. Note that when the leading edge of both reinforcements had displaced 40 mm, the tensile load in the steel reinforcement was 38.4 kN, compared to the 22.5 kN load measured in the polyester reinforcement. The inextensible reinforcement carried 170 percent of the load with only 2.5 percent as much elongation as the extensible reinforcement.

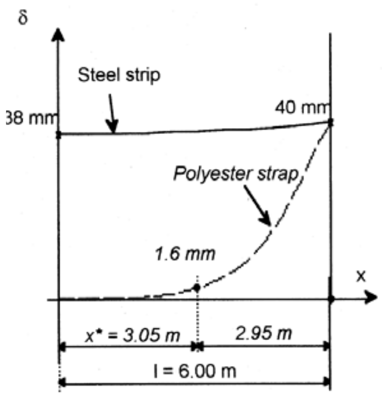

Figure 4. Reinforcement Displacement

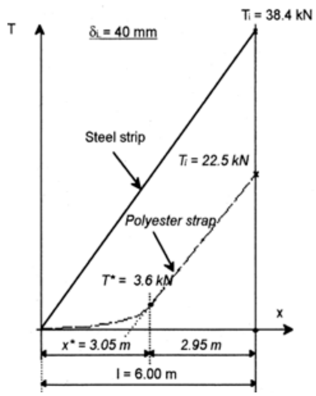

Figure 5. Reinforcement Load

Taken together, Figures 4 and 5 show clearly that inextensible (steel) reinforcements work along their entire length. The friction which is mobilized along the inextensible reinforcement is uniform, but less than the limiting shear stress of the soil. The safety factor against pullout is due to the extra shear stress which can be mobilized along the full length of the reinforcement. Conversely, extensible (geosynthetic) reinforcements make use of only the minimum adherence length necessary to transfer the load to the soil. The friction which is mobilized along this length is equal to the limiting shear stress of the soil. The extra reinforcement length which remains available, but is not mobilized, provides the safety factor in pullout.

Due to the extensibility of geosynthetic soil reinforcements, the reinforcement will deflect at the failure plane as shown in Figure 6. Tension in the reinforcement will be greatest along the failure plane and will decrease rapidly behind the failure plane, based on the limiting shear stress of the soil (Figure 7, Carrubba, et al., 1999). As was seen in Figure 5 and confirmed in Figure 7, pullout tests indicate the tension in extensible reinforcements may reduce to zero a short distance beyond the failure plane, depending on soil-reinforcement friction and reinforcement extensibility.

This analysis shows that extensible reinforcements, including polyester straps, are not mobilized over their full length, and confirms what was found from the monitoring of actual structures reinforced with geosynthetic soil reinforcements (Simac, et al., 1990, Carrubba, et al., 1999) and from finite element studies (Ho, et al., 1993), especially at the bottom of structures. These observations mean that MSE structures reinforced with extensible (geosynthetic) reinforcements do not behave as rigid bodies (coherent gravity structures), while MSE structures with inextensible (steel) reinforcements do behave as coherent gravity structures.

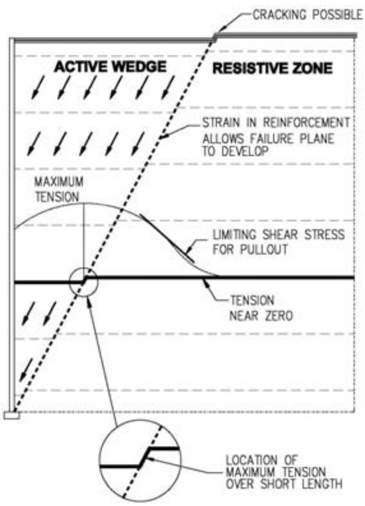

Figure 6. Extensible Reinforcement

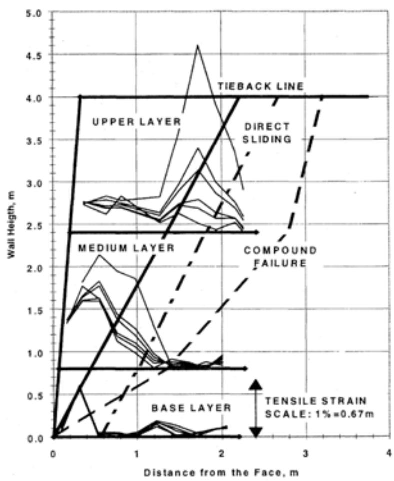

Figure 7. Extensible Reinforcement Tension

CONCLUSIONS

Inextensible (steel) MSE reinforcements are under tension over their full length, forming a coherent gravity mass. The measured reinforcement tensions clearly indicate an overturning effect consistent with Meyerhof (1953). The Coherent Gravity Method includes this overturning effect and predicts the measured tensions reasonably well. Extensible (geosynthetic) reinforcements are not under tension over their full length so an extensibly-reinforced MSE structure is not a coherent gravity mass. The Tieback Wedge Method is an accepted method for design of structures reinforced with extensible reinforcements and the Simplified Method is an MSE-specific version of the Tieback Wedge Method. Therefore, the Coherent Gravity Method should be used for design of MSE walls reinforced with inextensible (steel) reinforcements and the Simplified (Tieback wedge) Method should be used for design of MSE walls with extensible (geosynthetic) reinforcements.

ACKNOWLEDGMENTS

Figure 3 is adapted from an internal memorandum from Hart Crowser to members of the Sea-Tac Airport project team, which included the lead author's employer, The Reinforced Earth Company. Figures 4 and 5 were part of an internal Reinforced Earth Company report and were later published as cited (Segrestin and Bastick, 1996). Figure 7, from the cited paper by Carrubba et al., was originally published in the *Geosynthetics '99 Conference Proceedings, Volume* 2, and is reprinted with permission of the Industrial Fabrics Association International, all rights reserved.

REFERENCES

AASHTO (1990). *Task Force 27 Report, In Situ Soil Improvement Techniques*, AASHTO-AGC-ARTBA, subcommittee on New Highway Materials, Washington, pp. 4-38.

AASHTO (1991). *Standard Specifications for Highway Bridges, 1991 Interims*, American Association of State Highway and Transportation Officials, Washington, DC.

AASHTO (1997). *Standard Specifications for Highway Bridges, 1997 Interims*, American Association of State Highway and Transportation Officials, Washington, DC.

AASHTO (2009). *LRFD Bridge Design Specifications, 2009 Interims*, American Association of State Highway and Transportation Officials, Washington, DC.

Baquelin, F. (1978) “Construction and Instrumentation of Reinforced Earth Walls in French Highway Administration”, *Symposium on Earth Reinforcement*, ASCE Annual Convention, Pittsburgh, PA, pp. 186-201.

Bell, J.R., Stilley, A.N., and Vandre, B. (1975). “Fabric Retained Earth Walls,” *Proceedings of the Thirteenth Annual Engineering Geology and Soils Engineering Symposium*, University of Idaho, Moscow, ID, pp. 271-287.

Carrubba, P., Moraci, N., and Montanelli, F. (1999) "Instrumented Soil Reinforced Retaining Wall: Analysis of Measurements," *Geosynthetics 99 Conference*, Boston, MA, pp. 921-934.

Christopher, B.R., Gill, S.A., Juran, I., and Mitchell, J.K., (1990). *Reinforced Soil Structures, Vol. 1, Design and Construction Guidelines*, FHWA-RD-89-043.

Ho, S.K. and Rowe, R.K. (1993) "Finite Element Analysis of Geosynthetics-Reinforced Soil Walls" *Geosynthetics 93 Conference*, Vancouver, BC, pp. 203-216.

Huntington, W.C. (1957), "Trial Wedge Method," *Earth Pressures and Retaining Walls*, John Wiley & Sons, Inc., New York, NY, pp. 73-109.

McKittrick, D.P. (1978) "Reinforced Earth: Application of Theory and Research to Practice", keynote paper, *Symposium on Soil Reinforcing and Stabilizing Techniques*, Sydney, Australia.

Meyerhof, G.G. (1953) "The Bearing Capacity of Foundations under Eccentric and Inclined Loads," *Proc. 3rd International Conference on Soil Mechanics and Foundation Engineering*, Zurich, Switzerland, Vol. 1, pp. 440-445.

Ministry of Transport (1979). "Reinforced Earth Structures, Recommendations and Rules of the Art", Direction of Roads and Road Transport, (English Translation) Paris, France, pp. 1-194.

NCHRP 290 (1987), "National Cooperative Highway Research Program Report 290, Reinforcement of Earth Slopes and Embankments," Transportation Research Board, Washington, D.C.

Segrestin, P. and Bastick, M. (1996). "Comparative Study and Measurement of the Pull-Out Capacity of Extensible and Inextensible Reinforcements," International Symposium on Earth Reinforcement, Fukuoka, Kyushu, Japan, A.A. Balkema, pp. 139-144.

Schlosser, F. and Guilloux, A. (1979) "Friction between Soil and Strips in Reinforced Earth Structures", *International Conference on Soil Reinforcement*, Paris, France, Volume I, pp. 151-156.

Schlosser, F. and Segrestin, P. (1979) "Local Stability Analysis Method of Design of Reinforced Earth Structures", *International Conference on Soil Reinforcement*, Paris, France, Volume I, pp. 157-162.

Schlosser, F. (1990) "Mechanically Stabilized Earth Retaining Structures in Europe", *Specialty Conference on Design and Performance of Earth Retaining Structures*, Geotechnical Engineering Division, American Society of Civil Engineers, Cornell University, Ithaca, NY, pp. 347-398.

Simac, M.R., Christopher, B.R., Bonczkiewicz, C. (1990) "Instrumented Field Performance of a 6-m Geogrid Soil Wall," *Proceedings, 4th International Conference on Geotextiles Geomembranes and Related Products*, The Hague, Netherlands, pp. 53-59.

Stuedlein, A. (2005) "Third Runway Instrumentation Monitoring-October 2005", Hart Crowser Memorandum.

Effects of Second-Order Design Factors on the Behavior of MSE Walls

William J. Neely[1] and Siew L. Tan[2]

[1] Retaining Wall Services, Inc., 1660 Hotel Circle North, Suite 304, San Diego, CA 92108; email: wneely@retainingwallservices.com
[2] PanGEO, Inc., 2021A Minor Ave. E., Seattle, WA 98102; email: stan@pangeoinc.com

ABSTRACT

This paper examines a number of second-order design factors and gives practical examples of the types of problems that may develop in the field if they are not properly accounted for in MSE wall design. Each example includes a brief review of standard practice, results from field observations and measurements and practical guidance for designers.

INTRODUCTION

Mechanically stabilized earth (MSE) retaining walls are a common feature of urban highway and other construction projects. The technology is widely accepted and understood and the performance of MSE walls over the past thirty years has generally been excellent. The principal components are precast concrete facing panels, metallic or geosynthetic soil reinforcement and granular backfill. Today there are numerous comprehensive design manuals and computer codes available, allowing designers to analyze both internal and external stability of reinforced soil masses in great detail. However, the ease of carrying out calculations, taking into account complex loadings and wall geometries, leads many to believe that other, second-order factors, not specifically addressed in the calculations, do not need to be considered. The purpose of this paper is to draw attention to some of these factors.

BEARING PADS IN HORIZONTAL JOINTS

The principal function of bearing pads is to maintain horizontal joint width. This is necessary to provide in-plane flexibility in the event of differential settlement and to maintain facing permeability. They also act to prevent concrete-to-concrete contact and are the primary means of transferring axial loads in the plane of the wall face to the leveling pad at the bottom of the wall.

Bearing pads are manufactured from several different materials and are available in a range of sizes and shapes, depending on panel size and joint configuration. The most common materials are high density polyethylene (HDPE), ethylene propylene dimonomer (EPDM) and neoprene. MSE walls comprising nominal 1.5m square panels have two bearing pads per horizontal joint. Dimensions of individual bearing

 2010 Earth Retention Conference (ER2010)

pads range from 280mm x 64mm for a common HDPE waffle-type pad to 100mm x 85mm for a widely used EPDM bearing pad; nominal thickness is usually 20mm. One wall system uses 150mm x 70mm HDPE pads with 1.8m wide panels and another system uses 75mm x 50mm EPDM pads with 2.7m wide panels.

The nominal concrete-pad contact area (based on overall dimensions) varies by a factor of almost five, with the pads having the smallest contact area being used with the widest panels. For example, the nominal contact stresses on bearing pads in a joint 4.5m below the top of a wall range from 0.7MPa to about 6MPa, based only on the weight of 0.15m thick precast concrete panels above the joint, for panel widths between 1.5m and 2.7m.

Load-compression data for the HDPE waffle-type bearing pad (280mm x 64mm) are presented in Figure 1 where it may be seen that after an initial elastic response yield occurs at about 180kN, corresponding to a nominal contact stress of 10MPa. At yield the compression is about 3mm, representing a joint closure from 20mm to 17mm. Load deformation behavior may be very different for bearing pads of different geometry, contact area and material type; Figure 1 includes load-compression data for 110mm x 64mm x 25mm EPDM bearing pads.

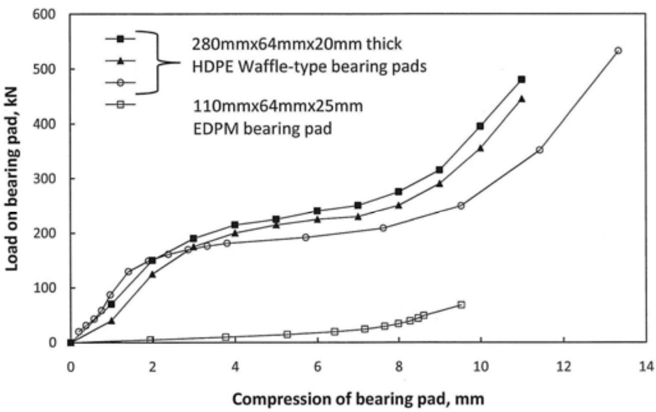

Figure 1. Typical load-compression data for HDPE and EDPM bearing pads

To avoid excessive compression, the design should consider the loads to be supported and the load-deformation behavior of the bearing pads. Excessive loads in horizontal joints may result in crushing of the bearing pads and spalling of the concrete; see Figure 2.

Figure 2. Spalling of concrete at bearing pad locations

Load cell measurements of vertical forces at the bottom of individual columns of MSE wall panels are available (Chida and Nakagaki, 1979; Bastick et al., 1993; Runser et al., 2001). Runser et al. (2001) found that the vertical load at the top of the leveling pad increased as wall height increased during construction and that the measured load was always greater than the weight of panels supported on the leveling pad. At the end of construction of the 17m high wall the measured vertical load at the top of the leveling pad exceeded two times the weight of the panels. These three sets of field measurements are summarized in Figure 3. These field measurements may be used as a basis for determining the vertical load in horizontal joints at depths up to 20m below the top of the wall. These loads can then be used in conjunction with the compression characteristics of the bearing pads to ensure that the specified joint widths are maintained.

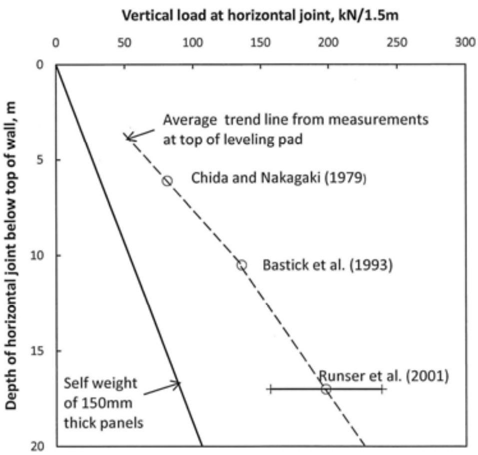

Figure 3. Variation in vertical load with height of column panels

The data in Figure 3 are based on 150mm thick panels and no top-of-wall treatments. Thicker panels and loads from a traffic barrier or sound wall should be accounted for in determining the loads to be supported by the bearing pads.

DESIGN OF LEVELING PAD

MSE wall panels are usually supported on an unreinforced concrete leveling pad, typically 300mm wide and 150mm thick. The minimum embedment depth for the leveling pad is usually 0.6m.

While careful inspection of the leveling pad to ensure correct line, grade, and offset is important, it is also important to make sure that the leveling pad can support the vertical loads in the plane of the wall face. This is especially so where walls are built on slopes and where embedment depth of short sections of leveling pad may be compromised by sloughing and/or erosion of the fill in front of the wall. In extreme cases, reduction of bearing capacity can lead to settlement of short sections of leveling pad and downward movement of the bottom one or two courses of panels. This, in turn, removes support to panels higher up the wall, often leading to unacceptably wide horizontal joints; see Figure 4.

Figure 4. Wide horizontal joint resulting from downward movement of panels due to undermining of leveling pad

These problems can be avoided by ensuring that sufficient embedment is provided to develop the necessary bearing capacity. Bearing capacity evaluations should be based on footing loads from Figure 3, where the depth to the lowest horizontal joint at the top of the leveling pad is equal to the height of the wall.

WIDE-ANGLE CONVEX CORNERS

Conventional design methodology for MSE walls is based on the tacit assumption of plane strain conditions, with design for different wall heights being based on typical sections one or two panel columns wide. This is conservative for sections well away from the ends of a wall. As illustrated in Figure 5, in design it is assumed that the section ABCD is free-standing, while in reality significant shear resistance is available on the sides AC and BD, adding to overall stability.

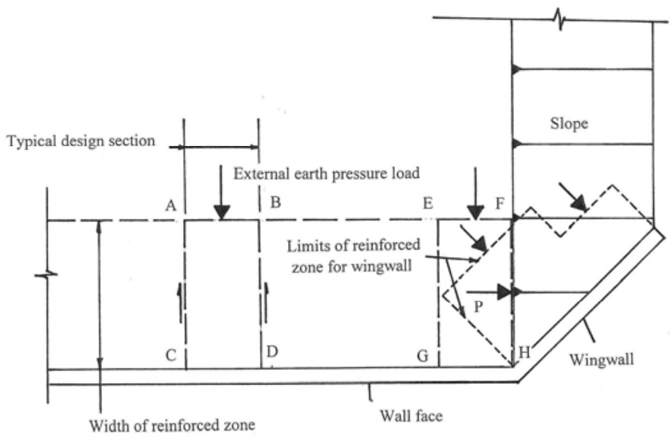

Figure 5. Analysis at convex corners

At the convex corner the design problem is three-dimensional. Block EFGH adjacent to the convex corner has less frictional resistance along EG and FH because of the reduced lateral restraint provided by the triangular wedge behind the wingwall. This is also likely to reduce pullout resistance of the soil reinforcement and increase the risk of wedge failures and opening up of panel joints in the convex corner, especially if the wingwall section supports a significant surcharge.

Convex corners are common at wingwalls to bridge abutments. As illustrated in Figure 5, there are several aspects of the three-dimensional problem that should be examined. First, the orientation of the soil reinforcement for the wingwall portion is not aligned with that of the downslope component of the lateral force from the backfill. The wingwall section is usually designed assuming lateral earth pressure at the back of the reinforced soil mass acts at right-angles to the face of the wall. However, there is an additional earth pressure load P from the main embankment fill on the plane FH. The importance of this force is accentuated where the fill slopes down from roadway level to the top of the wingwall, further reducing the weight of the triangular wedge. These factors should be taken into account in evaluating both the internal and external stability of the wingwall section beyond FH.

INTERNAL COMPRESSION OF MSE BACKFILL

Proper compaction of MSE backfill is critical to optimizing soil-reinforcement pullout resistance and minimizing wall movements. Inadequate compaction raises concerns about the effect of backfill settlement in creating additional stresses in the soil reinforcement and whether or not the stresses are large enough to cause failure at the panel-reinforcement connections.

To prevent high tensile stresses at panel-reinforcement connections should large differential settlements occur between the panels and the backfill, conventional practice is to have the surface of the fill 25-50mm above the level of the connection devices before the soil reinforcement is placed. By placing the reinforcing elements slightly above the connection level only compressive stresses, rather than tensile stresses, should exist, unless the backfill compression exceeds twice the differential height built in during construction.

Using relationships between relative density and volume change for Platte River sand (Hilf, 1991) backfill settlements have been calculated for a range of relative densities and fill thicknesses. This sand, classified as SW in the USCS system, is similar to many MSE backfill materials. Settlements were calculated using two different assumptions.

In the first calculation, the end-of-construction settlement is based on the assumption of instantaneous loading in which a thick layer of granular material possessing self weight is considered to compress as it is constructed. In this case, the maximum settlement develops at mid-height of the fill and is typical of granular materials with only a small amount of fines (<0.074mm) in which time-dependent and/or creep compressions are negligible. The pattern of internal compression is approximately parabolic, with the maximum occurring at mid-height and zero compression at the surface of the fill.

The second calculation is based on the assumption that all settlement occurs only once all the fill has been placed. In this case, which is more typical of fills containing appreciable fines and exhibiting significant time-dependent compression behavior, the maximum settlement develops at the top of the fill layer.

The end-of-construction settlements based on the assumption of instantaneous loading are presented in Figure 6, where the settlement at mid-height of the fill is shown as a function of fill height and relative density. The dominant effect of the relative density is clear, with end-of-construction settlements increasing by about 100 percent for a fill height of 20m as the relative density decreases from 73 to 50 percent.

As the fines content of the backfill increases, a greater portion of the end-of-construction settlement would be expected to be time dependent, in keeping with the second assumption where all compression occurs only after all the fill has been placed. For a fill height of 24m and a relative density of 73 percent, the end-of-construction settlement increases from about 60mm assuming instantaneous compression to 175mm assuming no compression occurs until all the fill has been placed. Actual settlement conditions would lie between these two extremes. However, poorer quality backfill containing significant fines will result in much larger internal compression which, if not properly accounted for in design and construction, could lead to overstressing and possible failure of reinforcing elements and connections.

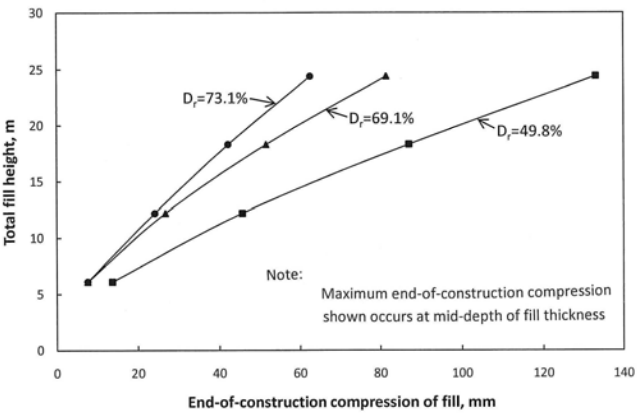

Figure 6. End-of-construction fill compression vs. fill height

SETTLEMENT OF EMBANKMENTS SUPPORTED BY BACK-TO-BACK MSE WALLS

MSE walls can accommodate significant differential settlements as a result of the in-plane flexibility of the facing panels. However, the presence of thick deposits of soft soils often means that anticipated total and differential settlements exceed those that can be safely tolerated by a conventional MSE structure. In such cases a common solution is to use a 2-stage MSE wall.

The first stage of a 2-stage wall comprises the construction of a reinforced soil mass which includes a permanent structural facing consisting of wire mesh and filter fabric. Settlement of the foundation soils under the weight of the reinforced soil mass must be completed before the precast concrete panels are attached to the soil reinforcement using specially designed adjustable connectors.

Settlement calculations are usually made considering vertical stress increases at depth based on the assumption of uniform, flexible loading. Summation of the associated vertical strains produces larger settlements at the center of the embankment than at the edges, resulting in a dish-shaped settlement profile across the width of the embankment. In reality, the embankment and MSE walls are not flexible in the transverse direction, but rigid. This has been verified in the field by Goodsen (2000) who used horizontal inclinometers to measure vertical displacements under a reinforced soil mass supported on soft, compressible soils. Goodsen's measurements show that the entire reinforced soil mass settles uniformly as a rigid block.

The difference between predicted and actual settlements at the wall face has important practical consequences. First, greater settlements at the edges of the embankment mean that the permanent wire-faced wall has to be extended to reach the final design grade, resulting in unanticipated additional costs. Second, and more important, the expectation of greater settlement in the center of the embankment than at the edges may result in instrumentation and monitoring efforts during the settlement phase being concentrated at the center. In some cases, embankments have been released for precast panel erection based on data at the center of the embankment, while settlement is still continuing at the edges where the panels are to be placed. This can lead to doglegging or buckling of the second-stage precast concrete panels; see Figure 7.

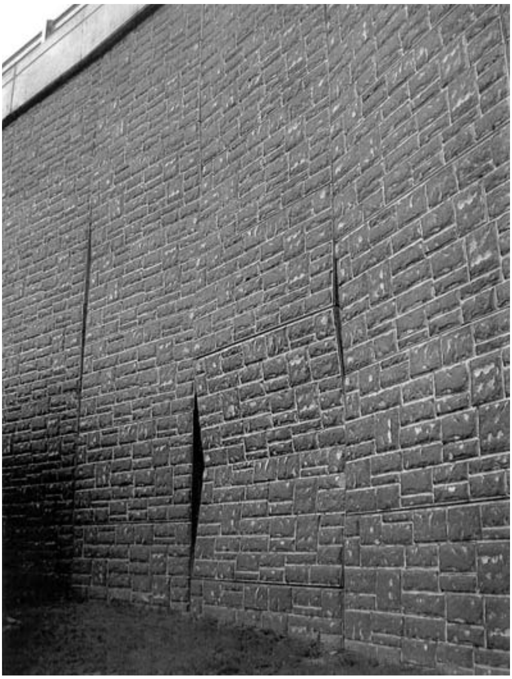

Figure 7. Doglegging of panels in 2-stage MSE wall due to continuing settlement after panel placement

While stress distributions for uniform flexible loading may be used in calculating settlements, a correction must be applied to the calculated values to account for the rigidity of the reinforced soil mass in the transverse direction. Experience suggests that a correction using Fox's (1948) method in which the vertical displacement of a vertically loaded rigid area may be approximated by the mean vertical displacement of a uniformly loaded flexible area of the same shape produces good agreement between predicted and measured settlements at the face of the wall. For a long embankment the settlement at any transverse section may be taken as one-half of the sum of the center and edge settlements, calculated by considering the embankment as a uniformly loaded flexible area.

CONCLUSIONS

Over the past several years increasing research efforts have been expended in refining and improving design methodologies for reinforced soil structures, particularly with respect to internal stability of the reinforced mass and the role played by soil-reinforcement relative stiffness. In contrast, other seemingly less important aspects of MSE wall design, construction and performance have received little or no attention from researchers, probably because they can only be studied in the field. Many of these aspects are handled on the basis of standard details or precedent, but this does not always ensure satisfactory performance. Several of these second-order factors have been discussed. Data from field observations and measurements have been presented which may be of use in evaluating the behavior of various MSE wall components or indicate areas where traditional simplified design approaches or practices may not be appropriate.

REFERENCES

AASHTO, (2002). Standard Specifications for Highway Bridges, 17th Edition, American Association of State Highway and Transportation Officials, Washington, D.C.

Bastick, M., Schlosser, F., Segrestin, P., Amar, S., and Canepa, Y., (1993). Experimental reinforced earth structure of Bourron Marlotte: Slender wall and abutment test. Proc. Intl. Symp. on Soil Reinforcement: Full Scale Experiments of the 80s, Presses de l'ENPC, Paris, France, 201-228.

Chida, S., and Nakagaki, M., (1979). Test and experiment on a full-scale model of reinforced earth wall. Proc. Intl. Conf. on Soil Reinforcement: Reinforced Earth and Other Techniques, Paris, France, Vol. II, 533-538.

Fox, E.N., (1948). The mean elastic settlement of a uniformly loaded area at a depth below the ground surface. Proc. 2nd Intl. Conf. on Soil Mech. & Found. Engrg., Vol. 1, 129.

Goodsen, M.W., (2000). Instrumentation and installation scheme on a mechanically stabilized earth wall on I-15. M.S. Thesis, Utah State University, Logan, Utah.

Hilf, J.W., (1991). Compacted Fill. Chapter 8, Foundation Engineering Handbook, 2nd Edition, Hsai-Yang Fang, Editor, Van Nostrand Reinhold, NY.

Runser, D.J., Fox, P.J., and Bourdeau, P.L., (2001). Field performance of a 17m-high reinforced soil retaining wall. Geosynthetics Intl., Vol. 8, No. 5, 367-391.

Design and Procurement Challenges for MSE Structures: Options going forward

Michael R. Simac, P.E., M.ASCE[1] and Blaise J. Fitzpatrick, P.E.[2]

[1] Earth Improvement Technologies, Inc., PO Box 1346, Fort Mill, South Carolina 29716, PH 803-548-8690; email: mike@earthimprovement.com

[2] Fitzpatrick Engineering Associates, P.C., 1237 Highfield Dr, Lawrenceville, Georgia 30043, PH 770-822-6022; email: fitzwall@bellsouth.net

ABSTRACT

Mechanically Stabilized Earth Walls (MSEWs) have been routinely used over the past 20 years. Experience with MSE structures has identified several challenging issues facing public and private owners using MSEWs for transportation corridors and land development to maximize useable land area. This paper discusses the current "state-of-practice" and offers recommendations relative to procurement and design of MSE structures to minimize short-term problems and ensure a service life consistent with nationally recognized design methods (AASHTO & NCMA). Specifically, the benefits and challenges of the owner controlled aspects of the process are discussed, such as; various options to contract for MSEWs, integration/coordination with civil site design, compatibility with geotechnical site investigation, testing, analysis, and recommendations, as well as MSE design methods, procedures, and guidelines that influence both cost and performance.

The division of professional design responsibility amongst the design team, a critical element to successful projects, is controlled by the owner. This paper provides guidance for future projects, primarily for owners, but also for design professionals, and contractors that balance prospective risks and rewards of the various procurement options available. Although focused specifically on MSEWs, Reinforced Soil Slopes (RSSs), and Segmental Retaining Walls (SRWs) encounter similar issues, such that the information presented is equally applicable to all types of MSE structures.

Successful MSEWs will be significantly influenced by the manner in which existing and improved MSE structure design standards (AASHTO / NCMA) are implemented on future projects. This paper examines that implementation process and how lessons from the last 20 years can positively influence MSEW performance going forward.

CONTRACTING FOR MSE DESIGNS – Role of the Owner

There are three general approaches currently used by owners to procure a design for MSE structures; designs supplied by the contractor, owner provided designs, or using the design-build approach. The owner may be unaware or uninformed of how the differences in each approach used to procure a MSE design, affect the design outcome. Described below are the advantages and drawbacks for each approach.

CONTRACTOR SUPPLIED DESIGNS: The most common approach used to procure an MSE design is through the contractor's material supplier. In this scenario a wall contractor provides (drawings, calculations and installation specifications) based on the Owner's contractual requirements and available civil and geotechnical information. Owners are typically steered toward the contractor supplied designs in an effort to allow competition between MSE systems and their lack of experience in producing designs. Usually the Owner's selection criteria are strongly influenced by cost, which is directly related to the design, and more importantly design assumptions. The most aggressive contractor supplied design, has a significant cost advantage. The owner must be aware that this aggressive design approach may include significantly more risk in; life-cycle costs, liberal soil strengths or available soil types, optimistic loading conditions, favorable groundwater conditions, etc. Also, some proprietary design approaches are aggressive by eliminating or altering minimum standards-of-practice, e.g. facing connection, bearing capacity, internal failure surface orientation, and global stability, etc. These designs are sometimes done by a third-party, without any contractual obligations to the owner, significantly complicating legal responsibilities when MSE performance is outside industry norms.

To minimize these disadvantages with contractor supplied designs the Owner must properly define the MSE design requirements and conditions. Owners can utilize standard specifications available through the professional organizations or material suppliers provided that the following items are clearly defined, which enhance the effectiveness of this method of procurement.

- Method of Analysis
- Minimum Design Safety Factors and Material Reduction Factors
- Designate minimum Reinforced Fill requirements, strength, and borrow source.
- Define the external / live loading conditions.
- Require a quality control testing program by the MSEW Installation Contractor.
- Owner provides MSEW specific geotechnical investigation.
- Owner assigns specific responsibility for global stability and foundation support.
- Owner to provide a third-party review and approval of contractor provided design.
- Owner provides through its civil designer a finalized site plan design with good surface water drainage design, accounting for wall batter and position.
- Owner implements a quality assurance testing program during construction.

DESIGN-BUILD APPROACH: Unfortunately the design-build approach is often confused with "Contractor Supplied Design" by many owners and site designers. Although similar, there are several procedural, contractual, and legal criteria necessary in the project specifications to invoke a true "design-build" scenario.

Design-build entities tend to follow more closely the standards-of-practice for design and construction because they are equally responsible for both, and unable to deflect criticisms or deficiencies as the other party's fault. Consequently, design-build MSEW firms with significant project experience can be trusted by the Owner. This approach requires the minimum amount of Owner involvement and knowledge.

To invoke a true design-build approach for the MSE structure, unless the entire project contract is already design-build, the Owner must define performance requirements in terms measurable limits of tolerable MSE structure movements over a specific service life, and then contractually make the Contractor responsible for:

- Selecting Design Method, Minimum Safety Factors, Material Reduction Factors
- Determining Wall geometry to meet contract finish grade.
- Determining Reinforced Fill requirements, strength, and borrow source.
- Obtaining all geotechnical information necessary to perform the design.
- Specific design responsibility for global stability and foundation support.
- Determining all internal, external and surface drainage for the MSE structure.
- Integrate design with all other buried and surface project design elements.
- Designing for all external/live loading conditions during and after construction.
- Executing a quality control testing program to verify proper installation.
- Providing MSE structure as-built drawings & survey of exact position.
- The design-build Contractor must be a licensed engineering firm in the state.
- The design-build Contractor must be a licensed "design-build contractor in state.
- Documenting professional liability insurance in its name by providing a "project policy" for twice the structure costs to cover at least 50 years or full design life.
- Repair or Replacement of MSEW for failure to meet performance requirements.

OWNER PROVIDED DESIGN: Owner Provided Design is an approach consistent with traditional (design-bid-build) method used for many construction contracts in which the MSE design is incorporated into the site design drawings. Some local plan review jurisdictions require complete MSEW plans as part of plan approval process of local jurisdictions. Routinely, the Owner retains a site (civil) designer to establish site grades, storm and surface water management, and utilities. The MSE designer simply becomes part of the Owners design team in the same manor as a structural engineer was traditionally retained for a cast-in-place reinforced concrete wall.

The key advantage of owner provided designs is integration of the MSE design into the overall site design early in the site planning process, providing the most cost effective design alternative by adjusting all site design components to accommodate constraints that are interdependent on each other. These cost savings are significantly greater than the nominal cost difference between competing MSE systems. The MSE designer develops design calculations, specifications and drawings through direct communication with other members of the Owner's design team, i.e. architect, civil engineer and geotechnical engineer. Issues related to geotechnical concerns and how the MSE is coordinated with the site grading are addressed early. Geotechnical information required for MSEW design can be obtained as part of the original site investigation streamlining geotechnical costs and design schedule for the MSE. The Owner is assured that all retaining wall design responsibility has been apportioned properly and installation costs are based on the same design, formulated specifically for their site location, and exact design requirements for owner defined risk tolerance. This ensures a true installed MSEW cost comparison, based on the same design.

Most MSE designers generally prefer the tighter controls and requirements an Owner provided design places on the Contractor. FHWA and manufacturer training has increased the number of qualified MSE designers available to the Owner. The Owner obtains much better control of the finished product, by integrating the MSE design with other design disciplines, and creating a quality assurance program ensuring construction compliance to the design. The Owner also obtains fair and equitable cost competition on the same MSE design. Contractors compete fairly on the same design, being judged on their ability to build, without incurring design liability. Material suppliers benefit by competing solely on their ability to manufacture products.

These are all favorable reasons for owners to move toward using the "owner provided design" approach, which benefit all the economic participants in the MSE market. It allows the Owner to harness the design professional's expertise to their benefit when building MSE structures. The "owner provided design" has the clearest and most direct contractual definition of responsibility amongst the design professionals, while fostering more and better communication on design and construction issues when it can best benefit the Owner from a cost and performance perspective.

COORDINATING THE DESIGN PROFESSIONALS

Coordinating the activities, responsibilities, and communication between the design professionals is the Owner's key role in building MSE structures and the focus of the contractual requirements in the three methods of contracting for those services outlined above. This coordination role is difficult because integration of the MSE system into the overall site design requires effective communication between three overlapping engineering disciplines, i.e. the site (civil) engineer, geotechnical engineer and MSE designer. The critical coordination is between MSE designer and geotechnical engineer, who need to work together, but clearly understand their division of responsibilities to achieve a successful project and outcome for the public. Understanding each professional's responsibilities should clarify the owner's coordination role for each contracting method.

SITE DESIGNER: The site/civil designer (civil engineer or landscape architect) works for the Owner to establish the site grading plan, based on existing topography, development objectives, and prevailing land use / environmental regulations. Using those constraints the site designer determines whether a steep change in grade structure (retaining wall or slope) is necessary, and the height, length, and location of such structure, to make the site development plan feasible. The site designer is also responsible for the design and layout of all site utilities; including water supply, sanitary sewer, and surface water drainage. Site surface water drainage design includes the hydrologic analysis to size; inlets, pipes, and storm water retention / detention ponds, along with their flow control (inlet/outlet). The site designer should follow the recommendations of the geotechnical engineer in establishing the site grading plan. The design-build contractor shall work to the geometric constraints established by the site designer, as shown in the contract documents.

GEOTECHNICAL ENGINEER: The project geotechnical engineer is responsible for investigating existing site conditions to determine the viability of the proposed site civil design, and makes recommendations on the suitability of existing site materials for use in construction. The geotechnical engineer should recommend; suitable slope inclinations for fills and temporary/permanent cuts, allowable soil bearing pressures, likelihood of encountering groundwater with drainage provisions to mitigate, earth pressures for retaining wall design, suitable fill types with compaction requirements, and specific recommendations to ensure global stability of slopes (and walls) or further examination of global stability of slopes, if warranted. The project geotechnical engineer is responsible for the MSE structure investigation, providing recommendations for soils properties (shear strength and unit weight), drainage systems, and analyzing/ensuring global stability of the MSE structure, except when these responsibilities are contractually assigned to the design-build contractor.

MATERIALS TESTING ENGINEER: The materials testing engineer (which often is, but does not have to be the project geotechnical engineer) is engaged to contemporaneously verify construction is proceeding according to the project plans and specifications. Likewise, a separate (or dual; i.e.; Contractor quality control, Owner quality assurance) materials testing engineer may be engaged specifically for the MSE wall or slope. This is a common requirement when the prevailing building code designates these structures for "special" inspection, dictating installation verification of; wall/slope facing elements, geosynthetic reinforcement, as well as the fill type, compaction, and allowable foundation pressures. The materials testing engineer also identifies conditions, inconsistent with the MSE designer's assumptions (as identified on plans) that may require design modifications, like; unsuitable foundation soils, groundwater flow into the reinforced soil mass, or substitution of available fill materials. Sometimes, the Owner engages the materials testing engineer to perform a third-party review of the MSE and/or site design to verify its consistency with standard design practices and make recommendations for any additional testing.

MSE DESIGNER: The MSE designer utilizes the site grading plan and geotechnical recommendations to prepare wall profiles and cross sections. The MSE designer is responsible for determining sufficient length, strength, and vertical spacing of soil (steel or geosynthetic)-reinforcement layers to ensure the external, internal, local/facing stability and compound internal stability of the reinforced soil mass for the wall geometry (height, length, and surcharge conditions) as defined on the site grading plan. The MSE design should consist of construction drawings showing proposed wall profiles with soil reinforcement layout (type, length, horizontal position and vertical spacing) along the wall length, typical wall cross sections, cross-sections for penetrations or conflicts with utilities, facing system details, and MSE construction specifications for materials, installation, and quality control testing.

GEOTECHNICAL INVESTIGATION FOR MSEWs

While it is recommended and extremely cost effective to perform site specific geotechnical investigations for MSE structures with the initial site development and/or building soils investigations, often project planning has not proceeded sufficiently to identify the exact locations of those structures. Once the site civil designer establishes the preliminary grading plan, with buildings and retaining structures, the geotechnical engineer should identify for the Owner all the geotechnical investigations necessary for site development. The geotechnical engineer should include investigation recommendations necessary for assessing slope stability and retaining structures, along with those routinely made for buildings, roadways, parking, and detention ponds. Direct input on investigation requirements from the MSE designer would be helpful, but the geotechnical engineer can proceed to consult the Owner based on the general requirements established in national MSE design guidance documents (AASHTO, Elias, et. al., Collin, Simac et. al.)

The subsurface exploration for MSE structures should consist of soil borings and test pits as performed by the geotechnical engineer. The type and extent of the exploration should be decided after review of the preliminary data obtained from a field reconnaissance by the geotechnical engineer, or MSE designer. The exploration must be sufficient to evaluate the geologic and subsurface profile in the construction area of the MSE structure, defining the groundwater and soil conditions within, behind, and beneath the proposed MSE structure.

National MSEW design guidelines provide detailed recommendations for subsurface exploration and laboratory-testing programs, consisting of: Soil borings at regular intervals to a depth of twice the structure height, and soil testing to determine the appropriate strength parameters, compressibility, and construction control values.

RESPONSIBILITY FOR GLOBAL STABILITY

Confusion over responsibility for global stability has plagued MSE structures for many years. MSE design guidelines require global stability be performed, which has lead some project geotechnical engineers to believe the MSE designer was responsible. However, consistent with building codes and long established professional practice for other retaining walls (i.e., concrete, rubble, gravity, tied-back, & sheet pile, etc.) most MSE designers exclude global stability from their work and indicate so on their construction drawings, believing the site designer and geotechnical engineer are responsible for ensuring global stability and adequate foundation support. Typically, public agency owners provide/enforce global stability measures and maximum foundation pressures. This is further complicated by differing levels of design services from various practicing MSE designers, some of whom are also qualified geotechnical engineers, which address global stability as an added benefit for their client and to minimize their own potential risk from liabilities due to the confusion.

This confusion emphasizes the owner's need to clearly define design responsibilities between these professionals. Although responsibilities vary slightly based on the contracting method chosen, by establishing the site grades and location of improvements the site civil designer has primary responsibility for global stability. The site designer and owner usually rely on the recommendations made by the project geotechnical engineer for global stability of the improvements. The very narrow set of circumstances for which the MSE designer has partial responsibility for global stability is also outlined below.

GEOTECHNICAL ENGINEER: For effective and comprehensive recommendations for site development, the project geotechnical engineer should evaluate the entire site for areas that may be subject to global instability, and provide recommendations to the Owner, site designer, and MSE designer to ensure safe performance of slopes and all types of walls throughout the project service life. The project geotechnical engineer is the most qualified professional to perform these analyses since they know more about the site conditions (soil and water) than any other party. The geotechnical engineer has the expertise to investigate, test, evaluate, and most importantly interpret the soils information to identify potential unstable areas for direct analysis. This ability to identify potentially unstable areas (by soil stratigraphy, groundwater conditions, geologic features, topographic geometry, and surcharge loadings) is much more vital to ensuring an accurate global stability analysis, than the ability to operate and manipulate a computer model.

Since the project geotechnical engineer has local knowledge of typical instability behavior, as well as the costs and capabilities for typical solutions for instability, they are better equipped to determine the most cost effective method to achieve the desired stability. The project geotechnical engineer generally understands the single solution the MSE designer can provide, increasing the length and/or strength and number of layers of geosynthetic-reinforcement necessary to ensure long term global stability. The project geotechnical engineer should analyze stability around the MSE structure, adjusting the reinforcement length, soil properties/materials, and surface geometry to obtain a stable configuration. Evaluating global stability around MSE structures is no different than any other road, embankment, earth dam or building on a hillside and for that matter any other type of retaining structure. The project geotechnical engineer recommendations ensure compliance with the Owner's selected level of risk (safety factor) relative to the desired performance.

MSE DESIGNER: In certain circumstances the MSE designer shares responsibility for ensuring global stability when the MSE structure consists of tiered walls, or is affected by compound internal stability. The setback of one single height retaining wall some distance (> 4 ft., but < 2H) from another, results in the MSE designer creating a reinforced slope, relative to the total change-in-grade. This type configuration creates unique stress concentrations and a reduction in sliding resistance at the base of the MSE structure. The influence of one or multiple walls above another in a tiered configuration must be examined using global stability analytical procedures by the MSE designer to ensure the full height interconnected reinforced soil structure is stable globally for the total change-in-grade. The MSE designer should check compound internal stability, for failure surfaces passing through the MSE structure face from behind or above the reinforced soil, which sometimes identifies portions of the MSE structure that require additional soil reinforcement (length, strength, or layers). These stability analyses for the MSE designer's share of responsibility do not relieve the geotechnical engineer from their responsibility to examine overall global stability independently.

SUMMARY and CONCLUSIONS

An owner faces numerous challenges when building MSE structures in integrating three major design disciplines; site/civil, geotechnical, and MSE designer. Three distinct contracting methods for MSE structures have been examined, with specific recommendations on making them more effective in the future, based on past experience. Effectiveness is increased by good coordination of responsibility and communication between these design disciplines, improving the likelihood of good performance. All three contracting methods seek to improve long-term performance of MSE structures by ensuring; the actual strength parameters of reinforced soil and foundation are known, global stability of the completed structure is performed, an adequate quality control / assurance testing is executed to verify compliance with plans and specifications, and appropriate internal and surface drainage has been incorporated into the MSE structure.

While all three methods of contracting for MSE structures will be used in the future. The owner-supplied design offers the owner the most control over the design, performance, and cost-benefits because the MSE structure design is accomplished using a team approach coordinated by the site designer on the owner's behalf. Having the three disciplines interact early and often through the design process, lead to streamlined design and construction costs for the entire project. Savings can not only be gained on the MSE structure itself, but also on the portions of the project affected by the MSE structure and vice-verse. Design changes during construction, due to changed soil or geometric conditions can be handled more efficiently with all three design disciplines working for the owner in a cooperative arrangement. After over twenty years experience MSE structures can now be designed and specified in a generic manner so as to not infringe on the uniqueness of proprietary systems.

Having the owner take control and provide the design up front, represents the best approach for all stakeholders to achieve the best performing MSE structure long-term at the lowest possible design and construction costs. At this stage of the market maturation process, the authors conclude Owner-provided designs appear to be the best way to improve both cost and quality of the finished product and should receive strong consideration for both public and private sector projects going forward.

REFERENCES

AASHTO (2002) "Standard Specifications for Highway Bridges," 17th Edition,

AASHTO (2007) "LRFD Bridge Design Specifications," 4th Edition, Nov. 2007 Interims

Bathurst, R.J. (1998) "Segmental Retaining Walls - Seismic Design Manual," National Concrete Masonry Association, 1st Edition, Herndon, VA, TR-160.

Collin, J., editor et. al. (1997) "Design Manual for Segmental Retaining Walls," National Concrete Masonry Association, 2nd edition. Herndon, VA, TR-127A.

Elias, V.E., Christopher, B.R. and Perkins, S. (1997) "Mechanically Stabilized Earth Walls and Reinforced Soil Slopes, Design and Construction Guidelines," prepared for Federal Highway Administration, Demonstration Project 82, Contract No.: DTFH61-93-C-000145, 371 p

Elias, V.E., Christopher, B.R. and Berg, R.R. (2001) "Mechanically Stabilized Earth Walls and Reinforced Soil Slopes, Design and Construction Guidelines," National Highway Institute Course No. 132042 prepared for Federal Highway Administration, Contract No.: DTFH61-99-T-25041, 394 p.

Simac, M.R., Fitzpatrick, B., (2007) "Part 1 – Three Challenges in Building SRWs and other Reinforced-Soil Structures - Geosynthetics Magazine, Vol 25, No 5, October-November 2007.

Simac, M.R., Fitzpatrick, B., (2007) "Parts 2A, 2B, 3A, 3B – Three Challenges in Building SRWs and other Reinforced-Soil Structures" Geosynthetics Magazine, Vol. 26, No. 2, February-March 2008, Vol. 26, No. 3, April-May 2008, Vol. 26, No. 4, June-July 2008, and , Vol. 26, No. 5, August-September 2008.

Effects of Corrosion Aggressiveness on MSE Wall Stability in Nevada

J. D. Thornley, A.M. ASCE, P.E.[1] and R.V. Siddharthan, M. ASCE, Ph.D., P.E.[2]

[1] Geotechnical Engineer, Hattenburg Dilley and Linnell Engineering Consultants, 3335 Arctic Boulevard, Suite 100, Anchorage, AK 99503; PH (907) 564-2139; FAX (907) 564-2122; email: jthornley@hdlalaska.com
[2] Professor, Department of Civil and Environmental Engineering, University of Nevada, Reno, Mailstop 258, Reno, NV 89557-0258; PH (775) 784- 1411; FAX (775) 784-1390; email: siddhart@unr.edu

ABSTRACT

Nevada Department of Transportation has over 150 mechanically stabilized earth (MSE) retaining walls at 39 locations. Recently, high levels of corrosion were observed due to accidental discovery at two of these locations. The resulting investigations of these walls produced direct measurements regarding the metal losses of the soil reinforcements and electrochemical properties of the MSE reinforced fill. One MSE wall (I-515/Flamingo) was replaced with a cast-in-place concrete tie-back wall at great expense because of the significant metal loss due to corrosion. There are two other walls at this intersection that were not mitigated.

It is now known that aggressive reinforced fill has been used in a number of MSE walls in Nevada. In its characterization of MSE reinforced fill the Nevada Department of Transportation has used the Nevada T235B soil resistivity test method. The Nevada test method under-predicts the corrosive nature of reinforced fill soils when compared to the AASHTO T-288 test method. As the MSE wall investigations show, this under-prediction has proved detrimental to the service lives of MSE structures.

The internal stability analyses (using AASHTO 2007 LRFD) of two remaining MSE walls at one intersection were performed using metal loss models developed from the statistical analysis of the direct measurements of metal loss. The results of an investigation that incorporates a statistical analysis in order to effectively undertake a prediction of the internal stability of the two remaining walls due to metal loss is presented in the paper. Other MSE walls in Nevada may also be experiencing similar high rates of corrosion which will result in a deteriorated internal stability.

INTRODUCTION

One of the most cost effective earth retaining structures used in transportation applications around the United States is the mechanically stabilized earth wall system, commonly referred to as MSE walls. In Nevada, the state Department of Transportation (NDOT) has constructed over 150 MSE walls, exclusively using metal reinforcements. It is well documented that when metals are buried they can experience corrosion due to the electrochemical interaction with the soil. This also holds true for metal soil reinforcements used in MSE walls. One part of the MSE wall design process involves adding extra cross sectional area or protective coating, also referred to as sacrificial thickness, to account for metal loss due to corrosion over the planned lifetime of the structure. Only MSE reinforced fill soils that are mild to non-corrosive are allowed by specifying a series of pass/fail controls (specifications) in order to limit the amount of corrosion. Metal loss models developed from corrosion studies are used to arrive at the sacrificial thickness estimates. When the combination of sacrificial thickness and mildly corrosive soils are used together, MSE walls are expected to perform as desired.

However, if adequate sacrificial thickness is not used or an aggressive environment exists in the reinforced fill, there will be higher than anticipated rates of corrosion. This can directly affect the internal stability of a MSE wall. At two locations in Las Vegas, Nevada, MSE wall soil reinforcements were found to have high amounts of corrosion. These two locations include the three MSE walls at the I-515/ Flamingo intersection, constructed in 1985 using welded wire fabric (WWF) that was not galvanized; the other MSE wall is at the I-15/Cheyenne intersection, constructed in 1998 using galvanized ribbed metal strips. The former wall reinforcement corrosion was found by accident during construction of a soundwall at the top of one wall. The later was also found by accident during demolition of a portion of an MSE wall for an expansion project. Due to length requirements, the Flamingo walls will be the focus of this paper. However, it should be noted that the Cheyenne MSE wall experienced a similar level of corrosion even though it was galvanized and the wall was approximately only nine years old.

The Flamingo intersection is of significant interest because the case study is well documented. In 2004, the reinforcements in the largest of the three walls were found to be highly corroded and the Federal Highway Administration recommended the wall be mitigated. A cast-in-place concrete tie-back wall was constructed in front of the existing MSE wall to provide adequate support. Also during that time, McMahon & Mann Consulting Engineers (MMCE) were hired to investigate the corrosion of all three MSE walls at this intersection (Fishman 2005). Their investigation evaluated the corrosive nature of the reinforced fill and collected direct measurements of the soil reinforcements at all the MSE walls at this intersection. From their analysis, uniform average metal loss rates were estimated. Stability analyses were also performed for the remaining two MSE walls at the intersection based on remaining reinforcement capacity from average uniform loss estimates.

The results from the Flamingo MSE wall investigation led NDOT to wonder how many other MSE walls may be experiencing stability issues due to high rates of corrosion. The research presented in this paper is a portion of the systematic approach used to answer this question.

A statistical evaluation of direct loss measurements to predict future stability is presented in this paper. The two remaining unmitigated walls at Flamingo are the focus of the stability analysis because they have not been mitigated and they possess the ability to cause disruption to the Las Vegas transportation corridor and potential loss of life if they fail. The results from the loss measurement statistical analyses performed also provide a framework to indentify other walls that may be experiencing similar rates of corrosion.

ANALYSIS OF CORROSION

The field investigation performed by MMCE in 2005 at I-515/Flamingo produced several interesting observations (*Fishman 2005*). The sampled reinforced fill was found to be categorized as very corrosive. The steel samples were observed to have corroded at least two feet from the front facing of the walls, to distances of at least five feet from the facing (the limits of excavation), which indicates that macro cell corrosion occurred. Direct measurements from metal reinforcements were used to calculate by a uniform metal loss over the entire reinforcement surface. The results of their investigation identified the MSE walls at the I-515/Flamingo intersection as highly corroded and in need of repair.

Metal Reinforcement Corrosion

In this paper, the diameter measurements performed by MMCE are revisited and further analysis of corrosion rates is presented. These calculations were performed for all measured wall locations. However, special focus has been placed on the remaining walls (Walls #2 and #3) because they have not been mitigated at this time. Summary statistics of 275 diameter measurements have been included in the second column of Table 1, where the original bar diameter is 0.298 inches, as specified by Hilfiker Retaining Walls.

An evaluation of the diameter measurements from Walls #2 and #3 shows that the metal loss distribution is not precisely normal. This observation requires careful evaluation of the descriptive statistics detailed in Table 1, where the mean and median values are not equivalent. The use of the mean or average value to approximate the corrosion rate that can be expected may not be appropriate in conservative analyses. Therefore, a statistics based approach may be more appropriate. The confidence interval of 95% was used so that the likely range of the mean can be estimated. Another statistical parameter, which is commonly used in earthquake risk analyses, is the 84th percentile corrosion rate. Using these statistical parameters, a corrosion model for future wall behavior at Flamingo has been developed. This can lead to a better characterization and will constrain the loss rates that will eventually lead to wall failure. The corrosion model that has been adopted here is based on the power loss equation,

$$P=kt^n \quad (1)$$

where P is the pit depth at time t, and k and n are constants that depend on the soil and metal characteristics, respectively. This power loss equation was suggested by a National Bureau of Standards (NBS) study (*Romanoff 1989*). In this evaluation the “k” values have been adjusted, using standard “n” values from existing literature, to “fit” the measured radial loss at the Flamingo walls with their twenty years of service life. Subsequently, one can extrapolate the loss rate over time using Equation 1.

Table 1. Summary Statistics from Diameter Loss Measurements at Flamingo Intersection for Walls #2 and #3.

Descriptive Statistic		Remaining Diameter (in.)	Loss Measurement "P" (µm)*	Parameter "k"**
	Mean	0.209	1129	103
	Median	0.222	965	88
	Standard Deviation	0.067	854	77
95% Confidence Interval	**Lower Bound**	0.201	1028	94
	Upper Bound	0.217	1230	112
	84th Percentile	0.142	1983	180

*Based on original bar diameter of 0.298"
**Assuming n = 0.8 (*Elias 1990*)

A comparison of metal loss estimates obtained by using different statistical parameters is useful when identifying how the MSE wall reinforcing elements will behave over time under the current corrosive environment. Table 1 also provides the "k" values calculated from the area loss statistics. Based on research conducted by the NBS (*Romanoff 1989*) and FHWA (*Elias 1990*), an "n" value of 0.80 is seen as a representative value for bare steel that did not have a galvanized coating. These models assist in the calculation of a sacrificial layer thickness. Once the sacrificial steel corrodes the structural section begins to experience metal loss. Corrosion beyond the sacrificial thickness is problematic because the structural section provides the tensile stability for the MSE wall. Failure can occur under static or seismic conditions due to localized corrosion creating cross sectional areas that cannot meet the tensile capacity required for wall support. Such a consequence questions the validity of using the average uniform loss model as it is not conservative.

Reinforced Fill Corrosivity

The reinforced fill electrochemical test data, which was used to characterize the corrosive nature of MSE reinforced fill, measured at the time of Flamingo construction in 1985, showed that the resistivity was suitably high enough to satisfy even today's FHWA and AASHTO requirements. The resistivity measurements were made using the Nevada T235B test method. Another more widely-used soil resistivity test is AASHTO T-288. It should be noted that the procedures associated with these tests are quite different. The Nevada T235B test method measures the conductivity of water from a saturated reinforced fill soil solution. This method of resistivity measurement is significantly different from the AASHTO T-288 test method which uses a soil box to measure reinforced fill resistivity directly. As a part of the study, reinforced fill soil resistivity was measured using both methods and then compared resulting in a correlation given by,

$$y = 0.859x^{0.963} \tag{2}$$

in which, x is the Nevada test values and y is the AASHTO test values. In subsequent analysis this relationship was used to convert Nevada resistivity results to corresponding equivalent AASHTO resistivity values.

It was found that there was significant difference between the 1985 reinforced fill approval data and the reinforced fill results from the subsequent 2005 investigation. While the 1985 data suggests that the MSE reinforced fill is only moderately corrosive, the 2005 data suggests that the reinforced fill is actually very corrosive. While these inconsistent results highlight the issues associated with the Flamingo walls, the results from the Cheyenne intersection (not reported here) were also similar.

POTENTIAL EFFECTS ON WALL STABILITY

As discussed in the introduction, only Wall #1 at the Flamingo intersection was mitigated by constructing a concrete tie-back wall in front of it. However, there are two remaining walls that have not been mitigated. With the development of predictive loss rates outlined in the previous section of this paper, it is possible to address the stability concern at other Flamingo wall locations.

The approach for the analysis of the two remaining MSE walls is based on the current practice for MSE wall design and analysis, as presented by AASHTO in the 4th edition of the Load and Resistance Factor Design (LRFD) Bridge Design Specifications (AASHTO 2007). Using this approach, an analysis of the existing wall internal stability, based on tensile strength of the soil reinforcements has been conducted for both of the remaining MSE walls at the Flamingo intersection. Both static and seismic evaluations were conducted. Two seismic cases were evaluated where the design motions at the surface have maximum accelerations of (1) a_{max} = 0.15g, a value traditionally used by NDOT Bridge Division in the Las Vegas region, and (2) a_{max} = 0.21g, estimated from United States Geological Survey (USGS) maps.

In LRFD static and seismic analyses, a capacity to demand ratio is calculated (C/D ratio), replacing the technique (Allowable Stress Design – ASD) of calculating the Factor of Safety. The load and resistance factors are included in each calculation instead of using a factor of safety, resulting in the need to have a C/D ratio greater than unity for adequate design and stability analysis. The evaluated sections of Walls #2 and #3 have effective heights of 32 and 15.5 feet, respectively. Using the predictive loss curves developed in the earlier section, the wall behavior can be evaluated over time.

When using the LRFD method, a factor is placed on the yield stress of the steel. This effectively keeps the yield stress of the soil reinforcements within the linear-elastic region of the stress-strain behavior of the steel. When evaluating the life expectancy of these MSE walls, the full yield strength of 70ksi is used for both static and seismic cases. It should be noted that the difference between static and seismic response may be smaller than one might expect. This is due to the fact that during design the yield strength is multiplied by a resistance factor for the seismic case of 0.85, while the static case uses a resistance factor of 0.65, thus allowing for higher stresses to develop during a seismic event while still staying at an acceptable level below the yield stress.

Two estimated loss models were used in the analyses. The first estimated loss model evaluates the results of corrosion if the soil reinforcements experience losses at the average power loss model (k = 103 in Equation 1; see Table 1) calculated from the diameter loss measurements. The second loss model uses the wall behavior expectations at the 84th percentile loss (k = 180 in Equation 1). When evaluating important structures it is common to evaluate the 84th percentile (average value plus one standard deviation) case when there is certain level of uncertainty and a conservative design is needed. For highway structures that have more importance and stringent safety requirements, such as these retaining walls, a more conservative estimate of the expected behavior is warranted. The results from these internal stability analyses have been summarized in Table 2. It can be seen that these walls will not likely to remain internally stable for a 75-year design life, either under static or seismic loading conditions. These stability calculations assume that the reinforcements will fail along the edge of the reinforced fill failure wedge at the interface of the active and resistant zones.

Table 2. Expected Failure Lifetimes for Wall #2 and #3 at Flamingo (C/D ratio < 1).

Load Case	**Expected Failure Lifetimes of Remaining Flamingo Walls**			
	Wall #2		**Wall #3**	
	Average Power Loss Model (yrs)	84th Percentile Power Loss Model (yrs)	Average Power Loss Model (yrs)	84th Percentile Power Loss Model (yrs)
Static	42	35	39	27
a_{max} = 0.15g	39	32	35	24
a_{max} = 0.21g	38	31	33	23

To predict wall failure the tensile capacity of the steel reinforcements should be compared to the tensile load introduced by the reinforced fill soil. As a baseline case, the original steel cross sections are used to calculate initial internal stability of Wall #2 (Figure 1). This baseline analysis has been used to evaluate the initial internal stability of Walls #2 and #3. However, this discussion will focus on Wall #2, as an example of the analyses performed, because it is significantly taller than Wall #3 and therefore will cause greater damage upon failure. With the baseline case established, further analysis accounting for corrosion using the power loss models has been conducted. The results of stability calculations estimating the corrosion of the

Flamingo walls are presented for three time periods in a snapshot fashion. These snapshots are in twenty-five year increments starting from a twenty-five year service life. As the time progresses, calculated capacity becomes smaller, due entirely to metal losses. In the case of Wall #2 the 84th percentile metal loss rate tensile values are presented in snapshot fashion in Figure 1. After fifty years there is very little to no structural capacity remaining in the reinforcements.

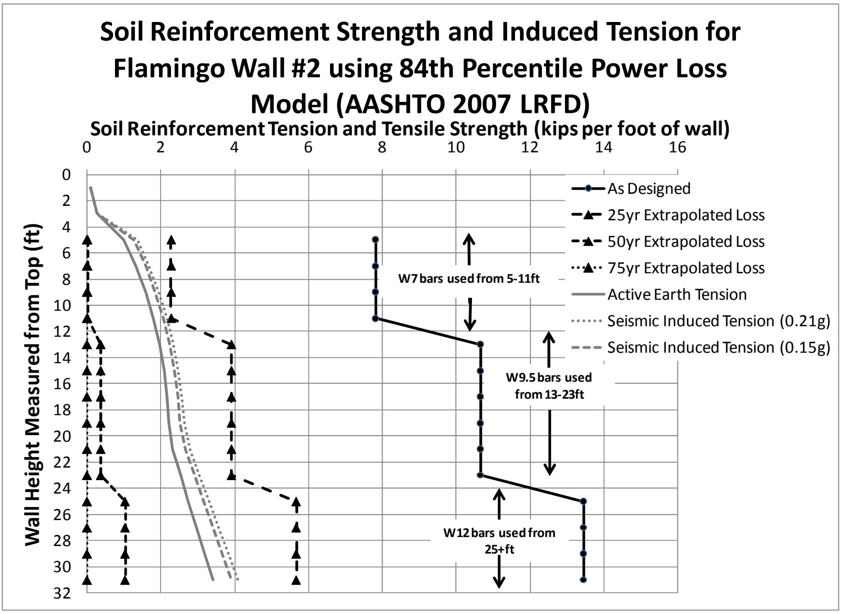

Figure 1. Soil Reinforcement Strength and Induced Tension for Flamingo Wall #2 – 84th Percentile Power Loss Model.

Wall #2 is constructed using three different WWF sizes, including W7, W9.5, and W12 with diameters of 0.298, 0.348, and 0.391 inches, respectively. Near the top of the wall, there is no remaining steel cross sectional area after about forty-five years of service life. However, it is more likely that Wall #2 would fail prior to complete loss of cross sectional area. Using the 84th percentile analysis with the larger longitudinal bars it is apparent that the remaining cross sections of the W9.5 and W12 bars will experience complete metal loss at approximately 55 years and 60 years of service life, respectively.

Figure 2 presents the possible seismic demand based on an input motion of 0.21g in the same snapshot method using the LRFD C/D values. In the case of Wall #2 with the 84th percentile metal power loss model we estimate that a 25 year service life would bring the wall to near failure. It should be reiterated that the walls at the Flamingo intersection have been in service approximately 24 years.

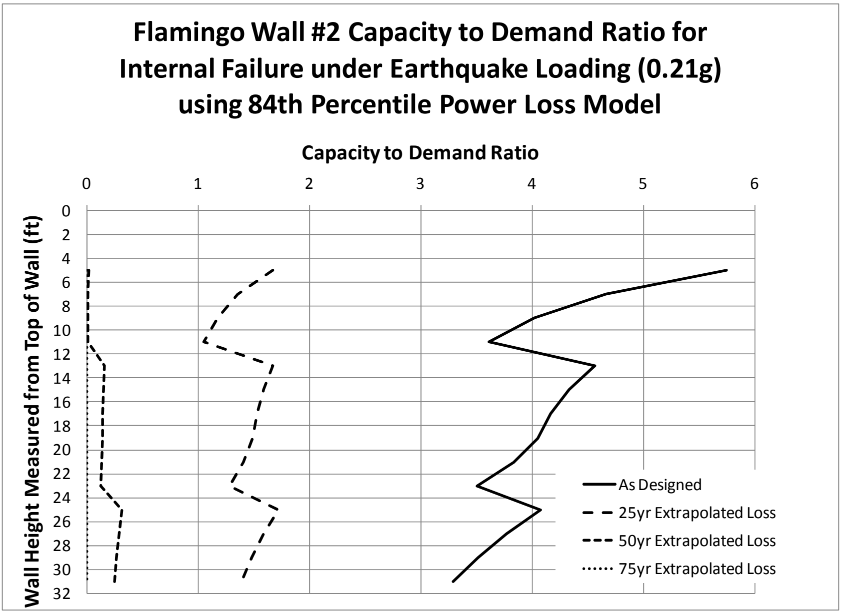

Figure 2. Flamingo Wall #2 C/D Ratio for Seismic Loading (a_{max} = 0.21g) – 84th Percentile Power Loss Model.

ANALYSIS OF OTHER NEVADA WALLS

As has been discussed previously, the Nevada test over-predicts the soil resistivity compared to the AASHTO T-288 soil resistivity test. The equivalent AASHTO resistivity estimates (Equation 2) for thirty of the total thirty-nine wall locations across the state where test data was found were evaluated. While there are many MSE walls across Nevada, low resistivity measurements appear to be present in the Las Vegas area. As many as seven (41%) of the wall locations in Las Vegas have pre-construction average resistivity lower than the 3, 000 ohm-cm minimum limit specified by AASHTO. There are four wall locations (24%) that do not have a single resistivity measurement above the 3,000 ohm-cm minimum limit. From this evaluation, it is clear that there are a number of walls that have lower resistivity values than is recommended by AASHTO design guidelines. Therefore, future evaluations should be conducted on other walls that have aggressive soils.

CONCLUDING REMARKS

Mechanically stabilized earth walls are very economical and have been incorporated in a large number of NDOT projects resulting in over 150 walls in Nevada. However, as is commonly practiced with other structures, these retaining walls require periodic monitoring and performance evaluations. It appears that corrosion monitoring is an important component in the successful performance of MSE walls. Corrosion monitoring can only be conducted by evaluation of the soil and reinforcement conditions behind the wall facing. This is evidenced by the fact that two Nevada MSE wall locations (I-515/Flamingo and I-15/Cheyenne intersections) have been found to have high rates of corrosion. One of the three MSE walls at the Flamingo intersection has been retrofitted with a cast-in-place concrete tie-back wall, at a great expense. Only accidental discovery of corroded reinforcements led to both of these discoveries. Outward observations of these walls showed no signs of distress that would lead to the conclusion that the soil reinforcements were not experiencing detrimental metal loss.

There is significant potential for other walls to have high rates of corrosion because of the unintentional use of aggressive MSE reinforced fill in Nevada. The use of the Nevada T235B test method, which over-predicts the soil resistivity, has allowed the use of more corrosive soils in Nevada MSE walls. A correlation between the Nevada T235B and AASHTO T-288 resistivity test methods shows that the Nevada test method is not conservative with respect to identifying aggressive soils.

Internal stability analyses of the two remaining Flamingo walls show that they are not likely to provide 75 years of service. After approximately 25 years of service a seismic event could impose enough stress on the corroded metal reinforcements to initiate failure. The results from these analyses and the past practice of using aggressive reinforced fill in other MSE walls point to a need for the immediate evaluation of other Nevada walls.

REFERENCES

Elias, V. Durability/Corrosion of Soil Reinforced Structures. FHWA-RD-89-186, Washington D.C., 1990.

Fishman, K. L. Consultant's Report: Corrosion Evaluation of MSE Walls I-515/Flamingo Road Las Vegas, Nevada. McMahon & Mann Consulting Engineers, P.C. May 2005.

Romanoff, M. Underground Corrosion. National Bureau of Standards Circular 579. Houston: National Association of Corrosion Engineers, 1989.

Mechanisms that generate pullout resistance of steel chain in non-cohesive soils

K. Abongo[1], T. Boonyatee[2], M. Kimura [3], A. Kitamura[4]

[1]Postgraduate student, Department of Urban and Environmental Engineering, Kyoto University, Kyoto 615-8520 Japan;abongo.k@ht3.ecs.kyoto-u.ac.jp
[2] Associate Professor, Department of Civil Eng., Chulalongkorn University,Phayathai Road,Putumwan, Bangkok 10330, Thailand; dr.tirawat@gmail.com
[3]Professor, Innovative Collaboration Center, Kyoto University, Kyoto 615-8520 Japan; kimura@iickyoto-u.ac.jp
[4]Engineer, Department of Reinforced Earth, Showa Kikai Shoji Co. Ltd., Suminoue-Ku ,Kitakagaya-1 Chome-3-23, Osaka 559-0011, Japan; kitamura@showa-kikai.co.jp

ABSTRACT

Notable features of steel chain are its flexibility and ability to generate high pullout resistance than those expected from other inclusions such as round steel rods flat plain bars and flat ribbed bars. Neverthess little is known about the mechanism that generates pullout force of steel chain. In order to identify the mechanisms that generate the pullout force of chain, special types of chains were fabricated and laboratory pullout test conducted using Toyoura sand. Test results obtained from these chains showed that the frictional resistance between the chain and the soil, the passive bearing developed in front of the chain and shear resistance of the soil enclosed in the inner space of the chain are the mechanisms that generate pullout force of chain. Test results also showed that the passive bearing resistance is the most predominant mechanism accounting for over 50% of the total pullout force of chain.

INTRODUCTION

The use of chain for reinforcing earth has gain prominence in Japan in recent times. Flexibility of chain hence its ability to be folded which eases its transportation is one factor that has led to its rapid use in recent times. In addition, due to its flexibility, chain can follow the deformation of soil around it. The other factor is high pullout force that is generated by steel chain. Previous studies (Fukuda et.al, 2007) showed that chain produces high pullout force that other reinforcement materials such as round bars and ribbed reinforcement. Despite the fact that little is known about the mechanisms that generate its pullout force, chain has been used to construct reinforced earth walls specifically in Japan. In the construction of chain wall, chain is integrated with steel frames which serve the purpose of the facing panel. A woven wire net of aperture size 2*cm* by 2 *cm* is laid around the facing panel during construction in order

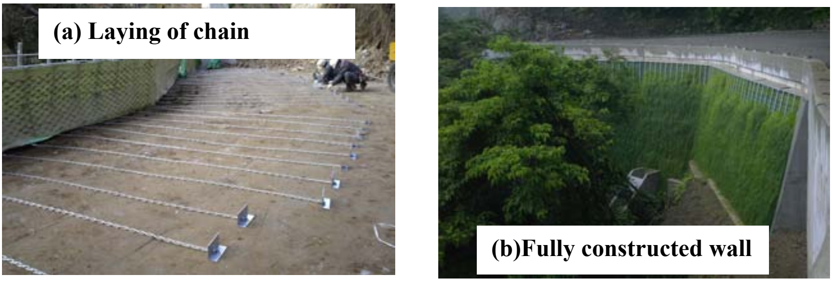

Figure 1 Construction of the chain reinforced wall (a) Integration of chain with steel frames (b) fully constructed

to firmly hold the soil. Figure 1 shows such constructed wall. Protection of the wall against erosion is achieved through wrapping a vegetation mat impregnated with grass seeds around the wire net as construction height progresses. Under suitable environmental condition, these seeds germinate and grown into grass that cover the entire wall. Additional resistance of the chain may be achieved by attaching an end bearing plate anchor at the end of the chain.

CHAIN PULLOUT FORCE

Previously, attempts have been made to formulate the pullout force of chain. Inoue et al. (1996) in particular proposed strip model shown in Figure 2 by decomposing the mechanisms that generated pullout force of steel chain into three components. The three components are the friction acting on the perimeter of the round bar portion, the shear resistance of the soil enclosed in the inner space of the soil and the passive bearing resistance acting on the front the chain. From this model, Inoue proposed equations (1) to (4) for the estimation of the pullout force of steel chain. However, when these equations are used to formulate the pullout force of chain, the values calculated are always lower than that measured from pullout test thereby casting doubt on the accuracy of these equations.

$$F_f = F_1 + F_2 + \mu F_3 \qquad (1)$$

$$F_1 = A_0 \times \left(\frac{1+K_0}{2}\right) \times \sigma_v \times \tan\left(\frac{\phi'}{2}\right) \times N \qquad (2)$$

$$F_2 = 2A_i \times \sigma_v \times \tan\phi \times N \qquad (3)$$

$$F_3 = \sigma_v \times K_p \times (B - D) \times D \times N \qquad (4)$$

Where, A_0 is the frictional area of the chain, A_i is the area of the inner space of the chain that is filled with soil, μ is a coefficient whose value ranges from 1 to 2.5, N is the number of links, K_0 and K_p are coefficient of earth pressure at rest and coefficient passive earth pressure respectively, ϕ is the frictional angle of the soil, σ_v is the applied pressure, B is the outer width of the chain while D is diameter of the bar.

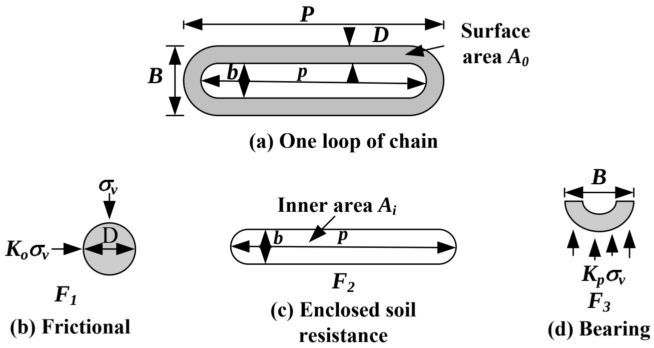

Figure 2. Components that generate pullout resistance of chain

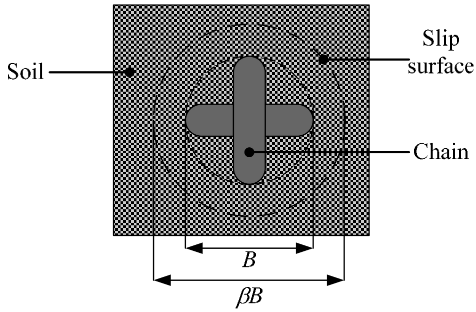

Figure 3. The cylindrical model of the chain

Fukuda et al. (2004) simplified the equation of strip model proposed by Inoue (1996) and proposed cylindrical model shown in Figure 3. The assumption in the formulation of the pullout force of steel chain from this model is that during pullout, the failure surface of the soil around the chain is circular. When chain is pulled out in the soil, the soil in its vicinity dilates resulting in the expansion of the diameter of the failure surface by an amount β of the outer width, B of the chain. From this model equation (5) to (7) were formulated. Equation (7) which gives the pullout force in terms of the frictional correction factor α, soil friction angle, ϕ the outer width, B and length, L and was proposed. The coefficient α is a chain-soil interaction parameter which depends on the type of soil, soil density and applied pressure.

$$F_f = \pi B \times \beta \times L \times \tan\phi \times \left(\frac{1+K_0}{2}\right) \times \sigma_v \qquad (5)$$

$$\alpha = \beta\left(\frac{1+K_0}{2}\right) \qquad (6)$$

$$F_f = \alpha \times \pi B \times L \times \sigma_v \times \tan \phi \qquad (7)$$

In this paper, attempt is made to evaluate the mechanism that generates pullout force of chain through laboratory pullout test. Special types of chains were fabricated with the aim of studying the interacting behavior between chain and soil.

LABORATORY PULLOUT TEST

Testing apparatus

Laboratory pullout tests were performed in order to make clear the mechanism that generates pullout force of steel chain. A cubic container of dimensions 0.5 *m* by 0.5 *m* by 0.5 *m* with an internal volume of 0.125 m^3 was designed for the purpose of conducting the pullout force. Pullout load and displacement were measured from load cell and displacement gauges fitted on the equipment. Confining pressure was applied through the loading plate using electric pump and the pullout test was conducted at a displacement controlled rate of 1 *mm*/minute. Pullout load and displacement were automatically registered to the data logger during the test

Testing chain and soil

Previous studies on full length chain yielded little information and therefore in order to obtain valuable information, three types of chain were fabrication that suited the requirements of this research. The fabricated chain included 800 *mm* long chain with one loop (herein referred to as two round bars). This type chain was fabricated with the aim of obtaining the contribution of the friction component acting on the perimeter of the chain. The second type of chain was a one link that was fabricated so as to obtain the contribution of the passive bearing component and the last type of chain was a two link chain (one loop) in which the pitch, P (distance between the two links was varied) in order to evaluate the effect of the soil enclosed inside the loop. Pitches of 2B, 5B, 10B, 15B were selected for this study. The chain used for this study had a diameter, D of 6 *mm* and outer width, B of 21 *mm*. Dry Toyoura was used as the testing ground. The soil had a dry unit weight of 15.8 kN/m^3. Direct shear test conducted on the soil at a relative density equal to 85 % of its unit weight gave a shear strength angle ϕ_p of 39°. Testing was conducted on the ground prepared at 85 % of its relative density. The desired relative density was achieved by raining sand into the container and them pressing the ground with a flat piece of ply wood in order to level

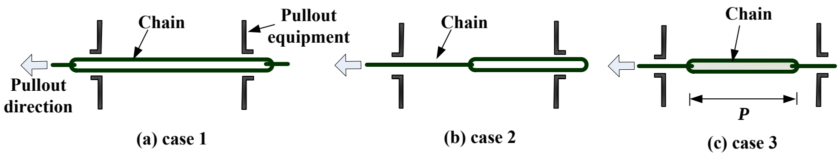

Figure 4. Schematic representations of test cases (a) Two parallel bars (b) one link of chain and (c) Two links of chain

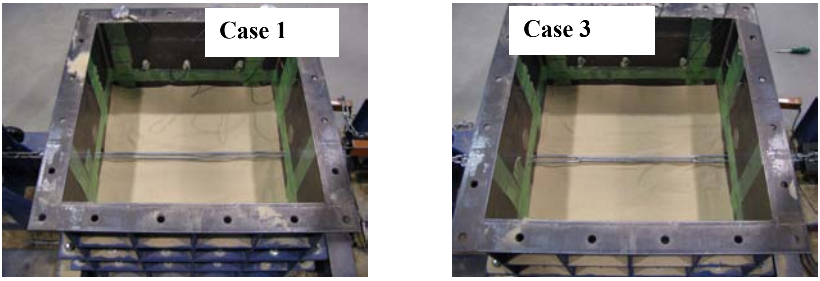

Figure 5. Chain inside the pullout box for (Case 1 and Case 3)

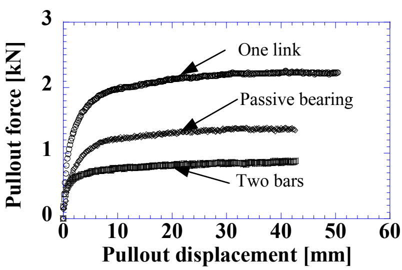

Figure 6 Force –displacement curves (case1 & case 2)

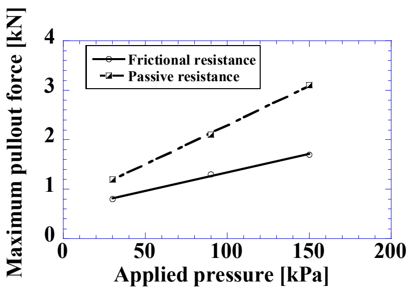

Figure 7 Variation of the components with pressure

the ground. Tests were performed under applied pressures of 30, 90 and 150 kPa. Figure 4 and Figure 5 shows the test cases conducted.

RESULTS AND DISCUSSION

Effect of one link

Figure 6 shows the shows the pullout force-displacement graphs obtained from pulling out two parallel bars and one link of chain under testing pressure of 30 kPa. Test results from two round bars showed a linear increase in pullout force till a displacement of about 1 mm (about 5%*B*) then the pullout force remained constant with displacement as the test continued. These graphs showed typical force-displacement curves similar to that of frictional pile. In the case of pulling out chain with one link, the pullout-displacement graphs showed a different pattern from the case of two round bars. In this case, the pullout graph increase linearly till the yielding value (5 *mm*) then increased again steadily but with a slope less steep than the initial (before 5 *mm*) before the ultimate value is reached in which pullout force remain constant as test increase. This ultimate value was achieved at a displacement of 40 mm. The passive bearing of the link was obtained by subtracting the graph gotten from two round bars from that obtained from contribution of chain with one link. Result obtained from this test revealed that in case 2 the total pullout force was 65-70% more that case 1. Figure 7 shows variation of the measured maximum frictional component and the maximum passive bearing component with the testing pressure. From both plots is can be seen that much of the pullout force of chain comes from passive bearing.

Effect of additional link (one loop)

Chain with two links form a loop in which the inner space is filled with soil. The filling of the inner space depends entire on the particle size of the soil. The shearing of this soil entrapped in the inner space of the chain produces additional resistance that contributes to the total pullout force of the chain. Figure 8 shows pullout displacement graphs obtained from pulling out two link chains (case 3) of various pitches (2*B*, 5*B*, 10*B* and 15 *B*). These curves show different pattern from those obtained from test on one link. Pullout–displacement curves show a linear increase until the yielding value then continues again to increase until the peak value. Until the yield value, the frictional resistance of the chain is fully mobilized however the passive bearing component and shear resistance of the soil in the inner space continues to be mobilized until the peak value is reached. After the peak value has been reached, the graphs show softening behavior which occurs suddenly until the residual value is reached in which the pullout force remains constant with displacement. The sudden drop of pullout force from peak to residual value can be attributed to the fact during pullout the chain loop is displaced at a faster rate than the soil entrapped inside it thereby leaving a gap behind the passive bearing member. When this gap become sufficiently large and the frictional resistance cannot accommodate the force transferred to it through the bearing mechanism, it suddenly burst thereby resulting in the reduction of the pullout force. The peak pullout force was obtained at different displacement levels for various pitches. In fact the as pitch increased, the displacement value at which the maximum pullout force occurred also increased. The reduction of pullout force from peak to residual value can be attributed to the effect of the inner space of the chain.

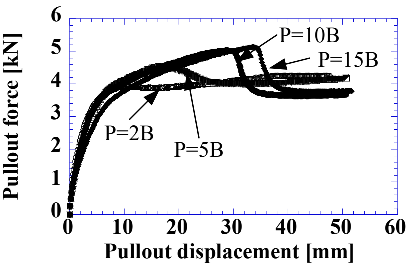

Figure 8 Pullout force for two link chain with various pitches

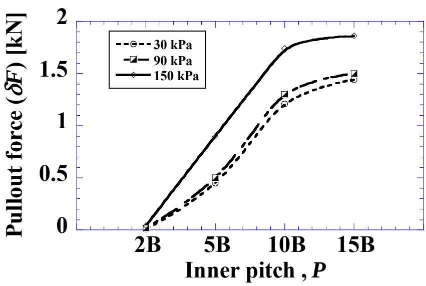

Figure 9 Variation of δF with various pitches

Figure 9 shows the plots of the variation of the difference of peak pullout value and residual pullout value (δF) with pitch for testing pressure of 30, 90 and 150 kPa. Clearly from the Figure 9 it is evident than δF is a function of the pitch and also the applied pressure. For a pitch of 2*B*, δF for all the testing pressure was found to be small. In the construction of chain retaining wall, chain whose pitch is equivalent to the 2*B* is employed and therefore based on this information it would be prudent if the effect of the inner is neglected in formulation of the pullout force of steel chain. The effect of the inner space however has been to be taken into account incase chains of wider pitches are to be used.

Contribution of the inner space

In order to clearly obtain the contribution of the inner space of chain on pullout force, test was performed on two links of chain with and without the inner space filled with a soft sponge. This test was done for chain of pitch equal to 2*B*. The blocking of the inner space restrained the soil from entering this space and therefore the difference of the graphs obtained from the two cases was taken to be the contribution of the inner space. Figure 10 shows the contribution of inner space obtained from the difference of the two graphs (blocked and unblocked). The curves showed in Figure 10 are for a testing pressure of 150 kPa. Figure 11 shows variation of pullout force of inner space with displacement at different testing pressures. From Figure 10 and Figure 11 is evident that the inner space produces small force when compared to the bearing force.

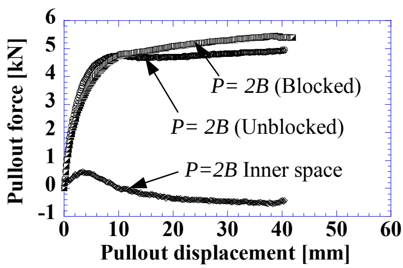

Figure 10 Isolation of the contribution of the inner space

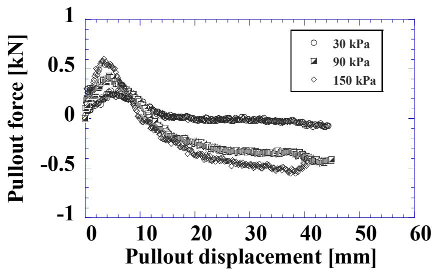

Figure 11 Variation of Isolated Inner spaces with displacement

Table 1 Summary of the contribution of each component for two links of chain of *P=2B* (value is bracked gives the percentage contribution)

Testing pressure [kPa]	Inner space kN(%)	Friction kN(%)	Bearing kN(%)	Total pullout kN
30	0.2 (8)	0.8 (32)	1.5 (60)	2.5
90	0.4 (10)	1.3 (33)	2.2 (56)	3.9
150	0.6 (12)	1.7 (34)	2.7 (54)	5.0

Table 2 Comparison of test result and calculated value from Inoue's equation (values from Inoue's equation)

Pressure	Friction (kN)		Inner space (kN)		Bearing (kN)		Total (kN)	
(kN)	*Inoue*	Expt.	*Inoue*	Expt.	*Inoue*	Expt.	*Inoue*	Expt.
30	*0.23*	0.80	*0.02*	0.20	*0.08*	1.5	*0.33*	2.5
90	*0.62*	1.30	*0.05*	0.40	*0.20*	2.2	*0.87*	3.9
150	*1.00*	1.70	*0.07*	0.6	*0.33*	2.7	*1.40*	5.0

The contribution of the inner space is however difficult to quality clearly and therefore may be neglected when computing the pullout force of steel chain.

Table 1 above gives a summary of the contribution of each component to the total pullout capacity with the percentage contribution give in bracket. From the table it can be concluded that the passive bearing contributes to over 50% of the total pullout force when two links of chain is taken into account. Table 2 shows a comparison of the experimental values and calculated values from Inoue's equation. In the computation of the bearing component from Inoue's equation, the value of μ was assumed to be 2.5. It can be concluded that in all the cases, when Inoue's equation is used in the computation of pullout force of steel chain, the value calculated is much lower than that obtain from experiment. It is therefore necessary that this equation is improved or another equation be developed that would accurately estimate the pullout force of chain adequately

CONCLUSION

From this study, the following conclusions can be drawn.

(1) Of the three components, passive bearing is the dominant mechanism that generates pullout force of steel chain.
(2) The contribution of the inner space is small and hence can be neglected in the computation of the pullout force of chain.
(3) The experimental and calculated values from Inoue's equation were not in agree and therefore there is need to develop an accurate formula for estimating pullout capacity of chain

REFERENCES

Fukuda, M., Kitamura, A., Mochizuki, Y., Hongo, T., Inoue, S., Fujimura, E. and Kimura, M. (2007) "Resistance of steel chain in pullout test with and without sliding box" *New Horizon in Earth reinforcement*, IS-Kyushu, pp. 299-305.

Fukuda, M., Hongo, T. and Konishi, K. (2004) "Frictional force of steel made chain reinforcement applied to fill slope". *Proc. Of Earth reinforcement*, IW-Shiga 2004, pp. 152-161.

Inoue, O. and Konami, K. (1996): Pullout force of steel-made chain reinforcement, 51st Civil Engineering Society Annual Conference (III), pp. 626-627 (In Japanese).

Effect of Soil Properties and Reinforcement Length on Mechanically Stabilized Earth Wall Deformations

Ömer Bilgin, P.E., M.ASCE[1] and Hugh Kim, P.E., A.M.ASCE[2]

[1] Assistant Professor, Department of Civil and Environmental Engineering, University of Dayton, 300 College Park, Dayton, OH 45469-0243; PH (937) 229-2985; email: bilgin@udayton.edu
[2] Civil/Structural Engineer, AMEC Paragon, Houston, TX

ABSTRACT

The design of mechanically stabilized earth (MSE) walls is primarily based on the limit equilibrium approach. Wall deformations which are especially important for serviceability usually are not considered in the design when methods using limit equilibrium approach are utilized. Most agencies require minimum reinforcement length of 70 percent of wall height for the design of MSE walls. However, in some cases, due to existing site conditions and limited space behind a wall, it is not possible to accommodate these required reinforcement lengths. This study was performed to investigate the effect of reinforcement length on wall deformations for varying soil conditions. The effect of reinforced soil, retained/backfill soil, and foundation soil properties were considered. The modeling and analyses were performed using finite element method. The results showed that although wall deformations increase as the reinforcement length decreases, the use of soils with more favorable properties can help reduce the wall deformations and compensate for the increased deformations due to the use of shorter reinforcement lengths.

INTRODUCTION

The use of mechanically stabilized earth (MSE) walls has increased tremendously since 1970's and they became one of the most commonly preferred wall types in transportation projects. Their relatively fast construction, cost-effectiveness, and adaptability to different site conditions contributed to their world-wide acceptance.

A design of an MSE wall using conventional methods usually requires minimum reinforcement length, L_{min}, of 0.7H, where H is the wall height. The Federal Highway Administration (FHWA) guidelines recommends a minimum reinforcement length of 0.7H and recognize that longer reinforcement lengths are required for structures subject to surcharge loads while shorter lengths can be used in special conditions (Elias et al. 2001). National Concrete Masonry Association design manual requires minimum reinforcement length of 0.6H to ensure stability (Collin 2002). British Standard BS8006 (1995) requires that L_{min} for walls with normal retaining function should be maximum of 0.7H and 3 m. Liu and Evett (2004) specifies L_{min} as 0.8H for overall stability. A study preformed by Bilgin (2009) showed that reinforcement lengths of approximately 0.5*H* are possible based on the current design performance criteria specified or recommended by design guidelines, e.g. FHWA, if favorable soil conditions exist. Kim and Bilgin (2007) reported that it is possible to reduce wall deformations by using the concrete key (leveling pad) below the wall as a structural element and by extending the length of the key under the reinforced soil zone.

The objective of this study was to analyze the effect of reinforcement length on the behavior of MSE walls for varying soil properties. A parametric study was performed using finite element analysis. Total of five parameters, unit weight and internal friction angle of reinforced soil and retained soil, and internal friction angle of foundation soil were considered for reinforcement lengths ranging from 0.7*H* to 0.4*H*. The wall behavior was analyzed by studying wall deformations, wall settlements, and axial force in reinforcement.

NUMERICAL MODELING AND ANALYSES

The effect of reinforcement length on wall behavior in terms of maximum wall deformation, $(\delta_h)_{max}$, maximum wall settlement, $(\delta_s)_{max}$, and maximum axial force acting in reinforcement, $(f_a)_{max}$ was investigated for varying soil properties used. The reinforcement lengths ranging from 0.7*H* (baseline model) to 0.4*H* were considered. The minimum reinforcement length of 0.4*H* was selected based on an earlier study showing that the wall deformations become excessive when the reinforcement lengths are reduced to 0.4*H* (Chew et al. 1990). Soil parameters considered in this study were unit weight and internal friction angle of reinforced soil, unit weight and internal friction angle of retained soil, and internal friction angle of foundation soil. The unit weight and friction angle for soils ranged from 16 kN/m^3 to 20 kN/m^3 and from 30° to 42°, respectively. For each case studied, only one parameter changed while the remaining variables were held constant at baseline model properties. Finite element analyses were performed using Plaxis finite element code (Brinkgreve et al. 2006) and two-dimensional plane strain analysis.

Description of Wall and Model Parameters. MSE wall modeled and analyzed in this study was a typical size of an eight-lane divided urban freeway overpass. It is a typical practice to elevate highways for overpasses by using a soil fill with MSE walls on both sides of the fill (Figure 1a). Due to a model symmetry as shown in Figure 1a, only half of the overpass was modeled and analyzed. A 10-m high wall with a reinforcement vertical spacing of 0.8 m was used. The geometry and material properties of the baseline model analyzed are shown in Figure 1, where γ, ϕ, and *c* are the unit weight, soil friction angle, and cohesion, respectively.

The model dimensions were set at a distance such that the boundaries would not affect the analysis results. The reinforcement length for the baseline model was 7 m (0.7*H*). The facing unit panels had dimensions of 0.35 m wide and 0.8 m high. Since the vertical spacing of reinforcement was 0.8 m, the block height was also set at 0.8 m for the ease of modeling of the construction sequence. The interface between the panels was modeled by introducing thin elements with rotational stiffness between the panels.

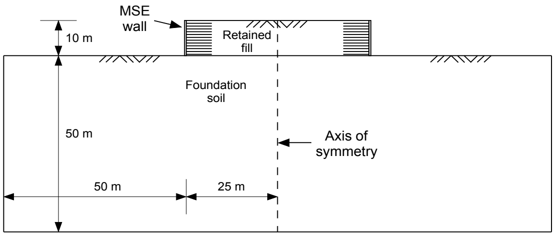

(a) Overall model (elevated highway overpass)

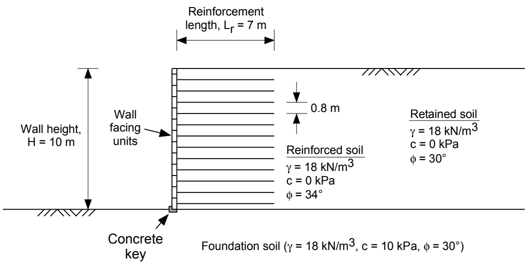

(b) MSE wall and baseline case properties

Figure 1. MSE wall model used in numerical analyses

The axial stiffness of EA = 980 kN/m was used for the reinforcement. The interface stiffness properties of the facing panels were back-calculated using the results of the full-scale field tests (Rowe and Skinner 2001). Based on the parametric study, the interface stiffness was selected as 0.5% of the panel stiffness.

RESULTS AND ANALYSIS

The results show that maximum wall deformations and maximum axial force in reinforcement increase as the reinforcement length is reduced from 0.7H to 0.5H and deformations increase more rapidly as the reinforcement lengths become shorter than 0.5H. The maximum wall settlements increase usually gradually as the reinforcement length decrease from 0.7H to 0.4H and the effect is not as significant compared to the deformations and reinforcement forces.

It should be noted that the reinforcement length of 0.6H was considered only for the baseline model. The analyses with baseline model showed that the effect of reinforcement length was more significant when the reinforcement lengths are reduced below 0.5H. Therefore, the effect of reinforcement length of 0.6H was not considered during the study, except for the baseline model.

Effect of Reinforced Soil Unit Weight, γ_r. The effect of reinforced soil unit weight, γ_r, (ranging from 16 kN/m^3 to 20 kN/m^3) on maximum wall deformation, maximum wall settlement, and maximum axial force in reinforcement for varying reinforcement lengths is shown in Figure 2.

As the reinforcement length decreases the wall deformation increases, regardless of the reinforced soil unit weight (Figure 2a). However, soils with higher unit weight cause more deformations when the reinforcement is longer (i.e., 0.7*H*), while soils with lower unit weight result in more wall deformations when the reinforcement is shorter (i.e., 0.4*H*). The unit weight of reinforced soil affects both horizontal forces acting on the facing unit and the friction between reinforcement and soil. At shorter reinforcement lengths, lower interface friction forces between the reinforcement and soil due to a lighter reinforced soil result in more deformations compared to the reinforced soils with higher unit weights.

An increase in the reinforced soil unit weight resulted in an increase in maximum settlement (Figure 2b), as expected. The results show that the maximum wall settlement is slightly affected by the reinforcement length and the settlements increased as the reinforcement length gets smaller.

Figure 2c shows the maximum reinforcement force for three different reinforced soil unit weights for varying reinforcement lengths. The results show that soils with higher unit weight result in more forces in the reinforcement. In addition, the reinforcement forces are slightly affected for the reinforcement lengths ranging between 0.7*H* and 0.5*H*, while the increase in forces are more significant for reinforcement lengths shorter than 0.5*H*.

Effect of Reinforced Soil Friction Angle, ϕ_r. The effect of reinforced soil friction angle, ϕ_r, ranging from 30° to 42°, on maximum wall deformation, maximum wall settlement, and maximum reinforcement force for varying reinforcement lengths is shown in Figure 3. The results show that the wall deformations are significantly influenced by the reinforced soil friction angle. A change in friction angle from 42° to 30° results in more than doubled wall deformations, regardless of the reinforcement length.

An increase in reinforced soil friction angle results in reduced wall deformations at all reinforcement lengths studied (Figure 3a). A decrease in the reinforcement length has more effect on wall deformations for reinforced soils with higher friction angles. For example, the reduction of reinforcement length from 0.7*H* to 0.4*H* results in approximately 65% increase in maximum wall deformations for ϕ_r=30° soils, while the increase is approximately 86% for ϕ_r=42° soils.

Figure 3b shows that while a reduction in reinforcement length results in slightly more settlements, the effect of reinforced soil friction angle on wall settlements is less significant.

The results show that the maximum reinforcement force increases as both the reinforcement length and the reinforced soil friction angle decrease (Figure 3c). The reinforcement force increases approximately 35% when the friction angle changes from 42° to 30°, regardless of the reinforcement length. On the other hand, the reinforcement force increases approximately 20% when reinforcement length changes from 0.7*H* to 0.4*H*, regardless of the reinforced soil friction angle.

Effect of Retained Soil Unit Weight, γ_f. The effect of reinforced soil unit weight, γ_f, (ranging from 16 kN/m^3 to 20 kN/m^3) on maximum wall deformation, maximum wall settlement, and maximum axial force in reinforcement for varying reinforcement lengths is shown in Figure 4.

Figure 4 shows that the unit weight of the retained soil has more effect on the wall behavior for shorter reinforcement lengths. The retained soil unit weight does not have any effect on the maximum wall displacement and the reinforcement force for the walls with reinforcement length of 0.7*H*. However, an increase of 4 kN/m^3 in unit weight (from 16 kN/m^3 to 20 kN/m^3) results in approximately 50% increase in maximum wall displacements (Figure 4a) and 12% increase in maximum reinforcement load (Figure 4c) for walls with 0.4*H* reinforcement length. The walls with denser retained soil experience more settlements, as expected (Figure 4b).

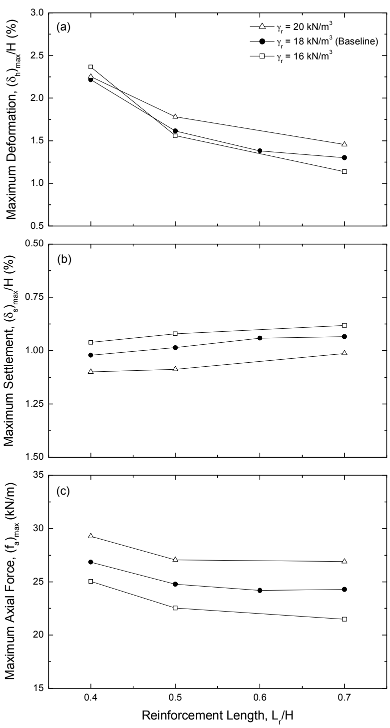

Figure 2. Effect of reinforced soil unit weight, γ_r, on maximum (a) wall displacement, (b) wall settlement, and (c) reinforcement force

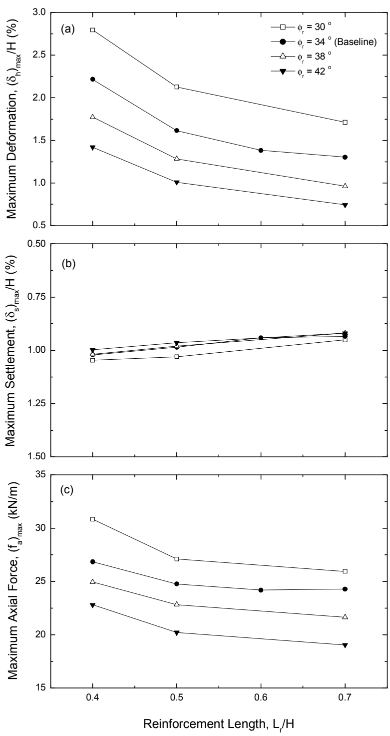

Figure 3. Effect of reinforced soil friction angle, ϕ_r, on maximum (a) wall displacement, (b) wall settlement, and (c) reinforcement force

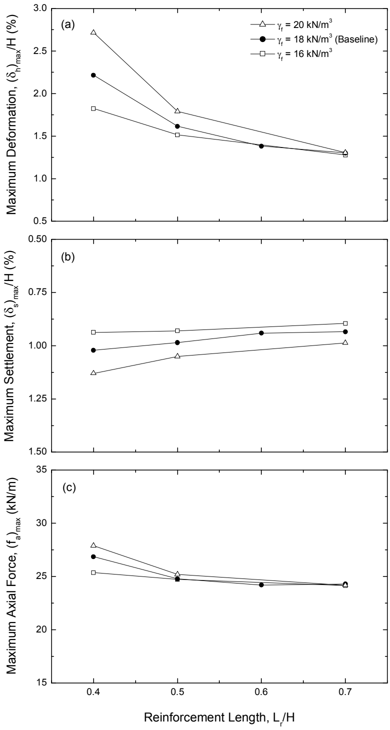

Figure 4. Effect of retained soil unit weight, γ_f, on maximum (a) wall displacement, (b) wall settlement, and (c) reinforcement force

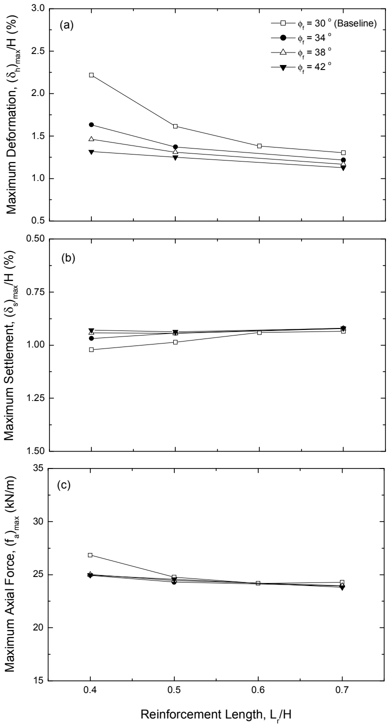

Figure 5. Effect of retained soil friction angle, ϕ_f, on maximum (a) wall displacement, (b) wall settlement, and (c) reinforcement force

Effect of Retained Soil Friction Angle, ϕ_f. The effect of retained soil friction angle, ϕ_f, ranging from 30° to 42°, on maximum wall deformation, maximum wall settlement, and maximum reinforcement force for varying reinforcement length is shown in Figure 5. The results show that the effect of retained soil friction angle increases as the reinforcement length decreases. The effect of reinforcement length and retained soil friction angle on wall settlements and reinforcement forces are minimal (within the reinforcement lengths studied 0.7*H* to 0.4*H*) when the retained soil friction angle is more than 34° (Figure 5b and c). Relatively loose retained soil, ϕ_f=30°, results in more wall settlements and reinforcement forces when the reinforcement lengths are shorter than 0.5*H* (Figure 5b and c). The retained soil friction angle has the most significant effect on wall displacements (Figure 5a). As the friction angle decreases wall deformations increase and the effect is more significant for walls with shorter reinforcement lengths. The displacements increase approximately 13% and 73% for soils with retained soil friction angle of 42° and 30°, respectively, when reinforcement lengths are reduced from 0.7*H* to 0.4*H*. The effect is more significant for relatively loose soils since the lateral earth pressure coefficient increases as the as the soil friction angle decreases.

Effect of Foundation Soil Friction Angle, ϕ_{fo}. The effect of foundation soil friction angle, ϕ_{fo}, ranging from 30° to 42°, on maximum wall deformation, maximum wall settlement, and maximum axial force in reinforcement for varying reinforcement length is shown in Figure 6. The results show that the foundation soil friction angle does not have any significant effect on the reinforcement forces (Figure 6c). On the other hand, both wall displacements and settlements are reduced as the foundation soil friction angle increases for all reinforcement lengths considered in this study. Figure 6b shows that settlements are slightly affected by the change in reinforcement length. The settlements slightly decreases as the reinforcement length gets shorter when the foundation soils are relatively stronger while the effect is reversed for relatively weaker foundation soils, i.e. settlements slightly increase as the reinforcement length gets shorter (Figure 6b). Foundation soil friction angle has the most significant effect on wall displacements and walls on relatively weaker foundation soils experience more deformations (Figure 6a). The results also show that the effect of reinforcement length on wall displacements is more significant for the walls placed over relatively weaker foundation soils. Reinforcement lengths reduced from 0.7*H* to 0.4*H* result in 50% and 73% increase in displacements for walls placed over foundation soils with friction angles of 42° and 30°, respectively.

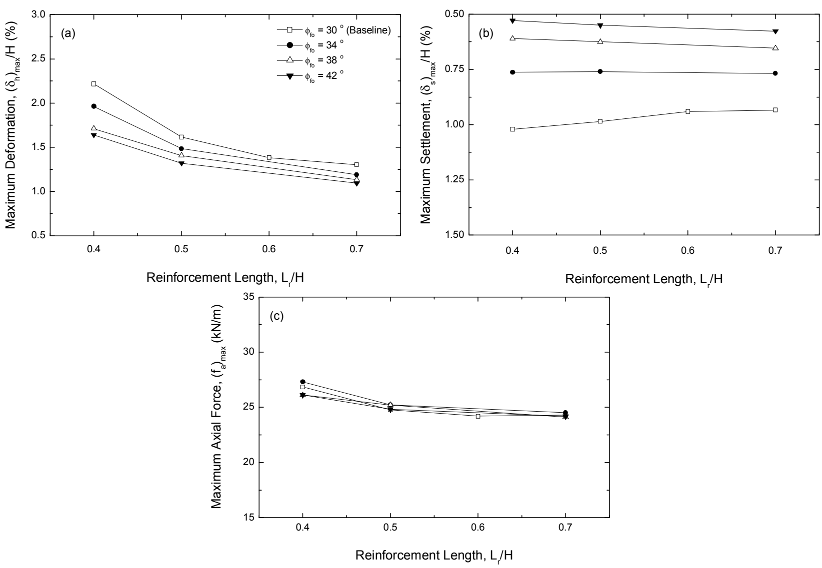

Figure 6. Effect of foundation soil friction angle, ϕ_{fo}, on maximum (a) wall displacement, (b) wall settlement, and (c) reinforcement force

CONCLUSIONS

Current design practice of MSE walls usually requires reinforcement length of 70% of wall height. The effect of the properties of soils involved in MSE walls (reinforced soil, retained soil, and foundation soil) on wall behavior has been investigated for varying reinforcement lengths. Wall displacements at the face, wall settlements, and axial loads in reinforcement have been studied. Based on the variables and ranges considered for the parametric study performed during this study, the following conclusions are drawn:

- Reinforcement length has the most significant effect on the wall displacements, compared to wall settlements and reinforcement force. In some cases, an increase of more than 80% in wall deformations was observed for the reduction of reinforcement length from 0.7*H* to 0.4*H*.
- Effect of shorter reinforcement lengths is minimal (usually around 5% or less) on wall settlements.
- Reinforcement loads can increase up to 20% when reinforcement length reduced from 0.7*H* to 0.4*H*, if relatively weak soils are present in and around the wall.
- Reinforced soil internal friction angle has significant effect on wall deformations. An increase in friction angle from 30° to 42° can reduce the maximum wall deformations up to 50%.

REFERENCES

Bilgin, Ö. (2009). "Failure mechanisms governing reinforcement length of geogrid reinforcement soil retaining walls." *Engineering Structures*. 31(9), 1967-75.

British Standards Institution (1995). *Code of practice for strengthened/reinforced soils and other fills, BS8006*. London.

Brinkgreve, R. B. J. et al. (ed.) (2006). *Plaxis 2D-Version 8 users manual*. Rotterdam: A.A. Balkema.

Chew, S. H., Schmertmann, G. R., and Mitchell, J. K. (1990). "Reinforced soil wall deformations by finite element method." *Performance of reinforced soil structures*. London: Thomas Telford, 35-40.

Collin, J. (2002). *Design Manual for Segmental Retaining Walls*. 2nd Edition, National Concrete Masonry Association, Virginia.

Elias, V., Christopher, B. R., and Berg, R. R. (2001). "Mechanically stabilized earth walls and reinforced soil slopes, design and construction guidelines." *Publication No. FHWA-NHI-00-043*, Federal Highway Administration (FHWA), Washington D.C.

Kim, H. S., and Bilgin, Ö. (2007). "Studying the effect of concrete key size on mechanically stabilized earth wall deformations using finite element method." *Computer applications in geotechnical engineering (GSP 157). Proceedings, Geo-Denver 2007-New Peaks in Geotechnics*, Colorado.

Liu, C., and Evett, J. B. (2004). *Soils and foundations*, 6th ed. Prentice Hall.

Rowe, R. K., and Skinner, G. D. (2001). "Numerical analysis of geosynthetic reinforced retaining wall constructed on a layered soil foundation." *Geotextiles and Geomembranes*, 19, 387-412.

Re-Visiting MSE Walls 20 Years After Construction: A Case History of Evaluation for Continued Use

J. E. Parkes, P.E.[1], P.L. Shank, P.E., C.M.[2], and J. E. Sankey, P.E.[3]

[1] PB Americas, Inc. 100 South Charles St., Tower 1, 10th Floor, Baltimore, MD, 21201; PH (410) 454-9763; email: parkes@pbworld.com
[2] Maryland Aviation Administration, P.O. Box 8766, Baltimore Washington International/Thurgood Marhsall Airport, MD 21240; PH (410) 859-7061; email: pshank@bwiairport.com
[3] The Reinforced Earth Company, 8614 Westwood Center Drive, Suite 1100, Vienna, VA, 22182-2233; PH (703) 821-1175; email: jsankey@reinforcedearth.com

ABSTRACT

Some of the first Reinforced Earth® MSE retaining walls built in the state of Maryland for public works projects were constructed at a rental car facility for BWI Airport in 1983. As part of later airport operations expansion, the site was considered for re-development and the rental car facilities were demolished in 2004. A comprehensive evaluation of the four existing MSE walls was performed to assess the suitability of the structures for continued use as part of new site development. In particular, several sinkholes had formed within the MSE wall envelope of one wall due to drainage alterations during demolition. In addition to evaluating the overall condition the four walls, the impact of these sinkholes was assessed. The evaluation included internal and external stability assessments. Field investigations included soil borings through the reinforced backfill, test pits to expose and inspect the integrity of the steel strip reinforcements, survey of the walls, and visual inspections. The walls were found to be suitable for continued use in the new development once remedial grouting, drainage, and maintenance measures were implemented. This case history presents a unique post-construction examination of the performance of MSE walls after more than 20 years of service and how such structures can be expected to perform over the remainder of the original 75 year design life.

INTRODUCTION

As part of a planning study for a new administration building for Baltimore Washington International Airport (BWI), a former rental car maintenance facility was identified as a possible site for redevelopment. The original structures on the site had been demolished, and the Maryland Aviation Administration (MAA) undertook an evaluation of four existing retaining walls for continued use in site redevelopment (Parsons Brinckerhoff, 2006). The walls are Mechanically Stabilized Earth (MSE) walls of proprietary design by the Reinforced Earth Company (RECO). The MSE walls are designed to act as gravity structures, with the stability of the structure derived from the overall weight of the reinforced mass. After demolition of the rental car facilities, two sinkholes developed behind one of the retaining walls. In order to assess redevelopment costs, the walls had to be evaluated for internal and external stability, as well as overall condition, to determine if they could be re-used, or if they needed to be rehabilitated or replaced.

Site Description and Construction. The site is located off of Elkridge Landing Road in Linthicum, Maryland, near BWI Airport. Access to the site is gained by a perimeter road entering the south side of the site, as shown in Figure 1. The perimeter road splits at a "T" intersection with one branch following the east perimeter of the site and the other branch following the west site perimeter. The site interior consists of paved parking areas gently sloping towards the entrance of the site. The four retaining walls on the site are labeled A-1, A-2, B, and C. Walls A-1 and A-2 support the eastern perimeter road. Wall B supports a parking area, providing grade separation between the "T" intersection and the parking area above. Wall C supports the western perimeter road. The walls are labeled on Figure 1 and photos of the Walls B and A-2 are shown in Figure 2. Wall dimensions are presented in Table 1. Most of the storm drains on the site drain to a manhole in the southeast corner of the site behind Wall B. A storm drain line runs behind and parallel to wall B, with inlets directly behind the wall within the MSE backfill zone.

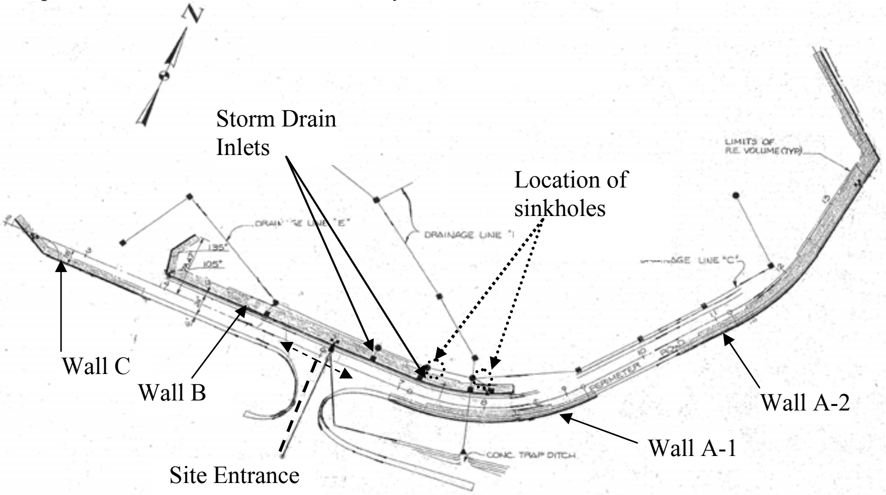

Figure 1: Site Plan Showing Retaining Walls and Sinkholes

Figure 2: Photos of MSE Retaining Walls B and A-2.

Table 1: Dimensions of the MSE Walls

Wall	Length, m (ft)	Max Height, m (ft)
A-1	76 (250)	4.3 (14)
A-2	125 (410)	7.2 (23.5)
B	101 (330)	6.1 (20)
C	38 (125)	2.3 (7.5)

The walls are proprietary design consisting of precast concrete panels with discrete steel reinforcing strips attached to the rear panel face. Typical panels have two strips in each of two rows offset from center, although several panels containing a fifth strip in the center or three rows of strips were used.

Design and Construction History. These walls are believed to be among the earliest MSE walls of the RECO design built in Maryland in 1983. These walls typically have a design service life of 75 years. On-site granular soils from cut areas were used as backfill to balance cut and fill quantities. These soils consisted of silty sand with 15 to 25% fines. Although current design standards include filter materials behind vertical joints for backfill with fines, these filter measures were not part of the original 1983 design. Instead, cork and/or foam were commonly placed in the joints.

Post Construction Site History. The site was used for maintenance and storage of rental cars. During Spring 2004, the rental car facilities were demolished, and storm drain inlets were covered with stone and fabric for sediment control during demolition. However, the stone and fabric were not removed, therefore long term drainage to the inlets was impaired. (Michael Baker Jr., Inc., 2004).

In September 2004, a sinkhole developed behind Wall B next to a storm drain inlet, as indicated in Figure 1 and shown in Figure 3. The sinkhole was approximately 2 m (6 ft) in diameter at the ground surface and approximately 1.5 m (5 ft) deep. Site drainage to this inlet could not enter the inlet because it was covered. The drainage ponded behind the wall, eventually overtopping the wall and creating a waterfall that eroded the soil at the toe of the wall. The erosion was severe and undermined several wall panels, which exposed the retained soil, allowing it to ravel out and erode (Michael Baker, Jr. Inc, 2004). As backfill soil raveled out from the panels, progressive collapse occurred in the MSE backfill, leading to a sinkhole at the ground surface behind the wall. The sinkhole was backfilled with a flowable fill mix consisting of cement, fly ash, sand, and water, with a layer of AASHTO No. 57 stone for drainage against the back of the wall. A concrete drainage swale was built at the wall toe to prevent further erosion. In July 2005, two additional sinkholes were observed at the adjacent inlet, as indicated in Figure 1 and shown in Figure 4. Approximate dimensions of these sinkholes were 2 m by 4 m in plan (6 by 12 ft) by 1.2 m (4 ft) deep and 2m by 1 m (6 ft by 3 ft) by 1 m (3 ft) deep. These were repaired in the same fashion as the first sinkhole.

Figure 3 – Photos of First Sinkhole and Erosion of Soil at Toe and Behind Panels

Figure 4 – Photos of Second Sinkhole

INVESTIGATIONS

Visual Inspection, Survey, and CCTV Inspections. Visual inspection of the walls indicated relatively sound structural condition without significant distress. In general, there was no visual leaning, settlement, or bulging. Wall B is the only wall in which concerns were identified during visual inspection, and the concerns identified related to issues resulting from poor drainage. The pavement behind Wall B coping had settled 5 to 10 cm (2-4 in), resulting in ponding of surface water that attempted to drain to the inlets. The ponded water seeped into the MSE backfill and out of the vertical joints in the wall. Since the wall was constructed with silty sand, and there was no continuous filter material at the joints, the fines had been washing out of the vertical joints over time. This is evident from staining at the joints as seen in Figure 2. Also, as a result of the sinkholes, several panels had experienced settlement, resulting in cracks and open joints.
A spot survey was performed to verify grading and check for excessive wall lean. Survey results indicated that the walls have a very slight lean outward of the vertical design alignment. Observed outward lean varied from 0.0% to 3.5%, with the highest occurring at Wall A-2. It is not clear if the wall lean is due to original construction or post-construction movement. However, the amount of wall lean is not significant and does not have a destabilizing effect on the walls (The Reinforced Earth Company, 2005).

A closed circuit television (CCTV) inspection of the storm drains was performed using a remote operated camera vehicle with a rotating view. No significant distress of the pipes that would adversely impact the retaining walls was found (Parsons Brinckerhoff, 2006).

Borings, Test Pits, and Laboratory Testing. A subsurface investigation consisting of six soil borings and six test pits was performed to obtain subsurface data. Test pits were performed directly behind the wall panels to investigate backfill soils and expose panels and reinforcing strips for inspection. The test pits were hand excavated to depths of 0.7 to 1.0 m (2 to 3 ft); just deep enough to expose the top layer of reinforcements. Excavation equipment, such as a backhoe, was not used due to the potential damage risk to the reinforcing strips. Excavating deeper than the upper row of reinforcements could have undermined or damaged the strips, and would have made backfilling underneath the strips difficult. The top row of strips were considered the most likely to experience corrosion, since chemical compounds in surface water infiltration would be more concentrated at shallower depths. Test pits were typically 1 m by 1m (3 ft by 3 ft) in plan as shown in Figure 5. Test pits were backfilled with excavated soils, fill was appropriately tamped, and pavement was restored.

Figure 5 – Photos of Test Pits in Reinforced Backfill

Borings were performed in order to characterize backfill, foundation soils, and groundwater conditions. Two borings were performed within the reinforced backfill, although one was terminated at shallow depth due to encountering a reinforcing strip in the side of the borehole wall. The remaining borings were performed outside of the MSE backfill zones. Standard Penetration Testing (SPT) was carried out in all borings at intervals of 0.75 m (2.5 ft) through the upper 5 to 6 m (15 to 20 ft) and at 1.5 m (5 ft) thereafter. Laboratory testing was performed to verify field soil classifications in accordance with the Unified Soils Classification System (USCS). Corrosion potential was evaluated using Electrochemical testing consisting of pH, resistivity, chloride content, and sulfate content on samples from the reinforced backfill zone. Electrochemical test results indicated low corrosion potential per criteria indicated for MSE walls in the AASHTO guidelines.

SUBSURFACE CONDITIONS

Site soils generally consist of granular fill overlying native granular soils. Fill, both within and behind the MSE backfill, generally consist of medium dense granular soils classified as silty sand with gravel, SM, in accordance with ASTM Standard D2487 and the USCS, respectively. It was noted that SPT N-values from the boring in the reinforced backfill in the area of the sinkholes were lower than the other Fill N-values, but still in the medium dense range. It was also observed from the test pits that fill against the wall panels at Wall B were saturated. Fill in other test pits were found to be moist, but not as wet as those at Wall B.

Beneath the fill, native granular soils consisting of coarse to fine silty sand with varying amounts of gravel were encountered, generally classifying as SM soils. Two strata of native sandy soils were found, separated by a thin layer of stiff lean clay (CL). The upper native sandy soils are medium dense silty sand with gravel, SM. This upper sand stratum is the bearing stratum for all of the walls and is where most of the fill appear to have come from. The lean clay layer is encountered within a 1 to 2 meters below foundation depths and is roughly 1.5 meters in thickness. Below the clay, the lower granular stratum consists of dense fine to medium grained silty sand.

Groundwater readings taken 24 hours after drilling through temporary piezometers in the completed borings indicated groundwater levels were below wall foundation grades.

ANALYSES AND EVALUATIONS

Site Drainage Impacts Relative to Walls. As mentioned previously, surface water drains to the area behind Wall B and ponds against the coping, resulting in infiltration of water into the MSE backfill and out through the vertical joints. Since the wall was not designed to accommodate the ponding and infiltration of water in this fashion, the infiltration led to washing out of fines from the backfill. It is noted that the fines content for the MSE backfill approaches 25%, and that current AASHTO practice is to maintain fines content less than 15% for MSE backfill. The loss of fines appears to have been localized to the area directly behind the panels, since samples from the borings and test pits behind all of the walls had consistent fines contents and did not indicate any washed or cleaner materials behind Wall B. However, the infiltration of ponded water through the backfill likely contributed to the propagation of the voids and sinkholes since the sinkholes appeared near the inlets. In addition, when the inlets were covered, the site drainage to Wall B ponded to the point where it overtopped the wall. The flow over the wall eroded the soil at the toe of the wall and behind the lowest panels, which led to the formation of voids and sinkholes. Since the sinkhole formation is a progressive collapse phenomenon, and since the backfill contains reinforcements that may have improved soil arching, it is possible that isolated voids remain in the backfill. Any remaining voids, however, are considered to be fairly small and not interconnected since no additional sinkholes or settlement has been noticed since the investigation.

Analyses of Wall Stability. Comprehensive internal and external stability analyses of the walls were performed to evaluate the remaining service life. Results of the borings, test pits, and lab testing were used to characterize backfill and foundation soils. Critical sections were selected with the shortest reinforcement length, L, compared to the maximum height, H. The minimum L/H ratio was determined to be 0.7 for all walls, and these ratios occurred at the maximum height of each wall. The maximum height results in the largest earth pressure, and the minimum reinforcement length provides the least amount of weight to counteract that driving force. A uniform surcharge of 12 kPa (250 psf) behind the walls was included in the analyses. External stability analyses included bearing capacity, sliding, overturning, and global stability. The investigations also included analyses for internal stability. All wall sections analyzed were found to have adequate factors of safety against sliding, overturning, and bearing capacity in accordance with current AASHTO requirements (2002). Based on borings and lab data, it was concluded that the MSE backfill is acceptable for all design requirements.

One critical section was analyzed for global stability. The maximum wall height at the site occurs at Wall A-2. At this location, the ground surface slopes down away from the toe of the wall, which results in lower global stability than if the ground surface were level. The other walls are not as high or have relatively level ground at the toe. Global stability was analyzed using limit equilibrium methods considering circular failure and sliding wedge failure modes. The critical wall section was determined to have an adequate factor of safety against global stability in accordance with AASHTO requirements (2002) (Parsons Brinckerhoff, 2006).

The internal stability of the walls was evaluated based on visual inspection as well as engineering analysis. Internal stability was analyzed using the Coherent Gravity Method, which was the original design method and is currently a standard AASHTO design method. The sinkholes occurred in the active zone of the backfill within 0.3H of the wall face, not the resistant zone where the reinforced backfill develops the resistance for stability; therefore the sinkholes did not significantly impact the internal wall stability. The sinkholes had been filled, therefore voids were not included in the analyses. Internal stability analyses included an allowance for metal loss based on observations, soil corrosivity test results, and assumptions regarding the loss of galvanization and underlying carbon steel. A metal loss formula for galvanization and carbon steel, consistent with AASHTO criterion, was used to determine remaining design life. Significant corrosion of the reinforcing strips was not observed in the test pits. Only one strip exposed during the investigation appeared to have lost the galvanized coating and even that was only in one isolated spot, as can be seen in Figure 5. The strip size, spacing, alignment, and depth were evaluated and determined to be consistent with design requirements (The Reinforced Earth Company, 2005). The connections of the strips to the panels appeared to be in good condition as well, with no significant corrosion. The results of the internal stability analysis indicated that the wall could be expected to last in excess of another 50 years, based primarily on potential metal losses in the steel strips, consistent with the initial 75 year design life of the walls. Considering the time passed since construction and this estimate of remaining service life the walls can be expected to perform satisfactorily for the remainder of their original design life.

REMEDIATION MEASURES

Preventative Site Remediation at Wall B. As mentioned previously, two sinkholes were repaired behind Wall B. In addition, since the issues observed at Wall B related primarily to drainage and infiltration of surface water, preventative site remediation measures were undertaken to reduce the potential for similar problems to occur in the future. The preventative measures included (a) construction of an asphalt speed berm behind Wall B to direct surface water away from the wall, (b) modifications to the drain inlets directly behind the wall to enable them to collect surface water that had been ponding behind the wall coping, (c) conversion of a manhole on the drainage line behind Wall B to a curb cut drain, and (d) construction of a second asphalt berm farther behind the wall to direct water to the reconstructed drain line. These modifications significantly reduced the amount of water draining directly to the wall, as well as improved the efficiency of the inlets and drain line behind the wall with regard to collection of surface runoff. In addition, a seal coat was applied to the pavement behind Wall B to further reduce infiltration of surface water into the backfill.

General Maintenance Measures for All Walls. As with any retaining wall, MSE walls require periodic maintenance. Maintenance measures as part of this remediation included inspection of wall joints to remove any vegetation and identify areas of excessive opening. Joints open wider than 1.5 inches were cleaned and caulked. Isolated joints with staining were also be caulked, as the staining indicates loss of material at these joints. Panels were cleaned to remove staining from previous seepage, in order to allow identification of similar seepage in the future. Finally, thick vegetation at the toe of Walls A-1 and A-2 was cut to allow easier inspection of the structures.

SUMMARY

A comprehensive field investigation and stability analyses were performed in order to assess the remaining design life of these four 20+ year-old MSE walls located at the former rental car maintenance facility at BWI airport. Minor drainage and maintenance issues were addressed based on the findings. All four retaining walls have been found to have performed as designed, and are anticipated to continue to perform as designed for the remainder of their original 75 year design life.

REFERENCES

American Association of State Highway Officials (AASHTO), *Standard Specifications for Highway Bridges*, 17th Edition, 2002.

Michael Baker, Jr., Inc., Letter Report, *Contract No. MAA-AE-01-008, Task 1963.1 Mechanically Stabilized Earth Wall*, October 1, 2004.

Parsons Brinckerhoff, *Evaluation of Existing Retaining Walls at the Former Rental Car Maintenance Facility, Elkridge Landing Road, Linthicum, Maryland, Contract No. MAA-AE-05-014,* March 2006.

The Reinforced Earth Company, Letter Report, *Wall Condition Survey, Elkridge Landing Road Near BWI Airport, RECO Project Number 11891*, November 22, 2005.

HEEDING NATURE'S CALL: REPLACING MSE WALL WITH A BRIDGE

Khamis Haramy[1], Scott A. Anderson Ph.D., P.E[2] and, Daniel E. Alzamora, P.E.[3]

[1] Geotechnical Engineer, Federal Highway Administration, Federal Lands Highway Division, 12300 W. Dakota Ave., Lakewood, CO 80228; Khamis.haramy@dot.gov
[2] Geotechnical and Hydraulics TST Leader, Federal Highway Administration, Resource Center, 12300 W. Dakota Ave., Lakewood, CO 80228; Scott.Anderson@dot.gov
[3] Geotechnical Engineer, Federal Highway Administration, Resource Center, 12300 W. Dakota Ave., Lakewood, CO 80228; Daniel.Alzamora@dot.gov

ABSTRACT: A wild forest fire that swept through the Catalina Mountains near Tucson, Arizona, burnt much of the vegetation along the General Hitchcock Highway and in the watershed above. This event was followed by several precipitation events which caused large amounts of sediment to reach and plug drainage-ditches and culverts along the roadway. Several months later an exceptional storm produced over 9 inches of rain in the watershed and caused the roadway drainage features to become overwhelmed with flowing water and debris. As a result, an approximately 60-foot segment of an existing MSE wall was overtopped and undermined, and subsequently collapsed. Evaluation after the wall failure indicated that the increased flows, bulked by debris, were too large to pass through the corrugated metal pipe culvert installed through the wall, and a larger opening was needed to prevent similar occurrences in the future. Several repair recommendations were evaluated for permanently repairing the failed roadway segment. The following factors were considered: 1) the presence of loose, easily eroded superficial materials, 2) steep slopes below the wall, 3) widely variable bedrock depths, 4) environmental restrictions, 5) maintenance of traffic, 6) hydraulic requirements, and 7) construction costs.

This paper summarizes the causes of the failure, the alternatives considered, and a rationale for the selection of the preferred alternative of a bridge to be constructed between the remaining MSE wall sections.

INTRODUCTION

The General Hitchcock Highway is an approximately 25-mile long route located in the Coronado National Forest near Tucson, AZ. This highway is the only paved access to Mount Lemmon and the Santa Catalina Mountain Range. It services a ski area and several hundred residences and businesses. As the highway ascends up the mountain it traverses steep rocky terrain, thin residual non-cohesive soils, high altitude arid or semi-arid climate, and low-density ground cover. The geology of the Santa Catalina Mountains is complex including ancient and recent episodes of volcanic activity, mountain building, sediment deposition, and metamorphism separated by periods of erosion. Faulting, fracturing, and differences in rock type and erosion resistance have resulted in a main high mountain mass separated from the rough, lower fore-range by several narrow canyons which the road follows. The rock types are mostly igneous and metamorphic, generally composed of granite, granitic gneiss, and gneiss. Soils range from very shallow, rocky, and arid soils in the low elevation foothills to deeper, more saturated, semi-humid soils in the higher areas. Topsoil is generally sparse throughout, especially at the lower elevations which are typical of a desert environment.

The highway was reconstructed in a series of 7 projects between 1988 and 2005. This project received much acclaim and national recognition for the context-sensitive design approach and innovative aesthetic treatments. To minimize impacts, the roadway embankments were retained by approximately 350,000 square-feet of MSE walls, many of which cross drainages. Surface water flows are managed by curbs, ditches, culverts and drop inlets, occasionally installed through walls as necessary.

Figure 1: (Left) Shows the wall prior to failure: (Right) Shows failed wall

In June of 2003, a large wild fire, known as the "Aspen Fire", swept through the forest burning much of the vegetation within an 85,000 acre area along the highway. As a result, the corridor began experiencing large amounts of sediment debris and natural erosion of bedrock onto the roadway during heavy precipitation events. These conditions clogged culverts, causing runoff and debris to flow over the roadway, significantly damaging existing embankments and retaining walls. Followed by a series of monsoon storms (between July 27th and 31st, 2006) produced over nine inches of rain on Mount Lemmon. This heavy rainfall caused rockslides, debris flows, flooding, and culvert overtopping at many locations along the highway, and resulted in partial embankment washout and wall failures. The most severe wall failures occurred at MP 9.8 where an approximately 60-foot long segment of an existing MSE wall partially collapsed, as shown in Figure 1.

The failed segment of the 20-foot high MSE wall at MP 9.8 was constructed only three years prior to the failure (2003) using a welded wire stone faced MSE wall system. The reinforcement lengths were designed to be 70% of the wall height. Within the failed area the reinforcement lengths were approximately 14-feet and were spaced 24 inch vertically. A 36-inch corrugated metal pipe culvert (CMP) was also installed within this wall segment to handle surface water runoff and uphill drainage. The CMP inlet for handling uphill drainage was located on the inboard side of the roadway with the outlet located near the base of the wall and extending approximately 10-feet in front of the wall face. A drop inlet near the roadway outboard edge was connected to an 18-inch vertical CMP located within the MSE wall approximately 24-inches from the face. This pipe was tied into the 36-inch CMP at the bottom of the wall.

INVESTIGATION OF WALL FAILURE

Extraordinary events such as wild fires and heavy rainfalls destroyed vegetation and greatly increased the runoff and sediment from that anticipated during design. To gain a better understanding of the effect of the fire on the surface runoff, the data of four gauged watersheds in the Santa Catalina Mountains were revised after the fire. The results indicated that post-burn peak runoff rates increased up to 6.5 times the pre-burn rates for those watersheds. Consequently, a two-year rainfall event could produce a 75-year runoff event.

In retrospect, it is not surprising that in the months following the wild fires, severe runoff from summer monsoon rains and sedimentation resulted in plugged culverts and ditches which overtopped the roadway curbs including the ones at the failed location. These conditions caused significant erosion to downhill slopes and damage to several retaining structures along the roadway. Steps were being taken to repair and maintain the MSE walls on the route through 2006, when the storm occurred. This storm was much larger than anything else experienced; it had an estimated return interval of approximately 1000 years.

The flooding shown in Figure 2 is from a very rare event but it also illustrates what could happen from several smaller storms, and what is believed to be the cause of the failure. Based on our forensic study of this and several other similar walls on the route, we believe the following processes are responsible. First, surface water exceeds the capacity of the curb and deposited debris on the road channelizes the water so that when it flows beyond the guard rail it erodes through the apron of compacted fill on the fore slope and reaches the wall facing rock. The wall facing rock is a zone of uniformly graded cobble size material that extends two to three feet back from the wall face for the full height and length of the wall. Water reaching the facing rock can flow vertically downward through the rock with ease, and reach the bottom of the wall. For these walls, water that reached the base of the wall could not easily flow laterally through the wire wall face because the wall was embedded by compacted fill that was intended to provide adequate bearing capacity and, ironically, keep surface water flowing away from the toe of the wall, where it could cause damage.

Figure 2: Surface water overtopping MSE wall

Instead of flowing perpendicular to the roadway and down the slope, the water at the base of the wall within the facing rock turned parallel to the face (and road), and flowed through the facing rock to a low point in the wall. At the MP 9.8 wall, the lowest point is where the culvert and drop inlet pipes met. When the water reached this point it was impeded by the pipes and by water flowing from the other side of the pipes. Water built up in the facing column below grade until it either caused failure of the compacted fill in front of the wall or it overtopped causing failure by erosion. Either way, the foundation of the facing rock was lost and there was nothing supporting it from running out the bottom of the wall except widely spaced reinforcement wires. Since the facing rock was uniformly graded and designed to be self-compacting, it was poor at bridging the opening between these wires. The wall failure extended approximately 60 feet along the roadway and to the roadway centerline. Following the failure, and to reestablish roadway access, the retained fill at this segment was temporarily supported with soil nails and shotcrete.

It is important for the investigation of failure to note that the road at MP 9.8 had previously experienced damage from debris flow and land sliding. In fact, the wall itself was part of an earlier emergency repair of an embankment failure. Giving consideration of this and the increased expectations of runoff and debris, a forensic engineering evaluation was performed of the adequacy of the design for the route, particularly the hydraulic and retaining wall features. It was determined that significantly greater capacity was needed for the cross drainages and that the conveyance of water beneath the road should be as large an opening as could reasonably be constructed, and that the grade of the cross drainage should be 25% or more to prevent build-up of debris.

RECONSTRUCTION ALTERNATIVES

Several repair recommendations were evaluated. Reconstruction recommendations for the failed MSE wall site are constrained by environmental restrictions, restrictions on traffic delays, hydraulic requirements, available geotechnical data, constructability, long-term maintenance requirements, and construction costs.

American peregrine falcons and Mexican spotted owls are known to exist within the project limits. Because these endangered species may be affected by noise, construction activity is limited to September through March. In order to construct this project in one season, the alternatives were limited to those which could be completed within a 6 month period, while providing public access with minimal traffic delays.

Due to loose highly eroded surficial materials and steep slopes, bedrock depths could have a significant impact on the costs of the various alternatives. For some alternatives, a deeper than anticipated bedrock surface or unforeseen scour vulnerability could cause a project redesign and delays. Therefore, a comprehensive geotechnical investigation program was completed to determine bedrock depths at various locations along the repair site. The field program consisted mainly of drilling ten borings within an 80-foot segment of the roadway near the failed wall to provide information for each proposed alternative. The subsurface materials at the site indicate that the overburden soils can be classified as well-graded gravels with less than 8% non-plastic fines. These soils were classified as GW-GM in the Unified Soil Classification System and as A-1-a (0) AASHTO Classifications system. Bedrock is granitic gneiss with high core recovery/RQD and a uniaxial compressive strength (UCS) varying between 5,000 and 25,000 psi. The boring results also depict bedrock at varying depth within the 80 foot segment along the roadway. Based on the field evaluation results, the following factors were considered during the development of repair alternatives:

1. Difficult setting constraints including traffic maintenance, construction schedule limits, available roadway width, wall stabilization, and steep channel bottom (>25%).
2. Failed MSE wall segments will be removed and remaining section will be repaired using in-kind materials for aesthetic reasons.
3. The failed culvert was determined to be undersized. Preliminary hydraulics evaluations indicate a larger drainage structure with a minimum opening width of 12 feet and height of 4 feet is required to provide adequate capacity and debris/sediment passage.
4. An open-bottom structure to minimize overflow velocities for erosion and down cutting of the lower slope was recommended by hydraulics.
5. The drainage structure should either be bearing or anchored into bedrock and should have armoring that is of sufficient strength to protect the remaining MSE wall from sediment flow.
6. The structure should be constructed so that routine maintenance is easily conducted with minimal disruption to traffic flow.

Several alternatives were identified to establish adequate flow and to rebuild the failed roadway segment. The hydraulic and structural capacity of the existing wall/culvert system was determined to be insufficient to handle heavy potential runoff and continuing debris flow at this location following the July 2006 event. Replacing the failed pipe with another pipe was therefore not considered.

Four alternatives were considered for repairing the failed MSE wall and improving hydraulic capacity at the site.

1) **Open-Bottom Culvert:** This alternative consists of MSE walls armored with engineered mega-modular blocks spanned by a metal culvert. The modular block systems are an attractive, economical, and durable alternative to cast-in-place concrete structures and can be rapidly installed. The inherent design flexibility can also accommodate a wide variety of site constraints. A wire-faced MSE wall along the length of the channel without an armored facing is not an option because large sediments or debris flow may damage the facing elements. The walls would be keyed into bedrock. The culvert would be a corrugated metal pre-fabricated system, spanning approximately 18 feet along the roadway. The culvert would be supported by cast-in-place footings poured on the newly constructed modular block walls. This structure would be sloped towards the outlet side with approximate opening heights of 18 feet at the outlet reducing to 7 feet at the inlet, depending on new invert elevation. The structure would have a minimum opening width of 12 feet. This structure would be erected in conjunction with the MSE wall reconstruction. This system may be time-consuming during construction because it is all custom-built in place.

2) **Close-bottom Culvert:** A10-foot span by 5-foot rise cast-in-place reinforced concrete box culvert or a corrugated metal box-shape culvert with a reinforced floor was evaluated. The culvert would be anchored in place and extended down the steep (25%) slope beyond the wall face. At the outlet, the flow would be conveyed using a rectangular-shaped channel built into the embankment or several drop structures, extending from the box outlet to the bottom of the embankment, adjacent to the creek, which would allow the flow to outlet directly onto solid rock or boulders embedded into the natural stream channel.

   An additional close-bottom culvert option is a 14-ft x 7-ft concrete box culvert with 3-ft of embedment. This type of configuration would provide an outlet velocity that is equivalent to the open bottom culvert and bridge alternatives.

3) **Bridge Supported by Spread Footings:** This option includes a bridge supported on a spread footing foundation within the MSE wall. The bridge superstructure would be constructed of precast pre-stressed concrete slab beams, tied together transversely with post-tensioned bar or strand. MSE wall armoring could be constructed of either modular block or cast in place concrete keyed into bedrock. This structure extends about 30-feet along the roadway, and will also be sloped towards the outlet side with an approximate opening height of 19 feet at the outlet and 8 feet at the inlet.

4) **Bridge Supported by Micropiles:** This option is the same as described above but the micropiles would transfer the loads deep into the bedrock to prevent settlement problems within the reinforced wall fill. The foundation elements increases the construction difficulty when mixed with existing wall elements and temporary repair elements all constructed in the same area. This alternative is self supported and is less affected by potential future wall concerns.

Prior to installing any structure, the failed wall segment must be removed. To prevent wall fill materials from falling out of the facing elements perpendicular to the cut, a large un-failed wall segment must also be removed stepping up every 2 feet at a 1V:1H slope ratio. An area extending about 180 feet along the roadway would be impacted by the excavation. The structure would be constructed and the MSE wall rebuilt to match existing.

A longer bridge option was proposed to eliminate the removal of un-failed segments of the MSE wall and to reduce the costs of the structure by replacing vertical wall segments along the culvert with slope paving. A 60-foot long bridge spanning the temporary soil nail repaired area provides a larger opening for debris passage. This option would utilize slightly deeper superstructure than the 30-foot span, but can be accommodated with a simple superstructure of pre-stressed box beam girders. This option more than doubles the available flow area of the 30-foot bridge options while minimizing the impacts of wall repair area. This bridge would also be supported on micropiles, (Figure 3).

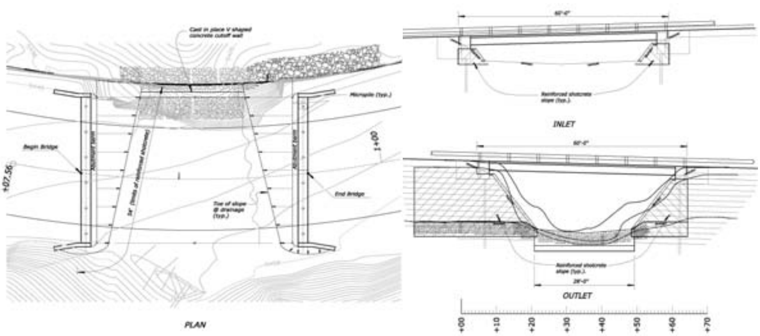

Figure 3: Plan View for a Sixty-Foot Span Bridge Option

A disadvantage of the longer span bridge alternative is accommodating the horizontal and vertical curvature and the superelvation transition of the roadway alignment. Variable depth wearing surface can be employed over the concrete boxes to accommodate the superelevation requirements while continuing to accommodate the required horizontal curve by providing a slightly wider than required superstructure. These disadvantages would be present with all the bridge alternatives but are magnified with the longer span lengths. A cut-off wall will also be required at the outlet and/or the inlet to minimize risks due to scour.

SUMMARY AND CONCLUSIONS

The 60-foot span bridge alternative was recommended and selected for this site because it provides the largest hydraulic capacity and the lowest construction cost. This alternative also requires shorter construction duration and can be constructed within the allowed period for construction. A plan view of the designed bridge is illustrated in Figure 3.

Regardless of which alternative was selected, improvements were required to the existing wall and the roadway drainage system around this area to manage surface water collection and transfer outside the structure limits. This was achieved by a combination of design features. A paved conveyance ditch was recommended to improve the collection of surface runoff and debris entering the roadway ditch at multiple locations. Curb removal within the project limits was recommended to allow water to sheet flow over the wall. The toe of the wall will be excavated down to the bottom of the wall and riprap will be placed along the toe of the wall to not only protect the base and foundation of the wall from future erosion but to also prevent hydrostatic pressure built-up in the wall facing.

The wire-faced MSE wall has been a very important wall type for this route. The wall type was selected initially because it met requirements for constructability, cost and aesthetics in a very difficult natural environment. The MP 9.8 wall and many others on the route have been tested in only a few years with extreme events, including fire and rain, and floods much greater than the walls were designed for. This has afforded us an opportunity to, in general, look at the wall performance under extreme conditions and, specifically for MP 9.8, recognize the limits of the wall with respect to managing overtopping from surface water and passing debris flows through culverts, and to redesign the structure as a bridge with MSE abutments to heed nature’s call.

Acknowledgement

The authors would like to thank the project manager, Tom Puto, and the Central Federal Lands project design team members Angela Johnson, Karl Eikerman, and Roger Kilgore for their contributions. We also would like to thank the construction team members Tom Bonar and Leo De Paula.

Collapse of MSE Wall Panels Due to the Effects of Freezing Temperatures

William J. Neely[1]

[1] Retaining Wall Services, Inc., 1660 Hotel Circle North, Suite 304, San Diego, CA 92108; email: wneely@retainingwallservices.com

ABSTRACT

This paper summarizes investigations and studies that were undertaken to identify the cause of the collapse of several panels in an MSE wall. The collapse was caused by the presence of frost susceptible backfill near the top of the wall. This material, combined with the large freezing index at the site, probably resulted in frost penetration depths of up to 2m behind the wall panels. After the collapsed section was repaired, outward movement of panels in the same area continued, aggravated by accumulation of water from snow melt in a shallow depression behind the wall.

INTRODUCTION

The development of a new mine in the western U.S. in the late 1970s included several mechanically stabilized earth (MSE) retaining walls. About eight years after construction, a number of precast concrete panels in a section of one wall collapsed. The collapse, which occurred in early spring, was preceded by outward bulging in several columns of panels in the upper 5m of the wall. No problems have been experienced with any of the other MSE walls on the project. The collapse was repaired by field-splicing replacement panels to the existing soil reinforcing strips; backfill lost in the collapse was replaced with No.57 stone, a coarse-grained material considered non-frost susceptible. The repaired section functioned satisfactorily for almost twenty years, but in the spring of 2006 outward bulging of panels was again occurring in the same section of wall. This paper describes the investigation and studies that were undertaken in 2007 to identify the causes of the earlier collapse and the continuing deformation of the wall face and to develop appropriate remedial measures. Description of the remedial work is beyond the scope of this paper.

BRIEF HISTORY OF MOVEMENTS AT WALL NO. 4

The collapse occurred near the west end of Wall 4, which is oriented in a northeast-southwest direction, with the MSE wall panels facing predominantly northward; see Figure 1. The collapse occurred where the wall height is about 11.2m. The panels are nominal 1.5m cruciform-shaped reinforced concrete sections having a thickness of 180mm. The soil reinforcing strips consist of 40 x 5mm and 60 x 5mm galvanized ribbed steel strips having a nominal yield strength of 248MPa. In the vicinity of the collapse an inclined conveyor crosses Wall 4 at right-angles to the wall face. The edge of a large spread footing supporting one of the conveyor bents is only 2.5m behind the MSE wall panels. Outward displacement of panels was first recognized in April 1986. The most severe distress was seen in the top four courses of panels. The fill surface behind the wall up to the edge of the conveyor footing had settled, although there was no evidence of any movement of the 11m long x 2.1m wide conveyor footing. Mine personnel measured outward horizontal displacements of panels of 90-120mm in some locations, with bulging evident to depths of 5m below the top of the wall. Subsequent measurements in May 1986 indicated no further movement. There were also reports of water seepage through panel joints in early spring.

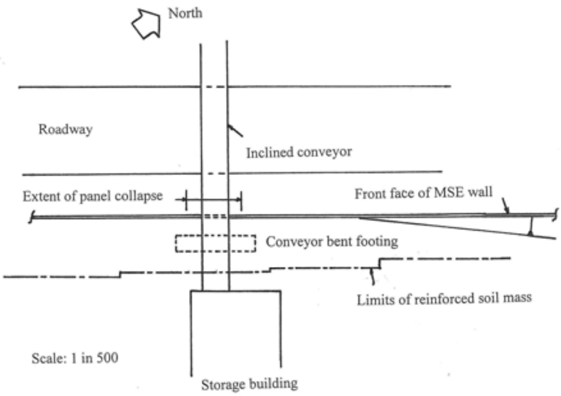

Figure 1. Plan view of MSE wall showing area of collapse.

An initial investigation by the MSE wall supplier focused on the possibility of accelerated corrosion of the reinforcing strips and saturation of the backfill material. Samples of backfill were recovered for testing. The fill material (SW-SM in terms of USCS system) has a mean grain size of 1.4mm and 5 percent finer than 0.075mm. Electrochemical testing showed pH=5.5, chloride and sulfate contents of 0.8 and about 80ppm respectively and a resistivity of 6,700 ohm-cm at 100% saturation. These data indicate that the backfill is practically inert, eliminating corrosion of soil reinforcement as the cause of panel displacements.

THE 1987 COLLAPSE

No remedial action was taken to correct the wall movements first seen in April 1986. About a year later, at the end of March 1987, collapse of seven full-size panels occurred in the bulged area. Figure 2 shows an elevation of the section of wall immediately underneath the conveyor, showing the panels that collapsed. Figure 3 shows that four of the panels fell to the ground while the other three were left hanging precariously, held in place by alignment pins or by soil reinforcing strips. This photograph was taken during a site visit in July 1987 about three months after the collapse. The three top-course panels did not bulge outwards appreciably. The reinforcing strips on these panels were intact and connected to the tie strips in the back of the panels; the reinforcing strips were bent downwards as they were pulled through the soil as backfill ran through the opening created by the collapsed panels.

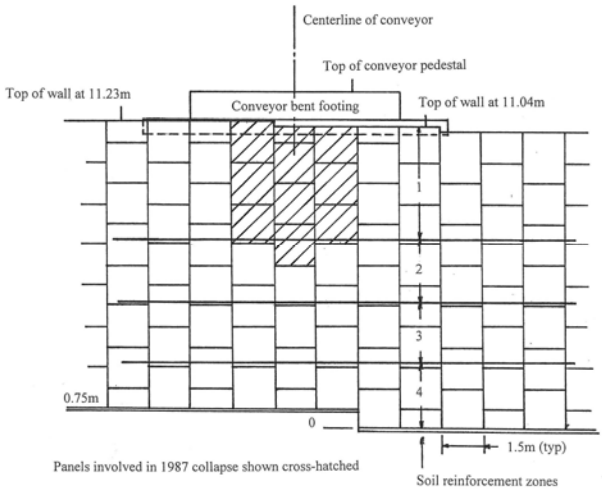

Figure 2. Partial elevation of wall face indicating panels involved in 1987 collapse.

The reinforcing strips for the panels which fell to the ground failed in tension at the bolt hole location. The strips were in excellent condition with the original galvanizing intact. Figure 3 indicates a series of reddish-brown/black vertical stains on the panels in the failure section, including those in the top course. This staining, which was not seen in other areas of Wall 4, suggests that flow occurred over the top of the wall, not through the joints, as suggested earlier. The collapse left a steep failure scarp about 1-1.5m deep in the reinforced soil mass to a depth of 5m.

Figure 3. Photograph of panel collapse showing inclined conveyor.

THE 1987 REPAIRS

The mine and the wall supplier together concluded that the collapse was due to poor surface drainage behind the wall, aggravated by cracked asphalt paving between the wall and the conveyor footing. However, no analyses were undertaken to estimate the forces needed to produce failure of the soil reinforcing strips at the bolt holes and whether or not such forces could be created by water pressure. The repairs in September 1987 consisted of replacing damaged panels and connecting them to the existing soil reinforcement using short lengths of reinforcing strips and double splice plates. The backfill lost in the collapse was replaced with No. 57 crushed stone.

FURTHER MOVEMENTS AT WALL NO. 4

The 1987 repairs functioned well for almost two decades, with no reports of any further panel movements until February 2006. It is possible that these new movements may have begun earlier but went unnoticed, as the mine had ceased operations for several years. By mid-March 2006 additional panel displacements of 25-75mm had occurred in exactly the same location as the 1987 collapse. In June 2006, after most of the snow had melted, it was noticed that water appeared to drain towards a low spot behind the wall, directly above the bulged panels and in the same area as the 1987 collapse. The ground surface behind the wall was covered by asphalt paving, except in the area of the original collapse where the backfill was topped with a tar sealing coat. The asphalt appeared to have moved about 150mm away from the edge of the conveyor footing, indicating lateral movement that had occurred since the 1987 repairs. There was no evidence of any movement of the conveyor footing.

INVESTIGATION OF PANEL COLLAPSE AND WALL MOVEMENTS

Wall Construction Records. The only records available are reports by the wall supplier made during periodic visits during construction of Wall 4. There is no mention of problems until the wall was almost complete when it was discovered that a section of the reinforced zone near the top of the wall had been backfilled with on-site material rather than the specified crushed rock material. The on-site material, which apparently contained an appreciable amount of fines (<0.075mm) was dug out after panels had moved out significantly during construction. The panels were pulled back into alignment and the area backfilled. Other comments make it almost certain that this problem occurred near the conveyor footing in the section of wall involved in the 1987 collapse. It also seems certain that only enough backfill material was removed (and then replaced) to allow the displaced panels to be pulled into proper alignment. A decision was made to monitor this section of wall and, if after a month, no further outward movement occurred, then it would be accepted. No movements were observed and Wall 4 was completed on schedule in September 1979, just before construction was shut down for the winter.

Wall Specifications and Design. The project specifications required that granular backfill meet gradation limits with 100 percent passing 150mm and a fines content (<

0.075mm) less than 15%. Surprisingly, the specifications also stated that materials not meeting these gradation limits could be used provided the plasticity index is less than five and the fraction finer than 0.015mm is less than 15%. Allowing such a large fraction of very fine particles in MSE backfill is very unusual. Gradation is a critical aspect of backfill for any type of retaining wall, given the environmental factors at this site. The mine is located at an altitude of more than 3,000m where the mean air freezing index is between 600 and 900 degree Celsius-days. The air freezing index is the area below zero degrees Celsius on a plot of temperature vs. time. Empirical correlations developed by U.S. Army Corps of Engineers (1961) suggest that the corresponding depth of frost penetration would be about 1.7-2.5m. No consideration appears to have been given in design to the susceptibility to frost damage of backfill material meeting the gradation limits in the specification. Casagrande (1932) found 0.02mm to be a critical grain size. A material with up to 15% finer than 0.015mm would certainly be classified as frost susceptible under this criterion. Grain size analyses are not available for the original crushed rock backfill used in the MSE walls, although field reports refer to it as having about 8% finer than 0.075mm. In contrast, the on-site material that was used in the section of Wall 4 where construction problems were encountered and collapse of facing panels occurred eight years later, was described as containing ‘amounts of clay’, with as much as 37% finer than 0.075mm. Given such a high fines content, it seems reasonable to expect that this material would be frost susceptible.

The design of the reinforced soil mass followed standards and methodologies similar to those in use today. The reinforcing strips were galvanized (thickness 86 microns). In the area of interest the reinforcing strips are 7.9m long. Reinforcement tensions due to loads on the conveyor footing were quite small and only affected reinforcing strips more than 5m below the top of the wall. Factors of safety with respect to sliding, overturning and bearing capacity are the same as those in current practice. The yield stress of the reinforcing strips averaged 338MPa, with an ultimate tensile strength of 470MPa. For design purposes, the nominal yield stress for the strips was taken as 248MPa, with an allowable tensile stress at the end of the nominal design life of 138MPa, corresponding to 55% of the nominal yield stress.

Effects of Freezing Temperatures. The high air freezing index could lead to frost penetration of up to 2m behind the face of the MSE walls. Frost action and the formation of ice lenses in soils require freezing temperatures, a source of water to supply moisture to the freezing front and a frost susceptible soil type. In retaining walls, the extraction of heat from the soil occurs primarily in a horizontal direction with ice lensing tending to occur parallel to the face of the wall. This can result in very large pressures on the wall. Rehman and Broms (1972) reported a field test in which a 2m high cantilever wall backfilled with uncompacted silty sand was allowed to freeze. The lateral earth pressures increased by 40-50kPa at some levels behind the wall. Broms and Stille (1976) measured an increase in the forces in tiebacks supporting a sheet pile wall and found that freezing of water which had percolated through cracks in the clay led to increases in lateral earth pressure of 15 to 30kPa. At a second site, freezing of soil behind a tied-back sheet pile wall resulted in increases in tieback loads corresponding to lateral pressures averaging 20kPa. On the basis of field experience Sui et al. (1993) classified frost heave and the resulting maximum horizontal pressure acting on fully restrained retaining walls into five categories; see Table 1.

Table 1. Frost Heave Pressures on Fully Restrained Retaining Walls.

Category	I	II	III	IV	V
Frost Heave (cm)	< 2	2 – 5	5 – 12	12 – 22	> 22
Lateral Heave Pressure (kPa)	< 50	50 – 100	100 – 150	150 – 200	200 - 250

The values Table 1 represent maximum values that are reached only in the middle third of the wall height. The distribution of horizontal frost pressure corresponds to an average pressure over the height of the wall of about 70% of the values in Table 1. In practice, a reduction in lateral heave pressure needs to be made to account for the inherent flexibility of tied-back sheet pile walls, where some lateral deformation occurs because of the flexibility of the sheeting and the extensibility of the tieback tendons. A similar situation arises in MSE walls where the increased pressures may lead to either tensile or geotechnical failure of soil reinforcing strips, although, unlike tiebacks which have long unbonded free lengths, soil reinforcing strips develop resistance to movement over their full length. In addition, the operating tensile stress in tieback tendons is much greater than for reinforcing strips; hence, greater restraint and larger frost heave pressures would be expected in an MSE wall.

Forces in Reinforcing Strips. The 1987 collapse occurred because of failure of reinforcing strips at the bolt holes used to connect them to the panels. Most of the strips that failed were 40 x 5mm. A total loss in thickness of 1.27mm was assumed to occur over the design life, leaving 149.2mm^2 per strip to resist internal lateral earth pressures. The allowable tensile stress was 136.5MPa, corresponding to a design reinforcement tension of 20.4kN per strip. When the collapse occurred, there had been no loss of strip thickness. The net cross-sectional area at the bolt hole is 128.6mm^2, implying that failure would require a force equal to the net area times the ultimate tensile strength (471MPa), or 60.6kN. The area of a full size panel is 2.25m^2. Since the panels that collapsed had four strips, then the average lateral pressure at failure would have been about 110kPa.

Using reinforcement tensions from the original MSE wall design gives an average lateral pressure of 34kPa on a panel near the bottom of the collapsed section between 3 and 4.5m below the top of the wall. Poor drainage conditions just behind the wall were originally cited as a cause of the 1987 collapse. Assuming the backfill is flooded to a depth of 4.5m, the average lateral pressure would increase to about 47kPa, or only about 40% of that needed to produce failure of the reinforcing strips at the bolt holes. Reinforcing strip forces may also increase because of temperature variations. During winter, temperatures may range from overnight lows around -40°C to daytime highs just above freezing. If the reinforced soil mass is frozen at 0°C followed by a temperature drop to -40°C, the difference in thermal expansion coefficients for the granular fill and the steel strips would lead to an increase in reinforcement stress of about 28MPa, giving a maximum stress at the bolt hole of 177MPa or only about one-third of that needed to cause rupture. The conveyor footing loads have no effect on tensions in the upper 5m of the wall, because of the 2V:1H spread of load from the edge of the footing. Increased lateral pressures due to frost heave are considered the most probable cause of the collapse. It is known that backfill containing appreciable fines and clay was placed in a section of Wall 4 as it neared completion. Although the panels displaced during construction were pulled back into alignment, it is almost certain that most of the clayey (and frost susceptible) fill was left in place.

Collapse Mechanism. As frost heave pressures increase, relative displacement or slip between the soil and the reinforcing strips occurs, particularly at shallow depths where pullout resistance is limited by low overburden pressures. When this happens, panels move outwards relieving some of the pressure. The next freezing cycle causes strip loads to build up again, resulting in further displacement. In this way, the strips are pulled through the soil in a series of frost-jacking actions, accumulating permanent displacements in some of the freezing cycles as a result of yielding and irrecoverable plastic strains.

Yielding and plastic straining cause some hardening of the load-displacement behavior of the strips, such that an increase in load is needed to produce slip in subsequent freezing cycles. Using the conservative default values in AASHTO (2002) for the pullout friction factor f* for ribbed strips, it can be shown that geotechnical failure at the soil/strip interface would be expected to occur at an average panel pressure of about 100kPa for a panel in the third course below the top of the wall. This is very close to the value of 110kPa, corresponding to the ultimate tensile capacity of four 40 x 5mm strips. Prior to the 1987 collapse, panel displacements averaged 20-90mm over the top 4.5m of the wall. Considering these displacements as the amount of frost heave, Table 1 suggests horizontal heave pressures of up to 150kPa on a fully restrained retaining wall. Using the method of Sui et al. (1993), a heave pressure of 100kPa would be consistent with Category III in Table 1 with a degree of restraint of about 80%.

Measurements of panel displacements about a year before the collapse showed average outward movements between 20 and 90mm over the top 4.5-5m of the wall, with some panels having bulged as much as 140mm. Equating the volume of the bulge in the wall face to that of the settlement trough between the back of the wall and the edge of the conveyor footing, it is estimated that before collapse the depression in the ground surface behind the panels may have been about 0.3m deep. During early spring, when daytime temperatures are often above freezing, water from melting snow would flow towards the low spot, creating a small reservoir. The low spot is in almost constant shadow in the spring. Some of the water probably flowed vertically down into the MSE backfill along the back of the panels. When temperatures fall during the night, the water and soil freeze, resulting in large lateral pressures on the panels and progressively greater outward displacements, ultimately leading to rupture of some of the reinforcing strips. This scenario, which is repeated almost daily for several weeks each year, is possible only in early spring, when daytime temperatures are regularly above freezing. Expanding ice lenses are capable of generating pressures as large as 2500kPa in confined conditions; however such large pressures are not possible in this case because the tensile capacity of the strips cannot sustain an average pressure of more than 110kPa. Figure 3 shows that the strips in the top course of panels did not rupture. The reason for this is that at shallow depths the pullout resistance is significantly lower than the tensile capacity of the strips. At greater depths, pullout resistance exceeds the tensile capacity of the soil reinforcing strips. Because of the higher pullout resistance, panels at greater depths below the top of the wall approach fully restrained conditions, leading to increased horizontal heave pressures until rupture of the strips occurs.

CONCLUSIONS

This case history demonstrates the consequences of failing to recognize the critical importance of grain size characteristics and frost heave potential of a small portion of the reinforced backfill. The need to complete the construction of Wall 4 before the winter shutdown probably meant that the problem of unsuitable backfill material was not investigated as thoroughly as it should have been. Although the potential for frost heave was not fully taken into account at the design stage, the excellent behavior of other sections of Wall 4 and other MSE walls on the project, shows that the high freezing index at the site can be safely dealt with, provided the backfill material meets the gradation requirements commonly specified for MSE fill. Nevertheless, where significant frost penetration depths are anticipated, extra care must be taken in preparing design and specification documents and testing and inspection procedures to ensure that the proper backfill material is used. More frequent testing may be necessary to ensure consistency of all MSE wall materials.

REFERENCES

Broms, B.B., and Stille, H., (1976). Failure of anchored sheet pile walls. Proc. ASCE, Jnl. Geot. Engrg. Div., Vol. 102, No. GT3, pp 235-251.

Casagrande, A., (1932). Disc. of “A new theory of frost heaving,” by A.C. Benkelman and F.R. Ohlmstead, Proc. Highway Res. Board, Vol. II, pp 168-172.

Rehnman, S.E., and Broms, B.B., (1972). Lateral pressures on basement wall: Results from full-scale tests. Proc. 5th Eur. Conf. on Soil Mech., Madrid, Vol. 1, pp 189-197.

Sui, T., Na, W., Li, D., and Jiang, W., (1993). The method of determining design values of horizontal heave force on retaining walls in seasonally frozen ground area. Proc. 16th Int. Conf. on Permafrost, Beijing, Vol. 1, pp 592-595.

US Army Corps of Engineers, (1961). Retaining Walls: Engineering and Design. Manual EM 1110-2502, 13 p.

Lessons Learned from Settlement of Three Highway Embankment MSE Walls

Marilyn D. Dodson[1], M. ASCE, P.E.

[1]Geotechnical Engineer, Federal Highway Administration, Central Federal Lands Highway Division, 12300 West Dakota Avenue, Lakewood, Colorado 80228; Marilyn.Dodson@dot.gov

ABSTRACT: Three MSE walls were constructed along a two-lane rural highway where the use of non-standard on-site material as wall backfill initially appeared to be a great cost-savings measure with relatively low risk to the overall performance of the walls. The MSE walls ranged in maximum height from 8 to 11 meters and extended from 119 to 332 meters in length. Settlement of 76 to 152 millimeters was observed in the outbound roadway lane less than six months after construction. Longitudinal cracking appeared near the centerline of the roadway above the MSE walls, with voids up to 2 meters deep at spot locations. Roadway distress above the MSE walls was caused by settlement and piping of the wall backfill material. Several site-specific issues contributing to the MSE wall distress, including; (1) up to 45% fines in the wall backfill material, (2) rigid temporary shoring (soil nail walls) at the back of the more flexible MSE wall, and (3) an unlined ditch at the top of the wall, allowing surface water to flow through the clean gravel roadway base course to the back of the MSE wall. Three main lessons were learned from this case history. First, using non-standard on-site material as wall backfill ended up costing more than if imported fill was used, even though initial project costs were less and it appeared to be low risk to the wall performance. Secondly, temporary shoring systems need to be considered in conjunction with the design of MSE walls due to the differences in potential deformation between the two systems, which could lead to cracking at the interface of the two walls. Thirdly, prevention of surface water infiltration into the MSE wall system would have prevented piping of the wall backfill material and drainage improvements are relatively inexpensive costs compared to the overall cost of the entire MSE wall.

BACKGROUND

Three wire-faced MSE walls with metal reinforcement were constructed as part of a 3.63 km long roadway improvement project in northern California in the Fall of 2004. The route resides in steep, mountainous terrain that is subject to short-duration, high precipitation events that cause notable erosion in exposed slopes. On-site materials consist of non-plastic sandy silts and silty sands. In the geotechnical report, it was noted that surface run-off and short-term saturation of silty soils would be significant issues to consider when working with the on-site materials.

MSE WALL DESIGN

The retaining walls were designed based on AASHTO (2002) and FHWA guidelines (Elias, 2001) for internal and external stability. Minimum base reinforcement lengths were equal to 0.7 times the total wall height and maximum vertical spacing was 0.6 m. Due to steep foreslopes, walls were embedded 20-percent of the total wall height. Foundation fill, consisting of 300 mm of select granular backfill, was placed under each wall to provide both a uniform foundation and an alternative drainage path. Temporary shoring was installed to maintain one travel lane during construction, but the retaining system selection and design was left up to the contractor. Table 1 contains the dimensional characteristics of each wall.

Table 1. MSE wall dimensions.

MSE Wall Designation	Approx. Wall Length[a] (m)	Max.Wall Height[a](m)	Approx. Wall Face Area[a](m^2)	Foreslope Ratio	Max. Roadway Grade (%)
Wall 50	119	8	560	1.0V:2.0H	2.88
Wall 60	124	11	940	1.0V:1.5H	4.72
Wall 70	332	10	2,000	1.0V:1.5H	6.88

Notes: (a) Approximate values used, rounded to the nearest meter or square meter.

The use of non-standard on-site materials as wall backfill was explored during the 30-percent design due to the lack of locally available fill meeting the requirements for select wall backfill and the potential cost savings of not importing material from the nearest borrow pit, approximately 45 miles away. Without this cost savings, the project was in jeopardy of being truncated to stay within the allotted construction budget. On-site materials did not comply with standard specifications for select wall backfill (FHWA, 1996) due to average fines content greater than 15 percent passing the No. 200 sieve (.075mm). The percent fines are also higher than NCMA guidance for MSE wall backfill (2002). The specified soil gradations are presented in Table 2.

Table 2. Select wall backfill gradation for reinforced zone of MSE walls.

Characteristic	AASHTO/ FHWA	NCMA	Wall 50, 60, 70 On-Site Soils
Percent Passing 100 mm (4 inch)	100	100-75	100
Percent Passing 4.75 mm (No. 4 Sieve)	--	100-20	75-100
Percent Passing 0.425 mm (No. 40 Sieve)	0-60	0-60	50-85
Percent Passing 0.075 mm (No. 200 Sieve)	0-15	0-35	0-45
Plasticity Index (PI)	<6	20	<6
Liquid Limit (LL)	--	--	<20
Internal Friction Angle (degrees)	34-degrees	--	32-degrees

Risks of using the non-standard materials initially appeared low to the project design team for several reasons. Although the on-site material contained high fines, they were generally non-plastic, indicating the soil behavior was likely to consolidate relatively quickly during construction and prior to paving operations. Additionally, the majority of investigated material was comprised of less than 35 percent fines, which would be similar to NCMA guidance that has been successfully implemented on several projects. However, it was recognized that special issues would need to be addressed when using on-site soils, including adequate drainage, interaction between soil and reinforcement elements, and higher corrosion potential.

At the 95-percent design, the use of on-site materials was reconsidered by the geotechnical and construction staff based on the estimated settlement of greater than 100 mm. Mistakenly, the recommendation to change the MSE wall backfill material to imported FHWA-compliant material was not implemented. The project went to bid with the allowed use of MSE wall backfill material with fines contents up to 45%.

DEFORMATION OBSERVATIONS AND CAUSES

Bulging Facing Baskets. Construction of the MSE walls was completed in the Fall of 2004 and issues with deformation immediately followed. Bulging facing baskets were observed in all three walls on 15% of the facing panels. Wall 70 had minor bows, but was generally performing well. Walls 50 and 60 had several major bulges, measuring as much as 152 mm horizontally, which are shown in Figure 1. Bulging of the facing panels was a construction and quality control issue with the placement of the baskets. The interlocking face panels did not allow vertical movement. Small movements downward on the face panels caused the center of the basket to bulge outward. Repairs were immediately made to the deformed panels by the MSE wall supplier, and no further distress was observed.

FIG.1. Bulging facing baskets (Wall 60, left; Wall 50, right).

Although aesthetically unpleasing, the bulges were not expected to impact the structural integrity of the walls. However, the MSE wall specification for future projects was changed as a result with the following verbiage added: “Design and construct the wire-faced wall and components to have the ability to compress up to 50-mm at each layer of reinforcement without creating outward bulging of the facing elements”. Additionally, the bulging baskets indicated that some kind of vertical settlement in the wall fill was occurring post-construction.

Wall 60 Distress. Following a rain-on-snow event in the six months after construction, cracks, depressions, and voids were observed at the top of MSE Wall 60 near the centerline of the roadway. Repairs were made a few months later, but additional settlement occurred near centerline within another six months. After the second winter season, the settlement extended the full length of Wall 60 and the road had to be closed to public traffic, as illustrated in Figure 2.

FIG. 2. Wall 60 distress - open cracks in the roadway (left) and void at the interface of the MSE wall and temporary shoring wall behind (right).

Observations from FHWA construction personnel indicated distress only occurred coincident with high and sustained inboard ditchline inundations, indicating water was transporting to the shoring wall interface via the road base gravel, which lead to piping out wall backfill material within the MSE wall. Piping could be attributed to:

1. Distress observations included higher than usual settlement (> 50 mm) occurring in the MSE wall backfill, which was expected due to the use of on-site materials. However, the soil nail wall was designed separately from the MSE wall and their interaction was not considered.
2. The soil nail temporary shoring was installed nearly vertically. This allowed for a stiffness disparity in the roadway fill, contributing to shear along the back of the wall during wall fill settlement.
3. The inboard ditch in the roadway above the MSE wall was unpaved. During high precipitation events, when the ditch was full, water could travel through the clean gravel base course to the back of the MSE wall like a blanket drain. In the field, water was observed pouring out of this layer into the voids.
4. The boundary between the soil nail wall and the MSE wall contained a geosynthetic sheet drain, which would have been the natural drainage path for water travelling through the clean gravel base course. However, the high volume of water observed during the initial storm event was not anticipated in the design of the drainage system, thus overflowing its boundaries into the MSE wall backfill material.

Wall 70 Distress. Three areas along MSE Wall 70 settled at the same time and in the same manner as Wall 60 with less magnitude, as illustrated in Figure 3. Unlike Wall 60, voids were not observed at the surface and the roadway was not closed. Distress did not correlate to the highest wall sections, but appeared to be associated with roadway drainage patterns for surface water flow paths down the steep gradients and around corners.

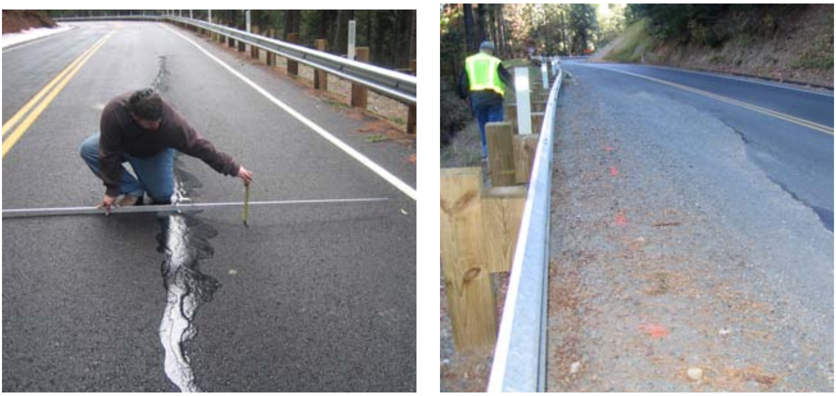

FIG. 3. Wall 70 distress consisted of vertical settlement and cracking.

Wall 50 Distress. Distress at Wall 50 did not occur until almost 5 years after construction. Distress was similar to that observed at Walls 60 and 70 with regard to piping of fine-grained backfill materials. However, deformation occurred near the guardrail posts rather than near the centerline of the roadway. Guardrail posts were driven into pilot holes and backfilled with gravel, which served as a vertical drain for surface water to infiltrate the MSE wall. Deformation at the soil nail wall and MSE wall interface was not observed, possibly due to lower wall heights at this location, resulting in less vertical settlement within the MSE wall. Deformation occurred where surface water overflows the ditchline and inundates the MSE wall behind the facing baskets, as illustrated in Figure 4.

FIG. 4. Wall 50 distress consisted of voids developing behind the guardrail posts.

MSE WALL REPAIRS

Repair work addressed temporary emergency repairs to open the roadway, as well as permanent repairs and new drainage elements. Voids were filled with hydro-patch, composed of modified asphalt base mixed with crushed aggregate. Pavement was milled and repaved, first with temporary overlay to prevent further surface water infiltration, and secondly to establish a permanent structural section.

Drainage was the most critical issue to address due to the piping of materials within the MSE wall. If water could be stopped from entering the wall, then the piping would not occur. The following drainage improvements were recommended:

1. **Cutoff wall.** Construct a cutoff wall (approximately 1-m wide by 2-m deep) upslope of the MSE wall perpendicular to the roadway to intercept subsurface water and divert it away from the structure. This was completed at Wall 60.
2. **Paved ditch.** Add paved ditches on the cutslope side of the road above Walls 50, 60, and 70 to prevent water infiltration into the exposed aggregate base.
3. **Underdrain.** Add 2-m deep standard underdrains under the paved ditches across from the MSE walls. This will be done for Walls 50, 60, and 70.
4. **Geomembrane.** Excavate the aggregate base and place an impermeable mat to prevent water flow down the face of the soil nail wall. Due to high impacts to the roadway travel lanes, excavation time, and cost, no geomembrane has been place. New walls along this route have been designed with this material.
5. **Curb Increased**. Increase paved ditch asphalt curb height from 152 mm to 203 mm. Increase the 102 mm asphalt curb height under the guardrail to 152 mm. This will divert surface water away from the MSE wall face. This has been implemented on all of the MSE walls.
6. **Cap Guardrail Post Holes**. Guardrail post holes should be capped with asphalt or concrete a minimum thickness of 152 mm to prevent surface water from entering the MSE wall reinforced zone. Every wall now has caps.

FIG. 5. Wall 60 repairs included filling the voids (left), and pouring cement caps at the top of the guardrail post holes (right).

COST COMPARISON

For purposes of evaluating the decision to use on-site materials rather than imported MSE select backfill material, rough cost estimates were made for the original construction, repairs, and imported material. These values are presented in Table 3.

Table 3. MSE wall estimated construction and repair costs.

MSE Wall Designation	Estimated Cost of Construction using On-site Soils in Reinforced Zone of MSE Wall[a]	Estimated Cost of Repairs[b]	Estimated Cost of Imported AASHTO-Compliant Soils for Reinforced Zone of MSE Wall[c]
Wall 50	$228,000	$75,000	$61,000
Wall 60	$382,900	$282,000	$164,000
Wall 70	$814,100	$336,000	$278,000
Total	**$1,425,000**	**$693,000**	**$503,000**

Notes:
(a) Construction costs were estimated based on square foot face of MSE wall, not including temporary shoring soil nail walls or the pavement structural section.
(b) Repair costs to date include temporary and permanent repair items such as remobilization to the site of equipment, construction of cutoff trench, void filling with hydropath, additional curb height, and concrete cap on guardrail holes, paved inboard ditch, inboard underdrain, temporary asphalt paving, permanent asphalt paving, painting and striping.
(c) Imported fill material costs estimated based on assumption of same source pit as project aggregate base course, approximately 45 miles haul. No other drainage improvements, such as geotextile separator material, roadway superelevation changes, paved ditches, or underdrain installation during original construction.

In this case, the estimated repair costs far exceed the estimated cost of importing material. Making repairs after construction can cost 20-30% more than during construction due to remobilization to the site, demolition of underperforming elements, and escalation of construction costs over time. Additional costs were also incurred due to performing both temporary and permanent fixes.

CONCLUSIONS

Three main lessons were learned from this case history. First, using the non-standard on-site material as MSE wall backfill ended up costing more than if imported fill was used, even though initial project costs were less and it appeared to be low risk to the wall performance.

Second, temporary shoring systems need to be considered in conjunction with the design of MSE walls due to the differences in potential deformation between the two systems. Consideration should be given to the long-term behavior of each individual wall systems (Morrison, 2006). Most of the lateral deformation of the soil nail wall is inelastic and expected to occur during excavation and prior to MSE construction. In contrast, settlement may continue during and beyond the construction of the MSE wall component. If the MSE wall rotates outward slightly due to lateral or vertical deformation, cracking can develop parallel to or along the MSE/shoring interface. The abrupt and relatively rigid interface will tend to focus differential settlement to the area immediately above the shoring, and cracking will likely result (Morrison, 2006). Recommendations should be provided to reduce the potential for differential behavior between the soil nail and MSE wall types, such as extending the upper two reinforcements beyond the shoring wall.

Lastly, prevention of surface water infiltration into the MSE wall system would have prevented piping of the backfill material. Additional drainage is needed when designing with higher fines percentage materials, which has been recommended by Sandri (2000) and demonstrated in this case history. The cost of additional drainage elements during design and/or construction of an MSE wall are relatively inexpensive compared to the total cost of the wall and can prove to be one of the most important factors in MSE wall performance.

ACKNOWLEDGEMENTS

The author would like to thank the FHWA Central Federal Lands Highway Division project team members for their contributions, especially the detailed efforts of the construction team members Orrin Lee, Ross Dawson, and Jeremiah Rogers.

REFERENCES

American Association of State Highway and Transportation Officials (AASHTO) (2002). *Standard Specifications for Highway Bridges*, Seventeenth Edition.

Cornforth, D. H. (2005). *Landslides in Practice,* Wiley, New Jersey. 596 p.

Elias, V., Christopher, B.R., and Berg, R.R. (2001). *Mechanically Stabilized Earth Walls and Reinforced Soil Slopes, Design & Construction Guidelines*. Report No. FHWA-NHI-00-043. Federal Highway Administration, March. 394 p.

Federal Highway Administration (FHWA) (1996). *Standard Specifications for Construction of Roads and Bridges on Federal Highway Projects*. FP-96.

Federal Highway Administration (FHWA) (2003). *Section 255- Mechanically Stabilized Earth Walls. Special Contract Requirements*.

Lazarte, C. A., Elias, V., Espinoza, R.D., and Sabatini, P.J. (2003). *Geotechnical Engineering Circular No. 7 – Soil Nail Walls*. Report No. FHWA-IF-03-017. Federal Highway Administration, March. 305 p.

Morrison, K. F., Harrison, F.E., Collin, J.G., Dodds, A., and Arndt, B. (2006). *Shored Mechanically Stabilized Earth (SMSE) Wall Systems Design Guidelines*. Report No. FHWA-CFL/TD-06-001. Federal Highway Administration, dated February. 212 p.

National Concrete Masonry Association (NCMA) (2002). *Design Manual for Segmental Retaining Walls*, Second Edition. J.G. Collin (ed.). 289 p.

Sandri, D. (2000), "Drainage Recommendations for MSE Walls Constructed with Marginal Fills", Conference Proceedings, NAGS/GRI-19.

Case History – Olympic Sculpture Park MSE Structures

George E. Charalambous[1], M. ASCE, P.E.
Dustin E. Bennetts[2], M. ASCE, P.E.
Kenneth P. Akins[3], M. ASCE, P.E.

[1]Senior Engineer, Tensar International Corporation, 5883 Glenridge Drive, Suite 200, Atlanta, GA 30328; gcharalambous@tensarcorp.com
[2]Regional Manager – Grade Separation Solutions, Tensar International Corporation, 350 Interlocken Boulevard, Suite 290, Broomfield, CO 80021; dbennetts@tensarcorp.com
[3]Technical Services Director, Tensar International Corporation, 5883 Glenridge Drive, Suite 200, Atlanta, GA 30328; kakins@tensarcorp.com

ABSTRACT

The nine-acre Olympic Sculpture Park (OSP) overlooks the Puget Sound and the Olympic Mountains, and required the import of approximately 164,000 cubic meters (215,000 cubic yards) of fill. The park is adjacent to Elliott Bay in downtown Seattle, Washington. Approximately 4,180 vertical square meters (45,000 vertical square feet) of wire basket face Mechanically Stabilized Earth (MSE) structures support the massive urban fill operation and provide the framework for the pedestrian park above. Pedestrian bridges over a busy street corridor and railroad tracks provide access to the urban waterfront. Design and construction of the MSE structures were completed by late 2006, and the park was opened for public access in early 2007. Unusual project features included:

- True abutment MSE applications with geogrid reinforcement supporting vertical and horizontal bridge loads
- MSE walls in pressure relief applications to eliminate lateral earth pressure on adjacent pedestrian bridge abutment walls
- Two-stage MSE structures with multiple face inclinations
- Back-to-back MSE walls with a narrow distance between parallel facings in a high seismic area

INTRODUCTION

The nine-acre Olympic Sculpture Park (OSP) in downtown Seattle, Washington overlooks the Puget Sound with the Olympic Mountains as a backdrop. Overall, the site has 16.5 meters (54 feet) of relief from the high ground in the park area to Elliott Bay of the Puget Sound. Pedestrian bridges over Elliott Avenue, a four-lane urban thoroughfare, and the double tracks of the Burlington Northern and

Santa Fe (BNSF) Railway link the segments of OSP over those urban elements for unobstructed views. The Seattle Art Museum (SAM) overlooks the park from the south. See Figure 1.

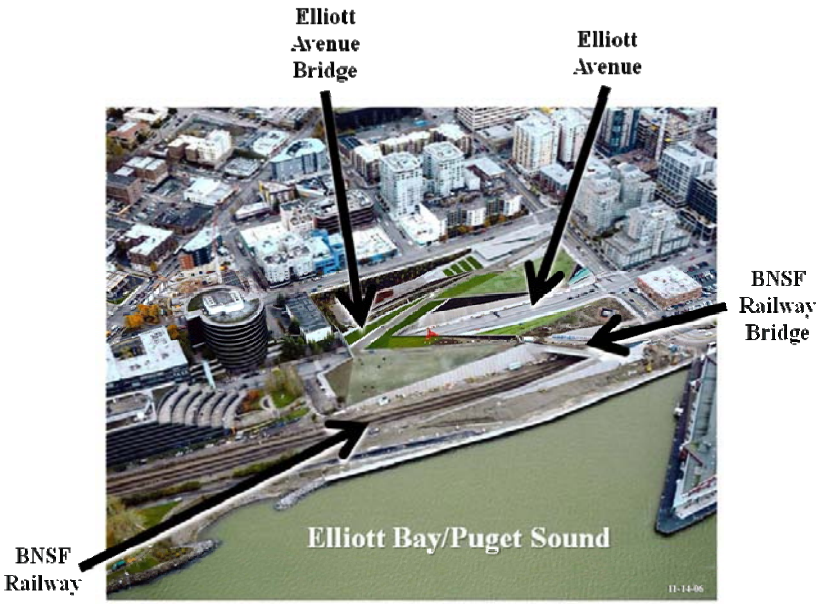

Figure 1. Aerial photograph (courtesy of Soundview Aerial Photography).

Approximately 4,180 vertical square meters (45,000 vertical square feet) of Mechanically Stabilized Earth (MSE) structures served to shape and support the massive urban fill, approximately 164,000 cubic meters (215,000 cubic yards), and provided the framework for OSP above. Unusual features of the MSE structures included “true abutment” walls with geogrid reinforcement that support the horizontal and vertical bridge loads, closely spaced back-to-back walls with overlapping reinforcement and unequal wall heights, and custom cast, irregularly shaped, overlapping precast panel facing to resemble “fish scales”. The MSE structures, built using the SierraScape® System from Tensar International Corporation (TIC), became part of the sculpture in the park.

The $85 million project had the feel of a “design-build” or “fast-track” project: very aggressive schedule, geometry evolving after construction started, sculptures, footings, large trees, and other structures added within reinforced volumes, multiple borrow sources, and multiple reviewers because of the high-profile nature of the project. Because the entire site was developed in consideration of appearance, the number of special details and transition considerations was extremely demanding.

MSE STRUCTURES

Design of the MSE structures was substantially completed by the middle of 2005, and construction was largely completed by late 2006. Unusual technical project features included:

- True abutment MSE applications with geogrid reinforcement supporting vertical and horizontal bridge loads
- MSE walls in pressure relief applications to eliminate lateral earth pressure on adjacent pedestrian bridge abutment walls
- Two-stage MSE structures with multiple face inclinations
- Back-to-back MSE walls with a narrow distance between parallel facings in a high seismic area

All MSE structures were designed in general accordance with Publication No. FHWA-NHI-00-043 (Elias, et al., 2001), although for some elements such as the unequal height back-to-back walls only limited guidance was available. Allowable Stress Design (ASD) was the conventional practice for MSE structures at the time. In terms of the project definitions, "Walls" have vertical facing and were analyzed using software developed for the MSE design firm. "Battered Walls" were typically inclined at 0.5H:1.0V batter (63.4° measured from horizontal) and analyzed as slopes (FHWA convention) using limit equilibrium methods in commercial software.

Design of the walls by the MSE design firm satisfied minimum factors of safety for the internal stability failure modes of reinforcement strength and reinforcement pullout, and the external stability failure modes of sliding at the base, overturning, and eccentricity. The project geotechnical engineer performed evaluations of global stability, compound stability, foundation bearing capacity, and settlements. With regard to design of the slopes, the MSE design firm satisfied minimum factors of safety for internal and compound stability failure modes while the project geotechnical engineer performed evaluations of global stability, foundation bearing capacity, and settlements.

Key considerations in design included a peak ground acceleration (PGA) of 0.38g for the project and 200 kPa (4,000 psf) for bridge abutment footings (maximum allowed under FHWA guidelines). Consistent with FHWA guidelines, full PGA was applied for internal stability of walls, ½ PGA for external stability of walls, and ½ PGA for stability of slopes. Other loads included:

- Horizontal load of 22 kN/m (1,500 lb/ft) from tie-back blocks for second stage facing
- Uniform live load traffic surcharge of 12 kPa (250 psf)
- Uniform dead load surcharge of 18 kPa (375 psf) due to soil overburden

True Abutment MSE Wall Applications. "True abutment" MSE applications support vertical and horizontal bridge loads from the Elliott Avenue

Bridge. Although geosynthetic reinforcement (extensible reinforcement) design procedures were included in Publication No. FHWA-NHI-00-043, they were not in the American Association of State Highway and Transportation Officials' "Standard Specifications for Highway Bridges" (AASHTO, 2002) at the time of design. True abutment MSE applications with geosynthetic reinforcement for vehicular loads did, however, have successful precedents. The Colorado Department of Transportation (CDOT) designed and constructed Founders Meadows Parkway overpass, the first fully mechanically connected, geosynthetically reinforced true abutment segmental block wall in public use (Abu-Hejleh, et al., 2000 and Abu-Hejleh, et al., 2001). Other vehicular loaded bridge abutments designed and supplied by the MSE design firm were in Idaho, Connecticut, Oregon, and Panama at the time of design (MSE design firm internal files).

Both east and west abutment MSE structures for the Elliott Avenue Bridge were approximately 9 meters (30 feet) tall overall (see Figure 2). The lower portion supporting the abutment footing was approximately 6.5 meters (21 feet) tall and the upper backwall portion was approximately 2.5 meters (9 feet) tall. The applied bridge footing stress was 200 kPa (4,000 psf) and earthquake horizontal bridge load was 205 kN/m (14,000 lb/ft). Thus, although this true abutment bridge primarily serves as a pedestrian bridge, it was designed to support vehicle bridge magnitude loads.

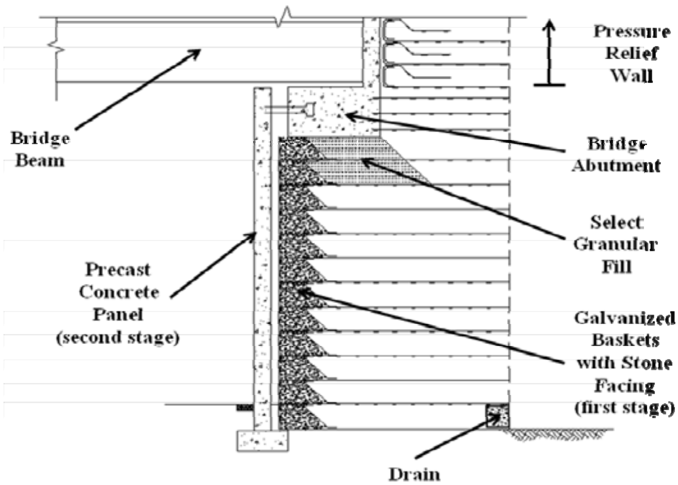

Figure 2. True abutment with pressure relief wall for abutment backwall.

The upper portion of the MSE structure was detailed as a Pressure Relief Wall so that earth pressure loads do not act on the abutment backwall. Geogrid reinforcement was also cast into the abutment footing to resist the earthquake loads applied to the footing. The selected geogrids are high density polyethylene (HDPE) and are unaffected by embedment into concrete. For the Elliott Avenue Bridge, MSE true abutments were more cost effective than reinforced concrete abutments.

Pressure Relief MSE Walls. MSE walls in pressure relief applications eliminated lateral earth pressure on adjacent walls. The presence of these pressure relief MSE structures resulted in a reduction in the reinforcement and concrete requirements for the adjacent reinforced concrete structures.

One pressure relief application, as described in the preceding section, was for the abutment backwalls for the Elliott Avenue Bridge. Another application was for the BNSF Railway Bridge. The 430 vertical square meters (4,600 vertical square feet) of pressure relief walls constructed with maximum heights of 10 meters (33 feet) eliminated earth pressures applied to the abutment walls resulting in significant savings on concrete and reinforcing steel. The detailing was similar to the lower portion of the Elliott Avenue Bridge abutment wall, except that the MSE zone did not support the bridge loads.

Two-Stage MSE Structure Selection. The MSE structures were built in two stages. The first stage included galvanized baskets that mechanically connect to the geogrid reinforcement. The second stage facing utilized precast concrete panels with concrete leveling pads and tie-back blocks. MSE structures were installed with either vertical batter, a typical batter of 0.5H:1V, or varied batter in transition zones. The two-stage construction offered important advantages:

- Settlement from the large fill loads occurred before final finishes were placed
- Pressure relief walls were easily incorporated wherever needed
- Precision placement of the unique architectural finish was possible

Figure 3. Photograph showing galvanized basket MSE structure and precast panel facing.

The custom cast, irregularly shaped, overlapping precast panel facing was developed to resemble “fish scales”. The concrete tie-back blocks and anchorages secured facing panels in place, with a gap to be maintained so that no lateral earth pressure was exerted on facing panels. See Figure 3.

Back-to-back MSE Wall Analysis. Back-to-back MSE walls constructed adjacent/parallel to the BNSF Railway support the path that leads from the upper park area to the waterfront garden beside Elliott Bay/Puget Sound. Approximately 1,100 vertical square meters (11,900 vertical square feet) of MSE walls were constructed in back-to-back configuration. The walls vary in height with a maximum height of 10 meters (32 feet) and the distance between parallel facings varies from approximately 8 meters (26 feet) to 3 meters (9.5 feet). The back-to-back portions are typically of unequal height. See Figure 4.

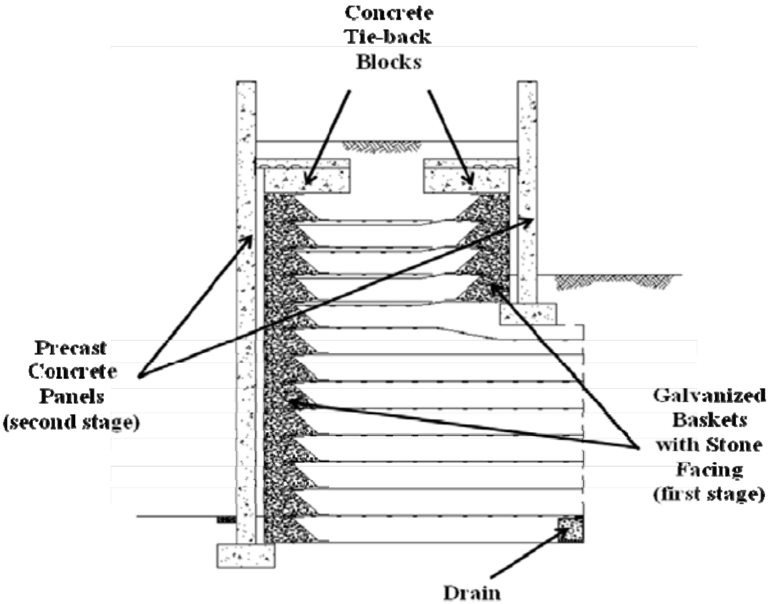

Figure 4. Unequal height back-to-back walls.

FHWA guidelines provided no specific guidance, other than a 1.1H to 1.2H separation distance between the back-to-back walls. Therefore, the MSE design firm and the project geotechnical engineer conducted numerous analyses for considering the effects of internal, external, and global stability within the components of the combined system. A specific result was the lengthening of geogrid reinforcement beyond the back-to-back limits for liquefaction concerns. The lengthening of the reinforcement came at the direction of the project geotechnical engineer.

CONSTRUCTION

As mentioned previously, the two-stage wall approach allowed settlement to occur before the precise final finish placement. Settlement evaluations were performed by the project geotechnical engineer. The approach also allowed the operations to proceed independently, so there were no coordination conflicts. The complexity and speed of the construction placed additional demands on the MSE design:

- Complex local geometric constraints required shortened geogrid reinforcement
- Trees, other plantings, and structures including sculpture foundations required modifications to the geogrid reinforcement, sometimes after initial construction
- Coordination with adjoining structures required special detailing to assure aesthetically pleasing boundaries and transitions

These demands meant that the MSE design firm needed to be readily available throughout construction.

CONCLUSIONS

The approximately 4,180 vertical square meters (45,000 vertical square feet) of MSE structures designed and constructed to support the substantial fill placement for the nine-acre OSP played a significant role in setting the scene and providing a good flow through the park. There were a variety of unique project aspects and challenges that were met by utilizing the selected wire basket face MSE system with a mechanical connection to the geogrid reinforcement, including:

- Ability to support bridge abutment loads, including true abutments and use of pressure relief walls
- Precise placement of unconventional facing elements
- Design and materials flexibility to provide cost effective solutions without sacrifice of appearance
- Modifications to conventional MSE methods to address complex geometries and construction conflicts, including back-to-back MSE walls with a narrow separation distance and two-stage MSE walls with multiple wall batters
- Cooperation with the design team to collaborate on design solutions when prescriptive design methods were not available

ACKNOWLEDGEMENTS

The writers gratefully acknowledge the opportunity to be a part of this noteworthy effort and the cooperation of the following team members:

- Owner = Seattle Art Museum
- Project Manager = Barrientos LLC
- General Contractor = Sellen Construction Company
- MSE Installer = Northwest Construction, Inc.
- Geotechnical Engineer = Hart Crowser, Inc.
- Civil/Structural Engineer = Magnusson Klemencic Associates, Inc.
- Architect = Weiss/Manfredi Architects
- Aerial Photographer = Soundview Aerial Photography

REFERENCES

Abu-Hejleh, N., Outcalt, W., Wang, T., and Zornberg, J.G. (2000). "Performance of Geosynthetic-Reinforced Walls Supporting the Founders/Meadows Bridge and Approaching Roadway Structures – Report 1: Design, Materials, Construction, Instrumentation and Preliminary Results", Report No. CDOT-DTD-R-2000-5, Colorado Department of Transportation, Denver, Colorado.

Abu-Hejleh, N., Zornberg, J.G., Wang, T., McMullen, M., and Outcalt, W. (2001). "Performance of Geosynthetic-Reinforced Walls Supporting the Founders/Meadows Bridge and Approaching Roadway Structures – Report 2: Assessment of the Performance and Design of the Front GRS Walls and Recommendations for Future GRS Abutments", Report No. CDOT-DTD-R-2001-12, Colorado Department of Transportation, Denver, Colorado.

American Association of State Highway and Transportation Officials (AASHTO). (2002). *Standard Specifications for Highway Bridges, 17th Edition*, Washington, D.C.

Elias, V., Christopher, B.R., and Berg, R.R. (2001). "Mechanically Stabilized Earth Walls and Reinforced Soil Slopes Design & Construction Guidelines" *FHWA-NHI-00-043*, Washington, D.C.

Soundview Aerial Photography, Arlington, Washington [Figure 1 of this paper].

Geosynthetic Reinforced Soil Walls as Integral Bridge Abutment Walls

Michael R. Simac, P.E., M ASCE[1] and David J. Elton, P.E. M. ASCE[2]

[1] Earth Improvement Technologies, Inc., PO Box 1346, Fort Mill, SC 29716, PH (803) 548-8690; email: mike@earthimprovement.com

[2] Professor of Civil Engineering, Auburn University Civil Engineering Dept.; USA PH (334) 844-6285 email: eltondj@eng.auburn.edu

ABSTRACT

The first use of geosynthetic reinforced soil walls for integral bridge abutment construction in North America occurred on the Greenville Southern Connector (I-185) toll road in 1999. A second bridge with a longer span and higher loads was constructed in 2000 for the same project. Each of these four bridge abutment walls were constructed over 20 ft. (6 m) high using modular concrete block wall (MCBW) facing units and geosynthetic reinforcement with a silty fine to medium sand backfill around vertically driven steel "H-Pile" foundation elements. While the piles were designed to carry all the vertical live and dead bridge loads, the lateral loads due to momentum, braking, and thermal movement would be transferred through the integrally cast-in-place concrete abutment to the piles to the wall facing elements through the piles, located just 3 ft. (1 m) behind the MCBW facing, and resisted by the geosynthetic reinforcement within the abutment wall.

This paper describes the engineering analysis, design procedures, and some of the installation details utilized for these geosynthetic reinforced Mechanically Stabilized Earth Walls (MSEWs) with MCBW facing for the traditional retaining wall loadings, plus the additional procedures to account for the pile induced lateral loads. The design procedures were based on the prevailing guidelines at the time, the 1996 AASHTO "Standard Specifications for Highway Bridges" as revised in 1998. Lateral loads were apportioned to the wall facing and geosynthetic reinforcement using "P-Y" curves for laterally loaded piles developed by Reese & Matlock. Seismic loadings were addressed by pseudo-static procedures. A review of the performance of these geosynthetic walls based on deformed shape measurement of the wall facing after ten years of service is also presented to begin to assess their performance.

KEYWORDS: Soil Reinforcement, Geosynthetic, Walls, MSEWs, Performance, Monitoring, Design, Bridge abutments, Lateral pile loads, Sliding analysis

Project Description: The Southern Connector toll road, I-185 in Greenville, SC, opened to commercial traffic in February 2001 connecting the major east-west highway I-85 to the primary north-south route I-385. The 16 mile toll road was built to FHWA standards in 1999 and 2000 by a private developer, but is now owned and operated by the South Carolina DOT. MSEWs were used extensively on the project, with a total face area over 40,000 sq. ft., in 3 roadway grade separation walls and 6 abutment walls. There are a total of 25 bridge structures along the route, three of which have geosynthetic reinforced MSEW abutment walls. Two of those MSEW

Table 1: MCBW Facing Unit Properties			
Height 8 inches	Setback 0.5 in.	Comp. Strength = 3,000 psi	
Depth 20 inches	Batter 3.6 degs.	Density = 134 pcf	Absorption = 6 %
Length 18 inches	Weight = 115 lbs.	Unit weight - filled = 126 pcf	
Shear Capacity (SC)	Top Concrete Lug	SC = 650 lbs/ft	+ NL tan 35.0 $^{\circ}$

bridge structures consisted of integral bridge abutments, where the bridge beams were rigidly fixed to the abutment bearing seat (i.e. cast into the concrete of). For straight short span bridges integral abutments reduce initial and maintenance costs by eliminating bridge bearings and battered piles to resist lateral loads. This rigid connection presented a unique MSEW design requirement not previously addressed in North America for MCBW facing units. This paper describes the engineering design for those four abutment walls, and details the engineering performance to date.

Bridge 19, with a total span of 175 feet, carries Log Shoals Road traffic over I-185, using equal spans of 87.5 ft long precast concrete beams to a center bent. Bridge 19 abutment walls are just 52 ft long to accommodate the two-lanes of local traffic. Bridge 24 supports I-185 traffic as it overpasses Laurens Rd (SC-417) in a single span of 137 feet using steel beams. Bridge 24 abutment walls are 99 ft long to support four lanes of interstate highway traffic. All four abutment walls are skew to the overpassed roadway creating acute or obtuse angles at each abutment corner.

Selection of MSEW System: Southern Connector project specifications allowed the general contractor to select the MSEW installation contractor and MSEW system for use in these locations. This flexibility of choice required the contractor provide detailed MSE design calculations and construction drawings for the system selected. The MSEW system selected by the retaining wall installation sub-contractor was the Anchor Wall System's VerticaPro™ MCBW facing system with Raugrid™ geogrid reinforcement. The specifications and engineering properties for the facing block and geogrid can be found in Table 1 and 2, respectively. The geogrid specific MCBW facing connection strength (CS) for the system is presented in Table 3, with each represented as a bi-linear strength envelope for both peak (ultimate), as well as deformation limited (0.75 in.) "service state" connection strengths.

Definition of Soil Conditions: The bridge designs were done by Florence and Hutcheson, Inc. in conjunction with Wilbur Smith Associates. A foundation

Table 2: Geogrid Reinforcement Properties in Main (roll) Direction

Grid Type	Tensile Strength (lbs/ft)	Creep Red. Factor	Durability Red. Factor	Damage Red. Factor	Allowable Strength (lbs/ft)	Overall Safety Factor	Design Strength (lbs/ft)	Pullout Coeff. Ci	Direct Sliding Cds
3	2,250	1.56	1.15	1.15	1,091	1.5	727	0.75	0.70
4	2,910	1.56	1.15	1.15	1,411	1.5	940	0.80	0.75
6	3,990	1.56	1.15	1.15	1,934	1.5	1,289	0.80	0.75
8	5,370	1.56	1.15	1.15	2,603	1.5	1,735	0.80	0.75

Table 3: Geogrid Reinforcement Connection Strength as a function of Normal Load (lbs/ft) MCBW unit

Grid Type	Peak-Lo Intercept (lbs/ft)	Peak-Lo Angle (degs.)	Peak-HI Intercept (lbs/ft)	Peak-HI Angle (degs.)	Service-Lo Intercept (lbs/ft)	Service-Lo Angle (degs.)	Service-HI Intercept (lbs/ft)	Service-HI Angle (degs.)
3	698	47	1207	0	607	9	1500	0
4	268	62	1447	5	411	21	804	2
6	442	54	2031	6	440	33	1170	3
8	813	48	1787	18	413	32	971	11

investigation for each bridge location, using standard penetration testing borings, provided subsurface information that was useful for the design of the MSEWs. The soil conditions for MSE designs were defined by the Owner's representative for both Bridge 19 & 24 (see Tables 5 & 6). The Owner stipulated a settlement controlled ultimate bearing capacity for each abutment, prescribed as a function of the effective foundation width, B (B = L-2e) which influenced both static and seismic design. Per design guidelines the cohesion strength component of the reinforced and retained soils was ignored throughout design, except for slope stability analyses.

The reinforced fill soil source was identified and tested by the contractor. A quarry manufacturing by-product, "course screenings," was selected based upon cost, available quantity, location, and consistency. The engineering properties of the reinforced fill used throughout this project are shown in Table 4, which complies with AASHTO's standard MSEW backfill specification, as required by the project.

The groundwater table was measured between 5-8 ft. beneath Bridge 19 MSEWs bearing elevations. This was close enough to the base of the Bridge 19 MSEWs to install a protective gravel blanket drain to intercept potentially rising groundwater levels and analytically model the ground water level at the base of those MSEWs. Bridge 24 groundwater levels were at sufficient depth to eliminate the blanket drain.

Design of MSEW System: The 1996 AASHTO Bridge Manual, as amended by the 1998 interim specifications, was used as the design guideline for these MSEWs. The lone exception was connection strength requirements, wherein a single lumped overall safety factor of 1.5 was applied to the peak strength defined by testing (Table 3). The 20 inch deep MCBW facing unit provided a residual friction connection, even after the geogrid would rupture, so a single lumped safety factor applied to friction connections subject to pullout failure was implemented for these MSEWs.

The wall height and foundation soil conditions at each of the four abutments varied enough to dictate a slightly different geogrid reinforcement layout. Each abutment

Table 4: Reinforced Fill Properties			Max. < 9.5 mm
c = 358 psf	SM	A-1-b	PI = Non Plastic
ϕ = 40 degs.	87% Sand	13 % < #200	MDD = 124.0 pcf
γ = 131 pcf	D_{60} = 0.672 mm	D_{15} = 0.092 mm	Opt. MC 11.5%

Table 5: Foundation Conditions Bridge **19**					Qult =(L-2e) **945** B1		**480** B3	
water table at base of MSEW **Soil Type** from Top of Roadway	Bent 1 C (psf)	Bent 1 Φ (degs.)	Bent 1 C' (psf)	Bent 1 Φ' (degs.)	Bent 3 C (psf)	Bent 3 Φ (degs.)	Bent 3 C' (psf)	Bent 3 Φ' (degs.)
Fill top 15' γ=125	1200	0	100	32	1200	0	100	32
Sandy Silt next 13' γ = 125	0	32	0	32	0	28	0	28
Silt Sand next 32' γ = 120	0	34	0	34	0	34	0	34
Silty Sand next 25' γ = 125	0	36	0	36	0	36	0	36

MSEW design utilized a 300 psf uniform surcharge to account for vehicle traffic loading, and 0.12g design seismic loading. The seismic loading conditions controlled both the number of reinforcement layers, and the length of the reinforcement layers, (i.e., internal and external stability, respectively) as affected by wall height and soil conditions. Figures 1 & 2 show typical sections for geogrid reinforcement layout at Bridge 19 and 24, respectively. Lateral sliding and settlement limited allowable bearing capacity during seismic loading, controlling length of the reinforcement at each MSEW. Seismic tensile capacity and static connection strength of the geogrid reinforcement controlled the type and number of reinforcement layers required at each MSEW. Overall global stability analyses for the seismic controlled geogrid lengths and strengths, under both seismic and static loading conditions found safety factors exceeding the minimum required by the AASHTO design method.

The vertical loads of the bridge superstructure where carried by "H" pile foundations driven to end bearing on bedrock, about 50'-70' deep. With the "H" piles rigidly connected to the concrete abutment seat, lateral movements of the bridge beams due to thermal expansion/contraction and braking loads placed additional lateral loads on the pile. The applied lateral pile load was calculated (Table 7) based on the design deflection provided by the bridge designer, which varied due to bridge beam material. P-Y curves, as presented by Reese & Matlock (1956, 1961, 1962) and later modified by Davisson (1963, 1970) were utilized to determine transfer of lateral load into the surrounding soil and directly apportioned into each geogrid layer, (Figures 3 & 4). This approach is conservative, ignoring pile spacing and stress distribution through the soil. These static lateral loads were utilized in calculating the total static tension, and included as a component of applied seismic tension, but were not directly increased pseudo-statically, for the seismic analysis. Combining these lateral loads with soil loads controlled the design, requiring stronger geogrids be used higher in the section. Figure 5 shows installation detail for geogrid reinforcement around the piles.

Table 6: Foundation Conditions Bridge **24**					Qult = **700** (L- 2e) both bents			
water table -12' base MSEW **Soil Type** from Top of Roadway	Bent 1 C (psf)	Bent 1 Φ (degs.)	Bent 1 C' (psf)	Bent 1 Φ' (degs.)	Bent 2 C (psf)	Bent 2 Φ (degs.)	Bent 2 C' (psf)	Bent 2 Φ' (degs.)
Fill top 25' γ=125	1200	0	100	32	1200	0	100	32
Sandy Silt next 11' γ = 125	0	28	0	28	0	28	0	28
Silt Sand next 15' γ = 120	0	34	0	34	0	34	0	34
Silty Sand next 25' γ = 125	0	36	0	36	0	36	0	36

Monitoring of the MSEW System: The authors received permission to begin performance monitoring these MSEW abutment structures in October 2009. Unfortunately, a baseline survey immediately after construction (1999/2000) was not performed, eliminating any possibility of separately evaluating all post-construction movements from construction in 1999-2000 to the present. Consequently, the authors will evaluate performance to date, using the current position of the wall facing relative to its original stacked batter, and the anticipated position after construction. A plot of the October 2009 wall face position for four monitoring sections on Bridge 19 are shown in Figures 6 & 7, and eight sections on Bridge 24 (Figures 8 & 9). Each section is located at the center of the travel lane supported above it. The measured existing wall facing position is about where expected after completion of construction except for Bridge 24 bent 1, which shows an increase in wall batter of about 1 degree from 3.57 to 4.44 degrees. Increase in wall batter, while unusual, is generally caused by settlement of fill immediately (< 3 ft.) behind the MCBW units, dragging the reinforcement down and pulling the MCBW facing units backwards. This is also probably affecting section "K" Bridge 24 bent 2. The October 2009 wall facing position for every section measured was within industry accepted performance tolerances of $\pm$ 2 degrees of the stacked batter of 3.57 degrees. Collectively these wall facing position measurements indicate that overall these MSEW abutments are performing well, in addition to looking good aesthetically. Additionally, the lack of any measured bulging near the top of wall indicates the geogrid reinforcement is adequately restraining the additional lateral loads being applied to the MCBW facing units by the "H" pile foundations over the first decade (10%) of service life.

Summary and Conclusions: The design requirements of the geogrid reinforcement for four MSEW integral abutment walls subjected to lateral loading from "H" pile foundations located immediately (1.8-3.0 ft.) behind the MCBW facing is presented. While seismic loading (0.12g) controlled the geogrid reinforcement length, lateral loading from pile foundations dictated geogrid reinforcement strengths necessary to restrain the MCBW facing from excessive horizontal displacement. The initial ten years of structure performance has been excellent, with no deleterious movements associated with the laterally loaded piles and or the typical imposed soil loading.

More research into long-term structural performance is needed. The authors intend to monitor these MSEW abutments over the next decade to quantify the amount and rate of horizontal movement to assess current performance prediction models for deformation, connection strength, and distribution of load into geogrid reinforcement.

REFERENCES:

AASHTO (1996) "Standard Specifications for Highway Bridges," & 1998 interims.

Davisson, M.T. and Gill, H.L. (1963) "Laterally Loaded Piles in a Layered Soil System," Journal Soil Mechanics & Foundation Engineering. ASCE Vol. SM3 May

Davisson, M.T. (1970) "Laterally Load Capacity of Piles," Highway Research Record, No. 333, pp. 104-112

Elias, V.E., Christopher, B.R. and Perkins, S. (1997) "Mechanically Stabilized Earth Walls and Reinforced Soil Slopes, Design and Construction Guidelines," prepared for FHWA, Demo Project 82, Contract No.: DTFH61-93-C-000145, 371 p

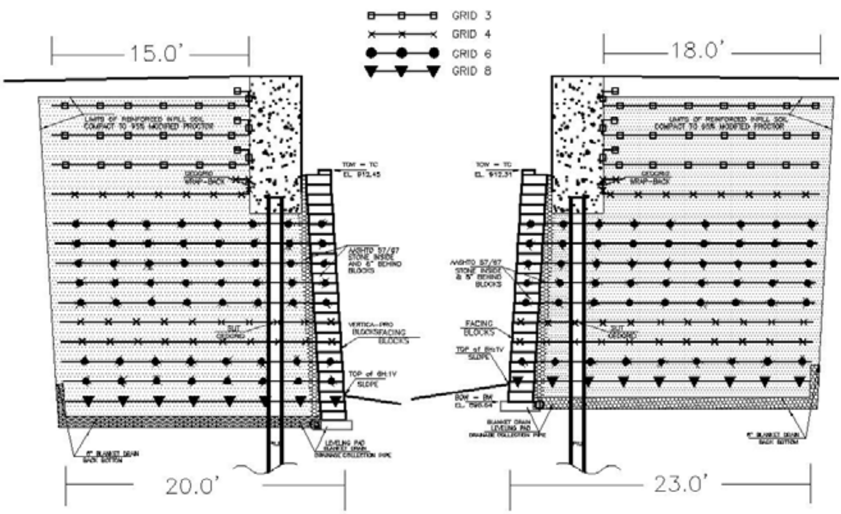

1a. Bridge 19 - Bent 1

1b. Bridge 19 - Bent 3

Figure 1: Bridge 19 Typical Abutment Sections

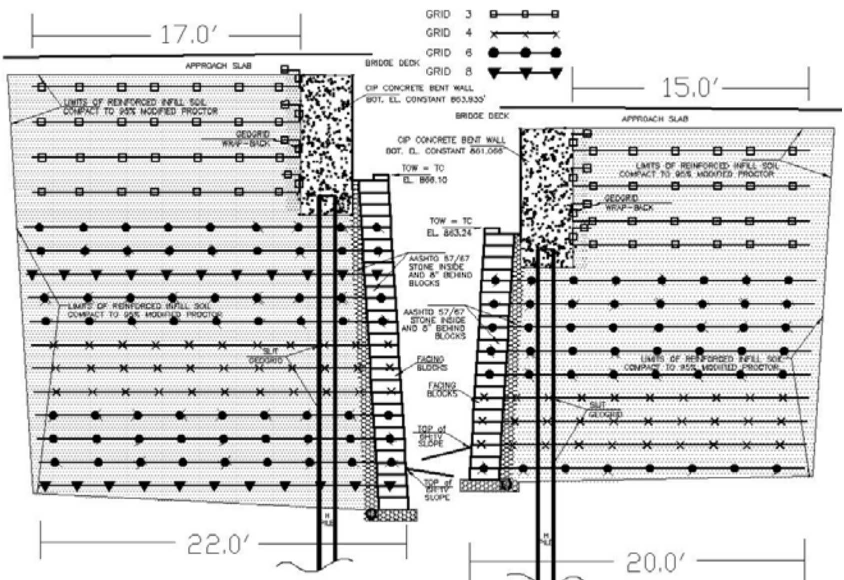

2a. BRIDGE 24 - Bent 1

2b. BRIDGE 24 - Bent 2

Figure 2: Bridge 24 Typical Abutment Sections

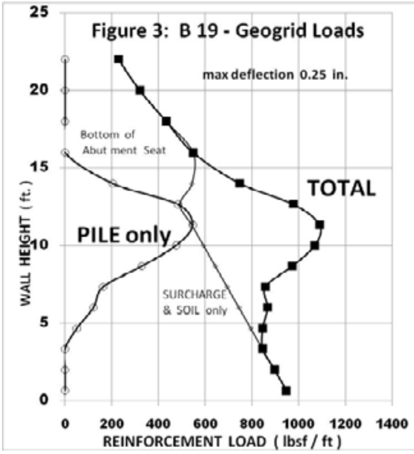

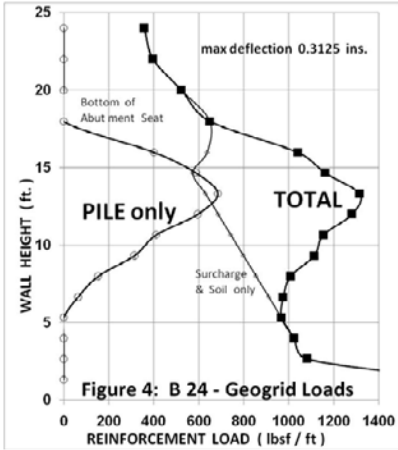

Figure 3: Bridge 19 – geogrid loads **Figure 4: Bridge 24 – geogrid loads**

Matlock, H. and Reese, L.C. (1962) "General Solutions for Laterally Loaded Piles", Trans. ASCE, Vol 127, Part I, pp. 1200-1247

Reese, L.C. and Matlock, H. (1956) "Non-Dimensional Solutions for Laterally Loaded Piles with Soil Modulus Assumed Proportional to Depth," Proceedings Eighth Texas Conference on Soil Mechanics & Foundation Engineering, Austin, Texas, ASCE

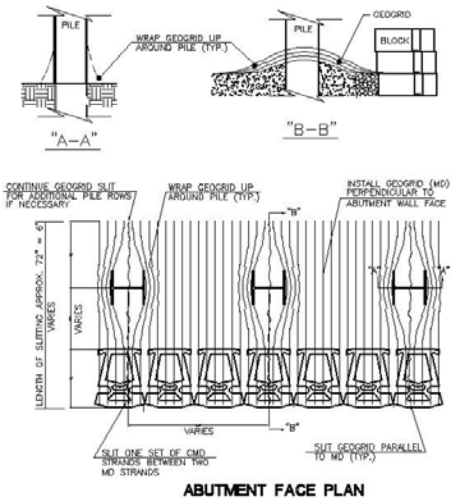

Figure 5: Geogrid Installation at Piles

Table 7: Lateral Load

PROPERTY	Bridge 19	Bridge 24
DESIGN DEFLECTION	0.25 in.	0.3125 in.
TYPE of PILE	H 12 x 53	H 12 x 53
STEEL	A36	A36
E – Modulus	29,000,000 psi	29,000,000 psi
I – Moment Inertia	127.3 in4	127.3 in4
E I	3,700,000,000 lbs–in2	
WIDTH of PILE	12.05 in.	12.05 in.
PILE Spacing	42 ins.	55 ins.
GROUP ACTION	NO	NO
FIXITY of PILE HEAD	50 %	50 %.
Conserv. Estimate – Nh	28 pci	28 pci
Calculate – T	3.51 ft.	3.51 ft.
Estimate – 5 T	17.53 ft.	17.53 ft.
Calculate – c Y	1.6803	1.6083
Calculate – Q lateral load	7,374.6 lbs.	9,218.2 lbs.
Calculate – Q / T	175.3	219.1

USE DIMENSIONLESS P–Y Curves to DISTRIBUTE DOWN PILE

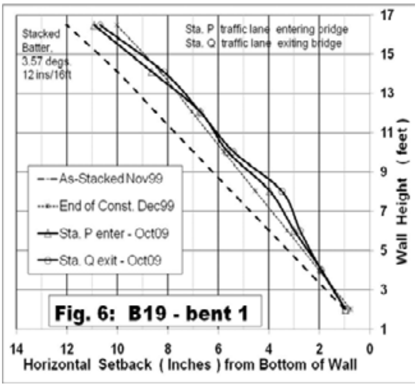

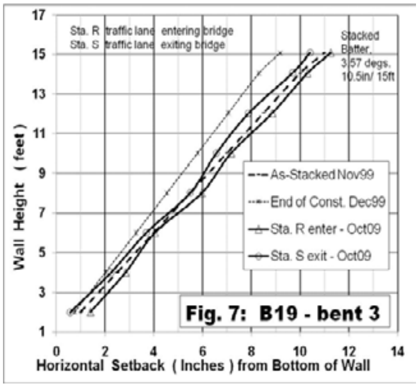

Figure 6: Bridge 19 – bent 1 **Figure 7: Bridge 19 – bent 3**

Notations:

B = Foundation Width = L-2e, L = Geogrid length, e = eccentricity found load
Ci , Cds = Coefficient of Interaction (pullout), Direct Sliding (friction)
CS = Connection Strength between MCBW and geogrid, ASTM D-6638
Max. = Maximum particle size
MDD & Opt. MC = Max.Dry Density & Optimum moisture ASTM D-1557
Peak, Service, HI, LO = HIgh & LOw strength envelope segments D-6638
NL = Normal Load (lbs/ft)
Qult = Ultimate bearing capacity, psf
SC = Shear Capacity between MCBW facing units, ASTM D-6916
T = Characteristic length dimension for laterally loaded piles

Acknowledgements: The authors appreciate of the cooperation of the SC-DOT and Southern Connector Toll Road Authority with monitoring these structures and CivilTek Associates for their precision surveying to document performance.

Figure 8: Bridge 24 – bent 1 **Figure 9: Bridge 24 – bent 2**

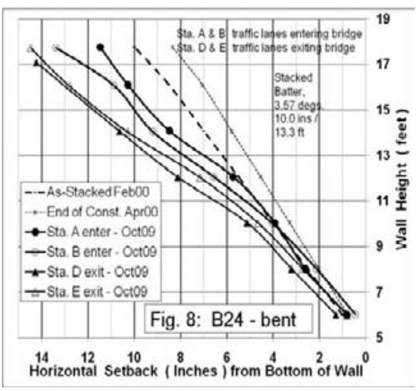

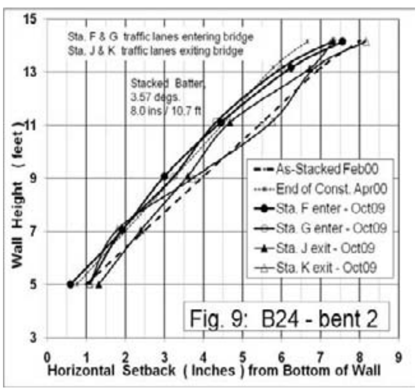

Preliminary Results for a GRS Integrated Bridge System Supporting a Large Single Span Bridge

K.A. Warren[1], W. Schlatter[2], M. Adams[3], T. Stabile[4], D. LeGrand[5]

[1]Department of Civil and Environmental Engineering, University of North Carolina at Charlotte, 9201 University City Boulevard, Charlotte, NC 28223-0001; PH (704) 687-6395; FAX (704) 687-6953; email: kawarren@uncc.edu
[2]Defiance County, Ohio, 500 Second Street, Defiance, OH 43512; PH (419) 782-4751; FAX (419) 782-3031; email: dce@defiance-county.com
[3]Turner Fairbank Highway Research Center, Federal Highway Administration, 6300 Georgetown Pike, McLean, VA 22101; PH (202) 493-3025; FAX (202); FAX (202) 493-3477; email: Mike.Adams@FHWA.DOT.GOV
[4]Turner Fairbank Highway Research Center, Federal Highway Administration, 6300 Georgetown Pike, McLean, VA 22101; PH (202) 493-3036; FAX (202) 493-3477; email: Thomas.Stabile@FHWA.DOT.GOV
[5]Department of Civil and Environmental Engineering, University of North Carolina at Charlotte, 9201 University City Boulevard, Charlotte, NC 28223-0001; PH (704) 687-2782; FAX (704) 687-6953; email: dmlegran@uncc.edu

ABSTRACT

In order to refine Geosynthetic Reinforced Soil Integrated Bridge System technology (developed by the FHWA), girders from a 42.7 m single span bridge were instrumented with strain gages, end pressures were measured using horizontal pressure cells, and the abutments were instrumented with vertical pressure cells and survey targets to measure girder footing and abutment wall movements. After a six month monitoring period, vertical deflections are within tolerable limits (ranging from 1.1 to 4.6 cm) and there are no visible cracks at the bridge-approach interface. The strain gages and earth pressure cells continue to collect meaningful data in terms of magnitude and trend. A change in ambient temperature causes a temperature induced strain in the steel, which affects the lateral pressure measured behind the steel girders as expected. Vertical pressures in the abutment are also affected by the thermal cycle. This paper will display the preliminary results from this project.

INTRODUCTION

A conventional bridge abutment with a 2:1 protected slope is not always a feasible solution due to space limitations. As a result, county and highway departments typically construct a full or partial-height abutment on deep foundations, which requires an earth retaining structure. However, this can be a cost prohibitive option especially if a deep foundation solution is not necessary. This paper describes the use of a unique GRS bridge abutment technology developed by the FHWA used to support a 42.7 m long, single span bridge constructed in Defiance County, Ohio.

In recent years, the Federal Highway Administration (FHWA) has developed, implemented, and continued to refine the Geosynthetic Reinforced Soil (GRS) Integrated Bridge System for use with typical, single span bridges. In comparison to conventional Mechanically Stabilized Earth retaining structures, GRS methods always specify 1) excellent fill between each reinforcement (a clean, crushed aggregate that meets AASHTO standards), 2) tight geosynthetic spacing (20.3 cm recommended), and 3) excellent compaction with special attention paid to the areas near the face of the wall. The use of high quality fill material and quality control during the construction process ensures that any movements associated with the earth retaining structures are minimal and within the tolerable limits of the structure. The "Integrated Bridge System" (IBS) component of this technology refers to the integration of the substructure with the superstructure. Box beams or steel girders are placed on the GRS abutment, and the same GRS construction technique is used behind the beam ends to serve as the foundation for the roadway approach. The use of this technology for this project eliminated the conventional need to hire specialty contractors with specialized equipment to install deep foundations (a costly alternative). Additionally, this system creates a seamless interface between the bridge and the approach, eliminating the "bump at the end of the bridge". Extensive research has been conducted (Adams, Schlatter, and Stabile 2008; Wu, Ketchart, and Adams 2001; Wu 2001; Wu et al. 2006, among others) to demonstrate the capabilities of GRS abutments when properly constructed.

Defiance County, Ohio has embraced this technology over the last several years to eliminate unnecessary deep foundation design and construction, which has saved their county significant money. With only the Defiance County maintenance personnel, GRS abutments have been constructed on 16 different projects, and these structures have experienced deflections well within the tolerable limits in addition to minimizing (if not eliminating) pavement cracks at the bridge-approach interface. Prior to this 42.7 m long, single span bridge, previous bridge lengths ranged from 4.6 m to 25.9 m. This bridge is currently the largest GRS Integrated Bridge System in the US.

In an attempt to refine GRS technology and study the interaction between GRS abutments and a steel superstructure, UNC Charlotte recently joined forces with the FHWA and Defiance County to instrument, monitor, and analyze the behaviour of a large GRS Integrated Bridge System constructed over the Tiffin River in Defiance, Ohio. This paper will outline the location of the field site, instrumentation and data acquisition plan, and provide preliminary results from this field project.

FIELD INSTRUMENTATION AND DATA ACQUISTION

The goal of this field project is to monitor the temperature dependent stresses, strains, and deflections associated with a newly constructed GRS Integrated Bridge System designed to replace the outdated bridge displayed in Figure 1(a). The newly constructed bridge (displayed in Figure 1(b)) is a 42.7 m long, 11 m wide, two lane bridge that crosses the Tiffin River on Stever Road oriented in the north-south direction.

The instrumentation plan was designed to monitor 1) the magnitude of the vertical stresses at two elevations below the girder footing within each GRS abutment, 2) changes in the girder end pressures measured behind the back wall due to thermal cycles, and 3) any vertical deflections of the girder footings or abutment walls. Figure 2 displays a profile of the instrumented GRS bridge abutment constructed for this project.

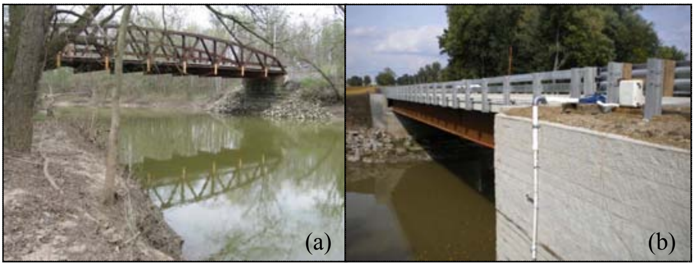

Figure 1. (a) Original Bridge; (b) Newly Constructed Bridge System.

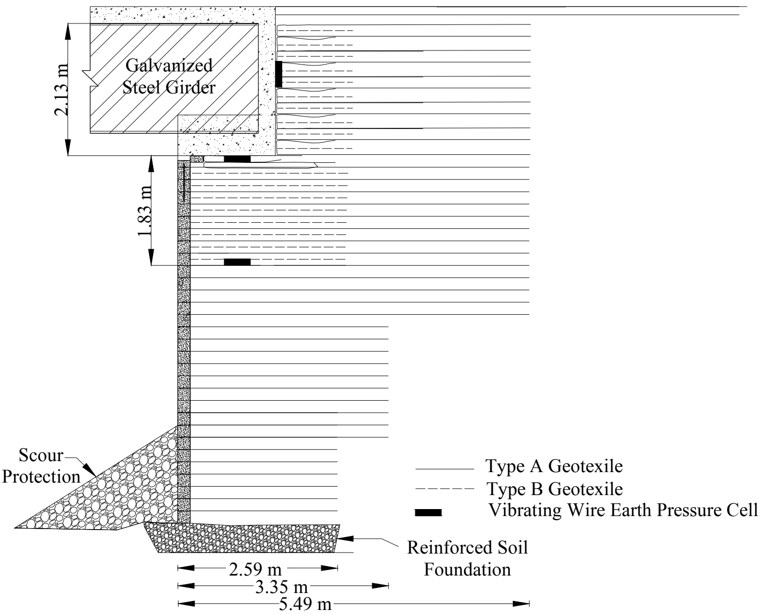

Figure 2. FHWA GRS Integrated Bridge System.

Three vibrating wire vertical pressure cells were installed at two depths on each abutment (a total of six vertical pressure cells per abutment). These cells were located 1.83 m below the girder footing and immediately below the girder footing (Figure 2). The center cell is located under the middle girder (girder 3) and the two outside pressure cells are located under girders 2 and 4 (2.74 m on either side of center).

Three vibrating wire lateral pressure cells were installed 1.07 m from the bottom of the concrete back walls (mid-height) to measure the horizontal soil pressure at each end of the bridge (Figure 2). These cells were also lined up with girders 2, 3, and 4. Sensor installation for all pressure cells was performed in accordance with the manufacturer's instructions with additional precautions to protect the integrity of the cells from experiencing excessive contact pressures by the AASHTO No. 89 stone backfill (3/8 in maximum grain size).

A total of 36 vibrating wire strain gages were attached to the web of all five steel girders, which were 42.7 m in length (fully constructed). The strain gages were installed at three locations along each fully constructed girder: at the midpoint and 3.1 m from each end. At each of the three locations along the length of the girder, there was a gage installed at the top and at the bottom of the web, approximately 7.6 cm from the base of the fillet. As a result, there are six strain gages installed to one side of each girder with the exception of the middle girder, which has strain gages on both sides. Note that all vibrating wire sensors collect static readings only and do not characterize the behavior of the structure as a result of live loading conditions.

The mounting blocks for each strain gage were arc welded at the fabrication plant before the girder sections were shipped and erected on site. Just prior to final girder placement, all 36 strain gages were installed in their mounting blocks and a GK-403 readout box was utilized to check functionality before the girders were moved to the GRS abutments by a 500 ton crane. Of all the sensors installed, one strain gage did not survive (98% sensor survivability). Each cable bundle was organized on the bottom flange of each girder and fed into a piping system attached to the bottom of the girders on the north side where the main data acquisition enclosure is located.

An electronic total station and 12 reflective targets are utilized to monitor the bridge settlement and any movement associated with the GRS abutments. A permanent total station mount installed on site provides a fixed point of reference for the measurements. Three targets were mounted on each girder footing and nine were installed on the face of each GRS wall to measure beam settlement and the settlement of the entire GRS abutment in addition to any wall deflection. Horizontal angle, horizontal distance, and vertical distance readings are recorded for each target to determine xyz coordinates of the targets to develop settlement plots. Baseline readings of the abutment and beam footing targets were collected at the completion of each abutment and just prior to girder placement. With each major loading event during the construction of the bridge (i.e. girder placement and concrete deck pour), survey readings were taken immediately after loading in addition to the daily observations to characterize the settlement behavior. Long term monitoring of the completed bridge will consist of monthly target readings collected over a 2 year period.

A CR1000 logger with two AVW200 vibrating wire interface modules and three 16-channel AM16/32B multiplexers was positioned on the north abutment to read the north abutment pressures and all strain data from the girders. A wireless vibrating wire interface module (AVW206) and AM16/32B multiplexer was positioned on the south abutment for use with a 900 MHz radio to transmit the south abutment pressure data to the north abutment so that all data could be retrieved from one point using a cell phone connection. Wireless technology eliminated the need for two data loggers and two modems so that all data is remotely retrieved from the north abutment enclosure. The data loggers are powered using regulated solar power with a battery, and strain and pressure data are recorded every two minutes. UNC Charlotte is responsible for the collection and analysis of the data for a two year time period subsequent to construction of this bridge, which was completed in September 2009.

PRELIMINARY RESULTS

The following figures illustrate the relationship between temperature induced strain and the stress changes within the GRS abutments (both lateral and vertical stress). Figure 3 displays the average girder strain for both the top and bottom strain gages near the north and south abutments (left side axis) and the average temperature (right side axis) as a function of time during a six month testing period. Note that a negative value of strain indicates compression and a positive sign indicates tension. To show the long term affect during the project duration, recorded strain (collected every two minutes) is averaged each hour and displayed in this figure. In general, as the temperature decreases through the end of 2009, the steel contracts with the colder temperatures, and the average strain moves towards a state of compression (becoming more negative with time).

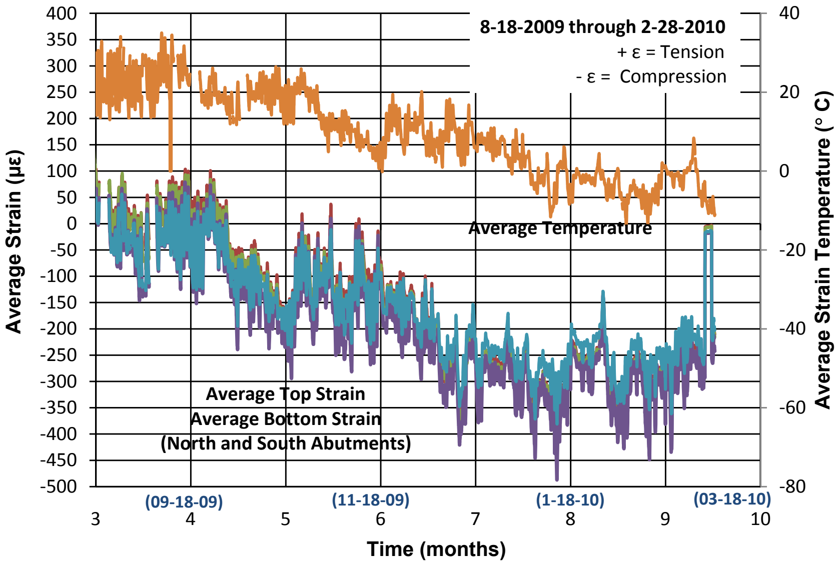

Figure 3. Top and Bottom Girder Strain with Time.

Figure 4 displays girder strains recorded every two minutes and the average temperature as a function of time during one week in October 2009. Note that noon is located at each major tick interval. On this figure, all strain measurements from all six top gages at each longitudinal location along the girder are averaged together (top-north, top-middle, and top-south) and all six strain measurements from the bottom gages at each longitudinal location are also averaged together (bottom-north, bottom-middle, and bottom-south). This figure shows the daily temperature cycles and corresponding changes in the temperature induced strain on the girders. As the temperature increases during the day causing the steel to expand, the strain moves towards a state of tension (magnitude increases) as expected. Similarly, as the temperature begins to decrease into the evening, the steel contracts and the strain moves towards a state of compression. The induced strains resulting from the daily thermal cycles are in line with the magnitudes expected based on the thermal expansion coefficient of steel.

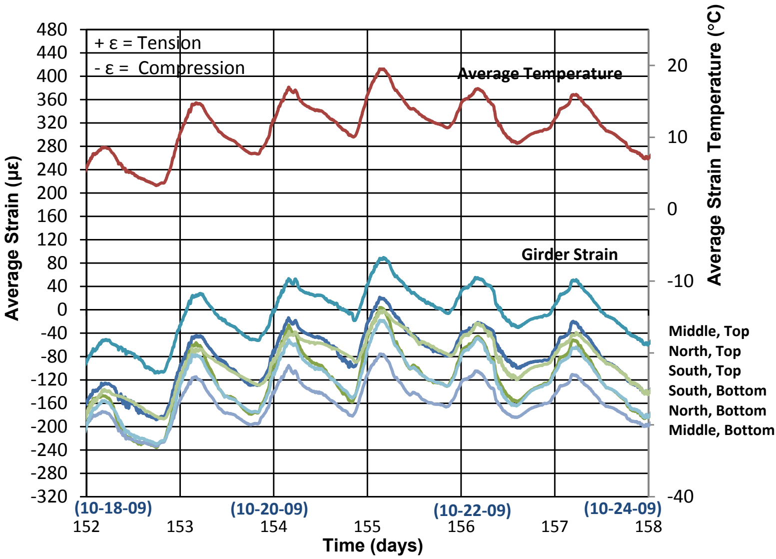

Figure 4. Girder Strain and Temperature with Time.

Similar to Figure 4, Figure 5 displays the relationship between average strain (for both top and bottom gages) and the average horizontal pressure as a function of time for the south abutment over the same time duration in October 2009. Note that strain is displayed on the left and temperature is displayed on the right. While Figure 4 illustrates thermal affects on the steel in terms of strain (an increase in temperature causes an increase in strain and an increase in the tensile state of the steel as an example), Figure 5 illustrates the corresponding increase in lateral pressure with an increase in tensile girder strain and vice versa. In summary, as the temperature increases, the girder steel expands (illustrated by the increase in tensile strain for each girder) and the horizontal pressure cells installed at the end of the beams measure an increase in lateral pressure as expected. The opposite is true for a temperature decrease.

Figure 6 displays the data from both the upper and lower vertical pressure cells on the south abutment and the average temperature over the six month testing period. Recall that the positions of the vertical pressure cells (upper and lower) are identified on Figure 2. Note that the lower vertical pressure cells are recording a higher stress than the upper cells due to their location within each abutment. As the temperature decreases each month, there appears to be a slight increase in vertical pressure within the abutment. In the latter part of January 2010, a sharp change in temperature creates a more significant change in the magnitude of the vertical pressure. This is more evident in the pressure cells located closer to the surface. Figure 6 illustrates an inverse relationship between the vertical stress in the abutment and the temperature.

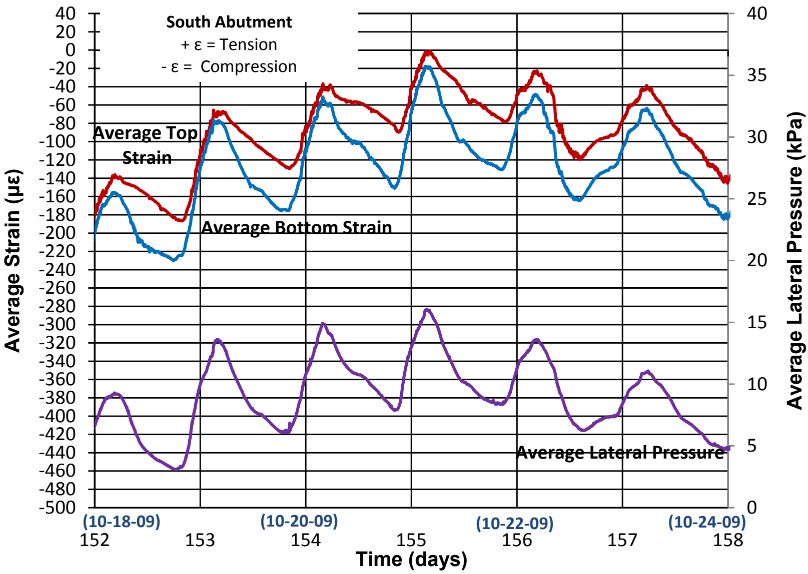

Figure 5. Top and Bottom Girder Strain and Lateral Pressure with Time.

CONCLUSIONS

The following conclusions and observations can be advanced regarding the preliminary results displayed in this paper:

1. With the exception of one strain gage, all instrumentation was successfully installed and is currently operational.
2. Six months into the project, minimal settlement has occurred. The average settlement for the north abutment wall and footing as of March 2010 is 4.6 cm and 2.2 cm, respectively. The average settlement for the south abutment wall and footing is 3.7 cm and 1.1 cm, respectively.
3. All data appears to be reasonable in magnitude and trend. As the ambient temperature increases, temperature induced tensile strain increases in accordance with the thermal coefficient of expansion for steel. The tensile strain (expansion of the steel) causes an increase in horizontal pressure at the

ends of the girders and a slight decrease in vertical stress within the abutment. The reverse holds true during temperature reductions.

4. The abutments and the steel girders continue to be monitored with the goal of refining this technology and studying the interaction between GRS abutments and a steel superstructure.

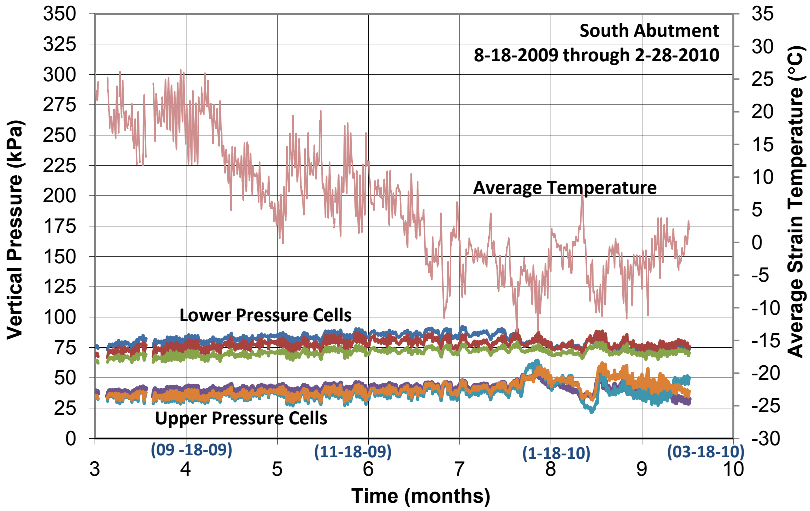

Figure 6. Vertical Pressure and Temperature with Time.

ACKNOWLEDGEMENTS

The first author would like to thank the FHWA for their financial support. Defiance County should be recognized for their efforts to utilize innovation to save money.

REFERENCES

Adams, M., Schlatter, W., and Stabile, T. (2008). “Geosynthetic Reinforced Soil Integrated Bridge System.” *Proceedings from the EuroGeo4 Conference*, Edinburgh, Scotland, September 2008.

Wu, J., Ketchart, K. Adams, M. (2001). *GRS Bridge Pier and Abutments*. Federal Highway Administration Report FHWA-RD-00-038.

Wu, J. (2001). *Revising the AASHTO Guidelines for Design and Construction of GRS Walls*. Colorado Department of Transportation Report CDOT-DTD-R-2001-16.

Wu, J., Lee, K., Helwany, S.,Ketchart, K. (2006). *Design and Construction Guidelines for Geosynthetic Reinforced Soil Bridge Abutment with a Flexible Facing*. Transportation Research Board, NCHRP Report 556.

Seismic Design Considerations for Underground Box Structures

Y. M. A. Hashash[1], Karina Karina[2], Demetrious Koutsoftas[3] and Nick O'Riordan[2]

[1]Department of Civil and Environmental Engineering, University of Illinois at Urbana-Champaign, 205 N. Mathews Ave., Urbana, IL 61801; PH: (217)333-6986, FAX (217)265-8041; email: hashash@illinois.edu
[2]Arup, 560 Mission St., Ste. 700, San Francisco, CA 94105; PH: (415)957-9445, FAX: (415)957-9096; email: karina.karina@arup.com, nick.oriordan@arup.com
[3]DKGC, Inc., 60 Joost Avenue San Francisco, CA 94131; PH: 415-465-4724, FAX: 415-584-1360; Email: deme@dkgeotech.com.

ABSTRACT

Underground structures have generally performed well during seismic events. Nevertheless the design of these structures has to consider seismic loading. Unlike above ground structures,the response of undergound structures to seismic loading is dominated by the seismic deformations of the surrounding soil. Seismic loading is characterized in terms of deformations imposed by the soil on the box structures and the interaction between them. This paper describes seismic analysis approaches for underground structures. The paper reviews available simplified solutions and describes procedures to conduct numerical analyses using pseudo-static and dynamic soil-structure interaction approaches. The paper describes some of the limitations associated with pseudo-static analyses for shallow structure and the need for dynamic soil-structure analyses under these conditions.

INTRODUCTION

Cut-and-cover box structures are commonly employed in urban transportation projects for mass transit or below ground roadways. These longitudinal box structures are either fully enclosed in soil or have three sides embedded in soil, while the roof is at the ground surface as illustrated in Figure 1. In addition to static loads, in seismically active areas these structures have to be designed to withstand significant seismic forces. The seismic response of underground box structures is dominated by that of the surrounding soil because the deformations and inertial response of the box structure are controlled by the deformations and inertial response of the surrounding soil mass (Arango, 2008; Hashash et al., 2001; Wang, 1993; Wu and Penzien, 1994). Unlike above ground structures, underground structures do not experience free vibration as a result of seismic shaking.

This paper discusses approaches used in the seismic design and analysis of underground box structures. The discussion focuses on the use of numerical analysis tools for pseudo static and dynamic analysis to evaluate the performance of these structures.

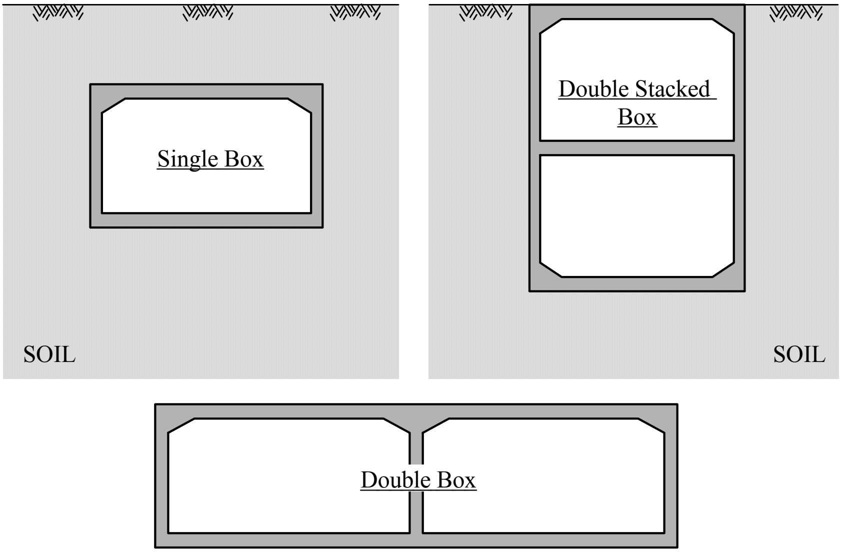

Figure 1 Typical cut-and-cover box structures

PERFORMANCE OF UNDERGROUND BOX STRUCTURES DURING EARTHQUAKES

Underground structures have generally performed well during seismic events (Arango, 2008; Hashash et al., 2001). The BART (Bay Area Rapid Transit) below ground box shaped stations in San Francisco did not experience damage during the 1989 Loma Prieta Earthquake. Similarly cut-and-cover box shaped stations for the Los Angeles Metro also performed well during the 1994 Northridge Earthquake. The recent 27 February 2010 M8.8 Mauli, Chile Earthquake resulted in significant shaking over large parts of Chile including the capital city of Santiago. Measured horizontal peak ground accelerations were up to 0.25g in Santiago. Inspection of two long and wide (3 lanes of vehicular traffic in each direction) below ground box structures over 1 km long that were constructed in relatively stiff gravel deposits showed no damage. Below ground stations of the Santiago Metro also showed no damage.

One of the cases in which the underground box structure did not perform well during an earthquake was the collapse of the Daikai Subway station during the 1995 Hyogoken-Nambu (Kobe) earthquake. The failure is attributed to deficiencies in reinforcement of the central columns (Iida et al., 1996; Parra-Montesinos et al., 2006) that resulted in insufficient confinement.

While the overall seismic performance of underground box structures has been satisfactory, the collapse of the Daikai subway station serves as a reminder of the need to consider seismic loading on such structures.

SEISMIC ANALYSIS APPROACHES

Seismic analysis of underground box structures starts with the definition of seismic hazard, followed by development of seismic performance criteria, selection of seismic input motions, site response analysis, and soil-structure interaction analysis.

Field and laboratory investigations. A detailed field investigation program is necessary to define site subsurface conditions and the variation of the soil stratigraphy across the site. The field investigation program should include definition of the depth to the depth of rock, as well as the shear wave velocity profile for some depth below the top of rock. of rock. Measurement of in situ shear wave velocity profiles across the site is essential. In addition to field investigation program, the characteristics of each major soil unit and bedrock are assessed through laboratory tests. The laboratory program should include standard soil index tests as well as definition of soil stress history and other engineering properties appropriate for the characterization of the various strata present at the site. Static and cyclic laboratory tests on the soil layers will provide needed information on strength of soil as well as the variation of shear modulus as a function of shear strain and number of loading cycles.

Seismic hazard analysis. For most major projects it is common to perform site specific probabilistic and deterministic seismic hazard analysis (Kramer, 1996) to define the seismic ground motion parameters. Relevant seismic sources are first identified and appropriate seismic parameters are selected for these sources. Applicable attenuation relationships are then selected to compute ground motion parameters at the site including spectral accelerations and velocities. The ground motion parameters, commonly in the form of acceleration response spectra, have to be defined at an equivalent rock outcrop.

Seismic performance criteria. A project seismic performance criterion is needed to define the structure performance objectives at one or more ground shaking levels. On many projects a two level criteria is often adopted that include operating basis earthquake (OBE) and maximum design earthquake (MDE). The structure is expected to survive the OBE event with very minor damage enabling the return to normal operations shortly after such a shaking event. Under an MDE, the structure might experience limited damage that requires some repairs after which the structure can be returned to normal service. Each of the OBE and MDE events are defined using response spectra developed based on probabalistic and deterministic analyses . and probabilistic

Seismic input motions. For each of the design earthquake levels a suite of three component motions is needed for site response analysis and soil-structure interaction modeling. Whenever possible it is preferable to use recorded motions in lieu of synthetic motions. The selected suite of motions is usually spectrally matched to the target spectra. The motions should reflect the duration of the controlling earthquake event(s), directivity effects if applicable and include appropriate velocity pulses due to near field effects.

For long box structures, it is necessary to include ground motion incoherency effects along the length of these structures. There are three sources of ground motion incoherency (Abrahamson et al., 1991; Hao, 1989; Tsai and Hashash, 2010) : (a) scattering and extended source effects, (b) wave passage effect and (c) local site effects. Local site effects are accounted for by performing appropriate site response analyses that capture the variability in site conditions accross the site. Scattering and extended source effects are generally not significant for many box structures, paricularly if they are of relatively limited length. Wave passage effects are accounted for by adding an arrival time delay of the ground motion along the length of the box structure.

Site response analysis. One-dimensional equivalent linear and nonlinear site response analyses are conducted to account for the effect of the soil column on the ground motion and are discussed in greater detail in the next section.

Soil-structure interaction analysis. Characteristic deformation of underground box structures caused by seismic shaking are illustrated in Figure 2 (Anderson et al., 2008; Hashash et al., 2001; Owen and Scholl, 1981; Wang, 1993).Deformations in the longitudinal and transverse directions must be considered in the design. In addition the effects of vertical shaking must be considered in the design. In the longitudinal direction underground structures are subject to bending and axial compression-tension as the seismic waves propagate along the structure. The response in the longitudinal direction is controlled by the extent of ground motion incoherency along the length of the alignment. The box structure will have to be designed to accommodate the resulting tensile and compressive strains.

In the transverse direction the box structure will be subjected to shear strains that will cause racking of the box structures. The extent of racking displacements will depend on the shear stiffness of the box structure relative to that of the surrounding soil. Box racking displacements can then be used in a structural analysis of the box structure to estimate the dynamic forcs in the box frame. Approaches using dynamic earth pressures such as those based on the Mononbe-Okabe method (Whitman, 1990) are not considered appropriate to the design of underground box structures due to kinematic and geometric constraints. Several papers published in this proceeding address the issue of dynamic earth pressures for retaining structures.

A number of authors have proposed solutions to calculate racking deformations for deep and shallow box structures (Bobet et al., 2008; Huo et al., 2006) and describe issues associated with numerical modeling of the racking soil-structure interaction (Anderson et al., 2008; Arango, 2008; Hashash et al., 2001; Hashash et al., 2005; Ostadan and Penzien, 2001; Parra-Montesinos et al., 2006; Sedarat et al., 2008; Wang, 1993; Wu and Penzien, 1994; Wu et al., 2008).

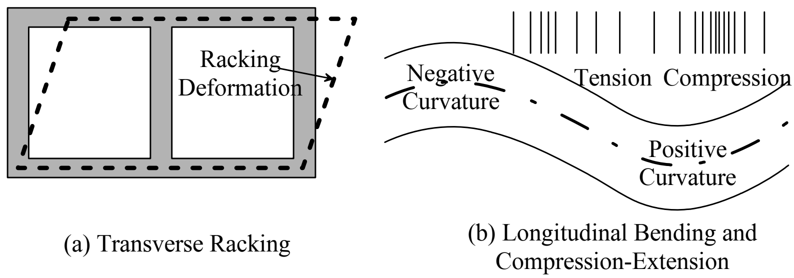

Figure 2 Seismic deformation modes of underground box structures

In the recent NCHRP 611 report (Anderson et al., 2008), a relationship is proposed between the racking ratio of rectangular conduits and the flexibility ratio: $R = \frac{\Delta_{Box}}{\Delta_{Free-Field}} = \frac{2F}{1+F}$, whereby the flexibility ratio: $F = \left(\frac{G_m}{K_s}\right)\left(\frac{B}{H}\right)$.

Where, B is the width of the box structure
H is the height of the box structure
G_m is the average strain-compatible shear modulus of the surrounding ground
K_s is the racking stiffness of the box structure, obtained by applying a unit lateral forces at the roof of the structure while restraining the base divided by the resulting lateral displacements (Figure 3).

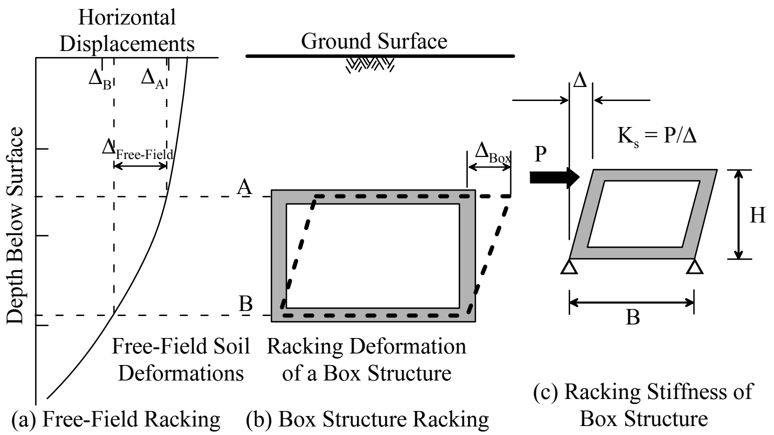

Figure 3 Racking ratio, free-field racking and structure racking.

The free-field racking deformations can be obtained from site response analyses. Numerical analyses can be employed instead of closed form solutions to estimate racking ratios for a wide range of box structure configurations. The following sections describe these analysis approaches.

SITE RESPONSE ANALYSIS

It is well established that local site conditions can significantly affect the propagating ground motions. One dimensional (1-D) site response analyses (Hashash et al., 2010; Idriss, 1990; Matasovic, 1993) are commonly used to characterize the change in the propagating ground motions through a soil column. In the analysis of box structures, 1-D site response analyses are used to provide:(a) free-field racking deformations along the box height which can be used in pseudo-static soil-structure interaction analysis, (b) input ground motions for dynamic soil-structure interaction analysis, (c) strain-compatible soil properties for use in pseudo-static and dynamic soil-structure interaction analyses, and (d) assessment of potential liquefaction and ground failure.

Site response analysis can be performed using equivalent linear frequency domain (Idriss and Sun, 1992) or nonlinear time domain analysis approaches (Kwok et al., 2006). Equivalent linear analysis is relatively easy to conduct and is widely used. Nonlinear analysis better incorporates soil-nonlinearity although significant expertise is required in developing input information. For moderate to strong ground shaking both equivalent linear and nonlinear site response analysis should be performed. While equivalent linear site response analysis might be sufficient for low levels of shaking. The following general steps are needed in site response analysis:

1. *Soil Profile.* The site stratigraphy is used to develop an idealized soil profile. The idealized soil profile is divided into sub layers with characteristic frequencies greater than 25 Hz.
2. *Model Parameters and dynamic curves.* Parameters needed in site response analysis include soil's unit weight, shear wave velocity, V_s, and soil stress history. Modulus reduction and damping curves as a function of shear strain can be obtained from laboratory tests data. In the absence of such data published curves based on empirical correlations (Darendeli, 2001; Vucetic and Dobry, 1991) can be adopted. The adopted curves have to be checked for implied shear strength or friction angle (Chiu et al., 2008; Hashash et al., 2010). Rate dependency of the shear strength should also be considered particularly in clays and cemented or locked sands.
3. *Selection of input Ground Motion.* The suites of ground motion time histories generated at an equivalent rock outcrop as described earlier are used as input motions in site response analysis. The motions should be base line corrected to minimize displacement drift in the computed response.
4. *Site Response Analysis and Results.* Equivalent linear and nonlinear site response analyses are then conducted. Output to be extracted from these analyses include: (a) the acceleration time history at the bottom of soil-structure interaction model, (b) free-field maximum racking deformation over the height of the box structure obtained from displacement and strain time histories over this height, (c) strain-compatible shear moduli and damping ratios (d) profiles of the PGA, maximum shear stress and shear strain levels.

Site response analysis results are used in the evaluation of seismic response of the box structures as well as in the assessment of ground failure potential of surficial soil susceptible to liquefaction and lateral spreading.

TRANSVERSE PSEUDO-STATIC SOIL-STRUCTURE INTERACTION ANALYSIS

The objective of the soil-structure interaction analysis is to compute the racking deformation of the box structure given the free-field racking deformations. In pseudo-static racking analysis, the inertia of the soil and structure due to seismic shaking is neglected. The soil-structure interaction problem is simplified to that of a frame in a soil medium subjected to simple shear on horizontal and vertical planes. Figure 4 illustrates the steps in pseudo-static analysis.

Site response analysis, described earlier, is conducted to simulate the ground motion propagation through the soil. The free-field racking (lateral displacement) over the height of the box structure is computed from the strains in the soil layers that span the height of the box in the site response analysis. Strain-compatible stiffness of the soil layers over the height of the box and some distance above and below the box, denoted as selected soil layers in Figure 4, are also obtained from the site response analysis.

In a two dimensional (2-D) numerical analysis, the box frame is represented in a uniform soil medium. The elastic properties of this soil medium are computed as the average strain-compatible elastic properties (Anderson et al., 2008) of the selected soil layers. Along the side and top boundaries of the model lateral displacements are imposed such that the free-field racking along the boundaries is equal to the free-field racking computed from the site response analysis as illustrated in Figure 4. The soil medium that surrounds the box will transmit the shearing displacement from the boundary to the modeled box structure. The box racking deformations are then computed in the analysis.

Pseudo-static soil structure analyses are computationally efficient and a large number of analyses can be performed to evaluate the sensitivity of the computed box response to input motions and types of site response analyses (equivalent linear and nonlinear). However, there are several important limitations of the pseudo-static analysis approach.

For shallow box structures, the shear displacements at the ground surface cannot be transmitted uniformly to the top of the buried structure. To overcome this limitation, the top boundary of the 2-D model can be artificially extended some distance above the top of the box and uniform elastic material is assigned as the medium that transmits the shearing to the box.

In the pseudo-static analysis, the racking deformations are assumed to vary uniformly over the height of the box structures in a uniform soil medium. Thus, the response of the individual soil layers is not represented. This becomes an important limitation if part of the box is embedded in a stiff soil while another part is in a soft soil.

Given the limitations discusse above, it is preferable that selected dynamic soil-structure interaction analyses be performed to verify the results of the pseudo-static analyses. Dynamic analyses, while more computationally demanding, are better suited to address problems associated with modeling of shallow box structures as well as significant variations in soil stiffness over the height of the box.

1. One-dimensional Site Response Analysis

- Obtain free-field racking deformation, $\Delta_{Free\text{-}Field}$ from site response analysis.
- Obtain strain compatible shear wave velocity.

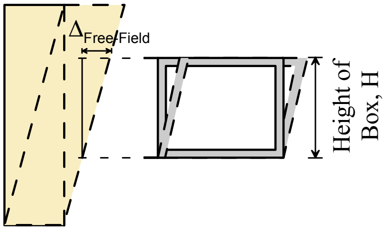

2. Two-dimensional Model Parameters Selection

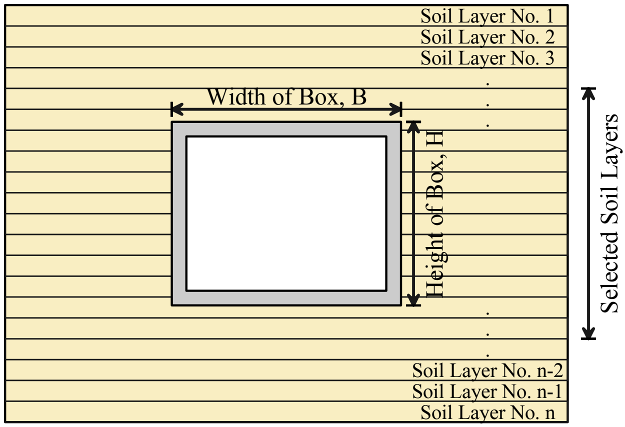

- Select soil layers that correspond to 4-10 ft above the top of the box structure to 4-10 ft below the bottom of the box structure.
- Use the strain compatible shear wave velocities from site response analysis to develop shear modulus values;
- Compute the average shear modulus over the selected soil layers.
- Obtain structural member properties (E, stiffness, I, moment of inertia, A, cross section area, EA and EI).

Figure 4 Pseudo-static racking analysis procedure (cont'd on next page).

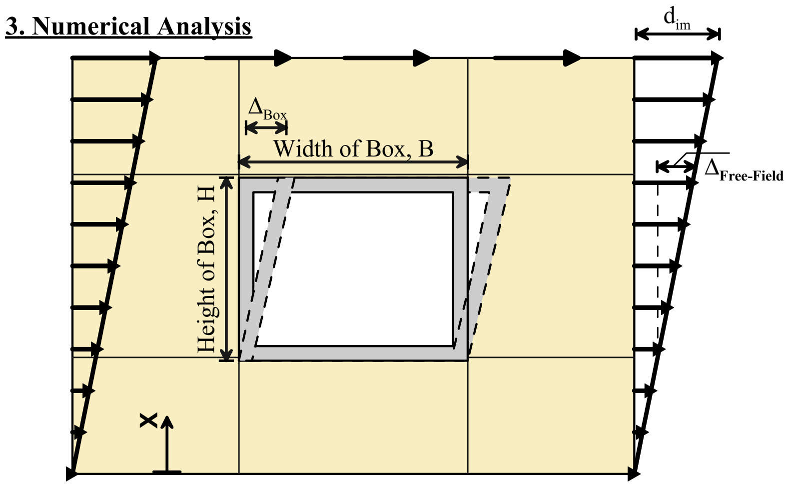

- Apply the free-field racking at left, right and top boundaries of the model.

$$d_{im} = \frac{x}{H}\Delta_{Free\text{-}Field}$$

- Obtain the box racking deformation from the numerical analysis.
- Calculate racking ratio:

$$R = \frac{\Delta_{Box}}{\Delta_{Free\text{-}Field}}$$

Figure 4 Pseudo-static racking analysis procedure (cont'd on next page).

TRANSVERSE DYNAMIC SOIL-STRUCTURE INTERACTION ANALYSIS

The dynamic soil-structure interaction analysis procedure is illustrated in Figure 5. In the numerical model the soil layers are modeled to reflect the idealized site stratigraphy. Each soil layer is modeled as a linear elastic material that is assigned strain-compatible shear modulus and damping values obtained from the site response analysis. The displacement time history applied at the bottom of the 2-D model is obtained from the corresponding soil layer in the site response analysis. The numerical analysis will then propagate the ground motion through the soil and simulate the soil-box interaction response. The maximum racking in the structure and in the free-field can be obtained from the analysis to compute the box racking ratio.

This procedure simplifies soil dynamic response using the equivalent linear analysis philosophy. This makes the computational effort manageable especially for design purposes. However, it is possible to account for the soil nonlinear behavior by using soil constitutive models that can represent soil nonlinear and hysteretic response at small strains. The use of such models requires additional model parameters and therefore there is a need for more advanced testing on the various soil formations to inform the selection of these additional model parameters.

1. One-dimensional Site Response Analysis

- Obtain acceleration and displacement time history for the layer corresponding to bottom of 2-D model.
- Obtain strain compatible shear wave velocity and damping ratio for layers corresponding to layers in the 2-D model.

2. Two-dimensional Soil Model Parameters Selection

- Obtain the soil properties from site response analysis
- Obtain structural member properties (E, stiffness, I, moment of inertia, A, cross section area, EA and EI).

3. Numerical Analysis

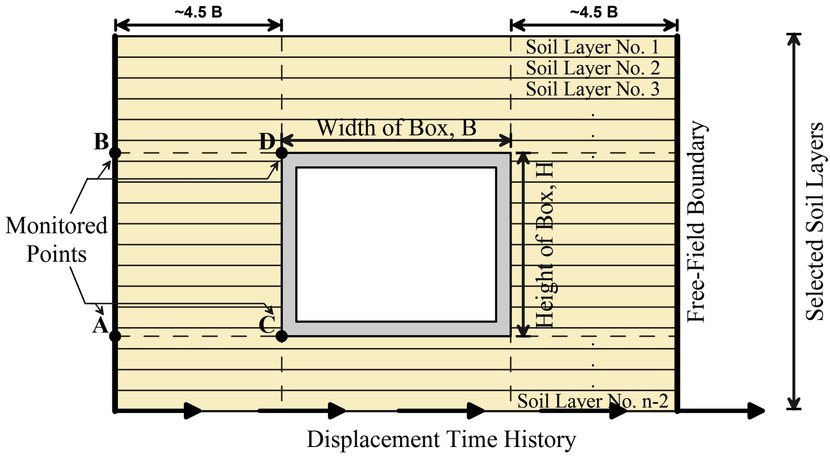

- Apply the displacement time history at the base of the model.
- Obtain the displacement time histories at four monitored points (A, B, C, and D)
- Obtain box relative displacement as follows:

$$\Delta_{box} = max[abs(\delta_{h,C} - \delta_{h,D})]$$

- Obtain free-field relative displacement as follows:

$$\Delta_{ff} = max[abs(\delta_{h,A} - \delta_{h,B})]$$

- Obtain Racking Ratio as follows: $R = \dfrac{\Delta_{Box}}{\Delta_{ff}}$
- Note that it is not necessary to include the full soil profile below the base of the box to the top of rock. A limited thicknes of soil that captures the characteristics of the wavw propagation is often sufficient.

Figure 5 Dynamic soil-structure interaction procedure.

TYPICAL RESULTS OF TRANSVERSE SOIL-STRUCTURE INTERACTION ANALYSES

A series of analyses were conducted on single and double box structures in stiff and soft soil profiles using 14 spectrally matched ground motion time series to a target response spectrum. The analyses included both pseudo-static and dynamic soil-structure interaction analysis. Equivalent linear and nonlinear site response analysis results were used as input in the soil-structure interaction analysis. The results of the analyses are summarized in Figure 6 whereby the computed racking ratio, R is plotted versus the flexibility ratio, F. Each cluster of data points represents the behavior of a single structure embedded in a specific soil profile. The variations of results in a cluster correspond to variation in input ground motion, site response analysis type and 2-D soil-structure analysis type. Figure 6 also plots the relationship of R vs. F proposed in the NCHRP 611 (Anderson et al., 2008) report for reference. When F<1, the racking stiffness of the box structure is larger than that of the soil. The soil is usually soft and the racking deformations are relatively large. When F>1, the racking stiffness of the box structures is smaller than that of the soil. The soil is usually stiff and racking deformations are small. Analysis results follow the general trend in the NCHRP 611 (Anderson et al., 2008) relationship. As the flexibility ratio increases the racking ratio also increases.

For the case of a box in a soft soil profile (F<1), a range of flexibility ratios is computed instead of a single value. This is a result of the variation in strain-compatible soil properties obtained from the equivalent linear and nonlinear site response analysis and the suite of 14 input motions. The dynamic and pseudo-static analysis results appear to be quite similar and they are slightly above the NCHRP 611 (Anderson et al., 2008) relationship.

For the case of a box in moderately stiff soil (4<F<9), similar to the structure in soft soil, a range of flexibility ratios is computed instead of a single value. The racking ratios computed from pseudo-static and dynamic soil-structure interaction analyses plot above the NCHRP 611 relationship. The dynamic analysis results show more scatter and give higher racking ratios compared to the pseudo-static analyses. The analyses imply that by accounting for dynamic interaction, the structure racking will be larger than that computed from the pseudo-static analyses.

For the structure in stiff soil (10<F<13) the pseudo-static and dynamic racking ratios are less than those for NCHRP 611 (Anderson et al., 2008). Dynamic analyses results in slightly lower racking ratios than pseudo-static analyses.

The results presented in Figure 6 show that the proposed numerical analysis approaches provide results and trends that are consistent with the results obtained from simplified closed-form solutions. The analyses highlight the need to account for variability in input ground motions and site response analysis methods as they affect the computed flexibility ratio. The flexibility ratio can vary substantially even under conditions represented by a single structure, embedded in a uniform soil profile and for a given target earthquake shaking level. The analyses also highlight the impotrance of dynamic analyses to verify and supplement the results of pseudo-static soil-structure interaction analyses.

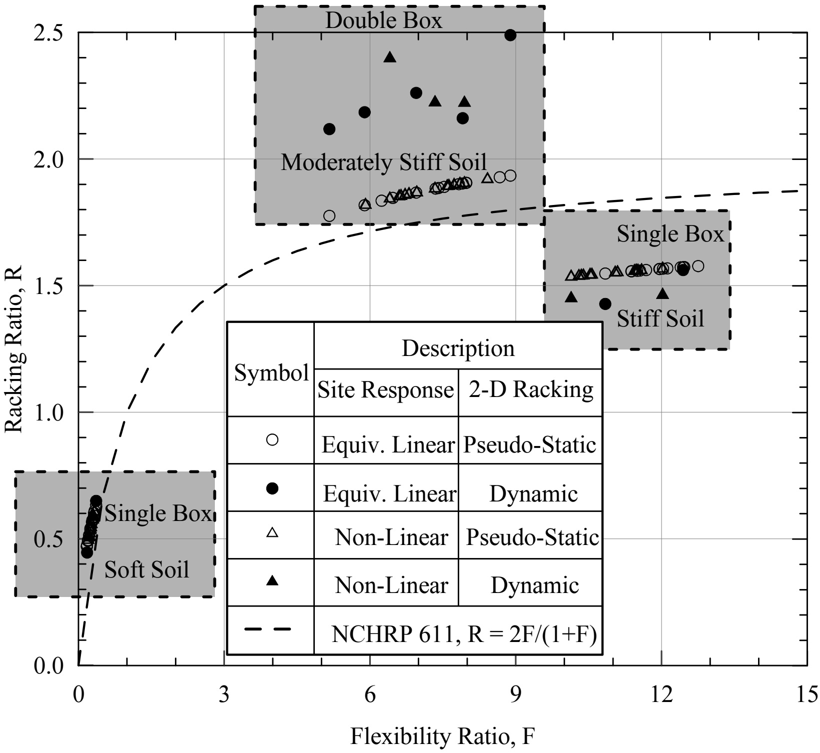

Figure 6 Typical results of pseudo-static and dynamic soil-structure interaction for underground box structures.

VERTICAL GROUND SHAKING AND RESPONSE

Vertical ground motions can be quite significant at a site and can impose vertical loads on the roof of a box structures. Figure 7 presents a schematic of the loading due to vertical acceleration on a relatively shallow box structure. Two possible approaches, 1-D site response analysis and 2-D soil-structure interaction, can be considered in estimating the vertical inertial load on the roof of the box structure.

In 1-D vertical site response analyses (Mok et al., 1998), the vertical input motions are propagated upward from the top of bedrock to the ground surface. The analyses will result in estimated vertical acceleration histories at various depths corresponding to the various soil sublayers. The vertical acceleration time histories can be used to evaluate the variations of acceleration with time and depth over the top of the box structure. These accelerations can be used in estimating the inertial loading of the soil mass on the roof of the box structure.

In 2-D soil-structure interaction analysis, the vertical ground motion is propagated from the bottom of the model that includes representation of the underground box structural components. The incremental loading on the roof of the box structure can be obtained directly from the analysis. Inertial loading of the soil mass above the box structure can be also obtained in the form of acceleration time histories from the analysis.

There is significant uncertainty in selecting appropriate dynamic soil properties for vertical site response analysis and the appropriate method for vertical propagation of ground motions. This is an area that remains a topic of ongoing research.

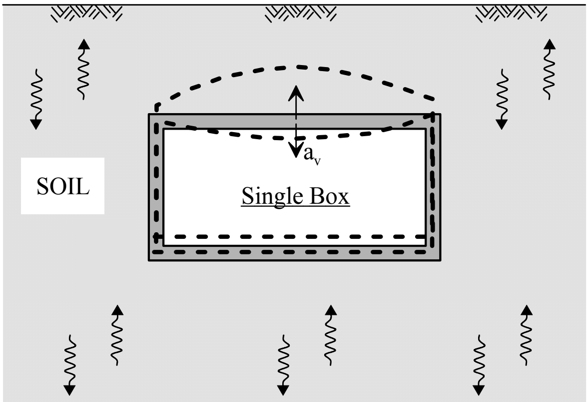

Figure 7 Schematic of vertical ground shaking effects on underground box structures

GROUND FAILURE AND LIQUEFACTION

The analysis approaches described thus far do not account for the potential of soil failure due to liquefaction and lateral spreading. Site response analyses can be used to evaluate the liquefaction potential of the various soil formations. The potential for lateral spreading will also need to be assessed. If liquefaction is limited to soil layers above the underground box structures, then liquefaction is unlikely to influence the racking response of the box. However, if the box is partially or entirely embedded in in liquefiable soil, additional evaluations are required. A check against box floatation is also needed. The box will also need to be designed to withstand the additional lateral pressures due to the presence of the liquefied soil.

CONSIDERATIONS DURING CONSTRUCTION

Braced excavations are often used to develop the space needed for underground box construction. Temporary excavations in urban areas with high levels of seismicity may have to be designed to withstand some level of seismic shaking. This level of shaking is usually less than that considered for the permanent box structures. Figure 8 illustrates the seismic racking response of a typical braced shoring system.

Transverse pseudo-static and dynamic analysis techniques described earlier for box structures can be used in the analysis of racking deformations of the braced shoring system. However, given the lack of soil cover, it is preferable that a dynamic soil-structure interaction analysis be conducted. The analysis can estimate the level of deformation that the shoring system will need to accommodate during the design seismic event. In addition the analysis can provide estimates of dynamic load increments on the shoring wall and the bracing.

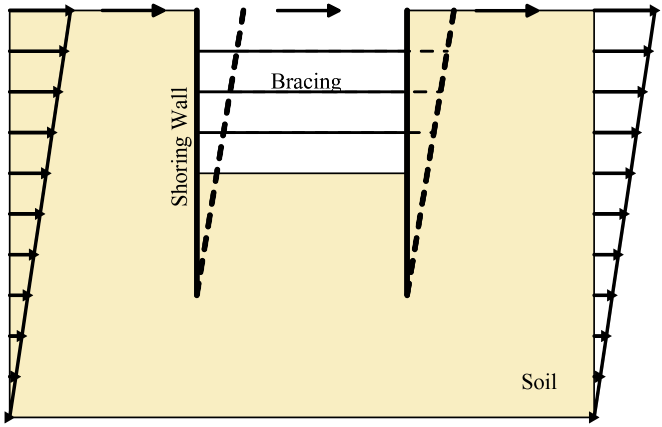

Figure 8 Racking of temporary braced sharing wall

Interaction of temporary and permanent structures

Analyses of seismic response of permanent box structures ignore the influence of temporary shoring walls on the overall system response. In situ, the temporary support will be left in place and only the first several feet of the top of the shoring wall will be cut-off. The response of the underground box structure with the presence of the temporary wall to racking might be altered. The effect of the presence of the shoring walls on the results of the racking analysis should be investigated.

The authors have performed an investigation of the effect of temporary shoring on box structures in soft soils. The same methodology for pseudo-static and dynamic analyses is employed. Three cases were considered as illustrated on Figure 9:

- Case 1: The shoring wall is not modeled
- Case 2: The shoring wall is modeled at the height of the box structure only.
- Case 3: The shoring wall is modeled to extend above and below the box structure

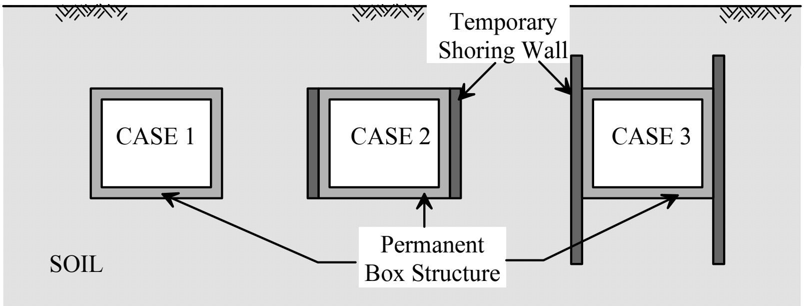

Figure 9 Cases considered in the evaluation of the interaction of the temporary shoring wall and the permanent underground box structure

The results of the analyses of the interaction of the box with the temporary shoring for the case of a single box embedded in soft clay (see also Figure 6) are summarized in Figure 10, and show that modeling the shoring wall only over the height of the box structure is similar to the analysis whereby the shoring wall is not modeled but the stiffness of the box structure is increased to account for the composite action of the shoring wall and the box wall. When the shoring wall is modeled to extend above and below the box structure, higher racking deformations are estimated as compared to the case where the shoring wall is not modeled. It appears that the shoring wall transfers soil loads from above and below the structure to the structure, acting as extended wings that capture more of the racking displacements above and below the box. The racking ratios increase by 15% to 20% for this case, and the differences decrease with increasing flexibility ratio.

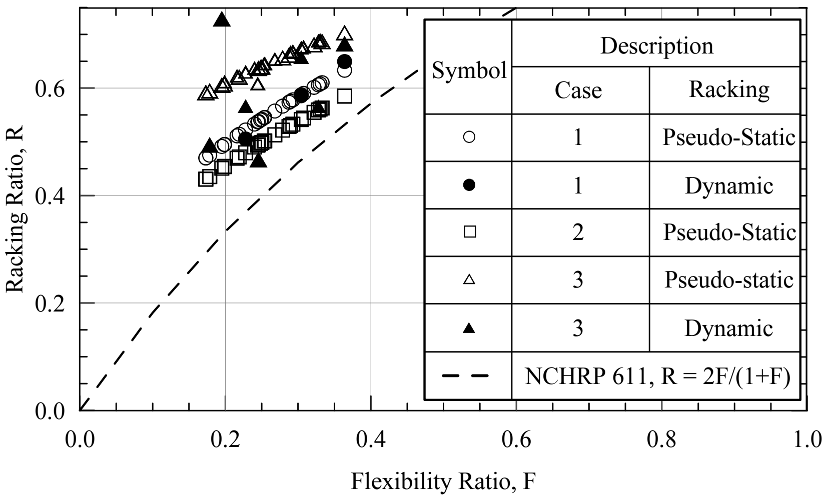

Figure 10 Results of pseudo-static and dynamic soil-structure interaction analyses to evaluate the interaction of temporary shoring wall

ADDITIONAL CONSIDERATIONS

There are a number of additional issues that will have to be considered in the evaluation of the seismic performance of box structures. Treatment of these issues is beyond the scope of this paper, but a brief discussion of some of them is presented.

Permanent changes in state of stress of soil. The analysis approaches described so far assume that the changes in the state of stress in the soil, especially beneath the box structure do not substantially alter the dynamic response of the soil. There are situations whereby the placement of wide box structures in relatively deep excavations in soft soil may lead to significant changes in soil properties which influence the long term dynamic response of the structure. The analyses will then have to specifically account for the influence of such changes on the overall dynamic response of the system.

Impact of superstructure. If an above ground structure is to be built on the box structures, the interaction of the superstructure with the below ground structure will have to be evaluated as well. Therefore a full seismic soil-box-superstructure interaction analysis is required to evaluate the system performance and seismic loads on the box structures.

Impact of adjacent structures. In heavily urbanized areas, underground box structures may be located in close proximity to the foundations of high-rise buildings. Seismic analyses will be needed to evaluate the impact of forces transmitted from the superstructure to its foundations, which would interact with the underground structure and influence its performance.

CONCLUSIONS

Underground box structures employed in urban transportation projects have generally performed well during seismic shaking with some notable exceptions. These box structures have to therefore be designed to withstand seismic in addition to static loading. The response of underground box structures to seismic shaking is dominated by the seismic deformations of the surrounding soil. The paper presented the steps required in the seismic evaluation of box structures. Pseudo-static and dynamic soil-structure interaction methods of analyses which can be used to evaluate the seismic behavior of box structures are described. The limitations of pseudo-static approaches in dealing with shallow box structures and soil profiles with significant stiffness variations are highlighted. Results of typical analyses of a range of box structure shapes, soil profiles and ground motions were presented. The influence of temporary shoring left in place on permanent box structure racking is also highlighted.

REFERENCES

Abrahamson, N.A., J. F. Schneider, and J. C. Stepp (1991) "Empirical Spatial Coherency Functions for Application to Soil-Structure Interaction Analyses," *Earthquake spectra*, Vol. 7, No. 1, pp 1-27.

Anderson, Donald G., Geoffrey R. Martin, Ignatius Lam, and J. N. Wang (2008) "Seismic analysis and design of retaining walls, buried structures, slopes and embankments," National Cooperative Highway Research Program, Transportation Research Board.

Arango, Ignacio (2008) "Earthquake engineering for tunnels and underground structures. A case history.," In: David Zeng, Majid T. Manzari, and Dennis R. Hiltunen, Eds., *Geotechnical Earthquake Engineering and Soil Dynamics IV*. Sacramento, CA: ASCE.

Bobet, Antonio, Gabriel Fernandez, Hongbin Huo, and Julio Ramirez (2008) "A practical iterative procedure to estimate seismic-induced deformations of shallow rectangular structures," *Canadian Geotechnical Journal*, Vol. 45, No. 7, pp 923-938.

Chiu, Peter, Daniel E. Pradel, Annie On-Lei Kwok, and Jonathan P. Stewart (2008) "Seismic Response Analyses for the Silicon Valley Rapid Transit Project," In: David Zeng, Majid T. Manzari, and Dennis R. Hiltunen, Eds., *Geotechnical Earthquake Engineering and Soil Dynamics IV*. Sacramento, CA: ASCE.

Darendeli, M. B. (2001) "Development of a new family of normalized modulus reduction and material damping curves," *Civil Engineering*. Austin: University of Texas at Austin, p 395.

Hao, H., Oliveria, C. S. and Penzien, J. (1989) "Multiple-station ground motion progressing and simulation based on SMART-1 array data," *Nuclear Engineering and Design*, Vol. 111.

Hashash, Y. M. A., J.J. Hook, B Schmidt, and J. I-C. Yao (2001) "Seismic design and analysis of underground structures," *Tunneling and Underground Space Technology*, Vol. 16, pp 247-293.

Hashash, Y. M.A., D. Park, and J. I-C. Yao (2005) "Ovaling deformations of circular tunnels under seismic loading, an update on seismic design and analysis of underground structures," *Tunneling and Underground Space Technology*, Vol. 20, No. 5, pp 435-441.

Hashash, Youssef M.A., Camilo Phillips, and David R. Groholski (2010) "Recent advances in non-linear site response analysis," *Fifth International Conference in Recent Advances in Geotechnical Eartqhuake Engineering and Soil Dynamics*. SanDiego, CA, p OSP 4.

Huo, H., A. Bobet, G. Fernández, and J Ramírez (2006) "Analytical solution for deep rectangular structures subjected to far-field shear stresses," *Tunnelling and Underground Space Technology*, Vol. 21, No. 6, pp 613-625.

Idriss, I.M. (1990) "Influence of Local Site Conditions on Earthquake Ground Motions," *Proceedings of the 4th U.S. National Conference on Earthquake Engineering*. Palm Springs, pp 55-57.

Idriss, I.M., and J.I. Sun (1992) "SHAKE91: A computer program for conducting equivalent linear seismic response analyses of horizontally layered soil deposits," Department of Civil and Environmental Engineering, University of California Davis.

Iida, H., T.Hiroto, N. Yoshida, and M. Iwafuji (1996) "Damage to the Daikai Subway Station," *Soils and Foundations Special Issue on Geotechnical Aspects of teh*

January 17, 1995 Hyogoken-Nambu Earthquake, pp 283-300.
Kramer, Steven Lawrence (1996) *Geotechnical earthquake engineering*, Upper Saddle River, N.J.: Prentice Hall.
Kwok, On-Lei A., Jonathan P. Stewart, Youssef M.A. Hashash, Neven Matasovic, Robert Pyke, Zhiliang Wang, and Zhaohui Yang (2006) "Practical Implementation of Analysis Routines for Nonlinear Seismic Ground Response Analysis," *Eighth National Conference on Earthquake Engineering*. San Francisco, CA.
Matasovic, Neven (1993) "Seismic response of composite horizontally-layered soil deposits," University of California, Los Angeles, pp xxix, 452 leaves.
Mok, Chin Man, C.-Y. Chang, and Dante E. Legaspi (1998) "Site response analyses of vertical excitation," *Geotechnical Earthquake Engineering and Soil Mechanics III*: ASCE, pp 739-753.
Ostadan, F., and J. Penzien (2001) "Seismic Design of Cut-and-Cover Sections of the Bay Area Rapid Transit Extension to San Francisco Airport," *Second US-Japan Soil Structure Interaction Workshop* Tsukuba, Japan.
Owen, G. Norman, and Roger E. Scholl (1981) "Earthquake engineering of large underground structures : final report." Washington, D.C.,: National Technical Information Service, pp xvi, 279.
Parra-Montesinos, Gustavo J., Antonio Bobet, and Julio A. Ramirez (2006) "Evaluation of soil-structure interaction and structural collapse in Daikai subway station during Kobe earthquake," *ACI Structural Journal*, Vol. 103, No. 1, pp 113-122.
Sedarat, Hassan, Alexander Kozak, Youssef M. A. Hashash, Anoosh Shamsabadi, and Alex Krimotat (2008) "Contact interface in seismic analysis of circular tunnels," *Tunneling and Underground Space Technology*, Vol. submitted for review.
Tsai, Chi-Chin, and Y. M.A. Hashash (2010) "Evaluation of Two Approaches to Simulate Spatially Variable Ground Motions," *Journal of Earthquake Engineering*, Vol. 14, No. 2, pp pp. 293 - 308.
Vucetic, Mladen, and Ricardo Dobry (1991) "Effect of soil plasticity on cyclic response," *Journal of Geotechnical Engineering*, Vol. 117, No. 1, pp 87-107.
Wang, J.N. (1993) "Seismic Design of Tunnels: A State-of-the-Art Approach," *Monograph 7*. New York, NY: Parsons Brinckerhoff Quade & Douglas, Inc.
Whitman, Robert V. (1990) "Seismic design and behavior of gravity retaining walls," *Design and Performance of Earth Retaining Structures, Geotechnical Special Publication*: Cornell University, pp 817-842.
Wu, C. L., and J. Penzien (1994) "Seismic Design of Muni Metro Turnback Project," *Fifth U. S. National Conference on Earthquake Engineering*. Chicago, Illinois, pp 799-808.
Wu, Ching L., Farhang Ostadan, Wen S. Tseng, and James Chai (2008) "Cut-and-Cover Structures: Seismic Response and Design," In: David Zeng, Majid T. Manzari, and Dennis R. Hiltunen, Eds., *Geotechnical Earthquake Engineering and Soil Dynamics IV*. Sacramento, CA: ASCE.

Seismic Displacement Design of Earth Retaining Structures

Jonathan D. Bray, F.ASCE[1], Thaleia Travasarou, M.ASCE[2], and Josh Zupan[3]

[1]Professor, Univ. of California, Berkeley, Depart. of Civil and Environ. Engineering, Berkeley, CA 94720-1710. E-mail: bray@ce.berkeley.edu
[2]Senior Engineer, Fugro-West, Inc., 1000 Broadway, Suite 440, Oakland, CA 94607
[3]Engineer, Cotton Shires and Assoc., Inc., 330 Village Lane, Los Gatos, CA 95030

ABSTRACT

Field performance observations and experimental evidence indicate that well-built retaining structures that are composed of or surrounded by materials that do not lose strength as a result of earthquake shaking perform satisfactorily at moderate levels of ground shaking. Thus, seismic earth pressures need not be considered when the peak ground acceleration is less than or equal to 0.3 *g*. At higher levels of ground shaking, the seismic evaluation should include the effects of the retained earth. The use of a Mononobe-Okabe-type method requires the selection of the seismic coefficient, which largely determines the magnitude of the seismic load increment. The rational selection of the seismic coefficient requires proper consideration of the seismic hazard at the site and the amount of seismic displacement that defines the threshold between satisfactory and unsatisfactory seismic performance of the earth retaining structure. Thus, a robust seismic design procedure should include a calculation of the potential seismic displacement of the earth retaining structure. In this paper, seismic displacement design procedures for earth retaining structures are examined.

INTRODUCTION

Most analytical procedures employed in earthquake engineering today have evolved significantly over the last two decades. However, the seismic design of earth retaining structures is still largely based on the application of the Mononobe-Okabe method that was proposed over eighty years ago. Although it is still widely used today, engineers understand that it is a coarse simplification of what is inherently a complex soil-structure interaction (SSI) problem. Yet, it is straightforward, and it is believed that it provides a reasonable estimate of the additional dynamic force exerted by the earth behind a yielding vertical retaining wall (i.e., gravity, cantilever, or tied-back earth retaining structure), so it is commonly used in engineering practice (e.g., Seed and Whitman 1970, Whitman 1990, and Kramer 1996). Its use satisfies the design objectives of straightforwardness, transparency, and reasonableness. However, it does not capture the actual dynamic response of the soil-structure system, and thus it does not provide the sound insight of an improved method that focuses on the most important seismic response and performance aspects of this problem. In this paper, several of these critical aspects are discussed and recommendations are made regarding methods that can be used when greater insight into this problem is desired.

STRENGTH LOSS POTENTIAL AND SEISMIC HAZARD ASSESSMENTS

The most critical component of the seismic evaluation of an earth retaining structure is the identification of materials within the earth structure or its foundation that could lose significant strength as a result of earthquake shaking. If such materials are present, the engineer should focus on evaluating their potential for strength loss and estimating their reduced post-cyclic shear strength. Therefore, a soil liquefaction triggering evaluation and an assessment of the post-liquefaction residual shear strength of materials that are likely to liquefy are critically important. Likewise, the evaluation of significant strength loss and its consequences in clayey soils (e.g., sensitive clays) is required, as is an evaluation of potential rock mass instability due to weak, unfavorably oriented bedding planes within in it. Foundation failures or severe strength loss in backfill materials are the most common causes of poor seismic performance of earth retaining walls that are properly constructed (Whitman 1991). The engineer should first focus on evaluating the strength loss potential of earth materials comprising and surrounding the earth retaining structure and its foundation.

The evaluation of cyclic-induced strength loss in earth materials requires a sound assessment of the potential seismic shaking at the site. The seismic hazard assessment, whether probabilistic or deterministic, is likely the second most important component of the seismic evaluation of an earth retaining structure. Fortunately, great strides have been made in this area, so although characterization of the seismic loading contributes significantly to the overall uncertainty in the evaluation, accepted methods for developing estimates of ground motion intensity parameters and in quantifying the level of uncertainty in their assessment are now widely available. Confusion and controversy still remain, however, in developing a suite of records (i.e., acceleration-time histories) for representing the seismic ground shaking hazard at a site. Thus, great care should be exercised when dynamic analyses are to be performed that require input ground motion records. The selection of ground motion records is critically important, and their selection should consider characteristics other than peak ground acceleration (PGA) or 5% damped elastic spectral acceleration (S_a) response spectrum. In many geotechnical problems, a record's duration of strong shaking or time-domain attributes such as pulse-type motions resulting from forward-directivity in the near-fault region can be equally important.

MONONOBE-OKABE METHOD

The Mononobe-Okabe (M-O) method resulted from the works of Mononobe and Matsuo (1929) and Okabe (1926). The M-O method is widely used in engineering practice, because it involves a straightforward modification of the widely accepted Coulomb (1776) lateral earth pressure theory for calculating static active earth pressures (see Figure 1). In the M-O method a horizontal force is added to the existing system of forces acting on the critical failure wedge of earth behind the wall. This force is the product of a selected horizontal seismic coefficient (k_h) and the weight of the critical failure wedge (W). The effects of vertical motions are believed to be relatively minor, so the vertical seismic coefficient (k_v) term is typically ignored.

Thus, the seismic load increment due to the earthquake loading is largely defined by the engineer's selection of the horizontal seismic coefficient.

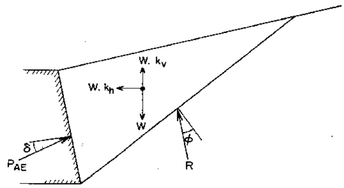

$$P_{AE} = 0.5\ K_{AE}\ (1\text{-}k_v)\ \gamma\ H^2$$

where γ is the unit weight of the backfill, H is the height of the wall, and K_{AE} is the dynamic active earth pressure coefficient that is a function of the seismic coefficients k_h and k_v and the friction angles of soil ϕ and soil-wall δ (see Kramer 1996); K_{AE} can be approximated by $K_{AE} = K_A + \Delta K_{AE}$, where K_A is the static active earth pressure coefficient and $\Delta K_{AE} = 0.75\ k_h$

Figure 1. Mononobe-Okabe method (Seed and Whitman 1970).

The horizontal seismic coefficient (k_h) represents the destabilizing effect of the earthquake shaking, which increases the horizontal force acting on the wall and leads to a more robust design in seismic regions. One constant parameter cannot possibly capture fully the complex interaction of the underlying earthquake ground motion, the seismic response of the potential sliding wedge of earth, and the dynamic response of the structural wall. Thus, it is recognized that the simplified M-O method must be calibrated against well documented case histories of the seismic performance of earth retaining walls during earthquakes or the results of validated advanced SSI dynamic analyses to be used with confidence. If well calibrated and understood, the M-O method provides a useful tool in the design of yielding earth retaining walls constructed on strong foundations with backfill materials that will not lose significant strength as a result of earthquake shaking, that is if the "correct" value of k_h is used.

The selection of k_h is often governed by precedence in engineering practice. For example, in several seismic design guidance documents (e.g., FHWA 1998, AASHTO 2007, and Anderson et al. 2008), k_h is assumed to be half of the ground surface PGA divided by the acceleration of gravity (g) (i.e., $k_h = 0.5\ PGA/g$) for earth retaining structures that may displace a few centimeters. The basis for using half of the PGA/g for k_h is that use of the full PGA/g value is overly conservative for walls that can displace some minor amount, and a value of about 0.5 PGA/g appears to capture most effects for this problem. Other recommendations for the selection of the seismic coefficient for the case of yielding walls includes $k_h = 0.33\ (PGA/g)^{0.33}$ (Okamoto 1984) and $k_h = 0.67\ PGA/g$ (several projects).

Recent centrifuge testing of cantilever retaining walls connected with a stiff floor slab (open channel structure) in dry cohesionless soil by Al Atik and Sitar (2010) confirms observations made previously (e.g., Whitman and Liao 1985, and Nakamura 2006) that the dynamic earth pressures from the backfill and the inertia forces on the wall do not act simultaneously. They state that the current practice of designing retaining walls for the maximum dynamic earth pressure increment and maximum wall inertia is "overly-conservative." Al Atik and Sitar (2010) recommend that seismic earth pressures can be ignored for well-designed walls for sites where the *PGA* is less than 0.4 *g*. This recommendation is consistent with the observations made by Clough and Fragaszy (1977) that open channel floodway structures that underwent shaking with *PGA* < 0.5 *g* during the 1971 San Fernando earthquake did not sustain damage even though the walls were not designed explicitly for seismic forces. For *PGA* greater than about 0.4 *g*, Al Atik and Sitar (2010) provide empirical relationships between the seismic earth pressure increment coefficient (ΔK_{AE}), which is defined in Figure 1, and the *PGA* measured in their experiments which show that ΔK_{AE} increases at about the same rate as *PGA*/*g* increases when *PGA* > 0.4 *g*. Importantly, their experimental evidence indicates that the seismic load increment acts at a height of one-third of the height of the wall up from the base of the wall. Thus, the total earth pressure resultant (P_{AE}) also acts at the one-third point up from the base of the wall, which greatly reduces the moment calculated at the base of a cantilever wall. In calculating the moment demand, the engineer must include the moment developed due to the inertia force acting on the wall itself at all levels of acceleration.

A key practical finding from the Al Atik and Sitar (2010) study is that seismic earth pressures can be ignored (i.e., $\Delta K_{AE} = 0$) for well-designed restrained cantilever retaining walls at lower levels of *PGA*. They define lower levels of *PGA* at the threshold of less than 0.4 *g*. Other researchers have suggested previously that due to the inherent conservatism in static design procedures, well-built retaining walls can undergo ground shaking with *PGA* levels less than 0.2 *g* to 0.3 *g* without incident. Earth retaining structures that are built on competent foundations with backfill materials that do not lose significant strength as a result of earthquake shaking have consistently performed well during major seismic events at ground shaking levels where the *PGA* was within the range of 0.2 *g* to 0.5 *g* (e.g., Clough and Fragazsy 1997, Whitman 1991, Lew et al. 1995, Sitar and Al Atik 2009, and Bray and Frost 2010). Therefore, it is reasonable to conclude that seismic earth pressures need not be considered for cases where the *PGA* ≤ 0.3 *g*. However, inertia forces on the wall are always considered. For projects, where the *PGA* exceeds 0.3 *g*, a rational design procedure is required for developing seismic earth pressures.

The rational selection of k_h requires proper consideration of the seismic hazard at the site and the amount of seismic displacement that defines the threshold between satisfactory and unsatisfactory seismic performance of the earth retaining structure. The seismic hazard at a site is function of the known tectonic framework and the level of risk that the owner decides is appropriate given the consequences of failure, uncertainty in the seismic assessment, and applicable building codes. Although a challenging problem, it is a tractable problem, once these issues are addressed. The key remaining seismic performance decision for a project involving an earth retaining structure is the selection of the seismic displacement threshold that defines satisfactory performance. Thus, a robust seismic analysis procedure should include, either explicitly or implicitly, the calculation of the potential seismic displacement of the earth retaining structure.

SEISMIC DISPLACEMENT ANALYSIS

The potential seismic displacement of an earth retaining structure and the backfill materials behind the structure depends primarily on shear-induced deformations from the accumulation of distributed deviatoric strains or sliding along a distinct failure plane that develops in the earth materials. Significant seismically induced volumetric strains may also develop in earth materials, and thus seismic compression of the compacted backfill materials, for example, can produce deformation of the ground surface behind a retaining wall. Seismically induced settlement of poorly compacted earth fill adjacent to vertical cantilever retaining walls is often observed after major earthquakes. Great care should be exercised in compacting soils adjacent to walls, and the use of approach slabs should be considered to alleviate this potential problem with bridge abutments. Ground displacements resulting from seismically induced volumetric strain of partially saturated soils can be estimated using procedures such as the Tokimatsu and Seed (1987) procedure. As seismic compression can often form a significant part of the overall seismically induced ground deformation, the potential for significant volumetric-induced ground strains should be evaluated. In this paper, however, the authors focus on methods that estimate seismic displacements resulting from shear-induced ground deformations, as these displacements are often the basis for evaluating the seismic design of yielding earth retaining structures.

Richards and Elms (1979) developed a procedure for the design of retaining walls that explicitly required the engineer and owner to select an allowable seismically induced permanent displacement of the wall (D_a). Utilizing the Newmark (1965) sliding block model to represent the earth materials behind the wall that may displace the wall outward as a result of cyclic-induced shear deformations, Richards and Elms (1979) developed an equation for calculating seismically induced permanent displacement (D) as a function of the ground motion's *PGA* and peak ground velocity (*PGV*) squared, and a higher order function of the ratio of the structure's yield coefficient (k_y, which is the seismic coefficient that produces a pseudostatic factor of safety, *FS,* of one) to its *PGA*/g, where g is the acceleration of gravity.

The Richards and Elms (1979) procedure required that D_a be selected. Then, the k-value that is compatible with this level of allowable seismic displacement given the design ground motion parameters of *PGA* and *PGV* could be calculated using their proposed equation. The M-O method is used with this value of k to calculate the total (static and dynamic) thrust on the retaining wall. The wall is then designed to resist this thrust from the earth backfill as well as the inertial force on the wall with the application of an appropriate *FS*, which is now often assumed to be about 1.1.

Whitman (1990) noted that although this procedure is essentially correct, it does not capture important aspects of the problem (such as the deformability of the backfill and the change in response during an episode of slip). This is not surprising as these shortcoming are inherent in the Newmark (1965) rigid sliding block method on which the Richards and Elms (1979) procedure is based. Whitman and Liao (1985) enhanced their procedure by using an idealized two-block model analogy initially proposed by Zarrabi (1979). They utilized a probabilistically based framework to account for the uncertainties associated with the dynamic response of the soil-structure system. They quantified the variability in the system's response resulting from ground motion variability. Additionally, they provided estimates of the error associated with not taking into account the deformability of the soil mass in their model, as well as not considering the vertical response and wall tilting. Whitman (1990) delineates the modified design approach as:

1. Select an allowable seismic displacement (D_a) for the system, which is often several centimeters (e.g., 5 cm, 10 cm, or 15 cm, depending on the system).
2. Set $k^* = PGA/g\ (0.66 - (1/9.4\ ln(D_a\ PGA/PGV^{\,2}))$, which provides for 95% confidence that the selected D_a value will not be exceeded for an earthquake with the design PGA and PGV values.
3. Use the M-O method with $k_h = k^*$ and analyze the adequacy of the system using a $FS \geq 1.0$ for sliding under the action of the calculated M-O earth thrust, which includes both the static and seismic increments, and the inertia force that acts on the wall itself.

The Whitman (1990) approach focuses appropriately on the importance of first selecting an allowable seismic displacement by which to judge seismic performance. However, considerable improvements may be made at this time, because of the large number of ground motion records that have become available over the last two decades. Earthquakes, such as the 1989 Loma Prieta, 1992 Landers, 1994 Northridge, 1995 Kobe, 1999 Kocaeli, 1999 Chi-Chi, and 1999 Duzce earthquakes, among others, have greatly increased the number of recorded ground motions. With a larger set of ground motions, a more robust relationship between simplified ground motion parameters and the seismic displacement resulting from Newmark-type sliding from these ground motions can be developed. Moreover, the backfill material can be appropriately modeled as a deformable earth mass, and the seismic response of the sliding mass during sliding can be more accurately captured.

UPDATED SEISMIC SLIDING DISPLACEMENT PROCEDURE

The concept of selecting D_a to guide design is tied to performance-based principles. It requires a representative model that captures the system's response. The dynamic response of an earth retaining structure is a complex phenomenon involving movement of a deformable mass of backfill soil and its interaction with the inertial response of the wall. Seismic performance is affected by: a) movement along a fully developed sliding surface or distributed deviatoric strain-induced movement of the deformable earth mass, b) incoherence of the dynamic response of the retained earth and wall, and c) co-seismic accumulation of displacements. An idealized model developed for earth embankments can be extended to provide estimates of the seismic displacement of an earth retaining structure. The Bray and Travasarou (2007) deviatoric seismic slope displacement calculation procedure is used for this purpose.

The Bray and Travasarou (2007) procedure is based on the dynamic response of the one-dimensional (1-D) nonlinear fully coupled stick-slip idealized soil model developed by Rathje and Bray (2000). This model is an improvement to a rigid block system in that it models the soil as a deformable mass while also modeling the nonlinear stick-slip episodes. Field performance and experiments (e.g., Zarrabi 1979) have shown that the critical failure surface is significantly flatter for the seismic case (i.e., angles of inclination of 30^o to 50^o from the horizontal), so the 1-D model is reasonable. The seismic response of the sliding and deformable mass is captured by an equivalent-linear visco-elastic modal analysis that considers the fundamental modal shape and uses strain-dependent material properties. Key model parameters representing the system properties are the fundamental period of the soil mass (T_s) and its yield coefficient (k_y). Key parameters representing the earthquake shaking are the spectral acceleration (S_a) at a degraded period of $1.5T_s$, and the earthquake moment magnitude (M), which is a proxy for the shaking duration.

The procedure used 688 records from 41 earthquakes, a significant improvement over the 14 records utilized by Whitman and Liao (1985). Hence, the variability in seismic displacement resulting from ground motion variability is better characterized. The seismic displacement corresponding to different probabilities of being exceeded is:

$$D_p = \exp\left(\Phi^{-1}\left[\left(1-\frac{p}{1-P(D="0")}\right),0,1\right]\cdot\sigma+\ln(D)\right) \tag{1a}$$

where p is the selected probability of exceedance, D_p is the displacement (in cm) that has a probability p of being exceeded given k_y, T_s, $S_a(1.5T_s)$ and M, Φ^{-1} is the inverse normal cumulative distribution function (NORMINV in excel) for mean 0 and standard deviation of 1, P(D="0") is the probability of negligible displacement (D < 1 cm) as a function of k_y, T_s, and S_a, $\sigma = 0.66$ is the standard deviation of the normally-distributed random error term, ε, with zero mean, and:

$$P(D="0") = 1-\Phi\left(-1.76-3.22\ln(k_y)-0.484\ln(k_y)T_s+3.52\ln(Sa)\right) \tag{1b}$$

$$\begin{aligned}\ln(D) = &-1.10-2.83\ln(k_y)-0.333\left(\ln(k_y)\right)^2+0.566\ln(k_y)\ln(S_a)+\\ &3.04\ln(S_a)-0.244\left(\ln(S_a)\right)^2+1.50T_s+0.278(M_w-7)\end{aligned} \tag{1c}$$

Φ is the cumulative normal distribution function (NORMDIST in excel). In (1c) the coefficient -1.10 should be replaced by -0.22 for a "rigid" soil mass (i.e., $T_s < 0.05$ s). As an example, for a system with $Ts = 0.2$ s, $k_y = 0.32$, and $S_a(0.3\text{s}) = 0.9\ g$ from a M 6.7 earthquake, the probability of negligible displacement P(D="0") from (1b) is equal to 0.05, and from (1c), D= 5.23 cm. The median estimated displacement and that with 16% probability of being exceeded can be calculated as:

$$D_{50} = \exp\left(\Phi^{-1}\left[\left(1-\frac{p=0.5}{1-0.05}\right),0,1\right]\cdot 0.66+\ln(5.23)\right) = 5.0 \text{ cm} = 5 \text{ cm}$$

$$D_{16} = \exp\left(\Phi^{-1}\left[\left(1-\frac{p=0.16}{1-0.05}\right),0,1\right]\cdot 0.66+\ln(5.23)\right) = 9.9 \text{ cm} = 10 \text{ cm}$$

Recently, a manipulation of the above equations was proposed by Bray and Travasarou (2009) to allow for estimating the seismic yield coefficient required for a target allowable displacement. Hence, a site-dependent and displacement-dependent value of the seismic coefficient can be obtained by:

$$k_h = \exp\left[\frac{-a+\sqrt{b}}{0.66}\right] \quad (2a)$$

$$a = 2.83 - 0.566\ln(S_a) \quad (2b)$$

$$b = a^2 - 1.33\cdot\left[\ln(D_a) + 1.10 - 3.04\ln(S_a) + 0.244(\ln(S_a))^2 - 1.5T_s - 0.278(M-7) - \varepsilon\right] \quad (2c)$$

ε is a normally-distributed random variable with zero mean and $\sigma = 0.66$.

These equations can be used in a M-O-based design approach as follows:

1. The allowable seismic displacement (D_a in cm) and the percent exceedance of this displacement threshold (e.g., median displacement estimate $\varepsilon = 0$, or 16% displacement estimate $\varepsilon = +1\sigma = 0.66$) should be established considering the consequences of unsatisfactory performance at displacement levels greater than this threshold. Normally, a few centimeters should be acceptable.
2. Calculate the seismic coefficient, k_h, compatible with the selected allowable displacement and level of exceedance from Equation 2. A higher seismic coefficient will be calculated for a smaller probability of exceedance of a certain displacement level (e.g., k_h corresponding to 16% probability of exceedance > k_h corresponding to median displacement).
3. Use the value of the coefficient calculated from Equation 2 in a pseudostatic slope stability analysis as the design seismic coefficient. If the calculated $FS \geq 1$, then the seismic displacement of the wall will be less than or equal to the selected allowable seismic displacement (D_a) at the specified level of exceedance.

We can use the previous example to estimate the k_h that is compatible with median displacement of 10 cm. From Equation (2b), $a = 2.89$. From Equation (2c) using $\varepsilon = 0$, $S_a = 0.9\ g$, $M = 6.7$, $T_s = 0.2$ s, and $D_a = 10$, then $b = 3.68$. From Equation (2a), $k_h = 0.23$. Key input parameters of the proposed displacement model are the initial fundamental period of the retained soil mass, T_s, representing the deformability of the backfill, and the spectral acceleration, S_a, at an assumed degraded period of $1.5T_s$, representing the earthquake loading. We recommend that those parameters are calculated in a manner compatible with the assumptions used in the idealized model proposed for empirical seismic displacement calculation:

- The input spectral acceleration at 5% damping should be calculated from the ground motion spectrum beneath the sliding mass, which is representative of the native soils beneath the backfill.
- The initial fundamental period of the retained soil mass can be approximated assuming a 1-D dynamic response of the retained earth with $T_s = 4H'/V_s$,

where H' is 0.8 times the height of the wall (H) and the equivalent shear wave velocity is computed as $V_s = \sum[(V_{si})(h_i)]/H$. Typical values of T_s range between 0.05 to 0.3 s for wall heights between 3 to 15 m retaining dry sand backfills with values of relative density between 70% to 90%.

Figure 2 presents an example of the seismic coefficient calculated using Equation (2) for a backfill soil with T_s = 0.2 s and different allowable displacement limits as a function of the shaking level. Allowing larger wall displacements for a given ground motion will typically result in smaller seismic coefficient. The right plot presents forward estimates of median wall displacement using Equation (1).

The key improvements of the proposed procedure relative to those previously developed are the consideration of deformability of the wall backfill, the modeling of the coupled occurrence of dynamic response and sliding episodes, and the significant number of earthquake recordings used in the model database. Additionally, the proper characterization of displacement variability associated with ground motion variability allows for estimating permanent wall displacements for specified probabilities of exceedance other than the median. Among the approximations of the proposed approach is the one-dimensional idealized model used to generate seismic displacements. Given the generally shallower failure wedges associated with seismic response, compared to static conditions, the 1D approximation although not accurate is likely not critical and is addressed in the proposed methodology by reducing the effective height of the retained soil in calculating the fundamental period. Similar to previous models the proposed approach does not explicitly account for the effect of vertical acceleration or tilting of the wall. Finally, its application is limited by the approximations of the M-O framework. Despite its approximations and limitations, the proposed methodology provides a refined tool for use in displacement-based seismic design of retaining structures.

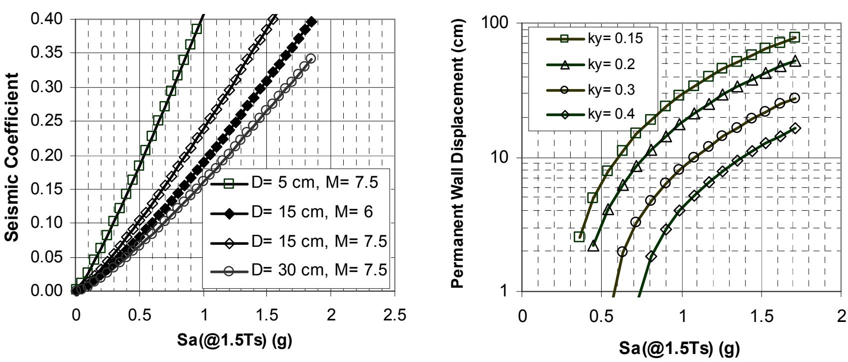

Figure 2. Example variation of seismic coefficient and median permanent wall displacement as functions of shaking intensity for retained earth with T_s= 0.2 s.

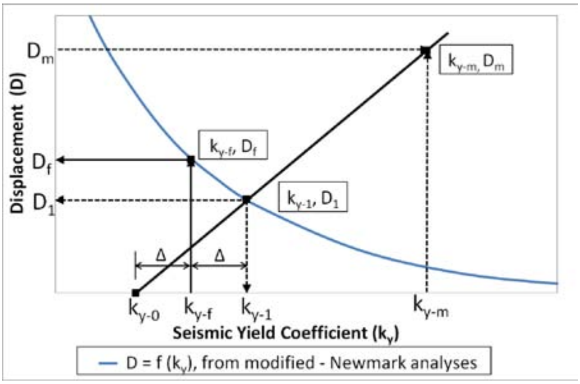

Figure 3. Simplified Procedure for Compatible SSI Sliding Displacements

SIMPLIFIED SSI SLIDING DISPLACEMENT ANALYSIS

In engineering practice, the dynamic loading of an earth structure is often represented by the seismic coefficient (i.e., horizontal equivalent acceleration/*g)*- time history for a potential sliding mass calculated utilizing equivalent-linear or fully nonlinear dynamic analyses. The dynamic resistance is represented by the seismic yield coefficient calculated utilizing a pseudostatic limit equilibrium slope stability analysis with FS = 1.0. The seismically induced permanent ground displacement is then calculated employing a Newmark (1965) procedure given the seismic coefficient-time history and the seismic yield coefficient. This procedure is referred to as decoupled, because the seismic displacement is calculated using a seismic coefficient-time history that was calculated assuming that no slip occurred. It provides reasonably conservative estimates of the seismic displacement calculated with a fully coupled dynamic stick-slip model for many practical cases (Rathje and Bray 2000).

There is additional complexity associated with a tied-back earth retaining structure, because its dynamic resistance increases as the tendons elongate as seismic displacement of the potential sliding mass increases (Whitman and Christian 1990). Thus, k_y increases with increasing seismic displacement until the tieback capacity is reached. This effect can be accounted for when performing a modified-Newmark sliding block analysis assuming that the tension in each tieback tendon is a linear elastic function of seismic displacement until its yield stress is reached and that k_y is approximately a linear function of the tension force that develops in the tiebacks. The simplified procedure for calculating compatible SSI sliding displacements consists of the following steps (Figure 3):

1) For several values of k_y, the Newmark displacement (D) is calculated for the seismic coefficient-time history calculated from each design input ground motion, and the median value at each k_y value is calculated from the suite of design ground motions to develop a plot of D vs. k_y.

2) The initial dynamic resistance of the system ($k_{y\text{-}o}$) is calculated with the tensions in the tieback anchors equal to the design static lock-off loads. Similarly, the maximum dynamic resistance of the system ($k_{y\text{-}m}$) is calculated with the tieback tendons at their maximum extension. D is assumed to increase linearly from 0 at $k_{y\text{-}o}$ to its maximum value at $k_{y\text{-}m}$.
3) The intersection of the line from step 2 with the D vs k_y curve from step 1 provides the first displacement estimate (D_1). It is based on $k_{y\text{-}1}$, which is the dynamic resistance reached at the end of shaking. During shaking, k_y increases from $k_{y\text{-}o}$ to $k_{y\text{-}1}$. Thus, this first displacement estimate is too low. The final (best) estimate of the seismic yield coefficient ($k_{y\text{-}f}$) is the average of $k_{y\text{-}o}$ and $k_{y\text{-}1}$. Accordingly, the final estimate of seismic displacement (D_f) is compatible with $k_{y\text{-}f}$ on the plot of D vs. k_y.

SSI DYNAMIC ANALYSIS OF AN EARTH RETENTION SYSTEM

SSI Analysis. SSI analyses utilizing the finite element (FE) or finite difference method with a nonlinear soil model can provide additional insight regarding the seismic performance of an earth retaining structure. Many of the restrictive and inaccurate assumptions and limitations of the M-O method can be overcome through the employment of a calibrated SSI FE analysis. The SSI FE analysis has the potential to capture the actual dynamic interaction of the retaining structure and the retained earth with the use of a time history analysis that provides both transient and permanent earthquake-induced loads and displacement. However, its use must be tempered by the relative complexity of a SSI FE analysis, and the requirement for additional earthquake and soil characterization efforts. When the earth retaining system is relatively sophisticated and the importance and complexity of the project warrants advanced analysis, a well-calibrated dynamic FE analysis can provide insights simply not possible through the use of the M-O method. In this section, a recent project that benefitted from SSI dynamic FE analysis utilizing the computer program PLAXIS 2D V9.02 (Brinkgreve et al. 2008) is described to illustrate its use.

Project Background. Following periods of heavy rainfall in the winter of 2004-2005, a pre-existing incipient landslide in Santa Barbara County, CA reactivated and damaged multiple residential properties and adversely impacted several roads. The areal extents and depths of landslide movement were investigated by Cotton, Shires and Associates, Inc. (CSA) and estimated to be 120 to 180 m wide by 210 to 240 m long and 10 to over 30 m deep, respectively. Based on their engineering geologic and geotechnical investigations and subsequent engineering analyses, CSA developed a multi-phase landslide repair design that included several tieback retaining structures to protect existing residential properties from further structural damage and to restore and protect residential roads. The "active landslide" repair design consisted of:

a) four, tied-back, shear pin wall systems consisting of large diameter (up to 1.2 m) reinforced concrete shear pins at 2.1 to 2.4 m on centers laterally with between 5 and 7 rows of tieback anchors at 1.5 m on centers vertically, tensioned to 1.4 MN each; the top 1.5 m of the shear pins were connected with reinforced concrete tie-beams;

b) one row of large diameter (up to 1.2 m) reinforced concrete shear cleats at 2.1 to 2.4 m on centers laterally; the shear cleats extend 6 m above and 6 m below the estimated landslide basal shear surface; and

c) excavation of landslide debris and the landslide basal shear surface at the toe of the slope and replacement of excavated materials with geosynthetic reinforced engineered fill materials.

The repair design was analyzed utilizing PLAXIS to evaluate if it could satisfy these criteria: 1) average calculated seismic displacement is less than or equal to 15 cm and also less than or equal to the available elongation in the tieback anchors so that rupture of the tiebacks does not occur, and 2) average calculated transient shear forces and bending moments induced on the wall systems during dynamic loading do not exceed the structural capacities of these systems.

Seismic Hazard. The project site is located near several significant potentially active and active faults, including the reverse-slip Mission Ridge/Arroyo Parida fault (M = 7.2 at distance R= 0.9 km) and the reverse-slip North Channel slope fault (M = 7.4 at R= 10 km. The design acceleration response spectrum was developed using the procedure outlined in the 1997 Uniform Building Code (UBC) and modified for near-fault effects using the procedure described by Somerville et al., (1997). Acceleration time histories were selected from the PEER_NGA database based on magnitude, distance, and near-fault characteristics (http://peer.berkeley.edu/nga/). The ground motions selected for design were: 1) Pacoima Dam 164 (1971 San Fernando EQ), 2) Los Angeles Dam 064 (1994 Northridge EQ), 3) Los Gatos Presentation Center 090 (1989 Loma Prieta EQ), 4) Lucerne 260 (1992 Landers EQ), 5) Joshua Tree 000 (1992 Landers EQ), and 6) Superstition Mountain 045 (1987 Superstition Hills EQ). The six ground motions were then scaled such that the average of the six acceleration response spectra reasonably matched the target spectrum (Figure 4).

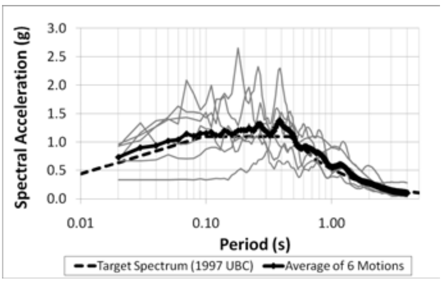

Figure 4. Acceleration response spectra (5% damping)

FE Modeling and Material Characterization. The subsurface stratigraphy and landslide geometry were characterized based on geologic and topographic mapping, large- and small- diameter exploratory boreholes, geophysical surveys, measured inclinometer offsets, and model calibration (CSA 2010). The subsurface was divided into four representative geotechnical units: engineered fill, landslide debris, the landslide shear zone, and relatively more competent foundation bedrock. The FE mesh was composed of 15-node triangular plane strain elements with a very fine global coarseness. The model side boundaries were placed 500 m apart to remain consistent with the dimensions of the cross section selected for analysis and minimize any potential adverse effects of the boundary conditions on the area of interest. The boundary conditions were set to the "Standard Earthquake Boundaries" which consisted of absorbent vertical side boundaries.

The "outcropping" rock design acceleration-time histories were converted to "within" rock motions with SHAKE2000 and then the corresponding "within" displacement-time histories were applied at the base of the model in PLAXIS to simulate earthquake ground motions. Analyses were performed as a series of calculation phases based on the anticipated construction sequence to establish the initial properties, followed by the application of the "within" base displacement-time histories to evaluate the effects of ground shaking after resetting FE nodal displacements to zero to differentiate between static and dynamic displacements.

Earth material strength parameters for the 2D dynamic FE model were selected in accordance with the calibrated strength parameters from previous static analyses, interpretation of laboratory tests on relatively undisturbed samples, results of a geophysical investigation, and engineering judgment (CSA 2010). Materials were described using the Mohr-Coulomb material model in PLAXIS utilizing an iterative scheme that developed the equivalent-linear dynamic soil properties of shear moduli and material damping. Initial estimates of the shear moduli and Rayleigh damping coefficients were based on SHAKE2000 analyses. To capture the relative changes in shear moduli, the subsurface profile for the dynamic PLAXIS analyses was divided into 10 units. To further refine and gain confidence in the shear moduli and Rayleigh damping parameters, a 2D calibration model was developed with PLAXIS.

The reinforced concrete shear pins and shear cleats were modeled using plate elements with an elasto-plastic material model. The axial stiffness and flexural rigidities were obtained through geometric relationships and correlations with the design unconfined compressive strength of the concrete. Unfactored axial force, bending moment, and shear force capacities were obtained from the project structural engineer, Hohbach-Lewin, Inc. The unbonded length of the tiebacks was modeled using node to node anchors with an elasto-plastic material model. Material parameters were obtained from the tieback manufacturer. The bonded length of the tiebacks was modeled using geogrid elements with an elastic material model. The axial stiffness of the bonded length was estimated using engineering judgment.

Results. The adequacy of the structural design of the retaining structure system was evaluated by examining the computed transient forces induced during dynamic loading and the after-shaking permanent forces that developed. The maximum values of axial force, shear force, and bending moment within each shear pin and shear cleat element during the ground motion time histories were recorded and used to construct force and moment 'envelope' plots. The tensile forces in each of the tiebacks were evaluated at the end of each ground motion time history. These calculated values were then compared with the developed structural capacities of each component to evaluate the design. In addition, displacements of the shear pin elements were evaluated at the end of each ground motion time history.

Figure 5 illustrates the deformed finite element mesh following the application of the Los Gatos Presentation Center 090 (LGPC090) ground motion. Figure 6 illustrates the bending moment and shear force envelope plots for the third uppermost wall system along with the corresponding structural capacities. The envelope plots presented correspond to the average envelope for the 6 design ground motions. Results such as those presented in Figure 6 were utilized for each of the wall systems to ensure the structural capacities would be sufficient to meet a reasonable estimate of the expected seismic demand. In general, it was observed that the maximum magnitude transient shear forces were located within the landslide basal shear zone (corresponding to EL 67.4 m (221 ft) to EL 69.2m (227 ft) in Figure 6) while the maximum magnitude transient bending moments were located slightly above and slightly below the landslide basal shear zone.

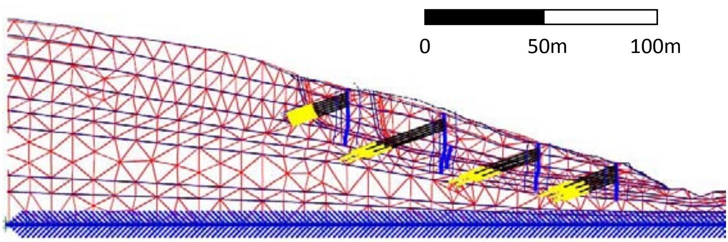

Figure 5. Deformed FE mesh after LGPC090 (Scale Factor = 20)

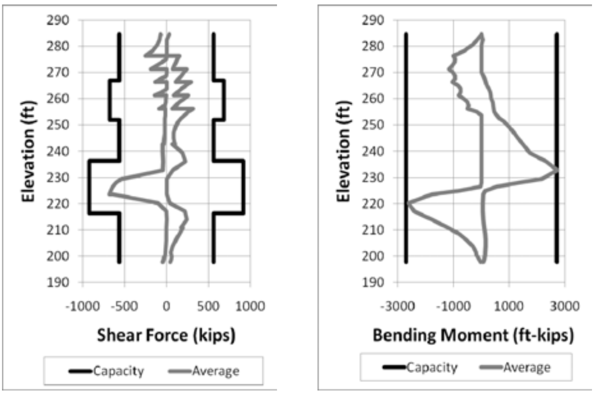

Figure 6. Average shear force and bending moment envelopes (Note: 1 kip = 4.45 kN and 1 kip-ft = 1.36 kN-m)

Differential displacement profiles were also generated for each of the wall systems to obtain estimates of localized seismically induced permanent displacements. The seismically induced permanent maximum differential displacements were on the order of 8 cm for the uppermost wall, the second uppermost wall and the third uppermost wall, 2 cm for the lowermost wall, and 10 cm for the shear cleats (which were located immediately down slope of the second uppermost wall). Thus, the calculated seismically induced permanent slope displacements of the repaired landslide were within the design criteria and judged to be acceptable.

COMPARISON OF SIMPLIFIED SSI AND FE ANALYSES

In addition to the FE analyses, CSA performed simplified SSI sliding displacement analyses using the procedure presented in this paper. The median seismic displacement calculated using the simplified SSI analyses for the six design ground motions was 10 cm. This result compares favorably with the seismically induced permanent displacements calculated from the FE analyses of 8 and 10 cm for uppermost wall, second uppermost wall, third uppermost wall, and the shear cleats. The FE analysis did calculate only 2 cm of seismic displacement for the lowermost wall, which was relatively more stable. This illustrates an obvious advantage of the FE analysis, because it calculates non-uniform wall displacements (if this is what is likely to occur); whereas the simplified SSI analysis employs a pseudostatic limit equilibrium slope analysis to develop one k_y value for the retrofit and hence one seismic displacement value for the overall system. The repair system was upgraded during the design process so that the FE analysis was of a slightly more robust system. Due to high transient shear forces and bending moments calculated with PLAXIS, a row of shear cleats was installed to ensure that the transient shear forces and bending moments would not exceed the structural capacities of the second uppermost wall. In addition, the steel reinforcements in the third uppermost and lowermost wall systems were redesigned to provide higher capacities in shear and bending. These changes to the repair design were made subsequent to the simplified SSI analyses, and thus, are not reflected in those analyses.

The tieback design loads from both analyses were around 1400 kN, indicating that the simplified SSI analyses could develop reasonable estimates of the tieback design load for this case. In many projects the tieback loads are established through static design with an overload factor, and if both analyses indicate similar ranges of tieback elongation, then both analyses should calculate fairly consistent seismic demands.

The simplified SSI analyses underestimated the shear forces and bending moments that developed in the reinforced concrete shear pins. The shear pin design loads calculated from the simplified SSI analyses do not include transient loads, only those due to permanent ground displacement. The shear pins in this case are designed using the reduced factored structural capacities so that the transient overload is accommodated for in an approximate manner. The FE analysis calculates the transient loads as well as the permanent loads that develop in the structural elements of the earth retention system. The structural capacity reduction factor in normal design was insufficient to accommodate the high transient loads produced by the intense, near-fault earthquake ground motions for this project. Therefore, the relative benefit of the more advanced FE analysis is apparent in this case.

CONCLUSIONS

The seismic design of earth retaining structures is still largely based on the application of the Mononobe-Okabe method. Although it is still widely used today, the M-O method is a coarse simplification of what is inherently a complex soil-structure interaction (SSI) problem. Yet, it is straightforward, and if employed with the appropriate input parameters that have been calibrated against field performance, experimental results, and the results of advanced analyses, it has been found to provide a reasonable estimate of the additional dynamic force exerted by the earth behind a yielding vertical retaining wall. However, it does not capture the actual dynamic response of the soil-structure system, and thus it does not provide the insight of an improved method that focuses on the most important seismic response and performance aspects of this problem.

Field performance observations and experimental evidence indicate that well-built retaining structures that are composed of or surrounded by materials that do not lose strength as a result of earthquake shaking perform satisfactorily at moderate levels of ground shaking. Thus, seismic earth pressures need not be considered when the $PGA \leq 0.3\ g$. However, the retaining wall should be designed to resist the inertia force acting on the wall itself as well as resist the static lateral earth pressures with an appropriate margin of safety. At higher levels of ground shaking, the seismic evaluation should include the effects of the retained earth.

The use of a M-O-type earth retaining structure seismic analysis requires the proper selection of k_h. The seismic coefficient largely determines the magnitude of the seismic load increment. Thus, its selection is critical. The rational selection of k_h requires proper consideration of the seismic hazard at the site and the amount of seismic displacement that defines the threshold between satisfactory and unsatisfactory seismic performance of the earth retaining structure. Therefore, the seismic design procedure should include a calculation of the potential seismic displacement of the earth retaining structure.

After reviewing the development of seismic displacement design procedures for earth retaining structures, an updated procedure is presented. The application of the Bray and Travasarou (2007) seismic slope displacement method to this problem incorporates results from thousands of coupled stick-slip deformable sliding block analyses. Nearly 700 recorded earthquake ground motion records were used in its development. This method can be used to estimate the seismic displacement of an earth retaining structure, or it can be manipulated to calculate the design seismic coefficient for use in a M-O-type analysis. The advantage of this approach is that k_h is based on the seismic hazard at the site and the amount of seismic displacement that defines the threshold between satisfactory and unsatisfactory seismic performance of the earth retaining structure.

Additional insights can be garnered through the use of advanced SSI FE analyses, especially for more complicated earth retaining systems. Their use is demonstrated through the discussion of a project in which the program PLAXIS was employed to examine the interaction of several tied-back retaining walls used to stabilize a landslide. A simplified SSI dynamic analysis procedure for tied-back walls was also presented, and its use provides meaningful insights as well.

ACKNOWLEDGMENTS

Support for some of the work referenced in this paper was provided by the National Science Foundation under award number EEC-2162000 through the Pacific Earthquake Engineering Research Center. Cotton Shires and Associates, Inc. was the engineer of record of the project described in the paper. Discussions with Patrick Shires, Dale Marcum, David Schrier, and Tim Sneddon of CSA were invaluable. Ben Mason performed some analyses. The authors would like to acknowledge discussions with Professor Nick Sitar of the Univ. of California, Berkeley and Marshall Lew of MACTEC Engrg. and Consulting, and Dr. Farhang Ostadan of Bechtel Corp.

REFERENCES

Al Atik, L. and Sitar, N. (2010). "Seismic Earth Pressures on Cantilever Retaining Structures," *J. of Geotechnical & Geoenvironmental Engineering*, ASCE, Vol. 136, doi:10.1061/(ASCE)GT.1943-5606.0000351, posted March 6.

AASHTO: American Association of State Highway and Transportation Officials (2007). *AASHTO LRFD Bridge Design Specifications*, U.S. Units." 4th Ed.

Anderson, D.G., Martin, G.R., Lam, I., and Wang, J.N. (2008). *Seismic Analysis and Design of Retaining Walls, Buried Structures, Slopes and Embankments.* NCHRP Report 611, Transportation Research Board, Washington, DC.

Bray, J.D. and Travasarou, T. (2007) "Simplified Procedure For Estimating Earthquake-Induced Deviatoric Slope Displacements," *J. of Geotechnical & Geoenvironmental Engineering*, ASCE, Vol. 133(4), 381-382.

Bray, J.D. and Travasarou, T. (2009) "Pseudostatic Coefficient for Use in Simplified Seismic Slope Stability Evaluation," *J. of Geotechnical & Geoenvironmental Engineering*, ASCE, Vol. 135(9), 1336-1340.

Bray, J.D. and Frost, J.D., Eds. (2010). "Geo-engineering Reconnaissance of the 2010 Maule, Chile Earthquake," a report of the NSF- Sponsored GEER Association Team, primary authors Arduino et al., http://www.geerassociation.org/

Brinkgreve, R.B.J. , Broere, W., and Waterman, D. (2008). *PLAXIS, 2D Version 9.0 Reference Manual.* http://www.plaxis.nl/shop/5/info/manuals/

Clough, G.W. and Fragaszy, R.J. (1977). "A Study of Earth Loadings on Floodway Retaining Structuresin the 1971 San Fernando Valley Earthquake." *Proc., 6th World Conference on Earthquake Engineering,* (3), 2455-2460.

Cotton, Shires and Associates, Inc. (2010). *Phases IV and V – Protect Lower Roads and Arrest Lower Portion of Active Landslide, Geotechnical Design*

Investigation, Sycamore Ranchito Landslide Repair Project, Santa Barbara County, CA.

FHWA: Federal Highway Administration (1998). "Geotechnical Earthquake Engineering." Pub. No. FHWA HI-99-012, Dec.

Kramer, S.L. (1996). *Geotechnical Earthquake Engineering.* Prentice Hall, Upper Saddle River, NJ.

Lew, M., Simantob, E., and Hudson, M.B. (1995). "Performance of Shored Earth Retaining Systems During the January 17, 1994 Northridge Earthquake." *Proc., Third International Conference on Recent Advances in Geotechnical Earthquake Engineering and Soil Dynamics,* St. Louis, MO, (3) 1417-1422.

Mononobe, N. and Matsuo, H. (1929). "On the determination of earth pressure during earthquakes." *Proceedings of the World Engineering Conference*, (9).

Nakamura, S. (2006). "Reexamination of Mononobe-Okabe Theory of Gravity Retaining Walls Using Centrifuge Model Tests." *Soils and Foundations*, (46) 2, 135-146.

Newmark, N. M. (1965) "Effects of earthquakes on dams and embankments." *Geotechnique*, London, 15(2), 139-160.

Okabe, S. (1926). "General theory of earth pressure." *Journal of the Japanese Society of Civil Engineers*, Tokyo, Japan, 12 (1).

Okamoto, S. (1984). *Introduction to Earthquake Engineering*. 2nd Ed., Wiley, NY.

Rathje EM, and Bray J.D. (2000) "Nonlinear coupled seismic sliding analysis of earth structures." *J. Geotech. & Geoenv. Engineering,* 126(11), 1002-1014.

Richards, R. and Elms, D.G. (1979). "Seismic Behaviour of Gravity Retaining Walls, *J. Geotech. Engrg.*, ASCE, 105(4), 449-464.

Seed, H.B. and Whitman, R.V. (1970). "Design of Earth Retaining Structures for Dynamic Loads." *ASCE Specialty Conf., Lateral Stresses in the Ground and Design of Earth Retaining Structures.* Cornell Univ., Ithaca, NY., 103-147.

Sitar, N. and Al Atik, L. (2009). "Seismic Response of Retaining Structures." *Proc. Inter. Conf. on Performance-Based Design in EQ Geotech. Engineering*, Kokusho et al., Ed., IS-Tokyo 2009, June 15-18.

Tokimatsu, K. and Seed, H.B. (1987). "Evaluation of settlements in sands due to earthquake shaking." *J. Geotech. Engrg.*, ASCE, 113(8), 861-878.

Whitman, R.V. (1990). "Seismic Design and Behavior of Gravity Retaining Walls." *Proc., Design and Performance of Earth Retaining Structures*, Geotech. SP No. 25, ASCE, NY, 817-842.

Whitman, R.V. (1991). "Seismic Design of Earth Retaining Structures." *Proc., Second International Conference on Recent Advances in Geotechnical Earthquake Engineering and Soil Dynamics*, St. Louis, MO., 1767-1778.

Whitman, R.V. and Liao, S. (1985). "Seismic Design of Gravity Retaining Walls," US Army Engr. Waterways Experiment Sta., Misc. Paper GL-85-1.

Whitman, R.V. and Christian, J.T. (1990). "Seismic Response of Retaining Structures," *Sym. Seismic Design for World Port 2020*, Port of Los Angeles, CA, March.

Zarrabi, K. (1979) "Sliding of gravity retaining wall during earthquake considering vertical accelerations and changing inclination of failure surface," S.M. Thesis, Dept. of Civil Eng., MIT, Cambridge, MA.

Seismic Earth Pressures: Fact or Fiction

Marshall Lew[1], Nicholas Sitar[2], and Linda Al Atik[2]

[1]MACTEC Engineering and Consulting, Inc., 5628 East Slauson Avenue, Los Angeles, California 90040. E-mail: mlew@mactec.com
[2]University of California, Berkeley, Department of Civil and Environmental Engineering, Berkeley, CA 94720

ABSTRACT

The current state of practice in the United States as implemented in the International Building Code now requires that structures with subterranean walls be designed for seismic earth pressures in addition to the normal static earth pressures. Since many design issues in the building code are introduced because of observed failure or deficiencies during earthquakes, the requirement to design for seismic earth pressures is peculiar because there is little or no evidence that any failures in engineered subterranean structures have occurred in past or even recent earthquakes. This paper examines how seismic earth pressures entered into the design practice and reviews some of the methodologies used to estimate seismic earth pressures in current engineering practice in the United States.

INTRODUCTION

The building code is a guiding document used to design and construct buildings to protect the public from man-made and natural hazards for an acceptable amount of risk. Many of the seismic provisions in the building code are a result of poor performance or observations from past and recent earthquakes. Examples of seismic provisions introduced into the building code as a result of poor performance have included ductile detailing of concrete, proper anchorage of floor and roof diaphragms in tilt-up buildings, consideration of liquefaction potential and mitigation, precautions about steel moment resisting frames, and accounting for near-source directivity effects near active earthquake faults. A list of changes to the U.S. building codes in response to observed earthquake performance was published in the SEAOC Blue Book (2009). However, damage attributable to seismic earth pressures have not been observed in United States earthquakes, yet provisions have crept into the building code with significant design and cost impact.

BRIEF HISTORY OF SEISMIC EARTH PRESSURE CODE PROVISIONS IN THE UNITED STATES

There were no specific requirements for the seismic increment of active earth pressure to be applied to walls retaining earth in any of the model building codes in the United States through 2003; this would include the Uniform Building Code, National Building Code, and Southern Building Code, which were all ultimately supplanted by the International Building Code (IBC). The 2006 edition of the IBC was the first national building code to include provisions to consider seismic earth pressures on earth retaining walls.

California Building Code

The California Building Code (CBC), which was based on the Uniform Building Code, did have provisions that included the issue of the seismic increment of active earth pressure. The CBC had jurisdiction over hospitals and public schools, as well as State of California public buildings. As early as the 1980s, the California amendments to the Uniform Building Code (UBC) had provisions mandating that the seismic increment of active earth pressure should be applied to buildings with walls that retain earth having exterior grades on opposite sides differing by more than 6 feet; this provision is shown below from Section 2312 (e) 1 E of the California amendments to the 1988 UBC (International Conference of Building Officials, 1988):

> ***Seismic increment of active earth pressure.*** *Where buildings provide lateral support for walls retaining earth, and the exterior grades on opposite sides of the building differ by more than 6 feet, the load combination of the seismic increment of active earth pressure due to earthquake acting on the higher side, as determined by a civil engineer qualified in soil engineering plus the difference in active earth pressures shall be added to the lateral forces provided in this section.*

The identical language was still present in the 2001 edition of the CBC (California amendments to the 1997 UBC) (California Building Standards Commission, 2002 and ICBO, 1997). In addition, the 2001 edition of the CBC had the following amendment to Section 1611.6 of the 1997 UBC regarding retaining walls:

> *Retaining walls higher than 12 feet (3658 mm), as measured from the top of the foundation, shall be designed to resist the additional earth pressure caused by seismic ground shaking.*

From the context of these two CBC amendments to the UBC, the former amendment clearly refers to building basement walls and the latter amendment refers to free-standing retaining walls as UBC Section 1611.6 describes the features of a retaining wall in some detail.

NEHRP Recommended Provisions

The "NEHRP Recommended Provisions for Seismic Regulations for New Buildings and Other Structures (FEMA 450)," 2003 Edition, Part 1 – Provisions, also known as the FEMA 450 report (Building Seismic Safety Council, 2004a), was intended to form the framework for future model building codes in the United States. It did not, however, contain any explicit recommended provisions for accounting of seismic earth pressures for design of retaining walls in the recommended provisions.

However, Part 2 – Commentary of the FEMA 450 report (Building Seismic Safety Council, 2004b) contains almost four pages of commentary on the consideration of lateral pressures on earth retaining structures. Section 7.5.1 of the commentary states that "In addition to the potential site hazards discussed in *Provisions* Sec. 7.4.1, consideration of lateral pressures on earth retaining structures shall be included in investigations for Seismic Design Categories D, E, and F." (The other hazards to be investigated are slope instability, liquefaction, and surface rupture due to faulting or lateral spreading, all as a result of earthquake motions.)

The FEMA 450 commentary states that "…increased lateral pressures on retaining structures during earthquakes have long been recognized; however, design procedures have not been prescribed in U.S. model building codes." The commentary notes that waterfront structures have often performed poorly in major earthquakes due to excess pore water pressure and liquefaction conditions developing in relatively loose, saturated granular soils based on a paper by Whitman (1991). The commentary also mentions that damage reports for structures away from waterfronts are generally limited with only a few cases of stability failures or large permanent movements, also according to Whitman.

The FEMA 450 commentary provides a discussion of the seismic design analysis of retaining walls for two categories of walls:

- "yielding" walls – walls that can move sufficiently to develop minimum active earth pressures
- "nonyielding" walls – walls that do not satisfy the movement condition

For yielding walls, the FEMA 450 commentary states that there is consensus in the geotechnical engineering practice that a simplified Mononobe-Okabe seismic coefficient analysis reasonably represents the dynamic (seismic) lateral earth pressure increment for yielding retaining walls (Mononobe and Matsuo, 1929; Okabe, 1926). The commentary presents an equation for evaluation of the dynamic incremental component (ΔP_{AE}) proposed by Seed and Whitman (1970):

$$\Delta P_{AE} \sim (1/2)\,(3/4)\,k_h \gamma H^2$$

where k_h is the "horizontal ground acceleration divided by gravitational acceleration." The commentary recommended that k_h be taken equal to the site peak ground acceleration that is consistent with the design earthquake ground motions as defined in the Provisions of FEMA 368 (k_h = $S_{DS}/2.5$). The resultant dynamic thrust was recommended to act at $0.6H$ above the base of the wall (which would be an inverted trapezoidal pressure distribution). It should be noted for the record that the Mononobe-Okabe theory also considers the vertical ground acceleration, denoted as k_v. Seed and Whitman (1970) had determined that the vertical ground acceleration, k_v, could be neglected for practical purposes because they made the observation that for most earthquakes, "…the horizontal acceleration components are considerably greater than the vertical acceleration components…"

For nonyielding walls, the FEMA 450 commentary presents an equation developed by Wood (1973) for a rigid nonyielding wall retaining a homogeneous linear elastic soil and connected to a rigid base. The dynamic thrust, ΔP_E, is approximately:

$$\Delta P_E = k_h \gamma H^2$$

As for yielding walls, the point of application of the dynamic thrust is typically taken at a height of 0.6H above the base of the wall.

The FEMA 450 commentary suggests that dynamic earth pressure solutions would range from the Mononobe-Okabe solution as a "lower" bound to the Wood solution as an "upper" bound.

Although the FEMA 450 report has an extensive commentary on consideration of increased lateral pressures on retaining walls during earthquakes, it does not provide any insight or guidance on what situations should be considered, especially in the case of nonyielding walls not connected to a rigid base. The commentary does not provide recommendations on the height of the retained earth (for "retaining" walls or level of unbalanced earth in the case of opposite building walls retaining earth, such as given in the earlier versions of the California Building Code.

ASCE/SEI 7-05 Minimum Design Loads

Minimum Design Loads for Buildings and Other Structures were published as ASCE Standard ASCE-SEI 7-05 (commonly referred to as ASCE 7-05) (American Society of Civil Engineers, 2006). For all earth retaining structures assigned to Seismic Design Category D, E, or F, lateral earth pressures due to earthquake ground motion are to be determined in accordance with Section 11.8.3 of ASCE 7-05. Section 11.8.3 just states that the geotechnical investigation report shall include: "The determination of lateral pressures on basement and retaining walls due to earthquake motions." A similar terse recommendation was also in the earlier edition of ASCE 7-02.

International Building Code

The 2006 edition of the International Building Code (IBC) adopts by reference the seismic requirements of ASCE 7-05. The 2009 IBC does not change this practice. Thus the requirements for seismic design pressures mandated by ASCE 7-05 are part of IBC.

DAMAGE TO BUILDING BASEMENT WALLS IN EARTHQUAKES

Although there are many reports of damage to earth retaining walls during earthquakes, almost all of the reports are for either poorly constructed non-engineered walls or walls that failed because of a soil-related failure, with many being in a marine or waterfront environment. Based on a search of literature by the authors, no reports of any damage to building basement walls retaining earth have been found for the 1971 San Fernando, 1987 Whittier Narrows, 1989 Loma Prieta, and 1994 Northridge earthquakes in the United States. Also, reports of damage to building basement walls in foreign earthquakes are few.

United States Experience

It is the authors' personal experience and the experience of colleagues in geotechnical engineering that engineered building basement walls did not experience damage in the recent United States earthquakes.

An extensive report on damage observed in the San Fernando earthquake of February 9, 1971 was published by the United States Department of Commerce National Oceanic and Atmospheric Administration (NOAA) (Murphy, 1973). In this report, the only reported damage to a building basement wall occurred at the Olive View Medical Center, Medical Treatment and Care Unit. A basement or retaining wall on the lowest level experienced pounding from movement of the structure against the wall, disturbing the soil behind the wall and also causing tension cracks on the inside (compression) face of the cantilever retaining wall; movement at the top of the wall was reported to be as much as 6 inches. Clough and Fragaszy (1977) reported on a study of floodway channels in the Los Angeles area that also experienced the San Fernando earthquake. They reported that no damage occurred to walls until accelerations of about 0.5g were reached, which was a surprisingly large value of acceleration in view of the fact that the walls were not explicitly designed for seismic loadings.

Damage to building basement walls was not reported in the two volumes of Earthquake Spectra (Earthquake Engineering Research Institute, 1988a and 1988b) which presented observations from the Learning from Earthquakes (LFE) program on the October 1, 1987 Whittier Narrows earthquake in Southern Califorina. Whitman (1991) also cited a reference on the behavior of ten tied-back walls in the Whittier Narrows earthquake that had no evidence of loss of integrity.

During the post-earthquake reconnaissance of the October 17, 1989 Loma Prieta earthquake by the Earthquake Engineering Research Institute (EERI), there were no observations or reports of damage to building basement wall structures (Benuska, 1990). A survey of mechanically-stabilized walls (for highways) was also cited by Whitman (1991); in the Loma Prieta earthquake region, no evidence of significant residual movements was observed in mechanically-stabilized walls.

Numerous geotechnical researchers and practitioners performed extensive reconnaissance of the effects of the January 17, 1994 Northridge earthquake (moment magnitude 6.6). No reports of damage to building basement walls were reported by Stewart et al. (1994), Hall (1995), and Holmes and Somer (1996). Lew, Simantob and Hudson (1995) reported that several deep excavations in Los Angeles secured with soldier beams and tieback anchors experienced no failures or excessive deflections. There are two examples of buildings in Los Angeles that retained a significant difference in height of soil from one side to the other: UCLA Boelter Hall and a 55-story office building in Downtown Los Angeles. Both buildings experienced strong ground motions during the Northridge earthquake. Boelter Hall has one wing constructed into a hillside and has 3 stories are below grade on the east side of the wing and it is daylighted on the west side, having an approximately 35 feet of unbalanced earth loading. The California Strong Motion Instrumentation Program had a free field ground response instrument on the UCLA campus and it is reported that the peak ground acceleration for one horizontal component at that instrument was

0.66g in the Northridge earthquake (Shakal et al., 1994). There were no reports of damage to the basement wall of Boelter Hall.

The 55-story office building is also constructed into a hillside having a base podium structure that extends about 100 feet below grade on the east and about 45 feet below grade on the west; there is approximately 55 feet of unbalanced earth retention from east to west. Because the 100-foot tall basement wall was constructed by slope cutting the natural materials at an inclination of 2/3:1 (horizontal to vertical) and then backfilling against the basement wall with soil, the basement wall was designed for lateral earth pressures consisting of a triangular distribution of earth pressure equivalent to that developed by a fluid having a density of 32 pounds per cubic foot. The peak ground accelerations during the Northridge earthquake within a few blocks of the 55-story office building were on the order of 0.2g (Shakal et al., 1994). There were no reports of damage to the basement wall of this building.

Experience outside the United States

Some comment is also necessary regarding the few retaining structures with documented significant movement that are away from waterfronts that were described in the paper by Whitman (1991) mentioned earlier. The retaining structures with significant movement that are cited include a few cantilever retaining walls, gravity walls, and a bridge abutment. Some of the failures were attributed to liquefaction. The references quoted by Whitman also mention retaining structures (away from waterfronts) that were not affected by earthquake. In one instance, there were low retaining walls in Tokyo where extensions were added to make higher retaining walls; these walls had no damage during earthquakes despite calculations by the Mononobe-Okabe formula that would have predicted failure. Whitman also reported that despite extensive earthquake damage to port facilities at Akita, Japan, 24 reinforced earth walls in the area performed well. Thus only a few actual cases of retaining structures with significant movement are documented. It is significant to observe that there are no reports of damage to building basement walls retaining earth in any of the references cited by Whitman.

A review of case history reports on geotechnical aspects of the January 17, 1995 Hyogoken-Nambu earthquake that devasted Kobe, Japan (Japanese Geotechnical Society, 1996) provided much evidence of failures and large displacements in waterfront walls and freestanding retaining walls supporting embankments, however, no evidence of damage to building basement walls was reported. However, there was some damage to subway stations in Kobe with the most severe damage to the Daikai Subway Station, part of the Kobe Rapid Transit Line (Iida, Hiroto, Yoshida and Iwafuji, 1996). Less severe damage occurred at four other stations in Kobe and at other locations in the subway system.

Iida et al. report that the Daikai station is the first subway structure completely damaged during an earthquake. The Daikai station was completed in 1964 and used the cut-and-cover method of construction. The station is about 120 meters long. Most of the Daikai station is a reinforced box type frame with columns at the center of the box and passenger platforms on the two sides. The box is about 17 meters wide and about 7.2 meters high (outside dimensions). The thickness of the overburden soils was about 4.8 meters above the one-story portion of the station. A small portion of the station was two stories with the upper floor serving as a ticket concourse and the lower floor with the passenger platforms. The two-story portion of the station also has center columns and is wider with additional column lines matching the exterior wall lines of the one-story portion of the station. The two-story portion is about 26 meters wide and about 10.1 meters high (outside dimensions). The thickness of the overburden soils above the two-story portion of the station is about 1.9 meters.

The most severe damage in the station occurred in the longer one-story portion of the station with failures of the center columns resulting in the ceiling slab subsiding along with the overburden soils above the station. Many cracks were also observed in the longitudinal walls as well as the few transverse walls at the ends the station and at the areas where the two-story portion abuts the one-story portions. Most of the columns failed at the base and Iida et al. opine that the initial mechanism of failure was from a combination of shear and bending moment. Once the initial damage occurred, the axial capacity of the columns was reduced which resulted in the complete failure of most of the center columns resulting in collapse of the ceiling of the station. The collapse of the center columns and ceiling caused cracking and tilting of the longitudinal walls; separations were seen near the top of the walls and near a bottom haunch for the station platforms.

An examination of the photographs in the article by Iida et al. reveals that the columns had very minimal lateral ties indicating that the columns would exhibit nonductile behavior. From the discussions in the paper, it appears that the station box structure was not designed for racking conditions due to earthquake, a practice that is common in design of subway stations in the United States for such systems such as the Bay Area Rapid Transit District in the San Francisco Bay area and the Metro Rail System in Los Angeles.

The Iida et al. paper does not mention the possibility that liquefaction may have occurred at the Daikai station. An examination of the soil profiles of boreholes drilled before and after the earthquake reveals that Holocene age sand materials are present in the vicinity of the station. One borehole drilled adjacent to the station after the earthquake encountered fill materials consisting of sandy soil. Soil profiles shown in the Iida et al. paper show that the standard penetration test (SPT) blowcounts (N-values) range from below 10 to above 30 in the Holocene sand materials, with many values in the 10 to 20 range. In the sandy fill soils, the N-values were typically about 10. The ground water level was reported to be about 3 meters in 1959 and between 6 to 8 meters in February 1995. Although Iida et al. do not mention the possibility of liquefaction, the data about the N-values and ground water levels strongly suggest that liquefaction may have occurred in the soils around the station, especially in fill materials adjacent to the station. This liquefaction may have contributed to the structural failures of the Daikai station whereby a liquefied soil exerts higher lateral pressures, even without directly considering the effects of lateral ground motions.

Damage to building basement walls were not reported in the EERI reconnaissance report for the August 17, 1999 Kocaeli, Turkey earthquake (Youd, Bardet and Bray, 2000).

Huang (2000) and Tokida et al. (2001) reported on the various types of soil retaining structures damaged by the September 21, 1999 Chi-Chi, Taiwan earthquake;

they both reported on damage to gravity-type retaining walls, wrap-around type geosynthetics-reinforced soil retaining walls, and segmental retaining walls with no damage to cantilever type retaining walls. However, a careful review of the damaged retaining structures shows that most, if not all, were located on steep slopes and their failures involved some combination of bearing capacity failure, overturning due to inadequate base width, slope instability above the walls, and in several cases direct fault offset. There was no mention of building basement walls in the two papers or in Abrahamson et al. (1999).

Rathje et al. (2006) reported that there was an absence of damage to basement walls and retaining walls in Duzce as a result of the November 12, 1999 Duzce, Turkey earthquake. However, Gur et al. (2009) does report that basement damage occurred in a school building in the Duzce earthquake. It was reported that a four-story school building had damage concentrated in the half-buried basement surrounded by partial height earth-retaining concrete walls. There were windows between the earth-retaining walls and the beams at the top of the basement and the exterior basement columns, which were captive along their weak axis, failed in shear. Gur et al. also report that the displacement demand was high enough to result in severe damage to masonry infill walls in the basement of the school building, but did not report about any damage to the earth-retaining concrete walls of the basement. The maximum horizontal ground accelerations near the school was reported as being 0.51g (east-west) and 0.41g (north-south). Gur et al. also report that in the May 1, 2003 Bingöl, Turkey earthquake, there was light damage to lateral basement walls even though the buildings had severe structural damage or collapse; the maximum horizontal ground accelerations in Bingöl were reported as being 0.28g (east-west) and 0.55g (north-south).

Summary

There are only few instances of documented damage to building basement walls due to seismic earth pressure in the United States or outside of the United States. The few reported instances that have occurred outside of the United States have only been minor in the damage amount. The available literature does not indicate that damage to building basement walls is a prevalent or even an occasional concern.

CURRENT STATE OF PRACTICE

Despite the lack of compelling damage that can be attributed to seismic earth pressures, the IBC Code (through the provisions of ASCE 7) requires the "determination" of seismic earth pressures for the design of earth retaining structures. The impetus for ultimate inclusion of seismic earth pressures probably dates back to the Seed and Whitman (1970) paper which essentially brought to the forefront the so-called Mononobe-Okabe seismic coefficient analysis (Mononobe and Matsuo, 1929 and Okabe, 1926). The interest aroused by this state-of-the-art paper sparked many researchers to conduct analytical, laboratory, and field analyses of the behavior of earth retaining structures to earthquake ground motions. Many of these studies, usually based on the same or similar assumptions made in the Mononobe-Okabe method, concluded that seismic earth pressures would be significant on earth retaining structures. On the basis of these studies and not actual experience, the concept of seismic earth pressures became an issue of concern that eventually led to its inclusion in the seismic design regulations embodied in the current ASCE 7 and IBC publications.

The present state-of-practice for evaluation of seismic earth pressures on building basement walls by geotechnical engineers in the United States is generally to rely upon an analysis based on the Mononobe-Okabe (M-O) method of analysis. The reasons for using the M-O method may be the simplicity of the method requiring only knowledge of the wall and backfill geometry, the soil's angle of internal friction, and the horizontal and vertical ground acceleration. Although other methods may be used in practice, the M-O method is the most common method of analysis by far.

USE OF THE MONONOBE-OKABE METHOD OF ANALYSIS

Despite the appearance of simplicity of the M-O method, suffice it to say that there is confusion among geotechnical practitioners regarding the evaluation of seismic earth pressures using this method for building basement walls. Part of the confusion stems from whether the M-O method is actually applicable for the intended analysis. The M-O method is based on Mononobe and Matsuo's (1929) experimental studies of a small scale cantilever bulkhead hinged at the base with a dry, medium dense granular backfill excited by a sinusoidal excitation on a shaking table.

The M-O method assumes that the Coulomb theory of static earth pressures on a retaining wall can be modeled to include the inertial forces due to ground motion (in the form of horizontal and vertical acceleration) in the retained earth as shown in Figure 1.

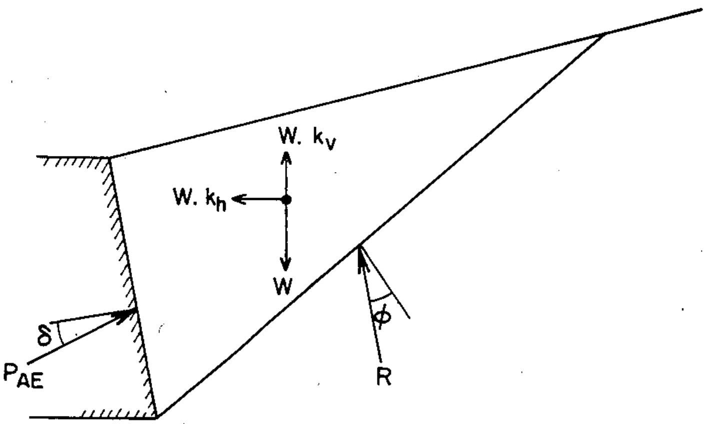

Fig. 1 Forces considered in the Mononobe-Okabe Analysis (after Seed and Whitman, 1970)

Seed and Whitman (1970) endorse the use of the method for gravity walls and list the following assumptions:

1. The wall yields sufficiently to produce minimum active pressures.
2. When the minimum active pressure is attained, a soil wedge behind the wall is at a point of incipient failure and the maximum shear strength is mobilized along the potential sliding surface.
3. The soil behind the wall behaves as a rigid body so that accelerations are uniform throughout the mass.

Despite these assumptions, the M-O method continues to be used for below ground structures. Ostadan and White (1998) have stated that "…the M-O method is one of the most abused methods the geotechnical practice." Ostadan and White list some reasons why they believe the M-O method is abused:

1. The walls of buildings are often of the non-yielding type. Wall movement may be limited due to the presence of floor diaphragms and displacements to allow limit-state conditions are unlikely to develop during the design earthquake.
2. The frequency content of the design ground motion is not fully considered as a single parameter (peak ground acceleration) may misrepresent the energy content of the motion at frequencies important for soil amplifications.
3. Appropriate soil properties are not considered as for soil dynamic problems, the most important property is the shear wave velocity, followed by the material damping, Poisson's ratio, and then the density of the soil.
4. Soil nonlinearity effects are not considered.
5. Soil-structure interaction (SSI) is not considered, such as building rocking motion, amplification and variation of the motion in the soil, geometry, and embedment depth of the building.

An area of abuse or perhaps more correctly misuse, is what to specify as the ground acceleration in the M-O method. Whitman (1991) had recommended that except where structures were founded at a sharp interface between soil and rock, the M-O method should be used with the actual expected peak acceleration. In the same vein, the seismic coefficient, k_h, is being recommended in future NEHRP documents to be equal to the site peak ground acceleration that is consistent with the design earthquake ground motions; in high seismic regions, such as California, these peak ground motions could easily exceed 0.5g. However, Kramer (1996) refers to the M-O method as a "pseudostatic procedure" and these accelerations as "pseudostatic accelerations." Arulmoli (2001) comments on the use of the M-O method and states that it has limitations, including the observation that the M-O method "blows up" for cases of large ground acceleration.

A study by the Washington State Transportation Center (Fragaszy, Denby, Higgins and Ali, 1987) on the seismic response of tieback retaining walls found that the M-O method overpredicted the dynamic soil pressures by a significant amount except for a small interval when compared with a finite element model using the full peak ground acceleration. Although a tieback retaining wall is not the same as a basement wall, tiebacks may be used for temporary shoring before the permanent basement wall is constructed and there may be application in this case as the shoring is usually not completely de-tensioned and left in place.

In practice, many geotechnical engineers have been using a seismic coefficient that is less than the expected peak ground acceleration for the design of building basement walls and other walls. The reason for the reduced value of the seismic coefficient compared to the peak ground acceleration is due to the following considerations:

1. The M-O method is a pseudo-static method of analysis, similar to many traditional slope stability methods that use a pseudo-static coefficient to represent earthquake loading.
2. There should be an intuitive reduction based upon the use of an effective ground acceleration rather than a peak ground acceleration (to take into effect the "repeatable" ground motion).
3. There should be a reduction to account for the averaging of the lateral forces on the retaining wall over the height of the wall (because of the out-of-phase nature of the ground movement as shear waves propagate vertically through the backfill soil).

The justification many geotechnical engineers use for using a reduced seismic coefficient comes from a Federal Highway Administration (FHWA) design guidance document for design of highway structures (Kavazanjian, Matasović, Hadj-Hamou, and Sabatini, 1997). In this document, it is stated that "…for critical structures with rigid walls that cannot accommodate any deformation and partially restrained abutments and walls restrained against lateral movements by batter piles, use of the peak ground acceleration divided by the acceleration of gravity as the seismic coefficient may be warranted." The document goes on to further state that "…however, for retaining walls wherein limited amounts of seismic deformation are acceptable…, use of a seismic coefficient from between one-half to two-thirds of the peak horizontal ground acceleration divided by gravity would appear to provide a wall design that will limit deformations in the design earthquake to small values." Thus many geotechnical engineers have been using a seismic coefficient of one-half of the horizontal peak ground acceleration.

Probably the biggest abuse of the M-O method is its application to retained earth that is not a truly cohesionless backfill. It seems logical that since soil cohesion reduces the active lateral earth pressure, it would also reduce the lateral seismic pressures. A very recent National Cooperative Highway Research Program (NCHRP) report (Anderson, Martin, Lam and Wang, 2008) provides guidance for use of the M-O method for soils with cohesion. Anderson et al. state that most natural cohesionless soils have some fines content that often contributes to cohesion, particularly for short-term loading conditions. Similarly, cohesionless backfills (for highway structures) are rarely fully saturated, and partial saturation would provide for some apparent cohesion, even for clean sands. Figures 2 and 3 present active earth pressure coefficient charts for two different soil friction angles with different values of cohesion for horizontal backfill, assuming no tension cracks and wall adhesion.

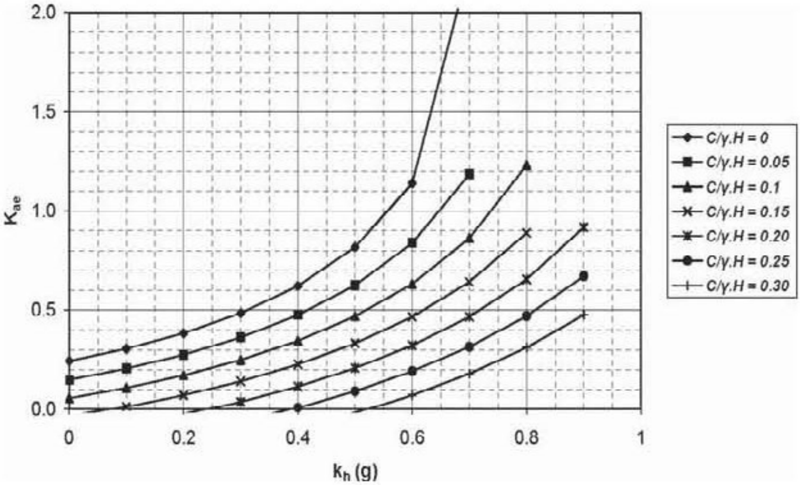

Fig. 2. Seismic coefficient chart for c-ϕ soils for angle of internal friction of 35 degrees (after Anderson et al., 2008).

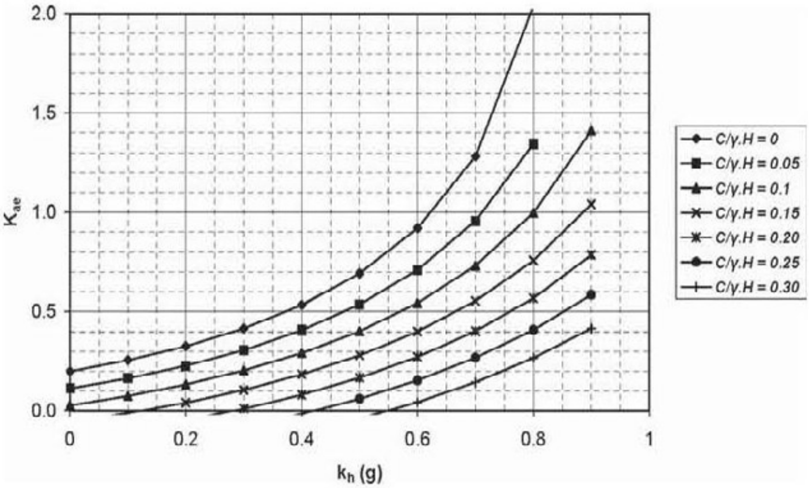

Fig. 3. Seismic coefficient chart for c-ϕ soils for angle of internal friction of 40 degrees (after Anderson et al., 2008).

These two charts show that a small amount of cohesion would have a significant effect in reducing the dynamic active earth pressure for design.

It should be noted that neglecting the vertical ground acceleration in the M-O analysis, as suggested by Seed and Whitman (1970), may be unconservative in cohesive soils. Recent events such as the 1994 Northridge, 1999 Chi-Chi (Taiwan), and 2008 Great Wenchuan (China) earthquakes have given recordings where the vertical ground motion components are comparable or even greater than the horizontal ground motion components. While some failures of retaining structures occurred in the epicentral region with high vertical ground motions in the Chi-Chi event, the absence of damage to retaining structures was striking in the 1994 Northridge and the 2008 Great Wenchuan events which also contained significant vertical components. Most recently, Gazetas et al. (2009) show that vertical accelerations have no influence on purely frictional analysis of sliding block motion using the Chi-Chi data, which is consistent with current analysis methods.

There are many reasons why the Mononobe-Okabe method is being used, misused and abused by geotechnical engineers in estimating seismic earth pressures on building basement walls. Geotechnical engineers are drawn to this method because of its simplicity, however, there are many assumptions that have to be made and some of the assumptions may simply not be applicable. The inclusion of cohesion in determining the M-O seismic increment of earth pressure may give more "reasonable" results. However, there is a lack of guidance as to what is a correct or reasonable seismic earth pressure.

RECENT RESEARCH ON SEISMIC LATERAL PRESSURES

As mentioned previously, the original experimental tests that formed the basis of the M-O method were based on the response of a small scale cantilever bulkhead supporting a dry, medium dense cohesionless backfill, excited by a sinusoidal input on a shaking table with accelerations up to 0.3g. Many of the researchers that followed have used similar experimental set-ups. However, the applicability of the test results from a small scale test based on idealized sinusoidal loading to full size structures has been called into question with new advances in testing, especially with the emergence of centrifuge testing.

Centrifuge testing allows for creating a stress field in a model that simulates prototype conditions in that proper scaling will provide correct strength and stiffness in granular soils. The granular soils, when having a scale model with dimensions of 1/N of the prototype and a gravitational acceleration during spinning of the centrifuge at N times the acceleration of gravity, will have the same strength, stiffness, stress and strain of the prototype (Kutter, 1995).

An early centrifuge test of a cantilever retaining wall was conducted by Ortiz, Scott and Lee (1983) to verify the M-O theory. One important finding in this study is the conclusion that "it is difficult or impossible to achieve in a (one-g) shaking table a pressure distribution which can be related quantitatively to that of the full-scale situation." Ortiz et al. also use dimensional analysis to show that "true representation of the dynamic prototype behavior cannot be attained in a (one-g) shaking table experiment, utilizing a reduced scale model and same soil as the prototype." Ortiz et al. also found that there was good agreement between the M-O theory and the centrifuge experiment that the point of application of the resultant of the static and dynamic earth pressure; i.e., the resultant was at about the one-third of the wall height above the base of the wall.

A more recent study by Nakamura (2006) also sought to reexamine the Mononobe-Okabe theory by centrifuge testing. An important finding by Nakamura was that the earth pressure distribution on the model retaining wall is not triangular (as assumed by M-O), and that its size and shape change with time. Nakamura also found that the earth pressure distribution for an input motion that was based on an actual earthquake time history was different from the distribution for sinusoidal shaking. The earth pressure in the bottom part of the wall, which greatly contributes to the total earth pressure, is not as great in an earthquake as it is for sinusoidal loading. Nakamura stated that the earth pressure increment is around zero when considering earthquake type motions, with the earth pressure nearly equal to the initial value prior to shaking when the inertia force is maximum.

Al Atik and Sitar (2007) also performed centrifuge experiments on model cantilever walls with medium dense dry sand backfill. Al Atik and Sitar found that the maximum dynamic earth pressures increase with depth that can be reasonably approximated by a triangular distribution analogous to that used to represent static earth pressure. They also found that the seismic earth pressures can be neglected at accelerations below 0.3g and state that the data suggest that even higher seismic loads could be resisted by cantilever walls designed to an adequate factor of safety. As the tests were conducted with medium sand backfill, they state that a severe loading condition may not occur in denser granular materials or materials with some degree of cohesion. Al Atik and Sitar also found that the maximum moment in the wall and the maximum earth pressure were out of phase and did not occur at the same time.

CONCLUSIONS

Despite the absence of compelling or even minimal evidence of structural distress or failure of building basement walls in earthquakes, the state of practice as dictated by the current building code (IBC) and engineering practice standards (ASCE 7-05) requires the consideration of seismic earth pressures for buildings and structures that have retained earth materials. Observations of the behavior of walls during earthquakes suggest that structural performance is quite good except for cases where there may be loss of strength in the soil due to liquefaction or other processes.

Because of the simplicity of the method, geotechnical engineers have generally been trying to apply the Mononobe-Okabe method of analysis to evaluate the seismic earth pressures for the building code's design earthquake criteria. Whether or not the Mononobe-Okabe method is really suitable for the evaluation of building basement walls may be debatable because the tests were made for cantilever walls retaining medium dense sand. As building basement walls are generally braced at several levels, comparisons with cantilever walls may be difficult. Also, medium dense sand backfill may not be representative of most of the retained earth behind building basement walls. Some attempts have been made to account for cohesion in the retained earth which will reduce the intensity of the seismic earth pressures. The profession has also struggled with the appropriate value of the seismic coefficient to use as high ground accelerations give very high seismic earth pressures that do not seem reasonable.

Recent research using centrifuge testing brings into question the validity of the M-O method. The applicability of the original test on a small scale shaking table with medium dense sand backfill excited by a sinusoidal wave to a large building basement wall appears to be suspect, if not valid at all. Centrifuge testing indicates model walls that have been properly scaled subjected to more realistic earthquake ground motions do not appear to experience large seismic earth pressures and the results indicate that the M-O method is very conservative, if just not applicable. However, centrifuge testing does indicate that the location of the resultant of the static and seismic earth pressures appears to match the M-O method at the one-third height above the base of the wall and is not located on the upper part of the wall as suggested by some researchers.

It appears that the current design practice for seismic earth pressures on building basement walls is conservative, uneconomical, and perhaps unnecessary. More importantly, the design practice is mostly based on experimental data that were extrapolated beyond the limits of their applicability.

REFERENCES

Abrahamson N., Bardet, J.P., Boulanger R,, Bray, J., Chan, Y.-W., Chang, C.-Y., Chen, C.-H., Harder, L., Huang, A-B., Huang, S., Ju, J.W., Kramer, S., Kuo, M.-J., Lee, W. F., Lin, H-L., Loh, C-H., Ou, C-Y., Seed, R., Shen, J.-D., Sitar, N., Stewart, J., Teng, L., Sun, J.I., and Wright R. (1999). *Preliminary Geotechnical Earthquake Engineering Observations of the September 21, 1999, Ji-Ji, Taiwan Earthquake,* GEER Association Report No. GEER-002

Al Atik, L. and Sitar, N. (2007). *Development of Improved Procedures for Seismic Design of Buried and Partially Buried Structures.* Pacific Earthquake Engineering Research Center, PEER 2007/06, Berkeley, Calif.

American Society of Civil Engineers. (2006). *Minimum Design Loads for Buildings and Other Structures.* ASCE Standard ASCE/SEI 7-05.

Anderson, D.G., Martin, G.R., Lam, I., and Wang, J.N. (2008). *Seismic Analysis and Design of Retaining Walls, Buried Structures, Slopes and Embankments.* National Cooperative Highway Research Program Report 611, Transportation Research Board, Washington, DC.

Arulmoli, K. (2001). "Earthquake Simulation in Geotechnical Engineering: Applications and Research Needs to Improve State of Practice." *Proceedings of NSF International Workshop on Earthquake Simulation in Geotechnical Engineering,* Cleveland, OH.

Benuska, L. (1990). "Loma Prieta Earthquake Reconnaissance Report." *Earthquake Spectra*, Supplement to Vol. 6.

Building Seismic Safety Council. (2004a). *NEHRP Recommended Provisions for Seismic Regulations for New Buildings and Other Structures (FEMA 450), 2003 Edition, Part 1 – Provisions.* BSSC, Washington, DC.

Building Seismic Safety Council. (2004b). *NEHRP Recommended Provisions for Seismic Regulations for New Buildings and Other Structures (FEMA 450), 2003 Edition, Part 2 – Commentary.* BSSC, Washington, DC.

California Building Standards Commission. (2002). *2001 California Building Code*. International Conference of Building Officials, Whittier, Calif.

Clough, G.W. and Fragaszy, R.J. (1977). "A Study of Earth Loadings on Floodway Retaining Structuresin the 1971 San Fernando Valley Earthquake." *Proceedings, 6th World Conference on Earthquake Engineering* (3), 2455-2460.

Earthquake Engineering Research Institute. (1998a). "1987 Whittier Narrows Earthquake Reconnaissance Report." *Earthquake Spectra*, (4) 1.

Earthquake Engineering Research Institute. (1998b). "1987 Whittier Narrows Earthquake Reconnaissance Report." *Earthquake Spectra*, (4) 2.

Fragaszy, R.J., Denby, G., Higgins, J.D. and Ali, A. (1987). *Seismic Response of Tieback Retaining Walls (Phase I).* Washington State Transportation Center, Pullman, Washington.

Gazetas, G., Garini, E., Anastasopoulos, L. and Georgakakos, T. (2009). Effects of Near-Fault Ground Shaking on Sliding Systems. *Journal of Geotechnical and Geoenvironmental Engineering,* ASCE, (135) 12, 1906-1921.

Gur, T., Pay, A.C., Ramirez, J.A., Sozen, M.A., Johnson, A.M., Irfanoglu, A., and Bobet, A. (2009). "Performance of School Buildings in Turkey During the 1999 Düzce and the 2003 Bingöl Earthquakes." *Earthquake Spectra*, (25) 2, 239-256.

Hall, J.F. (1995). "Northridge Earthquake of January 17, 1994 Reconnaisance Report – Volume 1." *Earthquake Spectra*, Supplement C to Vol. 11.

Holmes, W.T. and Somers, P. (1996). "Northridge Earthquake of January 17, 1994 Reconnaisance Report – Volume 2." *Earthquake Spectra*, Supplement C to Vol. 11.

Huang, C. (2000) "Investigations of Soil Retaining Structures Damaged During the Chi-Chi (Taiwan) Earthquake." *Journal of the Chinese Institute of Engineers*, (23) 4, 417-428.

Iida, H., Hiroto, T., Yoshida, N., and Iwafuji, M. (1996). "Damage to Daikai Subway Station." *Soils and Foundations Special Issue on Geotechnical Aspects of the January 17, 1995 Hyogoken-Nambu Earthquake*, Japanese Geotechnical Society.

International Code Council (ICC). (2003). *International Building Code*, Country Club Hills, Ill.

International Code Council (ICC). (2006). *International Building Code*, Country Club Hills, Ill.

International Conference of Building Officials (ICBO). (1988). *Uniform Building Code*, Whittier, Calif.

International Conference of Building Officials (ICBO). (1997). *Uniform Building Code*, Whittier, Calif.

Japanese Geotechnical Society. (1996). *Soils and Foundations Special Issue on Geotechnical Aspects of the January 17, 1995 Hyogoken-Nambu Earthquake.*

Kavazanjian, E., Matasović, N., Hadj-Hamou, T., and Sabatini, P.J. (1997). *Geotechnical Engineering Circular #3 – Design Guidance: Geotechnical Earthquake Engineering for Highways, Volume 1 – Design Principles.* Federal Highway Administration Report No. FHWA-SA-97-076.

Kramer, S.L. (1996). *Geotechnical Earthquake Engineering.* Prentice Hall, Upper Saddle River, New Jersey.

Kutter, B.L. (1995). "Recent Advances in Centrifuge Modeling of Seismic Shaking." *Proceedings, Third International Conference on Recent Advances in Geotechnical Earthquake Engineering and Soil Dynamics*, St. Louis, MO, (2) 927-942.

Lew, M., Simantob, E., and Hudson, M.B. (1995). "Performance of Shored Earth Retaining Systems During the January 17, 1994 Northridge Earthquake." *Proceedings, Third International Conference on Recent Advances in Geotechnical Earthquake Engineering and Soil Dynamics,* St. Louis, MO, (3) 1417-1422.

Mononobe, N. and Matsuo, H. (1929). "On the determination of earth pressure during earthquakes." *Proceedings of the World Engineering Conference*, (9).

Murphy, L.M. (1973). *San Fernando, California Earthquake of February 9, 1971 (in three volumes).* U.S. Department of Commerce, Washington, D.C.

Nakamura, S. (2006). "Reexamination of Mononobe-Okabe Theory of Gravity Retaining Walls Using Centrifuge Model Tests." *Soils and Foundations*, (46) 2, 135-146.

Okabe, S. (1926). "General theory of earth pressure." *Journal of the Japanese Society of Civil Engineers*, Tokyo, Japan, 12 (1).

Ortiz, L.A., Scott, R.F., and Lee, J. (1983). "Dynamic Centrifuge Testing of a Cantilever Retaining Wall." *Earthquake Engineering and Structural Dynamics*, (11), 251-268.

Ostadan, F. and White, W.H. (1998). "Lateral seismic soil pressure – an updated approach." *US-Japan SSI Workshop*, United States Geologic Survey, Menlo Park, CA.

Rathje, E.M., Stewart, J.P., Baturay, M.B., Bray, J.D., and Bardet, J.P. (2006). "Strong Ground Motions and Damage Patterns from the 1999 Duzce earthquake in Turkey." *Journal of Earthquake Engineering*, Taylor & Francis, 10 (5), 693-724.

Seed, H.B. and Whitman, R.V.. (1970). "Design of Earth Retaining Structures for Dynamic Loads." *ASCE Specialty Conference, Lateral Stresses in the Ground and Design of Earth Retaining Structures.* Cornell University, Ithaca, NY., 103-147.

Shakal, A., Huang, M., Darragh, R., Cao, T., Sherburne, R., Malholtra, P., Cramer, C., Sydnor, R., Graizer, V., Maldonaldo, G., Petersen, C., and Wampole, J. (1994). *CSMIP Strong-Motion Records from the Northridge, California Earthquake of 17 January 1994*, California Strong Motion Instrumentation Program Report No. OSMS 94-07, California Department of Conservation, Sacramento, Calif.

Stewart, J.P., Bray, J.D., Seed, R.B., and Sitar, N., eds. (1994). *Preliminary Report on the Principal Geotechnical Aspects of the January 17, 1994, Northridge*

Earthquake. Earthquake Engineering Research Center Report No. UCB/EERC 94/08. University of California, Berkeley.

Structural Engineers Association of California. (2009). *SEAOC Blue Book – Seismic Design Recommendations.* SEAOC, Sacramento, CA.

Tokida, K., Matsuo, O., and Nakamura, S.. (2001). "Damage of Earth Retaining Structures in the 1999 Chichi, Taiwan Earthquake." *Proceedings of the Joint Meeting of the U.S.-Japan Cooperative Program in Natural Resources-Panel on Wind and Seismic Effects,* (32) 495-512.

Whitman, R.V. (1991). "Seismic Design of Earth Retaining Structures." *Proceedings, Second International Conference on Recent Advances in Geotechnical Earthquake Engineering and Soil Dynamics*, St. Louis, MO., 1767-1778.

Wood, J.H. (1973). *Earthquake-Induced Soil Pressures on Structures.* Earthquake Engineering Research Laboratory Report EERL 73-05, California Institute of Technology, Pasadena, CA.

Youd, T.L., Bardet, J.P., and Bray, J.D. (2000). "1999 Kocaeli, Turkey, Earthquake Reconnaisance Report." *Earthquake Spectra*, Supplement to Vol. 16.

Seismic Design and Performance of Retaining Structures

Susumu Iai[1]

[1]Disaster Prevention Research Institute, Kyoto University, Gokasho, Uji, Kyoto 611-0011 Japan; Phone 81-774-38-4090; Fax 81-774-38-4094; e-mail: iai@geotech.dpri.kyoto-u.ac.jp

ABSTRACT

Which of the soil strengths should be used for seismic design of retaining walls with dry soil, peak or residual? The effort to answer this simple question leads to a generalized methodology that is based on the multiple-sliding plane concept using both the peak strength, for defining slip plane, and the residual strength, for evaluating earth pressure associated with the slip plane. Many of the assumptions made in the conventional seismic design, successfully applicable to retaining walls with dry soil, become questionable when the soil is submerged. Adequate characterization of the undrained behavior of sand under transient and cyclic loads is needed. Initial stress state of soil-retaining structure systems before the earthquake, often ignored in the simplified seismic design practice, can have a significant effect on the performance of the wall during earthquakes.

INTRODUCTION

The conventional practice for evaluating seismic stability of retaining structures has been based on a simplified approach, idealizing the soil mass around a retaining structure either by a sliding block or a spring (Seed and Whitman, 1970). By analyzing a sliding block of a soil mass, the earth pressures acting on a retaining structure are evaluated by modifying Coulomb's classical earth theory to account for inertia forces (Mononobe, 1924; Okabe, 1924). Using these earth pressures, permanent displacement of a retaining wall is evaluated based on a Newmark type analysis (Newmark, 1965; Franklin and Chang, 1977; Richards and Elms, 1979; Nadim and Whitman, 1983; Towhata and Islam, 1987). Tilt is also evaluated by extending the simplified analysis for rotation (Nadim and Whitman, 1983; Whitman and Liao, 1984; Prakash et al., 1995; Steedman and Zeng, 1996). By using a spring to idealize the soil mass around an embedded portion of a retaining structures, a reaction force is evaluated using the subgrade reaction coefficient (Rowe, 1952; Terzaghi, 1955). In deed, the simplified approach ha been the basis for the design of many retaining structures in north America, Japan and other seismically active regions around the world (PIANC, 2001).

When the soil is submerge, however, many of the assumptions made in the simplified approach become questionable. Under rapid shaking during earthquakes, the soil tends to dilate or contract depending on the density and stress state of the soil, changing the pore water pressure of the soil. A typical example is liquefaction in loose sand. Less acknowledged is the effect of negative excess pore water pressures due to the dilatant behavior of dense sand, suggesting a higher resistance and stability than in a dry condition.

Dry or submerged condition apart, intensity of shaking recorded during earthquakes has steadily increasing since the initiation of modern instrumentation in 1960's. The peak ground acceleration (PGA) recorded was 0.25g during 1968 Tokachi-oki, Japan, earthquake, the PGA was 0.5 to 0.8g during 1995 Hyogo-ken Nambu, Japan, earthquake, and the PGAs exceeded 1g since 2000 when much more modernized dense instrumentation with a spacing of every 25km is implemented throughout Japan, including the PGA exceeding 4g during 2008 Iwate-Miyagi Inland, Japan, earthquake. Just to appreciate what these values of acceleration imply with respect to the seismic design of geotechnical structures, let us take an example of a sand having internal friction angle of 35 degrees. The upper limit of the acceleration of a level ground consisting of this sand at dry condition can resist is 0.7g(=tan35$^{\circ}g$).

Development in seismic design of retaining structures over 20 years have been lead by the challenging issues described above; evaluating undrained cyclic behavior of sand and behavior of retaining structures during strong earthquake motions that can exceed the dry soil strength.

BEHAVIOR OF SAND UNDER TRANSIENT AND CYCLIC LOADS

Seismic behavior of retaining structures depends on the soil-structure-foundation interaction. The interaction is generally complex not only due to the geometry of the problem but also the highly non-linear behavior of soil during strong earthquake motions. Even before the earthquake shaking, the stress state of soil in the vicinity of the wall can be close to a shear failure condition, posing additional challenging problem when attempting to characterizing the seismic response and stress/strain state of the soil. "A long history of confusion" as brilliantly put in "Fifty years of lateral earth support" (Peck, 1990) may be interpreted as the confusion caused by the associated with the (wrong) assumptions made on the soil-structure interaction in the simplified method.

In order to discuss the complex soil-structure interaction in retaining structures, it is bet to begin by reviewing our basic understanding the soil behavior under transient and cyclic loads (Iai, 1998). For a dry condition, stress-train relationship of soil during cyclic shear is typically represented by a hysteresis loop as shown in Figure 1 (Hardin and Drnevich, 1972). The hysteresis loop depends on the shear strain level because the loop is bounded by the upper and lower limits specified by the soil strength. The behavior of soil discussed here, for example, explains the hysteretic subgrade reaction to an embedded foundation being forced in cyclic motion as illustrated in Figure 2. The upper and lower limits of the subgrade reaction correspond to the active and passive earth pressures, both of which play an important role in the conventional design practice of retaining structures.

The undrained behavior of soil under cyclic shear is completely different from the drained behavior and is strongly affected by the excess pore water pressures and the corresponding change in the effective stress of the soil as shown in Figure 3 (Ishihara, 1985). The upper and lower limits specified by the shear strength of the soil under a drained condition are non longer relevant to the hysteresis loop of the soil with an undrained condition because these limits are affected by the change in the effective confining stress during cyclic loading. Another important fact is the progressive increase in the shear strain amplitude without an increase in the cyclic stress level.

In two or three dimensional non-linear problem as is the case with analyzing the seismic behavior of retaining structures, soil stress condition has additional effects due to gravity. For example, the stress state of the soil behind the retaining wall indicated by the alphabet A in Figure 4 can be close to the active shear failure condition. that below the wall indicated by the alphabet B can be close to the failure condition in a compression shear mode. These anisotropic stress state before and during an earthquake, hereafter called initial shear, should certainly affect the behavior of soils subjected to the cyclic load afterwards during earthquakes.

The conceptual image of the deformation of a soil element B undergoing the stress and strain conditions discussed here is illustrated in Figure 5. As shown in this figure, the soil gradually deforms along the directions of the initial principal stresses (in this case, pointing downward). This type of cumulative deformation will induce settlement associated with lateral bulging, leading to residual deformation of retaining walls. The soil behavior under the anisotropic stress condition discussed above has been studied and confirmed by the laboratory study (Ishihara and Li, 1972).

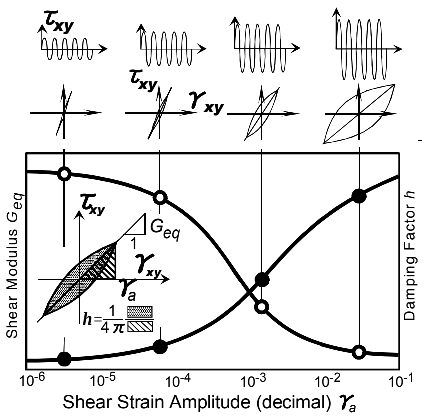

Figure 1. Sand Behavior under Drained Cyclic Shear

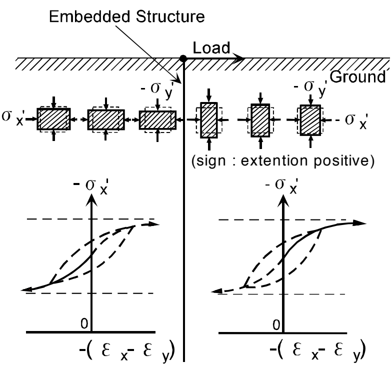

Figure 2. Hysteretic Subgrade Reaction in Drained Cyclic Shear Condition

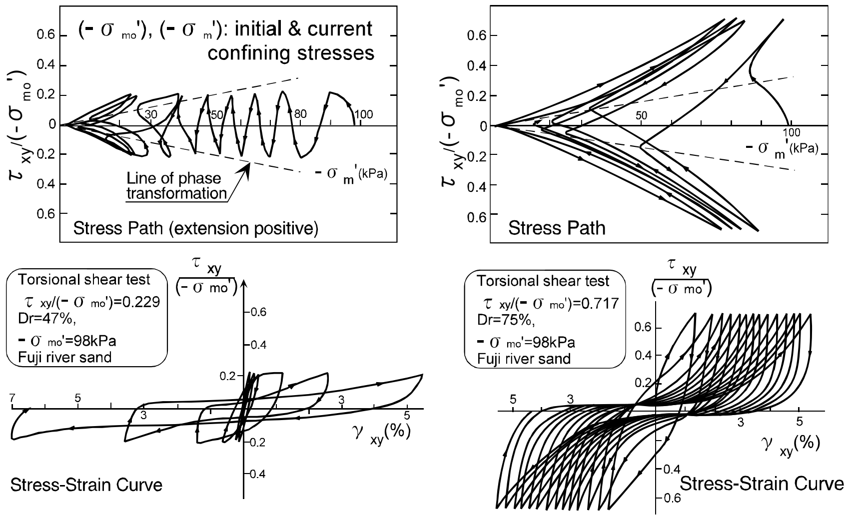

(a) Loose Sand (b) Dense Sand

Figure 3. Sand Behavior under Undrained Cyclic Shear (Ishihara, 1985)

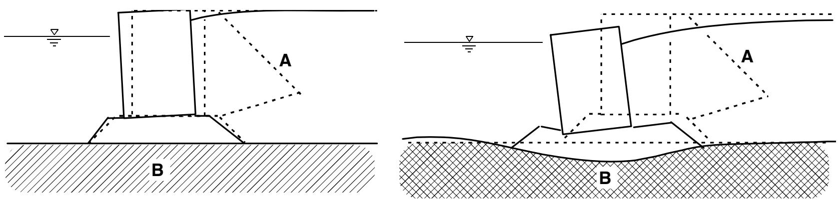

(a) On a Firm Foundation (b) On a Loose Saturated Sandy Foundation

Figure 4. Deformation/Failure Mode of Gravity Quaywall

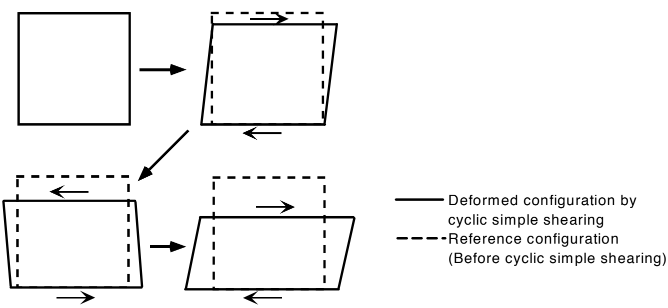

Figure 5. Schematic Deformation of Soil Element under Undrained Cyclic Loading with Initial Shear

In order to take into account the behavior of soil reviewed above in the analysis of soil-structure interaction of retaining structures, we need to develop a constitutive model being simple, numerically robust yet sophisticated enough to reproduce the essential features of the soil behavior. The essential requirements for the constitutive model include (Iai, 1998):

(1) the ability to follow the stress path close to the shear failure line such as shown in the upper figure in Figure 3,
(2) the ability to reproduce the hysteresis loop of a hardening spring type such as shown in the lower figure in Figure 3,
(3) the ability to reproduce the progressive increase in the shear strain amplitude such as shown in the lower figure in Figure 3, and
(4) the ability to analyze the cyclic behavior of sand under anisotropic stress field as shown in Figure 5.

SEISMIC EARTH PRESSURES FROM DRY BACKFILL

In the conventional simplified analysis, the earth pressures on the wall from the dry backfill are typically estimated using the Mononobe-Okabe equation (Mononobe, 1924; Okabe, 1924). In the uniform field of horizontal and (downward) vertical accelerations, $k_h g$ and $k_v g$, the body force vector, originally pointing downward due to gravity, is rotated by the seismic inertia angle, ψ, defined by (see Figure 6)

$$\psi = \tan^{-1}\left[\frac{k_h}{1-k_v}\right]$$

The Mononobe-Okabe equation is obtained by rotating the geometry of Coulomb's classical solution through the seismic inertia angle, ψ. A complete set of equations may be found in the design codes and manuals (Japan_Port_and_Harbour_Association_(ed.), 1989; Ebeling and Morrison, 1992).

With the increasing awareness in 1990s of the need to adopt high PGA in seismic design, a simple but fundamental question was asked: which of the soil strengths, peak or residual, should be used for seismic design of retaining walls with dry soil? It is well established that there is a significant difference between the peak and residual internal friction angles of sand. typical values for dense sand can be $\phi_{peak}=50^{o}$, $\phi_{res}=30^{o}$. This difference can have a significant effects on the earth pressures as schematically shown in Figure 7. First, the onset of failure should coincide with the full mobilization of peak internal friction angle rather than residual. Once a failure plane is formed, then the mobilized friction angle along this plane reduces to the residual internal friction angle. The important fact is that sliding remains to be trapped in the same failure plane until the effective seismic coefficient exceeds the threshold value for the onset of another failure plane that once again corresponds to the peak internal friction angle. The onset conditions of the initial and second failure plane among multiple choice of potential failure plane are schematically shown in Figure 8. This line of thought led to a proposal of a generalized method for estimating active earth pressures for dry backfill (Koseki et al., 1998).

Examples of the earth pressures computed through the generalized method are shown in Figure 9. In this figure, two examples are shown: one is associated with the initial sliding plane formed at static condition (i.e. $k_h/(1\text{-}k_v)=0$), the other at $k_h/(1\text{-}k_v)=0.2$. Once the initial sliding plane is formed, the sliding mode is entrapped with the same sliding plane. This process continues until the earth pressure associated with this sliding plane is overtaken by the Mononobe-Okabe earth pressure computed for peak internal friction angle. Then, the next sliding plane is formed. The results shown in Figure 9 indicate that the earth pressures computed using the residual internal friction angle in the conventional design practice may be too conservative especially in designing for the conditions with a high seismic coefficient.

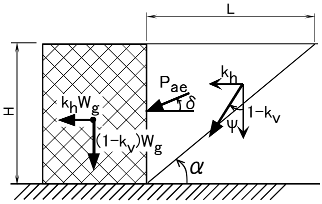

Figure 6. Active earth pressure

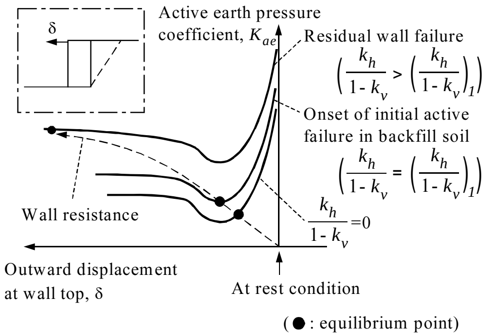

Figure 7. Wall displacement and active earth pressure coefficient, modified from (Koseki et al., 1998)

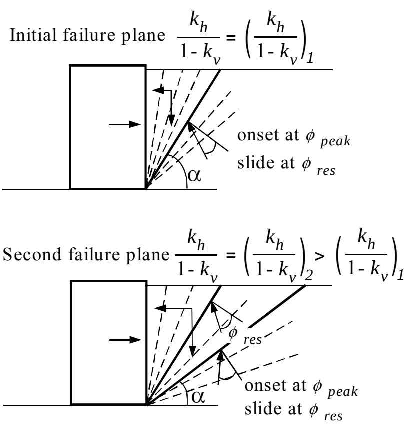

Figure 8. Multi-stage active failure

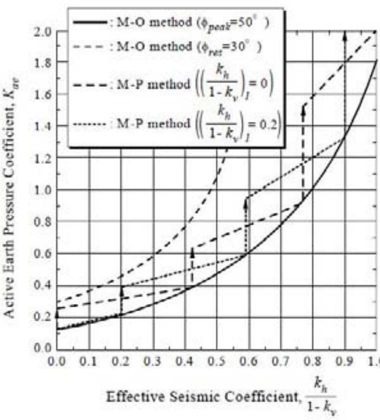

Figure 9. Active earth pressure by the generalized method ($\phi_{peak}=50^o$, $\phi_{res}=30^o$ and $\delta=25^o$), modified from (Koseki et al., 1998)

SEISMIC PERFORMANCE OF SUBMERGED RETAINING STRUCTURES

In the conventional simplified analysis, the effect of the pore water on the submerged soil was taken into account as buoyancy for modifying the Mononobe-Okabe equation (Japan_Port_and_Harbour_Association_(ed.), 1989; Ebeling and Morrison, 1992). The effect of dilatancy that characterizes the distinctive behavior of sand under undrained condition was ignored, most probably for the sake of simplicity. As described earlier, many of the assumptions made for dry soil become questionable when the soil is submerged. The stress-strain behavior of soil is completely different from that of dry soil as described earlier. The assumption of a sliding block type movement of soil becomes also questionable for a submerged sand, which tends to deform in a continuum rather than to slide along a well defined slip failure surface. Thus, since the late 1980's, more and more attention has been directed toward a full seismic response analysis of waterfront retaining structures using the finite element of finite difference technique based on the constitutive equation that has the ability to characterize the distinctive behavior of sand under undrained cyclic shear (Iai et al., 1998).

During the 1995 Hyogoken-Nambu, Kobe, Japan, earthquake of 1995, many of the caisson walls suffered damage as shown in Figure 10. These caisson walls were constructed on a loose saturated backfill foundation of decomposed granite, which was used for replacing the soft clayey deposit in Kobe Port to attain the required foundation bearing capacity. Subjected to a strong earthquake motion having peak accelerations of 0.54g and 0.45g in the horizontal and vertical directions, these caisson walls were displaced an average of 3 m (maximum displacement –5m) toward the sea, settled 1 to 2 m and tilted about 4 degrees toward the sea. Although a sliding mechanism could explain the large horizontal displacement of the caisson walls, this mechanism did not explain the large settlement and tilt of the caissons. Reduction in the stiffness of foundation soils due to development of excess pore water pressure was speculated as a main cause of the observed caisson damage at Kobe Port.

This speculation was confirmed by a series of effective stress analyses using a computer code FLIP, which incorporates a constitutive model based on strain space multiple mechanism model (Iai et al., 1992). The model parameters were evaluated based on the in-situ velocity logging, the blow counts of Standard Penetration Tests (SPT N-values) and the results of cyclic triaxial tests. The specimens used for cyclic triaxial tests were undisturbed samples obtained by an in-situ freezing technique. Input earthquake motions were those recorded at the Port Island site about 2km from the quay wall. The spatial domain used for the finite element analysis covered a cross sectional area of about 220 m by 40 m in the horizontal and vertical directions.

The effective stress analysis resulted in the residual deformation shown in Figure 11. As shown in this figure, the mode of deformation of the caisson wall was to tilt into and push out the foundation soil beneath the caisson. This was consistent with the observed deformation mode of the rubble foundation shown in Figure 12, which was investigated by divers.

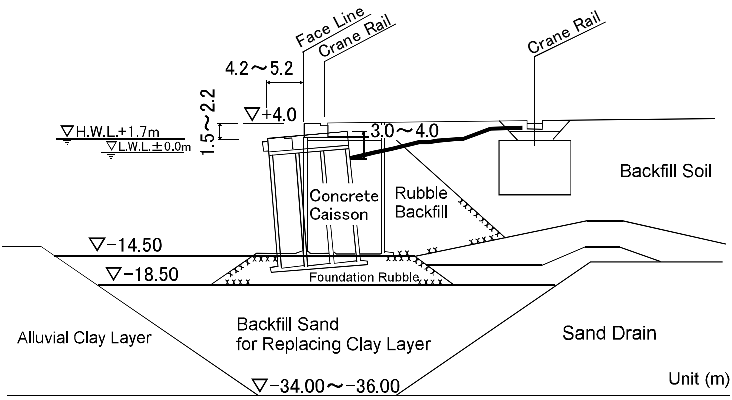

Figure 10. Deformation/Failure of Gravity quaywall at Kobe Port during 1995 Hyogoken-Nambu, Japan, earthquake

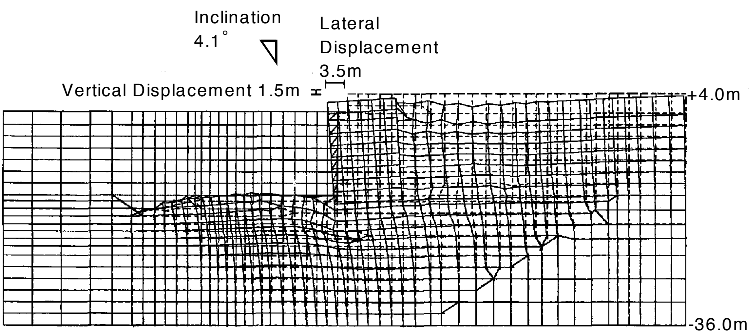

Figure 11. Computed deformation of a gravity quaywall

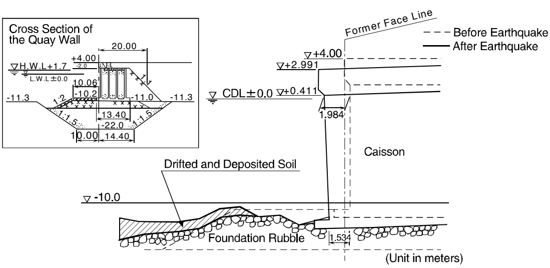

Figure 12. Deformation of rubble foundation of a quay wall investigated by divers

Since this case history of a gravity caisson wall is well documented with an ideal set of laboratory test results of soil and input earthquake motions, it has been frequently quoted among the geotechnical earthquake engineers, as a kind of a bench mark, for studying the applicability of constitutive models and computer code for numerical analysis. In this context, one can ask why this case history and analysis is important in the development in seismic design of retaining structures over these 20 years. The most important is not the capability of numerical analysis based on finite element or finite difference techniques or the constitutive models as often believed (wrongly) with a cursory glance of the results. The most important is the understanding of the mechanism that is associated with the undrained cyclic behavior of sand that does not have predefined shear strength but does have cumulative increase in shear strain. The mechanism does not involve the well defined slip failure surface, that was essential for the conventional simplified approach for evaluating the seismic earth pressure for dry backfill. The mechanism is governed by the cumulative increase in the shear strain induced in the soil around the retaining structures along the direction of initial stress due to gravity. Consequently, it is essential to evaluated the undrained cyclic behavior of soil for adequate seismic design of retaining walls in submerged condition.

As Whitman (1991) concluded his state-of-the art lecture (Whitman, 1991): "... Hopefully this pace will continue during the next 10 years, with new significant advances concerning the most perplexing of today's problems - more economical but adequate waterfront structures." The development described above proves that Whitman was correct in pointing out the most important direction of development in the seismic design of retaining structures.

EFFECT OF INITIAL STRESS

In the seismic response analysis of retaining structures based on linear or equivalent linear elastic model that had been, even might have been in some areas of application, widely used in practice, initial stress state in the soil and structure has nothing to do with the seismic response of the retaining structures. This practice, in the history of development in seismic design, unfortunately lead to the (wrong) understanding in the mind of engineers that initial stress conditions for the seismic analysis of retaining structures can be assigned, more or less arbitrarily, as a crude approximation.

The development in the seismic response analysis of retaining structures over these twenty years implies that initial stress conditions for seismic analysis plays a significant role. An example is shown on sheet pile retaining structure (Kameoka and Iai, 1993). In this study, cross section of a sheet pile quay wall is chosen from the case history of damage at Akita Port during 1983 Nihonkai-Chubu, Japan, earthquake, shown in Figure 13. initial earth pressures before the earthquake was varied by applying forced displacements between anchor and sheet pile wall as shown in Figure 14. The results of the seismic analysis shown in Figure 15 indicate that higher initial earth pressure applied on the wall results in smaller bending moments and displacements induced by the ground motions. In a sense, the high initial stress applied in the soil has a pre-stress to increase the confining stress, and thereby exhibiting higher resistance of soil to overcome the increase in the initial bending moment in the sheet pile. Based on these findings, it is recommended that the initial conditions for sheet pile quay walls be computed by step-by-step gravity analysis closely following the actually construction sequence (Miwa et al., 2003).

Figure 13. Damage to a sheet pile quay wall at Akita Port during 1983 earthquake

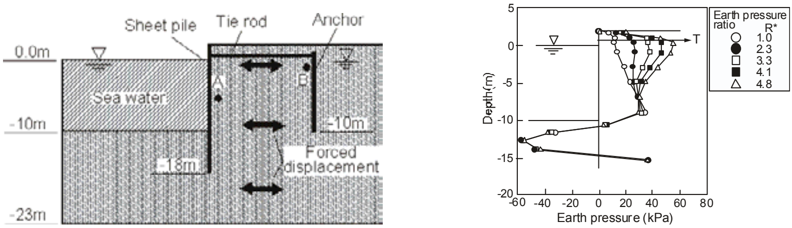

Figure 14. Cross section of quay walls (left) and earth pressure distribution given as initial condition (right)

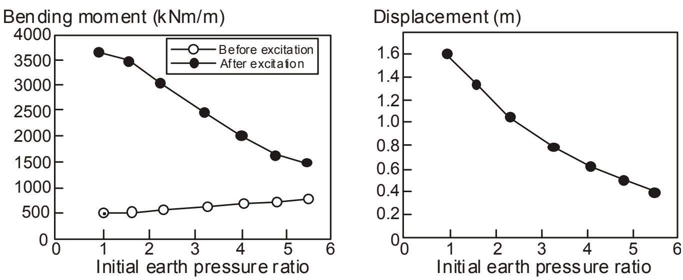

Figure 15. Computed earthquake-induced bending moment and displacement (Kameoka and Iai, 1993)

PERFORMANCE-BASED DESIGN

The development in seismic design of retaining structures in more recent years, especially since 2000, may be found in the area of collective efforts to put together a new design methodology that is more adequate in facing with the realistic performance of retaining structures discussed earlier. The principles in the performance-based approach relevant to the retaining structures may be summarized as follows (Iai, 2005).

In this approach, the objectives and functions of retaining structures are defined in accordance with broad categories of use such as commercial, public and emergency use. While the objectives and functions of retaining structures may be commercial use, there is a certain category of retaining structures designated as an essential part of emergency bases in Japan with objectives and functions being emergency use.

Depending on the functions required during and after an earthquake, performance objectives for seismic design of retaining structures are specified on the following basis:

-serviceability during and after an earthquake: minor impact to social and industrial activities, the port structures may experience acceptable residual displacement, with function unimpaired and operations maintained or economically recoverable after temporary disruption:

-safety during and after an earthquake: human casualties and damage to property are minimized, critical service facilities, including those vital to civil protection, are maintained, and the port structures do not collapse.

The performance objectives also reflect the possible consequences of failure.

For each performance objective, a reference earthquake motion is specified as follows:

-for serviceability during or after an earthquake: earthquake ground motions that have a reasonable probability of occurrence during the design working life;

-for safety during or after an earthquake: earthquake ground motions associated with rare events that may involve very strong ground shaking at the site.

Although these descriptions are very general, they constitute the essential principles of emerging methodologies for performance-based evaluation and design of retaining structures.

The increasing awareness of the high intensity of shaking we need to consider for seismic design of retaining structures also accelerated the process of incorporating the formal treatment of uncertainty with respect to seismic hazard and fragility in geotechnical structures (Iai et al., 2008). The methodology currently at the emerging state, not fully established or implemented yet, may be summarized as follows:

For ordinary retaining structures where primary objectives and functions are for commercial use, serviceability and economy become high priority issues and the methodology based on life-cycle cost has potential advantages over the conventional seismic design. In this methodology, failure is defined as the state where a structure does not meet the limit state or acceptable damage level. Probability of failure over design working life is computed based on fragility curve(s) and a seismic hazard curve. The fragility curve(s) reflect uncertainty in geotechnical and structural conditions. The seismic hazard curve allow consideration of ground motions with all (or varying) return periods. The performance is evaluated in terms of expected loss due to earthquake induced damage that reflects the consequence of failure. Life-cycle cost properly represents the trade-off between the initial construction cost and the expected loss. The design option that gives the minimum life-cycle cost is the optimum in terms of overall economy.

Apart from the ordinary retaining structures, higher priority should be assigned for safety if the retaining structures are essential parts of post-earthquake emergency strategies for recovery and restoration of urban areas as planned by local, regional, or federal governments. The methodology based on the life-cycle cost still plays an important role for arriving at the optimum design from the design options that have been already confirmed to meet the performance objectives of emergency facilities or safety requirements.

CONCLUSIONS

An overview of development over these 20 years is given for seismic design and performance of retaining structures.

For retaining structures with dry soil, seismic earth pressures may be more adequately evaluated through a generalized methodology that is based on the multiple-sliding plane concept using both the peak strength, for defining slip plane, and the residual strength, for evaluating earth pressure associated with the slip plane. The earth pressures evaluated using the residual internal friction angle in the conventional design practice may be too conservative especially in designing for the conditions with a high seismic coefficient.

Many of the assumptions made in the conventional seismic design, successfully applicable to retaining walls with dry soil, become questionable when the soil is submerged. Adequate characterization of the undrained behavior of sand under transient and cyclic loads is needed. The mechanism of seismic damage to retaining structures with submerged soil is due to the cumulative increase in the shear strain induced in the soil around the retaining structures rather than due to the slip failure often seen with dry soil.

Initial stress state of soil-retaining structure systems before the earthquake, often ignored in the simplified seismic design practice, can have a significant effect on the performance of the wall during earthquakes. Adequate evaluation of initial stress conditions before the earthquake is essential for seismic design of retaining structures.

A new methodology based on the concept of performance has been emerging and studied through corrective efforts of experts in earthquake geotechnical engineers. Hopefully this trends will continue to eventually lead us to a more adequate design methodology of retaining structures in the coming decades.

REFERENCES

Ebeling, R.M. & Morrison, E.E.Jr. (1992) "*The Seismic Design of Waterfront Retaining Structures,"* US Army Corps of Engineers, Waterways Experiment Station, 1-256.

Franklin, A.G. & Chang, F.K. (1977) "*Earthquake resistance of earth and rockfill dams, Report 5: Permanent displacements of earth dams by Newmark analysis,"* US Army Corps of Engineers, Waterways Experiment Station, 2-71-17.

Hardin, B.O. & Drnevich, V.P. (1972). "Shear modulus and damping in soils: design equation and curves," *Journal of Soil Mechanics and Foundations Division, ASCE,* 98(SM7), 667-692.

Iai, S., Matsunaga, Y. & Kameoka, T. (1992). "Strain space plasticity model for cyclic mobility," *Soils and Foundations,* 32(2), 1-15.

Iai, S. (1998). "Seismic analysis and performance of retaining structures," *Geotechnical Earthquake Engineering and Soil Dynamics III. , Geotechnical Special Publication No.75, ASCE*, 1020-1044.

Iai, S., Ichii, K., Liu, H. & Morita, T. (1998). "Effective stress analyses of port structures," *Soils and Foundations, Special Issue on Geotechnical Aspects of the January 17 1995 Hyogoken-Nambu Earthquake,* 2, 97-114.

Iai, S. (2005). "International standard (ISO) on seismic actions for designing geotechnical works - An overview," *Soil Dynamics and Earthquake Engineering,* 25, 605-615.

Iai, S., Tobita, T. & Tamari, Y. (2008). "Seismic performance and design of port structures," *Geotechnical Earthquake Engineering and Soil Dynamics VI, Geotechnical Special Publication 181, ASCE*, 1-16.

Ishihara, K. & Li, S. (1972). "Liquefaction of saturated sand in triaxial torsion shear test," *Soils and Foundations,* 12(2), 19-39.

Ishihara, K. (1985). "Stability of natural deposits during earthquakes," *Proceedings of 11th International Conference on Soil Mechanics and Foundation Engineering,* San Francisco, Balkema, 327-376.

Japan_Port_and_Harbour_Association_(ed.) (1989) *Technical Standards for Port and Harbour Facilities in Japan, English version (1991) by the Overseas Coastal Area Development Institute of Japan*, 1-438.

Kameoka, T. & Iai, S. (1993) "*Numerical analyses on the effects of initial stress conditions on seismic performance of sheet pile quay walls,"* Technical Note of Port and Harbour Research Institute, No.751 (in Japanese)

Koseki, J., Tatsuoka, F., Munaf, Y., Tateyma, M. & Kojima, K. (1998). "A modified procedure to evaluate active earth pressure at high seismic loads," *Soils and Foundations, Special Issue on Geotechnical Aspectsof the January 17 1995 Hyogoken-Nambu earthquake No.2*, 209-216.

Miwa, S., Ozutsumi, O., Ikeda, T., Oka, Y. & Iai, S. (2003). "Evaluation of earthquake damage to sheet pile type quay walls by effective stress analysis considering initial stress condition," *Proc. of Structural Engineering, JSCE,* 49A, 369-380.

Mononobe, N. (1924). "Considerations on vertical earthquake motion and relevant vibration problems," *Journal of JSCE,* 10(5), 1063-1094 (in Japanese).

Nadim, F. & Whitman, R.V. (1983). "Seismically induced movement of retaining walls," *Journal of Geotechnical Engineering, ASCE,* 109(GT7), 915-931.

Newmark, N.M. (1965). "Effects of earthquake on dams and embankments," *Geotechnique, 5th Rankine lecture,* 15(2), 139-160.

Okabe, N. (1924). "General theory on earth pressure and seismic stability of retaining wall and dam," *Journal of JSCE,* 10(6), 1277-1323.

Peck, R.B. (1990). "Fifty years of lateral earth support," *Design and Performance of Earth Retaining Structures, Geotechnical Special Publication No.25, ASCE*, 1-7.

PIANC (2001) *Seismic Design Guidelines for Port Structures*, International Navigation Association, Balkema, 1-474.

Prakash, S., Wu, Y. & Rafnsson, E.A. (1995). "On seismic design displacements of rigid retaining walls," *Proc. 3rd Int. Conf. on Recent Advances in Geotechnical Earthquake Engineering and Soil Dynamics,* St. Louis, 1183-1192.

Richards, R.Jr. & Elms, D. (1979). "Seismic behavior of gravity retaining walls," *Journal of Geotechnical Engineering, ASCE,* 105(GT4), 449-464.

Rowe, P.W. (1952). "Anchored sheetpile walls," *Proc. Institution of Civil Engineers, Part 1,* 1, 27-70.

Seed, H.B. & Whitman, R.V. (1970). "Design of earth retaining structures for dynamic loads," *ASCE Specialty Conference on Lateral Stresses in the Ground and Design of Earth Retaining Structures*, 103-147.

Steedman, R.S. & Zeng, X. (1996). "Rotation of large gravity walls on rigid foundations under seismic loading," *Analysis and Design of Retaining Structures against Earthquakes,* ASCE Geotechnical Special Publications 60, 38-56.

Terzaghi, K. (1955). "Evaluation of coefficients of subgrade reaction," *Geotechnique,* 5(4).

Towhata, I. & Islam, S. (1987). "Prediction of lateral movement of anchored bulkheads induced by seismic liquefaction," *Soils and Foundations, JGE,* 27(4), 137-147.

Whitman, R.V. & Liao, S. (1984). "Seismic design of gravity retaining walls," *Proc. 8th World Conference on Earthquake Engineering,* San Francisco, 533-540.

Whitman, R.V. (1991). "Seismic design of earth retaining structures," *Proc. of the Second International Conference on Recent Advances in Geotechnical Earthquake Engineering and Soil Dynamics,* St. Louis, 1767-1778.

Seismic Response of Retaining Wall with Anisotropic backfills

Bo Li[1], Xiangwu Zeng[2] and Haiyan Ming[3]

[1]Dept. of Civil Engineering, Case Western Reserve University, Cleveland, Ohio, 44106-7201, USA; PH (216)392-5978; Fax: (216)368-5229; Email: bxl102@case.edu

[2]Dept. of Civil Engineering, Case Western Reserve University, Cleveland, Ohio, 44106-7201, USA; PH (216)368-2950; Fax: (216)368-5229; Email: xxz16@case.edu

[3]Dept. of Civil Engineering, Shenzhen University, Shenzhen, 518060, China; PH (0755)2673-2830; Fax (0755)2653-4233; Email: Haiyan_ming@hotmail.com

ABSTRACT

In this study, eight earthquake centrifuge tests were performed on a model of a cantilever retaining wall to study the seismic response of a retaining wall with anisotropic backfills. A special rigid container was designed and used to prepare models with different directions of soil deposition. The eight centrifuge models had 0, ±45 and 90 degrees of sand deposition angles and with dry or saturated backfills. It was shown that the fabric anisotropy had a strong effect on the settlement of backfill and the response of the retaining wall. It was also clear that the acceleration in the soil was sensitive to the fabric anisotropy of granular materials.

1. INTRODUCTION

Failures of retaining walls have occurred many times during earthquakes, especially for port structures and bridge abutments. Based on the results of many laboratory tests and numerical analyses, fabric anisotropy of soil grains has significant influence on soil behavior. As a result, many researchers realized the importance of soil anisotropy. Meryerhof (1978) extended the theory of ultimate bearing capacity of shallow foundation on homogeneous isotropic soil to anisotropic cohesionless soils semi analytically. Cheng-Der Wang (2007) developed an analytical solution of lateral force induced by rectangular surcharge loads on a cross anisotropic soil. Arthur (1972, 1975) and Oda (1972, 1977, and 1979) studied anisotropic effect systematically using conventional lab tests and obtained some useful results. Guo (2008) used a new type of container to characterize strength variation of anisotropic sand in direct shear tests. Li and Dafalias (2000, 2002) incorporated fabric tensor concept into a constitutive model to simulate the anisotropic effect of granular material. However, there are hardly any real field data available to analyze the influence of anisotropy on response of retaining wall during earthquakes. Thus, verification and validation of design principles and numerical simulations have to rely on physical data obtained in full scale field tests or scaled centrifuge model test. Data from centrifuge tests have been used in recent years to study the mechanism of response and to verify the results of numerical simulations for seismic soil structure interactions in a number of important projects. For example, research was conducted to study the seismic response of a cantilever wall with dry or saturated backfill using centrifuge modeling and numerical simulation (Madbhushi and Zeng, 2006 and 2007).

In this project, eight scaled centrifuge model tests were conducted on a cantilever retaining wall model. Of these eight tests, four tests were conducted with dry backfills while the other four had saturated backfills. The angles of soil deposition were 0, ±45 and 90 degrees, respectively.

2. TEST PROGRAM

2.1 Toyoura Sand

Toyoura sand was used in the model tests, which has been widely used in the laboratory to study the effect of fabric anisotropy. The index properties of the sand are shown in Table 1.

Table 1. Index properties of Toyoura Sand

Parameter	Value
Particle shape	Angular or Subangular
C_u	1.59
C_c	0.96
Specific gravity	2.65
D_{50}	0.17
D_{10}	0.16
Max. Void Ratio	0.98
Min. Void Ratio	0.60

2.2 Testing Facility and Model Container

The centrifuge tests reported here were conducted on the geotechnical centrifuge at Case Western Reserve University that has an effective radius of 1.37m. The centrifuge payload capacity is 20 g-ton with a maximum acceleration of 200g for static tests and 100g for dynamics tests. The rigid box used in this test consists of 5 removable rectangular aluminum plates. The internal dimensions of the box are 53.3 cm (length) × 24.1 cm (width) × 17.7 cm (height). The centrifuge is equipped with a hydraulic shaker designed by the TEAM Corporation. The direction of shaking is perpendicular to the vector of rotation of the centrifuge. Before conducting the model tests a calibration test was performed on the box so as to simulate the earthquake that would have the desired amplitude and frequency. In theory a hydraulic shaker should be able to generate a specified earthquake. The earthquake simulated by the shaker was recorded by an accelerometer fixed on the shake table.

In this project, it was recognized that the use of a flexible-wall container was undesirable since there was an unbalanced lateral pressure on the model container. The explanation was reported by Kawai (1998). Therefore, a rigid model container made of aluminum was designed and manufactured for this project. As stated by Kawai (1998), to minimize the shear distortion, the container was design to be as rigid as possible. The container had removable end walls and a removable cover so that they can be taken out during model preparation. Hence sand deposition in the model in any specific direction can be made. Here the deposition angle defined in this project is shown in Figure 1. The models with ±45 degree deposition angles are presented in Figure 2. The model preparation procedures were reported by Zeng et al. (2009). The test configuration and schematic section of a model is shown in Figure 3.

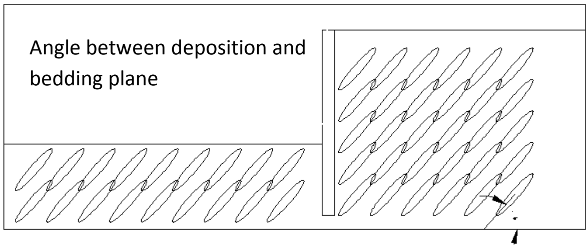

Fig. 1 Definition of deposition angle

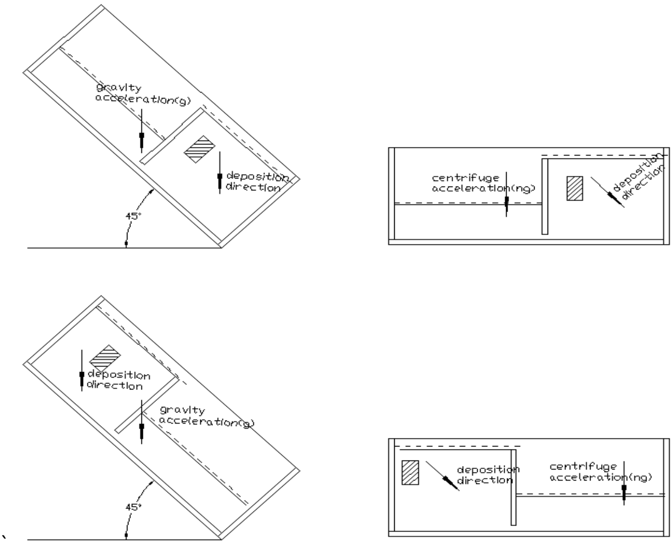

(a) Model preparation in ±45 degree (b) Model testing in ± 45degree

Fig. 2 Sketch of centrifuge models

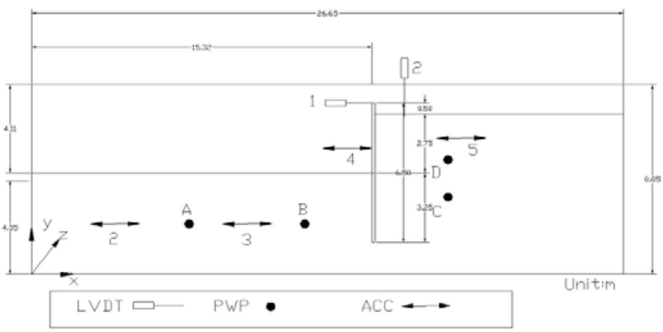

Fig. 3 Sketch of a centrifuge model (in prototype scale)

3. SELECTED RESULTS AND ANALYSIS

The input motion used in the tests is shown in Figure 4.

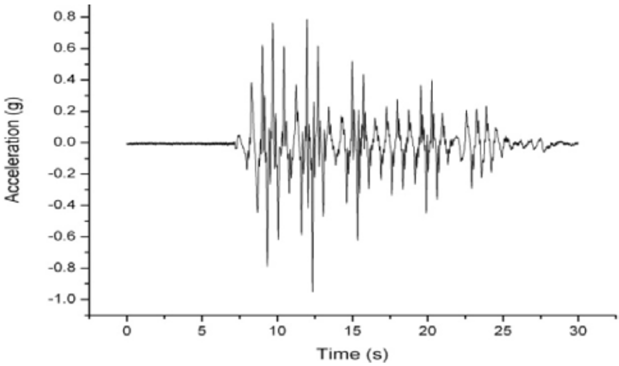

Fig. 4 Typical input acceleration

3.1 Effect of Fabric Anisotropy on Acceleration in the Model

The recorded acceleration time histories at the same location ACC3, which was located near the retaining wall in passive area about 1.25 m below the ground surface, in the saturated tests were illustrated in Figure 5. For the cases of 0, +45 and -45 degree, there was a sudden drop in the positive acceleration together with spikes in the negative direction but not in the case with 90 degree soil deposition angle. In contrast, the acceleration response of ACC5 which was located in the backfill behind the retaining wall was more symmetric for all models as shown in Figure 5. Therefore, the effect of fabric anisotropy was more significant near the retaining wall in the passive area.

To quantify the similarity and difference between models with soil deposition angles of 0, ±45 and 90 degrees, a correlation analysis between models was conducted and the results are summarized in Tables 2 and 3. The theory and procedures for a correlation analysis was described by Rangarao et al. (2005).

Table 2. Normalized correlation of acceleration by ACC 3 in saturated tests

Model types	0°	45°	90°	-45°
0°	0.87(repeat)	0.69	0.77	0.72
45°	0.69	—	0.57	0.47
90°	0.77	0.57	—	0.78
-45°	0.72	0.47	0.78	—

Table 3. Normalized correlation of acceleration by ACC 3 in dry tests

Model types	0°	45°	90°	-45°
0°	0.88(repeat)	0.87	0.81	0.76
45°	0.87	—	0.7	0.65
90°	0.81	0.7	—	0.89
-45°	0.76	0.65	0.89	—

As shown in Tables 2 and 3, the tests in each group have different results. The repeated test at 0 degree had the highest correlation coefficient, indicating a good repeatability. The most similar cases were the tests with 90 degree and -45 degree deposition angle with correlation coefficients of 0.78 and 0.89, respectively. On the other hand, the biggest difference existed between the cases with +45 and -45 degree deposition angles. The correlation coefficient was only 0.47 for the saturated tests. Similarly, for the dry models, the correlation coefficient was also minimum (0.65) between models with soil deposition angles of +45 and -45 degrees. The difference was more amplified from 0.65 in dry tests to 0.47 in saturated tests. As a result, these types of similarity or difference were reflected in the displacements recorded.

3.2 Effect of Fabric Anisotropy on Pore Water Pressure

For the four saturated tests, the recordings of PPT B and PPT C were presented here to show the influence of fabric anisotropy. As shown in Figure 6, PPT C in the model with 90 degree deposition angle had much higher pore pressure ratio than in the other three tests, where PPT C was located in lower part of backfill. In the same tests, PPT B which was located in passive area recorded similar high excess pore pressures in all the cases with the 45 degree model showed more cyclic variation. For this case, the model with a soil deposition angle of -45 degree had the smallest excess pore pressure buildup. The small amount of excess pore pressure recorded by PPT C may be caused by the large shear deformation in the region, as the failure zone in the backfill passed through there.

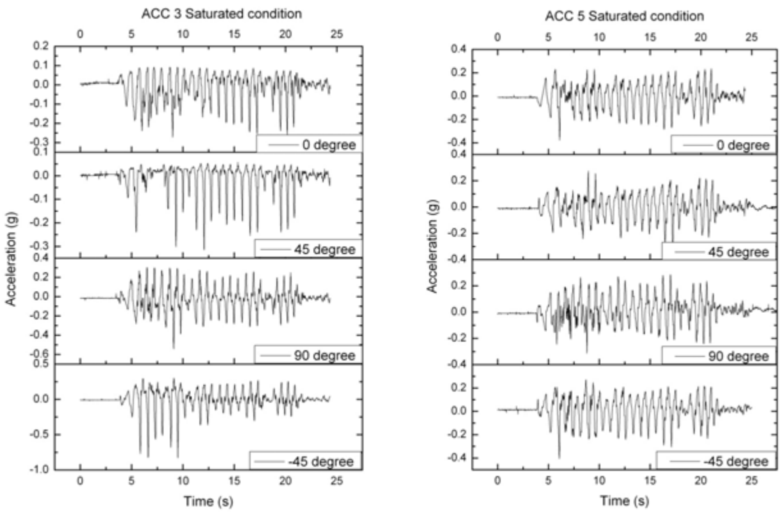

Fig. 5 Recorded time histories of ACC3 and ACC5

3.3 Effect of Fabric Anisotropy on Displacement

At the first stage of the project, the case of models with 0, +45 and 90 degree deposition angle were examined. We found the maximum horizontal displacement of retaining wall was 23 cm and maximum settlement of backfill was 12.9 cm in the dry case for the model with a soil deposition angle of +45 degrees. Since the failure zone in the backfill had an approximate 45 degree inclination, the model with +45 degree was the worst case among the tests. Typically, the soil was the strongest in the direction of soil deposition and the weakest in the direction perpendicular to the direction of deposition. Then the case with a soil deposition angle of -45 degree would be the strongest with the smallest deformation. Therefore, model tests with soil deposition angle of -45 degree were added to verify this hypothesis. The cross-sectional views of case ±45 degree models before and after earthquake tests are shown in Figures 7 and the displacements of eight tests were also summarized in Table 4. As observed in Table 4, the dry and saturated model with -45 degree angle of deposition had less settlement in the backfill and wall displacement than the model with a +45 degree angle of soil deposition. This difference in settlement was even more obvious in the saturated case, indicating the strong influence of anisotropy of backfill soil on the seismic response.

4. SUMMARIES AND CONCLUSIONS

Centrifuge tests were conducted to study the effect of fabric anisotropy of Toyoura sand on the seismic response of a retaining wall. The acceleration time histories, excess pore water pressure, the horizontal displacement of the retaining wall and settlement of the backfill in cases of 0, ±45 and 90 degrees of soil deposition angle and with both dry and saturated backfills were investigated.

The results of the tests reported here show:

(1) The differences in experimental results between the tests with different deposition angles clearly indicated the influence of anisotropic backfill on the seismic response of a cantilever wall.

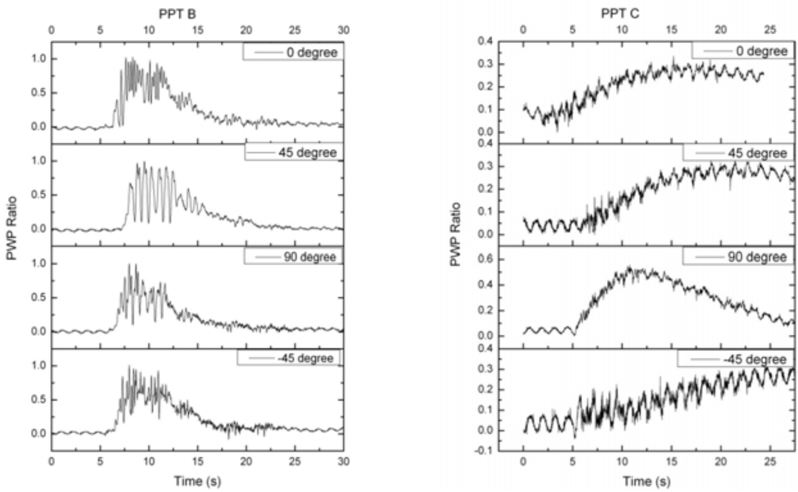

Fig.6 Time histories of excess pore water pressure

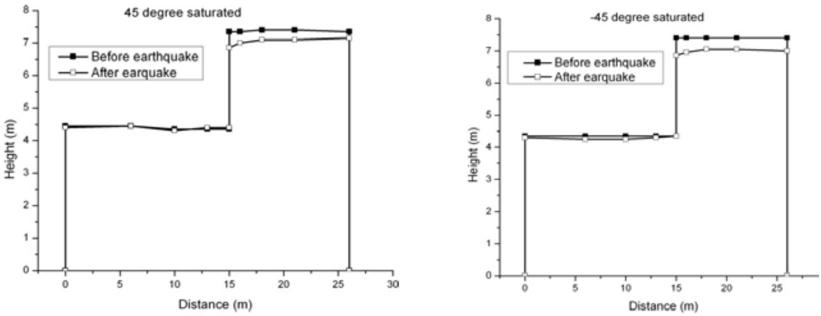

Fig. 7 Cross-sectional views of the models in ±45 degree saturated tests

Table 4 Summary results of deformation (in prototype scale)

Test No.	Deposition Angle (degree)	Dry/Sat	Relative Density (%)	Max. Disp. of wall (cm)	Max. Settlement of backfill (cm)
1	0	Sat	35	75	70
2	45	Sat	38	75	65
3	90	Sat	33	50	110
4	-45	Sat	35	50	55
5	0	Dry	40	12.7	8.5
6	45	Dry	35	23	12.9
7	90	Dry	33	18.2	11.5
8	-45	Dry	33	11.6	10.6

(2) The correlation analysis of the recording of ACC 3 shows that the most similar case was between case of 90 degree and -45 degree in both dry and saturated conditions, while the biggest difference existed between case of +45 and -45 degree in both conditions

(3) The excess pore water pressure buildup is more significant in the model with 90 degree deposition angle and smallest in -45 degree deposition.

(4) The settlement of backfill and the displacement of the wall in -45 degree angle of deposition cases was much less than in the model with 45 degree angle of deposition, especially in the saturated case. Thus the effect of anisotropy was most significant with these two deposition angles.

ACKNOWLEDGMENT

The first author would like to acknowledge the support provided by the Saada Family Graduate Fellowship for the work reported here. The research work report here was also partially supported by Natural Science Foundation of China, Grant No. 50678103 and Provincial Natural Science Foundation of Guangdong, China, Grant No. 7009408.

REFERENCES

Arthur, J.R.F. & Menzies, B.K. 1972. "Inherent anisotropic in sand." Geotechnique 22 (1), 115-128.

Arthur, J.R.F. & Philips, A.B. 1975. "Homogeneous and layered sand in triaxial compression." Geotechnique 25 (4), 799-815.

Guo, Peijun 2008. "Modified direct shear test for anisotropic strength of sand." Journal of Geotechnical and Geoenvironmental Engineering, ASCE 134 (9), 1311-1318

Kawai, T., & Kanatani, M. 1998. "Seismic performance of a caisson type seawall with an armored embankment." Proceedings, Centrifuge 98, 351-358.

Li, X. S. & Dafalias, Y. F. 2000. "Dilatancy for cohesionless soil." Geotechnique 50(4), 449-460.

Li, X. S. & Dafalias, Y. F. 2002. "Constitutive modeling of inherently anisotropic sand behavior." Journal of Geotechnical and Geoenvironmental Engineering, ASCE 128(10), 868-880.

Madabhushi, S.P.G., and X. Zeng, 2007 "Simulating Seismic Response of Cantilever Retaining Walls." Journal of Geotechnical and Geoenvironmental Engineering, ASCE 133(5), 539-549

Madabhushi, S.P.G., and X. Zeng, 2006 "Simulating Seismic Response of Flexible Cantilever Retaining Walls with Dry Backfill." Geomechanics and Geoengineering: An International Journal 1(4), 275-290

Meryerhof, G.G. 1978. "Bearing capacity of anisotropic cohesionless soils." Can. Geotech. J. 15(4), 592-595.

Oda, M. 1972. "Initial fabrics and their relation to mechanical properties of granular material." Soil and Foundations 12(1), 17-36.

Oda, M. & Koishikawa, I. 1977. "Anisotropic fabric of sands." 9th International Conference on Soil Mechanics and Foundation Engineering, Tokyo, Japan, Vol. 1,235-238

Oda, M. 1979. "Effect of Strength Anisotropy on Bearing Capacity of Shallow Footing in a Dense Sand." Soils and Foundations19 (3), 15-28.

Rangarao, Kaluri V. & Mallik, R.K. 2005. "Digital signal processing-a practitioner's approach." John Wiley & Sons, New York.

Wang, Chang-der 2007. "Lateral force induced by rectangular surcharge loads on a cross anisotropic backfill." Journal of Geotechnical and Geoenvironmental Engineering, ASCE 133 (10), 1259-1276.

Zeng, X., Li, B., and Min. H., 2010. "Effect of fabric anisotropy on seismic response of a retaining wall." Proceedings of the 7th International Conference on Physical Modelling in Geotechnics, Zurich, June 28- July 1.

ON SEISMIC DESIGN OF RETAINING WALLS

Yingwei Wu

Geotechnical Engineer, HNTB Corporation, Kansas City, Missouri, USA

Shamsher Prakash

Emeritus Professor, Civil Engineering Missouri S&T, Rolla, Missouri, USA

Vijay K. Puri

Professor, Civil and Environmental Engineering, Southern Illinois University, Carbondale, USA

ABSTRACT

Retaining walls have failed either by sliding away from the backfill or due to combined action of sliding and rocking displacements, during earthquakes. Performance based design of the retaining walls in seismic areas must account for these displacements, in addition to the usual factors of safety against failure in bearing, sliding and overturning. A realistic model for estimating dynamic displacement, which accounts for the combined action of sliding and rocking and takes into consideration, non-linear stiffness of soil and geometric and material damping and coupling effects is now available, Wu and Prakash (2009). This model has been used to calculate the displacement for several combinations of backfill and foundation soil conditions. Based on this study, typical design charts for preliminary design have been proposed.

1. INTRODUCTION

Retaining walls have failed during earthquakes by sliding away from the backfill or due to combined action of sliding and rocking displacements. Performance based design of the retaining walls in seismic areas must account for the likely displacements, the retaining wall may experience during an earthquake, in addition to calculating the usual factors of safety against failure in bearing capacity, sliding and overturning. A realistic model for estimating the dynamic displacement must account for the combined action of sliding and rocking vibrations and considering 1) non-linear soil stiffness 2) non-linear geometrical and material damping and 3) non-linear coupling effects.

This model has been developed by Wu (1999) and Design charts have been developed for performance based design. For further details see Wu and Prakash (2001, 2009 and 2010).

2. TYPICAL RESULTS

A wall 4m high (Figure 1) with granular backfill and foundation soil is used for illustration of typical results subjected to Northridge earthquake of January 17, 1994 (Figure 1). The displacements were computed on the assumption that the base width has been designed as for field condition 1(Table 1) and displacements computed for Northridge earthquake for field conditions 1 through 7. Nonlinear soil modulus and strain-dependant dampings are used in this solution.

Field conditions 1 through 4 have been specified in Eurocode 8 (1994). Field Conditions 3 and 4 refer primarily to quay walls and are outside the scope of present work. Conditions 5 and 6 refer to full saturation of backfill and earth pressure must be reduced by an appropriate drainage as a necessary design condition. Thus conditions 1, 2 and 7 are only important for these studies. The magnitude of this earthquake is M 6.7 and peak ground acceleration is 0.344g. Figure 3 shows displacements of the 4m high wall under 7 field conditions. Table 2 lists these displacements, for conditions for 1, 2 and 7 only.

Table 1: Loading conditions and corresponding parameters for dynamic displacements
(γ - Unit Weight, α_h and α_v - Horizontal and Vertical Seismic coefficients, P_{wd} - Hydrodynamic Pressure)

	Field Condition	Parameters for	
		Static Condition	Dynamic Condition
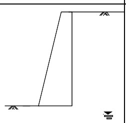	**Condition 1** moist backfill moist foundation soil	$\gamma^* = \gamma_t$ $P_{ws} = 0$	$\gamma^* = \gamma_t$ $\Psi = tan^{-1}\left(\frac{\alpha_h}{1 \mp \alpha_v}\right)$ $P_{wd}(t) = 0$
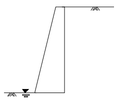	**Condition 2** moist backfill saturated foundation soil	$\gamma^* = \gamma_t$ $P_{ws} = 0$	$\gamma^* = \gamma_t$ $\Psi = tan^{-1}\left(\frac{\alpha_h}{1 \mp \alpha_v}\right)$ $P_{wd}(t) = 0$
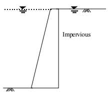	**Condition 3** submerged with impervious backfill	$\gamma^* = \gamma_{sat} - \gamma_w$ $P_{ws} = 0$	$\gamma^* = \gamma_{sat} - \gamma_w$ $\Psi = tan^{-1}\left(\frac{\gamma_{sat}}{\gamma_{sat} - \gamma_w} \frac{\alpha_h}{1 \mp \alpha_v}\right)$ $P_{wd}(t) = 7/12 \times \alpha_h \times \gamma_w \times H'$
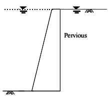	**Condition 4** submerged with pervious backfill	$\gamma^* = \gamma_{sat} - \gamma_w$ $P_{ws} = 0$	$\gamma^* = \gamma_{sat} - \gamma_w$ $\Psi = tan^{-1}\left(\frac{\gamma_d}{\gamma_{sat} - \gamma_w} \frac{\alpha_h}{1 \mp \alpha_v}\right)$ $P_{wd}(t) = 2 \times 7/12 \times \alpha_h \times \gamma_w \times H'$
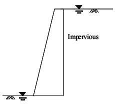	**Condition 5** perched with impervious backfill	$\gamma^* = \gamma_{sat} - \gamma_w$ $P_{ws} = \frac{1}{2} \times \gamma_w \times H^2$	$\gamma^* = \gamma_{sat} - \gamma_w$ $\Psi = tan^{-1}\left(\frac{\gamma_{sat}}{\gamma_{sat} - \gamma_w} \frac{\alpha_h}{1 \mp \alpha_v}\right)$ $P_{wd}(t) = 0$
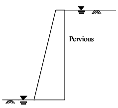	**Condition 6** perched with pervious backfill	$\gamma^* = \gamma_{sat} - \gamma_w$ $P_{ws} = \frac{1}{2} \times \gamma_w \times H^2$	$\gamma^* = \gamma_{sat} - \gamma_w$ $\Psi = tan^{-1}\left(\frac{\gamma_d}{\gamma_{sat} - \gamma_w} \frac{\alpha_h}{1 \mp \alpha_v}\right)$ $P_{wd}(t) = 7/12 \times \alpha_h \times \gamma_w \times H'$
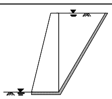	**Condition 7** perched with sloping drain	$\gamma^* = \gamma_{sat}$ $P_{ws} = 0$	$\gamma^* = \gamma_{sat}$ $\Psi = tan^{-1}\left(\frac{\alpha_h}{1 \mp \alpha_v}\right)$ $P_{wd}(t) = 0$

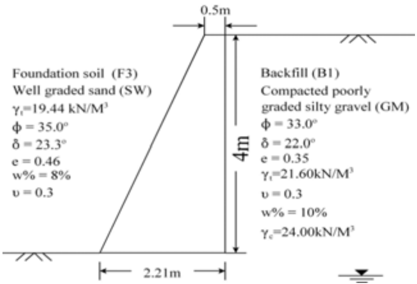

Figure 1a: Dimension of 4m high wall and soil properties used (γ_c – unit weight of concrete)

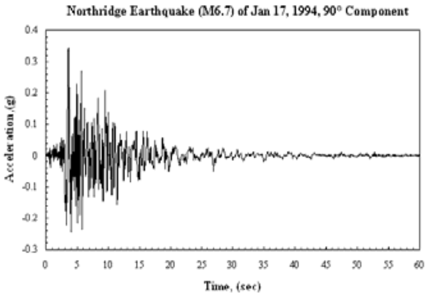

Figure 1b: Acceleragram of Northridge earthquake of Jan. 17, 1994, 90° Component

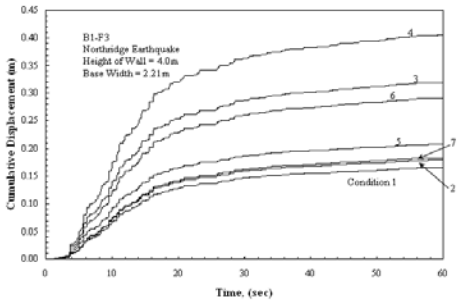

Figure 2: Computed displacement for 4m high wall and conditions 1 through 7 of Table 1

Table 2: Displacement of 4m high wall for Field Condition 1, 2,and 7

Field Condition	Displacement				%of Height
	Sliding	Rocking		Total (top)	
		Rotation	Translation		
	m	Heel, degree	m	m	
1	0.0622	1.48	0.1034	0.1656	4.1
2	0.0667	1.61	0.1126	0.1793	4.5
7	0.0682	1.64	0.1148	0.1830	4.6

An examination of Table 2 indicates that sliding displacements are close to 30 - 40 percent of the total displacement. According to Eurocode, the permissible displacement is 10.32cm (300×α_{max}, where α_{max} is 0.344 in Northridge earthquake). For practical design field conditions 1and 2 and for saturated soils but with a sloping drain in condition 7 are appropriate.

3. SOIL AND WALL HEIGHTS USED TO DEVELOP DESIGN CHARTS

Wu (1999) has studied seven soil conditions for foundation soil F1-F7 and three soils for backfill B1-B3. Thus 21 combinations for foundation and backfills soils were investigated (Table 3). Rigid walls heights investigated are 4m, 5m, 6m, 7m, 8m, 9m, and 10m. Table 5 lists cumulative displacements for B3-F4.

Table 3. Engineering properties for both foundation soil and backfill (Wu, 1999)

FOUNDATION SOIL (F)

F	Soil Type	γ_d kN/M^3	φ deg	δ deg	void ratio	v	c kN/M^2	PI	W%
F-1	GW	21.07	37.5	25.0	0.25	0.3	-	-	6
F-2	GP	19.18	36.0	24.0	0.36	0.3	-	-	6
F-3	SW	18.00	35.0	23.3	0.46	0.3	-	-	8
F-4	SP	16.82	34.0	22.7	0.56	0.3	-	-	10
F-5	SM	15.70	33.0	22.0	0.68	0.3	-	4	15
F-6	SC	14.00	30.0	20.0	0.88	0.3	-	13	25
F-7	ML	14.15	32.0	21.3	0.85	0.3	9.57	4	14

BACKFILL (B)

B	Soil Type	γ_d kN/M^3	φ deg	δ deg	void ratio	v	c kN/M^2	PI	W%
B-1	GM	19.6	33.0	22.0	0.35	0.3	-	-	10
B-2	GP	18.9	34.0	22.7	0.40	0.3	-	-	8
B-3	SP	15.6	34.0	22.7	0.69	0.3	-	-	8

*All properties of backfill are for the condition of 90 percent of the “Standard Proctor”.

4. VERTICAL VS INCLINED WALLS

In order to economize on design of walls, several cases of 6.0 m high retaining walls were analyzed for typical cases of foundation soil condition varying from well graded gravel (GW) to silt (ML) and the backfill soil varying from silty gravel (GM) to poorly graded sand (SP). Ground motions corresponding to El Centro, Loma Prieta and North Ridge earthquakes were used in the analysis. Typical case of a reference retaining wall 6.0 m high with nine different inclination angles of the wall face in contact with the backfill ‘α’ (0°, 1.25°, 2.5°, 3.75°, +5°, -1.25°, -2.5°, -3.75°, and -5°) subjected to Northridge earthquake is used for illustration. The negative angle at the back of the wall is the case of the wall resting on the backfill. Figure 3 shows cumulative displacement of the retaining wall away from the backfill due to combined sliding and rocking effects for $\alpha = -5^{\circ}, 0^{\circ}$ and $+5^{\circ}$ for a base width of 3.57 m. The foundation soil for this case was well graded sand (SW) and the backfill consisted of submerged silt gravel (GM). It can be observed from this figure that the negative values of ‘α’ result in somewhat smaller cumulative displacements compared to the case of vertical wall face (α = 0) or for positive value of α within the range considered Similar results were observed for other cases also. It, therefore, appears that retaining walls may be designed for permissible displacement for sliding only and then be built resting by a few degrees on the backfill as explained below. In this case this tilt is about 1.31° (Table 4).

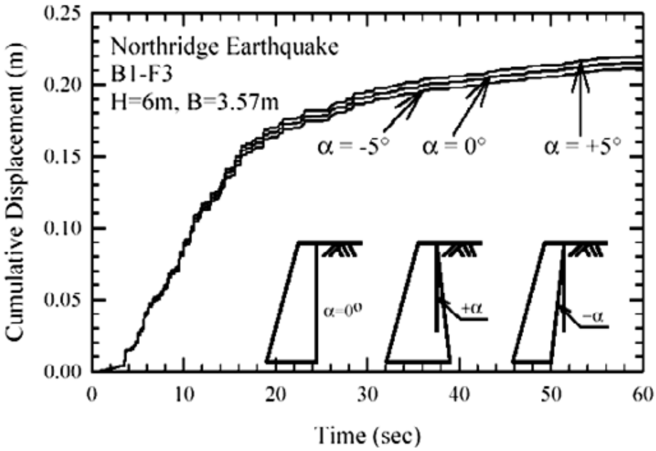

Fig: 3. Cumulative displacements of walls (B1-F3) with different inclinations with the vertical

Table 4.Cumulative displacement for several angles of inclination of the back of the wall subjected to Northridge earthquake condition (B=3.57m).

α angle (degree)	Base width (m)	Cumulative Displacement by Fixed Base Width (3.57m)			
		Sliding (m)	Rocking (degree)	Rocking (m)	Total (m)
+5.00°	3.81	0.08	1.31	0.13	0.21
+3.75°	3.76	0.08	1.30	0.13	0.21
+2.50°	3.70	0.08	1.30	0.13	0.21
+1.25°	3.63	0.08	1.29	0.13	0.21
0.00°	3.57	0.08	1.29	0.13	0.21
-1.25°	3.50	0.08	1.28	0.13	0.21
-2.50°	3.43	0.08	1.27	0.13	0.21
-3.75°	3.35	0.08	1.26	0.13	0.21
-5.00°	3.38	0.08	1.25	0.13	0.21

Table 4 shows a summary of new base widths and computed displacement for various inclinations. The computed cumulative sliding, rocking and total displacements are also shown in this table. The base widths decreased from 3.57m to 3.38m as the inclination changed from 0° to -5°, since the active earth forces decrease with negative inclination. Therefore, the base width was somewhat smaller for a wall with a negative inclination. The angular rotation in rocking (Table 4) decreased from 1.29° (α=0) to 1.25° (α=-5°), and the total displacements decreased slightly from 0.2155m to 0.2112m. The cumulative displacements for these walls will not be significantly altered by changing the inclination at the back of the wall.

For the wall built as a leaning-type rigid retaining wall with α = -5° lying on the backfill, the wall experienced a rocking movement of 1.25° during the Northridge earthquake. Therefore, when the wall was subjected to the same earthquake event up to 3 or 4 times, the wall experienced a total rocking close to 5°. At this time, the wall may become vertical.

Further analysis was conducted for 21 backfill and foundation soil combinations for a typical reference wall 6m high, subjected to three earthquakes. The backfill soil was varied from silty gravel to poorly graded sand, and the foundation soil varied from well graded gravel to silt of low compressibility.

The results generally indicated that the design widths of foundations for 21 cases of backfill – foundation soil combinations used in analysis generally reduced with values of α from 0° to -5°. This may result in saving of 8 -10 % in the material cost. It is, therefore recommended that rigid walls be constructed with the negative batter in the walls resting on the backfill. In this situation, these can be designed only for sliding displacements.

5. RECOMMENDED DESIGN PROCEDURE

1. Determine the section for static loading condition with FOS=2.5 in bearing, and FOS= 1.5 for sliding and tilting as a rigid body and no tension on the heel.
2. Estimate the sliding displacement from Wu (1999) design charts for comparable backfill and foundation soils and comparable ground motion.
3. Compare these displacements with permissible displacements as per Euro Code ($300 \times \alpha_{max}$).
4. If displacement in step 2 is less than that in step 3, then designs is OK, otherwise revise the sections of the wall for lower FOS in step 1.

6. TYPICAL DESIGN CHARTS

Table 5 lists the sliding and total displacement and rotation of walls 4m-10m high and subjected to 3-good motions of 1) El-Centro1946, 2) Northridge 1994, and 3) Loma Prieta 1979. Similar design charts for all 21 cases of table 3 have been prepared by Wu (1999)

Table 5: Cumulative Displacements for Walls 4 to 10m High with B3-F4 and Field Conditions 1, 2 and 7 (Table 2) subjected to El-Centro, Northridge and Loma-Prieta earthquakes

H and B[1] (m)	Field Con.	Cumulative Displacement								
		El-Centro[2]			Northridge[2]			Loma-Prieta[2]		
		Sliding m	Rocking degree (m)	Total m	Sliding m	Rocking degree (m)	Total m	Sliding m	Rocking degree (m)	Total m
4 (2.09)	1	0.0943	2.59 (0.1808)	0.2751	0.0642	1.67 (0.1164)	0.1806	0.0055	0.11 (0.0077)	0.0132
	2	0.0987	2.75 (0.1922)	0.2909	0.0673	1.79 (0.1248)	0.1922	0.0059	0.12 (0.0083)	0.0142
	7	0.1076	3.04 (0.2124)	0.3200	0.0739	1.99 (0.1386)	0.2125	0.0065	0.13 (0.0093)	0.0157
5 (2.51)	1	0.1113	2.74 (0.2395)	0.3509	0.0769	1.81 (0.1576)	0.2343	0.0073	0.13 (0.0116)	0.0189
	2	0.1156	2.89 (0.2526)	0.3681	0.0802	1.92 (0.1673)	0.2475	0.0078	0.15 (0.0127)	0.0205
	7	01256	3.20 (0.2760)	0.4046	0.0872	2.13 (0.1859)	0.2731	0.0086	0.16 (0.0142)	0.0228
6 (2.92)	1	0.1247	2.79 (0.2926)	0.4173	0.0868	1.87 (0.1955)	0.2823	0.0089	0.15 (0.0160)	0.0249
	2	0.1289	2.92 (0.3063)	0.4352	0.0896	1.97 (0.2060)	0.2956	0.0096	0.17 (0.0173)	0.0269
	7	0.1400	3.23 (0.3384)	0.4784	0.0977	2.18 (0.2283)	0.3260	0.0106	0.19 (0.0195)	0.0301
7 (3.35)	1	0.1359	2.78 (0.3398)	0.4757	0.0948	1.88 (0.2299)	0.3247	0.0106	0.17 (0.0205)	0.0311
	2	0.1399	2.90 (0.3540)	0.4939	0.0987	1.97 (0.2403)	0.3390	0.0114	0.18 (0.0221)	0.0335
	7	0.1519	3.20 (0.3911)	0.5430	0.1073	2.18 (0.2668)	0.3741	0.0215	0.20 (0.0248)	0.0373
8 (3.77)	1	0.1457	2.74 (0.3823)	0.5280	0.1025	1.87 (0.2606)	0.3631	0.0124	0.18 (0.0250)	0.0374
	2	0.1500	2.84 (0.3970)	0.5471	0.1051	1.95 (0.2720)	0.3771	0.0131	0.19 (0.0270)	0.0401
	7	0.1628	3.14 (0.4390)	0.6018	0.1144	2.16 (0.3015)	0.4159	0.0147	0.22 (0.0303)	0.0449
9 (4.19)	1	0.1544	2.68 (0.4209)	0.5754	0.1083	1.84 (0.2886)	0.3969	0.0140	0.19 (0.0296)	0.0436
	2	0.1584	2.77 (0.4356)	0.5941	0.1108	1.91 (0.3001)	0.4109	0.0147	0.20 (0.0319)	0.0466
	7	0.1718	3.07 (0.4817)	0.6536	0.1203	2.12 (0.3327)	0.4259	0.0160	0.23 (0.0358)	0.0519
10 (4.72)	1	0.1608	2.53 (0.4411)	0.6017	0.1123	1.74 (0.3033)	0.4156	0.0151	0.19 (0.0326)	0.0477
	2	0.1648	2.61 (0.4559)	0.6207	0.1153	1.80 (0.3144)	0.4297	0.0157	0.20 (0.0350)	0.0507
	7	0.1785	2.89 (0.5039)	0.6825	0.1250	2.00 (0.3484)	0.4734	0.0172	0.22 (0.0392)	0.0564

[1] H: height of wall, B: base width

[2] Permissible displacements for three earthquakes according to Eurocode = $300 \times \alpha_{max}$

El-Centro = 300*0.349 (mm) = 0.1047m

Northridge = 300*0.344 (mm) = 0.1032m

Loma-Prieta = 300*0.113 (mm) = 0.0339m

7. CONCLUSIONS

The following conclusions are drawn:

1. A realistic displacement model for rigid retaining walls under earthquake condition has been developed.
2. This model considers non-linear soil properties and any water condition behind the wall (Wu 1999).
3. Design charts for wall heights 4m-10m and 21 backfill foundation soils have been developed for use in preliminary design.

8. ACKNOWLEDGEMENT

The manuscript was typed by Khushboo Lall and Reformatted by Raghu Mutnuri, with great care.

9. REFERENCES

EUROCODE 8 (EUROPEAN PRESTANDARD 1994). "Design Provisions for Earthquake Resistance of Structures- Part 5: Foundations, Retaining Structures and Geotechnical Aspects", The Commission of the European Communities.

Wu, Y. (1999). "Displacement-Based Analysis and Design of Rigid Retaining Walls during Earthquakes", Ph.D. Dissertation, Univ. of Missouri-Rolla.

Wu, Y. and Prakash, S. (2001). "Seismic Displacements of Rigid Retaining Walls-state of the art"paper number 705, Proceedings Fourth Intrn Conf Recent Adv in Geot Eq Eng and Soil Dynamics CD ROM, San Diego, March

Wu, Y. and Prakash, S. (2009). "Design of Retaining walls in Seismic Areas "IS Tokyo 2009". Paper No 149, International conference on Performance based Design in Geo Earthquake Engineering (CD-ROM).

Wu, Y. and Prakash, S. (2010). "Design Charts for Retaining Walls in Seismic Areas". Paper No 178 , ASCE Conference . Geo-FL. (CD, ROM).

SEISMIC DEFORMATION OF BACK-TO-BACK MECHANICALLY STABILIZED EARTH (MSE) WALLS

Fransiscus S. Hardianto[1] and Kim M. Truong[2]

[1]The Reinforced Earth Company, 1660 Hotel Circle N, Suite 304, San Diego, CA 92108, USA, phone: 619-688-2400, fax: 619-688-2499, email: fhardianto@reinforcedearth.com
[2]The Reinforced Earth Company, 8614 Westwood Center Drive, Suite 1100, Vienna, VA 22182, USA, phone: 703-821-1175 ext 229, fax: 703-734-5794, email: ktruong@reinforcedearth.com

ABSTRACT

The continuing expansion of HOV lanes and limited right-of-way on urban freeways have led to increased use of back-to-back MSE walls. Because these lanes are often constructed in the existing median, many of the back-to-back structures have small aspect ratios, with the distance between the two walls often less than 0.7 times the wall height. There are no FHWA design guidelines for back-to-back walls closer than 1.2 times the wall height. In this paper, results from dynamic constitutive models are compared to those from the traditional Mononabe-Okabe pseudo-static approach. Compared to the results of conventional design methodology, data from the dynamic analyses show that walls with smaller aspect ratios exhibit greater deformation than walls having a higher aspect ratio, although this trend is obscured at lower accelerations. The study also shows that the current state-of-the-practice pseudo-static method is conservative.

INTRODUCTION

MSE (mechanically stabilized earth) walls are one of the most commonly used earth retaining wall types. The most widely used system uses ribbed steel strip reinforcing elements. More than 30,000 structures are in service worldwide, many of them in high seismic areas. These walls, including some back-to-back walls, have performed well during earthquakes even in the absence of specific seismic design consideration.

Presently, there are no formal design guidelines for narrow back-to-back MSE walls. Federal Highway Administration (FHWA) MSE design guidelines (Publication No. FHWA-NHI-00-043) for low seismic areas ($a < 0.05g$) allows aspect ratios as low as 0.6. For high seismic areas, where the width of back-to-back walls is less than 1.1 times wall height, detailed numerical analyses are required. Current state of the practice uses a modified Mononabe-Okabe pseudo-static method and simplified Newmarks's sliding block model, together with a displacement-based seismic load reduction.

OVERVIEW OF AASHTO METHOD AND FHWA GUIDELINES

The method described in AASHTO Standard Specifications for Highway Bridges (1996, 2002) is based on Mononobe-Okabe's pseudo-static approach considering inertial forces acting on the MSE mass, as shown in Figure 1.

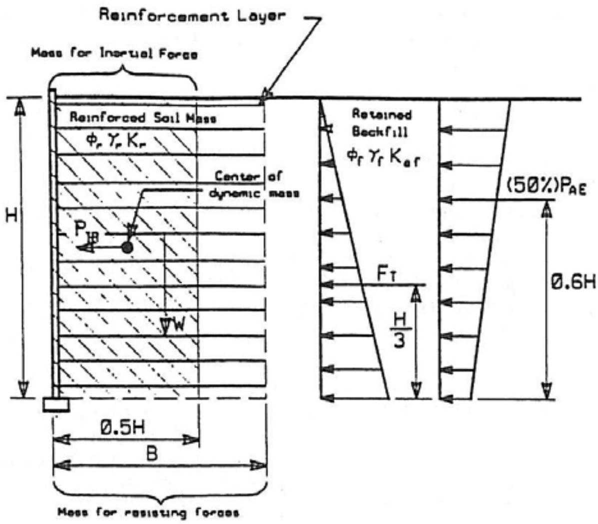

Figure 1. Schematic of seismic design forces for MSE walls

FHWA (2001) categorizes back-to-back MSE walls into two cases. Case 1 involves large aspect ratios, where soil reinforcing strips from each the back-to-back wall do not overlap. Considering the minimum soil reinforcement length of 70 percent of the wall height, the minimum aspect ratio for Case 1 back-to-back walls is 1.4, allowing them to be designed as independent walls.

Case 2 deals with narrower structures, where soil reinforcements overlap and the two walls interact. When the overlap is greater than 30 percent of the wall height there is no active earth thrust from the backfill. The narrow back-to-back MSE walls in this study are categorized as Case 2.

From the point of view of external stability, a back-to-back wall system can be considered as a rigid mass subjected to a seismic inertia force, as shown in Figure 1. The dynamic forces are a function of the maximum horizontal acceleration (A_m) within the MSE wall mass. The value of Am is a function of peak horizontal ground acceleration (A) as follows:

$A_m = (1.45 - A)\,A$ For the range of $A <= 0.45$ (1)

The use of the full value of A_m in Mononobe-Okabe stability evaluations is based on the assumption of zero wall displacement, resulting in overly conservative designs. In the interest of greater economy, AASHTO adopted a simplified version of the Newmark sliding block analysis to modify the horizontal seismic coefficient (k_h) based on inputs of A_m and an acceptable horizontal displacement (Kavazanjian, 1997). The reduced horizontal acceleration coefficient is then:

$$k_h = 1.66 A_m \left(\frac{A_m}{d} \right)^{0.25} \qquad (2)$$

where d = lateral wall displacement in mm

k_h is used in the external stability analyses instead of the full value of A_m.

Internal stability (tension and pullout) is handled conservatively by using a full value of A_m and designing each of the back-to-back walls independently, ignoring soil reinforcement from the opposite wall. The soil reinforcements are designed for the sum of the horizontal forces due to the internal seismic inertial force and the static forces, as described in AASHTO and FHWA.

SEISMIC DEFORMATION AND FIELD PERFORMANCE

Information regarding displacements of MSE walls during earthquakes is very limited. Some post-seismic observations show that although many older MSE walls were not designed for seismic, they performed well during earthquakes; no failures have been reported and most large displacements have been localized.

The Great Hanshin (Kobe) earthquake in 1995 ($a > 0.8g$) caused widespread damage. More than 800 metallically reinforced soil structures were affected, although only 124 structures were inspected after the earthquake. The structures ranged from 1.5 to 16.5 m in height with more than 70% higher than 5 m. Kobayashi et al. (1996) reported that 114 structures were undamaged. Ten structures had some panel cracking, opening of vertical joints, deformation up to 94 mm, and tilting movement of less than 2% of the wall height. These structures are located in areas that suffered relatively heavy damage. Despite the damage, the structures remained functional and structurally intact. From their study Kobayashi et al (1996) concluded that conventional pseudo-static design methods and global stability analyses are conservative.

The Izmit, Turkey earthquake (1999, $a \approx 0.4g$) affected an MSE structure located very close to the epicenter. The wall was designed for a ground acceleration of only 0.1g. The back-to-back ramp structure is 10 m high with an aspect ratio of 1.25. The wall was constructed on untreated alluvial subsoil that was prone to liquefaction. Pamuk et al. (2004) reported that the worst damaged occurred at the top of the wall, where the wall crossed a wide drainage culvert. Wall panels were displaced about 23 to 30 cm, both horizontally and vertically. The vertical ground subsidence appeared to be the significant factor in the damage. Although the bridge adjacent to the MSE walls collapsed, the walls remained stable.

CONSTITUTIVE MODEL

Due to the lack of information on the behavior of back-to-back MSE wall during seismic events and in order to verify whether the current AASHTO pseudo-static approach is appropriate for back-to-back walls, a series of numerical studies were performed to examine the behavior of the walls during earthquake loading. Only MSE walls using ribbed steel reinforcing strips were studied.

The numerical studies were done using a finite difference program, Fast Lagrangian Analysis of Continua (FLAC, version 6.0). The soil is considered as a linear elastic-plastic material using the Mohr-Coulomb model. The Mohr-Coulomb properties in Table 1 were selected through calibration based on correlating experimental data and prior static constitutive models of MSE walls. The facing panels are modeled as linear elastic beams. The soil reinforcing strips are modeled as strip elements and strip-to-soil interface resistance is defined by a non linear shear failure envelope that reflects the apparent friction angle defined in AASHTO and FHWA. FLAC's standard hysteretic damping, fitted to Seed and Idriss' (1970) data for sand, was used in conjunction with Rayleigh damping.

	Foundation Soil	Select Fill	Random Fill
Constitutive Model	Mohr-Coulomb	Mohr - Coulomb	Mohr - Coulomb
Bulk Modulus K	$9x10^4$ kPa	$5.9x10^4$ kPa	$3.9x10^4$ kPa
Shear Modulus G	$3.4x10^4$ kPa	$2.26x10^4$ kPa	$1.55x10^4$ kPa
Poisson's Ratio	0.3	0.3	0.3
Unit Weight	2000kg/m^3	2000kg/m^3	2000kg/m^3
Cohesion	2kPa	0	0
Friction Angle	40^0	34^0	30^0
Dilation	0	4	0

Table 1. Soil Material Properties for FLAC Analyses

RESULTS OF NUMERICAL ANALYSES - DISPLACEMENTS

Figure 2 shows the computed changes in horizontal displacements at the bottom of the wall with seismic time history for a 12 m high back-to-back wall with aspect ratio of 1.0. The seismic ground acceleration is 0.6g. The maximum displacement of 73 mm occurred at about 0.5 sec. After 1 second the bottom of wall had been displaced in the opposite direction by about 40 mm. Toward the end of the seismic event, at 1.8

sec, when the dynamic waves had been dampened, the walls have moved back to their original locations.

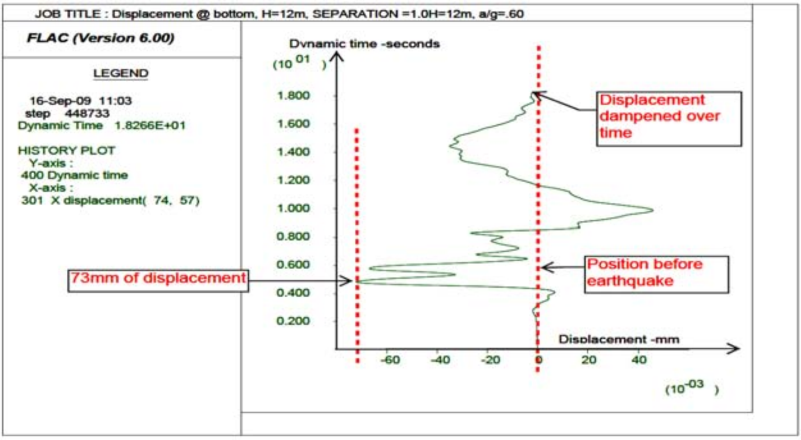

Figure 2. Displacements at the bottom of wall as a function of dynamic time

The results also show that back-to-back walls will displace in both directions during a seismic event. In contrast, a single conventional MSE wall will be displaced in the direction of failure because the dynamic thrust acts toward the wall face. Since back-to-back walls can move in both directions during an earthquake, while maintaining internal structural integrity at the end of seismic event, the final displacement may be much lower than for a single, conventional MSE wall, where increments of displacements accumulate in the direction of failure.

Figure 3 shows the horizontal displacements at the bottom and top of 12 m high walls with aspect ratios of 0.4 and 1.0, respectively. In both cases, as expected, the higher the ground acceleration the greater the displacements at the top and bottom. Displacements appear to increase linearly with ground acceleration.

Figure 3 also indicates that horizontal displacements at the top of the wall are greater than those at the bottom. On average, the displacements at the top are about 1.6 times those at the bottom. This non uniform pattern of wall deformation is at variance with the result from the single block model (based on Newmark's sliding block model and adopted in AASHTO). The trend in Figure 3 may also reflect some amplification of seismic acceleration near the top of wall, resulting in internal shear within the MSE mass. Interestingly, Figure 3 suggests that walls with an aspect ratio of 0.4 deformed less than those with aspect ratio of 1.0 (wider walls) for seismic coefficients less than 0.55g, although at higher accelerations wider walls deformed less. This may be the result of the much greater density of soil reinforcement in narrow structures designed using current methods, and not a seismic behavioral response. However, more sensitivity studies using a wider range of parameters are needed. Narrower back-to-back walls designed internally using standard AASHTO method will have more soil reinforcement than needed to resist pullout failure. The extra soil reinforcement results in a stiffer structure helping to reduce deformation. In addition, narrower structures have less mass, resulting in smaller seismic inertial forces. Therefore, in Figure 3 change in deformation patterns for aspect ratios of 0.4 and 1.0 may be a reflection of reinforcement density, as mentioned earlier. In this case, it may be appropriate to move the trend line for the narrow wall upward, to reflect the greater reinforcement density.

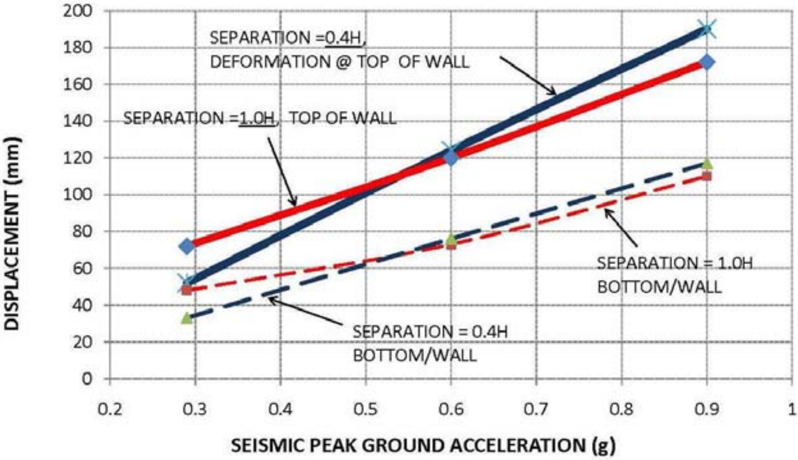

Figure 3. Displacements for 12-m high walls with aspect ratios of 0.4H and 1.0H

RESULTS OF NUMERICAL ANALYSES - TENSILE STRESSES

Figure 4 summarizes reinforcement tensions for a 12 m high wall with an aspect ratio of 0.4. The vertical spacing between reinforcements is 0.75 m. Horizontal acceleration coefficients of 0.29g, 0.60g and 0.90g were used as seismic input. The results of the numerical analyses show, as expected, that the higher the acceleration the greater the lateral forces and the tensile forces in the reinforcing strips. For an acceleration coefficient of 0.29g the lateral force increases almost linearly from the top of the wall to just above the bottom at 10.5 m. Below 10.5 m stresses decrease to the bottom of the wall. This pattern is similar to that observed in the field under static conditions, and is the result of shear resistance at foundation level. For higher seismic coefficients, however, the tensile forces near the bottom continue to increase linearly, suggesting that the soil may have strained beyond its peak strength.

Figure 5 compares the tensile stresses for walls with aspect ratios for 0.4 and 1.0. It can be seen that narrower walls result in lower tensile stresses than in the case for wider walls. This may be due to the reduced mass in the narrower structures.

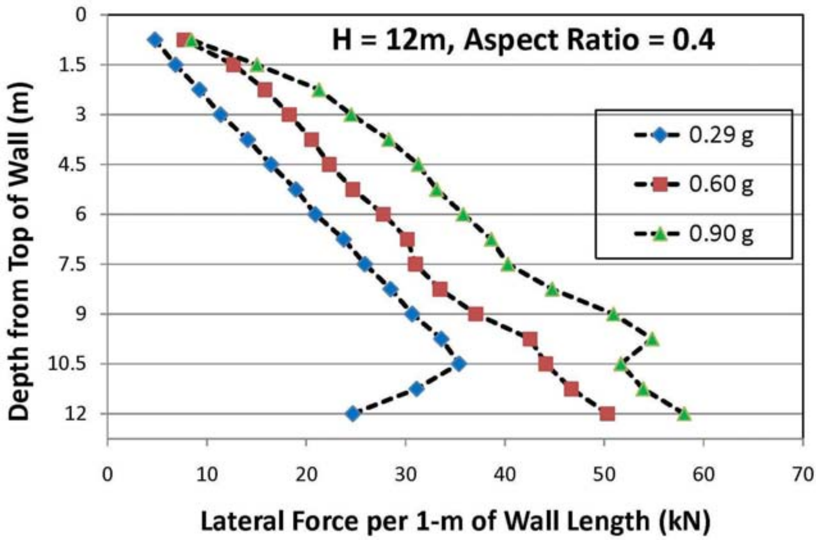

Figure 4. Tensile stresses for various seismic acceleration coefficients

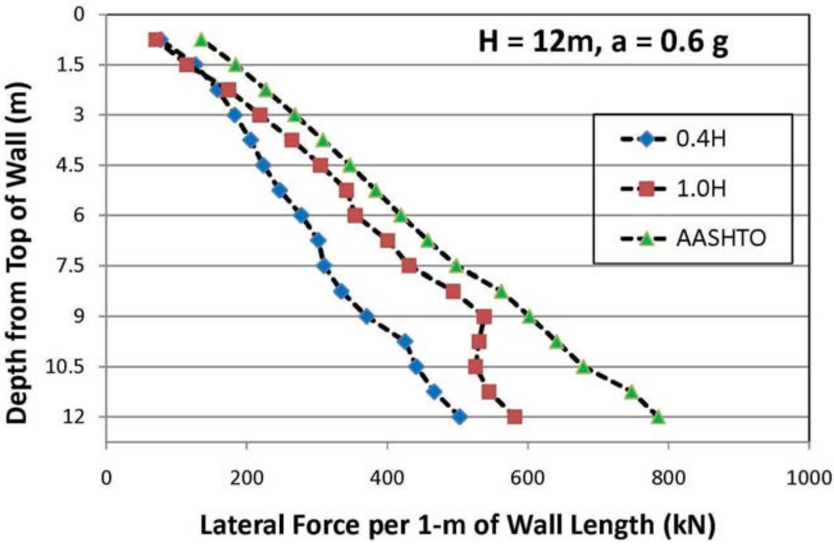

Figure 5. Comparison of tensile forces from numerical models and AASHTO

Figure 5 also compares reinforcement tensions from the numerical model and those calculated using state-of-the-practice AASHTO pseudo-static approach. It can be seen that for a wall height of 12 m and an aspect ratio of 1.0, the numerical model gives lower tensile stresses at all levels than the traditional AASHTO approach, indicating that the latter is conservative.

CONCLUSIONS AND RECOMMENDATIONS

Preliminary results from a numerical study of back-to-back MSE walls with various aspect ratios and acceleration coefficients show that the behavior of these walls differs from that of a single, isolated MSE wall. During shaking, back-to-back walls can move in both directions resulting in smaller final cumulative displacements. The displacements and deformations are proportional to seismic acceleration. An important preliminary finding is that narrow structures do not suffer significantly greater movements in a seismic event than a conventional MSE wall of the same height.

The tensile stresses in the soil reinforcement are directly proportional to the acceleration coefficient. However, since more steel is provided in narrower structures to increase the pullout resistance, the tensile stresses in such walls tend to be lower than those in wider structures. The tensile stresses from the numerical analyses were lower than those calculated using AASHTO pseudo-static method, indicating that the current AASHTO method is conservative. More numerical and experimental studies need to be performed to confirm the results obtained from this preliminary study of seismic behavior of back-to-back MSE walls.

REFERENCES

AASHTO (1996 , 1998, 2002). "Standard Specifications for Highway Bridges." and AASHTO (2004, 2007), "LRFD Bridge Design Specification."

Federal Highway Administration, Publication No. NHI-00-043. (2001). Mechanically Stabilized Earth Walls and Reinforced Slopes, Washington, D.C.

Kavazanjian, E., Matasovic, N., Hadj-Hamou, T. and Sabatini, P.J. (1997) "Geotechnical Engineering Circular #3 – Design Guidance: Geotechnical Earthquake Engineering for Highways." *FHWA-SA-97-076,* Washington, D.C.

Kobayashi, K., Tabata, H., Boyd, M., "The performance of reinforced earth structures in the vicinity of Kobe during the Great Hanshin Earthquake." *Proceedings of 1996 International Symposium on Earth Reinforcement / Fukuoka / Kyushu / Japan*, Vol. 1, Balkema, Netherlands: 395 – 400.

Pamuk, Ahmet, et at, "Behavior of Reinforced Wall System During the 1999 Kocaeli (Izmit), Turkey, Earthquake." Proceedings of Fifth International Conference on Case Histories in Geotechnical Engineering, New York, 2004.

The Golden Ears Bridge Design-Build Project:

Stabilizing Abutment-Wall System for Unnamed Creek Bridge

Casan King L. Sampaco[1], Ph.D., P.E, P. Eng., Dean E. Harris[2], P.E. and Donald G. Anderson[3], Ph.D., P.E.

[1] Senior Technologist and Geotechnical Engineering Specialist, *Design Oversight Management Team, Panama Canal Expansion Program*, CH2M HILL International, Republic of Panama; Phone (507) 6550-0274; e-mail: king.sampaco@ch2m.com

[2] Senior Geotechnical Technologist, CH2M HILL Inc., Boise, Idaho; Phone (208) 345-5314; e-mail: dean.harris@ch2m.com

[3] Principal Geotechnical Engineer, CH2M HILL Inc., Bellevue, Washington; Phone (425) 233-3418; e-mail: donald.anderson@ch2m.com

ABSTRACT

Geotechnical explorations for a bridge crossing an unnamed creek near Vancouver, British Columbia, identified a sloping layer of soft clay approximately 10 m below the ground surface at one of the bridge abutment slopes. The clay was interpreted to be sensitive, and stability analyses suggested that ground improvement or other stabilization was necessary for the bridge abutments. Various design options were evaluated, and a stabilizing abutment-wall system consisting of pipe piles to support the bridge and its approaches and to stabilize the east slope was selected for the project. This paper discusses the design concept and the numerical modeling performed for the stabilizing abutment-wall system and summarizes field monitoring that was carried out during construction of the foundation system.

INTRODUCTION

As part of infrastructure improvements for the 2010 Winter Olympics, a new crossing of the Fraser River was constructed approximately 30 km east of Vancouver, British Columbia. The project includes a 1-km-long extradosed cable-stayed bridge, 13 km of new roadway, 16 new structures, and 12 km of local street reconstruction. The project was a CDN $1.1 billion design-build-finance-operate project that was awarded in early 2006 to Golden Crossing Constructors Joint Venture (GCCJV) comprised of Bilfinger Berger Civil and CH2M HILL.

Approximately 8 km southwest of the Fraser River, the new highway crosses a small unnamed creek (UC) and ravine, where there is an existing 60-year-old oil pipeline, as shown in Figure 1. The ravine is approximately 120 m wide and 8 m deep, and a soft clay layer was found approximately 10 m below the ground surface at the East Abutment. The clay was interpreted to be highly sensitive, and there was concern that the eastern slope had experienced landsliding in the past.

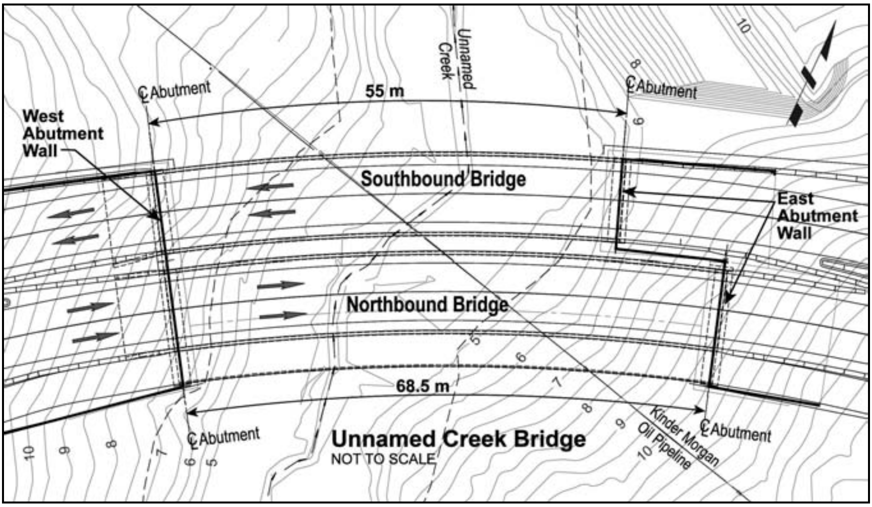

Figure 1. Plan View of Unnamed Creek Bridge

The GCCJV evaluated various bridge foundation design options for the structure and requested that CH2M HILL provide additional explorations and evaluations of stabilizing wall alternatives for the UC Bridge. This paper summarizes the site characterization, the stability and deformation analyses, and the field monitoring performed to support the design and construction of the abutment stabilization wall/abutment system for UC Bridge.

EXPLORATION AND LABORATORY TESTING PROGRAM

CH2M HILL conducted additional field and laboratory testing in early 2007. The field program consisted of six cone penetrometer test soundings with pore pressure measurements (CPTU) and four soil borings with field vane shear (VS) testing. CH2M HILL used the findings of the CPTU soundings to target specific depths for vane shear testing and collection of Shelby tube samples.

Laboratory testing included index testing, one-dimensional (1D) consolidation tests, monotonic direct simple shear (DSS) tests, and cyclic direct simple shear (CyDSS) tests. Results of laboratory testing revealed that the soil profile includes highly plastic clay with liquid limits higher than 60 and plasticity index (PI) values greater than 40, as well as layers of lower-plasticity clays. Liquidity indexes for the low-plasticity materials typically were greater than 1. Results of consolidation tests found no clear differences in estimated values of maximum past pressure (σ_p') or overconsolidation when comparing results from samples that targeted the soft layer to other clay. The tests showed a large range in C_C values (0.26 to 0.84) and estimates of the overconsolidation ratio (OCR) ranged from 1.2 to 2.1.

The estimated shear strength profile was developed by first considering the estimated undrained shear strength (s_u) based on CPTU tests and developing a linear representation for comparison to field VS tests. Figure 2 shows the profile of estimated s_u on the East Abutment slope. The findings indicate that the profile is stratified with strength increasing with depth, except for the soft layer which dips across the site and was encountered at varying elevations between 0 and -4 m, in the various cone soundings.

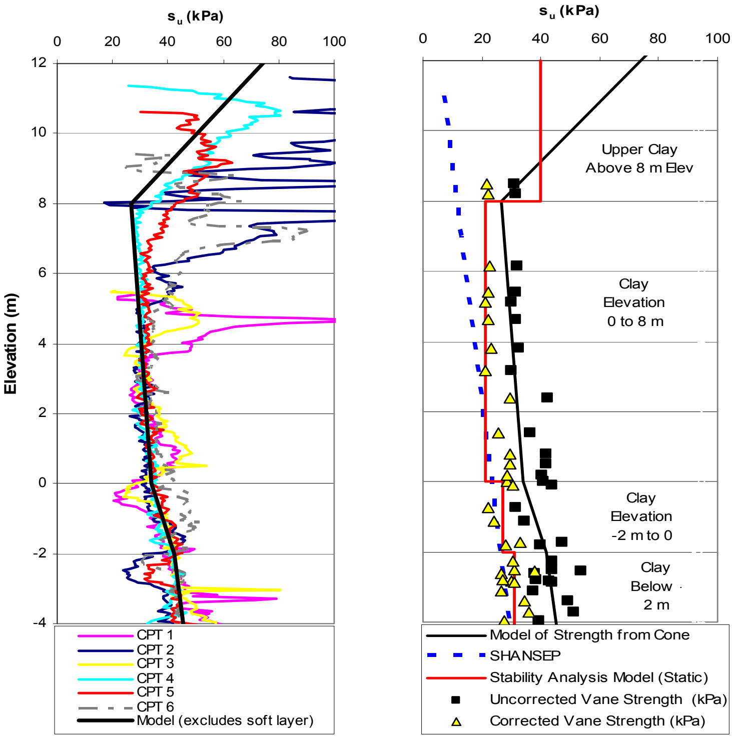

Figure 2. Soil Strength Profile

The uncorrected s_u values from the field VS tests were found to be consistent with estimates from the CPTU soundings assuming a cone factor (N_k) of 17. The uncorrected results appear to indicate that the clay is overconsolidated (OCR = 1.2 to 3.0). The results of VS tests that targeted the soft layer were generally much higher than the estimates from the CPTU soundings, with uncorrected peak s_u from VS tests of 32 to 54 kPa. Using a correction factor of 0.7 (for PI = 60), the corrected field VS strength for the soft layer ranged from 22 to 38 kPa. The remolded strength from the VS tests was less than 12 kPa.

DSS tests were performed on samples from the soft layer. Three specimens were consolidated to a vertical effective stress of 250 kPa. One was sheared immediately and two were unloaded to OCR values of 1.4 and 2. CyDSS and post-cyclic shear strength tests were performed on three specimens from the same sample. An initial shear stress of 30 kPa was applied to simulate the sloping ground conditions at the site. Each specimen was then cyclically sheared to predetermined ratios of the estimated undrained shear strength. The post-cyclic residual strengths from this testing were found to be approximately 10 to 20% lower than the monotonic strength, indicating limited loss in strength resulting from cyclic loading.

After evaluation of the various test results, a generic model of undrained strength for analysis was developed for different cross-sections, with strength increasing with depth as shown in Figure 2. The sloping soft layer was included in each cross-section, with the slope and depth based on the findings of relevant cone soundings for the given cross-section.

STABILITY ANALYSES – EXISTING SLOPE

Stability analyses were performed for the existing slope to compare the findings from different methods of analysis and so that the relative effects of the project could be better understood. Analyses were conducted for both static and pseudo-static loading conditions using limit-equilibrium and finite element (FE) analyses. Deformations associated with static and seismic conditions were estimated using a two-dimensional (2D) FE analysis program PLAXIS (2007). The FE analyses were initially conducted using only the East Abutment, but a full cross-section model was later used after the foundation option for the bridge was finalized.

The limit-equilibrium slope stability analyses were performed using the computer program SLIDE (Rocscience, 2007). Circular and sliding block failure surfaces were considered. Results of the limit-equilibrium analyses for static loading were checked using the c-phi reduction technique implemented in PLAXIS.

Stability analyses for existing static conditions at the East Abutment slope resulted in factors of safety (FS) of approximately 1.1 for block failure and 1.2 for circular failure surfaces (see Figure 3). FE analysis using PLAXIS also gave an FS of 1.2, with the critical failure surface resembling a circular shape. Pseudo-static analyses of earthquake conditions were performed using a peak ground acceleration (PGA) of 0.2g, the estimated peak ground motion within the sliding mass during the 975-year earthquake (EQ). An FS of approximately 0.7 was calculated for the seismic loading case. These results suggested that the existing east slope is marginally stable under gravity loads and could undergo large permanent displacements during the design earthquake.

DYNAMIC FINITE ELEMENT ANALYSES

Dynamic analyses were conducted using the dynamic version of PLAXIS for the following six EQ records:

- 1989 Loma Prieta NS and EW (magnitude = 6.6, duration = 39 seconds)
- 1971 San Fernando NS and EW (magnitude = 7.0, duration = 30 seconds)
- 1949 Olympia NS and EW (magnitude = 7.1, duration = 89 seconds)

Input motions for the PLAXIS analyses were developed from results of 1D, nonlinear site-response analyses conducted by others. The input motion for the site-response analyses had a firm-ground PGA of 0.25g and 0.33g, representing the 475- and 975-year design events, respectively. Each of the six ground motions was scaled to match the firm-ground PGA, and the motions were used as input at the base of the PLAXIS model.

A simplified shear strength model (Mohr-Coulomb) with a cohesion intercept equal to the estimated undrained shear strength of the soil and total stress friction angle equal to zero was used. The Rayleigh alpha and beta damping coefficients were adjusted to maintain consistency with the 1D, nonlinear site response analyses.

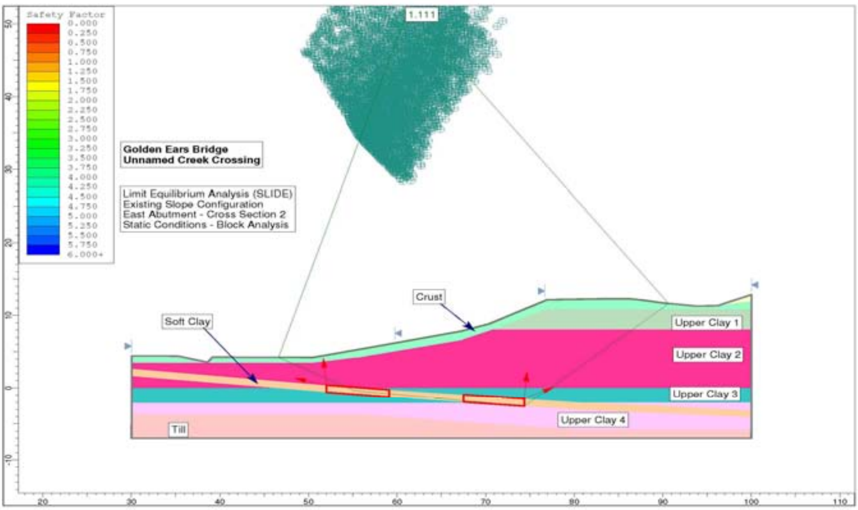

Figure 3. Typical Slope Stability Analyses

Findings from the PLAXIS analyses indicated a PGA of 0.2g and permanent displacements on the order of 75 mm to 180 mm at the base of the slope using the six EQ records. On top of the slope, a PGA of 0.18g and permanent displacements in the range of 100 mm to 200 mm were calculated.

DESIGN ALTERNATIVES FOR THE BRIDGE FOUNDATION

Ground improvement to stabilize the site was determined to be infeasible because of access and schedule issues and the existing pipeline. Therefore, the design and analysis focused on structural systems. to limit slope movement. Initially a conventional wall-fill system and a single, stabilizing abutment-wall system were evaluated using both limit-equilibrium and FE analyses. Results of these analyses showed that these options would not meet minimum FS and displacement criteria.

A two-wall "hollow abutment" system was considered in subsequent analyses. The hollow abutment-wall system consisted of lower and upper stabilizing walls with a concrete deck slab and diaphragm "jump span" connecting the walls, and transverse girders to connect the tops of the piles. The deck-pile system was designed as a pinned connection to allow freedom of rotation and translation. Extruded polystyrene (EPS) fill was selected for fill material, to further reduce demands on the wall system.

After first considering deep beam "king piles" with connecting sheet piles, a pipe-pile stabilization wall, comprised of single rows of 914 mm by 19 mm pipe piles at the East Abutment and East Backwall, was investigated. The pipe piles were spaced at 2.5 diameters to take advantage of soil arching behind the piles. The pipe piles extended on the order of 10 diameters below the critical failure surface to maximize lateral resistance.

DYNAMIC ANALYSIS OF STABILIZATION MEASURES

Because of the complex interaction between the opposing abutment slopes and the bridge structural elements, particularly during seismic loading, an evaluation of the full bridge (using FE analyses) was necessary. A model of the entire bridge, and both abutments was developed, as shown in Figure 4. Connections between the pipe piles and the jump spans and main span were modeled as "pin" connections. Piles were defined in the model as having stiffness values (EI) per unit width based on the number of piles and the width of the pile layout. Separate, closed-form analyses were performed to select a pile spacing that would minimize or eliminate squeezing of soil between the piles.

FE simulation was performed for three cases: construction, static gravity loading, and seismic loading. These analyses are summarized in the following text.

Construction Case. The evaluation of construction conditions assumed that the stabilizing piles were in place at each side of the bridge, but the jump span and main span were not in place during placement of fill. At the East Abutment, it was estimated that placement of the EPS and conventional fill could cause 128 mm of displacement at the backwall, and approximately 76 mm of displacement at the abutment wall. For the West Abutment, the estimated displacements were smaller, with estimated values of 10 mm at the backwall and less than 5 mm for the abutment wall.

The estimated maximum bending moment (Mmax) after placement of the final fill layer ranged from approximately 359 to 611 kN-m/m at the East Abutment Wall and Backwall, respectively. The estimated values for the West Abutment and Backwall ranged from 56 to 333 kN-m/m.

Gravity Loading. Load demands and displacements under gravity loading were determined by extending the analyses described previously to include erection of the bridge main span and the two jump spans. Findings from these analyses are summarized in the following text.

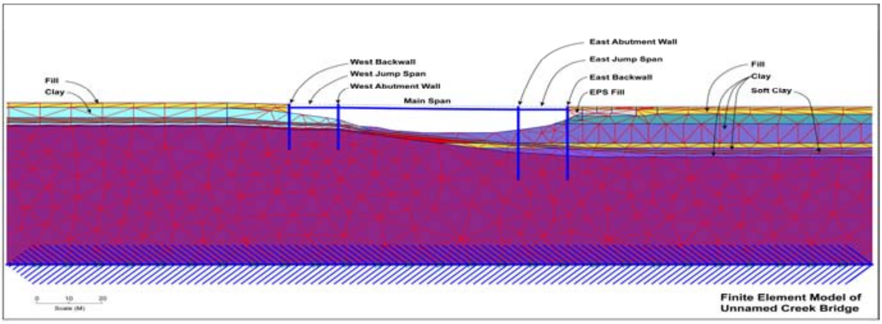

Figure 4. Finite Element Model of Unnamed Creek Bridge

For the East Abutment the maximum calculated lateral displacements under static conditions were 127 mm and 75 mm, at the East Backwall and East Abutment Wall piles, respectively. The maximum estimated lateral displacements for the West Backwall and West Abutment Wall piles were 36 mm and 5 mm, respectively.

The calculated Mmax on the pipe piles occurs at the East Backwall and was calculated to be 601 kN-m/m. The minimum Mmax occurs at the West Abutment pile and was calculated to be 66 kN-m/m.

Seismic Loading. A final evaluation was completed for the completed structure, and the ground motions from the 475- and 975-year EQs.

The horizontal acceleration of the bridge main span and the two jump spans during the EQs appeared to be of similar magnitude and direction, suggesting that movement of the bridge superstructures would be in-phase during the seismic event.

The calculated horizontal displacement at the center of the main span for the six EQ records varied between 17 mm and 78 mm, with the largest value resulting from the Loma Prieta NS record. The maximum transient dynamic displacement calculated using this record was approximately 200 mm for the 475-year EQ and 290 mm for the 975-year EQ. Using this record, the calculated permanent horizontal displacement varied between less than 5 mm to approximately 155 mm. The maximum calculated horizontal displacement occurred at a location behind the East Backwall.

The backwall piles are expected to experience the largest bending moments, which are estimated to range from 1,110 to 1,390 kN-m/m. The demands on the abutment piles are approximately 50% to 60% of the demands for the backwall piles. Moment demands for the 475-yr EQ are 60% to 70% of those calculated for the 975-yr EQ.

Results of the analyses described above for various loading conditions were provided to the bridge designers for use in detailing final structural design of the bridge. The calculated axial load, bending moments, and displacements of the pipe piles were used in establishing the design cross-sections and toe elevations of the pipe piles.

FIELD MONITORING DURING CONSTRUCTION

One of the key concerns for the project was the potential effects of vibrations associated with pile driving. Increases in porewater pressures in the clay created the potential for slope movements that could affect the pipeline or completed work.

The pipe piles were installed between April and June 2008, using a vibratory hammer to advance the initial segments of the pile. An impact hammer was used to drive the piles to the final toe elevation. Movement and vibration monitoring was performed along the oil pipeline during the pile driving. Surface monuments, inclinometers, and piezometers were used to monitor the slopes. Slope movements recorded during pile installation were lower than predicted by the analyses; however, pile driving was temporarily halted occasionally to allow porewater pressures to dissipate.

CONCLUSIONS

The Unnamed Creek geotechnical analysis presented challenges because of the soft soil conditions, the dynamic loads, and the complex soil-structure interaction. In particular, the earthquake loading and the effects of the bridge structure on the stabilizing piles (and the effect of slope movement on the bridge structure) made it difficult to analyze the site using traditional slope stability analyses. Traditional methods generally separate the problem into component pieces, which, in this case consisted of separate limit-equilibrium analysis of each abutment. It was not possible with traditional analyses to understand how the inertia of the bridge and the resistance of the opposite abutment could be considered. Finite element analysis of the entire bridge system made it possible to consider these effects.

Various bridge foundation design options were evaluated using this approach. A stabilizing abutment-wall system consisting of pipe piles was found to be the most effective in supporting the bridge and in stabilizing the east slope. The numerical modeling proved effective in establishing the design criteria for the bridge and in understanding soil-structure interaction effects among the bridge superstructure, its foundation, and the adjacent slopes under static and seismic loading. Field monitoring during construction verified that the oil pipeline and the marginally stable slope were protected. The bridge was completed in early 2009 and is now open for traffic.

ACKNOWLEDGMENTS

The success of this project resulted from the contributions of numerous groups including Trow Associates and AMEC Consultants for their early geotechnical work on the project, the CH2M HILL bridge designers, and the GCCJV construction group. This collaboration led to the project being completed in a short period of time under difficult site conditions.

REFERENCES

PLAXIS. 2007. *PLAXIS Version 8.6 User's Manual*. http://www.plaxis.com/.

Rocscience. 2007. *SLIDE User's Manual*. http://www.rocscience.com/.

Re-analysis of Deep Excavation Collapse Using a Generalized Effective Stress Soil Model

Gonzalo Corral[1] & Andrew J. Whittle[1]

[1] Department of Civil & Environmental Engineering, Massachusetts Institute of Technology, 77 Massachusetts Ave., Cambridge, MA 02139; PH (617) 253-7122; email: email: gcorral@mit.edu, ajwhittl@mit.edu

ABSTRACT

This paper re-analyzes the well-documented failure of a 30m deep braced excavation in underconsolidated marine clay using an advanced effective stress soil model (MIT-E3). The collapse of the Nicoll Highway during construction of cut-and cover tunnels for the new Circle Line in Singapore has been extensively investigated and documented. All prior analyses of the collapse have relied on simplified soil models with undrained strength parameters based on empirical correlations and piezocone penetration data. The current analysis use results from high quality consolidation and undrained triaxial shear tests that were only available after completion of the public inquiry. The current analyses achieve very reasonable estimates of measured wall deflections and strut loads using model parameters derived directly from the laboratory tests. The analyses confirm prior interpretations of the failure mechanism but provide a more rational basis for the modeling of soil-structure interaction.

INTRODUCTION

The collapse of the Nicoll Highway during excavations for the cut-and-cover tunnels for the new Circle Line in Singapore (Phase 1 contract C824) has been extensively documented in a Committee of Inquiry report (COI, 2005). Many local and international experts contributed to this report and have subsequently published detailed interpretations of the failure (e.g., Yong et al., 2006; Endicott, 2006; Davies et al., 2006). One key aspect was the under-design of the temporary lateral earth support system. Figure 1a shows the design for the (intended) 33.3m deep excavation comprising 0.8m thick diaphragm wall panels that extend through deep layers of Estuarine and Marine clays (Kallang formation) and are embedded a minimum of 3m within the underlying Old Alluvium (layer SW-2). The walls were to be supported by a total of ten levels of pre-loaded, cross-lot bracing and by two relatively thin rafts of continuous Jet Grout Piles (JGP). The Upper JGP raft was a sacrificial layer that was excavated after installation of the 9th level of struts. Collapse occurred on April 20th 2004 following excavation of the Upper JGP (to an elevation of approximately 72.3m RL, Fig. 1).

The design of the temporary lateral earth support system was based on a table of geotechnical design parameters (GIM, August 2001). This table included the unit weights, K_0 coefficients, hydraulic conductivities, k, elastic moduli, E, and both the Mohr-Coulomb (drained) effective stress strength parameters (c', ϕ') and undrained shear strength profiles, $s_u(z)$ for all of the main soil units and JGP layers. Many of these parameters were based on prior local experience (e.g., Bo et al., 2003; Tan et al., 2003; Chiam et al., 2003; Li & Wong, 2001).

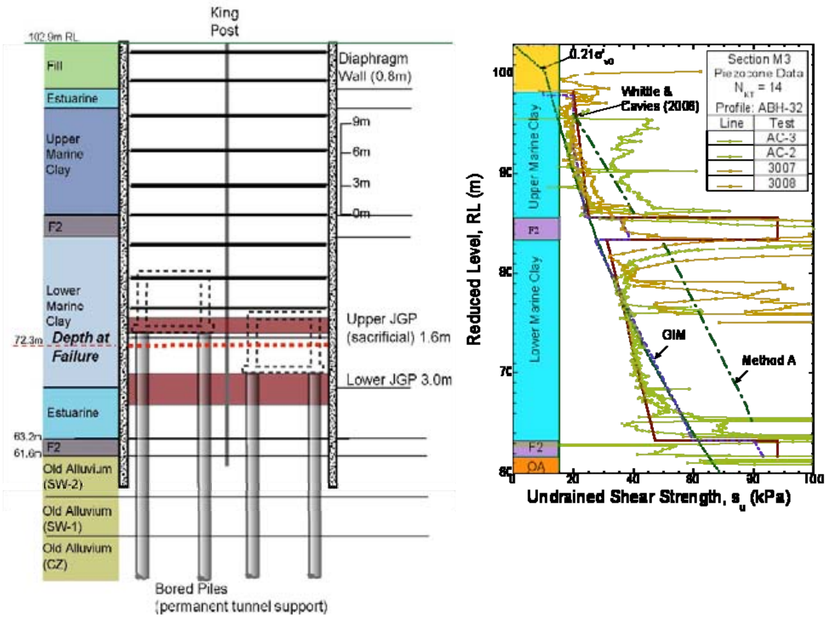

Figure 1(a). Cross-section of excavation support system design section, and (b) undrained shear strength profiles

Piezocone penetration data were the only reliable site-specific information on undrained shear strengths available at the time of design. Figure 1b compares the undrained shear strength profile specified in the GIM table with results from 4 piezocone tests interpreted using a cone factor N_{kT} = 14. The results show good agreement between the GIM and piezocone strengths in the Upper unit of the Marine Clay (UMC). However, the piezocone results also suggest that the Lower Marine Clay (below 75mRL) is weaker than the design strength profile. Whittle and Davies (2006) have attributed this to underconsolidation of the Lower Marine Clay associated with 5m of fill used to reclaim the land in the 1970's. This explanation assumes that the underlying units of Old Alluvium have low bulk permeability and/or low recharge potential.

The design of the lateral earth support system was based on finite element analyses of soil-structure interaction using an elastic-perfectly plastic (Mohr-

Coulomb, MC) model for the soil behavior. The analyses simulated undrained shear behavior of the clay layers using drained effective stress strength parameters (c', ϕ'). This approach, referred to as Method A (COI, 2005), led to gross overestimation of the undrained shear strength in the analyses (Fig. 1b). As a result the designers underestimated the wall deflections and bending moments and under-designed the bending capacity of the diaphragm wall and thickness of the two JGP layers.

Ironically, most of the experts involved in the investigations of the collapse used the same finite element program and MC constitutive model to diagnose the failure mechanism. These experts used total stress strength parameters (s_u = c', ϕ' = 0°) to represent directly the expected undrained strength profiles (e.g., GIM, 2001; Whittle & Davies, 2006; Fig. 1b). These Method B analyses were able to describe, to a reasonable first order approximation, the measured lateral wall deflections and strut loads. They also provided the basis for explaining the collapse mechanism in which the brittle failure of the 9th level strut-waler connections led to a redistribution of lateral earth pressures that could not be supported by the bracing system and led to catastrophic failure.

Extensive post-failure site investigation programs were carried out to resolve uncertainties associated with the complex stratigraphy (which includes a relic deep relic channel through the Old Alluvium). A detailed program of high quality laboratory consolidation and shear strength testing on high quality samples of marine clay was also performed (Kiso-Jiban, 2004). None of these data were analyzed in detail at the time of the inquiry but were included in a revised design manual (Amberg, 2005). This paper presents a re-analysis of the excavation performance based on the post-failure laboratory test program. The behavior of the Upper (UMC) and Lower (LMC) Marine Clay units is represented by the MIT-E3 model (Whittle and Kavvadas, 1994) which is able to simulate the anisotropic effective stress-strain-strength properties measured in the tests.

MODEL CALIBRATION

The MIT-E3 soil model (Whittle & Kavvadas, 1994) was developed to simulate the effective stress-strain-strength behavior of normally and moderately overconsolidated clays. The model describes a number of important aspects of soil behavior which have been observed in laboratory tests on K_0-consolidated clays including: 1) small strain non-linearity following a reversal of load direction; 2) hysteretic behavior during unload-reload cycles of loading; 3) anisotropic stress-strain-strength properties associated with 1-D consolidation history and subsequent straining; 4) post-peak, strain softening in undrained shear tests in certain modes of shearing on normally and lightly overconsolidated clays; and 5) occurrence of irrecoverable plastic strains during cyclic loading and shearing of overconsolidated clays. The model also has a number of key restrictions: It uses a rate independent formulation and hence, does not describe creep, relaxation or other strain rate dependent properties; and 2) it assumes normalized soil properties (e.g., the strength and stiffness are proportional to the confining pressure at a given overconsolidation ratio, OCR) and hence, does not describe complex aspects of soil behavior associated with cementation.

Calibration of the model for UMC and LMC clays follows the general procedure proposed by Whittle et al. (1994). Table 1 summarizes these input parameters, their physical meanings within the model formulation and laboratory tests from which they can be obtained, together with parameters selected for UMC and LMC units. The parameters have been derived principally from a set of 1-D consolidation tests (Fig. 2) and K_0-consolidated undrained triaxial shear tests (Fig. 3) on specimens reconsolidated to the in situ stress conditions.

Table 1: Input Parameters for MIT-E3 Constitutive Soil Model: UMC & LMC

Test Type	Parameter/ Symbol	Physical contribution/meaning	Upper Marine Clay (UMC)	Lower Marine Clay (LMC)
1-D Consolidation (Oedometer, CRS,etc.)	e_0	Void ratio at reference stress on virgin consolidation line	1.80	1.60
	λ	Compressibility of virgin normally consolidated clay	0.380	0.370
	C	Non-linear volumetric swelling behavior	10.0	9.0
	n		1.50	1.50
	h	Irrecoverable plastic strain	0.2	0.2
Ko-Oedometer or Ko-Triaxial	K_{0NC}	K_0 for virgin normally consolidated clay	0.52	0.52
	2G/K	Ratio of elastic shear to bulk modulus (Poisson's ratio for initial unload)	0.94	0.94
Undrained Triaxial Shear Tests: OCR=1; CKoUC OCR=1; CKoUE OCR=2, CKoUC	ϕ'_{TC}	Critical state friction angles in triaxial compression and extension (large strain failure criterion)	32.4°	27.0°
	ϕ'_{TE}		33.8°	27.1°
	c	Undrained shear strength (geometry of bounding surface)	0.96	0.96
	S_t	Amount of post-peak strain softening undrained triaxial compression	3.0	5.0
	ω	Non-linearity at small strains in undrained shear	0.40	0.40
	γ	Shear induced pore pressure for OC clay	0.5	0.5
Shear wave velocity	κ_0	Small strain compressibility at load reversal	0.0094	0.0094
Drained Triaxial	ψ_0	Rate of evolution of anisotropy (rotation of bounding surface)	100.0	100.0

The compressibilities of the normally consolidated UMC and LMC units are well-characterized virgin consolidation lines with $\lambda = 0.37 - 0.38$, Figure 2a. The upper marine clay generally has higher in situ void ratio ($e = 1.7 - 1.9$) than the lower unit ($e = 1.5 - 1.6$). The marine clays show significant elastic rebound when unloaded. Figure 2b shows that recoverable axial strains, $\Delta\varepsilon_a$ = 10-12% when the effective stress is reduced by one order of magnitude (ξ_v = OCR = 10). This behavior is consistent with laboratory measurements of the maximum shear modulus, G_{max}, (from bender elements), reported by Tan et al. (2003). The Authors have used these data to estimate the model input parameter, κ_0, and then selected input values of C, n (Table 1) to the swelling data as shown in Figure 2b.

A series of CAU normally consolidated triaxial compression and extension tests were performed on specimens from 4 depths within the UMC and LMC units, Figure 3.

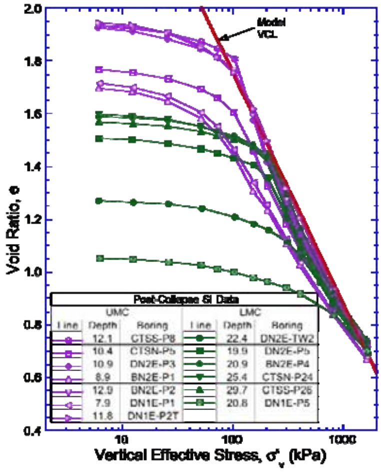

a) Compression behavior

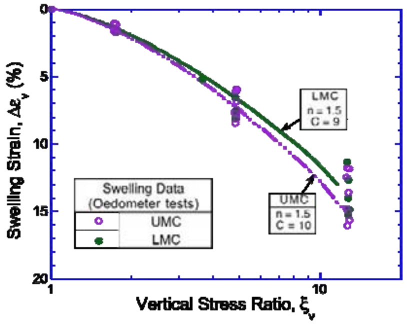

b) Swelling behavior

Figure 2: Compression and swelling properties of the Upper and Lower Marine Clays

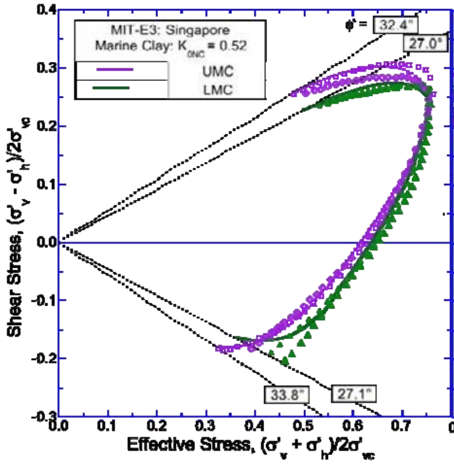

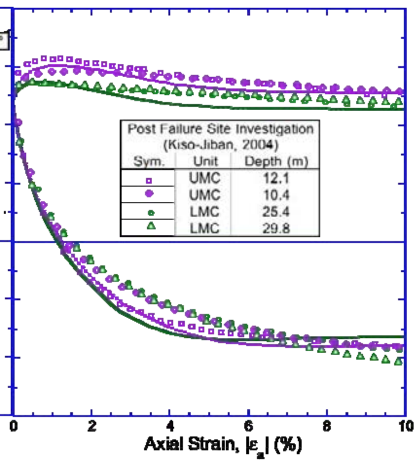

a) Effective stress paths b) Shear stress-strain behavior

Figure 3: Comparison of measured undrained shear behavior from laboratory CAU compression and extension tests on normally consolidated UMC and LMC specimens with numerical simulations using the MIT-E3 model

All of the specimens were consolidated to a common lateral stress ratio, K0 = 0.50 prior to shearing. The measured data show a significant different in the average undrained triaxial compression strength ratios measured in these tests, s_{uTC}/σ'_{vc} = 0.30 vs 0.27 for the UMC and LMC units, respectively. The data also show that UMC specimens mobilize higher friction angles when sheared to large strains (in both compression and extension), ϕ' = 32.4° -33.8° vs 27.0° - 27.1° for UMC and LMC. The UMC exhibits higher undrained strength anisotropy (s_{uTE}/s_{uTC} = 0.60 – 0.66) compared to LMC (0.80 – 0.88) and both exhibit relatively modest post-peak softening in compression shear modes for $\varepsilon_a > 2\%$.

Details of the measured effective stress paths and shear stress-strain properties are well characterized by MIT-E3 through model input parameters c, S_t, ϕ'_{TC}, ϕ'_{TE}, ω and γ (Table 1). The remaining parameters in Table 1 have been estimated from prior studies on similar clays.

FINITE ELEMENT MODEL

The numerical simulations of excavation performance have been carried out focusing on one specific cross-section (within the collapse zone) corresponding to the location of the instrumented strut line S335, Figure 4. Loads in each of the nine levels of struts installed at S335 were measured through sets of three strain gauges. These data have been extensively validated by each of the expert witnesses for the public inquiry (e.g., Davies et al., 2006). Measurements of the lateral wall movements at this section are obtained from inclinometer I-65 (installed through the north diaphragm wall panel) and I-104 located in the soil mass 1.5 – 2.0m outside the south wall.

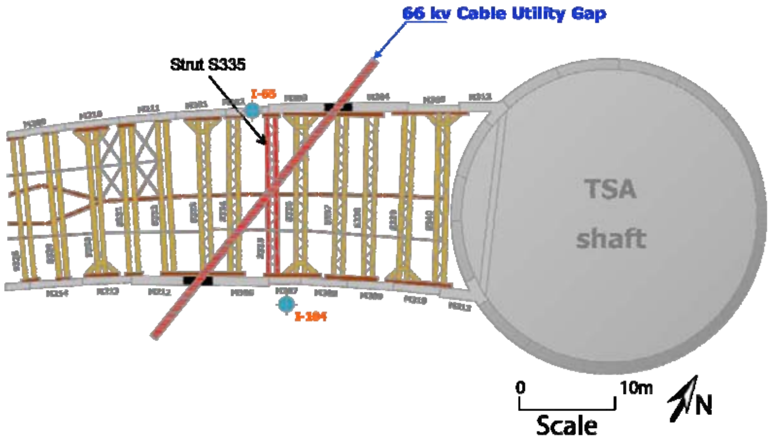

Figure 4: Plan showing the structural support system and 9th level strutting and monitoring instrumentation

Figure 5 shows the cross-sectional geometry for section S335 based on data from both pre-tender and post-failure site investigations: The section is notably more complex that the design section indicated in Figure 1. The base of the LMC dips notably to the south. This is part of a relic channel in the underlying Old Alluvium that was highlighted by Whittle and Davies (2006). On the south side, the LMC directly overlies the Old Alluvium, while units of fluvial sand, F1, and estuarine clay (E) separate the Marine Clay and OA on the north side. The post-failure investigations have established that the OA has relatively low bulk hydraulic conductivity, while the F1 layer has relatively limited extent and no ready source of recharge (although there is a hydraulic connection across the wall due to the absence of a diaphragm wall panel between S336 – S337 in Fig. 4). These details were critical in establishing that failure of the excavation was not caused by hydraulic uplift. The lateral earth support design includes two layers of continuous jet grout pile (JGP) rafts that were intended to provide additional passive resistance below the formation. At section S335 it is unlikely that the lower JGP raft is continuous within the Old Alluvium, as installation jetting parameters for the jet grout columns were based on parameters calibrated to marine clay conditions. Hence, the section shows a truncation of the lower JGP raft at the north wall.

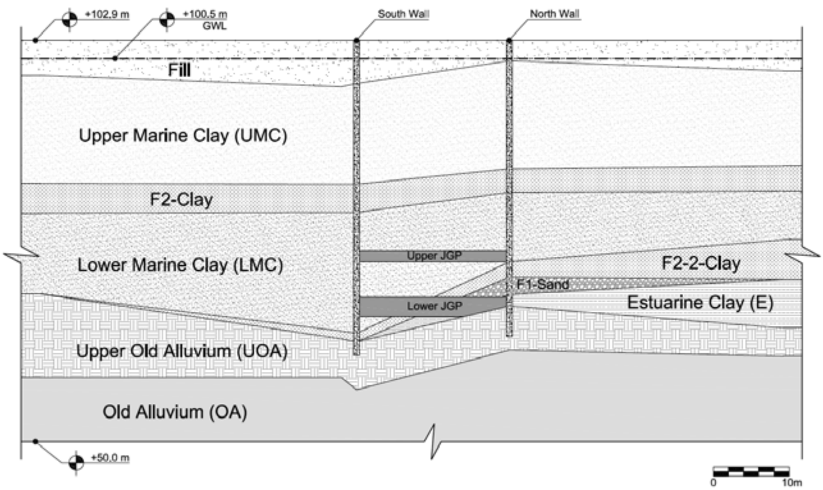

Figure 5: S335 Section geometry used in FE model

Section S335 has been modeled using the Plaxis^{TM} program. The MIT-E3 model has recently been integrated within the kernel of Plaxis (Akl, Bonnier; pers. comm., 2008). Following Whittle and Davies (2006), the current numerical simulations assume that the groundwater table in the Fill is at 100.5m RL and that there is small excess pressure in the underlying LMC and OA units (piezometric head, H = 103m). The UMC and LMC units[1] are modeled using the MIT-E3 model with parameters listed in Table 1, while engineering properties of all other soils and JGP rafts are simulated using the Mohr-Coulomb (MC) model with parameters reported in the prior studies (COI, 2005). It should be noted that the lower Estuarine clay (E, Fig. 5) is assumed to have the same properties and behavior as the LMC.

In order to apply the MIT-E3 effective stress soil model it is essential to specify carefully the in situ effective stress profile and the initial OCR. The current analyses assume $\sigma'_p/\sigma'_{v0} = 1.0$ in both UMC and LMC units (Fig. 6a). When combined with the assumed pore pressure conditions, this implies that the marine clays are slightly under-consolidated. The in-situ stresses also deviate from K_0-conditions due to the inclined stratigraphy. This is modeled using a standard drained relaxation of stress procedure within Plaxis.

Figure 6b summarizes the anisotropic undrained shear strength profiles within the marine clays obtained using the MIT-E3 model for three standard modes of plane strain shearing. The undrained plane strain active and passive strengths bound the best estimate profile recommended by Whittle and Davies (2006), based on their interpretation of piezocone tests (this assumes $s_{uDSS}/\sigma'_{v0} = 0.21$ for normally consolidated Singapore marine clay, after Tan et al., 2003). It is interesting to note that the undrained shear strength predicted by MIT-E3 in the DSS mode is 5-7kPa lower than the best estimate used in the prior MC analyses within the LMC.

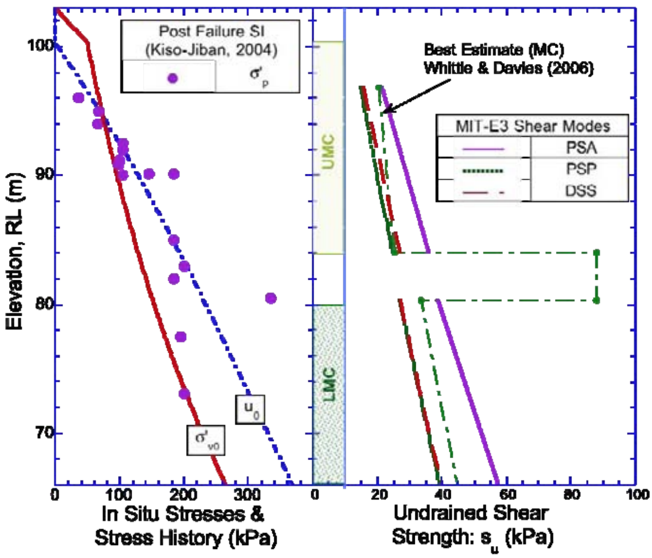

a) In situ stresses b) Undrained strengths in marine clay

Figure 6: Comparison of in situ stresses and undrained strengths of marine clay used in FE model

[1] The lower Estuarine clay (E, Fig. 5) is assumed to have the same properties and behavior as the LMC

All other parameters for the lateral earth support system including the as-built diaphragm wall embedment, capacity of the critical strut-waler connections and pre-load of the struts are based on prior interpretation of the construction records (Bell & Chiew, 2006).

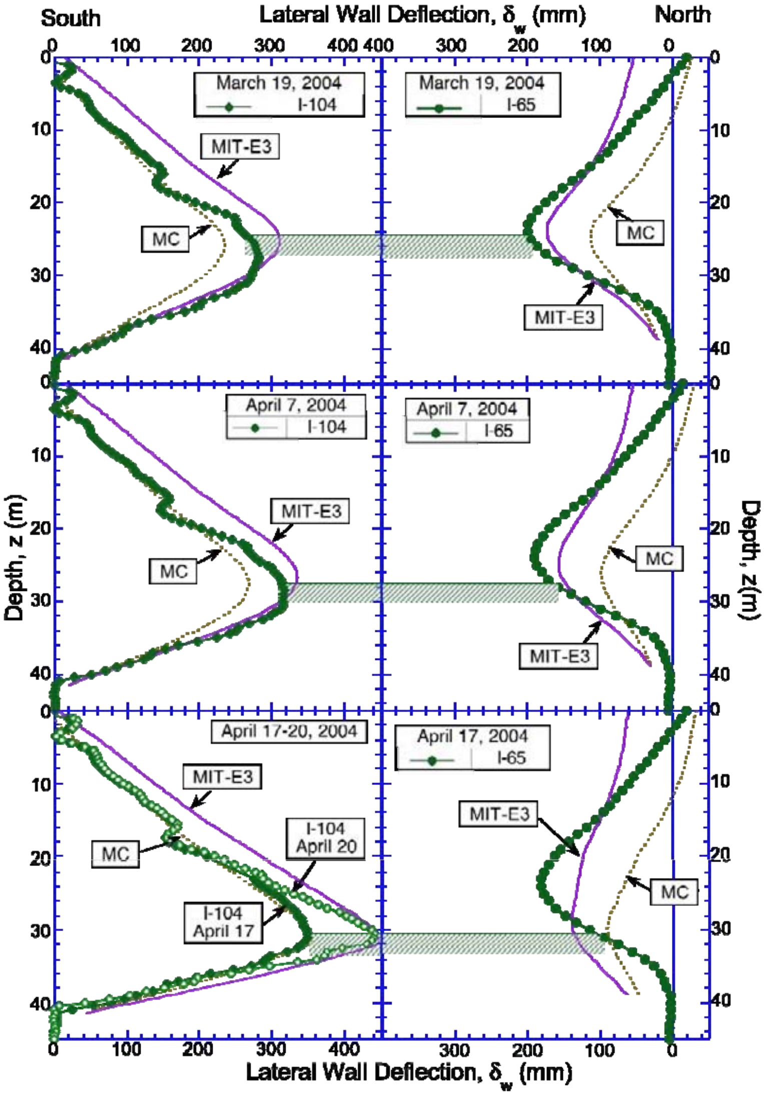

Figure 7: Comparison of computed and measured lateral wall deflections at Section S335, March – April 2004

RESULTS

Figure 7 compares predictions of lateral wall deflections from the current analyses with measured data from the two inclinometers (I-104, I-65) and with results of prior analyses (marked as MC) performed by Whittle & Davies (2006). The results are shown at three times during the month preceding the collapse (with excavation depths 24.6m, 27.6 and 30.6m). The current analyses predict very well the maximum lateral wall deflection on the south side of the excavation including the large deflections associated with removal of the upper JGP layer (April 17-20). At this stage, a plastic hinge formed in the south wall (at a depth of 32m) and there is very large rotation of the toe. The current analyses also describe very well the maximum lateral wall deflection on the north side through March. The analyses tend to overestimate inward movements of both walls within the upper 10-15m of the bracing system. This may be attributed to the assumption that the UMC is normally consolidated, while the pre-consolidation data show a small OCR in this layer (Fig. 6a). The analysis predicts significant lateral displacements at the toe of the north wall in April 2004 (70mm at time of failure on April 17-20). In contrast, inclinometer I-65 suggests that the north diaphragm wall panel remains well anchored. The net effect is that the analysis underestimates the deflections and flexure in the lower part of the north wall during April. This result is largely related to the complex stratigraphy and assumed truncation of the lower JGP at the north wall.

The current analyses using MIT-E3 predict larger inward wall deflections than the prior MC analyses and are in rather better agreement with the measured data. This result is encouraging as the current analyses are based on calibration of a complex constitutive model using laboratory test data (rather than a best estimate of a design strength line). However, it is clear that certain features of the measured data such as the toe fixity on the north wall are difficult to interpret and are not controlled by the properties of the marine clay. Similarly, the current analyses do require additional judgment in the selection of the OCR profile.

It is generally agreed that collapse of the Nicoll Highway initiated when the 9th level strutting failed due to sway buckling of the strut-waler connections. Overloading of the strut-waler connections occurred due to the absence of splays that had been designed for all struts (see Fig. 4). The strut-waler connections exhibited a brittle post-peak load response due to a mechanism of 'sway buckling' that was associated with the use of c-channel stiffeners at the strut-waler connections in levels 7-9 of the bracing system (this was a revised design used during construction; Bell & Chiew, 2006). Collapse occurred as the bracing system was unable to handle loads transferred upward through the bracing system. Figure 8 summarizes predictions of the strut loads at levels 7-9 on prior to collapse (April 20, 2004). The results show very reasonable agreement between the computed and measured loads in strut levels 7 and 8. The current analyses are also in close agreement with loads obtained by Whittle and Davies (2006) using the MC model. Both sets of analyses predict that the capacity of the 9th level strut-waler connection is fully mobilized at this stage of excavation (30.6m deep) immediately following removal of the upper JGP raft. In contrast the measured strut loads are much smaller. This is an inconsistency noted by all the experts to the public inquiry (COI, 2005). Hence, it can be concluded that the current analyses with MIT-E3 are able to predict the onset of collapse consistent with prior MC analyses but do not shed any insight to explain the measured loads at level 9.

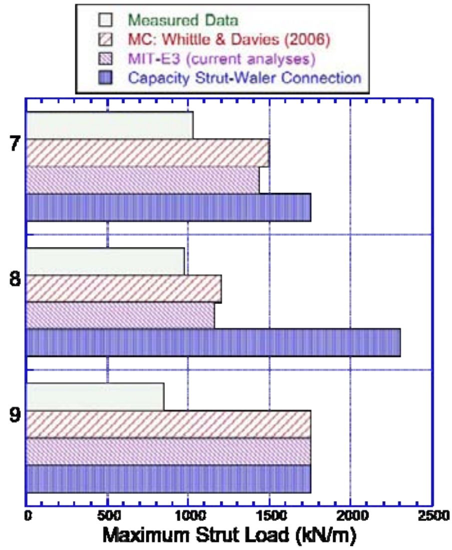

Figure 8: Comparison of computed and measured strut loads for excavation to 30.6m (April 17-20, 2004)

CONCLUSIONS

The Authors have re-analyzed the performance of the lateral earth support system for a critical instrumented section, S335, of the cut-and-cover excavations at the site where the Nicoll Highway collapsed in 2004. Engineering properties of the key Upper and Lower marine clay units have been modeled using the generalized effective stress soil model, MIT-E3, with input parameters calibrated using laboratory test data obtained as part of the post-failure site investigation. The model predictions are evaluated through comparisons with monitoring data and through comparisons with results of prior analyses using the Mohr-Coulomb (MC) model (Whittle & Davies, 2006). The MIT-E3 analyses provide a modest improvement in predictions of the measured wall deflections compared to prior MC calculations and give a consistent explanation of the bending failure in the south diaphragm wall and the overloading of the strut-waler connection at the 9th level of strutting. The current analyses do not resolve uncertainties associated with performance of the JGP rafts, movements at the toe of the north-side diaphragm wall or discrepancies with the measured strut loads at level 9. However, they represent a significant advance in predicting excavation performance based directly on results of laboratory tests compared to prior analyses that used generic (i.e., non site-specific) design isotropic strength profiles.

REFERENCES

Amberg & TTI (2004) Final geotechnical interpretative report CCL824 – reconstruction of Braced Excavation System, Project document.

Bell, B.C. & Chiew, S.P. (2006). "Nicoll Highway collapse: Some structural observations. Part 2: Soil retention system." *Proc. Int. Conf. on Deep Excavations*, Singapore, June 2006.

Bo, M.W., Choa, V. & Hong, K.H. (2003) "Material characterization of Singapore Marine Clay at Changi," *Quarterly Journal of Engineering Geology and Hydrogeology*, **36**, 305-319.

Chiam, S.L., Wong, K.S., Tan, T.S., Ni, Q., Khoo, K.S. & Chu, J. (2003) "The Old Alluvium," *Proc. Underground Singapore, 2003*, 408-427.

COI (2005). Report of the Committee of Inquiry into the Incident at the MRT Circle Line Worksite that Led to the Collapse of Nicoll Highway 20 April 2004. Report Submitted to the Minister of Manpower.

Davies, R.V., Fok, P., Norrish, A. & Poh, S.T. (2006). "Nicoll Highway Collapse: Field Measurements and Observations." *Proc. Int. Conf. on Deep Excavations,* Singapore, June 2006.

Endicott, L.J. (2006). "Nicoll Highway lessons learnt," *Proc. Int. Conf. on Deep Excavations*, Singapore, June 2006.

GIM (2001) Geotechnical Interpretative Memorandum C824/DES/DM/002A, Project Document.

Kiso-Jiban (2004) Factual reports on soil investigation at Nicoll Highway, 3 Vols., Project Documents.

Li, W.W. & Wong, K.S. (2001) "Geotechnical properties of Old Alluvium in Singapore," *Proc. Journal of the Institution of Engineers*, Singapore, 41(3), 10-20.

Tan, T.S., Phoon, K.K., Lee, F.H., Tanaka, H., Locat, J. & Chong, P.T. (2003) "A characterization study of Singapore Lower Marine Clay," *Proc. Conf. On Characterization and Engineering Properties of Natural Soils*, Eds. Tan et al., Swets & Zeitlinger, 1, 429-454

Whittle, A.J., & Davies, R.V. (2006). "Nicoll Highway Collapse: Evaluation of Geotechnical Factors Affecting Design of Excavation Support System." *Proc. Int. Conf. on Deep Excavations*, Singapore, June 2006.

Whittle, A.J. & Kavvadas, M.J. (1994). "Formulation of the MIT-E3 constitutive model for overconsolidated clays." *ASCE Journal of Geotechnical Engineering*, 120(1), 173-199.

Whittle, A.J., DeGroot, D.J., Ladd, C.C. & Seah, T-H. (1994). "Model prediction of the anisotropic behavior of Boston Blue Clay." *ASCE Journal of Geotechnical Engineering*, 120(1), 199-225.

Yong, K.Y., Teh, H.S. & Wong, K.S. (2006). "System failure of temporary earth retaining structure leading to collapse of Nicoll Highway." *Proc. Int. Conf. on Deep Excavations*, Singapore, June 2006.

One North Station Excavation in 30m of Jurong Residual Soils in Singapore

S.A. Tan[1]

[1.] Associate Professor, PE(Civil), PE(Geo), PhD (Univ Calif Berkeley), Department of Civil Engineering, National University of Singapore, 1 Engineering Drive 2, E1A 07-03, Singapore 117576; PH (+65) 65162278;
FAX (+65) 6779 1635 ; email: cvetansa@nus.edu.sg

ABSTRACT

The One-North MRT station is part of the Circle Line at Buona Vista Road in Singapore. The deep excavation involves a 30m deep cut into 20m of Jurong residual soils and 10m of Jurong sedimentary rocks to form a small stabilizing rock berm on the passive side of the wall, adjacent to the INSEAD building complex. The performance of the wall and excavation system is evaluated against field measurements and FEM analysis. Of significance is that the wall behavior showed that the Jurong residual soils behaved like a drained material despite its low permeability (k) values of less than 10^{-8} m/s. This project illustrate how allowing for judicious lowering of GWT can lead to a safe and economical design of a very deep excavation in tropical residual soils conditions, with very high GWT. For correct c-phi reduction analysis, allowance must be made for possible wall and anchor failure.

1. INTRODUCTION

The One-North MRT station is part of the Circle Line at Buona Vista Road in the research and commercial hub close to the National University of Singapore. The deep excavation involves a 30m deep cut into 20m of Jurong residual soils and 10m of Jurong sedimentary rocks to form a small stabilizing rock berm on the passive side of the wall, adjacent to the INSEAD building complex. At the time of excavation, INSEAD was also undertaking expansion works with bored piling activities close to the excavation boundary. This prohibits the use of multi-layers ground anchors as tied-back support system due to lack of space behind the wall on the INSEAD side of the land. The retaining wall system adopted is that of a 1.8 m diameter bored piles at 2.0 m centres to form a contiguous bored-piled (CBP) wall tied-back with a steeply inclined temporary ground anchor raker prop system through the capping beam near the top of the wall.

2. BRIEF DESCRIPTION OF EXCAVATION SYSTEM

2.1 Site plan

The One-North excavation consists of two parcels of basement construction works. The site covers an area of 14,725 m2, with the western half for the One-North MRT station, and the eastern part for a six-level basement of the Fusionpolis tower complex. The One-North station is situated adjacent to INSEAD building which is an existing campus of the European-based graduate business school in Singapore.

Due to the limited right of access space into INSEAD property, the ground anchor system employed is one where a steeply inclined (60^{o} to the horizontal) top row of raker anchors heavily preloaded to 80% of 150 ton per anchor at 2.0 m centres was used as the single prop tied-back wall. After 18 m of excavation a second row of short anchors at 2.0 m centres (75 tons and 125 tons working loads) were installed and another row at 20m depth was planned for possible installation as part of contingency measures if needed. These shorter ground anchors extended into Jurong sedimentary rocks in INSEAD land below the base of the newly installed bored piles closest to the boundary of the CBP wall.

2.2 Excavation sequence

Figure 1. showed the design cross sectional view of the tied-back CBP Wall Type 7 (WT-7), with the temporary ground anchors, and near horizontal sub-soil drains to lower GWT from RL115m to about RL 102.5m. The berm sizes varied in width due to the design of the Civil Defence (CD) shelter; making berm widths of about 4.0 m in Section 1, 9.5 m in Section 2 (see Fig.1) and 13.5 m in Section 3. The approximate timing and stages of construction is described in Table 1. below. In general, the 30 m deep excavation began in Jan 2004 and reached final levels of RL86.0 m by Dec 2004, and the pit was kept open for a period of more than a year. This has significant influence on the state of drainage and consolidation of the retained soils.

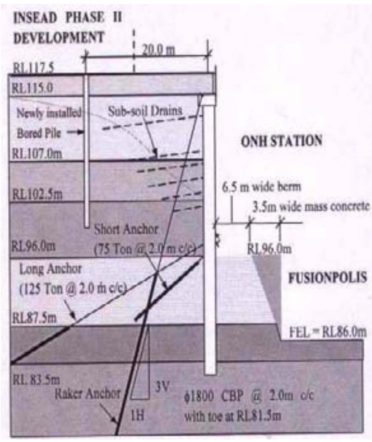

Figure 1. Tied-back CBP WT-7

Stage	Date	Construction Activity
1	15-Nov-03	Install 1.8m diameter CBP wall at RL117.0m
2	27-Nov-03	Excavate trench to RL115.0m to cast capping beam
3	15-Jan-04	Install Raker Anchor with 80% of 150T preload
4	16-Feb-04	Excavate trench to RL110.0m
		Install 1st row drain at RL112.5m
5	29-Mar-04	Excavate trench to RL102.5m
		Install drains at RL108.5, 106.5 and 104.5m
6	12-Jul-04	For Sect 1&2, excavate to RL96.5m
		Install drains at RL102.5m and 75T anchors at RL96.5m
		For Sect 3, excavate to RL98.5m
		Install drains at RL102.5m and 100T anchors at RL100.5m
		Excavate to formation level at RL95.9m
7	13-Sep-04	Cut rock berms to RL86.0m;gunnite exposed rock slope
8	18-Dec-04	Cast basement wall to RL95.9m and CD slab at RL86.0m
		For Sect 1&2, remove 75T anchors
9&10	18-Dec-04	Cast basement wall to RL102.5m and slab at RL98.05m
		For Sect 3, remove 100T anchors
11	3-Mar-05	Cast basement wall and slab at RL105.0m
12	26-Apr-05	Cast basement wall and slab at RL115.0m
13	1-Jun-05	Excavate to capping beam and remove raker anchors
14	1-Jun-05	Backfill to GL at RL 117.0m

Table 1. Construction sequence and timetable

3. SITE INVESTIGATION AND SOIL STRATIGRAPHY

A total of 10 boreholes with rock cores were done to define the stratigraphy along the wall boundary of the One-North station site. The soil and rock profiles of the Jurong formation in the three additional boreholes of ABH1, ABH2 and ABH3 describing the probable wall design cross-sections 1, 2 and 3 are shown in Fig.2. Relevant details of the Jurong sedimentary formation is described in CP4 (2003) of Singapore. The Jurong formation consists of bedded sedimentary and slightly meta morphosed rocks of conglomerate sandstone and siltstone with closely to very closely spaced fractures. The Jurong residual soils (Grade SVI) consists of firm to very stiff light yellow, grey, red to white fine to medium sandy clays and silts. The thickness of the residual soils ranged from 3 to 10 m with SPT N between 14 and 22. The completely weathered zone (Grade SV and SIV) consists of hard light to dark grey fine to medium sandy silts. These exist at depth from 5 to 20 m with SPT N between 30 and 100. Below these we have the Jurong rocks (Grade SIII to SI) ranging from highly weathered moderately weak to slightly weathered moderately strong to strong interbedded sandstones and siltstones.

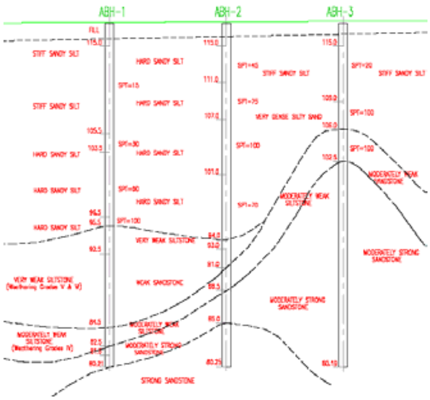

Fig.2 Soil stratigraphy along CBP wall WT- 7

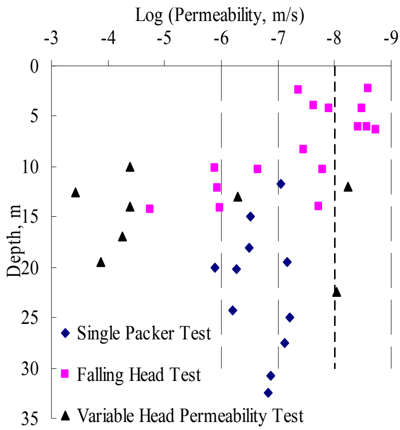

Fig.3 Field permeability tests data

The ground level (GL) of the CBP wall WT-7 is at RL117.0m, with ground water table (GWT) at about 2 m below GL. Several field permeability tests were done to determine the range of hydraulic conductivity or permeability coefficient (k) of the soils in the site. The results are shown in Fig.3; and it indicates that k is in the range of 10^{-7} to 10^{-9} m/s for the top 10 m of predominantly sandy clays. However for the next 10 m of sandy silts, the k value is one order higher in the range of 10^{-6} to 10^{-8} m/s. They are also areas of sands at these depths with k from 10^{-4} to 10^{-5} m/s, but these are at locations some distance away from CBP wall WT-7. This is consistent with the weathering profile which tends to show greater weathering towards the ground surface. The effects of more weathering are to produce large quantities of finer grained soils, and lower permeability as a result.

4. INSTRUMENTATION FOR EXCAVATION MONITORING

The key instruments for monitoring ground and wall deformations are the in-wall inclinometers (I18 in Section 1, I19 in Section2, and I1 in Section 3); and a series of settlement markers behind the walls. The effectiveness of the sub-soil drains for the design intent of lowering the GWT were monitored with water standpipes. Standpipe GW18 is close to I18 at 2m behind wall at Section 1, and GW17 is about 8m behind Section 1. Standpipe GW19 is close to I19 at about 2m behind wall at Section 2. The load cells on the raker anchors were also very important to check that the anchors were not loaded beyond its safe capacity.

5. FIELD PERFORMANCE OF EXCAVATION SYSTEM

Figure 4 depicts the history of the wall deflections recorded by in-wall inclinometers for WT-7 for Sections 1 to 3. It is apparent the largest increment in wall deflection is observed from Stage 3 to Stage 5 (excavation from GL117.0 m to top of rock berm at RL 96.0 m), and Stage 5 to Stage 7 (excavation of rock berm from RL96.0 m to RL86.0 m). It is also obvious that the passive resistance is somewhat proportional to berm size; with the stiffest response in Section 3 which has the largest width of rock berm. What are not so obvious are the effects of rock weathering and rock quality on the stiffness of the available passive resistance. From the rock core runs; the rock with the best quality is in Section 3 with the highest rock head as in Fig.2. Thus combining the effects of the largest rock berm with the best rock quality, it is observed that Section 3 showed maximum wall deflection of 40 mm, about half the values of Sections 1 and 2 with more than 80 mm maximum wall deflections.

Section 1 has about half the berm size of Section 2; and its smaller passive stiffness is observed in its larger wall deflections between 20 and 30 m depths in Fig.4. However, due to the stiffening corner effects of the steel struts in the left hand corner of the excavation pit, the overall maximum deflection of Section 1 is about the same at Section 2, at about 80 mm.

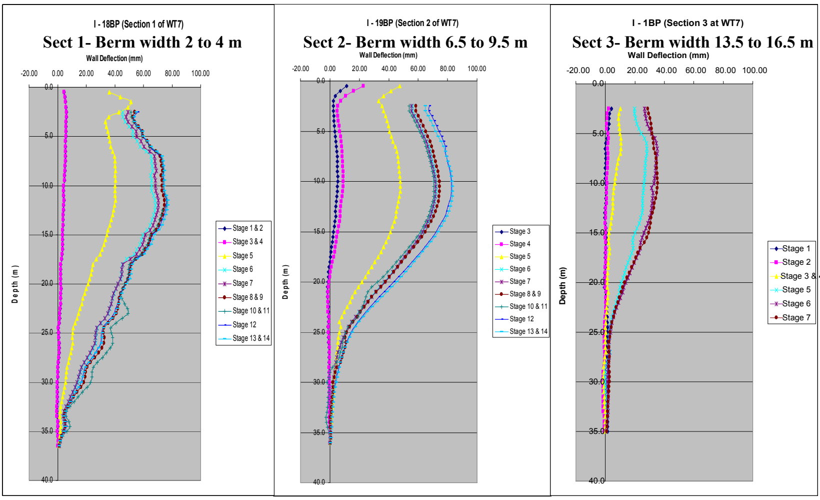

Fig.4 Horizontal deflections of CBP wall WT- 7 with 10m high bottom rock berms

Figure 5 showed the typical settlements profile behind the CBP wall in the INSEAD vicinity close to Section 1 of the wall. Comparing with the wall deflection, the maximum settlement is about 40 mm corresponding to maximum wall deflection of about 40 mm at Stage 7. The contributions to the settlements are partly from wall horizontal movements due to excavation only; and partly from soil compression and consolidation due to GWT lowering used in the design scheme to reduce lateral water pressures behind the CBP wall. Typically, without GWT lowering, local experiences of excavations in stiff Jurong residual soils will result in maximum settlements about 0.5 of maximum wall deflections. Therefore, it is inferred that half the settlements arise out of the excavation while the other half came from effects of GWT lowering.

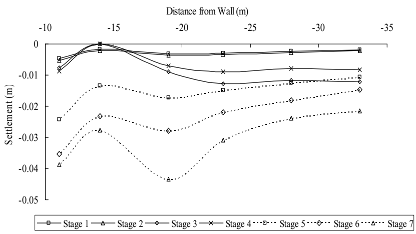

Fig.5 Ssettlements behind WT-7

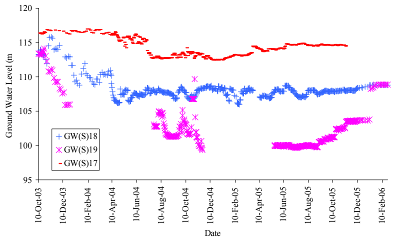

Fig.6 GWT lowering behind WT-7

The sub-soil drains were made of 75 mm diameter PVC piles perforated with several 5 mm diameter holes along its entire lengths, and protected from soil clogging with a thin geotextile filter wrapped around the closed-end pipes. The effects of sub-soil drains on GWT lowering can be observed from the water-standpipes readings of Fig.6. The sub-soil drains were very effective in lowering and maintaining a reduced GWT throughout the excavation works; as long as the pit were kept open, which is the design intent of the sub horizontal embedded drains.

6. SOIL PARAMETERS AND FEM MODEL STUDY

The rock mass properties were estimated using GSI method together with the Hoek and Brown criteria as contained in the program called RocLab (2002) from Rocscience. The best estimate of suitable Mohr Coulomb parameters for WT-7 is in Table 2. The correlation for soil stiffness is based on cu=5N kPa, and Eu/cu for stiff soils is about 400, that is, Eu=2000N kPa; which are widely accepted calibration obtained from many past projects in Jurong soils in Singapore (Tan & Tan, 2004). The drained strength parameters are obtained from the measured c' and phi' of CIU tests from undisturbed "Mazier" samples of stiff Jurong residual soils. The 2D plane-strain FEM model using Plaxis 2D-Version 8 (2002) of the typical tied-back CBP wall WT-7 at Section 2 is shown in Fig.7.

Name	v (-)	E_{ref} (kPa)	c_{ref} (kPa)	φ (○)
1 Fill Sandy Clay	0.2	7500	2	30
2 Stiff Sandy Silt	0.2	60000	20	31
3 Hard Sandy Silt	0.2	1.95E5	30	33
4 Hard Sandy Silt	0.2	2.55E5	85	33
5 Very Weak Siltstone	0.2	1.5E5	40	25
6 Mod Weak Siltstone	0.2	3.25E5	85	33
7 Mod Strong Sandstone	0.2	5E5	125	40
8 Strong Sandstone	0.2	5E5	150	40
5A Very Weak Siltstone	0.2	1.5E5	30	25
6A Mod Weak Siltstone	0.2	3.25E5	60	28

Table 2. MC soil parameters for FEM study

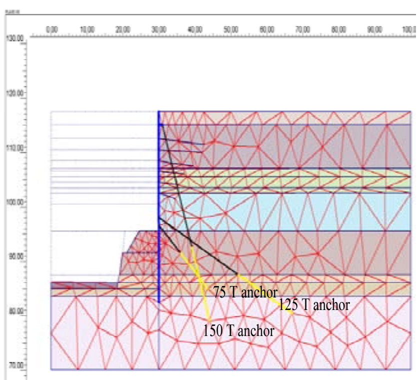

Fig.7 FEM model of WT-7 Section2

7. FEM STUDY

7.1 Drained or undrained excavation

The issue of drained or undrained behavior is not a straightforward matter for stiff residual soils. The problem is that these soils have low permeability between 10^{-6} to 10^{-8} m/s as in Fig.3, but very large stiffness usually greater than 10,000 kPa. Permeability on its own does not control the rate of consolidation in soils. The coefficient of consolidation is given by Terzaghi as:

$$c_v' = \frac{k_v E_{oed}}{\gamma_w}$$

k_v = *coeff of consolidation*

E_{oed} = *Oedometer stiffness*

γ_w = *unit weight of water*

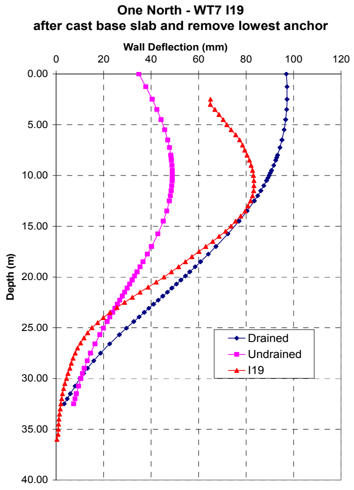

Fig.8 Comparison of drained/undrained analysis at Section 2

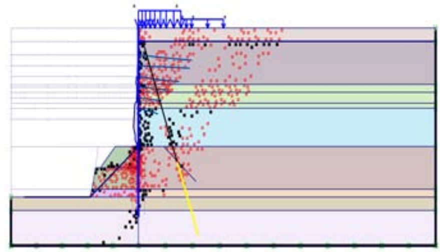

Fig.9 Simulated collapse of wall for Case where GWT is not Lowered behind WT-7

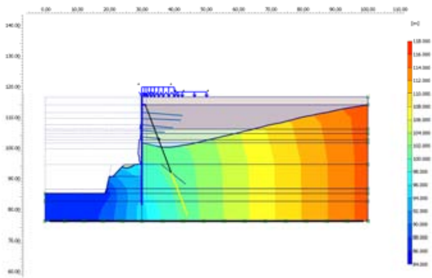

Fig.10 Seepage heads with sub-soil drains at WT7 Section 2

Measured c_v values in oedometer tests suggest c_v values between 20 and 300 m^2/yr. Thus, any soil of c_v greater than 100 m^2/yr would undergo very rapid consolidation much less than the construction period of about a year. The FEM analysis of the CBP wall WT-7 at Section 2 at the end of Stage 7 is shown in Fig.8. For the early stages of excavation in the first 3 to 6 months of progress, the wall response is closer to the undrained predictions. As the excavation progresses to the deeper levels, over a period of about 6 months to a year, the wall response is clearly much closer to the fully drained prediction as shown in Fig.8. An undrained analysis would predict maximum wall deflection at 50 mm, whereas a fully drained analysis with the same set of effective stress parameters predicts maximum wall deflection of 97 mm. The actual maximum wall deflection was about 85 mm when the excavation reached the formation level at 30 m depth from the top ground surface. Clearly a fully undrained analysis at all Stages for this wall design is inappropriate and unsafe.

7.2 CBP wall stability associated with drainage

The hypothetical case of the wall being subjected to full GWT loading at RL115.0 m is simulated in Fig.9. Using drained or undrained analysis, this case is unstable, and an equilibrium state cannot be obtained with the FEM showing collapse at M-Stage at about 0.5 (i.e. 50% to full equilibrium). The top of the wall would deflect horizontally by more than 0.5 m, and the wall would collapse by rotation about the rock berm, 20 m below the top of the wall. Fig.9 showed the typical failure Coulomb wedge where the soils within have all yielded with red dots indicating yielding at Mohr-Coulomb failure surface, and black dots indicating yielding at tension cut-off surface at low effective stresses. Thus, the wall design is critically dependent upon the effective lowering of the GWT behind the wall.

Using seepage modelling, the desired GWT levels can be achieved at steady state as shown in Fig.10. The water pressure behind the wall is reduced significantly to give stable wall conditions. The reality in the ground is that seepage is transient. Given the low permeability of the residual soils especially the upper crust layers which showed k of 10^{-8} to 10^{-9} m/s, it is not expected that steady state condition will be achieved during the early part of the construction period. Measured GWT in Fig.6 from water standpipes at 2 m to 8 m behind the walls showed GWT were lowered between 5 m to 13 m from RL115.0 m, and stayed at the depressed levels throughout the monitoring period of more than a year from Jul 04 to Sep 05 as in Fig.6, when the pit was kept open. This showed that the sub-soil drains had done its job, and is effective in achieving the design intention of lowering the GWT to reduce the water loading on the wall significantly so that the stability of the wall is not compromised. The data also suggests that steady state seepage conditions were reached in about 6 months to a year from the start of excavation works. This again gives another indication that the fully drained conditions for this kind of ground will be obtained within 6 months to a year from completion of excavation. Hence it is very critical to consider the fully drained condition for excavation in stiff residual soils.

The negative consequence of GWT lowering is that it is a form of soil loading that will increase the effective stress of the soil mass below the lowered GWT regime. This will lead to soil consolidation and hence delayed settlements of the ground behind the CBP wall. However, due to the relatively large stiffness of the residual soils, and in the absence of soft compressible clays, the additional soil compression from GWT lowering is small and has acceptable impact on the INSEAD property. From analysis, it is estimated that the ground will settle by less than 50 mm due to both the excavation works as well as the GWT lowering consolidation effects. Actual measured settlements behind the CBP wall on the INSEAD ground confirmed that settlements are in the order of 10 to 40 mm, over the 2 years of the excavation period.

7.3 Global FOS by c-phi reduction

Modern FEM programs like Plaxis provide a very powerful facility of determining the global factor of safety of geotechnical structures through a systematic strength reduction analysis. This is called the c/phi reduction option in Plaxis, whereby the strength reduction factor Msf is increased from 1 to whatever values it takes to form a soil body collapse mechanism in the FEM mesh.

The c/phi reduction method is applied to the final stage of the WT-7 FEM model when the excavation at reach 30m depth to the design base formation level in fully drained condition. The Msf factor is applied only to soil clusters in the FEM computations, where the operative strength of soil clusters at each computational step is set to c/Msf and tan (phi)/Msf. Therefore, it excludes the possibility of failure in structural components such as wall in bending or the anchors in tension pullout.

Figure 11 showed that if the CBP remains elastic without possibility of forming plastic hinge, the FOS will be about 1.75, and the wall can sustain a much larger deflection before it reached collapse state. On the other hand, if the CBP wall is set to have a limiting plastic moment of 4,300 kNm/m based on the steel input and Grade 40 concrete, the FOS will be only 1.40 in Fig.12, with a smaller maximum wall deflection at collapse state.

What is more significant is the different collapse mechanism that the two set of analyses produced. The first analysis with fully elastic CBP wall resulted in wall rotation about its toe as shown in Fig.14 by the incremental displacement vectors plot. This allows for larger zones of soil yielding and hence the higher FOS of 1.75 compared to 1.40. The mechanism of collapse for the case of an elastic-plastic CBP wall is shown in Fig.12. Here a plastic hinge is formed at 15 m from the top of wall, which resulted in a failure with smaller zones of soil yielding compared to Fig.11. Therefore to compute the correct value and mechanism for global factor of safety in FEM models, one must account for the possibility of collapse that includes the failure of any structural component in the earth retaining wall system.

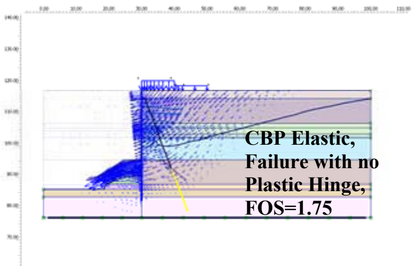

Fig.11 Failure mechanism with elastic wall

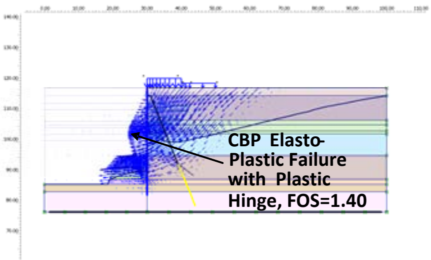

Fig.12 Failure mechanism with plastic wall

8. CONCLUSIONS

The performance of a deep excavation in stiff Jurong residual soils with a single tied-back raker anchor has been described. The key to the safety of the design is the lowering of GWT by sub-horizontal sub-soil drains in the active zone behind the wall. Monitored data and some FEM analysis demonstrate how this wall can work safely when the design intent of lowering ground water table is achieved during excavation. The response of the retaining system in stiff residual soils is closer to drained than undrained behavior. The correct simulation of collapse by a strength reduction approach must account for possibility of wall and anchor failure to correctly assess the true safety of the system.

ACKNOWLEDGEMENTS

Special thanks to LSW Consulting Engineers Pte Ltd, and Great Earth Construction Pte Ltd of Singapore, who has generously provide data and details of this very interesting deep excavation project for the author's study.

REFERENCES

CP4 Singapore Standard. (2003). *Code of practice for foundations*, SPRING Singapore, Singapore.
Plaxis 2D-Version 8. (2002). *Users manual*, AA Balkema, The Netherlands.
RocLab. (2002). *Users manual*, Rocscience Inc.
Tan, S.A. & Tan, R.Y. (2004). "Numerical Study of Two Braced Excavation in Singapore Marine Clay." *Journal of the Southeast Asian Geotechnical Society, April 2004.*

NUMERICAL STUDY ON A NEW STRUT-FREE COUNTERFORT EMBEDDED WALL IN SINGAPORE

S.S. Chuah[1] and S.A. Tan, Harry[2]

[1] PE(Civil), PE(Geo), M.Sc (Civil & Geotech), Former Graduate Student, National University of Singapore, 1 Engineering Drive 2, E1A 07-03, Singapore 117576; PH (+65) 91816850; FAX (+65) 63257482; email: chuah_s_s2000@yahoo.com.sg

[2] Associate Professor, PE(Civil), PE(Geo), AC(Geo), M.Eng, MSc, PhD (Berkeley), Department of Civil Engineering, National University of Singapore, 1 Engineering Drive 2, E1A 07-03, Singapore 117576; PH (+65) 65162278; FAX (+65) 6779 1635; email: cvetansa@nus.edu.sg

ABSTRACT**:** This paper highlights a new earth retention strut-free scheme for deep excavation using counterfort diaphragm wall in a Singapore excavation project. This scheme is not restricted to any particular shape on plan like circular, peanut, donut, or other regular shapes which are required for the enhancement of the hoop stresses for structural resistance against soil and water pressures. These counterfort walls in thick soft soils deposit were founded on good base support for it to work well without any strut or tied-back system. It can be used for a large enclosed excavation provided there is stiff ground reaction at the base of each counterfort wall. Three dimensional (3D) finite element (FE) modelling with Plaxis 3D Foundation v2.2 is used to study and analyse the reaction and stresses of such wall system. A study on panel joint effect can only be made in a 3D model. The need for 3D versus 2D FE analysis is discussed as they may affect the estimation of bending moments for wall design.

1. INTRODUCTION

There are many types of earth retention schemes being used to carry out deep excavation works in Singapore. Such retaining wall systems normally require a set of excavation support system such as steel or concrete struts to support the wall while excavation is being carried out. If strutting system is not used, tied-back wall system may be the other option to retain the wall back in the firm strata by means of ground anchors or soil nails. However, there are other types of retaining walls whereby regular shapes are being deployed to produce a self-supporting system with large hoop stresses generated around the wall/ring slab/beam. This paper highlights a new strut-free earth retention scheme which does not rely on any regular shapes of wall. It consists of counterfort walls, combined with embedded diaphragm retaining walls and counterfort slabs. It must be founded on a hard stratum base support for it to work well without any strut or tied-back system. It can be used for a large enclosed excavation provided there is stiff ground reaction at the base of each counterfort wall. This scheme has been used successfully in several excavation projects by the Koreans.

2. BRIEF LITERATURE REVIEW AND SINGAPORE FIELD CASE STUDY

Jung D.H. et al. (2005) described the Korean experience on using counterfort walls with the use of their two dimensional (2D) geotechnical, and three dimensional (3D) structures finite element programs to investigate various characteristics of the self-supporting counterfort diaphragm walls. They did not consider full 3D soil-structure interaction in their analysis. Their studies include the effect of end boundary condition of the wall toe embedded in a soft rock on the wall behavior. The fixity of the wall bottom was assumed to be either free, hinged, or fixed for comparison. Jeong G.H. et al. (2006) quoted many more Korean projects using the similar counterfort technique. Some were used in combination of raker props, tied-back ground anchors and with various layers of counterfort slabs.

The work on this paper is based on Plaxis 3D Foundation program version 2.2, which allows for the full 3D soil-structure interaction, to study the effects of panel joint in counterfort diaphragm walls. With reference to the earlier study made to compare the results from our own 2D and 3D model analyses [Chuah S.S and Tan S.A. (2009)], it was found that 2D analysis tends to simplify the problem to predict the wall deflection reasonably well, but it cannot produce realistic diaphragm wall forces when counterfort walls are present in the system. Under-estimation of bending moment in 2D model would be the result as compared with 3D bending moment of counterfort diaphragm wall model.

2.1 Singapore Tribeca Deep Excavation Project

The project is a 2-level basement excavation project called Tribeca, for a 30-storey residential development. The excavation depth varies at the second basement level with a maximum of -8m at formation level from the existing ground level.

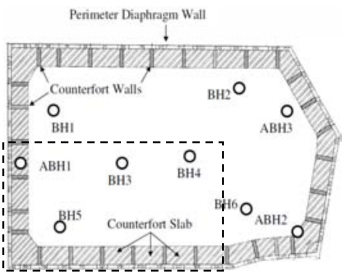

Fig 1 Site investigation boreholes, counterfort walls, counterfort slab and a quadrant model for numerical study

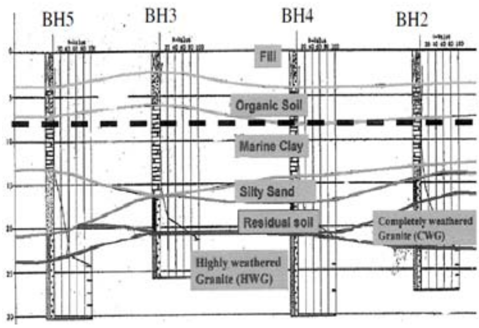

Fig. 3 Typical geological profile (shown for section along BH5-BH3-BH4-BH2)

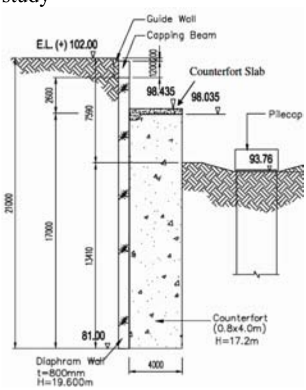

Fig. 2 Typical cross sectional view of diaphragm wall, counterfort wall and slab

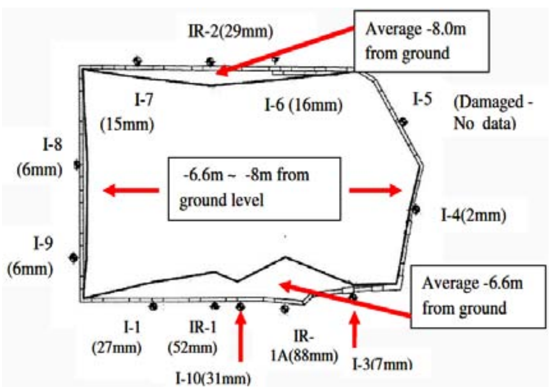

Fig. 4 Inclinometers layout plan and its measured walls' top deflections (unit in millimetres) when formation level was reached

In addition to this, 0.8m thick x 4m long x 21m deep counterfort walls at 7.0 to 7.5m c/c spacing were cast against the diaphragm walls as part of the supporting system to make the strut-free excavation system viable. These counterfort walls were connected by counterfort slab of 0.3m thick. The excavation site is approximately 48m wide and 75m long. Boreholes location, counterfort walls, slab layout and its cross section are shown in Figures 1 and 2 respectively; geological profile is depicted in Figure 3.

2.2 Field Measured Results

Figures 4 and 5 show the field measured results (all figures in millimetres) of wall lateral deflections by inclinometers around the wall perimeter.

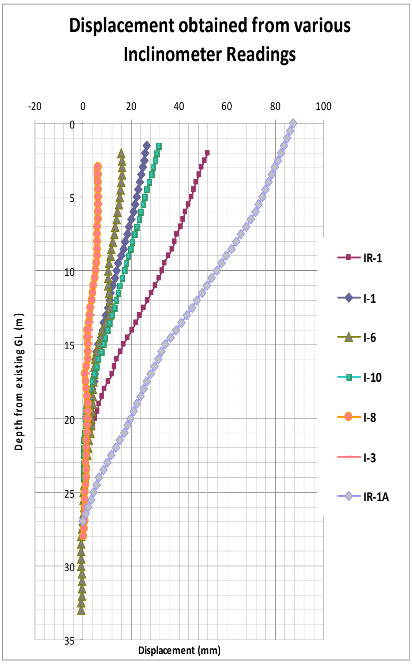

Fig. 5 Plots of various inclinometer readings with depth at Tribeca site, showing the mode of rotation of walls about the toe of counterfort walls

From Figure 5, the walls displaced mainly in a cantilever rotation mode about its toe, with larger movements at the wall top. Such rotation mode of wall movement is expected as the toe of the wall is supported firmly on a good hard base either in residual soil (30 < N < 50), or in completely or highly weathered granite.

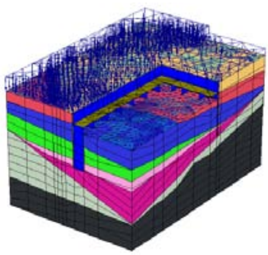

Fig. 6 One quadrant of 3D modeling showing the geological profiles based on various boreholes in that location.

A representative study with one quadrant of the site has been done using Plaxis 3D Foundation program version 2.2, with the calibrated soil parameters proposed as shown in Table 1 [Chuah S.S and Tan S.A. (2009)] to analyze the behaviour of such a wall system for comparison with field measurements.

It has been found that the soil parameters used can match well with the instrumented readings on wall movements and general behaviour of the walls during excavation to final formation level. For this numerical study, the soil parameters as shown in Table 1 have been selected as representative soil parameters with reference to our past experience in Kallang soils excavations in other Singapore projects [S.A. Tan et al (2004)]

Table 1 showed representative soil parameters used in the 3D model: Soil layers follow the sequence as listed below. It is to be noted that for modelling Undrained behaviour in Plaxis under Undrained Effective Stress Analysis with undrained strength parameters method, Plaxis offers the possibility of an undrained effective stress analysis (Material type = *Undrained*) for Mohr Coulomb model with direct input of the undrained shear strength, i.e. $\varphi = \varphi_u = 0$, and $c = c_u$. For this method, whenever the Material type parameter is set to *Undrained*, effective stress values must be entered for the stiffness parameters (Young's modulus E' and Poisson ratio *v'* in the case of Mohr-Coulomb model.)

Table 1: Representative soil parameters used in the numerical study

Soil	Model used in 2D & 3D PLAXIS	Type	γ_{unsat} (kN/m³)	γ_{sat} (kN/m³)	C_{ref} (kPa)	Φ (deg.)	E_{ref} (kPa)	ν	ψ	SPT N
Fill	Mohr-Coulomb	Drained	18	19	0	30	10000	0.3	0	4-7
Peaty CLAY	Mohr-Coulomb	Undrained	16	16	30	0	3000	0.35	0	1-2
Marine CLAY	Mohr-Coulomb	Undrained	16.5	16.5	20	0	4500	0.3	0	0-2
Fluvial Sand	Mohr-Coulomb	Drained	20	20	0	30	48000	0.3	0	5-30
Residual Soil (15<N<30)	Mohr-Coulomb	Drained	19.5	19.5	10	30	50000	0.3	0	15-27
Residual Soil (30<N<50)	Mohr-Coulomb	Drained	19.5	19.5	15	35	60000	0.3	0	30-48
Completely weathered Granite	Mohr-Coulomb	Drained	21	21	20	40	75000	0.3	0	33-80
Highly weathered Granite	Mohr-Coulomb	Drained	22	22	30	40	90000	0.3	0	100

3. NUMERICAL STUDY ON THE PANEL JOINT (PJ) EFFECT ON A 3D ACTUAL TWIN COUNTERFORT (CF) MODEL

Bending moment diagrams for an actual 3D counterfort wall system can be very complex due to the complexity of 3D counterfort diaphragm wall (D/Wall) itself. It has both the bending moment about the horizontal axis of the wall, M_{11} as well as the bending about the vertical axis of the wall, M_{22}.

However, the actual diaphragm wall has its weak panel joints due to the panel construction. The summary of the numerical run below is to show the effect of weak panel joint on the bending moments of diaphragm wall with the presence of counterfort walls. Panel joint properties are as follows:

For the real vertical wall bending about the horizontal axis, it is assumed that the flexural rigidity of the panel joint, EI is the same value as for other diaphragm walls. However, the vertical joint in the diaphragm wall will not be allowing the bending moment to cross over the panel joint. For such effect, the flexural rigidity, EI of vertical panel joint is given a very small value as compared with flexural rigidity, EI for bending about the horizontal axis. Following Plaxis 3D Foundation sign conventions, the E values used are taken as E_1 = 25E6 kN/m^2, and E_2, say 1.0 kN/m^2 to account for panel joint effect.

Table 2 Summary table for comparison between a 3D twin CF Walls with and without PJ:

<table>
<tr><td>Models</td><td colspan="2">3D twin CF Wall models</td></tr>
<tr><td><u>Without PJ:</u> 2D mesh plan view: 324 elements; ave. element size = 1.52m.
3D mesh generated: Total 7776 elements; Ave. element size = 2.06 m (15-noded 3D element)

<u>With PJ</u>: 2D mesh plan view: 397 elements; ave. element size = 1.37m.
3D mesh generated: Total 9528 elements; Ave. element size = 1.88 m (15-noded 3D element)</td><td>Without Panel Joint (plan view and isometric views):
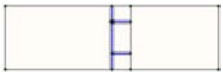
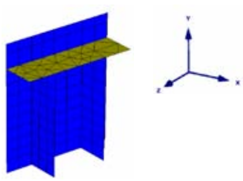</td><td>With Panel Joint (plan view):

Enlarged plan and isometric views:
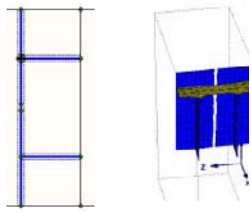</td></tr>
<tr><td>D/Wall Total displacement Ux (mm)</td><td> Max. value 95.0
Min. value 0</td><td>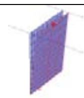 Max. value 97.5
Min. value 0</td></tr>
<tr><td>D/Wall bending moment (kNm/m), M_{11}
Max.
Min.
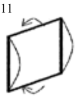</td><td>(see enlarged plots in Fig. 7)

179.0
43.4</td><td>(see enlarged plots in Fig. 8)

210.0
52.4</td></tr>
<tr><td>D/Wall bending moment (kNm/m), M_{22}
Max.
Min.
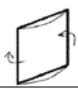</td><td>(see enlarged plots in Fig. 9)

427.0
271.0</td><td>(see enlarged plots in Fig. 10)

473.0
300.0</td></tr>
</table>

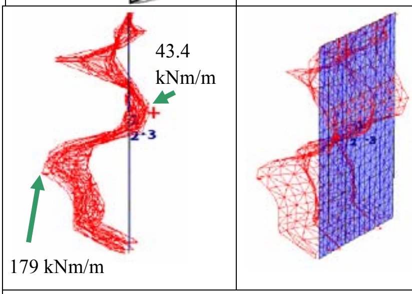

Fig. 7 Without PJ: Bending moment (BM) profile for M_{11}; M_{11} min. value = 43.4kNm/m (RHS). M_{11} max. value = 179kNm/m (LHS)

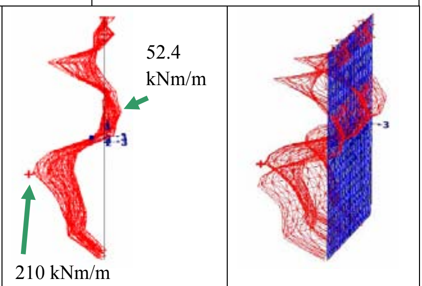

Fig. 8 With PJ: Bending moment profile for M_{11}: M_{11} min value =52.4 kNm/m (RHS). M_{11} max = 210 kNm/m (LHS)

From the table above, one observed that the results are comparable for both models without significant difference in bending moments $M_{11,}$ and M_{22} due to the presence of panel joint. However, with panel joint, M_{11} and M_{22} have been increased in bending moments in both directions.

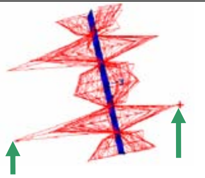 427 kNm/m 271 kNm/m (Looking from top view)	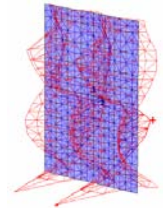	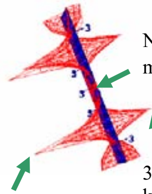 (Looking from top view)	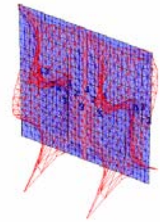
Fig. 9 Without PJ: Bending moment profile for $M_{22;}$ M_{22} min. value = 271 kNm/m; M_{22} max. value = 427 kNm/m		Fig. 10 With PJ: Bending moment profile for $M_{22;}$ M_{22} min. value = 300 kNm/m; M_{22} max. value = 473 kNm/m	

4. NUMERICAL STUDY ON 2 LONG CF WALL AND 4 SHORT CF WALL MODELS WITH PANEL JOINT

It can be shown that the due to smaller stiffness of the 4 short CF walls, the wall deflection is expected to be larger for 4 short CF walls model than that for 2 long CF walls model. M_{11} and M_{22} values for 4 short CF walls model would be smaller due to the span of the wall apart is shorter between the short CF walls. This study is to find out how the effective stresses may vary behind the diaphragm walls in response to the different stiffnesses of the counterfort walls. Effective normal stress is plotted with depth for various horizontal Z locations.

Table 3: Comparison between 4 Short CF Walls and 2 long CF Walls

Models	4 short CF Walls and 2 long CF Walls	
4 short CF Walls: 2D mesh plan view: 399 elements; ave. element size = 1.37m. 3D mesh generated: Total 9576 elements; Ave. element size = 1.88 m (15-noded 3D element) 2 long CF Walls: 2D mesh plan view: 397 elements; ave. element size = 1.37m. 3D mesh generated: Total 9528 elements; Ave. element size = 1.88 m (15-noded 3D element)	With Panel Joint 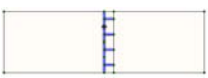 CF wall size 2m long x 0.8m thk each (4 nos at 3.75m c/c) (x, z) = (0,3.75m) (x, z) = (0,9.38m) 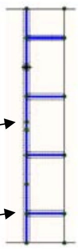	With Panel Joint 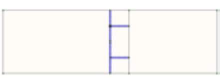 CF wall size 4m long x 0.8 m each (2 nos at 7.5m c/c) (x, z) = (0,3.75m) (x, z) = (0,7.5m) 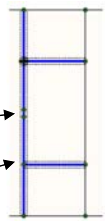

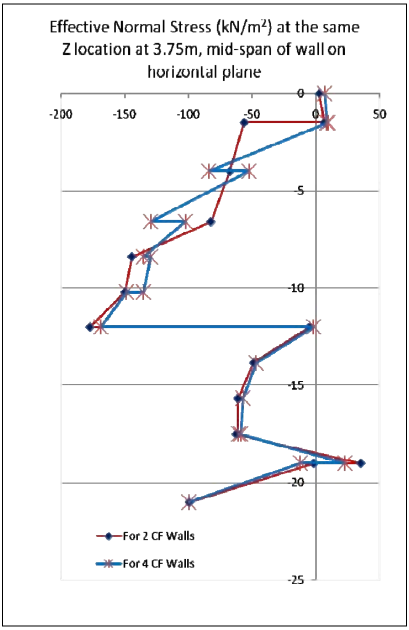

Fig. 11 Effective Normal Stress plot at location Z = 3.75m for both walls

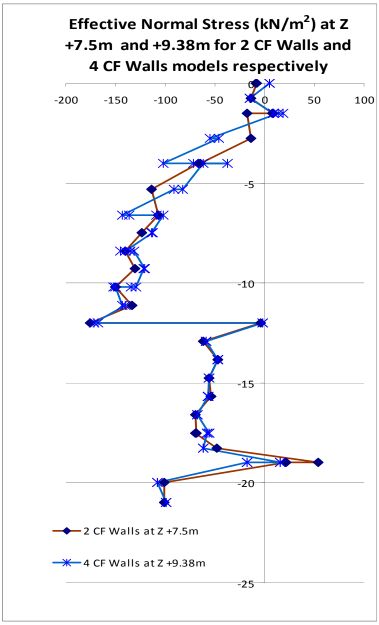

Fig. 12 Effective Normal Stress plot at Z=7.5m and Z=9.38m for 2CF and 4CF Walls respectively

From the above plots, one can notice that the effective normal stresses behind the walls do not vary much for the different types of Counterfort Walls.

5. CONCLUSIONS

Through this numerical study, conclusions below can be made in relation to the analysis and design of counterfort diaphragm wall system for having a strut-free excavation site (even at a site with deep soft soils deposit):

a) The founding soil/rock layer for the toe of counterfort walls must be a hard stratum for supporting the counterfort walls which tend to rotate about the toe of the counterfort walls.

b) 3D modelling is better in order to analyze and obtain the actual forces for design such as bending moments to the diaphragm wall in a counterfort diaphragm wall system.

c) Panel joints have no significant impact on the redistribution of diaphragm wall bending moments in M_{11} and M_{22} though there is an increase in values, where counterforts are present for this particular case. It is noted that only 3D modelling can produce such real forces in the complex behaviour of counterfort wall system where panel joints can be modelled appropriately.

d) Stiffness of counterfort wall system (for long CF walls at far spacing or short CF walls at close spacing) has minimum influence on the effective normal stress distribution behind the diaphragm walls.

2D analysis has its limitation to model the 3D effects. From the past 2D analyses done in plane strain conditions, they tend to simplify the problem by modelling well for the wall deflection but they cannot produce the actual diaphragm wall forces particularly when counterfort walls are present.

It is necessary to control wall deflection for not causing large ground movement if strut-free counterfort wall system is used. Such scheme may govern the design by wall deflection for very large depth of excavation such as very deep basement, underground rail station and tunnels. Hence, other mitigation measures such as additional layers of struts or tied-back at the top of wall may be required to avoid excessive wall deflection at the top.

ACKNOWLEDGEMENTS

The first Author would like to thank Building and Construction Authority (BCA), Singapore for allowing him to participate in the ER2010 Conference. Special thanks to Tiong Seng Contractors Pte. Ltd. and Dong-A Geological Engineering Co. Ltd. for their excellent support and assistance to the authors while writing this paper.

REFERENCES

Chuah S.S and Tan S.A, Harry (2009). Finite Element Analysis of a Counterfort Embedded Wall in a Strut-Free Excavation. Underground Singapore, 3-4 December 2009, Singapore

Jeong G.H. et al. (2004). Application of Self-Supported Diaphragm Wall Method Using Counterfort Technique. Korea Geotechnical Society, Spring Conference, March 25 -26, 2004, Seoul, Korea

Jeong G.H. et al. (2008). Singapore Case Study of Self Supported Diaphragm Wall Method using Counterfort Technique, KGS Fall National Conference, October 10-11, 2008, Gwangju, Korea

Jung D.H. et al. (2005). Characteristics of Self-Supported Counterfort Diaphragm Wall, Paper No. 2005-JSC-364

Ou C.Y., Teng F.C., Seed R.B. and Wang I.W. (2008). Using Buttress Walls to reduce excavation-induced movements, *Proceedings of the Institution of Civil Engineers Geotechnical Engineering* 161, August 2008 Issue GE4 pages 209-222

Tan S.A. and Tan R.Y. (2004). Numerical Study of Two Braced Excavation in Singapore Marine Clay. *Journal of the Southeast Asian Geotechnical Society, April 2004.*

Design of Permanent Soil Nail Walls using Numerical Modeling Techniques

King H. Chin [1], P.E., Member, Geo-Institute, Narong Trongtham[2], P.E., S.E., and Chris Wolschlag[3], Ph.D., P.E, S.E.

[1]Associate, GeoEngineers, Inc., 8410 154th Avenue NE, Redmond, WA 98052; PH: (425) 861 6000; FAX: (425) 861 6050; email: kchin@geoengineers.com
[2]Principal, ABKJ, 800 Fifth Avenue, Suite 2500, Seattle, WA 98104; PH: (206) 340 2055; FAX: (206) 340 2266; email: NarongT@abkj.com
[3]Partner, Ground Support PLLC., 2475 152th Avenue NE, Redmond, WA, 98052; PH: (425) 376 0177; FAX: (425) 376 0277; email: chrisw@groundsupport.com

ABSTRACT

This paper presents the numerical analysis completed for design of a 4,700-car underground parking garage located at the Microsoft Block C site in Redmond, Washington. The underground parking garage is about 335.3 m (1,100 feet) long in the east-west direction and 121.9 m (400 feet) wide in the north-south direction. The excavation and construction of the basement wall was completed using a permanent top down soil nail wall. Because of the length of the structure, the garage was designed as three separate sections with construction joints up to 152.4 mm (6 inches) wide in the east-west direction to accommodate the seismic movement of the soil as well as thermal expansion of the concrete. Permanent soil nails were utilized to resist the soil pressure and improve the seismic performance of the east and west walls. Finite element modeling was completed to estimate the seismic deformation of the east and west walls and to design gaps between floor slabs and the east and west walls. The purpose of the gaps was to prevent transfer of seismic soil pressures to the garage structure, hence, significantly reducing the number of the internal shear walls. Discussions on the effect of permanent soil nails on wall deformation and wall pressure under both the static and seismic conditions are also presented.

INTRODUCTION

The Microsoft Block C site is located southwest of the intersection of SR-520 and NE 40th Street in Redmond, Washington. The project included construction of four new office buildings of about 13,934 m^2 (150,000 ft^2) each and a four level, 4,700 car below-grade parking garage. The below-grade parking garage is about 335.3 m (1,100 feet) long in the east-west direction and about 121.9 m (400 feet) in the north south direction. Because of the length of the structure, the garage was designed as three separate sections with construction joints up to 152.4mm (6 inches) wide in the east-west direction to accommodate the seismic movement of the soil as well as thermal expansion of the concrete. Figure 1 shows a construction photo of the Microsoft Block C development.

Conventional force-based design methods would have required many internal shear walls in the east west direction to resist the soil pressure under both the static and seismic loading conditions. For this project, permanent soil nails were incorporated in the permanent basement wall design to reduce the seismic load on basement walls. Deformation based numerical analyses were completed to evaluate the performance of the permanent soil nails under both the static and seismic conditions. The results of the numerical analyses were used to design the gaps between the floor slabs and the east and west walls. The results also showed that the soil nails play a significant role in reducing the wall deformation under seismic conditions, hence reducing the soil pressure acting on the walls. This paper describes the numerical analysis and presents the conclusions and discussions on the positive effect of permanent soil nails on basement wall performance.

Figure 1. MS Block C Development

SITE CONDITIONS

The site is underlain by three general soil units: fill, glacial till, and advance outwash deposits. The fill is loose to medium dense silty sand with gravel and varies in thickness of 0.6 to 5.2 m (2 to 17 feet). The glacial till generally consists of medium dense to very dense silty sand with varying amounts of gravel and underlies the fill. The advance outwash deposits are present below the glacial till and consist of dense to very dense sand with silt and occasional gravel. Based on the monitoring well readings, static groundwater is located below the lowest finish floor elevation.

DESIGN ANALYSES

Soil Nail Wall Stability Analyses

The garage excavation was supported with soil nail shoring walls. The external stability of the soil nail walls was designed to meet the factor of safety per Federal

Highway Administration (FHWA) Geotechnical Engineering Circular No. 7. The design soil nail pullout resistance used for the fill was 29.2 kN per meter (kN/m, 2 kips per foot (k/ft)). The design soil nail pullout resistance used for the glacial till and advance outwash deposits was 58.4 kN/m (4 k/ft).

Based on the stability analyses, seven rows of soil nails were required for the east and west walls. The lower six rows of nails are permanent and epoxy-coated; the row 1 soil nails within the top 3 m (10 feet) of the wall (about 4 m (13 feet) from finished grade) are temporary to accommodate future utility work around the garage. The typical horizontal soil nail spacing was 1.8 m (6 feet) on center except for the soil nails in row 2, which has a horizontal spacing of 0.9 m (3 feet) on center to support the cantilever section of the walls. The required soil nail lengths range from 5.5 to 13.7 m (18 to 45 feet), and the required soil nail thread bar sizes range from #8 to #11 grade 75 steel bars and 25.4-mm (1-inch) to 31.75-mm (1¼-inch) grade 150 steel bars.

Figure 2 presents the typical sections of the east and west walls, which have similar height and soil conditions. However, soil nail rows 2 and 3 of the east wall are longer than the west wall because of the more stringent seismic performance required for the mechanical and HVAC equipment that is housed behind the east wall.

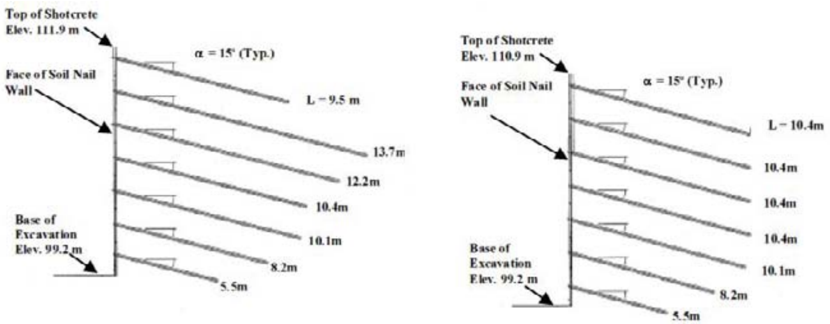

Figure 2. Typical Soil Nail Wall Section

Soil Nail Wall Deformation Analyses

The critical design criteria for the east and west walls are 1) determining the length of the permanent soil nails that will maintain wall movements to an acceptable level under seismic loading conditions, and 2) designing a gap between the garage wall and the floor slabs so that load is not transferred between the garage wall and the floor slab. Seismic performance of the east and west walls was evaluated by completing finite element modeling with the computer program PLAXIS V8.

Finite Element Design Sections. A total of four design sections were evaluated for the project's east and west walls. This paper presents only the results of the typical east and west wall sections. Figure 3 presents the typical PLAXIS design sections developed for the east and west walls.

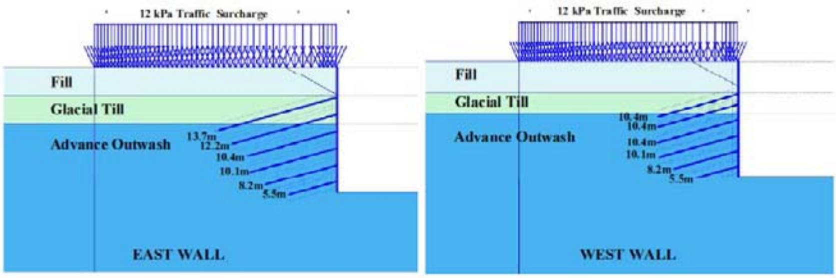

Figure 3. PLAXIS Typical Design Sections

Selection of Earthquake History. A recorded earthquake time history was selected for use in the PLAXIS analysis that was representative of the seismic hazard at the site and consistent with the design earthquake forces used in the structural design of the garage. For this project, the time history for the east-west component recorded at 13 BRAN station during the 1989 Loma Prieta Earthquake was selected for use in the finite element deformation analysis. Figure 4 shows the selected design earthquake response spectrum closely matches the IBC Site Class C generalized response spectrum for periods between 0 and 1 second, which is the structural period range of interest.

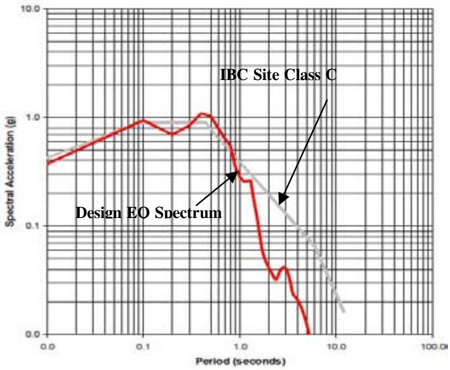

Figure 4. Design EQ Response Spectrum

PLAXIS Input Time History. The scaled time history discussed above represents a rock outcrop motion. This time history was deconvolved to the bedrock level and then propagated through the soil profile using the one-dimensional (1D) site response analysis program PROSHAKE. The time history computed at the elevation that corresponds to the bottom of the PLAXIS model was then used as the input time history in the PLAXIS analysis, as shown in Figure 5.

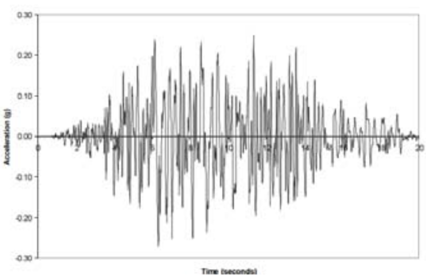

Figure 5. PLAXIS Input Time History

PLAXIS Input Soil and Structural Parameters. Table 1 presents the soil input parameters used in the PLAXIS analyses. Properties of the structural elements modeled in PLAXIS are summarized in Table 2 below. The axial stiffness was calculated using the soil nail load test results obtained from other soil nail projects with similar soil conditions. The permanaent basement wall was 228.6 mm thick where laterally supported by nails and 304.8 mm thick where cantilevered.

Table 1. Soil Parameters for PLAXIS Analysis

Parameter	Fill	Glacial Till	Advance Outwash
Soil Unit Weight, kN/m^3 (pcf)	19.6 (125)	20.4 (130)	20.4 (130)
Friction Angle, ϕ, degrees)	32	40	38
Cohesion, c, kPa (psf)	0 (0)	19.2 (400)	0 (0)
Unloading-reloading Soil Modulus, E, MPa (ksf)	239 (5,000)	1005 (21,000)	526 (11,000)

Table 2. Structural Input Parameters for PLAXIS Analysis

Structural Element	Bending Stiffness, (EI) kN-m^2/m (kip-ft^2/ft)	Axial Stiffness, (EA) kN/m (kips/ft)
Soil Nails GR 150 1¼" (6' horizontal spacing)	n/a	2.92×10^5 (2.0×10^4)
Soil Nails GR 150 1" (6' horizontal spacing)	n/a	2.63×10^5 (1.8×10^4)
Soil Nail GR 75 #11 (6' horizontal spacing)	n/a	3.06×10^5 (2.1×10^4)
Soil Nail GR 75 #10 (6' horizontal spacing)	n/a	2.92×10^5 (2.0×10^4)
Soil Nail GR 75 #9 (6' horizontal spacing)	n/a	2.77×10^5 (1.9×10^4)
9" Garage Soil Nail supported Wall	2.2×10^4 (1.6×10^4)	4.96×10^6 (3.4×10^5)
12" Garage Cantilever Wall	7.9×10^4 (5.9×10^4)	7.73×10^6 (5.3×10^5)

n/a – not applicable. Soil nails provide axial capacity only

Finite Element Modeling Results

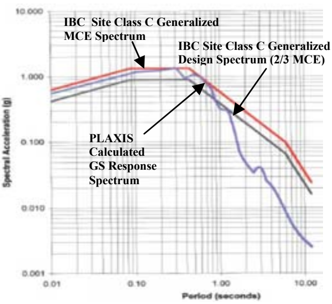

Figure 6. Ground Surface Response Spectrum

Ground Surface Response Spectrum. Figure 6 presents the response spectrum of the time history calculated at the ground surface by PLAXIS. By comparing the response spectra of the input time history (shown in Figure 4) and that of the output time history at the ground surface, the finite element model computes reasonable site amplification effects anticipated for a stiff site. In addition, the calculated ground surface response spectrum shown in Figure 6 indicates that the seismic forces of the time history used in the finite element model matches closely the IBC Site Class C generalized response spectra between 0 and 1 second.

Soil Nail Wall Deformation. Figure 7 presents the horizontal deformation contours of the east and west soil nail walls at the end of the design earthquake. These contours are generally consistent with the failure wedges analyzed using a traditional limit equilibrium pseudo static soil nail analysis. The development of the displacement wedge is consistent with outward rotation of the wall. The permanent relative wall deflections at different garage levels with respect to the bottom of the garage at the end of the design earthquake are summarized in Table 3. The results indicate that the east wall deforms less than the west wall due primarily to the longer west wall nails in rows 2 and 3.

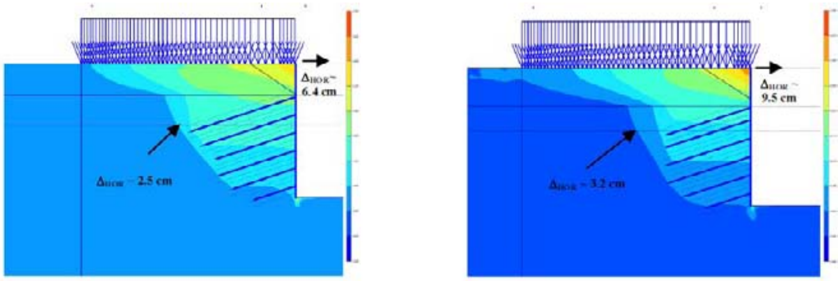

Figure 7. Horizontal Soil Deformation Contours

Table 3. East and West Wall Relative Horizontal Deformation at Garage Levels

Garage Level	West Wall, cm (inches)	East Wall, cm (inches)
Plaza Level	7.6 (3)	5.1 (2)
Level X1	5.1 (2)	2.5 (1)
Level X2	2.5 (1)	1.8 (0.7)
Level X3	1.3 (0.5)	1.0 (0.4)
Slab On Grade	0	0

Axial Soil Nail Forces. The maximum soil nail load during the design earthquake was calculated and used by the structural engineer in design of the connection between the soil nail shotcrete facing and the permanent garage walls. Table 4 presents the maximum axial nail force computed during the design earthquake event.

Table 4. Maximum Nail Force at East and West Walls during the Design Earthquake

Soil Nail Row	Max Nail Force at Garage Wall during Earthquake Loading, kN (kips)	
	West Wall	East Wall
2	235 (53)	289 (65)
3	80 (18)	107 (24)
4	102 (23)	120 (27)
5	58 (13)	76 (17)
6	62 (14)	116 (26)
7	62 (14)	116 (26)

Soil Nail Wall Bending Moment. Figure 8 presents the east and west wall bending moments calculated by PLAXIS at the end of top down soil nail wall construction. As shown in Figure 8, the predicted bending moment diagrams are consistent with a braced condition with the soil nail acting as struts. The primary benefit of using permanent soil nails under static conditions is the reduced wall bending moment because of the reduction in braced length.

Figures 9a and 9b present the predicted maximum east and west wall bending moments for the design earthquake time history. The bending moment increases under seismic loading as anticipated. Of special interest is the fact that the maximum bending moment in the east wall is much lower than that in the west wall. This is consistent with the displacement of the soil towards the east wall under seismic loading being lower for the soil mass containing longer nails. This is reflected by the higher soil nail axial forces in the east wall compared to the west wall, as presented above in Table 4.

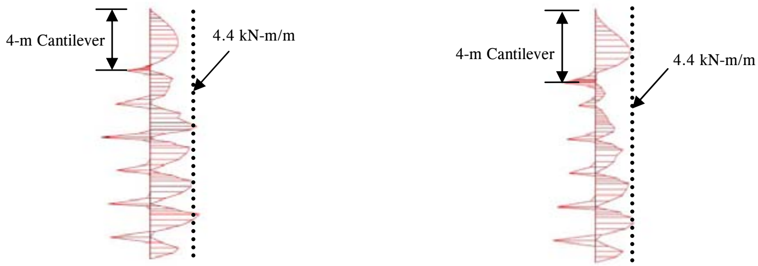

a) East Wall b) West Wall

Figure 8. Predicted Wall Bending Moment at the End of Construction

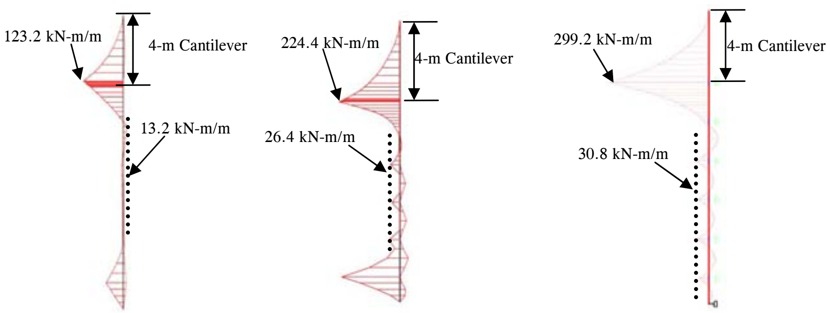

a) PLAXIS – East b) PLAXIS – West Wall c) STAAD – Earth Pressure Diagrams

Figure 9. Predicted Maximum Wall Bending Moment (Seismic Conditions)

Figure 9c presents the wall bending moment under the conventional apparent static and seismic earth pressure calculated using the structural computer program STAAD. Comparison of the bending moment diagrams shown in Figures 9a through 9c indicates the predicted maximum bending moments by PLAXIS are consistently lower than the values obtained using the conventional earth pressure diagram. This is because the conventional earth pressure method does not account for the lateral resistance provided by the permanent soil nails.

CONCLUSIONS

The authors conclude that for a competent soil site such as that presented in this paper:

1. Use of permanent soil nails can reduce the soil loads acting on the retaining walls which can result in more cost effective wall design. This is anticipated to benefit projects with long retaining walls (e.g. highways).
2. Wall design using conventional earth pressure for retaining walls with permanent soil nails will yield conservative design as the effect of the permanent soil nails is not accounted for.
3. Numerical analysis is an essential tool for realistically estimating soil loads acting on retaining walls with permanent soil nails.
4. Use of numerical analyses can optimize the design by considering the effect of the permanent soil nails and the soil-wall-soil nail interaction under seismic loading.
5. For projects where numerical analyses are used, peer review is critical and should be required to make sure that the results are reasonable and the design is sound.

ACKNOWLEDGEMENT

This paper has benefited greatly from the diligent review completed by Mr. Matthew Smith, P.E., Dr. Gordon Denby, P.E. and Mr. Shaun Stauffer, P.E. of GeoEngineers, Inc. The technical editing completed by Mr. Stephen Lynch is also acknowledged.

REFERENCES

Brinkgreve, R.B.J., Broere, W. and Waterman, D. 2004. "PLAXIS 2D" Version 8.

C. A. Lazarte, D. Espinoza, P. J. Sabatini and V. Elias (2003). *"Geotechnical Engineering Circular No. 7: Soil Nail Walls."* Report FHWA-IF-03-017, Federal Highway Administration, Washington D.C.

International Code Council (2003). *"International Building Code 2003."*

Finite-element Analysis of Lateral Pressures on Rigid Non-yielding Retaining Walls with EPS Geofoam Inclusion

Aurelian C. Trandafir, Jesse F. Moyles, and Benjamin A. Erickson

Department of Geology and Geophysics, Geological Engineering Program, University of Utah, 115 South 1460 East Rm. 383, Salt Lake City, Utah 84112-0101, USA, E-mail: atrandafir@yahoo.com, a.trandafir@utah.edu; Tel: +1-801-5850491; Fax: +1-801-5817065

ABSTRACT

An elasto-plastic constitutive model for expanded polystyrene (EPS) geofoam was employed with a finite-element analysis addressing the lateral pressures on a rigid non-yielding retaining wall with geofoam inclusion. Experimental results from laboratory uniaxial and triaxial compression tests were used to derive the parameters of the elasto-plastic constitutive models for the geofoam inclusion and the backfill soil used in the finite-element investigation. The numerical study revealed that for the analyzed EPS density, specific combinations of geofoam panel thickness and retaining wall height may induce plastic strains in the geofoam. The results were compiled into design charts providing the distribution of lateral pressures on the wall and the geofoam isolation efficiency as a function of EPS panel thickness and wall height.

INTRODUCTION

The application of the compressible inclusion function of EPS geofoam to rigid non-yielding retaining walls is known as the Reduced-Earth-Pressure (REP) concept (Horvath, 1997) and consists of placing a relatively thin geofoam panel between the wall and the retained soil (Figure 1). Due to its low stiffness, the geofoam will undergo horizontal compression allowing for a certain lateral deformation of the retained soil mass (i.e., controlled yielding) thus mobilizing the soil shear strength and bringing the soil mass closer to the active failure state. The result is a reduction in the lateral pressures on the wall, as they will approach the minimum value characterizing the active state. Partos and Kazaniwsky (1987) reported the installation of a 25-cm thick geofoam panel to reduce the lateral wall pressures on a rigid basement wall of an underground parking facility retaining a 10-m high granular backfill. Finite-element analyses of this field instrumented case predicted lateral wall thrust reductions of 26% for the short-term (i.e., rapid geofoam loading) and 29% for the long-term (i.e., geofoam creep loading) conditions compared to the at-rest state (Murphy, 1997). Numerical sensitivity studies based on the finite-element method were also conducted to investigate the effect of EPS panel thickness and geofoam elastic modulus on the reduction of lateral pressures on rigid non-yielding retaining walls for various wall heights and backfill properties (Karpurapu and Bathurst, 1992).

Most of the previous numerical analyses of lateral pressures on rigid non-yielding retaining structures with geofoam inclusion employed a linear-elastic model to describe the stress-strain behavior of EPS geofoam (e.g., Karpurapu and Bathurst, 1992). However, there is now considerable experimental evidence showing that this cellular geosynthetic exhibits an elasto-plastic response under monotonic loading with a relatively well-defined yield stress characterizing the onset of plastic behavior (e.g., Chun et al., 2004; Wong and Leo, 2006). Therefore, in the present investigation, an elasto-plastic model of EPS geofoam is employed with a finite-element sensitivity study addressing the lateral pressures on rigid non-yielding retaining walls with geofoam inclusion. The numerical analysis was conducted using the 2007 version of the Sigma/W finite-element module of the GeoStudio Office software package (GEO-SLOPE International Ltd., 2008).

PROBLEM SPECIFICATION

Figure 1 shows the finite-element mesh for a retained soil mass of height *H* with an EPS geofoam panel of thickness *t* placed against the face of the rigid non-yielding retaining wall. Smooth interfaces have been considered at the geofoam contact with the wall, the retained soil and the foundation ground. In these circumstances, the direction of the total wall thrust will be horizontal, and the orientation of the principal stresses within the geofoam will be along the vertical and horizontal directions. A smooth backfill-foundation interface has been considered in the present analysis. The boundary conditions for the finite-element model in Figure 1 involved restrained horizontal displacements along the vertical boundaries, and restrained vertical and horizontal displacements along the bottom horizontal boundary. The finite-element modeling was designed to simulate the evolution of lateral stresses on the rigid wall during a staged construction of the backfill with the soil placed in 1-m lifts up to a total height of 12 m.

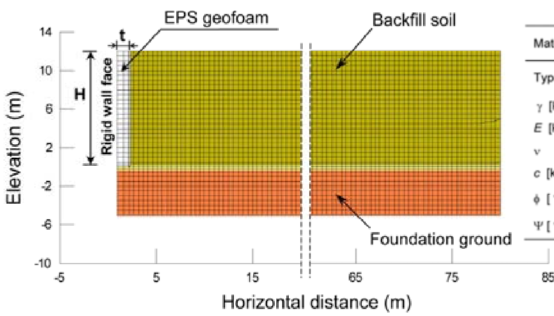

Material	EPS geofoam	Backfill soil	Foundation
Type	Elasto-plastic	Elasto-plastic	Linear elastic
γ [kN/m^3]	0.15	17	23.0
E [kPa]	3563	50500	5×10^7
ν	0.01	0.33	0.3
c [kPa]	$0.5(\sigma_{1y}-\sigma_3)$	0	------
ϕ [°]	0	43.4	------
Ψ [°]	-90	19.1	------

Figure 1. Finite-element model of the geofoam-backfill system behind a rigid non-yielding retaining wall and material properties used in the analysis.

The EPS geofoam stress-strain properties (Figure 1) were obtained from a multistage uniaxial compression test conducted in the Soil Mechanics Laboratory of the Department of Geology and Geophysics at the University of Utah on a 7-cm diameter cylindrical EPS specimen provided by the ACH Foam Technologies Llc, Salt Lake City, Utah, and characterized by a density of 15 kg/m^3 and a height to diameter ratio of 2:1. In the multistage uniaxial compression test, the axial stress (σ_a) was applied in relatively small increments (i.e., $\Delta\sigma_a$= 9 kPa), with each stress increment being added after the specimen has reached equilibrium (i.e., creeping has ceased) under the previous load step. This test is appropriate for the characterization of the long-term static behavior of the EPS geofoam panel behind the rigid non-yielding retaining wall since it incorporates the strains associated with the creeping of geofoam under static loads.

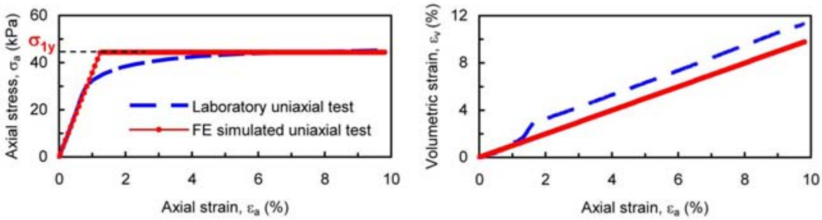

Figure 2. Experimental and finite-element (FE) simulated stress-strain response of EPS geofoam in the multistage uniaxial compression test.

As seen in Figure 2, the experimental results from the multistage uniaxial compression test agree quite well with the finite-element simulated response using the geofoam elasto-plastic model parameters depicted in Figure 1. In the present numerical investigation, a constant value of the major principal stress at yield (σ_{1y}) was assumed for the range of small confining stresses (i.e., σ_3 < 2 kPa) occurring throughout the EPS geofoam panel, as illustrated in Figure 4. In order to achieve a constant value of σ_{1y} for different minor principal stresses (σ_3), the *c* parameter of the Mohr-Coulomb yield function was set as a function of σ_3 (i.e., $c = 0.5(\sigma_{1y}-\sigma_3)$), whereas ϕ was set to zero (Figure 1). The geofoam plastic strain increments are provided by a non-associated plastic flow rule characterized by a negative dilatancy angle (Ψ= -90°).

The backfill soil was also modeled as an elastic-perfectly plastic material with Mohr-Coulomb yield function and non-associated flow rule (Figure 1). All backfill soil model parameters except for the Poisson's ratio were derived from the experimental results of consolidated-drained triaxial compression tests reported by Gomez (2000) on dense (relative density D_r= 92%) silica sand. Since the Poisson's ratio (υ) is controlling the value of the coefficient of lateral earth pressure at rest (K_0) in the present elasto-plastic finite-element analysis, the value of υ was carefully selected based on published experimental and numerical evidence reported by Gomez (2000). It is well recognized that Jaky's equation (K_0 = 1- sin ϕ), while providing reasonable K_0 values for loose sand, is a poor predictor yielding considerable underestimates of K_0 for densely compacted sand backfills. Therefore, laboratory measurements of the wall thrust due to at-rest lateral earth pressures acting on the instrumented panels of a rigid non-yielding retaining wall model performed by Gomez (2000) were used in selecting the υ and K_0 values for the present analysis. This experimental study indicates K_0 values within 0.43-0.48 for 1 to 2-m high compacted sand backfill characterized by a friction angle of 47°. Additionally, finite-element simulations of the backfilling process during the previously mentioned laboratory tests on instrumented rigid non-yielding retaining wall models provided a very good agreement between the predicted and measured at-rest lateral wall thrusts for a back-calculated υ value of 0.36 in the context of a compacted sand backfill with a friction angle ϕ =47° (Gomez, 2000). Hence, a value of the Poisson's ratio of 0.33 associated with K_0 = 0.493 was considered reasonable for the present finite-element study involving a densely compacted sand backfill with a friction angle ϕ = 43.4°. Figure 1 also provides linear elastic material properties within the typical range for sound, intact sandstone bedrock (Lambe and Whitman, 1969) assumed as foundation ground in the present numerical analysis.

NUMERICAL RESULTS AND DESIGN CHARTS

Figure 3 shows representative horizontal stress isolines (σ_h) within the geofoam-backfill system for various wall heights and an EPS panel thickness t = 1.2 m. For wall heights of 3 and 6 m, the entire EPS panel is subjected to stresses within the elastic range. On the other hand, for wall heights of 9 and 12 m plastic strains developed throughout a specific height H_y of the EPS panel, indicating yielding of geofoam in that area. The stress isolines become divergent in the vicinity of the yield zone of the EPS geofoam panel, and are shifted upward (Figure 3). This numerical outcome translates into stress transfer to the elastic region of the geofoam panel due to the redistribution of stresses associated with yielding of geofoam in the plastic region. As seen in Figure 3, the stress redistribution associated with plastic yielding of the EPS geofoam panel also propagates into the backfill soil, and the backfill volume undergoing stress redistribution increases with increasing height of the yield zone of the geofoam panel (H_y). It is worth mentioning that the intermediate-field horizontal stress state throughout the backfill with EPS geofoam inclusion shown in Figure 3 is different than the at-rest state since the backfill experiences stress relaxation due to the lateral compression of the geofoam panel. The at-rest condition involves no lateral deformations in the soil deposit, whereas the deviation from the vertical direction noted in the displacement vectors throughout the backfill with EPS geofoam inclusion for H = 6 m (Figure 3) indicates the occurrence of lateral strains in the retained soil mass. Thus the coefficient of lateral earth pressure in the intermediate-field region of the backfill with geofoam inclusion should be smaller than K_0.

The distribution of lateral pressures (σ_h) along the rigid retaining wall is illustrated in Figure 4 for an EPS panel thickness t = 1.2 m and various wall heights. In Figure 4, σ_h also stands for the horizontal stress in the geofoam panel in the vicinity of the wall-geofoam interface, whereas σ_v represents the vertical stress in the geofoam. The lateral earth pressures on the wall associated with the at-rest condition (p_0) and the active Rankine state (p_a) for the retaining wall with no geofoam inclusion were also plotted for comparison with the geofoam inclusion case (Figure 4). Throughout the geofoam panel, $\sigma_v < \sigma_h$ implying that the minor principal stress acts in the vertical direction (i.e., $\sigma_3 = \sigma_v$) and the major principal stress acts along the horizontal direction (i.e., $\sigma_1 = \sigma_h$). For wall heights of 3 and 6 m, σ_h throughout the geofoam is smaller than the major principal stress at yield (σ_{1y} = 45 kPa) indicating that the entire EPS panel is stressed in the elastic domain. The σ_h-diagram in such circumstances is quasi-linear and bounded by the p_0 and p_a cases (Figure 4). As discussed by Horvath (1997), the nonlinearity noticed in the horizontal stress distribution along the wall even for the cases associated with no plastic yielding of the geofoam panel (i.e., H = 3 m and H = 6 m in Figure 4) is due to the arching allowed to develop in the retained soil mass by the compressible geofoam inclusion. Murphy (1997) demonstrated that arching and associated nonlinear distribution of lateral wall pressures occurs even in the case of a geofoam panel of limited extent that does not cover the full height of the retaining wall down to the bedrock.

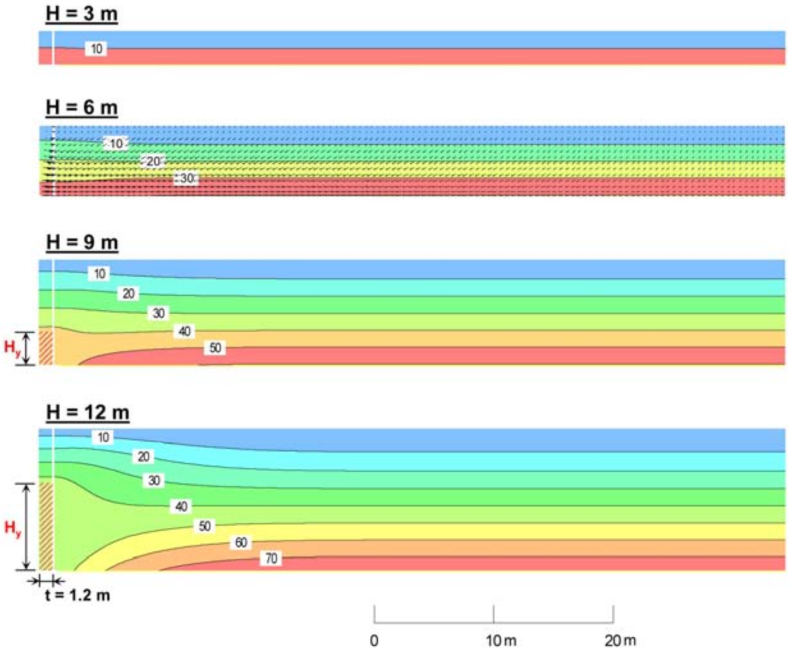

Figure 3. Finite-element computed horizontal stress (σ_h) isolines within the geofoam-backfill system (contour labels in kPa).

For wall heights of 9 and 12 m associated with the development of a plastic zone in the geofoam (Figure 3), σ_h becomes equal to σ_{1y} throughout the yield height H_y of the EPS panel (Figure 4). The stress transfer due to plastic yielding of the EPS panel becomes evident in Figure 4 for a retaining wall height of 12 m that shows a horizontal stress in the elastic region of the EPS panel greater than the lateral earth pressure at rest (i.e., $\sigma_h > p_0$). Based on the discrete data provided by the finite-element analysis, the following regression equation was developed to obtain the yield height (H_y) of the EPS panel in relation to the EPS thickness (t) for various retaining wall heights (H):

$$\boldsymbol{H}_{\mathrm{y}} = a_1 + a_2\, \boldsymbol{t} + a_3\, \boldsymbol{H} \tag{1}$$

with the regression coefficients $a_1 = -9.3023$, $a_2 = -1.99792$, $a_3 = 1.5809$, and H_y, t, H expressed in meters.

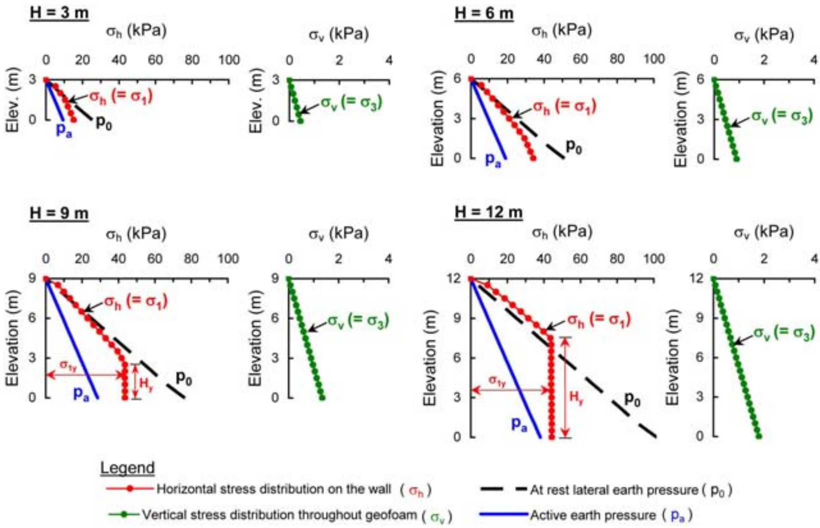

Figure 4. Finite-element computed horizontal (σ_h) and vertical (σ_v) stresses throughout the geofoam in the vicinity of the wall-geofoam interface (EPS panel thickness *t* = 1.2 m).

The results from the finite-element analysis were compiled into a design chart (Figure 5) providing the design relative EPS panel thickness (t/H) required to achieve a specific isolation efficiency (i) for a given retaining wall height (H). The isolation efficiency (i.e., percent reduction in the wall thrust) is obtained from the equation below

$$i = \frac{P_0 - P}{P_0} \tag{2}$$

where P_0 represents the total thrust on the non-yielding rigid retaining wall with no geofoam inclusion (i.e., the at-rest case), and P stands for the total thrust on the rigid wall with EPS geofoam inclusion. The dark dashed line in Figure 5 divides the design chart into two separate regions associated with two different shapes of the lateral pressure distribution diagram on the retaining wall. The region to the left of the dark separation line corresponds to H and t combinations that would result in elastic stresses throughout the entire EPS panel, whereas the region to the right corresponds to H and t combinations that would result in the development of a yield zone of height H_y in the geofoam.

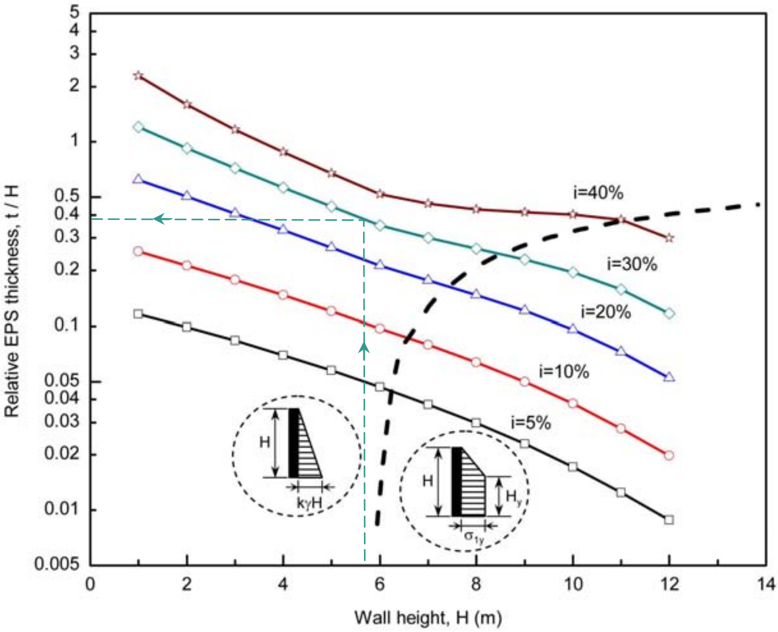

Figure 5. Relative EPS panel thickness (*t*/*H*) in relation to the retaining wall height (*H*) for various isolation efficiencies (*i*).

For the region to the left of the separation line (Figure 5), a linear distribution of the lateral wall pressure may be considered with the maximum pressure at the base of the wall given by ($K\gamma H$), where γ represents the unit weight of the backfill soil, and K stands for the coefficient of the wall thrust defined according to the equation below:

$$K = K_0\,(1\text{-}i) \qquad (3)$$

where K_0 represents the coefficient of earth pressure at rest for the rigid non-yielding retaining wall with no geofoam inclusion ($K_0 = P_0/(0.5\gamma H^2)$). The lateral pressure diagram for the region to the right of the separation line in Figure 5 is completely described by two parameters, i.e., the major principal stress at yield (σ_{1y}) of the EPS geofoam panel and the height of the yield zone (H_y) provided by Equation 1.

In the following, an example of using the developed design chart is provided. For a design non-yielding retaining wall height of 5.7 m and a required isolation efficiency of 30%, the chart yields a design value of the relative EPS thickness (t/H) of 0.38 (Figure 5) translating into a required geofoam panel thickness of 2.2 m. Since the point on the i = 30% line for H = 5.7 m is located to the left of the dark separation line, a linear distribution of the lateral wall pressure may be considered with the K

value characterizing the maximum lateral pressure at the wall base given by Equation 3, i.e., $K = K_0\ (1\text{-}i) = 0.7K_0$. For $K_0 = 0.493$ and $\gamma = 17$ kN/m^3 in this study, a maximum pressure of 33.4 kPa is obtained at the base of the 5.7-m high wall with a 2.2-m thick EPS panel.

CONCLUSIONS

The present study highlights the importance of an elasto-plastic constitutive model for EPS geofoam in performing accurate finite-element analyses of geofoam behavior in compressible inclusion applications. The elasto-plastic model has the advantage of capturing the development of plastic strains in the geofoam inclusion and the stress redistribution in the geofoam-backfill system due to the plastic yielding of geofoam. The design charts for rigid non-yielding retaining walls with EPS geofoam inclusion developed in the present investigation can be extended to incorporate various densities of geofoam and backfill properties.

ACKNOWLEDGMENT

This paper is based upon work supported by the National Science Foundation under Grant No. CMMI-0926042.

REFERENCES

Chun, B.S., Lim, H.S., Sagong, M., and Kim, K. (2004). “Development of a hyperbolic constitutive model for expanded polystyrene (EPS) geofoam under triaxial compression tests.” *Geotextiles and Geomembranes*, 22, 223-237.

GeoSlope International Ltd (2008). “Stress-deformation modeling with SIGMA/W 2007. An engineering methodology. Third Edition.” *GEO-SLOPE International Ltd.*

Gomez, J.E. (2000). “Development of an extended hyperbolic model for concrete-to-soil interfaces.” *Ph.D. Thesis*, Virginia Polytechnic Institute and State University, 248 pp.

Horvath, J. S. (1997). “The compressible inclusion function of EPS geofoam.” *Geotextiles and Geomembranes*, 15, 77-120.

Karpurapu, R., and Bathurst, R.J. (1992). “Numerical investigation of controlled yielding of soil-retaining wall structures.” *Geotextiles and Geomembranes*, 11, 115-131.

Lambe, T.W., and Whitman, R.V. (1969). “Soil Mechanics.” Wiley, New York, pp. 553.

Murphy, G.P. (1997). “The influence of geofoam creep on the performance of a compressible inclusion.” *Geotextiles and Geomembranes*, 15, 121-131.

Partos, A.M., and Kazaniwsky, P.M. (1987). “Geoboard reduces lateral earth pressures.” In: *Proceedings of Geosynthetics’87*, *Industrial Fabrics Association International*, New Orleans, LA, USA, 628-639.

Wong, H., and Leo, C.J. (2006). “A simple elastoplastic hardening constitutive model for EPS geofoam.” *Geotextiles and Geomembranes*, 24, 299-310.

An un-conventional earth retaining structure

Ashok K. Chugh

U.S. Bureau of Reclamation, Denver, Colorado 80225
PH (303) 445-3026; FAX (303) 445-6432; email: achugh@usbr.gov

ABSTRACT

An existing reinforced concrete barrel of the Weber Branch Siphon and Weber Coulee Siphon along East Low Canal in the State of Washington, U.S.A. is used as an earth retaining structure during required excavation for construction of an additional cast-in-place reinforced concrete barrel in close proximity. A continuum-based numerical model is implemented to simulate significant construction stages in sequential order so that soil-structure interaction effects are considered. Results of the numerical simulation demonstrate that at the end of required excavation, lateral forces on the existing barrel from the back and front soils are close to the corresponding lateral force values obtained using conventional earth pressure calculations with at-rest and passive earth pressure coefficients, even though the development of horizontal and vertical stresses is more complex.

INTRODUCTION

An unusual earth retaining structure is the existing 5.44 m diameter reinforced concrete barrel at Weber Branch Siphon (WBS) and Weber Coulee Siphon (WCS) along East Low Canal in the State of Washington, U.S.A. The WCS crosses interstate highway 90 (I-90) and a railroad line and is about 1.63 km long; the WBS crosses county road U and is about 0.90 km long. The depth of overburden soils on the existing barrel at the two siphon sites varies from about 1 m minimum to about 6 m maximum. Figure 1(a) shows the location of the project on the state map and Figure 1(b) shows an aerial view of the two siphons. Global coordinates of the project are: Latitude N 47° 05' 50", Longitude W 119° 02' 40".

The existing (1st) barrel was constructed in the mid 1950s; the project plans had envisioned construction of a second (2nd) barrel in the future to supplement the water conveyance capacity. Thus, during construction of the 1st barrel, foundation rock was prepared for the 2nd barrel in anticipation of the future construction in order to avoid rock blasting near the 1st barrel. Outside of the limits of the rock foundation, the 2nd barrel is to be founded on existing soil.

The 2nd barrel of 5.23 m diameter reinforced concrete is to be constructed with a clearance of 1.12 m from the 1st barrel at both siphon sites. The required phase 1 excavation in the overburden soils is in the form of a trapezoidal trench which includes the 1st barrel and is wide enough to accommodate construction of the 2nd barrel; the bottom of the phase 1 trench is level with the crown of the 1st barrel and then phase 2 excavation wraps around to the foundation level for the 2nd barrel. Figure 1(c) shows a cross-sectional view of the design excavation trench and the layout of the two barrels. During construction, the 1st barrel acts as an earth retaining structure for the back soil along its height and has front soil below the curved seating (cradle).

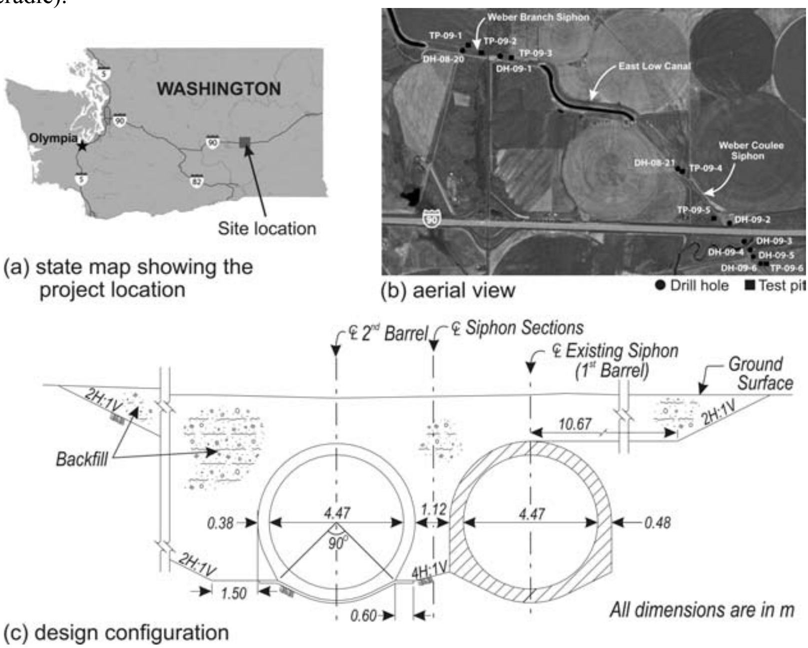

Fig. 1. Project location map and details of the siphon barrels under study.

Considering the broad scope of geotechnical items of interest (determination of: excavation slopes, dewatering, earth pressures, ground deformations among others) and significant soil-structure interaction effects, it was decided to use a continuum-mechanics based analysis procedure to analyze the problem in sequential order, i.e. starting with the existing condition and incrementally following the significant construction stages to completion of the project. The sequential problem solving strategy used could be implemented essentially in any continuum-mechanics-based solution procedure; however, a commercially available computer program FLAC (Itasca 2006) was used and its adoption was for convenience. The numerical model of the prototype field conditions was analyzed in plane strain, i.e. out-of-plane strains are zero. Continuum mechanics nomenclature for stresses and displacements is used.

The objectives of this paper are to present results of FLAC analyses on items of geotechnical significance in the construction of the 2nd barrel at the WBS and WCS sites, especially the lateral earth pressures due to the in-place soils behind and in-front of the 1st barrel. Deformation and stress results at select locations (considered relevant to the stability of the excavated trench) are also included.

For this paper, only geotechnical issues for design and construction of the 2nd barrel founded on soil foundation are considered. Also, the project is set in imperial units and numerical model studies were performed using imperial units; field data, design data, and numerical model results were converted to metric units and conveniently rounded for presentation in this paper.

PROJECT DETAILS

The existing siphon is an underground conduit to convey irrigation water from the upstream canal section to the downstream canal section; the 2nd barrel is to supplement the water conveyance capacity of the 1st barrel. The excavation geometry details (slopes and offsets) shown on Figure 1(c) are those that were determined via numerical model analyses that met acceptable design criteria for structural and hydraulic integrity of the 1st barrel as a retaining structure during construction of the 2nd barrel. Construction of the 2nd barrel is expected to extend over an irrigation season; therefore, the 1st barrel will be running under pressure during construction of the 2nd barrel. At the I-90 crossing, the 2nd barrel was constructed in 1968.

The in-side diameter (Ø) and wall thickness (t) of the 1st barrel are: Ø = 4.47 m, t = 48.26 cm; the corresponding dimensions for the 2nd barrel are: Ø = 4.47 m, t = 38.10 cm. The geometric configuration of the outside of the 1st barrel is such that it creates a cradle-like seat at the bottom such that the load on the soil under the barrel is distributed essentially over the projected width of the barrel (5.44 m). The cradle for the 2nd barrel corresponds to a 90° circular arc symmetric about the center of the barrel. The cast-in-place reinforced concrete 2nd barrel is to be constructed in 7.62 m long segments (with water seals between segments) using slip-forms. Clearance between the two barrels is 1.12 m.

Geologic Conditions

Locations of test pits and drill holes are shown on Figure 1(b). From the three test pits (TP-09-4 to TP-09-6) and six drill holes (DH-08-21 and DH-09-2 to DH-09-6) near the WCS site and three test pits (TP-09-1 to TP-09-3) and two drill holes (DH-08-20 and DH-09-1) near the WBS site, the following subsurface conditions were estimated to apply for this site: (a) the original backfill (b_fill) soil surrounding the existing siphon (1st barrel) to be sandy silt and silty sand with a dry density (ρ) of 1440 to1760 kg/m^3, average blow count (N) from Standard Penetration Tests (SPT) to be 0 to 10; and (b) the insitu soil (f_soil) to be silty sand to clayey gravel with interbedded silty sand and sandy silt with a ρ of 1600 to 2080 kg/m^3, and N of 20 to 50. Depth to ground water table is taken to be 0 to 4 m.

Construction Sequence

Working description of the planned construction sequence is: (i) lower ground water table to specified level over a specified length and width using dewatering wells and well points; (ii) excavate trench to specified dimensions; (iii) construct 2nd barrel; (iv) backfill the excavated trench; (v) repeat steps (i) to (iv) for the next incremental construction stretch (91.44 m).

NUMERICAL MODEL

Figure 2 shows the discretization and boundary conditions used for the construction stages modeled. The geometry of the model is referenced in x, y coordinates with $x = y = 0$ at the center of the model, at the bottom of the model. The sample locations shown are for the numerical model results included in this paper. Computed horizontal and vertical stresses along grid lines drawn darker than the rest of the grid lines are of interest in earth pressure calculations in engineering practice. Lowering of the ground water table and excavation of the trench were modeled in one step each because of the fast pace of construction (2.53 km of construction to be completed in one year). The constitutive model for soil is elasto-plastic, with a Mohr-Coulomb yield condition and a non-associative (dilation angle = 0) flow rule; for reinforced concrete, the constitutive model is linear elastic.

Table 1 shows the material properties for this project. For the in-place soils, density (ρ) is based on field measurements of dry unit weight (γ); the effective stress friction angle (φ) is based on available correlation between friction angle, N value from SPT, and effective overburden pressure (Craig 1994); and the elastic properties (bulk modulus (K) and shear modulus (G)) are selected from published values for similar materials. For the reinforced concrete, standard properties for concrete with compressive strength of 2.8×10^4 kPa were adopted.

Table 1. Material properties.

Material identifier	Density ρ kg/m^3	Elastic constants		Material strength	
		Bulk modulus K kPa	Shear modulus G kPa	Cohesion c kPa	Friction angle φ °
Concrete	2400	1.6×10^7	1.4×10^7	N/A	N/A
Native soil	1800	9.6×10^4	3.8×10^4	0	30
Backfill	1600	3.5×10^4	1.3×10^4	0	20

Unit weight (γ) = density (ρ) × gravity; N/A = not applicable

Interface properties: The normal and shear stiffness (k_n and k_s) values in kPa/m, cohesion (c) in kPa, and friction angle (φ) in ° are assumed to be:

Interface # 1 – between the cradle and the foundation soil: $k_n = k_s = 7.5\times10^6$, $c = 0$, $\varphi = 30$;
Interface # 2, 3, and 4 – between the backfill and the foundation soil: $k_n = k_s = 2.8\times10^6$; $c = 0$; $\varphi = 20$.

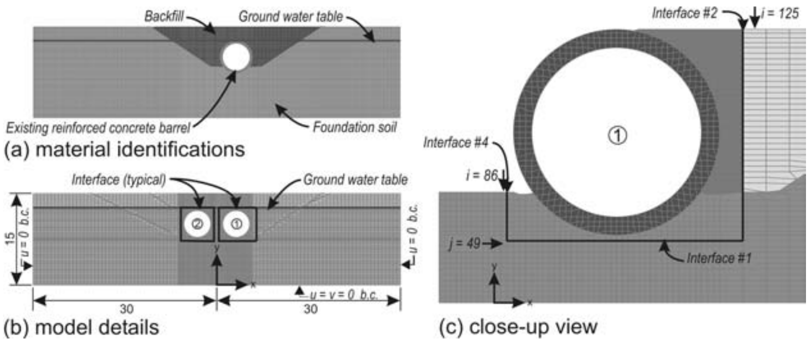

Fig. 2. Details of the numerical model. b.c. is boundary condition; ① is existing barrel; ② is new barrel.

The construction sequence was analyzed using a 2D numerical model in plane strain ($\varepsilon_{zz} = 0$) mode; specifically, the following stages were modeled: (i) existing condition in the field, i.e., barrel full of water but zero internal pressure and known ground water conditions; (ii) continuation of (i) with barrel under full internal pressure due to 43 m of water head; (iii) continuation of (ii) but ground water table lowered; (iv) continuation of (iii) but with full excavation for construction of the 2nd barrel; (v) continuation of (iv) with 2nd barrel constructed; (vi) continuation of (v) with trench backfilled and 2nd barrel filled with water; and (vii) continuation of (vi) with both barrels functioning under full internal pressure. Figure 3 shows the cross-sectional view of each of the seven construction stages analyzed in sequential order; the overburden is 3 m, excavation slopes are 2H:1V, and lowered ground water table is 1.5 m below the bottom of the 1st barrel.

Computed Results

For the existing siphon condition, Figure 3(b), computed v displacements in the model are small (maximum v = 10 mm at the ground surface), and the state of stress in the model is essentially elastic. These numerical model results agree with no indications of ground settlement or other signs of distress along the prototype siphons in the field and is taken to indicate that the material properties used are reasonable.

Results for the end of excavation stage, Figure 3(d), are of most significance for the structural stability and integrity of the 1st barrel during construction: Figure 4 shows the spread of plastic yielding at the end of the required excavation. Maximum displacement (resultant of u and v) at the floor of the excavation is 1.4 mm; the corresponding value for the entire model is 9 mm.

Figure 5 is for the computed stress results: Figure 5(a) shows the computed vertical stress (σ_{yy}) and computed horizontal stress (σ_{xx}) in zones adjacent to interface # 2 (marked i = 125 in Fig. 2(c)), and normal stress (σ_n) on interface # 2. Figure 5(b) shows the computed lateral earth pressure coefficient (σ_{xx}/σ_{yy}) for the back soil.

Figure 5(a) and 5(b) results are compared to the active and at-rest earth pressure conditions in Table 2. Figure 5(c) and 5(d) are similar to Figures 5(a) and 5(b) in layout and details and apply to zones adjacent to interface # 4 (marked i = 86 in Fig. 2(c)), and normal stress (σ_n) is on interface # 4. Figure 5(d) shows the computed lateral earth pressure coefficient ($\sigma_{xx}/\ \sigma_{yy}$) for the front soil. Figure 5(c) and 5(d) results are compared to the passive earth pressure conditions in Table 2. Figures 5(e) and 5(f) are for the bottom of the cradle: Figure 5(e) shows the computed vertical stress (σ_{yy}) in zones adjacent to interface # 1 (marked j = 49 in Fig. 2(c)), and normal stress (σ_n) on interface # 1. Figure 5(f) shows the computed subgrade modulus (σ_{yy}/v) for the cradle. Figure 5(e) results are compared to the values obtained using the flexural formula q = $\frac{P}{A} \pm \frac{M \times C}{I}$ in Table 2.

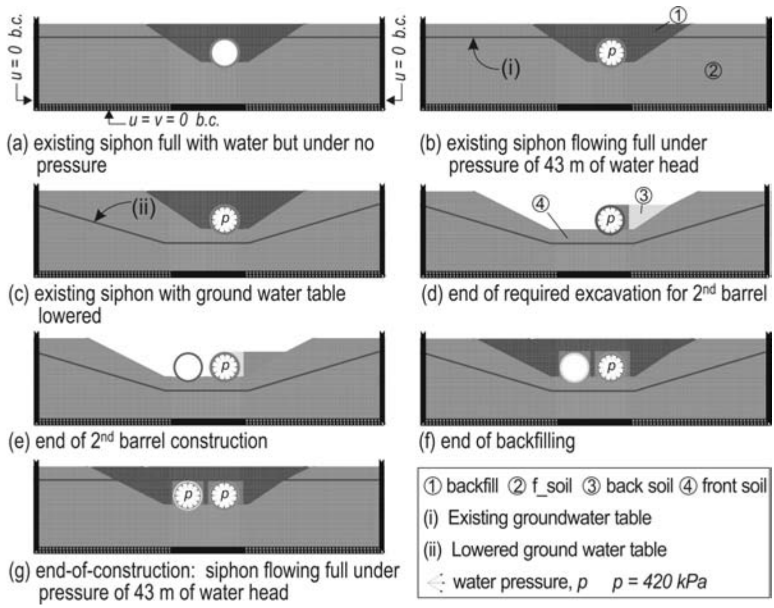

Fig. 3. Construction stages modeled – seven sequential stages.

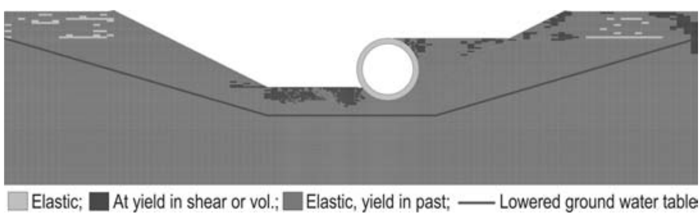

Fig. 4 Spread of plastic yielding at the end of excavation stage (Fig. 3(d)).

In both Figures 5(a) and 5(c) results: (i) the gravity stresses (σ_{yy}) vary linearly with depth; (ii) interface normal stresses (σ_n) are close to being equal to the horizontal stresses (σ_{xx}) in the zones next to the interfaces. In Figure 5(e), interface normal stresses (σ_n) are close to being equal to the vertical stresses (σ_{yy}) in the zones next to interface # 1.

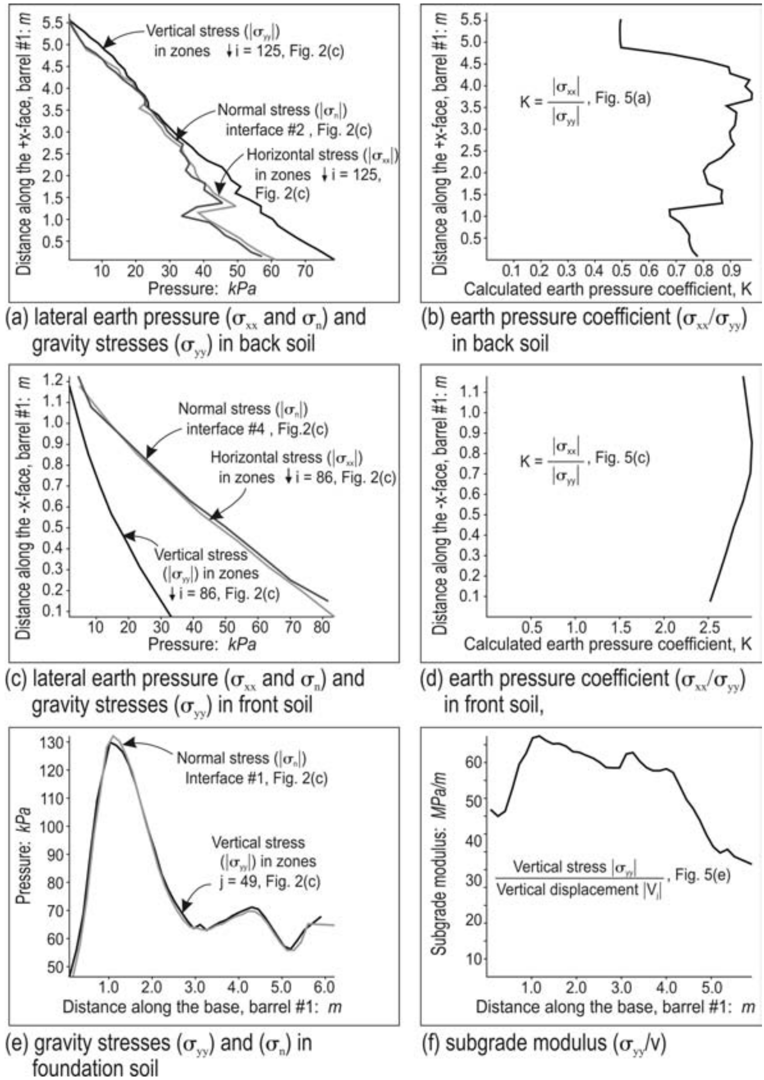

Fig. 5. Computed results at the end of required excavation (Fig. 3(d)).

Table 2 shows a comparison of results obtained using FLAC with those calculated using conventional earth pressure calculations employed in engineering practice for design of earth retaining structures; in general, the comparison is considered good.

Table 2. Comparison of results.

Item	Conventional calculations results			Fill height m	FLAC results	
	Condition	Source	Value		Value	Source
Lateral earth pressure coefficient	At-rest K_0	$1-\sin\varphi$	$\varphi = 20°$: $K_0 = 0.658$; $\varphi = 30°$: $K_0 = 0.500$	N/A	0.787	Fig. 5(b) average value
	Active K_a	$\frac{1-\sin\varphi}{1+\sin\varphi}$	$\varphi = 20°$: $K_a = 0.490$; $\varphi = 30°$: $K_a = 0.333$			
	Passive K_p	$\frac{1+\sin\varphi}{1-\sin\varphi}$	$\varphi = 30°$: $K_p = 3.000$		2.814	Figure 5(d) average value
Total lateral force on barrel # 1	Fig. 3 interface # 2 P_0, P_a	$\int_{h=0}^{5.43}(K_0 or K_a \times\gamma\times h)dh$	$P_0 = 140$ $P_a = 100$ kN/m	5.43	155 kN/m	Fig. 5(a) $\sum_{i=1}^{40}(\sigma_{xx}\vert_i \times\Delta_y\vert_i)$
	Fig. 3 interface # 4 P_p	$\int_{h=0}^{1.13}(K_p\times\gamma\times h)dh$	$P_p = 34$ kN/m	1.13	52 kN/m	Fig. 5(c) $\sum_{i=1}^{10}(\sigma_{xx}\vert_i \times\Delta_y\vert_i)$
Vertical earth pressure on barrel # 1	Fig. 3 Toe q_0, q_a	Flexural formulae: $q=\frac{P}{A}\pm\frac{M_z}{I_z}\times 2.72$	$q_0 = 128$ $q_a = 114$ kPa	Base width m	132 kPa	Fig. 5(e) Largest value in toe region
	Fig. 3 Heel q_0, q_a		$q_0 = 24$ $q_a = 38$ kPa	5.43	56 kPa	Fig. 5(e) Lowest value in heel region

N/A - not applicable

CONCLUSIONS

The numerical simulation of the proposed construction sequence for the second barrel supports the following:

1. FLAC analysis results are given more credence because the soil-structure interaction effects are taken into account in the numerical solution procedure.
2. Conventional earth pressure calculations based on earth pressure coefficients are not adequate (because of their limiting assumptions) for analysis of the unconventional earth retaining structure considered in this paper. However, they provided a check on the reasonableness of the FLAC results.
3. Continuum-based numerical analysis procedures provide an effective and efficient means to simulate construction sequences.

REFERENCES

Craig, R. F. (1994). “Soil Mechanics.” Chapman & Hall, New York.
Itasca Consulting Group (2005). FLAC – Fast Lagrangian analysis of continua. Itasca Consulting Group, Minneapolis, Minnesota.

Study of Mechanically Stabilized Earth Structure Supporting Integral Bridge Abutment

M. J. Grien[1], K. Truong[2] and M. R. Tavakolian[3]

[1]Michael J. Grien, P.E., Regional Engineer, The Reinforced Earth Company, 1331 Airport Freeway, Suite 307, Euless, TX 76040; PH (817) 283-5503; FAX (817) 354-6568; email: mgrien@reinforcedearth.com
[2]Kim Truong, P.E., Senior Engineer, The Reinforced Earth Company, 8614 Westwood Center Dr., Suite 1100, Vienna, VA 22182; PH (703) 821-1175; FAX (703) 821-1815; email: ktruong@reinforcedearth.com
[3]Reza Tavakolian, P.E., Senior Engineer, The Reinforced Earth Company, 8614 Westwood Center Dr., Suite 1100, Vienna, VA 22182; PH (703) 821-1175; FAX (703) 821-1815; email: rtavakolian@reinforcedearth.com

ABSTRACT:

This paper will present the effects of the loading from an integral bridge abutment on a Mechanically Stabilized Earth (MSE) retaining wall structure. The analysis will mainly concentrate on the effects of thermal deformation phenomenon (contraction and expansion) of the bridge deck on an MSE wall structure and more particularly the induced tensile force in soil reinforcements and lateral displacement at the front face of the wall as a result of the bridge movement.

A geotechnical numerical finite difference program, FLAC v5.0 2D, will be utilized to model a standard abutment (true bridge abutment on bearings) and an integral bridge abutment (bridge deck and beam seat rigidly connected). The paper will also discuss the concept, components and applications of numerical modeling results in design and construction of the MSE structures supporting standard and integral bridge abutments.

The results of the two models will be compared to an empirical design methodology as developed based upon American Association of State Highway and Transportation Officials (AASHTO) design guidelines. Increasingly more complex design and construction techniques are being used for MSE walls, similar to the cases discussed in this paper, which makes the use of accurate design tools such as numerical modeling an effective verification of design assumptions.

INTRODUCTION:

The use of integral bridge abutments, where the bridge beams, deck and footing are rigidly connected and constructed without joints, are becoming the more commonly specified bridge structures due to many advantages over traditional bridge abutments on bearings. These "jointless" integral bridge structures when compared to traditional bridge abutments, where the bridge beams are resting on bearings located on the footing, provide for a much less expensive and more maintenance-free bridge.

The overall design life is also more predictable due to the elimination of corrosion of the joints and bearings, caused by de-icing agents that leak through expansion joints. Corrosion to the joint material and bearings is expensive and difficult to replace, therefore increasing long-term costs associated with maintaining traditional bridge abutments in order to keep them functioning properly. In addition to durability issues associated with joints, integral abutments have performed well in seismic events and significantly reduced or avoided problems such as back wall and bearing damage (Mistry, 2005).

Regardless of bridge abutment type, Mechanically Stabilized Earth (MSE) retaining wall structures have been used for over 35 years with proven success of supporting bridge structures. Design of MSE walls supporting bridge abutments should be in accordance with AASHTO Standard Specifications for Highway Bridges, using the coherent gravity design method (Anderson, 2005). However, when the bridge structure is rigidly attached to the abutment footing, fluctuations in temperature cause the bridge to displace horizontally, varying the applied pressures below the abutment. Therefore, the bridge structure and MSE structure cannot be designed independently with dead and live loads alone, as the structural and geotechnical aspects are more interdependent.

OBJECTIVE:

To better understand the effects of an MSE wall supporting an integral bridge abutment (Figure 1), a geotechnical finite difference software, FLAC v5.0 is used to compare the induced tensile forces in reinforcing strip elements to those found from supporting a traditional (standard) bridge abutment (Figure 2). The analyzed section of MSE wall is approximately 6.5m tall, with 7.0m (50mm x 4mm) long discrete, high adherence metallic reinforcing strips, supporting a 92m wide x 18.48m long single span bridge.

The integral bridge abutment is modeled as a monolithic structure with live loads and horizontal loads caused by the phenomena of thermal deformation. The traditional abutment is modeled with appropriate dead and live loads from the bridge structure applied to the footing.

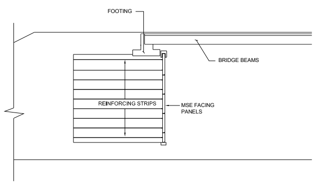

Figure 1. Integral Abutment

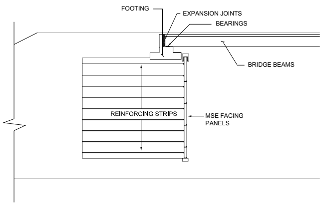

Figure 2. Traditional Abutment on Bearings

NUMERICAL ANALYSIS:

To determine the effects from thermal deformation within an integral bridge abutment, an applied horizontal force of 5,150kN (Equation 1) was used on each bridge abutment in the FLAC model to simulate the horizontal displacement based upon a temperature variation of approximately 50º F (Kunin, 1999), as shown in Figure 3. The backfill parameters for the MSE wall listed in Table 1 were modeled as Mohr-Coulomb and base material as elastic. The lateral earth pressure coefficient on the backwall of the abutment prior to thermal forces, during placement of the backfill was: 0.5, equivalent to k_o.

$$force = E * A * \varepsilon \quad (1)$$

Where:
E: modulus of elasticity of concrete = 2.5E+7kPa
A: section of bridge = $0.85m^2$
ε: strain = Δl/l = 2.24E-3m/9.24m = 2.42E-4
CTE: thermal coefficient for concrete = 18E-6 mm/mm/ºC
Δl: (assuming approx. ΔT = 13.5ºC) = 2.24mm

Table 1. Soil Parameters for FLAC Model

Soil Number	Name	Density of soil γ (kN/m^3)	Cohesion c' (kPa)	Friction angle ϕ' (°)	Stress-strain Modulus Es (kPa)	Poisson's ratio ν
1	R.E. Wall Backfill	20	0	36.0	60000	0.33
2	Random Backfill	20	0	30.0	40000	0.33
3	Class 1 Fill	20	0	36.0	60000	0.33
4	Base Material	20	20	30.0	20000	0.33

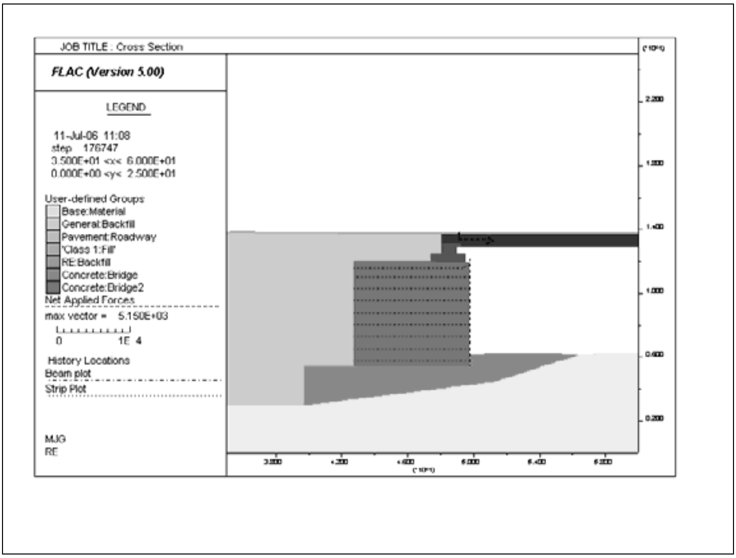

Figure 3. Typical FLAC Cross Section with Thermal Contraction

MODELING OF MSE WALL:

Initial construction sequences of MSE wall before placement of bridge abutments:

- FLAC Mesh defined for desired geometry,
- Parameters defined for existing soil,
- Initializing stresses in ground surfaces before construction of MSE wall and class 1 fill,
- MSE wall construction sequence:
    1. Placement of class 1 fill below reinforcing volume,
    2. First course of reinforced concrete panels,
    3. Select backfill within design length of reinforcing strips and random (general) fill placed beyond,
    4. First level of reinforcing strips within initial backfill lift.
        - Repeating steps 2-4; with multiple cycles of backfilling, compaction, strip placement and additional panels until design height is reached.
        - Bridge structures placed on top of MSE wall as shown in Figures 1 and 2.

VERTICAL STRESS BELOW FOOTING:

AASHTO (2007) equation 11.10.11-2 calculates the maximum horizontal stress required for internal stability of the MSE wall by including the effect of vertical soil stress due to footing load (Ds_v). For a standard abutment on bearings where the vertical loads are superimposed on the abutment footing, determining a conservative value for Ds_v is relatively simple, without taking into account rotation of the footing due to bearings separating the substructure from the superstructure. However, for the integral abutment case, this evaluation is slightly more complex, since the movement and rotation of the bridge will vary the vertical stress below the footing, depending upon bridge movement, as shown in Figure 4.

Figure 5 is the vertical stress taken from the FLAC model and shows the same results as Figure 4 for stresses directly below the abutment footing with the applied contraction forces within the bridge. The vertical stress increases from about -100kPa at the back edge of the footing to about -450kPa at the edge closest to the back face of MSE panel, then decreases to zero at back face of panel. Although no interface was modeled between the abutment footing and the MSE backfill, the overall rotation of the bridge foundation and distribution of the induced pressures below the footing will not be affected, only the actual values would be affected. Still the way in which the bridge deck is rigidly connected to the abutment footing, acting as a fixed support, when compared to a standard abutment, similar to a simply supported beam, the affects of the bending moments within the bridge deck, even before thermal forces are applied, resulted in the variations to the vertical stresses below the footing.

It is noted that although the maximum vertical stress below the footing exceeds the allowable of 200kPa (4ksf) for true bridge abutments (i.e. abutment without piles), the results show that the stress varies depending on the horizontal displacement of the bridge. The footing design for the integral bridge abutment should be sized and located properly with respect to the superstructure, so that the stress below the footing is limited to 200kPa for entire service life.

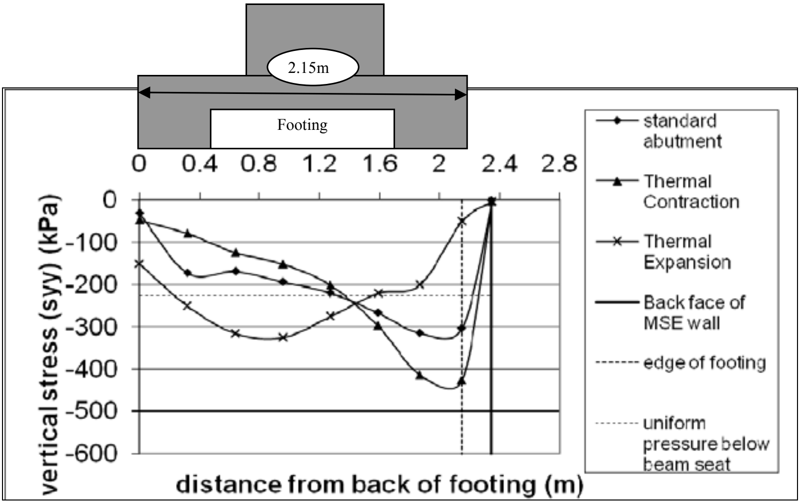

Figure 4. Vertical Stress Below Bridge Footing

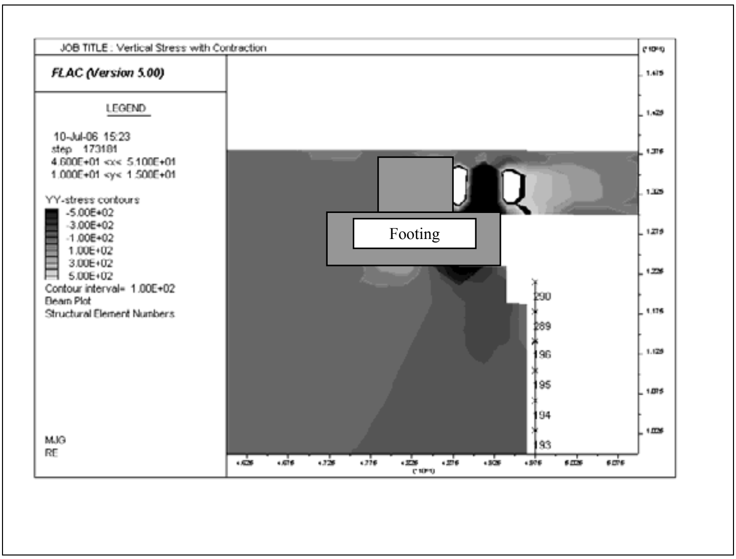

Figure 5. Vertical Stress from FLAC Model (With Contraction)

REINFORCING STRIP TENSION AND HORIZONTAL DISPLACEMENT OF WALL:

AASHTO Article 11.10.11 for MSE walls recommend a minimum reinforcement length of 6.71m and effective length determined from Article 11.10.10.1. This minimum length of reinforcement combined with high overburden pressures over the top layer of reinforcing strips typically limit the controlling factor for design to allowable strip tension, although verification of strip pullout is checked at every reinforcement level. It is shown in Figure 6 that the tensile forces per strip at all levels of the standard bridge abutment model exceed the tensile forces for the integral abutment for both thermal expansion and contraction. Therefore, one approach for design of the MSE wall for an integral bridge abutment would be to determine the horizontal forces acting on the wall similarly to those from a standard abutment.

As discussed in the 1985 FHWA study of tolerable bridge movements, over 75% of abutments experienced movement, more vertical movement than horizontal due to the fact that the abutments moved inward until they were stopped by the bridge beams and girders. This unanticipated lateral movement of standard abutments can be one cause for additional tensile stresses and increased lateral wall movement when compared to integral abutments, where the bridge deck provides lateral constraints.

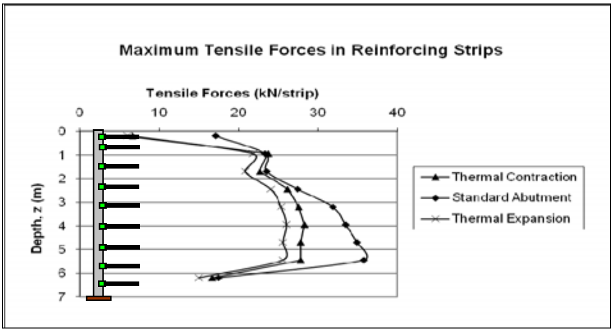

Figure 6. Reinforcing Strip Tensile Forces

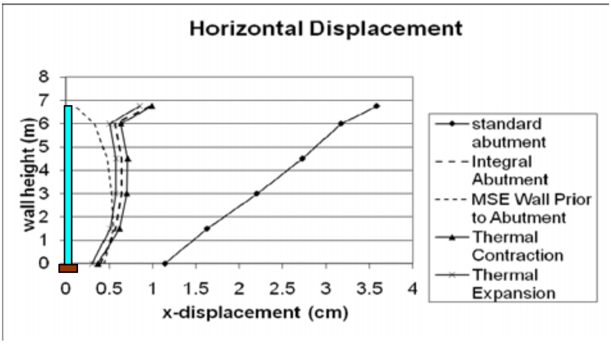

Figure 7. MSE Wall Horizontal Displacement

CONCLUSIONS:

Advances in bridge structures supported by MSE walls has made the use of numerical modeling as a tool for design verification of internal stability of MSE walls against standard AASHTO design methods very beneficial, since the affects to the retaining walls due to the global behavior of integral abutments are more complex than traditional abutments. Variations to the internal elements of MSE walls with different bridge structures shown in this report have increased the need for design coordination between the structural and geotechnical elements.

REFERENCES:

AASHTO (2007) “Standard Specifications for Highway Bridges.”

Anderson, P. L., and Brabant, K. (2005) “Increased Use of MSE Abutments,” proceedings from International Bridge Conference, Pittsburgh, PA.

FHWA (1985) “Tolerable Movement Criteria for Highway Bridges.”

Kunin, J. and Alampalli, S., “Integral Abutment Bridges: Current Practice in the United States and Canada.” Special Report 132, Transportation Research and Development Bureau, New York State Department of Transportation, Albany, NY, June 1999.

Mistry, V. C. (2005) “Integral Abutments and Jointless Bridges,” proceedings from The 2005 – FHWA Conference, Integral Abutment and Jointless Bridges, Baltimore, MD.

3D NUMERICAL ANALYSIS OF CONSTRUCTION PROCESS FOR TUNNELLING OF DONGHU METRO STATION

Hongjian Li

School of Civil Engineering, Shijiazhuang Railway Institute, Shijiazhuang 050043, China, Phone +860311/87935526, Fax +860311/87935526, lhjhh73@163.com

ABSTRACT

The Donghu station of No.6 line of Guangzhou rail transit is divided two parts: the embedded excavation part and the open excavation part. The kilometer of the embedded excavation part is from k13+462.752 to k13+519.452. The tunnel crown is located 19 m below the ground surface. Soil stratums are mix-filled soil, alluvial deposit to flooded alluvial deposit, wholly-weathered rock of red strata, highly weathered rock of red strata, moderately weathered rock of red strata and slightly weathered rock of red strata from the top down. The largest span of tunnel is 20 m. Its largest height is 10.349 m. Because the tunnel has large span and section, the construction is very difficult. In order to control the surface settlement and ensure the security of tunnel, the Finite Element Analysis method is used to analyze the construction process and find the rationality of construction method and support system. A three-dimensional numerical simulation model analyzes the construction process of the tube pre-support and center drift method in Donghu station by FLAC-3D. The results indicate that the reinforced and construction method can ensure the safety of construction, and control the surface settlement. The final conclusions are two: (1) the surface settlement and displacement are small and the tunnel is steady in the construction process. (2) The main step of influencing the surface settlement and crown settlement are step Ⅰ, step Ⅳ and removing of the temporary supporter. So the initial support must be installed in time and reinforced the supporter strength. The distance which is from working face to liner must be more than two times span of tunnel.

INTRODUCTION

The Donghu station of No.6 line of Guangzhou rail transit is divided two parts: the embedded excavation part, and the open excavation part. The kilometer of embedded excavation part is from k13+462.752 to k13+519.452. It passes through the Donghu road. The tunnel crown is located 19 m below the ground surface. Stratums are mix-filled soil, alluvial deposit to flooded alluvial deposit, eluvium and all regolith to medium regolith from the top down. The largest span of tunnel is 20 m. Its largest height is 10.349 m. Because the tunnel has large span and section, the construction is very difficult. In order to control the surface settlement and ensure the security of tunnel, the center drift method was adopted.

In actual tunnel construction process, the tunnel support system, excavation method, cycle advance and the various joint of all process have the tremendous influence to the stratum disturbance as well as the surface settlement. Therefore, a three-dimensional numerical simulation model analyzes the construction process of the selected pipe-roof pre-support and center drift method in Donghu station by FLAC-3D.

CALCULATING MODEL

FLAC-3D (Three Dimensional Fast Lagrangian Analysis of Continua) is widely used and advanced software in the world. The software is specially used to solve the soil mechanics questions, which is a Large-scale commercial finite difference program. Itasca Consulting Group Inc. of USA developed it.

The model size (xyz) is 160m, 70.31m and 21m with the horizontal direction 4 times tunnel span from tunnel center to the model boundary and the vertical direction is 4 times tunnel height from tunnel bottom to base boundary. The height above tunnel is from the tunnel crown to natural ground surface. The boundary conditions are as follows: ground surface is free, the left boundary and right boundary are fixed at x-axis direction, front boundary and rear boundary fixed at z-axis direction, and base boundary is fixed at y-axis direction. The uniform load of road surface is 10kpa. There are 38346 zones elements in this numerical model. An elastic-perfectly-plastic model using the Mohr-Coulomb failure criterion was adopted in this study.

Table 1. Analysis Parameters

Soils and support	Bulk density γ（kg/m3）	Cohesion c（kPa）	Angle of friction φ（°）	Young's modulus E（MPa）	Poisson's ratio μ
Mix-filled soil	1550	4	5	4	0.4
Fine sand deposit of alluvial to flooded alluvial t	1900	5	27	15	0.33
Medium-coarse sand deposit of alluvial to flooded alluvial t	1950	5	27	20	0.3
Wholly-weathered rock of red strata	1900	26.4	25	70	0.31
Highly weathered rock of red strata	2260	300	30	100	0.30
Moderately weathered rock of red strata	2420	1000	35	500	0.3
Slightly weathered rock of red strata	2560	2870	40.7	800	0.25
Reinforcement circle	2500	2870	40.7	800	0.25
Support (c25)	2300			29500	0.2
Second lining (c30)	2500			31000	0.2

The pre-support of pipe-roof was simulated by equivalent parameter method, namely through enhancing the parameter of pipe-roof reinforcement region to come equivalent simulation. The parameters were gotten by grading the class of soil that the pipe-roof reinforcement located. The physics mechanics parameter of reinforcement circle enhances a rank according to the locus level. The reinforcement circle scope is pipe-roof construction region of tunnel arch; reinforcement circle thickness is 200mm.

ANALYSIS PARAMETERS

The stratum, reinforcement circle and support structure parameter are list in table 1.

Analysis behaviour. The pre-support is pipe-roof. The excavation method is center drift method with bench method. The distance between top heading and bench is 3m. The abstract parameters are as follows: the pipe-roof is φ108mm seamless steel pipe, which was installed in tunnel arch with 0.4m circumferential spacing intervals. Spacing interval of steel grid is 0.5m. The excavation advance is 1m for each stage. The construction procedure, which has eight steps, is shown in figure 1.

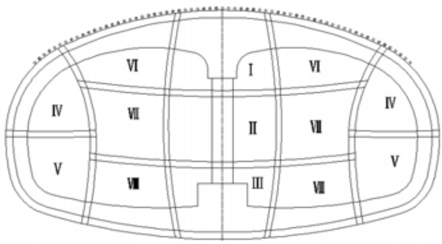

Figure 1. Construction Procedure

Table 2. The Inner Displacement and Ground Surface Settlement of Center

Behavior	Maximum crown displacement (mm)	Maximum step waist displacement（mm）			Maximum ground settlement (mm)
		Step Ⅰ	Step Ⅱ	Step Ⅲ	
StepⅠ: opening and support finished	3.02	1.7			0.85
Step Ⅱ: opening and support finished	3.18	1.84	0.9		0.98
Step Ⅲ: opening and support finished	3.22	1.87	0.93	0.26	1.02
Finished main structure of step Ⅰ, Step Ⅱ and Step Ⅲ	0.086	1.93	1.07	0.44	1.05

ANALYSIS RESULTS

The inner displacement and ground surface settlement of centre drift. The inner displacement and ground surface settlement of center drift is listed in table 2.

The inner displacement and ground surface settlement of other steps. The inner displacement and ground surface settlement of other steps are listed in table 3

Table 3. The Inner Displacement and Ground Surface Settlement of Other Steps

Behavior	Maximum crown displacement (mm)	Maximum arch waist displacement (mm)	Maximum arch foot displacement (mm)	Maximum spring displacement (mm)	Maximum ground settlement (mm)
Step Ⅳ: opening and support finished	0.6		1.83		1.86
Step Ⅴ:opening and support finished	0.59		1.91		1.91
From Step Ⅳ to step Ⅴ: lining finished	0.75		0.53	1.05	1.96
Step Ⅵ: opening and support finished	0.88	0.96	0.64	1.06	2.52
Step Ⅶ: opening and support finished	0.89	0.97	0.64	1.01	2.53
Step Ⅷ: opening and support finished	0.885	0.94	0.62	0.99	2.51
Finished Main structure	2.21	1.55	1.1	0.96	3.36

The ground surface settlement of finished main structure. The ground surface settlement of finished main structure is shown in figure 2.

The stress of finished main structure. The contour of minimum principal stress is shown in figure 3. The contour of maximum principal stress is shown in figure 4.

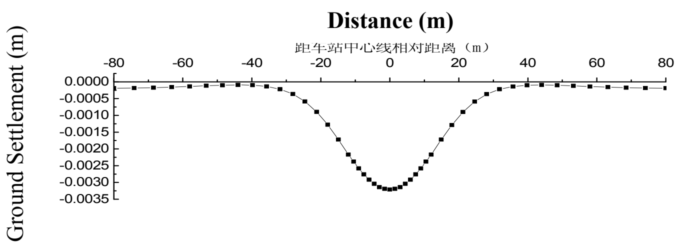

Figure 2. The Ground Surface Settlement Curve of Main Structure Finished

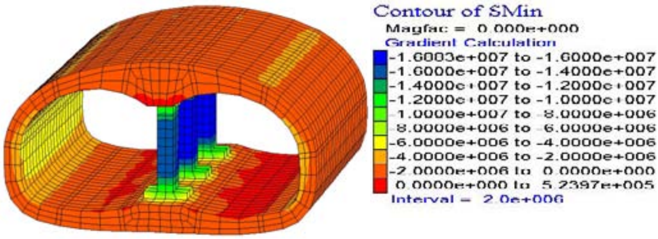

Figure 3. The Contour of Minimum Principal Stress

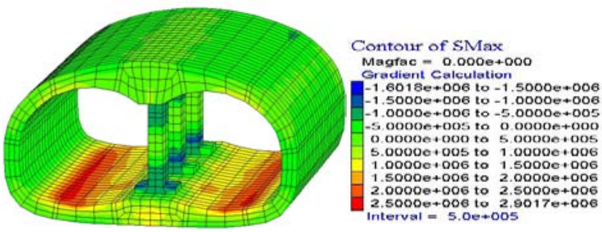

Figure 4. The Contour of Maximum Principal Stress

From the figure 4, the maximum compression stress located in center pillar of main structure. The maximum value is 16.88MPa. The maximum tensile stress is 2.5MPa, which lies right tunnel center and left tunnel bottom

Ground surface settlement of excavation steps. Ground surface settlement of excavation steps at z=0m is shown in figure 5.

Rock crown displacement of excavation steps. In order to know rock crown displacement of excavation steps, the rock vertical displacement of excavation steps at z=0m is shown in figure 6. It was observed that after excavation step Ⅰ, the vertical crown displacement of surrounding rock varies very little before removing the support, but after removing the support, it begins to increase rapidly. After main structure is finished, the crown vertical displacement of surrounding rock has increased 34 percent.

CONCLUSIONS

The final conclusions are as follows:

(1) Surface settlement and displacement are small and the tunnel is steady in the construction process.

(2) The main step of influencing the surface settlement and crown settlement are step Ⅰ, step Ⅳand removing of the temporary supporter. So the supporter must be installed in time and reinforced the strength. The distance that is from working face to temporary supporter must be more than two times span of tunnel.

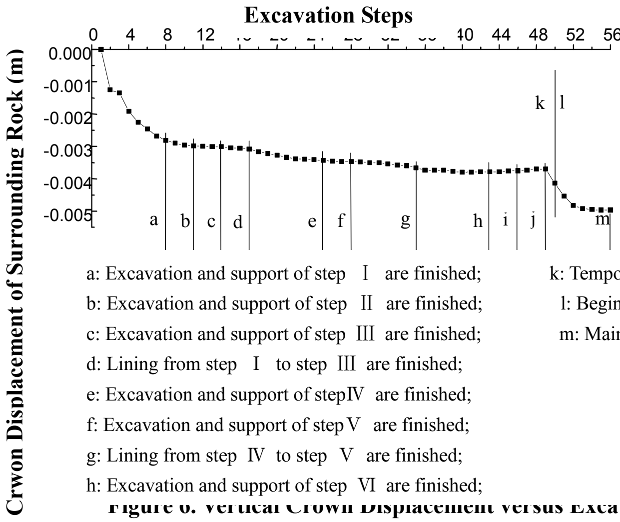

a: Excavation and support of step Ⅰ are finished;
b: Excavation and support of step Ⅱ are finished;
c: Excavation and support of step Ⅲ are finished;
d: Lining from step Ⅰ to step Ⅲ are finished;
e: Excavation and support of stepⅣ are finished;
f: Excavation and support of step Ⅴ are finished;
g: Lining from step Ⅳ to step Ⅴ are finished;
h: Excavation and support of step Ⅵ are finished;
k: Temporary support is removed
l: Begin to construct main structure
m: Main structure is finished

Figure 6. Vertical Crown Displacement versus Excavation Steps

REFERENCE

Xiao Ming. “Three-Dimensional Numerical Model of Construction Process for Underground Opening”. Chinese Journal Geotechnical engineering, vol. 22, 2000.7: 421- 425

X.D. Pan et. al, “Plane Strain analysis in Modelling Three-dimensional Tunnel Excavations”, Rock Mech. Min. Sci. & Gemech, Abstr. 1988,25 (5),331-337

Xu Linsheng, Sun Jun, Jian Shuping. “Study on the Numerical simulation of Excavation Face Space Effect in Yangpeng Highway Tunnel”. Geotechnical Engineering World, Vol. 4, 2001 (6): 42-44

Liu Heqing. “Mechanism of Initial Supporting system for Undercutting Subway Tunnel and Numerical analyzing”. Railway Investigation and Surveying, 2004 (5): 9-11

Implications of modern design codes for earth retaining structures

B. Simpson[1] and T. Hocombe[2]

[1]Arup, 13 Fitzroy Street, London W1T 4BQ, UK; PH +44 20 7755 3206; email: brian.simpson@arup.com
[2]Arup, Blythe Gate, Blythe Valley Park , Solihull, B90 8AE, UK; PH +44 121 213 3277, email: tim.hocombe@arup.com

ABSTRACT

The paper discusses the implications of recent developments in codes of practice related to retaining structures, concentrating on European and American codes. In contrast to traditional working stress design, recent codes are generally based on a Limit State approach, with safety margins specified by partial factors. Both European and American developments have factors applied to loads, but while the American preference (LRFD) is to apply factors to resistances, such as bearing capacity, Eurocodes use a mixture of factors on resistances and on material strengths.

Comparisons are provided for trial examples, a gravity wall and a propped embedded wall. It is shown that the precise way in which the factors are applied can have significant implications for the design result. The design to Eurocode of a new underground station for high speed trains in Florence is presented, illustrating some of the choices to be made in preparing calculations to satisfy code requirements.

DEVELOPMENT OF CODES AND STANDARDS RELATED TO RETAINING STRUCTURES

Simpson et al (2009) reviewed current international development of codes and standards for geotechnical design. The main recent developments have been in European, American and Japanese codes. A précis of the main points related to retaining structures in European and American codes is presented here, omitting details of the debates that led to differences between the codes. Specifically, the main documents noted are the Eurocodes, particularly Eurocode 7 – EN1997-1 (BSI 2004), Geotechnical design, and the AASHTO LRFD Bridge Design Specifications (2008).

Perhaps the greatest challenge for drafters of geotechnical codes is to find the best balance between fixed rules and personal expertise, both of which are essential to successful design. Geotechnical engineering relies heavily on the knowledge and judgment of individual designers. This is somewhat subjective, depending on the training and experience of each individual, but it is also indispensable, especially when shared in discussion with others. Codes must allow and encourage this.

Modern codes have generally been framed in terms of Limit State Design, in which attention is concentrated on "states beyond which the structure no longer satisfies the relevant design criteria". Attention is directed to states at or close to failure, which it is hoped will not occur in practice. The alternative is Working State Design in which attention is directed to the expected, desired state in which the structure is performing successfully under its expected loading. Its safety is then usually checked by requiring that the degree to which material strengths or ground resistances are mobilized is limited. Limit state design implies that the states studied should not occur. In this respect, working state design is easier to understand, but it has the danger of failing to highlight less probable, but critical, situations.

In the Eurocodes, *Ultimate limit states* (ULS) are "associated with collapse, or with other similar forms of structural failure". They generally relate to danger or severe economic loss. *Serviceability limit states* (SLS) "correspond to conditions beyond which specified service requirements for a structure or structural member are no longer met". The AASHTO Bridge Code has *Strength limit states* "relating to strength and stability during the design life". This is a more technical definition than the Eurocodes' ULS, but from most points of view it serves a similar purpose. The same code has *Service limit states* "relating to stress, deformation, and cracking under regular operating conditions". Both codes also consider accidental situations.

Assessment of parameter values. Prescribed values for partial factors provided by codes have little meaning unless it is clear how the parameter values are initially to be selected before being factored. These unfactored parameters are referred to as *characteristic values* of loads, strengths or resistances in Eurocodes, and as *nominal values* in AASHTO. EC7 defines characteristic values as "a cautious estimate of the value affecting the occurrence of the limit state", calling on the designer's understanding of what is really happening in the ground. In effect, modern codes provide safety margins by a combination of two features: somewhat cautious characteristic values, determined by the designer in the case of soil properties, and the application of partial factors, prescribed by the codes on behalf of society. To the authors' knowledge, the degree of caution assumed by AASHTO is not specifically stated, but it is recommended that a parametric study is carried out in cases of significant uncertainty, considering mean values for parameters and values that are 1 standard deviation from the mean. The alternative of varying resistance factors to accommodate uncertainty is also noted.

In both EC7 and AASHTO, the selection of characteristic (or nominal) values for ground parameters is seen as a combination of measurement with technical expertise related to established experience, geological interpretation and an understanding of construction processes. The need to consider the mode and extent of the failure is also noted. A pure statistical approach to parameter evaluation will rarely satisfy all these requirements, but for situations where a statistical approach could be relevant Schneider (1997) has interpreted EC7 as requiring a value that is about 0.5 standard deviations from the mean of test results. Figure 1 shows that this is very close to the recommendation of Dahlberg and Ronold (1993), who suggested that a "conservatively assessed mean" should be adopted, which is exceeded by 75% of the measurements. More recently, Foye et al (2006) have proposed an 80% exceedance. These approaches show good agreement, and Figure 1 shows that they are very different from the criterion of a 5% fractile of test results, or alternatively 2 standard deviations from the mean, often used in setting characteristic values for structural

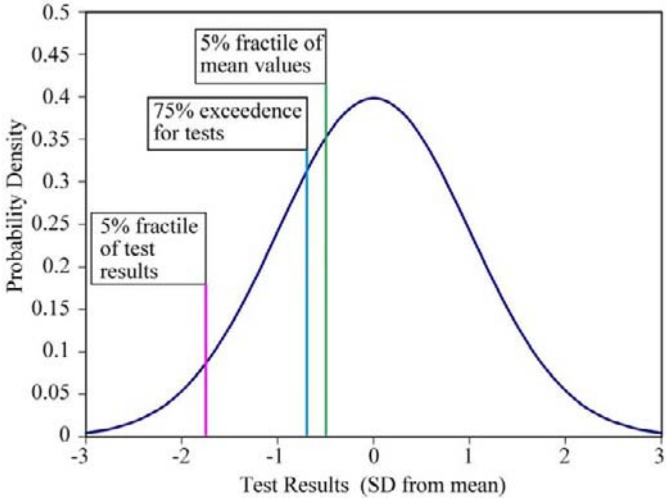

Figure 1. Alternative derivations of characteristic/nominal values

materials. These approaches are helpful when the failure mode averages the properties of the ground over a large volume or surface. EC7 notes that where a localized failure is concerned, a 5% fractile of test results may be more relevant.

Partial factors applied to materials or resistances. Generally, serviceability calculations are carried out with unfactored parameters, whereas partial factors are applied for ultimate or strength limit states.

On the resistance side, the main debate is whether to apply factors γ_M to material strength (c_u, c', $\tan\varphi'$) or factors γ_R or ϕ_R to derived resistances such as bearing capacity or lateral resistance. Becker (1996) put the case for resistance factors as follows:

- Resistance factors reflect not only uncertainty in strength but also uncertainties associated with the analytical models, site conditions, construction tolerances, and failure mechanisms.
- The factored strength approach also does not capture the true mechanism of failure when failure is influenced by nonlinear soil behaviour.
- The factored resistance approach is similar to WSD and therefore would allow for a smoother transition from WSD to LSD for foundation design.

Simpson (2007) and Simpson et al (2009) considered some of the advantages of a material strength approach in geotechnical design, in particular:

- It facilitates consistent analysis of combined problems, which are very common, involving, for example, a slope, loaded by a structure, supported by a retaining wall, itself supported by anchors and foundations.

- Because the strength of soil is derived from friction, non-linear, or disproportionate relationships between soil parameters and resistances are common. In these circumstances, it is important to check designs with factors of safety applied to the basic strength parameters of the soil.
- It can be used readily with both simple hand calculations and more complex finite element calculations. Introduction of resistance factors into finite element computations, which essentially require overall equilibrium, has proved to be difficult. In the authors' view, demonstration of equilibrium of complete systems is fundamental to good design practice.

Whereas the AASHTO code factors resistances, the Eurocode allows either approach, through its provision of alternative "Design Approaches". The UK decision, expressed in its National Annex (BSI 2007), is to use "Design Approach 1", with factors mainly on soil strengths.

In multi-stage analyses, as required for deep basements, the material or resistance factors could be applied throughout the analysis in all successive stages. Alternatively, the analysis could be run with unfactored parameters, and the factors applied separately in a re-analysis of individual critical stages. CIRIA Report C580 (Gaba et al 2003) favors the first of these strategies, whereas the second is probably more popular (Bauduin et al 2000, Simpson and Yazdchi 2003, Brinkgreve 2004). The significance of this distinction will be considered in a design example below.

Partial factors on loads. For loads, the point in the calculation at which factors are applied has a significant effect on the outcome. Simpson et al (2009) note that this was fundamental to the development of partial factor methods in the UK, as a result of the collapse of the Ferrybridge cooling towers. For retaining walls, this issue relates to whether the weight of ground or of groundwater should be factored. In the authors' view, this tends to lead to confusion, and the same intent is often better achieved by either factoring the strength of the ground (giving increased active pressures) or factoring resulting structural forces and bending moments. The UK approach using EC7 requires a combination of these two.

The sequence of calculation and factoring loads affects design of gravity retaining walls, since it changes the calculated eccentricity and inclination of the forces transmitted to the ground through the base. An example will be given below.

Features of Eurocode 7 related to retaining structures. EC7 provides minimum requirements for design but does not give detailed instruction on most issues. It provides values of partial factors to be used, but leaves the choice of calculation methods to the designer. EC7 allows three different "Design Approaches" to factoring for ultimate limit state calculations – each nation can choose its preferred approach. Typical factor values are shown in Figure 2, omitting pile design (for which see Bond and Simpson (2009-10)).

In Design Approach 1 (DA1), two "combinations" of partial factors are specified, and the design must be shown to accommodate both combinations. Essentially, they are used in the same way as load combinations, but the concept is extended to include material strengths and resistances. Partial factors are generally applied to either loads (before combination) or ground strengths (before calculation of resistances), though with some exceptions. The factors adopted in the United Kingdom are shown in Figure 2.

			Design Approach 1 Combination 1	Design Approach 1 Combination 2		DA2		DA3			AASHTO	
			A1	A2	M2	A1	R2	A1	A2	M2	Loads	Resistance
Actions	Permanent	unfav	1.35			1.35		1.35			1.25-1.5	
		fav									0.9	
	Variable	unfav	1.5	1.3		1.5		1.5	1.3		1.75	
		fav	0	0		0		0	0		0	
Soil	tan ϕ'				1.25			Struct actions	Geo actions	1.25		
	Effective cohesion				1.25					1.25		
	Undrained strength				1.4					1.4		
	Unconfined strength				1.4					1.4		
	Weight density											
Retaining walls	Bearing capacity						1.4					0.55
	Sliding resistance						1.1					0.8
	Earth resistance						1.4					0.5

Indicates partial factor = 1.0 A= Actions M= Material strength R= Resistance

Figure 2. Typical partial factor values for EC7 and AASHTO. UK values are shown for DA1. European factors divide strength and resistance; AASHTO factors multiply resistance.

In DA2, partial factors are applied to loads and to ground resistances. In a variant of DA2, DA2*, the equilibrium calculation is carried out using unfactored ("representative") loads, and the factors are applied to derived load effects. It has been found that DA2 and DA2* are unsuitable for slope stability problems and finite element calculations, so most countries that have adopted DA2 use DA3 for these. In DA3, factors are applied to material strength and to loads simultaneously.

For retaining structures, either limit equilibrium or more interactive calculations can be used for ultimate limit state calculations. Charts of earth pressure coefficients, based on the work of Kerisel and Absi (1990) are included; these are essentially the same as those in NAVFAC (1986) except that the values are resolved to give the pressures normal to the wall, rather than inclined at the angle of wall friction,□ □ . Programmable formulae for the coefficients are also provided, derived from plasticity theory. Simpson and Driscoll (1998) showed that these are slightly more conservative than the charts, though perhaps more soundly based.

For ultimate limit states, EC7 requires that the possibility of "unplanned excavation", including effects of erosion and scour, be carefully considered for material providing passive resistance to walls. For "a normal degree of [construction] control", excavations are to be designed as though they are 10% deeper for cantilevers, or 10% of the height below the lowest prop or tie for supported walls, with a limit on this additive element of 0.5m. This may add substantially to the length and required strengths of walls, and should only be disregarded if there is no possibility of loss of any of the passive soil.

EC7 does not allow reduction of partial factor values on the basis that a structure is "temporary works", except in cases "where the likely consequences justify it". This emphasis on consequences of failure, rather than merely on the temporary nature of the wall function, was supported by the report of the Committee of Inquiry in to the Nicoll Highway collapse in Singapore (Magnus et al 2005).

EC7 also requires consideration of serviceability limit states, both in terms of ground displacement, affecting existing structures, and deformation or cracking of the proposed structure. For retaining walls, displacements may be assessed by calculation, but there is also a strong emphasis on basing judgments on previously recorded observations, where this is possible. A formal approach to the Observational Method is also presented in the code.

Water pressures. One of the biggest challenges to both designers and code drafters is to specify adequate safety in regard to water pressures. EC7 allows "direct assessment" of design values for water pressure (meaning that they are severe values not to be subject to further factors) and the UK National Annex encourages this approach, stating that its load factors "might not be appropriate for self-weight of water, ground-water pressure and other actions dependent on the level of water". Similarly, AASHTO requires that "bearing resistance shall be determined based on the highest anticipated position of groundwater level at the footing location", but it does not apply factors to water pressures. Simpson et al (2009) suggest that making more than one check, effectively a parametric study, may be advisable, and describe how this can be done using EC7's "Design Approach 1". This difficult topic will be debated during a workshop on Eurocode 7 to be held in Pavia, Italy, in April 2010.

TYPCAL DESIGNS TO EUROPEAN AND US CODES

In 2005, a workshop was held in Dublin to compare designs to Eurocode and other European codes, submitted for typical examples (Orr 2005). The examples included three retaining walls, and lessons learned from two of them will be presented here. In addition, designs to AASHTO will be compared. One major lesson of the exercise is that very detailed specifications are needed in order to prevent respondents making widely different assumptions where precise information is missing. Full details of the examples are given in Simpson (2005).

Eurocode calculations shown below are to Design Approach 1, using partial factors taken from the UK National Annex (see Figure 2).

Gravity retaining wall. A simple gravity retaining wall was specified as shown in Figure 3. The surcharge is a variable load that might extend up to the wall (critical for bending moments in the wall), or might stop behind the heel of the wall, not surcharging the heel (critical for stability). The necessary width of the base, and the bending moment and shear force in the wall used for structural design are required.

The form of calculation is to adopt active earth pressures on the "virtual back" that extends up from the heel of the wall, with inclination parallel to the ground surface. Equilibrium with bearing capacity then has to be demonstrated, with due allowance for the eccentricity and inclination of the resultant force on the bearing area. For this case EC7 recommends that almost all the passive resistance in front of the wall is discounted, but the weight of soil in front of the wall may be used in the bearing capacity calculation.

The calculations required for the ULS check to DA1 of Eurocode 7 are shown in Figure 4. It is found that Combination 2 is critical for this design and the required footing width is 5m. Figure 4 shows how the soil strengths are reduced by partial factors before being combined into the equilibrium calculation.

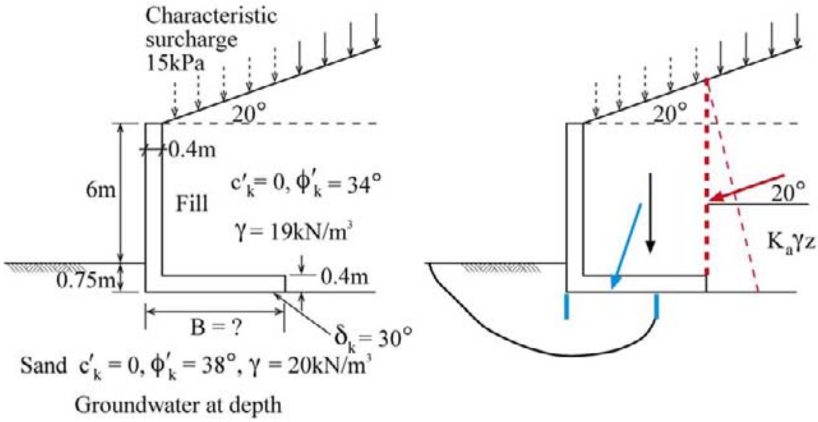

Figure 3. Gravity retaining wall.

Design approach:	DA1-C2	DA1-C1
Sand beneath wall		
γ(kN/m^3)	19	19
ϕ'_k (°) (c'_k =0)	34	34
$\gamma(\phi)$	1.25	1
ϕ'_d(°)	28.4	34.0
δ(k) on base (°)	30	30
$\gamma(\delta)$	1.25	1.00
δ(d) on base (°)	24.8	30.0
Fill behind wall (slope β=20°)		
γ(kN/m^3)$_k$	20	20
ϕ'_k (°) (c =0)	38	38
$\gamma(\phi)$	1.25	1
ϕ'_d(°)	32.0	38.0
Ka ($\delta/\phi=\beta/\phi$)	0.35	0.26
Ka (δ/ϕ=2/3)	0.35	0.25
γ(Ka)	1.00	1.00
Wall (concrete)		
γ(kN/m^3)	25	25
Surcharge (k)	15	15
(Surcharge)	1.3	1.1
Surcharge (d)	19.5	16.5
Base width	**5.0**	**5.0**
Max BM in wall (kNm/m)	436	297
γ (BM)	1	1.35
Design bending moment (kNm/m)	**436**	**400**
Max shear force in wall (kN/m)	184	127
γ (SF)	1	1.35
Design max SF in wall (kNm/m)	**184**	**171**

Design approach:	DA1-C2	DA1-C1
Footing width B (guess, check)	3.61	3.61
Bearing capacity		
γ(kN/m^3)	19	19
ϕ'_k (°) (c'_k =0)	34	34
$\gamma(\phi)$	1.25	1
ϕ'_d(°)	28.4	34.0
δ_k on base (°)	30	30
$\gamma(\delta)$	1.25	1.00
δ_d on base (°)	24.8	30.0
Overburden depth (m)	0.75	0.75
Overburden pressure (m)	14.25	14.25
γ(R)	1	1
Char. vertical force kN/m	886	855
Char. horizontal force kN/m	305	219
γ(V)	1	1.35
γ(H)	1	1.35
V_d/L	886	1154
H_d/L	305	297
ϕ'_d	28.4	34.0
c_d	0	0
N_q	15.3	29.4
N_c	26.5	42.2
N_γ	15.4	38.4
i_q	0.43	0.55
i_γ	0.28	0.41
i_c	0.39	0.54
Calculated base resistance R (kN/m)	877	2783
γ(R)	1	1
Design base resistance R_d (kN/m)	877	2783
Footing width B (checked)	3.63	2.32

Figure 4. Calculations required for gravity wall.

In comparing results, a major point of contention was found to be the point in the calculation at which factors were applied that would affect the inclination and eccentricity of the resultant force on the base. If factors are applied early in the calculation, by factoring material strength or by factoring active pressures, for example, the eccentricity and inclination of the force on the base are increased. This is true, for example, for the DA1-C2 calculations shown in Figure 4. However, an alternative approach has been proposed, known as DA2*, in which the equilibrium calculation is carried out using unfactored loads and materials, and the factors are applied to derived load effects (Vogt and Schuppener 2006). In this case, the inclination and eccentricity of the bearing load is not increased, but only its magnitude is factored. This results in a required base width that is about 25% less in this case. Figure 5 shows the 3.75m wide footing derived by this method. If the inclination and eccentricity are calculated without factoring, the footing appears to give an overall factor of safety on bearing capacity of 2.0. However, for pre-factored forces the inclination and eccentricity of the resultant force on the base are greater, and the factor of safety is only 0.68, suggesting an inadequate design. Simpson et al (2009) argue the case for applying factors early in the calculation.

Calculations have also been made for this example following AASHTO. To the authors' understanding, Section 10 of AASHTO, considering foundations, requires that eccentricity of load on a footing is calculated using factored loads, but inclination is calculated using unfactored values. Section 11, considering retaining structures, does not call up these clauses, and might imply that load inclination need not be considered. Using the AASHTO partial factors as listed in Figure 2, a footing width of only 2m is derived if load inclination is disregarded, whereas 4.7m is required if inclination factors are used, related to factored loads.

Requirements for service(ability) limit states are less specific in the codes. In the UK, advice can be found in a draft complementary document to be published by BSI, PD6694-1, *Recommendations for the design of structures subject to traffic loading to BS EN 1997-1*. This requires that for unfactored parameters the resultant force on the base should lie within the middle third and the bearing pressures should have a FOS of 3 on the maximum value.

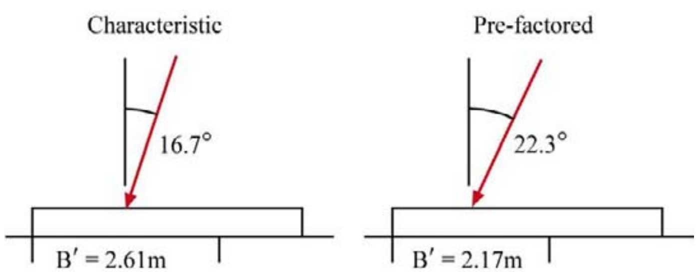

Figure 5. Resultant forces on a 3.75m wide base.

Tied sheet pile wall. For the wall shown in Figure 6, the minimum allowable length and corresponding design bending moment for structural design were required. The surcharge is a variable load and the wall is a permanent structure.

EC7 allows, but does not demand, that for propped walls earth pressures may be redistributed using some form of soil-structure interaction. This means that either of the earth pressure diagrams shown in Figure 7 could be used in the design. Traditional UK practice (CIRIA Report 104, Padfield and Mair 1984) would use a diagram similar to Figure 7a, with no allowance for redistribution, with factors on soil strength or resistance (eg passive pressure) when checking the wall length, but none in the calculation for bending moment (load factors would be applied to these). If Figure 7a is used more consistently for both length and bending moment with factors on soil strength, it is found that the computed bending moments are higher than have traditionally been used. Diagrams such as Figure 7b, derived using finite elements or other interaction programs such as *Oasys* FREW, give more economic designs when used with EC7. This approach is recommended by the replacement of CIRIA Report 104, ie Report C580.

EC7 DA1 calculations for this wall are shown in Figure 6. It is usually found that the minimum acceptable length and the design bending moment are determined by Combination 2, so it is normal practice to do this calculation first. It is sometimes found that the design tie or strut forces are determined by Combination 1, but this does not occur in this case.

As noted above, EC7 requires that the design depth of excavation is increased by 0.5m below the deepest support, unless exceptional measures are taken to justify reducing this. In this case, this increases the length of the wall by 0.6m, an increase of 21% in the penetration below dredge level – compare columns (a) and (c) in Figure 6. It is in this type of situation, where calculated penetration into relatively dense soils are small, that a small irregularity in the geometry can cause failure. Hence the consideration of "overdig" is very important. The code's recommended allowance would be reduced with great caution, and it should be increased if over-excavation or later erosion of the passive soil are thought likely.

Using the ASSHTO factors listed in Figure 2, a penetration of 2.5m has been calculated. This is slightly less than the 2.8m required by EC7 if "overdig" is disregarded. A contentious issue here was the factoring of ground weight, and related water pressures. With unfactored ground weight and water pressures, the AASHTO calculation gives about 2.7m.

While it might be thought that the geotechnical calculation ends at derivation of design bending moment, the choice of wall section also depends on the code requirements for structural design. Eurocode 3 Part 5, "Design of steel structures – piling", allows use of plastic design in which, for robust steel sheet piles, limited rotation is allowed to occur at a plastic hinge. It is claimed that this facilitates savings of up to 30% on steel sections.

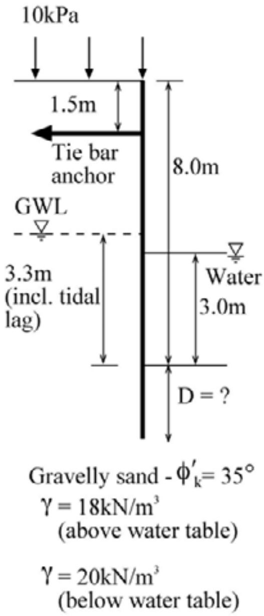

Sand	a	b	c
γ(kN/m³)	18 & 20	18 & 20	18 & 20
ϕ'_k(°) (c'_k =0)	35	35	35
$\gamma(\phi)$	1.25	1	1.25
ϕ'_d (°)	29.3	35.0	29.3
δ/ϕ active	0.67	0.67	0.67
δ/ϕ active	0.67	0.67	0.67
Ka	0.29	0.23	0.29
γ (on Ka or active pressure)	1	1	1
Ka (d)	0.29	0.23	0.29
Kp	4.43	6.51	4.43
γ (on Kp or passive pressure)	1	1	1
Kp (d)	4.43	6.51	4.43
Overdig (m)	0.5	0.5	0
Surcharge (k) (kPa)	10	10	10
γ (surcharge)	1.3	1.1	1.3
Surcharge (d) (kPa)	13	11	13
Embedment (m)	**3.4**	**3.4**	2.8
Bending moment kNm/m)	258	154	224
γ (BM)	1	1.35	1
Design bending moment (kNm/m)	**258**	**208**	224
Tie force (kN/m)	151	104	137
γ (SF)	1	1.35	1
Design tie force (kN/m)	151	140	137

Figure 6. Design situation for tied sheet pile wall.

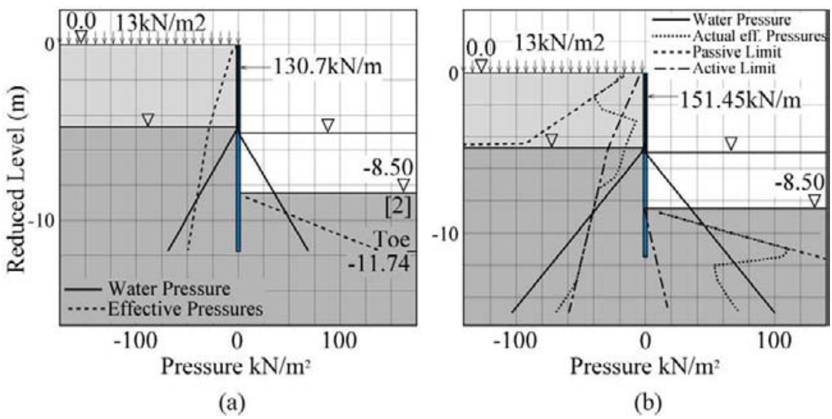

Figure 7. Earth pressure diagrams for tied sheet pile.
(a) No redistribution of active earth pressures; (b) redistribution computed by FREW.

EUROCODE CASE STUDY: FLORENCE HIGH SPEED RAIL STATION

Introduction. A large station box in Florence, Italy has been designed to Eurocode. This case study presents salient features of the design and the method adopted. Partial factors were applied to soil properties at all stages of excavation in the ULS analyses. Results are presented of a subsequent comparative study into the effects of applying partial material factors only at specific excavation stages.

The proposed station lies on a high speed rail line currently nearing completion between Milan and Naples and is situated just north of the historic centre of Florence. The Client for the station is Rete Ferroviaria Italiana (RFI) with construction scheduled for 2010. The structure is 454m long, 52m wide and 27 to 32m deep to underside of base slab (see Figure 8). The assumed excavation temporary works consisted of three levels of temporary steel props. Wall thickness required by initial design was 1.2m. This was subsequently increased to 1.6m for consistency with other structures on the Italian high speed network and to account for a possible prolonged cessation of work at final excavation stage (Hocombe et al 2007).

Ground conditions. The centre of Florence is underlain by Florence Clay, a stiff, over-consolidated, medium plasticity, fluvio-lacustrine blue-grey silty clay of Pliocene/ Pleistocene origin. It is overlain by more recent alluvial deposits comprising sandy gravels, generally finer deposits and Made Ground. Retaining wall design soil stratigraphy and Mohr-Coulomb soil parameters are shown in Figure 8.

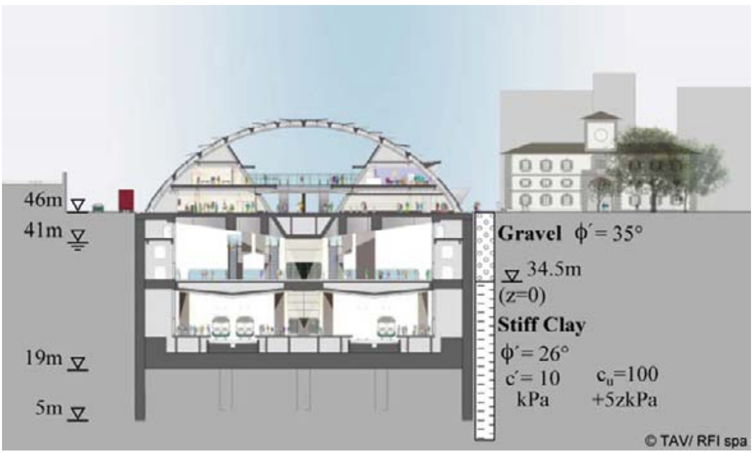

Figure 8. Florence station cross section with design Mohr-Coulomb soil parameters and stratigraphy

The Florence Clay has not been characterized in detail nor are there case histories of its behavior. In order to derive permeability and soil stiffness for this stratum a high quality site investigation was undertaken. Piezocone testing indicated permeabilities of the order of 10^{-10}m/s. A value of 10^{-9}m/s was adopted for design. Small strain stiffnesses from laboratory testing were found to exceed those predicted from stress history using empirical methods, e.g. Viggiani and Atkinson (1995). This may be due to some cementing, calcareous nodules being occasionally present.

Retaining wall design method. Eurocode 7, Design Approach 1 (EC7, DA1) was adopted by the design team. Design of the structure to Combinations 1 and 2 (C1 and C2) was more onerous than regulations applying at the time in Italy. The current Italian national standard specifies design of retaining structures and their supports to C1 only while C2 is checked for global failure due to collapse of the soil, not of the structure. It was, however, considered prudent for this project that the structure be checked for both combinations in accordance with EC7 DA1.

The decision to use EC7 DA1 did not, however, increase the number of analyses to be carried out since C2 was needed in any event to evaluate the depth of embedded walls for lateral stability.

Finite element SLS (SAFE) and elasto-plastic ULS (FREW) analyses. Coupled two-dimensional finite element analyses were undertaken using *Oasys* finite element (FE) program SAFE to model partial drainage of the clay during excavation. The non-linear constitutive model BRICK (Simpson 1992) was used for the Florence Clay. The FE analyses modeled SLS conditions, i.e. without soil material factors or unplanned excavation. These analyses used BRICK parameters derived for London Clay. Subsequent high quality testing suggested that higher stiffnesses could have been used.

Retaining wall design then used an analysis program applying linear elasto-plastic, Mohr-Coulomb soil parameters. This was for two reasons. Firstly, being quicker to run it allowed consideration of a number of design sections along the box. Secondly, the adoption of linear elasto-plastic parameters facilitated application of the partial material factors prescribed in DA1 analysis C2. The application of partial factors to soil strengths in non-linear constitutive models is not straightforward as parameters such as peak angle of shearing resistance and undrained shear strength are computed by the model, rather than being specified by the user (Simpson and Yazdchi 2003). The design program adopted was *Oasys* FREW (Pappin et al., 1986).

Mohr-Coulomb design soil parameters were derived from the SLS FE analyses by calibrating FREW analyses to the non-linear FE analyses. The calibration was conservatively based on FE analyses assuming a Florence Clay permeability of 10^{-8}m/s, an order of magnitude higher than the design value. Good matches between FREW and FE results were achieved using effective stress soil parameters on the retained side and total stress parameters on the passive side, as recommended by CIRIA Report C580, together with minor adjustment of the cantilever stage behavior. In this calibration the design "undrained" strength profile of the Florence clay was factored by 0.8 with respect to that shown in Figure 8 to account for partial drainage during construction.

Factors on soil strength and stiffness. The total and effective stress soil strength parameters derived from calibration with FE analyses were then factored as required by EC7 for ULS C2 (1.25 on $\tan\phi'$ and 1.4 on c_u). EC7 is not explicit on the requirement to factor soil stiffness at ULS. In the project design the soil stiffnesses for Florence Clay total stress parameters (as applied on the passive side of the wall) were derived from correlations with undrained shear strength. These stiffnesses in C2 were therefore factored down with respect to those in C1.

Investigation into effect of factoring soil strength at discrete construction stages. In EC7 DA1, application of partial factors to soil properties is required in ULS C2. As noted above, these factors were applied at all construction stages in the original design. EC7 is not explicit, however, as to whether partial factors should be applied at all stages or at salient, discrete stages.

An investigation has therefore been carried out, subsequent to the original design, into the effects of applying partial material factors only at specific excavation stages rather than at all stages. The results of these C2 analyses (with factored soil but unfactored wall moments and shears) are also compared with the results of C1 analyses (unfactored soil, factored wall moments and shears). The investigation considered three propped excavation stages based on a 1.2m thick diaphragm wall, applying the characteristic Mohr-Coulomb soil parameters presented in Figure 8 (plus the abovementioned 0.8 factor on "undrained" strength) in *Oasys* FREW. In this investigation soil stiffnesses parameters were not factored down along with soil strength in the C2 analyses.

Combination 1 and Combination 2 results with factored soil at all or discrete stages Bending moments derived using FREW are presented in Figure 9. The ULS C1 results have been factored up by the specified partial factor of 1.35 for comparison with those from ULS C2.

Maximum positive wall moments (tension on excavated face) are marginally higher from C1 compared to those from C2 in which partial factors are applied at all

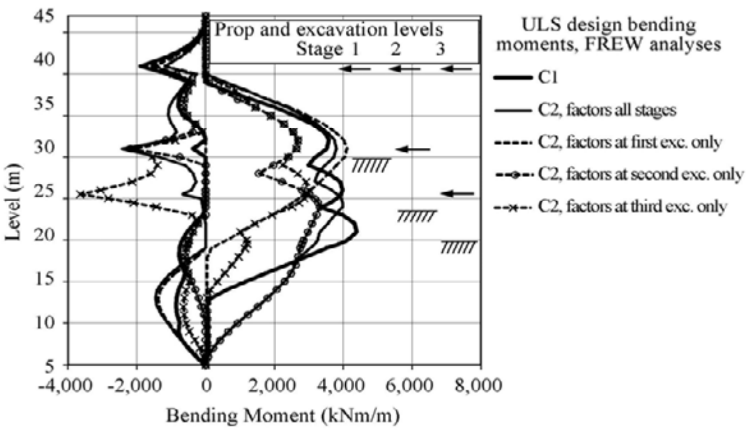

Figure 9. Comparison of ULS wall moments in EC7 DA1 between C1 and C2 and with partial factors at different stages in C2

stages, see the solid lines in the figure. Negative wall moments are, however, greater in C2 at the middle prop level (+31m). This may be a result of lower margin on lateral stability and higher wall deflection during the deeper stages of excavation in C2 compared to C1. The project design wall moments for the 1.6m wall gave similar comparisons of the two combinations.

Applying partial factors on soil strengths in C2 only at the respective excavation stages gave similar wall moments in stages 1 and 2 to the C2 analysis with factors applied at all stages. Application of partial factors only at excavation stage 3, however, resulted in larger negative wall moments at the lowest temporary prop, with greater wall deflection than the analysis with partial factors at all stages. Inspection of predicted soil pressures suggests that with partial factors applied during stages 1 and 2 more soil arching onto the higher props occurs, allowing greater reduction of soil pressure below the active limit than when partial factors are applied only in stage 3.

Results of the comparison in design prop forces using FREW are presented in Figure 10. The ULS C1 results have again been factored up by the specified partial factor of 1.35 for comparison with ULS C2. The C2 forces with factored soil strength at all stages are higher at the lower two levels than those from C1. In the project design analyses similar comparisons were seen, the lower prop force always governed by C2, with higher levels governed either by C1 or C2.

In the C2 analyses with soil strength factors only at discrete stages the design prop forces are similar at the upper two levels of props to those from C2 analysis with partial factors at all stages. In the lowest level of props, however, the force is significantly greater if partial factors are applied only at this stage, possibly due to the effects of soil arching mentioned above. (Analyses omitting soil arching showed forces in the lower prop did not change significantly in C2 with factors applied in all stages or only at the final stage.)

Effect of factoring soil stiffness as well as strength. The above analyses were performed factoring only soil strength, not soil stiffness, in C2. Repeat analyses with factored stiffness of the Florence Clay did not change the comparisons between C1 and C2 in terms of which combination governed design. C2 negative wall moments and forces in the lower prop were however, as expected, increased slightly due to the factoring of soil stiffness.

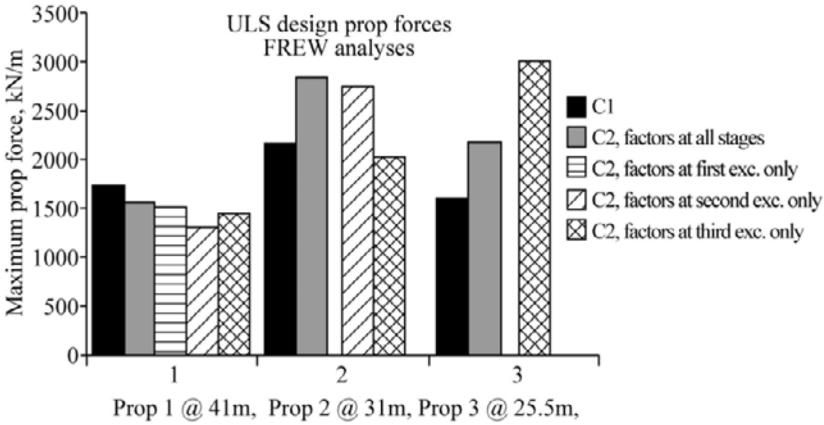

Figure 10. Comparison of prop forces between EC7 DA1 C1 and C2 and with partial factors at different stages in C2

Comparison of FREW with finite element analysis, partial factors at discrete stages

In addition to the comparison between factoring soil strengths at all or discrete stages in C2 in *Oasys* FREW, a comparison was made between results with factoring at discrete stages in FREW and factoring at discrete stages in coupled finite element analyses using the BRICK model, this time in PLAXIS. This allowed comparison of the effects of different analysis methods. Soil properties in PLAXIS were switched from the BRICK constitutive model to factored Mohr-Coulomb effective stress parameters using the Hardening soil model at three respective excavation stages. Consolidation stages were then used to model drainage during each excavation.

The use of Mohr-Coulomb effective stress parameters in finite elements allowed straightforward application of the specified EC7 C2 partial factors on strength as well as modeling of the ongoing partial drainage of the clay during excavation. This did, however, require derivation of specific effective stress parameters in addition to those shown in Figure 8. This was because the BRICK model behavior of the Florence Clay was found to correspond to relatively high effective stress parameters at the low effective stresses present on the passive side of the excavation. These effective stress parameters were derived in PLAXIS by calibrating Hardening model to BRICK analyses at SLS to obtain good matches in maximum bending moments and prop forces. The specified EC7 effective stress partial factor of safety of 1.25 on tan□ ′ was then applied in C2 at discrete excavation stages.

The maximum design wall bending moments from the PLAXIS analyses were, as in the FREW analyses, governed by C1. In C2, similar bending moments to those from FREW were observed with partial factors applied at the early construction stages. However, in C2 with partial factors at the final stage only, the high negative bending moment at the lowest prop in FREW was not observed in PLAXIS. This may be due to a higher margin of stability in the PLAXIS analyses, the partial factor on the passive side being 1.25 on $\tan\phi'$, rather than 1.4 on the "undrained" parameters used in FREW. This raises the question of appropriate partial factors on effective stress soil parameters when these are used to model an undrained or partially drained situation.

The force in the lowest level of props in PLAXIS was, as in FREW, governed by C2 rather than in C1. The increase in force above that derived from C1 was, however, smaller than from FREW, falling between the C1 and 'C2, factors at all stages' values shown in Figure 10.

The above example illustrates a number of issues to be considered in analyzing C2 in finite elements with partial drainage when the C1 analyses use an advanced constitutive soil model.

Conclusions. The above case history and subsequent investigation demonstrate:

a) EC7 DA1 is well suited to design methods using finite element analyses.
b) EC7 DA1, C2 (factored soil strength, unfactored wall moments, shears and prop forces) may govern the design of embedded walls (both dimensions and strength) as well as their supports.
c) Application of partial factors to soil strength in C2 at discrete stages of analysis may result in higher ULS wall moments, shears and prop forces than if they are applied at all stages of analysis.
d) The analysis of C2 using finite elements requires appropriate Mohr-Coulomb parameters to allow application of partial factors to soil strength. Derivation of such parameters may not be straightforward when using advanced soil models.

Conclusions b) and c) are considered especially relevant to the design of wall support systems that tend to fail in buckling. C2 was found to govern the design of most propping levels in the case history considered. It is recommended that conclusion c) be considered by those formulating future geotechnical design codes.

CONCLUDING REMARKS

Some developments in modern codes relevant to retaining structures have been discussed by reference to simple examples and a more practical one. The limit state format has been found to be viable, helping designers to address real issues and uncertainties. Successful use of Eurocode 7 Design Approach 1 has been illustrated for a major structure.

Areas of contention remain, notably related to factoring of water pressures, factors on soil strengths or derived resistances, and the point within calculations at which partial factors are applied. These are not new problems, but require critical and intelligent application of the limit state approach to specific situations.

The following points have been noted:

1. Geotechnical codes must provide a framework within which personal expertise can be used to best advantage.
2. American and European authors have made similar proposals about assessment of values for material parameters from varied and uncertain data.
3. On the materials side, partial factors can be applied either to material strengths or to resistances. In the United Kingdom, the first of these approaches is preferred and

some examples have been presented here. AASHTO uses resistance factors, except for slope stability.

4. The sequence adopted for calculation and factoring is important. It has a big effect on calculations of bearing capacity for footings with inclined, eccentric loading, such as occur beneath gravity retaining walls. The intentions of AASHTO are not fully understood in this regard.
5. Eurocode's recommendation to make an allowance for "unplanned excavation" has significant effects in some cases, illustrating its importance.
6. The factoring systems of Eurocode and AASHTO led to similar results for two examples considered, but issues of design for inclined loads and "unplanned excavation" could lead to significant differences.
7. For multi-propped walls, material factors may be applied throughout the analysis or only at individual stages. This choice significantly affects results.
8. Application of material factors to non-linear soil models may be difficult. One option is to switch to simple Mohr-Coulomb models at the individual stages at which factors are required.
9. Undrained materials can be modeled in finite element analysis using effective stress parameters. Clarity is needed about the partial factors then to be applied to soil strength or resistance.

ACKNOWLEDGEMENTS

The authors wish to acknowledge the support of their colleagues in Arup, particularly Terrence Carroll and Francesco Petrella for valued input to the calculations in this paper.

REFERENCES

AASHTO (2008). "LRFD Bridge Design Specifications, 4th edition, 2007 with 2008 Interim Revisions." American Association of State Highway and Transportation Officials.

C. Bauduin, De Vos, M. and Simpson, B. (2000). "Some Considerations on the Use of Finite Element Methods in Ultimate Limit State Design." LSD2000: Int. Workshop on Limit State Design in Geotechnical Engineering, ISSMGE, TC23, Melbourne.

Becker, D.E. (1996). "An overview of the foundation design process." Eighteenth Canadian Geotechnical Colloquium: Limit states design of foundations. Canadian Geotech J, 33(6), 956-983.

Bond, A.J. and Simpson, B (2009-10) "Pile design to Eurocode 7 and the UK National Annex (2 parts)." *Ground Engineering*, Dec 2009 and Jan 2010 (pp28-31).

Brinkgreve, R. (2004) "Plaxis and Eurocode 7". *Plaxis Bulletin*, Issue 16.

BSI (2004). BS EN 1997:1: 2004 "Eurocode 7: Geotechnical design - Part 1: General rules." BSI.

BSI (2007). "UK National Annex to Eurocode 7: Geotechnical design - Part 1: General rules." BSI.

Dahlberg, R. and Ronold, K.O. (1993) "Limit state design of offshore foundations." Proc Int Symp Limit state design in geotechnical engineering, Vol 2, pp491-500. Danish Geotechnical Society.

Foye, K.C. Salgado, R. and Scott, B. (2006). "Resistance factors for use in shallow foundation LRFD." J. Geotech. Geoenviron. Eng., 132(9), 1208–1218.

Gaba, A.R., Simpson, B., Powrie, W., and Beadman, D.R. (2003) "Embedded retaining walls: guidance for economic design." CIRIA Report C580.

Hocombe, T., Pellew, A., McBain, R., and Yeow, H-C. (2007) "Design of a new deep underground station structure in Florence." Proc. XIV ECSMGE, Madrid, Vol 2, pp 1049 – 1054.

Kerisel J. and Absi E. (1990). "Active and passive earth pressure tables." 3rd ed. A.A.Balkema, Rotterdam.

Magnus, R., Teh, C.I.and Lau, J.M. (2005). "Report on the Incident at the MRT Circle Line worksite that led to the collapse of the Nicoll Highway on 20 April 2004." Subordinate Courts, Singapore.

NAVFAC (1986) "Design Manual 7.02: Foundations and earth structures." US Naval Facilities Engineering Command, Alexandria, Virginia USA.

Orr, T.L.L. (2005). "Model Solutions for Eurocode 7 Workshop Examples." ISSMGE ETC23 workshop, Trinity College, Dublin.

Padfield, C.J. and Mair, R.J. (1984). "Design of retaining walls embedded in stiff clay." CIRIA Report 104.

Pappin, J.W., Simpson, B., Felton, P.J., and Raison, C. (1986) "Numerical analysis of flexible retaining walls." Symposium on computer applications in geotechnical engineering. The Midland Geotechnical Society, UK, April.

Schneider, H. R. 1997. "Definition and determination of characteristic soil properties." Discussion Session 2.3, XIV ICSMFE, Hamburg. Balkema.

Simpson, B. (1992) 32nd Rankine Lecture: "Retaining structures – displacement and design." Géotechnique 42, 4, 539-576.

Simpson, B. (2005). "Eurocode 7 Workshop – Retaining wall examples 5-7." ISSMGE ETC23 workshop, Trinity College, Dublin.

Simpson, B. (2007) "Approaches to ULS design - The merits of Design Approach 1 in Eurocode 7". ISGSR2007 First International Symposium on Geotechnical Safety & Risk pp 527-538. Shanghai Tongji University, China.

Simpson, B. and Driscoll, R. (1998). "Eurocode 7 - a commentary." Construction Research Communications Ltd, Watford, UK.

Simpson, B., Morrison, P., Yasuda, S., Townsend, B., and Gazetas, G. (2009) "State of the art report: Analysis and design." Proc 17th Int Conf SMGE, Alexandria, Vol 4, pp 2873-2929. IOS Press.

Simpson, B. and Yazdchi, M. (2003) "Use of finite element methods in geotechnical limit state design." LSD2003: International Workshop on Limit State Design in Geotechnical Engineering Practice. Cambridge, Massachusetts. 26 June, 2003.

Viggiani, G. and Atkinson, J.H. (1995) "Stiffness of fine-grained soil at very small strain." Géotechnique 45, 2, 249-265.

Vogt, N. & Schuppener, B. (2006). "Implementation of Eurocode 7-1 Geotechnical design in Germany." Proc TAIPEI2006 International Symposium on New Generation Design Codes for Geotechnical Engineering Practice Nov. 2~3, 2006, Taipei, Taiwan.

Design of deep excavations with FEM - influence of constitutive model and comparison of EC7 design approaches

H.F. Schweiger

Computational Geotechnics Group, Institute for Soil Mechanics and Foundation Engineering, Graz University of Technology, Rechbauerstr. 12, 8010 Graz, Austria; PH (+43316) 873-6234; email: helmut.schweiger@tugraz.at

ABSTRACT

Numerical analyses are performed on a routine basis in practical geotechnical engineering to assess the deformation behaviour of deep excavations under service load conditions, but it becomes increasingly common to use results from numerical analysis for ultimate limit state design (ULS). When doing so, compatibility of the design with relevant standards and codes of practice, valid in the respective country, has to be assured but there are no clear guidelines how this can be achieved. In this paper two aspects are addressed. First the influence of the constitutive model employed for modelling the mechanical behaviour of the soil on calculated structural forces of retaining walls is discussed and secondly the possibilities and limitations of introducing the partial factor concept as established in EC7 in combination with numerical analysis are highlighted.

INTRODUCTION

Numerical analyses are widely used in practical geotechnical engineering to assess the deformation behaviour of deep excavations, in particular when the influence on existing infrastructure such as buildings or adjacent tunnels has to be evaluated. In addition it becomes increasingly common to use results from numerical analysis as basis for the design. When doing so, compatibility of the design with relevant standards and codes of practice, valid in the respective country, has to be assured. In general this is a well established procedure when employing conventional design calculations based e.g. on limit equilibrium methods, but there are no clear guidelines how this can be achieved when numerical methods are used. Thus not much literature is available on this issue although some attempts have been made (e.g. Bauduin et al. (2000), Schweiger (2005, 2009), Simpson (2000, 2007)). An additional difficulty arises, namely the appropriate choice of the constitutive model for the soil, which has a direct consequence for the design because different constitutive models will lead to different design forces. Both aspects are addressed in this paper by means of a benchmark example. Finally, results form the analysis of a real case history, where a diaphragm wall with prestressed ground anchors is used as a retaining system are briefly presented. It follows from these examples that the choice of the constitutive model and the design approach has an influence on the results, but given the uncertainties inherent in any analysis in geotechnical engineering the differences due to the different design approaches seem acceptable provided a suitable constitutive model is employed.

BENCHMARK EXAMPLE - INFLUENCE OF CONSTITUTIVE MODEL

Problem definition and calculation steps

The basic geometry of the investigated deep excavation is depicted in Figure 1. In order to study the effect of different constitutive models for various ground conditions two different (homogeneous) soil conditions are assumed, namely dense sand and a soft soil. For simplicity the wall (EA = 2.53E06 kN/m, EI = 3.02E4 kNm^2/m) and the strut (EA = 1.5E06 kN/m) have been assumed the same for both ground conditions, only the length of the wall and drainage conditions vary. Wall friction was taken as 2/3 of the friction angle of the soil. The soil parameters have been determined based on experimental results which can be considered to be representative for the respective soil.
The following calculation steps have been performed, but only results for the final stage are presented in the following.

Step 0: Initial stress state ($\sigma'_v = \gamma.h$, $\sigma'_h = K_0\ \sigma'_v$, $K_0 = 1 - \sin\varphi'$)
Step 1: Apply surcharge load (permanent load of 10 kPa)
Step 2: Activate wall (wished-in-place), set displacements to zero
Step 3: Excavation to level -2.0 m
Step 4: Activate strut at level -1.5 m
Step 5: Lowering of GW-Table to -6.0 m inside excavation (only for dense sand)
Step 6: Excavation to level -4.0 m
Step 7: Excavation to level -6.0 m
Step 8: Apply variable load of 15 kPa (only for comparison of design approaches)

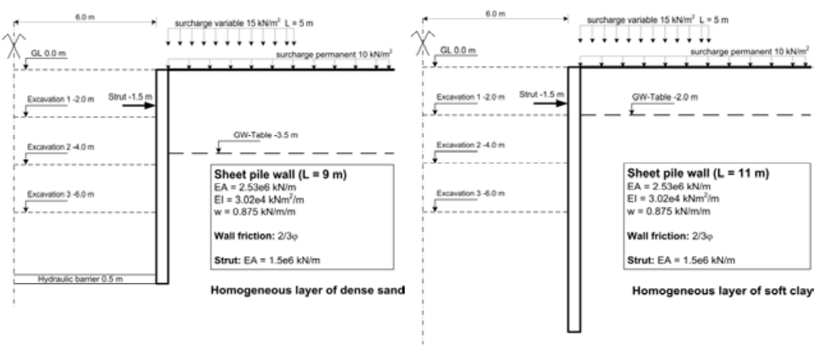

Figure 1. Geometry of benchmark problem for sand and clay layer

For the excavation in the sand layer a deep hydraulic barrier is assumed at the level of the base of the wall and thus no seepage flow is considered (see Figure 1). The analysis considering the soft soil layer has been performed under undrained conditions and it has been assumed that the water is excavated simultaneously with the soil and no modifications to the groundwater conditions are made. The original GW-table is assumed to be at -3.5 m for the sand and at -2.0 m for the clay (Figure 1). The clay above the water table has been modelled as drained material.

CONSTITUTIVE MODELS AND PARAMETERS

Sand layer

For the excavation in the sand layer three different constitutive models have been employed, namely the simple Mohr-Coulomb failure criterion (MC), the standard Plaxis Hardening Soil model (HS), which is a double hardening plasticity model, and the Hardening Soil Small model (HSS), which is the extension of the latter to account for small strain stiffness (Benz, 2007). The parameters are listed in Table 1. Strength parameters are the same for all models but stiffness parameters are different. They are stress dependent in the HS and HSS model (values in Table 1 are reference values) but constant in the Mohr-Coulomb model. The average value of loading and unloading stiffness which follows from the HS model at the base of the retaining wall has been assigned as stiffness in the latter.

Table 1. Parameters for dense sand for Hardening Soil Small Model (HSS)

Parameter		Meaning	Value
γ	[kN/m³]	Unit weight (unsaturated)	18
γ_r	[kN/m³]	Unit weight (saturated)	20
φ'	[°]	Friction angle	41
c'	[kPa]	Cohesion	0
ψ	[°]	Angle of dilatancy	15
ν_{ur}	[-]	Poisson's ratio unloading-reloading	0.20
E_{50}^{ref}	[kPa]	Secant modulus for primary triaxial loading	30 000
E_{oed}^{ref}	[kPa]	Tangent modulus for oedometric loading	30 000
E_{ur}^{ref}	[kPa]	Secant modulus for un- and reloading	90 000
m	[-]	Exponent of the Ohde/Janbu law	0.55
p_{ref}	[kPa]	Reference stress for the stiffness parameters	100
K_0^{nc}	[-]	Coefficient of earth pressure at rest (NC)	1-sin(φ')
R_f	[-]	Failure ratio	0.90
$\sigma_{Tension}$	[kPa]	Tensile strength	0
G_0	[kPa]	Small-strain shear modulus	112 500
$\gamma_{0,7}$	[-]	Reference shear strain where G_{sec}=0.7G_0	0.0002

Clay layer

For the clay layer the Plaxis Soft Soil model (SS) has been used in addition to the Hardening Soil models and the Mohr-Coulomb model. The Soft Soil model is a modification of the well known Modified-Cam-Clay model incorporating a Mohr-

Coulomb failure criterion and allowing for a modification of the volumetric yield surface in order to improve K_0-predictions. The parameters for the HSS model and the SS model are listed in Tables 2 and 3. All models are implemented into the finite element code Plaxis (Brinkgreve et al. 2006), which is used for all analyses presented in this paper. For the MC-model the same assumption with respect to the Young's modulus has been made as for the dense sand.

Table 2. Parameters for soft clay for Hardening Soil Small Model (HSS)

Parameter		Meaning	Value
γ	[kN/m³]	Unit weight (unsaturated)	15
γ_{sat}	[kN/m³]	Unit weight (saturated)	16
φ'	[°]	Friction angle (Mohr-Coulomb)	27
c'	[kPa]	Cohesion (Mohr-Coulomb)	15
ψ	[°]	Angle of dilatancy	0
ν_{ur}	[-]	Poisson's ratio unloading-reloading	0.20
E_{50}^{ref}	[kPa]	Secant modulus for primary triaxial loading	4 300
E_{oed}^{ref}	[kPa]	Tangent modulus for oedometric loading	1 800
E_{ur}^{ref}	[kPa]	Secant modulus for un- and reloading	14 400
m	[-]	Exponent of the Ohde/Janbu law	0.90
p_{ref}	[kPa]	Reference stress for the stiffness parameters	100
K_0^{nc}	[-]	Coefficient of earth pressure at rest (NC)	1-sin(φ')
R_f	[-]	Failure ratio	0.90
σ_t	[kPa]	Tensile strength	0
G_0	[kPa]	Small-strain shear modulus	25 000
$\gamma_{0.7}$	[-]	Reference shear strain where G_{sec}=0.7G_0	0.0003

Table 3. Parameters for soft clay for Soft Soil Model (SS)

Parameter		Meaning	Value
γ	[kN/m³]	Unit weight (unsaturated)	15
γ_r	[kN/m³]	Unit weight (saturated)	16
φ'	[°]	Friction angle	27
c'	[kPa]	Cohesion	15
ψ	[°]	Angle of dilatancy	0
ν_{ur}	[-]	Poisson's ratio	0.20
κ^*	[-]	Modified swelling index	0.0125
λ^*	[-]	Modified compression index	0.0556
K_0^{nc}	[-]	Coefficient of earth pressure at rest	1-sin(φ')

RESULTS

Sand layer

Figure 2 (left) shows the lateral displacement of the sheet pile wall for the final excavation stage. It is observed that the MC model predicts the smallest maximum displacement but of course this strongly depends on the chosen elasticity modulus. HS and HSS model show similar behaviour but including small strain stiffness effects reduces the maximum displacement slightly. It should be mentioned at this stage that the results from the HSS model may be quite sensitive on the choice of the parameter $\gamma_{0.7}$ (which is the shear strain at which the maximum small strain shear modulus is reduced to 70%) but reasonable values based on literature data have been chosen in this study. A similar trend is observed for bending moments (Figure 2, right). The notable difference between the simple and the advanced models become apparent when examining surface settlements behind the wall (Figure 3). The MC model shows unrealistic heave whereas the advanced models show the expected settlement, the maximum values being approx. 50% of the maximum horizontal displacement. Although this is not an issue from a design point of view it emphasizes the well known fact that simple elastic perfectly plastic models are not capable of representing the stress strain behaviour of soils correctly and therefore it remains questionable whether they should be used for design purposes. Strut forces obtained are -78 kNm/m for the MC model and -102 and -107 kNm/m for the HS and HSS model respectively.

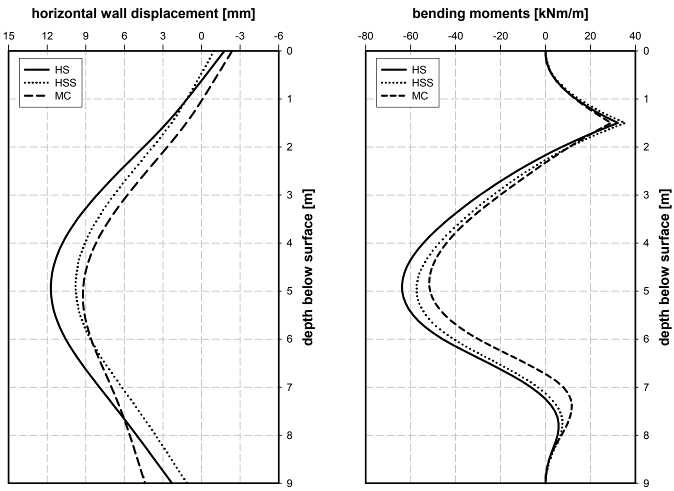

Figure 2. Comparison of wall deflection and bending moments - sand layer

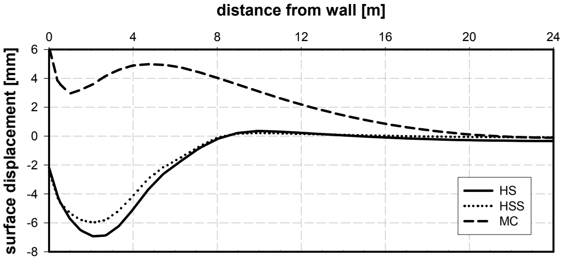

Figure 3. Comparison of surface displacements - sand layer

Clay layer

Figure 4 depicts lateral wall displacements and bending moments for the wall, now 11 m long, in the soft soil. The difference between HS and HSS models are similar as in the previous case but again this depends to a large extent on the value chosen for $\gamma_{0.7}$. The SS model gives the smallest displacements and the MC model shows a different shape of wall deflection, namely an almost parallel movement of the bottom half of the wall, which is in contrast to the other models. This behaviour also leads to differences in the bending moments.

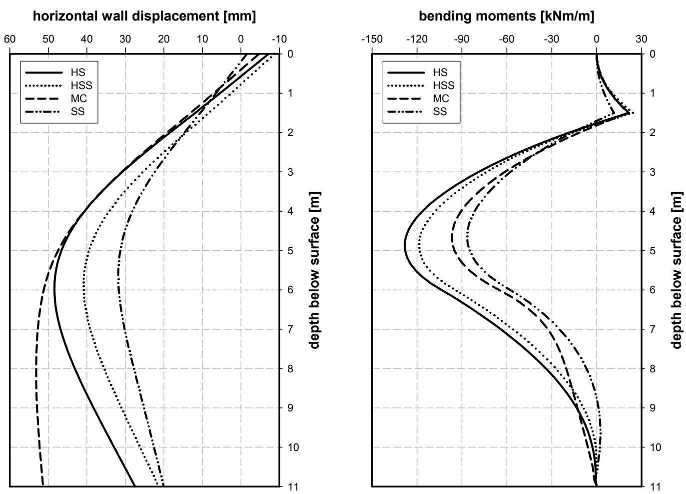

Figure 4. Comparison of wall deflection and bending moments - clay layer

For the settlement trough behind the wall (Figure 5) the same can be observed as in the previous section, namely that the MC model produces significant heave adjacent to the wall and – in this case due to undrained conditions – settlements in the far field (the lateral model boundary for this analysis was placed at a distance of 75 m from the wall). The calculated settlement troughs can be generally considered as too wide with the exception of the HSS model which is a consequence of taking into account small strain stiffness effects.

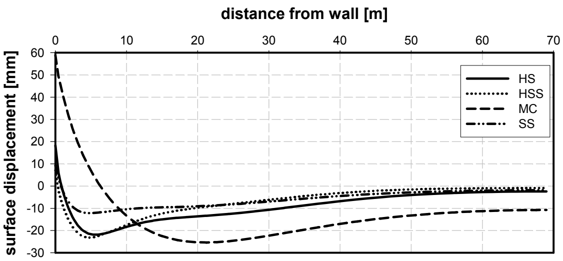

Figure 5. Comparison of surface displacements - clay layer

BENCHMARK EXAMPLE - INFLUENCE OF EC7 DESIGN APPROACH

EC7 design approaches

The same examples as discussed in the previous section is used to demonstrate the applicability of using the finite element method for ULS-design in accordance with Eurocode7. In Eurocode7 the partial factor of safety concept is introduced replacing the global factor of safety concept employed until now. Three different design approaches DA1 to DA3 have been specified which differ in the application of the partial factors of safety on actions, soil properties and resistances. They are given in Tables 4 and 5 for all three approaches. It is noted that 2 separate analyses are required for design approach 1. The problem which arises for numerical analyses is immediately apparent because DA1/1 and DA2 require permanent unfavourable actions to be factored by a partial factor of safety, e.g. the earth pressure acting on retaining structures. This is of course not possible because in numerical analyses the earth pressure is not an input but a result of the analysis. However, EC7 allows for the alternative of putting the partial factor on the *effect of the action* instead on the actions itself, e.g. bending moments or strut forces. This is commonly referred to as DA2*. In this way finite elements can be used because the analysis is performed with characteristic loads and characteristic parameters introducing the relevant partial factor at the end of the analysis. It is beyond the scope of this contribution to elaborate on the advantages and disadvantages of each of the approaches in detail but some discussion can be found e.g. in Simpson (2000, 2007), Bauduin et al. (2003)

and Schweiger (2005). However the differences in results with special emphasis on the constitutive model will be shown.

Table 4. EC7 partial factors for actions

design approach	permanent unfavourable	variable
DA1/1	1.35	1.50
DA1/2	1.00	1.30
DA2	1.35	1.50
DA3-Geot.	1.00	1.30

Table 5. EC7 partial factors for soil strength properties and resistances

design approach	tanφ'	c'	undrained shear strength	passive resistance
DA1/1	1.00	1.00	1.00	1.00
DA1/2	1.25	1.25	1.40	1.00
DA2	1.00	1.00	1.00	1.40
DA3-Geot.	1.25	1.25	1.40	1.00

The calculation steps are the same as in the previous section but an additional variable load of 15 kPa extending to a width of 5 m is added as a final calculation step in order to have the influence of a variable load taken into account (Figure 1). Again a sand and a clay layer are considered, but only two constitutive models, the HSS-model and the MC-model are compared. The (characteristic) parameters are the same as listed in Tables 1 and 2. For the clay layer an additional aspect is addressed, namely the consequences of performing the *undrained* analysis in terms of effective strength parameters φ' and c, or in terms of the undrained shear strength c_u because this does not only involve a difference in the method of analysis but different partial factors apply to effective strength parameters and the undrained shear strength respectively (Table 5), namely 1.25 versus 1.4. For the analysis in terms of undrained shear strength c_u, the following assumptions have been made. The distribution of c_u with depth has been worked out based on the Mohr-Coulomb criterion and this distribution has been also used for the HSS-model. It is noted at this stage that by doing so, some of the advanced features of the HSS-model are lost. It should also be mentioned that in the analysis in terms of effective strength parameters the undrained shear strength obtained from the HSS-model depends on a number of input parameters (not only strength) and is therefore different to the undrained shear strength in the MC-model. This approach yields the following distribution of characteristic undrained shear strength as used in DA2:
c_u at depth -2.0 m below surface: 23.9 kPa with an increase of 2.1 kPa/m

For DA3 the strength parameters have to be reduced by the partial factors listed in Table 5 resulting in values for the effective friction angle, the effective cohesion and the undrained shear strength as given in Table 6. The dilatancy angle ψ is also reduced by the partial factor which is however not explicitly mentioned in EC7. Finally a decision with respect to initial stresses has to be made. Here the value for K_0 has been kept the same for DA2 and DA3, i.e. it is based on the *characteristic* value for the friction angle ($1 - \sin\varphi'_{char}$) although an alternative would be to have it based on the *design* value in DA3. (For certain conditions K_0 based on φ'_{char} may however violate the yield function).

Table 6. Strength parameters used in DA3 (partial factors applied)

Parameter		Meaning	Value
φ'_{sand}	[°]	Friction angle	34.8
c'_{sand}	[kPa]	Effective cohesion	0
ψ_{sand}	[°]	Angle of dilatancy	12
φ'_{clay}	[°]	Friction angle	22.2
c'_{clay}	[kPa]	Effective cohesion	12
ψ_{clay}	[°]	Angle of dilatancy	0
$c_{u,clay}$	[kPa]	Undrained shear strength at 2.0 m depth	17.1
$\Delta c_{u,clay}$	[kPa/m]	Increase of undrained shear strength	1.5

RESULTS

In this section the differences in design strut forces and bending moments obtained from utilizing design approaches DA2 and DA3 (DA1 is basically a combination of the two) are presented.

Sand layer

Figure 6 shows a comparison of design bending moments (envelope over all construction stages) obtained for the two constitutive models for DA2 and DA3. The design moments for DA2 are obtained by the following procedure: *characteristic bending moments* are calculated without (M_1) and with (M_2) the variable load applied and from these the *design bending moments* are calculated by applying the appropriate partial factors. The same procedure is used for calculating design strut forces. It should be noted that this is an approximation only, due to the nonlinear behaviour of the soil.

$$M_{design,\ DA2} = M_1 \times 1.35 + (M_2 - M_1) \times 1.5$$

In DA3 results from the analysis are directly design values because the partial factors on soil strength and the variable load (15 kPa > 19.5 kPa) are taken into account in the input of the analysis.

It follows from Figure 6 that differences coming from the different design approaches are more pronounced for the MC-model than for the more advanced HSS-model. DA3 leads to significantly higher design moments for the MC-model whereas for the HSS-model very similar values are obtained. The same holds for strut forces where for the HSS-model actually a slightly lower design force is obtained from DA3 (Table 7). The reason for this behaviour is that a reduction in strength has a different effect in a linear elastic-perfectly plastic model than in an advanced hardening plasticity model due to the different stress paths followed.

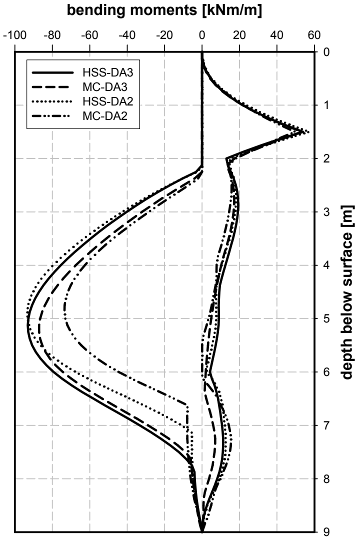

Figure 6. Comparison of design bending moments - sand layer

Table 7. Comparison of design strut forces - sand layer

DA2	Strut force after excavation	Strut force due to load	Design strut force
MC	78	21.6	**138**
HSS	108.6	23.1	**181**

DA3	Strut force after excavation	Strut force due to load	Design strut force
MC	122	39	**161**
HSS	140	36	**176**

Clay layer

Figure 7 shows design bending moments for both design approaches and both constitutive models for analyses in terms of effective strength parameters (denoted "A" in Figure 7) and undrained shear strength parameters (denoted "B"). The following can be observed: for the HSS-model again DA2 and DA3 yield similar results (DA2 slightly higher in this case) for analyses with effective strength parameters. For the MC-model the difference is higher and in contrary to the excavation in dense sand DA2 design bending moments are higher than the ones obtained from DA3. For analyses in terms of undrained strength parameters (c_u) it is different because the partial factor on undrained strength is higher than for drained strength parameters. Thus DA3 results in higher bending moments than DA2 for both models. For the MC-analysis with characteristic parameters (DA2) the differences in method A and B are negligible, which can be expected. For the HSS-model this is not the case because the analysis in terms of effective parameters will lead to a different undrained strength as the one specified in method B. Strut forces are summarized in Table 8.

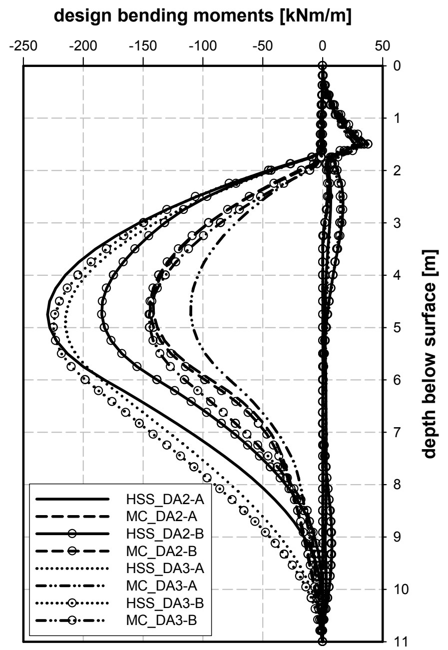

Figure 7. Comparison of design bending moments - clay layer

Table 8. Comparison of design strut forces - clay layer

DA2	strut force after excavation	strut force due to load	design strut force
MC	95.7	13.7	**150**
HSS	121	19.6	**193**
MC_B	100.6	15.3	**159**
HSS_B	121.4	19.4	**193**

DA3	strut force after excavation	strut force due to load	design strut force
MC	101.4	21.1	**123**
HSS	140.2	35.3	**176**
MC_B	116.7	35.1	**152**
HSS_B	161.9	43.8	**206**

PRACTICAL EXAMPLE

The benchmark examples presented in the sections above indicate that both design approaches DA2 and DA3 and consequently also DA1 can be applied in combination with the finite element method. It also follows from these examples that the differences in results due to the choice of the constitutive model are at least in the same order (or larger) than differences coming from the design approaches. However, for real practical problems details of the design may have more severe consequences for the choice of the design approach as compared to the simplified examples presented above. This will be illustrated as an example by considering a diaphragm wall with three rows of prestressed anchors. The excavation is about 17 m deep in a reasonably homogeneous layer of medium dense sand (Figure 8). The details of the analysis will not be discussed here because the goal of this section is only to highlight a particular aspect, namely the resulting design anchor forces. As described in the previous section, analyses were performed with characteristic soil strength parameters (DA2) and with design strength parameters (DA3). The permanent action is the earth pressure, there are no variable loads. Again DA2 is used in form of DA2*, i.e. the partial factor is applied to effects of actions rather than on the action itself. The resulting design anchor forces obtained from the two approaches are summarized in Table 9 and it can be seen that DA3 leads to significantly lower forces. The reason for this difference is the following: if anchors are highly prestressed, as it is the case here, a reduction in soil strength does not change calculated anchor forces significantly as compared to the analysis with characteristic soil strength. Thus in DA2 the result is multiplied by the partial factor for actions (= 1.35) whereas in DA3 the calculated forces are already design forces. It should be pointed out that in DA2 the effects of the water pressure are fully factored whereas they are not in DA3. It is acknowledged that, strictly speaking, an uncertainty in the water table should be considered in DA3 as a "geometric" factor, but this would not bring forces near the values obtained for DA2.

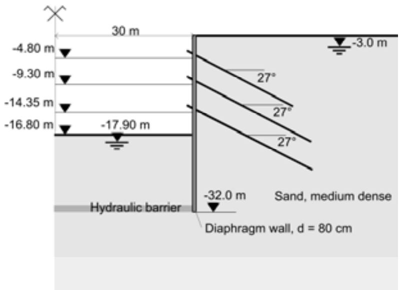

Figure 8. Layout of practical example

Table 9. Comparison of design anchor forces - practical example

	anchor force layer 1 (kN/m)	anchor force layer 2 (kN/m)	anchor force layer 3 (kN/m)
characteristic	334	756	755
DA2* (= char. x 1.35)	451	1021	1020
DA3	358	805	766

CONCLUSION

In the first part of this contribution the influence of the constitutive model on the results of finite element analyses of deep excavations has been demonstrated. The results clearly emphasize the well known fact that elastic-perfectly plastic constitutive models such as the Mohr-Coulomb model are not well suited for analysing this type of problems and more advanced models are required to obtain realistic results. Although reasonable lateral wall movements may be produced with simple failure criteria with appropriate choice of parameters, vertical movements behind the wall are in general not well predicted, obtaining heave in many cases instead of settlements. Strain hardening plasticity models including small strain stiffness behaviour are in general a better choice and produce settlement troughs being more in agreement with expected behaviour. As the goal of the study presented here was to qualitatively highlight the differences in results with respect to the constitutive model no quantitative comparison with in situ measurements has been provided.
The second part of the paper addressed the ULS-design of deep excavations by means of numerical methods. It has been shown that the concept of partial factors of

safety as established in Eurocode7 can be applied, but differences have to be expected depending on how this is done in the respective design approaches. Although more experience is needed in performing such analyses for practical examples, it emerges from this study that the differences in results depending on the design approach used are less pronounced for more advanced constitutive models as compared to simple elastic-perfectly plastic failure criteria. On first sight this seems to be in contradiction to practical experience but can be explained by different stress paths soil elements follow when different models are used. Postulating that advanced models are more reliable in describing the stress strain behaviour of soils for stress levels ranging from working load conditions up to failure it could be argued that advanced models have advantages not only for predicting displacements and stresses for working load conditions but have their merits also in ULS-design. Finally it should be mentioned that the models used in this study should be seen as representatives for certain classes of models and conclusions can be transferred to other constitutive models of similar type.

REFERENCES

Bauduin, C., De Vos, M. and Simpson, B. (2000). "Some considerations on the use of finite element methods in ultimate limit state design." Proc. Int. Workshop on Limit State Design in Geotechnical Engineering, Melbourne.

Bauduin, C., De Vos, M. and Frank, R. (2003). "ULS and SLS design of embedded walls according to Eurocode 7." Proc. XIII ECSMGE, Prague (Czech Republic), Vol. 2, 41-46.

Benz, T. (2007). "Small-Strain Stiffness of Soils and its Numerical Consequences." Publication No. 55, Institute for Geotechnical Engineering, University of Stuttgart.

Brinkgreve, R.B.J., Broere, W. and Waterman, D. (2006). "Plaxis, Finite element code for soil and rock analyses, users manual." The Netherlands.

Schweiger, H.F. (2005). "Application of FEM to ULS design (Eurocodes) in surface and near surface geotechnical structures." Proc. 11th Int. Conference of IACMAG, Turin, Italy, 19-24 June 2005. Bologna: Patron Editore. 419-430.

Schweiger, H.F. (2009). "Influence of constitutive model and EC7 design approach in FEM analysis of deep excavations." Proc. ISSMGE Int. Seminar on Deep Excavations and Retaining Structures (Mahler & Nagy, eds.), Budapest, 99-114.

Simpson, B. (2000). "Partial factors: where to apply them?" Proc. Int. Workshop on Limit State Design in Geotechnical Engineering, Melbourne, 145-154.

Simpson, B. (2007). "Approaches to ULS design – The merits of Design Approach 1 in Eurocode 7." First International Symposium on Geotechnical Safety & Risk, Oct. 18-19, 2007, Shanghai, Tongji University, China.

Advantages and limitations of ultimate limit state design methods for braced excavations

D. C. Konstantakos, P.E.[1]

[1]Deep Excavation LLC, 30-62 Steinway St. #188, Astoria, NY; PH (206)-279-3300; FAX (206)-279-3062; email: dimitrios@deepexcavation.com

ABSTRACT

This paper examines the advantages and limitations of employing ultimate limit state methods for the design of braced excavations. Braced excavation design requires both skill and careful evaluation of many factors that can affect performance. Traditionally in the US, braced excavations are designed with a serviceability approach where soil parameters are conservatively estimated and the performed analysis yields the service displacements, moments, and forces. Design forces are then calculated by applying a global safety factor on the service design results, while the wall embedment is determined by calculating limit equilibrium safety factors against wall rotation and passive resistance that range from 1.2 to 1.5.

In Europe, in contrast to the US, an ultimate limit state design approach has been adopted in geotechnical design including the design of braced excavations. In this design philosophy both wall and supports are designed based on an ultimate limit condition. The ultimate design forces are typically determined by reducing the characteristic soil strength parameters or by multiplying the effects of actions and dividing the effects of resistances by various safety factors. At the end, a safety factor of one or greater is required for all structures and other types of safety factors.

Back in the US, there is an increasing trend of promoting ultimate limit state design in geotechnical design, including braced excavations. In the author's experience the ultimate limit state method works reasonably well for most limit equilibrium methods but can produce very inconsistent results in many cases when numerical analyses are employed. Hence, the advantages and limitations of the ultimate limit state design should be carefully weighted by practitioners and academia in the US before, and if, the ultimate limit state philosophy is incorporated in a legally binding building code.

INTRODUCTION

Braced excavation design requires both skill and careful evaluation of many factors that can affect performance. Traditionally, braced excavations are designed with a service limit state (herein SLS) approach where soil parameters are conservatively estimated and the performed analysis yields the service displacements, moments, and forces at working conditions. Design forces are then calculated by applying a global safety factor on the service design results either as an allowable stress factor on structural material strength or as an overall safety factor that is used to multiply the SLS analysis results. Wall embedment is determined by calculating limit equilibrium safety factors against wall rotation and passive resistance that typically range from 1.2 to 1.5.

In the European Union, in contrast to the US, an ultimate limit state design approach (herein ULS) has been adopted in geotechnical design including the design of braced excavations. In this design philosophy both wall and supports are designed based on ultimate limit conditions that in essence represent a state with very large plastic displacements slightly before failure occurs. The ultimate design forces are typically determined by reducing the characteristic soil strength parameters or by multiplying the effects of actions and dividing the effects of resistances by various safety factors. At the end, a safety factor of one or greater is required for all structures and other types of safety factors. These types of checks may have to be examined for up to three basic design approach methods that in essence translate up to four ULS analysis models, not including the SLS conditions that have to also be examined.

Back in the US, in essence as an extension of Load Factor Resistant Design (LRFD) in structural design, there is an increasing trend of promoting the ULS philosophy in geotechnical design, including the design of braced excavations. The adoption of a similar ULS approach in the US can provide a more unified design philosophy if such a design approach is properly framed and calibrated to the US experience. Hence, the European experience should be carefully evaluated by US academia and practitioners before, and if, a ULS philosophy is adopted in deep excavation design. In this respect, this paper briefly reflects on the author's personal experience with European ULS design methods and aims to provide ground for further discussion.

OVERVIEW OF EUROCODE 7 DESIGN PROCEDURES FOR BRACED EXCAVATIONS

In 1975, the Commission of the European Community decided on an action program in the field of construction that aimed to eliminate technical obstacles to trade and harmonize technical specifications across member states. Within this action program, a set of harmonized technical rules for the design of construction works was established which from 2010 serve as the basis of design in each Member State. Design of braced excavations is mainly governed by the geotechnical standard that is Eurocode 7 (EN 1997 herein EC7). However, a designer has to also consider applications of Eurocode 2 for concrete members, Eurocode 3 for steel structures, and Eurocode 8 for earthquake resistant design.

EC7 specifies that, when applicable, the following Ultimate Limit States should not be exceeded:

- EQU: Loss of equilibrium of the structure or the ground, considered as a rigid body, in which the strengths of structural materials and the ground are insignificant in providing resistance.
- STR: Internal failure or excessive deformation of the structure or structural elements, including footings, piles or basement walls for instance, in which the strength of structural materials is significant in providing resistance.
- GEO: Failure or excessive deformation of the ground, in which the strength of soil or rock is significant in providing resistance.

- UPL: Loss of equilibrium of the structure or the ground due to uplift by water pressure (buoyancy) or other vertical actions.
- HYD: Hydraulic heave, internal erosion and piping in the ground caused by hydraulic gradients.

In the design of braced excavations, typically the STR, GEO, and HYD checks are of importance. Under all limit states, the designer should verify that:

$$E_d \leq R_d$$

E_d = Design value of the effect of actions (geotechnical, structural, etc)
R_d = Design value of the resistance to an action.

Partial factors on actions may be applied either to the actions themselves (F_{rep}) or to their effects (E) by applying either one of the following procedures:

$E_d = E\{\gamma_F F_{rep}; X_k/\gamma_M; a_d\}$ (EC7 equation 2.6a)
$E_d = \gamma_E E\{F_{rep}; X_k/\gamma_M; a_d\}$ (EC7 equation 2.6b)

Resistances to actions are determined in a similar manner where partial factors are applied to ground properties (X) or resistances (R) or to both with either one of the following:

$R_d = R\{\gamma_F\ Frep; X_k/\gamma_M; a_d\}$ (EC7 equation 2.7a)
$R_d = R\{\gamma_F\ Frep; X_k; a_d\}/\gamma_R$ (EC7 equation 2.7b)
$R_d = R\{\gamma_F\ Frep; X_k/\gamma_M; a_d\}/\gamma_R$ (EC7 equation 2.7c)

Where:

a_d = Design value of geometrical data
γ_E = Partial factor for the effect of an action
γ_F = Partial factor for an action
γ_m = Partial factor for a soil parameter (material property)
γ_R = Partial factor for a resistance
X_k = Characteristic value of a material property (soil friction, effective cohesion, undrained shear strength, etc).

Subsequently, the designer can apply up to three basic design modes that each provide one or more combinations of minimum partial factors that are applied concurrently to actions (A), material properties (M), and resistances (R). Actions on a retaining structure generally originate from external loads and from water or earth pressures. These actions are subsequently categorized as permanent or variable, and as favorable or unfavorable depending on the nature of the load. While EC7 provides suggested values for all the partial factors, each member state is free to adopt other factors. The combination modes are referred to as Design Approaches and are the following (quick designations DA-1/1 etc):

Design Approach 1:	Combination 1:	*A1* "+" *M1* "+" *R1*	(DA-1/1)
	Combination 2:	*A2* "+" *M2* "+" *R1*	(DA-1/2)
Design Approach 2:	Combination:	*A1* "+" *M1* "+" *R2*	(DA-2)
Design Approach 3:	Combination:	(*A1** or *A2†*) "+" *M2* "+" *R3*	(DA-3)

*on structural actions, †on geotechnical actions
Where "+" implies: "to be combined with".

The recommended partial factors by EC7 for actions (*A*), material properties (*M*), and resistances (*R*) are the product of statistical analysis and are summarized in Tables 1 through 3 respectively for each design case. Table 3 also includes recommended partial factors for the resistance of pre-stressed ground anchors since they are often used as external bracing in temporary excavations.

Table 1. Partial factors on actions (γ_F) or the effects of actions (γ_E)

Action		Symbol	Set	
			A1	A2
Permanent	Unfavorable	γ_G	1.35	1.0
	Favorable		1.0	1.0
Variable	Unfavorable	γ_Q	1.5	1.3
	Favorable		0	0

Table 2. Partial factors for soil parameters (γ_M)

Soil parameter	Symbol	Set	
		M1	M2
Angle of shearing resistance (applied to tan φ)	γ_{ϕ}'	1.0	1.25
Effective cohesion	γ_{c}'	1.0	1.25
Undrained shear strength	γ_{cu}	1.0	1.4
Unconfined strength	γ_{qu}	1.0	1.4
Weight density	γ_{γ}	1.0	1.0

Table 3. Partial resistance factors for earth resistance, pre-stressed anchors (γ_R)

Resistance	Symbol	Set			
		R1	R2	R3	R4
Earth resistance	$\gamma_{R;e}$	1.0	1.4	1.0	-
Ground anchors (temporary)	$\gamma_{a;t}$	1.1	1.1	1.0	1.1
Ground anchors (permanent)	$\gamma_{a;p}$	1.1	1.1	1.0	1.1

An interesting aspect of the above classification is that there is no specific definition for lateral earth actions and for lateral water pressures. However, it is common practice to consider both unfavorable lateral earth and water pressures as permanent loads (Bauduin et. al). Nevertheless, one could conceivably argue that unfavorable water under flow conditions can be considered as a variable load. The following two sections present examples of applying EC7 combinations for limit equilibrium and for nonlinear analysis methods.

SAMPLE APPLICATION OF EC7 FOR A SIMPLE BRACED EXCAVATION

In order to better illustrate how EC7 procedures are applied, a simple example solved with traditional limit equilibrium methods is first presented (Figure 1). This imaginary example comprises a 9m deep excavation, supported by an 18m long wall, braced by one ground anchor located at 3m below the wall top and inclined at 30 degrees from the horizontal. Retained ground water is located at 5m depth while water inside the excavation is maintained at subgrade.

For reasons of simplicity the analyses assume one soil type, Rankine active earth pressures on the retained side, and Rankine passive earth pressures on the excavated side. A simplified one-dimensional water flow is considered for all construction stages and the wall is analyzed with the free earth method. The excavation was analyzed for the service case (SLS), for a typical US approach with a typical 1.5 safety factor on the SLS results, and last for all EC7 ULS combinations (DA-1, DA-2, DA-3). Table 4 compares critical results computed with the aforementioned design scenarios. It is emphasized that this example does not represent an optimized design.

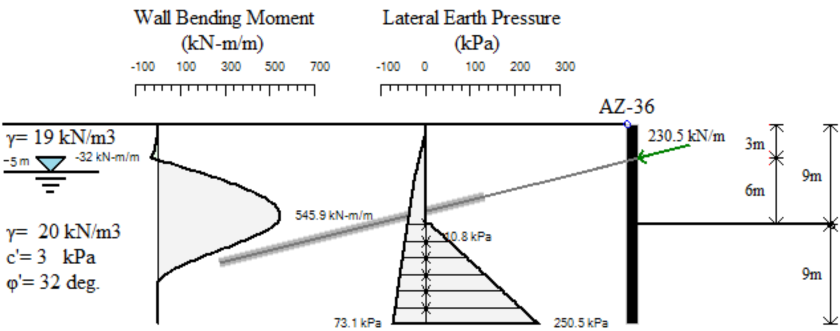

Figure 1. Example of typical braced excavation (with service analysis results)

Table 4. Comparison combination methods for braced excavation example with traditional limit equilibrium approach.

Case	M_{MAX} (kN-m/m)	R_{MAX} (kN/m)	*FS* ROT	*FS* HYD	$\sigma'_{A.MAX}$ (kPa)	U_{NET} (kPa)	q_{MAX} (kPa)	$\sigma'_{PASS.MAX}$ (kPa)
SLS	546	230.5	1.787	1.692	73.1	32.7	5.0	250.5
SLSx1.5	819	346.0	1.787	1.692	73.1	32.7	5.0	250.5
DA-1/1	931	354.1	1.324	1.128	98.7	44.2	7.5	250.5
DA-1/2	886	345.6	1.179	1.128	92.1	32.7	5.0	200.5
DA-2 [1]	1478[1]	476.5[1]	0.946	1.128	98.7	44.2	7.5	178.9
DA-3	884	348.5	1.179	1.128	92.1	32.7	7.5	200.5

Notes: 1. Case DA-2 model does not converge

$\sigma'_{A.MAX}$ = Maximum computed unfavorable active earth pressure (including partial factors)
$\sigma'_{PASS.MAX}$ = Maximum computed passive earth resistance pressure (including partial factors)
***FS* ROT** = Wall embedment safety factor against rotation (free earth method)
***FS* HYD** = Hydraulic heave safety factor
M_{MAX} = Maximum computed wall bending moment
R_{MAX} = Maximum computed support reaction at the anchorage direction
U_{NET} = Maximum computed unfavorable net water pressure (including partial factors)
q_{MAX} = Maximum computed unfavorable variable load (including effects of partial factors)

In this example, all EC7 combinations produced greater ultimate wall moments and support reactions when compared with the typical US approach (with a safety factor of 1.5). It is worth to note that EC7 combination DA-2 failed to converge as the earth resistance was not sufficient to fix the wall. While all methods that converged resulted in a similar ultimate anchor reaction, ultimate wall bending computed with EC7 combinations was from 8% to 13.5% greater compared to the SLS x 1.5 approach (where service analysis results are multiplied times 1.5). This difference is equivalent to applying a safety factor of 1.6 to 1.7 on the SLS wall bending results.

Next, the same example is examined with a well established nonlinear beam-on-elastoplastic foundation solution (DeepXcav 2010, Nova et. al. 1987). In this approach, the soil is modeled as a series of stage-dependent nonlinear soil springs on both the retained and the excavated sides. In addition to the limit-equilibrium method, nonlinear soil-structure interaction methods require the definition of the ground anchor prestress, the elastic soil and support properties, and equally important determination of the initial lateral earth pressures (i.e. at-rest lateral earth pressure coefficients). Table 5 compares critical results for the excavation of figure 1 computed with the nonlinear solution for the same design scenarios.

Table 5. Comparison of different combination methods for braced excavation example with beam-on-elastoplastic foundations approach.

Case	δ_{MAX} (cm)	M_{MAX} (kN-m/m)	R_{MAX} (kN/m)	**FS Passive Mobilized**	**FS Wall M vs. SLS**	**FS Support R vs. SLS**	**Comments**
SLS	6.0	528	263	1.606	1.00	1.00	-
SLSx1.5	6.0	792	394	1.606	1.50	1.50	Same as SLS
DA-1/1	6.0	712	356	1.606	1.35	1.35	Note 1
DA-1/2	12.7	874	365	1.154	1.66	1.39	-
DA-2	9.2	950	408	1.207	1.80	1.55	Note 1
DA-3	12.7	872	368	1.154	1.65	1.40	-

Note: 1. Combination performed by standardizing analysis by $\gamma_G = 1.35$
δ_{MAX} = Maximum horizontal wall displacement

Table 5 reveals many interesting points for discussion. First, combinations DA-1/1 and DA-2 are standardized by the partial safety factor for unfavorable permanent actions (1.35). In this procedure, initially all variable load actions are divided by γ_G, passive coefficients are adjusted for the (R) set of partial safety factors, and an equivalent service analysis is performed. The final results are then obtained by multiplying the standardized SLS analysis results by γ_G. This standardization is the only available analysis option when water levels differ between the retained and excavated sides (multiplication of water pressures by a safety factor in a nonlinear solution is virtually impossible and theoretically inconsistent since vertical effective stress and water pressures are coupled).

In this example, the EC7 design approach combinations result in wall bending moments that differ by -10% to 20% of the SLS x 1.5 case maximum wall bending (with corresponding safety factors ranging from 1.35 up to 1.80). EC7 results for the anchor reaction exhibit a smaller scatter compared to the wall bending around the SLS x 1.5 analysis scenario (from 90% to 103%, or overall safety factors from 1.35 to 1.55).

In the nonlinear solution, the standardization procedure essentially allows the DA-2 combination to be computed, whereas, the analysis could not converge for the limit-equilibrium approach. In a nonlinear analysis the passive mobilization safety factor can be particularly valuable in assessing excavation performance. Given that in a ULS approach a FS$\geq$ 1.0 is desired, one would immediately tend to render the safety factor FS= 1.2 in case DA-2 as acceptable. This apparent discrepancy can be misleading since the combination was analyzed with a standardized SLS approach. It can thus be argued, that in this case the minimum safety factor equal to the standardization factor is desirable (i.e. $FS_{Passive.Mobilized} \geq 1.35$).

ADVANTAGES AND LIMITATIONS OF ULS METHODS IN BRACED EXCAVATIONS

The main advantage of the ULS method is that it rationalizes the design approach by attempting to account for the relative importance of various factors that affect braced excavation design. Hence, in theory at least, the overall safety factor of 1.0 is desired globally to all items of interest, structures and ground alike. The partial factors should be in essence the product of statistical procedures that determine the acceptable probability of concurrent scenarios taking place. In this respect, the ULS approach is advantageous as it forces the designer to explore the overall design sensitivity by examining various scenarios. However, this unification may produce designs that are quite contradictory to the present SLS design experience.

Even though the braced excavation example in the previous section is relatively straightforward, the effort required to perform and evaluate the EC7 ULS combinations is considerably increased compared to the single SLS case. With this number of scenarios, a designer (including the author) is left with no option but to use computer software that performs all the necessary combinations automatically.

An important aspect not addressed so far is the calculation of the pullout resistance of ground anchors. In traditional SLS designs, ground anchorages are designed using published ultimate skin friction values with a safety factor of at least 2 (French T.A 1995, PTI 1996, et. all). Thus, in the previous nonlinear example the overall safety factor on the pull out of ground anchors is about FS= 1.4 x 1.1 = 1.54, well below the minimum 2.0 associated with skin friction design charts. Hence, some practitioners, including the author, recommend using an additional partial safety factor ξ_q when ultimate published skin friction values are employed (typically from 1.3 to 1.4 depending on the design assumptions). In essence in the DA-1/1 and DA-1/2 approaches one would end with:

DA-1: Comb. 1 $FS\ q_{skin} = \gamma_G$ "x" γ_a "x" ξ_q = 1.35 "x" 1.1 "x" 1.35 $\approx$ 2.00
Comb. 2 $FS\ q_{skin} = \gamma_{cu}$ "x" γ_a "x" ξ_q = 1.40 "x" 1.1 "x" 1.35 $\approx$ 2.08
"x" denotes approximate multiplication of effects.

Alternatively, the γ_{cu} "x" ξ_q product can be related to similar ξ factors for piles that depend on the number of ground anchor load tests performed on each project.

The current EC7 ULS design procedures seem to be geared mostly for traditional limit-equilibrium analysis. As already demonstrated, treatment of water in nonlinear solutions can be quite challenging. Furthermore, in a full finite-element model it can be particularly meaningless to simply adjust K_a and K_p by partial safety factors.

In the case of clays, the "*M2*" combination can produce quite meaningless results in nonlinear solutions if one for example adjusts the constant volume shearing friction angle φ'_{cv} and the peak friction angle of the clay φ'_{p}. For excavations in very soft clays, the "*M2*" case factors cannot be applied as the ground would be unstable even under minimal loading and the analysis will never converge.

What may not be immediately evident to most engineers is that nonlinear solutions are greatly affected by the initial stress level (or stress history). Hence, an unyielding wall (zero horizontal displacement) will only experience at-rest lateral earth pressures and in essence the ULS design can produce the same results as an SLS approach.

Last, in the author's opinion, the current EC7 ULS methods do not place sufficient importance on soil stiffness and the intrinsic nonlinear nature of soil. Perhaps a combination where soil stiffness is reasonably varied should be established and replace one of the combinations that produce quite conservative results.

CONCLUSIONS

From a theoretical standpoint ultimate limit state design procedures offer a unifying perspective on geotechnical design that is lacking in current braced excavation design practice in the United States. However, the European venture in ULS geotechnical world has demonstrated that proper application of the ULS methods can be particularly challenging by everyday practitioners especially when nonlinear effects have to be considered.

While in most cases little value appears to be added compared to traditional service designs, the ULS method forces designers to contemplate on the uncertainty of soil behavior. Unfortunately, this uncertainty has yet to persuade project managers to understand the importance of adequate soil investigation. In conclusion, the geotechnical community in the United States, including practitioners and academia alike, should carefully evaluate the impacts before moving away from current service design practices for braced excavations and geotechnical design in general.

REFERENCES

DeepXcav 2010 (2009). "A computer software program for the analysis of deep excavations", CeAS S.r.l Milano Italy, Deep Excavation LLC, New York, NY.

Frank R., Bauduin C., Driscoll R., Kavvadas M., Krebs Ovesen N., Orr T., Schuppener B, (2004). "Designers' Guides to EN 1997-1 Eurocode 7: Geotechnical Design-General Rules", Thomas Telford.

European Committee for Standardization (2004). "EN 1997-1, Eurocode 7: Geotechnical design – Part 1: General rules", CEN, Brussels.

French Recommendations T.A. 95 (1995). "Recommandations concernant la conception, le calcul, l'execution et le controle des tirants d'ancrage.", Eyrolles.

Nova, R., Becci, B. (1987) "A method for analysis and design for flexible retaining structures", *Proc. Conf. INTERACTIONS SOLS-STRUCTURES*, pp. 657-664

Post-Tensioning Insitute (PTI), (1996). "Recommendations for Prestressed Rock and Soil Anchors", Phoenix, Arizona.

LRFD for Earth Retaining Structures in U.S. Transportation Practice

Naresh C. Samtani[1], Ph.D., P.E. and Paul J. Sabatini[2], Ph.D., P.E.

[1] President, NCS Consultants, LLC, 640 W Paseo Rio Grande, Tucson, AZ 85737; Phone: (520) 544-2786; Fax: (520) 531-1194; E-mail: nsamtani@msn.com
[2] Associate, Geosyntec Consultants, 1420 Kensington Road, Suite 103, Oakbrook, IL 60523; Phone: (630) 203-3352; Fax: (630) 203-3341; E-mail: psabatini @geosyntec.com

ABSTRACT

This paper describes the geotechnical aspects of earth retaining structures in the context of U.S. transportation practice based on Load and Resistance Factor Design (LRFD) methodology as adopted by the American Association of State Highway and Transportation Officials (AASHTO). The paper provides information on: (1) basic concepts of LRFD; (2) limit states, loads, load factors and resistance factors for earth retaining structures; (3) comparisons with past practice based on allowable stress design (ASD); and (4) considerations for limit state analyses for earth retaining structures in an LRFD framework. Fill and cut walls are addressed.

INTRODUCTION

In the last three decades, reliability-based design methods have been formally implemented in design specifications across the world in various formats. In U.S. transportation practice, this design format has been labeled as Load and Resistance Factor Design (LRFD) by the American Association of State Highway and Transportation Officials (AASHTO). The first edition of the AASHTO-LRFD Bridge Design Specifications was introduced in 1994 followed by major editions in 1998, 2004 and 2007. Yearly interim revisions were released between each edition. Often the interim revisions contained significant changes. Herein, *LRFD-Specifications* refer collectively to the 2007 (4th) edition with 2008 and 2009 Interims (AASHTO, 2007).

The following sections of the *LRFD-Specifications* contain guidance for geotechnical features such as foundations and retaining walls:

- Section 3 – Loads and Load Factors
- Section 10 – Foundations
- Section 11 – Abutment, Piers and Walls

Although Section 11 of the *LRFD-Specifications* provides significant guidance related to the design of earth retaining structures, it is silent on many important issues. This paper presents the opinions of the authors related to implementation of LRFD for earth retaining structures in U.S. transportation practice.

EXPRESSION OF SAFETY IN THE AASHTO-LRFD APPROACH

The cardinal rule in the design of any type of structure is that it should be safe. Simply stated, safety is achieved by providing a resistance which is larger than the load. For design purposes, some quantification of safety is needed. In the allowable stress design (ASD) format, safety is deterministically quantified through a factor of safety, FS, which is the ratio of mean resistance to mean load. However, this definition of safety cannot be used to quantify the probability of failure.

In the AASHTO-LRFD approach, the variation of measured load, Q, and measured resistance, R, about their respective mean values is expressed through appropriate probability distribution functions (PDFs) as shown in Figure 1. The overlap zone between the PDFs for load and resistance qualitatively expresses the probability of failure because, in this zone, load is greater than resistance, i.e., $R – Q < 0$. The expression $R – Q$ can be thought of as a limit state, g, in the sense that the limit of $R < Q$ represents failure.

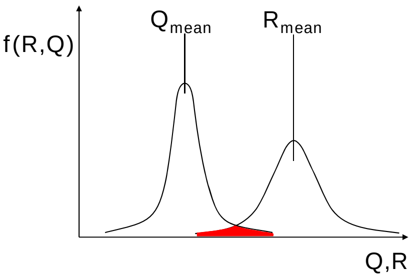

Figure 1. Basic LRFD framework for load, Q, and resistances, R.

By developing a PDF for the limit state $g = R – Q$, the probability of failure represented qualitatively by the overlap zone in Figure 1 can be quantified. Figure 2 shows the PDF for limit state $g = R – Q$. The following observations can be made:

1. The y-axis is the demarcation between failure and safety. In other words, failure is indicated to the left of the y-axis where resistance is less than the load.
2. The probability of failure is equal to the area under the PDF curve for limit state g on the left (negative) side of the y-axis.
3. Safety can be expressed in terms of how far the mean value of the limit state, g_{mean}, is from the y-axis. The distance between g_{mean} and the y-axis can be expressed in terms of the number of standard deviations of the PDF for g. The number of multiples of the standard deviation of g is denoted by β which is an alternative representation of safety and is known as the “safety” index or more commonly as the “reliability” index.

The term reliability index has an important psychological advantage because its use avoids the negative connotation of the word “failure.” Assuming that the load and the resistance are normally distributed and statistically independent (i.e., uncorrelated), the relationship between reliability index, β, and the probability of failure, P_f, is as shown in Figure 3.

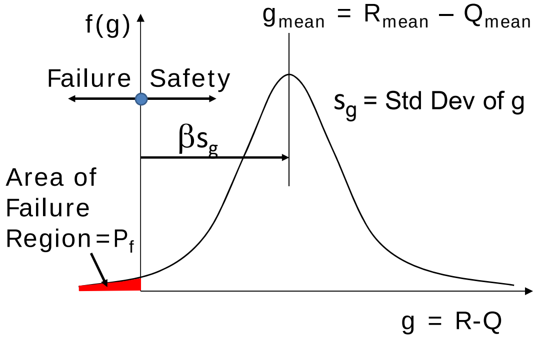

Figure 2. Expression of limit state and reliability index, β.

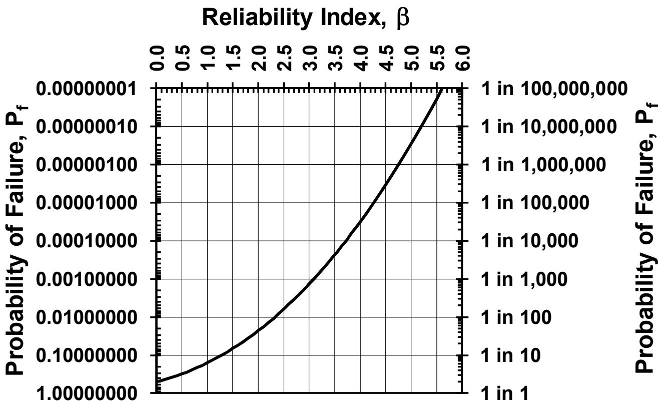

Figure 3. Relationship between reliability index, β, and probability of failure, P_f.

Figure 1 shows the mean value of measured load, Q_{mean}, and the mean value of measured resistance, R_{mean}. However, the design process is not based on mean measured values for loads and resistances, but rather on predictive models that provide nominal values of loads, Q_n, and nominal values of resistances, R_n. The variance of these nominal values from Q_{mean} and R_{mean} must be quantified so that the nominal values can be correlated to the measured mean values. This is achieved through the use of a bias factor, λ, which is expressed as the ratio of a mean value to a nominal value. Once the bias of the load and resistance is quantified, then the overlap zone can be controlled by use of a load factor, γ, and a resistance factor, ϕ, as shown in Figure 4. Basically, this control is accomplished by using a load factor greater than 1.0 and a resistance factor less than 1.0. The load factor accounts for variability of loads, lack of accuracy of load prediction models and the probability that different loads will occur simultaneously. The resistance factor accounts for variability of material properties, structural dimensions, and workmanship and uncertainty in the prediction of resistance (AASHTO, 2007).

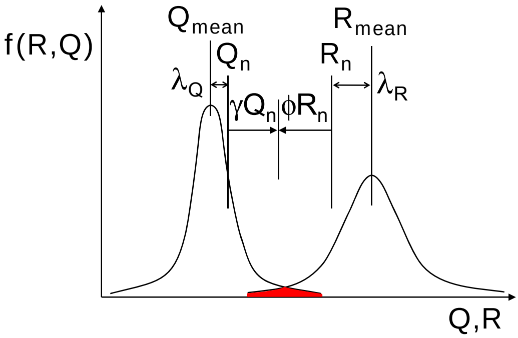

Legend

Q	Load	Q_{mean}	Mean measured load	γ	Load factor
R	Resistance	R_{mean}	Mean measured resistance	φ	Resistance factor
Q_n	Nominal load	λ_Q	Bias factor for force effect	f	frequency
R_n	Nominal resistance	λ_R	Bias factor for resistance		

Figure 4. Basic LRFD framework for force effects and resistances.

Since the overlap of the PDFs for load and resistance is correlated to reliability index, the load factor, γ, and resistance factor, φ, which control the extent of the overlap of the PDFs, can be calibrated to a given value of reliability index β. Details of various calibration processes are provided in Allen et al. (2005).

Once the load and resistance factors are incorporated into the LRFD framework as shown in Figure 4, the basic mathematical expression for a single load can be expressed as:

$$\gamma Q_n \leq \phi R_n \qquad \text{Eq. (1)}$$

Equation 1 represents a limit state in the sense that the factored load must be equal to or less than the factored resistance. When consideration is given to the force effect created by a combination of loads, then Equation 1 can be generalized as:

$$\Sigma \eta_i \gamma_i Q_i \leq \phi R_n = R_r \qquad \text{Eq. (2)}$$

where:

γ_i = load factor: a statistically-based multiplier applied to force effects
ϕ = resistance factor: a statistically-based multiplier applied to nominal resistance
η_i = load modifier: a factor relating to ductility, redundancy, and operational classification (see AASHTO, 2007 for more information)
Q_i = force effect
R_n = nominal resistance
R_r = factored resistance = ϕR_n

The term Q_i in Equation 2 represents the effects of combined loads on the component or structure being designed. Thus, for earth retaining structures, a suitable combination of vertical and horizontal loads can create force effects such as bearing pressure or sliding. In LRFD, the force effect, Q, and the resistance, R, can be any consistent set of variables. Examples of consistent variations include lateral pressure (Q) and lateral resistance (R); predicted settlement (Q) and tolerable settlement (R); and applied bending moment (Q) and flexural resistance (R). Each set of consistent variables thus defines a viable limit state that must be evaluated during the design process. This represents a significant advantage of LRFD over ASD since, for ASD, the formulation was primarily in terms of stress.

AASHTO LIMIT STATES

AASHTO (2007) defines a limit state as "A condition beyond which the bridge or component ceases to satisfy the provisions for which it was designed." In the AASHTO-LRFD framework, there are four distinct limit states: (1) strength (or ultimate) limit states; (2) service limit states; (3) extreme event limit states; and (4) fatigue limit states. The design of a wall or of a wall component is usually governed by either the strength or the service limit state and then checked for extreme event limit states. Fatigue limit states are generally not applicable for walls and will not be discussed here. The strength, service, and extreme event limit states are briefly described below:

- Strength (or ultimate) limit states pertain to structural safety and the loss of load-carrying capability. Strength limit states may be reached through either geotechnical or structural failure. Evaluation of strength limit states is based on inelastic behavior of the structure, which is accomplished by using increased or factored loads, and on modification of soil behavior, which is accomplished by using reduced or factored strengths. From a geotechnical viewpoint, strength limit states are reached when they involve the partial or total collapse of the structure due to sliding, bearing failure, etc. For well-designed structures, strength limit states have a very small probability of failure.
- Service limit states are the limiting conditions affecting the function of the structure under expected service conditions. Thus, service limit states address serviceability and include conditions short of the loss of load-carrying capability that may restrict the intended use of the structure, e.g., excessive total or differential settlements, cracking, local damage, poor ride quality, etc. Evaluation of service limit states is usually performed by using expected service loads, nominal strengths and elastic analyses. Compared to strength limit states, the service limit states have a greater probability of failure, but, if exceeded, involve less significant consequences.
- An extreme event is considered to be an event whose return period exceeds the design life of the structure. Examples include earthquakes, scour at super flood events, ice loads, and vehicle or vessel collisions. Once a wall has been designed based on strength and service limit states, it is then examined for its adequacy to withstand extreme events with the expectation to preserve life and not necessarily the serviceability of the structure. Based on these considerations, an earth retaining structure whose design has considered all appropriate failure modes based on strength limit states will likely be adequate when checked against an extreme event limit state.

Design of an earth retaining structure must provide adequate resistance against geotechnical and structural limit states. In general, the limit states for earth retaining structures include the following:

I. Strength and Extreme Event limit states
   1. External stability; e.g., sliding, limiting eccentricity, and bearing resistance.
   2. Internal stability; e.g., pullout resistance of mechanical inclusions in reinforced soil retaining structures such as mechanically stabilized earth (MSE) walls, soil nail walls and ground anchored walls.
   3. Depth of embedment for walls with deep foundations, e.g., cantilever or anchored walls
   4. Structural strength, e.g., tensile, compression, shear, bending or some combination of these limit states

II. Service limit states
   1. Excessive vertical movement (settlement)
   2. Excessive lateral movement (including rotation)
   3. Excessive vibration
   4. Overall (global) stability
   5. Deterioration of components due to cracking or corrosive environment

PRESSURE SURFACES AND WALL BACK-FACE

In all limit state analyses, the design engineer must be careful in defining the surfaces on which various pressures are applied. Figure 5 shows the case of reinforced concrete semi-gravity walls and reinforced soil walls. These walls can be in fill or cut. For the case of semi-gravity walls shown in Figure 5a, the geotechnical analysis for external stability is performed by considering the vertical plane CD through the back of the heel of the footing slab to be the back-face of the wall while the structural analysis for the stem wall is performed by considering lateral pressures on the actual plane AB. Similarly, for the case of reinforced soil walls shown in Figure 5b, external stability is evaluated by considering lateral pressures on the vertical plane XY while the structural stability of the wall face is evaluated by considering lateral pressures on wall front face plane VW. The configuration and application of vertical pressures on horizontal planes BE and WZ in Figures 5a and 5b, respectively, is a function of whether the vertical pressures create a stabilizing or destabilizing effect on the wall structure (as discussed subsequently).

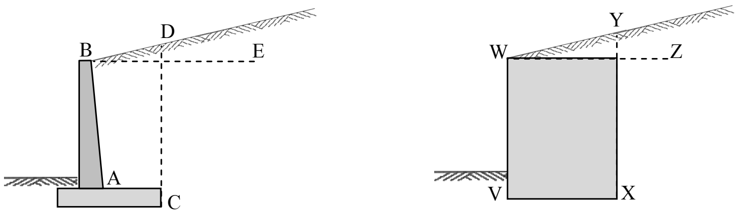

(a) Reinforced concrete semi-gravity walls (b) Reinforced soil walls

Figure 5. Typical pressure surfaces for analysis of walls.

OVERVIEW OF LOADS, LOAD FACTORS AND LOAD COMBINATIONS

A complete list of loads, load factors and load combinations considered in design of bridge structures and associated transportation structures, such as retaining walls is presented in Section 3 of the *LRFD-Specifications*. Many load types that are applicable to bridge structures are not applicable to earth retaining structures. Table 1 provides common loads and load designations for earth retaining structures. Tables 2 and 3 provide load combinations and load factors that are used for analysis and design of most earth retaining structures.

Table 1. Common Loads and Load Designations for Earth Retaining Structures

Permanent Load		**Transient Loads**	
Type	Designation	Type	Designation
Horizontal due to earth	EH	Vehicular collision	CT
Earth surcharge	ES	Earthquake load	EQ
Vertical due to earth	EV	Vehicular live load	LL
Components/attachments	DC	Live load surcharge	LS
Wearing surfaces/utilities	DW	Water/stream pressure	WA

Table 2. Load Combinations and Load Factors for Typical Earth Retaining Structures (after Table 3.4.1-1, AASHTO, 2007)

Load combination	**EH, ES, EV, DC**	**LL, LS**	**Use one of these at a time**	
			EQ	**CT**
Strength I	γ_p	1.75	-	-
Extreme Event I	γ_p	γ_{EQ}	1.00	-
Extreme Event II	γ_p	0.50	-	1.00
Service I	1.00	1.00	-	-

Notes: (1) For γ_p see Table 3; (2) The LRFD commentary suggests a load factor γ_{EQ} for live load = 0.5 during seismic events because the simultaneous occurrence of peak transient and seismic events is relatively unlikely; (3) The load factor for water/stream pressure (WA) = 1.00 for all limit states.

Table 3. Load Factors for Permanent Loads, γ_p for Typical Earth Retaining Structures (after Table 3.4.1-2, AASHTO, 2007)

Type of Load	**Load Factor**	
	Maximum	**Minimum**
DC: Components and Attachments	1.25	0.90
DW: Wearing surfaces and Utilities	1.50	0.65
EH: Horizontal Earth Pressure		
• Active	1.50	0.90
• At-rest	1.35	0.90
• Apparent earth pressure (AEP) for anchored walls	1.35	N/A
EV: Vertical Earth Pressure		
• Overall stability	1.00	N/A
• Retaining walls and abutments	1.35	1.00
ES: Earth Surcharge	1.50	0.75

Maximum and Minimum Load Factors. Two load factors, a maximum and a minimum, are listed in Table 3. Article 3.4.1 of the *LRFD-Specifications* states that: "*The factors shall be selected to produce the total extreme factored force effect. For each load combination, both positive and negative extremes shall be investigated. In load combinations where one force effect decreases another effect, the minimum value shall be applied to the load reducing the force effect. For permanent force effects, the load factor that produces the more critical combination shall be selected……Where the permanent load increases the stability or load-carrying capacity of a component or bridge, the minimum value of the load factor for that permanent load shall also be investigated.*"

In general, AASHTO's guidance can be applied by using minimum load factors if permanent loads increase stability and using maximum load factors if permanent loads reduce stability. For simple walls, e.g., level backfill without surcharges due to traffic or sloping backfill, the load factor (minimum or maximum) to use for a particular geotechnical limit state check may be readily identifiable by inspection as illustrated in Figure 6. Where a load is inclined such as the earth pressure load shown in Figure 6, the vertical and horizontal components of the inclined load are assigned the same load factor (minimum or maximum) that is applied to the inclined load.

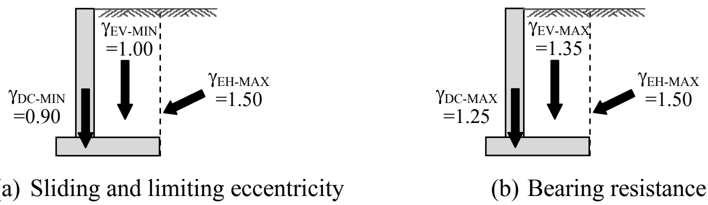

Figure 6. Typical application of load factors for evaluation of strength limit states of fill walls.

SURCHARGE LOADS

An earth retaining structure can be subject to additional vertical and lateral pressures due to loads from surcharges, which can be categorized broadly as transient and permanent. A common example of a transient surcharge load is traffic live load, while permanent surcharges may be in the form of sloping backfill (see Figure 5) or structural elements such as footings. Each of these loads has different levels of uncertainty. Transient and permanent surcharge loads are discussed below.

Transient Surcharge Loads. If a traffic load is within a distance equal to one-half of the height of the plane CD or XY shown in Figure 5, then it is included in the external stability analysis of the wall and is assigned a notation "LS", which means live load surcharge. The load type LS has only one load factor as shown in Table 2. In contrast to the maximum and minimum load factors for permanent loads such as EV and EH, the transient live load is considered to be either present or not. When its presence creates a more severe force effect, then it is included in the calculations and when its presence reduces the force effect then it is neglected.

The load type LS represents the effects of vehicular live load by equivalent uniform pressures expressed in terms of equivalent height of soil surcharge, h_{eq}. Using the example of an MSE wall, Figure 7 shows the manner in which load type LS is considered to maximize various force effects such as sliding, limiting eccentricity and bearing resistance. Similar considerations apply to other walls.

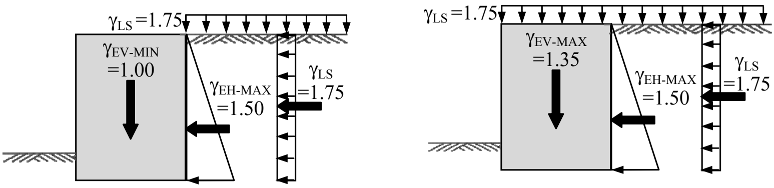

(a) Sliding and limiting eccentricity (b) Bearing resistance

Figure 7. Typical application of load factors for evaluation of strength limit states of MSE walls.

Tables 4 and 5 present the values of the equivalent height of soil surcharge, h_{eq}, depending on the direction of traffic with respect to the wall alignment, i.e., parallel or perpendicular to the wall. Table 4 is generally applicable to approach walls which are parallel to traffic while Table 5 is generally applicable to abutment walls which are perpendicular to traffic. The values in Table 5 apply to the case of walls without approach slabs. If approach slabs are used, then it is not necessary to account for the entire traffic surcharge within the length of the approach slab. However, depending on the configuration of wing walls, the traffic surcharge might be applicable for wing walls in which case the guidance in Table 4 should be used.

Table 4. Equivalent Height of Soil Surcharge, h_{eq}, for Vehicular Loading on Retaining Walls Parallel to Traffic (after Table 3.11.6.4-1, AASHTO, 2007)

Retaining Wall Height (ft)	h_{eq} (ft)	
	Distance from wall backface to edge of traffic = 0.0 ft	Distance from wall backface to edge of traffic ≥ 1.0 ft
5.0	5.0	2.0
10.0	3.5	2.0
≥ 20.0	2.0	2.0

Table 5. Equivalent Height of Soil Surcharge, h_{eq}, for Vehicular Loading on Abutments Perpendicular to Traffic (Table 3.11.6.4-1, AASHTO, 2007)

Abutment Height (ft)	h_{eq} (ft)
5.0	4.0
10.0	3.0
≥ 20.0	2.0

Permanent Surcharge Loads. Examples of permanent surcharges are soil loads due to sloping backfill or bearing pressure under a footing on top of a wall. If the vertical surcharge is area-wide and due only to soil, then it is assigned an EV load factor, while if the surcharge is concentrated, i.e., applied over a limited area and due to structural elements, then it is considered to be an ES-type load. The force effect due to a structural element may reflect the effect of many other load types. For example, the bearing pressure under a footing is affected by the dead load (DL) and live load (LL) that it may support. In this case it is not readily apparent which combination of loads will create the extreme force effect in the wall that supports such loads. Thus, the application of minimum and maximum load factors for ES-type loads requires a 2-step approach as noted in Article 3.11.6 of *LRFD-Specifications* which provides the following guidance: "*The factored soil stress increase behind or within the wall caused by concentrated surcharge loads or stresses shall be the greater of (1) the unfactored surcharge loads or stresses multiplied by the specified load factor, ES, or (2) the factored loads for the structure as applied to the structural element causing the surcharge load, setting ES to 1.0. The load applied to the wall due to the structural element above the wall shall not be double factored.*"

Basically, the *LRFD-Specifications* indicate that the ES load factors should be applied to the unfactored concentrated surcharge loads, unless the combined effect of the factored loads applicable to the foundation unit transmitting load to the top of the wall is more conservative. In the latter case, the ES load factor should be set equal to 1.0 and the factored footing loads used as the concentrated surcharge load in the wall design.

Complex Combinations of Surcharges. Permanent and transient surcharges can often occur in combination. Figure 8 shows the case of a bridge abutment with a spread footing on top of an MSE wall. This configuration is sometimes referred to as a "true" bridge abutment. In Figure 8, the load designations DL, LL and FR represent dead load, live load and frictional forces, respectively, from the bridge superstructure bearing on the spread footing. Consider the evaluation of the bearing resistance limit state at the base of the MSE wall. For the simple configuration shown in Figure 7b, it is straightforward to identify a suitable combination of maximum and minimum permanent loads as well as transient live load surcharge to evaluate the bearing resistance limit state. However, for the complex surcharge loading condition shown in Figure 8, it is not readily apparent what combination of maximum and minimum loads along with the transient live load (LL) and the live load surcharge (LS) will create the maximum bearing pressure at the base of the MSE wall. This is further compounded by the fact that the bearing pressure is also a function of the relative position and magnitude of the various loads.

The solution process for the case of a complex surcharge system is not straightforward and requires a detailed evaluation of various load combinations. The following guidance is provided for the bearing resistance strength limit state:

1: Compute maximum factored loads using maximum values of load factors.
2: Compute minimum factored loads using minimum values of load factors.
3: Appropriately combine the maximum and minimum values of factored loads to create an extreme force effect at significant component level. With respect

to Figure 8, one of the significant components is the spread footing. For the case of evaluation of bearing resistance below the base of the MSE wall, the bearing pressure distribution below the base of the spread footing must be evaluated; this bearing pressure distribution is then treated as an "ES" load type for further stability analyses. Using this logic, reduce the other loads to appropriate load types at the top of the MSE wall. For example, the weight of the soil above the top horizontal plane of the MSE wall and behind the vertical plane through the heel of the spread footing will be represented by a soil surcharge which will be assigned an "EV" load type. Since this soil surcharge is uniformly distributed, it will result in a rectangular lateral earth pressure distribution on the MSE wall block. This distribution will be assigned an "EH" load type.

4: Once the complex system of loading above the MSE wall has been reduced to appropriate load types in Step 3, the bearing pressure distribution at the base of the MSE wall can then be evaluated by using an appropriate combination of maximum and minimum load factors for such loads.

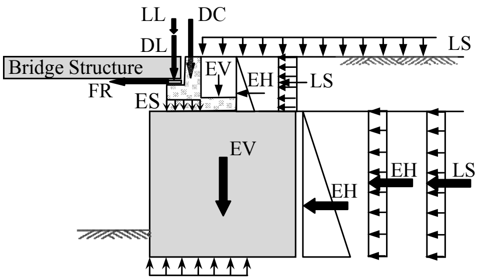

Figure 8. An example of complex surcharge system – bridge abutment with spread footing on top of MSE wall

The above approach allows construction sequencing to be addressed in the evaluation of extreme force effects. For the scenario depicted in Figure 8, the governing extreme force effect may occur when the bridge superstructure is placed while the backfill behind the spread footing is not completed. Use of a systematic step-by-step approach as noted above will permit development of correct solutions for other complex loading conditions, e.g., deep foundations through MSE wall backfill, seismic loads, vehicle/vessel collisions, etc.

CONUNDRUM FOR GEOTECHNICAL SPECIALISTS

Most of the loads, load factors and load combinations provided in the *LRFD-Specifications* were established based on bridge superstructure designs. When the concept of LRFD is extended to geotechnical features, the same load factors need to be applied for the sake of maintaining consistency in the treatment of loads between geotechnical and structural specialists. Take the example of the vertical earth load (load type EV) which is assigned a maximum load factor of 1.35 and a minimum load factor of 1.00 as shown in Table 3. In general, the typical range of geomaterial (i.e., soil or rock) unit weight variation is 3 to 7%. In this context, the maximum load factor of 1.35 could be construed to imply that the unit weight could be 35% larger than some mean value of unit weight commonly used in a site-specific analysis. Analyses of earth retaining structures in an LRFD framework are also complicated by the fact that unit weight is the primary component of geotechnical loads as well as resistances, e.g., pullout forces and resistances when evaluating internal stability of mechanically stabilized earth (MSE) walls or active and passive resistances for cut walls. This dominating effect of unit weight is further compounded by the use of maximum and minimum load factors. All of these considerations have created a conundrum for geotechnical specialists leading to confusion and the consequent development of hybrid approaches to work within the overall confines of the LRFD framework. These hybrid approaches include:

- development of resistance factors that are calibrated by "fitting" to past practice to achieve designs similar to those using the ASD approach;
- change in basic definitions for stability analyses, e.g., the conventional "middle-third" rule for the location of the resultant force to prevent overturning is no longer valid; and
- changes in basic definitions of load factors for stability analyses, e.g., use of load factor ES for external and internal stability analyses of MSE walls.

The remainder of this paper presents considerations for stability analyses of earth retaining structures in an LRFD framework in an attempt to resolve the seemingly counter-intuitive application of load and resistance factors.

CONSIDERATIONS FOR LIMIT STATE ANALYSIS OF EARTH RETAINING STRUCTURES IN AN LRFD FRAMEWORK

The behavior of an earth retaining structure is greatly influenced by construction techniques and the elements that comprise a given system. For example, the behavior of a reinforced concrete semi-gravity wall is different from a modular gravity wall such as a gabion wall. Similarly, the behavior of a reinforced soil fill wall, e.g., MSE wall, is significantly different from a reinforced soil cut wall, e.g., soil nail wall or anchored wall. As a frame of reference, a bridge superstructure might be comprised of AASHTO girders, post-tensioned box girders, an arch structure or something similar. AASHTO has expended significant effort to calibrate the behavior of various elements of bridges based on significant databases that exist for bridges. However, because of the seemingly endless possibilities in configurations and earth retaining structure types, it is virtually impossible to develop guidance within an LRFD framework that is appropriate for all earth retaining structures. However, despite this difficulty, significant considerations related to stability analyses in an LRFD framework are discussed in this paper. For each consideration discussed here, the letter "C" is used in square brackets for cut walls and the letter "F" is used for fill walls to identify the family of walls to which the consideration is applicable.

Calibration of resistance factors [C and F]. As noted earlier, the structural loads and load factors were established first by AASHTO. Then the resistance factors were computed to achieve a target reliability index, β_T. Where sufficient and high quality usable statistical data were available, the theory of reliability was used to develop the resistance factors. Where such statistical data were not available, the calibration was performed by "fitting" to achieve designs similar to those using the ASD approach, i.e. derive the resistance factors such that the designs using the LRFD approach are similar to those obtained by use of the ASD approach. Figure 9 presents the basic equations for calibration of resistance factors by "fitting" with ASD, where the left column starts with the ASD relationship between load and resistance and the right column with the LRFD formulation.

$$\Sigma Q_i \le \frac{R_n}{FS} \qquad \Sigma \gamma_i Q_i \le \phi R_n$$

$$FS\Sigma Q_i \le R_n \qquad \frac{\Sigma \gamma_i Q_i}{\phi} \le R_n$$

$$\phi = \frac{\Sigma \gamma_i Q_i}{FS\Sigma Q_i}$$

Legend

Q_i	Load
R_n	Nominal resistance
FS	Factor of safety
γ_i	Load factor
ϕ	Resistance factor

Figure 9. Basic equation for calibration of resistance factor by fitting with ASD.

The goal for future versions of the *LRFD-Specifications* is to develop all resistance factors based on reliability theory even though most currently used resistance factors were developed based on the "fitting" calibration approach shown in Figure 9. Regardless of the calibration approach, the following should be recognized:

- For permanent loads, Service I limit state uses a load factor and a resistance factor = 1.0. The practical implication is that designs based on deformation analyses should be identical for an ASD approach and an LRFD approach. It is important to recognize that this equivalence is correct only when the exact same resistance model and load definition equation is applied.
- Only the Strength I limit state has been calibrated thus far by AASHTO. Efforts to calibrate other limit states, including service limit states, are currently underway. Therefore, as further calibrations are conducted, one can expect modification of the current load and resistance factors for specific walls and/or their components.

Limiting Eccentricity [All F and some C walls, e.g., soil nail walls]. In the ASD approach (AASHTO, 2002) Group I loads (with load coefficients = 1.0) are generally used to evaluate overturning effects. Because of the specific separation of the uncertainty in loads and resistances in the LRFD approach, load factors generally greater than 1.0 are used to define various load combinations in the Strength limit state. Furthermore, in the LRFD approach, the overturning criterion has been replaced by limiting eccentricity (e) of the resultant load at the Strength limit state. The requirement in the LRFD approach is that the eccentricity does not exceed the following limits when Strength limit states are evaluated:

- One-fourth of the corresponding footing dimension, B (width) or L (length), for footings on soils; or
- Three-eighths of the corresponding footing dimensions, B (width) or L (length), for footings on rock.

The above criteria were developed by AASHTO based on a parametric study for cantilevered retaining walls having various heights. The base widths obtained using the LRFD load factors and an eccentricity of B/4 for soils are comparable to those of the ASD approach with an eccentricity of B/6. The design engineer must remember that the new eccentricity criteria apply only to the limiting eccentricity condition, which is evaluated at applicable Strength limit states. If the LRFD limiting eccentricity criteria are applied at the Service limit state, then the resulting footing sizes will be different than those found to be acceptable as per the ASD approach. The design engineer must further remember to apply the above criteria to eccentricity in the B direction (e_B) as well as eccentricity in the L direction (e_L).

For geotechnical analysis of wall footings, the concept of an effective area A' = (B')(L') is used, where $B' = B-2e_B$ and $L' = L-2e_L$. The definitions of effective foundation dimensions B' and L' remain unchanged in LRFD (as compared to ASD) since their purpose is to convert the non-uniform (trapezoidal or triangular) stress distribution due to eccentric load to an equivalent rectangular (uniform) stress distribution, also known as the "Meyerhof" stress distribution, over the effective foundation area. This exercise is performed to simplify the sizing of the foundation based on settlement (Service limit) and bearing resistance (Strength limit). Thus, while performing geotechnical analysis at an appropriate limit state, the design engineer should continue to apply the concept of effective foundation area using the eccentricity based on the limit state under consideration.

Once a wall footing is sized, the stress distribution (trapezoidal or triangular) under the foundation for structural design is based on the B/6 ("middle-third") criterion because the pattern of stress distribution has nothing to do with the LRFD approach or the ASD approach, but rather is related to fundamental theories of statics and equilibrium of forces, i.e., the free-body diagram.

The limiting eccentricity limit state is coupled with the bearing resistance limit state because the larger the tendency to overturn (as expressed by larger value of eccentricity of the resultant force), the larger the bearing pressure at the toe of the wall. Thus, by limiting the bearing pressure, the tendency to overturn is limited, and vice versa. However, since either state could govern, both limit states must be checked.

Global stability [F and C]. Article 11.6.2.3 of the *LRFD-Specifications* provides guidance for the evaluation of overall (or global) stability in the LRFD framework. The *LRFD-Specifications* indicate that the evaluation of the overall stability of earth slopes with or without a foundation unit should be investigated at the Service I Load Combination with an appropriate resistance factor. In lieu of better information, it is recommended by the *LRFD-Specifications* that the resistance factor, ϕ, at the Service I limit state be applied as follows:

- $\phi = 0.75$ for the case where the geotechnical parameters are well defined and the slope does not support or contain a structural element.
- $\phi = 0.65$ for the case where the geotechnical parameters are based on limited information or the slope contains or supports a structural element.

There are three considerations related to the above guidance:

- Since overall stability is evaluated at the Service I limit state (i.e. load and resistance factors of 1.0), it is possible to derive a straightforward relationship between FS in the ASD approach and ϕ in the LRFD approach. Substituting load factor (γ_i) = 1.0 in the relationship shown in Figure 9, $\phi = 1/FS$ is obtained. The practical aspect of this simple relationship is that all current limit-equilibrium based computer software can be used. Once a lowest reasonable FS is computed from routine slope stability analysis by using these computer programs, the resistance factor is obtained by simply taking the inverse of the FS, i.e. $\phi = 1/FS$.
- From the relationship, FS = $1/\phi$, it can be seen that the values of $\phi = 0.75$ and 0.65 mentioned above correspond to FS values of 1.33 and 1.54, respectively. The *LRFD-Specifications* do not intend to increase the traditional safety factors of 1.30 and 1.50 to 1.33 and 1.54, respectively. The equivalent FS values are simply a result of the AASHTO resistance factors being rounded to the nearest 0.05 because not doing so would imply an accuracy in the resistance factors that is not justifiable. Thus, in a practical sense, a resistance factor of 0.75 is intended to be the same as using FS=1.30 and rounding from 1.33 to 1.30 is appropriate. Similarly, rounding from 1.54 to 1.50 is appropriate.
- The phrase "*or the slope contains or supports a structural element*" is somewhat confusing in Article 11.6.2.3 of the *LRFD-Specifications*. Practically, this phrase means that the resistance factor should be 0.65 if the structure being supported by the slope cannot tolerate significant movement or if the consequences of the failure of the supported structure are severe, e.g. a bridge foundation, a critical pressurized utility, etc. For slopes that support relatively minor structures such as a sign foundation for which movements may not be detrimental or the consequences of the failure are not significant, a resistance factor of 0.75 may be more appropriate.

Pullout resistance for soil reinforcements in MSE walls [F]. The design of MSE walls includes an evaluation of external and internal stability. Internal stability involves two primary modes of failure of the soil reinforcements, pullout and tension breakage. In accordance with the AASHTO-LRFD framework, each of these failure modes is assigned a different resistance factor. The resistance factors for the tension breakage failure mode are related to the structural characteristics of the soil reinforcement. However, there is confusion regarding the treatment of live load surcharges from the viewpoint of external stability evaluations versus the pullout failure mode evaluations for internal stability.

It has been found that if a load factor of 1.75 is used for live load surcharge to check the internal stability of an MSE wall in the LRFD framework with respect to pullout, a larger amount of reinforcements would be needed as compared to ASD practice and when compared to instrumented MSE walls that have performed satisfactorily. This inconsistency occurs because the dissipation of live load surcharge through the reinforced soil mass is not considered correctly in current LRFD practice. Based on fitting with ASD, the amount of soil reinforcement is approximately the same as in ASD practice if a load factor of 1.35 for EV were to be used for modeling the live load surcharge for internal stability analysis. This simple modification clearly indicates the need to further refine and calibrate the LRFD approach for pullout resistance of soil reinforcements in MSE walls. Samtani (2009) provides further discussion regarding pullout resistance factors for MSE walls.

Pullout resistance for anchors [C]. The *LRFD-Specifications* include resistance factors for anchors installed in: (1) cohesionless (granular) soils with ϕ=0.65; (2) cohesive soils with ϕ=0.70; and (3) rock with ϕ=0.50. These resistance factors, however, were developed for minimum presumptive ultimate anchor pullout resistances. The *LRFD-Specifications* provide commentary that elaborates on these as prescriptive minimums, which may be used for preliminary design only. The *LRFD-Specifications* also provide a resistance factor of 1.0 where proof tests are conducted on every anchor to a load at least equal to the factored load. This provision recognizes typical U.S. anchor practice wherein the required length of the anchor bond zone for every production anchor is confirmed via proof or performance testing.

Evaluations of deformations for cut walls [C]. Earth retaining structures used in cut situations in urban settings are often designed based on consideration of strict lateral wall and ground movement requirements. The *LRFD-Specifications*, however, provide limited guidance for estimating lateral wall and ground movements. This is a limitation of designs performed under an ASD format as well. Also, cut walls are often designed by using soil-structure interaction or finite element analyses, which provide estimates of wall loads resulting from an assessment of staged construction. The simplistic loading diagrams provided in the *LRFD-Specifications* may therefore be inappropriate for applications involving, for example, flexible cantilevered or anchored walls in marginal ground for consideration of the Service limit state (where wall deformations are considered).

Temporary walls [F and C]. The current version of the *LRFD-Specifications* indicates that "some increase" in resistance factors for design of temporary walls may be appropriate consistent with increased allowable stresses for wall components in an ASD format. Historically, AASHTO has been used in consideration of permanent wall systems since temporary walls were typically procured under a Contractor design-build format. Since an LRFD platform for temporary walls does not exist, it is likely that some agencies will simply adopt the available permanent-wall LRFD platform for the design of temporary walls. At a minimum, it is recommended that load factors be developed that are consistent with typical time intervals for highway construction projects.

Wall element embedment depths for anchored walls [C]. The *LRFD-Specifications* require that vertical loads on anchored walls be supported by the embedded structural component of the wall, such as a soldier beam. This requirement may represent an inconsistency in that wall movement (and hence mobilization of side resistance in the excavated portion of the wall) would be required before vertical loads would be transferred to the embedded portion. Also, compared to ASD, LRFD designs result in larger embedment depths to resist vertical wall loads because resistance factors for deep foundations designed based only on static analyses are used. These resistance factors correspond to values less than traditional equivalent factors of safety used for wall embedment. Embedment designs in LRFD should be calibrated to provide similar embedment depths as for ASD.

Anchor load testing [C]. The magnitudes of the incremental test loads as provided in the *LRFD-Specifications* were developed for ASD. Therefore, the *LRFD-Specifications* indicate that the incremental test loads should be divided by the load factor for apparent earth pressure, i.e., 1.35 for anchors tested to factored loads. Simply stated, the intent is to test anchors to load levels nearly exactly the same as would have been done for the same anchor in an ASD format. This is important because the primary anchor acceptance criterion is related to a prescribed deformation at the maximum testing load. To test anchors to greater loads using the same prescribed deformation for acceptance would likely result in more anchor failures. However, where large surcharges are present (e.g., heavy cranes operating above a wall), test loads will be larger than those for ASD because load factors for such loads are greater than 1.35.

There may also be some confusion when evaluating the required size of the tendon in an LRFD format. For example, in ASD, tendons were selected such that: (1) the design load for the anchor did not exceed 60 percent of the guaranteed ultimate tensile strength (GUTS) of the tendon; and (2) the maximum test load, typically 1.33 times the design load, did not exceed 80 percent of GUTS. Based on discussions with contractors, the authors understand that some project specifications, which were written in an LRFD format, include the requirement that the maximum test load not exceed 60 percent of GUTS. This requirement is a misinterpretation of the *LRFD-Specifications*, especially when it is noted that the resistance factor for the tensile resistance of an anchor is 0.8. In LRFD, the intent is that the maximum test load, which is equal to the maximum factored load, should not exceed 0.8 GUTS.

SUMMARY

The AASHTO-LRFD framework has been developed to result in more efficient designs in terms of uniform levels of safety across various components in a given system. While such efficiency in designs is currently being realized for bridge superstructures, a similar level of efficiency is not clearly apparent at this time for earth retaining structures. A significant reason for this inefficiency is the wide variety of earth retaining structures and the lack of available high quality data required for proper reliability-based calibrations of load and resistance factors. However, the LRFD approach is superior to the ASD approach not only in terms of its rational basis for addressing uncertainty in designs, but also because it encourages and requires communication between structural and geotechnical specialists. Currently, there are many geotechnical specialists who are reluctant to embrace LRFD by citing issues such as lack of physical meaning of load and resistance factors for earth pressures or the confusion related to use maximum and minimum load factors. It should be realized that load and resistance factors are simply numbers to express uncertainty in loads and resistances in a rational manner based on the theory of reliability. As more high quality data are collected and calibrated, the benefits of the LRFD approach will become evident in the future.

The first edition of the Standard Specifications for Highway Bridges was issued in 1931 and the last (17^{th}) Edition was issued in 2002 (AASHTO 2002) – a span of 71 years. By comparison, the first edition of the *LRFD-Specifications* was introduced in 1994 and the industry is currently using the 4^{th} Edition released in 2007 with 2008 and 2009 Interims. As with the Standard Specifications, one can expect periodic revisions in the *LRFD-Specifications* as additional statistical data become available and current analysis methods are refined. The *LRFD-Specifications* are based on a framework of reliability theory that permits a rational platform to refine guidelines progressively so as to make civil engineering structures more efficient and consistent with uniform levels of safety. Thus, the industry should be anxious, not reluctant to transition from ASD to LRFD.

ACKNOWLEDGMENTS

The authors acknowledge the encouragement, support, and review effort provided by Dr. Edward A. Nowatzki, P.E., Principal Engineer, NCS Consultants, LLC and Professor Emeritus, University of Arizona, Tucson; Jerry DiMaggio, P.E., Retired Principal Bridge Engineer, FHWA, Washington D.C.; and Dr. Dennis R. Mertz, P.E., Professor, University of Delaware.

REFERENCES

AASHTO, (2002). ***Standard Specifications for Highway Bridges, 17th Edition.*** American Association of State Highway and Transportation Officials, Washington, DC.

AASHTO, (2007). ***LRFD Bridge Design Specifications, 4th Edition*** (with 2008 and 2009 Interims), American Association of State Highway and Transportation Officials, Washington, DC.

Allen, T. M., Nowak, A. & Bathurst, R, J. (2005). ***Calibration to Determine Load and Resistance Factors for Geotechnical and Structural Design.*** Transportation Research Circular E-C079, Transportation Research Board, Washington, D.C.

Samtani, N. C. (2009). "*Calibration of Resistance Factors for Pullout in MSE Walls Based on Fitting with ASD.*" Article # 01-0309-R0, www.ncsconsultants.com (Contact NSamtani@msn.com if a copy cannot be downloaded).

Metal Loss for Metallic Reinforcements and Implications for LRFD Design of MSE Walls

Kenneth L. Fishman, Ph.D., P.E., MASCE[1], James L. Withiam, Ph.D., P.E., D.GE, MASCE[2] and Robert A. Gladstone, P.E., MASCE[3]

ABSTRACT

Previous calibrations of resistance factors for load and resistance factored design (LRFD) of mechanically stabilized earth (MSE) retaining walls with galvanized metallic reinforcements have not considered cross-sectional area as a variable in the reliability analysis. The remaining cross section at the end of a 75- or 100-year design life is considered, however the metal loss from corrosion is estimated using recommended rates of metal loss that render conservative estimates of remaining cross section. This paper describes reliability-based calibration of resistance factors for the rupture limit state considering the variability of observed corrosion rates. Results are compared with resistance factors cited in the current American Association of State Highway and Transportation Officials (AASHTO) design specifications. The comparison identifies conditions for which the current AASHTO resistance factors achieve the targeted probability of failure inherent to the LRFD strategy.

INTRODUCTION

Most MSE walls owned by state departments of transportation are designed using some form of the AASHTO LRFD Specifications (AASHTO, 2009) as a guide. The approach to metal loss has been to calculate the expected loss of both zinc and steel, then add sufficient sacrificial steel to the reinforcement cross-section to satisfy resistance requirements for the intended design-life. Table 1 summarizes the AASHTO-recommended metal loss model for design of MSE structures and the corresponding fill material requirements.

Table 1. AASHTO Metal Loss Model and Fill Material Requirements

Metal Loss Model		Fill Requirements	
Component Type (age)	Loss (μm/yr)	pH	5 to 10
		Resistivity	≥ 3000 Ω-cm
Zinc (< 2 yrs), r_{z1}	15	Chlorides	< 100 ppm
Zinc (> 2 yrs), r_{z2}	4	Sulfates	< 200 ppm
Steel (after zinc), r_s	12	Organic Content	< 1%

Based on the metal loss rates (zinc and steel) in Table 1 the steel loss per side (X) in μm/yr for a given service life, t_f, and initial thickness of zinc coating, z_i, is computed as:

[1] Principal, McMahon & Mann Consulting Engineers, P.C., 2495 Main St., Suite 432, Buffalo, NY 14214, (716) 834-8932 (v), kfishman@mmce.net
[2] Principal, D'Appolonia Engineering Division of Ground Technology, Inc., 275 Center Road, Monroeville, PA, (412) 846-9440, jlwithiam@dappolonia.com
[3] Executive Director, Association for Metallically Stabilized Earth, McLean, VA, bobgladstone@amsewalls.org

$$X(\mu m) = 12\frac{\mu m}{yr} \times \left(t_f - 2yr - \frac{(z_i - 30\mu m)}{4\frac{\mu m}{yr}} \right) yr \tag{1}$$

LRFD is a reliability based design method whereby loads and resistances are factored as:

$$\sum \gamma_i Q_i \le \phi R \tag{2}$$

where, Q_i are loads from sources that may include earth loads, surcharge loads, impact loads or live loads, γ_i is the load factor for the i^{th} load source and is greater than 1, R is the resistance, and ϕ is the resistance factor and is usually less than 1.

Load and resistance factors are selected such that the probability of the load exceeding the resistance is relatively low. The AASHTO LRFD Specifications (2009) include resistance factors for the rupture limit state that were calibrated matching the safety factors that prevailed in the former allowable stress based design (ASD). The ASD employed safety factors of 1.8 (i.e., 1/0.55) or 2.1 (i.e. 1/0.48) relative to rupture of strip type reinforcements or grid type reinforcements respectively. The higher safety factor for grid reinforcing members connected to a rigid facing element (e.g., a concrete panel or block) accounts for the greater potential for local overstress due to nonuniform connection loads in grids (three or more longitudinal rods or wires) as compared to steel strips or bars (single element).

D'Appolonia (2007) described a reliability-based calibration to assess resistance factors for the rupture limit state, but did not considered metal loss from corrosion as a variable. This paper extends that study to consider variability of metal loss. Calibration of the resistance factors use load factors from the AASHTO LRFD Specifications (AASHTO, 2009) and the calibration methodology recommended by Allen et al. (2005). The resistance factor is calibrated with respect to a target reliability index (i.e. probability of failure) (β_T) that accounts for the redundancy of the system and load redistribution inherent to the rupture limit state. The bias of tensile strength and the corresponding statistics and distributions are used to calibrate resistance factors for LRFD. Monte Carlo simulations are performed considering each variable used to compute load and resistance.

PERFORMANCE DATABASE AND DATA ANALYSIS

The calibration relies on an extensive database of corrosion rate measurements from in service reinforcements. Performance data have been collected and archived from sites located in the Northeast, mid-Atlantic, Southeast, Southwest and Western United States, and includes data from 170 sites located throughout the United States and Europe. Corrosion rate measurements include direct physical observations of metal loss (e.g., weight loss measurements) and electrochemical measurements that render observations of corrosion rate at an instant in time (e.g., linear polarization resistance (LPR) measurements). The ages of reinforcements considered in the database range from less than two-years old to approximately 40-years old.

Data are grouped to consider the effects on observed corrosion rates of time (age since burial), fill character, climate and reinforcement type. Figure 1 depicts observations of corrosion and metal loss with respect to age of the reinforcements for fill conditions meeting the AASHTO criteria (Table 1). Observations included in Figure 1 are via electrochemical techniques (e.g., LPR) wherein corrosion rate is measured at an instant in time. For the purpose of MSE reinforcement design, the remaining metal loss at the end of the service life must be considered to estimate the metal resistance at that time. Since metal loss measurements at the end of service are not available (i.e., none of the monitored MSE walls depicted in Figure 1 have reached the end of their service life), there is a need to extrapolate existing observations of performance to the end of service condition. Measured corrosion rates are adjusted for the effects of time and metal loss considered as the product of corrosion rate over the applicable time interval.

Approximately 404 data points are included in Figure 1; 114 points from galvanized coupons and 290 points from galvanized reinforcements. The effect of time on corrosion rates is apparent in the data. In general, higher corrosion rates are observed during the first two years of service. On average, lower corrosion rates are realized from samples with ages between two and 16 years compared to those that are younger than two years, or older than 16. This is due to the attenuation of corrosion rate with respect to time as reported by Romanoff (1957), and the possibility that higher corrosion rates prevail after zinc is consumed from galvanized samples. The AASHTO line is a good upper limit for metal loss throughout the experience period and most of the data points lie well below the envelope described by the AASHTO model. Many of these data represent metal loss that is less than half of what is computed with the AASHTO model. This is consistent with the analysis of metal loss and corrosion rate measurements reported by Gladstone et al. (2006).

Observed corrosion rates are most affected by the quality of the reinforced fill. On average, observations from sites with fill resistivities less than 3,000 Ω-cm are approximately an order of magnitude higher than observations from sites with fill resistivity greater than 3000 Ω-cm. Observations from sites with fill resistivities between 3,000 and 10,000 Ω-cm have average corrosion rates slightly higher than those associated with resistivity greater than 10,000 Ω-cm.

There does not appear to be a significant effect of climate on measured corrosion rates. Therefore measurements from different regions are combined to evaluate the effects of fill character, time, and reinforcement type on corrosion rates and observations of metal loss.

RELIABILITY ANALYSIS

The reliability-based calibration of resistance factors for LRFD follows the procedure described by Allen et al. (2005). Figure 2 illustrates how the steel incorporated into the design of a reinforcement cross section can be construed to include three components including (1) nominal structural steel needed to resist the applied load without yielding, (2) steel consumed by corrosion, and (3) residual steel that was intended to serve as sacrificial steel, but not actually consumed by corrosion. Residual steel contributes to the reinforcement resistance, and consequently the bias inherent in the design. Differences between the metal loss model used in design and the prevailing corrosion rates determine the amount of residual steel at the end of the service life. Prevailing corrosion rates depend on the electrochemical properties of the fill, making fill quality an important factor to include in the calibration.

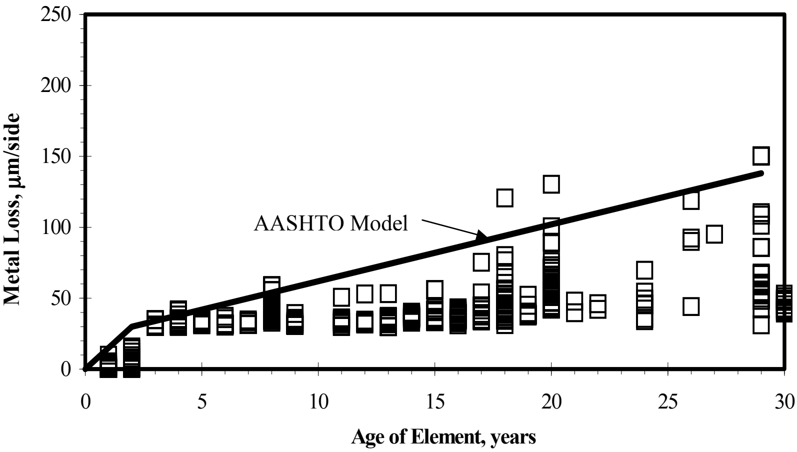

Figure 1. Metal Loss vs. Time for Galvanized Elements and Reinforced Fill Satisfying AASHTO Criteria Described in Table 1.

Reinforcement size is also important because the significance of residual steel becomes less as the cross sectional area of the reinforcement increases. In consideration of these factors the reliability-based calibration is performed in terms of the following design parameters:

- Service lives of 75 and 100 years.
- Different reinforcement thickness for strips of 3 mm, 4 mm, 5 mm and 6 mm, or wire diameters for grids W7, W9, W11, W14.
- Different reinforced fill conditions (all meet AASHTO criterion).

Resistance Bias

Corrosion rate measurements are extrapolated to compute remaining cross section at the end of a given design life considering the statistics and distribution of the corrosion rate measurements. The variation of remaining cross section and yield stress are then used to assess the statistics and distribution of remaining tensile strength. These results are compared to the nominal remaining tensile strength computed using Eq. (1).

The rupture resistance of the reinforcements is computed as:

$$R = \frac{R_c F_y A_c}{b} \tag{3}$$

where, R is resistance per unit width of wall, R_c is the coverage ratio, b is the width of the reinforcements, F_y is the yield strength of the steel, and A_c is the cross sectional area of the reinforcement at the end of the service life.

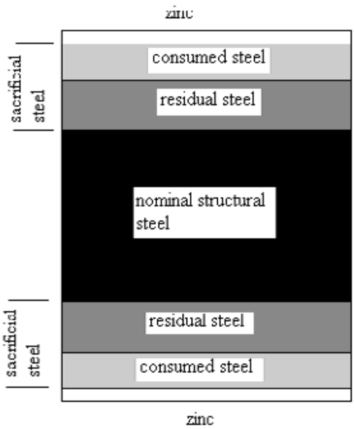

Figure 2. Idealized Reinforcement Cross Section

For strip type reinforcements:

$$A_c = bE_c \tag{4}$$

and for grid type reinforcements:

$$A_c = n \times \pi \times \frac{D^{*2}}{4} \tag{5}$$

where, E_c is the strip thickness corrected for corrosion loss; $E_c = b \times (S - \Delta S)$ for $\Delta S < S$ and 0 for $\Delta S \geq S$, S is the initial thickness, ΔS is the corrosion loss, n is the number of longitudinal rods/wires, D* is the diameter of the rod or wire corrected for corrosion loss and is equal to D_i-ΔS for $\Delta S < D_i$ and 0 for $\Delta S \geq D_i$, where D_i is the initial diameter.

For galvanized reinforcements:

$$\Delta S = 2 \times r_s \times (t_f - t_i) \qquad \text{For } t_i < t_f$$

$$\Delta S = 0 \qquad \text{For } t_i \geq t_f \tag{6a}$$

$$t_i = 2yrs + \frac{(z_i - 2 \times r_{z1})}{r_{z2}} \tag{6b}$$

where, r_s is the corrosion rate of steel after zinc has been consumed, t_f is the intended service life, t_i is the time to initiation of steel loss, z_i is the zinc initial thickness per side, r_{z1} is the initial corrosion rate for zinc, and r_{z2} is the corrosion rate for zinc after the first two years.

Variables for the resistance calculation include F_y, A_c, r_s, r_{z1}, r_{z2}, and z_i. The width of the reinforcements and the coverage ratio are taken as constants. Using the statistics and observed distribution for measurements of corrosion rate, the bias of the remaining strength is computed and used as input for the reliability-based calibration of resistance factor. The bias is computed as:

$$\lambda_R = \frac{F_y^* A_c^*}{F_y A_c} \tag{7}$$

The denominator includes nominal values used in design; A_c is based on the metal loss model recommended by AASHTO for design of metallic MSE reinforcements, and F_y is the nominal yield strength. The statistics of the observed corrosion rates from the database are used to describe the variable A_c^* and the statistics for F_y^* are taken from Bounopane et al. (2003). Bounopane et al. consider yield strengths to be normally distributed with a mean 1.05 times the nominal and COV = 0.1.

Calibration of Resistance Factor for LRFD

Monte Carlo simulations are employed to compute the relationship between β and φ. The Monte Carlo simulation method is used because the approach is more adaptable and rigorous compared to other techniques, and it has become the preferred approach for calibrating load and resistance factors for the LRFD specifications (Allen et al, 2005; D'Appolonia, 2007). The simulations are performed in terms of a given load factor, γ, load bias, λ_Q, and resistance bias, λ_R. The Monte Carlo technique utilizes a random number generator to extrapolate the limit state function, g = R-Q, for calibration of rupture resistance. Random values of g are generated using the mean, standard deviation, and the distribution (normal, lognormal, or Weibull) of the load and the resistance. The extrapolation of g = 0 makes estimating β possible for a given combination of γ and φ. A value of γ = 1.35 is adopted compatible with the static earth load calculations (AASHTO, 2007). A range of φ values is assumed and estimated values of β (by iteration) are checked against a target reliability index, β_T, of 2.3 as used in previous LRFD calibrations for MSE wall reinforcements (Allen et al., 2005; D'Appolonia, 2007).

The load bias depends on use of the simplified or coherent gravity method to compute maximum reinforcement tension and may depend on reinforcement type (strip or grid) as described by Allen et al. (2001), Allen et al. (2005), and D'Appolonia (2007). Results from these studies demonstrate that the load bias has a lognormal distribution with mean, μ_{λ_Q}, and standard deviation, σ_{λ_Q}, as shown in Table 2.

Since the oldest MSE walls are approximately 40 years old, direct measurements of remaining strength after a service life of 75 or 100-years are not available. Therefore, corrosion rate measurements must be extrapolated to estimate "measurements" of remaining strength used in the numerator of Eq. (7). The extrapolation also employs equations similar to Eqs. (3)-(7), but with corrosion rates r_{z1}, r_{z2}, and r_s from the observed performance of reinforcements during service. The corrosion rates used to extrapolate metal loss are considered constants over prescribed time intervals, and higher than those expected to prevail at the end of service. This approximation is considered conservative due to the likely attenuation of corrosion rate with respect to time.

Table 2. Mean (μ_{λ_Q}) and Standard Deviation (σ_{λ_Q}) of Lognormal Load Bias

Parameter	Strip		Grid	
	Simplified Method	Coherent Gravity Method	Simplified Method[1]	Coherent Gravity Method[2]
μ_{λ_Q}	0.973	1.294	0.973	1.084
σ_{λ_Q}	0.449	0.499	0.449	0.737

Good quality fill meets the AASHTO requirements for electrochemical and mechanical properties, and has ρ_{min} in the range between 3000 Ω-cm and 10,000 Ω-cm. Measured corrosion rates for zinc do not vary significantly with respect to the age of reinforcements, and the statistics for reinforcements that are between 2- and 16-years old are representative. Therefore, the measurements of corrosion rate for zinc are assumed to be constant with respect to time with a mean rate of 1.7 μm/yr (r_{z1} and r_{z2}) and standard deviation 1.09 μm/yr.

Given such a low rate of zinc loss, and since measurements were made on reinforcements that are less than 30-years old, very few measurements are available to describe the corrosion of steel after zinc has been consumed from a galvanized reinforcement. Two different assumptions are applied as described by Elias (1990) that either (1) consider that the base steel will corrode at the same rate as plain black steel (i.e., not galvanized) corresponding to the age of the reinforcement after the zinc coating is consumed, or (2) assume that the base steel will corrode at a rate similar to that prevailing as zinc is finally consumed (i.e. corrosion rate does not change abruptly after zinc is consumed). In addition, "measured" corrosion rates for steel were multiplied by two to render the loss of tensile strength from LPR measurements similar to that described by Elias (1990).

A conservative model for steel consumption assumes that the base steel corrodes at the same rate as plain steel (i.e. not galvanized) after the sacrificial zinc layer is consumed. Most of the data used for corrosion rates of steel embedded in fill materials meeting current AASHTO guidelines are from steel coupons installed at MSE sites located in California, New York, and Florida. The statistics of this data set render a mean corrosion rate and standard deviation of 27 μm/yr and 18 μm/yr, respectively; and the distribution can be approximated as lognormal.

A resistance bias is computed for different sizes of strip-type reinforcements (4 mm, 5 mm and 6 mm) and both 75 and 100-year service lives. The bias tends to decrease with respect to increase in reinforcement size, and is higher considering longer service life. The mean resistance bias, $\lambda_{R,}$ ranges between 1.2 and 1.5 with a coefficient of variation approximately 40% and a distribution that is approximated as a Weibull distribution.

The zinc residual model for steel consumption considers that the corrosion rate of the base steel is affected by the presence of zinc residuals. Zinc residuals include a zinc oxide film layer adhered to the metal surface and zinc oxides within the pore spaces of the surrounding fill. The presence of the zinc oxides tends to promote passivation of the steel. There are very few measurements describing corrosion rates of base steel after zinc has been consumed. A few observation may be applicable from the data set collected in Europe (Darbin, et al.,

1988) considering that some of the reinforcements only include a minimum zinc thickness of 30 μm and were placed within fills with less desirable electrochemical properties compared to AASHTO requirements such that zinc is consumed relatively rapidly (i.e., within a few years). A review of these data renders corrosion rates for steel that are close to 12 μm/yr. Since this is close to the metal loss model recommended by AASHTO it is adopted as a basis for comparison from calibrations performed by extrapolating measured corrosion rates with the conservative steel model. Similar to other data sets, a coefficient of variation of 60% and a lognormal distribution is used to describe the variation. The calibration was performed for both strip and grid type reinforcements. The mean of the resistance bias is approximately 1.4 with COV approximately 20%, and a distribution that is approximately normal.

High quality (select) reinforced fills have ρ_{min} > 10,000 Ω-cm and corrosion rates corresponding to these conditions were observed from sites in Florida (Sagues, et al., 1998; Berke and Sagues, 2009) and North Carolina. These data render mean and standard deviation of corrosion rates for the zinc coating of 0.8 μm/yr and 0.5 μm/yr, respectively. Corrosion rates observed from plain steel coupons older than 16 years correspond to mean and standard deviation values of 11.5 μm/yr and 9.4 μm/yr, and these parameters are assumed to represent the loss of base steel subsequent to depletion of the zinc coating for this case. The mean of the corresponding resistance bias is computed as ranging from 1.4 to 2.0 with COV approximately 10%. The bias distribution is approximately normal considering a 75-year service life, but is better represented by a Weibull distribution considering a 100-year service life.

DISUSSION OF RESULTS

Figure 3 presents results from Monte Carlo simulations considering strip type reinforcements and considering the load bias corresponding to the simplified method and the computed resistance bias for each of the cases described above. The AASHTO resistance factor corresponding to this case (ϕ = 0.75) is also shown for comparison.

In general, the computed resistance factors decrease with respect to initial reinforcement thickness (S). Resistance factors computed for select fill conditions correspond most closely to current AASHTO specifications, and for this case higher resistance factors are rendered considering a service life of 100-years compared to a 75-year service life. The 75-year service life corresponds to higher resistance factors considering good quality fill. The conservative steel model renders very low resistance factors that are between 0.25 and 0.50. The zinc residual model renders resistance factors that appear to be closer to the current AASHTO specifications.

Table 3 is a summary of typical resistance factors that were computed for different reinforcement types and considering either the simplified or coherent gravity methods for estimating reinforcement tension. In general, calibrations for grid type reinforcements rendered resistance factors that are 0.05 to 0.10 less than those computed for strip type reinforcements. Also the load bias corresponding to the coherent gravity method renders resistance factors that are approximately 0.10 less than those obtained considering the simplified method.

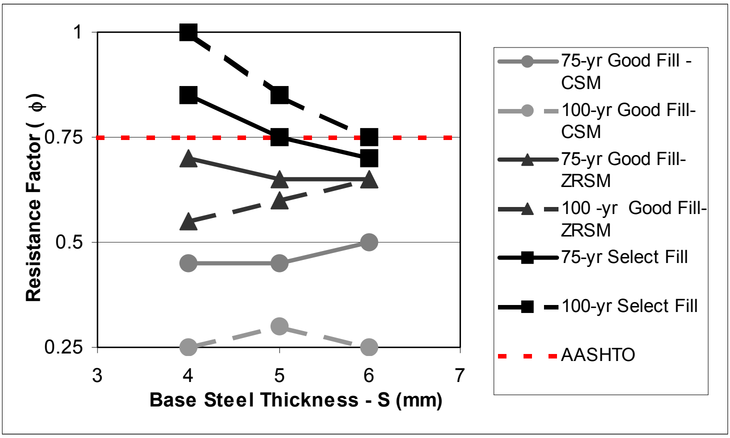

Figure 3. Resistance Factors Considering Strip Type Reinforcements and the Simplified Method of Analysis (CSM- conservative steel model; ZRSM – residual zinc steel model).

Table 3. Summary of Computed LRFD Resistance Factors

Fill Quality	Current AASHTO Resistance Factors (φ) Strip/grid	Computed Resistance Factors (φ)	
		Strip Simplified/Coherent	Grid Simplified/Coherent
Good	0.75/0.65	0.60/0.50	0.55/0.45
Select	0.75/0.65	0.75/0.65	0.65/0.55

CONCLUSIONS

Reliability-based calibration of resistance factors for MSE reinforcements is described considering the remaining cross section at the end of the design life as a variable. The computed resistance factors depend on fill conditions, reinforcement geometry, method used to compute reinforcement tension and service life. Current AASHTO specifications appear to employ resistance factors for the rupture limit state corresponding to select fill conditions. Lower resistance factors are obtained for fill conditions that are considered good, meaning they satisfy AASHTO requirements, but not by a very wide margin. More data are needed to identify the proper statistics describing the corrosion rates of steel after zinc is consumed from galvanized reinforcements.

ACKNOWLEDGEMENTS

A portion of the work described herein was conducted for the National Cooperative Highway Research Program (NCHRP) as part of NCHRP Project 24-28. The opinions and conclusions expressed are those of the authors and not necessarily those of NCHRP or its affiliates. Ms. Suzanne George, MSCE from McMahon & Mann Consulting Engineers, P.C. assisted with the resistance factor calibrations.

REFERENCES

1. AASHTO, 2009, *LRFD Bridge Design Specifications,* 4th Ed. With Interims, American Association of State Highway and Transportation Officials, Washington, D.C.
2. Allen, T., Christopher, B., Elias, V. and DiMaggio, J., 2001, *Development of the Simplified Method for Internal Stability of Mechanically Stabilized Earth Walls*, Report No. WA-RD 513.1, Washington State Transportation Center, Seattle WA, 108 p.
3. Allen, T.M., A.S. Nowak and R.J. Bathurst, 2005, "Calibration to Determine Load and Resistance Factors for Geotechnical and Structural Design," *Transportation Research Circular E-C079*, Transportation Research Board, Washington, D.C., 83p.
4. Berke, B.S, and Sagues, A.A., 2009, Update on Condition of Reinforced Earthwall Straps, Report No, BD544-32, Florida Department of Transportation, Tallahassee, FL http://www.dot.state.fl.us/research-center/Completed_StateMaterials.shtm, as BD544-32* [PDF - 11,209 KB].
5. Bounopane, S.G., Schafer, B.W., and Igusa, T., 2003, "Reliability Implications of Advanced Analysis in Design of Steel Frames," Proceedings ASSCCA '03, Sydney, Australia.
6. Darbin, M., Jailloux, J.M., and Montuelle, J., 1988, "Durability of Reinforced Earth Structures: the results of a long-term study conducted on galvanized steel", *Proceedings Institution of Civil Engineers*, Institution of Civil Engineers, Part 1, Volume 84, pp. 1029-1057.
7. D'Appolonia, 2007, "LRFD Calibration of Coherent Gravity Method for Metallically Stabilized Earth Walls," prepared for the Association for Metallically Stabilized Earth, available from http://www.amsewalls.org.
8. Elias, V., 1990, *Durability/Corrosion of Soil Reinforced Structures*, Report No. FHWA-RD-89-186, Office of Engineering and Highway Operations, R&D, McLean, VA, 173p.
9. Gladstone, R.A., Anderson, P.L., Fishman, K.L., and Withiam, J.L., 2006, *Durability of Galvanized Soil reinforcement: 30 Years + of Experience with MSE,* Journal of the Transportation Research Board, No. 1975, Transportation Research Board, National Research Council, Washington, D.C., pp. 49-59.
10. Romanoff, M., 1957, Underground Corrosion, *National Bureau of Standards, Circular 579*, U.S. Department of Commerce, Washington, D.C.
11. Sagues, A.A., Rossi, J., Scott, R.J., Pena, J.A. and Simmons, T., 1998. "Influence of Corrosive Inundation on the Corrosion Rates of Galvanized Tie Straps in Mechanically Stabilized Earth Walls", Final Report WPI0510686, Florida Department of Transportation Research Center, Tallahassee, FL.

Rockery Design and Construction Guidelines

Justin T. Henwood, P.E.[1] and Khamis Y. Haramy[2]

[1]Central Federal Lands Highway Division, 12300 West Dakota Avenue, Lakewood, CO 80228; PH 720-963-3362; email: justin.henwood@fhwa.dot.gov
[2]Central Federal Lands Highway Division, 12300 West Dakota Avenue, Lakewood, CO 80228; PH 720-963-3521; email: khamis.haramy@fhwa.dot.gov

ABSTRACT

Rockeries, also known as dry stack walls, consist of earth retaining and/or protection structures typically comprised of rough onsite rocks stacked in an interlocking fashion with no mortar, concrete, or steel to retain cut or fill slopes. They are context sensitive solutions that in many cases are also relatively low cost. Several rockeries exist as historic or cultural features on many Forest Highway and National Park roads. Many were apparently built in the Civilian Conservation Corps (CCC) era of the late 1930's; some are still performing well and others have required extensive maintenance or have failed.

Generally, rockeries have not been designed according to the AASHTO Standard Specifications or other accepted wall design procedures. The wide range of implementation suggests excellent performance can be expected when certain conditions are met. There is little guidance available to standard, acceptable design and construction guidelines. Therefore, a rationally based and tested design procedure is presented to provide designers and owners with the confidence that these structures can be used in modern highway engineering. Recommended guidelines for properly constructing rockeries are also presented.

INTRODUCTION

A rockery, also known as, "rockery wall, dry-stack wall, stone wall, and rock wall," is a retaining or protection structure that consists of stacked rocks without mortar, concrete, or steel reinforcement. Although the rocks are stacked in an "interlocking" pattern, there are no mechanical connections made between the individual rocks. Rather, these structures rely on the weight, size, shape, and interface friction of the rock elements to provide overall stability.

Un-reinforced stone structures have been constructed for thousands of years in many parts of the world. In the U.S., rockeries still exist that were constructed in the late 1800s. It is doubtful these historic rockeries were "engineered" in the current sense of the term. Rockeries were also constructed along many Forest Highway and National Park roads by manual labor in the 1930s-CCC era. Many of these roads have subsequently become part of the national highway system. Little is known about the design of these rockeries, although it is suspected many were constructed with little or no engineering. Nevertheless, while some have failed, many are still in use today.

These older rockeries, as well as more recent rockeries, are generally evaluated by the Federal Lands Highway (FLH) for conformance with design standards, as presented herein, as current and future transportation needs depend on their continued usage. Figure 1 shows typical rockery construction.

Figure 1. Typical rockery construction.

Although there is evidence the public sector was building rockeries in the 1930s, the private sector appears to have been somewhat slower to adopt commercial rockery construction. Rockeries have been constructed in the Pacific Northwest for the past four decades, and have seen increasing use in northern California and Nevada over the last 10 years. Because rockeries are a relatively inexpensive retaining alternative with a natural aesthetic appeal, they continue to gain popularity throughout the western United States. The FLH continues to find situations where new rockery construction would be advantageous or where repair or modification of existing historic rockeries is required. However, conventional highway design standards are not available to confirm adequate internal stability or factors of safety, even where rockeries have performed adequately for decades. Moreover, there is limited coverage of dry-stacked rockeries in engineering textbooks and literature. Although attempts have been made to develop guidelines for construction, these are typically local efforts and tend to be more procedural than analytical.

Based on review of available literature and the evaluation of several existing design procedures, a unified analysis and design framework was developed that can be used in modern highway engineering. The framework is rational and follows recognized engineering principles derived from analysis procedures for gravity retaining walls.

RECOMMENDED ROCKERY DESIGN GUIDELINES

Rockeries are composed of large blocks of stacked rock, heavy enough and dimensionally adequate to form a structure that resists overturning and sliding forces.

In this respect, rockeries can be treated as gravity walls, and can be analyzed rationally using modified forms of conventional gravity retaining wall design methodologies. Design of any retaining structure involves the determination of driving and resisting forces. For rockeries, driving forces include lateral earth pressures behind the rockery, surcharge pressures (both vertical and horizontal), and seismic pressures. Resisting forces can include the total weight of the rockery and individual rocks, inter-rock friction, base rock–foundation friction, and, in some cases, passive pressure at the toe of the rockery. Where Coulomb earth pressures are used, the vertical component of the active earth pressure can also aid in stabilizing the rockery. A typical rockery section is shown in Figure 2, along with the design parameters and dimensions that must be determined prior to rockery design.

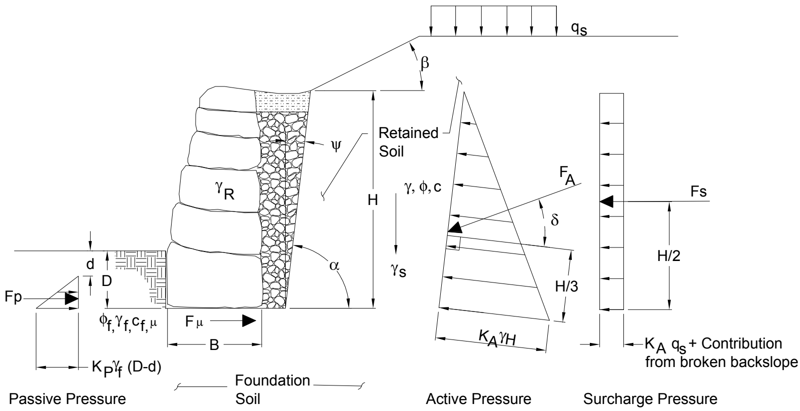

Figure 2. Schematic rockery section showing critical dimensions and parameters to be determined for design.

Design Parameters

For design, the following geotechnical parameters are required: 1) friction angle (Φ), unit weight (γ_s) and cohesion (c) for both retaining and foundation soils, 2) interface friction angle (δ) typically on the order 2/3Φ to Φ, 3) allowable back cut angle (Ψ), 4) unit weight for rock (γ_R)); typically assumed to be 23.5 kN/m^3, including void space, 5) minimum required embedment depth (D), 6) allowable bearing pressure and estimated settlement due to the weight of the rockery.

For rockery design, the theoretical failure plane crosses through two soil types (crushed rock used in backdrain and retained soil) and a compound failure wedge is developed. While it is feasible to develop closed-form equations for this condition, acceptable results can be obtained by making the simplifying assumption that the crushed rock is part of the rockery system and the lateral earth pressure is developed solely by the retained soil. Therefore, the lateral earth pressure acts on the back of the crushed rock layer at the crushed rock/slope interface rather than the back of the rockery facing elements. Because the friction angle of the crushed rock is almost always greater than that of the retained soil, this simplifying assumption is usually conservative.

Design requirements and pertinent factors of safety for the associated design component of rockeries generally follow AASHTO Standard Specification requirements for gravity retaining structures.

Sliding Resistance

Rockeries generally resist sliding primarily through friction along the bottom of the base rock, which is a function of the normal force acting on the base of the rockery and the coefficient of friction between the base rock and foundation soil. The normal force consists of the vertical component of the Coulomb active earth pressure ($F_{A,V}$, acting downward) and the weight of the rockery. The weight of the rockery can be estimated by assuming certain minimum dimensions for the rockery, breaking the rockery into a few easy to define geometric shapes, assuming a unit weight for the rockery mass, and computing the total weight as the sum of each component. The unit weight of the individual, sound, intact rocks is about 25.9 kN/m^3, which corresponds to a specific gravity of about 2.65. However, once the voids in the rockery are considered, a reasonable unit weight for a well-constructed rockery is about 23.6 kN/m^3.

Figure 3 shows a schematic of a rockery that has been divided into three sections for the computation of the rockery weight. Although the lateral earth pressures are assumed to act on the back of the crushed rock behind the rockery, the weight of the crushed rock is typically not included as a resisting force. Because the crushed rock is not physically connected to the back of the rockery and the facing rocks and crushed rock interact only through frictional contact, it is not clear that the weight of the crushed rock would provide a significant resistance to movement, particularly overturning. Therefore, the weight of the crushed rock is conservatively neglected. After the design is complete, the final rockery dimensions should be checked to verify the assumed geometry and weight are correct.

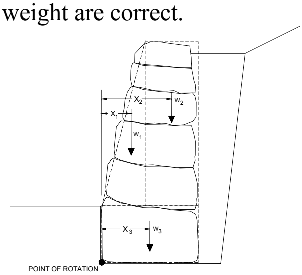

Figure 3. Estimation of rockery weight and centroidal distances.

The friction along the bottom of the base rock is computed by multiplying the friction factor for sliding between the rock and the foundation soil (μ) by the sum of the vertical forces acting on the base of the rockery. For the design procedures presented in this paper, a static factor of safety of 1.5 and a seismic factor of safety of 1.1 are recommended for sliding.

Inter-rock sliding is performed as a design check and is similar to external sliding, as described above, except that the total weight is only computed for the rocks above the point of sliding, which is generally taken between each lift of the rockery. A conservative friction factor is assumed unless additional data from laboratory testing or high rock roughness indices warrant a higher value.

Overturning

The horizontal forces include the horizontal component of the lateral earth pressure ($F_{A,H}$) and the additional horizontal pressure due to a vertical surface surcharge (FS). These will also tend to cause the rockery to tip forward about its toe. The overturning moments caused by these forces are counterbalanced by resisting moments due to the weight of the rockery (W), the vertical component of the lateral earth pressure ($F_{A,V}$), and the passive resistance at the toe of the rockery (F_P). The overturning and resisting moments are computed by summing moments about the toe of the rockery. The total resisting moment due to the weight of the rockery is computed for each component of the rockery weight (W_i), as shown in Figure 3, multiplied by the horizontal distance from the centroid of each rockery segment to the toe of the rockery (x_i). A minimum factor of static safety against overturning of 2.0 and seismic factor of safety of 1.5 are recommended.

Bearing Capacity

The final aspect of static design to be checked is the bearing capacity of the foundation soils. The allowable bearing capacity can be determined in accordance with the traditional Terzaghi bearing capacity equation. A minimum static factor of safety of 2.5 and seismic factor of safety of 1.5 are recommended, similar to AASHTO Standard Specification requirements for gravity retaining structures.

Seismic Considerations

In general, the Mononabe-Okabe procedure for earth retaining structures, as presented in the AASHTO Standard Specifications, is considered adequate for the seismic design of rockeries.

Global Stability

In some cases, the overall rockery design may be controlled by global stability considerations. This is especially true for cuts in previously placed fills or for walls with a sloping toe condition. The purpose of a global stability analysis is to check that the rockery or retained improvements will not be damaged by a slope stability failure through or below the wall facing.

Global stability analyses can be performed using most commercially available limit equilibrium slope stability programs. For static slope stability analyses, a minimum factor of safety of 1.5 is typically considered. For highway projects, it may be feasible to lower this factor of safety to 1.3.

Wherever global stability is checked for static conditions it should also be checked for seismic conditions. A minimum factor of safety of 1.1 should be used for seismic conditions. Depending on the results of the seismic slope stability analysis, a deformation analysis may also be required to check that estimated upslope movements are acceptable where upslope improvements exist or are planned.

ROCKERY CONSTRUCTION GUIDELINES

For most civil works, the performance of a structure is directly related to the quality of construction. For a rockery, this concept is magnified several times by the fact that rockeries are constructed from irregularly shaped, naturally occurring materials. Therefore, the skill of rockery placement has a large impact on its overall performance.

Rock Placement

Proper placement of rocks comprising the rockery requires skill and experience because of the irregular and non-uniform nature of the materials involved. Some rocks only fit in certain places and not others, and finding the proper match between rocks to form a stable structure can be a trial-and-error process even if the operator is highly experienced.

Base rocks should be placed on a properly prepared foundation excavation, as discussed previously. The minimum base rock width, B, should be specified on the plans and should be based on overall rockery height, retained soil properties, and any surcharge loads. All rocks, including the base rocks, should be placed with the longest rock dimension perpendicular to the face of the rockery. The second largest dimension should be parallel to the layout line of the rockery, and the smallest rock dimension should be its vertical dimension. The base rocks should be placed such that the tops of the rock are sloped back at least 5% towards the back of the rockery. The allowable tolerance for base rock widths should be 150 mm.

Because the rocks must be "finessed" into proper interlocking positions, the use of proper equipment for rock placement can be the difference between a successful and unsuccessful project. An excavator with a rotating clamshell attachment is useful for properly placing rocks. The clamshell allows the rock to be grasped uniformly on two sides, and the powered rotation capability allows the operator to quickly make adjustments to the rock orientation and alignment. In addition, a clamshell with rotation capability also allows one rock to be placed and replaced at multiple locations to determine the best fit without the need to move the excavator or regrasp the rock. An excavator with a rotating clamshell should be required, as it improves rockery construction and reduces time of installation.

Successive lifts of facing rocks should be placed above the base rocks in accordance with the design schedule. In general, the width of successive rows of facing rocks will be determined based on the design rockery face batter, which will generally vary between 4V:1H and 6V:1H. Each rock should be placed according to the following; 1) each rock should bear on at least two other rocks, 2) each rock should have at least three bearing points—two in front and one in back, 3) the front-most bearing points for each rock should be within 150 mm of the average face of the rockery, 4) the rear of the rocks should be aligned along an imaginary vertical plane. If rocks larger than the minimum specified B are used, they can extend beyond this imaginary plane provided they do not interfere with rockery drainage, and 5) the tops of each rock should be sloped back towards the backdrain as previously described for the base rock.

An example of a relatively well constructed rockery is shown in Figure 5. Although a few vertical seams can be located, the rocks are generally bearing at the proper locations and stacking in an approximate running bond pattern.

Figure 5. Example of a well constructed rockery.

Drainage System

As the base and facing rocks are placed, it is generally most convenient to construct the rockery drain and crushed rock zone concurrently. The drain pipe should generally consist of a 100 mm diameter perforated drain pipe surrounded on all sides by at least 100 mm of screened, 100 to 150 mm diameter, angular crushed rock. The drain pipe should consist of either corrugated high-density polyethylene (HDPE) pipe or smooth polyvinyl chloride (PVC) pipe.

In addition to subsurface water, surface water must also be controlled. To prevent a hydraulic connection between the rockery backdrain and surface water flows, the top of the crushed rock should be capped with at least 300 mm of “impermeable” soil over non-woven geotextile. This soil cap can generally consist of on-site soils and should be “impermeable” to the extent that rapid infiltration of surface water cannot occur.

As with any structure that retains soil or rock, surface water should also be directed away from the rockery where possible. Where the rockery is constructed at the toe of a slope or on a slope, a v-ditch consisting of concrete or impermeable soil should be constructed on the backslope above and behind the rockery to direct surface water to a suitable drainage outlet.

SUMMARY

In summary the design of a rockery that resists static and seismic earth pressures and lateral pressure surcharges is analogous to the design of a gravity retaining wall. The lateral pressures acting on the back of the rockery should be determined, and the rockery checked for an adequate factor of safety against sliding, overturning, and bearing capacity failure. The presented design procedure provides users a level of confidence in specifying and constructing rockeries.

More so than for other types of retaining walls, the stability and longevity of a rockery are controlled by the construction practice and the natural shape of the stones that are practically available. Proper and adequate construction inspection will likely improve the quality of construction and, thereby, improve the performance of the rockery; further reducing the likelihood of failure to a level that is believed to be generally consistent with other AASHTO designed retaining walls. Because this is not always achievable, it is recommended that rockeries be used where the consequence of failure is not excessive, such as for some lower volume roads, cuts requiring only nominal support (for example, short-term stability is sufficient to build the rockery without shoring), and where there is great benefit in cost and aesthetics for doing so.

ACKNOWLEDGEMENTS

The authors recognize the efforts of Sanders and Associates in completing a much more comprehensive and detailed technical report on the subject of rockery design and construction. This technical report was completed under the auspices of the Central Federal Lands Highway Division of the Federal Highway Administration and is available at the following website: www.cflhd.gov.

REFERENCES

AASHTO (2002), Standard Specifications for Highway Bridges, 17th Edition.

Lateral Pressure Reduction on Earth-Retaining Structures Using Geofoams: Correcting Some Misunderstandings

John S. Horvath[1], Ph.D., P.E., M.ASCE

[1]Professor, Manhattan College, School of Engineering, Civil and Environmental Engineering Department, Bronx, NY 10471, U.S.A.; jsh@jshce.com

ABSTRACT: Block-molded expanded polystyrene and related geofoam materials can reduce lateral pressures acting on a wide variety of earth-retaining structures to almost zero under both gravity and seismic loading. There are two distinctly different functional ways to achieve this: lightweight fill and compressible inclusion. This paper updates the state of knowledge in this area with an emphasis on seismic buffers. This particular application, which makes use of the compressible-inclusion function, has seen increasing research interest in recent years. However there appear to be significant misunderstandings about material behavior that require clarification.

INTRODUCTION

Geofoam has been used as the generic term for a category of *cellular geosynthetics* since the early 1990s (Horvath 1995). As such, "geofoam" when used alone does not mean one specific material or product as many mistakenly believe but rather a wide spectrum of polymeric, vitreous, and cementitious materials and derivative products, each with a characteristic texture of small, closed, gas-filled cells so relatively numerous that the material has a lower density than normal earth materials.

Experience to date is that the common white polymeric foam called *expanded polystyrene* (EPS) is the geofoam material of choice for virtually all functional applications. Therefore this paper is limited to a consideration of EPS geofoam, specifically its generic block-molded form, and materials related to it.

SCOPE OF PAPER

A comprehensive documentation of the geosynthetic functions and applications for all geofoams was presented in Horvath (1995) with an updated bibliography in Horvath (2001). More recently, an assessment was made of the relative usage of the various geosynthetic functions and applications of EPS geofoam (Horvath 2005b). This indicated that the use of EPS geofoam to reduce lateral pressures on both new and existing earth-retaining structures (ERSs) has been significantly and surprisingly underutilized and under-researched to date even though such use dates back at least to the 1970s and experience indicates that it has the promise to revolutionize how ERSs are designed and constructed (Horvath 2004b). This underutilization is especially true for applications involving seismic loading so recent publications by the author (Horvath 2008a, 2008b) focused on this important application.

These publication efforts have had a positive outcome as recent years have seen a surge in research interest in using EPS geofoam with ERSs, especially as a *seismic buffer* (defined subsequently). Unfortunately, it appears from the published record that there may not be a clear understanding of relevant EPS material behavior. This complicates the interpretation and practical utility of published research outcomes. Consequently, after a brief overview of the mechanisms for achieving lateral pressure reduction on ERSs this paper focuses on seismic buffers with an intent to clarify the apparent misunderstandings for the benefit of future research into this topic.

EPS GEOFOAM AND EARTH-RETAINING STRUCTURES

A common term used in discussions related to ERSs is *yielding*. In this context "yielding" is synonymous with horizontal (lateral) displacement and can be applied to either the ERS itself or the ground adjacent to the ERS. With this in mind, ERSs are broadly divided into those that are:

- *non-yielding* which defines an ERS that is inherently incapable of and/or constrained against both rigid-body displacement and deformation in the horizontal direction under service loads. Common examples include basement walls of buildings, conventional bridge abutments, and otherwise free-standing rigid retaining walls that are either physically or geometrically restrained against displacement. The hallmark of non-yielding ERSs is that they are logically designed assuming the *at-rest* earth-pressure state within the retained soil; and

- *yielding* which defines an ERS that can either displace or deform or both in the horizontal direction under service loads. The hallmark of yielding ERSs is that they are assumed to be capable of developing the *active* earth-pressure state within the retained soil although they may or may not under service loads due to excess capacity ('safety') intentionally built into the overall system.

Not considered in this paper due to space limitations is a third type of ERS called *self-yielding*. These are rigid ERSs that displace horizontally on their own (usually as a result of thermal changes in their environment) as opposed to displacing (or not) as a reaction to applied earth loads as in the above-defined cases of non-yielding and yielding ERSs. Examples include *integral-abutment bridges* as well as various types of circular water- and wastewater-treatment tanks (Horvath 2000, 2004a, 2005a).

There are two distinctly different physical mechanisms by which EPS geofoam can be used to reduce lateral pressures on ERSs, with each mechanism utilizing a different geosynthetic function:

- The *lightweight-fill* function makes use of the fact that EPS has a density that is considerably less (as low as 1%) than that of soil; is inherently self-supporting even when EPS blocks are stacked vertically; and has a Poisson ratio that is very small. This is what is called a *small-strain function* of EPS geofoam.

- The *compressible-inclusion* function makes use of the fact that EPS can be manufactured and designed to be relatively compressible compared to the other materials with which it is in contact in order to intentionally induce horizontal displacements and concomitant shear-strength mobilization within the retained-soil mass (*controlled yielding*). This is a *large-strain function* of EPS-geofoam.

LIGHTWEIGHT-FILL FUNCTION

Fig. 1 shows a generic cross-section where blocks of EPS are used for this function. This function can be used effectively with both non-yielding and yielding ERSs. A detailed discussion of the current state of practice concerning the correct model for analyzing this functional application can be found in Horvath (2008a).

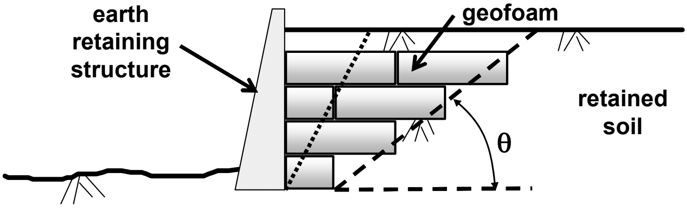

FIG. 1. Generic application of lightweight-fill function.

Of relevance to this paper is the common misconception that a classical active earth pressure wedge forms within the EPS blocks as indicated by the dotted line in Fig. 1. This simply does not occur. Rather, the EPS blocks act as an extension of the actual ERS so that the dashed line in Fig. 1 defined by the angle θ acts as a failure plane between the combined ERS + EPS mass and the retained soil, with the retained soil assumed to be in an active earth pressure state. The benefit of using EPS in this manner is due to the fact that a) the EPS blocks and overlying soil impart a relatively small lateral load on the ERS and b) the lateral earth pressure from the retained soil that is transmitted through the EPS blocks to the ERS under gravity and seismic conditions becomes zero if a sufficiently small value of θ as defined by Coulomb (for gravity loads) or Mononobe-Okabe (for seismic loads) theory is chosen.

COMPRESSIBLE-INCLUSION FUNCTION

The basic concept of a compressible inclusion is that a relatively low-stiffness geofoam material (EPS or related material) is intentionally placed between two stiffer materials (the ERS and adjacent ground). In such conditions the least-stiff material in the system (the EPS in this case) will compress much more readily than the others, resulting in load reduction through the classical soil mechanics mechanisms of shear-strength mobilization and arching within the adjacent ground (Handy 1985, Harrop-Williams 1989). These mechanisms were recognized and utilized at least as early as the early 20th century to reduce vertical loads on underground conduits (Spangler and Handy 1982). In these early conduit applications the compressible inclusion was some organic material such as bales of hay. The attraction of this concept is that it is very efficient and thus cost-effective material-wise as a relatively thin compressible inclusion, if properly designed, can result in significant load reductions on the ERS.

In its original and most basic form called the *Reduced Earth Pressure* (REP) concept (Fig. 2), a compressible inclusion is beneficial only for non-yielding ERSs as it is assumed the at-rest earth pressure state can be reduced only to the active earth pressure state through mobilization of the inherent shear strength of the retained soil.

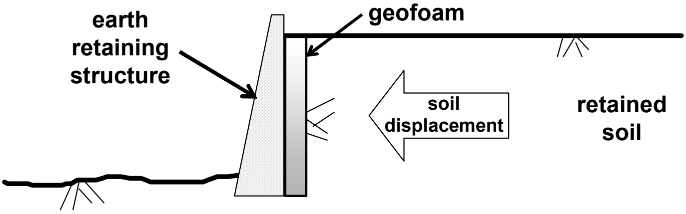

FIG. 2. Generic application of REP concept of compressible-inclusion function.

The original REP concept was subsequently extended by incorporating multiple horizontal layers of geosynthetic tensile reinforcement (geotextiles, geogrids, metallic strips or grids) within the retained soil and placed adjacent to the compressible inclusion in the classical arrangement of *mechanically stabilized earth* (MSE). This is called the *Zero Earth Pressure* (ZEP) concept because the system can be designed to allow the reinforcement to strain and behave in a classical *mechanically stabilized earth wall* (MSEW) mechanism. Thus the ZEP concept can produce benefits for both non-yielding and yielding ERSs as it is possible to reduce lateral pressures to less than the active state and approaching zero (hence the name used for this concept).

Space limitations preclude a detailed discussion of the current state of practice concerning models for analyzing the REP and ZEP concepts. Only an overview is presented here. Details concerning analytical models used to date can be found in Horvath (1996, 1997, 1998a, 1998b, 2008a).

The basic physical model used for analyzing both REP and ZEP applications is that of a mechanical system consisting of two axial springs aligned horizontally and placed in series. Each spring, which may be linear or non-linear as desired, represents the horizontal force-displacement behavior of a system component as follows:

- The retained soil, unreinforced or reinforced as appropriate, has an initial compressive force (typically assumed to be the at-rest state) that reduces with increasing horizontal displacement ('spring' extension) to either the active state (REP concept) or zero (ZEP concept). The magnitude of displacement required to reach these minima is problem-specific.

- The geofoam compressible inclusion has zero initial force that increases with increasing horizontal displacement ('spring' compression). Note this implies that the compressive stiffness normal to the primary direction of soil displacement (horizontal in this case) is the relevant physical property of the compressible inclusion. For the purpose of quantifying this stiffness it was found useful to define a new dimensionless parameter, λ, called the *normalized compressible inclusion stiffness* (Horvath 2000):

$$\lambda = \frac{E_{ci} \cdot H}{t_{ci} \cdot p_{atm}} \qquad \textbf{(1)}$$

where E_{ci} is the Young's modulus of the compressible-inclusion material; H is the 'geotechnical' height of the ERS (i.e. height of the retained soil against the back of the ERS); t_{ci} is the thickness of the compressible inclusion; and p_{atm} is atmospheric pressure (used solely to non-dimensionalize λ). The limiting values of λ are zero for the 'perfectly compressible' case of unrestricted displacement and infinity for the 'perfectly rigid' case of no displacement.

SEISMIC BUFFERS

In recent years the predominant area of research into the use of EPS geofoam to reduce lateral pressures on ERSs has been the REP concept (Fig. 2) under seismic loading. During this time the term *seismic buffer* has been coined by others and is now widely used for this specific application of the REP concept. Zarnani and Bathurst (2009) provide an overview and summary of recent research into seismic buffers that is current as of the time this paper was written (early 2010).

The most significant outcome of recent research is that the effectiveness of seismic buffers in terms of relative reduction of seismic forces compared to a baseline of no compressible inclusion depends on the natural frequency of the ERS-inclusion-retained soil system compared to the frequency of the applied cyclic load. Earlier work (Horvath 1997, 1998b) assumed load reduction was frequency-independent.

However, this recent research appears to unilaterally suffer from potentially significant flaws due to apparent fundamental misunderstandings of the mechanical (stress-strain-time-temperature) properties of the geofoam materials and products that were used in those studies as the compressible inclusions. To what extent these flaws impact the conclusions of this published work is unknown at this time and beyond the scope of this paper. The intent of this paper is to explain what these flaws are and what the correct interpretation should be. It is then left to others to revisit, revise, correct, and re-publish, as necessary, past research. Future research will hopefully be planned, executed, and interpreted correctly from the start.

The basic flaw in previous research involves proper understanding and assessment of the stiffness of the geofoam compressible inclusion. Compressive stiffness is the single most important behavioral characteristic of any compressible inclusion and as indicated in Eq. 1 Young's modulus is the material stiffness parameter of primary interest. However, most research to date (e.g. Bathurst et al. 2007) has placed undue focus and importance on the density of the EPS based on the assumption that EPS stiffness is proportional to its density. This is both misleading and simply incorrect as a general rule (Horvath 2009).

In general, the density of EPS in and of itself means absolutely nothing with regard to its stiffness. It is believed the common misconception that there is a relationship between EPS density and stiffness (in the form of Young's modulus) derives from the fact that in a very limited context involving relatively small compressive strains (less than 1%) and assuming certain important quality-assurance measures have been met then correlations (typically linear) between EPS density and Young's modulus have been observed by many researchers worldwide (Horvath 1995). However, as noted previously compressible-inclusion applications in general and seismic buffers in particular are inherently large-strain in nature. Therefore, any small-strain correlations between EPS density and modulus are simply irrelevant.

It appears that in more-recent publications (e.g. Zarnani and Bathurst 2009) researchers have begun to get away from using EPS density as a measure of its stiffness and are using Young's modulus directly as the primary correlation variable with material behavior in seismic-buffer applications. While this is certainly a step in the right direction it does not appear that the proper moduli have been used in analyses.

To begin with, there are two distinctly different EPS-based geofoam materials that have been studied by researchers and used in practice for compressible inclusions. The mechanical behavior of each material is markedly different even though the materials look identical and may even have identical densities. One material is 'normal' block-molded EPS that has the uniaxial unconfined compressive behavior depicted qualitatively by Curve 1 in Fig. 3. Upon initial loading, normal EPS has a very limited nominally linear-elastic range up to a compressive strain of approximately 1%. This is followed by a transition zone of significant yielding that is the result of physical distortion of the originally-spherical cells that comprise the EPS so that the cells become permanently ellipsoidal in shape. There is then an extended zone of slight work-hardening and finally a zone of significant work-hardening as the EPS is literally crushed back to solid polystyrene. Note that once the zone of yielding is passed even one time there is significant and permanent non-recoverable ('plastic') strain upon unloading as shown by a typical post-yield unload-reload portion of Curve 1. Note also that the scale of the stress axis in Fig. 3 is intentionally unlabeled as it is dependent on not only the EPS density but also strain-rate and temperature.

The most important point made here is that the Young's modulus of EPS, which is the slope of any point on Curve 1, is constantly varying once the initial nominal linear-elastic zone is passed. So the Young's modulus of normal EPS is dependent not only on the initial material density but also stress level, stress history, strain-rate, and temperature as well. All of these factors are significant for seismic-buffer applications where cyclic compressive strains well into double-digits and certainly well beyond the linear-elastic limit of approximately 1% strain are the rule.

Unfortunately, it appears that researchers to date have not appreciated the complex factors affecting the Young's modulus of EPS as they affect seismic-buffer applications, especially given the large strains and cyclic loading involved, as correlations for Young's moduli applicable for small-strain (i.e. $< 1\%$) applications have been used in research to date (e.g. Zarnani and Bathurst 2009).

The other material used for compressible inclusions is what is called *resilient* or *elasticized* EPS. This is normal block-molded EPS that has been subjected to an

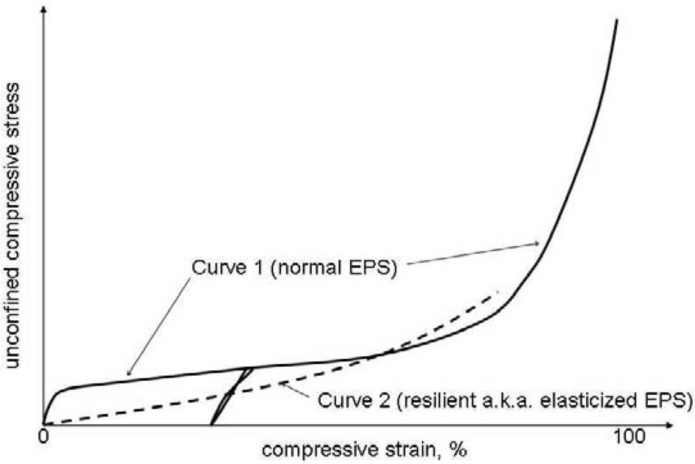

FIG. 3. Generic stress-strain behaviors of block-molded EPS and related materials

additional manufacturing step to permanently distort the cell shapes before the material is loaded in service for the first time. The benefit of doing this is that the stress-strain behavior of the material is permanently and markedly different compared to normal EPS. The behavior of resilient EPS is shown as Curve 2 in Fig. 3. Note that this comparison is for resilient EPS that originally had the same density as the normal EPS (Curve 1) depicted in the same figure. This emphasizes the point made previously that EPS that has the same density may have very different stiffness properties both qualitatively and quantitatively.

CONCLUSIONS

The efficacy of using block-molded EPS geofoam and related materials such as resilient EPS to reduce lateral pressures acting on ERSs is well established. However, research is still needed in many areas for both the lightweight-fill and compressible-inclusion functional applications to both better understand the behavior of the ERS-geofoam-retained soil systems as well as to both verify and improve, as necessary, current analysis and design methodologies. The key element in this overall process is that the very complex material behavior of EPS as it is relevant to a particular functional application must be clearly understood if research is to be properly formulated, executed, interpreted, and presented in publications.

REFERENCES

Bathurst, R. J., Zarnani, S., and Gaskin, A. (2007). "Shaking table testing of geofoam seismic buffers." *Soil Dyn. & Eq. Engr.*, 27: 324-332.

Handy, R. L. (1985). "The arch in soil arching." *J. Geotech. Engr. Div.*, 111 (3): 302-318.

Harrop-Williams, K. O. (1989). "Geostatic wall pressures." *J. Geotech. Engr. Div.*, 115 (9): 1321-1325.

Horvath, J. S. (1995). *Geofoam geosynthetic*. Horvath Engr., P.C., Scarsdale, NY.

Horvath, J. S. (1996). "The compressible inclusion function of EPS geofoam: an overview." *Proc. Intl. Sym. on EPS Construction Method (EPS Tokyo '96)*, Tokyo, Japan: 71-81.

Horvath, J. S. (1997). "The compressible inclusion function of EPS geofoam." *Geotex. & Geomem.*, 15 (1-3): 77-120.

Horvath, J. S. (1998a). "The compressible inclusion function of EPS geofoam: an overview of concepts, applications, and products." *Res. Rpt. No. CE/GE-98-1*, Manhattan Coll., Civ. Engr. Dept., Bronx, NY.

Horvath, J. S. (1998b). "The compressible-inclusion function of EPS geofoam: analysis and design methodologies." *Res. Rpt. No. CE/GE-98-2*, Manhattan Coll., Civ. Engr. Dept., Bronx, NY.

Horvath, J. S. (2000). "Integral-abutment bridges: problems and innovative solutions using EPS geofoam and other geosynthetics." *Res. Rpt. No. CE/GE-00-2*, Manhattan Coll., Civ. Engr. Dept., Bronx, NY.

Horvath, J. S. (2001). "Geomaterials research project - geofoam and geocomb geosynthetics: a bibliography through the second millennium A.D." *Res. Rpt. No. CGT-2001-1*, Manhattan Coll., Sch. of Engr., Ctr. for Geotechnology, Bronx, NY.

Horvath, J. S. (2004a). "Integral-abutment bridges: a complex soil-structure interaction challenge." *Geotech. Engr. for Trans. Proj.* (GSP 126), ASCE, Reston, VA: 460-469.

Horvath, J. S. (2004b). "Geofoam compressible inclusions: the new frontier in earth retaining structures." *Geotech. Engr. for Trans. Proj.* (GSP 126), ASCE, Reston, VA: 1925-1934.

Horvath, J. S. (2005a). "Integral-abutment bridges: geotechnical problems and solutions using geosynthetics and ground improvement." *Proc. IAJB 2005: The 2005 FHwA Conference on Integral Abutment and Jointless Bridges*, Baltimore, MD: 281-291.

Horvath, J. S. (2005b). "Expanding the use of expanded polystyrene (EPS) geofoam in practice." *Proc. BSCES ASCE Geo-Institute Fall 2005 Geotech. Engr. Sem.*

Horvath, J. S. (2008a). "Seismic lateral earth pressure reduction on earth-retaining structures using geofoams." *Geotech. Eq. Engr. & Soil Dyn. IV*, ASCE, Reston, VA.

Horvath, J. S. (2008b). "Extended Veletsos-Younan model for geofoam compressible inclusions behind rigid, non-yielding earth-retaining structures." *Geotech. Eq. Engr. & Soil Dyn. IV*, ASCE, Reston, VA.

Horvath, J. S. (2009). "Manufacturing quality issues for block-molded expanded polystyrene geofoam." *J. Matls. in Civ. Engr.*, ASCE, Reston, VA, submitted for publication.

Spangler, M. G. and Handy, R. L. (1982). *Soil engineering* (4^{th} ed.). Harper & Row, New York, NY.

Zarnani, S. and Bathurst, R. J. (2009). "Numerical parametric study of expanded polystyrene (EPS) geofoam seismic buffers", *Canadian Geotech. J.*, 46: 318-338.

NPS Retaining Wall Inventory and Assessment Program (WIP): 3,500 Walls Later

Matthew J. DeMarco[1], Richard J. Barrows[2], and Stephen Lewis[3]

[1]Geotechnical Group Lead, Central Federal Lands Highway Division, Federal Highway Administration, 12300 W. Dakota Ave, Ste. 210, Lakewood, CO 80228, 720-963-3520, Matthew.DeMarco@dot.gov.
[2]FLH Geotechnical Discipline Leader, Western Federal Lands Highway Division, Federal Highway Administration, 610 E 5th Street, Vancouver, WA 98661, 360-619-7704, Rich.Barrows@dot.gov.
[3]WIP/GIP Program Administrator, Central Federal Lands Highway Division, Federal Highway Administration, 12300 W. Dakota Ave., Ste. 210, Lakewood, CO 80228, 720-963-3492, Stephen.Lewis@dot.gov.

ABSTRACT: Beginning in 2004, the FHWA Office of Federal Lands Highway (FLH) teamed with the National Park Service (NPS) to develop and implement a retaining wall inventory and condition assessment program supporting roadway asset management efforts underway throughout U.S. Parks. The vast majority of Park earth retaining structures were built prior to 1960, with many built circa 1935, making the assessment of this aging asset a high priority within the NPS. This paper briefly describes key development and implementation aspects of the WIP, overviews the condition assessment approach taken for the range of wall types inventoried, and notes preliminary program findings.

INTRODUCTION

The National Park Service is responsible for the management and maintenance of nearly 5,500 miles of paved roads and parkways across more than 250 park properties nationwide. In addition to the primary paved roadway asset, the NPS is also responsible for appraising and managing deferred maintenance needs of numerous subsidiary roadway features - including bridges, retaining walls, culverts and traffic barriers. Although considered secondary assets, these subsidiary features are nonetheless major contributors to the safety and accessibility of the NPS roads system and represent substantial infrastructure investments. Given the wide range of geographic settings and public usage demands comprising the NPS network of roads, defining the backlog of secondary roadway asset needs in terms of location, quantity, condition, and failure consequence, is a major challenge to the NPS asset program.

Currently, park roadways and bridges are assessed within two inventory programs co-developed with the NPS and managed by the FHWA Office of Federal Lands Highway (FLH) – the Road Inventory Program (RIP) and Bridge Inventory Program (BIP). Both inventory programs provide asset data to the NPS Facility Management Software System (FMSS), the data hub for park asset documentation, management and planning efforts.

Beginning in 2004, the Park Facility Management Division of the NPS Washington Office (WASO) commissioned FLH to undertake development of a retaining wall inventory program similar in scope to the on-going RIP and BIP inventories. Both organizations are equally responsible for the continual development and management of the WIP program; the NPS is primarily responsible for integration of WIP wall data within the FMSS asset management system, while FLH has taken the lead for delivery of all field inventories. The program mission is to define and quantify wall assets associated with park roadways in terms of their location, geometry, construction attributes, condition, failure consequence, cultural concerns, apparent design criteria and cost of structure maintenance, repair or replacement. Wall inventory condition and cost data are readily transferred from the WIP database to FMSS. Ultimately, condition assessments for retaining wall structures are expressed as deferred maintenance costs, which are then divided by current year replacement costs to arrive at a "Facility Condition Index" (FCI). Coupling this condition prioritization index with an "Asset Priority Index" (API), which measures the feature's importance to the mission of the park, capital asset investments are made more efficiently. This approach appropriately focuses maintenance and construction priorities on value, rather than solely on cost.

In addition to providing asset information to FMSS, wall data are also provided to RIP to update wall assets associated with the parent roadway asset. Bridge, culvert and traffic barrier data are also provided to FMSS and RIP via other inventory programs. Similar to RIP, it is the intent of the WIP to periodically reassess retaining wall resources at programmed parks to ensure timely, accurate information is available to support NPS asset management initiatives.

WIP DEVELOPMENT

Following conceptual development of the WIP in 2006, FLH and NPS team members undertook (1) defining acceptance criteria for retaining wall inclusion within the inventory program; (2) defining approximately 65 wall data attributes that are logged, measured, calculated or assessed during field inventories; (3) developing field data collection procedures, field forms, and associated field guides and cost information; and (4) developing a MicroSoft Access-based, fully searchable WIP database. Several pilot studies were also conducted in the summer and late-fall of 2006, including developmental pilots at Sequoia and Crater Lake National Parks. Table 1 presents the general criteria for determining if an earth retaining structure should be included in the NPS wall inventory program.

Table 1. Wall acceptance criteria for the WIP.

Criteria Subject	Criteria Definition
Qualifying Roads	The inventory includes retaining walls, together with qualifying culvert headwalls, located on all classes of paved park roadways and parking areas as described in the RIP Route Inventory Report or identified by park facilities, maintenance, or resource staff.
Relation to Roadway Asset	Retaining walls and culvert headwalls, that meet the minimum height requirements, must reside within the known or assumed construction limits of the existing roadway or parking area and must support or protect the roadway or parking area.
Wall Height	The maximum wall height, measuring only that portion of the wall structure intended to actively retain soil and/or rock, must be greater than or equal to 4 ft. For culvert headwalls/wingwalls, maximum wall heights must be greater than or equal to 6 ft.
Wall Embedment	Include fully- or partially-buried retaining wall structures in the inventory that are known to meet the minimum wall height requirements, and when wall locations are known or verifiable.
Wall Face Angle	Individual walls are further defined by an internal wall face angle, measured at the wall face, greater than or equal to 45^{o} ($\geq$1H:1V face slope ratio). This criterion also applies to the internal angle of tiered wall systems (when considered as a single wall system), measured along the top edges of each wall tier.
General Acceptance	When wall acceptance based on the above criteria is marginal or difficult to discern, include the wall in the inventory, particularly where the intent is to support and/or protect the roadway or parking area and where failure would significantly impact the roadway or parking area and/or require replacement with a similar structure.

Although seemingly straightforward, the apparent simplicity of describing, measuring and evaluating earth retaining structures can be deceiving. In some circumstances it can be very difficult for inventory teams to determine whether a structure qualifies for inclusion in the inventory, or how to classify a particular wall's function. For example, is the wall present on the inside of a switchback a fill wall or a cut wall? Should a wall be considered a wall with a culvert, or a culvert headwall (Figure 1)? Is it an integral part of the bridge wingwall and, therefore covered under BIP, or does it primarily support the bridge approach? Is it a parapet extending above a wall, or is once-retained-earth missing from the top of the wall? During the development of this program, inventory teams were often challenged to best describe such unique wall conditions. It should be kept in mind that the WIP inventory only represents an initial screening of wall asset needs for a given park; more detailed wall assessments will be required to program repairs or complete structure replacements.

Wall attributes within five general data categories are described, measured, evaluated and/or rated to define and quantify WIP assets:

- **Wall Location Data**: Walls are located by park name, route number/name, side of roadway, RIP wall start and end milepoint, and calculated RIP wall start latitude/longitude (provided by an Automated Road Analyzer (ARAN) survey).

Fig. 1. Is it a large culvert headwall, or a retaining structure with a historic culvert? This retaining wall at Glacier National Park illustrates just one of the finer points captured within the WIP inventory. (FHWA photo)

- **Wall Description Data**: Walls are described by function, type, year built, architectural facings and surface treatments. Measurements are recorded for wall length, maximum height, face area, face angle, and vertical and horizontal offsets from the roadway. Photos are also logged for each wall, noting location relative to the roadway, major wall features, and overall element conditions.
- **Wall Condition Assessment**: Primary and secondary wall element conditions are described relative to extent, severity and urgency of observable distresses, and then numerically rated, giving due consideration to data reliability. The overall performance of the wall system (global performance of the entire wall system) is also evaluated and rated, with all ratings weighted and combined to arrive at a final, overall wall condition rating.
- **Wall Action Assessment**: Objective consideration is given to (1) the final wall element condition numerical rating, (2) any identified requirements for further site investigations (measure of data reliability), (3) the apparent design criteria employed (e.g., AASHTO), (4) any cultural concerns, and (5) the consequence(s) of wall failure to determine a recommended action: no action/monitor the wall; conduct maintenance-level work; repair wall elements; replace wall elements; replace the entire wall.
- **Work Order Development**: Brief, yet descriptive work orders are provided when maintenance, repair or replace actions are required. Unit costs for major work items are generated from the WIP Cost Guide, available park cost data, etc., to arrive at preliminary estimates of cumulative deferred maintenance.

Table 1 lists the various wall functions, types, architectural facings, surface treatments and rated wall condition elements included in the WIP inventory. Note that elements are visible parts of a retaining wall. An obvious limitation is that many key components of a retaining wall may not be visible, so overall wall performance is rated separately as a simple way of capturing whether or not non-visible components of the wall are functioning adequately. Detailed definitions and applications of each are beyond the scope of this paper, but available in the WIP Procedures Manual (FLHD, 2009).

Table 2. Key elements of the WIP program.

Wall Function	Wall Type	Architectural Facing	Surface Treatment	Wall Element
Fill Wall	Anchor, Tieback H-Pile	Brick Veneer	Bush Gun	Piles and Shafts
Cut Wall	Anchor, Micropile	Cementitious Overlay	Color Additive	Lagging
Head Wall	Anchor, Tieback Sheet Pile	Fractured Fin Conc.	Galvanized	Anchor Heads
Bridge Wall	Bin, Concrete	Form-lined Concrete	Painted	Wire/Geosynthetic Facing
Slope Protect.	Bin, Metal	Plain Concrete	Preservative	Bin or Crib
	Cantilever, Concrete	Planted Face	Silane Sealer	Concrete
	Cantilever, Soldier Pile	Sculpted Shotcrete	Stain	Shotcrete
	Cantilever, Sheet Pile	Shotcrete	Tar Coated	Mortar
	Crib, Concrete	Steel/Metal	Weathering Steel	Block/Brick
	Crib, Metal	Stone	Other	Placed Stone
	Crib, Timber	Simulated Stone		Stone Masonry
	Gravity, Block/Brick	Stone Veneer		Foundation Material
	Gravity, Mass Concrete	Timber		Wall Drains
	Gravity, Dry Stone	Other		Architectural Facing
	Gravity, Gabion			Traffic Barrier/Fence
	Gravity, Mortared Stone			Road/Shoulder
	MSE, Geosynthetic Face			Upslope
	MSE, Precast Panel			Downslope
	MSE, Segmental Block			Lateral Slope
	MSE, Welded Wire Face			Vegetation
	Soil Nail			Culvert
	Tangent/Secant Pile			Curb/Berm/Ditch
	Other			Overall Performance

Of the 23 primary and secondary wall elements defined in the WIP program, only those applicable (generally 5-15) are described in the field via a written "Condition Narrative" – a concise, descriptive narrative of element condition sufficient to characterize severity, extent and urgency of element distresses. Wall conditions are described within four distress categories: Corrosion/Weathering, Cracking/Breaking, Distortion/Deflection, and Lost Bearing/Missing Elements. Condition ratings are then determined through the application of a 1-10 Element Condition Rating scale, as shown in Table 3.

Table 3. Wall element condition rating criteria.

Element Condition Rating	Rating Definition
9-10 Excellent	No-to-very-low extent of very low distress. Any defects are minor and are within the normal range for *newly constructed or fabricated* elements. Defects may include those typically caused from fabrication or construction. Ratings of 9 to 10 are only given to conditions typically seen shortly after wall construction or substantial wall repairs.
7-8 Good	Low-to-moderate extent of low severity distress. Distress present does not significantly compromise the element function, nor is there significant severe distress to major structural components of an element. Ratings of 7 to 8 indicate highly functioning wall elements that are only beginning to show the first signs of distress or weathering.
5-6 Fair	High extent of low severity distress and/or low-to-medium extent of medium to high severity distress. Distress present does not compromise element function, but lack of treatment may lead to impaired function and/or elevated risk of element failure in the near term. Ratings of 5 to 6 indicate functioning wall elements with specific distresses that need to be mitigated in the near-term to avoid significant repairs or element replacement in the longer term.
3-4 Poor	Medium-to-high extent of medium-to-high severity distress. Distress present threatens element function, and strength is obviously compromised and/or structural analysis is warranted. The element condition does not pose an immediate threat to wall stability and closure is not necessary. Ratings of 3 to 4 indicate marginally functioning, severely distressed wall elements in jeopardy of failing without element repair or replacement in the near-term.
1-2 Critical	Medium-to-high extent of high severity distress. Element is no longer serving intended function. Element performance is threatening overall stability of the wall at the time of inspection. Ratings of 1 to 2 indicate a wall that is no longer functioning as intended, and is in danger of failing catastrophically at any time.

The requirement for sound engineering judgment in the WIP program is most apparent in the manner in which recommended wall actions are determined. Whereas similar condition-based inventory systems may directly correlate a numerical rating to a specific action, the WIP assessment methodology develops a numerical condition rating for applicable wall elements which is then considered in conjunction with other influencing factors to arrive at a recommended action. Other factors include such things as the consequences of wall failure, the cultural/historic significance of the structure – a very important aspect of the park program, and the reliability of the condition assessment data. The result is the selection of an appropriate action founded on a well-documented element condition and wall performance assessment, suitable for development of repair/replace work orders and preliminary cost estimates. The current wall assessment methodology meets the more comprehensive WIP program goals of identifying walls in need of maintenance, repair or replacement, allowing statistical assessments of wall elements throughout the entire WIP database, and provides the baseline for all future wall assessments.

INITIAL PARK INVENTORIES

Field data collection, storage within the WIP Database, and transfer to the NPS FMSS system began in April 2007. By October 2008, inventory teams had completed assessments on over 3,500 retaining walls in 32 National Parks, Parkways, Monuments, Seashores, Historic Sites and Recreation Areas. This initial inventory effort, thought to encompass the majority of retaining wall structures within the NPS roads system, serves as the basis for updated program developments included in the 2009 FLHD publication "National Park Service Retaining Wall Inventory Program - Procedures Manual" (FLHD, 2009).

Aside from providing wall-specific deferred maintenance data to the FMSS asset management system, the WIP database can also be queried to characterize and evaluate aspects of the entire NPS retaining wall asset – an asset that, until this time, had been undefined. General findings to date include…

Wall Functions: Of the six WIP wall functions inventoried – fill walls, cut walls, headwalls, switchback walls, bridge walls and slope protection – approximately half represent outboard fill walls. If culvert headwalls are also considered as a type of fill wall, then nearly 90 percent of all walls are designed and built to retain fill. Clearly, culvert headwalls supporting roadway assets comprise an overwhelmingly large percentage of the wall database. This leads to the question, as owners are moving toward inventorying culvert assets as well, as to where culvert headwalls should be included. The results show that culvert headwalls are typically small gravity structures in generally good condition. Inclusion of these structures within the inventory tend to bias and mask database performance trends for what could be considered the more traditional retaining walls – suggesting they are more appropriately assessed under culvert inventories. In comparison, cut walls comprise approximately 10 percent of the inventory, and a very small percentage of the walls are classified as slope protection, switchback walls, or bridge walls.

Wall Types: Although 17 unique wall types were inventoried, very few dominate the database. Nearly all culvert headwalls, and 50 percent of all walls, are mortared stone masonry gravity structures. Dry-laid stone masonry walls comprise another 25 percent of the inventory. It should also be noted that most of these stone masonry structures were built in the first half of the twentieth century. Of the 15 different wall types making up the remaining 25 percent, concrete gravity and concrete cantilever walls are relatively common. The inventory has only a few segmental block MSE walls and metal crib walls, and only one MSE wall with a geosynthetic wrapped face. The distribution of wall types is indicative of the setting where the walls are constructed and the relatively narrow time frame during which most were built.

Wall Element Ratings: As previously noted, the number of wall elements rated is different for different types of walls; generally ranging from 5-15 elements depending on the number of wall components and setting features. Nevertheless, when overall wall ratings are calculated the maximum, mean and minimum ratings remain generally consistent across the various wall types, indicating the WIP successfully quantifies wall condition within a reasonable band and with enough variation in scores that prioritization is possible.

Recommended Actions: Thus far in the program, and for most wall types with significant populations, about 25 percent of the walls require some type of corrective action – most commonly low-cost maintenance or minor repairs easily incorporated within a routine maintenance program. Only 3 percent of all walls have recommendations to replace all or part of the wall (less than 35 recommended for complete replacement), suggesting that the asset as a whole is still in acceptable condition, and that a recurring maintenance program would go along way towards keeping it that way. Bearing in mind that a large percentage of the walls inventoried were stone masonry structures, and half of all walls were culvert headwalls, the following maintenance and repair procedures were most commonly encountered:

- Removal of large brush and small trees from within and around wall structures to avoid pending root damage.
- Replacing missing, displaced and/or highly weathered masonry stones.
- Repointing and/or remortaring mortared joints in stone walls.
- Repairing wall foundations, generally suffering from a loss of foundation materials due to toe slope erosion, sliding, or scour.
- Reestablishing wall drainage systems.
- Treating wall element corrosion (e.g., wire baskets, steel piling, anchor heads).
- Sealing and replacing cracked or highly weathered concrete.

Work Order Cost Estimates: Work orders, defining general work items and associated costs, are prepared and submitted to FMSS any time a maintenance, repair or replace action is recommended. As expected, maintenance recommendations are most common and least expensive, averaging about \$4,000 per wall. Recommendations to repair or replace localized wall elements are less common, and have average costs ranging from \$25,000 to \$35,000. Total wall replacement costs average approximately \$150,000. Total deferred maintenance costs to date (end of 2008) are approximately \$18.5M, with an estimated inventory replacement cost of nearly \$407M. This equates to a program-wide FCI of 0.045 – a relatively low index value indicating the total wall asset is in reasonably good health.

REFERENCES

DeMarco, M.J., et.al. (2010), *National Park Service Retaining Wall Inventory Program (WIP) – Procedures Manual*, Central Federal Lands Highway Division, FHWA, Lakewood, CO.

The Stabilization of Major Landslides Using Drilled and Grouted Elements

John R. Wolosick, P.E., D.GE, M.ASCE [1]

(1) Director, Hayward Baker Inc., 515 Nine North Court, Alpharetta, GA 30004
jrwolosick@haywardbaker.com

Abstract: Many major landslides that have occurred throughout the U.S. in the last 15 years have been repaired using drilled and grouted elements. The projects include public and private facilities for many types of owners including State DOTs, railroads, casinos, shopping malls, and apartment complexes. The use of drilled and grouted elements such as tieback anchors and micropiles have enabled these owners to repair their problems for reasonable costs and within tight schedules.

Details of seven different landslides are presented in this paper. They are located in a wide range of geological conditions and terrains. These areas include Southern California, the Rocky Mountains, the Appalachian Mountains, middle Tennessee and the southern Mississippi River region. Massive stabilization forces have been imparted to the ground by the drilled and grouted elements to provide adequate factors of safety to stabilize the slide masses.

Introduction: The design for the repair of landslides is most often assessed in simple terms of forces and factors of safety. The factor of safety in its simplest form is defined as the ratio of the resisting forces divided by the driving forces. The drilled and grouted elements add to the resisting forces in this equation. The required factor of safety provided for any project depends on decisions made by the design team. Typical factors of safety provided usually vary between 1.3 and 1.5. However, slightly lower numbers such as 1.2 have been used when huge amounts of force have been required and technical or budget reasons have limited the installed systems. When the designer has a large amount of information on the landslide, including many well-executed borings, inclinometer results, accurate laboratory testing and a large amount of experience with the local geological setting, lower safety factors may be warranted. However, when these types of information are lacking, the use of higher safety factors is usually advised.

These repairs have been made on active slides, often times with significant ground movements occurring during construction. The installation of the elements can sometimes reduce the resisting forces by disturbing the adjacent ground or injecting water into the formation for drilling, etc. during construction. Therefore, the repair is often a delicate process of installing reinforcement to the slope as rapidly as possible, while attempting to end each day with as much of a positive effect on the slope as possible.

Grading solutions, such as the use of earthen berms, are often the first solutions considered to repair landslides by many engineers. While berms are a proven method, their use cannot be applied blindly. Most engineers are very familiar with earth moving operations and are therefore comfortable with their use. Conversely, they may not have a lot of experience with grouted element solutions, which are often considered to be expensive when compared to earth moving. However, many drilled and grouted element projects have been installed after berms have been attempted ineffectively on the same project, often doubling the cost of the fix. Four of the projects presented in this paper were originally unsuccessfully repaired with berms, only to be repaired again at a later date with drilled elements. In many instances, the location of the berm is force-fit within right-of-way limitations. Analyses may not accurately show that the berm actually may cause an increase in the driving force on the landslide or have a much lesser positive effect on the factor of safety than calculated. This is often due to the use of incorrect shear strength parameters for the soils in the analyses. Also, if the angle of the failure plane is very steep where the berm is located, the berm may be ineffective as placed.

Drainage provisions such as horizontal drains can also be used to help stabilize landslides. Reducing the peizometric pressure increases the resisting forces acting along the slide surface. However, clogging of the horizontal drains due to siltation or bacteria build-up, particularly in warm climates, often can limit their useful life. As drains clog, additional slope movements are typically observed as the effectiveness of the drains are reduced. Drilled and grouted elements can usually be upsized economically to resist water pressures, even for anticipated future high water events.

Table 1 presents the summary of the projects presented in this paper. The projects are listed in order, based on the required horizontal force applied by the drilled and grouted elements to achieve the desired factor of safety. As indicated in the table, huge forces can be applied to stabilize the slide mass using these systems.

Table 1: Summary of Projects

Project Name	**Location**	**Required Horizontal Force** Kips/Linear Foot, (kN/m)
Blue Trail Slide	Alpine, WY	172 (2,510)
Oso Creek Slide	Orange Co., CA	160 (2,335)
Ameristar Casino I	Vicksburg, MS	130 (1,900)
Ameristar Casino II	Vicksburg, MS	130 (1,900)
Mission Viejo Mall	Mission Viejo, CA	102 (1,490)
Signal Hill Slide, US 61S	Vicksburg, MS	100 (1,460)
Lexington Apartments	Nashville, TN	72 (1,050)

The two highest capacity systems shown in Table 1, The Blue Trail Slide and the Oso Creek Slide (as well as the Mission Viejo Mall project), were designed to high seismic criteria which contributed significantly to the required stabilization forces.

The Blue Trail Slide (172 Kips/LF, 2,510 kN/m): The Blue Trail Slide is located on US 26/89 within the Snake River canyon in west-central Wyoming, just north of the city of Alpine. The slide consists of a block failure of various types of detrital rocks with sand, silt and clay sliding on shales and siltstones. Most slide movements were observed during the spring melt when water levels within the slide mass rose simultaneously with the scour of the toe of the slope occurred due to increased runoff. Minor slide repairs and repaving were made over many years. However, a plan to widen the road through the landslide precipitated a fix to the existing slide which also had to carry the additional loading of a mechanically stabilized earth wall to accommodate additional space. The repair was bid in 1997 by the Wyoming Department of Transportation. Various general contractors bid the roadway work supported by various design/construct specialty subcontractors for the landslide repair.

A combination micropile retaining wall and tieback anchor system was employed to stabilize the slide. Due to the huge dimensions of the slide, which includes about 150 (46 m) feet in elevation change from the roadway level to the river, multiple retaining walls were required for stabilization. Figure 1 shows a cross-section of the system. The repair consisted of upper and lower micropile retaining walls and one small ancillary wall that were each supplemented with drilled tieback anchors (Turner, 1998).

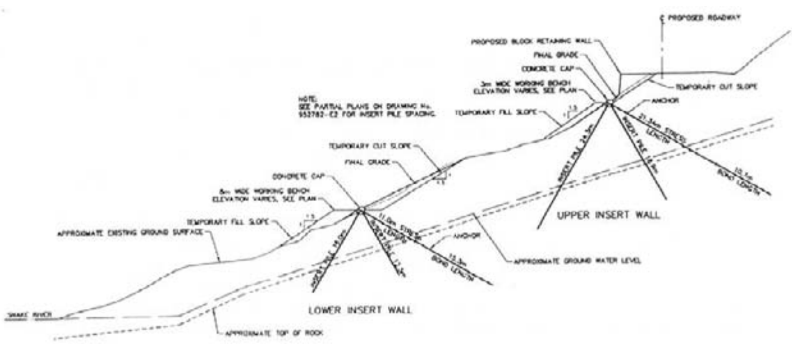

Figure 1: Blue Trail Slide Cross-Section

Table 2 shows the spacings and the design restraint provided by the drilled and grouted micropiles and tieback anchors to resist the landslide forces. A last minute uptick in the required horizontal ground acceleration to 0.11g required large tieback anchor forces for the lower wall to provide a seismic factor of safety of 1.1. The static factor of safety was in excess of 1.5.

Table 2: Design Details for the Blue Trail Slide

Wall	**Length** ft(m)	**Micropile Spacing** ft(m)	**Micropile Resistance** kip/ft(kN/m)	**Tieback Capacities** kip(MN)	**Tieback Spacing** ft(m)
Upper	308 (94)	1.67 (0.51)	51 (744)	350 (1.56)	25 (7.6)
Lower	289 (88)	1.25 (0.38)	57 (832)	630 (2.80)	12.5 (3.8)

The micropiles and tiebacks were installed through 4 foot by 4 foot (1.2 m by 1.2 m) reinforced concrete cap beams. The elements included 475 micropiles, 4-1/2 inch OD (114 mm) varying in length from 40 feet to 80 feet (12 m to 24 m) long. The tieback anchors included 16 anchors for the upper walls, 350 kips (10 strands, 1.6 MN), which were about 105 feet (32 m) long and 23 anchors for the lower wall, 630 kips (18 strands, 2.8 MN), which were about 85 feet (26 m) long. See Figure 2 for a view of the upper wall cap beam during construction. Corrugated plastic sleeves were cast into the beam for the micropile installation. The micropiles were drilled and grouted inside the sleeves, with cement grout bonding the piles to the cap beam. Figure 3 shows the anchors through the lower wall cap beam.

Figure 2: Micropile Wall Cap Beam

Figure 3: Anchors through Bottom Wall

Oso Creek Landslide (160 Kips/LF, 2,335 kN/m): In 2000, heavy rains saturated the hillside and caused Oso Creek in south Orange County, California to swell and undercut the toe of the slope downhill from a roadway called Camino Capistrano and the Orange County Transportation Authority railroad line. As a stop-gap measure, a rip-rap buttress was placed at the toe of the slope to slow movements. However, the buttress was on adjacent property and also encroached on the waterway which would exacerbate flooding in the area. The site consisted of loose fill materials overlying residual weathered Capistrano formation and deeper unweathered Capistrano. The Capistrano formation is a siltstone and mudstone formation that is well-known for frequent landslide tendencies due to its poorly consolidated nature and swell potential. It also frequently exhibits low shear strength along frequent slickensides within the formation.

Inclinometers indicated that the slide was occurring at the contact between the weathered and unweathered Capistrano formations. A design/build solution for a micropile retaining wall, including deep tieback anchors, was awarded to allow construction of the repair within the extremely limited available right-of-way. The micropile system was installed without the use of any cranes, which would have required substantially more access area. See Figure 4 for the limited access that was available for the construction. The drilled and grouted elements were installed through a 5 foot by 6 foot (1.5 m by 2.1 m) reinforced concrete cap beam shown on Figure 5. See the cross-section on Figure 6 for details of the installed system.

Figure 4: Drilling Anchors

Figure 5: Concrete Cap Beam

The construction was carried out over a six-month period in which the nearby roadway, Camino Capistrano, was closed but the adjacent rail line remained open. Initially, the slide was thought to be about 500 feet long, but as construction began and the heavy rains continued, it was discovered that the landslide encompassed almost 640 linear feet.

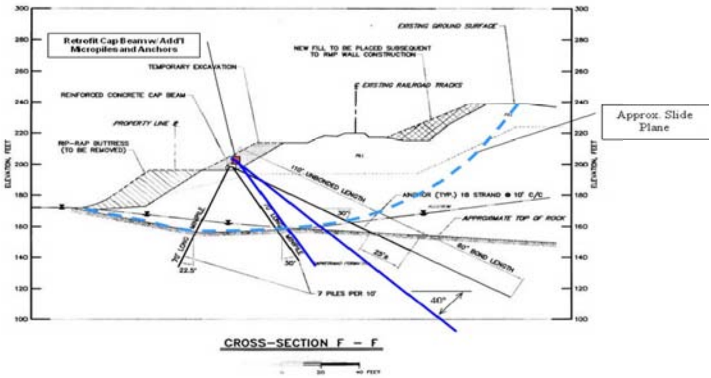

Figure 6: Oso Creek Landslide Repair Cross-Section

Additional micropiles and anchors were required for the final installation, which included 324 micropiles, 5-1/2 inch (140 mm) O.D., which were 70 to 75 feet (21-23 m) long. Sixty 400 kip (1.8 MN) and 550 kip (2.4 MN) 12 to 16 strand tieback anchors, 150 to 170 (46 to 52 m) feet long, constituted the landslide stabilization system. The system was designed for a static factor of safety of 1.5 and a seismic factor of safety of 1.1 for a design earthquake with a 0.15g horizontal acceleration.

Ameristar Casino I (130 Kips/LF, 1,900 kN/m): This project, completed in 1993, was located near the intersection of Interstate 20 and the Mississippi River in Vicksburg, Mississippi. Two retaining walls were required to support the existing bluff while providing grade separation for an access road (Wall A) to the Casino and for the upper parking lot (Wall B). Although a landslide had not occurred at the site, there is a history of landslide activity in the area along with the high plasticity soil profile created the potential for mass movements. See the Figure 7 plan view sketch for the location of the walls on the site and Figure 8 for the cross-section at Wall B. The walls consisted of driven steel soldier piles and treated wood lagging with steeply inclined tieback anchors. The surficial soils included a thick loess layer underlain by high plasticity clay terrace deposits overlying a relatively thin limestone shelf at depth. The limestone was utilized as a major part of the project to bear the soldier piles upon and also to found the tieback anchors within. Under the limestone was a weaker marl material consisting of hard silty clays.

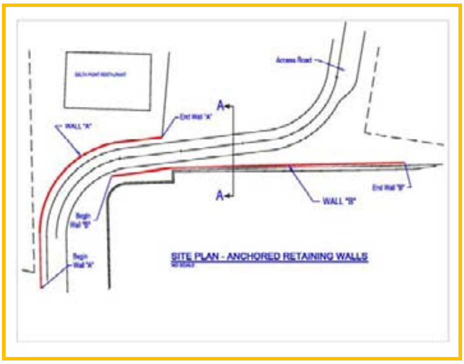

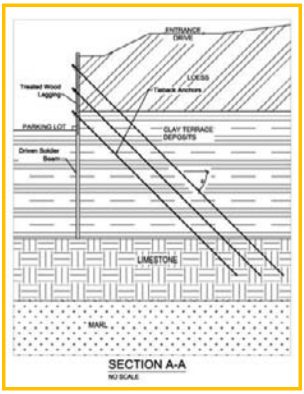

Figure 7: Plan View of Site **Figure 8: Cross-Section at Wall B**

The anchors were drilled into the underlying limestone at a 45 degree angle and were 480 kip (14 strands, 2.1 MN). Lengths varied from 100 ft (30 m) for the top row to 75 ft (23 m) for the bottom row. Huge wale beams as shown on Figure 9 were used to transfer the tieback loads to the soldier piles as shown on the photograph. Bearing the soldier piles on the limestone bedrock provided the necessary resistance to the large vertical component of load from the tiebacks. In addition, the soldier piles penetrated theoretical failure planes through the high plasticity clay terrace deposits, and the reinforcing effect of the piles passing through those planes was analyzed and relied upon for the overall factor of safety for the project, which was 1.3. Many questions were raised about the use of treated wood lagging as the facing as shown on Figure 10. The lagging is now approaching 20 years in age and has been maintained by pressure washing and is still in excellent condition. The system was designed for a global factor of safety (static) of 1.3.

Figure 9: Anchors with Large Wales

Figure 10: Wall B Retaining Wall

Ameristar Casino II (130 Kips/LF, 1,900 kN/m): A very large landslide was documented at the north end of the Casino and was repaired in 2005-2006 using tieback anchors. The landslide encompassed a large mechanically stabilized earth (MSE) wall. The MSE wall was incorporated into the fix as a back form for a cast in place concrete wall that included two rows of 220 feet (67 m) long tieback anchors drilled at very shallow angles of about 10 degrees. The extreme length of the anchors was required so the bond zones would be founded behind the failure plane of the landslide, which had been delineated by inclinometers. The limestone shelf used advantageously in the previous project in 1993 could not be used since this wall was at a much lower elevation. Therefore, the 385 kip (11 strands, 1.72 MN) anchors were installed within a hard marl layer. The anchors were spaced at 6 feet (2 m) horizontally and 15 feet (4.6 m) vertically. Since softer soils were located under the marl, an extremely shallow angle of installation was adopted for the tiebacks to ensure they were founded in the hard marl.

The wall was 550 feet (168 m) long. Large steel soldier piles were set and concreted into drilled holes on 12 feet (3.6 m) spacings and reinforced concrete panels were cast between the beams. Four block-outs were left for the tieback anchors in each panel. The anchors were drilled and grouted and then stressed against the new wall. Figure 11 shows the wall construction including the soldier pile placement and Figure 12 shows the anchor locations. The system was designed for an overall global factor of safety of 1.3.

Figure 11:Placing Soldier Piles for Wall

Figure 12:Anchors Through New Wall

Mission Viejo Mall (102 Kips/LF, 1,490 kN/m): In 1990, a huge landslide occurred at the Mission Viejo Mall in Orange County, California. The slide was located between the mall and Interstate 5 in a previously existing 2 (H):1 (V) slope that had been reworked extensively during the construction of both the highway and the mall. The slide mass was about 350 feet (107 m) long and 90 feet (27 m) high. Emergency measures were implemented, including removing 8,000 cubic yards (6,115 cubic meters) of soil from the site, the installation of deep dewatering drains, and the closing of the nearby Interstate ramp. A permanent fix of a tieback supported drilled shaft retaining wall was selected to stabilize the slope. See the Figure 13 for a plan view of the project.

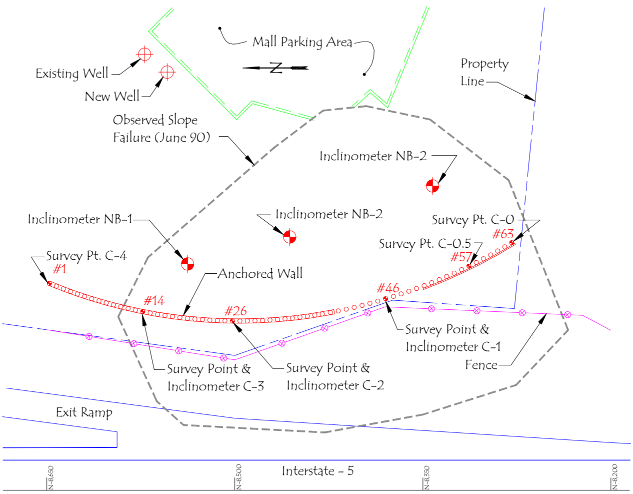

Figure 13: Mission Viejo Slide Plan View

The slope consisted of clay fill overlying weathered Capistrano formation and unweathered Capistrano formation materials. Numerous remolded clay seams were noted in the weathered zone. Bedding planes in the unweathered zone were noted to be locally weak and to be at an unfavorable angle to the highway. The Capistrano formation is a gray to black siltstone and clayey siltstone with numerous fractures, joints and frequent slickensides. The Capistrano formation typically exhibits swelling and collapse when drilled into.

The retaining wall consisted of 42 inch (1.1m) diameter reinforced concrete drilled shafts on 6 ft (1.8 m) center-to-center distances. Three rows of tieback anchors were drilled into the unweathered Capistrano formation, past the failure plane located by inclinometers. Anchor installation angles varied to separate the bond zones. The anchors were 250 kips (8 strands, 1.1 MN) each and varied from 95 ft (29 m) to 170 ft (52 m) in length. Drilling within the Capistrano formation created several challenges due to the slaking and collapsing nature of the rock. Foam injection was finally selected as the best method to keep the drill holes open during tieback installation. See the cross-section in Figure 14 for details of the installation and Figure 15 for a photo of the wall during construction (Wolosick, 1998). The design factor of safety (static) was 1.5, including assumed elevated groundwater levels. The seismic factor of safety including a magnitude 7.0 earthquake with a horizontal ground acceleration of 0.32 was 1.1.

Figure 14: Mission Viejo Slide Cross- Section

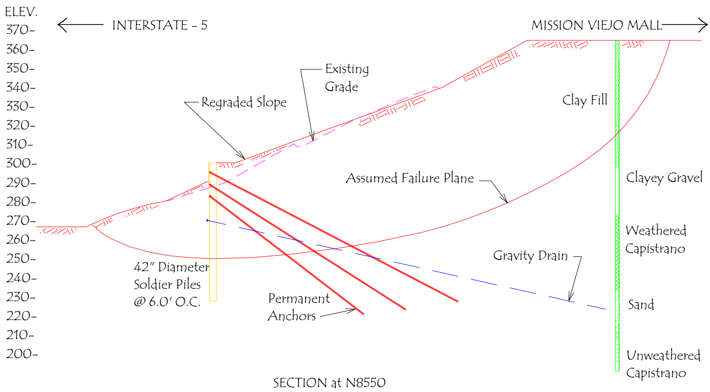

Figure 15: Mission Viejo Wall Prior to Concrete Facing Installation

Signal Hill Slide, US 61S (100 Kips/LF, 1,460 kN/m): In 2006, after the previous use of an earthen berm failed to stop movements, the Mississippi Department of Transportation decided to use deep tieback anchors to repair this huge landslide, which encompassed 20 acres (8 hectares). They received bids from prequalified contractors for a design/build tieback anchor installation after they specified the amount of force and the number of rows of anchors required. Five rows of anchors were specified due to the extremely flat nature of the landslide. However, the number of anchors and the anchor reaction system was left up to the builder. It was also specified that the anchors be bonded into a deep limestone formation. The slide threatened the four-lane highway, and forced the two southbound lanes to be closed. Traffic was rerouted onto the northbound lanes, with one lane utilized in each direction (Figure 17). The soils on site included loess fill, loess and terrace deposits overlying stratified deposits of sands and high plasticity clays. Analyses indicated that the multiple row installation was required for stabilization. If anchors had been placed only on the high side of the slide near US 61, the downhill portion of the landslide would have continued to move. Figure 16 shows the plan view layout of the site.

The anchors were installed in five rows and ranged from 170 feet (52 m) to 265 feet (81 m) long. The anchors were installed at an angle of 45 degrees from horizontal to reduce length but also provide a reasonable horizontal reaction. The presence of the previously installed earthen berm, which was about 20 feet (6 m) thick, required longer anchor lengths since the berm had to be drilled through. The anchor loadings were typically 466 kips (2.1 MN) each. Large pre-cast concrete reaction blocks, typically 13.7 feet (4.2 m) square, were pre-cast on site and utilized to transfer the loads from the tiebacks to the ground. A total of 253 anchors were installed in two phases due to right-of-way constraints. Figure 18 shows the drilling for the tiebacks.

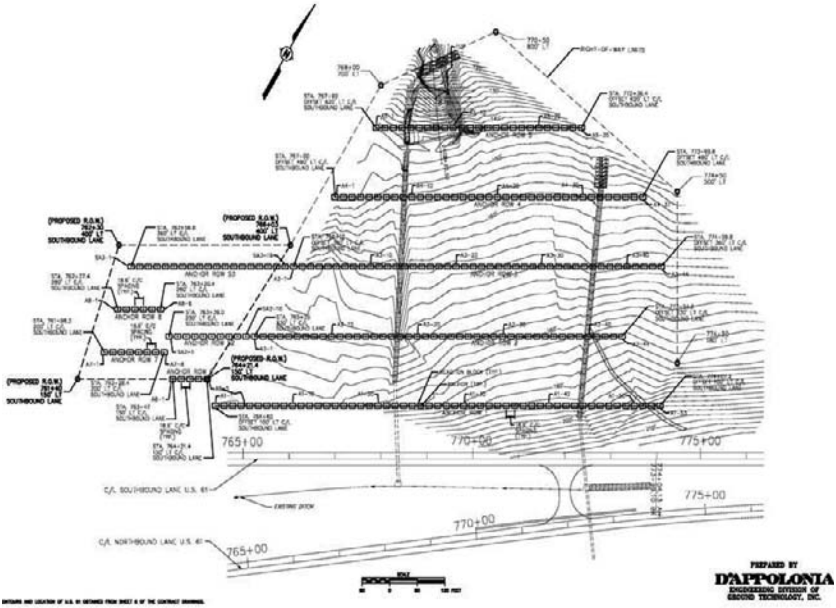

Figure 16: Plan View – Signal Hill Slide, US 61S Landslide Repair

The tieback anchors were highly effective in stabilizing the slide. As part of the project, highway drainage was also rerouted to bypass the site. The work was accomplished over the hot summer months of 2006. The anchors and concrete reaction blocks were completely buried by earth moving operations, and the system is completely underground, invisible to the traveling public. The system was designed for a factor of safety of 1.2.

Figure 17: Roadway Damage at Slide

Figure 18: Drilling Tieback Anchor

Lexington Apartments (72 Kips/LF (1,050 kN/m): In late February of 2003, after a very heavy rain, the 2(H):1(V) to 4(H):1(H) cut-slope behind three of the large units of the Lexington apartments began to move toward the buildings, which each contained 24 units. The apartments were evacuated prior to the slide mass ramming into the buildings as shown on Figure 19. Geotechnical exploration work was immediately initiated and a specialty contractor was hired to become part of the team to develop a repair. Inclinometers sheared shortly after installation, but gave enough information to show multiple failure surfaces within residual clay underlying wet colluvium and a deep failure surface just above the limestone bedrock (Figure 20). An emergency plan to place a temporary cantilevered soldier beam retaining wall, socketed into limestone bedrock was developed and implemented.

Figure 19: Landslide Rams Apartment Building

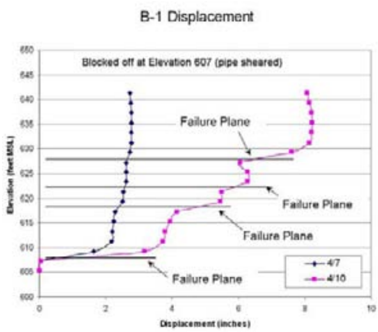

Figure 20: Inclinometer Results

As the design was developed, it was decided to keep the soldier pile wall as a permanent feature by adding tieback anchors and steel wale beams as shown on Figure 21. The wall was augmented with two additional rows of tiebacks uphill, installed through 10 feet by 10 feet (3 m by 3 m) pre-cast concrete reaction blocks (Figure 22). A temporary shot-rock berm was placed in front of the soldier pile wall to help provide stability and also provide access for the drill rig to install tiebacks into the limestone bedrock. The soldier piles and tieback anchors were bonded into the limestone bedrock.

Figure 21: Soldier Pile/Tieback Wall

Figure 22: Row of Anchored Blocks

The slope stabilization system was designed to provide a factor of safety of 1.3. A total of 80 tieback anchors were installed at a 30 degree angle, including 28 in the upper row and 29 in the middle row. Twenty three tiebacks were installed through the soldier pile wall. The anchor loadings were 300 kips (9 strands, 1.3 MN). Anchor lengths varied from 85 to 110 feet (26 to 34 m). See the cross-section on Figure 23 for an illustration of the system.

Other ancillary features of the repair included several rows of subsurface French drains and several tiers of surface ditches to divert water around the repaired area. In addition, the surface drainage in front of the soldier pile wall was improved.

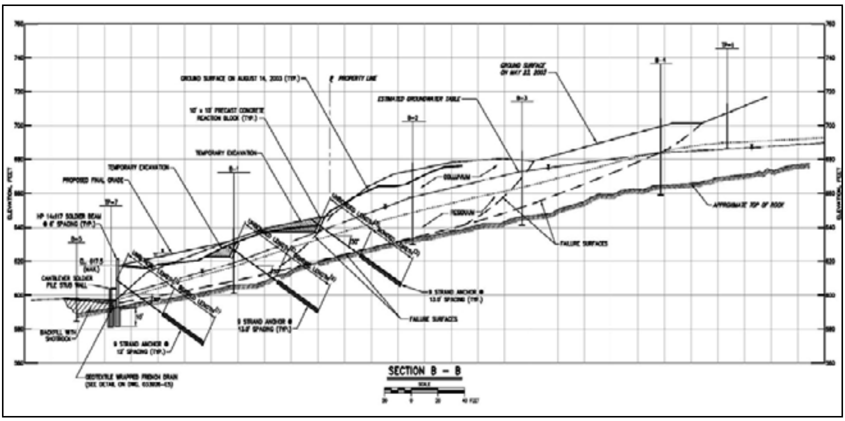

Figure 23: Lexington Apartments Landslide Repair Cross-Section

The repair encountered several challenges, including a rapidly moving slide mass and very wet conditions including one week where 10 inches (25 cm) of rain was recorded. Thirty-two thousand (32,000) cubic yards (24,466 cubic meters) of slide material were hauled off site. (Marasa, 2007).

Conclusions: Although drilled and grouted elements such as tieback anchors and micropiles are sometimes considered expensive by some engineers and owners, they often offer the best solution to repair major landslides. Earthen berms are often misapplied in these situations and can be ineffective if sufficient right-of-way or slide geometry preclude placement of the berm at an optimum location to provide resisting forces to stabilize the slide mass. When the berm solution fails, significant money is wasted when the drilled solution is implemented later. Horizontal drains can be an effective solution. However, particularly in warm climates, clogging with silts or bacteria can render drains ineffective in relatively short time frames. Drilled and grouted elements can be designed to resist large hydrostatic forces. These systems have been used very effectively in many varied geologic settings around the US to stabilize very large landslides. The design team working on these projects selected design factor of safety values that matched the needs of the project, considering technical concerns and budget constraints. The factors of safety for each project are shown on Table 3.

Table 3: Summary of Factors of Safety

Project	Static Factor of Safety	Seismic Factor of Safety
Blue Trail Slide	>1.5	1.1
Oso Creek Slide	1.5	1.1
Ameristar Casino I	1.3	-
Ameristar Casino II	1.3	-
Mission Viejo Mall	1.5	1.1
Signal Hill Slide, US 61S	1.2	-
Lexington Apartments	1.3	-

Acknowledgements: Construction project managers for the projects were Ron Triplett, Steve Buckner, Alan Ringen, Denny Glaser, and Mike Terry. Many of the projects were designed by Brad Campbell, formerly of D'Appolonia and now with Burns Cooley Dennis. The Ameristar Casino I project and the Mission Viejo Mall Slide were built by Nicholson Construction Company. The other projects were built by Hayward Baker Inc. Eddie Templeton of Burns Cooley Dennis performed the stability analyses at the Ameristar Casino I and the Signal Hill Slide, US 61S projects. Sandy Triplett helped to prepare this paper.

References:

Marasa, Michael J., Wolosick, J.R., and Campbell, B.D., "Real Time Response to the Landslide at the Lexington Apartments," Proceedings, 1st North American Landslide Conference, Vail, Colorado, AEG Special Publication 23, October, 2007, Association of Environmental & Engineering Geologists, CD-ROM.

Turner, John, Robert Hasenkamp, John Wolosick, "Micropile and Tieback Reinforced Walls for Landslide Stabilization, Snake River Canyon, Wyoming," *Proceedings*, 49th Highway Geology Symposium, Prescott, AZ, September, 1998, pp. 156-168.

Wolosick, J.R., P.B. Groneck, S.L. Pearlman, "Landslide Repair at Mission Viejo Mall," *Proceedings*, Ohio River Valley Soil Seminar, Louisville, KY, October, 1998, 12 pages.

PREHISTORIC LANDSLIDE STABILIZATION WITH GROUND ANCHORS AND SURFACE REACTION PADS

Edward P. Voytko[1], P.E., M. ASCE, Daniel D. Uranowski[2], P.E., M. ASCE, and Joseph W. Premozic[3], P.E., M. ASCE

[1] Principal Engineer, D'Appolonia Engineering Division of Ground Technology, Inc., 275 Center Road, Monroeville, PA 15146, epvoytko@dappolonia.com
[2] Chief Engineer - Foundation Division, Brayman Construction Corporation, 1000 John Roebling Way, Saxonburg, PA 16056, d_uranowski@braymanconstruction.com
[3] Civil Engineer, US Army Corps of Engineers, Pittsburgh District, 2200 William S. Moorhead Federal Building - 1000 Liberty Avenue, Pittsburgh, PA 15222, joseph.w.premozic@usace.army.mil

ABSTRACT

Corfu Street is perched on an isolated, lenticular plateau midway up the south valley wall of the Ohio River in the West End neighborhood of the City of Pittsburgh. This plateau represents the head of a prehistoric rockslide that likely occurred following a period of glacial meltwater erosion during the Pleistocene Epoch. The plateau comprises the surface of a 40-foot thick layer of landslide debris (soil and rock) resting on a mildly sloping claystone rock ledge. A steep, 150-foot high rock slope drops from this plateau to an active mainline railroad track below.

Following a year-long period of above-average rainfall, the landslide, involving more than 120,000 cubic yards of accumulated soil and rock debris, was re-activated by an apparent significant rise in the groundwater table and resulting saturation of the slide mass. This paper describes the geotechnical evaluation and monitoring of the landslide and the design and construction of a system of ground anchors and surface reaction pads installed to stabilize the landslide.

INTRODUCTION

Recent advances in earth retention have included the development of measures that reduce reliance on conventional structural systems, and employ earth reinforcements such as soil nails, geosynthetics and ground anchors, to retain the earth without extensive use of heavy structural facings and intermediate supports. The authors were responsible for the design and construction of measures to stabilize a massive, ancient landslide using a system of ground anchors to distribute support to the landslide mass through a series of relatively small, reinforced concrete reaction pads combined with regrading of the slope. This paper describes the geotechnical exploration and instrumentation used to characterize the slope failure mechanism and geometry, engineering design of the stabilization system, and the manner in which the construction was performed and sequenced to achieve stabilization without excessive and/or catastrophic slope movements.

BACKGROUND

The topographic bench supporting Corfu Street and adjacent properties encompasses the surface of a 40-foot thick mass of accumulated soil and rock debris overlying a very mildly sloping rock bench. This debris mass has been described (Hamel, 1998) as the remnants of a prehistoric landslide that occurred along a weak bedrock layer, during a time of rapid valley erosion that ultimately led to development of the current Ohio River valley. Hamel portrays the inferred post-landslide condition as a nearly flat top-of-intact rock surface beneath the “bench”, covered by an accumulation of transported/tilted rock with sloped bedding planes. The ancient slide mass had remained marginally stable since at least 1890, when residential development on the plateau was initiated. The authors hypothesized that saturation of the slide mass by a year of heavy rainfall culminating in Hurricane Ivan reactivated the slide in September 2004.

Prior to September 2004, the outslope of the debris mass was very steep (1 Horizontal to 1 Vertical), and marginally vegetated with brush and trees. Reactivation of the landslide initially caused gradual displacement of soil and boulders from the steep debris slope face and over the rock slope onto the railroad tracks below, ultimately disrupting the roadway and damaging the adjacent residential properties and homes. Although the homes were ultimately demolished and the roadway was closed, stabilization of the landslide was necessary to abate the threat it posed to critical rail traffic below.

A geotechnical exploration of the site confirmed the composition of the slide debris mass and geometry of the reactivated landslide. The exploration included 12 test borings and installation of slope inclinometers and vibrating wire piezometers to characterize soil and rock conditions, ground water levels and the of the landslide mass geometry. Whereas the bedrock units comprising the hillside between Corfu Street and the railroad tracks below consist of relatively horizontally bedded alternating strata of sedimentary rock (primarily shale, sandstone, claystone and limestone), thick beds of sandstone, shale and limestone tilted more than 30 degrees from horizontal were encountered above the bedrock surface. Inclinometers identified the base of the sliding mass as the surface of a claystone to clayey shale layer encountered at depths of 25 to 40 feet below the ground surface, and sloping mildly toward the slope face at about 5 to 6 degrees. The inclinometers indicated a rate of displacement along this shear plane of at least 0.3 inches per year.

IDENTIFICATION OF VIABLE STABILIZATION ALTERNATIVES

The authors concluded that the landslide involved the movement of a large mass of soil and rock over a weak, mildly sloping bedrock unit under the influence of elevated ground water conditions. Efforts to identify viable alternatives to stabilize the landslide, therefore, concentrated on reducing ground water levels and debris mass saturation, reducing driving forces (debris mass volume/weight) and increasing shear resistance to sliding.

Although a system of drains was initially designed in an effort to reduce ground water levels, the constructability and effectiveness of the drains were considered doubtful, and the drain system was abandoned due to the expected low permeability of the clay soil matrix, the likelihood that large boulders and rock slabs in the slide mass would hinder excavation of deep trenches for drain installation, and the probability that drain construction would interfere with structural or earthworks measures that might ultimately be implemented to effect a more positive improvement in slope stability.

Large scale excavation of the slide debris mass was considered as a possible means to reduce driving forces and eliminate the steep debris outslope and protruding boulders. However, site access considerations and the depth of excavation that would be necessary eliminated this as a potential solution The geometry of the slide shear plane presented a particularly difficult challenge to a bulk excavation approach to landslide stabilization, as the slide material of most immediate concern was the material comprising the steep face of the debris mass. However, this material was positioned directly above the toe of the sliding mass and over the flattest portion of the slide plane. Accordingly, this material, although locally unstable due to its steep face, exerted a vertical normal force on the slide plane that provided a significant net stabilizing effect with respect to global stability. As a result, excavation of material from the slope face would have actually caused more rapid destabilization of the slide mass unless a significant additional volume of material was removed from the "driving" portion of the mass (i.e., from the rear portion of the bench) to compensate. This effect was observed when an increased rate of movement of the slide mass was detected when excavations were made near the slope face to install the stabilization measures ultimately selected. As a result, inclusion of some form of structural slope stabilization was deemed necessary. To effectively stabilize the landslide, support elements would have to extend beneath the slide plane into bedrock. Two alternatives systems were considered:

- A steel soldier beam and reinforced concrete lagging retaining wall with soldier beams and ground anchors extending into bedrock, and
- A series of precast reinforced concrete reaction pads with ground anchors extending into bedrock

Either of these systems would be capable of achieving both local stabilization of the steep debris outslope and global stabilization of the entire slide mass. These two alternatives were evaluated further based on consideration of technical feasibility, constructability, and estimated construction cost. The anchored reaction pad system was selected for final design and implementation for the following reasons:

- The system could be installed using relatively light and mobile ground anchor drills, and there would be no need to mobilize large, heavy (i.e., caisson) rigs to the site over winding, narrow residential streets of questionable capacity. Also, this alternative would not require heavy equipment to operate on the surface of the unstable outer edge of the sliding mass,

- Materials required for construction (anchors and reaction pads) could be more easily delivered to the site through the residential streets as compared to long (40± feet) steel soldier beams,
- Installation of the reaction pads and anchors would likely be easier, quicker and would result in somewhat less ground disturbance than installation of soldier beams and anchors through the boulder-filled slide mass,
- The system would provide greater flexibility in regard to the sequence of construction, and would permit more expedient application of anchor forces in specific areas to obtain almost immediate support,
- The time frame for fabrication of construction materials (anchors and reaction pads) would be significantly shorter than for a conventional anchored soldier beam and lagging wall (soldier beams, anchors, and facing panels), and
- The estimated construction cost of the reaction pad system was less than one-third of the estimated construction cost of the soldier beam and lagging wall.

DESIGN OF ANCHORED REACTION PAD SYSTEM

A typical cross-section of the 500-foot long, unstable hillside depicting the anchored reaction pad system is shown in Figure 1. Stabilization of the steep debris face was accomplished by regrading the slope to a finished 2 to 2.5 horizontal to 1 vertical slope. Global stabilization of the landslide mass was accomplished by installing a system of 60, 100-foot long, 350 kip, 10-strand rock anchors bonded into bedrock below the slide plane. The anchors were installed in two rows along benches cut into the face of the slope. The anchors were inclined at about 30 degrees from horizontal, and with a spacing of about 16 feet horizontally and 10 feet vertically to distribute support throughout the limits of the slide mass. Anchors were corrosion-protected corresponding to the recommendations of the Post-Tensioning Institute (PTI, 2004) for Class I Protection. The anchor forces were transmitted to the face of the slope by means of 10-foot by 10-foot, approximately 2-foot thick, precast, reinforced concrete reaction pads installed on the slope face.

Stability analyses for evaluation of the landslide and design of stabilization measures were performed using the slope stability program STABL/G (GEOSOFT, 1994). STABL/G is a computer program developed at Purdue University for the general solution of slope stability problems by two-dimensional limiting equilibrium methods. Analysis of the global stability of the landslide mass was performed using the simplified Janbu method, which permitted modeling of the irregular (non-circular) failure plane identified by the slope inclinometer readings, and the application of anchor forces, which are input as tieback loads that are distributed through the retained earth mass and onto the failure surface as distributed normal and tangential forces along the slide plane. Analysis of the local stability of the steep face of the landslide mass was evaluated as an infinite slope.

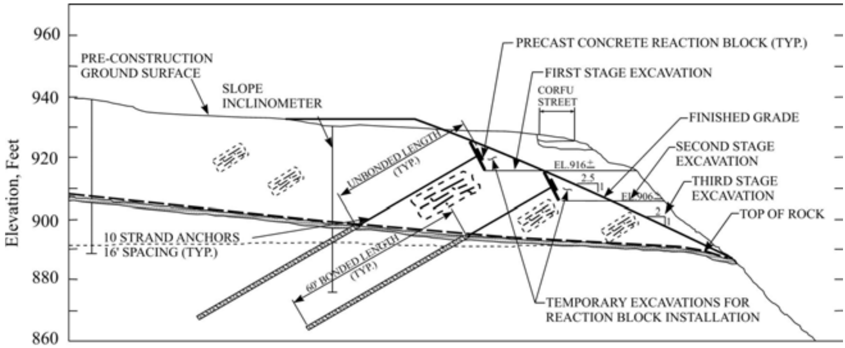

FIG. 1 Typical Section of Slope Stabilization Measures

The surface and slide plane geometry, subsurface soil and rock conditions and ground water levels considered in the analyses were based on the results of the test boring program, site topographic survey, visual observations and the results of instrumentation (slope inclinometer and vibrating wire piezometer) monitoring. Soil and slide plane shear strengths were estimated based on back-analysis of the existing slope conditions assuming a factor of safety of 1.0 against both global failure and failure of the slope face. Relative to the residual, zero-cohesion shear strength along the base of the failure surface, a previous assessment of the landslide (Hamel, 1998), based on less site specific information on the slide plane geometry and prevailing groundwater conditions, had suggested a possible range of 8 to 22 degrees. The back-analysis performed as part of the current study indicated a zero-cohesion shear strength of 13 degrees along the failure surface. Back-analysis of the face of the slide mass indicated a minimum, zero-cohesion shear strength of the soil and rock mass above the slide plane of approximately 34 to 35 degrees.

The stabilization measures (anchor forces and surface regrading) were designed to increase the factor of safety for both global and local slope failure to a minimum of 1.3 for the final slope, including a 2-foot surface surcharge over the site. Design anchor bond lengths were estimated based on assumed ultimate grout to rock bond values of 60 psi for medium hard siltstone and shale and 90 psi for medium hard sandstone, and applying a factor of safety of 3.0. Allowable anchor capacities were to be subsequently established by field load testing of production anchors. Since some excavation would be required on the face of the slope to install anchors and reaction pads, and because the soil comprising the slope face actually provided a vertical stabilizing surcharge load on the relatively flat slide plane, the factor of safety with respect to global stability was expected to drop below 1.0 in localized areas during excavation and prior to anchor installation and stressing. For this reason, the length of unanchored excavation along the slope face for each level of anchor installation was limited to a maximum of 170 feet at any time.

CONSTRUCTION AND PERFORMANCE

Following equipment mobilization and site preparation, construction operations were initiated in early February 2007 with first stage excavation for installation of the upper row of anchors, beginning at the north end of the site. Excavated soil and rock from the slide was generally hauled off-site for disposal, whereas large sandstone boulders were retained on site for further mechanical breakage prior to removal. Drilling for anchor installation started on March 5, again beginning at the north end of the site. Anchor holes were advanced with a Casagrande M9-1 drill using a roller bit and water to flush cuttings from the holes. The anchor holes were temporarily cased with 9-5/8 inch diameter steel casing. Typically, the construction was sequenced such that excavation was completed in stages which allowed 4 anchor pad locations to be prepared at a time. Drilling and installation of anchors followed shortly thereafter. Anchor drilling and installation typically proceeded at alternating (every other) anchors so as to limit excessive, local disturbance of the slide mass and failure plane due to drilling vibrations and water injection. Typically, the reaction pad was set and the anchor tested and locked off at each anchor location within one week after the anchor was drilled.

Anchor testing was performed and the results evaluated in accordance with the recommendations of the Post-Tensioning Institute (PTI, 2004). Each anchor was subjected to a single cycle proof test to 133 percent of the maximum design load of 348 kips before being locked off at the design load. Two of the anchors were subjected to four cycle performance tests to 133 percent of the design load prior to lock-off. All 60 anchors met the load-deformation acceptance criteria. Additionally, anchor grout cube samples were tested throughout the project to verify conformance of grout strengths to the required minimum compressive strength of 4,000 psi.

In conjunction with installation of the anchored reaction pad stabilization system, the surface of the outslope was regraded to reduce soil and boulder falls from the slope face onto the railroad tracks below. Localized areas of seepage encountered during the regrading were covered with crushed rock buttresses and drains constructed partially using rock from large boulders that were excavated from the face of the slide mass and processed on site for re-use. The finished slope was vegetated and the concrete reaction pads were covered such that they lie beneath the finished ground surface to provide an aesthetic, natural appearance.

As suspected, excavation and ground disturbance during construction resulted in a temporary increase in the rate of movement of the landslide mass. As depicted in Figure 2, slope inclinometers immediately above localized areas of excavation and anchor drilling for the upper level of anchors exhibited a rapid increase in movement rate along the slide plane (rock surface) almost immediately in response to disturbance. The inclinometer data represented in Figure 2 are for an inclinometer installed near the north end of the slide. Coincident with the initiation of anchor drilling on March 5, 2007, the rate of slope movement below the inclinometer accelerated to almost 1 inch per week. As the anchors in this area were locked off over the ensuing 2 week period, the rate of movement slowed almost immediately to less than 1/10 inch per week, and ceased completely within approximately 3 weeks. Approximately 1/10 inch of additional movement was experienced in this area when the second stage of excavation and lower level of anchors were installed approximately one month later, but the movement ceased when the lower level anchors were stressed and locked off. Inclinometer monitoring over a 14-month period following the completion of construction in July 2007 indicated no appreciable additional movement.

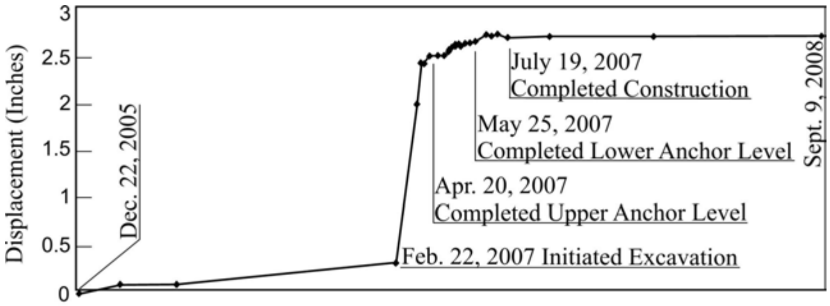

FIG. 2 Typical Inclinometer Behavior Over Time
Horizontal Movement at Bedrock Surface

CONCLUSIONS

A system of rock anchors and reinforced concrete reaction pads provided an effective and economical alternative to a conventional anchor soldier beam and lagging retaining wall for stabilization of a massive landslide in a relatively inaccessible urban area above an active railroad main line. The anchored reaction pad system offered a number of advantages over the more conventional retaining wall system:

- More prompt initiation and completion of construction due to less extensive fabrication requirements (e.g., for soldier beams), elimination of delays during soldier beam installation, and less vulnerability to site access restrictions,
- More rapid application of stabilizing forces to the landslide due to the relative independence of individual anchors afforded by reaction pads as compared to an integrated retaining wall beam and lagging facing system,
- Greater flexibility in the location and sequence of application of stabilizing anchor forces in response to slope movements detected during construction,
- Substantially reduced construction cost (estimated at one-third the cost of a more conventional soldier beam and lagging retaining wall), and
- Ability to easily produce a natural, aesthetic finished slope appearance unobstructed by structural elements, such as beams and facing panels.

Photographs of the slope before, during and after stabilization efforts are shown in Figure 3.

a. Preconstruction

b. Construction

c. Finished Slope

FIG. 3 Photographs – Progression of Landslide Repair

REFERENCES

GEOSOFT, Inc., (1994), "STABL/G, Slope Stability Analysis, Simplified Janbu, Simplified Bishop or Spencer's Method of Slices – An Engineering Analysis Program for Geotechnical Engineers," Orange, CA

Hamel, James V., (1998), "Mechanism of Pleistocene Rock Slides Near Pittsburgh, Pennsylvania," *International Journal of Rock Mechanics & Mining Sciences,* (Vol. 35, Issues. 4-5, Paper No. 032), Elsevier Science, Ltd., Amsterdam.

Post-Tensioning Institute (PTI), (2004), "Recommendations for Prestressed Rock and Soil Anchors," (fourth Edition), Phoenix, AZ.

PERMANENT SLOPE PROTECTION IN HIGHLY SEISMIC AND LANDSLIDE-PRONE AREA USING MULTI-LEVEL ANCHORED ALIGNED PILE WALL

Dr. Ing. Armando Cazzola[1] **Geronimo T. Reyes M. Eng'g**[2]

[1] Dr. Ing. Armando Cazzola, President – Foundation Specialists, Inc., Tel. no. (+63-2) 817-68-26; Fax no. (+63-2) 816-34-91; email dr.cazzola@foundation-specialists.com.
[2] Geronimo T. Reyes, M. Eng'g., D. Sc., – Philippine Technical Consultants, Inc., Tel. no. (+63-2) 812-70-32, Fax no. (+63-2) 813-71-24; email dr.reyes@philtech-engineers.com.

ABSTRACT

This paper presents the innovative analysis, design and construction of permanent slope protection in highly seismic and landslide prone areas.

The project scope of work consisted of creating a stable, large horizontal bench along a steep and long slope at the toe of an existing industrial complex, suitable for the construction site of a new industrial building complex 50 meters high. Several high slopes had to be developed, one after the other, and permanently stabilized to generate a safe and stable building site.

Originally, the contract called for an Anchored Diaphragm Wall (ADW) to support permanently the vertical slope. However, during an early stage of construction, discrepancies on the Owner-supplied Project Site Soil and Geological Conditions were discovered that necessitated design amendment. Anchored Aligned Pile Wall (AAPW) with Pervious Piles (PP) in between to serve as vertical draining elements was finally adopted to retain the 18-meter high vertical slope, thus allowing the construction of the new building complex on the slope, free from problems of high earth and hydrostatic pressures and external surcharges.

The ultimate purpose of the project was to provide local and global stability of the whole building complex during construction and ultimate service that required a design horizontal ground acceleration of 0.4g with performance objective of Immediate Occupancy after the earthquake.

This paper describes the design concept of the retaining wall systems, the problems encountered due to "change of site conditions", and the solutions designed and developed to cope with the actual site conditions.

1. INTRODUCTION

The new five-story building complex, 50 meters high, is located in a prominent industrial park in Baguio City, Philippines, which is within the tropical typhoon path and classified as a high seismic and landslide prone area. The mat foundations of the new building were constructed at the toe of a 32-meter high slope, with a preexisting 4-story industrial building complex and an access road located on the top of the slope.

Contractual requirements of the slope excavation project are to keep the existing access road open to traffic and permit no stress concentration, soil settlement or movement, or soil erosion capable of affecting the structural stability of the pre-existing building foundations. Hence, in order to excavate to the required depth of the mat foundation of the new industrial building, the Foundation Contractor had to address major challenges to laterally support the excavated or cut slopes.

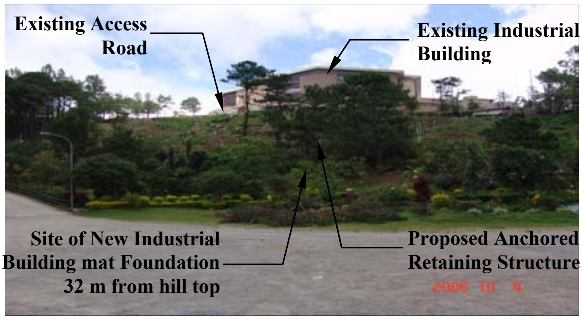

Figure 1. Project site before construction

2. SITE TOPOGRAPHY AND SUBSOIL CONDITIONS

The project site is on a slope of a hill, initially covered by thick vegetation shown in Figure 1. The subsoil condition was explored by the Project Owner Soil Contractor with twelve (12) boreholes drilled at maximum depth of 48 meters from top of the hill. The borehole logs located near the proposed retaining wall are shown in Figure 2. The soil investigation report shows a predominantly uniform mass of stiff to very stiff clay of low to medium plasticity and states that no water table was observed in any boreholes. The soil report of record was imposed as the basis for the design of the Anchored Retaining Wall System.

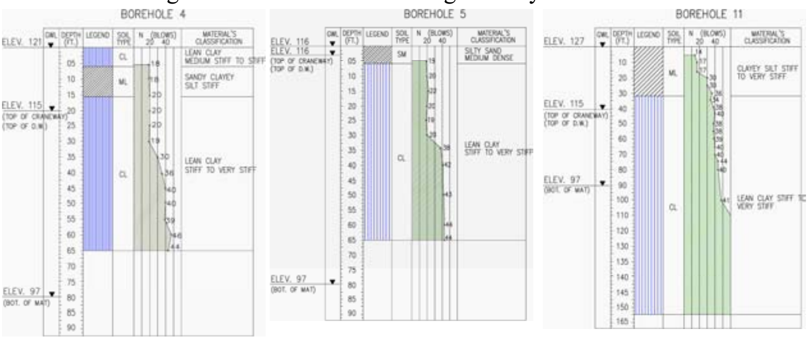

Figure 2. Boring Logs Located Along the Proposed Retaining Structure

3. DESIGN AND BUILT REQUIREMENTS

The project involves significant challenges for design and construct of permanent Anchored Retaining Wall Structures (ARWS) on the slope. The following are the general design requirements of the ARWS:

1.) Construction of permanent retaining structure to support the thirty two (32) meters deep excavation to allow the construction of a new building complex on the slope, free from problems of high earth and hydrostatic pressures and external surcharges.
2.) The new Industrial Building to be constructed simultaneously with the construction of Retaining Wall System.
3.) Design in accordance with NSCP (National Structural Code of the Philippines) 5th edition and applicable codes and specifications provided by the Project Owner.
4.) Performance Objective "Immediate Occupancy".
5.) Seismic Zone 4, Pseudo-ground horizontal acceleration value with 10 percent probability of exceedance in 50 years shall be assumed as 0.4g x 1.5 = 0.6g. The factor 1.5 came from Performance Objective "Immediate Occupancy" Owner's Specification (see Reference).
6.) Local and global slope stability analysis considering various load cases such as soil and water pressure, overburden pressure, surcharges and seismic forces.
7.) Structural and geotechnical design analysis of Anchored Retaining Wall System for various stages of construction to define wall stresses and deformations.
8.) Analyses of excavation that provide information on the ground movements outside of and inside the excavation.

4. DESIGN CONCEPT

The original, contract documents called for the design and construction of a diaphragm wall to support a 25-meter high vertical slope with ground anchors and another protection system for the upper 7-meter slope, in order to permit soil excavation to make way for the construction of a new industrial building on the slope of the hill. However, the Owner gave the contractors the option to propose the most effective and economical scheme, provided that the alternative proposal be in accordance with the project design requirements and criteria.

The project was awarded to Foundation Specialists, Inc. after several schemes and options were studied to obtain optimum design in terms of cost, safety and time schedule. The original awarded scheme was described as follows;

1.) Improvement of sloping ground at 60 degrees inclination from top of the hill down to 14 meters below and construction of 10-meter wide service road (spanning between the toe of inclined slope and top of vertical slope) to be used initially as working platform during construction (Figure 3). The 14-meter inclined slope was stabilized by soil nails and covered by plastic sheets during construction, to prevent scouring by rainwater. Then, at final stage, the slope was protected permanently by geotextiles and gabions as will be shown in Figure 14.
2.) The lower vertical slope, 18 meters high was initially designed to be supported by Anchored Diaphragm Wall (ADW) with four (4) levels of ground anchors, spaced horizontally at 1.75 meters. The diaphragm wall was 0.8 meters thick and the length of ground anchors ranged from 39 to 44 as shown in Figure 3.

5. DESIGN ANALYSIS

The staged excavation analyses of ARWS use numerical approaches to model stresses and deformations in normal condition and during earthquake actual sequence of excavation and anchor installation by considering each stage of the excavation as it is conducted, and as the anchors are installed.

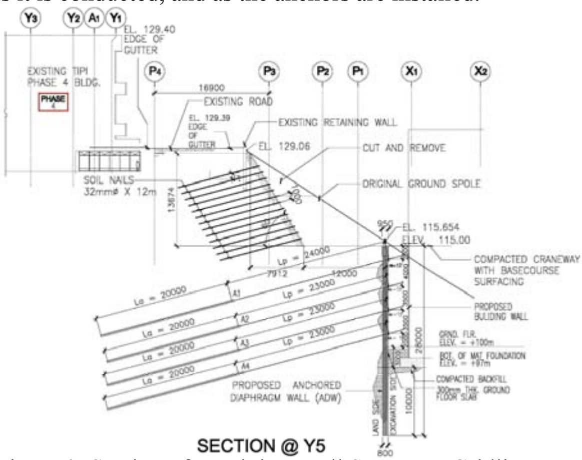

Figure 3. Section of Retaining Wall System at Gridline Y5

The analyses for the structural design of ARWS were performed using both Beams on Elastic Foundation (BEF) and Finite Element (FE) models. The BEF program, developed by Foundation Specialists Inc, was used for the structural design of the wall and permanent ground anchors. Using the BEF model, design profiles of wall stresses and deformations and anchor/props forces could be analyzed and evaluated. The FE model, using the commercial geotechnical computer program **PLAXIS**, was utilized to provide information on the ground movement outside and inside the excavation (Figure 4).

The slope stability analysis of Retaining Wall System excavations during construction and service condition with and without earthquake were analyzed using the commercial geotechnical computer program **SLOPE/W**, a slope stability software product used to compute factor of safety of earth and rock slopes. It can analyze both simple and complex problems for a variety of slip surface shapes, pore-water pressures conditions, soil properties, analysis methods and loading conditions. Figure 5 show a slope stability analysis during an earthquake.

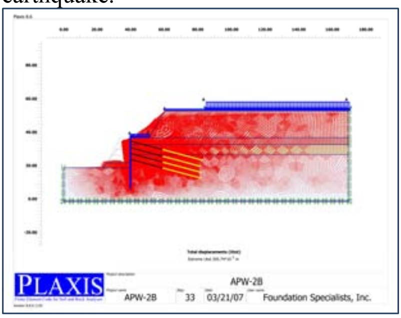

Figure 4. Displacement Vectors for FEM Analysis

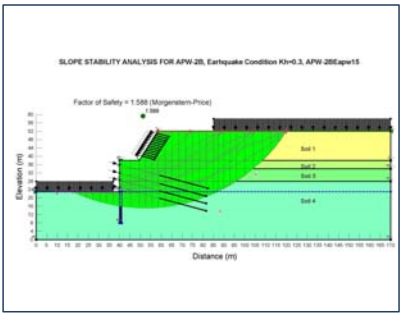

Figure 5. Slope Stability Analysis during Earthquake Condition

6. CONSTRUCTABILITY CONCERNS

In the early stage of construction the development and stabilization of the 14-meter high slope with 60-degree inclination was successfully implemented using 12-meter long soil nails arranged in a square grid of 1.5-meter spacing in both directions. The slope was covered by means of plastic sheets fixed on top of the nails to protect the topsoil from scouring due to rainwater.

During the construction of a temporary guidewall along the alignment of the ADW at El. 115 and partial excavation for the mat foundation for the new building at El. 97, a large landslide occurred and caused ground collapse and 4 meters vertical displacement from gridlines Y1' 25-meters stretch to Y4 within the areas prepared for the installation of the ADW as shown in Figures 6 and 7.

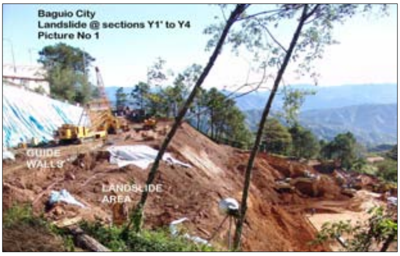

Figure 6. Landslide at gridlines Y1' to Y4 and guidewalls for executions of ADW.

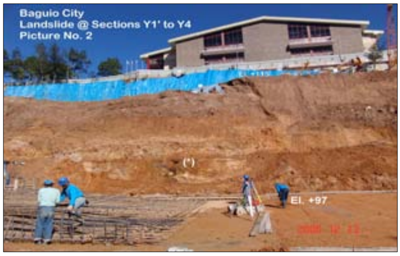

Figure 7. Landslide at gridlines Y1' to Y4 showing water to spring from soil marked as (*).

6.1 Causes of Landslide

Because of this incident at the project site, two basic questions had to be analyzed and answered regarding the causes of the landslide, to come up with corrective solutions that would not adversely affect the project cost and schedule:

1.) Was the soil that had collapsed, the original soil or excavated soil placed as backfill?
2.) What could possibly be the cause of the landslide?

A joint survey conducted on the landslide area showed that the soil involved in the landslide was entirely within the original ground, which is represented by the Owner's soil investigation report as a uniform mass of stiff to very stiff clay, with complete absence of water table.

From visual examination of the site, it was evident that the soil formation extending below elevation +115 contains pockets, lenses or levels of non-cohesive material a sandy soil. Figure 6 shows the area concerned by the proposed ADW in a photo taken after the landslide.

It was observed that, from the bottom of the ditch excavated from elevation +115 at the toe of the "nailed" slope, for the purpose of draining rainwater from the ADW working areas, there is what appears to be a water seep with a very small but constant water flow.

By observation of the landslide area and of the mechanics of the soil failure, the water gushing out from the collapsed soil immediately after the collapse then stopping, and again appearing intermittently, would seem to suggest the presence, within the surrounding clay formation, of small or thin water-bearing strata or of inter-communicating small lenticular structures made of non-cohesive soil, that could store water, probably in small quantity, but somehow under pressure because of the source being at higher elevations. This could explain the mechanics of soil during the landslide, with the rotation and slippage of relatively large soil masses down slope.

Clearly, what had happened at site constituted a "change of site conditions" that not only required remediation of the area to allow the safe construction of the ADW, but also made necessary further investigations and eventually led to a total re-design of the Retaining Wall System, taking into consideration the presence of hydrostatic pressure, and the introduction, at the back of the Retaining Structure, of a reliable drainage system that would prevent water impounding and consequent hydrostatic load build-up on the inner face of the Retaining Structure.

6.2 Technical Remarks

The landslide caused ground collapse and associated displacement within areas to be excavated for the installation of an ADW. The event resulted in unstable ground not suitable for excavation and pouring of concrete as needed for the construction of the cast-in-place ADW. To re-create conditions needed to safely install the ADW, it was necessary to improve the collapsed and destabilized ground by building up sufficient density and shear strength within the ground affected by the landslide.

Several technical solutions suitable for landslide remediation under the prevailing site conditions were studied, evaluated, quantified and translated into cost and related working time needed for implementation. The technical scheme that resulted to be most advantageous to the project for reliability of projected results, safety, costs and time schedule, was recommended for Owner approval.

6.3 Recommendations

In the light of the above observations, it was decided that no further excavation should be carried out on the existing slopes. The following schemes were recommended:

1.) Scheme 1: To implement the original solution with the ADW. In order to carry out expeditiously the construction of the retaining wall by means of cast-in-place, reinforced-concrete Anchored Diaphragm Wall (ADW), and in order to prevent major cave-in during execution, it would be necessary to execute an extensive ground improvement measure within the area affected by the landslide.

2.) Scheme 2: An alternative scheme for the Anchored Retaining Wall Structure (ARWS) by means of Anchored Aligned Piles Wall (AAPW) with diameter 1.5 meters, placed at a distance of 1.70 meters center-to-center. The piles would be constructed using long temporary casings to avoid extensive ground improvement.

In addition, construction of one line of temporary Soldier Piles along the 40-meter stretch most severely affected by the landslide on the excavation side of the Retaining Structure as shown in Figures 9 through 11. One-meter diameter Pervious Piles (PP) will be installed against the gap provided between the Bored Piles of the Anchored Aligned Piles Wall to serve as vertical draining elements to prevent hydrostatic pressure build-up on the inner face of the Retaining Structure. Perforated drains will also be installed and connected to a system of collector pipes leading to a ditch at the toe of the retaining structure. For layout and section of Anchored Aligned Pile Wall (AAPW), refer to Figures 8 to 11. The Anchored Aligned Piles Wall solution involves a shorter time schedule and no additional costs of the Owner.

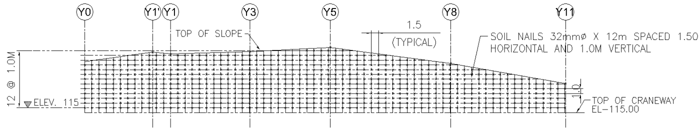

Figure 8. Soil nails at 14m high 60° slope

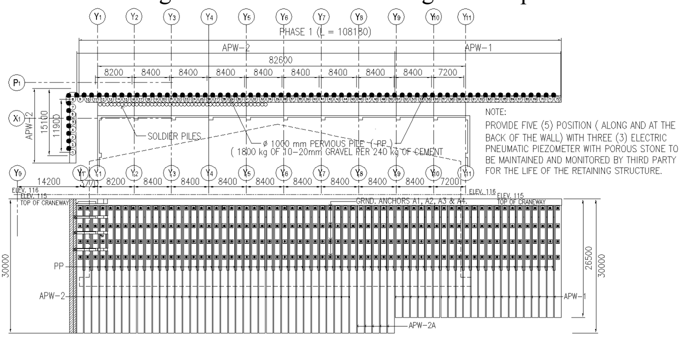

Figure 9. Anchored Aligned Pile Wall (AAPW) for 18-meters vertical slope.

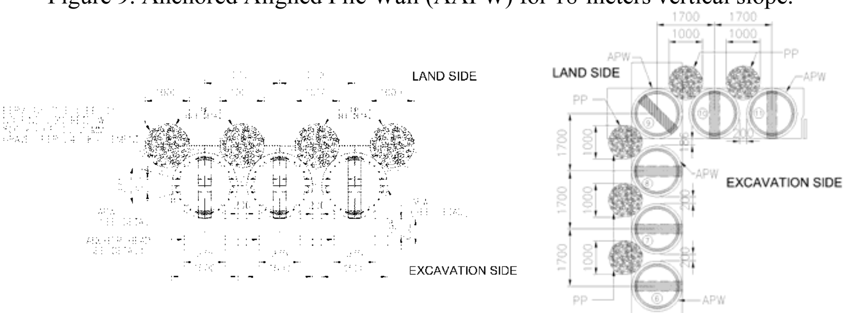

Figure 10. Layout Anchored Aligned Pile Wall (AAPW) with Pervious Piles (PP)

6.4. Owner Decision

The Owner's Consultants recommended the adoption of proposed Scheme 2, Anchored Aligned Pile Wall (AAPW), including Pervious Piles (PP), Permanent Ground Anchors and temporary Soldier Piles. Fig. 12 shows the AAPW under construction. Figure 14 depicts the finished project of AAPW. Fig. 15 shows the continuous monitoring of wall movement and of the anchors' prestressing load.

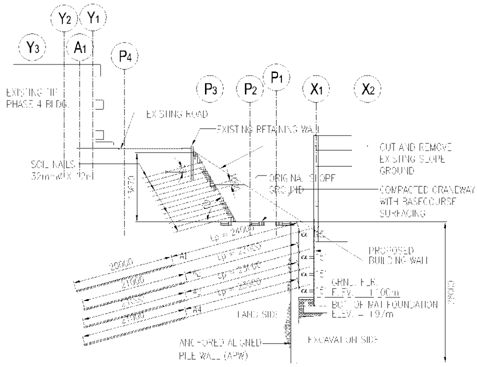

Figure 11. Section of Anchored Aligned Pile Wall at Gridline Y5

Figure 12. Anchored Aligned Pile Wall with 2 levels of Soil Anchor Installed

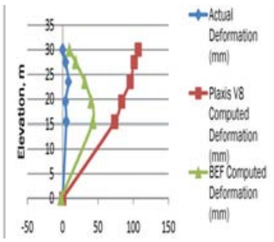

Figure 13. Computed and Measured Wall Displacement

Figure 14. AAPW, gabions and new industrial building

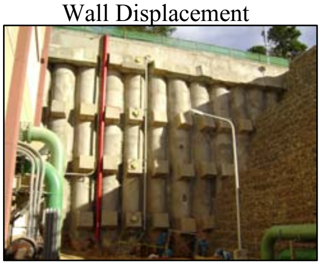

Figure 15. AAPW with load cells and for monitoring anchor and wall movement.

7. CONCLUSION

The chosen solution was key to the project's timely completion, in full compliance with the Design requirements and Specifications. In the two years since project completion the Project area has experienced a record number of destructive typhoons with rainfalls of up to 833 millimeters of rainfall measured in just two days (Typhoon Parma). The monitoring conducted to date by the Owner in the two years elapsed since the completion of the slope protection system (June 2007), shows that the overall wall movements for the entire site are less than the computed values (See Figure 13). The facilities are being used for their intended service purposes (Figs. 14 and 15).

8. REFERENCE - Performance Specification for the Construction of Diaphragm Wall and Soil Anchors, CCT Constructors Corp, Makati, Philippines, 2006

Using Tieback Anchors to Stabilize an Active Landslide in San Juan Capistrano, California

David H. Lee[1], PE, GE, M.ASCE, Colin E. Cunningham[2], PG, CEG, Karen E. Geraci[3], PE, GE, M.ASCE, D. Elliott Lee[4], PE

ABSTRACT

An ancient landslide was re-activated in 1998 in a hillside-graded area of San Juan Capistrano, California. The landslide occurred within a park site and threatened an adjacent residential development. The ensuing litigation led to the design and construction of a retention system with high-capacity tieback anchors in 2000. This system consisted of five levels of lateral support, with each level containing up to three rows of tiebacks and continuous walers. A total of 864 tieback anchors were installed, ranging in design load capacity from 300 to 365 kips. In order to account for the continuing slide movement that was expected to occur during the ongoing construction activities, the anchors were locked off at or above 50 percent of the design capacity. Post-construction monitoring has indicated that the measured loads in about 60 percent of the anchors continued to increase over a period of several years, up to 38 percent higher than the design capacity in some anchors. The anchor loads have now decreased to an equilibrium state at generally less than, or equal to, the design capacity (with few exceptions). This design approach has proven successful in resisting the active slide movement within the mitigated area.

INTRODUCTION AND SITE HISTORY

During the 1980s housing boom in Southern California, three residential developments and an adjacent park site were constructed in the coastal foothills of San Juan Capistrano, California. The site was underlain by numerous active and inactive shallow landslides, which were situated atop a much larger ancient landslide. Grading work in the 1970s and mid-1980s was attempted in order to stabilize the active landslides with earthen buttress fills. The final mass grading work produced small buttress keyways that were apparently intended to stabilize only the immediately adjacent slopes within the residential development. Consequently, this work was inadequate to stabilize one ancient landslide that re-activated over an area of about seven acres within the adjoining park site. In addition, partial removals of the landslide mass had the unintended result of reducing the resistant normal loads above the slide plane, which left the landslide in a failing condition. Grading was completed by 1988, and although the slide remained active, its movement within the undeveloped park site remained relatively undetected for some time.

1, 3, 4 –Principal Geotechnical Engineer, Project and Staff Engineers (respectively), David H. Lee & Associates, Inc., 23011 Moulton Pkwy, Ste D-11, Laguna Hills, CA 92653. Phone: (949)461-5690. Fax: (949)461-7901. Email: dhla@dhla.com

2 – Senior Engineering Geologist, formerly with David H. Lee & Associates, Inc., now with Geokinetics, Inc., 77 Bunsen, Irvine, CA 92618. Phone: (949)502-5353, Fax: (949)502-5354. Email: colin@geokinetics.org

The combined effects of higher-than-normal rainfall during the 1997-98 winter season, together with the remedial grading deficiencies, contributed to an overall acceleration in the active slide movement over the next two years. Some of the more noticeable distress features included (a) the steep natural slope southeast of the park site began to fail, (b) drainage swales within the park site became visibly offset and damaged, (c) ground cracks appeared near the active head scarp, and (d) compression features and cracks developed in the curbs and gutters, street pavements, and other flatwork within the adjacent residential development. It became evident that the landslide posed an immediate threat to the nearby streets and residences, and that continued movement could possibly lead to catastrophic failure within the toe area if repairs were not implemented promptly. As is often the case in these events, litigation ensued to determine the causes of the active landslide and the appropriate method for repair. As a consequence of that litigation, a fund was also established for the design and installation of a landslide retention system. A system of tieback anchors was constructed in 2000, using a design/build approach that teamed the park site's forensic geotechnical expert with the specialty repair contractor chosen for the project. This paper discusses the geotechnical design, construction, and long-term performance of this retention system.

GEOLOGIC CONDITIONS

The active landslide was principally confined to the park site area, immediately adjacent to a residential development to the west. The site is underlain by marine siltstone and claystone bedrock, assigned to the Capistrano Formation of upper Miocene to lower Pliocene geologic age (roughly 4.6 to 10 million years old). This formation is generally massive, with what little bedding observed being typically disturbed or disrupted to the point where the overall geologic structure is difficult to discern. However, the physical characteristics within this formation, which include high porosity, low permeability, high moisture retention, and high plasticity within the finer clay-rich portions, make it particularly susceptible to movement within slopes, and as such, this formation is locally notorious for landslides.

Regional geologic sources revealed that the adjacent residential developments were located on the eastern limb of a broad, north-trending structural feature known as the Capistrano syncline, implying that the overall trend of the bedding in the site vicinity should dip gently to the west. The slide plane was identified by a combination of subsurface exploration, employing both down-hole logging and observation of cores, geophysical borehole logging, and slope inclinometer data within the area of the active landslide. The slide plane was associated with relatively well-bedded zones that were planar, clay-rich, and appeared to extend for a considerable distance. The as-built topographic conditions at the site were forcing the landslide to move as a large "wedge" type failure, in a direction along which the slide plane had a maximum "apparent dip" of roughly 1 to 1 ½ degrees from the horizontal. A partial geologic map of the subject landslide is shown on Figure 1.

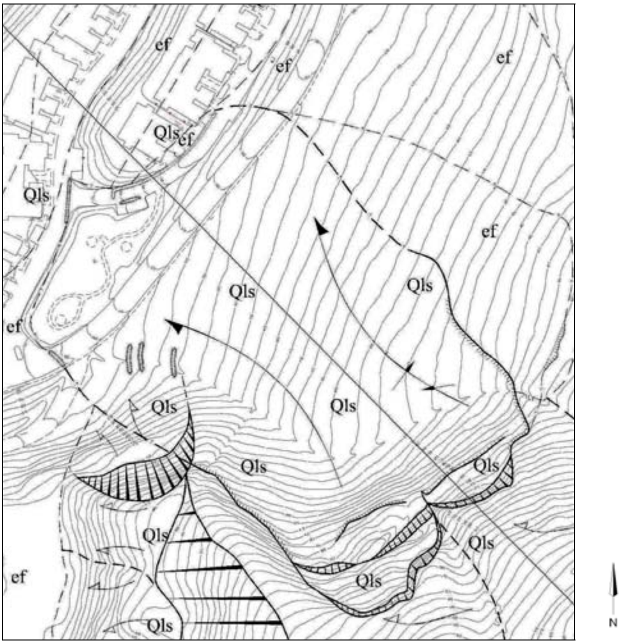

FIG 1. General Site Geologic Map (No Scale)
Qls = Active/Ancient Landslide; Ef = Engineered Fill; Tc = Capistrano Fm.

FIELD INSTRUMENTATION

The groundwater conditions beneath the site were monitored by pore pressure transducers (PPTs) and open standpipe observation wells. The PPTs consisted of one-inch-diameter pneumatic piezometers that were installed alongside the slope inclinometer casings, with the annular backfill of these boreholes consisting of a mix of cement with either hydrated lime or bentonite. The clayey nature of the landslide debris and formational bedrock beneath the site was characterized as having very high porosity and low permeability; such that these materials were found to be saturated below the apparent groundwater table, yet yielded no free moisture. Plots of the PPT data indicated that there were two separate groundwater systems within the landslide mass, with a general direction of flow toward the northwest. It also appeared that the groundwater was above most of the southeast half of the active slide plane, which further contributed to the active slide movement.

Slope inclinometer casings were installed throughout the affected slope to define and monitor the zone(s) of slide movement. An inclinometer probe was used to record the amount of deflection in the casing along two orthogonal directions. By calculation, the data were used to obtain resultant plots showing the magnitude and azimuth of the deflection, and the progressive change in the shape of the casing (or lack thereof) over time. The resultant magnitude and azimuth plots are crucial to the analysis of slope movement, and particularly to an active landslide, as the location of the slide plane, the magnitude of the slide mass and the rate at which the slide mass is moving can readily be seen from the resultant plots. At the toe of the active slide, the inclinometer casings showed rates of movement that ranged from 8 inches to 24 inches per year, when measured during periods of heavy rain in the winter of 1998-1999. The slide movement was detected at depths ranging from 35 feet beneath the residential street at the slope toe, to 95 feet at the head of the landslide along the east side of the park site. The rate of slide movement, and the fact that several inclinometer casings were crimped (or sheared) within two months of their installation, dictated that a means of stabilization needed to be found immediately in order to protect the nearby residences.

STABILITY ANALYSIS AND PRELIMINARY DESIGN

The existing stability of the active landslide was analyzed on several prepared cross sections, using the available surface and subsurface data obtained from the forensic geotechnical investigation. Based on the results of laboratory testing, the active slide plane was found to have a cohesion intercept of 100 pounds per square foot (psf), and an internal friction angle of 9.5 degrees (residual strength). The stability analysis was performed using PCSTABL6 software. The results indicated that the factors of safety were very sensitive to the designated location of the groundwater table. As such, the groundwater level was conservatively assigned based on a reasonably expected increase above the observed PPT piezometric data. Using this model, the active landslide was determined to have theoretical static factors of safety ranging from 0.78 to 1.2, with 1.0 representing impending failure.

The most critical cross section was then analyzed for approximately 90 different repair scenarios, in an initial attempt to design a feasible stabilization method. Due to the geometry of the landslide, the property boundaries, and various legal constraints, the most effective repair method precluded the use of either fill buttressing, large-diameter soldier piles, or cast-in-drilled-hole (CIDH) shafts to arrest the movement. Static factors of safety not much over 1.1 were attainable using these more traditional stabilization methods. The local regulatory grading code, and the geotechnical standard of practice, dictated that the long-term static factor of safety must be at least 1.5, with a corresponding pseudostatic (seismic) factor of safety of at least 1.1.

Based on our stability analysis, the only feasible repair that could be implemented on the park site property, which would bring the static factors of safety to at least 1.5 along most areas of the landslide, was the use of high-capacity tieback anchors. Our preliminary design included a total of over 1,000 tieback anchors ranging in design capacity from about 300 to 500 kips (although this design was later revised). Also, in a unique and localized portion of the active landslide mass, our analysis indicated that the static factor of safety along one cross section could only be improved to about 1.2 using a double-row of 500-kip tieback anchors, even though elsewhere the factors of safety would exceed 1.6. This anomaly was verified to demonstrate that there would be no adverse effect on the overall stability of the proposed repair if this immediate area could not be improved further. The design for this area required a code variance regarding the minimum factor of safety, which was satisfactorily demonstrated to the local regulatory agency in order to obtain the project approval.

FINAL DESIGN

Using the preliminary design, technical proposals were requested from a handful of specialty geotechnical contractors. In October 1999, three pre-bid test anchors were drilled and installed by the contractor who was ultimately chosen for this project. The data obtained from these tests were used by the contractor to prepare their design and cost estimate for the preliminary design. It soon became obvious that a design/build approach would provide a more efficient final design that would also result in a greater cost benefit to the client. As the structural design of the anchor blocks and tiebacks evolved, the contractor suggested the substitution of three rows of 365-kip anchors instead of two rows of 500-kip anchors, since in this case, it would be more economical to install a greater number of lower-capacity anchors than a lower number of high-capacity anchors. We then re-analyzed the landslide geometry and verified that the proposed design revisions would also meet the minimum accepted safety factor requirements.

The final design incorporated nearly 1,000 anchors, with design capacities of 300, 340, and 365 kips. However, some of these anchors would later be eliminated during construction (discussed below). As the geotechnical engineer of record, we specified the unbonded lengths, which ranged from 66 to 122 feet, based on the estimated location of the active slide plane along the anchor borehole. The tieback anchor contractor then designed the bonded lengths, which were either 45 or 54 feet, using an ultimate bond stress of 40 psi for the claystone bedrock. The anchors would have a down-angle of 45 degrees from horizontal, and spacings of either 5 or 5½ feet on centers within each anchor row, with one to three rows on each waler. Due to the low bearing capacities of the surficial soils, it was decided that continuous, cast-in-place, reinforced concrete grade beams would be installed, instead of individual reaction blocks, for the walers. The grade beams measured about 2.5 feet thick and 6 feet high, with lengths ranging from about 190 to 700 feet. Five tiers of walers were needed in the landslide stabilization area, as shown on the general repair plan in Figure 2. A typical cross section of the repair is also shown in Figure 3.

CONSTRUCTION

Pre-Production Test Anchors

In January 2000, the contractor installed four pre-production test anchors in order to verify that the design loads could be met. The results of the pre-production tests were used to verify the ultimate bond stress within the claystone bedrock, and the expected post-grouting criteria for the production phase.

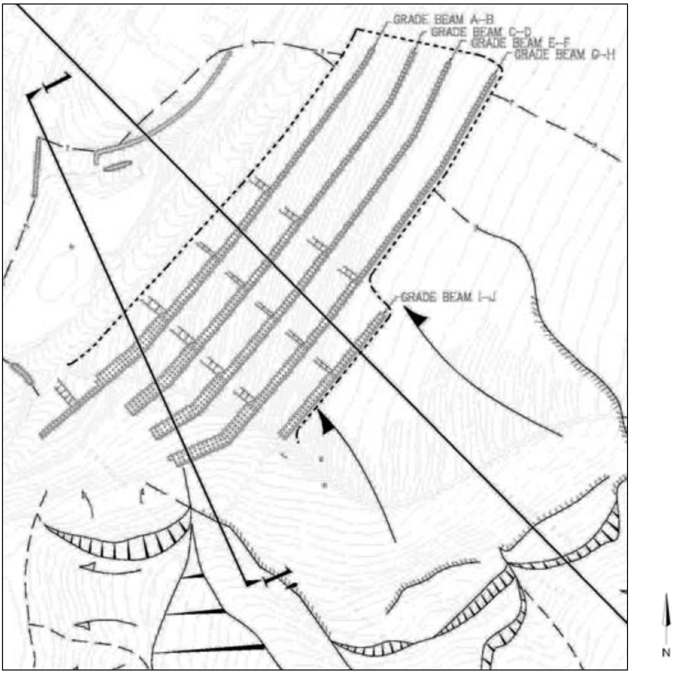

FIG. 2. General Repair Plan for Landslide Retention System (No Scale)

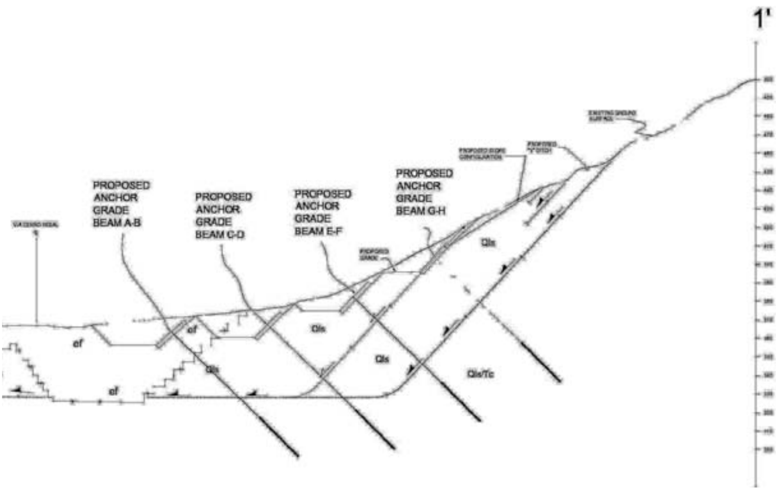

FIG. 3. Typical Cross Section for Landslide Retention System (No Scale)
Qls = Active/Ancient Landslide, Ef = Engineered Fill, Tc = Capistrano Fm.

Site Preparation and Grading

In February 2000, the grading contractor began excavating the uppermost tier for the anchor walers. Our geotechnical personnel observed the excavation to verify that the waler would bear against competent material. After the walers were constructed and the anchors were installed and stressed, this process would be repeated for each progressive tier, down to the lowermost level of anchors. Due to space limitations, a construction sequence of "flip-flopping" the excavated soils was required, such that after an upper anchor row was locked-off, it was backfilled with the soils being excavated for the lower adjacent tier. Final grading would then cover all the anchors with engineered fill and restore the park site to nearly its original configuration.

Production Anchors

Between April and October 2000, the tieback anchor contractor constructed the reinforced concrete walers, and installed and stressed the anchors. The anchor walers consisted of fabricated reinforced steel cages that were set against the soil subgrade and then sprayed with shotcrete. The boreholes for each anchor were drilled through cylindrical block-outs that were cast into the waler, using two types of hydraulically operated top-drive drill rigs equipped with air-rotary methods (Klemm KR-806D and Casagrande M-9). Isolated layers of very hard formational calcareous concretions were encountered during production drilling at several locations. When this occurred, the contractor switched to a down-the-hole pneumatic hammer (a standard carbide button bit with a drop-center face). The boreholes also tended to cave within the landslide debris (i.e., the unbonded zone), but the contractor had some success in keeping the shorter holes open by injecting small amounts of drill slurries at the cutting head, so that the rotary action mixed the slurry into the soil. On the longer holes that were more prone to caving, conventional casing was used. At seven anchor locations where concretions or other obstacles (pre-bid or pre-production anchors) were encountered, the drilled shafts were abandoned and grouted, and a new anchor was installed at a slightly steeper down-angle (46 to 49 degrees), which was verified to have no adverse effect on the overall design of the repair.

At each anchor location, the depth of the borehole (i.e., the anchor length) was established according to the design specifications. The anchors consisted of either 9- or 11-strand tendon bundles (depending on the design capacity), and ranged in total length from 111 to 176 feet. The anchors were encapsulated in a casing of corrugated PVC pipe (for Class I protection), with centralizers wired to the outside of the casing, and cable spacers in the bonded zone. Two 1-inch PVC grout lines were attached to the full length of the casing to facilitate post-grouting. The grout mix for the bonded zone consisted of Type V cement (due to the high corrosion potential of the site soils), mixed with sufficient water to maintain a maximum water/cement ratio of 0.44. After the initial grout had cured for at least 24 hours, the anchors were post-grouted under high pressure. Generally one post-grout was sufficient to enable the anchors to attain the required proof and performance test loads of 133 percent of the design capacity. However, there were 41 anchors that needed to be post-grouted twice, 3 that were post-grouted three times, and 2 that were post-grouted up to 4 times, before the required anchor capacities were attained.

The anchor tendons were stressed using either a 300- or 500-ton hydraulic jack. All of the production anchors were stressed to 133 percent of their design capacities using one of three test protocols, namely, the (a) proof test, (b) performance test, or (c) extended creep test. The test protocols were based on the criteria given in the Post-Tensioning Institute Manual (PTI, 1996). The locations for each test type were pre-determined by the geotechnical engineer of record, so as to provide an overall even distribution throughout the limits of the repair. If for any reason an anchor could not hold its test load for the required amount of time, the anchor was post-grouted and stress-tested again. This process was repeated until each anchor was able to pass its respective test. There were production totals of 864 tieback anchors ranging in capacity from 300 to 365 kips, which included 800 proof tests, 50 performance tests, 14 extended creep tests. Additionally, there were two anchors that failed the performance test but still maintained their design loads with minimal creep.

Design Modifications

The total number of as-built anchors was reduced from the original design due to the elimination of 167 anchors during the construction phase. As a result of our observations of newly exposed geologic conditions at the southwest end of the landslide, it became apparent that many anchors in that area would be installed in very loose graben and/or slide debris, likely derived from a smaller offsite landslide contiguous to the subject landslide. These materials lacked the strength necessary to support the anchor loads. Fortunately, the stability analysis indicated a higher factor of safety in this area, so these anchors were eliminated. This decision was confirmed when the contractor installed two isolated test anchors in these materials, and each anchor failed to achieve its test load. The southwest portion of the landslide was then left partially unmitigated, and future movement was expected to occur.

Anchor Lock-Off

Once an anchor passed its stress test, it was locked off at or above 50 percent of its design load. The minimum 50 percent lock-off load criterion was utilized to minimize the possibility of over-stressing the initial rows of anchors beyond their design loads, before a sufficient number of anchors could be installed to arrest the ongoing slide movement.

Strain gauges were factory installed on 53 anchors for long-term monitoring purposes, although only 46 remained operational when the anchor installation was complete. The actual lock-off loads ranged from 50 to 70 percent of the design loads, and the initial rows of anchors showed load increases of up to 30 kips (about 10 percent) as reflected by the strain gauges, before temporarily stabilizing during the remaining anchor construction.

Stability Analysis

Construction was completed by December 2000. The stability of the landslide was verified for the as-built conditions, using either the actual lock-off loads or the initial load increases indicated by the strain gauges. The most critical cross sections were found to have static factors of safety ranging from about 1.0 to 1.4, with an average of 1.2. In other areas, the factors of safety were even greater. The long-term factors of safety were expected to increase in accordance with the final design, once the anchor loads reached equilibrium at some point in the future. As such, long-term monitoring of the strain gauges would prove essential in order to verify the actual performance of the landslide retention system.

POST-CONSTRUCTION MONITORING

The long-term performance of this repair continues to be monitored, primarily by measuring the site instrumentation and evaluating the data patterns that have emerged since the time of anchor installation and lock-off. This work was performed by the geotechnical consultant of record until 2004, then by a subsequent consultant from 2004 to 2010. Long-term monitoring has generally occurred about once a year.

The most recent data was obtained in November 2009 and March 2010, when 7 inclinometers, 5 multi-stage piezometers, and 46 strain gauges remained operational. It should also be noted that the instrumentation for several strain gauges was recently repaired and re-measured, due to the 2009 discovery of poor electrical connections that had been damaged by water infiltration and corrosion. Based on an overall comparison between the most recent monitoring data with previous readings, the following data trends have been observed:

- Since November 2000, about 60 percent of the instrumented anchors have experienced a significant load increase (i.e., greater than 10 percent of lock-off load). These load increases have generally occurred across the entire width of the retention system. The greatest increases have occurred in the southwest portion of the landslide. The load increases have likely resulted from post-repair creep along the landslide failure surface, which was anticipated in the southwest area.

- Since August 2002, significant load increases (i.e. greater than 10 percent) have been recorded on only 17 percent of the instrumented anchors, and a decrease in load was recorded in approximately 40 percent of the anchors. Post-repair movements within the landslide have likely produced this response.

- Approximately 7 percent of the instrumented anchors are presently operating under loads in excess of their design capacity, by up to 12 percent. These anchors are located on the second-lowest tier in the southwest portion of the landslide, and on the uppermost tier. Importantly, the loads on these anchors have actually decreased from their maximum loads of 20 and 38 percent above the design capacity as recorded in 2004/2005, and appear to be performing favorably.

The overall data trend has been for the loads in the instrumented anchors to stabilize. There is also an absence of any detectable landslide movement in the two slope inclinometers that are being monitored within the mapped landslide limits. The long-term monitoring data suggest the retention system is functioning as intended.

SUMMARY AND CONCLUSIONS

The use of tieback anchors has become a popular method for landslide stabilization, especially where remedial grading may not be a viable option. In this case study, an unconventional approach was used to minimize the possibility of over-stressing the initial anchors while the slide was still moving, such that the anchors were locked off at, or above, 50 percent of their design capacities. Many of the anchor loads continued to increase over a period of several years. However, with few exceptions, long-term data trends indicate that the anchor loads have currently stabilized at generally less than, or equal to, their design capacities. The tieback retention system has proven successful in resisting active slide movement within the mitigated area.

ACKNOWLEDGEMENTS

The authors wish to thank Glenn Tofani of Geokinetics, who provided the results and data comparison for the current long-term monitoring at the site. We would also like to thank Karen Masterson, for her geotechnical engineering contributions on this project while employed at David H. Lee & Associates, Inc. We also acknowledge Garry Hove, Wil Fischetti, and Bret Rowan of Malcolm Drilling Company, Inc., for their structural design and construction of the tieback anchor system and their technical collaboration throughout the design/build process. We are especially grateful to the Mesa Loma Vista Park Association for this work on their property.

REFERENCES

1. Cheney, R.S. January 1984. *Permanent Ground Anchors.* Federal Highway Administration. FHWA-DP-68-1.
2. Johnson, L.M. and Turner, J.P. 2003. *Performance of Permanent Ground Anchors for Landslide Stabilization.* University of Wyoming. FHWA WY-03/03F.
3. Post-Tensioning Institute (PTI). 1996. *Recommendations for Pre-stressed Rock and Soil Anchors*.
4. Sabatini, P.J., Pass, D.G., and Bachus, R.C. June 1999, *Geotechnical Engineering Circular No. 4: Ground Anchors and Anchored Systems.* FHWA-IF-99-015.

SI UNITS

Convert From	To	Multiply by
inch	cm	2.54
feet	m	0.3048
acre	m^2	4046.856
gallon	liter	3.785
kips	kN	4.448
psf	kPa	0.0479

Design of Drilled Shafts to Enhance Slope Stability

Daniel Pradel[1], Jason Garner[2] and Annie On Lei Kwok[3]

[1]Dept. of Civil & Environmental Engineering, University of California, Los Angeles, CA 90095; dpradel@ucla.edu
[2]Shannon & Wilson Inc., 3990 Collins Way, Suite 100, Lake Oswego, OR 97035; jkg@shanwil.com
[3]Praad Geotechnical Inc., 5465 S. Centinela Ave., Los Angeles, CA 90066; annie@praad.com

ABSTRACT

This paper describes a numerical approach for the design of drilled shafts to reinforce slopes. The approach uses the program *FLAC* and the strength reduction method to predict the Factor of Safety of the improved slope. The method successfully predicted the maximum demands (shear force and bending moments) necessary for the structural design of stabilizing piles. The method also successfully predicted the critical mode of failure and slope stability Factors of Safety for piles with a plastic bending moment.

INTRODUCTION

In urban environments, drilled shafts are often used by geotechnical engineers to improve slope stability and stabilize existing landslides (e.g., Smethurst and Powrie, 2007). Permanent drilled shafts used in landslide stabilization must resist the large lateral loads imposed by the landslide. Typical shafts are closely spaced and have large diameters (1 to 3 meters). Because of the large bending moments to which they are subjected, these drilled shafts are generally reinforced with large steel I-beams instead of reinforcement cages and the design often incorporates several rows of tiebacks that extend below the landslide basal plane. Depending on the geographical area these stabilizing drilled shafts are often known as stabilizing piles, shear pins, caissons, or soldier piles.

DESIGN METHODS

The design methods used by geotechnical engineers for the design of stabilizing piles vary widely. To prevent movement of the stabilized slope and upper building pads, plastic flow of the soil between the shear pins must be prevented. Thus in practice geotechnical designs typically involve closely spaced drilled shafts with typical center-to-center spacing on the order of 2 to 3 shaft diameters. In frictional materials, a spacing of 3 shaft diameters is generally considered adequate to ensure full passive load transfer (Broms, 1964), prevent plastic flow (Smethurst and Powrie, 2007), and transfer the maximum lateral loads to the stabilizing piles by arching. In rare situations where a large spacing is specified, lateral deformations associated with soil flow between the piles should be anticipated and load transfer by arching must be verified (Ito et al., 1975 & 1981).

The lateral deflections depend on the depth of embedment of the stabilizing piles, the stiffness of the soils, diameter of the drilled shaft as well as the stability of the slope. In Southern California, in addition to Factor of Safety calculations, lateral capacity and deflection analyses of the stabilizing piles are often performed by geotechnical engineers using Broms' charts (e.g. Broms, 1964) and/or specialized computer programs for computing pile deflections (e.g., LPILE by Ensoft, 2004).

Although landslide stabilization using drilled shafts is a geotechnical repair method that has been used successfully to improve many slopes, there is no standard method used for the design of stabilizing piles. Numerous methods have been proposed for designing stabilizing piles. The proposed methods can be grouped into four general groups as described below:

- *Limit Equilibrium Methods:* Methods for the design of stabilizing piles using limit equilibrium methods are well documented in the geotechnical literature, e.g. Hassiotis et al. (1997). Design methods based on limit equilibrium generally obtain an equivalent force, which the drilled shafts must be capable of resisting. In their analyses, geotechnical engineers often replace the drilled shaft by an equivalent horizontal force, known as the unbalanced force (F_u in Figure 1), which is calculated using traditional slope stability methods. Depending on the selected slope stability method, the unbalanced force is obtained by the slope stability program through force and/or moment equilibrium. The review of numerous designs by the first author indicates that the slope stability methods that are most often used are: Bishop, Spencer and the simplified Janbu methods. Bishop's method, which requires moment equilibrium, is particularly well suited for this approach.
- *Earth Pressure Theory-Based Methods:* Designers sometimes use earth pressure theories, such as Coulomb and Rankine, to calculate lateral pressures on drilled shafts. This method is generally used to estimate the lateral load on stabilizing piles located near a top of slope, where a building pad needs protection and the slope below is allowed to move. Some designers use horizontal equilibrium, to balance active and passive loads. In these cases, the passive loads are typically reduced by a Factor of Safety. This method is problematic as it does not consider slope stability failure mechanisms and does not satisfy moment equilibrium. Thus it is unsurprising that in the first author's experience, this method is seldom encountered.
- *Pile Deflection Theory-Based Methods:* Reese (1992) proposed a method based on pile deflection theory, i.e. the p-y method. Reese's method is relatively complex and involves numerous steps. The required steps include: (a) conventional slope stability analyses of the subject slope, (b) selection of shaft diameter/stiffness and determination of the ultimate bending moment, (c) determination of the ultimate resistance of the soil against the pile, and (d) using the p-y curve method to analyze the pile. The procedure is iterative and must be repeated until the bending moment found using the p-y curve method and the ultimate bending moment are approximately the same for a given slip surface. Additional iterations are then needed as changes of the pile stiffness result in a new critical slip surface. The procedure is repeated until the critical

slip surface, the stiffness of the pile, and the resisting forces of the pile, are compatible. Poulos (1995) proposed a relatively similar method that involves three steps: (a) evaluating the total shear forces needed to bring the slope to a target Factor of Safety, (b) evaluating the maximum resistance that each pile can provide (using, e.g. Viggiani 1981), and (c) selecting the type and number of piles. The method uses a proprietary program called ERCAP to model the interaction of the slope and stabilizing piles. Due to the complexity of the Reese and Poulos methods, designers rarely use them in practice.

- *Numerical Solutions Methods:* Designs based on numerical methods, i.e., using the Finite Element Method (FEM) or Finite Difference Method (FDM), have previously been designed and implemented. Most designs use numerical modeling to predict the likely bending moments and deflections of the stabilizing piles and do not predict the Factor of Safety (FOS) of the improved slope. Thus these designs do not necessarily satisfy the requirements of customary building codes. As a consequence, reviewing government agencies will generally request that the geotechnical engineer demonstrates, in addition to the FEM/FDM model, that the design satisfies the minimum required calculated Factors of Safety using conventional slope stability methods.

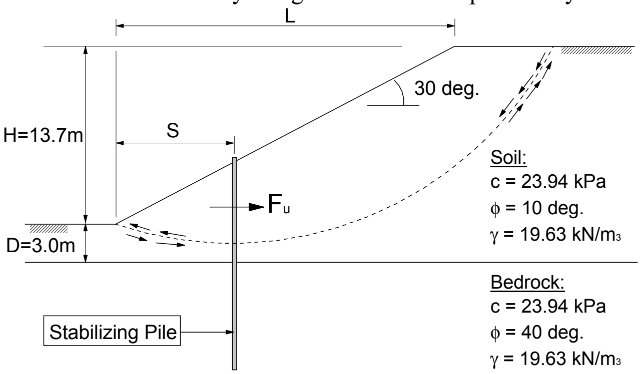

Figure 1. Slope geometry and material properties.

STRENGTH REDUCTION METHOD

The strength reduction method (e.g. Griffiths, 1999), which is incorporated into widely used computer programs such as FLAC (Itasca, 2008) and PLAXIS (2008), is a powerful tool to evaluate the Factor of Safety of a slope. The strength reduction method involves modeling the soil as an elastic-perfectly plastic material, and reducing the cohesion, c, and friction angle, ϕ, by a strength reduction factor, R, until the slope fails quasi-naturally:

$$c_d = \frac{c}{R} \tag{1}$$

$$\tan(\phi_d) = \frac{\tan(\phi)}{R} \tag{2}$$

The highest value of the strength reduction factor that satisfies equilibrium and is kinematically acceptable is the Factor of Safety, FOS, of the slope:

$$R_{max} = FOS \tag{3}$$

METHODOLOGY

To evaluate the capabilities of the strength reduction method for the analysis of a slope stabilized with drilled shafts, we adopted the soil strength, pile stiffness and slope geometry, similar to a previously published study (Hassiotis et al., 1997). The characteristics of the slope and stabilizing piles are shown in Figure 1.

We used the program FLAC (Itasca, 2008) to model the soil and piles, and programmed automated routines in FLAC to slowly lower the shear strength of the soil in accordance with equations 1 and 2. Since a row of closely spaced stabilizing piles will act as a wall due to arching, the piles were modeled using structural beam elements. FLAC's pile elements were also used in a limited number of runs without discernable geotechnical difference. Frictional interfaces connected the beam elements to the soil nodes on both the upslope and downslope sidesBeam elements are directly attached to the soil nodes on both the upslope and downslope sides, hence full friction between pile and soil is assumed to be mobilized. An elastic modulus of the stabilizing piles E = 200 GPa, a cross-sectional area A = 1 m^2/m, and moment of inertia I = 1 m^4/m were specified for elastic piles.

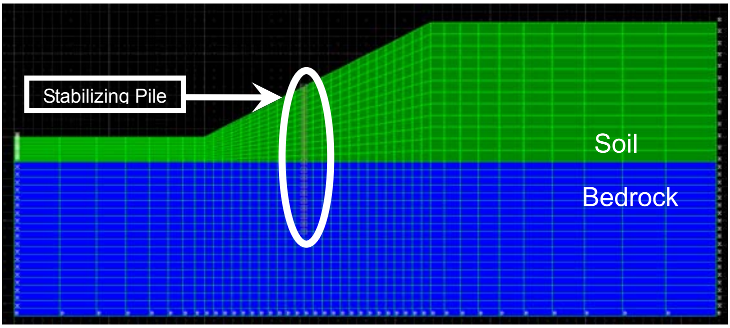

Figure 2. Finite difference grid used in FLAC

After bringing the original slope to static equilibrium, the drilled shafts were installed in the Finite Difference Model (Figure 2). Then very slowly, i.e., in thousands of steps, the strength of the soil and bedrock were decreased by a reduction factor, R. The procedure was programmed into FLAC and the reduction factor, R, was increased until the predicted maximum displacement, δ_{max}, exceeded 2 meters (e.g., Figure 3). The procedure was repeated for different pile locations and two different values of the angle of dilation ψ were used in our analyses, ψ = 0 and ψ = ϕ. In addition, the piles were modeled as both linear elastic (without a maximum bending moment), and with a maximum plastic moment, M_p = 2,000 kN.m/m.

The procedure worked flawlessly and the strength reduction technique easily predicted the Factor of Safety, FOS, for all the slope configurations. Results from a FLAC run with a row of elastic stabilizing piles located at S = 10.45 m from the toe of the slope (S/L = 0.44) are shown in Figures 3, 4 and 5b. Figure 3 shows that as R approaches R_{max} = 1.68, displacements become very large, which means that the slope is yielding. Figure 4 shows that the relationship between displacements and bending moments is roughly bilinear, and that as the slope starts to yield the bending moment remains approximately constant (M_{max} = 3750 kN.m/m). Hence, one of the main advantages of this procedure is that it provides the maximum structural demands in addition to the Factors of Safety of the slope.

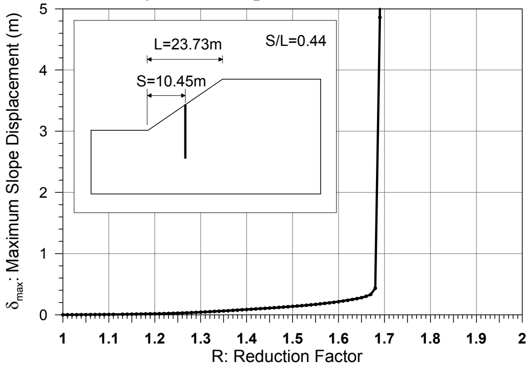

Figure 3. Maximum displacement vs. strength reduction factor for an elastic pile.

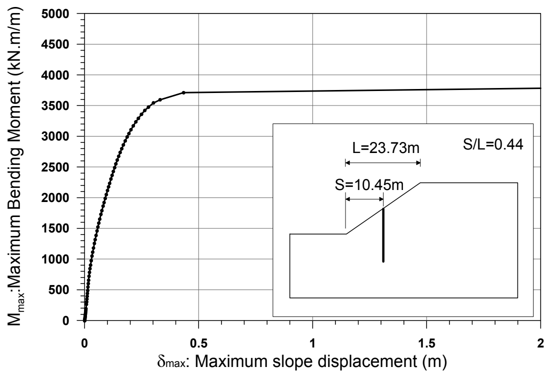

Figure 4. Maximum moment versus maximum displacement for an elastic pile.

Another advantage of the strength reduction technique is that the critical mode of failure can be easily determined. As the reduction factor, R, approaches the Factor of Safety of the slope, the predicted displacements become increasingly larger and a zones with large shear strain increments become apparent. The zone with maximum shear strain increments is the basal plane of the critical failure surface, and defines the critical mode of failure of the slope. Three different modes of failure were predicted in our analyses depending on the location of the stabilizing piles and the limiting bending moment, M_p:

- Slope failure below the stabilizing piles (Figure 5a).
- Slope failure above the stabilizing piles (Figure 5b). It should be noted that even when the failure involves slippage above the pile, bending moments are predicted because of the plastic yielding of soil (due to strength reduction).
- Development of a plastic hinge in the stabilizing piles and failure of the slope through the stabilizing shear pins (Figure 5c). This mode of failure only appeared when a small enough plastic moment was specified.

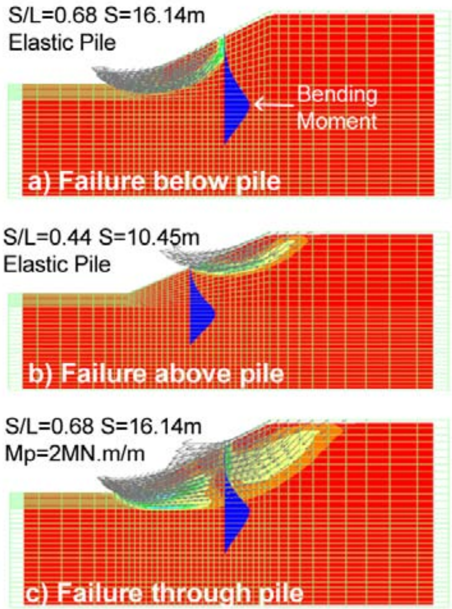

Figure 5. Bending moment, displacement vectors and shear strains for three different locations of the stabilizing pile and/or pile plastic moment, M_p.

Plastic Moment

Stabilizing piles used in practice have structural limitations in terms of depth, steel reinforcement and diameter. Hence, in practical applications, it is desirable to limit the moment capacity of the stabilizing piles, i.e. to specify a maximum design value. To analyze the effect of pile capacity on slope stability, our numerical analyses using elastic piles were repeated using shear pins having a limiting bending moment, M_p = 2000 kN.m/m.

The effect of limiting the moment capacity of the structural elements is shown in Figures 6 and 7. As expected, limiting the maximum bending moment results in a significant decrease in the Factor of Safety of the slope (from a maximum of 1.88 to a maximum of 1.48). Figure 6 also shows the effect of the pile location on the maximum Factor of Safety. For elastic stabilizing piles (without maximum plastic moment), the maximum Factor of Safety is achieved by placing stabilizing piles at S/L = 0.51. With a limiting bending moment, M_p = 2000 kN.m/m, the optimum location of the stabilizing piles changes and moves to S/L = 0.4. This change is important because it shows that the methodology presented here can be used to optimize the location of stabilizing piles in slopes. As shown in Figure 6 the Factors of Safety predicted by the strength reduction method compares well with those obtained by the conventional equilibrium method using simplified Bishop's method.

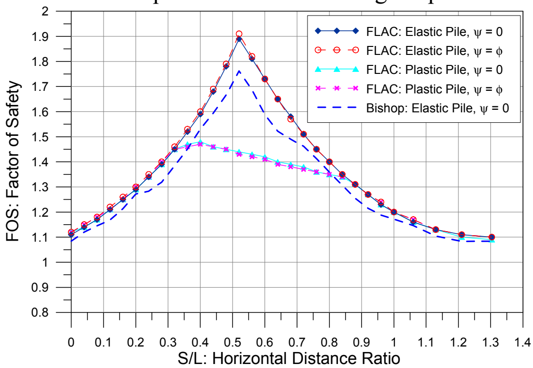

Figure 6. Comparison of horizontal distance ratio versus factor of safety for different pile and soil properties

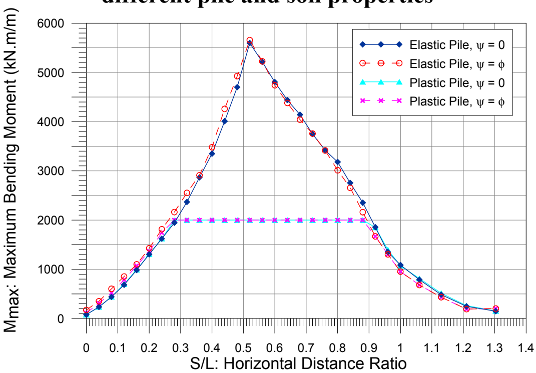

Figure 7. Comparison of horizontal distance ratio versus maximum bending moment for different pile and soil properties

Dilation Angle Effect

As R approached R_{max} = FOS, the solutions obtained with FLAC are both statically and kinematically admissible. Nevertheless, since most theoretical plasticity solutions in geotechnical engineering have been obtained using associated models, where the dilation angle is $\psi = \phi$ (Schofield and Wroth, 1968), it was considered worthwhile to study the effect of the dilation angle on the FOS and maximum bending moments. As can be seen in Figures 6 and 7, the effect of ψ is minor and can be neglected for the slope in Figure 1.

CONCLUSIONS

This paper describes a numerical approach for the design of drilled shafts to enhance the Factor of Safety of a slope using the strength reduction technique. Unlike conventional slope stability methods which require assumptions such as failure geometry, load distribution on the pile and distance to the point of fixity, the numerical modeling scheme requires no aforementioned assumptions and is able to predict the structural demand (bending moment and shear forces) of the pile directly. With the incorporation of strength reduction method, the Factor of Safety of an improved slope can be found easily. In addition, the method can be used to find the optimum location of stabilizing piles and predict the critical mode of failure. In our analyses, the angle of dilation did not appear to affect the results. In conclusion, the numerical approach with the use of strength reduction technique is straightforward, requires few hypotheses and is easy to implement.

REFERENCES

Broms, B. (1964). “The lateral resistance of piles in cohesionless soils,” *Journal of Soil Mechanics and Foundation Division, Proc. ASCE, 90 (SM3)*, 123-156

Ensoft (2004). Computer Program LPILE Plus Version 5.0, Austin, Texas.

Griffiths, D.V. and Lane, P.A. (1999). “Slope Stability analysis by finite elements,” *Geotechnique*, 49(3), 387-403.

Hassiotis, S., Chameau, J.L., and Gunaratne, M. (1997). “Design method for stabilization of slopes with piles,” *Journal of Geotechnical and Geoenvironmental Engineering*, 123(4), 314-323.

Itasca Consulting Group, Inc. (2008). FLAC – Fast Lagrangian Analysis of Continua and FLAC/Slope, *Ver. 6.0, User's Manual*, Minneapolis, Minn.

Ito, T. and Matsui, T. (1975). “Methods to estimate lateral force acting on stabilizing piles,” *Soils and Foundations*, 15(4): 43-59.

Ito, T., Matsui, T. and Hong, W.P. (1981). “Design method for stabilizing piles against landslide – one row of piles,” *Soils and Foundations*, 21(1): 21-37.

Plaxis (2008). Computer Program Plaxis 2D, Version 9.0, Delft, Netherlands.

Poulos, H.G. (1995). “Design of reinforcing piles to increase slope stability,” *Canadian Geotechnical Journal*, 32: 808-818.

Reese, L.C., Wang, S.T. & Fouse, J.L. (1992). “Use of drilled shafts in stabilizing a slope,” *Proceedings of Stability and Performance of Slopes and Embankments*, II 2, 1318-1332.

Schofield A. and Wroth P. (1968). *Critical State Soil Mechanics*, McGraw-Hill Publishing Company Limited

Smethurst, J.A. & Powrie, W. (2007). “Monitoring and analysis of the bending behavior of discrete piles used to stabilize a railway embankment,” *Geotechnique*, 57(8), 663-677.

Viggiani, C. (1981). “Ultimate lateral load on piles used to stabilize landslides,” *Proc. Int. Conf. Soil Mechanics and Foundation Engineering*, Stockholm, Vol. 3, 555-560.

STABILIZATION OF A 70-FT-HIGH SIDE-HILL FILL IN WEST VIRGINIA

Bernard Langan[1], Matthew Meyer[2] and George Siller[1]

[1]BF Langan Consultants, Inc., 200 Riverfront Boulevard, Elmwood Park, NJ 07407; PH (201) 791-4127; email: blangan@bflangan.com and gsiller@bflangan.com
[2]Langan Engineering and Environmental Services, Inc.; 15150 NW 79th Court Suite 200, Miami Lakes, FL; PH (786) 264-7200; email: mmeyer@langan.com

ABSTRACT
Stabilization of a 70-ft-high side-hill fill in West Virginia which was moving and damaging an occupied building was accomplished, by providing supplemental restraint through the use of tiered anchored sheet pile walls. The initial side hill fill, which was part of a development and served to level a large area for retail stores, was constructed in the fall of 2001. There was a slope failure at the completion of filling. Re-construction involved re-placement of the side hill fill after removing portions of the slide mass and after restraining the soil mass through the use of 8 ft by 8 ft anchored concrete thrust blocks. The thrust blocks were buried into the slope and the outer slope surface was surficially stabilized utilizing a mechanically stabilized earth system. A rock fill toe berm was also constructed downslope at the toe to buttress the side hill fill.

In 2002 there was minor cracking of the building's masonry walls. See Figures 1 and 2 below for an illustration of the observed damage in 2004.

Figure 1 Figure 2

Survey monitoring points were installed in the walls and a slope inclinometer (T-1) was installed at the southeast corner of the building. In the fall of 2004, additional cracking and structural damage to the steel x-bracing in the southeast corner of the building was noticed. The installed inclinometer and building monitoring points were not read but were still intact.

An extensive subsurface investigation and instrumentation program was implemented in the Winter of 2004 and the Spring of 2005. Based on the results of the supplemental subsurface investigation, instrumentation program and back-analysis utilizing the approximate failure geometry of the previous slope failure, a two-tiered, anchored sheet pile wall was implemented to provide supplemental restraint to the creeping side hill soil mass. The instrumentation detected increased rates of movement each month which required immediate remedial work. Installation of the supplemental restraint system was complicated by the presence of existing stabilization measures installed in 2001 and the increasing rates of movement indicated by the slope and building instrumentation. Immediate restraint was provided to the footing at the building corner at the top of the slope utilizing minipiles and soil anchors followed by expeditious implementation of mid-slope and down-slope restraint. Fast-track design and construction was implemented through a cooperative and coordinated effort by the Owner, Structural and Geotechnical consultants, General Contractor and specialty Contractors.

This paper will present the initial construction, subsequent repair, results of the instrumentation program and subsurface investigation, analyses and the stabilization measures implemented in 2004 to hold and restrain the side-hill fill. Since implementation of the two tiered, anchored sheet pile wall, monitoring has been on-going and the results of the monitoring program since completion of construction are presented.

INTRODUCTION

In June 2002 the authors were engaged for a short period to provide consulting services. The information presented prior to the author's engagement is provided as necessary background information to facilitate presentation of the initial construction and initial slide repair, which began in 2001. The authors were continually involved in 2004 and 2005 with all of the geotechnical phases of the project as a collaborative effort with numerous parties involved with the work previously.

PROJECT LOCATION AND DESCRIPTION

The development site is located along the north side of interstate 64 in Barboursville, WV. The site of the retail store was part of a large 25 acre retail development including several large anchor stores, miscellaneous strip type configured retail stores, large parking areas and vehicular access roadways. The site is located at the base of a ridge having a maximum height of 890 ft, msl. The lowest site elevation is approximately 560 ft, msl. Prior to development, the site was utilized as farmland, including a pond on the property.

The structure consists of a 1-level retail structure having an approximate building footprint area of 125,400 square feet. A 7 acre parking area was also constructed specifically to support the retail structure. Maximum column loads for the 1-story structure were approximately 120 kips and the ground floor slab consisted of a concrete ground floor slab on grade. Elevations within the limits of the project site ranged from approx el 630 ft to approx el 680 ft, which required up to 37 ft of cut and 45 ft of fill to establish the finished floor elevation of 667 ft for the proposed retail structure. Extending east of the proposed limits of the structure was a natural slope, which resulted in the need to construct a side hill fill to facilitate construction of the building pad, appurtenant infrastructure features of the project including, the access delivery road, stormwater management structures, the loading dock, truck turning areas, natural gas service, and an electric power loop for the development. The height of the side hill fill from the toe of slope to top of slope was approximately 70 ft.

SUBSURFACE CONDITIONS AND INITIAL LABORATORY TESTING

Based on published geologic information, the project site is underlain by both the Conemaugh and Monongahela group formations, which consist of sandstone, siltstone, shale, limestone and coal. Outcrops and observations of road cuts indicates the rock formations to consist predominantly of shale and siltstone bedrock. The general site subsurface conditions consist of residual silt and clay overlying shale bedrock. The transition between residual soil and competent shale rock is variable.

In January of 2001, a total of twenty-five (25) borings were drilled throughout the area of the proposed building footprint and proposed parking areas utilizing hollow stem auger drilling techniques. Typical SPT N-values within the residual silt and clay ranged from 10 blows/ft to 25 blows/ft within the upper approximate 10 ft. Increasing penetration resistance with depth below about 10 ft were recorded from 30 blows/ft to 100 blows/ft until the interface of residual soil to weathered rock. The weathered rock typically had SPT N-values ranging from 50 blows/ft to refusal type N-values (i.e., 50 or 100 blows over several inches of penetration). No borings were drilled in the area of the side hill fill.

INITIAL SLOPE DESIGN, FAILURE AND REPAIR

The side hill fill was placed on an existing slope by benching in and placing processed shale, sandstone and residual soil fill material, which was harvested by excavating and blasting other areas of the site. The initial slope was to be configured with a slope of 2H:1V and was subsequently revised to allow construction on a 1.75H:1V slope. Reportedly, the design factors of safety were on the order of 1.5 and 1.4, respectively for the 2H:1V and 1.75H:1V slope inclinations. Placement of fill within the building pad and side hill fill was completed between August and September of 2001. In late September of 2001, a side hill fill slope failure occurred immediately after completion of filling. Reportedly, the slide mass was approximately 100 ft to 150 ft wide, extended 5 ft to 10 ft west of the crest of the slope and a toe bulge extended approximately 75 ft beyond the toe of the slope. The results of the laboratory testing program indicated a range of effective stress strength parameters for remolded compacted fill of 28 degrees to 33 degrees with cohesion values of 100 lbs/ft^2 to 650 lbs/ft^2 based on consolidated undrained, triaxial testing with pore pressure measurements and large box direct shear tests. Typical remolded dry unit weights varied from 110 lbs/ft^3 to 115 lbs/ft^3 with remolded water contents of 10% to 15%. Back analysis of the slide geometry (i.e., for a factor of safety of 1.0), based upon a weak layer at the interface of the residual clay and silt indicated a friction angle within the weak layer of 13 degrees presuming a non-circular, block or wedge type failure mechanism.

The slope was repaired between October of 2001 and December of 2001 by removing a portion of the slide mass, placing a geosynthetic encased rock buttress (i.e., 12 inch to 24 inch diameter durable limestone rock in a trench) at the toe of the slope, installing individual thrust block restraints tied-back to the underlying shale bedrock and reinforcing the slope face with geosynthetics. The individual thrust block restraints were 8 ft by 8 ft by 2.5 ft thick, were embedded approximately 15 ft beneath the geosynthetic, reinforced slope face and consisted of two rows of individual square concrete blocks. The lower row of anchors consisted of fourteen (14), 210 kip design capacity, six strand, triple corrosion protected anchors spaced at 12 ft center to center. The upper row of anchors consisted of fifteen (15), 250 kip design capacity, seven strand, triple corrosion protected strand anchors spaced at 10 ft center to center. The strand anchors were installed at 2H:1V inclinations, embedded into the underlying shale bedrock and attached to reinforced concrete thrust blocks with embedded steel bearing plates. All strand anchors were reportedly tested to 120% to 133% of their design capacity in accordance with the Post Tensioning Institute's Guidelines and locked off near their respective design loads. The final resulting slope angle after applying restraint was reportedly 1.75H:1V. By mid April of 2002 building construction had been completed. See Figure 3 below for a schematic of the side hill fill restraint system, which was intended to address both surficial sloughing as well as the potential for a more deep seated slope instability.

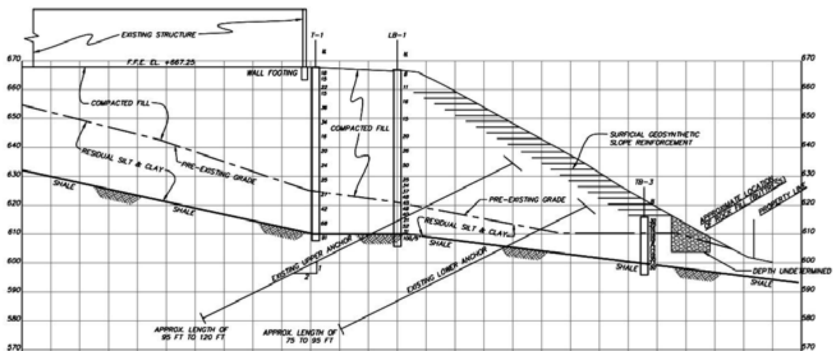

Figure 3. Initial Side Hill Restraint System and Subsurface Conditions

BUILDING, SLOPE MONITORING AND SUPPLEMENTAL SUBSURFACE INVESTIGATION

Between the completion of the initial slide repair in December of 2001 and early 2005, the slope and building were monitored to determine the rate and magnitude of both vertical and lateral deformations. In June 2004 there was a report of noticeable and significant damage in the southeast corner of the building. There had been 4 inches of settlement and 0.6 inch of lateral movement. A supplemental subsurface investigation was performed at the crest of the slope, which included drilling of nine (9) borings utilizing hollow-stem auger techniques. The photograph below shows the condition of the weak material at the residual clay and silt to weathered rock interface. This sample also correlated to the depth of the failure surface based on the slope inclinometer readings.

Figure 4. Slide Plane Sample at Residual Material to Weathered Rock Interface

The instrumentation consisted of both in-ground slope inclinometers as well as monitoring points installed at selected intervals along the exterior face of the block wall of the structure bordering the repaired slope. Between June of 2002 and April of 2005, the SE corner of the structure settled approximately 8 inches and the SE corner of the structure moved southeast approximately 2.25 inches as determined through the slope inclinometer readings. Additionally, the SE corner of the structure was surveyed and verified the southeasterly lateral movement relative to the construction as-built. The T-1 slope inclinometer readings indicated the slope movement to begin at a depth of approximately 45 ft from the surface grade. The rates of lateral movement between July 2002 and October of 2004 were on the order of 0.5 inch per year (0.04 inch/month). Between October of 2004 and March of 2005, increased rates of lateral movement on the order of 1.0 inch/year (0.08 inch/month) were measured. Between July of 2002 and October of 2004, vertical movements at the southeast corner were occurring at rates of 0.16 inch per month. Increased rates of movement of 0.2 inch per month and 0.33 inch per month were measured between October of 2004 and December of 2004 and December of 2004 and March of 2005, respectively. The zone of significant impact extended 75 ft north of the southeast corner and 50 ft west of the southeast corner. See Figure 5 below for the magnitude and trend of movement of selected data points installed along the façade of the structure and monitored utilizing optical surveying techniques.

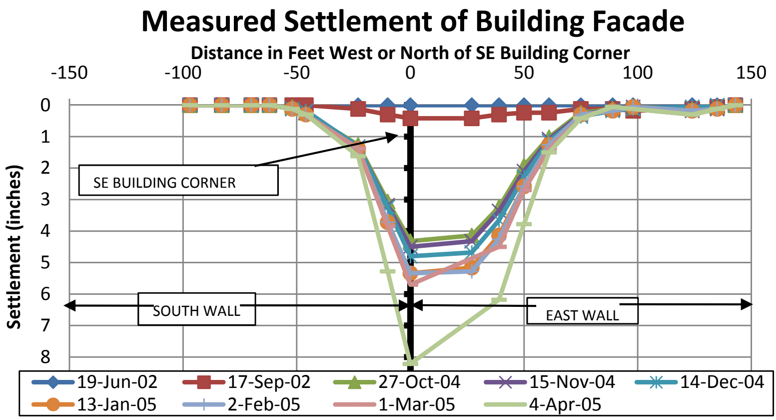

Figure 5. Magnitude and Trend of Building Façade Deformation

SECOND SLIDE REPAIR CONCEPT

Based on the results of the building and slope monitoring program, indicating increased rates of movement in both the vertical and lateral direction, supplemental slope stability analyses were performed to determine the extent and magnitude of supplemental restraint required based upon a deep seated non-circular slope failure. Slope stability analyses indicated for movements, "creep", to be on-going with the anchored thrust blocks in-place, the deep seated failure plane has a reduced shear strength (i.e., 10 degrees) as a result of continued movement.

A supplemental building and slope restraint program was designed and consisted of the installation of a two tiered anchored sheet pile wall. The footing located at the southeast corner of the structure was underpinned with nine (9), 50-ft-long, 8-inch-diameter mini-piles and laterally restrained with four (4), 90-ft-long soil anchors. The sheet pile walls and building stabilization measures were configured and installed such that the restraint applied in 2001 would remain, with the exception of the surficial geosynthetic. Both anchored steel sheet pile walls located mid-slope and toe of slope were installed. The toe of the mid-slope wall was terminated within the residual silt and clay and the toe of the wall at the bottom of the slope was driven to penetrate the surface of the weathered shale bedrock. At the mid-slope location, approximately twenty-one (21), 240-kip design capacity, double corrosion protected, 1-7/8 inch-diameter, high-capacity, 150-ksi, bar anchors were installed along the 200 linear foot AZ26 sheet pile wall. At the toe of slope location, approximately thirty-four (34), 240-kip design capacity, double corrosion protected, 1-7/8 inch-diameter, high capacity, 150-ksi, bar anchors were installed along the 300 linear foot AZ26 sheet pile wall. All anchors were installed to lengths ranging from 130 ft to 190 ft at the mid-slope location and lengths ranging from 90 ft to 105 ft at the toe of slope location. Minimum bond lengths were 55 ft to develop the design axial, tensile capacities with typical inclinations from horizontal of 25 to 35 degrees. All anchors were drilled utilizing casing to the surface of the rock and open hole drilled into the rock with a down-hole hammer having a minimum diameter of 5-inches. Neat cement grout having a design strength of 5,000 psi and grout tubes were utilized to facilitate post-grouting. Typically the anchors were load tested to 125% to 133% of their design load and locked off at 100% of their respective design loads. The figure below shows a schematic of the anchored, two tiered sheet pile walls as well as the restraint installed in 2001.

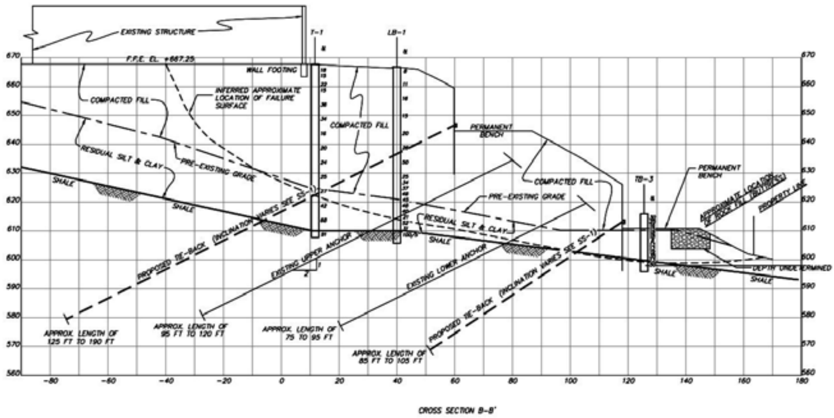

Figure 6. Anchored Two-Tiered Sheet Pile Wall Schematic

POST-CONSTRUCTION BUILDING AND SLOPE MONITORING

Upon completion of building and slope stabilization construction in June of 2005, two (2) slope inclinometers remained and were utilized as part of the post-construction monitoring program. Additionally, monitoring points were installed along the façade of the structure, at selected locations along the mid-slope and toe of slope sheet pile wall and at the ends of the tie-backs. The results of the inclinometers indicate maximum movements of 3/8 of an inch in a southeasterly direction at a depth of 10 ft between July of 2005 and February of 2007, with an average rate of movement of 0.02 inch per month. The results of lift off tests performed in November of 2006 indicate typically 5% to 15% reduction in tie-back load for the mid-slope wall and 0% to 5% reduction in tie-back load for the wall located at the toe of the slope. The results of building monitoring between July of 2005 and March of 2008 along the façade of the structure indicated the following: 1) less than 3/8 of an inch of movement along the south wall, 2) no movement of the southeastern column occurred, and 3) less than ½ of an inch of movement occurred along the east wall. Based on the observations made during a site visit in July of 2009, no significant change in building conditions have been observed between November of 2007 and June of 2009.

Conclusions

The following conclusions were drawn based on the author's involvement with this project over an extended period of time:

1) A cooperative effort between the original design team and contractors was essential to facilitate installation of supplemental side hill fill restraint in 2005.

2) Back analysis utilizing the original slide failure geometry concluded shear strengths along the slide plane had reduced resulting in the need for supplemental side hill fill restraint.

3) Execution and installation of supplemental restraint in 2005 was challenging and complicated by the presence of existing side hill fill restraint.

4) Monitoring of both vertical and lateral deformations throughout the installation of the restraint system in 2005 provided the necessary information to determine the required lateral extent for both the toe of slope and mid slope stabilization measures.

5) Post construction monitoring since June of 2005 indicates some post-construction movement was necessary to engage the lateral restraint and the sidehill fill has not undergone significant movement to date. Lift-off tests performed in November of 2006 indicate typically 5% to 15% reduction in tie-back load for the mid-slope wall and 0% to 5% reduction in tie-back load for the wall located at the toe of the slope. The reduction in load indicates the soil mass has not moved sufficiently down slope to add load to the tie-backs.

Acknowledgements

The authors would like to extend their appreciation to the owner, general contractor and specialty contractors involved with this challenging project. It is only through the owner's willingness to continue monitoring programs and understanding of the need for fast-track implementation of a stabilization program that this project has been a success to date.

References

American Society of Civil Engineers Manual, "Design of Sheet Pile Walls" October 22, 1996.

FHWA Publication IF-99-015 "Geotechnical Engineering Circular No. 4-Ground Anchors and Anchored Systems", FHWA, Washington, DC, 1999.

Post-Tensioning Institute Fourth Edition, "Recommendations for Prestressed Rock and Soil Anchors", 2004.

This page intentionally left blank

Author Index

Page number refers to the first page of paper

This page intentionally left blank

Subject Index

Page number refers to the first page of paper

